PHYSICAL REVIEW

Volume 99 Number 2

JULY 15, 1955

Published by the
AMERICAN PHYSICAL SOCIETY
Editorial Office, 175 Fifth Avenue, New York 10, N. Y.

THE PHYSICAL REVIEW

A journal of experimental and theoretical physics established by E. L. Nichols in 1893

Published by the American Institute of Physics
for the
AMERICAN PHYSICAL SOCIETY

Officers

President

E. T. Bowen
University of California
Berkeley, California

Vice-President

E. P. Wigner
Princeton University
Princeton, New Jersey

Secretary

K. K. Darrow
Bell Telephone Laboratories
Office
Columbia University
New York 27, New York

Treasurer

G. B. Pegram
Columbia University
New York 27, New York

Local Secretary
for the Pacific Coast

William A. Nierenberg
University of California
Berkeley, California

Managing Editor

S. A. Goudsmit
Brookhaven National Laboratory
Upton, Long Island
New York

BOARD OF EDITORS

Editor

S. A. Goudsmit

Associate Editors

1953–1957	1954–1958	1955–1959
W. A. Fowler	P. G. Bergmann	G. J. [illegible]
Kenneth Greisen	Gregory Breit	R. G. [illegible]
Charles Kittel	F. J. Dyson	K. G. [illegible]
R. E. Marshak	P. Kusch	J. R. [illegible]
W. K. H. Panofsky	E. Stuckelberg	Lewi [illegible]
V. F. Weisskopf	J. C. Slater	Gregory [illegible]

Manuscripts for publication should be submitted to S. A. [illegible], Brookhaven National Laboratory, Upton, Long Island, New York. Authors' institutions are requested to pay a publication charge of [illegible] page which, if honored, entitles them to 100 free reprints. Instructions will be sent with galley proofs.

Proof and all correspondence concerning papers in the process of publication should be addressed to the Publication Manager, American Institute of Physics, 57 East 55 Street, New York 22, New York.

Subscription Rates

United States and Canada.....$20.00
Elsewhere.....$22.00

Back Numbers

Yearly back number rate when complete year is available:
Prior to 1949: $25.00
Thereafter: $20.00
Single copies: $2.00 each, prior to July, 1941;
$2.50 each, July, 1941–December, 1945;
$3.00 each, January, 1946–December, 1948;
$4.50 each, thereafter.
General Index, 1893–1920: $6.00.
1921–1930: Paper binding, $10 (Members); $14 (Nonmembers);
Cloth binding, $12 (Members); $16 (Nonmembers).

Subscriptions, renewals, and orders for back numbers should be addressed to the American Institute of Physics, 57 East 55 Street, New York 22, New York.

Changes of address in the case of members of the American Physical Society should be addressed to the Treasurer; in the case of other subscribers to the American Institute of Physics.

[1] For Series I reprint of Physics Department, Cornell University, Ithaca, New York.

The Physical Review is published semi-monthly at Ithaca and Lancaster, Pennsylvania.

Entered as second-class matter March 6, 1917, at the Post Office at Lancaster, Pennsylvania, under the Act of March 3, 1879.

Acceptance for mailing at special rate of postage provided for in paragraph (d-2), section 34.40, P. L. and R., authorized January [illegible].

THE
PHYSICAL REVIEW

A journal of experimental and theoretical physics established by E. L. Nichols in 1893

SECOND SERIES, VOL. 99, NO. 2 JULY 15, 1955

Bipartition Angles for Compton Scattering by Free Electrons

H. M. CHILDERS AND J. D. GRAVES
Naval Research Laboratory, Washington, D. C.
(Received March 24, 1955)

In the Compton scattering of free electrons, the bipartition angles for the number of scattered photons, the number of secondary electrons, the energy of scattered photons, and the energy of the secondary electrons have been tabulated in terms of the incident photon energy from 10 kev to 10 Mev. (The bipartition angle for a quantity is the half-angle of the cone into which one-half of that quantity is scattered.) The average scattered photon energy and the average Compton electron energy have also been computed. In addition, a relation is given for the probability that the Compton electron energy will fall into the energy interval (E_1,E_2).

1. INTRODUCTION

MANY applications of Compton scattering theory result in very complex formulations which require numerical solutions. In some cases it is possible to assume that the recoiling electrons or photons will go in the direction of the bipartition angle for the number or energy of the recoiling particle and with the average energy of the particle. (The bipartition angle for a quantity which results from Compton events is the half-angle of the cone into which one-half of that quantity will be scattered.) The cone has its apex at the point of the event with axis along the incident photon direction, and opens in the direction of the incident photon. This in general simplifies the solutions to such problems considerably. These bipartition angles were calculated for application in cavity ion-chamber theory over the incident photon energy range from 20 kev to 3.0 Mev.

The bipartition angles for the number of photoelectrons, and curves from which some values for Compton-scattered photon bipartition angles can be estimated, are given by Davisson and Evans.[1] Graphs from which bipartition angles for Compton scattering may be obtained by "counting squares" or dividing the area under distribution curves into two equal parts have been prepared by Nelms.[2] The bipartition angles in this report have been computed directly by integrating the differential formulas and making use of available cross sections. The computations were carried out to the closest one-half degree or better.

[1] C. M. Davisson and R. D. Evans, Revs. Modern Phys. **24**, 79 (1952).
[2] Ann T. Nelms, National Bureau of Standards Circular 542 (U. S. Department of Commerce, Washington, D. C., 1953).

2. METHODS OF COMPUTATION

The angles θ and ϕ that the scattered photon and electron respectively make with the incident photon direction are related by

$$\cos\theta = 1 - \frac{2}{(1+\alpha)^2 \tan^2\phi + 1}, \tag{1}$$

where $\alpha = h\nu/mc^2$ is the incident photon energy in units of electron rest masses, $h\nu$ being the photon energy.

The bipartition angle $\bar{\theta}$ for the number of scattered photons is obtained through the relation

$$_e\sigma^{\bar{\theta}} = \tfrac{1}{2}\,{}_e\sigma, \tag{2}$$

where $_e\sigma$ is the total Klein-Nishina cross section, and $_e\sigma^{\theta}$ is the cross section for scattering between the angles 0 and θ.

The bipartition angle, $\bar{\theta}$, may be obtained by integrating the Klein-Nishina differential cross section between the limits zero and an angle which will give just one-half of the total cross section. Integrating the Klein-Nishina differential cross section between 0 and an arbitrary upper limit θ gives[1]

$$\begin{aligned} {}_e\sigma^{\theta} = \pi r_0^2 \{ & [4+10\alpha+8\alpha^2+\alpha^3 \\ & -(4+16\alpha+16\alpha^2+2\alpha^3)\cos\theta \\ & +(6\alpha+10\alpha^2+\alpha^3)\cos^2\theta - 2\alpha^2\cos^3\theta] \\ & \times [2\alpha^2(1+\alpha-\alpha\cos\theta)^2]^{-1} \\ & +\alpha^{-3}(\alpha^2-2\alpha-2)\ln(1+\alpha-\alpha\cos\theta)\}, \end{aligned} \tag{3}$$

TABLE I. Values of bipartition angle for number of photons, $\bar{\theta}$; bipartition angle for the energy of the photons scattered, θ'; bipartition angle for the number of electrons, $\bar{\phi}$; bipartition angle for the electron energy, ϕ'; average scattered photon energy, $\bar{E}_{ph}$, and average electron energy, $\bar{E}_{el}$.

$h\nu$ (Mev)	$\bar{\theta}$ deg	θ' deg	$\bar{E}_{ph}$ (Mev)	$\bar{\phi}$ (deg)	ϕ' (deg)	$\bar{E}_{el}$ (Mev)
0.010	88.0	88.0	0.0099	45.4		0.12×10^{-4}
0.020	86.6	85.2	0.0194	45.6		0.64×10^{-4}
0.040		79.8	0.0374			2.6×10^{-4}
0.050	83.0		0.0460	45.8	28.9	4.0×10^{-4}
0.060		76.5	0.054		28.9	5.6×10^{-4}
0.080	79.7	73.0	0.071	46.0	28.8	9.4×10^{-4}
0.100		70.5	0.086		28.8	0.014
0.150	73.8	65.0	0.123	45.8	28.5	0.027
0.200	70.9	60.8	0.156	45.3	28.2	0.044
0.300	66.6		0.219	43.8	27.3	0.081
0.400	63.7	50.5	0.276	42.1	26.4	0.124
0.600	59.9	44.5	0.379	38.6	24.4	0.221
0.800	57.3	40.5	0.474	35.6	22.5	0.326
1.00	55.5	37.5	0.56	33.0	20.7	0.44
1.50	52.1	32.0	0.76	27.5	17.5	0.74
2.00	49.8	29.0	0.94	23.7	15.2	1.06
3.00	46.2		1.27	18.8	12.2	1.73
4.00	44.2	20.3	1.58	15.0	10.2	2.42
5.00	42.4		1.87	13.0	8.5	3.13
6.00		17.3	2.14		7.7	3.86
8.00		15.3	2.67		6.2	5.33
10.00		14.5	3.16		5.0	6.84

where $r_0=e^2/mc^2$ is the classical electron radius. The right hand sides of Eqs. (2) and (3) were equated and numerically solved for $\bar{\theta}$. The values of $\bar{\theta}$ are given in Table I and Fig. 1, as a function of incident photon energy.

The bipartition angle for the number of electrons scattered is obtained as follows. Let $P(\phi)$ be the probability per unit solid angle that an electron will be scattered in the direction ϕ, then the probability that an electron will be scattered through an angle ϕ into the solid angle $d\omega'(\phi)$ is

$$d_e\sigma(\phi)=P(\phi)d\omega'(\phi). \tag{4}$$

The probability that an electron will be scattered into the solid angle $d\omega'(\phi)$ is equal to the probability, $K(\theta)d\omega(\theta)$, that a photon will be scattered through an angle θ into the solid angle $d\omega(\theta)$, hence

$$d_e\sigma(\phi)=K(\theta)d\omega(\theta), \tag{5}$$

where ϕ and θ are related by Eq. (1). This equation may be evaluated by changing the variable from θ to ϕ either before or after integration. Integration gives

$$_e\sigma(\phi)\Big|_{\phi_1}^{\phi_2}={}_e\sigma(\theta)\Big|_{\theta_1}^{\theta_2}.$$

If the right-hand side is evaluated between 0 and θ, it becomes Eq. (3), and corresponding to 0 and θ we have on the left-hand side $\pi/2$ and ϕ, which we write as

$${}_e\sigma^{\phi}={}_e\sigma^{\theta}.$$

Setting this equal to half the total cross section gives the bipartition angles for the number of photons scattered, Eq. (2), and the bipartition angle ϕ for the number of electrons scattered, that is

$${}_e\sigma^{\bar{\theta}}={}_e\sigma^{\bar{\phi}}=\tfrac{1}{2}\,{}_e\sigma, \tag{6}$$

where

$$\bar{\theta}=\cos^{-1}\left[1-\frac{2}{(1+\alpha)^2\tan^2\bar{\phi}+1}\right].$$

The values of $\bar{\phi}$ are given in Table I and Fig. 1, as a function of incident photon energy.

The bipartition angle θ' for the photon energy scattered is obtained from the relation

$${}_e\sigma_s^{\theta'}=\tfrac{1}{2}({}_e\sigma-{}_e\sigma_a), \tag{7}$$

where ${}_e\sigma_s^{\theta'}$ is the cross section for the photon energy scattered between 0 and θ', and ${}_e\sigma_a$ is the cross section for the energy absorbed by the electron. The cross section for the photon energy scattered between zero and θ is given by the relation[1]

$$\begin{aligned}{}_e\sigma_s^{\theta}=\pi r_0^2\{&\alpha^{-3}\ln(1+\alpha-\alpha\cos\theta)\\&-[6\alpha^2(1+\alpha-\alpha\cos\theta)^3]^{-1}\\&\times[6+15\alpha+3\alpha^2-12\alpha^3-8\alpha^4\\&-(6+30\alpha+27\alpha^2-18\alpha^3-24\alpha^4)\cos\theta\\&+(15\alpha+33\alpha^2-24\alpha^4)\cos^2\theta\\&-(9\alpha^2+6\alpha^3-8\alpha^4)\cos^3\theta]\}.\end{aligned} \tag{8}$$

Values for the right-hand side of Eq. (7) were calculated from the data of White.[2] These values were substituted into the left hand side of Eq. (8) which was then solved numerically for θ'. The values of θ' are given in Table I and Fig. 1, as a function of incident photon energy.

The electron energy scattered into the solid angle $d\omega'(\phi)$ is the probability that an electron will be scattered into $d\omega'(\phi)$ multiplied by the energy that an

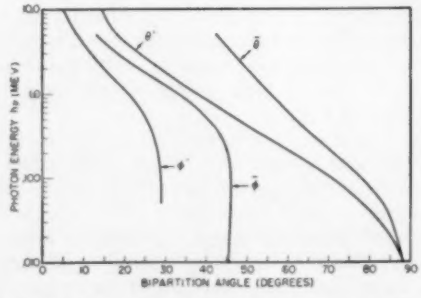

FIG. 1. Bipartition angles vs incident photon energy for Compton scattering. Bipartition angles $\bar{\theta}$, θ', $\bar{\phi}$, and ϕ' are for the number of scattered photons, scattered photon energy, number of scattered electrons, and scattered electron energy respectively.

[2] The cross sections by G. R. White, National Bureau of Standards Report 1003, 1952 (unpublished) were used throughout these computations.

electron scattered in the direction ϕ will have, i.e.,

$$dE_{el}(\phi)=E_{el}d_e\sigma(\phi)$$

$$=h\nu\left[1-\frac{1}{1+\alpha(1-\cos\theta)}\right]K(\theta)d\omega(\theta), \quad (9)$$

but the right-hand side of Eq. (9) is

$$h\nu[d\,{}_e\sigma(\theta)-d\,{}_e\sigma_s(\theta)],$$

which upon integration gives

$$\int dE_{el}=h\nu\,{}_e\sigma_a(\phi)\Big|_{\phi_1}^{\phi_2}=h\nu[{}_e\sigma(\theta)-{}_e\sigma_s(\theta)]\Big|_{\theta_1}^{\theta_2}.$$

Evaluating this expression between $\theta=(0,\theta)$ and $\phi=(\pi/2,\phi)$ gives

$$h\nu\,{}_e\sigma_a{}^{\phi}=h\nu[{}_e\sigma^{\theta}-{}_e\sigma_s{}^{\theta}]. \quad (10)$$

The bipartition angle for the electron energy scattered is obtained by setting Eq. (10) equal to one-half of the total energy absorbed by the electrons and solving for θ.

$${}_e\sigma_a{}^{\phi'}={}_e\sigma^{\theta}-{}_e\sigma_s{}^{\theta}={}_e\sigma_a/2. \quad (11)$$

Equation (11) may be solved either by changing variables from θ to ϕ' through Eq. (1), and then solving numerically for ϕ', or it may be solved numerically for θ and this value of θ substituted into Eq. (1) to give ϕ'. In terms of θ, Eq. (11) becomes

$$\begin{aligned}\pi r_0^2\{&[18+57\alpha+57\alpha^2+15\alpha^3-5\alpha^4\\&-(18+102\alpha+153\alpha^2+60\alpha^3-15\alpha^4)\cos\theta\\&+(45\alpha+129\alpha^2+81\alpha^3-15\alpha^4)\cos^2\theta\\&-(33\alpha^2+42\alpha^3-5\alpha^4)\cos^3\theta+6\alpha^3\cos^4\theta]\\&\times[6\alpha^2(1+\alpha-\alpha\cos\theta)^2]^{-1}\\&+[(\alpha^2-2\alpha-3)/\alpha^3]\ln(1+\alpha-\alpha\cos\theta)\}={}_e\sigma_a/2. \quad (12)\end{aligned}$$

The values for ${}_e\sigma_a$ given in reference 3 were employed in Eq. (12) to compute ϕ'. The values of ϕ' are given in Table I and Fig. 1, as a function of incident photon energy.

The energy distribution as a function of the number of Compton electrons is given in the appendix of reference 1 as

$$\frac{d_e\sigma}{dE_{el}}=\frac{2\pi k(\theta)}{\alpha h\nu}\left[\frac{(1+\alpha)^2-\alpha^2\cos^2\phi}{(1+\alpha)^2-\alpha(2+\alpha)\cos^2\phi}\right]^2. \quad (13)$$

This expression can be integrated between two arbitrary limits (E_1,E_2) to give the probability $P(E_1,E_2)$ that an electron will be scattered into the energy interval (E_1,E_2). This integration yields

$$\begin{aligned}P(E_1,E_2)=&\pi r_0^2\alpha^{-3}(h\nu)^{-2}\\&\times\left[\frac{(h\nu)^3}{h\nu-E}-h\nu(2\alpha+1)(h\nu-E)-\alpha^2(h\nu-E)^2/2\right.\\&\left.+(h\nu)^2(2+2\alpha-\alpha^2)\ln(h\nu-E)\right]\Big|_{E_1}^{E_2}, \quad (14)\end{aligned}$$

where $E_1<E_2\leq 2\alpha h\nu/(1+2\alpha)=$ the maximum energy a Compton scattered electron can assume. The bipartition energy E' may be computed by placing $E_1=0$ and $E_2=E'$ in Eq. (14) and setting this expression equal to ${}_e\sigma_a/2$.

It can be shown that the average energy, $\bar{E}_{el}$, of scattered electrons is given by

$$\bar{E}_{el}=h\nu({}_e\sigma_a/{}_e\sigma) \quad (15)$$

consequently, the average scattered photon energy $\bar{E}_{ph}$ is

$$\bar{E}_{ph}=h\nu(1-{}_e\sigma_a/{}_e\sigma). \quad (16)$$

Table I and Fig. 2 give the values of the average scattered photon energy $\bar{E}_{ph}$ and the average scattered electron energy $\bar{E}_{el}$.

The value of r_0 was taken as 2.8175×10^{-13} cm, and the rest energy of the electron was taken as $mc^2=0.5110$ Mev throughout the calculations in this paper.

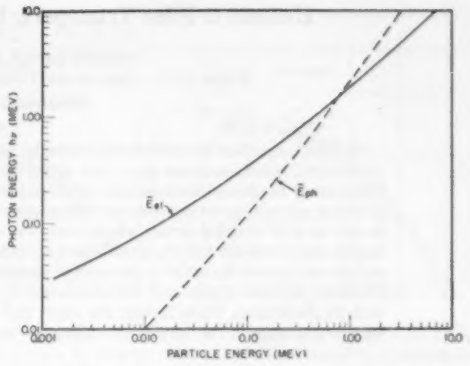

FIG. 2. Average energy $\bar{E}_{ph}$ of scattered photons and average energy $\bar{E}_{el}$ of scattered electrons *vs* incident photon energy for Compton scattering.

Helium II Film Transport. II. The Role of Surface Finish*

BERNARD SMITH† AND HENRY A. BOORSE‡
Pupin Physics Laboratories, Columbia University, New York, New York

(Received February 8, 1955)

The effect of surface finish has been studied by comparing transport rates measured on four metal beakers (aluminum, nickel, stainless steel, and nickel-silver), before and after they had been "superfinished." Deliberately roughened surfaces were employed in similar control experiments on glass. Measured values of beaker microfinish are reported for comparison with flow rates. The data obtained with these specimens, as well as with a nickel beaker whose inner wall was broached to provide, in effect, a capillary covered surface, are consistent with the hypothesis that transport rates adjust to the prevailing microscopic perimeter and do not require the added hypothesis of anomalous flow in surface cracks. A scheme for estimating the difference between macro- and micro-perimeter is proposed, and the flow data are found to be consistent with its predictions. These include the result that a large increase in surface roughness may not imply a very large change in the microscopic perimeter "seen by the film."

THE present study is concerned with the clarification of the answer to the question: How do measured transport rates vary with the surface finish of the substrate? Since the background of the problem has already been discussed in a previous paper,[1] further introduction is omitted here.

EXPERIMENTAL RESULTS[2]

The first results of interest were obtained from a preliminary investigation of the effect of systematic roughening of beaker surfaces. Various observers[3–6] have often speculated on the effect of what Daunt and Smith have recently aptly described as the "semi-capillary nature of the rough surfaces."[7] Nickel beaker specimen Ni-I (see Table I) was therefore broached, with the resulting longitudinal striations on the inner wall providing, in effect, a capillary covered surface. The original inner circumference of the beaker was covered by 100 equally spaced, slightly trapezoidal striations, 0.001 in. deep, 0.002 in. wide, and 0.010 in. apart. The size and distribution of these grooves were dictated by the mechanical requirements of the broaching operation. The broached surface extended from the rim to a depth of 0.985 in., the over-all inner depth being 1.530 in. By using a core with three calibrated regions (instead of the four shown in Fig. 2 of I),[1] with only two corresponding to liquid levels in the broached region, it was possible to compare flow rates obtained when the bottom of these narrow channels was above and below the liquid level in the beaker. In order to free the measurements from any ambiguity associated with a possible height dependence (to be described in paper III), a brief prebroaching control experiment (run 13) was performed using the same three-section core to check the average rates associated with these heights in the original bored beaker. The midpoints of Secs. 1, 2, and 3 were respectively 1.2 cm, 2.1 cm, and 3.0 cm from the rim, with Sec. 1 beginning 0.8 cm from the rim. The data for the broached beaker (runs 17 and 22) appears in Fig. 1, together with the average rates obtained at 1.25°K for the same heights before broaching. Transport rates

TABLE I. Identification of beakers. Since symbols (including the numbers assigned to identify runs) have the same meaning as in Table II of the preceding paper (I),[1] the composition of various specimens is omitted here.

Material	Specimen symbol	Condition of surface	Run numbers referred to in text
Aluminum	Al-II (B)	Bored	55
	Al-II (ES)	Externally superfinished	62,65
	Al-II (IS)	Internally superfinished	68
Glass: precision bore Pyrex	G-III	Untreated	56
	G-IV (FG)	Fine ground	54
	G-V (CG)	Coarse ground	57
Nickel	Ni-I (B)	Bored	13
	Ni-I (Br)	Broached	17,22
	Ni-II (R)	Reamed	53
	Ni-II (ES)	Externally superf.	60
	Ni-II (IS)	Internally superf.	67,69,70
Nickel silver	Ni-Ag II (B)	Bored	45,46,49
	Ni-Ag II (ES)	Externally superf.	52
	Ni-Ag-II (IS)	Internally superf.	64
Stainless steel	S.St. (B)	Bored	41-44,47
	S.St. (ES)	Externally superf.	50,51
	S.St. (IS)	Internally superf.	61,63

* Assisted by the Office of Naval Research and the Linde Air Products Company.

† Present address: Bell Telephone Laboratories, 463 West Street, New York 14, New York.
‡ Barnard College, Columbia University, New York 27, New York.

[1] B. Smith and H. A. Boorse, Phys. Rev. **98**, 328 (1955). (This paper is designated by the symbol I in the text.)

[2] Preliminary accounts of some of these results have already been presented in: (a) B. Smith and H. A. Boorse, Proceedings of the Third International Conference of Low Temperature Physics and Chemistry, Houston, December, 1953. (b) B. Smith and H. A. Boorse, Phys. Rev. **94**, 772 (1954). (c) B. Smith, Bull. Am. Phys. Soc. **30**, No. 1, 57 (1955).

[3] J. G. Daunt and K. Mendelssohn, Proc. Roy. Soc. (London) **A170**, 423 (1939).

[4] K. Mendelssohn and G. K. White, Proc. Phys. Soc. (London) **A63**, 1328 (1950).

[5] B. S. Chandrasekhar and K. Mendelssohn, Proc. Phys. Soc. (London) **A65**, 226 (1952).

[6] B. S. Chandrasekhar, Phys. Rev. **86**, 414 (1952).

[7] J. G. Daunt and R. S. Smith, Revs. Modern Phys. **26**, 172 (1954).

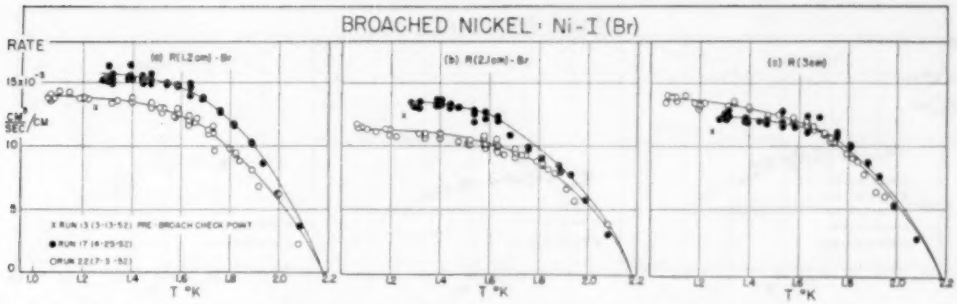

FIG. 1. Transport rates over broached nickel specimen Ni-I (Br), (a) between 0.8 cm and 1.6 cm from rim, (b) between 1.7 and 2.5 cm from rim, and (c) between 2.6 cm and 3.4 cm from rim. In each drawing, an average value at 1.25 °K, obtained in a prebroaching check run, is included for comparison. The key to symbols given in (a) also applies to (b) and (c).

were calculated using the added macroscopic volume and perimeter contributed by the broaching in Secs. 1 and 2, while the calculation for Sec. 3 was the same as before broaching. On the basis of the background variation in rates observed between runs 17 and 22, and similar evidence which will appear in subsequent discussion of other data, as well as the results reported in I,[1] it follows that surface capillaries of the size employed here did not enhance the flow of bulk liquid in an anomalous fashion.

A thorough study of the literature of metal surface finishing was undertaken to determine the feasibility of producing very smooth beaker surfaces. This led to the conclusion that the "superfinishing" process,[8] developed by the Chrysler Corporation, not only gave promise of producing the finest microfinish attainable,[8–11] but was also sufficiently flexible to be applicable to small scale cylindrical geometry. In the interests of brevity, the description of the process will be confined to the official definition formulated by D. A. Wallace: "Superfinishing is the name of a method of mechanically developing on metal parts a surface finish which is optically smooth and metallurgically free of any fragmented or smear metal, such as is created by the dimensional operations of turning, grinding, honing, lapping and/or burnishing. The superimposing of this process over previous machining operations removes the defective boundary layer material and exposes, for heavy duty load-carrying contact, the unworked and undisturbed crystalline base metal. The resultant superfinished surface is a true, geometrically developed, wear-proof bearing area, free of oil-film rupturing protuberances, and accurate to within submicroscopic range."[8] Aside from the purely industrial considerations of load carrying capacity and wear, which are irrelevant here, these specifications are seen to be admirable for transport vessel surfaces. For further information, including a complete description of the superfinishing process accompanied by many photomicrographs and profilograms illustrating the quality of the surfaces which may be produced using various techniques, as well as a discussion of the measurement of surface finish, one may consult the literature.[8–15]

A program for superfinishing metal beakers was arranged with the cooperation of the Production Research Department of the Chrysler Corporation. Specimens of nickel, aluminum, stainless steel and nickel-silver (in the compositions specified in I: Table II)[1] were selected as sufficiently representative of the materials which were deemed satisfactory for ultimate superfinishing. The design (shown in Fig. 2 of paper I)[1] incorporating four calibrated regions, was adopted as standard for all beakers. The undercut, labelled *U* therein, was added to facilitate the subsequent superfinishing operations.

Initial observations of film transport were made for each beaker in the original machined state, as delivered by the Columbia University Physics Department shop. The machining operations and the results of these measurements have already been described (for specimens Al-II, Ni-II, Ni-Ag-II, and S.St. in Table II of paper I)[1] in connection with the study of the role of substrate.

Prerun and installation procedures were the same as those previously described.[1]

Upon completion of the initial transport measurements, each beaker was mailed to Detroit for superfinishing of the outer surface only. During this operation the specimen was gripped by the approximately ½ in. long bearing surface provided by the solid base of the

[8] A. M. Swigert, *The Story of Superfinish* (Lynn Publishing Company, Detroit, 1940).
[9] G. Schlesinger, *Surface Finish* (The Institution of Production Engineers, London, 1942).
[10] J. J. Bikerman, *Surface Chemistry for Industrial Research* (Academic Press, Inc., New York, 1948).
[11] B. C. Brosheer, American Machinist, September 9 and 23 (McGraw-Hill Book Company, Inc., New York, 1948). The first article contains a valuable bibliography.
[12] *Surface Treatment of Metals* (American Society for Metals, Cleveland, 1941), pp. 392–427.
[13] Reason, Hopkins, and Garrod, *Report on the Measurement of Surface Finish by Stylus Methods* (Taylor, Taylor, & Hobson Ltd., Leicester, 1944).
[14] R. E. Reason, J. Inst. Production Engrs. (October, 1944).
[15] L. P. Tarasov, Trans. Am. Soc. Mech. Engrs. 67, 189 (1945).

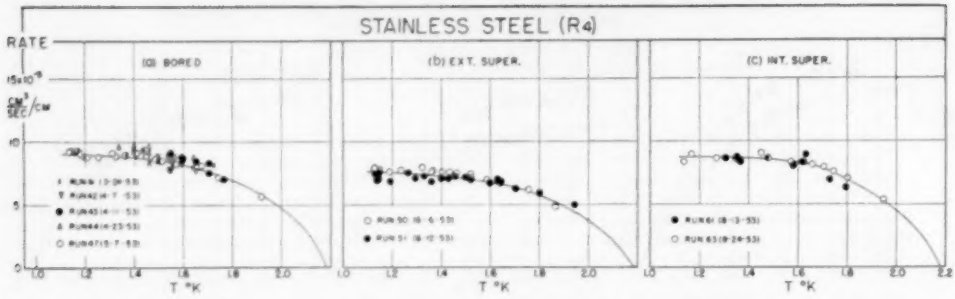

FIG. 2. Transport rates over a stainless-steel beaker in control experiments on surface finish. In each case the transport rates are averaged between 4.45 cm and 5.33 cm from the rim (R_4).

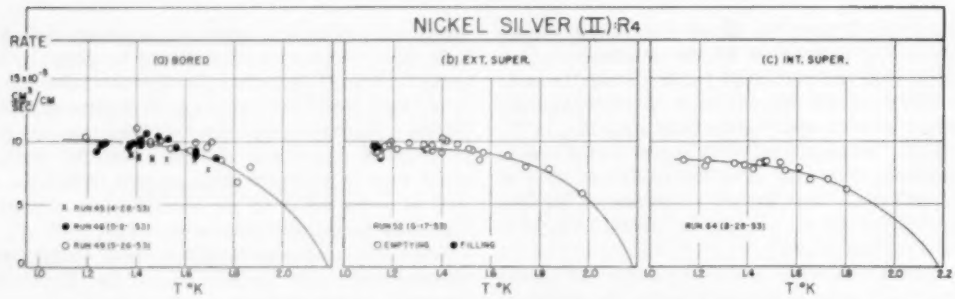

FIG. 3. Transport rates over a nickel-silver beaker (Ni-Ag-II) in control experiments on surface finish. All rates are averaged between 4.45 cm and 5.33 cm from the beaker rim (R_4).

capacitor shell (shown below *T*-5 in I: Fig. 2)[1]; thus the inner wall was absolutely untouched during this operation. Transport rates remeasured after this procedure are reported below under the general heading of transport over "externally superfinished" (ES) beakers. This step in each series of measurements was included to provide data under circumstances where the comparatively rough inner microperimeter might conceivably exceed the superfinished outer microperimeter.

Each beaker was then returned to the Chrysler Corporation for internal surface superfinishing. As before, specimens were gripped only at the unsuperfinished base so as to prevent marring of the already superfinished exteriors. The final series of transport measurements was then undertaken. All data reported below under the general heading "internally superfinished" (IS) will therefore pertain to beakers whose outer surfaces were still superfinished.

As a further precaution against inadvertent modification of the surface finish produced at any stage of the work, measurements of surface finish and exact beaker dimensions[1] were made only after the crucial transport measurements had been made. Microfinish was measured by the Chrysler Corporation, using Brush Surface Analyzers, models BL-103 and BL-110. All beakers were again forwarded to Detroit merely for additional measurements on the superfinished outer and inner walls after all transport data had been obtained. The microfinish of other specimens was measured under similar circumstances.

When it proved difficult to arrange a similar polishing program for glass beakers, a substitute program of systematic roughening of Pyrex beakers was evolved. Three identical containers were fashioned from lengths of precision bore Pyrex tubing obtained through the courtesy of the Corning Glass Works.[16] Specimen G-III was untreated while the other two had their inner surfaces ground with carborundum: No. 200 for "fine ground" (FG) specimen G-IV and No. 80 for "coarse ground" (CG) specimen G-V. The smooth outer surfaces and ground inner surfaces of these specimens are thus analogous to the surfaces of the metal beakers which have been described as "externally superfinished." The nickel-silver depth gauge used in conjunction with these glass vessels was designed to yield data for direct comparison of the Pyrex results with those obtained for identical heights in metal beakers.

It was recognized that the precautions specified in connection with previous work[1] would be of equal or

[16] We are indebted to Dr. Paul M. Sutton and his colleagues of Corning's Research Division for appraising our requirements and supplying the tubing.

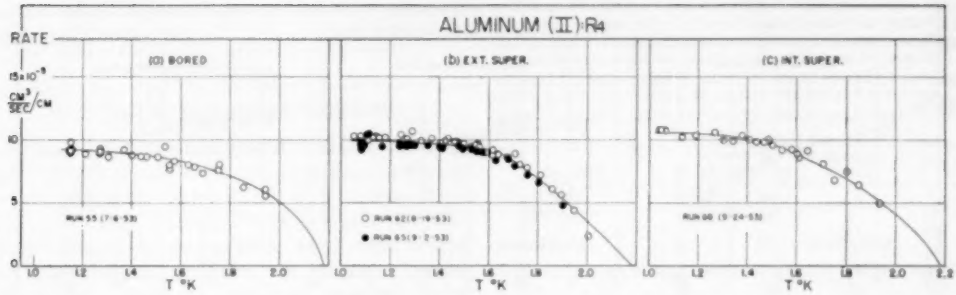

FIG. 4. Transport rates over an aluminum beaker (Al-II) in control experiments on surface finish. All rates are averaged between 4.45 cm and 5.33 cm from the beaker rim (R_4).

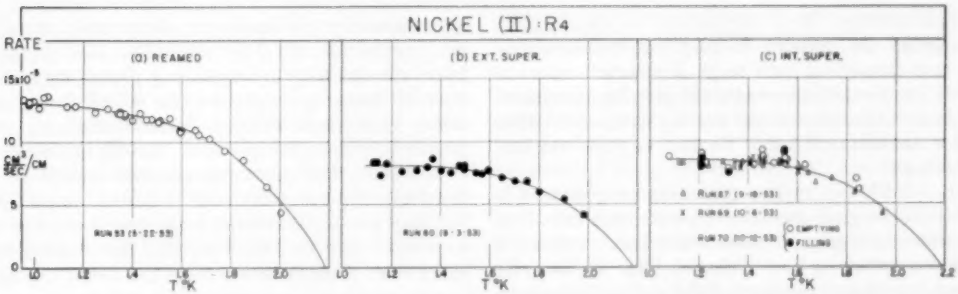

FIG. 5. Transport rates over a nickel beaker (Ni-II) in control experiments on surface finish. All rates are averaged between 4.45 cm and 5.33 cm from the beaker rim (R_4).

greater importance in the interpretation of the present experiments. The data previously acquired[1] on the "unavoidable background" variation observed after immediate and delayed reinstallation of a specimen in the cryostat were supplemented here in recognition of the necessity to establish statistical comparison as the dominant theme of the present work.

The data acquired in these control experiments are plotted in Figs. 2–6 where the horizontal display of the results for different finishes facilitates ready comparison. [It will be noted that part (a) of each figure reveals the original data from which the values tabulated for these specimens in Table III of paper I were obtained.][1] The corresponding tabulation of values obtained after special surface treatment is contained in Table II of the present paper, while similar tables of values obtained at other beaker heights will be found in paper III of this series.[17]

Values cited for the externally superfinished specimens, as well as for the ground Pyrex specimens G-IV and G-V were calculated using the geometrical inner circumference as the flow-limiting width of path, on the assumption that only a comparison of the results secured with all finishes would test the validity of this mode of calculation. This point will be discussed at greater length in a subsequent paragraph.

[17] B. Smith and H. A. Boorse, following paper [Phys. Rev. **98**, 358 (1955)], designated as III in the text.

Since the data seem noteworthy in regard to the rather narrow range of flow rates which were observed (in comparison with the reports of previous observers summarized in I: Table I),[1] averaged values of the tabulated rates at identical heights have been calculated for each group of similarly treated specimens. These averages are the plotted points of Fig. 7. A conservative statistical estimate of the observed variability is given by the vertical lines which are drawn so as to extend above and below each average value by an amount equal to the average of the absolute deviations of the individual runs from the mean. The horizontal bars represent the highest and lowest values which contribute

TABLE II. R_4: Average transport rate between 4.45 cm and 5.33 cm from beaker rim (midpoint at 4.89 cm); superfinished metals and ground Pyrex.

Specimen	Run No.	(Rate in cm³/cm-sec) ×10⁸ 1.1°	1.3°	1.5°	1.7°	1.9°	2.1°
Al-II (ES)	62,65	9.9	9.8	9.5	8.3	5.3	1.8
Ni-Ag-II (ES)	52	9.5	9.4	9.3	8.5	6.8	3.1
Ni-II (ES)	60	8.1	8.1	7.8	6.9	5.2	2.0
St.S. (ES)	50,51	7.6	7.4	7.2	6.3	4.8	2.1
Al-II (IS)	68	10.5	10.3	9.7	7.9	5.6	2.2
Ni-Ag-II (IS)	64	8.5	8.3	7.9	6.9	5.2	2.1
Ni-II (IS)	67,69,70	8.5	8.4	8.1	7.2	5.3	2.0
S.St. (IS)	61,63	8.8	8.7	8.5	7.8	5.6	2.3
G-IV (FG)	54	11.9	11.7	11.1	10.1	7.9	3.6
G-V (CG)	57	12.6	12.4	12.1	11.1	8.5	3.3

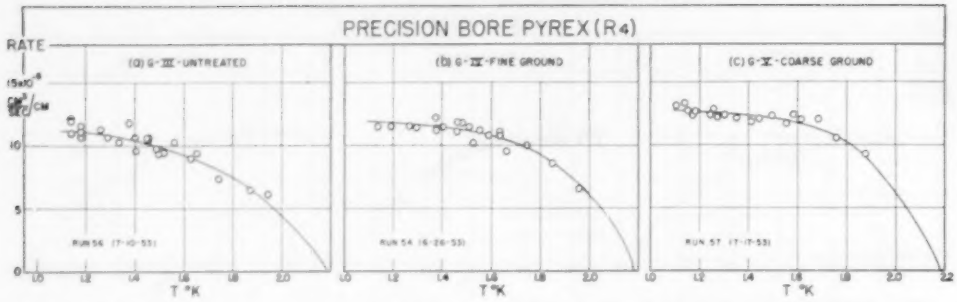

FIG. 6. Transport rates over three precision-bore Pyrex beakers in control experiments on the effect of surface finish. In each case the rate is averaged over the distance from 4.45 cm to 5.33 cm from the beaker rim (R_4).

to each average. As a further aid to visualization, histograms are included to map the distribution of the runs throughout each range of observed values at 1.1 °K. In calculating averages and plotting histograms, the basic statistical unit was one day's run, with values which are identical for a number of runs weighted accordingly.

Microfinishes of various specimens are presented in Table III. Original rms micro-inch readings have been converted to angstroms to facilitate direct comparison with the helium II film thickness. Gaps in the table reflect inadvertent omission of the necessary measurements before the surface in question was modified.

The chronology of microfinish measurement may be inferred by noting that tabulated finishes were measured *after* the completion of the last run listed in each row. It will be observed that the microfinishes of the outer walls of the (IS) beakers were always appreciably worse than those for the same specimen in the (ES) condition although, as previously noted, the external surfaces

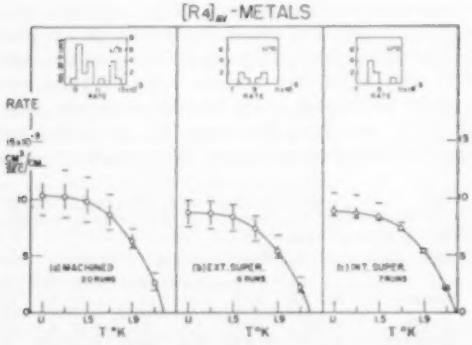

FIG. 7. Average values of transport rates for various metal surfaces, calculated from those listed in Table II of this paper and in Table III of the previous paper (reference 1). (R_4: 4.45 cm to 5.33 cm from rim). The plotted points are calculated arithmetic mean values; the vertical lines are drawn to extend above and below the points by an amount equal to the average absolute deviation from the mean and the horizontal bars represent the highest and lowest values contributing to each average. The histograms show the frequency distribution of the observed rates at 1.1 °K.

were ostensibly the same in the two cases. However, the microfinish of (ES) specimens was measured *before* the handling accompanying precise determinations of beaker geometry for use in calculating flow rates, while these external microfinishes were then purposely remeasured *after* such handling in the case of (IS) beakers. This precaution provided a check on the durability of finish under such conditions. Similarity of handling and measurement sequences thus leads one to suspect that the tabulated (IS) bore finishes may differ from those present during the actual transport measurements by an amount comparable to the variations observed in the adjacent column for outer wall finishes.

As is evident from the graphical and tabular summaries in this and the previous paper,[1] variations from run to run were usually small enough to compare favorably with the scatter of the data on a given run. However, larger variations were observed sufficiently often to justify their careful consideration in the interpretation of the data, and so such behavior has been summarized in Table IV. The table includes the results of analysis which will be found in a subsequent paper[17] for data obtained with these specimens at different heights. These data account for the entries corresponding to beaker sections other than 4 (see Fig. 2 of paper I). Since omitted entries indicate agreement at some beaker heights, the observed discrepancies are seen to vary irregularly with height.

The results of the following paper (III)[17] have also been employed in compiling Table V, which indicates the degree of reprodubility which was observed for similarly prepared specimens of the same material. In spite of the fact that much more data were available for the compilation of Table IV than for Table V, the latter required roughly twice as many entries. Study of the data (in papers I[1] and III[17] as well as the present paper) thus indicates that the excellent reproducibility frequently exhibited from run to run by one specimen was not duplicated in observations on different specimens of the same material, although such varia-

tions as were observed were of the same order of magnitude in both cases.

DISCUSSION

I. Extent of Background Variation

A comparison of the background variations shown in Tables IV and V with those characterizing the reports of other observers (summarized in I: Table I)[1] is difficult since most investigators have usually preferred to seek the more interesting effects which might appear when experimental conditions are purposely varied between runs. Although variations observed under such altered conditions have frequently been attributed to deliberate beaker and cryostat treatment, many of the discrepancies among results appearing in Table I of paper I for similar materials fall within the range observed here in the absence of special treatment. In this connection it is of interest to note the following remarks of Eselson and Lazarev: "One must still note that the data obtained in different series of similar experiments differed. This circumstance was noted by all authors and the same is true in the work under our conditions. In all probability this scatter (within 20 percent) is caused by the influence of very minute quantities of impurities, the avoidance of which is very difficult."[18] Further evidence of widespread recognition of the limitations on agreement to be expected among various observations is implicit in the prevailing judgment that the different results obtained by many investigators for glass (see Table I of paper I) are in satisfactory agreement.[7,19–21]

It therefore seems clear that, in evaluating the significance of fairly small changes which may be observed for rates measured after subjecting a beaker to special treatment, one must take careful cognizance of the background variations which characterize the transport measurements. The source of such variations will be considered in subsequent discussion of the nature of beaker surfaces.

TABLE III. Measured microfinish of various specimens: root-mean-square deviations from the mean surface in angstrom units. (Some specimens not subjected to special surface treatment but employed in the study of the substrate dependence[1] are also included.)

Specimen	Run Nos.	Surface condition	Rms microfinish in angstroms: Inner wall	Outer wall
Al-II	55	(B)	···	3560
Al-II	62,65	(ES)	···	50.8
Al-II[a]	68	(IS)	635	508
Cu	59,66	(B)	4064	11 430
Ni-Ag-I	33–35,37	(B)	8128	8636
Ni-Ag-II	52	(ES)	···	76.2
Ni-Ag-II[a]	64	(IS)	762	355
Ni-II	53	(R)	···	17 780
Ni-II	60	(ES)	···	25.4
Ni-II[a]	67,69,70	(IS)	610	254
Ag	58	(B)	12 192	22 352
S.St.	50,51	(ES)	···	76.2
S.St.[a]	61,63	(IS)	457	228
G-III	56	···	203	152
G-IV	54	(FG)	20 300	152
G-V	57	(CG)	50 292	152
Aluminum core[b]			12 700	
Nickel silver core[b]			39 624	
Nickel core[b]			13 208	
Stainless steel core[b]			35 576	

[a] Finishes in this row were determined after the handling described in the text. The extent of deterioration in each case is indicated by comparison of each (IS) result for outer wall finish with the one immediately above it in the table.
[b] These entries are included to supplement the data on the finishes which may be produced by turning solid cylindrical specimens.

TABLE IV. Background variation in transport rates observed for metal beakers which were untreated except for removal from the cryostat, reinstallation and outgassing between runs. Percentages were calculated by dividing the difference in rates at 1.1°K by the arithmetic mean of these two rates. Variations comparable to the scatter of the data on a given run are not tabulated.

Specimen	Comparing Run No. vs run No.		Beaker section	Percent variation at 1.1°K
Al-I (B)[a]	38,39	48	2[b]	9.6
Al-I (B)[a]	38,48	39	4	15
Al-II (ES)	62	65	1[b]	25
			3[b]	27
Cu[a]	59	66	1[b]	10
			3[b]	15
			4	7
Ni-Ag-I (B)[a]	33,34,37	35	1[b]	20
Ni-I (Br)	17	22	Various heights	11–20

[a] See reference 1 for data pertaining to this specimen.
[b] See reference 17 for data pertaining to beaker sections other than 4.

II. Role of Microfinish

A. Previous Views.—In the absence of a satisfactory theoretical formulation, the original observation that rates on metals were much higher than on glass[4] led to consideration of two alternatives: "either that the difference in intermolecular forces between the film and the different substrates causes a change in the flow rate or that simply, owing to its micro-structure, the effective perimeter of the underlying surface varies from case to case."[4] The intermolecular force picture seemed to involve excessive complexity since it leads to a variation of film thickness with height whereas the transport rates were believed to be independent of height (see paper III).[17] Consequently it was concluded that a purely geometrical increase in the solid surface carrying the transfer was somewhat more probable. In view of the range of rates which had been observed it was apparent that "the required increase in perimeter to account for the higher transfer on metal would have to be about threefold."[4] Moreover, this threefold difference between macroscopic and microscopic perimeters would

[18] B. N. Eselson and B. G. Lazarev, J. Exptl. Theoret. Phys. (U.S.S.R.) **23**, 552 (1952). We are grateful to Dr. B. S. Chandrasekhar for supplying us, in April, 1954, with a translation of this paper prepared at the University of Illinois.

[19] K. Mendelssohn, Report of Proceedings of the Oxford Conference on Low Temperature Physics, August, 1951, discussion, p. 70.
[20] D. F. Brewer and K. Mendelssohn, Phil. Mag. **44**, 340 (1953).
[21] Dyba, Lane, and Blakewood, Phys. Rev. **95**, 1365 (1954).

TABLE V. Variation in transport rates observed for similarly prepared specimens of the same material. See Table II for surface finishes. Percentages were calculated as in Table IV. Results of comparison of data for different heights, necessitated by non-standard beaker geometry, were corrected (by less than 5 percent) in accordance with the results to be presented in paper III, and are therefore listed as approximate. Variations comparable to the scatter of the data on a given run are not tabulated.

Specimen—runs	vs	Specimen—runs	Beaker section	Percent variation at 1.1°K
Al-I: 38,39,48[a]		Al-II: 55	1[b]	24
Al-I: 38,39[a]		Al-II: 55	2[b]	30
Al-I: 48[a]		Al-II: 55	2[b]	20
Al-I: 38,39,48[a]		Al-II: 55	3[b]	17
Al-I: 38,48[a]		Al-II: 55	4	8
Al-I: 39[a]		Al-II: 55	4	21
Ni-Ag-I: 33,34,37[a]		Ni-Ag-II: 45,46,49	1[b]	15
Ni-Ag-I: 35[a]		Ni-Ag-II: 45,46,49	1[b]	34
Ni-Ag-I: 33–35,37[a]		Ni-Ag-II: 45,46,49	2[b]	11
			3[b]	16
			4	18
G-I: 9,10[a]		G-II: 30,31[a]	···	~14
G-I: 9,10[a]		G-III: 56	···	~30
G-II: 30,31[a]		G-III: 56	···	~14
Q-I: 23[a]		Q-III: 24,25[a]	···	~ 8
Ni-I: 22		Ni-II: 53	···	~10

[a] See reference 1 for these data.
[b] See reference 17 for data pertaining to beaker sections other than 4.

have to characterize the smoothest portion of each beaker since "a region of smooth surface on the wall of the beaker would clearly limit the transfer anywhere along the beaker wall below this level."[4] Since such a threefold variation might appear excessive, it was remarked that "once one admitted the existence of surface cracks allowing some kind of capillary flow, which would still be pressure independent, the required increase in effective perimeter would be much smaller."[4]

The view that surface roughness may thus enhance the flow of bulk liquid to an extent greater than would be indicated by purely perimetric considerations has been restated on a number of occasions.[5,6] Although the influence of the chemical nature of the substrate is still assigned a negligible role in this later work, one finds that high transport rates are ascribed to the "microstructure of the substrate" on the assumption that "narrow surface cracks of the order of magnitude of the film thickness or somewhat larger might be filled up with liquid helium and thereby produce a much greater transport of liquid,"[5] while mention of the simple picture of a large microscopic perimeter is now omitted. The experiment designed to test this hypothesis yielded a transfer rate "practically the same as that for a baked-out glass surface" for two stainless steel beakers "of a much better finish than any metal surface that had previously been used for helium transfer."[5] Later it was found that when "one of the beakers was brought to red heat, thus destroying the smooth surface finish, and it was then lightly polished with cotton wool to remove any deposit of oxide···the flow rate had changed considerably, being now more than three times the original value."[5]

On the other hand, the view that flow rates simply adjust to the prevailing microscopic perimeter continues to attract support as may be seen from the recent analysis of Daunt and Smith, which ends with the remark that "it presumably must also be concluded that the increase in transfer rate over rough surfaces is due to their increased periphery available for flow···."[7] However, apparently as a result of associating a plotted curve with the wrong set of ordinates, Daunt and Smith evaluated available data on the assumption that the experiments on polished stainless steel which have just been described, indicated a change of only about 50 percent due to the destruction of polish by heating,[7] instead of the change to three times the original value which was actually reported.[5] In view of the crucial role accorded this experiment in their discussion, this oversight had the regrettable effect of eliminating all but passing reference to the larger discrepancies which have induced others to postulate an anomalous flow in metal surface cracks.

B. Present Observations.—The effect of altered microfinish of metal beakers on the average rates exhibited in Fig. 7 is summarized in Table VI (which also includes additional results for beaker Secs. 1–3 from paper III).[17] The size of the observed diminution of rate with improved microfinish is much smaller than would be expected from many previous reports. It is abundantly clear that, in the face of the background variation, the resolution of this effect is made possible only by averaging of the data obtained for different specimens on many separate occasions.

The results for untreated and ground Pyrex beakers (see Fig. 6 and Table II) are in accord with those obtained for metal beakers. In fact, contrary to many previous reports, transport rates measured over the comparatively rough bored metallic specimens were found to exhibit a reproducibility and simplicity comparing favorably with that obtained with glass and quartz.[1,22] Such similarity of behavior appears consistent not only with the previously cited[1] calculation of Schiff,[23] but also with the known physical

TABLE VI. Comparison of average transport rates at 1.1°K for machined and superfinished (internally as well as externally-IS) metal specimens. Data for beaker SecS. 1–3 (see Fig. 2 of Paper I), tabulated in the columns headed R_1, R_2, and R_3 were obtained from the results to be presented in Paper III.

	(Average rate in cm³/cm-sec) ×10⁴			
	R_1	R_2	R_3	R_4
Machined metals	15.0	11.9	10.7	10.3
Superfinished metals (IS)	11.4	9.9	9.3	8.9
Percent difference with respect to mean	27%	18%	14%	15%
Ratio of machined to (IS) average rate	1.32	1.2	1.15	1.16

[22] B. Smith and H. A. Boorse, Phys. Rev. **92**, 505 (1953).
[23] L. I. Schiff, Phys. Rev. **59**, 839 (1941).

properties of glass surfaces.[24–27] For example, in a section entitled "The Universal Corrosion of Glass Surfaces," McBain[24] remarks that "glass owes its power of resisting agents generally to the existence of an insoluble film of silica or highly silicated matter upon its surface. The silica is mostly left behind as a coating of silica gel upon the surface of the glass. This is amplified when the usual corrosive cleaning agents are employed. Surfaces so prepared for use are no longer glass and they possess appreciable depth and porosity." He therefore concludes that "the true extent of the surface of glass in its ordinary condition is not even approximately known; the uncertainty amounts to an order of magnitude." In commenting on what he terms the spongy nature of glass surfaces, Adam[25] observes that "glass is also rather liable to minute surface cracks" and adds that "glass surfaces seem to become dirty more quickly than most others; this is very likely due to the contamination having penetrated below the surface into cracks, and coming out gradually after cleaning the actual surface." Thus the observation of conventional transport rates for glass surfaces, including those cleaned with chromic acid,[4] is also in accord with the present indications of the small degree to which altered microfinish may influence transport rates.

Although the extent of the possible difference between macroscopic and microscopic perimeters for machined metals has always been discussed on intuitive grounds in connection with helium film transport,[3–7,28–30] it appears feasible to estimate this difference quantitatively. Consider the simple model of a rectangularly corrugated surface shown in cross section in Fig. 8, where p_0 represents the superficial macroscopic perimeter whose microscopic counterpart, p, is to be estimated. Let the average combined width of each adjacent hill and valley be designated by λ, which therefore equals the ratio of the measured geometrical perimeter p_0 to the number, n_0, of such elevation-depression pairs, where of course $p_0 \gg \lambda$. This definition of λ as an average width, frees the model from the restriction to the perfectly regular periodicity which has been depicited in Fig. 8 merely for convenience in drawing. If the depressions have a depth given by 2δ, then the sum of p_0 and vertical contributions to the perimeter yields an expression for the total microscopic perimeter given by

$$p = p_0[1 + 4\delta/\lambda], \tag{1}$$

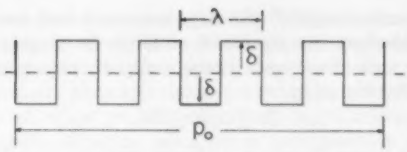

FIG. 8. Simple model of cross section of rough surface (not to scale).

where the definition of λ,

$$p_0 = n_0\lambda, \tag{2}$$

has been employed to eliminate n_0. Thus the dimensionless ratio $(4\delta/\lambda)$ is a direct measure of the contribution of surface roughness to p. It is of course assumed that only irregularities for which 2δ exceeds the helium II film thickness ($\gtrsim 200$ A) would qualify in altering the perimeter "seen" by the film.

Suitable numerical estimates of δ for various beakers are given by the measured values of rms microfinish (deviations from the mean surface) shown in Table III, whereas corresponding values of λ are not available for these metal specimens. However, study of the literature of machined surface finish[8–18] reveals that δ and λ are not entirely unrelated. The correlation between δ and λ is reflected by the necessity to employ different scales of horizontal and vertical magnification whenever it is desired to study surface contours as revealed by photomicrographs and profilograms. One usually chooses that ratio of vertical to horizontal magnification which will reduce δ and λ to a comparable scale much as is shown in Fig. 8. In practice, "experience shows that in the vertical direction the range of useful magnification extends from about 1000 to 100 000" while "in the horizontal direction, values from 6 to 800 have been used."[13] When fixed distortion of horizontal and vertical dimensions in a collection of such graphs is desired, "the best all-round value for measuring roughness would seem to be 100"[13] (i.e., ratio of vertical to horizontal magnification). Thus Reason[14] has observed that "what appear on these graphs to be slender projections and narrow crevasses are in reality nothing of the sort and are merely the compressed representation of gentle hills and broad valleys. A certain amount of care and practice is required to use these distorted graphs, and all the time to think correctly about them. There is a terrible tendency to forget the distortion and to discuss the effect of the various shapes just as though the graph were actually a true representation of the surface. On the graph it looks as though the slender projections could easily bend over or snap off: but when you consider reality you will see that this could hardly happen, for the actual inclinations of the flanks of the undulations to the horizontal are so small that there can be no question of simple bending or breaking." Therefore, an estimate of the range to be expected for (δ/λ) with actual machined metal surfaces may be made by observing the distortion ratios employed in most graphical

[24] J. W. McBain, *The Sorption of Gases and Vapours by Solids* (Routledge, London, 1932). Most references are to Chapters 7 and 10.
[25] N. K. Adam, *The Physics and Chemistry of Surfaces* (Oxford University Press, London, 1941), third edition, Chaps. 5 and 7.
[26] S. Brunauer, *The Adsorption of Gases and Vapors* (Princeton University Press, Princeton, 1954), Vol. 1.
[27] J. E. Stanworth, *The Physical Properties of Glass* (Oxford University Press, London, 1950).
[28] J. G. Daunt and K. Mendelssohn, Nature **142**, 475 (1938).
[29] J. G. Dash and H. A. Boorse, Phys. Rev. **82**, 851 (1951).
[30] W. C. Knudsen and J. R. Dillinger, Phys. Rev. **91**, 489 (1953).

representations,[8,12,14] showing horizontal and vertical irregularities for machined surfaces to roughly the same scale. From such study it appears reasonable to consider the range

$$20 \lesssim (\lambda/\delta) \lesssim 200, \tag{3}$$

where larger numbers indicate greater smoothness. Fragile projections characterized by smaller values of (λ/δ) seem unable to survive the rigors of the machining process. In combination with Eq. (1) this yields:

$$1.02 \lesssim (\rho/\rho_0) \lesssim 1.2. \tag{4}$$

The replacement of the rectangular contour shown in Fig. 8 by another regular curve (e.g., sinusoid or sawtooth) would also lead to a correction term small compared with ρ_0 for contours satisfying the empirical condition (3). Furthermore, in view of (3), the transition from an ideally regular model to actual surface irregularities should not cause an appreciable modification of these conclusions.

These considerations therefore argue against the possibility that the smoothest portion of each beaker might be characterized by values of (ρ/ρ_0) even approaching two, while values of three or more such as are required by previously reported transport measurements would appear to be extremely unlikely. This lends support to the rejection of a purely perimetric explanation of such results by Mendelssohn and White[4] and Chandrasekhar and Mendelssohn.[5]

On the other hand, comparison of entries in the last row of Table VI with Eq. (4) indicates that the present data for metals are consistent with the hypothesis that transport rates adjust to the prevailing microscopic perimeter, while the added hypothesis of a large, anomalous flow in surface cracks is completely unnecessary. Recently Dyba, Lane, and Blakewood have also reported the absence of anomalous flow in transport from glass capillaries.[21]

Further support of the present view is provided by the data for Pyrex specimens G-III, IV, and V, if one assumes that the order of magnitude of λ is given by the diameter of the abrasive particles used in grinding the walls of beakers G-IV and V. Using measured microfinish values for δ, and particle size for λ, one obtains Table VII. Although G-V appears more than twice as rough as G-IV (from comparison of microfinish values), the calculated increase in perimeter over that of untreated specimen G-III is about the same in each case. Furthermore, $(4\delta/\lambda)$ is so small that one might expect the observed background variation to tend to blur the correlation of transport rates with (ρ/ρ_0) since only one run was taken on each specimen. This is indeed observed at various heights,[17] whereas averages of transport rate ratios observed at all heights yield the values shown in Table VII. The agreement of the data with the proposed model is most satisfactory, although the virtual identity of the last two columns of Table VII must be regarded as somewhat fortuitous. Thus, the assumption that increased surface roughness in general leads to higher transfer rates[21] is seen to involve considerable oversimplification.

TABLE VII. Comparison of calculated increase in perimeter with observed changes in transport rates for Pyrex specimens G-III, IV, and V. Tabulated values of (ρ/ρ_0) were calculated from Eq. (1), using measured microfinish for δ and carborundum grit size as a measure of λ. Transport rates observed at 1.1°K, for ground beakers G-IV and V were divided by the corresponding rate for untreated specimen G-III at each height; ratios obtained at different heights were then averaged to obtain the entries in the last column. (Data for beaker sections other than 4 were obtained from Paper III.)

Specimen	δ in microinches (rms)	λ (inches)	Calculated (ρ/ρ_0)	Measured $(R/R_{G\text{-}III})_{4.2}$
G-IV (FG)	80	0.005	1.06	1.05
G-V (CG)	198	0.0125	1.06	1.04

In judging the quality of finish imparted to the superfinished beakers it is desirable to provide some standard of comparison. As previously noted, the most reliable estimates of the originally imparted superfinish appear to be those measured on the outer walls of (IS) beakers before handling. Such measurements, of which there is one for each of four metal beakers, range from 25.4 A to 76.2 A for rms surface irregularities on the cylindrical surfaces (see Table III). These values will be compared with the results of a recent study of the microscopic nature of optical flats, since specifications for such flats are generally regarded to impose the most stringent tolerances attainable. Using multiple beam interferometry to resolve irregularities that could not be revealed by the electron microscope, Koehler[22] offers the following description of an optical flat: "If one could obtain a collection of cones with conchoidal sides, mean height less than 60 A, average deviation from the mean about one-third the mean, and bases less than 0.01 mm in diameter, and then place them as close together as possible with their bases on a supersmooth surface, then one would have a model of a polished glass surface." The value of 60 A is in excellent agreement with the range of electromechanically determined microfinishes on superfinished metal beakers. Furthermore, substitution of 60 A for δ and Koehler's observed average distance between adjacent cusp points of 0.004 mm for λ, yields satisfactory agreement with the undisputed smoothness of optical flats as well as the previously specified correlation between λ and δ for mechanically prepared metal surfaces.

In the past, the proposed correlation of a very large range of transport rates for metals with changes in perimeter appeared incompatible with the lack of clear evidence of changes of comparable magnitude accompanying the surface modifications which would be expected to result from the mere aging and handling of beakers.[29] The present results are not open to this

[21] D. F. Brewer and K. Mendelssohn, Phil. Mag. **44**, 559 (1953).
[22] W. F. Koehler, J. Opt. Soc. Am. **43**, 743 (1953). We are grateful to Dr. Koehler for communicating these results to us prior to publication.

objection since changes of the same order of magnitude as those to be expected from Eq. (4) have been observed as background variations with individual beakers (Table IV), in variations among similarly prepared beakers (Table V), and in changes resulting from deliberate alteration of microfinish (Tables VI and VII). The details of the background variations as previously discussed are thus seen to play a vital role in any scheme which attributes differences in transport rates to substrate microstructure. Their existence is to be expected, and only their absence from the data would require special explanation.

In this connection, another aspect of the virtual impossibility of exact duplication of microscopic surface conditions is deserving of attention. Since the discovery, by Bowers and Mendelssohn,[23] that anomalously high transport rates were associated with condensed layers of solidified gases, all investigators have taken great pains to exclude foreign gases from their apparatus. The preventive measures employed by Atkins[24] (outgassing etc.) were very similar to those already described for the present experiments.[1] Mendelssohn and White[4] outgassed glass vessels at temperatures up to about 130°C for 1½–2 hours in a vacuum of about 10^{-3} mm Hg. Both metal and glass beakers were cleaned with acid. Their treatment of platinum and nickel specimens included degassing at about 600°C at a pressure of approximately 10^{-3} mm Hg for an hour. In what appears to be the most ambitious effort thus far undertaken to minimize contamination, van den Berg used glass apparatus which was evacuated for four hours at 300°C and then sealed off, following which it was immersed in the liquid helium where the pressure was reduced to about 1 mm Hg before the seal was broken.[25] He reports a transport rate of 11×10^{-5} cm³/cm-sec (presumably at temperatures below 1.5°K) when the level was not very close to the rim. The same rate was observed in a separate experiment where helium was condensed into the measuring beaker through a spiral and several charcoal traps immersed in liquid hydrogen as well as a spiral immersed in liquid helium.[25] (We note in passing that this rate of transport is in excellent agreement with the present data for glass and quartz[1] as well as with the recent work at Yale.[21]) Eselson and Lazarev[18] repeatedly refer to "measures which excluded the contamination of the walls of the vessel by solid impurities" although they furnish no description of these measures other than the statement that "before starting the experiment, the apparatus is carefully evacuated and filled with pure gaseous helium."

Although these precautions have proven sufficient to exclude obvious contamination of the sort described by Bowers and Mendelssohn,[23] it is by no means clear that they are sufficient to remove the "foreign matter in a thin layer" with which "a solid surface is nearly always contaminated."[25] It has already been noted that glass, particularly when acid cleaned, tends to be covered by a layer of silica gel. In commercial applications, for adsorption of water, silica gel is used probably more than any other adsorbent.[10] It has also been observed for borosilicate glasses like Pyrex, that 300°C is required to remove most *adsorbed* gases while *absorbed* gases begin to come off at the softening point (600°C).[26] It is therefore not surprising that suspicions of adsorbed water on glass transport vessels which have yielded conventionally low flow rates in previous measurements, have been voiced by Mendelsshon and White.[4] The possibility of contaminating metals in the machining process is obvious; furthermore, when cleaned by etching, "the metal surface is covered by the products of the reaction between metal and liquid or at least by their concentrated solution in the etching liquid."[10] Thus, "in many instances cleaning attempts only accentuate the chemical difference between the interior and the surface of a solid."[10] Furthermore, as has been observed by Bikerman[10]: "A complete removal of these adsorption layers requires a prolonged heating in high vacuum. For instance, Holm and Meissner[27] had to heat platinum wires for hours at 1100° in a perpetually evacuated glass vessel the walls of which were cooled with liquid hydrogen to prevent gas molecules striking these walls from returning to the wires. If the material to be cleaned cannot stand up to a degassing of such intensity, its surface will never have the composition of its interior." Adam[25] also observes that "if the surface is prepared by etching, chemical changes may be produced on the surface, oxide or other films being present" and that "most surfaces would have their structure much altered by heating, however, the small ridges and projections becoming sintered and rounded off." Consequently, complete cleanliness appears highly incompatible with the study of surfaces of known microstructure at helium temperatures.

Insofar as fluctuations in the composition and extent of minute residual contamination of "clean beaker surfaces" might alter the microscopic periphery of a beaker, such effects are completely consistent with the preceding discussion of present observations. This is also the mechanism used by Eselson and Lazarev to explain the background variation they observed for transport over glass.[18]

However, the probable existence of such residual deposits is disturbing when one endeavors to proceed further and dissociate the role of the helium-substrate interaction from purely geometric effects. It has already been noted[1] that differences in this interaction, as calculated by Schiff[28] for copper, silver and glass, are too small to permit their systematic resolution in the

[23] R. Bowers and K. Mendelssohn, Proc. Phys. Soc. (London) **A63**, 1318 (1950).
[24] K. R. Atkins, Proc. Roy. Soc. (London) **A203**, 241 (1950).
[25] G. J. van den Berg, Report of Proceedings of the Oxford Conference on Low Temperature Physics, August, 1951, p. 67.
[26] J. E. Harris and E. E. Schumacher, J. Ind. Eng. Chem. **15**, 174 (1923).
[27] R. Holm and W. Meissner, Z. Physik **74**, 715 (1932).

present experiments. The apparent consistency between the present observations and Schiff's calculations,[1] however, may be fortuitous, since in the absence of precise knowledge of the composition of the surface of a "clean beaker," it is not known to what extent the direct helium-substrate interaction assumed in the calculation is applicable.

Contamination in the sense employed by Bowers and Mendelssohn has been observed to cause transport rates between ten and twenty times larger than the conventional "clean beaker" rates observed here.[35–41] It has frequently been assumed, "in view of many of the results obtained with the transfer over metal surfaces, that the increase in the transfer rate over contaminated surfaces is due to the increased perimeter due to the deposit."[7] Since this assumption now seems inadequate to explain many of the high rates previously reported for machined metals, its applicability to contamination must be re-evaluated. If the effect of contamination is truly one of enlarged perimeter, then it should be possible to show that values of λ and δ required in Eq. (1) to produce such large changes in perimeter are indeed compatible with the kinetics of the condensation process and the amount of gaseous impurity which is introduced. On the other hand, just as has been shown for machined metals, it may prove very improbable for the condensate to form needle-like projections of the requisite density and fragility to produce large enough values of (δ/λ). (This of course assumes that one must consider only irregularities larger than the film thickness so that mere granularity on an atomic scale would not suffice.) Solidified gases might then prove to be extremely useful in the study of the direct helium-substrate interaction. For example, Ham and Jackson[42] have already observed the formation of discrete drops from the helium II film only when the polished surface of the mirror was free from condensed gaseous impurities; otherwise, the bulk liquid could just be observed as a stream of liquid of uneven thickness flowing on an irregular substrate. Some unpublished results obtained at Leiden also appear to be of interest in this connection.[35] In any event, further theoretical and experimental study of these questions would be very valuable. Temperley's recognition of the importance of bound states of helium atoms which "are presumably present on any boundary wall, even if it is submerged in the liquid" and which "certainly will affect the transport properties profoundly"[43] might prove to be a useful point of departure for future studies.

Attention must also be directed to previous observations of transport over "clean metal beakers" for which measured rates greatly exceed those to be expected from a mere increase in perimeter. Since such observations now seem to be anomalous even for machined metal beakers, it appears that a completely satisfactory explanation must await further experiments in which such results are reproduced at will by controlled beaker treatment after normal, low rates have been observed for the same beaker in the original machined state. In those cases where some details of beaker history are available, it may be significant that very high rates have been associated with beakers which had previously been heated to 600°C in a vacuum of about 10^{-3} mm Hg,[4] heated (apparently in air) to "red heat,"[5] otherwise oxidized,[29] and/or etched in acid,[4,29] whereas lower rates such as those reported here have been observed in the past over metals[2,28,29,44–46] for which no mention of such treatment was made. Thus, in the absence of further experimental and theoretical knowledge of the role of surface impurities and the manner in which oxidation, heating, and chemical treatment may alter microfinish, it is difficult to judge the merits of the hypothesis of anomalous flow in surface cracks in explaining usually high rates. In this connection McBain remarks that "when discussing impermeable crystals, it is well to remember that it is now recognized that perfect crystals will spontaneously develop a network of surface cracks spaced about 100 atoms apart owing to contraction due to the unbalanced forces at the surface. This must appreciably increase the area available for the sorption of small molecules. The remarkable experiments of Griffith with fibres of glass and silica show than even a 'virgin fire-polished' surface of fused silica does not remain intact if exposed even for a few hours."[24]

Finally it must be noted that the statistical analysis of the data embodied in Fig. 7 (and similar graphs to appear in III),[17] reveals a somewhat curious situation which is not apparent from tabular summaries. Although tabulated and plotted values of transport rates over (ES) beakers were calculated by assuming that the limiting perimeter was still provided by the unchanged inner wall (just as for bored specimens), average (ES) transport rates as shown in Fig. 7 (and paper III) were virtually identical with average (IS) results. In terms of Eq. (1) of paper I,[1] it therefore appears that, on the average, the time Δt taken to empty identical volumes was different in the bored and (ES) cases. Such a result might be interpreted to mean that the rough microscopic inner circumference sometimes exceeded the smooth outer perimeter. However, if this were so, the use of the outer circumfer-

[35] K. R. Atkins, Nature **161**, 925 (1948).
[36] W. J. deHaas and G. J. van den Berg, Revs. Modern Phys. **21**, 524 (1949).
[37] R. Bowers and K. Mendelssohn, Nature **163**, 870 (1949).
[41] R. Bowers and K. Mendelssohn, Proc. Phys. Soc. (London) **A63**, 1318 (1950).
[42] A. C. Ham and L. C. Jackson, Phil. Mag. **44**, 214 (1953). Also see reference 40 of paper III.
[43] H. N. V. Temperley, Proc. Roy. Soc. (London) **A198**, 438 (1949).
[44] B. V. Rollin and F. Simon, Physica **6**, 219 (1939) with the added explanation offered by H. A. Fairbank and C. T. Lane in Phys. Rev. **76**, 1209 (1949).
[45] J. G. Daunt and K. Mendelssohn, Proc. Phys. Soc. (London) **A63**, 1305 (1950).
[46] E. Ambler and N. Kurti, Report of the Proceedings of the Oxford Conference on Low Temperature Physics, August, 1951, p. 70.

ence in the calculation would be proper in certain cases. Some (ES) graphs in Figs. 2–5 would be lowered by about 20 percent and would then include results as low as 5.9 (10^{-5}) cm³/sec-cm at 1.3°K, which is lower than any previous report for glass, metal, or plastic substrates. Furthermore, since the results for (IS) beakers would be expected to be just as low, one would be led to assume that some superfinished outer microcircumferences were smaller than their superfinished inner counterparts.

It is important to note that a revision of the data along these lines, if applied uniformly to all superfinished metal and ground glass beakers, would increase the consistency of some sets of results only at the expense of a comparable diminution of consistency in control experiments on other beakers. However, the background variations which were observed, when coupled with the small size of the statistical sample involved, argue against the propriety of applying such a correction only to those results whose consistency would be improved thereby. Fortunately, the fact that the corrections which might conceivably be applied are too small to permit their unambiguous justification, has the added effect of guaranteeing that the discussion of results as already presented would survive such revisions intact. Furthermore, the added possibility, however remote, that a polished outer wall can to some extent affect film flow, without providing the controlling perimeter, should not be overlooked in view of the incompleteness of the present state of knowledge. For example, the flow of the film is sometimes coupled with drop formation on the outer beaker walls[42,47] in a manner which varies with surface condition in a way that is not fully understood.[42] Consequently, until such time as conclusive evidence for the necessity of such revision may be forthcoming, it would be imprudent to alter the presentation of the data.

Although the question of outer *vs* inner perimeter is thus seen to be of relatively minor importance in these experiments, it appears to be crucial in the interpretation of some previous observations on stainless steel.[5] Apparently as a result of the difficulty of polishing the inner walls of small bore specimens, only the outer walls were polished,[48] thereby providing beakers similar to those labeled (ES) in the present work. Published rates were calculated using the polished outer circumference as the limiting perimeter.[48] If it be assumed that machined metals always yield spuriously high flow rates as a result of anomalous flow in surface cracks,[4] then the observed low rate of emptying of these steel beakers would appear to justify the assumption that the smooth outer surface was limiting the transport. However, previous observations of low rates on polished stainless steel and iron,[29] as well as the present observations on various machined metals indicate that, in the absence of a pre-polishing control experiment, the reported data on such externally polished beakers do not justify conclusions as to the effect of enhancing surface finish. On the contrary, the observations are in excellent agreement with the present results for ordinary machined metals.[1] Furthermore, polishing similarly restricted to the outer surface of a platinum beaker, had no appreciable effect in other experiments.[4] Although the polishing therefore may be irrelevant to the experiments on stainless steel,[5] these considerations do not affect the observation that the flow rate increased to more than three times the original value[5] after heat treatment of the beaker. However, the use of these data to draw conclusions about the surface smoothness required for the observation of low transport rates,[7] rather than on the effect of damaging beaker specimens by bringing them to red heat in air, is unjustified. This distinction is of particular importance in the interpretation of work in which flow rates are used in the calculation of other physical quantities.[20,45,49]

SUMMARY OF CONCLUSIONS

Variations observed from run to run with the same specimen, and from specimen to specimen of the same material in these and previous experiments,[1] indicate that trustworthy generalizations cannot be based on small amounts of data. In this connection, the line of demarcation between "clean" and "contaminated"[50] beaker surfaces is not sufficiently clear. Consequently, the apparent compatibility of the data for various materials with the calculations of Schiff (noted in I)[1] may be fortuitous, since the calculations assume a direct interaction between the helium film and a surface whose properties are identical with those in the interior of the solid.

The data are consistent with the hypothesis that transport rates adjust to the prevailing microscopic perimeter presented to the film. The effect of improved microfinish could be discerned only from a statistical comparison of the results for various groups of similarly treated specimens. The size of the observed background variations, as well as the effect of improved microfinish are in good agreement with the proposed calculations of the difference between microscopic and macroscopic perimeters "seen" by the film for mechanically finished substrates (considering irregularities greater than or equal to the film thickness). The calculated difference is much smaller than many previous intuitive estimates and it has been shown that an increase in surface roughness (as manifested by an increase in the height of surface irregularities) is not sufficient to guarantee an appreciable change in the microscopic perimeter

[47] D. G. Henshaw and L. C. Jackson, National Bureau of Standards Circular 519 (U. S. Government Printing Office, Washington 25, D. C., 1952), pp. 189–190.
[48] B. S. Chandrasekhar (private communication).
[49] L. C. Jackson and D. G. Henshaw, Phil. Mag. 44, 14 (1953).
[50] In this context, "contamination" includes chemical and physical surface damage as well as the condensation of foreign gases in the sense of Bowers and Mendelssohn.

presented to the film. The present estimates of the difference between geometric and microscopic perimeters give quantitative support to the rejection by some authors of a purely perimetric explanation of anomalously high flow rates which have sometimes been reported for metals. The inapplicability of the perimetric explanation to such results suggests the desirability of re-examining the accepted perimetric explanation of the very high rates which result from contamination (in the sense of Bowers and Mendelssohn), with specific attention to the probable values of the ratio (δ/λ) as employed in Eq. (1).

ACKNOWLEDGMENTS

The authors wish to express their appreciation to Arnold Berman, Raymond Kaplan, Leonard Lesensky, Robert D. Worley, and Professor Adam H. Spees for valuable assistance during the course of the measurements; to Mr. G. T. Poirier and Mr. P. DePalma and their associates in the Department of Production Research of the Chrysler Corporation whose splendid cooperation in the superfinishing program was vital to the completion of the research; and to Professor Mark W. Zemansky for his active and stimulating interest in these experiments.

PHYSICAL REVIEW VOLUME 99, NUMBER 2 JULY 15, 1955

Helium II Film Transport. III. The Role of Film Height*

BERNARD SMITH† AND HENRY A. BOORSE‡
Pupin Physics Laboratories, Columbia University, New York, New York
(Received March 22, 1955)

Transport rates have been measured for film heights up to 5.3 cm. A variation with film height, whose average behavior is similar to that which has been reported for the film thickness, was observed. This height dependence of the flow rates was found to be temperature independent in the range under investigation ($1°K \lesssim T < T_\lambda$). The results are also relatively insensitive to changes in substrate and microfinish. Consideration of this height dependence was essential to the analysis of the role of substrate and microfinish presented in the previous papers of this series.

INTRODUCTION

IN proceeding with the study of film transport rates inaugurated in previous papers,[1,2] the present investigation is concerned with the clarification of the answer to the question: How do measured transport rates vary with the distance of the liquid source from the rim of the beaker?

In the earliest relevant investigation, it was found that the rate decreased "only by 20 percent when the level had dropped from within 0.5 mm of the rim to some 20 mm from the rim."[3] It was concluded that "the rate of transfer depends only on the temperature and is practically independent of the difference in height between the two levels (except if the higher level is very near—1.5 cm or less—the top of the barrier)."[4] In a recent review, Daunt and Smith have given the following more quantitative description of these early results: "Daunt and Mendelssohn observed a small variation of the rate of transfer with height when observations were made over height differences as large as 6 cm. The variation in the rate was approximately 2 percent per cm change in height."[5] It was concluded that "the change in gravitational potential does influence the transfer but that this influence plays only the role of a correction of higher order."[6] Consequently, "to avoid the small error which might have been introduced by the slight influence of gravity, the determinations were all carried out in the same range of the beaker."[7] Later, on the basis of these experiments, the following summary was offered: "The most striking feature of the film transfer is its independence of the pressure head and of the length of the path over which it takes place. A beaker filled with liquid helium will empty itself at a steady rate · · · which does not depend on the position of the level or on the height of the intervening wall. These facts indicate that the film transport must be free of friction, since dissipation of the kinetic energy of flow would introduce a dependence of the flow rate on the pressure head and the length of path."[8]

* Assisted by the Office of Naval Research and the Linde Air Products Company.
† Present address: Bell Telephone Laboratories, 463 West Street, New York 14, New York.
‡ Barnard College, Columbia University, New York 27, New York.
[1] B. Smith and H. A. Boorse, Phys. Rev. **98**, 328 (1955), designated as I in the present text.
[2] B. Smith and H. A. Boorse, preceding paper [Phys. Rev. **99**, 346 (1955)], designated as II herein.
[3] J. G. Daunt and K. Mendelssohn, Nature **141**, 911 (1938).
[4] J. G. Daunt and K. Mendelssohn, Nature **142**, 475 (1938).
[5] J. G. Daunt and R. S. Smith, Revs. Modern Phys. **26**, 172 (1954).
[6] J. G. Daunt and K. Mendelssohn, Proc. Roy. Soc. (London) **A170**, 423 (1939).
[7] J. G. Daunt and K. Mendelssohn, Proc. Roy. Soc. (London) **A170**, 439 (1939).
[8] K. Mendelssohn, Report of International Conference on Fundamental Particles and Low Temperatures, Phys. Soc. (London) **2**, 35 (1947).

Later some observers,[9,10] using glass beakers, reported very high rates characterized by a severe height dependence and a variability which was excessive even by the standards previously enumerated for such results in paper I.[1] Bowers and Mendelssohn,[11,12] as a result of impressive detective work, were able to show that such high transfer rates are produced by the contamination of glass surfaces with solidified gases. This conclusion was promptly confirmed in other laboratories.[13–15] (The data previously alluded to in the present summary as well as in I[1] and II,[2] have been limited to results generally considered to be unaffected by such contamination. This restriction will also apply to subsequent references unless otherwise specified.)

The fact remains that most observers have agreed that, in the absence of such contaminating influences, proximity of the liquid level source to the rim is associated with increased transport rates. The magnitude of this variation, as well as the distance along the beaker over which the variation is pronounced, is however not clear. For example, in addition to those already quoted, the following observations have been reported: "Although the stainless steel beaker has mono-layers of barium stearate on the outside, it apparently behaves as a 'clean beaker' in the sense of Bowers and Mendelssohn, since the creep rate is practically independent of the height of the inner liquid level except for the first few millimeters, where, as usual, the creep rate is considerably greater."[16] In another paper it was reported that the motion of the liquid surface "was invariably a linear function except in the initial stages of an emptying process when the liquid · · · was very near the rim of the tube."[17] The routine acceptance of this effect is indicated by statements such as "the dependence of the transport rate on the position of the liquid level below the container rim was found to correspond qualitatively with the results of other investigators."[18] Other authors have reported that "the increased transfer near the rim still persisted after baking out and can therefore hardly be ascribed to adsorbed water or air. · · · Thus while it is tempting to see in the observed variation of R a true, if slight, dependence on the height of the film above the liquid level, the effect is so small that we hesitate to regard it at present as being of fundamental significance."[19] Consideration of these data has often led to the conclusion that "the flow rate height dependence, if it exists at all, cannot be large."[20]

On the other hand, it has also been observed that even "when adequate precautions were taken to prevent the formation of solid deposits on the surface holding the film, this characteristic rate of flow · · · varied with the height of the film · · · .This type of behaviour was observed in all the experiments. · · · In their original experiments, Daunt and Mendelssohn observed an increase in the rate of flow when one level was near the rim of their beaker, but they suggested that it was due to surface-tension effects. In actual fact the surface-tension rise of a liquid helium meniscus near a wall is about 0.7 mm, whereas · · · there is a significant variation of the rate of flow at film heights of several centimeters, and this must be regarded as a genuine film effect."[12] However, on reproducing an apparent flow rate height dependence, Brown and Mendelssohn have been "inclined to ascribe the small variation which was actually observed not so much to a real change in the flow rate but to a slight variation of the diameter of the beaker over its length. This is the more probable since in the following experiment the same variation was observed."[21]

With few exceptions, it has been common practice to exploit the diminution of this ill-defined effect with increased distance from the rim by calculating flow rates from data taken with the liquid source far removed from the rim (see papers I and II)[1,2] while according only cursory attention to the extent of the observed variation. This practice makes it rather difficult to analyze and compare much of the existing data on the magnitudes of the rates for the various substrates, since the aforementioned precaution[7] of comparing only those determinations carried out in the same range of the beaker has fallen into disuse. (This problem was also noted in I, where the data reported in Table III and Fig. 8 were therefore acquired at identical film heights.)[1]

Thus, in order for the companion studies of the role of substrate[1] and surface finish[2] to be meaningful, it has likewise been necessary to chart the variation of rate with film height.

Furthermore, the quantitative data on this subject have hitherto been acquired only for transport over glass surfaces, and to the best of our knowledge had been restricted to the plotting of four isotherms.[13,22] Further work of this nature,[22] also restricted to glass surfaces, was brought to our attention after the completion of the work described herein. The paucity of such data for glass, and its nonexistence for metals, serve to emphasize the need for a systematic study of this effect. Interest in this variation is further stimulated by various

[9] K. R. Atkins, Nature **161**, 925 (1948).
[10] W. J. deHaas and G. J. van den Berg, Revs. Modern Phys. **21**, 524 (1949).
[11] R. Bowers and K. Mendelssohn, Nature **163**, 870 (1949).
[12] R. Bowers and K. Mendelssohn, Proc. Phys. Soc. (London) **A63**, 1318 (1950).
[13] K. R. Atkins, Proc. Roy. Soc. (London) **A203**, 241 (1950).
[14] K. R. Atkins, Proc. Roy. Soc. (London) **A203**, 119 (1950).
[15] E. J. Burge and L. C. Jackson, Phil. Mag. **41**, 205 (1950).
[16] L. C. Jackson and D. G. Henshaw, Phil. Mag. **41**, 1081 (1950).
[17] Webber, Fairbank, and Lane, Phys. Rev. **76**, 609 (1949).
[18] J. G. Dash and H. A. Boorse, Phys. Rev. **82**, 851 (1951).
[19] K. Mendelssohn and G. K. White, Proc. Phys. Soc. (London) **A63**, 1328 (1950).
[20] J. G. Dash, Phys. Rev. **94**, 825 (1954). We are grateful to Dr. Dash for providing us with these results prior to publication.
[21] J. B. Brown and K. Mendelssohn, Proc. Phys. Soc. (London) **A63**, 1312 (1950).
[22] B. N. Eselson and B. G. Lazarev, J. Expti. Theoret. Phys. (U.S.S.R.) **23**, 552 (1952). We are grateful to Dr. B. S. Chandrasekhar for supplying us, in April, 1954, with a translation of this paper prepared at the University of Illinois.

TABLE I. R_1: average transport rate between 0.45 cm and 1.33 cm from beaker rim (midpoint at 0.89 cm).

Specimen	Run No.	(Rate in cm³/cm-sec) ×10⁵ 1.1°	1.3°	1.5°	1.7°	1.9°	2.1°
Al-I (B)	38, 39, 48	16.0	15.7	14.9	13.1	9.7	3.9
Al-II (B)	55	12.5	12.3	11.6	10.4	7.8	3.5
Cu	59	17.3	16.8	16.0	13.5	10.2	4.7
Cu	66	15.5	15.2	14.3	12.6	9.3	3.7
Ni-Ag-I (B)	33, 34, 37	15.6	15.4	14.8	13.1	9.6	4.0
Ni-Ag-I (B)	35	...	18.9	17.9	16.1	12.0	...
Ni-Ag-II (B)	45, 46, 49	13.4	13.2	12.6	11.4	8.4	3.5
Ni-II (R)	53	16.0	15.8	15.2	13.9	10.4	4.4
Ag	58	14.3	14.1	13.3	12.0	9.5	3.9
S.St. (B)	41–44, 47	14.9	14.7	14.0	12.6	9.4	4.3
Al-II (ES)	62	15.5	15.5	15.4	14.4	10.9	4.4
Al-II (ES)	65	12.1	12.0	11.6	10.4	7.9	3.5
Ni-Ag-II (ES)	52	10.8	10.7	10.5	9.4	7.4	3.1
Ni-II (ES)	60	11.2	11.1	10.9	9.9	7.7	3.8
S.St. (ES)	50, 51	11.1	10.8	10.3	9.2	7.3	3.7
Al-II (IS)	68	17.0	16.7	15.3	13.1	9.9	4.0
Ni-Ag-II (IS)	64	11.2	11.1	10.7	9.7	7.3	3.3
Ni-II (IS)	67, 69, 70	11.1	10.9	10.3	9.1	6.9	2.8
S.St. (IS)	61, 63	9.0	9.0	8.9	8.4	6.6	3.0
G-III	56	16.2	15.9	15.0	13.0	9.1	3.6
G-IV (FG)	54	18.4	18.2	17.8	16.2	12.8	6.1
G-V (CG)	57	15.5	15.3	14.7	13.3	10.2	4.2

TABLE II. R_2: average transport rate between 1.78 cm and 2.67 cm from beaker rim (midpoint at 2.22 cm).

Specimen	Run No.	(Rate in cm³/cm-sec) ×10⁵ 1.1°	1.3°	1.5°	1.7°	1.9°	2.1°
Al-I (B)	38, 39	13.1	13.0	12.6	11.3	8.2	3.3
Al-I (B)	48	11.9	11.7	10.9	9.5	6.9	2.9
Al-II (B)	55	9.7	9.5	9.0	8.0	6.2	2.7
Cu	59, 66	11.5	11.4	11.3	10.2	7.4	3.2
Ni-Ag-I (B)	33–35, 37	12.8	12.7	12.3	10.3	7.1	2.6
Ni-Ag-II (B)	45, 46, 49	11.5	11.4	10.9	9.8	7.1	2.7
Ni-II (R)	53	12.2	12.1	11.7	10.0	7.1	2.9
Ag	58	11.4	11.3	10.9	10.0	7.4	2.6
S.St. (B)	41–44, 47	11.4	11.2	11.0	9.5	6.8	2.8
Al-II (ES)	62, 65	11.7	11.5	11.0	9.6	6.7	2.4
Ni-Ag-II (ES)	52	9.4	9.3	8.8	7.8	6.0	2.8
Ni-II (ES)	60	8.2	8.1	7.8	7.2	5.7	2.3
S.St. (ES)	50, 51	9.0	8.9	8.5	7.8	5.9	2.6
Al-II (IS)	68	11.9	11.5	10.7	9.2	6.8	2.5
Ni-Ag-II (IS)	64	9.2	9.0	8.6	7.7	5.5	2.2
Ni-II (IS)	67, 69, 70	9.8	9.5	8.9	7.8	6.0	2.4
S.St. (IS)	61, 63	9.5	9.4	9.3	8.6	6.4	2.5
G-III	56	13.3	12.8	11.7	10.0	7.4	3.3
G-IV (FG)	54	14.2	14.1	13.9	12.6	9.1	3.6
G-V (CG)	57	13.2	13.0	12.3	11.0	8.2	3.1

theoretical correlations[5,18,20,22] between the height dependence of the film thickness and the transport rates.

Consequently, the objective of the present investigation has been the study of the variation of film transport rates with the height of the film, with particular emphasis on a possible systematic variation with material[1] and surface finish.[2] The temperature independence of this effect, hitherto tacitly assumed when not completely ignored, has also received careful attention.

EXPERIMENTAL RESULTS[24]

The data to be reported were acquired for transport from "4-section" beakers of the design shown in paper I (Fig. 2 therein).

Each complete emptying of these capacitor-beakers yields four transport rates which will be designated by R_n, where $n=1, 2, 3, 4$, corresponding to the similarly numbered sensitive regions of the capacitor core shown in I, Fig. 2. Thus, four rate *vs* temperature characteristic curves result from each day's run. A complete summary of the data for beaker sections 1–3 inclusive is provided in Tables I–III, where numerical values, abstracted from smooth curves drawn through the experimental points, are reported at conveniently spaced temperatures. The corresponding data for R_4 have already been tabulated elsewhere[1,2] and are consequently omitted here. Since the notation of the present paper is identical with that introduced in the preceding papers,[1,2] correlation of symbols, specimen composition, surface condition, run chronology, etc., may be established with the aid of tables in papers I and II. Since each row in Tables I–III of the present paper represents a separate rate *vs* temperature curve, it is clear that space does not permit the graphical exhibition of all the experimental points, although as has previously been noted,[1,2] a rather complete display of the data is vital in a field whose history is so filled with conflicting reports. However, the original data for R_4 have already been pre-

TABLE III. R_3: average transport rate between 3.11 cm and 4.00 cm from beaker rim (midpoint at 3.56 cm).

Specimen	Run No.	(Rate in cm³/cm-sec) ×10⁵ 1.1°	1.3°	1.5°	1.7°	1.9°	2.1°
Al-I (B)	38, 39, 48	10.9	10.7	10.0	8.7	6.3	2.8
Al-II (B)	55	9.2	9.1	8.7	7.8	5.8	2.2
Cu	59	11.0	10.9	10.7	9.8	7.3	2.7
Cu	66	9.5	9.4	9.1	8.2	5.9	2.2
Ni-Ag-I (B)	33–35, 37	12.3	12.2	11.9	10.4	7.0	2.1
Ni-Ag-II (B)	45, 46, 49	10.5	10.4	10.0	9.0	7.1	3.4
Ni-II (R)	53	13.4	13.0	12.1	10.4	7.1	2.6
Ag	58	9.1	9.1	9.0	8.5	6.9	2.9
S.St. (B)	41–44, 47	9.8	9.7	9.5	8.6	6.3	2.6
Al-II (ES)	62	12.2	11.8	10.9	9.5	6.7	2.3
Al-II (ES)	65	9.3	9.3	8.9	7.4	5.2	2.4
Ni-Ag-II (ES)	52	8.8	8.8	8.7	8.1	5.9	2.4
Ni-II (ES)	60	8.4	8.3	8.2	7.6	5.9	2.3
S.St. (ES)	50, 51	8.0	7.9	7.8	6.8	5.1	2.2
Al-II (IS)	68	10.8	10.5	9.7	8.4	6.3	2.6
Ni-Ag-II (IS)	64	8.7	8.6	8.2	7.3	5.6	2.5
Ni-II (IS)	67, 69, 70	9.4	9.3	8.8	7.6	5.9	2.5
S.St. (IS)	61, 63	8.6	8.5	8.4	7.5	5.5	2.3
G-III	56	12.3	11.9	11.1	9.3	6.6	2.7
G-IV (FG)	54	11.7	11.5	11.1	10.1	8.1	3.7
G-V (CG)	57	13.3	13.1	12.9	11.6	8.6	3.7

[23] J. G. Dash, Phys. Rev. **94**, 1091 (1954). We are indebted to Dr. Dash for acquainting us with these results prior to publication.

[24] Preliminary accounts of some of these results have already been presented: B. Smith and H. A. Boorse, Proceedings of the Third International Conference on Low Temperature Physics and Chemistry (Rice Institute, Houston, 1953); B. Smith and H. A. Boorse, Phys. Rev. **94**, 772 (1954); B. Smith, Bull. Am. Phys. Soc. **30**, No. 1, 57 (1955).

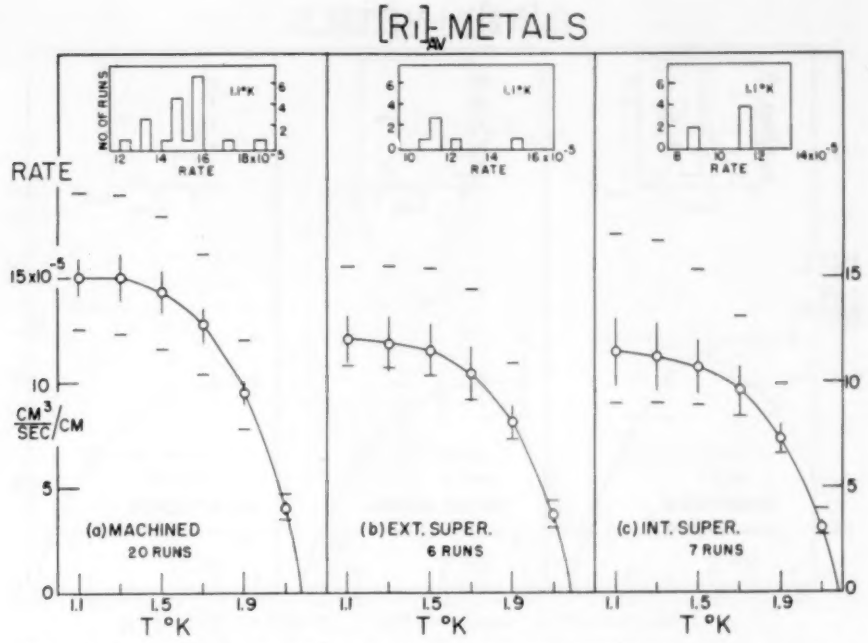

FIG. 1. Average values of transport rates calculated from those listed in Table I for various metal surfaces (R_1: 0.45 cm to 1.33 cm from beaker rim). The plotted points are calculated arithmetic mean values; the vertical lines are drawn to extend above and below the points by an amount equal to the average absolute deviation from the mean and the horizontal bars represent the highest and lowest values contributing to each average. The histograms show the frequency distributions of the observed rates at 1.1°K.

sented (see I: Fig. 8 and II: Figs. 2–6); this should prove adequate since there exist one to one correspondences between the plotted experimental values of R_4 and those for R_1, R_2, and R_3, which will not be shown.

As previously noted,[2] the striking similarity of the data for all materials and finishes at each height suggests an analysis based on the statistical comparison of average behavior illustrated in Figs. 1–3 of the present paper and Fig. 7 of paper II. Indeed, these results have already been invoked in the previous analysis of the role of substrate[1] and surface finish.[2]

The variation of transport rate with height for each complete isothermal emptying of the capacitor may be obtained by plotting R_n against abscissas corresponding to the distance of the midpoint of the nth section from the rim. Thus, each emptying yields a height dependence isotherm similar to those plotted by Eselson and Lazarev[22] and Atkins.[13] The prohibitive number of such graphs (one for every experimental point shown in the graphs of R_4 *vs* T in papers I and II) may greatly be reduced by making use of the fact that this effect was found to be temperature independent over the range of temperatures which was investigated. This may conveniently be observed by plotting a separate graph of the dimensionless ratio (R_n/R_4) against temperature for each value of n; a complete isothermal emptying provides a point on each such graph. Representative results are portrayed in Fig. 4 in plots of (R_3/R_4) *vs* T obtained for a number of materials and surface finishes. Since such graphs failed to reveal any dependence on temperature, an arithmetic mean of values obtained over all temperatures was then calculated for each ratio. A complete summary of these average values appears in Table IV. Individual values for the three glass runs are also plotted in Fig. 5(d). The rows in Table IV reflect the observed temperature independent average height variation in a conveniently normalized fashion since the value $(R_4/R_4)=1$ (omitted in the table) is common to each row. This normalization may further be exploited by averaging items in each column of Table IV which correspond to groups of similarly prepared metal beakers. This operation yields the graphs shown in Fig. 5(a–c), which thus represent a distillation of the information available in hundreds of height dependence isotherms. The points, vertical lines, and horizontal bars in Fig. 5 were drawn using the conventions previously described in reference to Figs. 1–3. Histograms are included in the insets of Fig. 5 to exhibit the frequency distribution of actual values in the range observed for one particular ratio. For reasons which will later become apparent, it is of interest to investigate the possibility of representing the data in Fig. 5 by algebraic expressions of the form

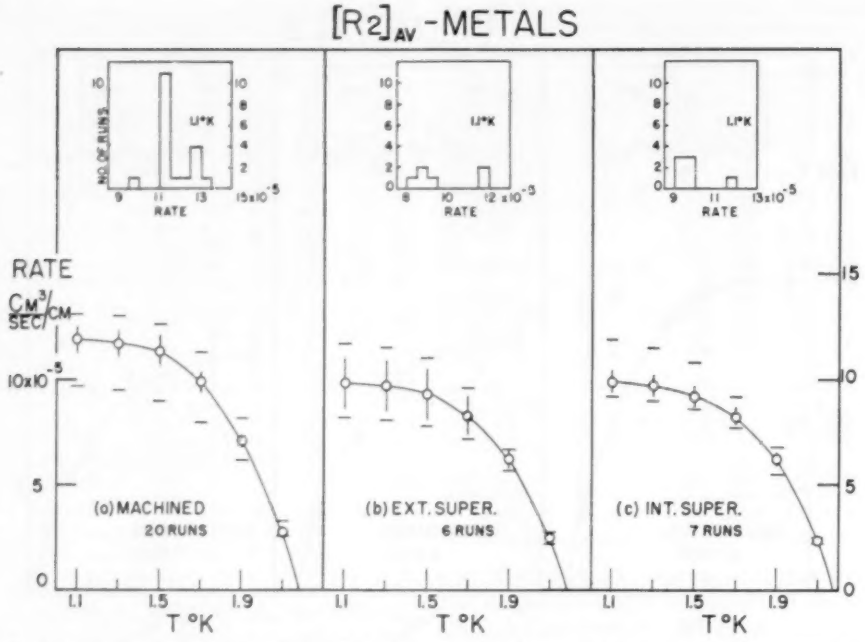

FIG. 2. Average values of transport rates calculated from those listed in Table II for various metal surfaces (R_2: 1.78 cm to 2.67 cm from the rim). Symbols have the same significance as in Fig. 1.

$h^{-1/z}$. Consequently, the average data have been replotted logarithmically in Fig. 6, where successful representation by the expression $h^{-1/z}$ should produce linearity with slope $(-1/z)$. Except for the average data for bored specimens, it is clear that the departures from linearity are rather pronounced. A rough measure of this departure may be inferred from the line segments which have been drawn connecting adjacent points on the two lower curves. Values of z appropriate to each segment are indicated on the graphs. The curves shown in Fig. 5 were drawn for integral values of z suggested by the range of slopes in Fig. 6; each curve has been scaled to correspond to the observed data at a distance of 1 cm from the rim. These curves are included only for reference in the discussion to follow and are not intended to convey an adequate representation of the experimental results.

Direct verification of the consistency of earlier observations (shown in I: Figs. 4–7 and II: Fig. 1) with those just described is rendered difficult by the different heights appropriate to the earlier data. However, graphs of R *vs* h similar to Fig. 5 but differing in the omission of normalization, serve to verify the complete consistency of all the data which have previously been presented.[1,2] Thus, although the uniform geometry characterizing specimens in the final series of control experiments[1,2] provides a fertile source of easy and direct comparisons, thereby encouraging almost exclusive reference to these results in subsequent discussion, the conclusions drawn will be equally applicable to the other data.

DISCUSSION

As mentioned in the Introduction, the present study of the height dependence of the transport rate was undertaken as a precautionary measure intended to minimize ambiguity in the analysis of the dependence on substrate[1] and microfinish.[2] An undeniable variation of transport rate with film height, regardless of its origin, has indeed been observed. The value of the precaution of comparing only those "determinations carried out in the same range of the beaker"[7] has therefore amply been demonstrated.

The arguments most frequently cited for judging previously observed height dependences to be spurious do not seem to apply here. For example, the results cannot be ascribed to uncertainties in beaker geometry, because the effect was observed for so many beakers whose inner diameters had been accurately measured (see I for discussion of bore measurement). The results cannot simply be ascribed to surface roughness since the height dependence persisted even for (IS) beakers.[2] There is no reason to believe that contamination in the sense discussed by Bowers and Mendelssohn[11,12] is responsible for the observations, in view of the leak tightness and outgassing precautions which were adopted.[1] Furthermore, the observed rates not only fail to exhibit the anomalously high values characteristic of

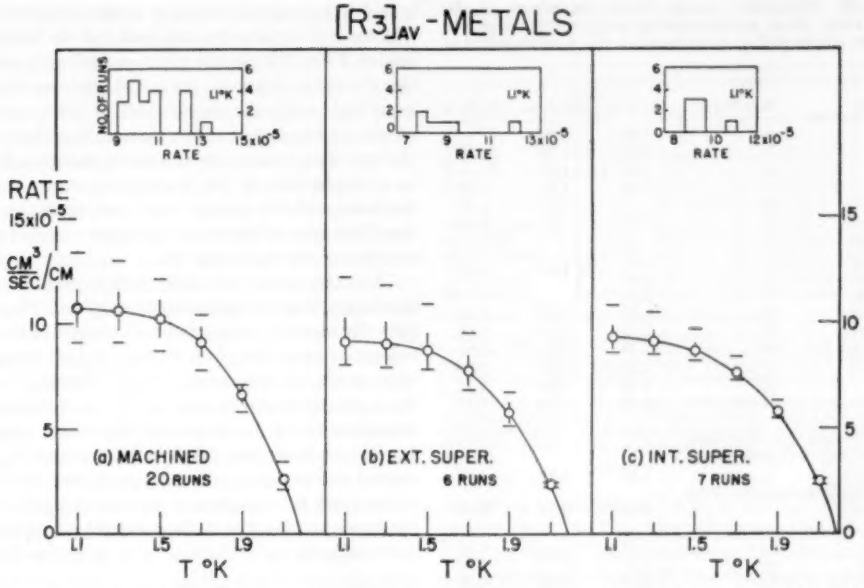

FIG. 3. Average values of transport rates calculated from those listed in Table III for various metal surfaces (R_3: 3.11 cm to 4.00 cm from rim). Symbols have the same significance as in Fig. 1.

contaminated surfaces, but are even lower than most previous results for "clean metal beakers."[1] Finally, as will be discussed in a subsequent paper,[25] the temperature dependence of the flow was observed to be the same (on the average) at all heights.

The present observations are similar to those described by Atkins[13] and Eselson and Lazarev,[22] both with respect to order of magnitude and also with respect to their conclusion that the film height (i.e., the distance of the level of the liquid source from the beaker rim) is the significant parameter with which the observations may be correlated. Since detailed evidence for this conclusion is available elsewhere,[13,22] the present discussion will be limited to the observation that the effect of film height is most vividly observed by comparison of filling rates, measured at effectively constant film height, with those obtained on emptying which takes place at continuously varying film height.

As a result of the primary interest of the present work in comparing the behavior of beakers of various materials and finishes under identical conditions,[1,2] most of the systematic observations were made on the emptying of beakers which had previously been filled by immersion. Those filling rates which were measured did not appear appreciably different from emptying rates obtained at comparable film heights (see graphs in papers I and II), although other observers have noted measurably higher,[22] as well as lower[19] rates on emptying. The present measurements did not extend to the small level differences which have been the concern of some investigations.[13,22,26]

In the absence of any clear evidence for an alternative explanation, it seems reasonable to identify the observed dependence on height with the similar behavior of the film thickness, as has been done by Atkins.[13] However,

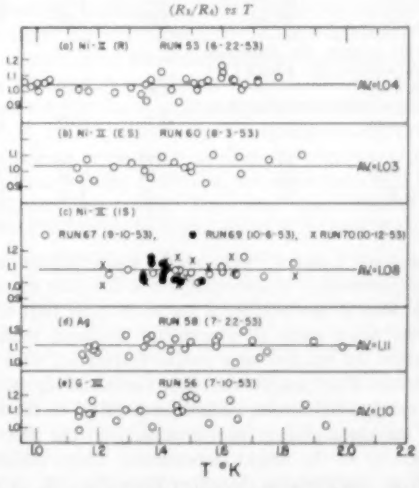

FIG. 4. Typical plots of (R_3/R_4) as a function of temperature for some metal and glass specimens. These and similar graphs reveal the temperature independence of this ratio for all specimens, thereby providing a single average value for each run as shown. Averages so obtained are listed in Table IV.

[25] B. Smith and H. A. Boorse, following paper [Phys. Rev. **99**, 367 (1955)], designated as IV in the present text.

[26] G. S. Picus, Phys. Rev. **94**, 1459 (1954).

TABLE IV. Normalized average height dependence of the transport rates. These are temperature independent values (obtained from graphs such as those shown in Fig. 4) as explained in the text.

Specimen	Run Nos.	$(R_2/R_4)_{h_2}$	$(R_3/R_4)_{h_3}$	$(R_3/R_4)_{h_4}$
Al-I (B)	38	1.63	1.29	1.02
Al-I (B)	39	1.35	1.19	
Al-I (B)	48	1.65	1.21	
Al-II (B)	55	1.35	1.05	1.01
Cu	59	1.64	1.11	1.12
Cu	66		1.31	1.03
Ni-Ag-I (B)	33	1.35		
Ni-Ag-I (B)	34	1.40	1.06	1.01
Ni-Ag-I (B)	35	1.49		
Ni-Ag-I (B)	37	1.33		
Ni-Ag-II (B)	45	1.38	1.23	1.14
Ni-Ag-II (B)	46	1.33	1.19	1.04
Ni-Ag-II (B)	49	1.28	1.03	1.01
Ni-II (R)	53	1.29	0.96	1.04
Ag	58	1.68	1.34	1.11
S.St. (B)	41–44, 47	1.54	1.33	1.11
Over-all average for machined [i.e., (B) and (R)] metals [See Fig. 5(a)]		1.47	1.19	1.06
Average absolute deviation from the mean		0.12	0.11	0.04
Al-II (ES)	62	1.57	1.21	1.13
Al-II (ES)	65	1.27		0.95
Ni-Ag-II (ES)	52	1.19	0.96	0.92
Ni-II (ES)	60	1.41	1.01	1.03
S.St. (ES)	50	1.49	1.24	1.09
S.St. (ES)	51		1.19	
Over-all average for externally superfinished (ES) metals [See Fig. 5(b)]		1.39	1.14	1.04
Average absolute deviation from the mean		0.13	0.10	0.07
Al-II (IS)	68	1.57	1.14	1.01
Ni-Ag-II (IS)	64	1.34	1.09	1.02
Ni-II (IS)	67, 69, 70	1.27	1.10	1.08
S.St. (IS)	61, 63	1.09	1.06	0.97
Over-all average for internally superfinished (IS) metals [See Fig. 5(c)]		1.27	1.09	1.03
Average absolute deviation from the mean		0.13	0.02	0.04
G-III	56	1.49	1.18	1.10
G-IV (FG)	54	1.58	1.24	1.00
G-V (CG)	57	1.23	1.02	1.06

Eselson and Lazarev,[22] upon noting a lack of instantaneous adjustment to a new equilibrium flow rate when the liquid level progressed from the wide upper part to the narrow lower part of a specially designed beaker,[27] question the validity of a simple correlation with film thickness. They suggest that only the initial high rate of emptying a full beaker should be ascribed to the large film thickness arising from proximity to the rim. The remainder of the height dependence, which manifests itself at considerable distances from the rim, is then depicted as the result of a tendency of the rate to resist changes from the initial high value. This inertial effect is said to be more pronounced under conditions of poor thermal contact between the bath and the helium in the beaker. Even this picture relies on the height dependent film thickness to furnish the initial tendency for the rate to be high, while the exact nature of the special effects, as well as the details of the inertial hypothesis, remain obscure. The present discussion will therefore be limited to a comparison of the known properties of the film thickness with the present flow rates, on the assumption that "the rate of transfer is probably a rather sensitive measure of the thickness."[28]

The calculation of Schiff[29] which predicts that the stationary film thickness should vary as $h^{-\frac{1}{2}}$ has already been discussed in connection with the size of the helium-substrate interaction [see I: Eq. (2)]. Although somewhat similar considerations also led Frenkel[30] to predict the same functional dependence of the thickness on h, a variation with $h^{-\frac{1}{3}}$ was derived from other assumptions by Bijl, deBoer, and Michels.[31] Consequently, experimental results are traditionally compared with functions of the form $h^{-1/z}$ to provide numerical estimates of the appropriate values of z. Temperley[28] incorporated features of both these theories in a quantum-mechanical

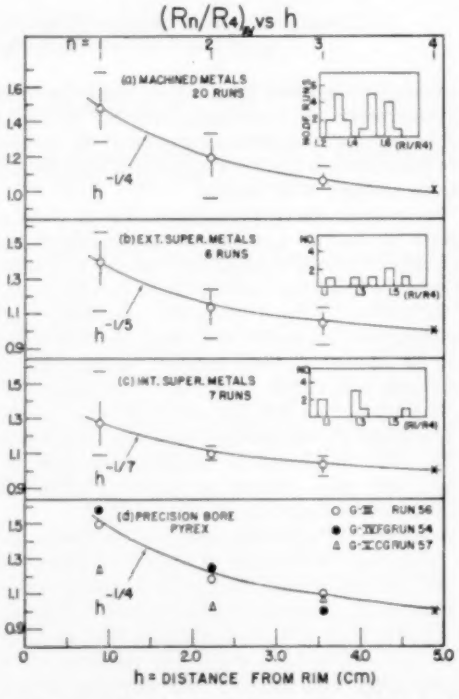

FIG. 5. Average normalized dependence of transport rates on film height for various materials and surface finishes.

[27] Although not specifically discussed in their paper, it appears that Daunt and Mendelssohn observed a similar effect in their original experiments (see reference 6, Fig. 7).

[28] H. N. V. Temperley, Proc. Roy. Soc. (London) **A198**, 438 (1949).

[29] L. I. Schiff, Phys. Rev. **59**, 839 (1941).

[30] J. Frenkel, J. Phys. (U.S.S.R.) **2**, 365 (1940).

[31] Bijl, deBoer, and Michels, Physica **8**, 655 (1941).

treatment which leads to a qualitatively similar result which cannot be reduced to such a simple algebraic relation between thickness and height. Atkins[32] has also deduced a more complicated result which yields a value of z between 2 and 3, if an approximation of the form $h^{-1/z}$ is sought. A discussion of the merits and limitations of the various theories will be omitted here in view of the availability of two excellent review articles which have recently appeared.[5,33]

It must first be noted that the variation with height of the present transport rates has been found to be temperature independent over the range which was investigated (see Fig. 4). This compares favorably with a similar temperature independence exhibited by the film thickness in both optical[34] and gravimetric[35] studies.

Only Temperley[28] has made a serious attempt to propose a theory of the variation of film thickness with temperature. His work leads to three possible results depending on three different assumptions which can be made in comparing the energy attributed to the lowest state of the liquid with the energies of the film states. One assumption leads to a constant film thickness below the lambda point, another leads to a vanishing of the film at absolute zero, and the third implies that the film thickness should exhibit a maximum below the lambda point. Temperley notes that "it is not possible to predict *a priori* which of these three assumptions should be made," although he suggests "a little evidence" in favor of the third possibility. This consists, in part, of the fact that the observed proportionality of transport rates to the minimum perimeter presented by surfaces can be correlated with the third assumption in a fairly obvious manner. Supplementary evidence is based on experimental data available at the time (1949), from which it was inferred that "the rate of transfer seems to pass through a maximum at 1.6°K to 1.8°K," thereby suggesting that "the film thickness passes through a maximum here also." Since later measurements have shown that neither the thickness[34,35] nor the transport rates[1,2,25] normally exhibit such maxima, it might be profitable to develop the consequences of the previously ignored first assumption in a more quantitative fashion. The fact that Temperley's calculation does not predict a maximum on an *a priori* basis seems to have received inadequate attention in the literature.

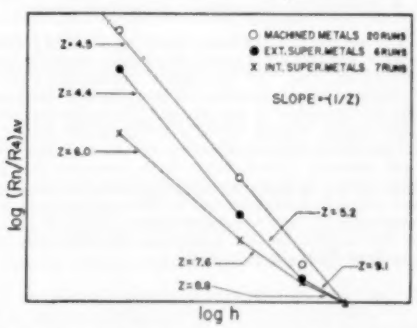

FIG. 6. Logarithmic replot of the average data of Fig. 5 to determine the applicability of the functions shown therein to the data.

TABLE V. Comparison of values of z obtained by fitting measured variation of film thickness with height[a] to the functional dependence $h^{-1/z}$.

Substrate	Range of film height (cm)	T°K	z	Method	Reference
Glass	0.5–5.0	1.47	7	Oscillations	36
Glass	0.3–1.0	1.47	~2	Oscillations	36
Glass	1.0–4.5	1.47	~10	Oscillations	36
Glass		1.3–1.9	1–2	Oscillations	26
Stainless steel covered by barium stearate	0.25–1.2	1.5	2.9–3.1	Optical, static film	34[b]
	0.15–1.5	1.1	3.3	Optical, static	34[b]
	0.15–1.5	2.1	2.5	Optical, static	34[b]
	0.4–1.6	2.05	2.3	Optical, static	40
	0.25	?	2.5	Optical, mobile	34[b]
	1	?	8–12	Optical, mobile	34[b]
Aluminum	0.3–7.9	1.25–2.15	2±0.3	Gravimetric	35

[a] In a paper which appeared after the preparation of this manuscript, L. Meyer [Phys. Rev. **97**, 22 (1955)] offers an interesting discussion and interpretation of "the great variety of the experimental evidence" to be found in reports of the thickness of the static helium film as a function of height.

[b] As noted by Daunt and Smith (see reference 5), these values must presumably be corrected in accordance with later observations reported by L. C. Jackson and D. G. Henshaw [Phil. Mag. **44**, 14 (1953)]. See reference 40 for those details of the required modifications which have thus far been reported.

The results for individual runs have been listed in Table IV so as to provide a basis for detailed comparison of the present observations with future theoretical and experimental studies. In view of the current status of both theory and experiment,[5,34,35] it seems reasonable to restrict the present discussion to the average dependence of the transport rate on height which is shown in Fig. 5. In such a discussion it must always be remembered that Table IV and Fig. 5 indicate variations from run to run and specimen to specimen to which the remarks made in connection with the analysis of the role of substrate[1] and microfinish[2] also apply. Here too, the difficulty of exactly duplicating beaker surfaces is worthy of attention. For example, the film thickness data which will be cited for "clean surfaces" may be compared with Atkins' report[36] that the film thickness varied as h^{-1} on contaminated glass surfaces. Atkins has also observed a thickness on soda glass which had been cleaned with hot distilled water, which differed from the thickness he measured for lead glass cleaned in hot chromic acid, although the film "had the same shape in the two cases."[26]

Table V summarizes the available data on the functional dependence of film thickness on height as reflected by values of z in expressions of the form $h^{-1/z}$. Comparison with Fig. 6 indicates that the results are

[32] K. R. Atkins, Can. J. Phys. **32**, 347 (1954).
[33] R. B. Dingle, Phil. Mag. Suppl. (Advances in Physics) **1**, 111 (1952).
[34] E. J. Burge and L. C. Jackson, Proc. Roy. Soc. (London) **A205**, 270 (1951). (Also, see reference 40.)
[35] R. Bowers, Phil. Mag. **44**, 1309 (1953); Phys. Rev. **91**, 1016 (1953).
[36] K. R. Atkins, Proc. Roy. Soc. (London) **A203**, 119 (1950).

indeed similar; although the function appears too simple for an adequate description of the logarithmic plots of Fig. 6, this inadequacy is virtually masked in the curves shown in Fig. 5. These curves were drawn solely for the purpose of demonstrating this observation and do not reflect any attempt to provide the best possible fit to the data. In both thickness and flow rate determinations, the trend is toward larger values of z at greater heights. The scatter of the present height dependence data, as well as the actual transport rate data, was found to be greatest at small film heights. While this effect cannot be dissociated from the increased uncertainty inherent in measurements of the shorter times associated with higher rates,[1] one must not overlook possible correlation with other effects such as the drop formation which has on occasion been observed in association with proximity of the liquid level to the rim.[37] It must also be noted that the validity of the comparison of values in Table V with the present data on flow rates may be limited by the different geometrical conditions of the various experiments. For example, the gravimetric measurements[25] refer to the film thickness on a sheet of aluminum foil, the optical measurements[34] determine the thickness of the film on the outside wall of a beaker, and the oscillation studies[26,36] are performed only at small level differences, whereas the present flow data should be correlated with the thickness of the film on the inner beaker wall during emptying. Comparison should also be confined to measurements of the thickness of mobile rather than stationary films.

It has been suggested that the expression

$$(mv_c)d \sim h, \tag{1}$$

where (mv_c) is the average critical momentum of the superfluid particles and d is the film thickness or channel width, might describe superflow in liquid helium II.[5] If m is then associated with the atomic mass of helium, rather than some effective mass which might depend implicitly on other parameters, it would be expected that any variation of d with height should be counteracted by a variation of v_c tending to maintain the constancy of the product $v_c d$. Consequently the transport rate, which is expected to vary as $v_c d$ on dimensional grounds, would also be height independent.[5] In spite of the interesting features embodied in Eq. (1), its status with respect to the helium II problem is not sufficiently established in theory or experiment to justify the rejection of experimental observations which seem to conflict with its consequences. For example, although Eq. (1) implies $v_c \propto d^{-1}$, Mott[38] has proposed a model in which $v_c \propto d^{-\frac{1}{2}}$, and a recent calculation by Dash[20] also leads to the latter dependence. Experimental evidence for the invariance of the product $v_c d^{\frac{1}{2}}$ is cited by Dash,[20] while Daunt and Smith[5] conclude that the experimental evidence "does not allow a completely clear choice" between the two alternative relations connecting v_c and d. Atkins[39] has called attention to evidence that "$v_c d$ is not a constant but increases with d."

Dash[22] has also suggested that the transport rate might vary with height as the square root of the thickness dependence on height. Such a variation (i.e., $R \propto h^{-\frac{1}{2}z}$, when $d \propto h^{-1/z}$) would also be consistent with the present data if one uses the smaller values of z shown in Table V for the film thickness. A more complete comparison must await further study of the film thickness as a function of material, finish, temperature,[40] etc., in both theory and experiment.

ACKNOWLEDGMENTS

The authors wish to express their appreciation to Arnold Berman, Raymond Kaplan, Leonard Lesensky, Robert D. Worley, and Professor Adam H. Spees for valuable assistance during the course of the measurements; to Mr. G. T. Poirier and Mr. P. DePalma for their cooperation in the superfinishing program conducted by the Department of Production Research of the Chrysler Corporation; and to Professor Mark W. Zemansky for his active and stimulating interest in these experiments.

[37] D. G. Henshaw and L. C. Jackson, National Bureau of Standards, Circular 519 (U. S. Government Printing Office, Washington 25, D. C., 1952) pp. 189–190.

[38] N. F. Mott, Phil. Mag. **40**, 61 (1949).

[39] K. R. Atkins, Phil. Mag. Suppl. (Advances in Physics) **1**, 169 (1952).

[40] A. C. Ham and L. C. Jackson, Phil. Mag. **45**, 1084 (1954). In this paper, it is reported that a thick film persists above the lambda temperature, and that "the thickness of the helium II film was greatly increased by the presence of an extremely thin layer of solid air on the surface of the mirror." These observations are obviously of great interest, not only in the present context, but also in connection with the previous discussion of the roles of substrate (reference 1) and surface finish (reference 2). Further discussion of these findings must however await the publication of the more complete report promised by Ham and Jackson, as well as the extension of these new measurements to mobile films and greater film heights. In this connection, Meyer's recent paper (cited in Table V) is also of interest.

Helium II Film Transport. IV. The Role of Temperature*

BERNARD SMITH† AND HENRY A. BOORSE‡
Pupin Physics Laboratories, Columbia University, New York, New York

(Received March 22, 1955)

The study of film transport, inaugurated in previous papers in this series, is concluded with a statistical analysis of the temperature dependence of the transport rates, with particular attention to the possibility of detecting systematic variations with substrate, surface finish, and film height. Analysis of 153 rate *vs* temperature characteristic curves reveals that the temperature dependence of the transport is relatively insensitive to changes in the aforementioned parameters. The functional dependence of the *normalized*, *average* transport rates for all materials, finishes, and film heights discussed in papers I–III, is given by $[1-(T/T_\lambda)^7]$, in the temperature range under investigation ($1.1°K \leqslant T < T_\lambda$). These results are compared with various theoretical predictions based on the two-fluid model of liquid helium as well as with relevant reports of other observers.

INTRODUCTION

THIS, the fourth and final paper in the current series of studies of helium II film transport,[1–3] is concerned with the clarification of the answer to the question: How do measured transport rates vary with temperature?

A suggestion by Daunt and Mendelssohn[4] that the variation of transport rate with temperature might be a measure of the concentration of superfluid atoms was subsequently bolstered, in a modified form, by a theoretical argument due to London.[5] Although London was then forced to conclude that the experimental evidence was too scant to permit safe generalization and that it would be very desirable to have more data available, only one previous study[6] of transport rates includes data (for glass, platinum and nickel) which have been analyzed with respect to the actual functional form of the temperature dependence. Furthermore, unusual rate *vs* temperature characteristic curves (observed for Lucite)[7,8] have been the source of suggested interpretations of the role of surface finish.[8] A recent theoretical prediction by Dash[9] has also emphasized the need for more experimental evidence.

The present objective has therefore been to study the functional dependence of the transport rate on temperature, with particular emphasis on possible systematic variations with material, surface finish, and film height.

EXPERIMENTAL RESULTS[10]

In analyzing the functional dependence on temperature, it has been found convenient to normalize the rates to unity at 1.1°K; although measurements have been made at lower temperatures, this represents the lowest temperature at which data were obtained with satisfactory consistency. The characteristic curves are automatically coincident at the high temperature extreme (lambda point). Further normalization anywhere other than at the low temperature extreme would then yield a deceptively exaggerated similarity of plotted curves, since little opportunity for departure of the curves from one another would be available within the resultant short range of all points from the normalization temperature. Using data and notation cited in previous papers,[1–3] division of each value of $R(T)$ by the corresponding value of $R(1.1°)$ accomplishes the desired normalization. The similarity of the results so obtained for all heights and finishes (see papers I–III) is striking, and may be observed for metals from the average values and average absolute deviations from these mean values as indicated in Table I. In order to insure that the deviations represent appropriately conservative estimates, all values of deviation less than 0.01 have arbitrarily been listed as 0.01. For comparison of the over-all average obtained from 132 curves for metals, the results of similar calculations for all glass and quartz specimens[1–3] (including those studied with other than "4-section" depth gauges)[1] are also given. The latter two sets of averages are plotted in Fig. 1 where the calculated average absolute deviations from the mean are in all cases no greater than the size of the plotted points. The horizontal bars showing the extreme values encountered at each temperature, as well as the histograms portraying the frequency distribution of observations at 1.7°K, where the distance from both normalization temperatures accentuates the dispersion, serve to complete the statistical picture. The calculated curves, based on the indicated seventh power dependence on temperature, were drawn after suitable logarithmic

* Assisted by the Office of Naval Research and the Linde Air Products Company.

† Present address: Bell Telephone Laboratories, 463 West Street, New York 14, New York.

‡ Barnard College, Columbia University, New York 27, New York.

[1] B. Smith and H. A. Boorse, Phys. Rev. **98**, 328 (1955). (I. The Role of Substrate, designated as I in the present text.)

[2] B. Smith and H. A. Boorse, this issue [Phys. Rev. **99**, 346 (1955)]. (II. The Role of Surface Finish, designated as II herein.)

[3] B. Smith and H. A. Boorse, this issue [Phys. Rev. **99**, 358 (1955)]. (III. The Role of Film Height, designated as III herein.)

[4] J. G. Daunt and K. Mendelssohn, Nature **150**, 604 (1942).

[5] F. London, Revs. Modern Phys. **17**, 310 (1945).

[6] K. Mendelssohn and G. K. White, Proc. Phys. Soc. (London) **A63**, 1328 (1950).

[7] J. G. Dash and H. A. Boorse, Phys. Rev. **82**, 851 (1951).

[8] B. S. Chandrasekhar, Phys. Rev. **86**, 414 (1952).

[9] J. G. Dash, Phys. Rev. **94**, 825 (1954). We are grateful to Dr. Dash for providing us with these results prior to publication.

[10] Preliminary accounts of some of these results have already been presented: B. Smith and H. A. Boorse, Phys. Rev. **94**, 772 (1954); B. Smith, Bull. Am. Phys. Soc. **30**, No. 1, 57 (1955).

TABLE I. Summary of average normalized temperature dependence of the transport rates. Entries represent average values of the quantity $[R(T)/R(1.1°K)]$ appropriate to the temperatures indicated in column headings. Average absolute deviations from the mean are given in columns headed "A.d." (where values less than 0.01 have been listed as 0.01 as noted in the text). For a description of heights pertaining to beaker sections 1–4, finishing procedures, specimen composition and other experimental details, see papers I–III.

Beaker section (n)	1.3°K Av	1.3°K A.d.	1.5°K Av	1.5°K A.d.	1.7°K Av	1.7°K A.d.	1.9°K Av	1.9°K A.d.	2.1°K Av	2.1°K A.d.
Machined metals: Data for 8 specimens, averaged over 20 runs.										
1	0.98	0.01	0.94	0.01	0.84	0.01	0.62	0.01	0.29	0.03
2	0.99	0.01	0.96	0.01	0.84	0.02	0.60	0.02	0.24	0.02
3	0.99	0.01	0.96	0.02	0.85	0.03	0.67	0.04	0.25	0.04
4	0.99	0.01	0.95	0.02	0.84	0.02	0.62	0.02	0.25	0.03
Externally superfinished metals: Data for 4 specimens, averaged over 6 runs.										
1	0.99	0.01	0.96	0.02	0.87	0.03	0.67	0.02	0.32	0.02
2	0.99	0.01	0.94	0.01	0.85	0.03	0.63	0.04	0.26	0.04
3	0.99	0.01	0.96	0.03	0.85	0.04	0.64	0.04	0.26	0.02
4	0.99	0.01	0.96	0.01	0.85	0.02	0.62	0.05	0.25	0.05
Internally superfinished metals: Data for 4 specimens, averaged over 7 runs.										
1	0.99	0.01	0.95	0.03	0.85	0.05	0.65	0.05	0.28	0.04
2	0.97	0.01	0.91	0.01	0.80	0.01	0.60	0.01	0.24	0.01
3	0.99	0.01	0.94	0.02	0.83	0.03	0.63	0.01	0.27	0.01
4	0.99	0.01	0.95	0.01	0.84	0.04	0.61	0.02	0.24	0.01
Over-all average[a] from above 132 $R(T)$ curves for metals (all heights and finishes), plotted in Fig. 1(b).										
All	0.99		0.95		0.84		0.63		0.26	
Over-all average[a] from 21 $R(T)$ curves for glass and quartz (all heights and finishes), plotted in Fig. 1(a).										
All	0.98		0.94		0.84		0.62		0.25	

[a] Average absolute deviations calculated for these over-all averages are in all cases less than 0.01 and are therefore unlisted.

plots yielded straight lines of slope seven. Comparison of the plotted points with the calculated curves and other values indicated in Fig. 1 is reserved for the discussion to follow.

DISCUSSION

It may be observed from Table I and Fig. 1 that the temperature dependence of the transport rates was so insensitive to variations in beaker material, microfinish, and height of the film, that observed differences were unsystematic and could not definitely be ascribed to changes in these parameters. The difficulty of exactly reproducing beaker surface conditions[1–3] must again be considered in any attempt to evaluate the significance of small differences between the results obtained on separate runs. Although enough tabular information has already been presented[1–4] to permit the analysis of the temperature dependence of many individual runs, the current status of theory and experiment does not seem to warrant the extension of the present discussion beyond the consideration of the average values shown in Table I and Fig. 1. The shape of the histogram in Fig. 1(b) also encourages reliance on the statistical picture.

Before discussing this average behavior, it is well to recall that departures from the pattern exhibited in Fig. 1 have received some attention in the literature. According to Chandrasekhar,[8] the maxima he observed in the R vs T curves for transport over methyl methacrylate polymers, "seem to indicate that the observed flow on Lucite and Perspex can be regarded as being composed of two parts: (1) pure film flow giving a characteristic similar to the one observed on glass; (2) a pressure dependent flow of bulk helium, which takes place when the surface irregularities are of a shape and size favorable to this type of syphon flow. The maxima in the flow characteristics would require this type of flow to decrease with decreasing temperature." Support of this conclusion is adduced[8] from the observation that the most pronounced maximum was obtained for a Perspex surface which showed a rough streaky structure with ridges and valleys about 10^{-3} cm wide.

It has already been noted[1,11,12] that the results obtained for Lucite in the current study of the role of

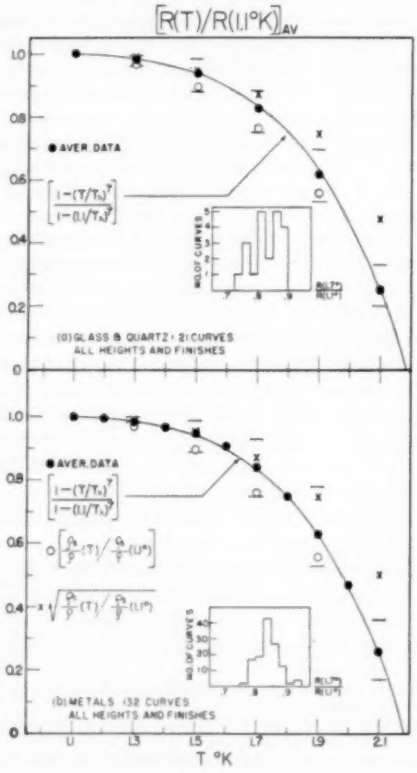

FIG. 1. Average, normalized temperature dependence of the transport rates at all heights (see Table I), (a) averaged over 21 curves for glass and quartz, and (b) averaged over 132 curves for metals. The apparent absence of (ρ_s/ρ) values at some temperatures stems from the identity of these values with the average data close to the normalization temperatures. Details of specimen composition, beaker identification, machining and superfinishing procedures, film heights appropriate to various beaker sections, and other relevant experimental details may be determined by reference to the previous papers in this series (I–III).

[11] B. Smith and H. A. Boorse, Phys. Rev. **90**, 156 (1953).
[12] J. G. Daunt and R. S. Smith, Revs. Modern Phys. **26**, 172 (1954).

substrate do not exhibit such a maximum (see I: Fig. 7). Furthermore, the 10^{-3} cm wide ridges do not seem very significant in view of the conventional results obtained for the channels about $5(10)^{-3}$ cm by $2.5(10)^{-3}$ cm in size which covered the surface of a broached nickel beaker in work previously described.[2] A recent search for anomalous flow in glass capillaries has also yielded negative results.[13] Transport rates, for the comparatively rough specimens of glass and metal used in control experiments on the role of microfinish,[1,2] did not display maxima in R *vs* T curves.

It is also noteworthy that transport rate characteristic curves with and without such maxima have now been reported not only for plastics, but also for platinum[6] and glass,[14] while Mendelssohn and White[6] remark that this "peculiar fall of the rate with lower temperatures · · · was also observed on glass beakers by Daunt and Mendelssohn." The evanescent nature of such behavior was vividly portrayed in some of our early experiments,[11] in which capacitor design and reproducibility from run to run were being investigated. As is evident from Fig. 2, a maximum was observed for transport over a machined nickel beaker (run 5) which, except for outgassing,[1] was left undisturbed in the cryostat between prior and subsequent runs which did not reveal such behavior (runs 4 and 6). Thus the size and shape of surface irregularities were unchanged while the rate-temperature characteristics varied. (Since later work[3] indicated that the transport rates vary considerably with height in the range used here (between 0.5 cm and 3.5 cm from the rim), the absolute values of transport rate in Fig. 2 can be interpreted only in connection with the discussion of height dependence presented in paper III. When so interpreted, these data are consistent with the other results obtained for nickel.)[1–3]

It thus seems appropriate to add a note of caution about the interpretation of data from which the existence of transport rate maxima has been inferred. On perusal of the graphs illustrating this effect,[6–8] one is immediately struck by the comparatively small number of experimental points which serve to justify the curvature ascribed to the rate-temperature characteristics. This is also true in Fig. 2, where run 5 ended before more data could be secured at the lower temperatures. Furthermore, on some occasions, it appears from plotting experimental values in chronological order in the present experiments that, had some runs ended earlier, a somewhat distorted view of the final rate-temperature characteristic would have been obtained. Consequently, it would appear that only repeated and painstaking traversals of the entire range of accessible temperatures may be used to gauge the true scatter of the data with sufficient accuracy to establish the shape of a particular curve.

In view of these considerations, it will henceforth be assumed that the occurrence of maxima in R *vs* T curves is not a fundamental property of the transport.

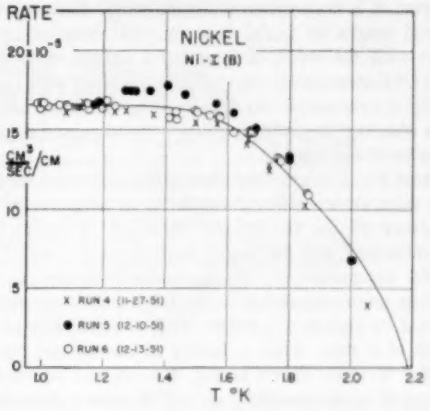

FIG. 2. Transport rates over nickel specimen Ni-(B) (see papers I and II for beaker identification), averaged over region between 0.5 cm and 3.5 cm from the rim. Interest in these results centers in the variation of curve shape from run to run, although the specimen remained in the cryostat and was merely outgassed between runs. The magnitudes may be compared with data obtained in other experiments only if the previous discussion of height dependence (reference 3) is used to interpret the results; such a comparison indicates that these data are consistent with the results obtained for this and other specimens on other occasions (see papers I–III).

Mendelssohn and White[6] observed that their data on glass, platinum and nickel, when normalized at 1.4°K, were fairly well represented by an expression of the form

$$[1-(T/T_\lambda)^\sigma], \tag{1}$$

with σ equal to 6, except for the lowest rates obtained with an unbaked glass specimen for which $\sigma=8$ seemed preferable. They noted that in spite of the variation in absolute value by up to a factor of approximately 3, the shape of the transfer curves was almost identical. The present data, when averaged over all heights, materials and finishes, follow expression (1) with $\sigma=7$, very closely throughout the entire temperature range under investigation. The extent to which this is really characteristic of all the data is revealed by the separate analysis of the data for glasses and metals (Fig. 1), as well as by the size of the absolute deviations from the mean listed in Table I.

Since it has been suggested that the analogy between superfluidity in helium and superconductivity proposed by Daunt and Mendelssohn[4] implies that "the ratio of the density of the normal constituent to the total density can be evaluated from the curves for the rate of volume flow,"[12] values of the ratio of superfluid to total density (ρ_s/ρ), are included for comparison in Fig. 1. (These have also been normalized to unity at 1.1°K.) Although expression (1), with a value of about 5.5 for σ, is a convenient first approximation[5,9] to the concentration of superfluid atoms in the temperature range of

[13] Dyba, Lane, and Blakewood, Phys. Rev. **95**, 1365 (1954).
[14] H. A. Fairbank and C. T. Lane, Phys. Rev. **76**, 1209 (1949).

interest, it is known that a careful study of the experimental results for (ρ_s/ρ) does not yield detailed agreement with the result of inserting a unique value of σ in (1).[12] Consequently, the points associated with (ρ_s/ρ) in Fig. 1 were calculated directly from the experimental data obtained in oscillating disk[15,16] and second sound[17] experiments above 1°K.

From Fig. 1 it is evident that although the normalized flow rates show a definite similarity in temperature dependence to the normalized variation of (ρ_s/ρ), the resemblance[18] may be largely superficial in view of the forced agreement of the normalized curves at the lambda point and at 1.1°K. In judging such agreement it must be kept in mind that (1) is so insensitive to the value of σ that, when a family of normalized curves similar to those shown in Fig. 1 is plotted for various values of σ, comparison, at 1.75°K where differences appear most pronounced, shows that the result for $\sigma=6$ differs from those for $\sigma=4$ and $\sigma=8$ by only 20 percent and 12 percent, respectively.

Since the experimental values of (ρ_s/ρ) are regarded as well established, the significance to be attached to the seventh-power dependence of the average flow rates is not clear. The expectation that the transport rate should reflect the variation of (ρ_s/ρ) in a detailed rather than a superficial manner is not sufficiently rooted in an explicit theory for the consequences of the apparent contradiction to be discussed.[12] Preliminary studies[19,20] have indicated that valuable information may be forthcoming from extension of the measurements to very low temperatures.

Dash[9] has recently proposed a model which includes the possibility that the flow rates should vary as the square root of (ρ_s/ρ). Typical normalized values of this quantity, based on the experimental data for (ρ_s/ρ), are also shown in Fig. 1. This function appears to rise too steeply from the lambda point to be consistent with the present data.

ACKNOWLEDGMENTS

The authors wish to express their appreciation to Arnold Berman, Albert Brown, Raymond Kaplan, Leonard Lesensky, Robert D. Worley, and Professor Adam H. Spees for valuable assistance during the course of the numerous measurements upon which the present analysis was based; to Mr. G. T. Poirier and Mr. P. DePalma and their associates in the Department of Production Research of the Chrysler Corporation for their splendid cooperation in superfinishing various specimens; and to Professor Mark W. Zemansky for his active and stimulating interest in these experiments.

[15] E. L. Andronikashvili, J. Exptl. Theoret. Phys. (U.S.S.R.) (a) **18**, 424 (1948); (b) **18**, 429 (1948).
[16] A. C. Hollis-Hallett, Proc. Roy. Soc. (London) **A210**, 404 (1952).
[17] deKlerk, Hudson, and Pellam, Phys. Rev. **93**, 28 (1954).
[18] In this connection, the recent investigation, by R. T. Swim and H. E. Rorschach [Phys. Rev. **97**, 29 (1955)], of the isothermal, pressure-induced volume flow rates through narrow glass slits, is also of interest. From their data between 1.4°K and the lambda point, normalized to equal (ρ_s/ρ) at 1.81°K, they conclude that "the temperature dependence of the flow is essentially the same as that of the superfluid concentration."
[19] E. Ambler and N. Kurti, Phil. Mag. **43**, 260 (1952).
[20] L. Lesensky and H. A. Boorse, Phys. Rev. **87**, 1135 (1952).

Radiation Flux Field Outside of Stars and Spherical Reactors

M. A. MELVIN
Department of Physics, Florida State University, Tallahassee, Florida
(Received December 23, 1954; revised manuscript received March 23, 1955)

The energy density U, flux density F, and pressure P in the field of a hot spherical system, are here investigated along with their neutron-flux analogs. General expressions for U, F, and P are obtained and evaluated in particular (1) outside of spherical bodies radiating according to Lambert's law of isotropic radiance, I=constant, and (2) outside of stars or spherical reactors. Radiative (or transport) balance within a star (or reactor) leads to an angularly dependent radiance, $I(\cos\theta)$, from the outer surface. Assuming I to be given up to quadratic terms in $\cos\theta$, analytic expressions for U and P are obtained. It is further shown how one may use known exact numerical values for the radiance and its derivatives, at $\cos\theta=0$ and 1, to give still better analytic representations. For many purposes where one wishes to carry out calculations involving U or P, it is convenient to have simple analytic approximations for these quantities; such approximations, are here given in the form of simple Lambert-law expressions multiplied by suitable factors.

1. DENSITY, FLUX, AND PRESSURE IN THE FIELD OUTSIDE AN EMITTING SPHERE

THE problem of neutron transport through a spherical shell of scattering material is the same mathematically as that of radiative transfer through the photosphere of a star.[1] The corresponding plane-parallel problem has been discussed extensively in the literature. In the plane-parallel case, the problem of the field outside the photosphere is of course solved once the emergent angular distribution of intensity is known. For the spherically symmetric case there remains the subsidiary problem of determining the way in which the flux field falls off with distance, and it is with this problem in its general setting that we are here concerned. A point-source approximation is valid only at large distances and may lead to significant errors if applied locally.

The transfer problem in astrophysics is older than the neutron transport problem, and there exists a considerable literature on it. It is therefore perhaps advisable to use the astrophysical terminology, or the necessary generalizations thereof to the spherical case. Suppose that we are given a general flux of radiation in matter-free space. We consider a field point P, and wish to know the radiation energy contained in a unit volume located there. For simplicity of imaging, and for use in the subsequent discussion, we take as a test volume at P a little sphere of unit projected area; i.e., the radius is $1/\sqrt{\pi}$ and the volume is $4/3\sqrt{\pi}$. Let us call this the test sphere. Clearly, if the amount of energy flowing through the test sphere per second in any single direction is $\mathcal{S}$, the amount contained in it at any moment is $4\mathcal{S}/3c\sqrt{\pi}$. Thus the *energy density* of the singly directed radiation is simply $\mathcal{S}/c$. To find the total energy density at P, $U(\mathrm{P})$, we must integrate $\mathcal{S}/c$ over all directions.

In practice one usually has to deal not with singly directed but rather with angularly distributed streams of radiation. Thus, as a basic photometric quantity, we adopt the standard definition of the *intensity* I in a a given direction at any point: I is the directed energy-current density at the point. More explicitly, consider a unit test area normal to the given direction; construct on it, and about the given direction as axis, the truncated cone flaring out with a unit solid angle. Then I is defined as the amount of energy, with directions within the unit truncated cone, which enters the unit normal test area per unit time (erg cm^{-2} sec^{-1} sterad^{-1}).

So far we have been considering the intensity anywhere in space. Now, given a steadily radiating spherical body of radius R with center at S (Fig. 1), take any surface element on the body $d\sigma$ at a point Q. Let θ be the angle between the normal to $d\sigma$ and the line in the test direction. The angular distribution of intensity I, outwardly directed, in the field just in front of $d\sigma$ is called the "radiance" of the surface at that point.[2] In general it is some function of θ, but if Lambert's law holds it is constant. For convenience in the later analysis we write it rather as some function of $\cos\theta$, $I(\cos\theta)$. The amount of radiation emitted from $d\sigma$, which

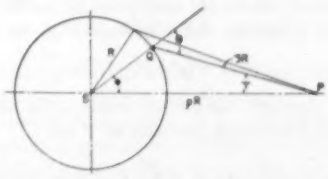

FIG. 1. Geometrical relations governing the field at an outside point P due to a flux from Q. The angle θ is measured from QP to the outward-directed normal at Q.

[1] This is true provided one makes the assumption that the photosphere is "grey", i.e. that the absorption coefficient is the same for all frequencies; the corresponding assumption in the neutron case is that the neutrons are scattered without change in their velocity. The astrophysical-diffusional correspondences are discussed by V. Kourganoff in *Basic Methods in Transfer Problems* (Oxford University Press, London, 1952), pp. 19, 21, 37–39. We indicate below how one may translate from astrophysical terms to neutron transport terms.

[2] This is the term used in the astrophysical literature. See M. Minnaert, *The Sun*, edited by G. P. Kuiper (University of Chicago, Chicago, 1953), p. 88. In the general physical literature Lambert's law is often assumed to start with, and I is then expressed in terms of the concept of "photometric brightness" or "luminance."

will just intercept the test sphere at P, is then

$$dF = I(\cos\theta)d\sigma\cos\theta, \quad \Delta\omega = I(\cos\theta)\cos(1/z^2)d\sigma, \quad (1)$$

where $\Delta\omega$ is the element of solid angle subtended by the unit projected area of the test sphere at the distance z from Q.

Introducing the dimensionless measures of distance,

$$\rho \equiv r/R, \quad \zeta \equiv z/R,$$

and the abbreviation

$$\mu \equiv \cos\theta = (\rho^2 - 1 - \zeta^2)/2\zeta$$

[therefore $\zeta = \sqrt{(\mu^2+\rho^2-1)} - \mu$], the flux contribution from an elementary ring around SP as axis may be shown to take the form

$$\frac{2\pi}{\rho} I(\mu) \frac{\mu}{(\mu^2+\rho^2-1)^{\frac{1}{2}}} d\mu, \quad (1')$$

where we have made use of the relation

$$d\zeta/\zeta = -d\mu/(\mu^2+\rho^2-1)^{\frac{1}{2}}.$$

There are three quantities in which one would be interested in an astrophysical or spherical reactor problem. First there is the total *energy density* U at P, which is $1/c$ times the integrated flux from all the contributing surface elements on the radiating sphere. The corresponding quantity for a spherical reactor is the *neutron flux* density, commonly denoted Φ; in a parallel stream it is equal to the volume density of neutrons times their velocity. The two other quantities which are of interest are the normal *radiation-flux density* F (corresponding to the *neutron-current density*, commonly denoted J) and the *radiation pressure* P at any point in the field. Consider the energy flux through a unit area at P normal to PS. Clearly the elementary contribution to this flux from an element of surface at Q will differ from (1) only by the factor $\cos\Psi$, where Ψ is the angle between PS and PQ. The integral over the total contributing area gives the normal flux density at P.

Correspondingly, assuming the unit area to be perfectly absorbing, the contribution to the normal pressure on it will be (1) multiplied by $\cos^2\Psi$. With the help of the geometry of the triangle PQS, we find:

$$\cos\Psi = (\mu^2+\rho^2-1)^{\frac{1}{2}}/\rho. \quad (2')$$

Thus, all together, the energy density, the normal flux density, and radiation pressure at P are

$$U = (\pi/c)u(\rho), \quad u(\rho) = 2\rho^{-1}\int_0^1 d\mu I\mu/(\rho^2-1+\mu^2)^{\frac{1}{2}}, \quad (3)$$

$$F = \pi f/\rho^2, \qquad f = 2\int_0^1 d\mu I\mu, \quad (4)$$

$$P = (\pi/c)p(\rho), \quad p(\rho) = 2\rho^{-3}\int_0^1 d\mu I\mu(\rho^2-1+\mu^2)^{\frac{1}{2}}. \quad (5)$$

We see that, unlike U and P, F continues to be given by an expression of the same form as in the case of a point source. The quantity πf is the net flux of radiation per unit area per second from the sphere, and f is the *mean intensity over the apparent disk* of the sphere, as viewed from an infinitely distant point ($\theta = \phi$):

$$f = \int I\mu d\sigma \Big/ \int \mu d\sigma = 2\int_0^1 I\mu d\mu.$$

Further, it will be noticed that between the first and third integrals there is a simple relation which allows one to check any independent evaluation of the two:

$$u = 3p + \rho dp/d\rho. \quad (6)$$

The first term on the right reminds one of the relation which holds for isotropic radiation in an enclosure, $U = 3P$.

From the form of the integrals (3) and (5) it is easy to establish that, whatever be the law of radiance at the surface of a spherical radiator, the following inequalities hold between its field and that of the equivalent point source located at the center of the sphere and emitting the same total flux: *For any spherical radiator the radiation density is greater and the pressure is less than for the equivalent point source.* Equality with the point source field is approached as the distance from the sphere goes to infinity; and the familiar relations $U = P = F/c$ then hold.

For $\rho = 1$, the three integrals (3), (4), and (5) go over smoothly into familiar astrophysical (neutron-transport) integrals,[1] which apply in the interior of the steliar atmosphere (neutron scattering shell). These are listed in Table I. Up to this point, I was the surface radiance. Within the atmosphere, I becomes the local intensity, $I(\tau,\mu)$ where τ measures the depth below the surface; the change in the lower limit of the integrals for the interior case is connected with the fact that the radiation now comes from all directions and is not limited to the angular region $0 \leqslant \mu \leqslant 1$. At the surface there is no inward flow of radiation, i.e.,

$$[I(\mu)]_{\text{surface}} = 0 \quad \text{for} \quad \mu \leqslant 0,$$

and the corresponding integrals join smoothly. In Table I we have also attempted to clarify the correspondences between the various confusing notations and terminologies used in the astrophysical and neutron-transport literature.

In the neutron-transport case, Placzek and Seidel[2] use z for depth and consider the inward direction as positive. For the density of neutrons having direction cosines between μ and $\mu+d\mu$, they introduce the function

$$\psi(z, -\mu) \sim 2I(\tau,\mu)/f(0),$$

which corresponds, as we have indicated, to the astrophysical I. One sees that ψ represents the neutron dis-

[2] G. Placzek and W. Seidel, Phys. Rev. **72**, 550 (1947).

TABLE I. Classification and interpretation of the radiation density, flux, and pressure integrals, u, f, and p, which occur in the problem of radiative transfer through a photosphere (or neutron transport through a scattering shell). In the tier labeled "Significance" are given first the physical interpretations or relations which u, f, and p satisfy under general conditions (i.e., inside or outside the radiating sphere). Then the special relations which apply when the integrals are evaluated at the surface of the photosphere are given. In the tier labeled "Interior continuation" are listed three familiar transfer theory integrals which may be regarded as the continuation into the photosphere of our outside u, f, and p integrals. In the remaining tiers, an attempt is made to correlate the various notations and terminologies used for these integrals in the astrophysical and neutron-transport literature.

Suggested name and symbol:	Radiation-density quantity u Neutron-flux quantity	Radiation-flux quantity f Neutron-current quantity j	Pressure quantity p
Significance:	*General:* Uc/π: energy density$\times c/\pi$ $4\bar{I}$: $4\times$average intensity	*General:* F/π: normal flux density$/\pi$ *Evaluated at surface:* mean intensity over disk as viewed from infinity intensity of equivalent Lambert radiator	*General:* Pc/π: radiation pressure$\times c/\pi$
Interior continuation:	$u \to u(\tau)=2\int_{-1}^{1} I(\tau,\mu)d\mu$	$f \to f(\tau)=2\int_{-1}^{1} I(\tau,\mu)\mu d\mu$	$p \to p(\tau)=2\int_{-1}^{1} I(\tau,\mu)\mu^2 d\mu$
Symbols for the interior continuation used by: Woolley and Stibbs[a]	$4J$: $4\times$"average flow of radiation" (p. 4)	$\mathfrak{F}=4H$: "mean intensity over disk" (p. 6)	$4K$
Kourganoff[b]	$4\bar{I}$: $4\times$"mean intensity" (p. 12) (Schwarzschild)	$\mathfrak{F}$: "integrated flux" (p. 16)	$4\mathfrak{N}$
Chandrasekhar[c]	$4J$: $4\times$"average intensity" (p. 4)	F: "net flux$/\pi$" (p. 2)	$4K$
Placzek and Seidel[d] (plane case)	$u(\tau)/f(0)\sim\psi_0(z)$ "neutron density" (normalized to unit current density)	$f(\tau)/f(0)\sim j(z)$ "current density"	

[a] Woolley and Stibbs, *The Outer Layers of a Star* (Clarendon Press, Oxford, 1953).
[b] V. Kourganoff, *Basic Methods in Transfer Problems* (Clarendon Press, Oxford, 1952).
[c] S. Chandrasekhar, *Radiative Transfer* (Clarendon Press, Oxford, 1950).
[d] G. Placzek and W. Seidel, Phys. Rev. **72**, 550 (1947).

tribution normalized so that the *current density* j is equal to unity.

$$j=-\int_{-1}^{1}\mu\psi(z,\mu)d\mu=1.$$

That the integral is always equal to 1 follows from its being the expression for $f(\tau)/f(0)$ in our notation; by reason of the conservation of energy, f in the interior, just as in the exterior, is always a constant, for a system in a steady state. This is true not only in the plane case considered by Placzek and Seidel but also in the spherical case considered here. This conclusion can, of course, also be established formally from the transport equation for the spherically symmetric case. We omit the formal argument here since the transport phenomena within the sphere are not our immediate problem.

We note that, in a second paper[4] on the angular distribution of neutrons emerging from a plane surface, Placzek uses a distribution (intensity) function $\varphi(\mu)$ normalized to unit density rather than to unit current. The relation to his earlier notation and to ours is

$$\varphi(\mu)=\psi(0,-\mu)/\sqrt{3}=2I(\mu)/\sqrt{3}f(0).$$

In his paper Placzek gives a detailed numerical evaluation of $\varphi(\mu)$ from an exact Wiener-Hopf solution of the radiative balance (transport) problem. We shall later indicate how this exact numerical solution for the radiance in the plane case may be used to advantage in getting a good approximate representation of U and P in the corresponding spherical case.

[4] G. Placzek, Phys. Rev. **72**, 556 (1947).

2. CASE OF LAMBERT'S LAW. CASE OF RADIATIVE TRANSFER IN THE QUADRATIC APPROXIMATION

If Lambert's law of emission is obeyed, as is true exactly for a black body[5] and approximately for many surfaces, we have

$$I(\mu)=I=\text{constant},$$

and we find

$$u=2I[1-(1-1/\rho^2)^{\frac{1}{2}}]=I\left[\frac{1}{\rho^2}+\frac{1}{4\rho^4}+\frac{1\cdot3}{4\cdot6\rho^6}+\cdots\right], \quad (7)$$

$$f=I, \quad (8)$$

$$p=\frac{2I}{3}[1-(1-1/\rho^2)^{\frac{1}{2}}]$$
$$=I\left[\frac{1}{\rho^2}-\frac{1}{4}\left(\frac{1}{\rho^4}+\frac{1}{6\rho^6}+\frac{1\cdot3}{6\cdot8\rho^8}\right)+\cdots\right]. \quad (9)$$

By comparing Eq. (4) with (8), we see that f in the general case (i.e., with any law of radiance) has another simple physical significance. It is the intensity with which a spherical surface would have to radiate according to Lambert's law in order to send out the same flux as the given surface. The actual dependence of U and P upon ρ, in the Lambert case, is plotted in Figs. 2 and 3. At or near the surface of the radiating body ($\rho=1$) the radiation density is numerically three times as great as the pressure, just as in the case of isotropic radiation. In absolute magnitude $U(1)$ is twice, while $P(1)$ is

[5] See M. A. Melvin, Am. J. Phys. (to be published).

TABLE II. Functions which occur in the calculation of the normalized energy density $u(\rho)$ and radiation pressure $p(\rho)$ in the field of a spherical radiator. The functions u_L and p_L are the energy density and pressure which would obtain if the surface were to radiate according to Lambert's law. u_β, p_β, and u_γ, p_γ result from first and second powers of $\mu=\cos\theta$, respectively, appearing in the formula for the radiance I.

1 ρ	2 u_L	3 u_β	4 u_γ	5 p_L	6 p_β	7 p_γ
1.00	2.000	1.000	0.667	0.667	0.500	0.400
1.05	1.380	0.819	0.572	0.648	0.472	0.373
1.10	1.167	0.709	0.503	0.618	0.444	0.348
1.20	0.895	0.560	0.404	0.554	0.390	0.302
1.30	0.722	0.459	0.335	0.493	0.332	0.264
1.40	0.600	0.386	0.282	0.438	0.302	0.232
1.60	0.439	0.285	0.210	0.350	0.239	0.182
1.80	0.337	0.220	0.164	0.283	0.192	0.146
2.00	0.268	0.176	0.133	0.233	0.158	0.120
3.00	0.155	0.076	0.056	0.108	0.062	0.055
5.00	0.040	0.027	0.017	0.040	0.026	0.020
10.00	0.010	0.007	0.005	0.010	0.007	0.005

only two-thirds of the value which one will find for a point source with the same total flux, located at S.

We turn now to the astrophysical situation. We consider the outer layers of a star, i.e., the absorbing photosphere region, from which comes the bulk of the visible and thermal radiation. The limb-darkening effect observed in the light from the solar disk, and other data, confirm the theory that radiative balance approximately governs the physical conditions in these layers. The basic problem in the theory of radiative balance is that of determining the intensity at any point in this photosphere. This intensity is a function of μ and of the depth. If one has a solution for the intensity distribution with depth, one also has the desired emergent intensity. In this way a second approximation in the theory of radiative balance leads to the following formula for the intensity emitted from the boundary, or the radiance:

$$I(\mu)=f(1+\beta\mu+\gamma\mu^2)/(1+2\beta/3+\gamma/2), \qquad (10)$$

where β and γ are constants and the expression has

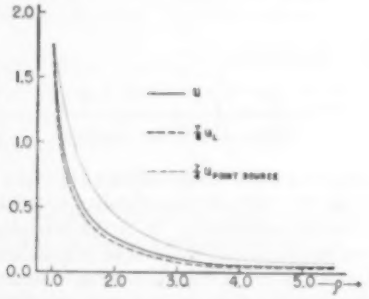

FIG. 2. The energy density u as a function of the distance ρ from the center of a sphere whose surface is radiating according to a linear law of radiance $I=f(1+\frac{3}{2}\cos\theta)/2$. The distance is expressed in units of the sphere radius, and the energy density is normalized to unit flux quantity f. (f is the mean intensity over the apparent disk of the sphere as viewed from an infinite distance.) For comparison, the expressions for u obtained with Lambert's law of radiance ($I=$constant), and for a point source are also given. Each of these has been normalized to agree with u at $\rho=1$.

been normalized so that f continues to represent the mean intensity over the apparent disk of the sphere, as follows from Eq. (4). The empirical data on the limb-darkening in the sun verify the general form of (10) with fair approximation, but give varying parameters β, γ for different wavelengths. A detailed analysis is given by Chalonge and Kourganoff.[6] For a first approximation to the integrated radiance, one may set $\gamma=0$ and take the Milne-Eddington value, $\beta=\frac{3}{2}$, or the Fermi value,[7] $\beta=\sqrt{3}$.

Let the Lambert-law values for u and p, both taken per unit I (or f) be represented by u_L and p_L. Then, upon substituting (10) into (3), and (5), we find

$$u(\rho)=f[u_L+\beta u_\beta+\gamma u_\gamma]/[1+\tfrac{2}{3}\beta+\tfrac{1}{2}\gamma], \qquad (11)$$

$$p(\rho)=f[p_L+\beta p_\beta+\gamma p_\gamma]/[1+\tfrac{2}{3}\beta+\tfrac{1}{2}\gamma], \qquad (12)$$

where we have introduced abbreviations for the extra

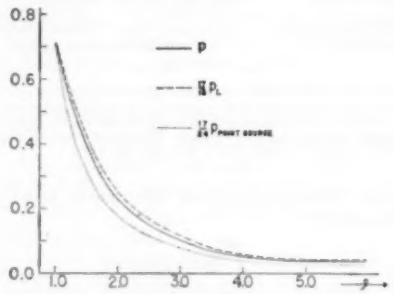

FIG. 3. The radiation pressure p as a function of the distance ρ from the center of a sphere whose surface is radiating according to the linear law of radiance $I=f(1+\frac{3}{2}\cos\theta)/2$. The normalization is again to unit flux quantity f. For comparison, the expressions for p obtained with Lambert's law of radiance, and for a point source, are given. These have been normalized to agree with p at $\rho=1$.

non-Lambertian terms:

$$u_\beta(\rho)=[1-(\rho-1/\rho)\coth^{-1}\rho]$$

$$=2\sum_{n=1}^{\infty}1/(4n^2-1)\rho^{2n}, \qquad (11')$$

$$u_\gamma(\rho)=2[1-\tfrac{3}{5}\rho^2+\tfrac{3}{5}\rho^2(1-1/\rho^2)^{\frac{5}{2}}]\to 1/2\rho^2+\cdots, \qquad (11'')$$

$$p_\beta(\rho)=\tfrac{1}{4}[1+1/\rho^2-\rho(1-1/\rho^2)^2\coth^{-1}\rho]$$

$$=-2\sum_{n=1}^{\infty}1/(4n^2-1)(2n-3)\rho^{2n}, \qquad (12')$$

$$p_\gamma(\rho)=(4/15)\rho^2[-1+5/2\rho^2+(1-1/\rho^2)^{5/2}]\to$$
$$1/2\rho^2+\cdots. \qquad (12'')$$

Confining ourselves to the linear approximation ($\gamma=0$), a detailed analysis leads to upper and lower bounds for both u and p throughout their range. We find for

[6] D. Chalonge and V. Kourganoff, Ann. astrophys. **9**, 69 (1946).
[7] E. Fermi, Ricerca sci. **7**, [2] 13 (1936).

TABLE III. Functions involved in calculating the energy density in terms of the numerical values for I, $dI/d\mu$, and $d^2I/d\mu^2$ at $\mu=0$ and $\mu=1$, when these are known.

ρ	$u_0'=(\rho-1/\rho)\ln(\rho^2-1)^{\frac{1}{2}}$	$-u_1'=1+(\rho-1/\rho)\ln(\rho+1)$	$u_0''=\frac{1}{2}\rho^2(1-1/\rho^2)^{\frac{1}{2}}$	$u_1''=1-2\rho^2/3+(\rho-1/\rho)\ln(\rho+1)$
1.00	0.0000	1.0000	0.0000	0.3333
1.05	−0.111	1.0701	0.0209	0.3351
1.10	−0.1489	1.1416	0.0583	0.3349
1.20	−0.1505	1.2891	0.1621	0.3291
1.30	−0.0985	1.4421	0.2944	0.3154
1.40	−0.0140	1.6003	0.4475	0.2936
1.60	+0.2167	1.9316	0.8115	0.2249
1.80	0.5019	2.2812	1.2418	0.1212
2.00	0.8240	2.6479	1.7334	−0.0198
3.00	2.7725	4.6968	5.0280	−1.3032
5.00	7.6272	9.6006	15.6750	−8.0661
10.00	22.7462	24.7392	65.6667	−41.9275
20.00	59.7403	61.7378	265.6800	−204.9289

example

$$\frac{1+\beta/2}{1+\frac{2}{3}\beta}u_L \leqslant u \leqslant u_L.$$

The upper bound function is independent of the value of β. The lower bound depends on β, and takes the value $(7/8)u_L=0.875u_L$, for $\beta=\frac{2}{3}$. (For Fermi's value, $\beta=\sqrt{3}$, the lower bound is $0.866u_L$.) Summing up we may say: *Under the law of radiance (10) with $\beta=\frac{2}{3}$ and $\gamma=0$, u increases from $(7/8)u_L$ to u_L as ρ goes from 1 to ∞. On the other hand, p decreases from $(17/16)p_L$ to p_L as ρ goes from 1 to ∞.*

These results suggest that we may get a fair approximation to the rigorous u in the important neighborhood near the source by using 7/8 times the Lambert-law value. The comparison of $(7/8)u_L$ with u is exhibited graphically in Fig. 2. We have made use of this approximate representation recently in analyzing the reinterpretation by Freundlich of the stellar and galactic redshifts.[8] The corresponding approximate representation, for p in terms of $(17/16)p_L$ is given in Fig. 3. The various functions of ρ occurring in (11) and (12) are tabulated in Table II.

3. USE OF EXACT NUMERICAL RADIANCES TO IMPROVE THE ANALYTIC APPROXIMATION

Examination of the exact solution from transport theory for I in the plane parallel case[9] shows that it follows a straight-line variation with μ only imperfectly; a quadratic fit is naturally better. In Sec. II, assuming the quadratic radiance law (10), we obtained analytic expressions for u and p. We may get even more realistic, though still analytic, expressions by following an integration-by-parts procedure up to the second derivative of I with respect to μ; this derivative is small over the range of μ, as an examination of second differences in the table of the exact solution of the plane parallel case[4] shows, and higher derivatives may be expected to be still smaller. Integrating Eq. (3) by parts three times, and dropping the remaining integral which involves $d^3I/d\mu^3$, we find

$$u=2[I_1-(1-1/\rho^2)^{\frac{1}{2}}I_0]+(u_1'I_1'+u_0'I_0')+(u_1''I_1''+u_0''I_0''), \quad (13)$$

where the functions u_0', u_1', u_0'', u_1'' are given in Table III. Similar approximate expressions in terms of initial and final values for I and its derivatives may be obtained for p, but we shall not present them here.

If one assumes that the third derivative of I is rigorously zero, then one may set

$$I_1''=I_0''=I'',$$
$$I_1'=I_0'+I'', \quad I_1=I_0+I_0'+\tfrac{1}{2}I'',$$

and the expression (13) goes over into the form (11) obtained in Sec. II. Greater fidelity to the exact solution can be obtained by substituting for I and its derivatives values obtained from the exact solution for the radiance[4] in the plane-parallel case. These values are (ignoring I''):

$$I_0/f=\sqrt{3}/4=0.4330 \quad (0.5), \quad I_1/f=1.2591 \quad (1.25),$$
$$I_0'/f=1.4835 \quad (0.75), \quad I_1'/f=0.766 \quad (0.75).$$

In parentheses we have indicated the corresponding values on the linear approximation with $\beta=\frac{2}{3}$. It will be noted that the biggest error results from the use of the linear value for I_0'.

In concluding, the author wishes to express his appreciation to Dr. A. E. S. Green and Dr. Conway Snyder for reading and commenting on this paper, and to Mr. John Burgeson for his help in the computations and illustrations.

[8] M. A. Melvin, Phys. Rev. **98**, 884 (1955).

[9] A graph and a numerical table (following Placzek) of this solution are given on pages 100 and 187 respectively of Kourganoff's book.

Physical Theory of Semiconductor Surfaces

C. G. B. Garrett and W. H. Brattain
Bell Telephone Laboratories, Inc., Murray Hill, New Jersey
(Received December 20, 1954)

The properties associated with the space-charge region and with surface states at a semiconductor surface are discussed. A theory of the space-charge region that takes into account charge-densities arising from immobile impurities and from both signs of mobile carrier is presented. The properties of the space-charge are discussed in terms of the surface potential and of the electrochemical potentials of holes and electrons, and related to the transport of added carriers in a homogeneous semiconductor. The change in surface conductivity arising from nonvanishing surface excesses of holes and electrons is treated. The space-charge systems at a free surface and at a p-n junction are compared, and the range of validity of the Mott-Schottky space-charge theory evaluated. The arrangement of surface states is discussed with reference to the Brattain-Bardeen model. Theories for the surface photoeffect and field-effect experiments are given, with and without surface states: it is concluded that the existence of surface states is without gross effect on the former, while relevant quantitative evidence from the latter is not yet available. The question of the relation between surface potential and contact potential is discussed. The properties of "channels" are discussed in terms of the theory. The paper concludes with a short section on long-time effects.

INTRODUCTION

THE purpose of this paper is to summarize the conclusions which may be drawn from physical theory as to the electrical properties of the surface of a semiconductor. The surface of a semiconductor, like most phase boundaries, is the seat of a space-charge double layer. In many one-dimensional problems, it suffices to consider the case that the field outside the semiconductor is zero: this means that the net surface charge density is also zero. The double-layer may in principle arise in several ways, such as preferential adsorption of ions of one sign, or alignment of adsorbed atoms or molecules having an electrical dipole moment. In a metal, such charge can be compensated by a high density of electrons or holes in the immediate vicinity, i.e., within a few atomic diameters, of the geometrical surface. In a semiconductor, part at least of the electron or hole distribution must be spread over a relatively wide space-charge region, owing to the combined requirements of electrostatics and statistical mechanics. At the same time, there may still be an extra population of holes and electrons bound in the near vicinity of the surface, since one must not expect bulk statistical considerations to hold over atomic distances. The concept of "surface states" was proposed some years ago by Tamm,[1] and discussed in detail by Bardeen.[2] It should, however, be noticed that the distinction between charges consisting of electrons and holes in surface states, and charges deriving from impurity atoms adsorbed onto the surface, is far from clear. Specifically, the lack of dependence on work function of the rectifying properties of metal semiconductor contacts might be due to Tamm-type surface states, or to charges associated with adsorbed gases: one does not know. One may distinguish, a little artificially perhaps, between these two kinds of surface charge as follows. That part of the surface charge which, while not forming part of the extended space-charge region, is yet in good electrical contact with the conduction or valence band, will be described as charge in surface states; that part which can only change relatively slowly, with some sort of "activation energy," is thought of as associated with adsorbed ions. How far this distinction can be maintained operationally must be left for experiment to decide. Another convenient assumption is that the surface states are associated with recombination processes at the surface; that is, the surface states are trapping centers of the type discussed by Shockley and Read.[3]

In Sec. A of this paper, we shall be concerned only with the properties of the space-charge region itself. The problem is to write down expressions for the surface excesses Γ_n and Γ_p of electrons and holes, as functions of the *surface potential* (the difference between the mean electrostatic potential just inside the surface and in the interior) and the electrochemical potentials for holes and electrons. From this one can write down (*i*) the net surface charge density due to the space-charge region, (*ii*) the shape of the space-charge region, i.e., the dependence of potential on distance, and (*iii*) (with some reservations) the excess conductivity due to mobile carriers near the surface.

In Sec. B, an attempt will be made to use the theoretical concepts to describe the results of experiments which have been or can be made on semiconductor surfaces. In the understanding of many of these measurements, it is unfortunately necessary to make some assumption about the surface states. On the basis of surface recombination measurements made on germanium surfaces prepared in a certain way, Brattain and Bardeen[4] proposed a particular model, in which the surface states are supposed to be either of donor character, lying high in the forbidden band, or of

[1] I. Tamm, Physik Z. Sowjetunion **1**, 733 (1932).
[2] J. Bardeen, Phys. Rev. **71**, 717 (1947).
[3] W. Shockley and W. T. Read, Phys. Rev. **87**, 835 (1952).
[4] W. H. Brattain and J. Bardeen, Bell System Tech. J. **32**, 1 (1953).

acceptor type lying low. In this paper we shall predict the results of various experiments on two extreme assumptions: (*i*) that there are negligibly few surface states, and (*ii*) that there are surface states of the type proposed by Brattain and Bardeen.

The problem of the apportionment of charge between space-charge and surface states has also been considered by Pikus,[5] who has discussed such questions as the variation of work function with temperature and the effect of applying an electric field normal to the surface. For a detailed discussion of the properties of Tamm states, as opposed to the questions of ionic charge discussed by Brattain and Bardeen, we refer the reader to this paper.

A. PROPERTIES OF THE SPACE-CHARGE REGION

1. Fundamental Considerations

The theory of the space-charge region at the surface of a semiconductor has been given by Schottky,[6] Schottky and Spenke,[7] and Mott.[8] For convenience we shall develop here the considerations applicable to rather high-resistivity germanium or silicon, at or near room temperature. It will be assumed that impurity atoms (donors and acceptors) are completely ionized at all points. The space charge then may be written down in terms of the local concentrations p and n of holes and electrons, which may be taken to obey Boltzmann statistics, so long as the impurity concentration in the semiconductor is low enough to make the Fermi-Dirac assembly nondegenerate. The considerations to be given are applicable either to a step (abrupt) junction within a single crystal between regions of differing impurity content, or to a free surface.

Following Shockley[9] we wri e

$$p=n_i e^{\beta(\varphi_p-\psi)}, \qquad n=n_i e^{\beta(\psi-\varphi_n)}, \tag{1}$$

where φ_p and φ_n are the "quasi-Fermi levels"[9] for holes and electrons respectively; ψ is the electrostatic potential, n_i the density of holes and of electrons in intrinsic semiconductor, and $\beta=e/kT$, e being the electronic charge, k Boltzmann's constant, and T the absolute temperature. The quasi-Fermi levels have, apart from a change in sign of φ_n, the properties of electrochemical potentials. The zeros of φ_p and φ_n have been chosen in such a way that, in thermodynamic equilibrium, $\varphi_p=\varphi_n$: we shall denote this common value by φ_0. Now in equilibrium φ_0 is uniform throughout the system; in particular, it is constant right up to the surfaces of the sample. In the body of the semiconductor the electrostatic potential ψ is also uniform, but this ceases to be true in the vicinity of the surface.

In order to determine the form of the electrostatic potential near the surface, one must solve Poisson's equation:

$$\nabla^2\psi=-4\pi\rho/\epsilon\epsilon_0. \tag{2}$$

(Unrationalized quantities are used in writing this equation.) Here ϵ is the dielectric constant for the semiconductor, and ρ is the charge density at each point, which, for a completely ionized semiconductor, is given by

$$\rho=e[(p-p_0)-(n-n_0)], \tag{3}$$

where p_0 and n_0 are the hole and electron concentrations in the body of the semiconductor. With some reservations, to be discussed below, the charge distribution near the surface is completely determined (in the case of thermodynamic equilibrium) by substituting Eqs. (1) and (3) into Eq. (2), and solving with the appropriate boundary conditions.

Before following this procedure, one generalization is required. In dealing with semiconductor problems, it is often important to consider steady-state distributions which, although not corresponding to strict thermodynamic equilibrium, are sufficiently close to it to be regarded as quasi-equilibrium configurations. The lifetime of minority carriers in high-resistance germanium is so long that it is permissible to treat the holes and electrons as separate components in the thermodynamic sense, so that the sum of the electrochemical potentials (the *difference* of quasi-Fermi levels) is no longer to be held constant. Each electrochemical potential, however, is uniform throughout the system; in particular, we may consider a steady-state configuration of the semiconductor surface, such as may be produced by shining light on it, in which φ_p and φ_n are different from φ_0, but each is constant throughout the space-charge region. This approximation holds good so long as (*i*) the diffusion length of minority carriers in the semiconductor is long in comparison with the thickness of the space-charge region; (*ii*) currents (arising from either carrier) to or from the surface are not too large, nor the depletion of carriers, such as may be produced by an externally applied voltage, too extreme.[10]

In a moment we shall proceed to calculate the space-charge configuration in terms of arbitrary values for φ_p and φ_n. It is not possible, however, to choose φ_p and φ_n independently, because, in the body of the semiconductor, there must be net space-charge

[5] G. E. Pikus, Zhur. Eksptl. i. Teort. Fiz. **21**, 1227 (1951).
[6] W. Schottky, Z. Physik **113**, 367 (1939); **118**, 539 (1942).
[7] W. Schottky and E. Spenke, Wiss. Veröffentl. Siemens-Werken **18**, 3 (1939).
[8] N. F. Mott, Proc. Roy. Soc. (London) **A171**, 27 (1939).
[9] W. Shockley, Bell System Tech. J. **28**, 435 (1949).

[10] The assumption of constancy of "quasi-Fermi levels" cease to be true for a p-n junction that is subjected to a reverse bias considerably larger than kT/e. In order that the hole and electron currents I_p and I_n may be solenoidal (no recombination), the products $\rho\nabla\varphi_p$ and $n\nabla\varphi_n$ must be constant, and since p and n are greatly reduced in value near the junction on the n and p sides respectively, $\nabla\varphi_p$ and $\nabla\varphi_n$ must be quite large there. Calculation suggests that, in a typical case, the assumption of constancy of φ_p and φ_n is reasonably good up to about 10 times kT/e, that is, about 0.2 volt. An exact treatment of the case of still larger reverse biases has not been attempted, involving as it does the solution of the bipolar conduction problem in the presence of space charge.

neutrality, so that one electrochemical potential is determined if the other is known. The relation between them is obtained from Eqs. (1) and (3) by setting $\rho=0$, and will appear as Eq. (10) below.

There are two limitations on the validity of a treatment that starts from Eqs. (1) and (2). Equations (1) apply rigorously to the case of a statistical assembly extending indefinitely in all directions; we wish to apply them to a space-charge region in which the potential is varying very rapidly with distance. A rigorous discussion of this difficulty, which occurs also in the Debye-Hückel theory of strong electrolytes, has been given by Kirkwood.[11,12] Another limitation is set by the wave nature of the electron; one would not expect statistical considerations to apply down to distances of the order of an electron wavelength. In the absence of any alternative method, we shall assume that Eqs. (1) and (2) will be a fair approximation so long as the variation of ψ is not so great that the semiconductor becomes degenerate at the surface. The total extent of the space-charge region in high-resistivity germanium is of the order of 10^{-4} cm, but certain of the properties associated with it depend on the distribution of carriers within only 100 A of the surface. In the light of the above considerations, any conclusions concerning these latter properties must be regarded with caution.

Substituting Eqs. (1) into Eq. (3), we obtain

$$\rho=en_i\left[e^{\beta(\psi_0-\varphi_0)}-e^{\beta(\varphi_0-\psi_0)}+e^{\beta(\varphi_p-\psi)}-e^{\beta(\psi-\varphi_n)}\right], \quad (4)$$

in which we have written ψ_0 for the value of the electrostatic potential in the body of the semiconductor. Now suppose that ψ and ρ vary only in the direction perpendicular to the surface; and let x stand for the distance along this direction, with $x=0$ at the surface, and x going positive inwards. Integrating Eq. (2), we obtain

$$\left(\frac{d\psi}{dx}\right)^2=-\frac{8\pi}{\epsilon\epsilon_0}\int_{\psi_0}^{\psi}\rho\,d\psi. \quad (5)$$

Into this we substitute Eq. (4) and carry out the integration, so obtaining

$$\frac{d\psi}{dx}=\frac{2}{\beta\mathfrak{L}}F(y,\lambda,P,N), \quad (6)$$

where

$$\mathfrak{L}=\left[\epsilon\epsilon_0/2\pi en_i\beta\right]^{\frac{1}{2}},$$
$$\lambda=\left[p_0/n_0\right]^{\frac{1}{2}}=p_0/n_i=n_i/n_0=e^{\beta(\varphi_0-\psi_0)},$$
$$P=\beta(\varphi_p-\varphi_0),$$
$$N=\beta(\varphi_n-\varphi_0),$$
$$y=\beta(\psi-\psi_0),$$

and

$$F(y,\lambda,P,N)=\mp\left[\lambda e^{P}(e^{-y}-1)+\lambda^{-1}e^{-N}(e^{y}-1)+(\lambda-\lambda^{-1})y\right]^{\frac{1}{2}},$$

with the following sign convention: when $y<0$, the positive branch of the square-root function must be chosen; when $y>0$, the negative branch. Note that $\mathfrak{L}$ is a characteristic length for the semiconductor, having the value 1.4×10^{-4} cm for germanium at room temperature.

From Eq. (6) we can write down expressions for the surface excesses Γ_p and Γ_n of holes and electrons. The idea of "surface excess," first introduced by Gibbs,[13] implies the difference between the total amount of some component in the actual system, per unit area of surface, and that which would be found if the phases were homogeneous right up to some chosen dividing surface. We choose the dividing surface in such a way that the surface excess of the component forming the semiconductor is zero; and write Y and ψ_s for the values of y and ψ at this surface (averaged over distances of the order of atomic dimensions). Then

$$\Gamma_p=\int_0^{\infty}(p-p^*)dx$$
$$=-\int_0^{Y}(p-p^*)\left(\frac{dx}{dy}\right)dy$$
$$=-\tfrac{1}{2}n_i\mathfrak{L}\lambda e^{P}\int_0^{Y}\frac{(e^{-y}-1)}{F(y,\lambda,P,N)}dy, \quad (7)$$
$$\Gamma_n=\int_0^{\infty}(n-n^*)dx$$
$$=-\tfrac{1}{2}n_i\mathfrak{L}\lambda^{-1}e^{-N}\int_0^{Y}\frac{(e^{y}-1)}{F(y,\lambda,P,N)}dy,$$

where p^* and n^* are the steady-state values of hole and electron concentration at a point just inside the space-charge region, and are given by $p^*=p_0e^{P}$ and $n^*=n_0e^{-N}$. Notice that in the limit of $-Y$ large,

$$\Gamma_p\to n_i\mathfrak{L}e^{\beta(\varphi_p-\psi_s)}, \quad (8a)$$

while for Y large,

$$\Gamma_n\to n_i\mathfrak{L}e^{\beta(\psi_s-\varphi_n)}. \quad (8b)$$

The total surface charge density due to excess holes and electrons is

$$e(\Gamma_p-\Gamma_n)=en_i\mathfrak{L}F(Y,\lambda,P,N) \quad (9)$$

[11] J. G. Kirkwood, J. Chem. Phys. 2, 767 (1934).

[12] The question concerns the statistical fluctuations in electrostatic potential at each point, and the resulting fluctuations in the local densities of holes and electrons. It is assumed that the mean distribution functions are obtained, to sufficient accuracy, by inserting into the Boltzmann expressions the mean electrostatic potential at each point. The error involved in so doing becomes larger, the greater the departure of the mean electrostatic potential from its value in the body of the semiconductor. It has been shown for the electrolyte case that the method usually breaks down as soon as it ceases to be a good approximation to write $e^{\beta\Delta\psi}\sim1+\beta\Delta\psi$. Fortunately, the restriction in the semiconductor system is less severe. C. Herring has pointed out to us that the approximation used is satisfactory so long as $e^2/\epsilon\epsilon_0\mathfrak{L}'\ll kT$, where $\mathfrak{L}'=(\epsilon\epsilon_0/2\pi Ne\beta)^{\frac{1}{2}}$, in which N stands for the local concentration of holes or electrons, whichever is the greater. This condition is easily satisfied in most cases of practical interest.

[13] J. Willard Gibbs, *Collected Works* (Longmans Green and Company, London, 1906), Vol. 1, p. 219.

as may be proved in a more straightforward manner by considering the value of $d\psi/dx$ at the surface. Notice that the integrals for Γ_p and Γ_n separately cannot easily be evaluated explicitly, but the difference $\Gamma_p-\Gamma_n$ can.

So far we have said nothing as to what determines the values of φ_p and φ_n. Since, however, φ_p and φ_n are constant right through the space-charge region, we may invoke the condition of space-charge neutrality in the body of the semiconductor, and write

$$(\epsilon^{-N}-1)/(\epsilon^{P}-1)=\lambda^2, \tag{10}$$

as may easily be proved from Eqs. (1) and (3), setting $\rho=0$.

2. Shape of the Space-Charge Region

The form of the space-charge region at a semiconductor surface or interface has usually been treated in the following way. If the electrostatic potential near the surface is greater than in the interior for n-type semiconductor, or less for p-type semiconductor, there will be an enrichment of the majority carrier in the surface region, which may be described by a simple Boltzmann expression. In the contrary case, there is a depletion of the majority carrier, which may be treated by thinking of an exhaustion region of appropriate depth containing no carriers of either sign. At the same time it has been realized that, on base material of high resistivity, one may have the state of affairs in which there is an appreciable concentration of minority carriers at the surface. Such a surface region is usually called an inversion layer. The purpose of this section is to consider more exactly the shape of the space-charge region, with particular reference to material that is not too far from intrinsic, in order to show clearly the limits within which the usual simple treatment is allowable.

To find ψ as a function of x, one integrates (6):

$$x=\tfrac{1}{2}\mathfrak{L}\int_0^Y \frac{1}{F(y,\lambda,P,N)}dy. \tag{11}$$

This integral cannot easily be evaluated explicitly. In order to illustrate the shape of the space-charge region, we shall consider the behavior of the integral for the case of a change in potential near the surface tending towards the production of an inversion layer. Three parts of the space-charge region may be distinguished:

(*i*) $0<|y|\ll 1$

Expanding the exponentials, and using (10), we have

$$F(y,\lambda,P,N)\rightarrow -y[\tfrac{1}{2}(\lambda^{-1}-\lambda)+\lambda\epsilon^{P}]^{\frac{1}{2}}. \tag{12}$$

The integral therefore diverges logarithmically: the space-charge region extends indefinitely far into the semiconductor. In this region, however, the properties are not greatly different from those of the bulk semiconductor.

(*ii*) *The "Parabolic" Region*

In the usual, simplified form of the space-charge theories of Mott and Schottky, it is assumed that all of the space-charge arises from absence of both holes and electrons in a certain well-defined region. Using this approximation, it is easy to show that the potential should vary as the square of the distance. This approximation is equivalent to ignoring all terms under the square root sign except $(\lambda^{-1}-\lambda)y$. It may be checked that this is a poor approximation except under the following conditions:

$$\begin{aligned} &\text{(a)}\quad y\ll -1,\quad \epsilon^{-y}/(-y)\ll\lambda^{-2}\epsilon^{-P},\\ \text{or}\quad &\text{(b)}\quad y\gg 1,\quad \epsilon^{y}/y\ll\lambda^{2}\epsilon^{N}. \end{aligned} \tag{13}$$

These conditions specify that the potential must vary in the direction tending to produce an inversion layer, by an amount that is large in comparison with kT/e, but still small in comparison with that which would actually produce an inversion layer. The conditions are most clearly satisfied at a reverse-biassed p-n junction, but at the free surface of a block of semiconductor that is not too far from intrinsic the range of potentials in which they are satisfied is small.[14]

In the range of x for which y satisfies condition (a), one has

$$x_1-x\rightarrow \mathfrak{L}\lambda^{\frac{1}{2}}(1+\tfrac{1}{4}\lambda^2)[(-y)^{\frac{1}{2}}-(-y_1)^{\frac{1}{2}}], \tag{14}$$

where $x=x_1$ is the limit of this region on the inside, and y_1, the value of y there, is of the order of -1.

(*iii*) *Inversion Region*

When $\lambda<1$ and y is sufficiently large and negative, or when $\lambda>1$ and y is sufficiently large and positive, the greatest contribution to the space-charge comes from carriers of the opposite kind to those predominating in the bulk. Here it is sufficient to neglect all except the first or the second term in the expression under the square-root sign in Eq. (6), so that we have: For

$$\begin{aligned} &\lambda\ll 1,\quad \epsilon^{-y}/(-y)\gg\lambda^{-2}\epsilon^{-P},\\ &x_2-x=\mathfrak{L}\lambda^{-1}\epsilon^{-\frac{1}{2}P}(\epsilon^{\frac{1}{2}y_2}-\epsilon^{\frac{1}{2}y}), \end{aligned} \tag{15}$$

where $x=x_2$ represents the inside limit of this third region, and y_2 is the value of y there. This third region corresponds to an inversion layer: in the case considered, a hole-rich region over an n-type semiconductor. The inversion layer is, as we shall see below, very thin in comparison with $\mathfrak{L}$ in a practical case, and the drop in potential across it is usually insignificant in compari-

[14] One physical system where such conditions do exist is the surface of the base region of an npn junction transistor having a channel across it. Here a reverse bias can be applied between the p-type body and the n-type surface. So long as the applied voltage is rather greater than kT/e, the parabolic approximation will hold for most of the space-charge region.

son with the drop across the parabolic region. It is important to remember however, that most of the positive space-charge may be concentrated in the inversion layer.

A similar analysis may be carried out for the case that the potential near the surface is varying in such a sense as to enhance the concentration of the majority carrier. Here there is of course no exhaustion region, and the distribution of carriers near the surface is similar to that worked out for region (*iii*) as may easily be checked from Eq. (11).

The complete space-charge region consists of regions where (*i*) and (*ii*) are applicable, with or without region (*iii*) depending on the boundary conditions. The exact profile may of course be determined by numerical integration of Eq. (11).

3. Space-Charge at a *p-n* Junction

For the sake of completeness, we shall see how the foregoing considerations apply to the case of an "abrupt" *p-n* junction,[9] in which the impurity concentration changes in a distance small in comparison with $\mathfrak{L}$. The following notation will be used:

$$\begin{array}{c|c} x=0 & \\ \hline p & n \\ \hline & \rightarrow x \end{array}$$

On the *p*-side, $\lambda_p=[p_0/n_0]^{\frac{1}{2}}>1$, $V_p=\beta(\psi_s-\psi_{0p})$. On the *n*-side, $\lambda_n=[p_0/n_0]^{\frac{1}{2}}<1$, $V_n=\beta(\psi_s-\psi_{0n})$. For other quantities, suffixes *p* and *n* denote values referring to the *p*- and *n*-side, respectively.

It is required that, at the junction, the quantity $(d\psi/dx)$ shall be continuous. Using Eq. (6), and paying attention to the sign-convention for the square-root function (note that $V_p/V_n<0$), we have

$$\frac{e^{P_p}\lambda_p(e^{-V_p}-1)+e^{-N_p}\lambda_p^{-1}(e^{V_p}-1)+(\lambda_p-\lambda_p^{-1})V_p}{e^{P_n}\lambda_n(e^{-V_n}-1)+e^{-N_n}\lambda_n^{-1}(e^{V_n}-1)+(\lambda_n-\lambda_n^{-1})V_n}=1. \tag{16}$$

In addition, we have two relations of the form of Eq. (10) to be satisfied; and, as pointed out by Shockley,[9] the quasi-Fermi levels must be related to the applied voltage V in the following way:

$$\begin{aligned} \beta V&=P_n-P_p=N_n-N_p,\\ V_p-V_n&=-\beta V-\ln(\lambda_n\lambda_p^{-1}). \end{aligned} \tag{17}$$

The above equations may now be solved for N_p, N_n, P_p, P_n, V_p and V_n:

$$\begin{aligned} e^{-N_p}&=e^{\beta V}\frac{(1-\lambda_n^2)+\lambda_n^2e^{\beta V}(1-\lambda_p^{-2})}{1-\lambda_n^2\lambda_p^{-2}e^{2\beta V}},\\ e^{-N_n}&=e^{-\beta V}e^{-N_p},\\ e^{P_n}&=e^{\beta V}\frac{(1-\lambda_p^{-2})+\lambda_p^{-2}e^{\beta V}(1-\lambda_n^2)}{1-\lambda_n^2\lambda_p^{-2}e^{2\beta V}},\\ e^{P_p}&=e^{-\beta V}e^{-P_n}, \end{aligned} \tag{18}$$

$$V_p=-\frac{\beta V+\ln\lambda_n\lambda_p^{-1}}{1+(\mathcal{P}/\mathcal{R})}+\left\{\frac{1-\lambda_n\lambda_p^{-1}e^{\beta V}}{1+\lambda_n\lambda_p^{-1}e^{\beta V}}\right\}\times\left\{\frac{(\mathcal{P}/\mathcal{R})-1}{(\mathcal{P}/\mathcal{R})+1}\right\}, \tag{19}$$

$$V_n=\frac{\beta V+\ln\lambda_n\lambda_p^{-1}}{1+(\mathcal{R}/\mathcal{P})}-\left\{\frac{1-\lambda_n\lambda_p^{-1}e^{\beta V}}{1+\lambda_n\lambda_p^{-1}e^{\beta V}}\right\}\left\{\frac{(\mathcal{R}/\mathcal{P})-1}{(\mathcal{R}/\mathcal{P})+1}\right\},$$

where $\mathcal{P}=(\lambda_p-\lambda_p^{-1})$ and $\mathcal{R}=(\lambda_n^{-1}-\lambda_n)$. The foregoing expressions represent exact solutions of the problem. We now consider approximate solutions to the following topics: (*i*) the dependence of the V's on the resistivity of the two sides, and (*ii*) the capacity of the space-charge region.

We first note that, since the maximum forward bias that can be applied across a junction is $\beta^{-1}\ln(\lambda_p/\lambda_n)$, it is permissible to drop terms of order $\lambda_n\lambda_p^{-1}e^{\beta V}$ from Eqs. (18) and (19). This excludes only the case of extreme forward bias. One then sees from Eq. (19) that, for the case $\lambda_p\lambda_n\gg1$ (implying that the *p*-type side is much more heavily doped than the *n*-type side):

$$\begin{aligned} V_n&\sim\ln\lambda_n\lambda_p^{-1}+\beta V_a+1,\\ V_p&\sim+1; \end{aligned} \tag{20a}$$

while in the contrary case,

$$\begin{aligned} V_n&\sim-1,\\ V_p&\sim-\ln(\lambda_n\lambda_p^{-1})-\beta V_a-1. \end{aligned} \tag{20b}$$

This confirms the usual conclusion that "most of the space-charge region is on the side of higher resistivity." But note that, however heavily doped one side may be, there is still a potential drop of kT/e across it when the junction is reverse-biased.

To illustrate these results, consider a junction between, say, 10 ohm-cm *n*-type and 0.1 ohm-cm *p*-type. If a reverse bias of 0.25 volt is applied, all except 0.025 volt appears across the *n*-side. There is a negative space charge (extending $\sim10^{-6}$ cm) on the *p*-side, which is largely compensated by excess holes in a narrow region (again $\sim10^{-6}$ cm) on the *n*-side of the junction; beyond this there lies the remaining positive space charge, in a region $\sim10^{-4}$ cm in width in which the "parabolic" approximation applies.

The *capacity* associated with the junction is a quantity that is rather difficult to define. The easiest approach is to consider the ac admittance of the junction $G+iS$, and take the quantity $(S/\omega)_{\omega\rightarrow0}$ as describing the low frequency shunt capacitance of the device. The term S is made up of two parts: that arising from diffusion of excess or deficit hole-electron pairs out to distances of the order of a diffusion length, and that due to the creation of a space-charge region in the immediate vicinity of the junction. The first of these, considered by Shockley[9] decreases exponentially with reverse bias, whereas the latter decreases only as

$\sqrt{(-V)}$. In consequence it is the space-charge capacity which is of principal interest for reverse biased junctions.

The analytical difficulty in discussing both sources of capacity at the same time arises from the fact that in the presentation given here we have evaded the whole question of the mechanism of carrier transport in the space-charge region, replacing it by the condition of constancy of the quasi-Fermi levels. We shall therefore consider only the space-charge capacity. First we note that $d^2\psi/dx^2$ passes through zero once and once only, to wit at the geometrical junction. The stored charge on each plate of the equivalent condenser is therefore given directly by Eq. (9), which may of course be evaluated either for the p side or for the n side. Into this one substitutes for the P's and V's from Eqs. (18) and (19), and differentiates with respect to V. The general expression for the capacity is too complicated to be useful. One special case of interest is that in which one side (say the p side) is much more heavily doped than the other. For sufficient reverse bias, the capacity is given by

$$C\sim e n_i \mathfrak{L}\beta/2\lambda_n^{\frac{1}{2}}[-\beta V-2-\ln(\lambda_n/\lambda_p)]^{\frac{1}{2}}. \qquad (21)$$

By comparing this with the diffusion capacity discussed by Shockley, one sees that the space-charge capacity predominates as long as $2\lambda_n^{\frac{1}{2}}(L_p/\mathfrak{L})e^{\beta V}\times\sqrt{(-\beta V)}$ is small in comparison with unity. In a practical case this condition is well satisfied for reverse voltages of 0.2 volt or more. Note that Eq. (21) is nearly the same as one gets by straight-forward application of the Mott-Schottky "exhaustion layer" theory, in which the potential drop occurs entirely on the high-resistivity side, and the potential varies parabolically with distance. One may conclude with one or two remarks as to the conditions under which the Mott-Schottky exhaustion layer theory is justified. When both sides of a p-n junction are equally heavily doped, the exhaustion layer model, and the parabolic potential, apply well to both sides, with zero or negative bias across the junction. When, however, one side of the junction is much more heavily doped than the other, the exhaustion layer model can be used only for the high-resistance side, and then only if one excludes the region in the immediate vicinity of the junction. The extent of the region over which the potential is parabolic increases, of course, with negative bias; so, at high reverse bias, and so long as one is not interested in the precise field distribution near the junction itself, it is reasonable to regard the whole of the potential drop as occurring across a Mott-Schottky exhaustion region.

4. Surface Conductivity

It is possible to evaluate the change in conductivity of the surface region due to the presence of a space-charge layer:

$$\Delta G=e\mu_p(\Gamma_p+b\Gamma_n), \qquad (22)$$

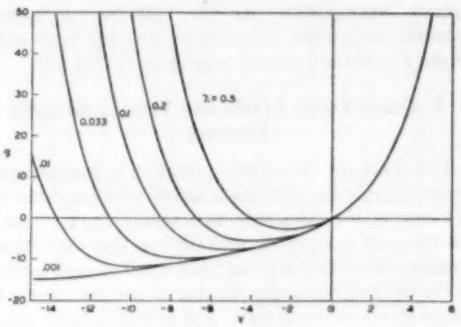

FIG. 1. The surface-conductivity integral as a function of the surface potential V for various values of the parameter λ (for n-type).

where μ_p is the mobility for holes and b is the ratio of the electron mobility to hole mobility. This equation, however, however, assumes that it is sufficient to suppose that the mobilities of holes and electrons in a differentially thin slice of semiconductor are the same as the bulk mobilities. This will not be too bad unless the thickness of the space-charge region is comparable with the mean free path of the carriers. This latter quantity is of the order of 10^{-5} centimeter, which is not very much smaller than $\mathfrak{L}$, so that this approximation is not very good. In consequence, the actual change in surface conductivity would be expected to be rather smaller than the values to be predicted below. The errors arising from this approximation have been investigated by Schrieffer.[15]

Substituting from Eqs. (6) and (7), one finds

$$\Delta G=+\tfrac{1}{2}e\mu_p n_i \mathfrak{L} g\lambda^{-1}, \qquad (23)$$

where g is the integral

$$g=\lambda^{\frac{1}{2}}\int_Y^0 \frac{\lambda(e^{-y}-1)+b\lambda^{-1}(e^{y}-1)}{F(y,\lambda)}dy. \qquad (24)$$

Values of this integral are shown in Fig. 1. Notice that if, for n-type semiconductor, the potential at the surface is greater than that in the interior, the change in surface conductivity arising from extra electrons at the surface is positive. If, however, the surface potential is a little bit less than the potential in the interior, the change in conductivity is negative, because there are now fewer electrons in the surface region at $x=0$, and not yet any appreciable contribution from holes. Only for very low surface potentials does the change in conductivity begin to rise again, as extra holes are created. The minimum surface conductivity is at the potential

$$V=\ln(\lambda^2/b). \qquad (25)$$

Thus, one sees that the surface must be more p than the interior is n before there is any appreciable hole

[15] J. Robert Schrieffer, Phys. Rev. **94**, 1420 (1954).

surface conductivity. At the extremes of surface potential the surface conductance is of the form $g\mu_p\Gamma_p$ or $gb\mu_p\Gamma_n$, where Γ_p and Γ_n are given by Eq. (8).

5. Quasi-Fermi Levels and Flow of Minority Carriers

The transport of added carriers in a homogeneous semiconductor has been discussed by van Roosbroeck.[16] We restrict the discussion to a semiconductor that is not too close to intrinsic, and suppose that any current crossing the surface is at any rate small enough for flow in the body of the semiconductor to proceed largely by diffusion rather than drift. For a semi-infinite block, the small signal solution for hole density at points inside the space-charge region is of the form

$$\Delta p = Be^{-x/L_0}, \tag{26}$$

where $L_0=\sqrt{(D_0\tau)}$ and $D_0=D_n$ for n-type, D_p for p-type.

The hole current at a point just inside the space-charge region, arising partly from flow of minority carriers into the surface traps, is

$$I_p'=I_p-\text{surface recombination flow}, \tag{27}$$

where I_p is the hole current actually crossing the surface. But, from Eq. (26), the current I_p' is given by $-eD_0\ \text{grad}\Delta p$, which is equal to $I_s'[(p^*/p_0)-1]$ for n-type semiconductor, where p^* is the hole concentration just inside the space-charge region, and I_s', the body saturation current, equals eD_pp_0/L_p. Now the recombination flow may be written $es_s(p^*-p_0)$, where s_s is the surface recombination velocity, so that

$$I_p=I_s[(p^*/p_0)-1]=I_s(e^P-1), \tag{28}$$

where I_s, the total saturation current, is given by

$$I_s=ep_0[(D_p/L_p)+s_s]. \tag{29}$$

The net hole inflow I_p could arise from injection of minority carriers from a metal or electrolyte in contact with the surface. If the surface is illuminated with light that is absorbed within a distance from the surface short in comparison with a diffusion length (not necessarily short in comparison with a Debye length), it may be shown[17] that the effect is equivalent to a minority carrier flow L across the surface equal to eN, where N is the number of hole-electron pairs created per unit area per second. The effect on the distribution of carriers inside the semiconductor is then given by adding L to the current I_p in the above equations.

Equation (28) represents the linear approximation to surface and body recombination. If I_p is very large, this linear approximation is usually no longer adequate. Under many conditions one might expect a mass-action recombination law to hold,[16] so that one can write instead:

$$\begin{aligned} I_p&=(I_s/n_i^2)(p-p_0)(n_0+p),\\ &=I_s(e^P-1)(1+\lambda^2e^P). \end{aligned} \tag{30}$$

This equation is quadratic in e^P.

B. PROPERTIES OF THE SURFACE CHARGE

6. Space Charge and Charge in Surface States

Equations (7) for Γ_p and Γ_n are correct only so long as it is assumed that Eqs. (1) hold right up to the dividing surface, and that there are no free electrons or holes beyond. As mentioned in the introduction, there are reasons for believing in the existence of surface states into which electrons can be bound in such a way that they cannot take part in lateral conduction. It is reasonable to assume further that these surface states are associated through trapping with recombination of minority carriers at the surface. Brattain and Bardeen proposed that these trapping centers were either of donor type lying high in the band, or of acceptor type lying low, or both. Such a model enables one to understand how the surface recombination velocity can be insensitive to variations of surface potential produced by changes in chemical environment, as found experimentally.[4,18] The argument goes like this. Consider low-lying acceptor-like traps. The flow of current between the conduction band and the traps will be proportional both to the number of *electrons* in the conduction band at the surface, and to the number of *empty* traps; this flow will be much less than that between the traps and the valence band, which is proportional both to the number of *holes* and to the number of *occupied* traps, unless the electrochemical potential of the traps is almost equal to that of the holes: so the main resistance to recombination occurs in the former process. Since variation of surface potential affects the densities of electrons near the surface and of empty traps by compensating factors, surface recombination should be unaffected by changes in surface potential that do not affect the number of traps. Note that either donor or acceptor traps are sufficient to account for recombination in both n- and p-type.

With this model, the charge in surface traps is

$$\sigma_{tr}=e[N_be^{P-Y}-N_ae^{Y-N}], \tag{31}$$

in which N_a and N_b represent densities of donor and acceptor traps multiplied by the appropriate Boltzmann factors, and P, N, and Y have their previous meanings.

In the following sections we shall assume that the charge in surface states may be written as in Eq. (31); it is easy to proceed to the limiting case of no surface states by setting $N_a=N_b=0$.

[16] W. van Roosbroeck, Phys. Rev. **91**, 282 (1953).
[17] W. H. Brattain and C. G. B. Garrett, Physica **20**, 885 (1954); Bell System Tech. J. **34**, 129 (1955).
[18] R. J. Keyes and T. G. Maple, Phys. Rev. **94**, 1416 (1954).

7. Surface Photoeffect

The total charge in both space charge and traps is given by

$$\Sigma = e(\Gamma_p - \Gamma_n) + \sigma_{tr}, \tag{32}$$

where $\Gamma_p - \Gamma_n$ is given by (9) and σ_{tr} by (31). We are concerned with calculating the change in ψ_s produced on illumination of the surface, the illumination being supposed to take place so abruptly that the ionic charge, and therefore the total charge Σ in the surface of the semiconductor, to which it is equal in magnitude and opposite in sign, does not have time to change. Differentiating the right-hand side with respect to L, the light current, using Eqs. (10) and (28), and setting the result equal to zero, we find (for n-type)

$$\frac{d\psi_s}{dL} = \frac{1}{\beta I_s}\left[(e^{Y}-1)+(e^{-Y}-1)-Z(\lambda^2 N_a e^{Y} - N_b e^{-Y})\right] \div \{-\lambda^{-2}[(1+\lambda^2 L/I_s)e^{Y}-1]+[(1+L/I_s)e^{-Y}-1] + Z[(1+\lambda^2 L/I_s)N_a e^{Y}+(1+L/I_s)N_b e^{-Y}]\}, \tag{33}$$

where

$$Z = 2F(Y,\lambda)/n_i \mathfrak{L}\lambda. \tag{34}$$

The theory of Brattain and Bardeen gave an expression equivalent to ignoring all those terms in (33) not multiplied by Z, since charge in the space-charge region was ignored. The following approximations to (33) should be noted:

$$\begin{aligned} Y \to -\infty &: \frac{d\psi_s}{dL} \sim \frac{1}{\beta I_s}\frac{1}{1+L/I_s} \to \frac{1}{\beta I_s} \quad \text{for } L \text{ small}, \\ Y \to +\infty &: \frac{d\psi_s}{dL} \sim \frac{-1}{\beta I_s}\frac{\lambda^2}{1+\lambda^2 L/I_s} \to -\frac{\lambda^2}{\beta I_s} \quad \text{for } L \text{ small}. \end{aligned} \tag{35}$$

For N_a, $N_b = 0$, L small:

$$\frac{d\psi_s}{dL} = \frac{1}{\beta I_s}\frac{1-e^{Y}}{1+\lambda^{-2}e^{Y}}. \tag{36}$$

With the Z terms only (i.e., N_a, $N_b \to \infty$)

$$\frac{d\psi_s}{dL} = \frac{1}{\beta I_s}\frac{1-e^{2Y'}}{1+\lambda^{-2}e^{2Y'}}, \tag{37}$$

where $Y' = Y + \frac{1}{2}\ln(\lambda^2 N_a/N_b)$.

Let us consider the import of Eqs. (36) and (37). In each, the surface photovoltage is given as that change in surface potential which is required in order to keep the semiconductor surface charge constant when the imrefs of holes and electrons inside are altered. The reasoning leading to Eq. (37) is relatively simple; most of the surface charge is in donor and acceptor traps, and the populations of these traps would alter when the imrefs change, if it were not for the change in surface potential. The physical interpretation of Eq. (36) is harder to picture. First it is worth noting that if the space-charge region were accurately described by a Mott-Schottky exhaustion layer, and if there were no surface states, there would be no surface photovoltage at all, because the charge associated with the space-charge region would then be a function only of the surface potential, and would be unaffected by the change in imrefs produced on illuminating the sample. The surface photovoltage given by Eq. (36) arises precisely because the Mott-Schottky exhaustion layer model is not exact. In this view (with no surface states) in order to maintain the total charge in the space-charge region constant, the surface potential must change and the only way in which this can happen is by rearrangement of the distribution of that charge. One point to notice is that the limiting values of surface photovoltage are the same, whichever model one uses. As we have emphasized elsewhere,[17] the limiting values of photovoltage may be derived by a thermodynamic argument, and are therefore independent of the precise model assumed; all that the model adds is the dependence of surface photovoltage on surface potential in the intermediate region, which depends, in chemical language, on rate process considerations.

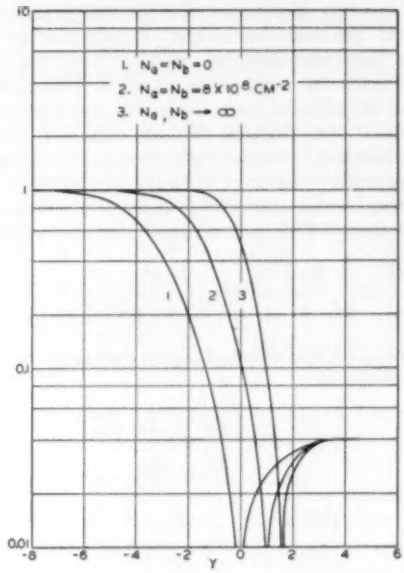

FIG. 2. Surface photoeffect as a function of Y, with and without surface states (relative values).

In Fig. 2, Eq. (33) has been evaluated for $\lambda = 0.2$ for the two extreme conditions represented by (36) and (37) and also for an intermediate case in which $N_a = N_b = 8\times10^{8}$ cm^{-2}. It will be seen that there is little difference between the shapes of the three curves.

The quantity $d\psi_s/dL$ describes the change in surface potential produced by sudden illumination of the surface. Experimentally, one can measure the change in contact potential or electrode potential. This includes changes in potential drop across the material itself, such as IR drop. Suppose that the current I, if any, is kept constant: then there still remains the change in the potential difference $[(b-1)/(b+1)]\beta^{-1}\ln(\sigma/\sigma_0)$ that arises because of the difference in mobilities of holes and electrons.[16] This gives an additional photoeffect:

$$\frac{dV_i}{dL}=\frac{1}{\beta I_s}\frac{b-1}{b}\frac{\lambda^2}{1+(\lambda^2/b)[(b+1)(L/I_s)+1]}, \tag{38}$$

so that the limiting values of the net surface photoeffect for $L\to 0$ should be

$$\begin{aligned} &V\to -\infty, \quad \frac{dV}{dL}\sim\frac{1}{\beta I_s};\\ &V\to \infty, \quad \frac{dV}{dL}\sim -\frac{\lambda^2}{b}\frac{1}{\beta I_s}. \end{aligned} \tag{39}$$

Expressions for p-type are analogous.

8. Surface Potential and Contact Potential

Let us now turn from the question of variation of surface potential with illumination to that of the dependence of surface potential on chemical environment. One way of investigating this is to measure the contact potential difference between the semiconductor and a reference electrode, of which one has reason to believe that the work function is adequately independent of environment.

The question arises as to how much of the change in contact potential observed, for example, in the Brattain-Bardeen cycle, is change in surface potential ψ_s, and how much is to be ascribed to changes in the ionic double layer. Brattain and Bardeen[4] have concluded that only about 20 percent of the change in contact potential arises from ψ_s. Measurements by Morrison[19] of surface conductivity as a function of gaseous environment suggest that this estimate is too low. If there were no surface states, the predicted result would be close to 100 percent, since the capacity of the space-charge region is two orders of magnitude or more lower than that normally associated with an ionic layer (~ 30 μf/cm^2). Even with $N_a=N_b=10^{13}$ cm^{-2}, the capacity associated with the semiconductor surface is negligibly small except at the extremes of ψ_s. As we shall see below from the field-effect experiment, it is unlikely that the density of surface states is greater than this by more than an order of magnitude or two, so that one would not be surprised to find that changes in ψ_s account for almost all of the observed change in contact potential.

[19] S. R. Morrison, J. Phys. Chem. **57**, 860 (1953).

One possible test is the behaviour of contact potential in very strong light. First assume $N_a=N_b=0$. In order to derive expressions for the surface potentials in a very strong light we use the strong form for the recombination (30). On physical grounds one would expect that the difference between the surface potential and the potential in the body would become very small in strong light: now that there is a copious supply of both holes and electrons the charge in the space-charge region has become very sensitive to the exact value of surface potential. Let us then take Eq. (9) and expand the exponentials in a power series in y. In this case, the first-order terms cancel, giving

$$V_L\sim\frac{[\lambda(e^{-Y_0}-1)+\lambda^{-1}(e^{Y_0}-1)+(\lambda-\lambda^{-1})Y_0]^{\frac{1}{2}}}{[\lambda^2 L/I_s]^{\frac{1}{2}}}. \tag{40}$$

From this, one sees that $V\to 0$ in strong light as the fourth root of the intensity of the light.

A similar analysis can be carried out for nonvanishing N_a and N_b. The point is that in all cases the effect should be to shift that portion of contact potential arising from ψ_s to a standard value ($V=0$ for $N_a=N_b=0$; $V'=0$ for $N_a, N_b\to\infty$) irrespective of the starting-point: any contributions from the ionic double layer, however, should be unchanged.

The experimental difficulty in this lies in the high light-intensity required. One rough experiment on an n-type sample was carried out, the results of which are shown in Fig. 3. (The measurements were made on an ac basis, with a low duty-cycle, to minimize heating.) The upper curve was obtained in an atmosphere of humid oxygen (about 70 percent relative humidity); the lower in an atmosphere of dry oxygen. For the upper curve $V>0$, the surface is more n-type than the interior, and the surface photovoltage is small; for the lower curve $V<0$, the surface is strongly p-type, and the small-signal photovoltage is large and of the opposite sign. The fact that, in the latter case, it was possible to shift the contact potential nearly half-way to the zero point, shows that the original estimate of Brattain and Bardeen of $\Delta\psi_s/\Delta$cp~ 0.2 is assuredly too low, as

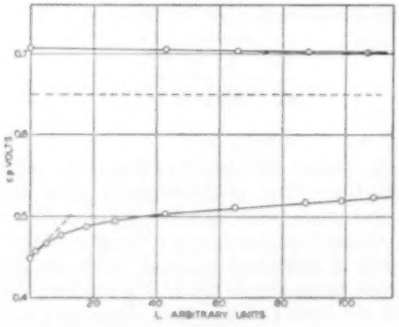

FIG. 3. Experimental behavior of contact potential in strong light.

concluded by Morrison, but it was not possible to attain a light intensity sufficiently great to reach the region where Eq. (40) might apply.[20]

The conclusions of this section may be summarized thus: (1) The surface photo-effect, in combination with measurements of surface recombination velocity (in order to calculate I_s) is the most reliable tool for determining whether the surface is p-type or n-type, and how much so; (2) Such measurements do not, however, shed much light on the problem of determining the location and density of surface traps.

9. Field Effects

In the field-effect experiment of Shockley and Pearson,[21] measurements were made of the change in surface conductivity produced by applying a high normal electric field. The results of such a measurement are best described by quoting an effective mobility μ_{eff}, defined by $d\Delta G/d\Sigma$, the differentiation being carried out at constant ionic charge. Using (32), (7), (23), and (31) we find

$$\mu_{eff}=\mu_p\frac{1-\lambda^{-2}be^Y}{1+\lambda^{-2}e^Y-Z(N_ae^{2Y}+N_b)/(e^Y-1)}, \quad (41)$$

where Z again has the significance of Eq. (34). Equation (41) is illustrated in Fig. 4, for the case $\lambda=0.2$, with $N_a=N_b=0$ and with $N_a=N_b=8\times10^8$ cm^{-2}. (For N_a, $N_b\to\infty$, $\mu_{eff}\to0$ for all Y).

Results of measurements on germanium generally give values of $|\mu_{eff}|$ lower than μ_p by about a factor of 2.[22] Although such experiments have not been carried out in a controlled environment such as the Brattain-Bardeen cycle, there is a suspicion that μ_{eff} is much more nearly independent of Y than one would gather from Fig. 4. If this turns out to be the case, either the Brattain-Bardeen trap model is wrong, or the traps responsible for surface recombination are different from the surface states that cause $|\mu_{eff}|$ to be less than for the case of space-charge only. It is clear, however, that N_a and N_b cannot be very much greater than 10^9 cm^{-2}, or there would be no field effect at all.[23]

Two other possible experiments may be mentioned here: (*i*) the influence of applied field on the surface photo-effect; (*ii*) the influence of light on the effective mobility as measured in the field-effect experiment.

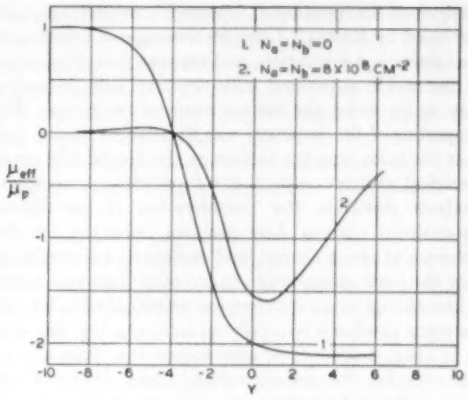

FIG. 4. The "effective mobility" in the field-effect experiment, with and without surface states.

The first of these measures the quantity

$$\left(\frac{\partial}{\partial V}\right)_L\left(\frac{\partial\psi_s}{\partial L}\right)_\Sigma=\frac{\epsilon_{air}\epsilon_0}{4\pi D}\frac{\partial^2\psi_s}{\partial\Sigma\partial L}, \quad (42)$$

where D is the gap across which the voltage ΔV is applied. This may be evaluated from Eqs. (32) and (33). The resulting expressions are very cumbersome. For the case of N_a, N_b smaller than $n_i\mathfrak{L}$, and in the vicinity of the change in sign of the photo-effect ($|Y|<1$), it may be shown that

$$\Delta\left(\frac{d\psi_s}{dL}\right)=\frac{\epsilon_{air}\lambda^{-1}\mathfrak{L}}{\epsilon_{Ge}\sqrt{2D}}(\beta V)\left(\frac{1}{\beta I_s}\right), \quad (43)$$

independently of the magnitude of N_a and N_b, to first order in these quantities. The effect should be easily measurable, but gives no direct information as to the surface states. The second experiment measures the quantity

$$\left(\frac{\partial}{\partial L}\right)_\Sigma\left(\frac{\partial\Delta G}{\partial\Sigma}\right)_L=\left(\frac{\partial\psi_s}{\partial L}\right)_\Sigma\left(\frac{\partial}{\partial\psi_s}\right)_L\left(\frac{\partial\Delta G}{\partial\Sigma}\right)_L+\left(\frac{\partial}{\partial L}\right)_{\psi_s}\left(\frac{\partial\Delta G}{\partial\Sigma}\right)_L. \quad (44)$$

This may be evaluated, using Eqs. (23) and (33). The general result is too complicated to be worth quoting here, but it may be shown for the case $N_a=N_b=0$ that, in the vicinity of the point at which μ_{eff} changes sign, illumination of the surface with light of intensity of the order of I_s should produce significant changes in μ_{eff}. Such an experiment ought to give an additional check on the theory.

10. "Channel" Conductance

The formulation of space-charge theory which we have presented in this paper makes possible a simple

[20] The lower branch of Fig. (3) fits well to an equation of the form $L=I_s(e^{\beta\Delta\psi}-1)(1+\lambda^2e^{\beta\Delta\psi})$, obtained by setting $P-Y=$ const [see Eqs. (9) and (31)] and using Eq. (31). This shows that, even at the highest light, the surface potential has not yet shifted to the point at which electrons or donor traps have become of appreciable importance.

[21] W. Shockley and G. L. Pearson, Phys. Rev. **74**, 232 (1948).

[22] J. Bardeen and S. R. Morrison, Physica **20**, 873 (1954). H. C. Montgomery and W. L. Brown, Bull. Am. Phys. Soc. **30**, No. 2, 42 (1955).

[23] Remember that N_a and N_b are the numbers of traps *multiplied by a Boltzmann factor*. The actual numbers should be much greater than this.

analysis of the question of "channel" conductance, first discussed by Brown.[24] Consider a sample of germanium containing a p-n junction, and suppose that the surface of the n-side is covered with negative ions, in such a way as to make the surface everywhere p-type. The properties of the structure will be affected by the fact that the holes near the surface on the p-type side are in electrical contact with the n-type side. A complete analysis demands the consideration of the three-dimensional current flow problem, allowing for the presence of space charge, and requires a knowledge of how the ionic charge will change with time as a result of the change in electrochemical potential of holes and electrons produced by applying a bias to the junction. It is easy, however, to write down the channel conductance for the one-dimensional case, in which the ionic charge and electrochemical potentials are supposed uniform in the direction parallel to the surface and constant with time. The channel conductance is then that surface conductance arising from minority carriers in the inversion region near the surface. Since the channel conductance is significant only when the inversion region is well developed, it is sufficient approximation to set the actual number of minority carriers per unit area near the surface equal to the surface excess of minority carriers. We shall suppose that the base material is n-type, so that holes are the minority carriers. In our agreed approximation, the channel conductance is thus equal to $e\mu_p\Gamma_p$. The magnitude of this quantity depends on the density of absorbed anions, and therefore on the chemical environment. The interesting question is then how the channel conductance depends on the voltage applied to the nearby junction in the bulk semiconductor. If the section of the channel considered is very near the bulk junction, it is sufficient to make our usual assumption that the electrochemical potentials are everywhere uniform, so that the applied voltage V and the quantity P on the n-type side are related approximately by $V=P/\beta$ [see Eq. (18)].[25,26] The voltage is imagined to be applied suddenly, so that the ionic charge on the surface has not time to change. The change in the space-charge region so produced still depends on the assumption made in regard to the surface states. We start first with the assumption $N_s=N_0=0$. From Eq. (9), one can write $\Gamma_p-\Gamma_n$ constant. For the case of interest (βV, $Y\ll-1$) the only terms in $F(Y)$ that need be considered are $\lambda e^{\beta V-Y}$ and $\lambda^{-1}Y$, we have the following equation for Y:

$$\lambda^2 e^{\beta V-Y}-Y=\lambda^2 e^{\Delta}+\Delta, \tag{45}$$

where Δ is the value of $(-Y)$ for the case $\beta V=0$. By using Eq. (7), it may then be shown that the channel conductance G_{ch} is well described by the following approximations:

$$-\beta V<-\beta V_0,\quad -Y\sim-\beta V+\Delta,$$
$$G_{ch}\sim K\{[-\beta(V+V_0)]^{\frac{1}{2}}-(-\beta V)^{\frac{1}{2}}\}. \tag{46}$$

$$-\beta V>-\beta V_0,\quad -Y\sim-\beta V_0+\Delta,$$
$$G_{ch}\sim K(-\beta V_0)^{\frac{1}{2}}\{[e^{\beta(V-V_0)}+1]^{\frac{1}{2}}-1\}, \tag{47}$$

where $\beta V_0=-\lambda^2 e^{\Delta}$ and $K=e\mu_p\lambda^{-\frac{1}{2}}n_i\mathfrak{L}$.

It will be seen that, in the model of no surface states, the channel conductivity should vary rather slowly with reverse bias until a voltage V_0 is reached, and should fall off very rapidly thereafter. The point is that, for zero bias, the (negative) ionic charge is compensated partly by holes, partly by ionized donors in the exhaustion region; as negative voltage is applied, the exhaustion region widens, until finally all of the (fixed) negative ionic charge can be compensated by ionized donors. There being no holes left, the channel is described as having been "pinched off."

With an appreciable density of surface states, this pinching off does not occur. Using Eq. (31), we see that there is now no linear term in V in the expression for surface charge: therefore the approximation $-Y\sim-\beta V+\Delta$ should continue to hold indefinitely. In the limit, for $-V$ very large, we should have

$$G_{ch}\sim\tfrac{1}{2}K(-\beta V_0)/(-\beta V)^{\frac{1}{2}}, \tag{48}$$

the conductivity decreasing as the inverse square root of applied voltage. For high reverse bias, however, as pointed out by Kingston,[26] the thickness t of the region in which holes can flow becomes small in comparison with the bulk mean free path l. Following Kingston, we take this thickness to mean the distance X in which the electrostatic potential falls through kT/e; then, from Eq. (11), for the limit $-\beta V\gg-\beta V_0$, one has

$$X=\tfrac{1}{2}\mathfrak{L}\int_{Y+1}^{Y}\frac{dy}{(\lambda e^{\beta V-y}-\lambda^{-1}y)^{\frac{1}{2}}}\sim\frac{\lambda^{\frac{1}{2}}\mathfrak{L}}{2(-\beta V)^{\frac{1}{2}}}, \tag{49}$$

so that, because of the reduction in available thickness, the hole mobility is reduced in the ratio $\lambda^{\frac{1}{2}}\mathfrak{L}/2l(-\beta V)^{\frac{1}{2}}$. Thus $K=e\mu_p n_i\mathfrak{L}^2/2l(-\beta V)^{\frac{1}{2}}$, and

$$G_{ch}\sim\frac{e\mu_p n_i\mathfrak{L}^2}{4l}\left(\frac{V_0}{V}\right) \tag{50}$$

Therefore $G_{ch}\sim3\times10^{-6}(V_0/V)$ mhos per square for germanium at room temperature. This agrees with Kingston's conclusion[26] that, at high reverse bias, the conductivity should be proportional to $1/V$. The remarkable feature of (50), however, is that the channel conductivity at $V=V_0$ is, under these conditions, *independent of the resistivity of the base material.* The reason for this is that the quantity λ enters both into the concentration of minority carriers at the surface

[24] W. L. Brown, Phys. Rev. **91**, 518 (1953).

[25] Since, as we shall see, the channel conductance is comparatively low, this assumption is incorrect for regions distant from the bulk junction, because, as Kingston has pointed out,[26] the current carried by the channel sets up an ohmic drop in potential along the channel, which makes the effective voltage applied between the channel and the n-type body smaller and smaller, the further one proceeds away from the body junction.

[26] R. H. Kingston, Phys. Rev. **98**, 1766 (1955).

and into the width of the channel, so that the channel conductance depends only on Δ, and on this only through the "pinch-off" voltage V_0.

For a channel of length c and perimeter d, the channel conductance should thus be $\approx 3\times 10^{-6}(d/c)$ at $V_0 \sim V$. In the junction transistor structure, (d/c) may be of the order of 50 or more for a channel over the base region: the channel conductance should therefore be $\sim 10^{-4}$ mhos at $V_0 \sim V$. Experiments of Kingston[26] and of Brown[24] give just this order of magnitude. In an alloyed structure, no appreciable channel can form over the base, but a channel over the emitter or collector would have $(d/c) \sim 500$, so that channel conductances of 10^{-3} mho would not be surprising.

The general conclusion of this section is to confirm Kingston's observation that, for sufficient reverse bias, $G \propto 1/V$, and to show that the coefficient in this relation depends on the bulk properties and surface treatment through the factor V_0. In comparing with the experimental results, however, one must remember that, if sufficient time is allowed after the application of bias, the ionic charge itself may change.

11. Time Effects

It has been assumed throughout that surface states are in extremely good electrochemical contact with the conduction or valence band of the semiconductor, while charges associated with ions are fixed. That the former is a reasonable assumption is shown by the observation that the "effective mobility" observed in a field-effect experiment is consistently less than the space-charge-only value even when measurements are made in a time of the order of 10^{-3} second after switching on the field.[22] The assumption about the constancy of ionic charge implies that there are no further time constants in the surface system. This is not true. When the surface of a lump of germanium is illuminated by a fairly intense light, it is found that the contact potential returns over a period of seconds or minutes towards its initial (dark) value; on switching off the light, the contact potential overshoots, and only recovers the original value some time later. Similar effects have been observed by the authors in experiments on germanium electrolyte systems.[17] These experiments can be described by saying that the ionic charge tends to change in such a sense as to restore the surface potential ψ_s to the value corresponding to chemical equilibrium. This is what one would expect from the theoretical treatments of chemisorption on a semiconductor given by Aigrain and Dugas, Engell and Hauffe and by Weisz.[27]

The question of long-time effects introduces considerable uncertainty in the application of the results of section B of this paper to actual systems. In addition, there is the complication that, in structures involving body p-n junctions, ions on the surface may drift under the influence of applied fields[28] thereby introducing further long-time changes in surface properties.

12. Conclusion

In this paper we have considered the theoretical interpretation of experiments on the electrical properties of semiconductor surfaces. The theory of the space-charge region may be written down fairly precisely, but considerable ignorance still prevails as to the exact structure of surface states, under given chemical conditions. Measurements of surface photoeffect are not in themselves sufficient to answer this question. The most promising line of attack appears to be a combination of the field-effect experiment with a controlled variable chemical environment.

ACKNOWLEDGMENTS

The authors have had the advantage of several discussions with R. C. Fletcher and W. L. Brown. We wish also to thank R. W. Hamming and the staff of the computation laboratory for the numerical evaluation of the surface conductivity integral (Fig. 1).

[27] P. Aigrain and C. Dugas, Z. Elektrochem. **56**, 363 (1952); H.-J. Engell and K. Hauffe, Z. Elektrochem. **56**, 366 (1952); **57**, 762 (1953); P. B. Weisz, J. Chem. Phys. **20**, 1483 (1952); **21**, 1531 (1953).

[28] J. T. Law, Proc. Inst. Radio Engrs. **42**, 1367 (1954).

Effect of Pressure on the Electrical Properties of Indium Antimonide*

DONALD LONG
University of Pennsylvania, Philadelphia, Pennsylvania
(Received March 24, 1955)

The electrical resistivity and Hall coefficient of indium antimonide have been measured as a function of pressure to 2000 atmospheres at 0°C, 24.3°C, and 54.3°C. The sample was p-type at low temperatures and became intrinsic with respect to the type of conductivity-temperature variation at about 220°K. It was found that the resistivity and Hall coefficient both increase exponentially with pressure, but at different rates, the resistivity curves having the greater slopes. The experimental results indicate an increase in the energy gap of 14.2×10^{-6} ev/atmosphere and a decrease in the electron mobility of 14 percent for 2000 atmospheres pressure at room temperature.

INTRODUCTION

INDIUM antimonide is one of a series of semiconducting compounds formed between elements of columns IIIB and VB of the periodic table. The lattice has the zincblende structure and therefore exhibits cubic symmetry.

This paper presents the results of measurements of the effect of pressure on the resistivity and Hall coefficient of a sample of InSb which was intrinsic at the temperatures of the experiments and p-type below about 220°K. It was found that the energy gap increases linearly with pressure and that there is an accompanying decrease in the electron mobility.

APPARATUS AND MEASUREMENTS

The hydrostatic-pressure vessel used in these experiments was constructed of nonmagnetic stainless steel, and the lower section in which the sample was located could be placed in a temperature bath between the pole-pieces of a magnet. Electrical leads passed out of the vessel through a plug in the top. Tri-cresyl phosphate was used as the pressure-transmitting fluid, and the pressure was measured by a Bourdon-tube gauge. A thermocouple junction was placed next to the sample inside the pressure vessel to measure the temperature.

Electrical lead wires of copper were soldered to the sample with pure indium. The resistivity was measured by the usual four-probe potentiometric method. The Hall voltages were read from a Leeds and Northrup indicating dc microvolt amplifier. All thermomagnetic effects except the Ettingshausen were eliminated from the Hall voltage readings by reversing the current and magnetic field directions and taking the appropriate averages. The Ettingshausen effect has the same current and field dependence as the Hall effect and so cannot be eliminated in this way. Thermocouples were soldered to the sample in the Hall probe positions, and an attempt was made to measure an Ettingshausen temperature difference due to the magnetic field under the same experimental conditions present inside the pressure vessel. No such temperature difference was detected, however, and thus no correction for the Ettingshausen effect was necessary in the Hall voltage readings. Changes in the sample dimensions with pressure were not taken into account in any case, since the compressibility of InSb is as yet unknown; however, the effects of any such changes would undoubtedly be negligible.

The experimental results are shown in Fig. 1 in which log resistivity and log Hall coefficient are plotted against the pressure at three different temperatures. The resistivity and Hall coefficient both increase exponentially with pressure but at different rates, the resistivity rate being the larger at each temperature.

An auxiliary experiment in which the Hall coefficient was measured as a function of temperature from liquid

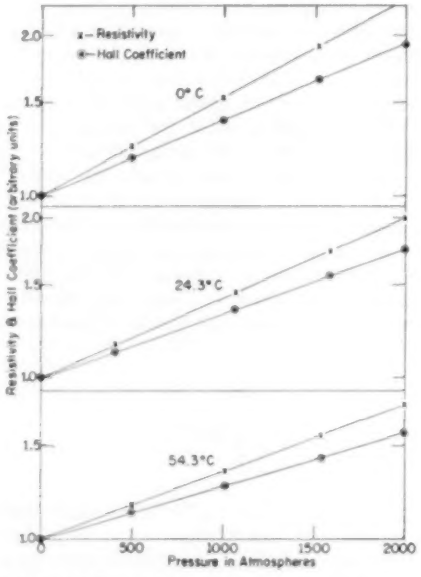

FIG. 1. Resistivity and Hall coefficient *versus* pressure for InSb. The zero-pressure actual values of resistivity and Hall coefficient are as follows:

Temp. °C	Resistivity (Ω cm)	Hall coeff. (cc/coul)
0	1.13×10^{-3}	547
24.3	0.670×10^{-3}	294
54.3	0.387×10^{-3}	153

* Work supported by a contract with the Office of Naval Research.

air to room temperature was also performed in order to determine the density of impurity holes in the sample and the electron-hole mobility ratio. These data are shown in Fig. 2 and are typical of the behavior of p-type InSb. The impurity density p_0 as found from the value of the Hall coefficient in the extrinsic range,

$$R_{ext} = -\frac{3\pi}{8}\frac{1}{p_0 e}, \tag{1}$$

was 3.26×10^{15} per cm³. A mobility ratio c of 32 was found from the condition that the Hall coefficient pass through a maximum in the negative region, *viz.*,

$$R_{max}/R_{ext} = (c-1)^2/4c. \tag{2}$$

Other important properties of InSb are listed in Table I, including an electron mobility of about 40 000 cm²/volt-sec for the sample used in these experiments.

The Hall *vs* pressure data were taken using the rather small magnetic field of 870 gauss in order to minimize the field dependent term of the Hall coefficient. Simple theory[1] predicts that this term should be approximately $0.4u_n^2H^2\times10^{-16}R$, which for a mobility of 40 000 cm²/volt-sec and a magnetic field of 870 gauss would have a value of $0.05R$, where R is the zero-field Hall coefficient. The Hall coefficient of the sample was measured as a function of field strength from 870 gauss down to 290, but no measurable field dependence was observed. Thus, the value at 870 gauss must closely approximate the zero-field Hall coefficient. In order to verify that any small field dependence had no effect on the results,

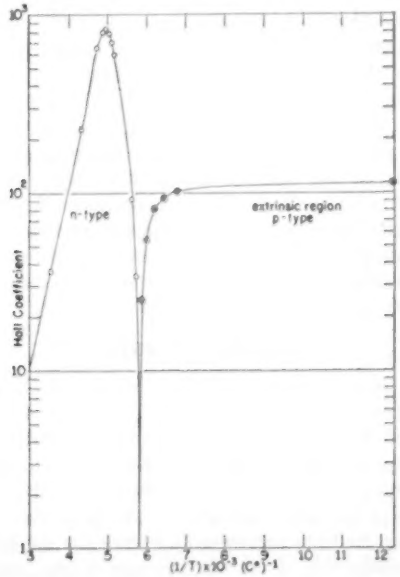

FIG. 2. Hall coefficient *vs* inverse temperature for InSb.

[1] A. H. Wilson, *The Theory of Metals* (Cambridge University Press, Cambridge, 1936).

TABLE I. Properties of InSb.

Energy gap at room temperature	0.18 ev,[a] 0.16 ev[b]
Electron mobility at room temperature	~40 000 cm²/volt-sec
Mobility ratio	32
Electronic effective mass	$0.03m_0$,[a] $0.04m_0$;[b] where m_0 is the true mass

[a] O. Madelung and H. Weiss, Z. Naturforsch **9a**, 527 (1954).
[b] Breckenridge, Blunt, Hasler, Frederikse, Becker, and Oshinsky, Phys. Rev. **96**, 571 (1954).

the Hall *vs* pressure experiment was repeated at 24.3°C using a field of 290 gauss. The same slope was obtained on the log Hall coefficient *vs* pressure plot as that for the measurements at 870 gauss.

INTERPRETATION OF MEASUREMENTS

Because of the extremely small effective mass of an electron in InSb it is possible for a sample to become degenerate at relatively low conduction electron concentrations. For an effective mass of $0.03m_0$ classical statistics may be used with accuracy in the analysis if the density of conduction electrons does not exceed about 2×10^{16} per cm³; the criterion used is that the Fermi level should not lie closer than $2kT$ below the bottom of the conduction band. This condition is satisfied in the experiments at 0°C and 24.3°C. Even though it is not quite satisfied at the higher temperature, the error involved in using classical statistics should not be significant.

It is possible to explain the experimental results in terms of decreases in the density and mobility of the conduction electrons with the application of pressure to the sample, and to relate these decreases in turn to increases in the energy gap and the electronic effective mass. The conductivity and Hall coefficient are expressed as functions of the carrier densities and mobilities by the following two equations:

$$\sigma = e(n\mu_n + p\mu_p), \tag{3}$$

$$R = -\frac{3\pi}{8e}\frac{nc^2-p}{(nc+p)^2}, \tag{4}$$

where the factor $3\pi/8$ is used in (4) because Harman *et al.*[2] have shown that thermal scattering dominates InSb above 125°K. The constant value of the Hall coefficient over a wide range of temperatures in the extrinsic range indicates that nearly all the acceptor impurities become ionized at a very low temperature, and for this case it is possible to make the substitution, $p = n + p_0$, into the above equations which then become

$$\sigma = e\mu_p[n(c+1)+p_0] \simeq ne\mu_n\left[1+\frac{p_0}{n(c+1)}\right], \tag{3a}$$

$$R = -\frac{3\pi}{8e}\frac{n(c^2-1)-p_0}{[n(c+1)+p_0]^2} \simeq -\frac{3\pi}{8e}\frac{1}{n}\left[1-\frac{2p_0}{nc}\right], \tag{4a}$$

[2] Harman, Willardson, and Beer, Bull. Am. Phys. Soc. **30**, No. 2, 9 (1955).

TABLE II. Results.

Temperature °C	$(\partial E_g/\partial P)_T$ ev/atmos	$(\Delta\mu_n/\mu_{n0})P=2000$ atmos	$(\Delta m_n/m_{n0})P=2000$ atmos
0	$+(14.2\pm0.3)\times10^{-6}$	−0.16	−0.060
24.3	$(14.2\pm0.3)\times10^{-6}$	0.14	0.053
54.3	$(13.1\pm0.4)\times10^{-6}$	0.12	0.046

where the approximations are valid because of the high mobility ratio in InSb and because in these experiments n was always greater than p_0.

The value of n at any pressure is calculated by using Eq. (4a) from the measured value of R at that pressure and the values of p_0 and c, providing the assumption is made that c does not vary with pressure. It is evident though from the above approximate expressions for σ and R that a change in c would not produce an appreciable effect anyway.

An expression for μ_n at any pressure is obtained by multiplying (3a) by (4a) and neglecting terms which are very small. The result is,

$$\sigma R=-\frac{3\pi}{8}\mu_n\left[1-\frac{p_0}{n(c+1)}\right]\left(1-\frac{1}{c}\right). \tag{5}$$

Now, according to Bardeen and Shockley,[3] μ_n is related to the electronic effective mass in the thermal scattering range by the following equation:

$$\mu_n=\frac{(8\pi)^{\frac{1}{2}}eh^4}{3(kT)^{\frac{1}{2}}}\frac{c_{ii}}{E_1^2m_n^{5/2}}, \tag{6}$$

where c_{ii} is the elastic constant in the direction of propagation of thermal vibrations, and E_1 is the change in energy gap per unit dilation. No data are available on the change in c_{ii} with pressure in InSb. Lazarus[4] has measured the changes in elastic constants with pressure for KCl, NaCl, CuZn, Cu, and Al. Only in KCl and NaCl, which are strongly ionic crystals, did any elastic constant change by more than 1.5 percent for 2000 atmospheres, the changes in these crystals being as large as 6 percent. It seems probable that in InSb, which is only slightly ionic, the change is not much greater than 1.5 percent. This change is small compared to the approximately 14 percent decrease of mobility of InSb. A change in E_1 would represent the existence of a nonlinear change in the energy gap, but this is unlikely because of the true exponential nature of the data. Thus, it can be assumed that the observed decrease in mobility of InSb is the result of an increase in the electronic effective mass, the magnitude of which is then determined from Eqs. (5) and (6).

The energy gap is related to the free carrier densities and effective masses at a temperature T by the following equation.

$$n(n+p_0)=4(2\pi kT/h^2)^3(m_nm_p)^{\frac{3}{2}}\exp(-E_g/kT). \tag{7}$$

[3] J. Bardeen and W. Shockley, Phys. Rev. **80**, 72 (1950).
[4] D. Lazarus, Phys. Rev. **76**, 545 (1949).

The change in energy gap due to the application of a pressure P to the sample is then calculated from the equation below, which follows from (7), where the values of n and m_n at zero and high pressure are obtained by the methods previously described.

$$\Delta E_g=-kT\left[\ln\left(\frac{n_p}{n_0}\right)+\ln\left(\frac{n_p+p_0}{n_0+p_0}\right)\right]+\tfrac{3}{2}kT\ln\left(\frac{m_{np}}{m_{n0}}\right). \tag{8}$$

No allowance has been made for a change in the effective mass for holes, since it cannot be deduced from the data. Further justification for this procedure is that the mass of the holes is nearer that of the free electron mass and should be less sensitive to pressure. The calculated values of $(\partial E_g/\partial P)_T$ are given in Table II along with the corresponding values of $(\Delta\mu_n/\mu_{n0})$ and $(\Delta m_n/m_{n0})$ for 2000 atmospheres pressure.

The lower value of $(\partial E_g/\partial P)_T$ at 54.3°C may be due to the onset of degeneracy at this temperature. The apparent value of $(\partial E_g/\partial P)_T$ would be lower than the true one when degeneracy is present in InSb, because the conduction band empties as the energy gap increases thereby decreasing the difference in energy between the bottom of the conduction band and the lowest state into which an electron may be excited. The variation in the fractional changes in electron mobility at the different temperatures might be explained either as a true effect or as the result of neglecting any variation of mobility ratio with pressure when calculating μ_n from Eq. (5). It can be seen from (5) that a decrease in c would tend to bring the three mobility decrease values into closer agreement.

ACKNOWLEDGMENTS

The author wishes to express his gratitude to Professor Park H. Miller, Jr., of the University of Pennsylvania for his guidance and assistance during the course of this work. Thanks are also due to Dr. R. G. Breckenridge of the National Bureau of Standards for providing the sample of InSb, to Mr. John Bowen of Pressure Products Industries for assisting in the design and construction of the high-pressure system, and to Professor H. B. Callen of the University of Pennsylvania for several suggestions regarding interpretation of the results.

Infrared Stimulation and Quenching of Photoconductivity in Luminescent Powders*†

HARTMUT KALLMANN, *Department of Physics, New York University, Washington Square, New York, New York*

BERNARD KRAMER, *Department of Physics, New York University, Washington Square, New York, New York and Physics Department, Hunter College, Bronx, New York*

AND

ARNOLD PERLMUTTER‡, *Department of Physics, New York University, Washington Square, New York, New York*

(Received October 19, 1954; revised manuscript received January 28, 1955)

Ac measurements of impedance changes in (ZnCd)S fluorescent powders upon addition of infrared radiation (a) simultaneously with the exciting ultraviolet and (b) various periods after excitation by ultraviolet or gamma radiation are described. A decrease (quenching) of conductivity is always observed in the steady state (a), but in case (b) a strong increase (stimulation) is often observed. The simultaneous quenching shows two maxima, one in the 7500 A region, the other about 12 500 A, but the stimulation decreases monotonically with increasing wavelengths. These two effects (quenching and stimulation) are superimposed; quenching can most easily be observed at relatively high conduction electron density, while stimulation is most easily observed long after excitation has ceased. The conductivity stimulation can be observed with most (ZnCd)S phosphors many days after cessation of excitation; thus these materials act as storage phosphors in which, however, the storage properties are observed by conductivity stimulation. Their light stimulability is often small. A specially activated Fonda-type storage phosphor with a very high light stimulability, however, shows only small conductivity stimulation. An explanation of this behavior and the wavelength dependence of the stimulation and quenching in terms of the action of infrared irradiation on trapped and valence-band electrons is given.

INTRODUCTION

THE change in conductivity of (ZnCd)S phosphors during and after excitation by light or high energy radiation has been investigated by means of dc and ac measurements.[1,2] The change of impedance observed in ac measurements was shown to be due to the increase in conductivity (more electrons in the conductivity band) of the phosphor rather than an increase in dielectric constant due to highly polarizable filled traps.[3] A simple model of conducting and nonconducting layers (the latter due to air spaces between separate grains, and between the electrodes and the sample) explains the main features of the capacitance saturation and shape of the Q-value curve.[2,4,5] In addition, the fact that the application of infrared light after excitation temporarily increased the capacitance change indicated even more conclusively that the impedance changes stemmed from changes in the conduction electron density rather than changes in the number of occupied traps.

It is well known that if infrared radiation is applied simultaneously with the exciting radiation, a quenching is observed in both the fluorescence and dc photoconductivity. Such quenching has been explained on the basis of the infrared light producing new possibilities of transitions of excited electrons to the ground states. However, the fact that some phosphors show first an increase in conductivity or light emission or both indicates that there is also an increased probability of transitions from traps to the conduction band.

After special activation, some (ZnCd)S phosphors display an increase in light emission due to infrared irradiations which may be observed many days after excitation has ceased (storage phosphors). A corresponding stimulation of conductivity has not been previously investigated, but should be expected if some electrons enter the conduction band when expelled from traps.

It should be noted that since some electrons may leave traps and recombine with the positive charges without emitting light, glow curves may not be a completely valid way of detecting traps. However, it is possible that such traps may empty into the conductivity band under infrared irradiation and thus will be detected by ac conductivity measurements (dc measurements are far less sensitive than ac measurements because of the existence of blocking layers). All traps, whether leading to radiative or nonradiative transitions can be also detected by the so-called "rise time" curves for photoconductivity and for light emission, since steady photoconductivity or light emission sets in only when all traps are filled to their equilibrium values. Such measurements, which will be reported in a later paper, show that practically all (ZnCd)S phosphors have deep traps whose number (for all substances) are of the same order of magnitude so that obviously a lack

* This work was supported by the Signal Corps Engineering Laboratories, Evans Signal Laboratory, Belmar, New Jersey.

† In partial fulfillment of the requirements for the Ph.D. degree (A.P.), Graduate School, New York University.

‡ Now at The Cooper Union, Department of Physics, Cooper Square, New York 3, New York.

[1] H. Kallmann and B. Kramer, Phys. Rev. **87**, 91 (1952); see also E. A. Taft and M. H. Hebb, J. Opt. Soc. Am. **42**, 249 (1952).

[2] Kallmann, Kramer, and Perlmutter, Phys. Rev. **89**, 700 (1953); for a general review article on this subject see J. Roux, J. phys. radium **15**, 176 (1954).

[3] G. F. J. Garlick and A. F. Gibson, Proc. Roy. Soc. (London) **A188**, 485 (1947).

[4] C. G. Koops, Phys. Rev. **83**, 121 (1951).

[5] M. Borisov, Isvest. Bulgar. Akad. Nauk. **2**, 281 (1951).

TABLE I. Characteristics of phosphors investigated.

Powder	Composition	Color	Light[a] persistence After 1 min	After 5 min	Conductivity quenching (Simultaneous ultraviolet and infrared) Short wavelength A	$\delta C/C_0$, %	Long wavelength A	$\delta C/C_0$, %	Relative[b] light stimulability	Relative[c] current stimulability
Powder *A*[d]	ZnS(Cu)	Green	1.2×10^4	1.9×10^3	8500	4.5	12 500	3	5×10^5	100
LG-2150[e]	ZnS(Cu, Pb)	Green	3.5×10^5	2.9×10^4	6500	35	12 000	8	5×10^6	Negligible
Powder *O*	(ZnCd)S(Cu)	Orange	1.2×10^3	90	7500	6	12 000	1	1.6×10^4	100
Powder *N*	ZnS(Ag)	Blue	5.1×10^3	7.3×10^2	7000	1	12 500	0.7	1.8×10^3	3
Powder *R*[f]	ZnS(Cu)	Green	1.1×10^5	7.4×10^4	6500	12	12 000	2	7×10^5	1000
Powder *B*[d]	ZnS(Ag)	Blue	1.7×10^3	50	7000	1.5	12 500	1	1.7×10^5	100
Powder *M*[f]	ZnS(Cu)	Green	1.5×10^5	1.9×10^5	7000	2	12 500	1	3.8×10^5	10
Powder *K*	(ZnCd)S(Cu)	Yellow	5	2.5	7500	4	12 000	2	2.8×10^5	Negligible

[a] Arbitrary units; initial fluorescence about 150×10^6.
[b] Arbitrary units; 1 hour after ultraviolet excitation to trap saturation; 7-69 filter for infrared stimulation.
[c] Arbitrary units; 7-69 filter for infrared stimulation; values given are very approximate, since the exact determined ΔC peak cannot accurately be converted to induced conductivity.
[d] Supplied by the courtesy of Philips, Eindhoven; glow curve indicates only shallow traps [H. A. Klasens, J. Electrochem. Soc. 100, 172 (1953); W. Hoogenstraaten, J. Electrochem. Soc. 100, 356 (1953)].
[e] Manufactured by New Jersey Zinc Company.
[f] Powder *R* has Cu concentration of 0.007 percent; Powder *M* has Cu concentration of 0.004 percent.

of light or current stimulation is due to other causes than a mere lack of deep traps.

The measurements to be described in this paper are a continuation of the ac measurements previously discussed,[2] but in which the effect of application of infrared irradiation simultaneously with excitation, or during the decay period is more thoroughly investigated. It will be shown that almost all (ZnCd)S phosphors (even those with no light stimulation) contain deep traps which, when emptied, increase the conductivity of the powder sample, and that their photoconductivity is stimulable by infrared light days after excitation even without special activation. In addition, it will be shown that the infrared wavelengths most suitable for light stimulation in storage phosphors are also very important in photoconductivity, but that there is no direct correlation between current and light stimulation.

It will be recalled[2] that an increase in conductivity results in an increase in the measured capacity of the powder sample up to the point where the saturation value of the capacitance is reached. The Q-curve, on the other hand, goes through a minimum with increasing excitation, and is steep only at low or high intensities. Thus, for most cases, the change in measured capacity will be used as an indication of the conductivity; however, at low intensities where the capacitance curve is flat or at high intensities where the capacitance curve is close to saturation, the Q-values are more sensitive to conductivity changes.

The experimental results will be described in two parts; the first dealing with the effects obtained with simultaneous application of infrared irradiation (steady state), the second dealing with the effects obtained when infrared is applied after excitation.

The powders investigated were chosen to represent a wide range of characteristics as far as composition, activators, and light persistence and stimulation are concerned (see Table I).

2. EXPERIMENTAL RESULTS

A. Apparatus

The impedance measurements described were obtained with a General Radio 716-C Bridge (Schering type) with an oscilloscope used as a detector.[6] The powder samples were made using a small amount of Duco cement as a binder, the areal density ranging between 5 and 25 milligrams/cm². The electrodes were Nesa glass on one side and a flexible aluminum foil under pressure on the other side. With foils of several cm² in area, dark capacitance values up to 100 micromicrofarads were obtained. (The foils must be pressed strongly against the powder, otherwise a thin air layer adjacent to the electrode may diminish the capacity in an uncontrolled way.)

The excitation was provided by either a Mineralight or Hanovia ultraviolet source filtered so that most radiation was around 3650 A. The actual intensity incident on the powder was about 10 microwatts.

Infrared irradiation was supplied either by a 250-watt tungsten source through suitable filters or with a

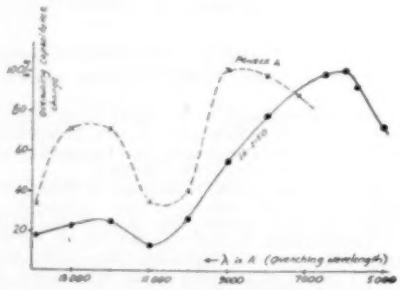

FIG. 1. Capacitance quenching (simultaneous ultraviolet and infrared) as a function of infrared wavelength for powders *A* and *LG*-2150. (Normalized.)

[6] Measuring frequency 1000 cps or 10 000 cps.

Bausch & Lomb monochromator. The intensity of the former over the entire infrared region was about 10 milliwatts/cm²; the latter was adjusted so that about 100 microwatts/cm² was obtained at any wavelength setting. The particular filters used with the tungsten source will be described below. The substances used are listed in Table I together with their electrical and optical characteristics.

The gamma source used in the experiments is a 1-millicurie radium source placed at an average distance of about 1 inch from the sample (1.3 r/hour).

B. Simultaneous Infrared Irradiation

All (ZnCd)S luminescent powders investigated display a quenching[7] of conductivity in the steady state under infrared irradiation (0.7 to 1.5 microns) added to existing ultraviolet excitation; that is, the capacitance decreases, and Q increases for low excitation intensities (left side of the Q-curve, Fig. 2 of reference 2). This

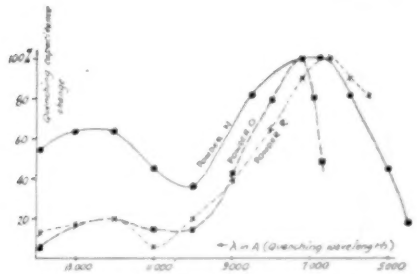

FIG. 2. Capacitance quenching (simultaneous ultraviolet and infrared) as a function of infrared wavelength for powders N, O, and R. (Normalized.)

quenching is also observed in the fluorescence and dc conductivity of all (ZnCd)S powders measured.

Figures 1 and 2 show this quenching effect for five different samples. Table I also includes information on 3 additional powders. The quenching there is given in terms of the change of capacitance from ultraviolet to ultraviolet plus infrared excitation $\delta C = (C_{uv} - C_{uv+ir})$ divided by the dark capacitance (C_0); and the abscissa gives the wavelength of infrared irradiation. In the curves (Figs. 1, 2) the ordinates are given in percentage of the maximum quenching, which can be taken from Table I. It can be seen that for these substances there are two quenching maxima; one in the 12 500 A region; the other below 9000 A. Only powder A gives approximately equal quenching in both bands; the others show much stronger quenching at the shorter-wavelength region.

Since the capacitance for all these powders changes

[7] There is also a temporary increase in conductivity immediately after infrared application; this is especially noticeable at low ultraviolet intensities and is due to a release of trapped electrons into the conductivity band or due to the creation of free holes in the valence band.

TABLE II. Correlation of capacitance change and intensity at about 0.1 microwatt/cm².

Phosphor	Percentage change for factor of 10 in intensity
Powder *A*	12
Powder *LG*-2150	8
Powder *O*	13
Powder *N*	10
Powder *R*	10

by 5 to 20 percent[8] when the intensity of excitation in the range used is changed by a factor of 10 (see Table II for actual percentage for each powder), these measurements show that the highest capacitance quenching (*LG*-2150) corresponds to a change in excitation greater than two orders of magnitude at the short-wavelength band, and by a factor of almost one order of magnitude at long wavelengths. All other samples show a quenching by a factor smaller than one order of magnitude at short wavelengths, with a smaller quenching at long wavelengths. All these infrared quenching measurements were carried out with constant ultraviolet excitation of about 0.1 microwatt/cm².

The quenching curve for powder A shows that a peak is reached at about 9000 A rather than about 7500 A as for most other substances. It will be shown below that this may be due to a simultaneous infrared-induced stimulation of conductivity that is particularly strong in the 7500 A region for this substance. This stimulation is always overridden by the quenching effect in the steady state with simultaneous excitation as will be discussed below. However, during the decay it shows up clearly immediately upon application and removal of infrared irradiation; as noted before, it also shows up as a temporary increase in conductivity during excitation before the over-all quenching sets in. It may be noted that the over-all shape of quenching *vs* wavelength curve (Figs. 1, 2) does not show much dependence either upon the Cd content, type of activator, or luminescent properties, except that the quenching drops

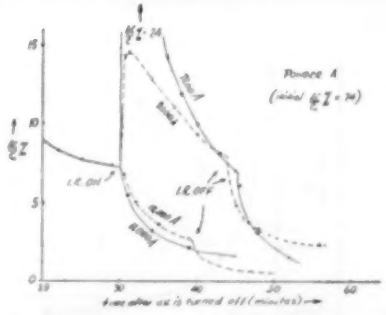

FIG. 3. Change in capacitance upon application of various infrared wavelengths after ultraviolet excitation for powder A.

[8] For the general shape of capacitance *versus* intensity curves see reference 2.

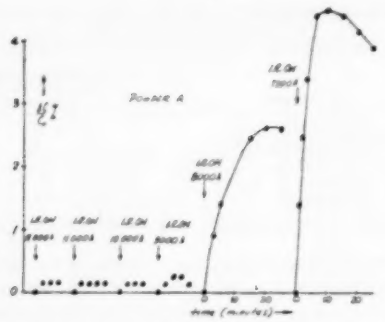

FIG. 4. Change in capacitance upon application of various infrared wavelengths three days after ultraviolet excitation for powder *A*.

off more steeply at the short wavelength end for (ZnCd)S powders, since they can already be excited in this wavelength region.

C. Infrared Irradiation after Excitation

Figure 3 shows the effect of infrared radiation of various wavelengths during the current decay of a powder *A* one-half hour after removal of 10 microwatts of ultraviolet excitation. Infrared at 7200 A and 8000 A shows a strong increase in capacitance (stimulation of conductivity) contrary to the quenching obtained with simultaneous ultraviolet excitation (Fig. 1); these changes of capacitance are described by $\Delta C = C_{uv} - C_0$. When the infrared light is turned off there is a sharp instantaneous drop in capacitance even below the normal decay curve. This is another indication of conductivity stimulation[7] and allows the detection of such stimulation even when the over-all effect is that of quenching. Using 10 000 A and 12 000 A infrared irradiation, a strong quenching of the decaying conductivity is observed. Although these wavelengths show a pronounced quenching, the instantaneous sharp drop when these wavelengths are turned off indicates some stimulation is occurring although it is almost negligible at 12 000 A.

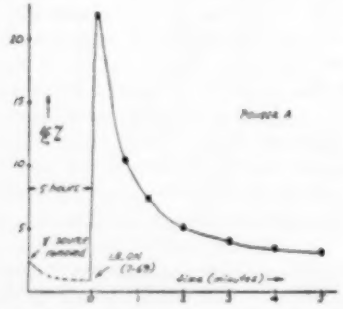

FIG. 5. Change in capacitance due to infrared irradiation five hours after gamma excitation for powder *A*.

A long-time stimulation (performed a long period of time after excitation) of this powder is shown in Fig. 4. The powder was excited by ultraviolet and, after a three-day period in the dark, was irradiated successively by infrared of 12 000, 11 000, 10 000, 9000, 8000 and 7200 A in that order. Down through 10 000 A there was very little stimulation (the small increase in capacity may be due to some stray light), but at 8000 A and 7200 A there is a marked increase of capacitance reflecting the increase of conductivity.

This experiment shows conclusively that the capacity changes noted in (ZnCd)S powders cannot be due to electrons while they are in traps since these curves show that the capacitance is increased when the traps are emptied, presumably into the conduction band.

These capacitance changes may be compared to the light emission obtained with storage phosphors when irradiated with infrared a long time after excitation; these changes of capacitance are due to a stimulation in conductivity and are thus not limited to the presence of a second activator which makes a luminescent material a good light stimulable phosphor. It will be shown

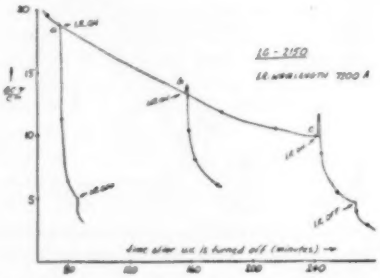

FIG. 6. Change in capacitance due to infrared irradiation during conductivity decay of Fonda phosphor *LG*-2150.

that light stimulation does not necessarily require an increase of the density of electrons in the conductivity band; thus such a storage phosphor may not show current stimulation because the probability of recombination accompanied by light emission is so large that the lifetime of the electrons in the conductivity band may be quite short.

Powder *A* also shows a strong stimulation 5 hours after gamma irradiation (Fig. 5). After the capacitance change had decreased from 2.5 percent to 1 percent, a stimulation greater than 20 percent was observed when infrared irradiation was applied. The capacitance change rises to a peak of 20 percent at this time although the capacity change during excitation was only about 2.5 percent, indicating that the gamma excitation was utilized mainly in filling traps, rather than building up a large conduction-electron density. A 7-69 filter was used in this experiment; this passes a band of infrared between 7200 A and 10 000 A with an intensity of about 1 milliwatt/cm^2. Thus in the case of very weak excitation such as with high-energy radiation (the gamma

excitation corresponded to an absorbed energy of only 4×10^{-11} watt/cm^2), radiation is much more easily detectable by stimulating the sample after a certain time of irradiation and observing its capacitance change than by measuring this change during excitation.

Figure 6 shows the effect of infrared irradiation during the decay of the conductivity of powder *LG*-2150, a strong light-stimulable phosphor. Although this particular powder is a Fonda-type[9] phosphor [ZnS(Cu,Pb)] and shows tremendous light stimulation, the over-all current stimulation is quite small (when observed) and a large quenching is obtained when infrared of 7200 A is applied. This is in agreement with the strong simultaneous infrared conductivity quenching for this powder. This strong quenching is presumably caused by recombinations accompanied by light emission which are very frequent in this substance (see conclusions). The current stimulation cannot be observed until after several hours of decay [points (b) and (c) of Fig. 6], earlier (a) only the quenching can be seen. However, after the infrared is removed, a further drop is observed, indicating that

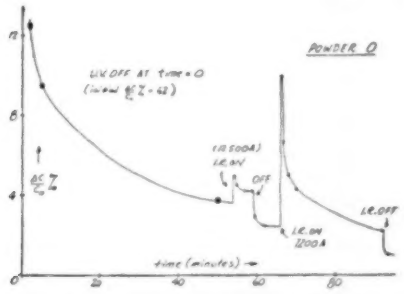

FIG. 7. Change in capacitance due to infrared irradiation during conductivity decay of powder *O*.

some current stimulation was occurring during the quenching. Another factor tending to decrease any current stimulation is the fact that this powder has an extremely slow rate of decay; that is, even after several hours the remaining conductivity is still large. Thus, the quenching effect (which is already large for this particular phosphor) is far more important than the stimulating effect. This highly light-stimulable substance is the one which shows the weakest current-stimulation, even when this long decay of conductivity is taken into account.

A decay curve starting with full (ultraviolet) excited sample shows a slow decrease similar to Fig. 6; 15 hours after excitation the application of infrared of 7200 A shows a stimulation, but much smaller than with powder *A*, then a quenching; radiation with 12 500 A, however, shows only quenching.

The effect of infrared irradiation on the conductivity of an orange-luminescent phosphor with very short light decay (powder *O*) is shown in Fig. 7. A much

[9] G. R. Fonda, Trans. Electrochem. Soc. **87**, 339 (1945).

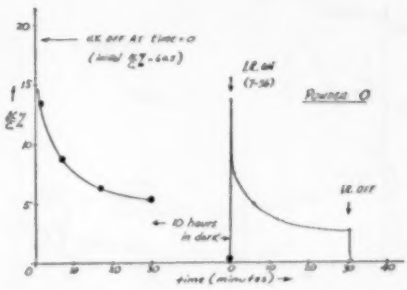

FIG. 8. Change in capacitance due to infrared irradiation 10 hours after ultraviolet excitation for powder *O*.

faster conductivity decay is observed (few shallow traps) than with the long decaying 2150 substance. About 1 hour after excitation, the application of 12 500 A infrared results in a small but noticeable capacitance increase (current stimulation). Following this, 7200 A infrared is applied, and a much stronger stimulation is observed. A still stronger stimulation is observed (Fig. 8) when the sample is left in the dark for 10 hours and irradiated using a 7-56 filter.[10] Thus, again, a long-time stimulable conductivity is observed, even with a short persistent, practically nonlight-stimulable (ZnCd)S phosphor.

Previous gamma excitation also yields a stimulation of conductivity. About one-half hour after the gamma radiation has been removed, a strong current stimulation is observed with 7-56 infrared irradiation. All the traps were not emptied in the first infrared application; after 2.5 hours in the dark a second infrared application again resulted in a noticeable further stimulation.

Powder *N* is also a relatively fast-decaying powder, dropping from a capacitance change of 62 percent to 20 percent in less than 10 minutes, again indicating only a small density of shallow traps. Short-wave infrared irradiation (7-69 filter) shows a strong stimulation 20 hours after full ultraviolet excitation (Fig. 9) indicating a considerable number of deeper traps. If infrared irradiation of longer wavelength (7-56) is applied,

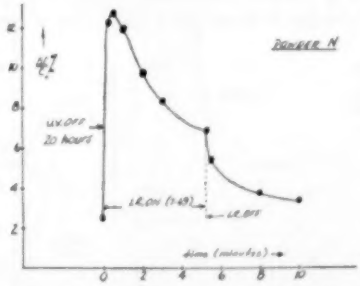

FIG. 9. Change in capacitance due to infrared irradiation 20 hours after ultraviolet excitation for powder *N*.

[10] Passing wavelengths greater than 8000 A, intensity about 10 milliwatts/cm^2.

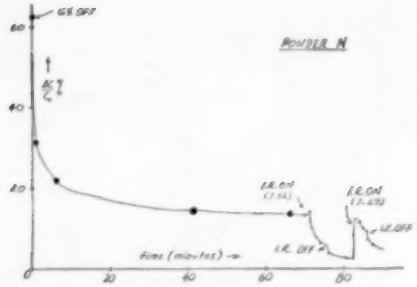

FIG. 10. Change in capacitance due to infrared irradiation during conductivity decay for powder *N*.

about 70 minutes after full ultraviolet excitation (Fig. 10), only a short stimulation pulse is noted followed by a pronounced quenching. If infrared is applied by using a 7-69 filter after application of the longer wavelength infrared, a stimulation peak similar to that of Figs. 9 and 11 is obtained. One hour after gamma excitation, stimulation by 7-69 infrared irradiation is also observable (capacity changes from 4 to 10 percent) with this powder (Fig. 11).

Powder *R* displays a very long light decay and weak stimulated light emission; its conductivity is also slow-decaying but shows strong stimulability. In Fig. 12 can be seen the very slow decay followed by the quenching when infrared of various wavelengths are applied 20 minutes after excitation has ceased. The wavelength showing the strongest quenching is 7200 A followed by 9000 A, 12 000 A, and 10 500 A, respectively, exactly as could be inferred from the simultaneous quenching curve (Fig. 2). It should be noted that the two short wavelengths show small stimulation peaks before quenching sets in; this stimulation can also be seen from the further drop in the decay of conductivity when these wavelengths are turned off. The long wavelengths, however, produce no noticeable stimulation although the quenching effect is weaker. The stimulation using 12 500 A twelve hours after full ultraviolet excitation is scarcely noticeable (about 0.25 percent capacity change) followed by a quenching of the same

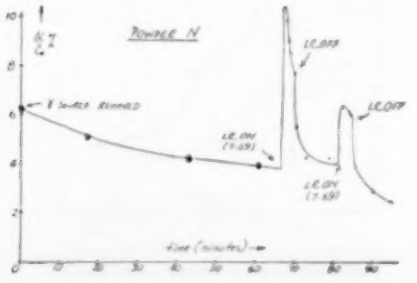

FIG. 11. Change in capacitance due to infrared irradiation after gamma excitation for powder *N*.

order of magnitude. When the infrared was turned off there was a further drop of 1 percent capacity change.

This powder however shows strong stimulation using 7200 A infrared irradiation about one hour after gamma excitation (Fig. 13). A tremendous increase in capacity is observed (25 percent) although the equilibrium capacitance change after 15 hours of gamma excitation is only 12 percent. The reason for the large stimulation peak in this run is due to the much smaller conductivity present immediately before stimulation (see Sec. 3).

Besides these substances, other phosphors have been investigated with similar results. These are given in Table I. It is seen that one of the two substances with weak current stimulation is 2150, which showed the highest stimulated light emission.

It may be noted that there is a definite similarity between the light decay curves and the capacity decay curves when the relation between $\Delta C/C_0$ and intensity of excitation is taken into account (Table II). Thus

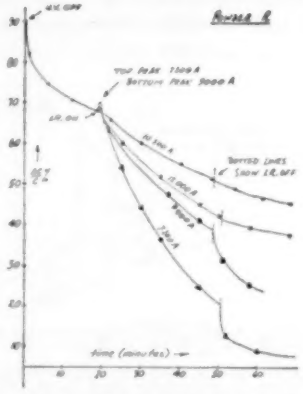

FIG. 12. Change in capacitance due to various infrared wavelengths during conductivity decay for powder *R*.

powders *LG*-2150 and *R* which show the longest light persistence also show the longest conductivity persistence, while powder *O* which has almost no light persistence shows an extremely fast current decay. After several minutes the conductivity of powder *R* has decreased to approximately one-tenth the initial value, while in the same time interval powder *O* has decreased to 10^{-5} of the initial value.

The increase in capacitance under infrared irradiation can be transformed to equivalent excitation intensity (Table II), and the stimulations observed can thus be compared with each other. This is done in the last column of Table I for stimulation after previous excitation. Thus the last two columns give an approximate comparison between light stimulability and current stimulability for the powders investigated. It is quite evident that the powder with the highest current stimulability has a relatively weak light stimulability, while the highest light-stimulable powder has one of the weakest current stimulabilities.

It should be mentioned that all the capacitance changes observed under illumination or stimulation can be duplicated by observing the dissipation factor or the Q-value instead. In this case, however, it must be considered that the Q-factor changes with increasing conductivity quite differently from the capacitance. With increasing conductivity it first drops sharply, goes through a minimum and rises again with increasing conductivity (see Fig. 4 of reference 2). Hence, with current stimulation, for instance, a decrease of Q is obtained if one works on the descending branch of the Q-curve, but an increase will result on the ascending branch of the Q-curve; with current quenching just the converse effects are obtained. Since it is not always possible to say in which part of the Q-curve the observations are performed, especially if fast changes in conductivity occur, it is more convenient to investigate the changes in C in order to gain information about the changes in conductivity. As an example, the corresponding changes of C and Q for a sample of powder O are described in Fig. 14 for excitation, decay, stimulation, and quenching. In the first 40 minutes the conductivity buildup is seen and the rise in C is accompanied by a drop in Q. When the exciting ultraviolet illumination is turned off (first broken line), C drops and Q rises but not quite to its original dark value. When infrared is turned on (second broken line), C abruptly jumps to a high value and Q drops just as fast; then C drops slowly again because of the decay of conductivity under infrared irradiation. Q, however, drops even further at the beginning because with this stimulation a point was reached which was on the right side of the Q-minimum. After passing this minimum, the Q-value rises since at low conductivity the Q values increase with decreasing conductivity.

3. CONCLUSIONS AND DISCUSSION

In general, the discussion of stimulation and quenching of light emission or conductivity in the (ZnCd)S phosphors by infrared radiation has involved the release of electrons from traps and the production of free holes in the valence band. On the basis of the above experiments it is possible to complement this mechanism.

First, it must be stressed that these experiments on conductivity stimulation and quenching show that different elementary processes are induced by the same infrared wavelengths. Quenching is most obviously observed in the steady state (simultaneous excitation and infrared irradiation). Here infrared irradiation decreases the light emission and also the conductivity over the whole range of infrared wavelengths with two maxima of quenching, around 12 500 A and 7000–8000 A. It must, however, be borne in mind that this observed decrease in conductivity is a superposition of a stimulation and a quenching process in which the quenching effect always prevails. This is noteworthy since it is not as evident as it is in the case of light

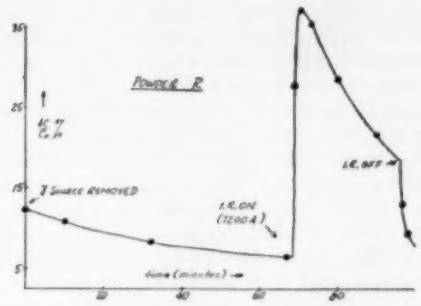

FIG. 13. Change in capacitance due to infrared irradiation after gamma excitation for powder R.

emission. Without infrared irradiation, most excited electrons return to the ground state accompanied by light emission; hence additional infrared irradiation cannot increase the light emission in the steady state, since almost all excited electrons emit light in any case. Therefore, if infrared creates nonradiative transitions, the over-all effect must be that of light quenching, and this is correct even when some slight quenching also occurs under normal conditions without infrared.

This is not necessarily the case with conductivity, which depends upon the density of electrons in the conduction band (and perhaps to a lesser degree on that of holes in the valence band). The density in the conduction band would be increased if infrared irradiation only releases additional electrons into this band from traps and would be decreased if infrared irradiation only produces new transitions to the valence band (recombination); the experiments show that both processes occur simultaneously and thus it is not evident which process will prevail. The experiments show that in the steady state the density of electrons in the conduction band is always decreased by infrared irradiation (at least at room temperature); this means that the

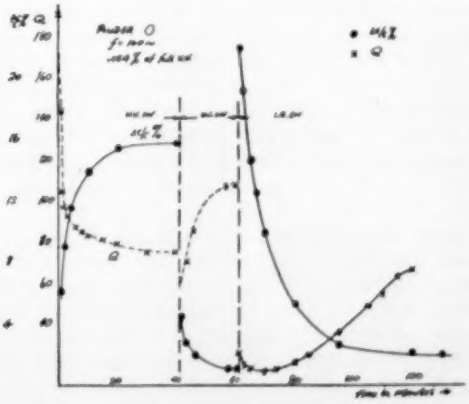

FIG. 14. Capacitance change and Q-curve for powder O showing excitation, decay, and infrared stimulation.

drain of electrons from this band by recombinations created by infrared irradiation surpasses the stimulation of electrons into the conductivity band.

Stimulation is more easily observed in the nonsteady state, along the decay curve of conductivity. Here the net effect also depends on the magnitude of both stimulation and quenching. Since the amount of quenching depends on the density of electrons already present in the conduction band before infrared is applied, the absolute amount of quenching is low when only a small conductivity (low-conduction density) is available to be quenched. But stimulation can then be easily observed since electrons are released from deep traps (filled by previous strong excitation) into the nearly empty conduction band. Thus at high-electron density in the conduction band (immediately after excitation) the net effect is often that of quenching or of only small stimulation, whereas further along the decay curve stimulation becomes more pronounced particularly for shorter infrared wavelength; at very low conductivity (very long after excitation) quenching obviously cannot be detected at all. These effects are similar to those observed with dc conductivity.[1]

It may be emphasized again that stimulation into the conduction band can still be observed even when the over-all effect is that of quenching along the decay curve. If, during the ac conductivity decay, the infrared radiation is turned off, a further instantaneous drop in conductivity occurs (see Fig. 6, for instance). This drop is caused by the sudden cessation of the electron transfer from traps into the conduction band due to infrared. The magnitude of this drop is thus also a measure of the stimulation by infrared.

It is found that stimulation decreases monotonically with increasing λ and practically vanishes in the region of 12 000 to 13 000 A. Thus, the wavelength dependence of current stimulation and of quenching seem to be quite different since the quenching displays two maxima, one in the region where stimulation has practically vanished.

The maxima of the quenching process can be observed, not only in the steady state (simultaneous excitation and infrared irradiation) but also along the decay curve. The drop in the decay curve due to infrared irradiation (see for instance Fig. 12—powder *R*) is stronger for 7200 A than for 9000 and 10 500 A but increases again for 12 000 A in complete agreement with the steady-state quenching curve of this substance (Fig. 2).

Light stimulation and quenching differ in behavior from that of the conductivity. The observed light quenching curves show similar maxima as the current quenching curve, indicating that both are in some way connected with each other, but when the influence of infrared on the light decay is studied, especially in the Fonda-type phosphors, strong light stimulation often occurs at the same wavelengths where current quenching prevails. Further, the light-stimulation curve is not monotonic but displays the same maxima as the quenching curve. Strong-light stimulation occurring a long time after excitation has ceased and due to special activation is relatively rare, whereas current stimulation of such a type occurs in many substances.

To explain these observations together with the known effects of light stimulation in Fonda-type phosphors,[11] it is assumed that the current stimulation is always due to the release of electrons from traps ranging down to approximately one volt (measured from the bottom of the conduction band); that traps of such depth are present in appreciable number follows from the fact that stimulation of conductivity (not the conductivity itself) decays only extremely slowly with time (three days after excitation considerable conductivity is still stimulated; Fig. 4). Before the addition of infrared, the number of trapped electrons are in equilibrium with the number in the conduction band (n_c) in accordance with the equation[1]

$$n_c/n_t = n_c/n_{0t} + \delta_t/\beta n_{0t},$$

where n_t is the number of electrons occupying the traps of kind t, n_{0t} is the total number of traps of kind t available (both per unit volume), β is the probability for trapping, assumed equal for all traps, and δ_t is the probability per unit time of release of electrons from traps. Such an equation holds separately for each trap level. The addition of infrared irradiation effectively increases the δ_t term, as if a higher temperature were applied. The effect, therefore, for $n_c \ll n_t$, is that a larger number of electrons is now transferred into the conduction band, and an increase in conductivity would occur if the infrared induced no additional recombinations.

The quenching of light[12] and conductivity by infrared has been ascribed to the production of free-moving holes (*E* in Fig. 15) in the valence band by lifting electrons out of the valence band into some higher energy level (perhaps an ionized activator). The holes thus created are free to move and recombine with free (*D*)

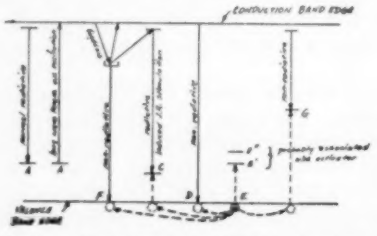

FIG. 15. Energy-level diagram for (ZnCd)S phosphors. *A* activators; *B* traps; *C* special activators (i.e., Pb); *D* radiationless recombination of hole and free electron; *E* hole; *F* radiationless recombination of trapped electron and hole; *G* radiationless recombination at quenching center.

[11] See Fig. 15 for transitions discussed in the following paragraphs.

[12] M. Schon, Z. Physik **119**, 470 (1942); Ann. Physik **3**, 333 (1948).

or trapped (F) electrons directly or indirectly via centers (C, G), thus tending to decrease the density of conduction electrons. Light quenching, however, will only occur if some of these recombinations are nonradiative. It will be also assumed for the purpose of explaining the two quenching maxima, that there are at least two different energy levels involved in the production of holes (E', E'').

We attribute these two levels to the hole production process rather than to the release of electrons from traps because these maxima only occur in the current quenching and not in current stimulation. Besides this, there is evidence from investigation of light stimulation[13] indicating that these two maxima are not connected with different levels of trap. Of course, if this assumption is made, one must explain why two maxima occur in light stimulation and not in current stimulation. This will be done below.

The free holes moving in the valence band do not essentially contribute to conductivity since no indication of current stimulation is found for long wavelengths where a quenching maximum occurs. This may be due to the fact that the holes recombine quickly with the available electrons or are otherwise immediately retrapped.

In all (ZnCd)S phosphors tested up to now in this laboratory there was a definite quenching of the conductivity under additional infrared radiation (also noted in fluorescent light emission). This may be understood as follows. The electron density in the conductivity band at a certain ultraviolet intensity is mainly determined by the many shallow traps and not as much by the deep traps which are filled to saturation. From the shallow traps there is a constant release of electrons into the conduction band by thermal action (δ_t). Infrared irradiation increases this release, but not by a very large amount relative to this constantly present release by thermal action; the recombinations with the valence band, however, occur relatively seldom without infrared and are tremendously increased by such irradiation (as radiative or radiationless transitions) and the experiments show that this increase surpasses the increase in total release of electrons into the conductivity band.

The results obtained with light stimulation may be explained as follows. In the long-time light-stimulable substances (Fonda phosphor), two maxima in light stimulation occur corresponding to the quenching maxima of the light[9,14] and conductivity; the stimulability at the long infrared wavelength does not persist very long but decays considerably within one day.[15] To explain the coincidence of the light-stimulation maxima with those of conductivity-quenching maxima, it is assumed that at least two types of current-quenching centers exist; one which induces recombination accompanied by light emission (C), and the other which gives rise to radiationless transitions (D, F, and G). Both induce current quenching but only the second type causes light quenching. If the recombinations via the radiative centers are more probable (perhaps because of a larger recombination cross section) than the normal radiative transition via the activators and via the nonradiative centers, then light stimulation will be at its maximum when hole production is at a maximum and thus the quenching maxima and the light stimulation maxima will coincide in wavelength. The long wavelength light stimulation comes about by a recombination of electrons still in the conduction band or in shallow traps with the freed holes (via the aforementioned centers) whereas the short-wave maximum comes about by the simultaneous release of electrons from deep traps and of holes and their recombination thereafter. Thus in the case of special radiative centers, hole production induces light stimulation and strong current quenching since the probability of transitions to the ground state is augmented by the additional radiative centers. Thus it is found, particularly with light stimulable substances, that the net effect on conductivity (even at short wavelengths) is that of strong quenching soon after excitation; only at the later parts of the conductivity decay curve does stimulation become noticeable. However, in any case in such a substance the current stimulation is found to be weak since it is simultaneously counterbalanced by strong recombinations. In accordance with these ideas it was found that some substances with weak light stimulation show strong current stimulation.

The investigations reported in this paper show that the so-called storage phosphors are not as much distinguished by their storage properties as by their capability of light stimulation. The stimulation of conductivity long after excitation is very common and occurs in nearly all substances, indicating that many of them have equal storage qualities, but they differ tremendously in their capability of light emission when they are stimulated.

In this connection it may be noted that three methods of detecting electrons stored in deep traps have been discussed, namely the rise-time method, the infrared stimulation of light emission, and the infrared stimulation of conductivity. There is still another effect which can be used to detect such filled traps, the effect of persistent polarization in such photoconductive substances.[16] The persistence of this polarization depends on the time that electrons stay in these traps, and by measuring the decay of this polarization it is possible to obtain information about the number and depth of these traps.

In conclusion, it should be stressed that the given

[13] (to be published).
[14] Polytechnic Institute of Brooklyn, Final Report for Contract NObsr 39045, June 30, 1949 (unpublished).
[15] (to be published).
[16] H. Kallmann and B. Rosenberg, Phys. Rev. **97**, 1596 (1955).

explanation may not be the only one that can be chosen to account for the stimulation and quenching with infrared radiation of conductivity and light in (ZnCd)S phosphors. Since it explains, with a minimum number of assumptions, the basic experimental results, and fits into the general band picture for these phosphors, it seems a reasonable starting point in a quantitative theory of the electronic transitions in such phosphors.

PHYSICAL REVIEW VOLUME 99, NUMBER 2 JULY 15, 1955

Electrical Properties of p-Type Indium Antimonide at Low Temperatures*

H. FRITZSCHE AND K. LARK-HOROVITZ
Department of Physics, Purdue University, Lafayette, Indiana
(Received April 11, 1955)

The electrical resistivity ρ, Hall coefficient R, and transverse magnetoresistive ratio $\Delta\rho/\rho$ of p-type single crystals of indium antimonide have been measured between 370°K and 1.5°K. Low-temperature anomalies similar to those observed by Hung on germanium have been found, a steep maximum in the log$R$ *versus* $1/T$ curve and a change of slope of the logρ *versus* $1/T$ curve. Contrary to the case with germanium, the magnetoresistive ratio of InSb does not vanish in the lowest temperature range, but it changes its sign from positive to negative as the sample is cooled to a temperature somewhat lower than that at which the Hall coefficient reaches its maximum value. Negative values of the magnetoresistive ratio cannot be explained by the usual theory of semiconductors. At the present time it also is not clear how Hung's model of impurity band conduction can account for negative values of the magnetoresistive ratio.

INTRODUCTION

At temperatures above 78°K indium antimonide behaves like a conventional semiconductor, as previous measurements[1,2] of the Hall coefficient and the resistivity have shown.

Several materials, however, which show the normal behavior of semiconductors at higher temperatures exhibit anomalous electrical properties at low temperatures which cannot be explained by the usual semiconductor theory. Germanium, for instance, shows large deviations from the normal behavior in the range below 50°K, as Hung[3] discovered in 1950. The Hall coefficient of germanium does not increase indefinitely as the temperature is lowered, but reaches a maximum value and decreases thereafter by orders of magnitude. In the logρ *vs* $1/T$ curve, one can distinguish a larger slope in the higher temperature range, before the Hall maximum is reached, and a much smaller slope at still lower temperatures.

Anomalies similar to those discovered by Hung on Ge have been found by Busch and Labhart[4] on SiC. Also, TiO_2 seems to show the same abnormal behavior at low temperatures, as recent measurements in this laboratory indicate.

As an explanation for the anomalous behavior of germanium at low temperatures, Hung[5] suggested that a small but finite conduction takes place in the impurity band, in addition to conduction in the ordinary conduction band.

A detailed theory of conduction in impurity bands has not yet been worked out. In any theoretical discussion, however, the explanation of the formation of a conducting impurity band with impurity concentrations as low as 10^{15}/cc is rather difficult. It would be of interest, therefore, to investigate whether other materials also exhibit anomalies at low temperatures and how they differ from those in germanium. This might throw some light on the conduction properties of impurity bands or even suggest a different explanation for the anomalies. For this reason, an investigation of the electrical properties of indium antimonide at very low temperatures has been undertaken.

This paper reports the measurements of electrical resistivity, Hall coefficient, and magnetoresistive ratio on several p-type single crystals of indium antimonide down to 2°K.[6]

EXPERIMENTAL PROCEDURE

A. Preparation of Samples

The samples used were prepared by Miss L. Roth of this laboratory. The indium obtained from the Indium

* Supported by U. S. Signal Corps.

[1] H. Welker, Z. Naturforsch. **7a**, 744 (1952) and **8a**, 248 (1953), Physica **20**, 893 (1954), also Scientia Electr. **1**, 2 (1954); H. Weiss, Z. Naturforsch. **8a**, 463 (1953); R. G. Breckenridge, Phys. Rev. **90**, 488 (1953); M. Tanenbaum and J. P. Maita, Phys. Rev. **91**, 1009 (1953); Cunnel, Saker, and Edmond, Proc. Phys. Soc. (London) **B66**, 1115 (1953); O. Madelung and H. Weiss, Z. Naturforsch. **9a**, 527 (1954).

[2] Breckenridge, Blunt, Hosler, Frederikse, Becker, and Oshinsky, Phys. Rev. **96**, 571 (1954).

[3] C. S. Hung and J. R. Gliessman, Phys. Rev. **79**, 726 (1950) and **96**, 1226 (1954); see also H. Fritzsche and K. Lark-Horovitz, Physica **20**, 834 (1954).

[4] G. Busch and H. Labhart, Helv. Phys. Acta **19**, 463 (1946).

[5] C. S. Hung, Phys. Rev. **79**, 727 (1950).

[6] Some low-temperature measurements on InSb have also been made by the Oxford group, without giving the details reported here. See J. Hatton and B. V. Rollin, Proc. Phys. Soc. (London) **A67**, 385 (1954).

Corporation of America and the antimony obtained from Bradley Mining Company were zone heated separately in a hydrogen atmosphere until they were spectroscopically pure. The metals were then melted together and zone heated sixteen times in a hydrogen atmosphere. No impurities were added to the melt intentionally. Single crystals of indium antimonide were grown by the Czochralski method at a rate of 2 inches per hour in a hydrogen flow of about two liters per minute. Single crystals weighing up to 130 grams have been obtained. One crystal was annealed at 375°C in a vacuum of about 10^{-6} mm Hg for 77 hours.

The top parts of the crystals usually have a smaller conductivity than the bottom parts. This makes it possible to cut samples with different conductivity from the same ingot. The samples were cut to a size of about 10 mm×4 mm×1 mm with their large areas transverse to the concentration gradient in order to minimize the error due to such a gradient inside the sample. The sample surfaces were then ground with No. 600 carborundum.

Measurements of the resistivity along the length of the samples at 300°K and 78°K showed the samples to be homogeneous.

TABLE I. Properties of samples of p-type InSb on which measurements were made.

InSb Sample	R (78°K) cm³ coulomb⁻¹	ρ (78°K) ohm-cm	R_{ss}/ρ (2.5°K) cm² volt⁻¹ sec⁻¹	N_A $m^*=m_0/6$ cm⁻³	N_D $m^*=m_0/6$ cm⁻³	Crystal orientation of current flow I	Crystal orientation of mag. field H
a[a]	7300	1.23	0.6	1.6×10^{16}	1.5×10^{16}	(110)	(112)
b[a]	6300	1.23	0.8	1.8×10^{16}	1.6×10^{16}	(110)	(112)
c	1200	0.19	5.9	1.6×10^{16}	6.8×10^{15}	(110)	(112)
d	200	0.072	120			(110)	(100)
e	76	0.065	180			polycrystalline	

[a] Sample a is annealed at 375°C, whereas sample b is not.

Teflon insulated 0.0003-in. copper wires were attached to the sides of the sample with Cerroseal-35 solder to serve as current and potential leads in the usual arrangement for Hall and resistivity measurements.

B. Apparatus

The cryostat and the electrical measuring circuit are identical with those used and described before.[3] The cryostat allows one to take measurements at any temperature between 1.3°K and 300°K. Care was taken that no light or room temperature radiation could reach the sample during the measurements at low temperatures.

All voltages were measured with the conventional compensating method using a type K-2 potentiometer and a Leeds and Northrup high-sensitivity galvanometer.

EXPERIMENTAL RESULTS

The samples on which measurements were made are listed in Table I. The samples a, b, c, and d are single crystals. The polycrystalline sample e is included for comparison with the other samples in the lowest temperature region. The samples a and b are identical but for the fact that b was measured before and a after it was annealed for 77 hours at 375°C.

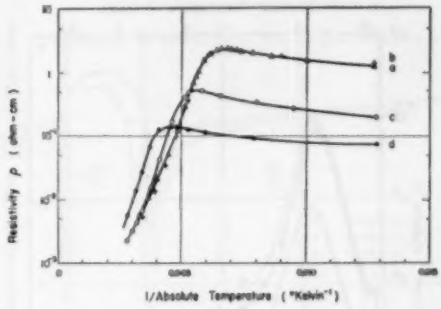

FIG. 1. Resistivity of p-type indium antimonide as a function of $1/T$ between 78°K and 370°K.

All samples were found to be p-type. In order to show that these samples of indium antimonide behave completely normally at higher temperatures and in agreement with the results of other investigators, the temperature dependences of their resistivity and Hall coefficients between 370°K and 78°K are shown in Figs. 1 and 2, respectively.

For these measurements the low-magnetic-field approximation was used for the Hall coefficient. Resistivity and Hall coefficient are independent of the current for electric fields between a hundred microvolts/cm and a hundred millivolts/cm. No breakdown measurements have been performed with higher electric fields.

A. Hall Measurements

The Hall coefficient was measured with magnetic fields between 450 and 900 gauss. Since it was found that R is independent of the magnetic field strength up to fields of about 1000 gauss, above which R begins to decrease with increasing field strength, the values of R reported here follow the low-field approximation. A

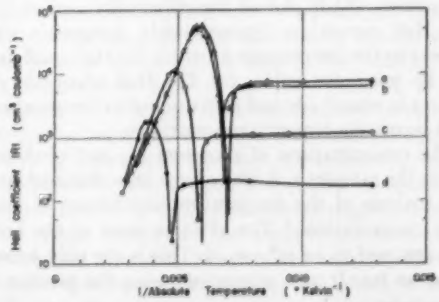

FIG. 2. Hall coefficient of p-type indium antimonide as a function of $1/T$ between 78°K and 370°K.

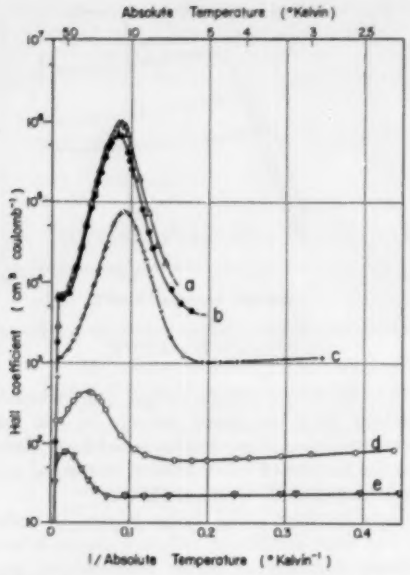

FIG. 3. Hall coefficient of p-type InSb as a function of $1/T$. Note the small slopes of the Hall curves of the samples c and d at temperatures below 5°K. These slopes are much smaller than those of the corresponding resistivity curves in the same temperature range.

larger field of 3500 gauss was used only in the lowest temperature range where the Hall coefficient becomes very small. Electric fields between a few millivolts/cm and several hundred millivolts have been used. In this range the Hall coefficient is independent of the current through the sample.

Figure 3 shows how the Hall coefficient of indium antimonide containing various amounts of impurities depends on temperature between 78°K and 2°K. The main features of these curves can be summarized as follows:

(a) The Hall coefficient reaches a maximum value with decreasing temperature and then drops rapidly as the temperature is lowered, down to a value which is of the same order of magnitude as the Hall coefficient at exhaustion. (b) If plotted logarithmically against $1/T$ the Hall curves are approximately symmetric with respect to the temperature at which the Hall coefficient has its maximum value. (c) The Hall maximum decreases in magnitude and shifts to higher temperatures with increasing impurity concentration.

The concentrations of acceptors N_A and of donors N_D in the samples a, b, and c have been obtained from the analysis of the temperature dependence of their hole concentrations.[7] The effective mass of the holes was assumed to be $m^*=m_0/6$. This is the only known value so far. It was calculated[8] using the product of hole and electron concentrations in the intrinsic range, the ratio of electron to hole mobility at room temperature and the temperature dependence of the intrinsic energy gap as determined optically.

Because of the large number of assumptions involved in the calculation, the effective mass is uncertain to a large degree.[8] The concentrations of acceptors N_A and of donors N_D listed in Table I can, therefore, be used only for qualitative comparison of the samples.

This comparison yields the following results. The samples a and b which, due to their large Hall coefficients at exhaustion, were thought to be the purest samples obtained actually contain large concentrations of both acceptors and donors which compensate each other. Sample c is the purest sample, although it also contains a large number of compensated impurities.

Evidence for this is found also in the measurements of resistivity and magnetoresistive ratio as will be shown later.

B. Resistivity Measurements

The log resistivity *versus* $1/T$ curves are shown in Fig. 4. The log resistivity *versus* $1/T$ curves have large slopes at temperatures above the Hall maximum and much smaller slopes at temperatures below the Hall maximum. The resistivity can be described approxi-

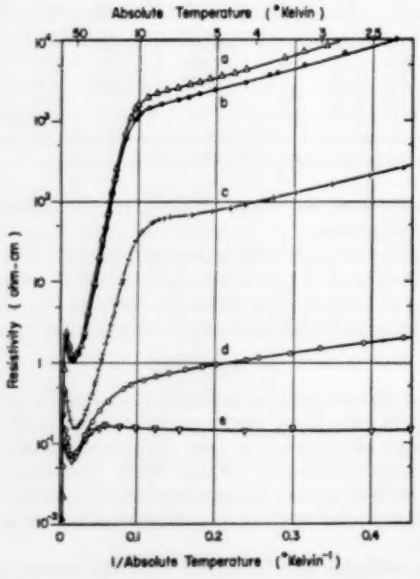

FIG. 4. Resistivity of p-type InSb as a function of $1/T$. The $\log\rho$ *versus* $1/T$ curves are straight lines from about 5°K down to 1.5°K, which is the lowest temperature at which measurements have been performed.

[7] H. Fritzsche, Ph.D. thesis, Purdue University, 1954 (to be published).

[8] We are indebted to C. Kittel for letting us see a manuscript on cyclotron resonance in InSb [Dresselhaus, Kip, Kittel, and Wagoner, Phys. Rev. **98**, 556 (1955)], which suggests tentatively one effective mass value for holes in InSb as $m^*=0.18m_0$.

mately by an equation

$$1/\rho = C_1 e^{-\epsilon_1/kT} + C_2 e^{-\epsilon_2/kT}, \quad (1)$$

with $\epsilon_1 \approx 8\times10^{-3}$ ev and $\epsilon_2 \approx 4.5\times10^{-4}$ ev, where the C_i may depend slightly on temperature.

The first exponential term of this equation is due to the temperature dependence of the hole concentration in the valence band, as can be seen from the exponential increase of R with increasing $1/T$ before the Hall maximum is reached. The second term, however, cannot be explained as being due to excitation of electrons from the valence band into lower-lying acceptor levels, as the completely different behavior of the Hall coefficient in the lowest temperature range shows. The measurement of the resistivity has been extended down to temperatures of about 1.5°K. The resistivity of the samples continues to increase as described by Eq. (1), and no further change has been observed.

The logarithm of the Hall mobility R/ρ of these samples is plotted against $\log T$ in Fig. 5. The Hall mobility passes through a maximum at a higher temperature than that at which the Hall coefficient reaches its maximum value. At lower temperatures R/ρ decreases, first slowly, and then very rapidly at temperatures below that at which the Hall maximum occurs. This last part is certainly not proportional to any drift mobility because the Hall coefficient ceases to be proportional to the reciprocal of the carrier concentration as long as it decreases with decreasing temperature.

The Hall mobility of sample c is much larger than that of the samples a and b despite the fact that sample c has a smaller Hall coefficient at exhaustion. This can be understood because the samples a and b contain a larger concentration of compensated impurities which act as additional ionized scattering centers. In other words, in samples a and b the concentration of ionized impurity centers $N_I = 2N_D + n$ is larger, although the concentration of electrons at exhaustion $n_{exh} = N_A - N_D$ is smaller, than in sample c.

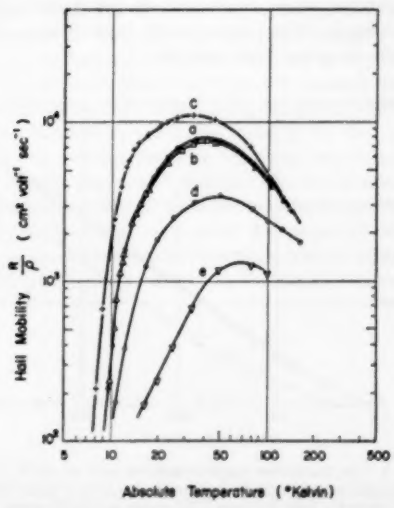

FIG. 5. The temperature dependence of the Hall mobility R/ρ. The Hall mobility of sample c is larger than those of samples a and b indicating the smaller impurity content of sample c.

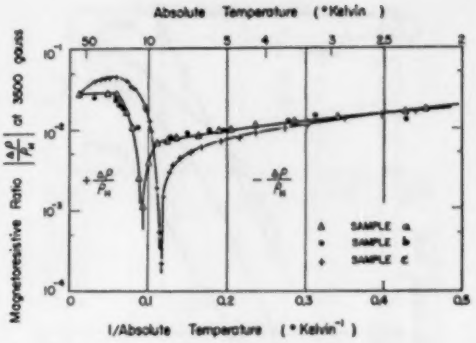

FIG. 6. The absolute value of the transverse magnetoresistive effect, as measured with a magnetic field of 3500 gauss, as a function of $1/T$. The temperature at which the magnetoresistive ratio changes from positive to negative values depends on the impurity content of the InSb samples. It is somewhat lower than the temperature of the Hall maximum.

All resistivity curves have a finite slope in the lowest temperature range which, however, is larger than the slope of their corresponding Hall curve.

The measurements on the polycrystalline sample e are included in these graphs because they show one characteristic which is found to be not only a property of indium antimonide but also of germanium. In the lowest temperature range, the resistivity and Hall curves of polycrystalline samples, plotted logarithmically against $1/T$, always have a much smaller slope than those of single crystals.

C. Magnetoresistive Ratio

The transverse magnetoresistive effect of the three samples a, b, and c was measured as a function of temperature using a field of 3500 gauss. For each measurement of the resistivity in the presence of the transverse magnetic field, four readings were taken with opposite directions of sample current and opposite directions of magnetic field to eliminate thermal emf's and pick-up in the circuit and to see whether the magnetoresistive ratio is an even function of the magnetic field strength. This was found to be the case within the limits of accuracy of the measurements.

In Fig. 6 are shown the magnetoresistive ratio *versus* $1/T$ curves for the samples a, b, and c. At about the temperature of the Hall maximum the magnetoresistive ratio drops sharply as the temperature is lowered, reverses its sign, and then remains negative down to the lowest temperature investigated, which is about 2°K. At temperatures below the reversal, the absolute magnitude of the magnetoresistive ratio first increases

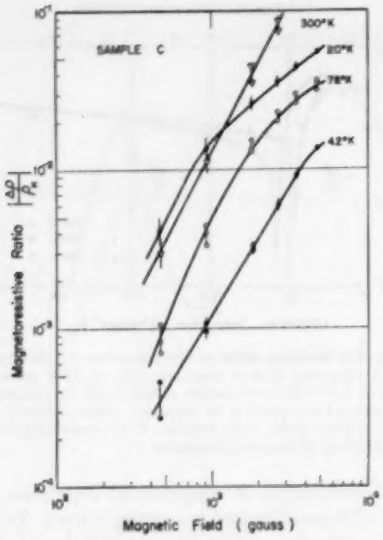

FIG. 7. The transverse magnetoresistive ratio of sample *c* as a function of magnetic field strength at various temperatures. $\Delta\rho/\rho_H$ is negative at 4.2°K and positive at 20°K, 78°K, and 300°K.

quickly, then slower with decreasing temperature, and is still rising at about 2°K. In the lowest temperature range the slopes of the $\log(\Delta\rho/\rho_H)$ *versus* $1/T$ curves seem to be comparable with those of the log resistivity *versus* $1/T$ curves.

Between 78°K and 20°K, the magnetoresistive ratio of samples *a* and *b* is smaller than that of sample *c* indicating a smaller mobility in agreement with the assumption that samples *a* and *b* contain a larger concentration of compensated ionized impurities than sample *c* does.

The magnetic field dependence of the magnetoresistive ratio is shown in Fig. 7 for one sample measured at 300°K, 78°K, 20°K, and 4.2°K. At 300°K and 78°K the curves start with a slope of about two at low fields and then bend over as the field strength is increased. At the lower temperatures the quadratic field dependence either does not exist or is limited to smaller fields than those with which measurements could be made. For these temperatures a linear plot of the magnetoresistive ratio *versus* field strength seems to be appropriate. Such a plot is shown in Fig. 8 for samples *a*, *b*, and *c* at 4.2°K. At fields larger than about 1000 gauss, the magnetoresistive ratio increases linearly with increasing field strength. The slopes of these curves are the same for all the samples despite their different values at a particular field.

A linear variation of $\Delta\rho/\rho_H$ with fields between 3500 and 800 gauss, with no indication of saturation, has been observed before[9] for *p*-type material at temperatures above 80°K.

[9] Harman, Willardson, and Beer, Phys. Rev. **93**, 912 (1954).

DISCUSSION

The experimental results show clearly that at low temperatures the electrical properties of indium antimonide deviate strongly from those of a normal semiconductor. The kind of anomalies observed in the temperature dependence of the Hall coefficient and resistivity are identical with those found in germanium: the maximum of the Hall curve, the small slope of the resistivity curve in the lowest temperature range and the strong dependence of these effects on the concentration of impurities. This last factor has always been the strongest argument in favor of Hung's model of impurity band conduction, because on the basis of this model one expects a rapid decrease of the mobility in the impurity band with increasing separation between the impurity atoms.

The simplest model which assumes additional conduction in an impurity band is that of Hung.[5] The impurity band of his model is formed by the interaction between the ground states of the impurities.

Assuming that at low temperatures practically all charge carriers, which at exhaustion are in the conduction band, contribute to the conduction in the impurity band, Hung defines an impurity band mobility by[10]

$$\mu_i(T)=R_{ex}/\rho(T), \qquad (2)$$

for all temperatures low enough so that conduction in the ordinary conduction band can be neglected. For impurity concentrations less than about 10^{16} atoms/cc, the impurity band mobility is found to be many orders of magnitude smaller than the ordinary conduction band mobility. From this, one would expect that the magnetoresistive ratio is vanishingly small at low temperatures where conduction in the impurity band predominates. This has actually been found experimentally on germanium samples.

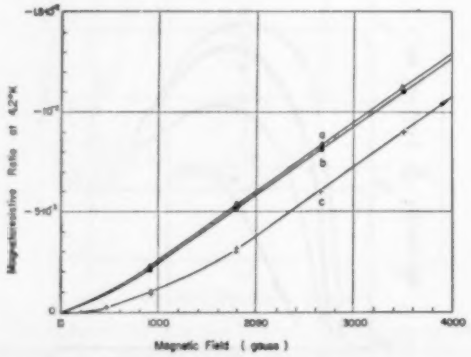

FIG. 8. The transverse magnetoresistive ratio at 4.2°K plotted linearly against magnetic field strength. $\Delta\rho/\rho_H$ is a linear function of the magnetic field between 2000 gauss and 4600 gauss which is the largest field with which measurements have been performed.

[10] R_{ex} is the value of the Hall coefficient in the exhaustion range.

The magnetoresistive ratio of p-type indium antimonide samples, however, exhibits a completely different behavior. As the temperature is lowered, the magnetoresistive ratio reverses its sign from positive to negative values shortly after the Hall maximum is reached and remains negative in the whole temperature range in which the anomalous conduction predominates.

The strong relation between the anomalies observed in the resistivity, Hall coefficient, and magnetoresistive ratio becomes evident in Fig. 9, in which the results measured on one sample are plotted on the same temperature scale.

A negative magnetoresistive ratio cannot be explained by the usual theory which calculates the effect of a magnetic field on the motion of the charge carriers. That one has to deal with a different process in the case of negative magnetoresistive ratios is also indicated by the linear magnetic field dependence in contrast to the quadratic field dependence of the ordinary magnetoresistive ratio.

It is difficult to estimate how far the splitting of the electronic energy levels in the impurity band due to a magnetic field affects the conduction in the impurity band or how the model of impurity band conduction can account for a negative magnetoresistive ratio, because no detailed theory has been worked out yet.

The definition (2) of the impurity band mobility implies many crude assumptions, as was pointed out in the discussion of behavior of germanium.[7] However, it still might be a useful parameter for describing the conduction process at low temperatures. For this reason, the values of μ_i as calculated from the resistivity of the indium antimonide samples at 2.5°K are listed in Table I.

Comparing the μ_i value of sample a with that of sample c, which has the same concentration of acceptor levels, one finds that the impurity band mobility is not only determined by the concentration of impurities which form the impurity band, but it depends also on the concentration of carriers occupying the band. This one has to expect, since the mobility of Eq. (2) is actually an average mobility involving many carriers which occupy states with different effective masses.

The higher values of μ_i of these indium antimonide samples as compared to those of p-type germanium of similar acceptor concentrations might also be explained as being partly due to this fact. The samples of indium antimonide contain a large concentration of compensated impurities and therefore a smaller carrier concentration in the impurity band at low temperatures than the germanium samples of equal acceptor concentration do.

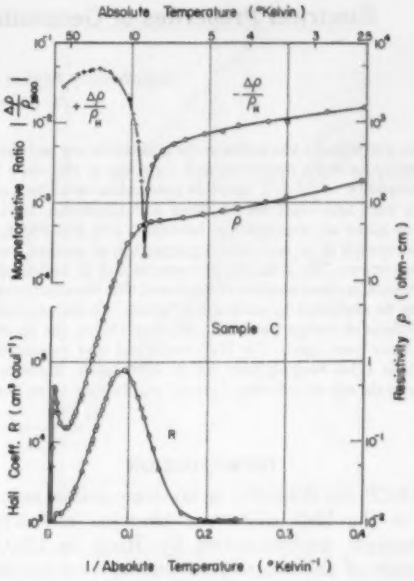

FIG. 9. Hall coefficient, resistivity, and magnetoresistive ratio of sample c plotted logarithmically against $1/T$. All three quantities deviate from their normal behavior in the same temperature range, indicating that one and the same process gives rise to these anomalies.

The measurements on indium antimonide show that the low-temperature anomalies are not restricted to germanium but seem to be a more general property of semiconductors. The negative value of the magnetoresistive ratio in the lowest temperature range, however, constitutes an additional problem.

ACKNOWLEDGMENTS

The authors are indebted to Miss L. Roth for the preparation of the InSb samples, to D. Waldorf for the measurements which are shown in Figs. 1 and 2, and to P. H. Keesom for providing us with the low-temperature equipment.

Electrical Properties of Germanium Semiconductors at Low Temperatures*

H. FRITZSCHE
Department of Physics, Purdue University, Lafayette, Indiana
(Received April 11, 1955)

Low-temperature anomalies in the Hall coefficient and electrical resistivity—a steep maximum and a change of the slope of the log resistivity *versus* $1/T$ curve in germanium semiconductors—which were first observed by Hung and Gliessman, have been reinvestigated at temperatures between 1.5°K and 300°K using single crystals of n- and p-type germanium of various impurity concentrations. The influence of contacts and of various surface treatments has been studied. It was found that the effects observed cannot be explained by surface conduction. To exclude electrical field effects at low temperatures, fields well below the breakdown field have been used. The Hall coefficient was measured with magnetic fields ranging from 100 to 3500 gauss. Measurements on crystals cut in different crystal orientations show that the anomalies cannot be due to directional effects. In the same temperature region where the Hall effect and resistivity become anomalous, the magnetoresistive ratio also shows a drastic change. Throughout the whole temperature range the sample type, n or p, is retained. The results indicate that in order to describe the observations it seems necessary to assume conduction in at least two bands, the regular conduction band (valence band in the case of p-type material) and one band with a very small mobility. Hung's model of impurity band conduction has to be refined considerably or altered to account for the complicated behavior of germanium samples with impurity contents between 2×10^{16} and 7×10^{16} acceptors/cc or between 3×10^{16} and 1×10^{17} donors/cc.

INTRODUCTION

SINCE the discovery of low-temperature anomalies in the Hall effect and electrical resistivity of germanium semiconductors by Hung in 1950,[1] the question of the accuracy of the experimental results and of alternate explanations to the one given by Hung[2] has been discussed.

The observations of Hung[1,3,4] can be summarized: with decreasing temperature the resistivity and Hall coefficient first increase exponentially, as expected from the usual theory of semiconductors, but at a certain temperature the Hall coefficient reaches a maximum value and then decreases sharply by orders of magnitude. In the temperature range of the Hall maximum the resistivity seems to reach a saturation value. With increasing concentration of impurity atoms in the germanium, the onset of the anomalies shifts to higher temperatures and the Hall maximum as well as the low-temperature resistivity decrease rapidly.

For the explanation of these results Hung[2] postulated that conduction in an impurity band is the dominating process at the low temperatures.

By assuming that at low temperatures the number of carriers in the impurity band is equal to the number of carriers in the conduction band observed at higher temperatures, in the exhaustion range, and that the mobility in the impurity band is extremely small compared to the ordinary mobility in the conduction band, Hung obtained reasonable agreement with the experiments.

Although the conduction properties of an impurity band have been discussed by several authors,[5] a detailed theory has not been worked out so far.

The probability of a charge exchange from occupied to unoccupied impurity atoms decreases very rapidly with increasing distance between the impurity atoms. It, therefore, is very difficult to explain the formation of a band with impurity concentrations of the order of 10^{16}/cc, which corresponds to an average impurity separation of about 500 atomic distances.

Before developing such a theory, one should first investigate whether the irregular behavior of the Hall coefficient and the resistivity of germanium at these low temperatures might be caused by some other effects which have been overlooked in previous measurements.

For this reason, Lark-Horovitz suggested a reinvestigation of germanium using the most recent methods of purification and extending the range of observation to about 1.5°K by use of more sensitive detecting devices.

This paper reports experiments which were performed to study the effects of surface treatment, of different kinds of contacts and of the electric and magnetic field strength on the low temperature anomalies. The germanium samples were cut in different crystallographic orientations to investigate whether the anisotropy of the constant energy surfaces might give rise to the observed anomalies.

Measurements of resistivity, Hall coefficient, and magnetoresistive ratio on a large number of germanium samples containing various amounts of impurities are reported. The extent of agreement with the proposed models of impurity band conduction is discussed.

EXPERIMENTAL PROCEDURE

Preparation of Samples

The germanium crystals were grown by Miss L. Roth of this laboratory. The germanium was first purified

* Work supported by U. S. Signal Corps Contract. Based partly on Ph.D. thesis at Purdue University.
[1] C. S. Hung and J. R. Gliessman, Phys. Rev. **79**, 726 (1950).
[2] C. S. Hung, Phys. Rev. **79**, 727 (1950).
[3] C. S. Hung and J. R. Gliessman, Phys. Rev. **96**, 1226 (1954).
[4] H. Fritzsche and K. Lark-Horovitz, Physica **20**, 834 (1954).
[5] B. Gudden and W. Schottky, Z. tech. Phys. **16**, 323 (1935); W. Schottky, Z. Elektrochem. **45**, 33 (1939); G. Busch and H. Labhart, Helv. Phys. Acta **19**, 463 (1946); H. M. James and A. S. Ginzbarg, J. Phys. Chem. **57**, 840 (1953); C. Erginsoy, Phys. Rev. **80**, 1104 (1950), also Phys. Rev. **88**, 893 (1952); X. Baltensperger, Phil. Mag. **44**, 1355 (1953); P. Aigrain, Physica **20**, 978 (1954).

either by repeated pulling of single crystals or by the method of zone refining until it contained less than 10^{13} impurity atoms per cc. This starting material was *n*-type and had a resistivity of about 40 ohm-cm at room temperature. *P*-type germanium with the desired concentration of impurity atoms was obtained by doping this starting material with an appropriate amount of indium or gallium and drawing a new single crystal. For *n*-type germanium the doping material was antimony which was zone-refined until spectroscopically pure.

The crystal orientation was determined in the Purdue x-ray laboratory by I. G. Geib and J. Radavich. Some indium-doped samples used originate from older melts and were found to consist of several crystals.

The samples cut from the crystals normal to the gradient of the impurity concentration were of about 1.5 cm in length, 0.3 cm in width, and 0.08 cm in thickness. The sample surfaces were either ground with No. 600 carborundum or etched with CP4 etching solution. For some experiments the surface was electropolished by using the germanium as cathode and platinum wire as anode. The electrolyte was diluted chemically pure HCl.

Teflon-insulated 0.003-in copper wires were attached to the sides of the sample with Cerroseal-35 solder to serve as current and potential leads in the usual arrangement as described before.[3]

All samples were found to be electrically homogeneous at room temperature by measuring the potential distribution along the surface with the aid of a movable point contact probe.

TABLE I. R and ρ at 298°K and at 78°K and the crystal orientation of the samples.

Sample code number	298°K R cm³ coul⁻¹	298°K ρ ohm cm	78°K R cm³ coul⁻¹	78°K ρ ohm cm	Crystal orientation of Current flow I	Crystal orientation of Mag. field H
In-1	15 300	4.40	11 600	0.48	a	a
In-2	4900	1.69	4590	0.306	(110)	(100)
In-3	281	0.171	320	0.070	polycrystalline	
In-4	165	0.0932	225	0.0488	polycrystalline	
In-5	79.2	0.0785	130	0.054	polycrystalline	
Ga-1	3180	1.055	2570	0.140	(100)	(110)
Ga-2	2360	0.809	1900	0.115	(100)	(110)
Ga-3	1850	0.620	1640	0.098	(100)	(110)
Ga-4	1350	0.494	1220	0.0883	(100)	(110)
Ga-5	940	0.375	850	0.0754	(100)	(110)
Ga-6	450	0.190	420	0.0568	(100)	(110)
Ga-7	230	0.090	300	0.044	(100)	(110)
Ga-4-1	380	0.174	420	0.0545	(211)	b
Ga-4-2	240	0.1186	282	0.0494	(211)	b
Ga-4-3	176	0.0965	224	0.0439	(211)	b
Ga-4-4	120	0.0755	160	0.0423	(211)	b
Ga-6-1	215	0.1106	270	0.0459	(101)	(100)
Ga-7-1	170	0.0938	223	0.0445	(100)	(110)
Sb-15-1	−985	0.281	−1130	0.0746	(100)	(010)
Sb-15-2	−1000	0.290	−1150	0.0755	(110)	(010)
Sb-15-3	−770	0.245	−935	0.066	(110)	(010)
Sb-15-4	−860	0.252	−955	0.070	(110)	(101)
Sb-19-1	−205	0.0695	−295	0.0356	(110)	(100)
Sb-19-2	−128	0.0508	−191	0.0350	(110)	(100)
Sb-19-3	−66	0.0284	−110	0.0251	(110)	(100)

[a] No prominent orientation.
[b] 26° off (111).

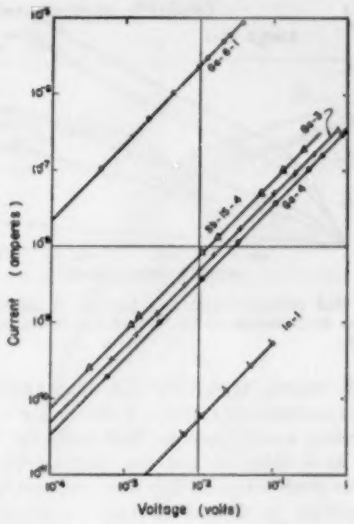

FIG. 1. Current as a function of applied voltage at $T=4.2$°K. A voltage of 1 volt corresponds to a field of about 2 volts/cm.

Apparatus

The cryostat and the electrical measuring circuit used have been described before.[3] Few alterations assured a more stable temperature control and a higher insulation resistance for the electrical leads.

For sample resistances larger than 10^5 ohms a vibrating reed electrometer made by the Applied Physics Corporation is used as zero indicating instrument, in order to increase the input impedance of the voltage reading circuit. The voltages to be measured are applied directly to the vibrating condenser and the compensating voltage from a type *K*-2 potentiometer is used as bias for the amplifying circuit. The current flowing into the electrometer from the sample circuit is smaller than 10^{-16} ampere.

EXPERIMENTAL RESULTS

The samples which were investigated are listed in Table I. The sample code number indicates the doping element, Ga, In, or Sb.

The Hall coefficient and resistivity at 298°K and 78°K of the samples investigated are listed in columns 2, 3 and in columns 4, 5, respectively. The last two columns give the crystallographic orientations of the current flow I and the directions of the magnetic field H.

Ohmic Behavior and Surface Effects

If the applied electric field is high enough, the charge carriers may gain enough energy between two collisions

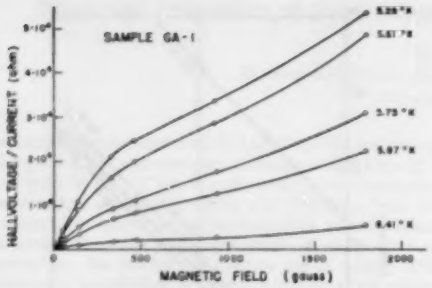

FIG. 2. Hall voltage/current as a function of magnetic field strength at temperatures above that of the maximum in the Hall curve.

to ionize neutral impurities and thus produce an avalanche excitation of carriers. This increase in carrier concentration would cause the Hall coefficient to drop sharply, as is observed and thus might explain[6] the anomalous phenomena. In this case, one would expect the resistivity to depend strongly on electric field strength.

Figure 1 shows the current-voltage relation of several samples (n-type and p-type) at 4.2°K. The resistivity is ohmic in the voltage range used. Special care was taken in the lower temperature range, which was extended down to about 1.5°K and for some samples down to 1.2°K.

No field dependence of the resistivity was observed at any temperature between fields of 10^{-3} volt/cm and 0.5 volt/cm which have been used. One, therefore, has to discard this explanation.

It has been reported before[4] that no errors seem to be introduced by soldering voltage probes directly to the germanium sample. This technique of attaching probes was used throughout all measurements.

To study the effect of surface treatment, ground, etched, and electropolished samples with various ratios of volume to surface area and different recombination rates have been compared. The results[4] show that measurements on etched germanium samples yield the resistivity and the Hall coefficient of the bulk material. All measurements reported below were performed on etched samples.

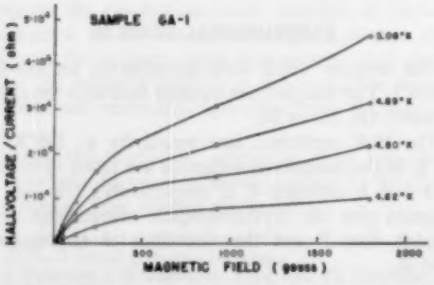

FIG. 3. Hall voltage/current as a function of magnetic field strength at temperatures below that of the maximum in the Hall curve.

[6] Dresselhaus, Kip, and Kittel, Phys. Rev. 92, 827 (1953).

Hall Coefficient as a Function of Magnetic Field

Figures 2 and 3 show the ratio of the Hall voltage to the sample current as a function of the magnetic field for sample Ga-1 at various temperatures above and below the Hall maximum, respectively.

Already at fields as small as 250 gauss deviations from the linear relationship become noticeable. The large field dependence of the Hall coefficient of p-type material at higher temperatures has been explained successfully by taking into account the double-band structure of the valence band which gives rise to the existence of a small percentage of high-mobility holes.[7] These fast holes having a very small effective mass are strongly influenced already by weak magnetic fields.

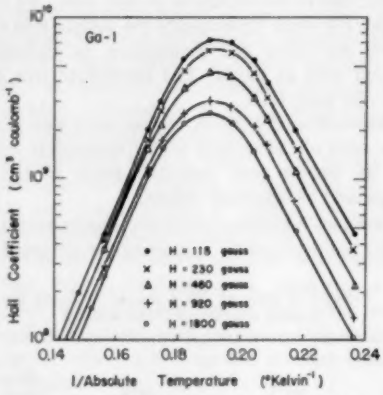

FIG. 4. The maximum of the Hall coefficient at various magnetic fields.

Since the same arguments hold also for low temperatures, the strong field dependence of the Hall coefficient can be understood.

The low-temperature Hall maximum does not disappear in the limit of zero-field slopes in Fig 2 at decreasing temperature (6.41°K to 5.26°K); the slope and therefore the Hall coefficient increases as the temperature is lowered. However, in going from 5.08°K to 4.62°K (Fig. 3) the slope decreases, indicating a maximum at about 5.15°K.

Throughout the temperature range investigated, the condition that the transverse Hall electric field be small compared to the applied electric field was fulfilled. Although the Hall coefficient depends on the magnetic field used, the shape of the Hall curve is not significantly altered by the magnetic field strength. This behavior is illustrated in detail in Fig. 4. The Hall coefficient has an even greater anomaly at larger mag-

[7] Willardson, Harman, and Beer, Phys. Rev. 96, 1512 (1954).

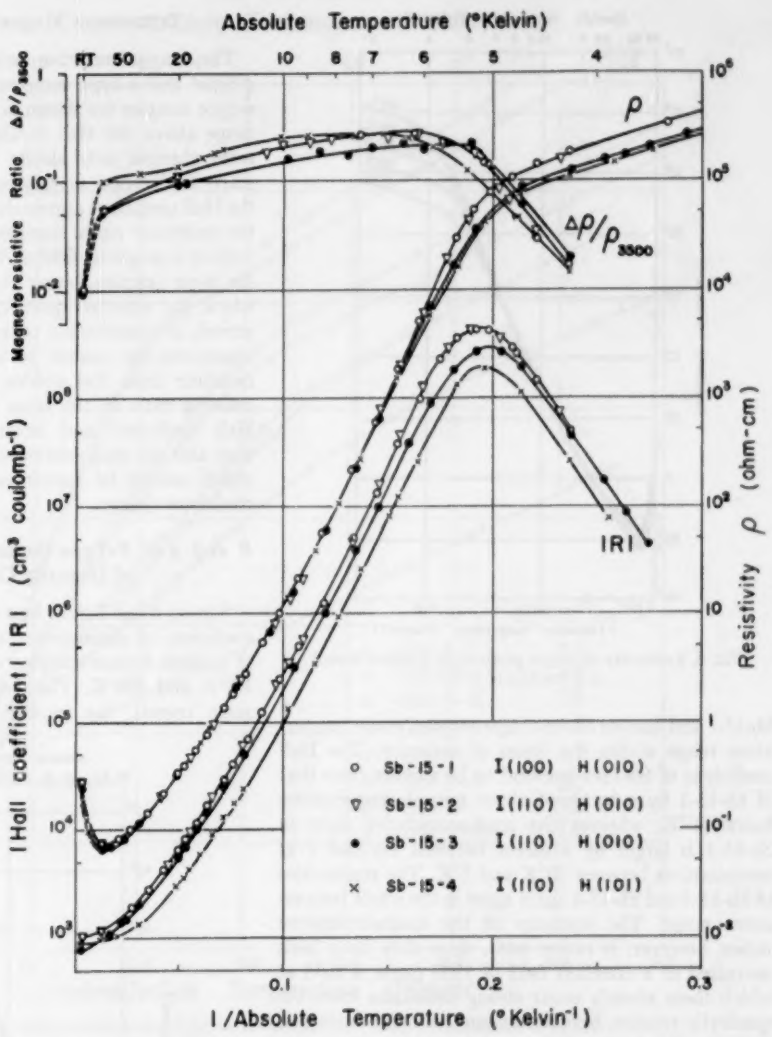

FIG. 5. R, ρ, and $\Delta\rho/\rho_H$ of n-type samples with different crystallographic orientations of I and H.

netic fields, since at low temperatures the Hall coefficient decreases with increasing field strength.

The measurements of the Hall coefficient were performed with a magnetic field of between 115 gauss and 230 gauss. Higher fields up to 4600 gauss were used only at very low temperatures where the Hall angle, which is proportional to R/ρ, becomes very small.

Directional Effects

The work on the directional properties of the magnetoresistive ratio[8] and on the cyclotron resonance[9] in germanium shows a structure of the conduction band in which the surfaces of constant energy consist of ellipsoids of revolution lying along the (111) axis. The warped energy surfaces of the valence band on the other hand are anisotropic to a much smaller degree.

In order to investigate the anisotropy effect of the Hall coefficient and the resistivity and to see whether the low temperature anomalies depend significantly on the choice of crystal orientation, four n-type samples of almost equal impurity content have been measured. These are Sb-15-1, Sb-15-2, Sb-15-3, and Sb-15-4 listed in Table I.

The resistivity of these samples is measured between 1.5°K and 300°K, the Hall coefficient and magnetoresistive ratio between 4.2°K and 300°K. The results are plotted in Fig. 5. The measurements on sample

[8] G. L. Pearson and H. Suhl, Phys. Rev. **83**, 768 (1951).
[9] Lax, Zeiger, Dexter, and Rosenblum, Phys. Rev. **93**, 1418 (1954).

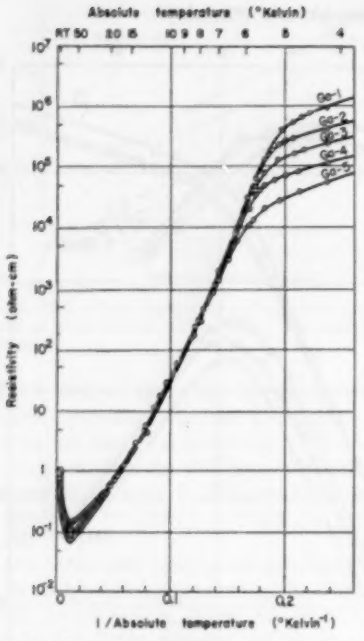

FIG. 6. Resistivity of p-type germanium (gallium-doped) as a function of $1/T$.

Sb-15-1 and sample Sb-15-2 agree in the whole temperature range within the limits of accuracy. The Hall coefficient of Sb-15-4 is found to be smaller than that of Sb-15-3 by a factor of about two at temperatures below 20°K, whereas the magnetoresistive ratio of Sb-15-4 is larger by a factor between 1.5 and 2 at temperatures between 20°K and 7°K. The resistivities of Sb-15-3 and Sb-15-4 again agree in the whole temperature range. The accuracy of the magnetoresistive ratios, however, is rather poor, since they have been measured at a constant field of 3500 gauss, a field at which there already occur strong deviations from the quadratic relation between magnetoresistive ratio and field. Smaller fields will have to be used to check this point.

Although the samples originate from the same region of the ingot and those samples which are being compared differ in resistivity at room temperature only by about 5 percent, one cannot be certain that they contain the same amounts of n-type and p-type impurities. The quantitative comparison of the results is, therefore, uncertain to that degree.

However, since the small difference which has been found in the Hall coefficient of two of the oriented samples (Fig. 5) is the same before and after the onset of the anomaly and since the Hall curves of all four samples go through a maximum at 5.2°K, one can conclude that the low-temperature anomalies cannot be due to anisotropy effects.

Transverse Magnetoresistive Effect

The magnetoresistive ratio has been measured on p-type[4] and n-type samples. The results obtained on n-type samples are shown in Fig. 5. In the temperature range above the Hall maximum the magnetoresistive ratio changes only slowly with temperature, but it starts to decrease sharply near the temperature where the Hall coefficient approaches the maximum and where the resistivity curve changes slope.

Since a magnetic field of 3500 gauss is used, which is, for these samples, larger than the critical field below which the expected quadratic field dependence is observed, a quantitative comparison with the low field approximation cannot be made. However, one can conclude from the sudden change of the magnetoresistive ratio in the same temperature region where Hall coefficient and resistivity become anomalous, that also the magnetoresistive ratio shows a behavior which cannot be accounted for by the usual semiconductor theory.

R and ρ of P-Type Germanium as a Function of of Impurity Concentration

Figures 6 and 7 show how the resistivity and the Hall coefficient of germanium containing various amounts of gallium impurities depend on temperature between 1.5°K and 300°K. These samples originate from the same crystal, the impurity concentration of which

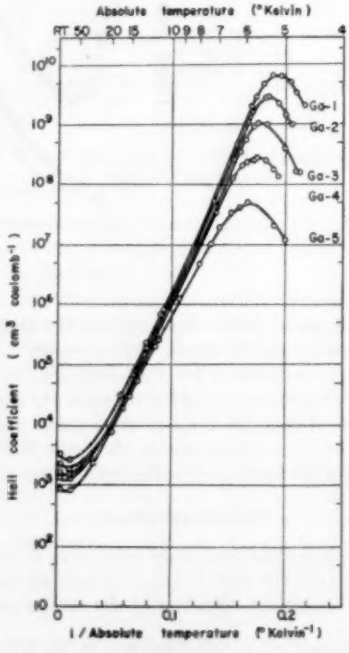

FIG. 7. Hall coefficient of p-type germanium (gallium-doped) as a function of $1/T$.

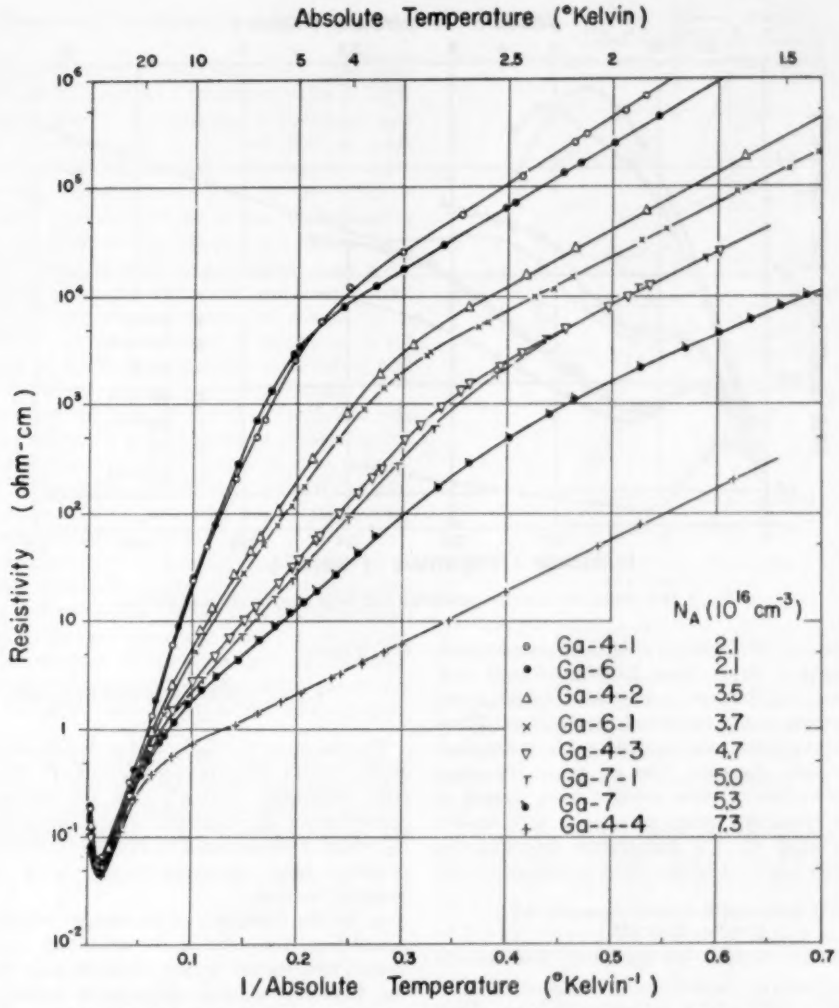

FIG. 8. Resistivity measurements of p-type germanium with large concentrations of gallium.

extends from 3×10^{15}/cc to 10^{16}/cc. The low-temperature behavior observed by Hung is essentially confirmed. The main features will be summarized here.

(a) The Hall coefficient reaches a maximum value with decreasing temperature and decreases thereafter by orders of magnitude. (b) The log resistivity *versus* $1/T$ curves have a large slope at temperatures above the maximum and a much smaller slope at temperatures below the maximum in the Hall curve. The resistivity can be described approximately by the equation[10]

$$1/\rho = C_1 e^{-\epsilon_1/kT} + C_2 e^{-\epsilon_2/kT}, \qquad (1)$$

with $\epsilon_1 \approx 1\times10^{-2}$ ev and $\epsilon_2 \approx 2\times10^{-3}$ ev. (c) The Hall maximum shifts to higher temperatures and decreases in magnitude with increasing impurity content.

The Hall coefficient could not be measured at still lower temperatures because the Hall angle becomes too small. The lowest temperature region was investigated to find out whether the Hall voltage again becomes large enough to be measured but with no success.

It is difficult to interpret the temperature dependence of the resistivity in the lowest temperature region without knowing the concentration and sign of the charge carriers. For this reason samples with impurity contents larger than 2×10^{16} atoms/cc were measured. The Hall coefficient of these samples could be followed down to much lower temperatures.

[10] Where the C_i may be temperature dependent. C_1, C_2, C_3 will be used later, but in this concentration range only C_1 and C_2 are measurable.

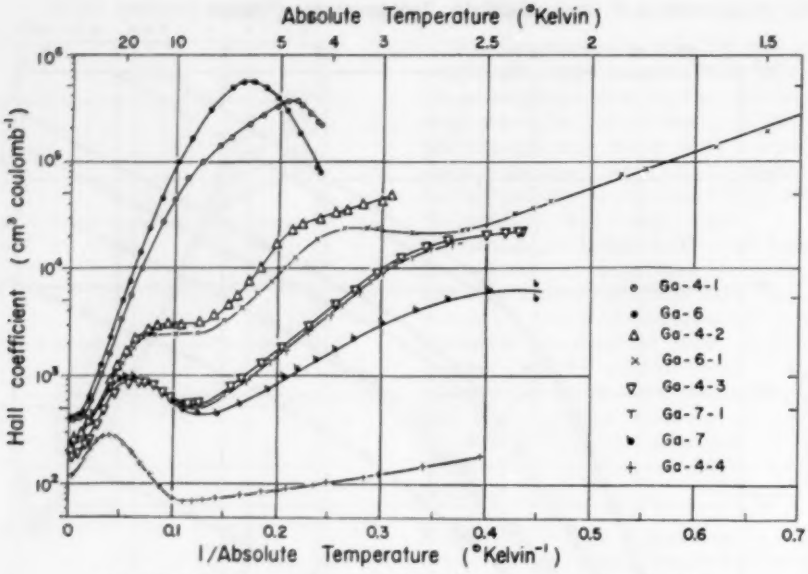

FIG. 9. Hall coefficient of p-type germanium with large concentrations of gallium.

Resistivity and Hall coefficient of these samples with gallium contents larger than 2×10^{18} atoms/cc and smaller than 7×10^{16} atoms/cc are shown in Figs. 8 and 9 as a function of the reciprocal temperature. These curves exhibit a much more complicated behavior than those previously discussed. The log resistivity *versus* $1/T$ curves consist of three straight lines, instead of two as the resistivity curves of samples with smaller impurity content do. The temperature dependence of the resistivity can thus be described approximately by the equation

$$1/\rho = C_1 e^{-\epsilon_1/kT} + C_2 e^{-\epsilon_2/kT} + C_3 e^{-\epsilon_3/kT}. \qquad (2)$$

TABLE II. Resistance temperature parameter for Ge.
[See Eq. (2) of text.]

	N_A cm^{-3}	N_D cm^{-3}	C_2 ohm^{-1} cm^{-1}	ϵ_2 ev	C_3 ohm^{-1} cm^{-1}	ϵ_3 ev
In-1	9.3×10^{16}	3.1×10^{16}			4.0×10^{-2}	5.3×10^{-4}
In-2	3.0×10^{18}	1.4×10^{18}			1.8×10^{-4}	5.9×10^{-4}
In-3	3.6×10^{18}	1.1×10^{18}				
In-4	5.2×10^{18}	7.5×10^{18}			1.54×10^{-3}	7.0×10^{-4}
In-5	1.3×10^{17}	3.3×10^{16}			1.43	5.0×10^{-4}
Ga-1	2.9×10^{18}	1.1×10^{18}				
Ga-2	3.9×10^{18}	1.3×10^{18}				
Ga-3	4.4×10^{18}	1.0×10^{18}			2.5×10^{-2}	1.4×10^{-4}
Ga-4	6.1×10^{18}	1.7×10^{18}				
Ga-5	9.0×10^{18}	5.1×10^{18}			7.7×10^{-4}	1.3×10^{-3}
Ga-6	2.1×10^{18}	2.1×10^{18}			5.03×10^{-3}	1.1×10^{-3}
Ga-4-1	2.1×10^{18}	1.5×10^{18}	4.30	4.04×10^{-3}	2.78×10^{-3}	1.2×10^{-3}
Ga-4-2	3.5×10^{18}	3.9×10^{18}	4.30	2.87×10^{-3}	1.00×10^{-3}	1.0×10^{-3}
Ga-6-1	3.7×10^{18}	2.9×10^{18}	4.00	2.75×10^{-3}	1.17×10^{-3}	0.95×10^{-3}
Ga-4-3	4.7×10^{18}	4.5×10^{18}	4.25	2.44×10^{-3}	3.90×10^{-3}	1.0×10^{-3}
Ga-7-1	5.0×10^{18}	6.7×10^{18}	4.16	2.1×10^{-3}	3.90×10^{-3}	1.0×10^{-3}
Ga-7	5.3×10^{18}	2.0×10^{18}	4.09	1.74×10^{-3}	6.66×10^{-3}	0.8×10^{-3}
Ga-4-4	7.3×10^{18}	7.0×10^{18}	4.09	0.93×10^{-3}	4.09	0.9×10^{-3}
Sb-15-1	4.7×10^{14}	6.9×10^{15}			10^{-3}	1.6×10^{-3}
Sb-15-2	4.0×10^{14}	6.7×10^{15}			10^{-3}	1.6×10^{-3}
Sb-15-3	5.0×10^{14}	8.7×10^{15}			10^{-3}	1.6×10^{-3}
Sb-15-4	9.0×10^{14}	8.3×10^{15}			10^{-3}	1.6×10^{-3}
Sb-19-1	2.8×10^{15}	3.4×10^{16}			2.33×10^{-3}	1.06×10^{-3}
Sb-19-2	1.5×10^{16}	6.5×10^{16}			2.5×10^{-1}	8.6×10^{-4}
Sb-19-3	2.6×10^{16}	1.2×10^{17}			4.45	4.7×10^{-4}

[a] The $\log\rho$ *vs* $1/T$ curves of these samples have a continuously increasing slope at the lowest temperatures. The values listed here for comparison have been determined at 2.5°K.

The values for C_2, C_3, ϵ_2, and ϵ_3 determined from the experimental curves are listed in Table II. It is particularly remarkable that C_2 does not depend on the concentration of p-type and n-type impurities at all. C_3, which is proportional to Hung's "mobility" in the impurity band, decreases rapidly with decreasing impurity content.

ϵ_3—of the dimension of an energy—which is determined from the slope of the resistivity curve in the lowest temperature region, depends only slightly on the impurity content, whereas ϵ_2 increases rather strongly with decreasing impurity concentration. The latter increases from 9.2×10^{-4} ev for sample Ga-4-4 to 4×10^{-3} ev for sample Ga-4-1, and it would become larger than ϵ_1, which is about 8×10^{-3} ev, in the case of samples with impurity concentrations smaller than 10^{16}/cc if it continues to increase at the same rate. An ϵ_2 equal to or larger than ϵ_1 would make the second term in the Eq. (2) negligible compared to the first term and, therefore, unnoticeable in the resistivity curve. This might be the reason why an intermediate slope in the resistivity curve, and with it the complicated behavior of the Hall coefficient, were never observed on samples with impurity concentrations smaller than about 10^{16}/cc.

In contrast to the behavior of samples with smaller impurity content (Fig. 7), the Hall curve of these samples do not have one sharp maximum, but a very

irregular shape which is different for different impurity contents.

The only exception is sample Ga-4-4, the Hall coefficient of which reaches a maximum value at 27°K and decreases then with decreasing temperature to a minimum value which is lower than that at room temperature. After this, the Hall coefficient rises exponentially with $1/T$ with an $\epsilon = 3.4_5 \times 10^{-4}$ ev, which is smaller than $\epsilon_3 = 9.3 \times 10^{-4}$ ev of the corresponding resistivity curve in the same temperature region.

No Hall curve approaches its exhaustion range value at low temperatures, as was predicted and also observed by Hung on three neutron-bombarded samples. The Hall coefficient of sample Ga-6-1 in particular is 10^3 times larger at 1.5°K than at room temperature and continues to increase at still lower temperatures.

A reversal of the sign of the Hall coefficient was looked for, particularly in measurements of these impure samples, which could be carried out at very low temperatures. In all cases thus far, the sign of the Hall coefficient is the same throughout the whole temperature range in which observations were made.

It is very unlikely that the complicated behavior of the samples with gallium concentrations higher than 2×10^{16}/cc and lower than 7×10^{16}/cc is only accidental and caused by spurious impurities which are not present in the other samples. If this were the case one could not understand the remarkable agreement of the results obtained on Ga-4-3 and Ga-7-1, which were cut from different crystals.

The fact that the samples Ga-6 and Ga-7 (Figs. 8 and 9) show a quite different temperature dependence of the Hall coefficient and resistivity than the samples Ga-1, Ga-2 to Ga-5 (Figs. 6 and 7), although they are cut from the same crystal, also indicates that the more complicated behavior is a general property of samples with higher gallium concentrations. Measurements on *n*-type samples with large antimony concentrations will be reported below. They also show a complicated behavior of Hall coefficient and resistivity as the *p*-type samples do which contain corresponding concentrations of gallium.

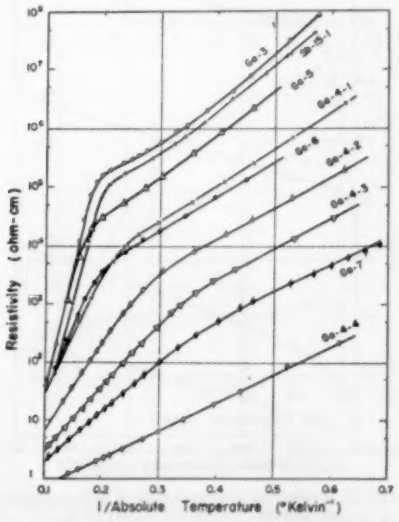

FIG. 10. Resistivity as a function of $1/T$ between 1.5°K and 10°K. Note the similar resistivity curves of Ga-3 and Sb-15-1.

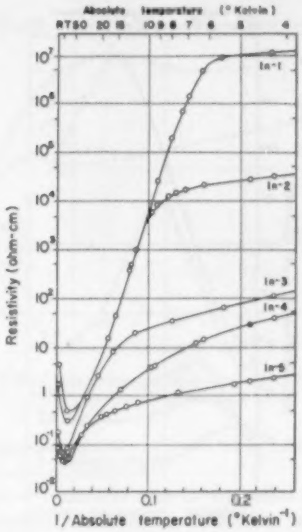

FIG. 11. Resistivity of indium-doped germanium (*p*-type) as a function of $1/T$.

The temperature dependence of the resistivity of the germanium samples, which have been doped with gallium, is shown in Fig. 10 for temperatures between 1.5°K and 10°K. With the exception of the highest resistivity curves, the slopes of which continue to increase with decreasing temperature, the curves have a constant slope at the lowest temperatures which increases slowly as the impurity content of the samples is decreased.

The results of measurements on germanium containing various amounts of indium impurities are shown in Figs. 11, 12, and 13. The Hall and resistivity curves of these samples also exhibit the anomalies at low temperatures. One again finds that the Hall maximum shifts to higher temperatures and decreases in magnitude if the impurity content is increased (Fig. 12). The behavior of indium-doped samples, however, differs from that of gallium-doped samples in some respects.

(a) The slopes of the log resistivity *versus* $1/T$ curves as determined in the lowest temperature range vary between 4×10^{-4} ev and 7×10^{-4} ev in the case of indium-doped samples and between 1×10^{-3} ev and 1.8×10^{-3} ev in the case of gallium-doped samples. (b) The Hall curves of the samples In-4 and In-5 are

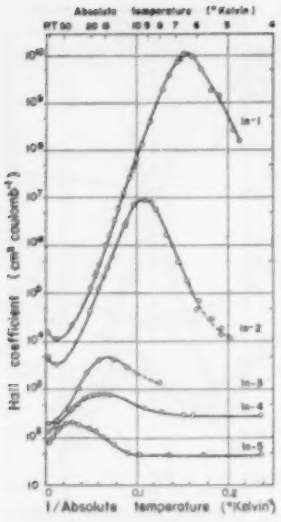

FIG. 12. Hall coefficient of indium-doped germanium (p-type) as a function of $1/T$.

flat in the lowest temperature region. There is no indication of a slope.

Upon comparing the gallium-doped samples with the indium-doped samples one has to keep in mind, however, that several of the samples doped with indium are polycrystalline.

Electrical Properties of N-Type Germanium

Four n-type samples containing about 7.5×10^{15} antimony atoms/cc have been discussed above and the results are plotted in Figs. 5 and 10. These samples show the same behavior at low temperatures as the p-type samples which contain corresponding amounts of gallium or indium impurities. The resistivity curves have a large slope at temperatures above the Hall maximum, and in the lowest temperature range a much smaller slope, which is the same as the slopes of the resistivity curves of the p-type samples which are doped with gallium. This can be seen from Fig. 10, where sample Sb-15-1 is included for comparison.

Three samples with antimony concentrations between 3 and 12×10^{16} atoms/cc have been investigated to find out whether also highly doped n-type samples exhibit the more complicated behavior which is shown in Figs. 8 and 9 for highly doped p-type samples. The results are shown in Figs. 14 and 15. It is uncertain whether the conductivity of these samples can be described by a sum of three exponential terms as in Eq. (2).

The Hall curves of the samples Sb-19-1 and Sb-19-2 show a behavior similar to that of highly doped p-type samples. They do not approach their exhaustion range value at very low temperatures but after reaching a maximum they decrease only slightly with decreasing temperature and then continue to increase down to the lowest temperatures at which measurements could be performed. The slopes of the Hall curves of these two samples are considerably smaller than the slopes of their corresponding resistivity curves in the lowest temperature range. The Hall coefficient and the resistivity of sample Sb-19-3 are almost independent of temperature below 10°K. This behavior has to be compared with that of other samples of this impurity range before one can discuss it.

Concentration of Impurities

The problem of calculating the concentration of majority impurities and of minority impurities to a reasonable degree of accuracy has become very complicated, since the discovery of high-mobility holes in the valence band. Although the percentage of the fast holes is small, they affect considerably the magnetic field dependence of the Hall coefficient and the ratio of Hall mobility to drift mobility. This makes the calculation of the impurity concentration from the scattering due to ionized impurities as well as the calculation based on the temperature dependence of the carrier concentration very difficult. There are other uncertainties especially in the latter calculation, one of which is the presence of excited states of the impurities and another the dependence of the impurity activation energy on the concentration of charge carriers.[11]

Because of these complications the concentrations of

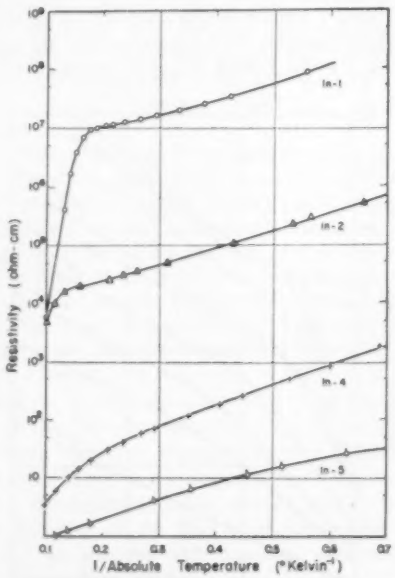

FIG. 13. Resistivity measurements on indium-doped germanium between 1.5°K and 10°K.

[11] I am indebted to E. M. Conwell for very valuable discussions about this problem.

donors and acceptors listed in columns 2 and 3 of Table II can be taken as order of magnitude values only. They were calculated from the mobility data at 78°K with the aid of the Brooks-Herring formula[12] for scattering by ionized impurities, assuming an effective mass of $m_e^*=0.125m_0$ for electrons[13] and $m_h^*=0.33m_0$ for holes[13] and ignoring the presence of the high-mobility holes in p-type material. The polycrystalline nature of In-3, In-4, and In-5 constitutes an additional factor of uncertainty for the concentration values obtained for these samples.

The indium-doped samples contain on the average a much larger concentration of minority impurities (donors) than the gallium-doped samples. This is to be expected[4] because of the difference in the segregation coefficients of indium and gallium in germanium.

DISCUSSION

The fact that the Hall maximum, the onset of the small slope of the log resistivity *versus* $1/T$ curve, and the sharp drop of the magnetoresistive ratio occur always at one and the same temperature for a given sample seems to indicate that one and the same process causes all three properties to deviate from their normal behavior.

In the following, the various explanations for the observed anomalies will be compared with the experimental results, and it will be shown why one has to discard them.

(1) Conducting surface layers cannot be the reason for the observed phenomena because measurements made on etched samples are independent of sample thickness; hence, conducting surface layers, although found on ground samples, are not detectable on etched or electropolished samples.[14]

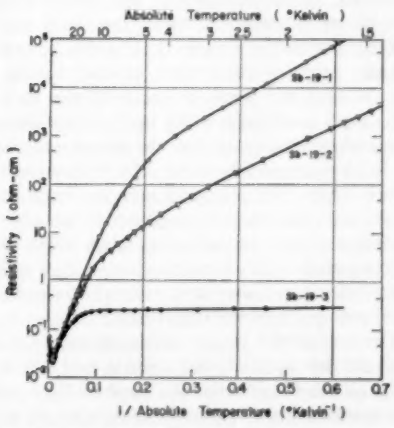

FIG. 14. Resistivity measurements on n-type germanium with large concentrations of antimony.

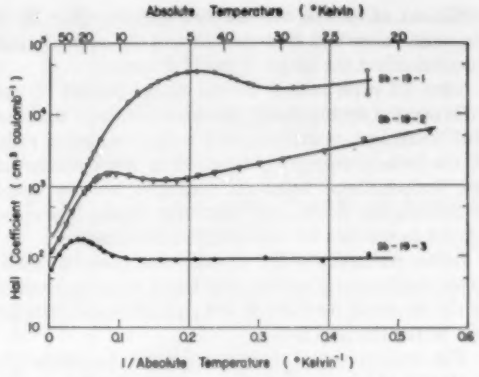
Absolute Temperature (°Kelvin)
50 20 10 5 4.0 3.0 2.5 2.0
Sb-19-1
Sb-19-2
Sb-19-3
Hall Coefficient (cm³ coulomb⁻¹)
1/ Absolute Temperature (°Kelvin⁻¹)

FIG. 15. Hall measurements on n-type germanium with large concentrations of antimony.

(2) Soldered contacts also do not seem to influence the measurements, since cross-shaped samples and ordinary Hall plates show the same results. Furthermore, no difference is found after removing and resoldering the leads several times.

(3) In the very low electric fields applied, it is very difficult to picture an avalanche excitation of charge carriers, particularly in view of the ohmic behavior of the resistivity (Fig. 1).

(4) The possibility of light excitation of charge carriers at low temperatures due to radiation from warmer parts of the cryostat or to stray light from outside has to be excluded. The sample is surrounded by a copper cylinder of the same temperature and thus is shielded against radiation from warmer parts. The experimental arrangement excludes also the possibility that stray light reaches the samples.[15]

(5) The strong magnetic field dependence of the Hall coefficient might suggest that the anomalies are purely a magnetic field effect which disappears in the limit of vanishing fields. This, without doubt, is not the case. The resistivity is measured without an applied magnetic field, and even the limiting value of the Hall coefficient as the magnetic field goes to zero passes through a maximum (Figs. 2 and 3).

(6) The possibility of explaining the anomalies as being due to the fact that the surfaces of constant energy are nonspherical has to be excluded, because the small difference which has been found in the Hall

[12] H. Brooks, Phys. Rev. **83**, 879 (1951).
[13] Lax, Zeiger, and Dexter, Physica **20**, 818 (1954); C. Kittel, Physica **20**, 829 (1954).

[14] If one plots the maximum value of the observed Hall coefficient against sample thickness, then for etched samples one obtains a horizontal line indicating a Hall coefficient independent of sample thickness. The same experiment carried out with ground samples shows a Hall coefficient which increases with increasing thickness approaching the value of the etched samples.

[15] Further evidence for this is that heating effects due to light were never observed even at very low temperature where the atomic heat of the sample is exceedingly small and absorption of radiation would lead to a rise in temperature, which was not observed.

coefficient of two of the oriented samples (Fig. 5) is the same before and after the onset of the anomaly and does not affect the shape of the Hall curve.

Since all explanations offered so far do not fit the experimental arrangement, one must conclude that the Hall coefficient, resistivity, and magnetoresistive ratio of the bulk germanium do not show the behavior at low temperatures which is predicted by the usual semiconductor theory, and that this theory has to be altered to account for the observed phenomena.

Before discussion of the theories that postulate additional conduction in an impurity band, some regularities in the electrical behavior of the gallium-doped samples will be summarized here.

The conductivity of these samples can approximately be described by a sum of three exponential terms as in Eq. (2). The first term represents conduction by holes in the valence band. The second term is only found in the case of samples with impurity content larger than about 10^{16}/cc; it becomes much smaller than the first term when the impurity content is smaller than 10^{16}/cc, since ϵ_2 increases rather strongly with decreasing concentration of impurities, whereas the factor C_2 remains constant (see Table II).

The third term consists of an exponential with an ϵ_3 of the order of 10^{-3} ev and a factor C_3 which decreases very rapidly with decreasing impurity concentration. Since the second and the third terms depend on the concentration of impurities in quite different ways, two different mechanisms are probably responsible for their appearance.

The strong decrease of the factor C_3 with decreasing impurity concentration makes the assumption of additional conduction in an impurity band a very plausible explanation for the presence of the third term and for the maximum in the Hall curve, since the mobility in such a band would be expected to decrease rapidly with increasing distance between the impurity atoms.

At the present time, nothing can be said about the mechanism which gives rise to the presence of the second term in the expression for the conductivity and to the complicated behavior of the Hall coefficient which is always connected with it. Since this mechanism seems to be not effective in purer samples, it will be tried to discuss the possibility of a conducting impurity band as an explanation for the anomalies without considering this additional effect which becomes noticeable only in the electrical behavior of samples in a certain impurity concentration range.

If one tries to compare the experimental results with any kind of model which assumes conduction in impurity bands, one encounters great difficulties.

According to James and Ginzbarg,[5] an impurity band is formed by the interaction between localized impurity states, or the overlapping of their electron wave functions. The distribution of energy states of a perfect crystal differs from that of a crystal in which one n-type impurity atom replaces a regular lattice atom by the fact that in the latter case two energy states are missing from the conduction band and one doubly degenerate energy state appears in the forbidden gap. The degeneracy is due to the two alternative spin directions. The two corresponding eigenfunctions are localized in that they have an appreciable amplitude only in the neighborhood of the impurity. If two impurities replace regular lattice atoms, two doubly-degenerate energy states appear in the forbidden gap and a corresponding number of states are missing from the conduction band. The energy difference between these two states can be computed in terms of an exchange integral involving the single-impurity wave functions. The eigenfunctions belonging to these energy states again have an appreciable amplitude only in the neighborhood of the two impurities. When there are many impurities, the group of energy states in the forbidden energy gap is called an impurity band.

In the hypothetical case of a periodic arrangement of the impurity atoms, the impurity band is separated from the bottom of the conduction band (or from the top of the valence band in p-type) by a forbidden gap, and it contains twice as many energy states as there are impurity atoms. James and Ginzbarg[5] have shown that, if the random distribution of impurities is taken into account, then the impurity band appears as an energy range of high-level density, separated from the conduction band merely by a range of smaller level density and that the number of states in the impurity band is less than twice the number of impurity atoms.

Some difficulties, which arise in discussing conduction in an impurity band, will be given in the following. For this discussion, a periodic arrangement of impurity atoms will be assumed. The realistic case of a random distribution of impurity atoms will probably be more complicated, although Aigrain[5] has shown that the band-type approximation holds for lower impurity densities rather in the random than in the ordered case.

A basic property of a band, formed by an ideal lattice, is that the average value of the ratio free electron mass to effective mass, m_0/m^*, over the whole band vanishes. This means that the net current vanishes if the band is completely filled. The ratio m_0/m^* must therefore depend on energy inside the band, and it must assume positive and negative values. Since at most temperatures the impurity band width will be small compared to kT, carriers with positive and with negative effective masses will exist at the same time and will move in opposite directions.

The excess carrier concentration which produces a net current flow in an applied electric field will depend strongly on the distribution of charge carriers over the quantum states in the impurity band, hence on temperature, and will, therefore, be quite different from the true concentration of carriers occupying the band. The average mobility will also depend on temperature through the averaging process which involves states with very different effective masses.

The theory for the Hall coefficient and the resistivity of an impurity band has not yet been worked out. The formulas will certainly look very different from those of the ordinary band because of the drastic changes of the effective mass within the impurity band. One cannot expect, for instance, that the Hall coefficient is proportional to the reciprocal of the concentration of charge carriers occupying the impurity band. Some factors similar to $r=|R|/en$ of the ordinary conduction band might depend on temperature since the averaging process includes states of very different properties.

The simplest model which assumes conduction in an impurity band is that of Hung.[2,3] The impurity band of his model is formed by the interaction between the ground states of the impurities. The approximate agreement obtained by Hung is based on the assumption that (a) the expressions for the Hall coefficient and the resistivity for simultaneous conduction in two bands still hold in this case[16]

$$R=-\frac{1}{e}\frac{r_c n_c \mu_c^2+r_i n_i \mu_i^2}{(n_c\mu_c+n_i\mu_i)^2}, \tag{3}$$

$$\rho=1/(en_c\mu_c+en_i\mu_i), \tag{4}$$

where the subscripts refer to the conduction band and the impurity band, respectively, and (b) that the factors r_c and r_i do not deviate appreciably from unity.

With these assumptions the concentration of charge carriers in the impurity band at very low temperatures is equal to the carrier concentration in the conduction band at exhaustion and the calculated curves of the resistivity and the Hall coefficient are both flat in the lowest temperature region.

The finite slopes of the resistivity curves and the Hall curves in the lowest temperature region and the fact that the Hall coefficient does not approach its exhaustion value as the temperature is lowered disagree with Hung's picture. One concludes that either the model of a conduction in the ground states of the impurities or the Eqs. (3) and (4) must be altered so that they account for the special properties of the impurity band which were mentioned above.

Since at the present time, Eqs. (3) and (4) are the only ones available for the Hall coefficient and the resistivity of two-band conduction, it will be attempted to show that they can describe the observations obtained from the purer samples without making use of Hung's original assumption that the impurity band is formed by the ground states. It will only be assumed that a certain concentration of charge carriers flows in another band with an impurity band mobility μ_i much smaller than the mobility μ_c in the valence band so that

$$r_c n_c \mu_c^2 \gg r_i n_i \mu_i^2 \tag{5}$$

in the temperature range under consideration.

[16] In general, one might write $R=\Sigma_i R_i\sigma_i^2/(\Sigma_i\sigma_i)^2$.

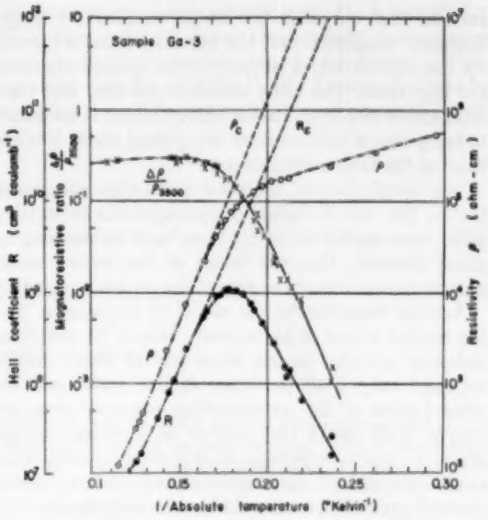

FIG. 16. $\Delta\rho/\rho_H$ and R calculated from ρ, R_c and ρ_c (see text).

If one denotes by

$$R_c=r_c/en_c,\quad \rho_c=1/en_c\mu_c,\quad R_i=r_i/en_i,\quad \rho_i=1/en_i\mu_i, \tag{6}$$

the Hall coefficient and the resistivity in the conduction band and in the impurity band, respectively, one obtains by use of Eqs. (3), (4), and (5):

$$R/R_c=\rho^2/\rho_c^2. \tag{7}$$

From Eqs. (4) and (8), one obtains the magnetoresistive ratio for two-band conduction as follows:

$$\sigma(H)=\sigma_c(H)+\sigma_i(H),$$
$$\sigma_c(H)=\sigma_c(0)(1-B_cH^2),$$
$$\sigma_i(H)=\sigma_i(0)(1-B_iH^2).$$

One can neglect B_iH^2 as being small compared with unity as found experimentally.[4] By using resistivities instead of conductivities, one finds

$$(\rho_H-\rho_0)/\rho_H=\Delta\rho/\rho_H=B_cH^2\rho/\rho_c. \tag{8}$$

Here ρ_c may be calculated from the n_c extrapolated from the Hall curve and μ_c extrapolated from the mobility curve. The Hall coefficient R and the magnetoresistive ratio $\Delta\rho/\rho_H$ calculated from ρ and ρ_c by using (7) and (8) show that this description is self-consistent (see Fig. 16).

These considerations are very hypothetical, and the agreement which was demonstrated previously does not yet prove the validity of the assumptions in the case of such a complicated picture.

Because of the finite slopes of the resistivity curves

and the Hall curves in the lowest temperature range, Erginsoy[4] suggested that the impurity band is formed by the excited states instead of the ground states of the impurities. The finite slopes would then find their explanation in the excitation energy which is necessary to bring charge carriers from the ground states into the band of the first excited states.

The calculations of the lower band-edge energies of the $2s$, $2p$, and $3s$ bands of hydrogen-like impurities, which were carried out by Erginsoy[4] and Baltensperger,[5] show, however, that the bands of the excited states are concentrated near the edge of the conduction band.[17]

Another objection to the model of Erginsoy is that the excited states of an impurity cannot be treated as ordinary acceptor states, since one of them can be occupied only if all the other excited states and the ground state of the corresponding impurity atom are empty. This limits the number of available excited states so much, expecially at low temperatures when most of the ground states are occupied, that conduction through excited states should be extremely small.

Busch and Labhart[6] used a slightly different model to explain their experimental findings on SiC. They assumed a conducting acceptor band in an n-type crystal (a corresponding donor band between the acceptors and the valence band in the case of a p-type crystal). These authors determined the energy gap between their postulated band and the impurity states, as well as the number of states forming the additional band, from the experimental curves using Eqs. (3) and (4).

In order to explain the temperature dependence of the Hall coefficient and resistivity of the gallium-doped samples on the basis of Busch's model, it is necessary to assume a conducting impurity band about 10^{-3} ev below the acceptor states. This band should be filled with electrons at 0°K and partly empty at elevated temperatures, to account for the observed positive sign of the Hall coefficient. This discussion shows clearly that additional experimental work will be necessary to provide an adequate foundation for theoretical discussion.

SUMMARY

The resistivity ρ, the Hall coefficient R, and the transverse magnetoresistive ratio $\Delta\rho/\rho$ of single-crystal samples of n-type and p-type germanium have been reinvestigated in the temperature range from 300°K to 1.5°K. It was found that Hung's observations of an anomalous behavior of resistivity and Hall coefficient are correct.

The $\log\rho$ *versus* $1/T$ curve has either two or three different slopes at temperatures below about 25°K, depending on the range of impurity concentrations.

The Hall coefficient first increases with decreasing temperature, as expected from semiconductor theory, but, in the temperature range in which the slope of the resistivity curve changes, the Hall coefficient goes through a maximum. At still lower temperatures, the Hall coefficient decreases by orders of magnitude in the case of samples with lower impurity concentrations. At the lowest temperatures the Hall coefficient of samples with high impurity concentrations is either completely constant with temperature or shows one or even two slopes in the $\log R$ *vs* $1/T$ plot. These slopes are significantly different from the corresponding slopes of the resistivity curves in the same temperature range.

Throughout the whole temperature range the Hall coefficient does not change sign. Samples which are found to be p-type at higher temperatures remain p-type down to the lowest temperature investigated and the same holds for n-type samples.

In the same temperature range where Hall coefficient and resistivity become anomalous, the magnetoresistive ratio decreases when the temperature is lowered.

Special precautions were taken to exclude the effect of surface conduction, the influence of heat radiation, and electric field excitation.

Investigation of the Hall coefficient as a function of magnetic field strength shows clearly that the anomaly cannot be due to a magnetic field effect. That the effects observed can also not be due to the influence of the direction of the current flow, and the magnetic field with respect to the symmetry axes of the Brillouin zones, has been shown by measurements on carefully selected and crystallographically oriented specimens in which the symmetry axes of the sample had different crystal orientations.

The explanation of these observations due to Hung, who assumed that the localized impurity states interact and form a conduction band, seems plausible for the following reasons. The width of the impurity band should drastically decrease with increasing separation between the impurity atoms. Therefore one would expect the mobility of the charge carriers in the impurity band to decrease rapidly with decreasing concentration of impurities. This effect is demonstrated by the following observations: (a) In the lowest temperature range where conduction in the impurity band should outweigh conduction in the ordinary conduction band, the resistivity increases rapidly, if the impurity concentration of the sample is decreased; (b) the Hall maximum decreases in magnitude and shifts to higher temperature when the impurity concentration is increased, and (c) the magnetoresistive ratio is exceedingly small in the lowest temperature range where conduction in the impurity band should predominate.

Hung's hypothesis on the other hand cannot account for the complicated behavior of Hall coefficient and resistivity of germanium samples with impurity concen-

[17] There is reason to believe that excited states are much closer to the ground state in antimony-doped n-type germanium, as E. M. Conwell [Phys. Rev. (to be published)] pointed out to me.

trations larger than 2×10^{16}/cc and smaller than about 10^{17}/cc.

ACKNOWLEDGMENTS

The author expresses his sincere gratitude to K. Lark-Horovitz for suggesting this problem and for his guidance in the course of this work. He is indebted to H. Y. Fan and H. M. James for very helpful discussions, to Miss L. Roth for her help in supplying the germanium samples, and to P. H. Keesom for making available the equipment of his low-temperature laboratory.

PHYSICAL REVIEW VOLUME 99, NUMBER 2 JULY 15, 1955

Cohesive Energy of Noble Metals

K. KAMBE*
Harvard University, Cambridge, Massachusetts
(Received December 31, 1954)

The method, developed by Kuhn and Van Vleck, and later simplified and extended by Brooks, for calculating the cohesive energy of monovalent metals, is here further extended to include the effects of the deviation of the effective ion-core potential from pure hydrogenic form in the vicinity of the surface of the s-sphere. A formula is derived for calculating the logarithmic derivative of the wave function at the surface of the s-sphere. From the logarithmic derivatives of the s- and p-functions the ground-state energy and the Fermi energy can be evaluated. The method thus extended is applied to the calculation of the cohesive energy of the monovalent noble metals. For these metals, the repulsion between ion cores is important. Combining the repulsive energy, which is calculated by Fuchs with a modified Thomas-Fermi method, with the energy of valence electrons calculated by the present method, we obtain the total cohesive energy of copper. Since there is no calculation of the repulsive energy for silver and gold, the ion cores are assumed to be rigid and the energies of the valence electrons at the observed lattice spacings are determined and considered as the approximate total energies. The cohesive energies calculated at the observed lattice spacings with the rigid ion-core assumption are 61.7 for Cu, 55.8 for Ag, and 49.2 for Au in comparison with the experimental values of 81.2, 68.0, and 92.0 respectively. Here the energy unit is kcal/mole.

1. INTRODUCTION

VAN VLECK and Kuhn[1] have given simplified methods of calculating the cohesive energies of monovalent metals. Recently, Brooks[2] has pointed out a number of simplifications of their methods and obtained reasonable theoretical predictions of the cohesive energy and lattice constants of all the alkali metals. The Van Vleck-Kuhn method is based on the following facts: (1) The effective potential in the vicinity of the surface of the s-sphere in the Wigner-Seitz sphere approximation[3] is essentially hydrogenic, therefore, (2) the wave function in the same region can be excellently approximated by a linear combination of the confluent hypergeometric functions, *viz.*,

$$U_k^{(l,n)}(r)=\bar{W}^{(l,n)}(r)+k_l\bar{W}^{(l,n)}(r), \tag{1}$$

where the functions $\bar{W}^{(l,n)}$ and $\bar{W}^{(l,n)}$ are related to the standard Whittaker functions by Eqs. (11a, b) in Van Vleck and Kuhn, and (3) k_l can be determined by the function matching method. Brooks, however, has shown that

$$k_l=-\tan(\delta_l\pi), \tag{2}$$

where δ_l is the quantum defect.

In the present paper, the cohesive energy of the noble metals will be computed by the Brooks method, incorporating the correction due to the deviation of the effective potential from the pure hydrogenic form. In the case of copper, Fuchs[4] has calculated the cohesive energy by numerical integration of the radial wave equation in a Hartree-Fock potential. His results for copper as well as the observed values for all noble metals will be compared with our results in the last section.

2. EXTENSION OF THE BROOKS METHOD

We shall first explain a further extension of the Brooks method of determining k_l, and then derive the expression for the logarithmic derivative of the wave function with the correction due to the deviation of the effective potential from the pure hydrogenic form.

In calculating s- as well as p-functions by (1) and (2), Brooks has determined the dependence of δ_l on the energy ϵ by straight forward extrapolation from the free atom term values for both s- and p-levels. For s-levels, $l=0$, the straightforward extrapolation of δ_0 is legitimate and nearly linear in most cases. For $l\geq1$, however, Ham[5] has pointed out that the straight-forward extrapolation of δ_l is often not adequate. Instead of δ_l the quantity η_l, which is related to δ_l by

$$\tan(\eta_l\pi)=\frac{\tan(\delta_l\pi)}{1+\epsilon}, \tag{3}$$

* Now at the College of Electro-Communications, Tokyo, Japan.

[1] J. H. Van Vleck and T. S. Kuhn, Phys. Rev. **79**, 382 (1952).
[2] H. Brooks, Phys. Rev. **91**, 1027 (1953).
[3] E. P. Wigner and F. Seitz, Phys. Rev. **43**, 804 (1933).
[4] K. Fuchs, Proc. Roy. (London) **A151**, 585 (1935).
[5] F. Ham (private communication).

should be extrapolated in case of $l=1$. If the x-ray term values or the energy parameters in the self-consistent field equation of Hartree-Fock type are known, these energy values will give further information on the dependence of η_l on ϵ.[6] For alkali metals, the wave function calculated by (1) with (2) yields excellent results for the usual solid-state parameters, if we carry out the δ_0 and η_l extrapolation for s- and p-functions, respectively.

For monovalent noble metals, however, the effective potential in the vicinity of the surface of the s-sphere is not completely hydrogenic, because the actual lattice spacings of these metals are relatively small. Therefore, the wave function also is not purely hydrogenic, and we have to make corrections due to the deviation of the effective potential from the pure hydrogenic form in this region. These corrections can be obtained in the following way.[7]

In calculating the ground-state energy ϵ_0 and the Fermi energy ϵ_F, we need only the knowledge of the logarithmic derivatives of the s- and p-functions, if we take only the first two terms of the expansion of the energy in powers of k. Hence, we shall derive the corrected expression of the logarithmic derivative of the wave function.

The uncorrected wave function $U_k^{(l,n)}(r)$ satisfies the radial wave equation with the pure hydrogenic potential:

$$\frac{d^2U_k^{(l,n)}}{dr^2}+\left[-\frac{1}{n^2}+\frac{2}{r}-\frac{l(l+1)}{r^2}\right]U_k^{(l,n)}=0, \qquad (4)$$

where $1/n^2=-\epsilon$. The true wave function $U^{(l,n)}(r)$ should satisfy the wave equation with the true effective potential $V(r)$:

$$\frac{d^2U^{(l,n)}}{dr^2}+\left[-\frac{1}{n^2}-V(r)-\frac{l(l+1)}{r^2}\right]U^{(l,n)}=0. \qquad (5)$$

Here and elsewhere, the energy is in Rydberg units, and r is in Bohr units. We assume that the potential $V(r)$ and the wave function $U^{(l,n)}(r)$ become essentially hydrogenic for all $r\gtrsim R$. From (4) and (5), we find that

$$\int_{r_s}^{R}\left[\frac{d^2U_k^{(l,n)}}{dr^2}U^{(l,n)}-U_k^{(l,n)}\frac{d^2U^{(l,n)}}{dr^2}\right]dr$$
$$=-\int_{r_s}^{R}\left[\frac{2}{r}+V(r)\right]U_k^{(l,n)}U^{(l,n)}dr, \qquad (6)$$

where r_s is the radius of the s-sphere. By integration by parts, (6) can be reduced to

$$U^{(l,n)}\frac{dU_k^{(l,n)}}{dr}-U_k^{(l,n)}\frac{dU^{(l,n)}}{dr}\Bigg|_{r_s}^{R}$$
$$=-\int_{r_s}^{R}\left[\frac{2}{r}+V(r)\right]U_k^{(l,n)}U^{(l,n)}dr. \qquad (7)$$

Since at $r=R$,

$$U^{(l,n)}(dU_k^{(l,n)}/dr)-U_k^{(l,n)}(dU^{(l,n)}/dr)=0,$$

we have

$$\frac{r}{U^{(l,n)}}\frac{dU^{(l,n)}}{dr}\Bigg]_{r=r_s}=\frac{r}{U_k^{(l,n)}}\frac{dU_k^{(l,n)}}{dr}\Bigg]_{r=r_s}$$
$$-r_s\int_{r_s}^{R}dr\left(\frac{2}{r}+V(r)\right)\frac{U_k^{(l,n)}(r)}{U_k^{(l,n)}(r_s)}\cdot\frac{U^{(l,n)}(r)}{U^{(l,n)}(r_s)}. \qquad (8)$$

Here, $U_k^{(l,n)}(r)$ can be calculated by (1), and (8) is the equation to be solved with respect to $U^{(l,n)}(r)$. If we put $V(r)=-2Z(r)/r$. Where $Z(r)$ is the effective nuclear charge, $Z(r)$ is not much different from unity in the vicinity of r_s. The quantity

$$\Delta V(r)=-\frac{2}{r}-V(r)=\left(\frac{Z(r)}{r}-\frac{1}{r}\right)2, \qquad (9)$$

which is involved in (8), is the deviation of the true potential from the pure hydrogenic form, and is small near r_s, and vanishes for all $r\gtrsim R$. Since, therefore, the integral on the righthand side of (8) is small, and $U^{(l,n)}(r)$ may not be appreciably different from $U_k^{(l,n)}(r)$, we may assume, as the first approximation, that $U^{(l,n)}(r)$ in the integrand can be replaced by $U_k^{(l,n)}(r)$. Thus, we obtain the first approximation formula for the logarithmic derivative of the true wave function:

$$\phi_l(r_s)=\left[\frac{r}{U^{(l,n)}}\frac{dU^{(l,n)}}{dr}\right]_{r=r_s}=\frac{r}{U_k^{(l,n)}}\frac{dU_k^{(l,n)}}{dr}\Bigg]_{r=r_s}$$
$$+r_s\int_{r_s}^{R}\Delta V(r)\left(\frac{U_k^{(l,n)}(r)}{U_k^{(l,n)}(r_s)}\right)^2dr. \qquad (10)$$

If we want more accurate values of $\phi_l(r)$, we may employ successive approximations. First the values of ϕ_l are calculated by (10) at several values of r. For large values of r, $r\gtrsim R$, $U^{(l,n)}(r)$ should be equal to the uncorrected $U_k^{(l,n)}(r)$ which can be obtained by (1). Then, we integrate $\phi_l(r)$ numerically, starting at a large value of r toward smaller values of r. The values of $U^{(l,n)}(r)$ thus obtained will give a better approximation to the true values of $U^{(l,n)}(r)$, and will be used in computing the integral on the righthand side of (8). In this way, one obtains the second approximation to the logarithmic derivative ϕ_l. This procedure can be repeated until we get the self-consistent solution of (8).

[6] The use of η_l and of the deep-lying levels was suggested by H. Brooks.

[7] The procedure described in the following paragraphs was worked out by H. Brooks, to whom I am indebted for the loan of his notes on the method.

3. COHESIVE ENERGY OF THE NOBLE METALS

The method developed in the preceding section will be applied to the calculation of the cohesive energy of the monovalent noble metals, *viz.*, copper, silver, and gold.

The uncorrected wave function $U_k^{(l,n)}(r)$ is calculated by (1). The confluent hypergeometric functions involved are evaluated from the tables calculated by Ham[8] who has revised and extended the tables published by Kuhn.[9] In calculating k_l for the uncorrected s-function, the extrapolation of δ_0 from the free-atom term values listed by Bacher and Goudsmit[10] is employed for all three metals.

In the case of p-levels, however, the information from the free atom term values is not sufficient for determining the dependence of the quantity η_1 defined by (3) upon the energy parameter ϵ. Moreover, the term values of the p-series of copper show marked irregularity which is attributed to configuration interactions. Whitelaw[11] has given a theory which permits the estimation of the unperturbed positions of the p-series. The unperturbed positions of the $4p$ and $6p$ term assigned by Whitelaw and the energy parameter of the Hartree-Fock equation for the $3p$ electron[12] are used in deriving the $\eta_1-\epsilon$ relation for copper. The $5p$ term is not used because the influence of the other perturbing multiplet on this term seems to be appreciable and is not properly incorporated in the treatment of Whitelaw. For silver and gold, the x-ray term values together with the spectroscopic term values are used in deriving the relation. Thus η_1 is expressed as a function of ϵ for all three metals, and from η_1 we can calculate k_l involved in the calculation of p-functions by (1).

We now apply Eq. (10) to the evaluation of the logarithmic derivatives, if ΔV is known. For copper, the values of the effective nuclear charge $Z(r)$ calculated by the Hartree-Fock method are available.[12] For silver and gold, $Z(r)$ will be extrapolated from that of copper as follows. As we shall see later, the lattice spacing of copper is mainly determined by the repulsive force between ion-cores when they come into contact. We shall call this repulsion the ion-core repulsion hereafter. Now, we may assume that the size of the ion core determines the lattice spacing of silver and gold as well. Therefore, by comparing the observed lattice constants of silver and gold with that of copper, we can estimate the form of the ion-core potential of silver and gold. The Hartree-Fock values of $\Delta V(r)$ for copper can be approximated by means of the analytical expression

$$\begin{aligned} \Delta V(r) &= \beta r^{-1}\exp-\alpha_1 r \quad \text{for} \quad 1.4\leqq r\leqq 3.4, \\ &= 0 \qquad\qquad\qquad\quad \text{for} \quad r\geqq 3.4, \end{aligned} \tag{11}$$

with

$$\alpha_1=2.438, \quad \beta=27.53. \tag{12}$$

Let us assume that the form of $\Delta V(r)$ for silver as well as for gold is analogous to (11), and also that the values of β and ΔV at r corresponding to the observed lattice spacings are identical for all three metals. Then, remembering the observed lattice constant is 3.60 A for copper, and 4.06 A for silver and gold, we find that $\alpha_1=2.113$ for silver and gold. The radius R_c outside of which ΔV vanishes, is assumed to be proportional to the observed lattice constants, and we have $R=3.4$ for copper and $R=3.8$ for silver and gold. Thus the form of ΔV for silver as well as gold is determined.

The logarithmic derivatives $\phi_0(r_s)$ of s-functions are computed by (10) for several s-sphere radii, and the values of ϵ_0 which satisfy the boundary condition $\phi_0(r_s)=1$ are determined as the ground state energy. The logarithmic derivatives $\phi_1(r_s)$ of p-functions are also calculated by (10), where the energy parameter is taken to be equal to ϵ_0. The Fermi energy ϵ_F is evaluated by the well-known formula[13]

$$\epsilon_F=2.21\alpha r_s^{-2}, \tag{13}$$

where

$$\alpha=\gamma[\phi_1(r_s)-1]. \tag{14}$$

$$\gamma=-\tfrac{1}{3}r_s^2(\partial\phi_0(r_s)/\partial\epsilon_0)^{-1}. \tag{15}$$

Finally, Coulomb, exchange, and correlation energies are approximated by means of the expression

$$\epsilon_C=0.284r_s^{-1}-0.576/(r_s+5.1) \tag{16}$$

given by Wigner.[14]

In the case of copper, we carried out the successive approximations until we obtained the self-consistent solution of (8), but we found that the accuracy of (10) was sufficiently good for our purpose. Therefore, the logarithmic derivatives involved in the calculation of ϵ_0 and ϵ_F are evaluated by (10).

The results of our calculation are summarized in Table I. The cohesive energy ϵ_{coh} in this table may be regarded as the cohesive energy resulting from the valence electrons. The lattice structure of the monovalent noble metals is face centered cubic. The lattice constant is 3.60 A for copper and 4.06 A for silver and gold. The corresponding sphere radius is 2.66 for copper, and 2.99 for silver and gold, all in Bohr units. We readily see from Table I that the cohesive energy due to the valence electrons does not have a maximum at the observed lattice spacing for any of these metals. This means that the ion-core repulsion is of importance in realizing the maximum of the cohesive energy at the observed lattice spacing.

Fuchs[4] has estimated the ion-core repulsion energy of copper by a modified Thomas-Fermi method. He has

[8] F. Ham (private communication).
[9] T. S. Kuhn, Quarterly of Appl. Math. **9**, 1 (1951).
[10] R. F. Bacher and S. A. Goudsmit, *Atomic Energy States* (McGraw-Hill Book Company, Inc., New York, 1932).
[11] N. G. Whitelaw, Phys. Rev. **44**, 544 (1933).
[12] D. R. Hartree and W. Hartree, Proc. Roy. Soc. (London) **A157**, 490 (1936).
[13] J. Bardeen, J. Chem. Phys. **6**, 367 (1938); R. A. Silverman, Phys. Rev. **85**, 227 (1952); W. Kohn, Phys. Rev. **87**, 472 (1952).
[14] E. P. Wigner, Phys. Rev. **46**, 1002 (1934); Trans. Faraday Soc. **34**, 678 (1938).

TABLE I. The calculation of the energy of valence electrons. ϵ_{coh} is the difference between the binding energy $\epsilon_0+\epsilon_P+\epsilon_C$ and the first ionization potential. α and γ are defined by Eqs. (14) and (15) respectively. z_s is equal to $(8r_s)^{\frac{1}{2}}$. The values in brackets are those obtained by assuming a pure hydrogenic potential, in which case $\Delta V=0$.

Metal	z_s	ϵ_0	γ	α	ϵ_P	ϵ_{coh}
	4.0	−1.406 *Ry*	1.189	0.933	0.515 *Ry*	0.262 *Ry*
		(−1.508)	(1.264)	(0.918)	(0.507)	(0.372)
Copper	4.5	−1.147	1.034	0.983	0.339	0.203
		(−1.158)	(1.046)	(0.983)	(0.339)	(0.214)
	5.0	−0.952	0.891	0.987	0.223	0.140
		(−0.953)	(0.893)	(0.988)	(0.224)	(0.140)
	4.5	−1.175	1.096	0.988	0.333	0.248
		(−1.210)	(1.124)	(0.949)	(0.327)	(0.289)
Silver	5.0	−0.967	0.929	1.010	0.229	0.160
		(−0.971)	(0.934)	(1.006)	(0.228)	(0.165)
	5.5	−0.819	0.789	1.003	0.155	0.097
		(−0.819)	(0.789)	(1.003)	(0.155)	(0.097)
	4.5	−1.293	0.897	0.984	0.339	0.239
		(−1.321)	(0.916)	(0.861)	(0.297)	(0.309)
Gold	5.0	−1.062	0.781	1.006	0.228	0.135
		(−1.066)	(0.786)	(1.004)	(0.227)	(0.140)
	5.5	−0.903	0.639	0.969	0.150	0.065
		(−0.903)	(0.639)	(0.969)	(0.150)	(0.065)

shown that the ion-core repulsion begins to be appreciable at an interatomic distance of 5.5 a.u., which corresponds to $r_s=3.03$ or $z_s=4.93$, and it increases very rapidly as the interatomic distance decreases. This means that the ion-core is almost rigid. Combining values of ϵ_{coh} given in Table I with the ion-core repulsion energy given by Fuchs, we find that the equilibrium lattice constant is 4.2 A, and the total cohesive energy is 1.89 ev (43.5 kcal/mole) for copper. The observed values for these constants are 3.6 A and 3.52 ev, while the values obtained by Fuchs are 4.2 A and 1.45 ev. From the comparison of the calculated and observed values of lattice constant, one can conclude that the ion-core repulsion estimated by Fuchs starts to rise at too large an interatomic distance. In the present paper, however, we will not try to improve the calculation of the ion-core repulsion. Instead, we shall make use of the fact that the ion core is almost rigid. If we assume that the ion cores of the noble metals are rigid spheres, the interatomic distances are determined by the ion-core radii, while the total cohesive energies are equal to the cohesive energies due to the valence electrons. We calculate the radii of the s-spheres from the observed lattice constants for these metals, and determine the cohesive energy at those radii by interpolating values of ϵ_{coh} given in Table I. Since the ion-core repulsion contributes very little to the total cohesive energy, as is shown for copper by Fuchs, the cohesive energy due to the valence electrons calculated at the observed lattice spacings should be a good approximation to the total cohesive energy. The results are given in Table II, where values of α at the observed lattice spacings are included as well.

CONCLUSION

The agreement with the observed values of the cohesive energy is fairly good for copper and silver, but not so good for gold. We shall point out some of the shortcomings in the present calculation: (I) The calculation of the uncorrected p-function is relatively inaccurate, because the information from the spectroscopic term value on the dependence of η_l on ϵ is insufficient. In the case of copper, the configuration interaction aggravates the situation. (II) The ion-core potentials for silver and gold are extrapolated from that of copper. Although the corrections due to ΔV are small, the errors in ΔV may have introduced small errors in the final results. (III) The ion-core repulsions are not treated accurately. In fact, we have assumed the rigidity of the ion-core, and neglected the contributions from the repulsive energy to the cohesive energy. (IV) We have neglected terms with powers higher than the second in the expansion of the energy into the power series of k.

TABLE II. The calculated and observed values of cohesive energy and the calculated values of α. The theoretical values are calculated at the observed lattice spacings.

Metal	Cohesive energy in kcal/mole			α	
	Corrected[a]	Uncorrected[b]	Observed	Corrected[a]	Uncorrected[b]
Copper	59.3	59.9	81.2	0.988	0.989
Silver	55.8	58.9	68.0	1.008	0.985
Gold	48.9	53.3	92.0	1.006	0.987

[a] Calculated with corrections due to the deviation of the effective ion-core potential from the pure hydrogenic form.
[b] Calculated by assuming a pure hydrogenic potential.

The fourth-power term may contribute appreciably to the Fermi energy.

Finally the values of α listed in Table II are the reciprocal values of the ratios of the effective electron mass to the free electron mass. Hence, the effective electron mass calculated near the bottom of the lowest Brillouin zone is almost equal to the free electron mass for all three noble metals.

The author wishes to thank Professor H. Brooks for his advice and helpful suggestions throughout this work. He is also indebted to Dr. F. Ham for the use of his results before publication.

Compression of the Alkali Metals to 10 000 Atmospheres at Low Temperature

C. A. SWENSON
Cryogenic Engineering Laboratory, Massachusetts Institute of Technology, Cambridge, Massachusetts
(Received April 13, 1955)

A technique originally developed by Bridgman has been used to measure the total compressions of the alkali metals (Li, Na, K, Rb and Cs) for pressures up to 10 000 atmospheres at 4.2° and 77°K. The unusual features found were an abnormally low decrease in compressibility with pressure for cesium, probably connected with a smearing out of the electronic transition found at 45 000 atmos at room temperature, and a possible transformation in rubidium at 77°K which resulted in a permanent increase in the room temperature density of about ten percent. A comparison of these data with theoretical work by Bardeen shows better agreement than was obtained with an extrapolation of room temperature data to absolute zero, although the agreement is satisfactory only for sodium. Approximate densities also were obtained at these temperatures, and the agreement with unpublished calculations by Brooks is excellent for all the metals except lithium, where a deviation could be expected to occur.

INTRODUCTION

THE work done in compressing a solid can in general be broken up into two parts: the first involving changes of entropy with volume (heating effects), and the second involving only changes in internal energy. From a theoretical point of view, calculations involving the temperature as an independent variable are extremely difficult, so that theoretical calculations of compressibilities are usually confined to absolute zero where the volume is the only independent variable. Because it is as difficult to extrapolate high-temperature compressibility data to low temperatures as it is to make the initial high-temperature calculations, a proper comparison of theory with experiment can be made only if the range of experimental data is extended into the temperature region where thermal effects will be unimportant.

The substances which are of the greatest theoretical interest are the condensed rare gases and the alkali metals, since they represent, respectively, the simplest dielectric solids and the simplest metals. Because of their low Debye θ's, it is necessary to go to liquid helium temperatures (4.2°K) to make sure that thermal effects for these substances are negligible, and it is unfortunate that conventional methods for measuring the change in volume with pressure cannot be used in this temperature region. However, exploratory work by Stewart[1,2] has shown that many of the solidified gases and also the alkali metals are quite plastic at 4.2°K, so that a technique which was used by Bridgman for very high pressure work[3,4] has been adapted for compressibility work at these temperatures. Results obtained using this method have been published recently for some solidified gases,[2,5] and the work described below concerns similar measurements on the alkali metals; lithium, sodium, potassium, rubidium, and cesium.

EXPERIMENTAL DETAILS

The method which was used is essentially that due to Bridgman,[4] and is illustrated in Fig. 1. The sample was placed in a thick-walled cylinder which was closed at either end by a piston. A compressive force was applied to the pistons, and the motion of the pistons as a function of applied force was used to give, with suitable corrections, the hydrostatic compression of the sample as a function of pressure.

The major problem with this method is to make sure that the sample is plastic enough so that the pressure on the sample is approximately hydrostatic; or, in other words, it must not be possible for an appreciable pressure difference to exist between the ends and sides of the sample. This will be true if the shear yield strength of the sample material is much less than the applied pressure. Stewart's measurements have shown that this is true at 4.2°K for sodium and potassium,[1] and since cesium and rubidium are much more plastic than these at room temperature, it was assumed that they would also be sufficiently plastic at low temperature. Lithium is perhaps less satisfactory and represents a borderline case, so that the results on it must be taken with some reservation.

The major pieces of equipment needed to perform these experiments, other than the sample holder, are a

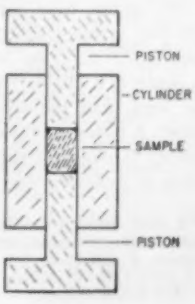

FIG. 1. The type of sample holder used in these experiments.

[1] J. W. Stewart, Doctoral thesis, Harvard University, May, 1954 (unpublished).
[2] J. W. Stewart, Phys. Rev. **97**, 578 (1955).
[3] P. W. Bridgman, Proc. Am. Acad. Arts Sci. **74**, 425 (1942).
[4] P. W. Bridgman, Proc. Am. Acad. Arts Sci. **76**, 1 (1945).
[5] J. W. Stewart and C. A. Swenson, Phys. Rev. **94**, 1096 (1954).

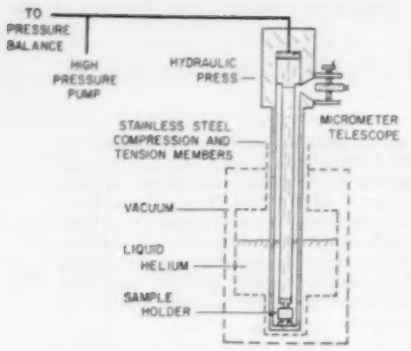

FIG. 2. A sketch of the hydraulic press and the liquid helium (or liquid nitrogen) dewar. The surrounding liquid nitrogen jacket is not shown.

hydraulic press with long supports to compress the sample holder at low temperature, a means for measuring both the initial length and the changes in length of the sample, and a dewar vessel for containing liquid helium or liquid nitrogen. These essential parts of the apparatus which was used are sketched in Fig. 2. The force on the sample holder was calculated from the oil pressure (given by the pressure balance) and the area of the hydraulic piston, while apparent changes in the length of the sample were indicated by the motion of the hairline as measured by the micrometer telescope (sensitivity about 0.002 mm). The maximum force available was four tons, which corresponds roughly to 10 000 atoms pressure on a 0.250-in. diameter sample.[6]

In principle, the taking of compression data at liquid nitrogen or liquid helium temperatures was quite simple, since it was only necessary to increase the pressure and record the motion of the hairline. However, three basic corrections had to be made which formed a large part of the readings actually taken; namely, the corrections for friction, background stretch (that is, the motion of the hairline with no sample in the holder), and the expansion of the holder under hydrostatic pressure. In order to guard against systematic errors in making these corrections, sample holders of two different sizes were used for each of the five alkali metals.

The holders were similar to that shown in Fig. 1, with the outside diameter of the cylinder being in all cases 0.875 in. Two holders were used with inside diameters of 0.250 in.; the first was made from hardened tool steel, and the second from hardened beryllium copper. A piston on the original steel holder was broken midway through the runs, and when difficulty arose in trying to replace it due to repeated breakage, a beryllium copper holder of the same dimensions was substituted. These holders were useful for sample pressures from 1500 to 10 000 atmos, and will be referred to below as the "small" holders. The other or "large" holder, with twice the piston area (0.354-in. diameter), was also made from hardened tool steel and was used for pressures from 750 to 5000 atmos. The background stretch correction was relatively about twice as great for the "large" as for the "small" holder, while the friction and expansion corrections were less.

The effects of friction are illustrated by the hysteresis loop in Fig. 3, where the experimental data for one cesium run are plotted. As the pressure was increased slowly and monotonically by placing weights on the pressure balance, the friction opposing the motion of the piston built up fairly quickly until it reached a steady value. When a maximum pressure was reached (determined only by the danger of permanently deforming the apparatus), the pressure was slowly reduced, so that the direction of this frictional force was reversed. It did not reverse instantaneously, but eventually became constant again in the opposite direction at slightly lower pressures. This was shown by the fact that the pressure increasing and pressure-decreasing curves were parallel for intermediate pressures, and in this region the true pressure corresponding to a given displacement could be calculated as the mean of the two curves, as is shown.[6] The dotted curve which gives this average pressure was extrapolated to higher pressures beyond the parallel region on the assumption that the friction remained at a constant value.

At low pressures, the friction decreased, and the true pressure was again the mean for a given displacement. If there was no permanent deformation of the sample,[7] the reading at zero pressure was unchanged, although because of uncertainties in the friction, this did not necessarily correspond to the true sample length at zero pressure. To eliminate this effect and to allow a determination of the sample length to be made, a calibration setting of the hairline (taken with respect to a fiducial mark on the hydraulic head and corrected for friction) was always recorded at a pressure at 1500 atmos, to be compared with a similar setting with no sample in the holder. This length (good to about 0.03 mm) and the weight of the sample were then used to calculate a density at 1500 atmos which was subsequently extrapolated to zero pressure by using the $\Delta V/V$ data. It is worth noting that the absolute values of the lengths as obtained in this way were far less accurate than changes in lengths, since hairline settings could be reproduced to about 0.002 mm when the pressure was released and then reapplied during a given run. Great care was always taken to ensure that the

[6] A more detailed description of this apparatus, which was similar to that described in reference 5, will be found in C. A. Swenson, J. Inst. Soc. Am. (to be published), and also in the U. S. Army Office of Ordnance Research Technical Memorandum, TM-55-1 (unpublished).

[7] There was always a zero shift on the initial compression due to the compacting of the material in the sample. For this reason, the sample was subjected to full pressure several times ("seasoned") at each temperature until the zero remained constant after cycling.

temperature gradient down the support members was constant during each run and reproducible from run to run, since any change in gradient could affect both the background stretch correction and the calibration setting of the hairline, as well as cause spurious changes in readings.

The major source of the friction has been discussed by Bridgman,[3] and is undoubtedly due to polycrystalline grains of the sample being forced to move with respect to each other. This is supported by the fact that the friction increased with decreasing temperature. It is interesting to note that at 4.2°K the half-height of the hysteresis loop represented about ten percent of the total change in sample length observed for all the metals except lithium, where it was slightly more. This was surprising, since the lengths, the total compressions, and the sample areas all varied indiscriminately over a factor of at least two. Thus, if the two sides of the loop were parallel to ten percent (as was usual), the effect on $\Delta V/V_0$ was of the order of one percent.

The background stretch due to the hydraulic press and the sample-holder pistons was determined by performing an identical experiment at each temperature for each holder in the absence of a sample. The resulting curves were quite linear, and gave a total compression in 10 000 atmos, which was reproducible to about one-half percent. The magnitude of this correction is shown also in Fig. 3, where it can be seen to represent about thirty percent of the data which was taken. This was the most favorable case, and the correction varied with sample material and length until in the least faborable cases (short samples of lithium and sodium) it represented about sixty percent of the data. This introduced an uncertainty into the final calculations of less than two percent.

The last correction, that due to the expansion of the sample holder under hydrostatic pressure, had to be determined experimentally. The sample holders were filled with a soft metal (such as lead, indium or thallium), and a measurement of the room temperature compression of this metal was taken as described in the aforementioned. The difference between the total compression as given by using the background stretch and friction corrections only, and the true value as given in the more accurate results of Bridgman,[4] was assumed to be due to the cylinder expansion. This difference was measured as a function of length for each holder at room temperature and was extrapolated to 77° and 4.2°K by assuming that it was inversely proportional to the Young modulus of the metal.[5] This correction at room temperature amounted to less than 0.005 in $\Delta V/V_0$ for the full compression in the large holder, while the maximum effect was about 0.020 in $\Delta V/V_0$ for the small beryllium copper holder. The inaccuracy in $\Delta V/V_0$ due to this

[5] Unpublished results at this laboratory have shown that the increase in Young's modulus for steel and beryllium copper as the temperature is decreased is roughly ten percent from room temperature to 77°K and practically zero from 77°K to 4.2°K.

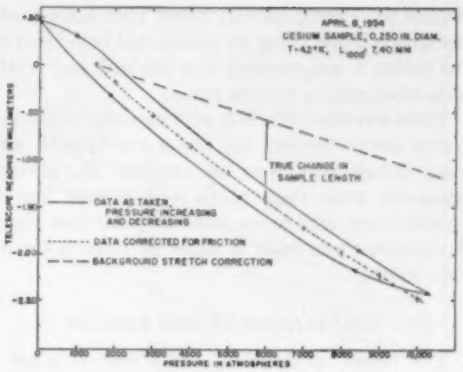
APRIL 8, 1954
CESIUM SAMPLE, 0.250 IN. DIAM.
T=4.2°K, L 7.40 MM
TRUE CHANGE IN SAMPLE LENGTH
DATA AS TAKEN, PRESSURE INCREASING AND DECREASING
DATA CORRECTED FOR FRICTION
BACKGROUND STRETCH CORRECTION
TELESCOPE READING IN MILLIMETERS
PRESSURE IN ATMOSPHERES

FIG. 3. Typical experimental data obtained in a cesium run at 4.2°K.

cause can be shown to be absolute, independent of the compression to a first approximation, and it was never greater than 0.001. It was consequently more serious for the least compressible metals, lithium and sodium. The necessity for determining the correction in this manner means that the results quoted are relative to Bridgman's results. Making a correction in this way also serves to eliminate errors due to small effects which might otherwise be overlooked.

A fourth correction, due to thermal expansion, was not serious except in the density calculations. The volume change between room temperature and 4.2°K was assumed to be $-0.5(\pm 0.3)$ percent for the steel holders, and $-0.9(\pm 0.3)$ percent for the beryllium copper holders. The weights of the samples were obtained by weighing the holders when empty and when full, and the volume was calculated from the value of the length at 1500 atmos extrapolated to zero pressure. The values of the densities so obtained for each holder usually agreed to about one-half percent, and the experimental accuracy is estimated to range from 0.5 percent for the heavier metals to one percent for lithium.

The metals were obtained from A. D. Mackay, Inc., who estimated the purities as 99.9 percent for the sodium, rubidium, and cesium, and as better than 99 percent for the lithium and potassium. Except for the lithium, they were furnished in evacuated glass ampules containing from 0.5 to 1 gram. These were broken and manipulated under dry benzine into a glass funnel arrangement which could be evacuated and in which the metal was melted from the ampule into the cylinder (closed at its bottom by its lower piston), either under vacuum or in a helium atmosphere. The sample holder was then cooled considerably below room temperature so that the top piston could be placed in the cylinder. The chances for the introduction of oxide were very slight, since all operations were done as quickly as possible, and no film was ever observed on the metal surfaces after melting. The lithium was immersed in

benzine while being cut with a cork borer and placed in the sample holder. After the pistons had been fitted into the holder, it was removed from the bath and dried in a chamber using a vacuum pump.

There was some difficulty with extrusion of the more plastic metals between the piston and cylinder walls, even though they were an excellent fit, so small, triangular brass rings which were pressed into the cylinder were used as an additional seal (see Fig. 1). A correction was made to allow for these in the final calculations.

CALCULATION OF THE RESULTS

The values for $\Delta V/V_{1500}$ which were obtained for each metal in each sample holder, suitably corrected, were plotted against pressure on a large sheet of graph paper, and a smoothed curve drawn through them for each temperature. The lower pressure limit of 1500 atmos for the small holders and 750 atmos for the large holder was caused by a limitation in the minimum weight which could be used on the pressure balance. No great effort was made to rectify this, since at lower pressures the friction was changing so rapidly. The agreement of the two curves between 1500 atmos and 5000 atmos was never worse than five percent of $\Delta V/V_{1500}$, and was usually much better, giving a considerable confidence in the correctness of the data obtained and the corrections made.

These values of $\Delta V/V_{1500}$ were then extrapolated to zero pressure by means of an expression derived by Birch from Murnaghan's theory of finite strain[9]:

$$P=(3/2\beta_0)[y^7-y^5][1-\xi(y^2-1)], \qquad (1)$$

where $y=(V_0/V)^{\frac{1}{3}}$, V is the volume at the pressure P, V_0 is the volume at zero pressure, β_0 is the initial compressibility $[\beta=-(1/V_0)(\partial V/\partial P)_T]$, and ξ is an adjustable constant which must be found by trial and error. For this extrapolation, β_0 is actually β_{1500}, and V_0 is V_{1500}. Good fits were found for moderate values of ξ except for the case of lithium.

$\Delta V/V_0$ could then be calculated from the values of V_{1500}/V_0 which were found. These compressions are plotted as a function of pressure in Fig. 4 for all the alkali metals at both 77° and 4.2°K, while the actual 4.2° smoothed data are given in Table I. It must be emphasized that the differences in the $\Delta V/V_0$'s between 1500 and 10 000 atmos are known more accurately than those from zero to 1500 atmos, since these latter are due to an extrapolation. The probable error in $\Delta V/V_0$ was estimated to be less than three percent at 10 000 atmos for potassium, rubidium, and cesium, and to be slightly higher for lithium and sodium. This corresponds to an error in the pressure for a fixed $\Delta V/V_0$ of less than five percent. The data for lithium are the least dependable, both because of its low compressibility, and its lack of plasticity at 4.2°K. Final $\Delta V/V_0$ curves were again fitted to Eq. (1) in order to obtain compressibilities at zero pressure, and the resultant values of β_0 and ξ are given in Table I for both 77° and 4.2°K.

TABLE I. The smoothed results for the compression experiments on the alkali metals.

P(atmos)		Li	Na	K	Rb	Cs
0		0.000	0.000	0.000	0.000	0.000
500		0.004	0.007	0.014	0.016	0.022
1000		0.007[5]	0.013	0.028	0.031	0.044
1500		0.011	0.020	0.039	0.046	0.063
2000		0.014	0.026	0.049	0.060	0.081
3000	$\Delta V/V_0$	0.021	0.038	0.070	0.084	0.113
4000		0.028	0.049	0.090	0.106	0.141
6000		0.040	0.070	0.123	0.142	0.188
8000		0.051	0.088	0.152	0.171	0.229
10 000		0.061	0.105	0.177	0.196	0.263
$\beta_{0,77}(10^{-6}$ atmos$^{-1})$		0.88	1.56	2.96	3.88	4.93
$\beta_{0,4.2}(10^{-6}$ atmos$^{-1})$		0.78	1.39	2.88	3.48	4.41
$\xi_{0,77}$		−2.5	−0.9	0	−0.3	+0.4
$\xi_{0,4.2}$		−2.0	0	0	−0.15	+0.6
$\rho_{0,300}$(g/cc)		0.53[3]	0.971	0.862	1.53(1.71)	1.90
$\rho_{0,77}$(g/cc)		0.56[3]	1.01[5]	0.91[5]	1.64(1.79)	2.09
$\rho_{0,4.2}$(g/cc)		0.56[4]	1.01[6]	0.92[5]	1.63	2.13

The average densities at 77° and 4.2°K as found in these experiments are also given in Table I, together with the room temperature densities.[10] In general, within the limits of error, the density was greater at 4.2° than at 77°K, although as would be expected, the change was quite small. The agreement with the 77°K x-ray

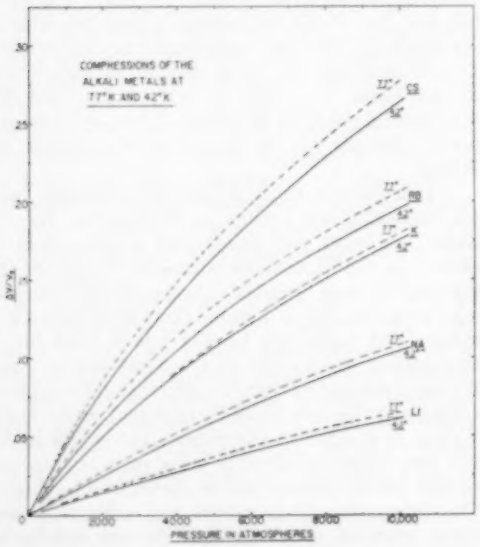

FIG. 4. The $P-V$ relationships to 10 000 atmos for the alkali metals at both 77° and 4.2°K.

[9] F. Birch, J. Geophys. Research **56**, 227 (1952).

[10] J. D'Ans and E. Lax, *Taschenbuch fur Chemiker und Physiker* (Springer-Verlag, Berlin, 1949), p. 211.

data of Simon and Vohsen[11] is satisfactory, although their results give slightly lower densities.

An exception for rubidium (noted by the figures in brackets at room temperature and 77°K) deserves special mention, and a rather detailed account of its occurrence. The small and large holders were both filled with rubidium and run at 4.2°K, giving results for $\Delta V/V_{1500}$ and the density which agreed quite well with each other. The next day, the small sample was run at 77°K, giving the density of 1.64 g/cc which is recorded. The large sample and holder were then placed in the press and cooled, after which the pressure was increased slowly to "season" the sample, as was the usual practice. At a sample pressure of a few hundred atmos, a sharp crack was heard, with a coincidental decrease in the sample length of about ten percent. The resulting $\Delta V/V_{1500}$ curve agreed very well with the same curve for the small sample holder, in spite of the difference in density (1.64 to 1.79 g/cc) and consequent change in V_{1500}.

When the holder was warmed to room temperature and its length and weight checked, a sample density of 1.71 g/cc was obtained in place of the correct 1.53 g/cc which was obtained for the small holder. This sort of phenomenon was not found for any other substance, and could not be reproduced in two other runs with different fillings of rubidium. The weight was checked twice, and gave good agreement at 4.2°K with the small holder, so that an error here seems unlikely. Since an error in the measurement of a length at room temperature to a few percent is unlikely, this isolated effect is reported as unexplained, and as being a *possible* new form of rubidium of higher density, stable at room temperature.

Before the sample was destroyed (in the firm belief that the sample holder had changed its characteristics), an attempt was made to measure the melting point of the material in the sample holder. Normally, rubidium melts at about 38°C, while no evidence of melting was found as high as 100°C. A slight decrease of density was found after this heating, which is probably significant. These effects may have some connection with the rather strange, irreversible effects which have been found by Pearson in the thermal expansion of rubidium,[12] and also by others in its specific heat[13] and electrical resistance.[14]

DISCUSSION OF THE RESULTS

The 4.2°K data of Table I were extrapolated to 50 000 atmos and were replotted as molar volumes in Fig. 5 to compare them with the room temperature results given by Bridgman.[15] This extrapolation of over a factor of five in pressure, made by using Eq. (1), is qualitatively justified by the success which Birch has had in fitting this function to compression data for pressures up to 100 000 atmos.[9] Birch found that most substances obeyed the simpler form of Eq. (1) given by $\xi=0$, and this is the case for sodium, potassium and rubidium to 10 000 atmos at 4.2°K. If this behavior is to be taken as "normal" (realizing that Eq. (1) is semiempirical in nature), then one can conclude that lithium is too hard ($\xi<0$) with its compressibility dropping off more rapidly than one would expect, and that cesium is too soft ($\xi>0$), with its compressibility dropping off more slowly than "normal" with increase of pressure. While the data for lithium are suspect because of the mechanical strength of the metal, there is no reason to mistrust either the actual data or the extrapolation for cesium.

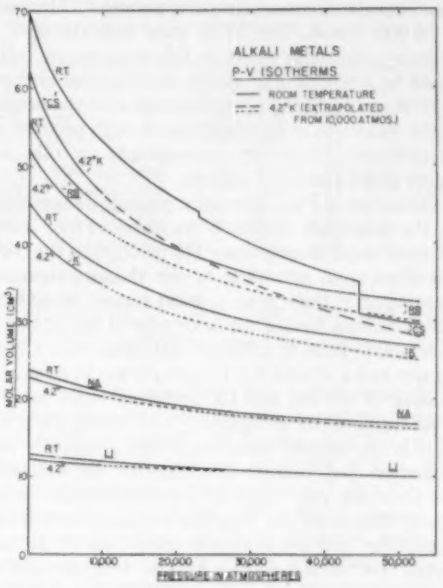

FIG. 5. A comparison of the extrapolated low temperature data for the alkali metals with the data obtained by Bridgman at room temperature.

This "softness" in cesium and a possible explanation can be seen in the curves of Fig. 5. The two transitions for cesium shown in the room temperature curve are due to a change in crystal structure from body centered cubic to face centered cubic at 23 000 atmos, and a presumed change in electronic structure (a $6s$ electron moving into a $5d$ orbit) at 45 000 atmos.[15,16] The crystallographic transformation is too small to be of significance for the extrapolation, but the excess softness of the cesium seems to be connected with a smearing out of the electronic transition, as is seen by the.

[11] F. Simon and E. Vohsen, Z. physik. Chem. **133**, 165 (1928).
[12] F. M. Kelley and W. B. Pearson, Can. J. Phys. **33**, 17 (1955).
[13] T. M. Dauphinee and H. Preston-Thomas (unpublished results). See reference 12.
[14] D. K. C. MacDonald, Phil. Mag. **43**, 479 (1952).
[15] P. W. Bridgman, *The Physics of High Pressure* (G. Bell and Sons, London, 1949), second impression, p. 178.
[16] R. Sternheimer, Phys. Rev. **78**, 235 (1950).

coincidence of the room temperature and 4.2° isotherms at 50 000 atmos. The 77°K data indicate that the softening effect also exists at this temperature, and it would be interesting to obtain experimental isotherms at 77°K and higher to try to discover what the behavior of the transition is as a function of both pressure and temperature. Electrical measurements in this same region would also be of interest.

The curves of Fig. 5 give some grounds for speculation on the suspected rubidium transition. First, it is of the same order of magnitude (10 percent) as the cesium transition, and, according to the theoretical work of Sternheimer,[16] there is no *a priori* reason for excluding rubidium from having the same type of transition. If a more stable form of rubidium did exist, with a higher density and a similar $P-V$ curve, it would remove the crossing of the Rb and Cs isotherms which has been commented on by Bridgman,[17] and would place rubidium in its "proper" position at high pressure between potassium and cesium. The grounds for conclusions like these are very vague at the moment, but they do give guidance for the direction of future experimental work. The only other known transitions in the alkali metals are shear-sensitive at low temperatures and occur in lithium[18] and sodium,[19,20] but since the volume changes are very slight, they would not show up in this work.

The 77°K data were not plotted in Fig. 5, since they tended to coincide with the 4.2°K data at pressures above 5000 atmos. The relative contributions to the pressure of the internal energy and the entropy terms have been discussed by Bridgman,[21,22] and it is of interest to try to estimate the entropy contribution for relatively low pressures near 80°K, where it should be small. The thermodynamic relationship,

$$TdS = PdV + dU, \tag{2}$$

can be rewritten at constant temperature to give

$$P = T\left(\frac{\partial S}{\partial V}\right)_T - \left(\frac{\partial U}{\partial V}\right)_T = -\left[T\frac{(\partial V/\partial T)_P}{(\partial V/\partial P)_T} + \left(\frac{\partial U}{\partial V}\right)_T\right]. \tag{3}$$

In this expression, the first term vanishes at low temperatures, where the pressure is determined solely by the volume derivative of the internal energy. At higher temperatures, it would be possible to calculate the magnitude of the first term if thermal expansion data as a function of pressure and temperature were available, but, except for some average values at room temperature, these data do not exist for the alkali metals. Bridgman has estimated that at room temperature $(\partial U/\partial V)_T = 0$ at pressures of a few thousand atmospheres for sodium and one would expect this term to increase rapidly with decreasing volume, while the first term decreases in importance. The indications are, however, that the entropy term is still significant at room temperature for pressures of 50 000 atmos.

There is a second way of estimating the relative importance of this entropy term. The total work done in an isothermal compression can be calculated from the integral of $-PdV$, part of which appears as heat $(-\int TdS)$, and the rest of which appears as a change in the internal energy. In general, the entropy decreases with pressure with the total decrease limited by the third law of thermodynamics, since the entropy can never be less than its value at absolute zero for a system in thermodynamic equilibrium. Thus, if the value for the entropy difference between absolute zero and a given temperature is known for zero pressure $[(S-S_0)_{p=0}]$, then it is possible to calculate the maximum heat which can be evolved in a reversible isothermal compression at that temperature as $Q \leq T(S-S_0)_{p=0}$.

If this calculated heat is large compared with the total work done in the compression, it is highly probable that the entropy contribution to the pressure will be considerable. If, however, the two are comparable, then one would expect that the substance has been compressed to the point where the contribution of its entropy term is negligible, since $T(\partial S/\partial V)_T$, or the thermal expansion, will decrease with pressure, and $(\partial U/\partial V)_T$ will increase.

These quantities have been calculated for the alkali metals and are given in Table II. The values of $T(S-S_0)_{p=0}$ decrease by a factor of about ten from room temperature to 77°K and are negligible at 4.2°K,[23] while (except for the previously discussed softness of cesium) the work done in a compression to 10 000 atmos changes only slightly. Thus, one would expect a relatively large pressure difference between the room temperature and 77° isotherms for a given value of the molar volume, but only a slight change between 77° and 4.2°K. This, in fact, is what is observed. In effect, the molar volumes obtained for 10 000 atmos and 77°K would seem to differ only slightly from those at 10 000 atmos and 4.2°K, so that preliminary experimental work in the higher pressure region can probably be done as profitably at 77° as 4.2°K.

[17] Reference 15, p. 182.
[18] C. S. Barrett and O. R. Trautz, Trans. Am. Inst. Mining Met. Engrs. **175**, 579 (1948).
[19] C. S. Barrett, Am. Mineralogist **33**, 749 (1948).
[20] John Rayne, Phys. Rev. **95**, 1428 (1954).
[21] Reference 15, p. 172.
[22] P. W. Bridgman, Revs. Modern Phys. **7**, 1 (1935).

[23] The room temperature values of the entropy were taken from J. D'Ans and E. Lax, *Taschenbuch fur Chemiker und Physiker* (Springer-Verlag, Berlin, 1949), pp. 214–256. The low-temperature entropies for lithium and potassium were estimated from the Debye θ's given in the survey of F. M. Kelley and D. K. C. MacDonald [Can. J. Phys. **31**, 147 (1953)]. The entropy at 77°K for sodium was taken from G. L. Pickard and F. E. Simon [Proc. Phys. Soc. (London) **59**, 1 (1948)], while the rubidium and cesium data are from unpublished results of Dauphinee and Preston-Thomas (reference 13), kindly furnished by Dr. Martin of the National Research Council, Canada.

While speculations as to the change of internal energy with temperature are amusing, the chief value in obtaining experimental results at temperatures where the entropy term is negligible lies in a comparison with theoretical calculations. Very little has been done along these lines which is quantitative enough in nature to allow a check with the experimental results of Table I.[24] Some time ago, Bardeen reported detailed calculations for lithium and sodium using the Wigner-Seitz model, while also giving an analysis of Bridgman's room temperature results for all of the alkali metals in terms of a semiempirical model.[25] Even though the latter is probably too simple, it is of interest to repeat Bardeen's analysis using the data in Table I and his quoted experimental values for the cohesive energy at absolute zero. Very briefly, Bardeen assumed that the energy of a simple metal is given by

$$E_{\text{coh}}=Ay^3+By^2-Cy, \tag{4}$$

where $y=(V_0/V)^{\frac{1}{3}}$, and the first and third terms refer to the energy of the electron in its lowest state, while the second term represents the Fermi energy. By using values for V_0, β_0 and E_{coh} at absolute zero and zero pressure, it is possible to evaluate the constants A, B, and C, and to compare them with theory.[25] This comparison is made in Table III, lines 3 to 7. As would be expected, the agreement is better than was obtained by Bardeen's use of the extrapolated room temperature values. In particular, all the constants now have the expected sign, and vary in the expected direction.

By evaluating $P=-(\partial E/\partial V)_P$, Bardeen derived the following expression from this three-constant energy equation[25]:

$$PV_0=y^4(y-1)[2A+2B/3+a(y-1)], \tag{5a}$$

or

$$P=y^4(y-1)[3/\beta_0+A(y-1)/V_0]. \tag{5b}$$

The second term in the brackets in (5b) is quite small (of the order of a few percent at most), so that the shape of the $P-V$ curve is almost uniquely determined once β_0 has been specified. The easiest method for comparison here is to compute the theoretical pressure which would correspond to the value of (V_0/V) given by an experimental pressure of 10 000 atmos. This comparison is shown in the last line of Table III. The indications are that all the metals except cesium are less compressible than would be expected from the observed β_0 and theoretical curve, while cesium is too compressible, in agreement with the earlier conclusion. The deviations are outside the limits of experimental error (±500 atmos) and can be interpreted as meaning that the three constant equation does not provide the correct form of the pressure-volume curve. This is not surprising in view of the approximations involved. In particular, when these calculations are compared with Bardeen's earlier work, the anomaly found for rubidium disappears, although anomalies appear for lithium and cesium.

More recently, Brooks has published an outline of some new and more exact calculations on the alkali metals which are currently being refined.[26] The latest, unpublished, values for the lattice constant as given by these calculations[27] agrees well with the experimental values at 4.2°K (see lines 1 and 2 in Table III), except for the case of lithium, where the free electron approximation of the theory does not really apply.

TABLE II. The work done in compressing the alkali metals to 10 000 atmos at 298° and 4°K, compared with the maximum heat which can be produced in an isothermal compression for the same metals at 298° and 77°K. The 4.2°K entropies, and hence the heat developed in a reversible compression at 4.2°K (not shown), are negligibly small.

		Li	Na	K	Rb	Cs
		(All calculations in calories per mole)				
$-\int_{p=0}^{p=10\,000} PdV$	298°K	90	270	(800)	(1050)	1350
	4°K	84	260	770	1020	2000
$T(S-S_0)_{p=0}$ [a]	298°K	2000	3640	4530	5000	5900
	77°K	100	344	520	726	880

[a] See reference 23.

TABLE III. Comparison of the experimental results with theory. a is the lattice constant. The parameters A, B, and C are defined in Eq. (4).

	(Units)	Li	Na	K	Rb	Cs
a(exp)	(10^{-8} cm)	3.43	4.22	5.20	5.56	5.92
a(th)	(10^{-8} cm)	3.31	4.25	5.19	5.57	5.90
A(exp)	(10^{13} ergs/mole)	0.46	1.48	1.60	2.08	1.94
B(exp)	(10^{12} ergs/mole)	5.76	3.06	1.92	0.72	0.63
B(th)	(10^{12} ergs/mole)	2.73	1.81	1.39	1.03	0.91
C(exp)	(10^{13} ergs/mole)	12.90	10.56	8.74	7.68	7.08
C(th)	(10^{13} ergs/mole)	12.7	9.82	8.00	7.46	6.91
Theoretical pressure in atmos for $P_{\text{exp}}=10\,000$ atmos		8900	9500	9250	9000	11 400

CONCLUSIONS

The information about the density and pressure-volume relationships for the five alkali metals near absolute zero is useful chiefly as a basis for comparison with theory, and the check with Brooks' calculations for lattice parameter at absolute zero is reassuring, and gives promise for the future. The existence of an excessive softness for cesium, which seems to be an indication of a smearing out of the large room temperature electronic transition found at high pressure, and the probable existence of another modification of rubidium, ten

[24] F. Seitz, *Modern Theory of Solids* (McGraw-Hill Book Company, Inc., New York, 1940), Chap. 10.
[25] J. Bardeen, J. Chem. Phys. **6**, 364, 372 (1938); also F. Seitz, reference 24, p. 381–3.
[26] H. Brooks, Phys. Rev. **91**, 1027 (1953).
[27] H. Brooks (unpublished results). The author is indebted to Professor Brooks for allowing him to quote these results prior to publication.

percent more dense than normal, would indicate that these data should be extended to pressures of at least 25 000 and preferably 50 000 atmos. This is not quite the formidable task which it would appear to be, since the similarity of the 4.2° and 77°K isotherms above 5000 atmos shows that for pressures above this figure these metals are effectively at absolute zero at liquid nitrogen temperatures. It also would be of interest to obtain isotherms at temperatures between 77°K and room temperature, especially for cesium, so that the effect of temperature on the internal energy could be calculated.

The agreement with Bardeen's theoretical model is acceptable only for sodium, with the deviations, especially in the shape of the $P-V$ curve, outside experimental error. It is to be hoped that more refined calculations will show a better agreement between theory and experiment.

ACKNOWLEDGMENTS

The author wishes to express his appreciation to Professor Harvey Brooks for many discussions of the theoretical aspects of this work, and for allowing the use of some of his unpublished results. He is very grateful to Professor S. C. Collins for providing this opportunity to work in his laboratory, and for furnishing, along with constant encouragement, the quantities of liquid nitrogen and helium which were required.

This work was performed under a contract with the U. S. Army Office of Ordnance Research.

PHYSICAL REVIEW VOLUME 99, NUMBER 2 JULY 15, 1955

Surface Adsorption and Migration Energies for KCl†

JOHN E. HOVE
Nuclear Engineering and Manufacturing, North American Aviation, Downey, California
(Received January 10, 1955; revised manuscript received March 7, 1955)

The binding and migration energies for a K^+ ion on a (100) KCl surface are calculated. It is found that the most stable K^+ site is about an interionic lattice spacing above a Cl^- surface ion and the binding energy is 0.68 ev. The activation energy for lateral diffusion is 0.23 ev and the estimated vibration frequencies are 10^{13} sec^{-1} along the surface and 2.8×10^{13} sec^{-1} normal to the surface. From these figures it is shown that the mean path length of the ion is about 2×10^{-4} cm; the binding energy for an absorbed KCl molecule is found to be about 0.36 ev. This leads to the conclusion that the molecule will travel at most a few lattice spacings before evaporating. Some effects of this on crystal growth and additive coloring are discussed briefly.

I. INTRODUCTION

BASIC to most problems concerning defects in crystals is the energy required to form the defect and the energy required for it to migrate through the crystal.

One defect (although perhaps not usually considered as such) of interest is an absorbed ion or molecule on a crystal surface. Possibly the simplest materials of importance for which a study of adsorbed particles can be readily carried out are the alkali-halides with a NaCl-type lattice. Typical problems, involving the binding and diffusion energies for these solids are crystal growth from a vapor phase (or, conversely, evaporation) and the detailed mechanism of additive coloring from the metal vapor. The first step, in calculating the total energies involved, is to find the energies for an isolated defect of one kind only. This problem will be considered in the present paper. Thus (although there will be dislocation ledges on the surface[1]), the configuration considered will be a perfectly smooth (100) surface with a single ion or molecule adsorbed. For the numerical results the crystal will be taken as KCl and the adsorbed ion will be considered as K^+ ion. This has the advantage that covalent effects are small, so that the semiempirical Born-Mayer interaction energies may be used.[2]

In this case, an important problem is that of evaluating the long-range energy contributions. To facilitate such evaluations, use has been made of the convergence transformation developed in a previous paper.[3] This is of special value for the lattice polarization energy contribution which is quite long-range in character, although it is convenient to so transform even the short-range overlap repulsive energy. As mentioned in reference 3, this lattice sum transformation permits many non-Coulomb interactions to be handled as easily as those of a Coulombic nature.[4] A secondary purpose of the present paper is to demonstrate this.

† This paper is based on work performed at Cornell University, Ithaca, New York, under a predoctoral Cornell Aeronautical Laboratory Fellowship.

[1] Burton, Cabrera, and Frank, Trans. Roy. Soc. (London) **243**, 299 (1951).

[2] N. F. Mott and R. W. Gurney, *Electronic Processes in Ionic Crystals* (Oxford University Press, London, 1948), second edition.

[3] J. E. Hove and J. A. Krumhansl, Phys. Rev. **92**, 569 (1953).

[4] J. E. Lennard-Jones and B. M. Dent, Trans. Faraday Soc. **24**, 92 (1928).

As far as the author is aware, there has been no previous treatment of the crystal polarization, due to an adsorbed ion in a general position, which has not involved a direct summation plus an integration.

II. SURFACE ADSORPTION ON A KCl (100) PLANE

We shall consider a K^+ ion above a (100) face of a perfect, semi-infinite KCl crystal. The surface structure will be assumed to be the same as that of the interior; justification for this has been given by Lennard-Jones and Dent[4] who have calculated that the maximum change in the lattice spacings of the surface layer is about 6 percent of the bulk values (for both the in-plane ionic spacing and the distance between the top plane and that underneath). In addition, Patterson[5] has shown that there is no polarization surface structure in the alkali-halides.

The energy may be separated into additive contributions from Coulomb, overlap repulsive, and polarization interactions. Van der Waals and covalent effects are assumed negligible. The physical constants are given by Mott and Gurney[2] except for the polarizabilities. The ion polarizabilities were calculated from the optical dielectric constant by assuming their ratio to be the same as in a free ion state. The values obtained are $\alpha_+=0.75$ A^3 and $\alpha_-=3.66$ A^3 for K^+ and Cl^-, respectively. The displacement polarizability was calculated in the usual manner[2] as $\alpha_d=3.74$ A^3. The dipole moments induced on lattice ions by the adsorbed ion were computed by the macroscopic approximation used by Mott and Littleton.[6] It was assumed for simplicity that the induced dipoles in the surface layer are also given by this approximation. While this is not a desirable assumption for a given surface ion, the total effect over the crystal should be satisfactory, since the errors committed for the near neighbors in the surface will tend to be cancelled by those for the far neighbors. Moreover, because the polarization energy is quite long-range, the interior lattice ions contribute significantly to the total energy, tending to reduce further the relative error of the surface layer.

The central problem in this section is that of determining the minimum-energy surface of the adsorbed ion as a function of the coordinates (x,y). The coordinate system is chosen so that the (x,y) axes are in the surface plane and the z-axis pointing out of the crystal; a Cl^- ion is chosen as an origin and all coordinates are in units of r_0, the interionic spacing. After thus obtaining the most stable site, parabolas can be fitted to the energy well to find the approximate classical vibration frequencies and hence the diffusion constant. The several contributions to the total energy will each be considered separately, below, for arbitrary positions of the K^+ ion.

[5] D. Patterson, Trans. Faraday Soc. **48**, 877 (1952).
[6] N. F. Mott and M. J. Littleton, Trans. Faraday Soc. **34**, 485 (1938).

1. Coulomb Energy

The total Coulomb interaction of the lattice and the adsorbed ion is immediately found by the expression[4]

$$V_c=\frac{8e^2}{r_0}\sum_{\substack{l_1,l_2=1\\(\text{odd})}}^{\infty}(\cos\pi l_1 x)(\cos\pi l_2 y)(l_1^2+l_2^2)^{-\frac{1}{2}},$$
$$\times\{1+\exp[-\pi(l_1^2+l_2^2)^{\frac{1}{2}}]\}^{-1}$$
$$\times\exp[-\pi z(l_1^2+l_2^2)^{\frac{1}{2}}]. \quad (1)$$

Since we expect z to be of the order of unity, the (1,1) term is a sufficient approximation. For KCl, r_0 is 3.14 A and Eq. (1) thus becomes

$$V_c=-(25.38)(\cos\pi x)(\cos\pi y)\exp(-4.45z)\text{ ev}. \quad (2)$$

It is of interest to note that at $z=1$ and $(x,y)=(0,0)$, this is (-0.296) ev. This illustrates how small is the out-of-plane contribution to the Madelung energy, since the total Madelung energy for KCl is (-7.94) ev.

2. Polarization of Adsorbed Ion

The electric field of the crystal can be found above the surface from the gradient of Eq. (2). Using the free ion polarizability,[2] the polarization energy of the K^+ adsorbed ion in this field is

$$V_p^+=-(18.70)(\cos^2\pi x+\cos^2\pi y)\exp(-8.90z)\text{ ev}. \quad (3)$$

At $z=1$ and $(x,y)=(0,0)$, this equals (-0.005) ev which is of the order of the Van der Waals energy. We shall thus neglect these contributions here although they would represent most of the binding of an adsorbed rare gas atom.

3. Crystal Polarization

The presence of a single adsorbed ion will polarize the crystal; the polarization field then interacts with the ion to produce a long range attractive coupling. Using the macroscopic approximation of Mott and Littleton,[6] the total interaction energy of the crystal polarization is

$$V_p=-\tfrac{1}{2}e^2r_0^{-1}[M_-S_-+M_+S_+]. \quad (4)$$

Here

$$S_\mp=r_0^4\sum(r_\mp)^{-4} \quad (5)$$

is the sum over the semi-infinite crystal of the face-centered sublattice of either Cl^- or K^+ ions, where $r_\mp$ is the distance from the adsorbed ion to one of the lattice ions. $M_\mp$ are constants for a given type of ion, involving the polarizabilities and the dielectric constant, and are derived in reference 6. For KCl, the respective numerical values of M_+ and M_- are (0.0156) and (0.0690) for a rigid lattice and (0.0488) and (0.0764) for a displaceable lattice. It should be noted that the Cl^- ions will contribute most of the polarization energy and furthermore that their contribution is not greatly altered by considering the lattice to be displaceable. The ions in

the surface layer just underneath the adsorbed ion will not, of course, be displaced upward; rather they will pull the adsorbed ion down. For this reason, in the present calculations, it will be assumed that the lattice is rigid. Since there is little numerical difference involved for KCl, this is not a major assumption.

The lattice sum of Eq. (5) converges quite slowly. It may, however, be transformed into a form which converges rapidly for values of z of the order of unity. This has been done explicitly in reference 3, and it is easily shown that only the following terms of the transformed series must be retained:

$$S_{\mp}=\tfrac{1}{2}\pi\zeta(z,2)\pm(22.62)\pi^2(8z)^{-1}(\cos\pi x)(\cos\pi y)\times K_1(4.446z)+2\pi^2z^{-1}(\cos2\pi x+\cos2\pi y)\times K_1(6.284z)+(45.25)\pi^2(8z)^{-1}(\cos2\pi x)\times(\cos2\pi y)\times K_1(8.880z)\text{ ev}. \quad (6)$$

In this expression,

$$\zeta(z,2)=\sum_{l=0}^{\infty}(z+l)^{-2}$$

is the generalized zeta function which is tabulated[7]; K_1 is the Bessel function of first order and the second kind for imaginary argument. For $z=1$, the first term in Eq. (6) is readily shown to be $(\pi/2)(\pi^2/6)$, while an integration of a continuum of r^{-4} interaction centers gives $(\pi/2)$. Thus the first term in Eq. (6) is the result of a discrete summation over all the (100) planes, but smearing out each individual plane. The remaining terms represent the lowest order effect of the actual discreteness of the (100) planes. For $z=1$ and $(x,y)=(0,0)$, the value of V_p becomes (-0.528) ev, which is almost twice the Coulomb energy. This is therefore a very important contribution to the binding energy.

4. Overlap Repulsion

Although the overlap repulsion is a very short-range interaction, it is more convenient for our purpose to write it as a sum over the lattice and transform in a similar manner to the polarization energy. Since the transformation separates the interaction into sums of products of (x,y) terms (simple cosine functions) and z terms, this procedure simplifies the calculation when many (x,y) points (each with several z points) are desired. The resulting expression for the total overlap energy for KCl is

$$V_r=(81.20)(1+9.12z)\exp(-9.12z)+(75)\times(1+10.15z)(\cos\pi x)(\cos\pi y)\exp(-10.15z)+(90.1)(1+11.07z)(\cos2\pi x+\cos2\pi y)\times\exp(-11.07z)+(119)(1+12.73z)(\cos2\pi x)\times(\cos2\pi y)\exp(-12.73z)\text{ ev}. \quad (7)$$

The magnitude of the largest neglected term is about 10^{-3} times that of the first term. At $z=1$ and $(x,y)=(0,0)$, this yields a value of 0.1615 ev, while a direct sum over nearest and next-nearest neighbors gives 0.1618 ev. A much more severe test of the accuracy of Eq. (7) is for $z=\frac{1}{2}$ and $(x,y)=(\frac{1}{2},\frac{1}{2})$, which will never arise in the present calculations. Nevertheless, Eq. (7) then gives 1.568 ev while a direct sum gives 1.623 ev, a satisfactory agreement. The individual ion pair repulsion energies used in obtaining the above are those given in reference 2. Since Eq. (7) is capable of an independent check, the exact series is not presented here, although it may be found in reference 12.

5. Surface Dipole Layer

The surface layer in an ionic crystal will always have some degree of permanent polarization due to the unbalanced electric field of the rest of the lattice. In obtaining the dipole moments of the surface ions, the results of Lennard-Jones and Dent[4] will be used. They have computed the total electric field at any ion, including that from the other surface dipoles. Considering a positive dipole moment to be pointing out of the surface, the moments on Cl^- and K^+ surface ions are found to be $(0.780)e/r_0^2$ and $(-0.286)e/r_0^2$, respectively, where the constant has units of A^2. The total interaction energy with an absorbed ion is

$$V_d=e\sum[\mathbf{p}_k\cdot(\mathbf{r}-\mathbf{r}_k)]\,|\mathbf{r}-\mathbf{r}_k|^{-3},$$

where the sum is over the surface layer only and $\mathbf{p}$ is always normal to the (100) plane. This is readily trans-

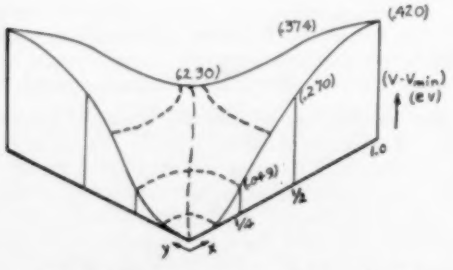

FIG. 1. Minimum energy surface. The numbers in parentheses are $V-V_{\min}$, in ev.

[7] E. Jahnke and F. Emde, *Tables of Functions* (Dover Publications, New York, 1945). This actually tabulates the logarithmic derivative of the Γ function, but these are simply related to the generalized zeta function (see, for example, reference 3).

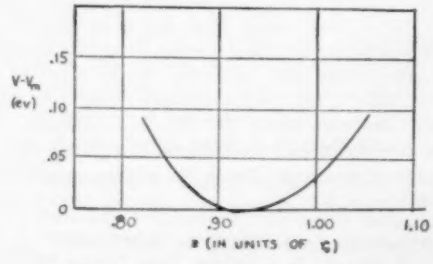

FIG. 2. Plot of V *versus* z at $(x,y)=(0,0)$.

TABLE I. The coefficients (in ev) of Eq. (9) as a function of z (normalized to r_0).

z	1.5	1.4	1.3	1.25	1.20	1.15	1.01	1.05	1.00	0.95	0.90	0.85	0.80	0.75	0.70	0.65	0.60	0.55	0.50
$-A$	0.281	0.306	0.335	0.350	0.365	0.380	0.393	0.403	0.406	0.401	0.376	0.326	0.235	0.085	−0.162	−0.531	−1.090	−1.965	−3.235
$-B$	0.031	0.048	0.075	0.088	0.115	0.143	0.176	0.218	0.267	0.323	0.385	0.470	0.542	0.631	0.714	0.757	0.752	0.642	0.471
C	0.000	0.000	0.000	0.001	0.001	0.002	0.004	0.008	0.013	0.023	0.038	0.076	0.108	0.180	0.297	0.486	0.797	1.285	2.079
D	0.000	0.000	0.000	0.000	0.000	0.001	0.001	0.002	0.004	0.008	0.014	0.025	0.045	0.080	0.142	0.252	0.445	0.787	1.339

formed by the method of reference 3 into a rapidly convergent sum which is given in reference 12. The result, when one retains only the lowest order term, is

$$V_d = (1.964)(\cos\pi x)(\cos\pi y)\exp(-4.45z)\text{ ev}. \quad (8)$$

There is also a constant term which arises and which is characteristic of dipole layers. This has no significance in the present calculation and has been dropped. At $z=1$ and $(x,y)=(0,0)$, V_d has a value of 0.025 ev, which is quite small compared to other interaction energies.

6. Total Energy

By combining all the above terms, an expression for the total energy may be written as

$$V = A + B(\cos\pi x)(\cos\pi y) + C(\cos 2\pi x + \cos 2\pi y) + D(\cos 2\pi x)(\cos 2\pi y). \quad (9)$$

The coefficients are functions of z only and are tabulated in Table I.

The minimum value of V was found for various values of (x,y). This minimum energy surface is shown in Fig. 1; the stable position is at (0,0) with the K^+ ion at $z=0.90$, and a binding energy of 0.683 ev. The saddle point for surface diffusion is at $(\frac{1}{2},\frac{1}{2})$ with $z=0.85$ and a binding energy of 0.453 ev. Thus the activation energy for surface diffusion is 0.230 ev. By fitting the energy minimum near (0,0) with a paraboloid, the classical frequency of vibration parallel to the surface can be estimated as 10^{12} sec^{-1}. Figure 2 shows a plot of V *vs* z at $(x,y)=(0,0)$. By fitting this with a parabola also, the classical frequency normal to the surface is estimated to be 2.8×10^{12} sec^{-1}. It might be mentioned that the crystal polarization energy, while very important for the binding energy, does not greatly affect the diffusion activation energy. The latter is mostly made up of the change in Coulomb energy, which is about 0.3 ev.

The rate of diffusion or evaporation of an adsorbed K^+ ion can be written as[8]

$$R = (Q_2'/\alpha Q_1)(kT/h)\exp(-\epsilon/kT), \quad (10)$$

where α is the number of equivalent paths, ϵ is the activation energy, Q_1 is the partition function in the normal state, and Q_2' is that in the activated state excluding the translational degree of freedom along the diffusion path. This assumes a transmission coefficient of unity. Applying standard rate theory, Eq. (10) can be very closely approximated as

$$R = \nu\exp(-\epsilon/kT), \quad (11)$$

where ν is the classical vibration frequency, for both diffusion and evaporation.

For surface diffusion, the mean time for a single jump is thus found to be 10^{-8} second at room temperature. This gives a diffusion constant of about 2×10^{-7} cm^2 sec^{-1}. From the calculated evaporation rate for a single ion the mean time which that ion spends on the surface is found to be 0.29 second. The product of the surface diffusion constant and the mean time spent on the surface is the square of the mean path length traveled on the surface. From the above calculation, this length is 1.9×10^{-4} centimeter. This is quite long since a reasonable figure for the linear dislocation density is about 10^4 per centimeter; thus the ion has an excellent chance of finding a more stable site at a dislocation ledge.[1]

It is probably true that the vapor above the surface will be mostly molecular, since the heat of sublimation of KCl is 2.2 ev,[9] half the dissociation energy of the molecule.[10] Thus, it is also of interest to calculate the above quantities for an adsorbed KCl molecule. The chief difference between this case and that of the K^+ ion is that there is no longer any long range polarization energy. In computing the binding energy, the KCl molecule was assumed to be purely ionic with a separation equal to the crystal spacing (3.14 A). This was done for obvious reasons of convenience but the observed spacing of the free molecule is less (2.67 A).[11] It is not difficult to show that the lattice interaction is insufficient to stretch the molecule appreciably,[12] so that our result will be an overestimate of the binding energy. Without presenting the details of the calculation (which are similar to those for the single ion and are given in reference 12), a binding energy of 0.36 ev was found for the molecule, with a classical vibrational frequency normal to the surface of 1.9×10^{12} sec^{-1}. An additional difference between this case and that of a single ion is that the molecule will gain at least one rotational degree of freedom by evaporating from the surface. It may gain two, if the molecule on the surface is assumed fixed, but it is probably more nearly correct to consider it as free to rotate in the surface plane. In

[8] See, for example, Eyring, Walter, and Kimball, *Quantum Chemistry* (John Wiley and Sons, Inc., New York, 1944), Chap. 16.

[9] Gmelin, Handb. der Anorgan. Chem. (Kalium) **22**, 373 (1938).

[10] A. G. Gaydon, *Dissociation Energies and Spectra of Diatomic Molecules* (John Wiley and Sons, Inc., New York, 1947).

[11] Fabricand, Carlson, and Rabi, Phys. Rev. **86**, 607 (1952).

[12] J. E. Hove, Ph.D. thesis, Cornell University, 1953 (unpublished).

either case, this will introduce rotator partition functions into Eq. (11). The partition function for two angular degrees of freedom becomes[8]

$$Q_r = 8\pi IkT/h^2,$$

and that for a plane rotator

$$Q_r = (2\pi)^{\frac{1}{2}}(IkT/h^2)^{\frac{1}{2}} - 1,$$

in the classical (high-temperature) approximation. The moment of inertia (I) was estimated as 2.4×10^{-38} gram-cm^2 for KCl.[11] At room temperature, therefore, the mean time which the molecule spends on the surface is calculated as 0.35×15^{-7} second if it can rotate freely in the surface plane and 0.42×10^{-9} second if it cannot. We assume that there is no change in the internal vibrational entropy. The jump time for motion on the surface was not computed by the author. However, this would be of the same order of magnitude as that for the single ion (10^{-8} second) if the molecular spacing were equal to the lattice spacing, since translation would probably occur by alternate rotations similar to a walking motion. The molecular spacing is actually less than the lattice spacing; this will reduce somewhat the jump time for surface migration, but will also reduce the mean time spent on the surface. Thus a jump time of 10^{-8} second will give the correct order of magnitude of the mean path length, using the evaporation time computed above. Depending on whether the molecule is considered to gain one or two rotational degrees of freedom, this path varies from zero to two lattice spacings. We must therefore conclude that a KCl molecule will leave a perfect surface almost immediately after hitting it. It should perhaps be explicitly noted that the molecule will not dissociate on the surface, since only 1.0 ev of binding energy will be gained, while the dissociation energy is about 4.4 ev.[10]

III. SUMMARY

The results of a calculation of the binding energy of a K^+ ion and a KCl molecule on a perfect (100) surface of a KCl crystal have been presented. The value for the ion was found to be 0.68 ev, and that for the molecule 0.36 ev. The activation energy for lateral migration of the ion is 0.23 ev; that for the molecule was not computed, but is assumed to be of the same order of magnitude. These values lead to the conclusions that the ion has a mean path length of about 2×10^{-4} centimeter on the surface before evaporating and that the molecule will leave the surface before it has migrated more than one or two lattice spacings. This has some implication on the problem of crystal growth from a supersaturated vapor phase. Thus, since the vapor would be largely molecular, growth would be very slow, because only those molecules which hit the surface very near a dislocation ledge, or other defect, would remain. If the vapor could be made ionic (say by electron bombardment, or if the present calculations can be considered essentially valid for a solution), however, the growth would be much more rapid, since practically all ions which hit the surface will migrate to a surface defect. This assumes that a Cl^- ion would have about the same surface characteristics as does a K^+ ion; since the only essential differences are the polarization energy of the adsorbed ion, which is a negligible contribution anyway, and the overlap repulsion energy of the next-nearest neighbors, this should be a good assumption. The author has not made a study of the actual growth rates to be expected, but the present results indicate that, for an ionic vapor, a procedure of the type used by Burton, Cabrera, and Frank[1] must be modified to include ion recombination on the surface. This is necessary because such a recombination would result in a KCl molecule, which would then evaporate almost immediately.

We would also like to mention some possible effects of our results on the description of the additive coloring process in KCl. The usual picture[2] is that the K atom yields an electron to the conduction band of the crystal and the resulting K^+ ion moves to a surface ledge, where it attracts a negative ion from the layer beneath. The resulting vacancy will migrate into the crystal and trap the electron to form an F-center. It can be seen, from our results, that it is not energetically feasible for a K atom to ionize upon approaching a perfect surface. Thus the ion would gain a little less than 0.68 ev, but the ionization energy of K is about 4.1 ev. It is difficult to imagine a state where the electron could gain enough energy to make up this difference, so that only those K atoms near a surface defect would be expected to contribute to the formation of F-centers. Another mechanism could also occur, namely the approach of a K atom near an adsorbed Cl^- ion. The formation of a KCl molecule would thus be energetically feasible since the dissociation energy is 4.4 ev, and the electron could enter the conduction band of the crystal, thus gaining further energy of the amount of the electron affinity of KCl. Therefore, such a process could be an appreciable competitor of the first mechanism mentioned. The essential difference would be that one mechanism increases the crystal volume and mass while the other decreases them since the KCl molecule will quickly evaporate. While there is enough of a mass change in a heavily colored crystal to be measurable, it is difficult to avoid oxidation and other effects of the same order of magnitude and the author is unaware of any such measurements.

ACKNOWLEDGMENTS

The author wishes to thank J. A. Krumhansl and D. R. Westervelt for many discussions.

Optical Bleaching of *F* Centers in X-Rayed Alkali Halide Crystals*

ROBERT HERMAN AND RICHARD F. WALLIS
Applied Physics Laboratory, The Johns Hopkins University, Silver Spring, Maryland
(Received March 24, 1955)

When *F* light is absorbed by *F* centers it is assumed that electrons leave negative-ion vacancies and are transferred to the conduction band. Conduction electrons may be captured by holes and by negative ion vacancies. It is assumed that the cross sections for the latter two processes are equal and that the conduction electron concentration is small and stationary. Under these conditions the local *F*-center concentration, n, is specified by the equation $\partial n/\partial t = -bIn^2$, where I is the local *F*-light intensity assumed to be given by the Beer-Lambert law and b is a constant. Exact expressions for n and I have been obtained for the case of a uniform initial *F*-center distribution. The theoretical results are compared with quantitative measurements of the *F*-center concentration as a function of *F*-light irradiation time in x-rayed NaCl for a range of incident light intensities and initial *F*-center concentrations. It is found that the behavior of the model is consistent with experimental data in lightly x-rayed crystals having initial concentrations in the range $\sim 10^{16}$–$\sim 10^{17}$ cm^{-3}. In more heavily x-rayed crystals, appreciable growth of *M* and *R* bands occurs during the bleaching and deviations from the behavior of the model are observed.

I. INTRODUCTION

DURING the course of a recent investigation on the production and bleaching of color centers in x-rayed alkali halide crystals,[1] we became interested in the possibility of describing the optical bleaching process by means of a model. Such a model should take into account the spatial distribution of the centers produced by the x-rays and the nonuniformity of the bleaching light intensity throughout the crystal. The model should also be consistent with the fact that photoconductivity[2] is associated with optical bleaching at temperatures that are not too low and with the possibility that there is an appreciable concentration of unfilled negative ion vacancies in an x-rayed alkali halide crystal. Mathematical descriptions of this kind have been studied in connection with the luminescence and conductivity of phosphors.[3] Similar models have been applied to the case of electronic conductivity in semiconductors.[4]

Relatively little work on the above type of models has been done for color center phenomena in the alkali halide crystals. We feel that the investigation of the properties of theoretical models is important as a means of interpreting quantitative experimental data. Even the study of simple models may yield some understanding of the gross features of the data and provide a basis for more "realistic" models.

The present paper deals specifically with the bleaching by *F* light of *F* centers produced by x-rays in crystals of various thicknesses. A range of bleaching light intensities and initial color-center concentrations was employed.

II. EXPERIMENTAL

All of the experimental work described in this paper concerns single crystals of NaCl obtained in various lots from the Harshaw Chemical Company. The x-ray coloration was done at room temperature using a Picker-Waite diffraction unit with a Machlett x-ray tube and an accelerating voltage of 50 kv. The optical absorption measurements and bleaching were carried out at room temperature with a Beckman Model DU spectrophotometer having a 2-volt and 6-volt Sorensen power supply.

The *F*-center concentration in an x-rayed crystal is nonuniform in the direction of the x-ray beam. For this reason the direction of the bleaching *F* light as well as the light used for the optical absorption measurements was taken perpendicular to the x-ray beam direction. In this way the bleaching process was initiated in a portion of crystal containing an essentially uniform distribution of *F* centers. The details concerning experimental arrangements and techniques are discussed fully in reference 1.

III. THEORETICAL MODEL

In a previous paper,[1] a discussion was given for the optical bleaching of an initially uniform distribution of *F* centers with the restriction that only a small fraction of the incident light is absorbed and that, consequently, negligible concentration gradients develop during the bleaching process. The present work extends this treatment by removing this restriction.

The electron transfer processes during bleaching involve the elevation of an electron from an *F* center into the conduction band by the absorption of a quantum of radiation and a phonon, and the capture of conduction electrons either by positive holes or by negative ion vacancies.[5] The nonlinear kinetic equations

* This work was supported by the Bureau of Ordnance, Department of the Navy.
[1] Mador, Wallis, Williams, and Herman, Phys. Rev. **96**, 617 (1954).
[2] J. J. Oberly and E. Burstein, Phys. Rev. **79**, 217 (1950).
[3] See, for example, Herman, Meyer, and Hopfield, J. Opt. Soc. Am. **38**, 999 (1948) as well as numerous other references in *Bibliography on Physical Electronics* prepared by W. B. Nottingham and staff (Massachusetts Institute of Technology, Cambridge, 1954).
[4] See report of Conference on Photoconductivity held at Atlantic City, November 4–6, 1954 (to be published).
[5] It should be noted that the *F*-center concentration after optical bleaching was determined after the thermally unstable *F'*

for these processes may be written as follows,[1] remembering that all dependent variables are both space- and time-dependent:

$$\partial n_F/\partial t = -\sigma_F I n_F + k_1 n_c n_v, \tag{1a}$$

$$\partial n_c/\partial t = \sigma_F I n_F - k_1 n_c n_v - k_2 n_c n_h, \tag{1b}$$

$$\partial n_v/\partial t = \sigma_F I n_F - k_1 n_c n_v, \tag{1c}$$

and

$$\partial n_h/\partial t = -k_2 n_c n_h, \tag{1d}$$

where I is the local intensity of the bleaching F light; n_F, n_c, n_v, and n_h are the local concentrations of F centers, conduction electrons, negative-ion vacancies, and holes, respectively; σ_F is the cross section for the optical decomposition of F centers and k_1 and k_2 are rate constants.[6] The conservation of negative-ion vacancies, filled or unfilled, and the balance between holes and electrons lead to the following equations of condition:

$$n_v^0 + n_F^0 = n_v + n_F = N, \tag{2a}$$

and

$$n_h = n_c + n_F, \tag{2b}$$

where n_v^0 and n_F^0 represent the initial concentrations of unfilled single negative-ion vacancies and of F centers, respectively.

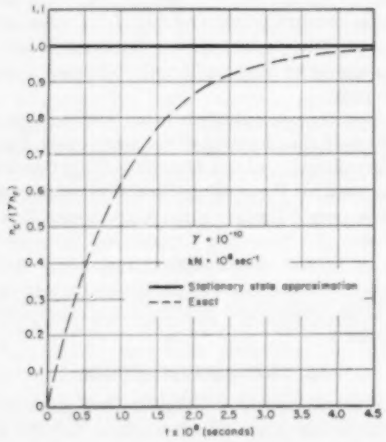

FIG. 1. Comparison of the exact and stationary state solutions for the conduction electron concentration, n_c, as a function of time of bleaching.

centers were allowed sufficient time to decay. In the theoretical treatment the influence of the F' center has been neglected. See reference 1. The small thermal decay of F centers in NaCl at room temperature has also been neglected.

[6] Note that if σ_p is the cross section for the absorption of a photon by the F center yielding an excited F center, then $\sigma_F = q_1 \sigma_p$ where q_1 is the primary quantum efficiency for the destruction of F centers, i.e., the fraction of the electrons elevated into the excited state which are then transferred to the conduction band by the absorption of a phonon. The constants k_1 and k_2 may be written as $\sigma_1 v$ and $\sigma_2 v$, respectively, where σ_1 and σ_2 are the corresponding cross sections and v is the average speed of the conduction electrons. For orders of magnitude, $\sigma_1 \sim \sigma_2 \sim 10^{-16}$ cm^2, $v \sim 10^7$ cm/sec, and $k_1 \sim k_2 \sim 10^{-9}$ cm^3/sec.

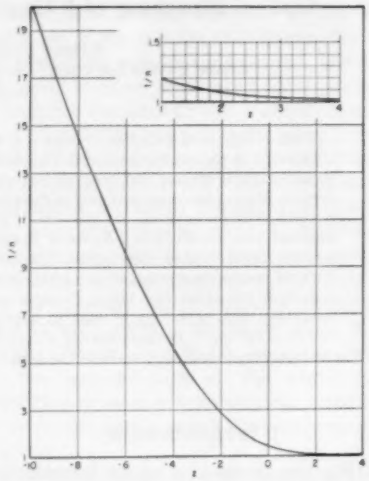

FIG. 2. Exact solution of Eqs. (4) and (6) giving the F-center concentration as a function of z which depends on the depth and time of optical bleaching.

As in previous work,[1,7] we again make certain simplifying assumptions, namely, that the conduction electron concentration is stationary in time, $dn_c/dt = 0$, the rate constants k_1 and k_2 are equal, $k_1 = k_2 = k$, and that $n_F \gg n_c$. From these assumptions and Eqs. (2a) and (2b), it follows from Eq. (1b) that

$$n_c \cong (\sigma_F I/kN) n_F. \tag{3}$$

An exact expression for n_c for the case $k_1 = k_2$ with the initial condition $n_c = 0$ for $t = 0$ is given by[3]

$$n_c = \frac{\gamma\{1 - \exp[-(1+\gamma)kNt]\}}{1 + \gamma \exp[-(1+\gamma)kNt]} n_F, \tag{3a}$$

where

$$\gamma = \sigma_F I/(kN). \tag{3b}$$

For $\sigma_F \sim 10^{-16}$ cm^2, $I \sim 10^{16}$ quanta cm^{-2} sec^{-1}, $k \sim 10^{-9}$ cm^3/sec, and $N \sim 10^{17}$ cm^{-3}, $\gamma \sim 10^{-10}$ and may be neglected compared with unity. The exponentials in Eq. (3a) may then be neglected for times $t \gg 1/(kN) \sim 10^{-8}$ sec and the approximation given in Eq. (3) is obtained. These results are presented graphically in Fig. 1. It is clear that for physically interesting values of γ and kN the stationary state solution is a very good approximation except for the initial rise time.

Using Eqs. (2a) and (3), Eq. (1a) may be transformed to the simplified form

$$\partial n_F(x,t)/\partial t = -b I n_F^2, \tag{4}$$

where

$$b = \sigma_F/N, \tag{4a}$$

and x is distance measured from the illuminated face

[7] R. V. Hesketh, thesis, University of Durham, Durham, England, 1953 (unpublished).

of a crystal of thickness x_0 in the direction of the bleaching light beam. In the limiting case where the initial optical density is very low the light intensity I can be assumed to be a constant I_i. Equation (4) then yields upon integration[1]

$$n_F^0/n_F = 1 + n_F^0 b I_i t. \tag{5}$$

In the more general case, we assume that the Beer-Lambert law is obeyed so that one may write

$$\partial I(x,t)/\partial x = -\sigma_p n_F I, \tag{6}$$

where σ_p is the cross section for the absorption of a photon by an F center.

An exact solution to Eqs. (4) and (6) has been found for the case that $n_F(x,t)$ and $I(x,t)$ satisfy the boundary conditions:

$$n_F(x,t) = n_F^0 \text{ at } t=0 \text{ for all } x, \tag{7a}$$

and

$$I(x,t) = I_i \text{ at } x=0 \text{ for all } t. \tag{7b}$$

If one introduces the dimensionless variables

$$n = n_F/n_F^0, \tag{8a}$$

$$\mathcal{I} = I/I_i, \tag{8b}$$

$$y = \sigma_p n_F^0 x, \tag{8c}$$

$$\tau = s_0 t, \tag{8d}$$

where

$$s_0 = n_F^0 b I_i, \tag{8e}$$

then the exact solution may be written as

$$z = -\mathrm{Ei}[\ln(1/n)], \tag{9}$$

where

$$z = y - \mathrm{Ei}[\ln(1+\tau)] \tag{9a}$$

and $\mathrm{Ei}(\xi)$ is the exponential integral function[2] defined by

$$\mathrm{Ei}(\xi) = \int_{-\infty}^{\xi} \frac{\exp\phi}{\phi} d\phi \tag{9b}$$

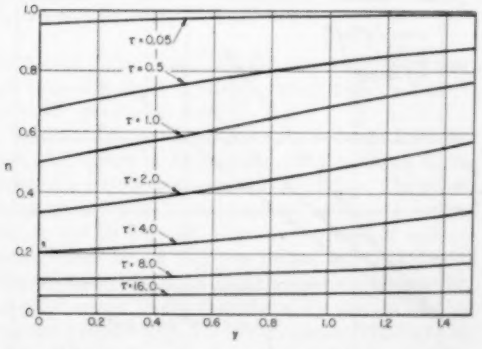

FIG. 3. The F-center concentration as a function of depth in the crystal for various times of optical bleaching according to the exact solution.

[2] See *Tables of Sine, Cosine, and Exponential Integrals* (Works Projects Administration, Mathematical Tables Project, New York, 1940).

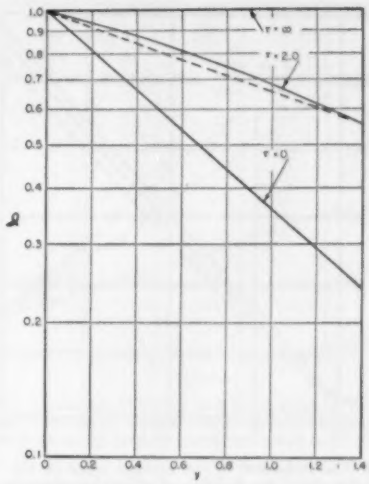

FIG. 4. The bleaching light intensity as a function of depth in the crystal for various times of optical bleaching. The dashed curve shows $\mathcal{I} = f(y)$ for a uniform distribution of F centers having the same average concentration as the solid curve at $\tau = 2.0$.

where the principal value of the integral is to be taken. A derivation of Eq. (9) is given in Appendix A.

The local light intensity $\mathcal{I}$ is shown in Appendix A to be given by

$$\mathcal{I} = \ln(1/n)/\ln(1+\tau). \tag{9c}$$

In Fig. 2, is given a plot of $1/n$ *vs* z as obtained from Eq. (9). The value of n for any given depth y and time τ is readily found by first computing z using Eq. (9a) and then determining $1/n$ from Fig. 2.

Equations (4) and (6) may also be integrated numerically by using the finite difference equations,

$$\Delta n_F = -b I n_F^2 \Delta t, \tag{10a}$$

$$\Delta I = -\sigma_p n_F I \Delta x, \tag{10b}$$

and the boundary conditions on n_F and I given in Eq. (7). Some of the calculations reported in this paper were made by numerical integration prior to the finding of the exact analytical solution. Spot checks indicated that the numerical results are within ~10 percent of the exact values.

The nonuniformity of the bleaching light in the crystal leads to the formation of concentration gradients during the bleaching. The effect of a concentration gradient has been shown[1] to increase the average bleaching rate compared with the rate for a uniform concentration of the same average value. The variation of n with distance y at various times τ is shown in Fig. 3. It may be seen that for $\tau = 2$ the concentration is ~40 percent higher at $y=1$ than at $y=0$.

The variation of light intensity, $\mathcal{I}$, with y at various values of τ is shown in Fig. 4. The presence of a positive F center concentration gradient for $\tau = 2$ causes $\mathcal{I}$ to be

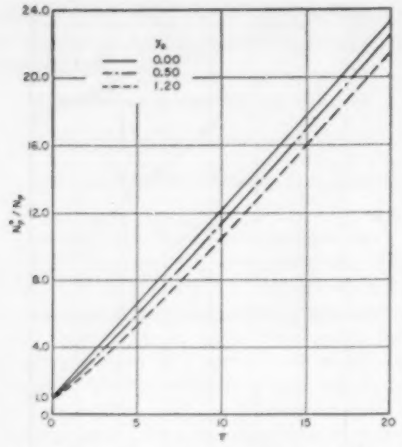

FIG. 5. The reciprocal of the average value of the F-center concentration *versus* the duration of optical bleaching for various crystal thicknesses according to the exact solution.

somewhat larger at interior points of the crystal than the values corresponding to a uniform concentration of the same average value.

The measurement of the optical density yields the average value N_F of the F-center concentration over the thickness of the crystal. In Fig. 5 are plotted theoretical values of N_F^0/N_F against τ for various values of the crystal thickness y_0. In the limit $y_0 \to 0$, the curve is a straight line in agreement with Eq. (5). For any y_0, the initial slope of the curve is proportional to the average initial bleaching light intensity. As y_0 increases, the initial slope accordingly decreases. For given $y_0 > 0$, as τ increases, the slope increases and approaches that of the limiting case $y_0 = 0$.

IV. EXPERIMENTAL RESULTS AND DISCUSSION

The optical bleaching experiments on NaCl described below were carried out on both thin ($\sim$0.1 cm) and thick ($\sim$1.0 cm) crystals covering an initial F-center concentration range of $\sim 10^{15}$–$\sim 4\times 10^{17}$ cm^{-3}. The theoretical model discussed in Sec. III appears to agree rather well with the results for initial F-center concentrations of $\sim 10^{16}$–$\sim 10^{17}$ cm^{-3}. Outside this range of concentrations deviations were observed which will be discussed later.

It should be emphasized that there does not appear to be a general theoretical treatment for the optical bleaching of a crystal containing an arbitrary non-uniform initial concentration distribution of F centers. The theory discussed above treats the case of a uniform initial distribution. For this reason the experiments were carried out by bleaching x-rayed crystals in the direction perpendicular to the x-ray beam. The bleaching light beam was sufficiently narrow so that the change in F-center concentration over the beam width was small. Various initial F-center concentrations were obtained by bleaching at various distances from the x-rayed crystal face. The experimental and theoretical results were compared in the following manner. The experimentally measured optical density, $\log_{10}(I_i/I_{x_0})$, for a crystal of thickness x_0, can be directly related to the average F-center concentration along the light path, N_F, if the Beer-Lambert law is assumed. The relation is

$$\left(\frac{\ln 10}{\sigma_p x_0}\right)\log_{10}\left(\frac{I_i}{I_{x_0}}\right)=\int_0^{x_0} n_F dx \Big/ \int_0^{x_0} dx = N_F, \quad (11)$$

where I_{x_0} is the transmitted bleaching light intensity. The cross section for the absorption of photons, σ_p, can be determined assuming Smakula's equation relating the absorption coefficient to the F-center concentration.[9] By using an oscillator strength $f=0.7$ and an F-band half-width of 0.51 ev, σ_p for NaCl was computed to be 1.32×10^{-16} cm^2.

The theoretical value of N_F at any time t is obtained by evaluating the integral in Eq. (11) using the values of n_F *vs* x given by Eqs. (9) and (9a). This result depends on the value of the quantity $s_0 = n_F^0 b I_i$ which defines the dimensionless time coordinate in Eq. (8d). The quantity s_0 was adjusted to secure the best agreement between theory and experiment. If one assumes that the quantum yield $q_1 = 1$ (see footnote 6) then $\sigma_F = \sigma_p$. Since I_i and σ_p are known and since n_F^0 can be determined by using Eq. (11), the adjustment of s_0 yields the value of N which is the total number of filled and unfilled single negative-ion vacancies.

The values of N_F^0/N_F derived from experiment on an NaCl crystal are plotted against the time of bleaching t in Fig. 6 for initial F-center concentrations between 0.34×10^{16} and 1.42×10^{16} cm^{-3}. The incident bleaching light intensity was maintained constant at 0.87×10^{14} quanta cm^{-2} sec^{-1}. The theoretical values of N_F^0/N_F

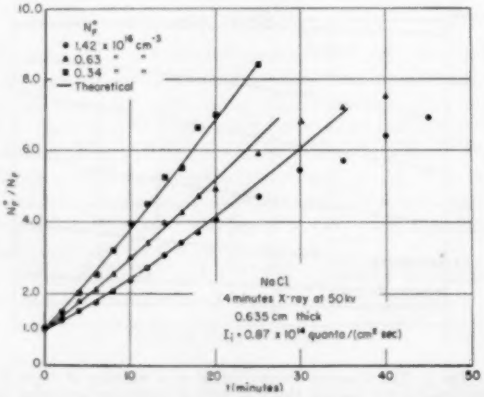

FIG. 6. A comparison of theory with experiment for the optical bleaching of F centers in x-rayed NaCl for initial F-center concentrations in the range $\sim 10^{16}$–$\sim 10^{16}$ cm^{-3}.

[9] A. Smakula, Z. Physik **59**, 603 (1930).

with s_0 chosen to give the best fit to experiment are indicated by the solid lines. The agreement between theory and experiment is quite good except for the bleaching of the last 25 percent of the F centers in the case of the two highest initial concentrations. The origin of this discrepancy is not clear.

Experimental data and theoretical curves for the bleaching of an NaCl crystal at initial concentrations between 0.32×10^{17} and 1.44×10^{17} cm^{-3} are presented in Fig. 7. The intensity of the bleaching F light was the same as in the former case. The experimental results are seen to be consistent with the behavior of the model.

A series of bleaching experiments were carried out at the same initial F-center concentration but different incident bleaching light intensities. The results are given in Fig. 8 for $n_F{}^0=0.31\times10^{17}$ cm^{-3} and in Fig. 9

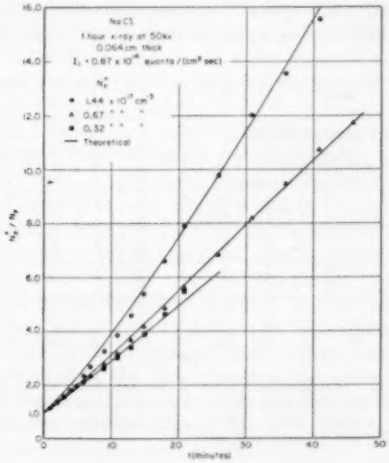

FIG. 7. A comparison of theory with experiment for the optical bleaching of F centers in x-rayed NaCl for initial F-center concentrations in the range $\sim10^{16}$–$\sim10^{17}$ cm^{-3}.

for $n_F{}^0=1.4\times10^{17}$ cm^{-3}. In this series of experiments the bleaching light intensity varied from $\sim3\times10^{13}$–$\sim9\times10^{13}$ quanta cm^{-2} sec^{-1}.

Values of the parameter $N=n_F{}^0+n_V{}^0$ were computed from the values of s_0 obtained by the fitting of the theoretical curves to the experimental data. The results are given in Table I. The quantity $n_F{}^0+n_V{}^0$ is plotted against $n_F{}^0$ in Fig. 10. Now an increase in $n_F{}^0$ unaccompanied by an increase in the total number of filled or unfilled single negative ion vacancies, i.e., $n_F{}^0+n_V{}^0$, would imply that the x-ray process fills but does not produce negative ion vacancies. The fact that $n_F{}^0+n_V{}^0$ is roughly proportional to $n_F{}^0$, as can be seen in Fig. 10, is evidence that the x-ray process produces single negative ion vacancies.

Reference to Table I shows that for a given value of $n_F{}^0$ the value of $n_F{}^0+n_V{}^0$ determined by a bleaching

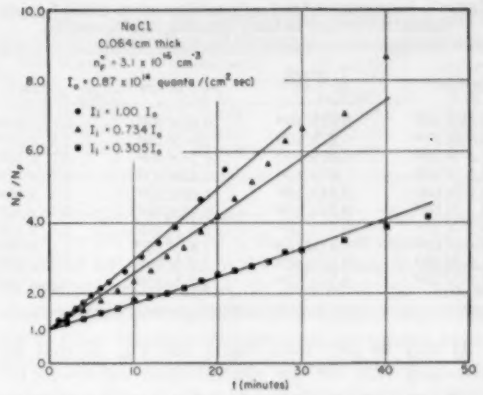

FIG. 8. A comparison of theory with experiment for the optical bleaching of F centers in x-rayed NaCl for various bleaching light intensities at an initial F-center concentration of $\sim3\times10^{16}$ cm^{-3}.

experiment is essentially independent of the bleaching light intensity, I_i. This result is consistent with the foregoing theoretical model in that I_i occurs only in the product $s_0 t$ as shown in Eqs. (8d) and (8e).

For initial F-center concentrations outside the range $\sim10^{16}$–$\sim10^{17}$ cm^{-3} we consider first the case of crystals x-rayed for a prolonged period and having initial concentrations between $\sim1\times10^{17}$ and $\sim4\times10^{17}$ cm^{-3}. In Fig. 11 is shown $N_F{}^0/N_F$ *vs* t for a NaCl crystal x-rayed for ~40 hr at 50 kv. Two features of the curves should be noted, namely, that the rate of bleaching is considerably lower than for lower initial F-center concentrations and that the curvature is different than in the former cases and is not in agreement with the proposed model for the case $k_1=k_2$.[11] During these optical bleaching experiments it was noted that the R and M bands grew to a significant extent as the F band was bleached. However, this was not observed for crystals having shorter x-ray irradiation times.

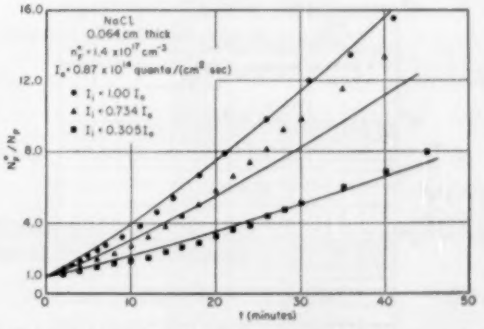

FIG. 9. A comparison of theory with experiment for the optical bleaching of F centers in x-rayed NaCl for various bleaching light intensities at an initial F-center concentration of $\sim1\times10^{17}$ cm^{-3}.

[11] See Fig. 5 which shows the curvature predicted by the model for $k_1=k_2$.

TABLE I. Parameters n_V^0 and $n_V^0+n_F^0$ for various initial F-center concentrations and incident bleaching light intensities.

n_F^0 cm^{-3}	I_i quanta cm^{-2} sec^{-1}	$n_V^0+n_F^0$ cm^{-3}	n_V^0 cm^{-3}
0.34×10^{16}	0.87×10^{14}	0.82×10^{16}	0.48×10^{16}
0.63×10^{16}	0.87×10^{14}	2.0×10^{16}	1.4×10^{16}
1.4×10^{16}	0.87×10^{14}	5.1×10^{16}	3.7×10^{16}
3.2×10^{16}	0.87×10^{14}	1.13×10^{17}	8.1×10^{16}
3.1×10^{16}	0.64×10^{14}	1.00×10^{17}	6.9×10^{16}
3.2×10^{16}	0.27×10^{14}	0.89×10^{17}	5.7×10^{16}
6.7×10^{16}	0.87×10^{14}	2.0×10^{17}	1.3×10^{17}
1.4×10^{17}	0.87×10^{14}	2.8×10^{17}	1.3×10^{17}
1.4×10^{17}	0.64×10^{14}	2.8×10^{17}	1.3×10^{17}
1.4×10^{17}	0.27×10^{14}	1.9×10^{17}	0.5×10^{17}

It may be seen from Fig. 7 and Fig. 11 that the bleaching rate for the concentration $n_F^0=\sim1\times10^{17}$ cm^{-3} was considerably slower in the crystals x-rayed for a prolonged period (heavily x-rayed crystals) than in those x-rayed for a short time (lightly x-rayed crystals). This difference may be due only to a difference in the particular crystals or it may be due to the difference in the intensity and hardness of the x-rays at different depths in the crystal. To attempt to clarify this point, two specimens cleaved from the same crystal were x-rayed, one for one hour and the other for ~40 hours. They were then re-x-rayed in a direction perpendicular to the original direction of x-ray at depths for which the F-center concentration was $\sim5.5\times10^{16}$ cm^{-3} in each case. It was found that the rate of production of F centers during the second irradiation was significantly larger in the crystal initially irradiated for 40 hours than in that irradiated for one hour. This result and the difference in the optical bleaching rates appear to be consistent with a larger value of n_V^0/n_F^0 at a given value of n_F^0 in a crystal irradiated for a prolonged period at low x-ray intensity than in a crystal irradiated for a short period at a high intensity of somewhat softer x-rays.

Another possible explanation for the slowness of bleaching in heavily x-rayed crystals and for the shape of the curves in Fig. 11 is that some of the holes are trapped in an aggregate of positive-ion vacancies such that the resulting V center has a small cross section for capture of conduction electrons. It has been observed by Casler, Pringsheim, and Yuster[12] that the so-called V_3 band is present in a KCl crystal x-rayed for two hours at room temperature, that this band does not bleach appreciably when the F band is bleached by F light, and that it is difficult to bleach the F band completely. Seitz[13] has suggested that the V_3 center consists of a hole trapped at a pair of positive-ion vacancies. Such a model would have a net negative charge and would repel conduction electrons. Further experimental work on lightly and heavily x-rayed crystals is required to clarify the role of the V bands during the F-light bleaching of the F band.

For initial concentrations in the range 1.0×10^{15}–7.0×10^{15} cm^{-3} optical bleaching rates of the F band were studied using a very thick (1.67 cm) NaCl crystal and short x-ray irradiation times (~3 min). The results were qualitatively similar to those obtained for the heavily x-rayed crystals (Fig. 11) rather than those for n_F^0 values in the range 10^{16}–10^{17} cm^{-3} (Fig. 7). No explanation has been established for the deviation of the results for very thick crystals from the behavior of the model. It is possible that impurities are playing a significant role in the concentration range under 10^{16} cm^{-3}.

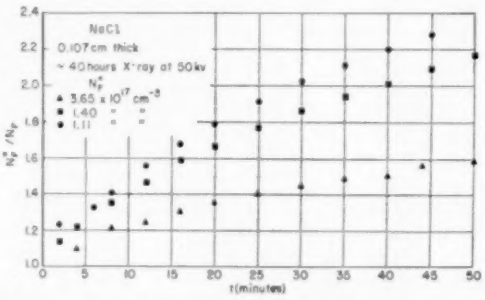

FIG. 11. Experimental values of the reciprocal of the average F-center concentration *versus* time of optical bleaching in a heavily x-rayed NaCl crystal. The bleaching light intensity $I_i=0.87\times10^{14}$ quanta/(cm^2 sec).

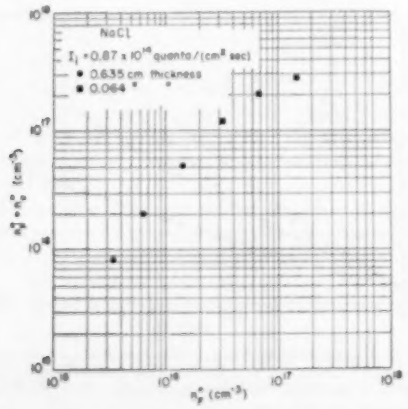

FIG. 10. The total concentration of filled and unfilled negative ion vacancies *versus* the initial F-center concentration.

The work of Etzel and Maurer[14] on the electrical conductivity of NaCl indicates that positive-ion vacancies diffuse at an appreciable rate at room temperature. It is possible that association of positive- and negative-ion vacancies may occur with the result that the effective capture cross section of negative-ion vacancies for conduction electrons does not remain constant

[12] Casler, Pringsheim, and Yuster, J. Chem. Phys. **18**, 1564 (1950).
[13] F. Seitz, Revs. Modern Phys. **26**, 57 (1954).
[14] H. W. Etzel and R. J. Maurer, J. Chem. Phys. **18**, 1003 (1950).

during the bleaching. This possible association of positive and negative ion vacancies was investigated by optically bleaching a NaCl crystal ~22 hours after x-raying and comparing the results with those for a specimen cleaved from the same crystal and x-rayed in the same manner but optically bleached ~1 hour after x-raying. The values of n_V^0 calculated for runs at the same value of n_F^0 were 15–30 percent lower in the former case than in the latter. This result indicates that during the course of a bleaching experiment (<3 hours duration) effects arising from association of positive and negative ion vacancies are probably negligible.

A number of experiments were performed to test the effect of the initial state of the crystal on the optical bleaching rate. A given crystal was found to give reproducible results if it was heated to 350°C for two hours between runs. Different batches of Harshaw NaCl crystals, when treated in the above manner, gave qualitatively the same results. Various batches differed somewhat in the largest value of n_F^0 for which the behavior of the model agreed with experiment and in the value of $n_V^0+n_F^0$ which gave the best fit to the data for a given n_F^0 value.

Several experiments were carried out using lead-free (<0.0001% Pb) NaCl single crystals prepared by Mrs. E. W. Claffy at the Naval Research Laboratory and kindly supplied to us by Dr. H. W. Etzel. For n_F^0 values in the range 3.1×10^{16}–1.3×10^{17} cm^{-3} the experimental results agree rather well with the behavior of the model. The values of n_V^0/n_F^0 were roughly double those obtained from the data given in Fig. 7. For n_F^0 values in the range 3.5×10^{15}–1.7×10^{16} cm^{-3} the experimental values of N_F^0/N_F are significantly lower during the last one-third of the bleaching than the values given by the theoretical curves fitted to the data for the first two-thirds of the bleaching. This effect is shown in a somewhat less pronounced manner in Fig. 6.

A cursory investigation was made of the effect of various heat treatments prior to x-ray irradiation on the optical bleaching rate of F centers. Two crystals cleaved from the same source were heated to 750°C for two hours. One crystal was cooled quickly (~2 min) to room temperature while the second was cooled slowly to room temperature over a period of ~18 hours. The crystals were then x-rayed and the rates of optical bleaching of the F band determined. The bleaching rate for the slowly cooled crystal was more rapid than for the rapidly cooled crystal. Both rates were more rapid than for a crystal (Fig. 7) heated to 350°C before x-raying and bleaching. Typical values of n_V^0/n_F^0 calculated from the data are tabulated in Table II. For the crystals heated to 750°C the quantity n_V^0/n_F^0 was found to be considerably smaller in the crystal cooled slowly than in that cooled rapidly. The n_V^0/n_F^0 values for the latter case were smaller than those for the crystal heated to 350°C. Optical bleaching rates for a crystal heated to 600°C and cooled quickly before x-raying gave values of n_V^0/n_F^0 somewhat smaller than those for the crystal heated to 350°C. The crystals heated to 600°C and 750°C showed more rapid bleaching of the last one-third of the F band than is predicted by the theoretical model. It is possible that besides single negative-ion vacancies other imperfections which act as traps for conduction electrons are present in the crystals heated to the higher temperatures.

TABLE II. Effect of heat treatment on optical bleaching rates.

Heat treatment	Cooling period	n_F^0 (cm^{-3})	n_V^0/n_F^0
2 hr at 750°C	18 hr	5.4×10^{16}	0.15
2 hr at 750°C	2 min	6.6×10^{16}	0.61
4 hr at 600°C	20 min	5.9×10^{16}	1.3
2 hr at 350°C	20 min	6.7×10^{16}	1.9

V. ACKNOWLEDGMENTS

We are greatly indebted to Dr. James W. Follin, Jr., who obtained the exact solution to Eqs. (4) and (6). We are also indebted to Dr. Bernard Fleishman who pointed out the possibility of numerically integrating these equations. We wish to thank Professor F. Seitz for a profitable discussion. We should like to express our appreciation to Dr. H. W. Etzel of the Naval Research Laboratory for supplying us with lead-free NaCl crystals prepared by Mrs. E. W. Claffy. We wish to thank Miss M. C. Williams for carrying out the experimental measurements and Miss Jacquelyn Siler for performing the numerical calculations. Finally we thank Miss Doris Rubenfeld who prepared the figures and Miss Shirley Thomas for assistance with the manuscript.

APPENDIX A

Equations (4) and (6) may be written in terms of the dimensionless quantities defined in Eq. (8) as follows:

$$\partial n/\partial\tau=-\mathcal{J}n^2, \tag{A1}$$

$$\partial\mathcal{J}/\partial y=-\mathcal{J}n. \tag{A2}$$

This pair of equations may be written as

$$\partial\eta/\partial\tau=\mathcal{J}, \tag{A3}$$

$$\partial\mathcal{J}/\partial y=-\mathcal{J}/\eta, \tag{A4}$$

where

$$\eta=1/n. \tag{A5}$$

Differentiating Eq. (A3) with respect to y and making use of Eq. (A4), one obtains

$$\partial^2\eta/\partial\tau\partial y=-\partial\ln\eta/\partial\tau. \tag{A6}$$

Integrating with respect to τ,

$$\partial\eta/\partial y=-\ln\eta+f(y). \tag{A7}$$

Making use of the boundary condition given by Eq. (7a), we have for $\tau=0$, $\eta=1$ for all y so that $\ln\eta=0$,

$\partial\eta/\partial y=0$, and finally $f(y)=0$. Thus

$$\partial\eta/\partial y=-\ln\eta, \tag{A8}$$

which becomes

$$e^{u}\partial u/\partial y=-u \tag{A9}$$

if

$$u=\ln\eta.$$

Integrating Eq. (A9) yields

$$y=-\int_{1}^{u}\frac{e^{\phi}}{\phi}d\phi+g(\tau). \tag{A10}$$

Equation (5) may be written as

$$u=\ln(1+\tau) \tag{A11}$$

and specifies u for $y=0$. Evaluating $g(\tau)$ yields

$$y=-\int_{1}^{u}\frac{e^{\phi}}{\phi}d\phi+\int_{1}^{\ln(1+\tau)}\frac{e^{\phi}}{\phi}d\phi, \tag{A12}$$

or

$$y=-\mathrm{Ei}(u)+\mathrm{Ei}[\ln(1+\tau)], \tag{A13}$$

which is equivalent to the result stated in Eqs. (9), (9a), and (9b).

By differentiating Eq. (A13) with respect to τ and making use of Eq. (A3), one may show that

$$s=\ln\eta/\ln(1+\tau). \tag{A14}$$

By using the series expansion for $\mathrm{Ei}(u)$ given by

$$\mathrm{Ei}(u)\simeq\gamma+\ln u+\sum_{p=1}^{\infty}\frac{u^{p}}{p\cdot p!},$$

where γ is Euler's constant defined by

$$\gamma=\lim_{\epsilon\to 0}\int_{-\infty}^{\epsilon}\frac{\exp\varphi}{\varphi}d\varphi+\int^{1}\frac{d\varphi}{\varphi}=0.577216\cdots,$$

one can show that Eq. (A13) is consistent with the boundary condition $\eta=1$ for all y at $\tau=0$. By eliminating η from Eqs. (A13) and (A14), one may verify that these equations are consistent with the boundary condition $s=1$ for all τ at $y=0$.

PHYSICAL REVIEW VOLUME 99, NUMBER 2 JULY 15, 1955

Specific Heat of Bismuth at Liquid Helium Temperatures

K. G. RAMANATHAN AND T. M. SRINIVASAN
National Physical Laboratory of India, New Delhi, India

(Received March 8, 1955)

The specific heat of bismuth has been investigated in the liquid helium region down to 1.3°K by means of a new vacuum calorimeter. The Debye θ is found to increase from 103.5 to 120 in the range 4.1 to 2°K and appears to attain a constant value at lower temperatures. Evidence is obtained for an electronic contribution of $0.114\times10^{-4}T$ calories/°K to the atomic heat of bismuth.

1. INTRODUCTION

THE specific heat of bismuth does not seem to have been investigated accurately at very low temperatures.[1] The measurements of Keesom and van den Ende[2] appear to be the only work that has extended down to liquid helium temperatures. From these they concluded that the atomic heat obeys a T^3 law to a first approximation in the entire range covered by them (3 to 20°K). However, the results they obtained at temperatures below 4°K are not claimed to be very accurate. Since this happens to be the region where the electronic contribution to the specific heat becomes appreciable, it was decided to obtain fresh data with an improved calorimetry technique.

[1] Since this work was completed, we have come across the recent measurements of P. H. Keesom and N. Pearlman [Phys. Rev. **96**, 897 (1954)], with which our results show good agreement.

[2] W. H. Keesom and J. N. van den Ende, Communs. Kamerlingh Onnes Lab. Univ. Leiden, No. 203d: Proc. Koninkl. Ned. Akad. Wetenschap. **33**, 243 (1930); Leiden Communs. 213c, Proc. Koninkl. Ned. Akad. Wetenschap. **34**, 210 (1931).

2. EXPERIMENTAL DETAILS

The results described below were obtained with a new vacuum calorimeter[3] which was recently developed in this laboratory, capable of an accuracy better than 3 percent in the range 4.2 to 1.3°K. In this apparatus the specimen is suspended inside a hermetically sealed can, the air in which is frozen out while cooling with liquid helium. The use of an exchange gas and the operation of high-vacuum equipment which are essential in conventional methods, are avoided by means of a mechanism which can make or break a thermal contact of the specimen with the bath as necessary. The heat capacities are measured by thermally isolating the specimen and dissipating a known amount of electrical energy through a heating coil wound around it. The temperature rise (this is always kept below 0.04°K) is then measured with a carbon resistance thermometer (a ½-watt 100-ohm resistor manufactured by Speer Resistor Corpora-

[3] K. G. Ramanathan and T. M. Srinivasan, Phil. Mag. **46**, 338 (1955).

tion) calibrated against the helium vapor pressure temperature scale.[4] The thermal isolation obtained in this method is so good that the specimen temperature remains steady within detectable limits (0.0001°K) for several minutes after the heating power is switched off.

The performance of the calorimeter has been tested by measuring the specific heat of tin in the range 4.2 to 1.5°K. The results obtainedco mpare well with those of Keesom and van Laer.[5] The observed jump (0.0025 calorie) in the atomic heat at the superconducting transition point 3.71°K, also agrees well with the theoretical value (0.0026 calorie) calculated from Rutgers' formula by using the known value of the gradient dH/dT in the critical magnetic field temperature curve at the transition point.

Two specimens of bismuth (51.56 g and 61.85 g) made out of a Johnson-Matthey sample of purity 99.95 percent, were used for the measurements. They were cast free from strains from the molten metal in a cylindrical form with diametrical holes provided in the casting itself for embedding thermometers.

3. RESULTS AND DISCUSSION

Figure 1(a) shows the variation of the atomic heat of bismuth in the range 4.1 to 1.3°K. The points obtained by Keesom and van den Ende are also plotted in the graph for comparison. The variation of C/T^3 with temperature is shown in Fig. 1(b). It is seen that this quantity decreases progressively in the range 4.1 to 2°K, below which there is a region of apparent constancy. The Debye θ increases from 103.5 at 4.1°K to about 120 below 2°K. The region of apparent constancy below 2°K ($T<\theta/50$) could be the result of a genuine T^3 variation of the lattice specific heat.

Figure 1(c) is a plot of C/T against T^2. If we assume the atomic heat below 2°K to be represented by $C_v=aT+bT^3$, then a is the intercept of the graph on the C/T axis and b is its gradient. Estimating these constants by the method of least squares from 28 readings we get the expression for the atomic heat

$$C_v=10^{-4}[(0.114\pm0.146)T+(2.71\pm0.05)T^3] \text{ calories/°K}$$

containing a small linear term in temperature.

The Sommerfeld formula for the electronic specific heat per gram atom of a metal is

$$C_e=\pi^2nRT/2T_0,$$

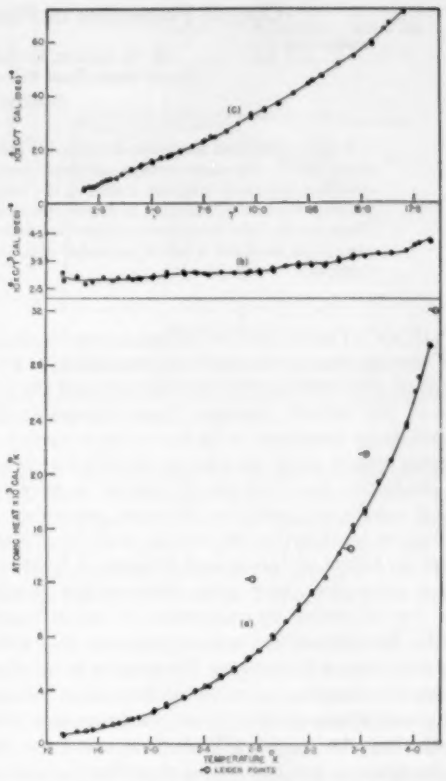

FIG. 1. (a) Variation of atomic heat of bismuth in the temperature range 4.1 to 1.3°K. (b) Variation of C/T^3 with temperature. (c) Plot of C/T against T^2.

where R is the gas constant, n is the effective number of free electrons per atom and T_0 is the degeneracy temperature of these electrons. Equating this to the linear term in the expression for the atomic heat we get $n/T_0=1.2\times10^{-4}$. From measurements of the De Haas-van Alphen effect in bismuth, Shoenberg[6] has estimated T_0 to be 210°K. When we use this estimate to eliminate T_0, n turns out to be 2.5×10^{-4}.

ACKNOWLEDGMENTS

The authors are thankful to Sir K. S. Krishnan, F.R.S., Director of the National Physical Laboratory, for his kind interest in this work. Our thanks are also due to Dr. J. K. Hulm, of the Institute for the Study of Metals, Chicago, for supplying us with the carbon thermometer used in this work.

[4] D. Shoenberg and H. van Dijk, Nature **164**, 51 (1949).
[5] W. H. Keesom and P. H. van Laer, quoted in D. Shoenberg, *Superconductivity* (Cambridge University Press, London, 1938), p. 63.
[6] D. Shoenberg, Trans. Roy. Soc. (London) **A245**, 54 (1952).

Optical Properties of Plastically Deformed Germanium

H. G. Lipson, E. Burstein, and Paul L. Smith
United States Naval Research Laboratory, Washington, D. C.

(Received March 15, 1955)

N-type germanium specimens of 1 ohm-cm resistivity were plastically deformed from 3 to 15 percent at about 700°C. The more strongly deformed specimens were found to be converted to *p*-type. All of the deformed specimens exhibited a shift in the intrinsic absorption edge as well as an extended tail. Those samples which were converted to *p*-type also exhibit the characteristic absorption bands due to free holes. These results differ from those obtained for neutron-bombarded germanium which exhibits no shift of the absorption band and a tail of somewhat different character from that found in the plastically deformed material.

DISLOCATIONS produced in germanium by plastic deformation at elevated temperatures have been shown to affect the electrical conductivity and the lifetime of the minority carriers. These changes in the properties are considered to be due to the formation of acceptor centers which have energy levels 0.2 ev below the conduction band.[1] It was of interest to carry out optical studies on plastically deformed germanium in order to see what further information could be obtained about the effects of dislocations. Samples of 1-ohm-cm *n*-type germanium were given deformations ranging from 3 to 15 percent by compression at approximately 700°C. The deformation was accomplished in a stainless steel furnace by pressing the samples in a helium atmosphere between cylinders of Burundum.* Resistivity and thermoelectric power measurements indicated that the larger deformations converted the originally *n*-type germanium to *p*-type. Heating without deformation was found to increase the resistivity from 1-ohm-cm *n*-type to 3-ohm-cm *n*-type. The material remained *n*-type after a 3 percent deformation, changing from 1-ohm-cm to 15-ohm-cm. On the other hand, a 15 percent deformation converted the material to 16-ohm-cm *p*-type.

Optical transmission measurements were carried out from 1 to 15 microns by means of a Perkin-Elmer spectrometer with LiF and NaCl prisms. Measurements were made on the original material and on the heated, but undeformed, control samples as well as on the deformed samples. Typical room temperature transmission and absorption curves are given in Figs. 1 and 2.

Transmission measurements out to 15 microns are in agreement with the resistivity data. The original material, the heated control, and the 3 percent deformed samples have high transmissions in this range corresponding to relatively pure *n*-type germanium. The

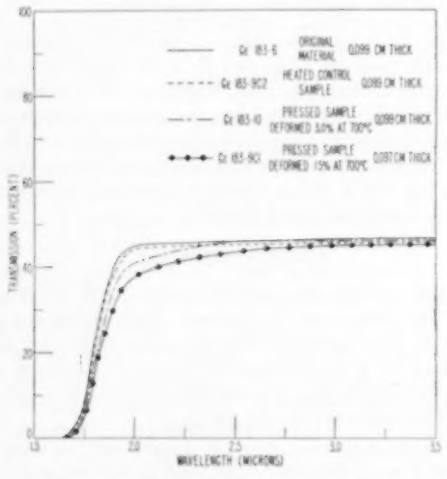
Ge 183-6 ORIGINAL MATERIAL 0.099 CM THICK
Ge 183-9C2 HEATED CONTROL SAMPLE 0.099 CM THICK
Ge 183-10 PRESSED SAMPLE DEFORMED 3.0% AT 700°C 0.099 CM THICK
Ge 183-9C1 PRESSED SAMPLE DEFORMED 15% AT 700°C 0.097 CM THICK
TRANSMISSION (PERCENT)
WAVELENGTH (MICRONS)

FIG. 1. Transmission of germanium specimens before and after heat treatment and deformation.

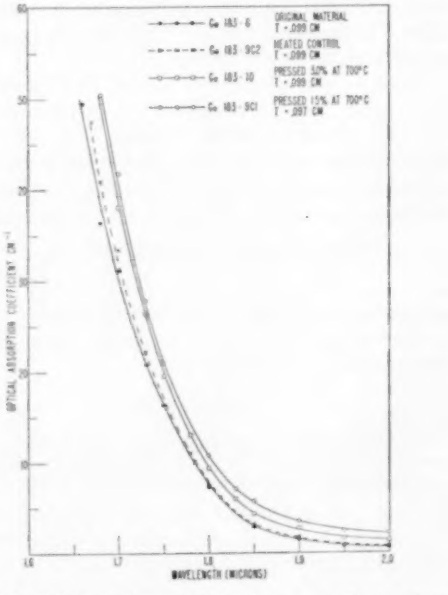
Ge 183-6 ORIGINAL MATERIAL T = .099 CM
Ge 183-9C2 HEATED CONTROL T = .099 CM
Ge 183-10 PRESSED 3.0% AT 700°C T = .099 CM
Ge 183-9C1 PRESSED 15% AT 700°C T = .097 CM
OPTICAL ABSORPTION COEFFICIENT CM⁻¹
WAVELENGTH (MICRONS)

FIG. 2. Optical absorption coefficients for same specimens whose transmissions are shown in Fig. 1.

[1] Pearson, Read, and Morin, Phys. Rev. **93**, 666 (1954).

* Trade name for Al_2O_3 ceramic made by U. S. Stoneware Company.

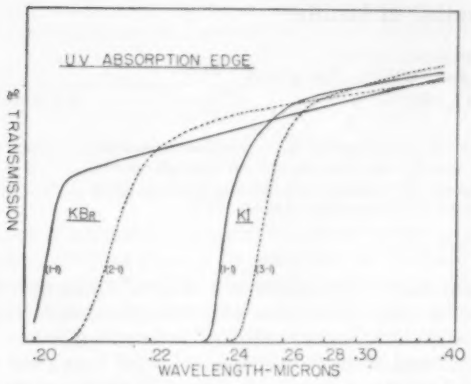

FIG. 3. Transmission of KBr and KI specimens before and after plastic deformation. The numbers in parentheses indicate the change from the initial final thickness in mm.

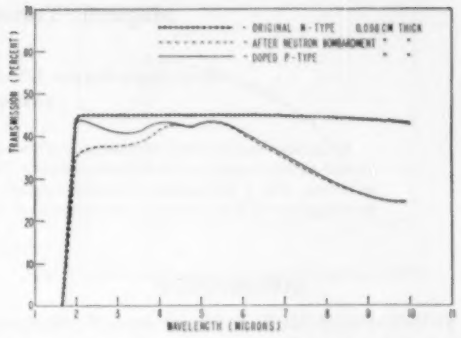

FIG. 4. Transmission of germanium specimens converted from *n*- to *p*-type by neutron irradiation compared with the original *n*-type material and with an unirradiated *p*-type specimen of the same final charge carrier concentration.

strongly deformed germanium samples also exhibited characteristic absorption bands due to free holes[2] which further confirms the change to *p*-type character.

All of the deformed samples are found to exhibit an extended tail and a shift in the intrinsic optical absorption edge toward longer wavelengths which increased with the amount of deformation. This shift is similar to one previously observed in plastically deformed KBr and KI as shown in Fig. 3.[3] At liquid nitrogen temperature the strongly deformed samples have a high resistance and exhibit photoconductivity to approximately 6 microns.

It has long been recognized that lattice imperfections affect the long wavelength edge of the fundamental "electronic" absorption band of insulators.[4] Seitz, for example,[5] has suggested that the long-wavelength tail observed in the silver halides is due to the presence of dislocations which cause a relaxation of the selection rules affecting nonvertical transitions. More recently Blakney and Dexter[6] investigated theoretically two additional mechanisms by which dislocations affect optical properties (a) the effect of local density variations on the energy gap and (b) the effect of defect centers which introduce discrete levels in the forbidden band. Their calculations indicate that phonon interactions[7] are more effective than dislocations in breaking down selection rules. In addition they point out that the dislocations will influence the absorption only near the edge and therefore cannot account for the extended tail.

We may accordingly attribute the shift of the absorption edge observed in plastically deformed germanium to the effect of local changes in density on the energy gap and the tail to defect centers and their associated energy levels. The long-wavelength tail observed in germanium seems to have a break at 2.5 microns corresponding to an energy gap of 0.5 ev. It is tempting to attribute the absorption associated with this tail to transitions from the dislocation acceptor levels to the valence band. The extended tail beyond 2.5 microns is presumably associated with other simple lattice defects. The photoconductivity observed at liquid nitrogen temperatures is probably also due to such centers. An extended tail has also been observed in neutron bombarded germanium[8] as shown in Fig. 4 by the difference in transmission between a sample converted from *n*-type by neutron bombardment and a doped *p*-type sample of the same final charge carrier concentration. This tail is attributed to a distribution of centers associated with simple lattice defects.

[2] H. B. Briggs and R. C. Fletcher, Phys. Rev. **87**, 1130 (1952).
[3] Burstein, Smith, and Davisson, Phys. Rev. **86**, 615 (1952), and unpublished data.
[4] N. F. Mott and R. W. Gurney, *Electronic Processes in Ionic Crystals* (Oxford University Press, London, 1940), second edition; F. Seitz, Phys. Rev. **80**, 239 (1950).
[5] F. Seitz, Revs. Modern Phys. **23**, 328 (1951).
[6] R. M. Blakney and D. L. Dexter, Phys. Rev. **96**, 227 (1954); D. L. Dexter, paper presented at Atlantic City Photoconductivity Conference, November, 1954 (unpublished).
[7] Hall, Bardeen, and Blatt, Phys. Rev. **95**, 559 (1954).
[8] Unpublished data from work at Naval Research Laboratory in collaboration with J. H. Crawford and J. W. Cleland of Oak Ridge National Laboratory.

Magnetic Transformation in MnBi†

R. R. HEIKES
Westinghouse Research Laboratories, East Pittsburgh, Pennsylvania
(Received April 7, 1955)

Manganese bismuth loses its spontaneous magnetization very sharply at 633°K. At the same temperature drastic changes occur in the lattice constants. Previous workers have interpreted both these phenomena as arising from a ferromagnetic-antiferromagnetic transition. The present work indicates that the phase existing above 633°K is actually a ferromagnetic one with a Curie temperature of about 470°K.

INTRODUCTION

PREVIOUSLY MnBi had been studied principally by Guillaud.[1] The present investigation was initiated because the interpretation of the transition at 633°K as a ferromagnetic-antiferromagnetic change was felt to be unsatisfactory. (MnBi loses its ferromagnetism very sharply at 633°K. Coincident with the loss of ferromagnetism are a decrease in the *c*-axis of the order of 3 percent and an increase in the *a*-axis of the order of 1.5 percent.)

The samples used in the present work were prepared by Dr. A. J. Cornish of this laboratory. X-ray analysis[2] showed the room-temperature phase of MnBi and that quenched from above 633°K to have essentially the same lattice constants as reported by Guillaud. The results are summarized in Table I.

EXPERIMENTAL RESULTS AND DISCUSSION

All measurements of saturation magnetization and susceptibility were made by using the gradient method, which is considered accurate to within ±1 percent. The saturation magnetization curve shown in Fig. 1 possesses the same general characteristics as that recorded previously[1]: (1) the sudden loss of magnetization at 633±2°K,[3] and (2) the thermal hysteresis at the transition point. The important difference is the fact that I_s extrapolates to a value of $3.9\mu_B$ at 0°K rather than $3.52\mu_B$ as recorded previously.[1] This present value agrees well with a theoretical value of $4\mu_B$ based on the assumptions that MnBi has a *g*-factor of 2 (MnSb, a compound chemically and structurally similar to MnBi, has a measured *g*-factor of 1.96[4]) and that Mn is present as Mn^{+++}.

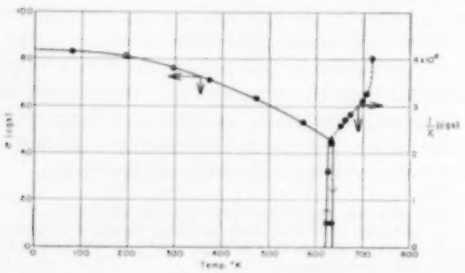

FIG. 1. Saturation magnetization and susceptibility of MnBi.

Also shown in Fig. 1 is the curve of reciprocal susceptibility *versus* temperature. It has been predicted[5] that the behavior of MnBi above its "Curie point" should be similar to that of MnAs (Fig. 2). This is found not to be the case. It should be noted that the extrapolation of the reciprocal susceptibility to zero value occurs at 440°±10°K. (The sharp bend in the curve at 720°K is due to the decomposition of the compound at the peritectic temperature.) For a normal ferromagnet one finds that this extrapolated value is very close to the Curie point. However, in the present case a different phase exists above 633°K. Therefore, the fact that the curve of $1/\chi$ extrapolates to 440°K would indicate that the high-temperature phase (the phase existing above 633°K) would be ferromagnetic with a Curie point of 440°K if it could be retained at room temperature. To test this hypothesis a sample of MnBi was quenched from 650°K. The x-rays showed the sample to be mainly the high-temperature phase. The measurement of saturation magnetization as a function of T is shown in Fig. 3. The point at which the curve turns up is dependent on the rate of heating, indicating that the quenched

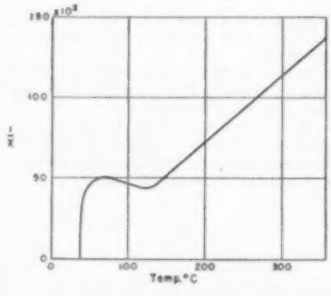

FIG. 2. Reciprocal susceptibility *versus* temperature for MnAs.

† Work supported in part by Wright Air Development Center, U. S. Air Force.

[1] C. Guillaud, thesis, Strasbourg, 1943 (unpublished).

[2] Only lines attributable to MnBi appeared in the x-ray photograph.

[3] A few samples were measured which did not possess the transition at 633°K but instead had a normal Curie temperature at about 700°K. At present their occurrence is not understood.

[4] F. Galavics, Helv. Phys. Acta **12**, 581 (1939).

[5] C. Guillaud, Grenoble Conference Papers, 1950.

TABLE I. Lattice constants of MnBi (NiAs structure).

	Room-temperature phase	High-temperature phase
Present data	c—6.118 A a—4.287 A	c—5.964 A a—4.339 A
Guillaud's data	c—6.12 A a—4.30 A	c—5.83 A a—4.32 A

material is transforming into the stable low-temperature phase. If, after heating to just below the transition temperature of 633°K, the MnBi is cooled, it then returns along the original curve of the low-temperature phase. It can be seen that upon extrapolation to $I_s=0$, a Curie point is found at about 470°K. Because of the inaccuracies involved, this second estimate of the Curie point of the high-temperature phase is considered to be in good agreement with the value derived from the reciprocal susceptibility curve. (The fact that the quenched form of MnBi is ferromagnetic was first observed in our Laboratories by Himmel and Jack.[6])

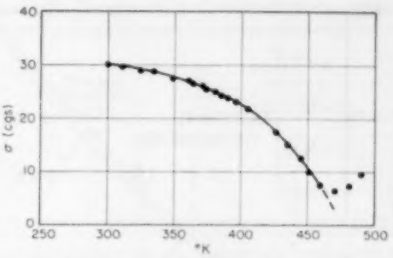

FIG. 3. Saturation magnetization of quenched MnBi.

ACKNOWLEDGMENTS

The author wishes to thank Miss Erlena Schilling for her work on the magnetic measurements.

[6] L. Himmel and K. Jack, (unpublished work).

PHYSICAL REVIEW VOLUME 99, NUMBER 2 JULY 15, 1955

Heat Capacities of Vanadium and Tantalum in the Normal and Superconducting Phases*

R. D. WORLEY,† M. W. ZEMANSKY,‡ AND H. A. BOORSE§
Pupin Physics Laboratories, Columbia University, New York, New York

(Received March 21, 1955)

The heat capacities of two samples of vanadium and two of tantalum have been measured in the normal and superconducting phases in the temperature interval between 1.7° and 5°K. Below the transition temperature T_0, the superconducting heat capacity of both metals could be represented accurately by the relation $C_s=AT+BT^3$. In the normal phase the data obeyed the usual relation $C_n=\gamma T+(464/\theta^3)T^3$. From these data H *vs* T curves were calculated and values of H_0, the threshold field at absolute zero, were obtained. For the better vanadium sample the values of the various constants were found to be $T_0=4.89$°K, $A=-1.97\times10^{-3}$ cal/mole deg^2, $B=1.69\times10^{-3}$ cal/mole deg^4, $\gamma=21.1\times10^{-4}$ cal/mole deg^2, $\Theta=273$°K, and $H_0=1340$ oersteds; for the better tantalum sample $T_0=4.38$°K, $A=-1.45\times10^{-3}$ cal/mole deg^2, $B=1.33\times10^{-3}$ cal/mole deg^4, $\gamma=13.0\times10^{-4}$ cal/mole deg^2, $\Theta=231$°K, and $H_0=860$ gauss. The measured heat capacities were compared with the predictions of the Koppe theory and the α model.

1. INTRODUCTION

AN experimental study of the electronic contribution to the heat capacity of metals in the superconducting phase is of fundamental interest in the theory of superconductivity. Vanadium and tantalum are well suited to such a study for they have a high zero field transition temperature, a large electronic heat capacity, and a relatively small lattice heat capacity. In addition, the heat capacities of these two metals are of interest in their own right for comparison with the results of magnetic measurements of the threshold fields which destroy their superconductivity.

There is a great disparity in the threshold fields which have been reported for vanadium,[1,2] and, prior to the present measurements, no calorimetric data existed for the purpose of comparison. The more recent work[2] indicates that the threshold fields for this metal depend markedly on the amount of internal strain in the sample, due either to mechanical work or to the presence of interstitial gaseous impurities which distort the lattice structure. The effect of these quantities on the heat capacities of vanadium has been studied in these experiments.

Tantalum has been the subject of two earlier heat capacity investigations. The first of these was carried out by Keesom and Désirant in 1941.[3] Since their results did not agree with the magnetic measurements

* This work was assisted by the Office of Naval Research and Linde Air Products Company.

† Now at Bell Telephone Laboratories, Inc., Whippany, New Jersey.
‡ Permanent address: The City College of New York, New York, New York.
§ Permanent address: Barnard College, Columbia University, New York, New York.

[1] Webber, Reynolds, and McGuire, Phys. Rev. **76**, 293 (1949).
[2] A. Wexler and W. S. Corak, Phys. Rev. **85**, 85 (1952).
[3] W. H. Keesom and M. Désirant, Physica **8**, 273 (1941).

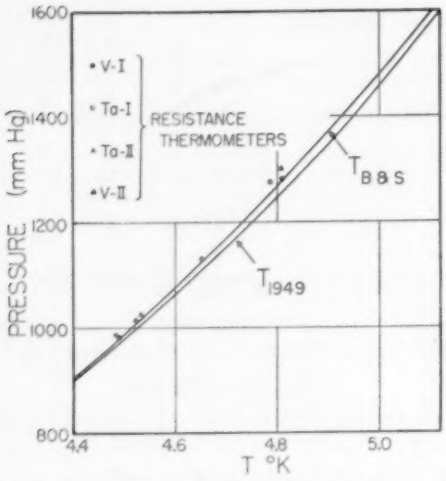

FIG. 1. The vapor pressure of helium between 4.4° and 5°K. T_{1949} is the relation given by the 1949 temperature scale; $T_{B\&S}$ is the relation determined by Berman and Swenson.

of Daunt and Mendelssohn,[4] particularly in the vicinity of the zero field transition temperature, Mendelssohn and Désirant[5,6] repeated the heat-capacity measurements in this temperature range on a sample of tantalum taken from the same batch as the sample used by Daunt and Mendelssohn. They obtained reasonable agreement with the magnetic measurements. Since the results of these two measurements of the heat capacity of tantalum are not in agreement and since the later measurements cover only a very limited temperature interval, it was deemed worth while to repeat the measurements in greater detail. No study of the effect of internal strain due to interstitial gaseous impurities or to mechanical work was attempted.

2. EXPERIMENTAL PROCEDURE

The experimental techniques and apparatus used in these measurements have been described in an earlier paper from this laboratory on the heat capacities of niobium.[7] The only modification of the apparatus described therein has been the addition of an improved system of manometers to increase the range and accuracy of the measurement of the vapor pressure of the liquid helium bath. This system consisted of a mercury manometer and a butyl phthalate oil manometer each 135 cm long and each equipped with brass scales and verniers. The oil manometer was used over the range of pressures from 0.1 to 9 cm Hg and the mercury manometer over the range from 9 to 135 cm Hg. Column heights were measured to 0.2 mm and corrected for the temperature variation of the density of the mercury and oil. To facilitate measurements at pressures above 76 cm Hg a heater at the bottom of the helium bath was used to warm the bath to the required temperature.

All vapor pressure measurements at temperatures above the λ point of liquid helium were corrected for the hydrostatic pressure of the liquid helium above the level of the resistance thermometer. Since the helium Dewar was not transparent, the height of the helium bath level was determined by measuring the efflux of helium gas with a flowmeter attached to the exhaust from the mechanical pumps. The initial bath level was established by completely filling the Dewar with liquid helium at the start of the experiment. Starting with a full Dewar the hydrostatic pressure correction was equivalent to 0.004° at the normal boiling point and to 0.040° after pumping the bath down to a temperature just above the λ point.

Each sample contained an Allen-Bradley carbon resistor whose resistance was measured at each vapor pressure determination. The conversion from vapor pressure to temperature and the calibration of these carbon resistance thermometers have been described in detail in a previous communication[8] which called attention to possible errors in the 1949 "agreed" relation[9] between vapor pressure and temperature above 4.2°K. These errors were later confirmed by Berman and Swenson[10] but found to be of smaller magnitude than those reported by us. When our data, however, were modified by the application of the Kistemaker[11] corrections the results were found to be in good agreement with those of Berman and Swenson, as shown in Fig. 1. The data obtained with four different resistance thermometers, each mounted in a different sample, are shown in Fig. 1 as separate points. The points obtained with each thermometer are designated according to the tabulation which will be given later in Table II.

The heat capacities were determined in the manner described by Brown, Zemansky, and Boorse[7] from the equation

$$C=(i_H)^2R_H\Delta\tau/nJ\Delta T, \tag{1}$$

where n is the number of moles, J the mechanical equivalent of heat, i_H the heater current, R_H the heater resistance, $\Delta\tau$ the time interval during which energy was supplied to the heater, and ΔT the temperature difference brought about by this energy input. ΔT was obtained from the relation

$$\Delta T=\frac{\Delta R}{dR/dT} \tag{2}$$

[4] J. G. Daunt and K. Mendelssohn, Proc. Roy. Soc. (London) **A160**, 127 (1937).
[5] K. Mendelssohn, Nature **148**, 316 (1941).
[6] M. Désirant, *Report of the International Conference on Fundamental Particles and Low Temperatures* (Physical Society, London, 1947), Vol. 2, p. 124.
[7] Brown, Zemansky, and Boorse, Phys. Rev. **92**, 52 (1953).
[8] Worley, Zemansky, and Boorse, Phys. Rev. **93**, 45 (1954).
[9] H. van Dijk and D. Shoenberg, Nature **164**, 151 (1949).
[10] R. Berman and C. A. Swenson, Phys. Rev. **95**, 311 (1954).
[11] J. Kistemaker, Physica **12**, 272 (1946).

where ΔR is the change in the resistance of the thermometer during the heating interval and dR/dT is the slope of the calibration equation described earlier.[8] In all of the measurements i_H was chosen to make the energy input at least ten times the natural heat leak, and ΔR was then chosen to make $\Delta\tau$ of the order of 10 to 30 seconds.

i_H, R_H, and $\Delta\tau$ were each measured to better than 0.1 percent. Errors in these three quantities were unimportant compared to those introduced into the measurements through dR/dT and ΔR. Errors in dR/dT were due primarily to systematic errors in calibrating the resistance thermometers. At worst, an error of 0.02° at 5°K would introduce an error of 1.5 percent in the heat capacity at that temperature. Such systematic errors should not appreciably affect the comparison of the results obtained for different samples since all thermometers were calibrated in the same manner and the errors in calibration should be much the same for all. The uncertainty in reading ΔR from the heating curves was of the order of 1 percent. The corresponding uncertainty in the curve of heat capacity as a function of temperature, obtained from a large number of heat capacity determinations, should be much smaller if the errors in ΔR were random. They were not completely random since personal judgment was required for the extrapolation of the fore and after periods of the heating curves. Consequently the use of the method of least squares, which will be described in the presentation of the results, must be regarded merely as a systematic method for handling the data. For this reason no attempt was made to compute precision measures for the least square calculations. From these considerations it is estimated that for the purpose of intercomparison the results are good to better than 1 percent, while the absolute values for the heat capacities are good to better than 2 percent. For the smaller sample of tantalum these figures should be increased to 2 percent and 3 percent, respectively, for in these measurements the slopes of the fore and after periods of the heating curves were steeper and ΔR could not be read with as great accuracy.

The contributions to the heat capacity of each sample from the resistance thermometer and from the glyptal varnish used to bond the thermometer and heater to the sample were estimated from the data of Gurney[12] for the heat capacity of carbon and from that of Keesom and Pearlman[13] for the heat capacity of glyptal. These contributions were of the order of 2 percent for the small tantalum sample and appropriate corrections were made. No corrections were made to the measured heat capacities of the other samples since the contributions were at most 0.6 percent and were very nearly equal for all samples.

TABLE I. Properties of vanadium and tantalum samples.

Sample	No. of moles	Density (g/cm³)	% impurities (by weight) N_2	O_2	H_2	C	Fe
V–I	3.802	6.098	0.132	0.13	0.0055	0.045	0.1
V–II	2.674	6.098	0.04	0.08	0.008	0.054	...
V–IIA	2.650	6.100	0.04	0.08	0.0005	...	...[a]
			0.05	0.05	0.001	...	...[b]
Ta–I	3.029	16.09	...	...	...	0.03	0.03
Ta–II	0.5545	16.65	...	...	...	0.03	0.03

[a] Center of bar.
[b] Surface layer.

TABLE II. Characteristics of resistance thermometers.

Sample	Nominal resistance (ohms)	Power dissipation (watts)	Room temperature resistance (mounted in sample) (ohms)	Approx. resistance at NBP of helium (ohms)
V–I	22	1	36	335
V–II	27	½	37	465[a]
V–IIA	27	½	37	465[a]
Ta–I	27	1	43	605
Ta–II	27	½	35	435

[a] The same thermometer was used for both series of measurements.

3. EXPERIMENTAL RESULTS

A. Description of Samples

The physical properties of the samples of vanadium and tantalum used in these experiments are given in Table I. Table II gives the characteristics of the resistance thermometers used in the various samples.

The vanadium samples were supplied by the Union Carbide and Carbon Corporation. Each was forged under atmospheric conditions to a one-inch diameter bar from a two-inch square ingot at a temperature of 1125°C. The finishing temperature for this process was 750°C. After cooling in air the surface oxide layer was machined away. Since the recrystallization temperature for vanadium is about 750°–800°C, the samples presumably contain a considerable amount of stress due to cold-working. The analysis of nonmetallic impurities was made by the Union Carbide and Carbon Research Laboratories. A spectrographic analysis of turnings from sample V–I was made by the Analytical and Research Measurements Laboratories of the Department of Chemistry of Columbia University. This analysis indicated that, with the exception of iron, metallic impurities were present in amounts of 0.01 percent or less.

Preliminary heat capacity measurements were made on sample V–I in the condition in which it was received. The measurements were repeated after annealing the sample at a temperature of 950°C for 10 hours at a pressure below 10^{-6} mm Hg. In the interim between the measurements the accuracy of the measurement of temperature was greatly improved by the installation of the new manometer system. Within the accuracy of the earlier measurements no significant changes were

[12] R. W. Gurney, Phys. Rev. 88, 465 (1952).
[13] P. H. Keesom and N. Pearlman, Phys. Rev. 88, 398 (1952).

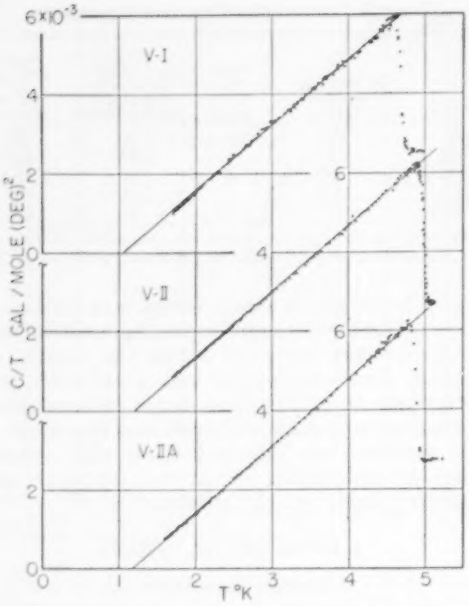

FIG. 2. C/T *versus* T for the vanadium samples in the superconducting phase.

observed in the heat capacity of the vanadium sample. In particular, the zero field transition temperature, which later measurements showed to be quite sensitive to changes in physical properties, was not affected.

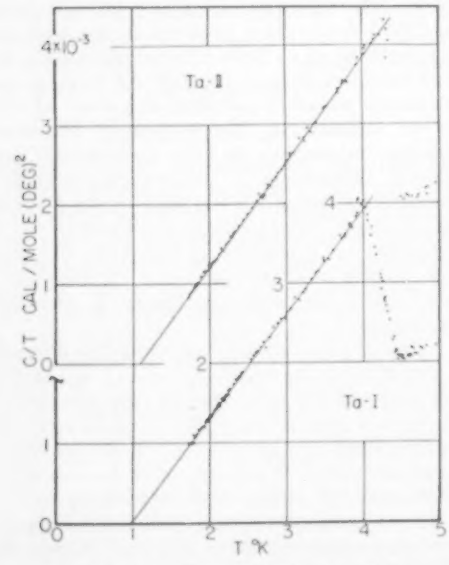

FIG. 3. C/T *versus* T for the tantalum samples in the superconducting phase.

The results which are reported for this sample are those obtained after the heat treatment.

A similar series of measurements were carried out on a vanadium sample of higher purity. This sample is designated in the table as V–II before annealing and as V–IIA after annealing. In view of the results of the measurements on sample V–I it was decided that this second sample should be annealed at a temperature just below the melting temperature, 1900°C.[14] Since this temperature was well beyond the range of the available furnace, arrangements were made with the Materials Laboratory of the Wright Air Development Center at Wright-Patterson Air Force Base, Ohio, to carry out the heat treatment in their resistance furnace. In the annealing cycle the sample was heated to a temperature of 1800°C in thirty minutes, held at that temperature for one hour, and then cooled without quenching in twenty minutes. The pressure throughout the cycle was 4×10^{-4} mm Hg. After this heat treatment the sample consisted of polycrystals with a grain size of 1 to 2 mm easily visible to the unaided eye. Originally gray, the sample had acquired a yellowish luster. The Materials Laboratory ascribed the change in color to a slight pickup of oxygen or nitrogen at the end of the heating cycle when the furnace was opened to the atmosphere. At the conclusion of the second series of heat capacity measurements the sample was returned to the Union Carbide and Carbon Research Laboratories for an analysis of gas content. Samples for the analysis were taken from a surface layer, after hand polishing to remove the temper color, and from the center of the bar. The results of the analysis are included in Table I. They indicate a definite reduction in the hydrogen content. The oxygen content was reduced in the surface layer, although this figure can probably be taken as an indication of no change. There was no change in the nitrogen content.

The tantalum samples were purchased from the Fansteel Metallurgical Corporation, the only commercial source of tantalum. Massive tantalum metal is prepared commercially by compacting electrolytic powder at moderate pressures and then sintering in vacuum. The bar is purposely left rather porous to enable the hydrogen which is evolved during sintering to escape. Hydrogen is not present in the original electrolytic powder but is absorbed by the metal during the chemical cleaning process preparatory to compacting and sintering. After sintering, the metal is worked to higher density by cold swaging and rolling until there is a considerable reduction in cross section. The larger rod sizes cannot be supplied at the proper density because Fansteel is not able to effect the necessary reduction. When the bar has been worked to the proper size it is annealed at 1150°C at a pressure of 5×10^{-6} mm Hg. In order to minimize cold-working,

[14] Adenstadt, Pequiquot, and Raymer, Trans. Am. Soc. Metals 44, 990 (1952).

considerable care was exercised in the machining necessary to prepare the samples for the heat capacity measurements. The initial measurements were made on the larger sample of low density. Because this sample did not exhibit a sharp transition from the superconducting to the normal phase in the absence of a magnetic field, further measurements were made on the smaller sample with the proper density. The impurities quoted in Table I do not refer to these particular samples but are merely typical of tantalum metal refined by Fansteel. No estimate of gaseous impurities was available.

B. Results of the Heat-Capacity Measurements

The experimental results for the heat capacities in the superconducting phase for all the samples are shown in Figs. 2 and 3. The data are presented as plots of C_s/T *versus* T, where C_s is the superconducting heat capacity in calories per mole-degree. This form of presentation was chosen because it was found that the

TABLE III. Coefficients for Eq. (3) and zero field transition temperatures.

Sample	A (cal/mole deg^4)	B (cal/mole deg^2)	T_0 (°K)	Width of transition (°K)	Number of points
V–I	-1.73×10^{-3}	1.65×10^{-3}	4.69	4.66–4.85	129
V–II	-2.01×10^{-3}	1.67×10^{-3}	4.99	4.93–5.05	115
V–IIA	-1.97×10^{-3}	1.69×10^{-3}	4.89	4.82–4.96	99
Ta–I	-1.26×10^{-3}	1.29×10^{-3}	···	4.02–4.42	83
Ta–II	-1.45×10^{-3}	1.33×10^{-3}	4.38	4.36–4.41	77

equation

$$C_s = AT + BT^3 \tag{3}$$

describes the experimental results remarkably well in the temperature range covered by the measurements. The coefficients of Eq. (3) were obtained from the data by a least-squares fit to a straight line on the plot of C_s/T *versus* T, assuming that errors were present only in the y-coordinate. These coefficients are given in Table III, and the lines which they represent are shown in the figures. The number of experimental points used in each least squares calculation is also tabulated. It is emphasized that Eq. (3) cannot be valid at much lower temperatures since the parameters given in the table yield a negative heat capacity below 1°K. Table III also contains a tabulation of the zero-field transition temperature, T_0, for each sample and the approximate width of the transition region. In this tabulation, T_0 is defined as that temperature at which the heat capacity is midway between the values in the normal and superconducting phases.

The normal data for each sample are shown in Figs. 4 and 5, where C_n/T is plotted against T^2. C_n is the heat capacity in the normal phase in calories per mole-degree. These data were obtained in applied fields of 5000 gauss, although some of the results for

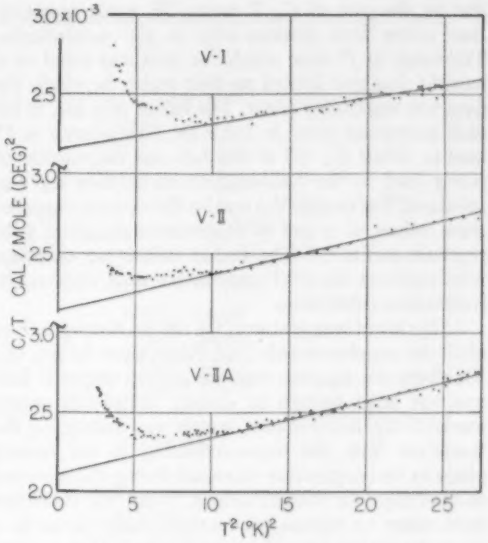

FIG. 4. C/T *versus* T^2 for the vanadium samples in fields of 5000 gauss.

Ta–II at the lower temperatures were obtained in smaller fields. The straight line on each plot represents the equation

$$C_n = \gamma T + (464/\Theta^3)T^3. \tag{4}$$

This is the Debye-Sommerfeld relation which expresses the heat capacity as the sum of a term linear in T representing the electronic contribution and a term cubic in T representing the lattice contribution. Θ is the Debye characteristic temperature. γ and Θ were obtained from the data by a least-squares fit to a straight

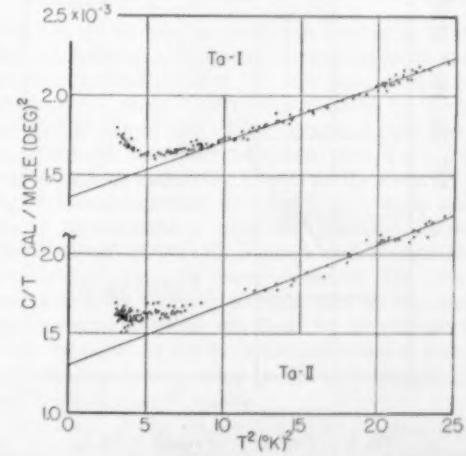

FIG. 5. C/T *versus* T^2 for the tantalum samples in fields of 5000 gauss. Below $T^2=10$ some of the data for sample Ta–II were obtained in smaller fields.

line on the plot of C_n/T *versus* T^2, again assuming that errors were present only in the y-coordinate. The range in T^2 over which the data was fitted to a straight line was limited to that region in which the data was reasonably linear. The values of γ and Θ for each sample are given in Table IV. The interval in T^2 used in fitting Eq. (5) to the data and the number of points used in the least-squares calculations are also tabulated. For sample V–I and for the tantalum samples these values of γ and Θ supercede those which were reported earlier.[15,16] The earlier values for tantalum were based on the 1949 temperature scale without the Kistemaker corrections.

At the lower temperatures, the normal heat capacities of all the samples exceeded the values given by Eq. (4). This behavior suggests that the applied magnetic field was not large enough to destroy completely superconductivity and that each sample was undergoing the transition from the superconducting to the normal phase as its temperature increased during the sequence of heat capacity determinations. When the transition from super to normal conductivity takes place in a magnetic field a latent heat is absorbed. If the superconductor has a zero demagnetizing coefficient and if the magnetic field is uniform, then the transition will take place in an infinitesimal temperature interval and the apparent heat capacity will be infinitely large. If the field is not homogeneous or if the demagnetizing coefficient is not zero the transition will be spread over a finite temperature interval. In this temperature interval the sample is in a mixed phase, partially normal and partially superconducting, called the intermediate state. As the sample passes through the intermediate state its heat capacity will rise above that in the superconducting phase, pass through a maximum, and descend to the value appropriate to the normal phase. If the magnetic field is increased and the process repeated, the position of the maximum will be shifted to lower temperatures. Because the samples used in these experiments had a demagnetizing coefficient greater than $\frac{1}{2}$, and because the applied magnetic field was not homogeneous over the region occupied by the sample, the intermediate state would be spread over a wide range in temperature if the magnetic field were not sufficient to destroy completely superconductivity.

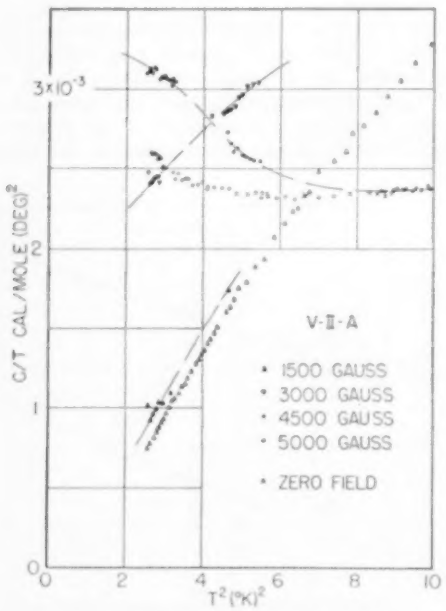

FIG. 6. C/T *versus* T^2 for sample V–IIA in the intermediate state.

To determine if the intermediate state were present in these samples at the largest field strengths employed, a series of measurements of the heat capacities of three of the samples were made at lower field strengths. The results for samples V–IIA and Ta–I are shown in Figs. 6 and 7 as plots of C/T *versus* T^2. The preceding discussion of the behavior of C as a function of T applies equally well to C/T as a function of T^2. In Fig. 7, it may be seen that the curve for Ta–I in a field of 500 gauss behaves in the manner just described. Although the complete curve for the heat capacity in the intermediate state was not traced out for each of the magnetic fields that was used, it is possible to estimate the position of the maximum in the curve from the measurement of a small portion of the curve. The results for V–IIA show that the maximum was shifted to lower temperatures as the applied field was increased, for all values of the field. This confirms that the intermediate state was present in the vanadium sample at the lower temperatures for all field strengths and that at the lowest temperature superconductivity was never completely destroyed. A similar behavior has been observed by Goldman[17] who has made magnetic measurements at low temperatures and high field strengths on the samples of vanadium used by Wexler and Corak.[2] He found evidences of superconductivity in fields as large as 6000 gauss at 2°K. These results

TABLE IV. Electronic constants and Debye temperatures.

Sample	γ (cal/mole deg²)	Θ (°K)	Range in T^2 (°K²)	Number of points
V–I	21.5×10^{-4}	308	12.5–25	32
V–II	21.4×10^{-4}	274	12.5–25	18
V–IIA	21.1×10^{-4}	273	12.5–25	49
Ta–I	13.6×10^{-4}	237	9 –25	65
Ta–II	13.0×10^{-4}	231	11 –25	32

[15] J. Eisenstein, Revs. Modern Phys. **26**, 277 (1954).
[16] Worley, Zemansky, and Boorse, Phys. Rev. **93**, 1567 (1953).
[17] J. E. Goldman, remarks at Third International Conference on Low Temperature Physics and Chemistry (Rice Institute, Houston, 1953).

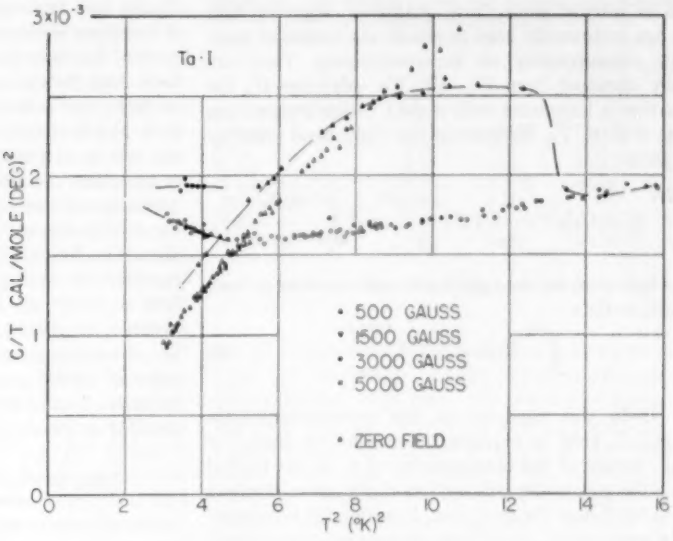

FIG. 7. C/T *versus* T^2 for sample Ta-I in the intermediate state.

show that a magnetic field larger than the one currently available is necessary if the heat capacity measurements in the normal phase on the vanadium samples used in these experiments are to be extended below 3°K.

The results of the measurements on the two tantalum samples are not as readily interpreted in terms of the intermediate state. For sample Ta-I in fields lower than 3000 gauss the maximum in the heat capacity was indeed shifted to lower temperatures as the field was increased. In larger fields, however, the maximum was no longer shifted and the heat capacity was independent of the magnetic field. For Ta-II no systematic variation with field strength was observed in the heat capacity in fields of 1200, 2800, and 5000 gauss within the precision of the measurements. The results of all the measurements made on this sample at different field strengths have been plotted in Fig. 5. Although the results for both samples show no variation with field strength for sufficiently large fields, nevertheless the heat capacities at the lowest temperatures are larger by about 20 percent than the values given by Eq. (4) using the constants from Table IV.

4. DISCUSSION

A. Calculation of the H_T *versus* T Curve

The heat capacities in the normal and superconducting phases are related to the threshold field H_T by the equation

$$C_s - C_n = \frac{VT}{4\pi}\frac{d}{dT}\left(H_T\frac{dH_T}{dT}\right); \tag{5}$$

V is the molar volume. If Eqs. (3) and (4) are used for C_s and C_n, then H_T can be obtained as a function of temperature in a straight forward manner by dividing Eq. (5) by T and integrating twice with respect to the temperature from T_1 to T_0, where T_1 is the lowest temperature attained in the calorimetric measurements. The constants of integration are evaluated by putting $T=T_0$ after each integration. The threshold fields which are obtained for samples V-II and Ta-II are given by

$$\text{V-II: } H_T = 10\{17\,680 + 1077T - 2621T^2 + 351.5T^3 - 2.38T^4\}^{\frac{1}{2}}, \quad 1.7° < T < 4.99°\text{K}; \tag{6}$$

$$\text{Ta-II: } H_T = 10\{6997 + 366.8T - 1327T^2 + 214.07T^3 - 3.057T^4\}^{\frac{1}{2}}, \quad 1.7° < T < 4.38°\text{K}. \tag{7}$$

V-II was chosen for this calculation because its transition temperature, purity, and mechanical state most nearly resembled those of the vanadium sample for which an H_T *versus* T curve was obtained by Wexler and Corak[3]; Ta-II was chosen because it exhibited a much sharper zero field transition than Ta-I. The results for both metals are plotted as H_T *versus* T^2 in Fig. 8. This type of plot was used since it shows most clearly the departures from the parabolic relation $H_T = H_0(1-T^2/T_0^2)$ which is often used to represent the threshold fields of superconductors. The points representing the magnetic measurements on vanadium are the results of Wexler and Corak for their sample *B*. Those for tantalum are the smoothed values of Daunt and Mendelssohn[4] corrected to the 1949 temperature scale by Shoenberg.[18]

The value of the threshold field at absolute zero, H_0, and the slope of the threshold field curve at T_0 are

[18] D. Shoenberg, *Superconductivity* (Cambridge University Press, London 1952), pp. 224–227.

also of interest since these quantities, together with T_0, are customarily used to report the results of magnetic measurements on superconductors. They are easily obtained from Eq. (5). To solve for H_0 the equation is integrated with respect to the temperature from 0°K to T_0, integrating the right-hand member by parts:

$$\int_0^{T_0}(C_s-C_n)dT=\frac{V}{4\pi}\left\{TH_T\frac{dH_T}{dT}\bigg|_0^{T_0}-\tfrac{1}{2}\int_0^{T_0}\frac{dH_T^2}{dT}dT\right\}.$$

The first term on the right-hand side vanishes at both limits, so that

$$\int_0^{T_0}(C_s-C_n)dT=\frac{VH_0^2}{8\pi}. \tag{8}$$

To apply this equation to the experimental data C_s and C_n must be extrapolated to absolute zero. The exact nature of the extrapolation of C_s is not critical since the area under this portion of the curve is only a small fraction of the total area. Equation (4) is assumed to be correct for C_n over the entire temperature interval. $dH_T/dT)_{T=T_0}$ follows directly from Eq. (5) when the indicated differentiation is performed. Since H_T is zero when $T=T_0$, Eq. (5) reduces to Rutgers' equation,

$$(C_s-C_n)_{T=T_0}=\frac{VT_0}{4\pi}\left\{\frac{dH_T}{dT}\right\}^2_{T=T_0}. \tag{9}$$

The results for the three vanadium samples and the small sample of tantalum are assembled in Table V. Included for comparison are the values for sample B of Wexler and Corak and the values for tantalum of Daunt and Mendelssohn as corrected by Shoenberg. A complete summary of the work on tantalum prior to 1947 has been given by Webber.[19] Much of this has been done by measuring the resistance of the sample to detect the onset of superconductivity. While resistance measurements can be of value when comparing the effects of purity and annealing on the behavior of tantalum, the magnetic measurements of Daunt and Mendelssohn are presumed to represent more closely the equilibrium values of the threshold fields. Work on vanadium has not been as extensive. Since its superconductivity was discovered by Meissner and Westerhoff in 1935,[20] the only other work has been that of Webber, Reynolds, and McGuire.[1] They found very broad transitions and very large critical fields, of the order of 10 000 gauss at 2°K, for two samples. Their measurements of the threshold field curve were not as detailed as those of Wexler and Corak.

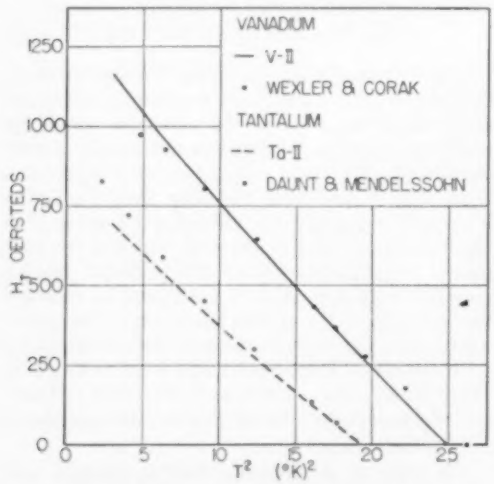

FIG. 8. Threshold fields for vanadium and tantalum. The curves represent the fields calculated from the calorimetric data; the individual points represent the results of magnetic measurements.

TABLE V. Magnetic properties of superconducting vanadium and tantalum.

Sample	T_0 (°K)	H_0 (gauss)	$dH/dT)_{T=T_0}$ (gauss/deg)
Vanadium			
V-I	4.69	1260	−471
V-II	4.99	1360	−477
V-IIA	4.89	1340	−482
Wexler and Corak[a]	5.13	1190	−436
Tantalum			
Ta-II	4.38	860	−334
Daunt and Mendelssohn[b,c]	4.4	975	−310

[a] Reference 2.
[b] Reference 4.
[c] Values corrected to 1949 temperature scale by Shoenberg, reference 18.

B. Effects of Purity and Annealing on the Heat Capacity of Vanadium

Vanadium is typical of the so-called hard superconductors whose properties depend strongly on the chemical and physical state of the metal. As a rule the hard metals have very high melting points so that it is difficult to prepare samples of high purity, and once prepared it is difficult to anneal them without contamination. Presumably the distinction between hard and soft superconductors would vanish if each could be obtained in an ideal state, i.e., a single crystal. The present investigation of the effects of purity and mechanical state on the heat capacity of vanadium was launched in an effort to ascertain if the differences in properties from sample to sample observed in magnetic measurements would be reflected in the heat capacity, and if they were, to obtain data for a sample which most nearly approximated the ideal case for the purpose of comparison with theory.

[19] R. T. Webber, Phys. Rev. **72**, 1241 (1947).
[20] W. Meissner and H. Westerhoff, Z. Physik **87**, 206 (1934).

The results of the measurements show that C_n, C_s, and T_0 are all sensitive to the state of the sample. The closest correlation between these results and those of magnetic measurements arises in the behavior of T_0 as a function of purity. Wexler and Corak observed that the zero field transition temperature of vanadium was markedly dependent on the amount of nitrogen and oxygen present in the sample; in small concentrations these strain the lattice by entering the structure interstitially. The correlation between transition temperature and purity is shown in Table VI. Since the measurements do not distinguish between the effects of nitrogen and oxygen impurities, the sum of these impurities has been tabulated in the last column as an aid in making the correlation. Wexler and Corak did not report a threshold field curve for all of their samples, so that in the preparation of this table the transition temperature for samples *D* and *E* were obtained directly from their *B versus H* curves; the spread in temperature given in the table represents the interval which bracketed T_0 in the actual measurements and does not relate to the actual width of the transition. These authors reported the same transition temperature for their samples *A*, *B*, and *C*. Since the purities of these samples did not differ appreciably, only sample *B* is included in the table. The transition temperature of sample *D* probably lies near the lower limit given in the table. Since the sample was melted in its preparation it is not surprising that its transition temperature lies below that of sample V–I in view of the effect of annealing on the transition temperature of vanadium which was observed in the present measurements.

The depression of the zero field transition temperature of sample V–II following the removal of mechanical strains by annealing was unexpected. Many independent investigators have found just the opposite effect for the hard superconductors niobium[21] and tantalum.[19,22,23] Since all three metals are found in the same column in the periodic table and all have very similar superconducting and physical properties, one might expect their transition temperatures to respond in a similar way to the amount of cold work present. It must be noted, however, that with the exception of niobium and tantalum, the reduction of T_0 with the removal of cold work is typical of most superconductors; it has been observed for zirconium[24] and thorium[25] among the hard superconductors, and for tin,[26] thallium,[26] indium,[26,27] and mercury[27] among the soft.

Changes in the amount of impurity and the amount of cold work present in the vanadium samples produced small but measurable changes in the superconducting heat capacity, while only changes in the amount of impurity affected the normal heat capacity. In the normal phase, within the accuracy of the measurements, there was no change in the electronic heat capacity. The small differences in γ among the three samples are not deemed significant in view of the rather long extrapolation necessitated by the presence of the intermediate state at lower temperatures. The change in the Debye Θ with purity is in the direction to be expected from simple Debye theory. Although no measurements of the elastic constants of vanadium are available, it is known that the hardness of the metal increases with increasing oxygen and nitrogen content.[28] Since the Debye Θ is proportional to the velocity of sound, it will be larger for the sample in which the velocity is greater, that is the harder, and more impure sample. The behavior of the Debye Θ indicates that the impurities in vanadium are the primary cause of internal strains. Thus it is not surprising that the intermediate state persisted in very high fields in the annealed vanadium sample, since this behavior is typical of severly strained superconductors.[29] The insensitivity of Θ to the large change in hydrogen impurity which resulted from the high vacuum anneal is an indication that small amounts of hydrogen do not appreciably distort the lattice structure.

TABLE VI. The effect of oxygen and nitrogen impurities on the zero field transition temperature of vanadium.

Sample	T_0 (°K)	% impurities (by weight) O_2	N_2	O_2+N_2
Wexler and Corak[a] Sample *B*	5.13	0.038	0.021	0.059
V–II	4.99	0.08	0.04	0.12
V–IIA	4.89	0.08	0.04	0.12
Wexler and Corak[a] Sample *D*	4.60–4.70	0.075	0.106	0.181
V–I	4.69	0.13	0.132	0.262
Wexler and Corak[a] Sample *E*	4.11–4.19	0.15	0.189	0.339

[a] Reference 2.

C. Intermediate State Measurements on Tantalum

The calculations described earlier yielded values for the threshold fields several times smaller than those actually applied to the samples during the heat capacity measurements. Yet the results for samples V–IIA and Ta–I show that the application of fields larger than the threshold values will not guarantee the destruction of superconductivity. For sample Ta–I, a more realistic estimate of the fields necessary to destroy superconductivity completely can be made by utilizing the results of the measurements in a field of 500 gauss.

[21] L. C. Jackson, *Proceedings of the International Conference on Low Temperature Physics* (Oxford, 1951), p. 16.
[22] Silsbee, Scott, and Brickwedde, J. Research Natl. Bur. Standards **18**, 295 (1937).
[23] Ziegler, Brucksch, and Hickman, Phys. Rev. **62**, 354 (1942).
[24] T. S. Smith and J. G. Daunt, Phys. Rev. **88**, 1172 (1952).
[25] D. Shoenberg, Proc. Cambridge Phil. Soc. **36**, 84 (1940).
[26] W. I. Khotkevitch and V. R. Golik, J. Exptl. Theoret. Phys. (U.S.S.R.) **20**, 427 (1950).
[27] E. Maxwell and O. S. Lutes, Phys. Rev. **95**, 333 (1954).
[28] S. Beatty, J. Metals **4**, Trans., 987 (1952).
[29] B. G. Lasarew and A. A. Galkin, J. Phys. (U.S.S.R.) **8**, 371 (1944).

TABLE VII. Calorimetric properties of normal and super-conducting tantalum.

Sample	γ $\left(\frac{\text{cal}}{\text{mole deg}^2}\right)$	Θ (°K)	A $\left(\frac{\text{cal}}{\text{mole deg}^6}\right)$	B $\left(\frac{\text{cal}}{\text{mole deg}^8}\right)$	T_0 (°K)	Purity (%)
Ta–I	13.6×10^{-4}	237	-1.26×10^{-8}	1.29×10^{-8}	4.02–4.42	99.9+
Ta–II	13.0×10^{-4}	231	-1.45×10^{-8}	1.33×10^{-8}	4.36–4.41	99.9+
Keesom and Désirant[a]	14.1×10^{-4}	246	-1.14×10^{-8}	1.22×10^{-8}	3.96–4.16	99.95
Mendelssohn[b] and Désirant[c]	...	...	...	...	4.36–4.40	99.9+
Chou and White[d]	13.6×10^{-4}	250	-1.45×10^{-8}	1.33×10^{-8}	4.39[e]	...

[a] Reference 3.
[b] Reference 5.
[c] Reference 6.
[d] Reference 30.
[e] The width of the transition was not reported.

The disappearance of superconductivity in this field at 3.6°K determined a point on the H–T curve. Using the relation $H=H_0(1-T^2/T_0^2)$ and taking T_0 equal to 4°K, one obtains a value of 2700 gauss for H_0. Although no other H–T points were obtained in this manner, these parameters are consistent with the observations that superconductivity persisted in a field of 1400 gauss at 2°K while it was destroyed in a field of 2600 gauss at 1.7°K. This H–T curve is strong evidence against the presence of the intermediate state in the tantalum samples in fields of 5000 gauss. If the behavior of C_s was not due to the presence of the intermediate state, sample Ta–II comes closer to being an ideal sample, for 1200 gauss was sufficient to destroy superconductivity at 1.7°K and even smaller fields may have been adequate.

D. Comparison with Other Heat Capacity Measurements

In view of the anomalous behavior of C_s for both tantalum samples it is particularly instructive to compare these results with those of other measurements of the heat capacity of tantalum. Since the inception of the present experiments the results of Chou and White[30] for a sample of tantalum annealed in high vacuum at 2400°C have become available in addition to those of the references cited in the introduction. The results for all samples are assembled in Table VII. γ and Θ for C_s are those quoted by the original authors. A and B for C_s were obtained from the results of Keesom and Désirant[3] and of Chou and White by replotting their data as C_s/T *versus* T and drawing a straight line through the points. The agreement for Ta–II and the sample of Chou and White is striking, although the fit of their data to the straight line at temperatures near T_0 is not as good as at lower temperatures. The purity of each sample has been tabulated, but in the absence of an analysis of gaseous impurities it is not particularly significant. No information was given on the mechanical state of the samples of Keesom and Désirant and of Mendelssohn and Désirant; presumably they were unannealed.

At very low temperatures and in large magnetic fields, a rise in C_s/T was not observed for any of the other samples. Keesom and Désirant carried out their measurements in a field of 3000 gauss. The scatter of their data did not preclude such a behavior, but if present, it was of smaller magnitude than that observed for Ta–I and for Ta–II. The critical fields necessary to destroy superconductivity in their sample were very similar to those for Ta–I; measurements of the heat capacity in fields of 450 and 700 gauss showed that superconductivity was destroyed at 3.79° and 3.55°K respectively. Chou and White measured C_s in a field of 2000 gauss. They did not find a rise in C_s/T but they made only 6 determinations of the heat capacity below 3°K. They also observed the disappearance of superconductivity in smaller magnetic fields and found good agreement with those calculated from the calorimetric measurements.

In discussing the behavior of C_s for these samples it is instructive to review the results obtained by Webber for the effects of annealing and gaseous impurities on the superconducting properties of tantalum.[19] Making resistance measurements on tantalum wires near T_0, Webber observed that an anneal by the supplier, the Fansteel Metallurgical Corporation, at 1000°C was ineffectual. He was able, however, to raise the transition temperature from 4.16° to 4.30°K by additional annealing at 2400°C and to reduce $dH/dT)_{T=T_0}$ from -1200 to -600 gauss per degree. Measurements on another sample, which was annealed at 2400°C and then contaminated by heating to 1200°C and exposing to air at 10^{-3} mm Hg, yielded values of 4.32°K and -600 gauss per degree for T_0 and $dH/dT)_{T=T_0}$. The sample had absorbed an estimated 9 volumes of oxygen. Webber concluded that the state of anneal was the predominant factor influencing the superconducting properties of tantalum. Bearing in mind that Chou and White found agreement between

[30] C. Chou and D. White, Eighth Annual Calorimetry Conference, Chicago, Sept. 1953 (unpublished). The authors are indebted to Dr. Chou and Dr. White for making their results available prior to publication.

the threshold fields calculated from their calorimetric data and those which destroyed the superconductivity of their sample, one would surmise that their sample was the best of those which have been studied and that the rise in C_n/T at low temperatures is not typical of an ideal sample of tantalum. Indeed, Eq. (4) has proven adequate to describe the heat capacities of most metals, including superconducting metals in the normal phase, which have been studied in the helium temperature region. For this reason the departure of C_n from Eq. (4) has been neglected in the calculations of the threshold fields for Ta–II. If it were not neglected the derived H–T curve would be slightly depressed at lower temperatures.

Corak, Goodman, Satterthwaite, and Wexler[31] have recently reported the results of heat capacity measurements on a sample of vanadium in the superconducting phase over the temperature range from 1.2°K to its transition temperature at 5.05°K. They compared their results with those of the present measurements and found good agreement in the temperature interval common to both measurements. A more detailed comparison will not be attempted here. They fitted their data to an exponential dependence on temperature which represents their results to 5 percent or better from 1.2° to 4.5°K. Above this temperature range the fit is not as good.

E. The Two-Fluid Model of Superconductivity

These experimental results will be compared with two theoretical calculations, each of which has been carried out within the framework of the two-fluid model of superconductivity. This model was proposed by Gorter and Casimir[32] in 1934 to describe the second order phase transition in zero field and the temperature dependence of the threshold field and the heat capacity. The superconducting phase is envisaged as a mixture of two electronic fluids, the superconducting fluid which carries no entropy and the normal fluid which carries the entropy

$$S_n = K(\omega)\gamma T. \tag{10}$$

As the temperature is lowered below T_0 the electrons are presumed to condense from the normal into the superconducting fluid. ω is the degree of condensation; it varies from 1 at 0°K to 0 at T_0. $K(\omega)$ measures the effect of the condensation on the normal fluid; it is proportional to the effective number of normal electrons and varies from 0 at 0°K to 1 at T_0. At and above T_0, S_n is just γT, the electronic entropy given by the free electron theory of metals. Gorter and Casimir assumed that $K(\omega)=(1-\omega)^\alpha$, and, by assigning to α the constant value $\frac{1}{2}$, they obtained the parabolic threshold field curve and the heat capacity in the superconducting phase proportional to T^3, in substantial agreement with the experimental data available at that time.

Recent precise measurements of the critical fields of a number of superconductors incident to the investigation of the isotope effect[27,33,34] have confirmed that the parabolic relation is not an accurate representation of the threshold field curve for most superconductors. Prompted by the results of these measurements, Marcus and Maxwell[35] re-examined the assumptions on which the two fluid model is based. They have shown that a much better description of the experimental results can be obtained if the parameter α in the form of $K(\omega)$ chosen by Gorter and Casimir is not fixed at $\frac{1}{2}$ but is allowed to vary from one metal to another. This form for $K(\omega)$ is called the α model. Values of α ranging from 0.38 to 0.55 have been found among the superconductors investigated.[27] Furthermore, if $K(\omega)$ is taken to be independent of the isotopic mass then the two fluid model also exhibits the experimentally observed property that the threshold field curve for each superconductor is independent of the isotopic mass when it is expressed in terms of the reduced field $h=H/H_0$ and the reduced temperature $t=T/T_0$. Expressing the heat capacity in reduced terms, the α-model gives the following expression for the electronic heat capacity in the superconducting phase:

$$c/t = C_s^{el}/\gamma T = (1+\alpha)/(1-\alpha)t^{(3\alpha/1-\alpha)}. \tag{11}$$

C_s^{el} is the electronic contribution to the heat capacity in the superconducting phase, and γT is the normal electronic heat capacity.

In 1947, Koppe[36] calculated $K(\omega)$ by making an explicit assumption for the effect of the onset of superconductivity on the distribution in energy of the free electrons in the normal phase. Prompted by the Heisenberg theory of superconductivity[37] he assumed that a fraction ω of all momentum states with energies above ϵ_0, the Fermi energy at absolute zero, are not available to the normal electrons after the condensation has begun. $K(\omega)$ is obtained by modifying the distribution in energy by the factor $(1-\omega)$ for energies above ϵ_0 and evaluating the integrals for the total number of electrons and the total energy by the method of Sommerfeld and Bethe.[38] The result is an expression which cannot be given in simple form. Representative values for the electronic heat capacity given by this function have been tabulated by Brown, Zemansky, and Boorse.[7]

Since these calculations are concerned only with the electronic heat capacity, the lattice heat capacity must be subtracted from the measured values. This

[31] Corak, Goodman, Satterthwaite, and Wexler, Phys. Rev. **96**, 1442 (1954).
[32] C. J. Gorter and H. B. G. Casimir, Physik. Z. **35**, 963 (1934).
[33] Serin, Reynolds, and Lohman, Phys. Rev. **86**, 162 (1952).
[34] E. Maxwell, Phys. Rev. **86**, 235 (1952).
[35] P. M. Marcus and E. Maxwell, Phys. Rev. **91**, 1035 (1953).
[36] H. Koppe, Ann. Physik **1**, 405 (1947).
[37] W. Heisenberg, Z. Naturforsch. **2a**, 185 (1947).
[38] A. Sommerfeld and H. Bethe, *Handbuch der Physik* (Verlag Julius Springer, Berlin, 1933), Vol. **24**, Part 2.

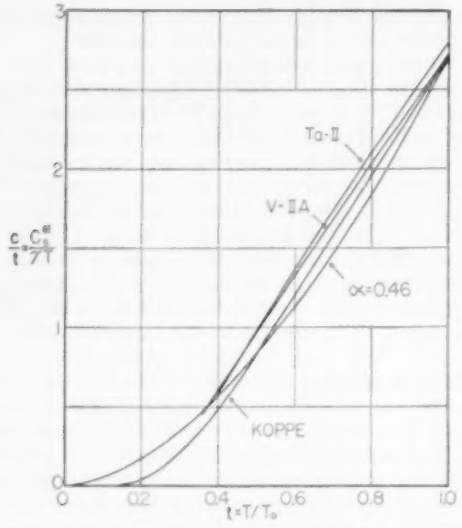

FIG. 9. The reduced electronic heat capacities of vanadium and tantalum in the superconducting phase plotted as c/t *versus* t. The values predicted by Koppe's theory and the α model ($\alpha=0.46$) are also shown.

can be done if it is assumed that the lattice contribution is unaffected by the transition to superconductivity. Then the electronic heat capacity in the superconducting phase is given by the equation

$$C_e^{sl}=C_s-(464/\Theta^3)T^3. \tag{12}$$

The results for samples V–IIA and Ta–II, expressed in terms of the reduced temperature and the reduced heat capacity, are shown in Fig. 9. $c/t(=C_e^{sl}/\gamma T)$ has been plotted against t since it was found that the relation given by Koppe is very nearly linear above $t=0.4$ on this plot. The curve representing the α model corresponds to the value $\alpha=0.46$. This value was chosen to fit the results for vanadium at $t=1$. Other values for α do not improve the agreement with the experimental results.

Considering the simple assumption on which Koppe's calculation is based, the agreement with the experimental results for V–IIA and Ta–II is rather striking. The measurements of Corak, Goodman, Satterthwaite, and Wexler[21] extend the results on vanadium down to $t=0.23$. These data cross the Koppe curve at $t=0.3$ and lie slightly below it at lower t. This behavior is similar to that observed for niobium,[7] although the departure from the Koppe curve is somewhat greater in this case. Although the results for tantalum and vanadium are in close agreement, those obtained for niobium indicate that the heat capacity when expressed in reduced form is not a universal function and that the primary defect of Koppe's calculation is that it predicts the same reduced heat capacity, as well as the same reduced threshold field curve, for all superconductors. The α model does possess the added flexibility of an adjustable parameter, however the agreement with the calorimetric data for tantalum and vanadium is not as good as for the Koppe model.

The magnetic measurements agree with the calorimetric measurements in so far as they show that the reduced threshold field curve is not a universal function for all superconductors. Consequently the α-model with its adjustable parameter does give a somewhat better description of many of the experimental results than does the Koppe calculation. There is evidence to show that both models represent a considerable improvement over the simple cubic heat capacity and the parabolic threshold field curve, but the models must be refined if there is to be agreement in detail with the experimental results.

V. ACKNOWLEDGMENTS

The authors would like to express their gratitude to the Union Carbide and Carbon Research Laboratories and their representative Mr. C. M. Brown for placing the vanadium samples at their disposal and for supplying the analyses of gaseous impurities; to Professor T. I. Taylor of the Department of Chemistry of Columbia University for a spectrographic analysis of turnings from the first vanadium sample; to the Materials Laboratory of the Wright Air Development Center for annealing the second vanadium sample; to Professor Jack Steinberger, Professor A. M. Sachs, and Dr. David Bodansky of the Nevis Cyclotron Laboratories for supplying liquid hydrogen; and particularly to the members of the Columbia Cryogenic Laboratory for their assistance in making the measurements and in analyzing the data: Arnold Berman, Albert Brown, Raymond Kaplan, Leonard Lesensky, Dr. Bernard Smith, and Professor A. H. Spees.

Low-Field Magnetic Resonance

M. A. GARSTENS AND J. I. KAPLAN
United States Naval Research Laboratory, Washington, D. C.
(Received March 24, 1955)

Low-field magnetic resonance has been investigated for linearly and circularly polarized radio-frequency radiation for both the saturated and unsaturated case using modified Bloch equations for both. For the circularly polarized case, a quantum-mechanical solution is presented. Experimental verification for the linearly polarized case has been obtained.

INTRODUCTION

IN previous papers[1,2] we have investigated low-field magnetic resonance for linearly polarized radio-frequency radiation using power sufficiently weak not to cause saturation. We now consider what happens when the rf source is intense. To do this, we use modified Block equations,[3] allowing the relaxation to occur along and at right angles to the instantaneous external magnetic field. This method is applied to both the linearly and circularly polarized cases. In the latter case a quantum mechanical solution is also presented.

LINEARLY POLARIZED CASE

If the Bloch equations[4] are modified[3] so that longitudinal relaxation takes place along the field which is the resultant of the steady state field H_0 and the instantaneous radio-frequency field, and the lateral relaxation at right angles to it, we obtain the following equations of motion:

$$\dot{M}_x=\gamma M_y H_0-(M_x-\chi_0 H_1\cos\omega t)/\tau, \tag{1a}$$

$$\dot{M}_y=\gamma M_z H_1\cos\omega t-\gamma M_x H_0-M_y/\tau, \tag{1b}$$

$$\dot{M}_z=-\gamma M_y H_1\cos\omega t-(M_z-H_0\chi_0)/\tau, \tag{1c}$$

where γ is the gyromagnetic ratio, M_x, M_y, M_z the x, y, and z components of the magnetization, $H_1\cos\omega t$ the oscillating magnetic field in the x direction, τ the relaxation time, and ω the rf frequency. At low fields and for strong interactions, a single parameter τ characterizes both longitudinal and lateral relaxation times. We seek the steady-state solutions of Eqs. (1) under the assumption that $\bar{M}_z$ is time-independent, where $\bar{M}_z$ is the average value of M_z over one cycle of the rf field. Let

$$\begin{aligned} M_x&=A_1\cos\omega t+B_1\sin\omega t,\\ M_y&=A_2\cos\omega t+B_2\sin\omega t. \end{aligned} \tag{2}$$

From the above assumptions, substituting (2) in (1c) and averaging over one cycle, we get

$$0=-\tfrac{1}{2}\gamma H_1 A_2-(\bar{M}_z-H_0\chi_0)/\tau.$$

Therefore,

$$\bar{M}_z=H_0\chi_0-\tfrac{1}{2}\gamma H_1\tau A_2. \tag{3}$$

Substituting (2) and (3) back into (1), we obtain

$$\begin{aligned} -\omega A_1+B_1/\tau-\omega_0 B_2&=0,\\ A_1/\tau-\omega_0 A_2+\omega B_1&=\chi_0 H_1/\tau,\\ -\omega A_2+\omega_0 B_1+B_2/\tau&=0,\\ \omega_0 A_1+(\tfrac{1}{2}\gamma^2 H_1^2\tau^2+1/\tau)A_2+\omega B_2&=\gamma H_1 H_0\chi_0, \end{aligned} \tag{4}$$

where $\omega_0=\gamma H_0$.

The absorption χ'' corresponds to the out-of-phase component B_1 of M_x in (2). From Eq. (4), therefore,

$$\chi''=\frac{B_1}{H_1}=\chi_0\omega\tau\left((1+\omega^2\tau^2+\omega_0^2\tau^2)-\frac{4\omega_0^2\omega^2\tau^4}{(1+\omega^2\tau^2+\omega_0^2\tau^2)+\tfrac{1}{2}\gamma^2H_1^2\tau^2}\right)^{-1}. \tag{5a}$$

Figure 1 is a plot of χ'' against $\omega_0\tau$ for varying values of the saturation term $\frac{1}{2}\gamma^2H_1^2\tau^2$. For small values of this parameter compared to $1+\omega^2\tau^2+\omega_0^2\tau^2$ (no saturation), χ'' reduces to the well-known formula previously derived[1]:

$$\chi''=\tfrac{1}{2}\chi_0\omega\tau\left(\frac{1}{1+(\omega_0-\omega)^2\tau^2}+\frac{1}{1+(\omega_0+\omega)^2\tau^2}\right). \tag{6}$$

This appears in Fig. 1 as the upper curve marked unsaturated. As the rf power increases, we obtain the successive lower curves indicated, until at a point of total saturation (very large H_1) χ'' approaches the limiting curve,

$$\chi''=\chi_0\omega\tau/(1+\omega^2\tau^2+\omega_0^2\tau^2), \tag{5b}$$

indicated as 100 percent saturated in the figure. It is of interest to note that all of the curves terminate at

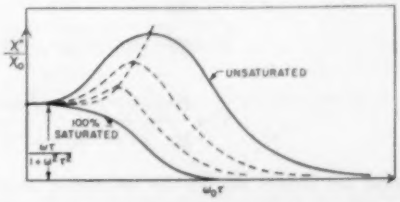

FIG. 1. Absorption in a coil oriented along the z axis for varying rf intensities.

[1] M. A. Garstens, Phys. Rev. **93**, 1228 (1954).
[2] Garstens, Singer, and Ryan, Phys. Rev. **96**, 53 (1954).
[3] Codrington, Olds, and Torrey, Phys. Rev. **95**, 607 (1954).
[4] F. Bloch, Phys. Rev. **20**, 460 (1946).

the same Debye value,

$$\chi''=\chi_0\omega\tau/(1+\omega^2\tau^2),$$

when $\omega_0=0$ and have the same zero slope at this point.

The maximum absorption points shift successively to the left with increasing saturation, approaching zero in the limit with 100 percent saturation.

The corresponding dispersion formula is given by

$$\chi'=\frac{A_1}{H_1}=\chi_0\times\left\{\frac{1+\dfrac{(\frac{1}{2}\gamma^2H_1^2\tau^2+1+\omega_0^2\tau^2-\omega^2\tau^2)\omega_0^2\tau^2}{\frac{1}{2}\gamma^2H_1^2\tau^2+(1+\omega^2\tau^2+\omega_0^2\tau^2)}}{(1+\omega^2\tau^2+\omega_0^2\tau^2)-\dfrac{4\omega_0^2\omega^2\tau^4}{\frac{1}{2}\gamma^2H_1^2\tau^2+(1+\omega^2\tau^2+\omega_0^2\tau^2)}}\right\}. \quad (7a)$$

For low rf levels ($\frac{1}{2}\gamma^2H_1^2\tau^2\ll 1+\omega^2\tau^2+\omega_0^2\tau^2$), this reduces to

$$\chi'=\chi_0\left\{\frac{1+\dfrac{(1+\omega_0^2\tau^2-\omega^2\tau^2)\omega_0^2\tau^2}{(1+\omega^2\tau^2+\omega_0^2\tau^2)}}{(1+\omega^2\tau^2+\omega_0^2\tau^2)-\dfrac{4\omega_0^2\omega^2\tau^4}{(1+\omega^2\tau^2+\omega_0^2\tau^2)}}\right\}. \quad (7b)$$

At zero field, these reduce to the Debye dispersion formula:

$$\chi'=\chi_0/(1+\omega^2\tau^2).$$

Figure 2 is a plot of Eq. (7) for varying degrees of saturation and for several values of $\omega\tau$. For large saturation values, Eq. (7) reduces to

$$\chi'=\chi_0\left(\frac{1+\omega_0^2\tau^2}{1+\omega^2\tau^2+\omega_0^2\tau^2}\right). \quad (8)$$

For each of $\omega\tau=0$, 1, and 20, the figure first shows the unsaturated curve Eq. (7b), a partially saturated curve indicated by the first arrow, and fully saturated curve Eq. (8) indicated by the second arrow.

We have been able to verify Eq. (7) for the unsaturated case by fitting curves of the type indicated in Fig. 2 to experimental data obtained at this Laboratory by Waddel.[5] These were dispersion measurements taken at 16.9 Mc/sec at low rf levels on diphenylpicryl hydrazyl and tris-p-nitro phenyl methyl. The theoretical unsaturated curves for both cases fitted experimental dispersion curves over their entire range within experimental error. For the hydrazyl an $\omega\tau$ of 5.9 was found to fit the data while for the methyl radical $\omega\tau$ was equal to 19.2, yielding a τ of 0.06×10^{-6} for the former and 0.18×10^{-6} for the latter.

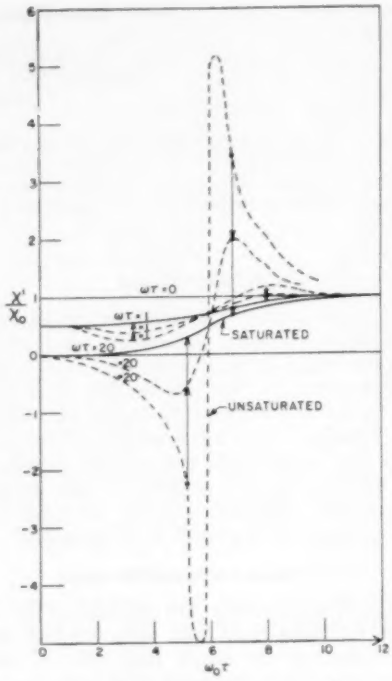

FIG. 2. Dispersion in a coil oriented along the x axis for varying rf intensities and values of $\omega\tau$.

In an attempt to obtain direct confirmation of low-field saturation effects at high rf levels an experiment was carried out using a Bloch type of apparatus with enough power to partially saturate diphenyl hydrazyl.

To obtain the χ'' and χ' values in this case, the M_y components of magnetization must be computed. Thus

$$\chi''=\frac{A_2}{H_1}=\frac{2\omega_0\omega^2\tau^3\chi_0}{[1+\tau^2(\omega_0-\omega)^2][1+\tau^2(\omega_0+\omega)^2]+\frac{1}{2}\gamma^2H_1^2\tau^2(1+\omega^2\tau^2+\omega_0^2\tau^2)}, \quad (9)$$

$$\chi'=\frac{B_2}{H_1}=\frac{2\omega_0\omega\tau^2\chi_0(\omega^2\tau^2-\omega_0^2\tau^2-1-\gamma^2H_1^2\tau^2)}{[1+\tau^2(\omega_0-\omega)^2][1+\tau^2(\omega_0+\omega)^2]+\frac{1}{2}\gamma^2H_1^2\tau^2(1+\omega^2\tau^2+\omega_0^2\tau^2)}. \quad (10)$$

These are shown plotted for increasing saturation in Figs. 3 and 4. Figure 5 shows some observed curves for χ' and χ'' at increasing saturation values using a detection coil at right angles to the rf coil.

[5] R. C. Waddel (private communication). Further publication on this is to appear.

$\bar{M}_z$ can be obtained from Eq. (3). Thus

$$\bar{M}_z=\chi_0\left\{H_0-\frac{\gamma^2\omega^2H_1^2\omega_0\tau^4}{[1+(\omega_0-\omega)^2\tau^2][1+(\omega_0+\omega)^2\tau^2]+\frac{1}{2}\gamma^2H_1^2\tau^2(1+\omega^2\tau^2+\omega_0^2\tau^2)}\right\}. \tag{11}$$

Of interest is the fact that $\bar{M}_z$ can have negative values for certain values of magnetic field, frequency and relaxation time.

CIRCULARLY POLARIZED CASE

The circularly polarized case has been solved by two methods, one in a manner similar to the previous case, the other, quantum mechanically.

(a) Classical Solution

If the equations of motion are modified to describe a circularly polarized rf, we obtain

$$\dot{M}_x=\gamma[M_yH_0+M_zH_1\sin\omega t]-(M_x-\chi_0H_1\cos\omega t)/\tau,$$
$$\dot{M}_y=\gamma[M_zH_1\cos\omega t-M_xH_0]-(M_y+\chi_0H_1\sin\omega t)/\tau,$$
$$\dot{M}_z=\gamma[-M_xH_1\sin\omega t-M_yH_1\cos\omega t]-(M_z-\chi_0H_0)/\tau.$$

The average value of M_z for the steady-state solution now becomes $\bar{M}_z=H_0\chi_0-\frac{1}{2}\gamma\tau H_1(B_1+A_2)$, and

$$\chi''=\frac{B_1}{H_1}=\frac{\chi_0\omega\tau}{1+(\omega_0-\omega)^2\tau^2+\gamma^2H_1^2\tau^2},$$

$$\chi'=\frac{A_1}{H_1}=\chi_0\frac{1+\omega(\omega_0-\omega)\tau^2+\gamma^2H_1^2\tau^2}{1+(\omega_0-\omega)^2\tau^2+\gamma^2H_1^2\tau^2};$$

also

$$\bar{M}_z=\chi_0\left(H_0-\frac{\gamma H_1^2\omega\tau^2}{1+(\omega_0-\omega)^2\tau^2+\gamma^2H_1^2\tau^2}\right).$$

As in the linearly polarized case, we note that $\bar{M}_z$ can take on negative values at low fields.

(b) Quantum-Mechanical Solution

In this method the spin resonance equations for the circularly polarized case are solved under the following assumptions:

(a) The system can be described by one relaxation time τ.

(b) That immediately after a collision the spin will achieve equilibrium with the resultant magnetic field at the time of the collision.

(c) That the rf field is monochromatic and of a constant value over the sample (i.e., no skin effects).

The solution of the time dependent Schrödinger equation for a spin $\frac{1}{2}$ particle acted on by a magnetic field **H** whose components are $H_1\cos\omega t$, $-H_1\sin\omega t$, and H_0, has been solved by Archibald[6] in a simple form. He finds that the ratio of the components of the spin wave function $\binom{a_+}{a_-}$ is given as

$$a_+/a_-=fe^{i\omega t}, \tag{12}$$

where

$$f=-(1/\omega_1)\{\alpha-i\Delta\tan[(t-t_0)\Delta/2+b]\},$$

$\alpha=\omega-\omega_0$, $\omega_1=\gamma H_1$, $\Delta^2=\alpha^2+\omega_1^2$, and b is an integration constant. By using this solution of the wave function, the expectation value of the three Pauli spin vectors is found to be

$$\langle\sigma_z\rangle=\frac{e^{-i\omega t}f^*+e^{i\omega t}f}{1+ff^*},$$

$$\langle\sigma_y\rangle=i\frac{[-e^{-i\omega t}f^*+e^{i\omega t}f]}{1+ff^*}, \tag{13}$$

$$\langle\sigma_x\rangle=\frac{f^*f-1}{1+ff^*}.$$

The value for the integration constant b is chosen so that just after a collision at time t_0 the components of the spin vector will be equal to the direction of the magnetic field at the time t_0. Thus we find that

$$\langle\sigma_x\rangle_{t=t_0}=H_1\cos\omega t_0/(H_1^2+H_0^2)^{\frac{1}{2}}, \tag{14a}$$

$$\langle\sigma_y\rangle_{t=t_0}=-H_1\sin\omega t_0/(H_1^2+H_0^2)^{\frac{1}{2}}, \tag{14b}$$

$$\langle\sigma_z\rangle_{t=t_0}=H_0/(H_1^2+H_0^2)^{\frac{1}{2}}=z. \tag{14c}$$

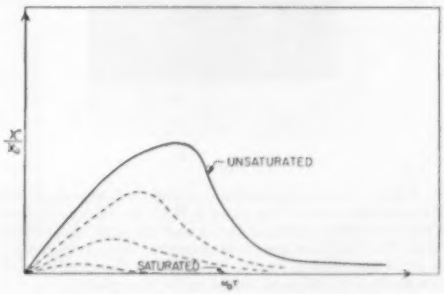

FIG. 3. Absorption in a coil oriented along the y axis for varying rf intensities.

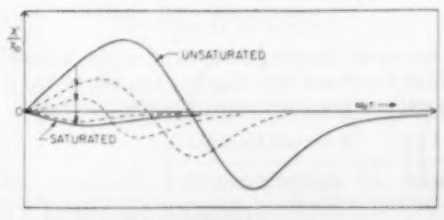

FIG. 4. Dispersion in a coil oriented along the y axis for varying rf intensities.

[6] J. Archibald, Am. J. Phys. **20**, 368 (1952).

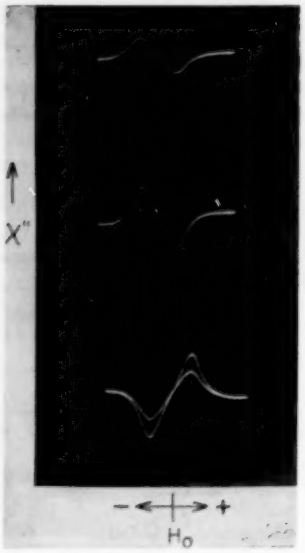

(a)

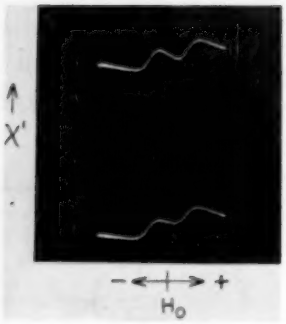

(b)

FIG. 5(a,b). Observed absorption and dispersion curves. These are to be compared with Figs. 3 and 4. With increasing rf intensity the absorption curves become flatter and the peak shifts towards zero field. The field H_0 is zero at the center of the curves increasing to the right and diminishing to the left. The third curve of 5(a) shows a saturated and unsaturated curve superposed.

It is seen from Eqs. (14)(a) and (b) that f must be real and from Eq. (14c) that

$$f=[(1+s)/(1-s)]^{\frac{1}{2}}=\delta. \tag{15}$$

We next write the integration constant b as a complex number $A+iB$ and then expand f as given in Eq. (12) into real and imaginary parts. The result is that

$$f=\frac{1}{\omega_1}\left[\left\{-\alpha-\frac{\Delta\tanh B(1+\tan^2 A)}{1+\tan^2 A\tanh^2 B}\right\}+i\left\{\frac{\Delta\tan A(1-\tanh^2 B)}{1+\tan^2 A\tanh^2 B}\right\}\right]. \tag{16}$$

The requirement that f must be real is satisfied by setting $\tan A=\infty$; then the real part becomes

$$f=(1/\omega_1)[-\alpha-\Delta\coth B]. \tag{17}$$

From Eqs. (15) and (17), the value of B is found to be

$$\coth B=-(1/\Delta)[\omega_1\delta+\alpha]. \tag{18}$$

All that remains to be done is to average $\langle\boldsymbol{\sigma}\rangle$ over all collision times t_0 by the prescription

$$\langle\langle\boldsymbol{\sigma}(t)\rangle\rangle=\int_{-\infty}^{t}\frac{e^{-(t-t_0)/\tau}}{\tau}\langle\boldsymbol{\sigma}(t-t_0)\rangle dt_0, \tag{19}$$

which is just the sum of contributions from all collision times t_0 weighted by an exponential law of decay. The final result for the x component is that

$$\langle\langle\sigma_x\rangle\rangle=-\frac{2\omega_1}{\varphi}\left\{\cos\omega t\left[\alpha\left(\frac{\frac{1}{2}\tau^2\Delta^2}{1+\Delta^2\tau^2}+\sinh^2 B\right)+\Delta(\sinh B\cosh B)\right]-\sin\omega t\left(\frac{\Delta}{2}\frac{\tau\Delta}{1+\tau^2\Delta^2}\right)\right\}, \tag{20}$$

where

$$\varphi=\Delta^2(2\sinh^2 B+1)+2\alpha\Delta(\sinh B\cosh B). \tag{21}$$

Substituting for $\cosh B$ and $\sinh B$ from Eq. (18) and recalling that the difference between the number of spin up and spin down states was assumed to be proportional to

$$\chi_0(H_1^2+H_0^2)^{\frac{1}{2}},$$

according to assumption (b), we have for the x component of magnetization

$$M_x=-\chi_0 H_1\omega\left[\cos\omega t\left(\frac{\alpha\tau^2}{1+\tau^2\Delta^2}-\frac{1}{\omega}\right)-\sin\omega t\left(\frac{\tau}{1+\tau^2\Delta^2}\right)\right]. \tag{22}$$

Identifying the in-phase component as the dispersion and the out-of-phase component as the absorption, we have that

$$\chi'=-\chi_0\left(\frac{\omega\alpha\tau^2}{1+\tau^2\Delta^2}-1\right), \tag{23}$$

and

$$\chi''=\chi_0\left(\frac{\omega\tau}{1+\Delta^2\tau^2}\right), \tag{24}$$

which are identical with the expressions obtained in the previous section. Equation (24) is identical with Bloch's[7] equation for absorption except that his ω_0 in the numerator is replaced by ω. This, of course, is a small effect except where ω varies appreciably in going through resonance. The dispersion on the other hand has an

[7] F. Bloch, Phys. Rev. **70**, 460 (1946).

added constant value χ_0 over the value derived by Bloch. Thus in the case of complete saturation the dispersion will have a constant finite value other than zero.

Further experimental work is planned to verify Eq. (5b) under conditions of complete saturation.

We are indebted to Dr. R. K. Wangness of the Naval Ordnance Laboratory for allowing us to see his manuscript on magnetic resonance for arbitrary field strength prior to publication. In this paper, the circularly polarized case has been worked out by a quantum-mechanical method different from that used here.

PHYSICAL REVIEW VOLUME 99, NUMBER 2 JULY 15, 1955

Multiple Resonances in Cobalt Ferrite*

P. E. TANNENWALD
Lincoln Laboratory, Massachusetts Institute of Technology, Lexington, Massachusetts
(Received April 1, 1955)

Double microwave resonances have been observed in cobalt ferrite when a magnetic field was applied in crystal directions near the hard axis. One resonance occurs before the magnetization vector is lined up with the external magnetic field and another occurs in the aligned state. The experimental results exhibit characteristic features expected before complete line-up and yield, at 90°C, $K_1/M=2200\pm200$ and $g=2.7\pm0.3$.

IN the past, microwave resonance experiments on ferromagnetic single crystals have been carried out on the assumption that the material was magnetized to saturation and the magnetization vector was fully aligned with the applied magnetic field. This is probably justified when the anisotropy field is of the order of 10 percent of the effective field necessary for resonance. Some materials, like cobalt ferrite, exhibit an anisotropy so large that at ordinary microwave frequencies the internal field puts the crystal already above resonance, according to the relation $\omega=\gamma H_{\text{eff}}$. However, as will be described now, the resonance frequency can be lowered by applying an external magnetic field in the hard direction of the crystal,[1] and furthermore, one resonance can be expected in the nonaligned state of the magnetization vector M and another in the aligned state.

Zeiger has given a general solution of the equation of motion[2] which includes the effects of anisotropy in terms of energy rather than effective demagnetizing factors. This has the advantage that it yields resonance conditions even when M is not lined up with the applied field. The results are shown for a cubic crystal on the assumption of single-domain structure, in Figs. 1 and 2, and clearly indicate the possibility of two resonances as a function of applied field H_0 in certain crystal directions.

Figure 3 shows the results of absorption measurements on a cobalt ferrite single crystal at 90°C as a function of magnetic field applied in various crystal directions Ψ in the (110) plane. The operating frequency (23 800 Mc/sec) is evidently above the "critical frequency" $\omega_c=2\gamma K_1/M$, because resonance was achieved in the easy axis ($\Psi=0°$) by application of an external field. A plot of the position of the high field peaks as a function of crystal orientation is shown in Fig. 4. This anisotropy curve, although similar, differs from that obtained in the usual effective demagnetizing theory.[3] As can be seen from Fig. 1, near the easy axis

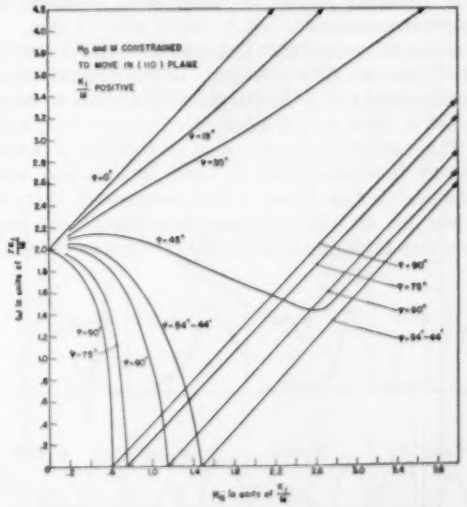

FIG. 1. Resonance condition in (110) plane. The microwave frequency ω is expressed in units of $\gamma K_1/M$ and external magnetic field H_0 is expressed in units of K_1/M.

* The research reported in this document was supported jointly by the Army, the Navy, and the Air Force under contract with the Massachusetts Institute of Technology.

[1] This idea is similar to that used by H. Suhl, Phys. Rev. **97**, 555 (1955) in achieving very-low-resonance frequencies in materials with low anisotropy.

[2] H. J. Zeiger, Lincoln Laboratory (unpublished notes). A similar solution was first given by J. Smit, Conference on Ferrimagnetism, October 11, 1954 (unpublished). See, also, reference 1.

[3] C. Kittel, Phys. Rev. **73**, 155 (1948).

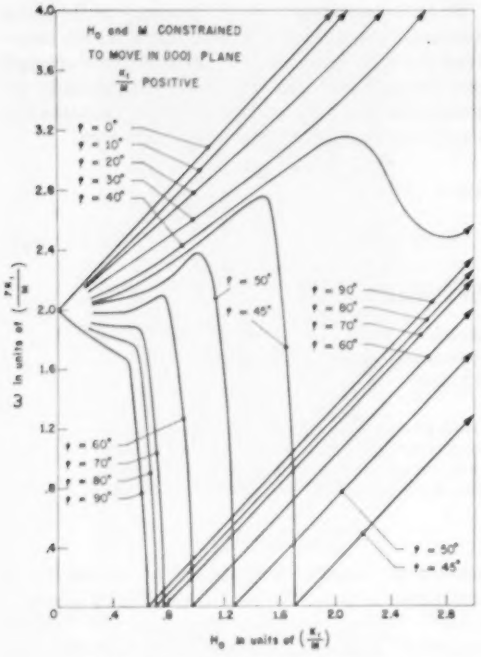

FIG. 2. Resonance condition in (100) plane.

above ω_c, the resonance condition is modified by lack of complete alignment of M with H_0. But even the present theory does not give satisfactory agreement yet with the experimental data. One probable reason is that allowance should be made for a second-order anisotropy constant.

If one attempts a best fit to the theory as it stands, at 90°C $K_1/M = 2200 \pm 200$, $g = 2.7 \pm 0.3$. The anisotropy has decreased to $K_1/M \cong 200$ at 200°C, and has vanished at 280°C. Here $g = 2.27 \pm 0.05$.

The question of why two peaks are observed in certain crystal directions above ω_c must be answered with reference to Figs. 1 and 2. If it seems most likely to expect the M vector to come from the nearest easy axis, then for Ψ's up to 55° in the (110) plane, the (110) curves apply; for $\Psi = 90°$ in the (110) plane, the 45° curve of the (100) curves applies; and for angles between $\Psi = 55°$ and 90°, other calculations would have to be carried out. Since in the experiment the operating frequency was above ω_c, the origin of the double peaks up to $\Psi = 55°$ is not clear. However, at $\Psi = 90°$, it can be seen from the (100) curves (here $\Psi = 45°$) that double resonances are possible.

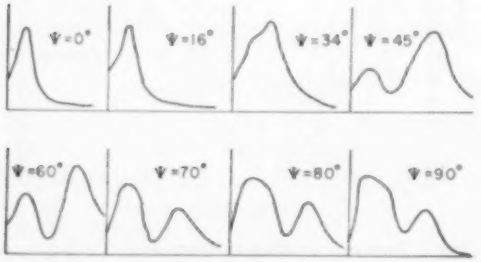

FIG. 3. Absorption *versus* magnetic field in cobalt ferrite at 90°C and 23 800 Mc/sec, with H_0 applied in (110) plane. Range of H_0 is to approximately 11 000 oersteds.

Optimum results have been achieved at 90°C because below ω_c the broad resonance lines lead to continuous absorption from $H_0 = 0$ to $H_0 \cong 11\,000$ oersteds. Consideration must also be given the possibility that the material is not a single domain and hence M can be turned towards H_0 from a variety of crystal directions; and that the dynamic demagnetizing fields from domain walls[4] shift and broaden the nonaligned resonances. Finally, it should be pointed out that the mechanism described in this note may be responsible for the double peaks observed at very low temperatures in other ferrites. In fact, multiple resonances should occur whenever the anisotropy field becomes comparable to the effective field necessary for resonance in spherical samples.[5]

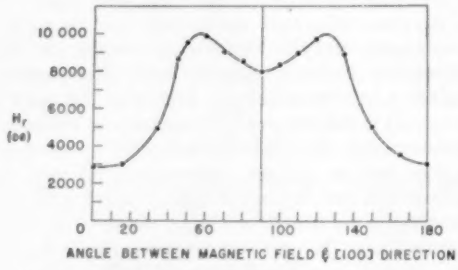

FIG. 4. Cobalt ferrite anisotropy curve in (110) plane, at 90°C and 23 800 Mc/sec.

The author is grateful to Benjamin Lax for suggesting this investigation and for his helpful criticism and constant encouragement; to H. J. Zeiger for valuable discussions and suggestions; to Mrs. M. Campbell for carrying out the theoretical computations; to D. Wickham of the Laboratory for Insulation Research for growing and furnishing the sample; and to E. P. Warekois for performing the x-ray orientation.

Note added in proof.—J. O. Artman of Lincoln Laboratory is making more refined calculations which will correct errors appearing in Figs. 1 and 2 due to oversimplification of the situation. The lowest energy position of M may actually be out of the principal crystal planes. Consequently, the curves between 55° and 90° in Fig. 1 and between 45° and 90° in Fig. 2 need revision.

[4] D. Polder and J. Smit, Revs. Modern Phys. **25**, 89 (1953); T. Nagamiya, Prog. Theor. Phys. Japan **10**, 72 (1953).

[5] A. F. Kip and R. D. Arnold [Phys. Rev. **75**, 1556 (1949)] observed double peaks in a sheet of iron single crystal when the applied magnetic field was of the order of the anisotropy field.

Optical Properties of Indium-Doped Silicon

R. NEWMAN
General Electric Research Laboratory, Schenectady, New York
(Received February 21, 1955; revised manuscript received March 31, 1955)

Absorption and photoconduction have been studied in indium-doped silicon at low temperatures. The optical properties indicate a level at about that obtained from thermal-resistivity measurements, i.e., 0.16 ev. Sharp absorption lines are observed at 20°K which broaden and essentially disappear by 77°K.

INTRODUCTION

THE ionization energies of Groups III and V elements, as impurities in silicon, were recently obtained by Morin *et al.*[1] from resistivity measurements. The ionization energies were all approximately 0.05 ev with the exception of that of indium, which was measured as 0.16 ev.

The case of indium, with its large ionization energy, was of especial interest because it afforded an opportunity to study impurity optical phenomena over a convenient range of temperature (e.g., $T \leqslant 77°K$) with the important condition satisfied that the carrier population in the impurity centers remained essentially constant over this range. In addition a possibility existed of preparing a material which would be a useful infrared detector out to 7 or 8μ and which could be operated at the readily accessible temperature of liquid air.

The work reported here paralled that of another group.[2] Where the results of the two efforts overlap they are essentially identical. The present paper may in part, therefore, be considered as corroboration of the work of Burstein's group.

EXPERIMENTAL

Six single crystals of indium-doped silicon were prepared by conventional doping and crystal-pulling techniques. The original starting material was zone-melted DuPont silicon of approximately 40 ohm cm, *p*-type. It was, therefore, necessary to compensate the starting material with *n*-type impurity and back dope with indium to get a crystal with the desired property, i.e., all uncompensated acceptors derived from the indium. In practice the starting material was doped with enough Sb-Si alloy so that the initial portions of the pulled crystal prior to indium doping were 1 to 10 ohm cm *n*-type. Indium was added in different runs to give initial concentrations in the melt which ranged from 0.01 percent to 1 percent by weight. In all cases, because of the segregation, the minimum room temperature resistivity that could be obtained was 1 ohm cm, which corresponded to 5×10^{16} carriers/cm^3. In all the ingots grown, polycrystalline growth would develop at a concentration of about 2 percent indium by weight in the melt.

Samples were mounted in a cryostat equipped with NaCl windows. For photoconductive measurements the cryostat was at the exit port of a Perkin Elmer spectrometer. For absorption measurements the crystat was placed in the sample section of the spectrometer. CaF_2 and NaCl optics were employed. The photoconductive spectra were taken in 13-cps chopped light by using a constant-voltage-input circuit and the Perkin Elmer 13-cps amplifier system. Equivalent data were obtained in 450 cps chopped light by using a Baird phase-sensitive amplifier. Indium soldered contacts were used. The energy output of the globar source was monitored with a thermocouple.

RESULTS AND DISCUSSION

Figure 1 shows the absorption spectra of indium-doped silicon at 77°K and 21°K for a sample having 5×10^{16} holes/cm^3 at room temperature. Figure 2 shows a detail of these spectra in the region from about 0.14 to 0.16 ev with this sample at several temperatures in the 77°–20°K range. The region of lattice absorption is not shown in the latter figure.

Figure 3 shows a plot of the photoconductive spectrum at 77°K of a sample again having a room temperature carrier density of 5×10^{16}/cm^3. Figure 4 shows the same for a sample having a room temperature carrier density of $\sim1\times10^{16}$/cm^3.

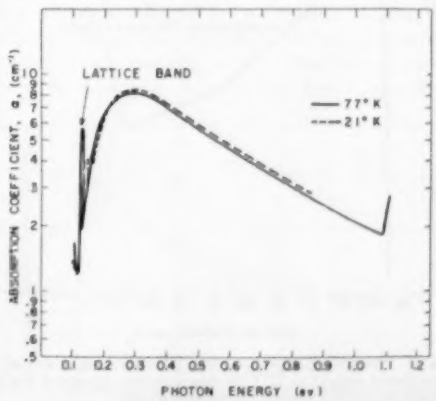

FIG. 1. Absorption spectrum of indium-doped silicon at 77°K and 21°K. Sample had 5×10^{16} holes/cm^3 at 300°K.

[1] Morin, Martin, Shulman, and Hannay, Phys. Rev. **96**, 833 (1954).
[2] Burstein, Picus, Henvis, Schulman, and Lax (to be published), quoted in Burstein *et al.*, Atlantic City Photoconductivity Conference, November, 1954 (unpublished).

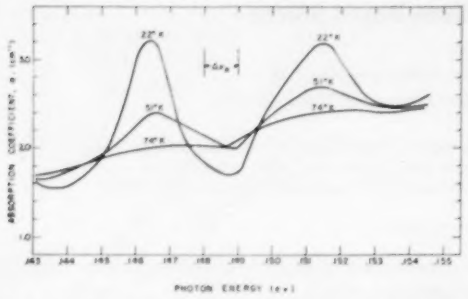

FIG. 2. A detail of the absorption spectrum of indium-doped silicon showing the effect of temperature on the absorption lines.

Conductivity-temperature measurements on one of our samples were made by W. W. Tyler. They showed a 0.16$_4$ ev ionization energy in agreement with Morin's results and indicated a room temperature mobility of 180 cm^2/volt sec and a mobility maximum at about 80°K.

The model employed to describe the optical properties of a hydrogen-like atom has been carried over to explain the optical properties of the so-called hydrogen-type impurities in semiconductors, notably silicon.[3] The model has met with success in predicting the existence of discrete excited impurity levels and in explaining the form of the continuous absorption corresponding to photoionization. Since the application of the model to the case of indium-doped silicon has already been described,[3] only brief comment will be made here.

Referring to Fig. 1, the continuous absorption extending toward higher energy from about 0.15 ev is identified with the photoionization of holes from the indium centers. The low-energy threshold of absorption at about 0.15 ev is in agreement with the ionization energy that has been determined by resistivity measurement (0.16 ev). The photoionization can also be studied through a measurement of the impurity photoconductivity. For a sample in which the product of absorption constant (α) and sample thickness (d)$\ll$1 (case 1), it would be expected that the photocurrent/incident quantum would be proportional to α. On the other hand, for the case where $\alpha d \gg 1$ (case 2), the sample should show a flat response in photocurrent/incident quantum over the range where this condition is satisfied. Under the conditions for which the data of Fig. 3 were obtained, $\alpha d > 1$ should be satisfied out to about 0.15 ev. Conversely, for the data of Fig. 4, the condition $\alpha d < 1$ should be satisfied over the entire impurity range.[4] Thus the photocurrent/incident quantum curve of Fig. 4 should be superposable with the absorption curve of

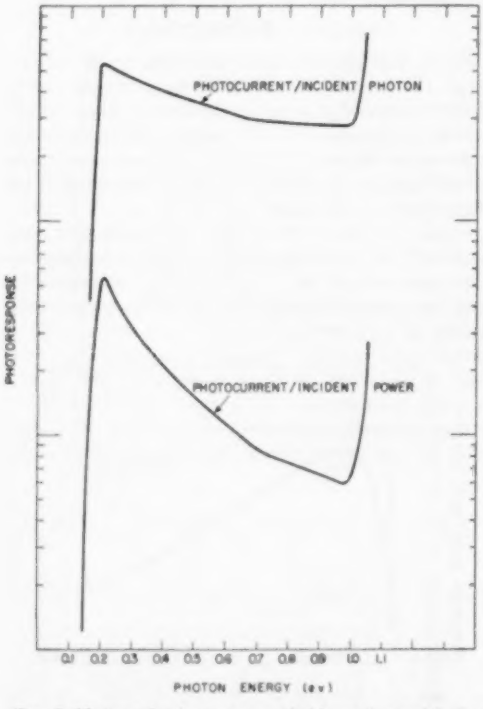

FIG. 3. Photoconductive spectrum (arbitrary log scale) of an indium-doped sample at 77°K having a carrier density of 5×10^{15} holes/cm^3 at 300°K. Sample thickness 0.65 cm.

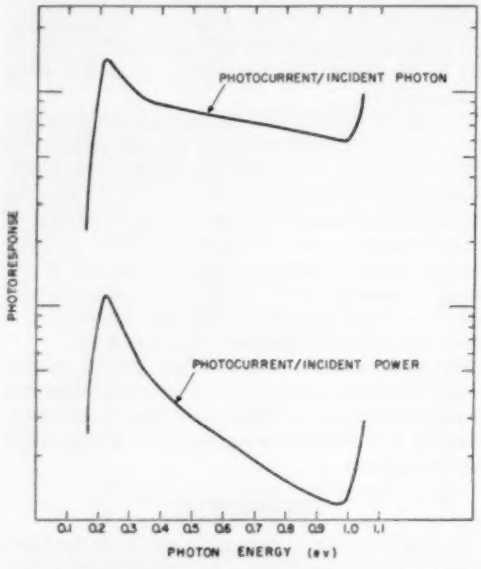

FIG. 4. Photoconductive spectrum (arbitrary log scale) of an indium-doped sample at 77°K having a carrier density of $\sim1\times10^{16}$ holes/cm^3 at 300°K. Sample thickness 0.30 cm.

[3] Burstein, Bell, Davisson, and Lax, J. Phys. Chem. **57**, 849 (1913).

[4] Absorption coefficient was not measured for this sample. It is assumed from the room temperature carrier density (1×10^{16}) that α would be $\frac{1}{3}$ of that shown in Fig. 1.

Fig. 1. This is only roughly so. The reason for the discrepancy between them is not understood.

As remarked previously, one of the predictions of the hydrogen-like model of impurities is the existence of discrete excited levels. Such levels may be evidenced by the existence of relatively sharp absorption lines in the spectra of doped materials at low temperatures. Two such lines are found in indium-doped silicon (see Figs. 1 and 2). We have located them at 0.147 ev and 0.152 ev. Burstein has identified these lines respectively, with the $1s \rightarrow 3p$ and $1s \rightarrow 4p$ transitions.[5]

An interesting feature of these lines is their temperature dependence as illustrated in Fig. 2. Unfortunately our measurement of this dependence was hindered by an inferior resolving power ($\Delta\nu_R \sim 10^{-3}$ ev). It is, however, obvious from the figure that at about 74°K the line width is greater than 10^{-3} ev (i.e., resolving power), at about 50°K it is comparable to 10^{-3} ev and at about 20°K it is less than or equal to 10^{-3} ev. This type of temperature dependence has been previously observed in boron-doped silicon.[3] It has been treated theoretically by Lax and Burstein.[5] They indicate that the line broadening is due to a broadening of the ground state of the impurity due to an interaction with lattice vibrations. The temperature range over which the line width transition is observed in the present case is essentially that predicted by their theory.

ACKNOWLEDGMENTS

I should like to express my appreciation to W. W. Tyler for resistivity and Hall measurements and to J. H. McTaggart for his assistance.

[5] M. Lax and E. Burstein, Phys. Rev. **91**, 208 (1953).

PHYSICAL REVIEW VOLUME 99, NUMBER 2 JULY 15, 1955

Electrical Conductivity and Seebeck Effect in $Ni_{0.80}Fe_{2.20}O_4$

F. J. Morin and T. H. Geballe
Bell Telephone Laboratories, Murray Hill, New Jersey

(Received March 25, 1955)

Electrical conductivity and Seebeck effect have been measured as functions of temperature on single-crystal samples of $Ni_{0.80}Fe_{2.20}O_4$. A thermal hysteresis has been observed in the conductivity but not in the Seebeck effect. This suggests that the hysteresis involves the charge carrier transfer process but not the production of carriers. The activation energy associated with the transfer process is estimated to be 0.10 ev in the high-temperature state and 0.06 ev in the low-temperature state.

1. INTRODUCTION

MAGNETIC losses in ferrites have been interpreted[1,2] as being due to an electron transfer of the type

$$Fe^{2+} + Fe^{3+} = Fe^{3+} + Fe^{2+},$$

with an activation energy required for the transfer process. It is generally believed that the process of electrical conduction in ferrites also involves such a transfer. We have therefore made measurements of electrical conductivity and Seebeck effect as functions of temperature in order to determine an independent value of the energy required for the electron transfer. This result is presented below. In the course of measurements, an unexpected thermal hysteresis was encountered for which we offer no explanation at the present time.

2. EXPERIMENT

The two crystals of nickel ferrite used were obtained from Linde Air Products Company. Chemical analysis indicated the composition to be $Ni_{0.80}Fe_{2.20}O_4$. The growth direction was within a few degrees of [111].

A rectangular bar 0.608 in. long (in the growth direction), 0.206 in. wide, and 0.0600 in. thick was cut from the crystal. Electrical contacts were fired on in air at about 660°C for 5 minutes using a silver paste. The contacts were arranged so that 4-point electrical conductivity, Hall effect, and Seebeck effect measurements could be made. The contacts were nonrectifying. The Hall voltage was found to be too small to detect. The Seebeck voltage per degree, or thermoelectric power proved to be a smoothly varying function of temperature. The results are shown in Fig. 1 and interpreted in

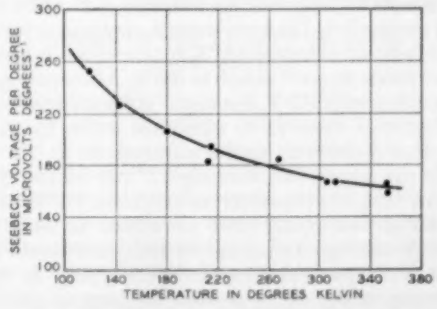

FIG. 1. Seebeck effect as a function of temperature.

[1] J. K. Galt, Bell System Tech. J. **33**, 1023 (1954).
[2] H. P. J. Wijn and H. van der Heide, Revs. Modern Phys. **25**, 99 (1953).

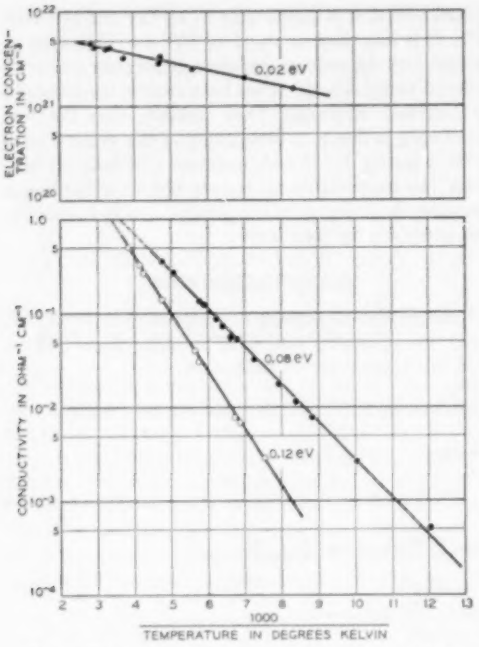

FIG. 2. Electron concentration and electrical conductivity as a function of reciprocal temperature.

the next section. The results of the electrical conductivity are shown in Fig. 2, where log conductivity is plotted against reciprocal absolute temperature. Between 130° and 210° the points fall on either of two straight lines. Below 130° the points fall on the upper line with the smaller negative slope. The points above 210° all fall on the lower line with the greater negative slope. Four times while cooling, the conductivity "jumped" from the lower curve to the upper curve; and four times while warming, the conductivity jumped from the upper curve to the lower curve. We were unable to effect a jump from one curve to the other by mechanical shock, magnetic field, or discharging a spark coil near the sample. However, there is some evidence that the magnetic field may have "conditioned" the sample to jump near the temperature at which the field was applied. The lower-curve to upper-curve jumps initially occurred around 120°K and the upper- to lower-curve jumps occurred as high as 200°K. After applying a magnetic field at 170°K, the upper- to lower-curve jump was actually observed to take place within the time constant (3 seconds) of the galvanometer at 176°K, while the sample was warming 0.3° per minute. The reverse jump was then observed to occur at 170°K while the sample was cooling 0.090° per minute. In the latter case, the cooling rate in a high vacuum was followed for over 90 minutes, with no observable change in rate occurring before, during or after the jump in conductivity. This indicates there is no latent heat associated with the jump and there is no sharp change in heat capacity near the jump.

A longitudinal section amounting to about one-third of the sample was cut off and new contacts fired on. The piezoresistance of this new sample was measured at room temperature using a stress of 5×10^7 dynes/cm^2. The effect was only that to be expected from dimensional change. The conductivity was measured several times over the critical temperature range and repeated the upper curve of Fig. 2, no jump was observed. A slice was cut from a second crystal and conductivity *vs* temperature was measured several times. The upper curve was repeated, no transition was found. Thus, the upper conductivity curve appears to be the one typical of these crystals.

3. ANALYSIS

The data of this experiment are interpreted in terms of a model[3] for conduction in a d-level semiconductor. Conductivity, as usual, is taken as the product of carrier concentration, carrier mobility, and electronic charge:

$$\sigma = n\mu e. \tag{1}$$

The relation between carrier concentration and Seebeck effect Q is assumed[4] to be

$$n = N\exp^{-Q/k}, \tag{2}$$

where N is the concentration of electronic levels involved in the conduction process. In this case, $N=2.8\times10^{22}$, the number of octahedral cation sites/cm^3 of ferrite. The thermoelectric effect, which depends on carrier concentration, did not undergo a transition. The results therefore, in terms of the model, suggest that the conductivity transition involves only the charge transfer process. Carrier concentration computed from measured Q and Eq. (2) is shown in Fig. 2. The slope of this plot is 0.02 ev, the energy required for the production of carriers. The two conductivity slopes are 0.12 and 0.08 ev. Thus the energy involved in the mobility (transfer) process is 0.10 ev in the high-temperature state and 0.06 ev in the low-temperature state.

Chemical analysis indicated the first crystal to be 52.60 percent Fe and 20.05 percent Ni by weight. Assuming a complete oxygen lattice and electrical neutrality, the composition of the crystal is calculated to be

$$Ni_{0.80}^{2+}Fe_{0.21}^{2+}Fe_{1.99}^{3+}O_4^{2-}$$

Ten percent of the iron, or $\sim3\times10^{21}$ atoms/cm^3, is Fe^{3+}. Since Fe^{3+} acts as a donor center with respect to Fe^{3+}, this result is in agreement with the carrier concentration determined from thermoelectric effect and thereby lends support to that calculation.

We wish to thank G. W. Hull for preparing the sample and his aid in making the measurements.

[3] F. J. Morin, Phys. Rev. **93**, 1195 (1954).

[4] However, the assumption about the Fermi level is doubtful here since the handling of the kT term is doubtful and QT is about the magnitude of kT.

Application of the Augmented Plane Wave Method to Copper*

D. J. HOWARTH†
Massachusetts Institute of Technology, Cambridge, Massachusetts
(Received March 31, 1955)

An application of the augmented plane wave method of solving the periodic potential problem has been made to metallic copper. The aim is to investigate the value of the method and to learn details of the energy band structure of copper. The method has been found to converge very rapidly; eigenvalues of three- or four-figure accuracy can be obtained for any point in k-space without involving the solution of very large secular determinants. Throughout, good results can be obtained by considering only a single augmented plane wave; these appear to be good one-electron wave functions by themselves, and the possible use of these as a starting point in a self-consistent calculation is discussed. The method proves suitable ground for the application of a high-speed computer, by which the present computation has been carried out.

The numerical results for copper are not in agreement with the results of a cellular calculation. Recalculation of certain states by the cellular method indicates that the dominant reason lies in the different potentials employed, the augmented plane wave method dealing with a potential constant in a region between the atoms. The sensitivity of the energy levels upon the exact crystal potential has become more apparent, though copper may be expected to show greater sensitivity than other materials. The present calculation of the width of the $3d$ band is 3.935 ev, compared with 3.46 ev by the cellular method and 2.7 ev by the tight-binding method. The appearance of a high density of states near the top of the $3d$ band is confirmed.

IN recent years, various methods have been used in attempts to make accurate solutions of the periodic potential problem. By limiting consideration to points in momentum space possessing high symmetry, the cellular method has proved capable of accurate results; calculations have been made on sodium,[1,2] lithium,[3] copper,[4] and lead sulfide,[5] using this method. The orthogonalized plane wave method originally proposed by Herring[6] can also be used with accuracy at certain points in momentum space, and studies have been made by this means of beryllium,[7] lithium,[8,9] and, more recently, of diamond[10] and germanium.[11–13]

An alternative approach to the periodic potential problem was suggested by Slater[14] and extended by Saffren and Slater[15]; the purpose of the present paper is to describe an application of this method and to estimate its value as a practical approach to the investigation of energy band structures. The method is obviously simple mathematically; its practical value depends upon the rate of convergence of an expansion of the wave function in terms of "augmented plane waves," and it is hence of immediate interest to apply the method to a particular substance. Metallic copper has been selected for two reasons. Firstly, the form and relative positions of the $4s$ and $3d$ bands are of interest, in particular since it is an indication of the band structure of the transition elements preceding copper in the periodic table. Secondly, a calculation by the cellular method has already been carried out for copper,[4] and confidence in such calculations would be greatly improved by obtaining equivalent results by the two approaches. Comparison can also be made with the calculations in the $3d$ band in nickel using the "tight-binding" approximation,[16,17] although this makes no claims to be an exact solution of the problem.

The conclusion arising from the present work is that the method provides an excellent approach to the solution of the periodic potential problem. Without undue numerical labor, it is possible to obtain eigenvalues of greater accuracy than those resulting from the cellular method as it is used at present. In addition, it is possible to extend the calculation to deal with points in momentum space possessing no symmetry properties. The numerical results for copper are not in agreement with the results of the cellular calculation; the difference is apparently due to the different crystal potential assumed in the two calculations. The present work is to be regarded as an analysis of the practical use of the augmented plane wave method rather than an evaluation of physically significant results for copper.

THEORY OF THE AUGMENTED PLANE WAVE METHOD

The mathematical details of the method used here have been given by Saffren and Slater,[15] subsequently referred to as I. Only a brief recapitulation of the necessary formulas will be given here.

We assume the crystal potential in which the electron moves to be spherically symmetrical inside a sphere, radius r_s, surrounding each atom and constant between these spheres. We shall here consider a material con-

* Work assisted by the Office of Naval Research.
† Now at Radar Research Establishment, Gt. Malvern, Worcestershire, England.
[1] F. C. von der Lage and H. A. Bethe, Phys. Rev. **71**, 612 (1947).
[2] D. J. Howarth and H. Jones, Proc. Phys. Soc. (London) **A65**, 355 (1953).
[3] B. Schiff, Proc. Phys. Soc. (London) **A67**, 2 (1954).
[4] D. J. Howarth, Proc. Roy. Soc. (London) **A220**, 513 (1953).
[5] Bell, Hum, Pincherle, Sciama, and Woodward, Proc. Roy. Soc. (London) **A217**, 71 (1953).
[6] C. Herring, Phys. Rev. **57**, 1169 (1940).
[7] C. Herring and A. G. Hill, Phys. Rev. **58**, 132 (1940).
[8] C. Herring, Phys. Rev. **55**, 598 (1939).
[9] R. H. Parmenter, Phys. Rev. **86**, 552 (1952).
[10] F. Herman, Phys. Rev. **88**, 1210 (1952).
[11] F. Herman and J. Callaway, Phys. Rev. **89**, 518 (1953).
[12] F. Herman, Phys. Rev. **93**, 1214 (1954).
[13] F. Herman, Phys. Rev. **95**, 847 (1954).
[14] J. C. Slater, Phys. Rev. **92**, 603 (1953).
[15] M. M. Saffren and J. C. Slater, Phys. Rev. **92**, 1126 (1953).
[16] G. C. Fletcher and E. P. Wohlfarth, Phil. Mag. **42**, 106 (1951).
[17] G. C. Fletcher, Proc. Phys. Soc. (London) **A65**, 192 (1952).

taining only one atom per unit cell. Inside the sphere, the wave function is expanded in a series of spherical harmonics of angle, and radial wave functions of r, $u_l(r)$, satisfying the equation

$$\frac{d^2(ru_l)}{dr^2}=\left(\frac{l(l+1)}{r^2}+V(r)-E\right)ru_l, \tag{1}$$

$V(r)$ being the potential inside the sphere.

Outside the sphere, we assume the solution to be a single plane wave of propagation constant $\mathbf{k}$; if we choose the constant potential to be zero in this region, the energy of this wave is $|\mathbf{k}|^2$. By suitable choice of constants in the expansion inside the sphere, the two functions can be made equal at the boundary of the sphere. The wave function so obtained may be written in unnormalized form [see I, Eq. (2)] as

$$\psi=\epsilon_1\exp(i\mathbf{k}\cdot\mathbf{r})+\epsilon_2\cdot 4\pi\sum_l(2l+1)j_l(|\mathbf{k}|r_s)\times i^lP_l(\cos\theta)u_l(E,r)/u_l(E,r_s). \tag{2}$$

$j_l(|\mathbf{k}|r_s)$ are spherical Bessel functions, θ is measured relative to the direction of $\mathbf{k}$ as polar axis, and ϵ_1, ϵ_2 are defined as

$$\epsilon_1=1,\quad \epsilon_2=0,\quad \text{when}\quad r>r_s;$$
$$\epsilon_1=0,\quad \epsilon_2=1,\quad \text{when}\quad r<r_s.$$

The function (2) we call an augmented plane wave. It will, in general, possess a discontinuity in first derivative at the boundary of the sphere; to obtain the "best" single function of the type (2) possible, the parameter E is chosen to make the expectation value of the energy of (2) a minimum. The result of this process, which can be carried through analytically, is to set the expectation value of the energy equal to the parameter E. The spurious contribution arising from the plane wave outside the sphere is exactly cancelled by the contribution to the kinetic energy integral of the discontinuity in first derivative over the surface of the sphere. The resulting equation for E [see I, Eq. (5)] is

$$\Omega(E-|\mathbf{k}|^2)-4\pi r_s^2\sum_l(2l+1)j_l^2(|\mathbf{k}|r_s)\times[d\ln u_l(E,r)/dr]_{r=r_s}=0. \tag{3}$$

Ω is the volume of the unit cell lying outside the sphere.

The dependence of E upon $|\mathbf{k}|^2$ implicit in (3) has been discussed previously from theoretical considerations;[13] a typical example is shown in Fig. 1. By solving (3), we have determined an augmented plane wave for a given $\mathbf{k}$. Such functions are used as initial functions in a variational procedure. As pointed out by Slater,[14] we can use functions with the same propagation vector $\mathbf{k}$ but corresponding to different energies E; we can also use functions with $\mathbf{k}$ ranging through a number of Brillouin zones, arising from the same reduced wave vector, corresponding to energies E which join smoothly to each other as $\mathbf{k}$ is varied. The overlap integrals and matrix components of energy between the various augmented plane waves are easily determined. We find three contributions to the energy matrix elements, arising from the regions inside and outside the sphere, and from the discontinuity in first derivative over the surface of the sphere. The calculation of these matrix elements follows the treatment of reference 14. For completeness, we give here the resulting formulas for matrix elements between two augmented plane waves $\psi_1(E_1,\mathbf{k}_1)$ and $\psi_2(E_2,\mathbf{k}_2)$. If we denote the Hamiltonian operator H and the unit operator I by the symbol 0, we find that

$$[\psi_1,0,\psi_2]=J(\psi_1,0,\psi_2)+4\pi\sum_l(2l+1)j_l(|\mathbf{k}_1|r_s)\times j_l(|\mathbf{k}_2|r_s)P_l(\mathbf{k}_1\cdot\mathbf{k}_2/|\mathbf{k}_1||\mathbf{k}_2|)K_l(\psi_1 0,\psi_2), \tag{4}$$

where

$$J(\psi_1,I,\psi_2)=-4\pi r_s^2j_1(|\mathbf{k}_1-\mathbf{k}_2|r_s)/|\mathbf{k}_1-\mathbf{k}_2|,\quad(\mathbf{k}_1\neq\mathbf{k}_2) \tag{5}$$
$$=\Omega,\quad(\mathbf{k}_1=\mathbf{k}_2) \tag{6}$$
$$J(\psi_1,H,\psi_2)=\mathbf{k}_1\cdot\mathbf{k}_2J(\psi_1,I,\psi_2), \tag{7}$$
$$K_l(\psi_1,I,\psi_2)=r_s^2[d\ln u_l(E_2,r)/dr-d\ln u_l(E_1,r)/dr]\times[E_1-E_2]^{-1},\quad(E_1\neq E_2) \tag{8}$$
$$=\left[\int_0^{r_s}u_l^2(E_1,r)r^2dr\right]u_l^{-2}(E_1,r_s),\quad(E_1=E_2) \tag{9}$$
$$K_l(\psi_1,H,\psi_2)=r_s^2[E_1d\ln u_l(E_1,r)/dr-E_2d\ln u_l(E_1,r)/dr][E_1-E_2]^{-1},\quad(E_1\neq E_2) \tag{10}$$
$$=E_1K_l(\psi_1,I,\psi_2)+r_s^2[d\ln u_l(E_1,r)/dr]_{r=r_s},\quad(E_1=E_2). \tag{11}$$

The functions ψ_1, ψ_2 are unnormalized. The normalization constant $n(E,\mathbf{k})$ is easily seen from (6) and (9) to be given by

$$n^2=\Omega+4\pi\sum_l(2l+1)j_l^2(|\mathbf{k}|r_s)\times\left[\int_0^{r_s}u_l^2(E,r)r^2dr\right][u_l^{-2}(E,r_s)]. \tag{12}$$

With the exception of (9) and (11), these matrix elements have a dependence on the radial wave functions only through their logarithmic derivatives at the surface of the sphere. Formulas (9) and (11) can be reduced to a similar form by use of the relationship

$$\int_0^{r_s}u_l^2(E,r)r^2dr=-r_s^2u_l^2(E,r_s)\frac{d}{dE}[d\ln u_l(E,r)/dr]_{r=r_s}. \tag{13}$$

[13] M. M. Saffren, Quarterly Progress Report, Solid-State and Molecular Theory Group, Massachusetts Institute of Technology, October 15, 1953 (unpublished), p. 16.

For computational purposes, however, accuracy is most easily maintained by using (9) and (11) as they stand.

As shown by Slater,[14] we find that when $\mathbf{k}_1$ and $\mathbf{k}_2$ are equal and when (3) is satisfied both energy and overlap matrix elements are zero (except when E_1 and E_2 are also equal). Hence, in particular, the augmented plane waves corresponding to electrons in the valence or conduction bands will be orthogonal to those corresponding to electrons in the ion core states, so that, if we restrict our discussion to the former, the lowest eigenvalue will converge to the required eigenvalue in the valence or conduction band.

If we include augmented plane waves of different wave vectors in the variational problem, however, both overlap and energy matrix elements are nonzero; the resulting secular equation will thus, in general, be one involving a nondiagonal overlap matrix, i.e., with the energy parameter occurring in nondiagonal terms as well as along the diagonal. The method used to solve such an equation will be outlined in the following section.

METHOD OF COMPUTATION

It is obvious that the computation involved in this work is simple, but laborious. It must also be borne in mind that when a method of solving the periodic potential problem has been found, a desirable feature of such a process would be the ease with which it could be used in a self-consistent type of calculation (that this may be necessary even in calculations on simple metals is apparent from the results of the present work). These features of the calculation suggest the use of a high-speed computer; throughout this work therefore, use has been made of the Whirlwind I high-speed digital computer to enable the entire process to be carried out automatically and at high speed.

The first step is to solve Eq. (3). For this we require the radial wave functions $u_l(E,r_s)$ for various l and E; these are obtained by the Noumerov process.[19] The spherical Bessel functions $j_l(|\mathbf{k}|r_s)$ are most accurately determined[20] by use of the auxiliary function Λ_l, defined by

$$\Lambda_{l+\frac{1}{2}}(x)=(2/x)^l(2/\sqrt{\pi})\Gamma(l+\tfrac{3}{2})j_l(x). \qquad (14)$$

For high l, simple series expansions of $\Lambda_{l+\frac{1}{2}}(x)$ are possible, from which functions of lower l may be generated from the recurrence relation

$$\Lambda_{l-\frac{1}{2}}(x)=\Lambda_{l+\frac{1}{2}}(x)-\frac{x^2}{(2l+1)(2l+3)}\Lambda_{l+\frac{1}{2}}(x). \qquad (15)$$

In practice, this was found to produce negligible loss in accuracy for all l and $x(=|\mathbf{k}|r_s)$ required here.

Having computed the function on the right-hand side of (3), we wish to specify a value of $|\mathbf{k}|$ corresponding to a particular point in the Brillouin zone, and to determine the solutions $E(\mathbf{k})$ of (3). Regarded as a function of E, however, (3) has the undesirable property of discontinuities at values of E such that $u_l(E,r_s)$ is zero. In addition, the computation of (3) at values of E forming a fine enough mesh for accurate interpolation of zeros is a lengthy calculation owing to the occurrence of the radial wave functions. A more tractable approach is to regard (3) as a function of $\mathbf{k}$ for a given value of E, and to determine the zeros of this function, which varies slowly with $\mathbf{k}$.[3] Graphical interpolation then yields the desired values of E for the particular wave vectors required.

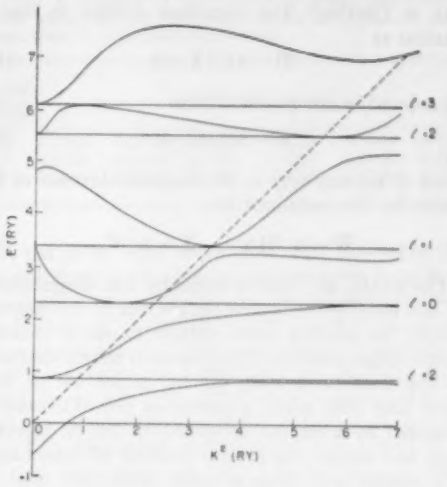

FIG. 1. Energy of augmented plane wave, E, as a function of wave vector, $|\mathbf{k}|$, of plane wave portion (Hartree atomic potential for Cu^+, $(3d)^{10}$ configuration, touching radius of sphere). Asymptotes corresponding to zeros of $u_l(E,r_s)$ are shown with relevant values of l. Broken line indicates $E=|\mathbf{k}|^2$.

One fact of some importance arises as a result of this method of solution. The values of E and $\mathbf{k}$ subsequently used to calculate the matrix elements do not necessarily satisfy (3) exactly, since they depend upon the accuracy with which one can select points from a graph. Hence, the orthogonality relations mentioned in the preceding section are not exactly satisfied. It has been found that the eigenvalues of the resulting secular equation are highly sensitive to small changes in the matrix elements, and considerable errors can arise by assuming that overlap and energy matrix elements between functions of the same k are zero. The original formulas (4) to (11) were therefore used to calculate these matrix elements also. By this means, the formulation of the variational problem remains consistent, although the augmented plane waves with which we start are not the "best" functions possible.

The method used to solve the secular equation is

[19] For a detailed account of this method, see G. W. Pratt, Phys. Rev. 88, 1217 (1952).

[20] *Tables of Spherical Bessel Functions* (National Bureau of Standards, Washington, 1948), Vols. I and II.

that of Löwdin.[21] The equations written in matrix notation as

$$(\mathbf{H}-\mathbf{\Delta}E_j)\mathbf{X}_j=0 \tag{16}$$

are reduced to the canonical form

$$(\mathbf{H}'-\mathbf{1}E_j)\mathbf{C}_j=0, \tag{17}$$

where E appears only in the diagonal elements of the matrix by the transformation

$$\mathbf{H}'=\mathbf{\Delta}^{-\frac{1}{2}}\mathbf{H}\mathbf{\Delta}^{-\frac{1}{2}}, \quad \mathbf{X}_j=\mathbf{\Delta}^{-\frac{1}{2}}\mathbf{C}_j. \tag{18}$$

The matrix $\mathbf{\Delta}^{-\frac{1}{2}}$ can be found by first diagonalizing $\mathbf{\Delta}$, and forming the inverse square root of the diagonal matrix; the problem hence reduces to one of ordinary matrix diagonalization. The process of matrix diagonalization, used twice here, can be carried out at high speed and with great accuracy on the Whirlwind I computer by a routine developed by Dr. A. Meckler. This fact makes the present method of determining $\mathbf{\Delta}^{-\frac{1}{2}}$ simpler and more accurate than that used by Löwdin.

APPLICATION TO METALLIC COPPER

In order to apply this method to any material, suitable choice must be made of the spherically symmetric potential $V(r)$ around each atom. In the cellular calculation on copper, an atomic potential was used as an approximation to the crystal potential. In order to conform as closely as possible to the data used in this previous investigation, the same potentials have been used, modified to be continuous with the zero constant potential at the boundary of the sphere. In the present work, the spheres were taken to be touching, giving the best facilities for approaching as closely as possible to the actual crystal potential with this form of potential. In all cellular calculations, the electron under consideration is supposed to move in the field of the nucleus and all other electrons. In the case of the 4*s* band, therefore, a suitable potential is that for Cu^+ in configuration $(3d)$.[10] Two atomic potentials are available for this configuration, the Hartree atomic potential,[22,23] and the Hartree-Fock potential[24] which includes exchange between the ion core electrons. Separate calculations have therefore been carried out using both of these potentials, in order to investigate the difference in energy band structure arising from the two different assumptions. In the case of the 3*d* band, a modified Hartree potential was formed to represent the $(3d)^9(4s)$ configuration by subtracting from the Hartree Cu^+ potential the contribution from one 3*d* electron and adding that of an atomic 4*s* electron, both normalized to unity inside the atomic sphere. It is recognized that these potentials are probably only crude approximations to the actual crystal potential, and the marked dependence of the relative positions of the electronic energy levels upon the potential found subsequently indicates that greater care is necessary in the choice of potential in order to obtain results of real physical significance.

The computation was carried out as already described. A typical plot of the energy of an augmented plane wave as a function of $\mathbf{k}^2$ is shown in Fig. 1. The example shown is obtained by using the Hartree Cu^+ potential inside the sphere; the lattice constant is taken to be the observed value, 6.8124 Bohr units. The asymptotes shown correspond to values of E for which $u_l(E,r_s)$ is zero; the relevant values of l are shown for each asymptote. In carrying out the summation over l, the series in (3) is in practice terminated at a given l, determined by the properties of the spherical Bessel functions. However, it may be observed that the aim in solving (3) is simply to obtain the best possible one-electron wave functions to use as unperturbed functions in the subsequent variational calculation. It has been found that this latter process converges so rapidly that functions which only satisfy (3) approximately are still sufficiently good unperturbed wave functions. Hence, a reduction in numerical labor can be achieved at this stage of the computation by including only terms of low l in the summation in (3). Results for copper have shown that inclusion of terms for which $l<7$ in (3) gives values of E determining wave functions which are equally good unperturbed functions for the variational process as are functions resulting from the inclusion of all terms for which $l<13$. In setting up the matrix elements between two augmented plane waves, however, we maintain sufficient values of l to ensure accuracy in the summations in (4). Although the augmented plane waves determined by this means possess, in general, a discontinuity in first derivative at the boundary of the sphere, the contribution of this discontinuity to the energy vanishes if $E=|\mathbf{k}|^2$.[25] It is seen from Fig. 1 that over much of the range the curves E *versus* $|\mathbf{k}|^2$ lie close to the line $E=|\mathbf{k}|^2$, indicating that the individual augmented plane waves are themselves quite good approximations to the true solutions of the wave equation.

To form a wave function corresponding to a point $\mathbf{k}$ in the Brillouin zone as a linear combination of augmented plane waves, we can use functions with wave vectors $\mathbf{k}_n=\mathbf{k}+\mathbf{K}_n$, $\mathbf{K}_n$ being a vector of the reciprocal lattice. The expression for the wave function is hence

$$\Psi(\mathbf{k},E)=\sum_{n,m} a_n{}^m\psi(k_n,E_{m,n}), \tag{19}$$

ψ being an augmented plane wave, and $a_n{}^m$ being constants to be determined by solution of a secular equation. The index m refers to functions with differing E but the same $\mathbf{k}$. It is immediately apparent that in general a large number of terms can appear in (19).

[21] P. O. Löwdin, J. Chem. Phys. **18**, 365 (1950).
[22] D. R. Hartree, Proc. Roy. Soc. (London) **A141**, 282 (1933).
[23] D. R. Hartree, Proc. Roy. Soc. (London) **A143**, 516 (1934).
[24] D. R. Hartree and W. Hartree, Proc. Roy. Soc. (London) **A157**, 490 (1936).
[25] See analysis in references 14 and 15.

For a face-centered cubic crystal such as copper, the lowest nonzero $\mathbf{K}_n$ are of the form $\mathbf{K}_{004}=(0,0,4\pi/a)$, the next of the form $\mathbf{K}_{044}=(0,4\pi/a,4\pi/a)$ and so on, together with similar vectors formed by interchange of the three components and alteration of signs. Thus, inclusion of only terms in which $\mathbf{K}_n=(0,0,0)$ and $\mathbf{K}_n=(0,0,4\pi/a)$ results in $7m$ unknown constants in (19) and hence a secular equation of order $7m$, where m is the number of "branches" of Fig. 1 being used. Inclusion of the next set of $\mathbf{K}_n$ gives a secular equation of order $19m$. Thus, unless the series (19) converges very rapidly in both n and m, the resulting secular equation will be of very high order.

At points in the Brillouin zone possessing high symmetry, however, the permissible wave functions possess known symmetry properties.[26] In such case, some of the coefficients a_n^m are interdependent, and, compared with the general case described above, an equivalent number of terms can be included in (19) with fewer undetermined coefficients. For example, at the center of the zone, $\mathbf{k}=(0,0,0)$, for the state possessing s-like symmetry (referred to in reference 26 as the state Γ_1), we find that

$$a_{004}{}^m=a_{040}{}^m=a_{400}{}^m=a_{00-4}{}^m=a_{0-40}{}^m=a_{-400}{}^m,$$

and similarly, all coefficients of the type $a_{044}{}^m$ are equal. Hence, to consider the Γ_1 state, a secular equation of order $2m$ replaces one of order $7m$ in the general case, and one of order $3m$ replaces one of order $19m$, and so on. Thus, as in all such calculations, this method will be most powerful at points possessing high symmetry in k-space, for this allows the inclusion of more terms in (19) without involving secular equations of an equivalently high order. Much of the present calculation has therefore been limited to points of high symmetry in k-space.

To discuss the convergence of the sum (19), it is convenient to consider an example; that selected is the state X_s,[27] having reduced wave vector $(0,0,2\pi/a)$, and having the symmetry of the free electron function $\cos(2\pi z/a)$. After applying the symmetry conditions, the following independent coefficients remain in (19):

$$a_{002}{}^m,\ a_{042}{}^m,\ a_{006}{}^m,\ a_{442}{}^m,\ a_{406}{}^m,\ \cdots.$$

Table I shows the lowest eigenvalue resulting from solutions of a secular equation involving varying numbers of these coefficients. The first entry in the first column shows the energy of the single symmetry combination of augmented plane waves, coefficient $a_{002}{}^1$. The second entry in this column shows the result of including $a_{002}{}^1$, $a_{042}{}^1$; the second entry of the second column results from the inclusion of $a_{002}{}^1$, $a_{042}{}^1$, $a_{002}{}^2$, $a_{042}{}^2$, and so on. More terms have been included in this example than in any other state considered in order to demonstrate the convergence. The excellent convergence shown in Table I is typical of results for all the states considered here; in no case was any improvement obtained by inclusion of more than two values of E for each $\mathbf{k}$ ($m=1$, 2 in the notation given above), and in no case was it necessary to consider values of $\mathbf{K}_n$ greater than $\mathbf{K}_{044}$. This latter observation is not surprising in the case of copper, and may not be true for other substances. Previous calculations[4] have shown that the energy of a conduction electron in copper approximates closely to that of a free electron, and hence the wave function, except in the immediate vicinity of the nucleus, can be well approximated by a single plane wave. In the case of the electrons in the $3d$ band, the wave functions are principally concentrated inside the atomic sphere, and are small in the region of constant potential between the spheres. The accurate representation of this part of the wave function is therefore of little importance in determining the energy.

TABLE I. Example of convergence of lowest eigenvalue of secular equation, using different numbers of augmented plane waves. State X_s using Hartree potential.

Number of wave vectors	Number of E per k 1	2	3	4	5	6
1	0.3760	0.3752	0.3747	0.3747	0.3746	0.3746
2	0.3754	0.3746	0.3746	0.3746	0.3746	0.3746
3	0.3748	0.3746	0.3746	0.3746	0.3746	0.3746

The rapid convergence obtained for states of high symmetry in the Brillouin zone, of which Table I is a typical example, suggest that the method could be applied at points of no symmetry in k-space. A calculation has been made at one such point, the point $A=(\pi/2a,\pi/a,3\pi/2a)$. Results of four figure accuracy can be obtained from the solution of a secular equation of order 14. This is the highest order equation it has been found necessary to solve in the present work.

The method is hence more powerful than the cellular method, which has so far only been applied with accuracy at points of high symmetry in k-space. The orthogonalized plane wave method has also been used to investigate general points in k-space[28]; approximately the same numerical labor is required in the two methods, and the present method would appear to show a more rapid convergence.

Higher eigenvalues of the secular equations possess slower convergence and, in most cases, it is necessary to include further $\mathbf{K}_n$ to obtain accurate results for such states. No attempt has been made to complete the calculation of these eigenvalues except in a few cases; for this reason, the results given here do not exhaust the data of interest. The aim of the present calculation has been to demonstrate the power of the

[26] Bouckaert, Smoluchowski, and Wigner, Phys. Rev. **50**, 58 (1936). See also reference 4 for a general description of these symmetries.

[27] The notation used to denote the states of various symmetries is an adaptation of that used by Bouckaert *et al.* (reference 26), and is fully described in references 2 and 4.

[28] F. Herman (private communication).

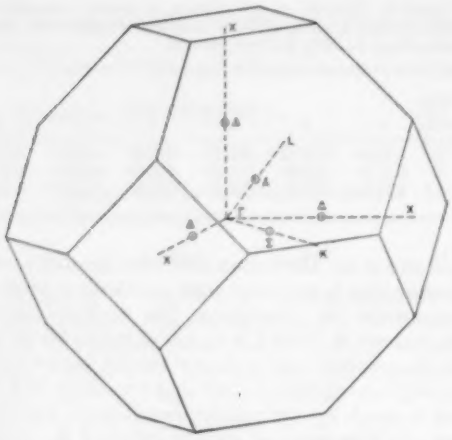

FIG. 2. Brillouin zone for a face-centered cubic crystal, showing points of high symmetry.

augmented plane wave method rather than to calculate every eigenvalue of interest for copper. The ultimate aim in such a calculation is the determination of the entire density of electronic energy states; this would be possible by the augmented plane wave method, but, even making full use of a high-speed computer, would be a very laborious operation. The calculation of an eigenvalue at a general point in k-space involved here the solution of a secular equation of order 14, and the evaluation of over 70 radial wave functions. However, there have recently been suggested methods of interpolating, from accurate results at a few points in momentum space, the energy at any point in k-space, and hence obtaining the density of electronic states.[29,30] Such methods become more powerful if there exist accurate results at more points in momentum space. Thus, the ability to investigate any point in momentum space with accuracy, even at the cost of extensive numerical labor, affords very valuable assistance in applying any such interpolation scheme.

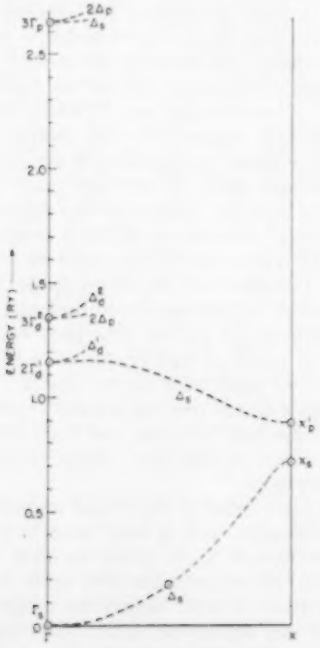

FIG. 3. Energy as a function of wave vector in [002] direction: Conduction band using Hartree potential. Energy in Rydberg units relative to the ground state Γ_1. Figure preceding description of state indicates degree of degeneracy.

DISCUSSION OF RESULTS

The numerical results obtained for copper are shown in Tables II and III. For convenience of reference, the states are given both in the notation of the previous cellular calculation[4] (HJ notation) and in that of Bouckaert *et al.*[28] (BSW notation). The points of high symmetry in the Brillouin zone are shown in Fig. 2. The results are quoted to the accuracy that has been obtained by investigating the successive convergence of the secular equations. The points along the axes of high symmetry referred to as Δ, Λ, Σ represent the center points along these axes [i.e., Δ is the point $(0,0,\pi/a)$]. The dependence of E upon k along the principal directions in k-space is shown in Figs. 3–11. The calculated points are shown, together with schematic diagrams of the $E-k$ curves through these points. The manner in which the various states are connected along the axes can be derived from the compatability conditions of Bouckaert *et al.*[28]

TABLE II. Eigenvalues of conduction band of copper using (a) Hartree and (b) Hartree-Fock atomic potentials. Energies in Rydberg units.

State			
HJ notation	BSW notation	(a)	(b)
Γ_s	Γ_1	−0.558	−0.354
Γ_d^1	Γ_{12}	0.671	0.803
Γ_d^2	Γ_{25}'	0.7982	0.907
Γ_p	Γ_{15}	1.697	2.308
Σ_s	Σ_1	−0.451	−0.240
K_s	K_1	−0.147	0.086
K_p^1	K_3	−0.136	0.0951
Λ_s	Λ_1	−0.391	−0.1702
L_s	L_1	−0.0519	0.2219
L_p^1	L_3'	0.0887	0.3263
Δ_s	Δ_1	−0.471	−0.174
X_s	X_1	0.080	0.375
X_p^1	X_4'	0.2409	0.502
A	...	0.124	0.361

The eigenvalues of the conduction band show that the states at the top of this band are predominantly

[29] J. C. Slater and G. F. Koster, Phys. Rev. **94**, 1498 (1954).
[30] L. Allen (private communication); Phys. Rev. **98**, 993 (1955).

s-like in character along each of the principal directions. The energy gap across the faces of the first Brillouin zone varies from 2.18 ev along the [002] direction to 0.15 ev along the [011] direction when the Hartree potential is used, and from 1.72 ev in the [002] direction to 0.12 ev in the [011] direction in the case of the Hartree-Fock potential. There is a considerably closer correspondence between the results for the two potentials than was observed in the cellular calculation. The use of the Hartree-Fock potential results in a larger width for the conduction band, and a smaller energy gap across the faces of the zone along each of the principal directions, but the relative positions of the states possessing s- and p-like symmetries at the edges of the zone is unaltered. The eigenvalues lie close to the "free-electron" values along the [002] and [111] directions, but are lower than these values along the [011] direction. Calculations at the center points along these axes confirm the approximate parabolic dependence of E upon $\mathbf{k}$, with the consequence of an effective mass slightly less than unity in the [002] and [111] directions, and considerably less than unity in the [011] direction. The presence of an s-like state at the top of the conduction band in the [111] direction does not agree with the prediction of Mott,[21] based on x-ray absorption measurements by Cauchois[22] that this state would be predominantly p-like in character.

TABLE III. Eigenvalues of d band of copper. Energies in Rydbergs.

State HJ notation	State BSW notation	Eigenvalue	State HJ notation	State BSW notation	Eigenvalue
Γ_d^1	Γ_{12}	−0.155	Δ_s	Δ_1	−0.235
Γ_d^2	Γ_{25}'	−0.0541	Δ_d^1	Δ_2	−0.13
Σ_s	Σ_1	−0.2853	Δ_d^2	Δ_2'	−0.067
K_s	K_1	−0.3448	Δ_p	Δ_5	−0.0643
K_s	K_1	−0.14	X_s	X_1	−0.335
K_d	K_2	−0.1621	X_d^1	X_2	−0.1062
K_p^1	K_3	−0.1528	X_d^2	X_3	−0.0742
K_p^2	K_4	−0.0688	X_d^3	X_3	−0.066
Λ_s	Λ_1	−0.1355	X_p^2	X_5'	+0.64
Λ_p	Λ_3	−0.152	X_f^1	X_3'	+1.527
Λ_p	Λ_3	−0.061	X_f^2	X_3'	+1.60
L_s	L_1	−0.2756			−0.2693
L_d	L_3	−0.1456	A	A	−0.194
L_p^2	L_3'	−0.0652			−0.127

The eigenvalues of the $3d$ band show a spread of 3.935 ev from the Γ_d^2 state at the center of the zone to the state K_s at $\mathbf{k}=(0,3\pi/4,3\pi/4)$. This value is in general agreement with the predictions of x-ray absorption measurements by Cauchois,[22] who predicts a value of less than 5 ev, and by Gyorgy and Harvey,[23] who predict a width of 3.5 ev. It also agrees with the result of 3.8 ev quoted by Chodorow[24] obtained from an application of an earlier form of this method,[25] using the same form of potential. The width of the band in the [002] direction in fact agrees exactly with that of Chodorow.

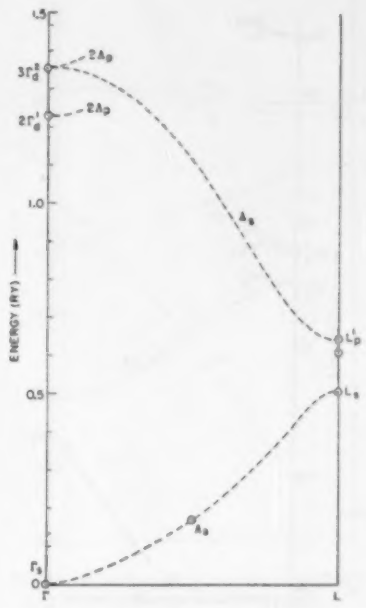

FIG. 4. Energy as function of wave vector in [111] direction: Conduction band using Hartree potential.

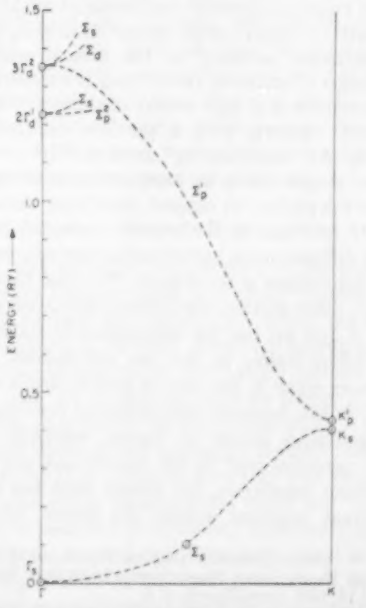

FIG. 5. Energy as function of wave vector in [110] direction: Conduction band using Hartree potential.

[21] N. F. Mott, Phil. Mag. **44**, 187 (1953).
[22] Y. Cauchois, Phil. Mag. **44**, 173 (1953).
[23] E. M. Gyorgy and G. G. Harvey, Phys. Rev. **93**, 365 (1954).
[24] M. Chodorow, Phys. Rev. **55**, 675 (1939).
[25] J. C. Slater, Phys. Rev. **51**, 846 (1937).

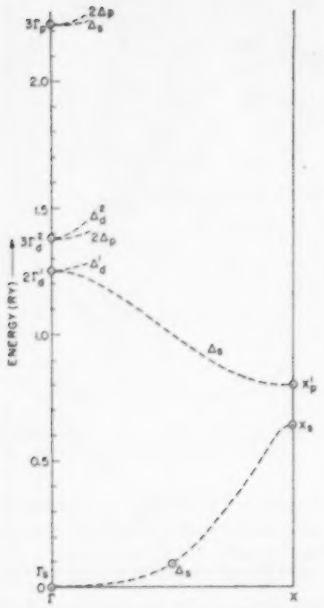

FIG. 6. Energy as function of wave vector in [002] direction: Conduction band using Hartree-Fock potential. Energy in Rydberg units relative to the ground state Γ_s.

It will be seen from the figures quoted that not all the states in the d band have been evaluated at each point in k-space considered; further states would involve the solution of higher order secular equations, which is not considered necessary in the present work. The distribution of states in the d band is consistent with the assumption of a high density of states at the top of the band, agreeing with a previous calculation for nickel by the "tight binding" method.[16,17,36]

These results are to be compared with those of the cellular calculation on copper[4] since both claim to be accurate solutions to the periodic potential problem. Serious differences are immediately apparent, especially in the eigenvalues in the d band. The total band width does not differ greatly, the cellular calculation giving a width of 3.46 ev, but the distribution of states in the band differs widely in the two calculations. Similar differences occur in the case of excited levels of the d band.[37] It has, however, been observed previously that the eigenvalues appear to depend markedly on the crystal potential used in the calculations, and, unlike the cellular calculation, the present work has assumed a constant potential outside the atomic spheres. A cellular calculation has therefore been repeated using the exact potential employed in the present work. In particular, the two states at the center of the zone in the d band were considered, both of which are easily amenable to an accurate cellular calculation. The results agreed with those of the augmented plane wave method to within the accuracy one can claim from the cellular method. It is therefore concluded that the difference in the results is predominantly due to different potentials used in the two calculations.

The same may be assumed to be true in the case of the conduction band. The augmented plane wave method may be the more reliable for these states. Doubt has recently been cast on the accuracy of cellular calculations involving the matching of boundary conditions at points on the cell boundaries,[38] and this may affect the reliability of the results for the conduction band of copper carried out by that method. The agreement with experiment is equally good for both sets of results.

It must be pointed out that the use of two different potentials in considering the $3d$ and $4s$ bands makes it impossible to predict the relative positions of the bands by direct use of the augmented plane wave method. This method is only used to solve the periodic potential problem for a single assumed potential. The two calculations are therefore to be regarded as distinct energy

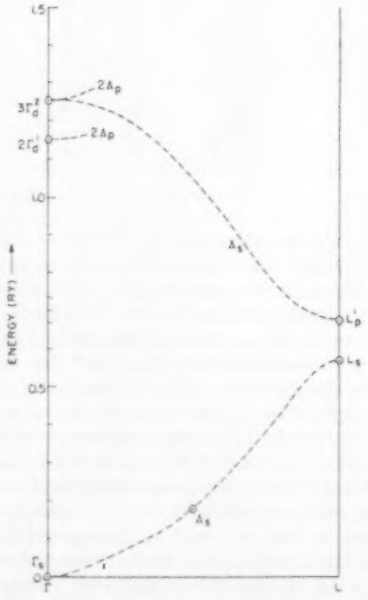

FIG. 7. Energy as function of wave vector in [111] direction: Conduction band using Hartree-Fock potential.

[37] I am indebted to Mr. J. Hubbard for permission to see results on the excited states of the d band carried out by the cellular method.

[38] F. Ham, Ph.D. thesis, Harvard University, 1954 (unpublished). I am indebted to Dr. Ham for several discussions on this matter.

band calculations. In the cellular calculation, an attempt was made to determine the relative positions of the two bands by an approximate solution of the Hartree equations for the crystal. Such a calculation is necessarily very approximate in the absence of a full self-consistent treatment of the two bands, and no such attempt has been made in the present work.

The sensitivity of the eigenvalues upon the exact crystal potential has been noted previously in the case of copper and of germanium. Copper and the transition metals preceding it in the periodic table may be expected to show more sensitivity than other materials, for it is known that the radial wave functions for $l=2$ are exceptionally sensitive to the potential; in the crystal, this effect will be particularly noticeable in the *3d* band. It becomes more apparent that a self-consistent type of calculation is necessary even in the case of simple metals. In this connection, the augmented plane wave method has a marked advantage over other existing methods of solving the periodic potential problem. It has already been observed from Fig. 1 that a single augmented plane wave may well be a good approximation to the true wave function. This is borne out in Table I and in every other state considered. Energies in error by not more than 0.003 Rydberg unit can be obtained before entering upon the variational problem, that is, by considering an augmented plane wave to be a sufficiently good wave function. Although the wave functions themselves may be expected to show greater error, it still appears that an augmented plane wave forms a fair approximation to the true solution. This is a significant observation when the problem of self-consistency is approached. The contribution to the potential of these one-electron functions could be estimated; this new potential could then be used to repeat the calculation and to obtain self-consistency. Alternatively, the new potential could be regarded as a perturbation to the original potential, to be included in the variational calculation. Hence, a practical consequence of the extremely rapid convergence of the augmented plane wave method is the feasibility of a self-consistent energy band calculation.

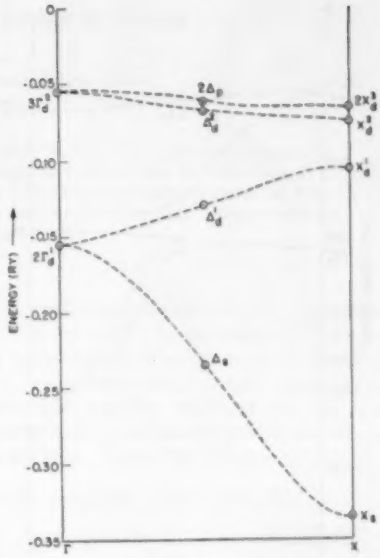

FIG. 9. Energy as function of wave vector in [002] direction: *3d* band. Energy in Rydberg units.

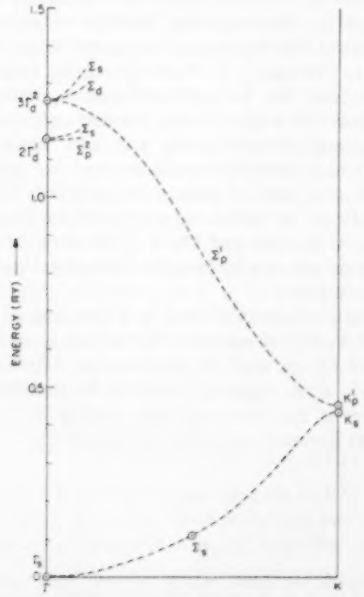

FIG. 8. Energy as function of wave vector in [110] direction: Conduction band using Hartree-Fock potential.

CONCLUSION

The work on copper has shown that the augmented plane wave method is among the most powerful of the existing methods for the solution of the one-electron periodic potential problem. Results of greater accuracy than those obtainable by the cellular method as currently used can be obtained with no greater numerical difficulty. In addition, the application is not so severely limited to points of high symmetry in momentum space. The method thus compares favorably with the method of orthogonalized plane waves, which has also been applied to points of no symmetry in momentum space. Although the method used here deals with a restricted form of potential, it has been pointed out by Slater that more general forms of potential could be considered with some ease; it remains to be seen whether the rapid

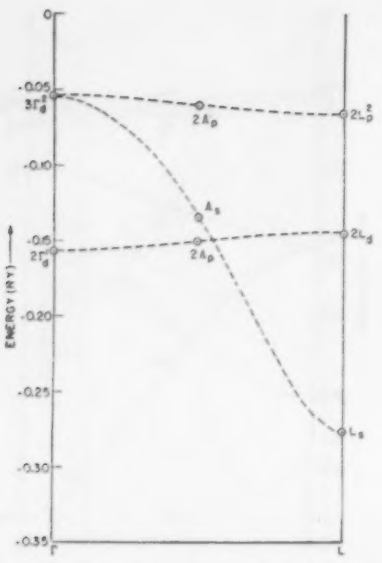

FIG. 10. Energy as function of wave vector in [111] direction: 3*d* band.

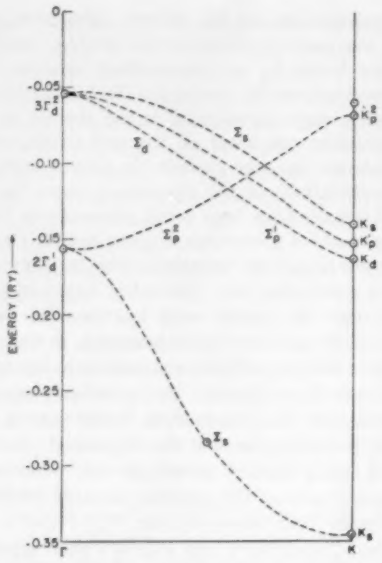

FIG. 11. Energy as function of wave vector in [110] direction: 3*d* band.

rate of convergence observed in the present work would also result from the inclusion of different forms of potential. Although the calculation of an entire density of states by the augmented plane wave method would be a calculation of prohibitive length, the ability to obtain accurate eigenvalues at any point in k-space affords a valuable means of checking any interpolation procedure used to obtain a density of states curve.

In view of the differences between the results of the present calculation on copper and those of the cellular calculation, which difference appears entirely due to the different potentials employed, it cannot be claimed that the results of such solutions to the periodic potential problem necessarily bear any great physical significance. As more accurate solutions are carried out, it becomes increasingly apparent that the exact form of the potential inside the atomic cell is an important factor in determining the energy levels. The need for a self-consistent calculation is obvious, and the present method would appear to make such a calculation feasible. Such a calculation has not been carried out for copper, and the present work is therefore to be regarded as an investigation into the value of the augmented plane wave method, rather than an investigation of the physical properties of metallic copper.

ACKNOWLEDGMENTS

The work described here was carried out during a year spent in the Solid-State and Molecular Theory Group at the Massachusetts Institute of Technology. I am glad of this opportunity of expressing my deepest thanks to Professor J. C. Slater for making such a visit possible, and for his guidance and encouragement throughout the work. Thanks are due to all members of the group for making my stay with them such a pleasant and valuable experience, and for many discussions and pieces of advice. In particular, I wish to thank Mr. M. M. Saffren for several helpful discussions, and Dr. A. Meckler and Mr. F. J. Corbató for making possible the use of a fast matrix diagonalization routine on the computer.

The entire numerical work has been carried out on the M.I.T. digital computer Whirlwind I, and I wish to thank all the staff of the computer laboratory for their help at all stages of the work. Availability of the computer at this time was made possible by the Office of Naval Research, to whom thanks are due.

Spin Resonance of Impurity Atoms in Silicon

CHARLES P. SLICHTER
Department of Physics, University of Illinois, Urbana, Illinois
(Received April 11, 1955)

An explanation is proposed for the weak satellite lines observed in the microwave electron spin resonance of Group V impurity atoms in silicon. The satellites occur halfway between the main hyperfine lines. It is proposed that the satellites represent the resonance of pairs of impurities close enough together for their exchange interaction to be very large compared to the hyperfine coupling. Mathematical details are worked out.

THE microwave spin resonance of Group V impurity atoms in silicon such as As or P has been studied by Fletcher, Yager, Pearson, Merritt, Holden, and Read.[1] They find the resonance consists of $2I+1$ equally spaced lines of equal intensity, where I is the nuclear spin of the impurity atom. They interpret the splitting of the electron line as arising from the hyperfine interaction with the nuclear magnetic moment. The theoretical splitting has been worked out by Kohn and Luttinger.[2] Although the wave function of the electron bound to the impurity atom is complicated in silicon, they are able to obtain excellent agreement with the experimental splitting. Thus the main features of the resonances appear to be well understood. Fletcher and his co-workers find, however, that a close examination reveals that there are very weak satellite lines half-way between each of the main pairs.

Although Fletcher *et al.* propose in their second paper that the lines are from forbidden transitions, in a private communication they point out that the observed intensity is too high for this explanation. The purpose of this note is to propose a possible alternative explanation.

In essence, our proposal is that the satellite lines arise from the resonance of impurity atoms sufficiently close together that they should be considered as pairs whose electron spins are coupled strongly by the exchange interaction. In this case the electrons act as a unit which effectively responds to the average magnetic field produced by the hyperfine coupling to the two nuclei involved. As a consequence, the pattern for pairs consists of lines spaced at half the interval of single impurities, but extending over the same total range. Let us examine the mathematical details.

We consider a system of pairs of impurities in a static magnetic field H_0. The Hamiltonian is

$$\mathcal{H}=a(\mathbf{I}_1\cdot\mathbf{S}_1+\mathbf{I}_2\cdot\mathbf{S}_2)+A\,\mathbf{S}_1\cdot\mathbf{S}_2 +\gamma_e\hbar(S_{1z}+S_{2z})H_0+\gamma_n\hbar(I_{1z}+I_{2z})H_0,$$

where $\mathbf{I}_1$ and $\mathbf{I}_2$ are the nuclear spins, $\mathbf{S}_1$ and $\mathbf{S}_2$ are the electron spins, γ_e and γ_n are the electron and nuclear gyromagnetic ratios, and a is the hyperfine coupling constant evaluated theoretically by Luttinger and Kohn. The term $A\,\mathbf{S}_1\cdot\mathbf{S}_2$ represents the electron exchange interaction between pairs of electrons.[3] In its absence, we obtain energy levels which to a first approximation may be described by the quantum numbers m_1 and m_2 for the two nuclei, and M_1 and M_2 for the electrons. We find for the energy

$$E=a(m_1M_1+m_2M_2)+\gamma_e\hbar(M_1+M_2)H_0 +\gamma_n\hbar(m_1+m_2)H_0.$$

The interaction $\gamma_e\hbar(S_{1x}+S_{2x})H_x\cos\omega t$ will then induce transitions in which $\Delta M_1=\pm1$, $\Delta M_2=0$ or $\Delta M_1=0$, $\Delta M_2=\pm1$, giving us a set of lines at energies $\gamma_e\hbar H_0+am_1$, where $m_1=I, I-1, \cdots -I$. There are then $2I+1$ lines all told, of spacing a.

When $A\gg a$, it is appropriate to consider the electrons as forming a system described by quantum numbers S and M, where $S=1$, 0 and $M=S, S-1\cdots -S$, but the nuclei are still described by m_1 and m_2. Now the states $S=1$ and 0 are the well-known singlet or triplet states. Then the diagonal terms become (since the triplet is symmetric and the singlet antisymmetric)

$$E=a(\tfrac{1}{2}m_1M+\tfrac{1}{2}m_2M)+\tfrac{1}{2}A[S(S+1)-\tfrac{3}{2}] +\gamma_e\hbar MH_0+\gamma_n\hbar(m_1+m_2)H_0.$$

The term $\gamma_e\hbar H_x(S_{1x}+S_{2x})\cos\omega t$ gives us transitions $\Delta S=0$, $\Delta M=\pm1$, so that we get lines at $\gamma_e\hbar H_0+\tfrac{1}{2}a(m_1+m_2)$ which will give $4I+1$ lines. The spacing is $a/2$ rather than a. The intensity will *not* be uniform. To compute the intensity pattern we must find the number of ways of getting the same sum $m_1+m_2\equiv M_F$. This procedure is a straight forward problem which can be solved by vector addition of the two angular momenta I to form $F=2I, 2I-1, \cdots 0$. For each value of F we get a given value of M_F once. Moreover, each value of F occurs only once. Thus, $M_F=2I$ occurs once, $M_F=2I-1$ occurs twice, etc. The relative intensity of lines starting from one end of the pattern will then be 1-2-3-4$\cdots$4-3-2-1. Therefore in the case of As we get an intensity pattern 1-2-3-4-3-2-1. The three lines of intensity 2-4-2 will be seen. The 1-3-3-1 lines will be

[1] Fletcher, Yager, Pearson, Holden, Read, and Merritt, Phys. Rev. **94**, 1392 (1954); Fletcher, Yager, Pearson, and Merritt, Phys. Rev. **95**, 844 (1954).
[2] W. Kohn and J. M. Luttinger, Phys. Rev. **97**, 883 (1955).
[3] We have omitted the magnetic dipole coupling between the electrons as being small compared to the exchange interaction.

masked by the resonance of single As impurities. Thus the central *satellite* should be twice as large as the outer satellites.

As the concentration increases, we would have resonances coming from clusters of more than two, but we might expect such clusters to be rather infrequent in the concentration range in which clusters of two are rare. The extreme case is the one in which the exchange coupling is so strong that we have a metal with completely nonlocalized electrons. Thus our case of interacting pairs is simply the first step in the process of turning the sample into a metal.

We note, finally, that if $A \sim kT$ or larger, there should be a temperature dependence of the satellite intensity of $\exp(-2A/kT)$, assuming the triplet states are higher in energy. The presence of satellites should also be a function of concentration (approximately proportional to c for low concentrations) and possibly of the mechanical treatment of the material if it causes the distribution of As in the lattice to be appreciably altered.

The predicted greater intensity of the central satellite for As is confirmed experimentally. The weakness of the lines makes it difficult to check the intensity ratio accurately, although Dr. Fletcher states that the experimental values scatter in the vicinity of the theoretical prediction

The author wishes to thank Dr. Fletcher for interesting conversations. This paper grew out of discussions on another problem with Professor David Pines and Professor John Bardeen. The author is indebted to them for numerous stimulating conversations and helpful comments.

PHYSICAL REVIEW VOLUME 99, NUMBER 2 JULY 15, 1955

Melting Curves of He^3, He^4, H_2, D_2, Ne, N_2, and O_2 up to 3500 kg/cm²*

R. L. MILLS AND E. R. GRILLY
Los Alamos Scientific Laboratory, University of California, Los Alamos, New Mexico

(Received April 13, 1955)

New and more accurate measurements were made on the melting pressure-temperature relationship of seven substances below 120°K and up to 3500 kg/cm². New regions were covered for He^3 and O_2. The blocked-capillary method was used. The data were fitted to the Simon-type equation, $P=a+bT^c$, with more success than to a quadratic, $P=A+BT+CT^2$. Rather straightforward shifts were obtained in the melting curves of the isotope pairs, He^3-He^4 and H_2-D_2. Superpressuring in the O_2 measurements was unusually great.

1. INTRODUCTION

OUTSIDE of the pioneering work of Simon and his collaborators,[1,2] there is a surprisingly small amount of data on melting[3] temperatures as a function of pressure over a wide range and in the region below 100°K. They covered He, H_2, Ne, N_2, and A up to about 5000 kg/cm² using the blocked capillary technique first used by Kamerlingh Onnes and van Gulik.[4] Bridgman[5] also determined the the melting curves of N_2 and A to about 6000 kg/cm² but used the discontinuity in the specific volume as the criterion of melting. His P–T curves lay below those of Simon *et al.*; he felt that their data were in error as a result of the shear stress in the capillary plug. Recently, Robinson,[6] using the freedom of a pellet as the criterion of melting, measured A and N_2 to about 9400 kg/cm²; his P–T curve for A lay below those of both Simon[2] and Bridgman,[5] while his N_2 curve lay between those of Simon and Bridgman (if one believes Robinson's actual data rather than his conclusions).

Helium has been studied in the 4000–7300 atmos (35–50°K) region by Holland, Huggill, and Jones[7] and in the 140–780 atmos (4–12°K) region by Dugdale and Simon.[8] All of these He data agree substantially with those of Simon.[1,2]

An interesting isotopic comparison resulted from the observations of Chester and Dugdale[9] on H_2 and D_2. They found the D_2 P–T curve to be consistently 170 kg/cm² lower than the H_2 curve up to their maximum pressure of 2800 kg/cm². However, their quantitative results were expressed only as the difference between the two isotopes and are therefore inadequate for general use.

One of the most debated points concerning solid-gas equilibria is the maximum temperature at which solid exists.[10–13] According to Simon,[10] the substance most

* Work done under the auspices of the U. S. Atomic Energy Commission.

[1] F. Simon, Z. physik. Chem. **B2**, 340 (1929).

[2] Simon, Ruhemann, and Edwards, Z. physik. Chem. **B6**, 62 (1929); **B6**, 331 (1930).

[3] Used in its most general sense: solid to either fluid phase, liquid or gas.

[4] H. Kamerlingh Onnes and W. van Gulik, Leiden Comm. 184a (1926).

[5] P. W. Bridgman, Phys. Rev. **46**, 930 (1934); Proc. Am. Acad. Arts Sci. **70**, 1–32 (1935).

[6] D. W. Robinson, Proc. Roy. Soc. (London) **A225**, 393 (1954).

[7] Holland, Huggill, and Jones, Proc. Roy. Soc. (London) **A207**, 268 (1951).

[8] J. S. Dugdale and F. E. Simon, Proc. Roy. Soc. (London) **A218**, 291 (1953).

[9] P. F. Chester and J. S. Dugdale, Phys. Rev. **95**, 278 (1954).

[10] F. E. Simon, Z. Elektrochem. **35**, 618 (1929); Trans. Faraday Soc. **33**, 65 (1937); Proc. Roy. Soc. (London) **A218**, 291 (1953).

likely to show this phenomenon, if it exists at all, is He. Since He^4 has not yet shown the effect, it seems that measurements on He^3 will provide the last chance for an experimental test. Up to now the only melting point measurements on He^3 have been those below 1.5° K and 56 atmos by Osborne, Abraham, and Weinstock.[14]

A review of the melting curves measured heretofore indicates their deficiencies in both extent and accuracy. Greater accuracy or, at least, internal consistency is especially desirable for deriving thermodynamic quantities from the slope of the melting curve. Therefore, we felt that there was a need for a comprehensive program of measurements, repetitive as well as new. We report here the results of the first phase: melting curves to 3500 kg/cm² for He^3, He^4, Ne, N_2, and O_2 and to 1800 kg/cm² for H_2 and D_2.

2. APPARATUS

A. General

The apparatus is shown schematically in Fig. 1. Here the gas source is a metal tank containing the gas at low pressures, from 1 to 150 atmos. The cryogenic pump is a heavy-walled steel vessel into which is condensed the gas when the pump is cooled by an appropriate bath. When the pump is warmed, the resulting high-pressure gas is sent into the steel capillary tubing, the mercury pusher, and the coil gauge. The process is repeated, if necessary, until the system is loaded to ~1000 kg/cm² with the mercury in the right leg of the pusher at a minimum. From the left leg of the pusher, an oil line leads to a free-piston gauge and its manually operated oil injector. The capillary of Type 347 stainless steel, 0.69 mm o.d., by 0.25 mm i.d., is bent into a long, narrow loop, the tip of which can be cooled to any temperature down to 1.9°K. On the other side of the cold loop is a Bourdon helical coil gauge whose degree of uncoil, a measure of pressure, is observed by means of mirror, telescope, and scale.

The following procedure was used in making a melting-point measurement. The cold loop was adjusted to an appropriate temperature. The piston gauge was loaded stepwise with weights, and the oil injector was adjusted accordingly, thus increasing the pressure in the capillary until no movement of the coil gauge was observed, which indicated plugging in the cold capillary loop. Removal of weights caused unplugging. The initial freezing and melting pressures were usually within 1 percent of each other but, at times, differed by 10 percent. (In some cases, the temperature was varied at constant pressure; the supercooling found was approximately equivalent to the superpressuring.) If, during the melting transition, a weight was immediately added, freezing could be induced at a pressure lower

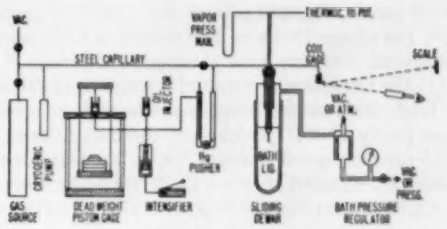

FIG. 1. Schematic diagram of the melting point apparatus.

than the initial freezing pressure. By successive freezings and meltings, we approached a pressure which needed smaller and smaller changes in weight to cause a freezing or melting. When melting and freezing were caused within ~±1 kg/cm², the point was taken as our "melting point."

B. Source and Purity of Gases Used

All the gases used in the melting-point determinations, and in the vapor pressure thermometer, were analyzed in our mass spectrometer, which generally is sensitive to ~0.05 percent for each impurity. However, considerable discretion must be used if impurities are indicated; many of these indications are false because of residues in the instrument.

(*a*) The helium-3 was obtained from the radioactive disintegration of tritium (T or H^3); the T was kept as UT_3, which has a negligible chemical decomposition pressure at 300°K, therefore the He^3 could be simply pumped off. Our analysis showed the He^3 to contain: <0.10 percent He^4, <0.01 percent H_2, <0.06 percent DT, <0.03 percent T_2, <0.03 percent N_2. The 4, 5, 6 masses are probably residues of HT, DT, and T_2 in in the spectrometer.

(*b*) The helium-4 was obtained directly from an AEC helium cylinder which had been filled by the Bureau of Mines. The Bureau's precautions are generally adequate to allow it to quote a purity of 99.99 percent in the filled cylinder. Our analysis showed <0.02 percent H_2, <0.01 percent Ne, <0.05 percent N_2.

(*c*) The hydrogen was produced through water electrolysis by the National Cylinder Gas Company. The more condensable gases were removed by adsorption on silica gel at 77°K. Our analysis showed <0.02 percent N_2 and <0.01 percent O_2 on the mass spectrometer and <1 ppm O_2 on a Beckman magnetic susceptibility analyzer.

(*d*) The deuterium was produced through heavy water electrolysis by the Stuart Oxygen Company, who claimed >99.5 percent purity. Our analysis showed 1.10 (+0.00 or −0.37) percent HD, <0.02 percent H_2, <0.12 percent N_2, and 0.01 percent O_2.

(*e*) The neon was produced through air distillation by the Linde Air Products Company, who designated it "spectroscopically pure." Our analysis showed 0.09 (+0.00 or −0.05) percent He, <0.05 percent H_2,

[11] P. W. Bridgman, Revs. Modern Phys. **7**, 1 (1935).
[13] J. E. Lennard-Jones and A. F. Devonshire, Proc. Roy. Soc. (London) **A170**, 464 (1939).
[13] J. de Boer, Proc. Roy. Soc. (London) **A215**, 4 (1952).
[14] Osborne, Abraham, and Weinstock, Phys. Rev. **82**, 263 (1951); **85**, 158 (1952).

<0.05 percent N_2, 0.28 percent Ne^{21}, and 10.0 percent Ne^{22}. The adopted value of Ne^{22} content is 8.82 percent, but several observers have obtained 9.72 percent.[15]

(*f*) The nitrogen was produced through air distillation by Linde Air Products Company, who claimed a minimum purity of 99.7 percent and the impurities to be <0.3 percent O_2 and traces of Ne, A, Xe. Our analysis showed 0.11 (±0.01) percent O_2, 0.06 (±0.01) percent A, <0.06 percent Ne, <0.03 percent He, <0.04 percent H_2.

(*g*) Melting measurements were made on three kinds of oxygen: (1) Air distillation oxygen by Linde Air Products Company, who claimed >99.5 percent purity with <0.5 percent N_2 and traces of Ne, A, and CO_2. Our analysis showed 0.14 (±0.01) percent A, <0.05 percent He, <0.03 percent H_2. Mass spectrometric observations on N_2 and Ne were meaningless because of interference from other molecules. (2) Electrolytic oxygen by Stuart Oxygen Company labeled "Medical grade." Our analysis showed 0.30 (±0.03) percent H_2, <0.05 percent He, 0.03 (±0.01) percent A (the presence of A is difficult to explain). (3) The same as (2) but with the H_2 removed by distillation of the liquid. The resulting liquid showed a vapor pressure independent of amount evaporated. Our analysis of the gas showed <0.03 percent H_2, 0.03 (±0.01) percent A. This is the only O_2 that we consider gave reliable results.

C. Temperature Control and Measurement

The capillary cold loop, wherein freezing and melting occurred, went through a small copper block, 6 mm diam and 10 mm long, which had been split open and shaped to receive the tube and a thermocouple. All these parts were soldered together with "Cerrobend" (an alloy melting at ~70°C). Into the top of the copper block was drilled a hole to act as a vapor pressure thermometer well. This was connected to a manometer by means of steel capillary tubing. The vapor pressure thermometer system could be loaded with an appropriate gas: He, Ne, H_2, N_2, or O_2. Into the bottom of the copper block was soldered a steel rod whose purpose was to bridge the gaps between those temperatures obtained directly with liquid baths. This was accomplished by adjusting the bath level below the copper block until the temperature gradient was suitable to get the desired temperature at the block. This technique was aided by use of a Dewar with a sliding seal at top. The Dewar, 4 cm diam and 35 cm long on the inside, was of double construction, so that liquid nitrogen could be used as a shield, and had unsilvered strips for windows. The Dewar sat on a screw-type leveling ring so that its height could be adjusted closely with minimum effort on the part of the observer.

The liquid baths used were He, H_2, N_2, O_2, and CH_4; they were thermally stirred to promote temperature uniformity. With each, various temperatures could be chosen by adjustment of its vapor pressure from several to 2000 mm Hg. The bath pressure was controlled to the equivalent of 0.02° by a valve which was actuated by the difference between control and controlled pressures across a metal bellows.

The melting temperatures were determined by the vapor pressure thermometer wherever possible, otherwise by a thermocouple. Both were in intimate contact with the coldest point of the high pressure capillary. Where it was advantageous, a platinum resistance thermometer suspended in the bath was also used, but this was not entirely reliable in liquids like air, O_2, and N_2, which often have large temperature gradients. The thermocouple was made of Cu and an alloy of Cu containing 0.015 wt percent Fe, both wires being ~0.005 in. in diameter. The alloy, suggested by the work of Borelius,[16] was mixed, drawn, and annealed in this laboratory. The sensitivity in μv/deg was 10 at 5°K and 14 at 15° to 30°K, then dropped off to 5.5 at 60°K and finally to 1 at the ice point, which was used as the reference junction.[17]

Table I gives the thermometers used in various temperature ranges.

Wherever possible, concurrent comparisons were made between temperatures from vapor pressure, resistance thermometer, and thermocouple so that the last would have maximum interpolation value. In general, the vapor pressure thermometer was considered most reliable. In another type of apparatus, a similar resistance thermometer had been compared with vapor pressures of the gases used in this research; a maximum deviation of $T_{RT}-T_{VP}=0.08°$ was obtained at 75°K with N_2. Simultaneously emf *vs* T data

TABLE I. Thermometers used in various temperature ranges.

T range, °K	Thermometer used	Reference
1.9–5.2	v.p. He	a
5.2–12; 31–55	Cu−Cu Fe thermoc.	This research
12–24.5	v.p. $n-H_2$	b
24.5–31	v.p. Ne	c
55–78	v.p. N_2	d
75–101	v.p. O_2	e
14–24.5; 58–121	Pt resis. therm.	f

[a] The 1948 agreement at Amsterdam, and published by the Royal Society Mond Laboratory, Cambridge, in 1949, up to 4.2°; R. Berman and C. A. Swenson, Phys. Rev. **95**, 311 (1954) for 4.2–5.2°.
[b] Woolley, Scott, and Brickwedde, J. Research Natl. Bur. Standards **41**, 379 (1948) for 12–20°; E. R. Grilly, J. Am. Chem. Soc. **73**, 843 (1951) for 20–24.5°.
[c] F. Henning and J. Otto, Physik Z. **37**, 633 (1936) for 24.5–27.5°; E. R. Grilly (unpublished) for 24.5–31°.
[d] F. Henning and J. Otto, Physik Z. **37**, 633 (1936) for 66–78°; W. F. Giauque and J. O. Clayton, J. Am. Chem. Soc. **55**, 4880 (1933) for 55–66°.
[e] H. J. Hoge, J. Research Natl. Bur. Standards **44**, 321 (1950).
[f] Leeds & Northrup Company, serial No. 1008495, calibrated at the international fixed points and in the region 10–91° by the National Bureau of Standards against a gas thermometer.

[15] K. T. Bainbridge and A. O. Nier, "Relative Isotopic Abundance of the Elements," Preliminary Report No. 9, Nuclear Science Series, Div. of Math. and Physical Sciences, National Research Council, Washington, D. C. (unpublished).

[16] G. Borelius, Physica **19**, 807 (1953).

[17] An alloy of Cu and 0.008 wt percent Sn, suggested by the work of Dauphinee, MacDonald, and Pearson [J. Sci. Instr. **30**, 399 (1953)], was also made up and tried, but it failed to give the proper sensitivity. Perhaps the mixture was not of uniform composition.

were obtained for two other Cu–Cu Fe thermocouples; these two and the thermocouple used for the present melting points gave parallel and only slightly separated calibration curves. In view of the various checks on the thermometry, it is estimated that the greatest possible error in melting temperature was 0.1°, which applied to the midpoints of the 5.2–12° and 31–55° regions, where interpolation by thermocouple was necessary; in other regions, the possible errors probably averaged about 0.03°.

The temperature control and measurement system used here was simple in principle and construction. Besides doing its main job of accurately measuring the melting temperature, it provided a means of rapidly changing the temperature whenever desired. This proved useful when melting points obtained in the normal way were checked by keeping the pressure constant and varying the temperature. Operation of the system was more tedious than that of the conventional system whereby the cold point is isolated from the bath by vacuum after reaching the lowest temperature desired. Whether the advantage was worth this is not readily discernible.

D. Pressure Measurements

On one side of the cold loop, high pressures were established and measured precisely with a free-piston gauge. Pressure changes on the other side of the loop were observed by means of a highly sensitive Bourdon helix. The two pressure devices will be described separately.

(*a*) *Free-Piston Gauge*

In the range of 350 to 3500 kg/cm², pressures were measured with a controlled-clearance free-piston gauge. The advantages of a controlled-clearance gauge, i.e., high sensitivity, manageable leakage of fluid past piston, and knowledge of effective area, have been discussed by its inventors, Johnson and Newhall.[18] Our instrument, shown in Fig. 2, was similar to theirs with minor modifications.

The jacket was designed to cover the range 0–3500 kg/cm² although the inner components could be pressured somewhat higher. The inner cylinder was machined from a manganese tool steel, hardened to Rockwell C-65, and then ground and lapped. The cylinder bore, nominally 0.0646 cm² in cross-sectional area, was 3.56 cm long.

The piston was made from a rod of Kennametal,[19] 2.5 cm long and 0.32 cm in diameter, brazed to a larger steel support. The piston was ground with a diamond wheel and lapped with diamond dust until it slipped into the cylinder without interference. In the completed assembly, the piston was free to move 5 mm, the tip moving 2.5 mm above and below the center of the cylinder bore. The piston was rotated at 24 rpm after the method of Myers and Jessup.[20] A height gauge of calibrated spring tension was firmly mounted to follow the travel of the piston. In practice the piston was floated to within ±0.012 mm of its center position with a manually operated oil injector.

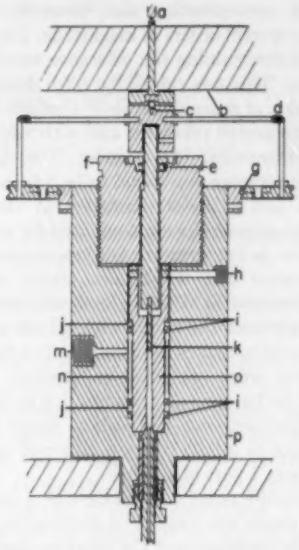

FIG. 2 The controlled-clearance free piston gauge. (*a*) height gauge; (*b*) yoke; (*c*) tungsten carbide insert and hardened ball; (*d*) light spring; (*e*) ball bearing guide; (*f*) packing nut; (*g*) ball bearing for rotating pulley; (*h*) oil overflow; (*i*) steel rings; (*j*) lead washer; (*k*) tungsten carbide piston; (*m*) jacket inlet; (*n*) thrust sleeve; (*o*) inner cylinder; (*p*) outer cylinder.

The hydraulic fluid employed was an aviation instrument oil. Oil pressure was developed with a hand pump and a 10-to-1 intensifier. The outer jacket of the free-pistion gauge was pressured with oil from the same intensifier. Its pressure was read on a 0–1400 kg/cm² (0–20 000 psi) Heise[21] gauge of guaranteed 0.1 percent accuracy.

The piston gauge is a primary pressure standard in its own right if careful attention is given the measurement of force and effective area. The force exerted by the various pan loadings was calculated as the product of the masses, calibrated to 0.001 percent and corrected for air buoyancy, times the gravitational acceleration, determined at our location to the same accuracy. Slight corrections for the spring force of the height indicator gauge and for piston buoyancy in oil were made. The effective area of a free piston gauge is the mean of the cylinder and piston areas. Our piston area was calculated from an average diameter measured with an electrolimit gauge to a few microinches. The result at 20°C was 0.064570 cm². Direct measurement of a bore

[18] D. P. Johnson and D. H. Newhall, Trans. Am. Soc. Mech. Engrs. **75**, 301 (1953).

[19] Trade name of a tungsten carbide-cobalt mixture manufactured by Kennametal Inc., Latrobe, Pennsylvania.

[20] C. H. Myers and R. H. Jessup, J. Research Natl. Bur. Standards **6**, 1061 (1931).

[21] Heise Bourdon Tube Company, Newtown, Connecticut.

diameter of corresponding size, however, suffers in accuracy by several orders of magnitude. The expedient was used of determining the clearance between piston and cylinder. This was calculated from direct observation of the flux of *n*-propyl alcohol[22] through the crevice at various measured pressures and with various jacket pressures surrounding the cylinder. The clearance at atmospheric pressure was found to be $5.64\pm0.08\times10^{-5}$ cm. Piston and cylinder diameters at the different experimental pressures were computed by substituting values of the jacket pressure and approximate experimental pressure into well-known elastic equations.[23] The effective area at 3500 kg/cm² was less than 0.2 percent larger than the piston area quoted above.

All indicated pressures obtained by dividing force by effective area were converted to absolute values by addition of the barometric pressure. It is estimated that the controlled-clearance free-pistion gauge gave pressures accurate to ±0.05 percent, although its observed sensitivity was 1 part in 100 000.

In the pressure range 3.5–350 kg/cm², a commercial[24] free-piston gauge was used. The platform weights were calibrated by weighing and the effective area, 0.080640 cm² at 35.5445 kg/cm², was determined by balancing the gauge against a pressure standard, the vapor pressure of pure CO_2 at 0°C.[25] Effective areas at other

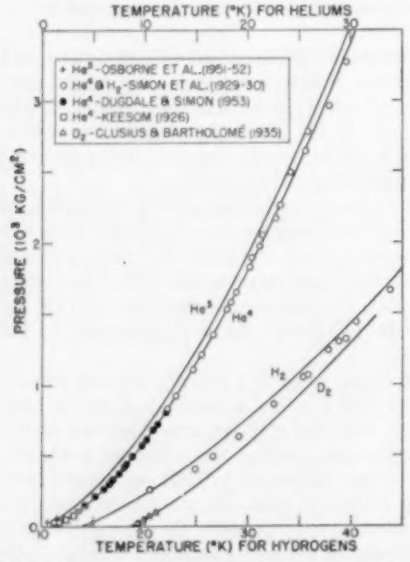

FIG. 3. Melting curves of helium and hydrogen isotopes. Present measurements are represented by the curves (no deviations are visible on this scale).

[22] The viscosity of *n*-propyl alcohol as a function of pressure has been determined by P. W. Bridgman, *The Physics of High Pressure* (G. Bell and Sons, Ltd., London, 1949), pp. 330–356.

[23] See for example R. J. Roark, *Formulas for Stress and Strain* (McGraw-Hill Book Company, Inc., New York, 1943), p. 264.

[24] Ashcroft Gauge Tester 1312–50, Manning, Maxwell and Moore, Inc., Stratford, Connecticut.

[25] O. C. Bridgeman, J. Am. Chem. Soc. **49**, 1174 (1927).

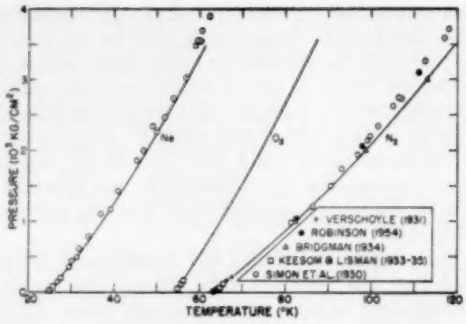

FIG. 4. Melting curves of Ne, O_2, and N_2. Present measurements are represented by the curves (no deviations are visible on this scale).

pressures were calculated from elastic theory. Pressures measured with this gauge were accurate to within 0.05 percent. A comparison of the commercial pistion gauge with the controlled-clearance gauge at 350 kg/cm² showed no significant deviation.

(*b*) *Bourdon Helix Gauge*

A 45-cm length of 0.69-mm o.d. by 0.25-mm i.d., Type 347, stainless steel capillary tubing was flattened by rolling until its major diameter was 1.5 times the minor diameter. The flattened tubing was then soldered shut at one end and coiled into a 2-cm diameter helix. The helix was fixed to a support just above the flattened section so that the closed end was free to describe angular rotation as a function of pressure. Such rotation was observed by means of a mirror, telescope, and scale. Scale deflections could be read to 0.1 mm which corresponded to a 0.2- or 0.3-kg/cm² pressure change in the helix gauge. This fixed the limit of resolution for all freezing- and melting-pressure determinations.

The helix gauge was initially pressure-seasoned at 3900 kg/cm², then calibrated *in situ* with He against the free-piston gauge. The calibration changed somewhat with time due to zero shifts, but the helix gauge was used to approximate absolute pressures only when the high-pressure system was charged initially from the cryogenic pump or subsequently bled to a lower range of pressures. Its primary function was that of sensing small pressure changes.

Response of the Bourdon helix gauge to pressure changes in the piston gauge became noticeably slower at low pressures. This was caused by the smaller density and larger compressibility of communicating gases in the capillary loop and resulted in somewhat more uncertain melting- and freezing-pressure determinations in the low-pressure region. At pressures greater than 350 kg/cm², the response was essentially instantaneous.

3. RESULTS

Putting 240 melting points into tabular form seemed impracticable; therefore, the measurements are given

herein graphically and analytically. Figures 3 and 4 show the character of the melting curves in general and the comparison of our data (represented without visible deviations by the drawn curves) with those of other observers. Table II gives the results of fitting by least squares our measured pressures and temperatures to the melting equation advocated by Simon[1] and to be discussed later as Eq. (2): the constants, the pressure range of application, the root-mean-square deviation, and the number of points fitted. Figures 5 and 6 show the difference between measured and equation-computed pressures as a function of pressure. Of the three types of O_2 measured, only the results for the purest are reported in the table and figures.

Following the suggestion of Bridgman[5] that there should occur a transition point in solid N_2 in the 110–700 kg/cm² region, we measured melting points in this region at about every 30 kg/cm². We found no discontinuity in the slope of the melting curve.

4. DISCUSSION

A. Isotopic Effects

In each pair of isotopes observed here, He^3-He^4 and H_2-D_2, there is an approximate parallelism shown in Fig. 3 with the heavier isotopes displaced to lower pressures. The difference between the helium curves appears to increase from 40 to 120 kg/cm² over the range 2 to 30°K. Between the H_2 and D_2 curves there is a slight decrease in the difference, 170 to 140 kg/cm², in going from 19° to 43°K. The melting data of Clusius and Bartholomé[26] on D_2 up to 100 kg/cm² (21°K) first indicated a constant pressure (but not temperature) difference of ~170 kg/cm² between the H_2 and D_2 curves. Chester and Dugdale[9] reported a constant difference of 170±6 kg/cm² over the 25 to 57°K range. (Since they gave no absolute values, their results do not appear on our graph.) Unfortunately, we could not extend our measurements on H_2 and D_2 to 3500 kg/cm², nor include T_2, both of which were our intentions.[27]

TABLE II. Constants in the Simon melting equation, $P_m = a + bT^c$.

	a	b	c	P range kg/cm²	$\left[\frac{\Sigma(P-P_m)^2}{n}\right]^{\frac{1}{2}}$	n [a]
He^3	25.16	20.08201	1.517083	76–3500	2.68	61
He^4	−17.80	17.31457	1.555414	37–3500	3.87	68
H_2	−270.52	2.534870	1.764739	0–1920	3.57	17
D_2	−418.29	1.812821	1.855812	0–1530	2.58	14
Ne	−1057.99	6.289415	1.599916	0–3500	4.91	37
N_2	−1638.30	0.976780	1.791000	0–3600	1.75	26
O_2	−2786.83	2.635754	1.742594	0–3600	5.09	17

[a] n = number of fitted points.

[26] K. Clusius and E. Bartholomé, Z. physik. Chem. **B30**, 237 (1935).

[27] Among the readily available metals, we could not find any which would contain H_2 above 2000 kg/cm² in the Bourdon helical coil of rolled capillary necessary for determining small pressure changes. The capillary tubing used throughout to contain the high-pressure gases was Type 347 stainless steel, supposedly resistant to H_2 embrittlement. In other apparatus, the unrolled and uncoiled capillary withstood H_2 pressures of 3200 kg/cm² for at least a day and 2500 kg/cm² for at least a month. But in rolled and coiled form the capillary burst within a few minutes at H_2 pressures slightly greater than 2000 kg/cm². A similar effect resulted from using a capillary of the same steel but with heavier wall (0.79 mm o.d., 0.15 mm i.d.). A hard-drawn *K*-monel capillary (0.79 mm o.d., 0.33 mm i.d., manufacturer's specification of 3200 kg/cm² working pressure) also failed at 2300 kg/cm², probably purely the result of insufficient strength. Therefore, further measurements on the hydrogens will have to be delayed until we find a suitable substitute for the present coil gage.

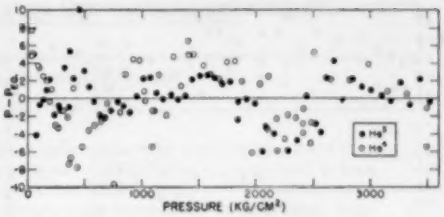

FIG. 5. Deviations of observed melting pressures from Simon equation.

B. Comparison of Present Measurements with Those of Other Observers

Also shown in Figs. 3 and 4 are results of other observers. The data of Simon, Ruhemann, and Edwards[1,2] show fair agreement with our He^4 results, less with our H_2 and Ne data, and give distinctly higher pressures than our N_2 curve. The recent work of Dugdale and and Simon[8] on He^4 up to 800 kg/cm² agrees with ours within ±5 kg/cm². Other observations, up to ~200 kg/cm², on He^4 by Keesom,[28] on Ne, O_2, and N_2 by Keesom and Lisman,[29] and on N_2 by Verschoyle,[30] also agree with ours. The only previous measurements on He^3, by Osborne, Abraham, and Weinstock,[14] covered 0.5 to 1.5°K. Below 0.5°, their melting curve approached 29.3 atmos. corresponding to the constant pressure reached by He^4 at somewhat higher temperatures. As well as we can presently determine, our data, down to 1.9°, meet theirs smoothly.

Since both Bridgman[5] and Robinson[6] gave their published results on N_2 as smoothed, we cannot examine the reliability of the individual measurements but must be content with the trends shown by their measurements. The status of the N_2 melting curve is now as follows: Simon *et al.*,[2] using the blocked-capillary technique, and Robinson,[6] using the moving-pellet method, agree with each other and give pressures 8 percent higher than the results of Bridgman,[5] using the volume-discontinuity criterion, and of our observations, using the blocked-capillary technique. Bridgman's smoothed data agree with ours to 5 kg/cm², thereby negating his objection to the blocked-capillary technique.

[28] W. H. Keesom, Leiden Comm. No. 184b (1926).

[29] W. H. Keesom and J. H. C. Lisman, Physica **1**, 735 (1934) and **2**, 839, 901 (1935); Proc. Acad. Sci. Amsterdam **36**, 378 (1933) and **38**, 808 (1935).

[30] T. T. H. Verschoyle, Trans. Roy. Soc. (London) **A230**, 200 (1931).

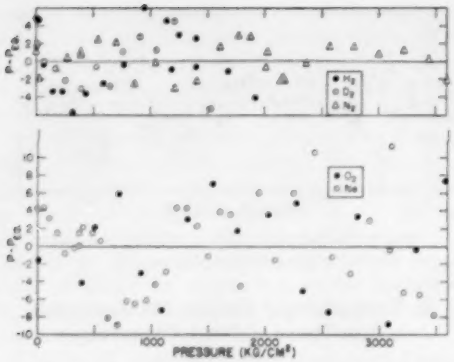

FIG. 6. Deviations of observed melting pressures from Simon equation.

C. Simon Melting Equation

Simon,[1,2,8,10] Lennard-Jones and Devonshire,[12] de Boer,[13] Domb,[21] and Salter[22] have advocated, on empirical and theoretical grounds, a universal melting formula

$$P/\alpha=(T/T_0)^c-1, \tag{1}$$

in which α is related to the "internal pressure" of the solid, T_0 to the triple-point temperature, and c to the intermolecular potential. The formula has, indeed, been successful in expressing all the measurements made on the low-boiling elements. We undertook fitting our data by the method of least squares, minimizing $\sum(P-P_{eq})^2$, to the empirical form of Eq. (1)

$$P=a+bT^c, \tag{2}$$

and to a simple quadratic

$$P=A+BT+CT^2. \tag{3}$$

Compared with Eq. (3), Eq. (2) gave a much better fit for He^3 and He^4, moderately better for H_2, D_2 and Ne, and about equally as good for N_2 and O_2. As shown in Figs. 5 and 6, the deviations of our data from Eq. (2) show some definite oscillations, indicating that minor corrections should be made to the equation. In the case of the heliums, the different characters of the deviation plots at low pressures reflect the different temperatures at which the pressures level off to constant values.

In spite of the generally good agreement between measurement and Eq. (2), we cannot consider any one set of the constants a, b, and c unique. With proper compensation between terms, we could vary the constants considerably without affecting $\sum(P-P_{eq})^2$ appreciably, and with different sets of data we could get significant variations in the best-fitting constants. Therefore, we cannot attach much quantitative significance to the relations between the empirical constants and the fundamental properties noted in Eq. (1). On the other hand, it is difficult to disregard the positive value of a for He^3, which would mean, on the basis of Eq. (1), that the "internal pressure" is negative or that the isothermal increase of volume causes a decrease in the internal energy of the solid.

D. Unusual Melting-Freezing Transition in O_2

A rather speculative conclusion we reach is that there must be something unique in the melting-freezing transition in O_2. For all the other substances observed, we found the initial freezing pressure to be within 1 percent of the melting pressure and could easily bring the two to within 1 kg/cm² by the previously described procedure. But for O_2, the initial freezing pressure was usually 10 percent higher than the melting pressure, which remained fairly constant with alternate meltings and freezings; then only by considerable manipulation could the superpressuring be removed. It does not seem possible to blame this effect entirely on impurities. For example, the Ne and N_2 were more impure than some of the other substances (see 2-B) yet gave no anomalous reversibility; in fact the N_2 was remarkable in its overall reproducibility and adherence to the Simon melting equation. Moreover, the three types of O_2 that we observed showed no definite variation in reversibility although they gave three different melting curves.[23] We surmise there is some connection between the melting-freezing characteristics as observed in the present work and the behavior of the N_2 and O_2 impurities in a hydrogen liquefier. As is often observed in the liquefier, solid N_2 readily blows through the expansion valve while solid O_2 usually plugs the valve.

5. ACKNOWLEDGMENTS

We wish to thank the following persons who contributed to this research: Frederick J. Edeskuty for his large part in the development of the controlled-clearance piston gauge and for assistance in observations; Robert Chrisman for his skilful fabrication of the piston gauge; Isaac Valdez and Guadalupe Garcia for assistance in observations; and Max Goldstein for assistance in computations.

[21] C. Domb, Phil. Mag. **42**, 1316 (1951).
[22] L. Salter, Phil. Mag. **45**, 369 (1954).

[23] The O_2 and 0.3 percent H_2 curve was 1 to 2 percent higher in pressure, while the O_2 and 0.14 percent. A curve was ½ percent lower in pressure than the curve of the purest O_2. This result is fairly consistent with the expected types of solid phase: single component and solid solution with H_2 and A, respectively.

Magnetic Susceptibility of Indium Antimonide

D. K. Stevens and J. H. Crawford, Jr.
Oak Ridge National Laboratory, Oak Ridge, Tennessee

(Received March 31, 1955)

The magnetic susceptibility of both *n*- and *p*-type InSb has been measured by the Faraday method from 65°K to 650°K. The carrier contribution has been obtained by subtracting the lattice component in both the intrinsic range and the extrinsic range. These data indicate that the energy gap at 0°K is 0.262 ev and that the electron effective mass is 0.028 m_0. The hole contribution to the susceptibility in the extrinsic range for the *p*-type specimen used was too small to permit a determination of the effective mass of holes.

THE magnetic susceptibility of several *n*- and *p*-type single crystals of InSb[1] have been measured by the Faraday method from 68°K to 650°K. The results of these measurements[2] are shown in Fig. 1. In specimen *N*-1 the extrinsic electron concentration $n_0 = 1.6\times10^{16}$ cm^{-3}, in *N*-2 $n_0\simeq4\times10^{14}$ cm^{-3}, and in *P*-1 the extrinsic hole concentration $p_0=1.1\times10^{16}$ cm^{-3}.

It can be shown[3] that the susceptibility of a semiconductor can be written as the sum of three components: the diamagnetic lattice contribution χ_L, the paramagnetic contribution of impurity atoms χ_I containing unpaired electrons, and the contribution of the carriers χ_c. Since the impurity content of the specimens is too small to contribute significantly to the susceptibility, we are concerned here only with χ_L, which is usually only slightly temperature dependent, and χ_c. In the range of classical behavior,

$$\chi_c=(\beta^2/3\rho kT)n(3-f_e^2) \qquad (1)$$

for electrons, a similar expression holding for holes. Here, β is the Bohr magneton, ρ the density of the crystal, n the electron concentration, and $f_e=m_0/m_e^{(M)}$, where m_0 is the electron rest mass and $m_e^{(M)}$ is the effective electron mass averaged appropriately for motion in the magnetic field.[4] In the case of appreciable carrier degeneracy Eq. (1) gives too large a value for χ_c. For classical intrinsic behavior the carrier contribution is

$$\chi_c=CT^{\frac{1}{2}}\left[\frac{m_e^{(N)}m_h^{(N)}}{m_0^2}\right]^{\frac{1}{2}}e^{-E_g/2kT}\left[6-f_e^2-f_h^2\right], \qquad (2)$$

where $C=2\beta^2(2\pi m_0)^{\frac{1}{2}}k^{\frac{1}{2}}/3\rho h^3$ and $E_g=E_g^0+BT$.

In view of Eq. (2), the rapid increase in diamagnetism above 200°K exhibited by the curves in Fig. 1 is attributed to intrinsic ionization. The maximum at 600°K is probably due to two effects: (1) the onset of carrier degeneracy which in itself would not cause a maximum and (2) a temperature dependence of χ_L similar to that observed in Ge[5] and Si,[6] i.e., decreasing diamagnetism with increasing temperature. From Eq. (2), it is evident that a plot of $\log(\chi_c/T^{\frac{1}{2}})$ *vs* $1/T$ should yield a straight line of slope $E_g^0/2k$. Such a plot is shown in Fig. 2 for *N*-2. In order to obtain χ_c, it was assumed that χ_L is temperature independent and is given by the low-temperature value of χ in Fig. 1. The curve is indeed linear over most of the range with a slope corresponding to $E_g^0=0.262$ ev, in reasonable agreement with values obtained from electrical measurements.[7,8] Because of the assumption concerning χ_L, this value may be somewhat small.

The curve for *N*-1 in Fig. 1 shows the extrinsic contribution at low temperature (<200°K). Because of

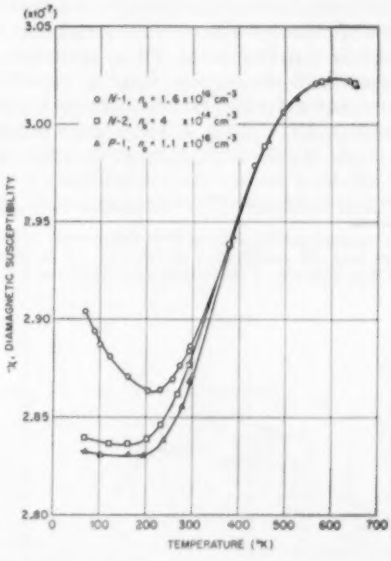

FIG. 1. Diamagnetic susceptibility as a function of absolute temperature for three specimens of InSb.

[1] We are indebted to H. J. Hrostowski and M. Tanenbaum of Bell Telephone Laboratories for these specimens.

[2] The relative precision of points on a given curve is better than ±0.1 percent. The absolute precision, relative to the reported value of O_2 gas at N.T.P. is not better than ±0.5 percent. For comparison purposes the curves were adjusted to correspondence at 600°K.

[3] G. Busch and E. Mooser, Helv. Phys. Acta **26**, 611 (1953).

[4] $m^{(M)}$ becomes identical with the density of states mass $m^{(N)}$ only when the energy surfaces are spheres in *K*-space and the bands are nondegenerate.

[5] D. K. Stevens and J. H. Crawford, Jr., Phys. Rev. **92**, 1065 (1953).

[6] D. K. Stevens (unpublished data).

[7] M. Tanenbaum and J. P. Maita, Phys. Rev. **91**, 1009 (1953).

[8] Breckenridge, Blunt, Hosler, Frederikse, Becker, and Oshinsky, Phys. Rev. **96**, 571 (1954).

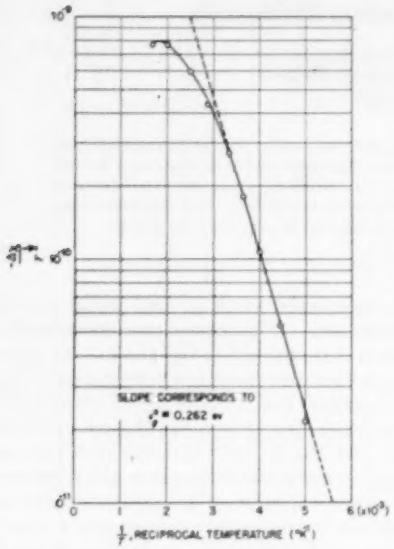

FIG. 2. Carrier susceptibility divided by $T^{\frac{3}{2}}$, $(\Delta\chi T^{-\frac{3}{2}})$, as a function of reciprocal temperature in the intrinsic range for sample N-2.

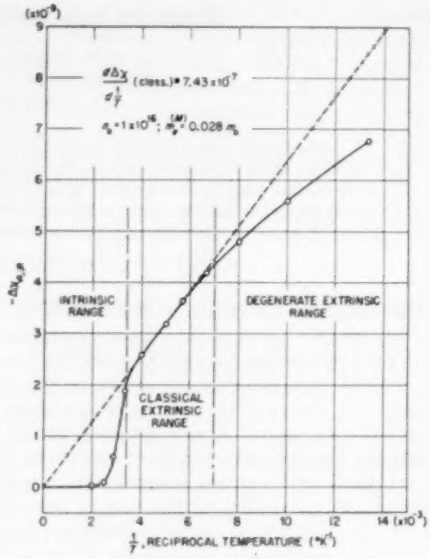

FIG. 3. $-\Delta\chi_{n,p} = (\chi_{P\text{-}1} - \chi_{N\text{-}1})$ as a function of reciprocal temperature.

the smaller temperature dependence of χ_e and the expected temperature dependence of χ_L, χ_e cannot be obtained in this case as was done for the intrinsic contribution. However, because of the larger hole mass,[9] the extrinsic contribution of N-1 is given to a good approximation in the extrinsic range by the difference in the curves for N-1 and P-1. This difference is plotted as a function of $1/T$ in Fig. 3. Three ranges of behavior are evident: (1) the intrinsic range in which the extrinsic difference between the two specimens is reduced by intrinsic ionization, (2) the approximately classical extrinsic range due only to N-1, and (3) the extrinsic range in which degeneracy becomes appreciable. It is evident from Eq. (1) that the slope of the χ_e vs $1/T$ curve is proportional to $m_e^{(M)}$ in the classical extrinsic range. From Fig. 3, this corresponds to $m_e^{(M)} = 0.028 m_0$. This value is somewhat smaller than that determined electrically.[8] A similar analysis was made for the difference between N-1 and N-2, yielding $m_e^{(M)} = 0.032 m_0$. Because of the higher purity of N-2 than P-1, the intrinsic range extended to a much lower temperature. Consequently, the slope was obtained on a portion of the curve deeper in the degenerate range which would give too small a slope and too large a value of $m_e^{(M)}$. Hence the first value is the most reliable.

[9] The reported mobility ratio of 85 in this material (reference 7) indicates that the contribution of holes in P-1 is perhaps no greater than 2 percent of the electron contribution in N-1.

Electrical Conductivity Induced in MgO Crystals by 1.3-Mev Electron Bombardment*

M. A. Pomerantz, R. A. Shatas, and J. F. Marshall
Bartol Research Foundation of The Franklin Institute, Swarthmore, Pennsylvania

(Received March 8, 1955)

Currents induced by the passage of a pulsed beam of essentially monoenergetic 1.3-Mev electrons through thin single crystals of MgO have been observed. The bombardment-induced current is proportional to the applied voltage in accordance with theoretical expectation. The lifetime of the charge carriers before trapping is approximately 3×10^{-11} sec.

CONDUCTIVITY pulses arising from the passage of ionizing particles through various crystals have been observed by a number of investigators seeking materials suitable for application as solid conduction counters.[1] Bombardment-induced currents in very thin dielectric films,[2] in zinc blende crystals,[3] and in diamond[4] have also been measured. Thin samples of germanium were bombarded by 340-kev electrons from an electrostatic generator in 1-μsec pulses, and a variation of the resistance as a function of time was observed.[5] The only comprehensive series of experiments from the point of view of the properties of solids were performed by McKay,[4] who bombarded a diamond with electrons having energies up to 14 kev. In this case, the range of the primary electrons is very short compared with the thickness of the target.

By irradiating a thin target with 1.3-Mev electrons, it has been possible to observe currents induced by the passage of essentially monoenergetic primaries through a single crystal of MgO. The collimated beam from the linear accelerator, in the form of 1-μsec rectangular pulses, impinges upon the specimen and is stopped in a carbon trap after emergence. Internal secondary electrons produced uniformly along the path of the primary through the crystal are thereby lifted from the filled band to the conduction band, where they (and the corresponding holes in the filled band) drift under the influence of the field maintained by the application of a potential difference between very thin silver films deposited on the two faces. As a consequence of trapping of the carriers, the mean drift distance is very short ($<10^{-4}$ cm). When the primary electron beam is on, a flow of charge which may be regarded as a displacement current is observed by means of an integrating micromicroammeter which measures the average crystal current, I_c. The corresponding primary (trap) current, I_p, is measured simultaneously.

Alternatively, the 1-μsec conductivity pulses may be displayed oscillographically. In this case, the relatively small space-charge effects which are observed to occur as a result of the trapping of carriers can be eliminated by reversing the polarity of the crystal voltage, V_c, prior to each successive pulse by means of a flip-flop circuit. No buildup of space charge is visible during an individual microsecond pulse, but a slight decrease in I_c occurs some time after the onset of bombardment if the direction of the field remains constant.

Since the mean drift distance in the direction of the field is short compared with the thickness of the crystal, the bombardment-induced current per unit primary current, $m\equiv I_c/I_p$, is given by

$$m=\delta v V_c \tau/d, \tag{1}$$

where δ is the number of internal secondary electrons raised into the conduction band by one primary electron per cm of path, v is the average mobility of the carriers, V_c is the voltage applied across the target of thickness d, and τ is the lifetime of the carriers before trapping.

A plot of typical data obtained under space-charge-free conditions is shown in Fig. 1. The experimental arrangement is also represented schematically.

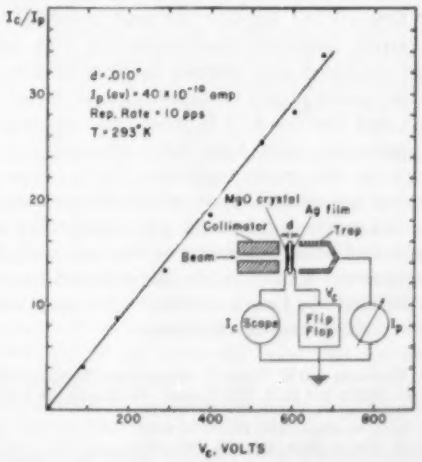

FIG. 1. Plot of bombardment-induced current per unit primary current, $m=I_c/I_p$, as a function of voltage across crystal, V_c. Schematic diagram of the experimental arrangement is also shown.

* Assisted by the Office of Ordnance Research, U. S. Army.

[1] See review articles by R. Hofstadter, Nucleonics **4**, 2 (1949); **5**, 29 (1949); Proc. Inst. Radio Engrs. **38**, 726 (1950); also F. C. Champion in *Progress in Nuclear Physics* (Pergamon Press, Ltd., London, 1953), Vol. 3, Chap. 6.

[2] F. Ansbacher and W. Ehrenberg, Nature **164**, 144 (1949).

[3] M. F. Distad, Phys. Rev. **55**, 1146 (1939).

[4] K. G. McKay, Phys. Rev. **74**, 1606 (1948); **77**, 816 (1950).

[5] K. Lark-Horovitz, in *Semi-Conducting Materials* (Butterworths Scientific Publications, London, 1951), p. 64.

The mobility, v, can be estimated theoretically[6] as about 100 cm/sec per volt/cm for MgO. Similarly the value of δ is approximately 4×10^{5} cm^{-1}. According to Fig. 1, $md/V_c = 1.2\times10^{-4}$ cm volt^{-1}. Hence τ, the lifetime of the carriers, is roughly 3×10^{-11} sec. This is consistent with the fact that, at room temperature, no time effects compatible with a lifetime as long as 10^{-6} sec have been observed in oscillographic display of the pulses.

In accordance with Eq. (1), the bombardment-induced current follows Ohm's law up to the highest applied fields (~200 kv/cm). Furthermore, for peak primary currents ranging from 2.5 μa to 2.5 ma, the induced current is proportional to the primary current.

[6] N. F. Mott and R. W. Gurney, in *Electronic Processes in Ionic Crystals* (Clarendon Press, Oxford, 1950), p. 107; H. Fröhlich and N. F. Mott, Proc. Roy. Soc. (London) **171**, 496 (1939).

PHYSICAL REVIEW VOLUME 99, NUMBER 2 JULY 15, 1955

Effect of Pressure on the Electrical Conductivity of InSb

ROBERT W. KEYES
Westinghouse Research Laboratories, East Pittsburgh, Pennsylvania

(Received March 28, 1955)

The electrical conductivity of InSb has been measured as a function of temperature from −78°C to +300°C and pressures up to 12 000 kg/cm². It is found that the activation energy increases at a rate 15.5×10^{-6} ev/(kg/cm²), that the electron mobility is approximately inversely proportional to the activation energy, and that the hole mobility is independent of pressure. On the basis of these mobility effects it is concluded that the k of the valence band energy extremum is not zero. An examination of the effects of pressure and temperature above 200°C suggests that there are three or four equivalent energy minima in the conduction band.

1. INTRODUCTION

THE unusual properties of the semiconducting compound InSb, in particular the extremely high electron mobility and the partial degeneracy of the electron gas,[1–3] have recently attracted much interest. The significant variations in the energy gaps of semiconductors[4,5] which are produced by hydrostatic pressure suggested that some light might be cast on these unusual properties by a study of their variation with pressure and inspired the work reported here. For certain quantities characteristic of InSb which are not evaluated here reference has been made to the extended investigations of Madelung and Weiss[1] and Austin and McClymont.[2] In some cases constants of the conduction band have been estimated, in the absence of any more acceptable theory, from the perturbed free electron model of the electronic states.[6] The small values of the energy gap and effective mass in InSb lend some plausibility to this approximation. An experiment similar to the one reported here has been performed by Long and Miller[7] over a considerably more restricted range of conditions.

[1] O. Madelung and H. Weiss, Z. Naturforsch. **9a**, 527 (1954).
[2] I. G. Austin and D. R. McClymont, Physica **20**, 1077 (1955).
[3] E. Burstein, Phys. Rev. **93**, 632 (1954).
[4] J. Bardeen, Phys. Rev. **75**, 1777 (1949).
[5] R. W. Keyes, Phys. Rev. **92**, 580 (1953).
[6] C. Kittel, *Introduction to Solid State Physics* (John Wiley and Sons, Inc., New York, 1953).
[7] D. Long and P. H. Miller, Jr., Bull. Am. Phys. Soc. **30**, No. 1, 53 (1955).

2. MATERIAL

n- and *p*-type specimens of InSb were generously provided by Dr. S. W. Kurnick of the Chicago Midway Laboratories. The *n*-type material was of high purity, having in the exhaustion region a low-field Hall constant of −6000 cm³/coul, indicating a donor concentration of 10^{15} cm^{-3}, and a mobility (δ/σ) of 80 000 cm²/volt sec at 77°K. The Hall constant of the *p*-type material at low temperatures was 70 cm³/coul and the acceptor concentration thus was 10^{17} cm^{-3}.

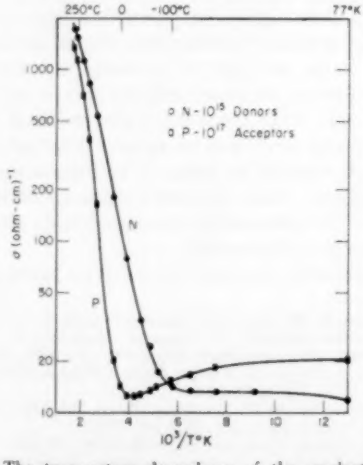

FIG. 1. The temperature dependence of the conductivity at atmospheric pressure of the materials used for this experiment.

The conductivity of both materials at atmospheric pressure is shown in Fig. 1 throughout the temperature range of interest.

3. EXPERIMENTAL

The high-pressure system used was of the usual Bridgman type.[8] The temperature was controlled by immersing the high-pressure vessel containing the sample in a heated or cooled liquid bath. The pressure generating and measuring apparatus was separated from the sample container by a connecting pipe as described by Kurnick.[9] From $-80°C$ to $+100°C$ isopentane was used as the pressure transmitting fluid; from $+100$ to $+300°C$ a silicone oil was used. Pressure was measured in the conventional Bridgman way with a manganin wire resistance gauge calibrated at the freezing point of mercury.

For the determination of the conductivity, samples 1 mm×2 mm×1 cm were cut from the original ingots. Spring contacts of Nichrome wire were used as electrodes. The conductance of the samples was determined by the direct current-potential probe method; a Leeds and Northrup Type K potentiometer was used to measure the potential drop in the sample and the potential across a standard resistor in series with the sample. Readings were taken for both directions of sample current.

4. RESULTS AND DISCUSSION

The principle data are presented in Figs. 2 and 3, which show the conductivity as a function of pressure for several temperatures between $-80°C$ and $+100°C$.

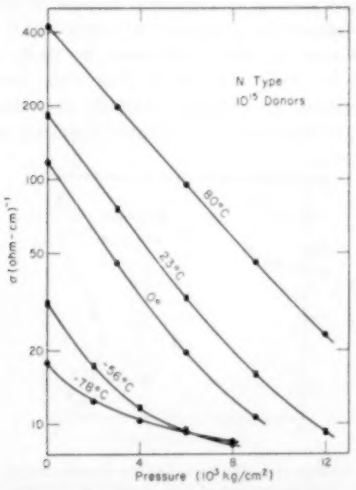

FIG. 2. The conductivity of the n-type InSb as a function of pressure at several temperatures.

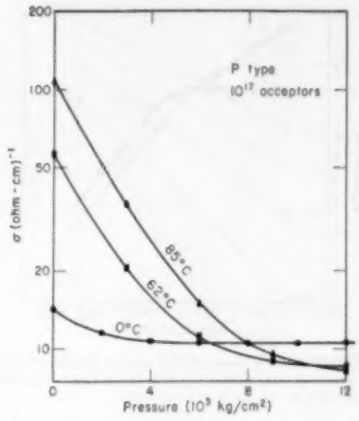

FIG. 3. The conductivity of the p-type InSb as a function of pressure at several temperatures.

The qualitative features of the data are immediately apparent; the initial rapid decrease in the conductivities is indicative of an activation energy which increases with pressure. At all temperatures for which curves are given, an appreciable number of "intrinsic" carriers, or carriers due to electrons excited across the gap from the valence to the conduction band, are present at atmospheric pressure. As the activation energy increases, the number of intrinsic carriers decreases, and the sample approaches the "exhaustion" region of conductivity, in which the number of carriers is constant and is determined by the impurities in the sample. This accounts for the leveling of the curves at high pressure. The P sample at 0°C is in the exhaustion region above 6000 kg/cm², and the constancy of the conductivity from 6000 to 12 000 kg/cm² shows that the hole mobility is independent of pressure

The phenomena in the n-type sample are slightly more complex. Use of the value to be derived for the rate of change of activation energy with pressure shows that at $-78°C$ the conductivity due to intrinsic carriers is negligible above 4000 kg/cm². The continuing decrease of conductivity above this pressure is therefore due to a decreasing electron mobility. It can be seen from Fig. 1 that the donor impurities are just beginning to deionize at 100°K, and a very large change in donor ionization energy would be required if we attribute the decrease in conductivity above 4000 kg/cm² to a change in the number of current carriers. In addition, the constancy of the conductivity from $-78°C$ to $-56°C$ at 8000 kg/cm² reinforces the belief that the donors are completely ionized.

The analysis of the results in terms of a few parameters will be described in some detail, since its understanding is necessary in evaluating the significance of these parameters. The conductivity is given by the formula

$$\sigma = (n\mu_n + p\mu_p)e, \qquad (1)$$

[8] P. W. Bridgman, *Physics of High Pressure* (G. Bell and Sons, London, 1939).
[9] S. W. Kurnick, J. Chem. Phys. **20**, 218 (1952).

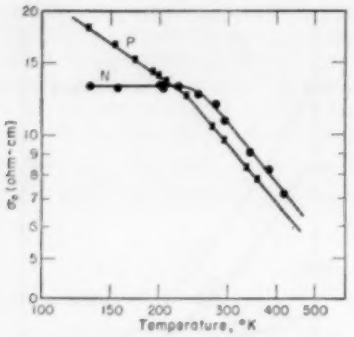

FIG. 4. The quantities $N_D\mu_n e$ and $N_A\mu_p e$ as functions of temperature. The electron mobility referred to is Hall mobility, while the hole mobility is conductivity mobility.

where the carrier densities are determined by

$$np = n_0^2 e^{-W/kT} \tag{2}$$

and

$$n + N_A = p + N_D. \tag{3}$$

In the p-type sample, we have set $N_D = 0$ and in the n-type sample $N_A = 0$, and in addition neglected the conductivity due to the holes in the n-type sample. The impurity concentrations were determined by measurement of the Hall constant in the exhaustion range. The temperature variation of the electron mobility was found by measuring the Hall constant from 77°K to 144°C. The temperature variation of the hole mobility was found from the impurity conductivity, which was in turn determined by fitting the σ *vs* P curves at the high pressure end. These mobility variations are shown by Fig. 4, in which $N_A\mu_p e$ and $N_D\mu_n e$ are plotted against temperature. Data from the low-temperature exhaustion range of the p-type sample are also included.

To take account of pressure variation in Eq. (2), it was rewritten

$$np = n_0^2 e^{-(W_0 + Pv)/kT} = [n_1(p)]^2 e^{-Pv/kT}. \tag{4}$$

The pressure dependence of n_1 is due to the fact that it includes a factor $(m_e^* m_h^*)^{\frac{3}{4}}$ which may depend on the energy gap. Because the hole mobility is independent of pressure we assume that m_h^* is also indepent of pressure. We estimate the pressure variation of m_e^* from the perturbed free electron calculation of energy levels in a periodic potential,[6] according to which $m^* \sim W$. At $P = 0$, $n_1(0)$ is calculated from Eqs. (1), (3), and (4), and then $n_1(P)$ by the formula $n_1(P) = (1 + Pv/W_0)^{\frac{3}{4}} n_1(0)$. In order to represent the mobility variation in terms of a physically significant parameter we write $\mu_n \sim W^{-s}$. A value of W_0 is not obtained in the present experiment and for the purpose of these calculations a value $W_0 = 0.25$ ev has been used throughout, in agreement with thermal energy gap and infrared absorption measurements at low temperatures.

The quantities to be determined are now v and s. At each temperature values of these quantities which gave a reasonable representation of the observed curves were found by trial. The curves drawn in Figs. 2 and 3 were calculated from the selected values of s and v. It was found that a single value of v, namely $v = 15.5 \times 10^{-6}$ ev/(kg/cm²) = 15.3 cm³/mole, was satisfactory for all the data. The necessary values of s were all of the order of one and are shown in Fig. 5.

It should be pointed out that the effect of pressure on the conductivity over most of the region studied is primarily due to the variation of the activation energy and that the calculated value of v is very insensitive to the assumptions made about the variation of mobilities and density of states. These details were presented in order to explain what is meant by s. Values of s are determined most accurately by the data at −78°C and −56°C, where the exhaustion range is attained at high pressure.

5. DISCUSSION OF THE MOBILITY

The large change of electron mobility with pressure suggests that the band separation at the k value characteristic of the electrons has changed by an appreciable fraction, which implies that the separation of the order of the thermal activation energy. On the other hand, the negligible change of hole mobility means that the band separation at the K of the holes is large. Since there is evidence that the electrons have k near zero,[10,11] this means that the holes are not at $k = 0$. Thus the $E(k)$ curves must have roughly the form of Fig. 6, in which the band separation increases rapidly as k goes away from zero because of the small effective mass of the electrons ($m^* = 0.013 m_0$).[10]

It is of some interest to compare the result $\mu \sim W^{-1}$ obtained in the preceding section with theoretical interpretations of mobility. Explicit formulas have been derived for three mechanisms: (1) ionized impurity

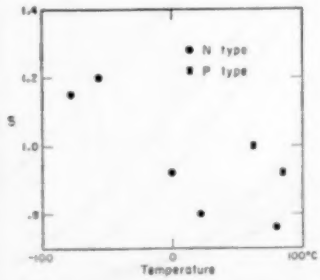

FIG. 5. Values of s, the exponent in the expression $\mu \sim W^{-s}$, obtained by fitting the data of Figs. 2 and 3 in the way described in the text.

[10] Dresselhaus, Kip, Kittel, and Wagoner, Phys. Rev. **98**, 556 (1955).

[11] G. L. Pearson and M. Tannenbaum, Phys. Rev. **90**, 153 (1953).

scattering, (2) neutral impurity scattering,[12] and (3) deformation potential scattering.[13] Dependence of the mobility on the energy gap enters these formulas through the effective mass and the dielectric constant. For the former we assume as previously $m^* \sim W$, for the latter we assume the Moss relationship, $\kappa^2 W = \text{constant}$,[14] where κ is the effective dielectric constant.

(1) The well-known Conwell-Weisskopf formula is

$$\mu = \frac{2^{7/2}\kappa^2 (kT)^{3/2}}{N\pi^{3/2} e^3 m^{*1/2}} \left\{ \log\left[1 + \left(\frac{6\kappa dkT}{e^2} \right)^2 \right] \right\}^{-1}, \qquad (5)$$

and thus, with our assumptions, $\mu \sim W^{-1}$. The exponent $-\frac{3}{2}$ cannot be regarded as inconsistent with the data presented above. Figures 1 and 4 show however that the temperature dependence of the mobility is not correctly described by this formula, and in addition the numerical result for the mobility at 200°K using $N = 10^{15}$ cm^{-3} is $\mu = 3 \times 10^6$ cm^2/volt sec, much larger than the observed value in the n-type sample.

(2) The constancy of the electron mobility over a large range of temperature would be expected according to the formula of Erginsoy,

$$\mu = e\tau/m^* = 8\pi^3 m^* e^3 / 20\kappa N h^3.$$

The pressure dependence of μ according to this formula is $\mu \sim W^1$, a result not in agreement with the data.

(3) The deformation potential formula is

$$\mu T^{3/2} = \left(\frac{(8\pi)^{1/2} e h^4 C}{m^{*5/2} k^{3/2} E_1^2} \right), \qquad (6)$$

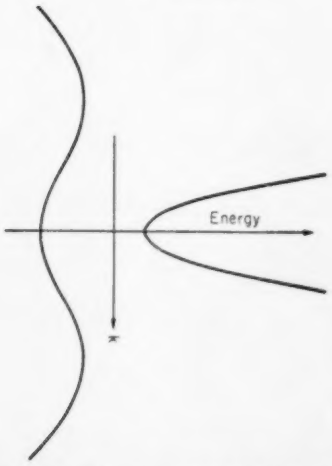

FIG. 6. A dependence of energy on k which explains the variation of the mobilities with pressure and is consistent with the magneto-resistance and cyclotron resonance experiments.

[12] C. Erginsoy, Phys. Rev. **79**, 1013 (1950).
[13] J. Bardeen and W. Shockley, Phys. Rev. **80**, 72 (1950).
[14] T. S. Moss, *Photoconductivity in the Elements* (Academic Press, Inc., New York, 1952).

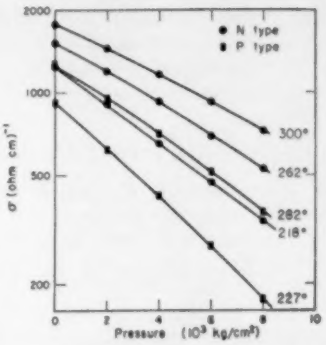

FIG. 7. The conductivity of n- and p-type InSb as a function of pressure at temperatures between 200°C and 300°C.

where C is the elastic constant for longitudinal sound waves and $E_1 = V(dW/dV)$. In the perturbed free electron approximation W is a Fourier coefficient of the potential in which the electrons move. Since this potential is not expected to exhibit any unusual features when W is small the pressure variation of E_1 should not be marked. Consequently $\mu \sim W^{-5/2}$, suggesting a somewhat stronger pressure dependence of mobility than that which is actually found.

In order to calculate μ numerically, the elastic constants must be known. An estimation of these by using a Lindemann relation in the form $CV/T_m = \text{constant}$ with C = elastic constant, V = molar volume, T_m = melting temperature to compare InSb with germanium suggests that the elastic constants of InSb are about half those for germanium. Thus, attributing the entire gap variation to the conduction band, we use $E_1 = 6$ ev and $C = 0.75 \times 10^{12}$ dynes/cm^2 and find at 300°K that $\mu = 10^7$ cm^2/volt sec. The main reason for this extremely high value is the small effective mass. Dilation may, of course, shift both band extrema in the same direction, and if $E_{1c} = 60$ ev the calculated mobility is of the correct magnitude. This possibility cannot be definitely rejected.

6. HIGH-TEMPERATURE MEASUREMENTS

Some data obtained up to 8000 kg/cm^2 in the temperature range 200°C–300°C are presented in Fig. 7. Comparison of these curves with those of Figs. 2 and 3 shows that the ressure dependence of the conductivity is distinctly smaller. The reason for this can be seen from the work of Madelung and Weiss,[1] who have concluded that at high temperatures the Fermi level approaches the bottom of the conduction band and the Boltzmann approximation to the Fermi distribution function is not adequate, or, in other words, the electron gas becomes degenerate. In order to confirm and amplify the picture of the high-temperature conductivity formulated by Madelung and Weiss the high-temperature data of Fig. 7 have been examined

closely and an attempt has been made to derive values of some parameters characteristic of InSb which allow a consistent representation of this data.

At high temperatures the equation which determines the Fermi level is

$$N_v g_v \alpha_v^{-\frac{3}{2}} F_{\frac{1}{2}}(-w-\xi) = (\tfrac{1}{2}\sqrt{\pi}) N_A + N_c g_c \alpha_c^{-\frac{3}{2}} F_{\frac{1}{2}}(\xi). \quad (7)$$

(The donor concentration in our samples is entirely negligible at the temperatures in question and has been set equal to zero.) In this equation

$$N_c = 2(2\pi m_c kT/h^2)^{\frac{3}{2}},$$

g_v and g_c are the degeneracies of the extrema of the of the valence band and the conduction band, respectively, and the α's are the effective mass ratios, m_0/m^*, in the case of spherical energy surfaces and more complicated functions of the effective mass tensor which give the density of states in the case of ellipsoidal surfaces. Energies are measured from the bottom of the conduction band; the magnitude of the gap is wkT and the energy of the top of the valence band is $-wkT$. The Fermi level is at energy ξkT. The acceptors are assumed completely ionized. $F_{\frac{1}{2}}(\xi)$ is the Fermi integral, tabulated by McDougall and Stoner.[15] By using the Boltzmann approximation for the holes in the valence band and defining $\gamma = (g_c/g_v)(\alpha_v/\alpha_c)^{\frac{3}{2}}$ and $f = (\sqrt{\pi}) N_A \alpha_c^{\frac{3}{2}} / 2 N_c g_c$, we transform Eq. (7) to

$$e^{-w} = \gamma e^{\xi}[F_{\frac{1}{2}}(\xi) + f]. \quad (8)$$

If an energy-independent mean free path for the electrons is assumed and the hole mobility is neglected, the conductivity is related to the Fermi level[1] by $\sigma = \bar{\sigma} \log(1+e^{\xi})$ with $\bar{\sigma} = N_c \alpha_c^{-\frac{3}{2}} g_c \mu_n$.

Since no temperature dependence of v appeared in the low temperature data, the value derived there, $v = 15.5 \times 10^{-6}$ ev/kg/cm^2, is used here. In view of the scatter of the points of Fig. 5 and the uncertainty of the value of s to be expected theoretically, the introduction of additional parameters to describe the mobility variation would not be meaningful, and the expression $\mu \sim (W_0 + Pv)^{-s}$ is used in this section in the identical form as before, with $W_0 = 0.25$ ev and $s = 1.0$, the arithmetic mean of the values given in Fig. 5.

By using the m^* of reference 10 and an electron mobility $\mu_n = 3 \times 10^4$ cm^2/volt sec at 500°K,[1] we calculate $\bar{\sigma}$ to be $400 g_c$ (ohm cm^{-1}). If $g_c = 1$, the observed conductivity requires that $\xi = +4$, and reconciliation of this value with the infrared energy gap requires $\gamma = 2 \times 10^{-4}$. When the Fermi level is this high the dependence of the conductivity on ξ is very weak, and the conductivity calculated as a function of temperature or pressure varies much too slowly. We therefore conclude that $g_c > 1$ and use $g_c = 3$ in trying to reproduce the pressure effect, since, although higher values are not excluded by the data, very high multiplicity is not to be expected for spherically symmetrical energy surfaces. Another possibility is that the effective mass measured at 4°K is not the correct one to use at high temperatures.

Knowing g_c and N_A allows us to calculate f for the p-type material, while for the n-type material, $f = 0$. Then Eq. (8) can be solved for ξ and the conductivity obtained as a function of γ and w. The rate at which σ changes with pressure depends on γ and on the value of w at $P = 0$. The energy gaps at $P = 0$ which best reproduce the data of Fig. 7 are shown for two choices of γ in Fig. 8. It is seen that $\gamma = 0.02$ gives fair agreement between the gap derived from the N sample and the extrapolated infrared absorption edge of Austin and McClymont,[4] while $\gamma = 0.01$ results in better consistency of the data from the n- and p-type samples. Because the mobility effects discussed previously and the cyclotron resonance experiment[10] suggest considerable complexity in the structure of the valence band extrema, no attempt has been made to draw inferences from the values of α_v and g_v suggested by these values of γ.

7. CONCLUSIONS

The compound InSb is somewhat similar to germanium in the magnitude of the dependence of energy gap on dilation, but the very small effective mass leads to a deformation potential scattering 100 or 1000 times smaller for InSb. However, none of the conventional scattering mechanisms appear to provide sufficient scattering to limit the electron mobilities to the observed values. Adams[16] has pointed out that electron-

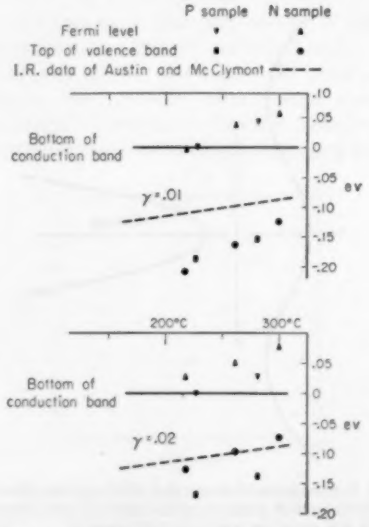

FIG. 8. The values of the energy gap at $P = 0$ and the corresponding Fermi levels which give the best fit to the pressure dependence of the conductivity illustrated in Fig. 7.

[15] J. McDougall and E. C. Stoner, Trans. Roy. Soc. (London) **A237**, 67 (1938).

[16] E. N. Adams (private communication).

hole collisions[17] provide sufficient scattering to limit the mobility to the observed values at high temperatures and may be the dominant mechanism there. Using the estimate of E_1 previously given and the thermal expansion coefficient $\alpha = 14.4 \times 10^{-6}$ deg^{-1} of Mokrowski and Regel,[18] the change of activation energy with temperature due to thermal expansion of the lattice can be calculated. It is 1.0×10^{-4} ev/deg, which is to be compared with the value 2.6×10^{-4} ev/deg derived from the shift of the infrared absorption edge by Austin and McClymont.[2] Even allowing for possible error in the compressibility, a considerable portion of the temperature variation of the gap must be attributed to direct electron-phonon interactions.

[17] F. J. Morin and J. P. Maita, Phys. Rev. **94**, 1525 (1954).
[18] H. P. Mokrowski and A. R. Regel, J. Tech. Phys. (U.S.S.R.) **22**, 1281 (1952).

8. ACKNOWLEDGMENTS

The author is indebted to the Chicago Midway Laboratories and Dr. S. W. Kurnick for the InSb used in this experiment and to Dr. C. Kittel and co-workers at the University of California for communication of their cyclotron resonance results prior to publication. He also wishes to thank Dr. E. N. Adams, Dr. R. L. Longini, and Dr. F. Keffer for critical reviews of the manuscript.

PHYSICAL REVIEW VOLUME 99, NUMBER 2 JULY 15, 1955

Distribution of Electrons Scattered by Gold*

L. Marton, J. Arol Simpson and T. F. McCraw
National Bureau of Standards, Washington, D. C.
(Received April 14, 1955)

The distribution in energy and angle of 20-kev electrons scattered by gold has been measured. The energy resolution is better than 0.1 percent and the angular resolution better than 10^{-3} radian. Data are presented for gold of different thickness and degree of crystal orientation and for grazing angle reflection.

ALTHOUGH the interactions of electrons with matter have been extensively studied in the past, most of the interest has been directed either to incident energies so high that the most important contribution to the scattering is nuclear, or to energies of at most a few hundred electron volts where secondary emission is of primary interest. With a few notable exceptions,[1] the range of energies from a few kev to one hundred kev has until recently been neglected. Yet this region of the energy spectrum can give information on the imaginary part of the complex dielectric constant used in the semi-classical theory of stopping power, or from another point of view, information on the density effects on the elementary interactions processes. This knowledge is of interest both to the solid state and radiation physics. Interest in this region was revived in Germany just after the war when Mollenstedt[2] with the aid of an improved electrostatic analyzer, began to study the energy losses of electrons in the forward direction (0–10^{-3} rad). This work was extended by the studies of Marton and Leder[3] in America and workers in Japan and Germany.[4] The interest was centered on the characteristic losses of the scatterers which are more or less discrete losses ranging from 1 to 100 electron volts. With a modified Mollenstedt apparatus Leonhard[5] and Watanabe[6] have extended these measurements to include the distribution in angle. The electrostatic analyzer when used in this manner is somewhat unsatisfactory, being nonlinear in energy and intensity and having a poorly defined acceptance angle.

To overcome these limitations we have constructed an apparatus using a double-focusing magnetic analyzer and the geometry shown in Fig. 1. This instrument, which will be described in detail elsewhere, is automatic in operation and gives a record of the energy spectrum of the scattered electrons with an energy resolution of better than 0.1 percent at angular intervals of less than 10^{-3} radian over a range of 300 degrees. The relative value

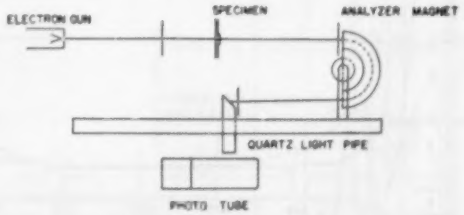

FIG. 1. Electron trajectory showing relative placement of principal elements of the scattering instrument.

* This work was in part supported by the Office of Naval Research.
[1] G. Ruthemann, Naturwiss. **29**, 648 (1941); Ann. Physik (6) **2**, 113 (1948); W. Lang, Optik **3**, 233 (1948).
[2] G. Mollenstedt, Optik **5**, 499 (1949); **9**, 473 (1952).
[3] L. Marton and L. B. Leder, Phys. Rev. **94**, 203 (1954); L. B. Leder and L. Marton, Phys. Rev. **95**, 1345 (1954).
[4] H. Watanabe, J. Phys. Soc. Japan **9**, 920 (1954); **9**, 1035 (1954); Phys. Rev. **95**, 1684 (1954); W. Klein, Optik **11**, 226 (1954).
[5] F. Leonhard, Z. Naturforsch. **99**, 727 (1954).
[6] H. Watanabe (private communication).

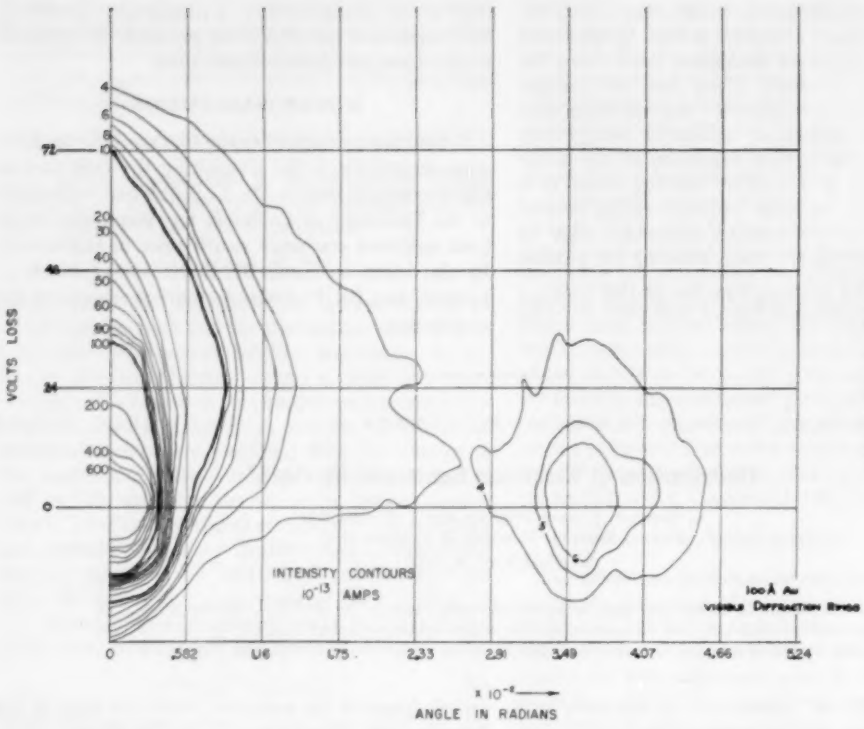

FIG. 2. Cartographic plot of the distribution of 20-kev electrons scattered by 100 A polycrystalline gold. The abscissa is angle, the ordinate energy loss in ev, and the contours of equal intensity, in 10^{-13} ampere.

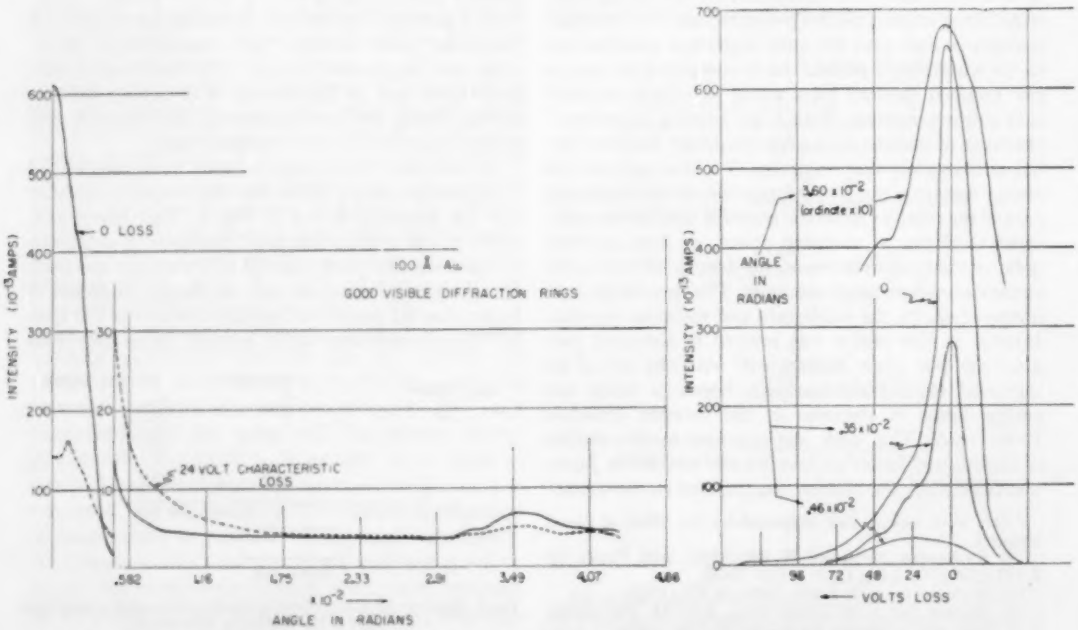

FIG. 3. Left: Graph of scattered intensity as a function of angle. Both elastic and 24-ev characteristic energy loss curves are shown. Right: Graph of scattered intensity as a function of energy loss in ev at selected angles. Polycrystalline 100 A gold, 20-kev incident energy.

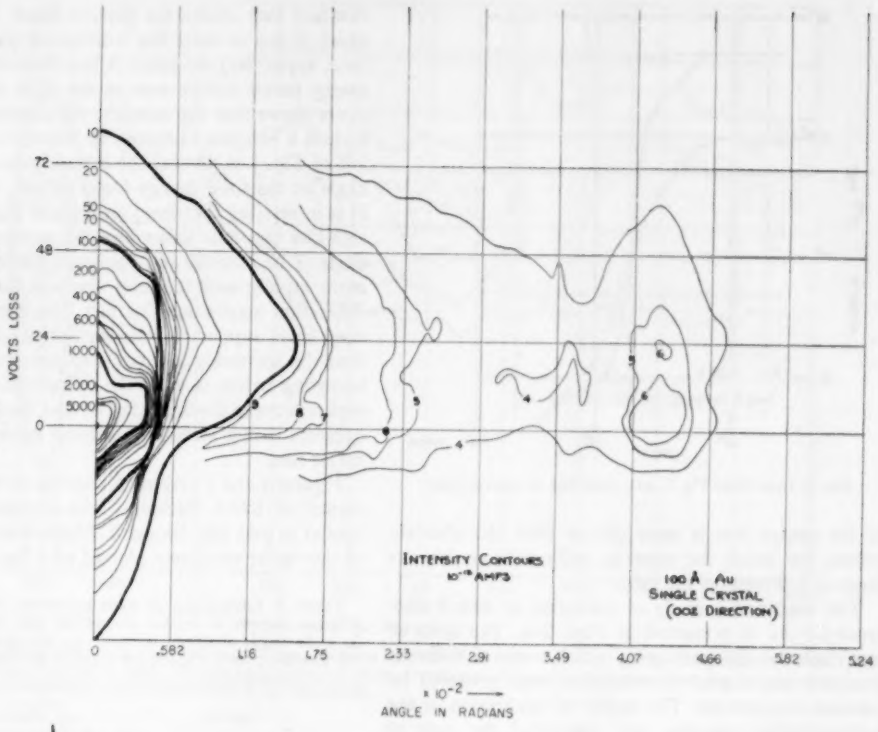

FIG. 4. Cartographic plot of the distribution of 20-kev electrons scattered by 100 A single crystal gold. The abscissa is angle, the ordinate energy loss in ev, and the contours of equal intensity in 10^{-13} ampere.

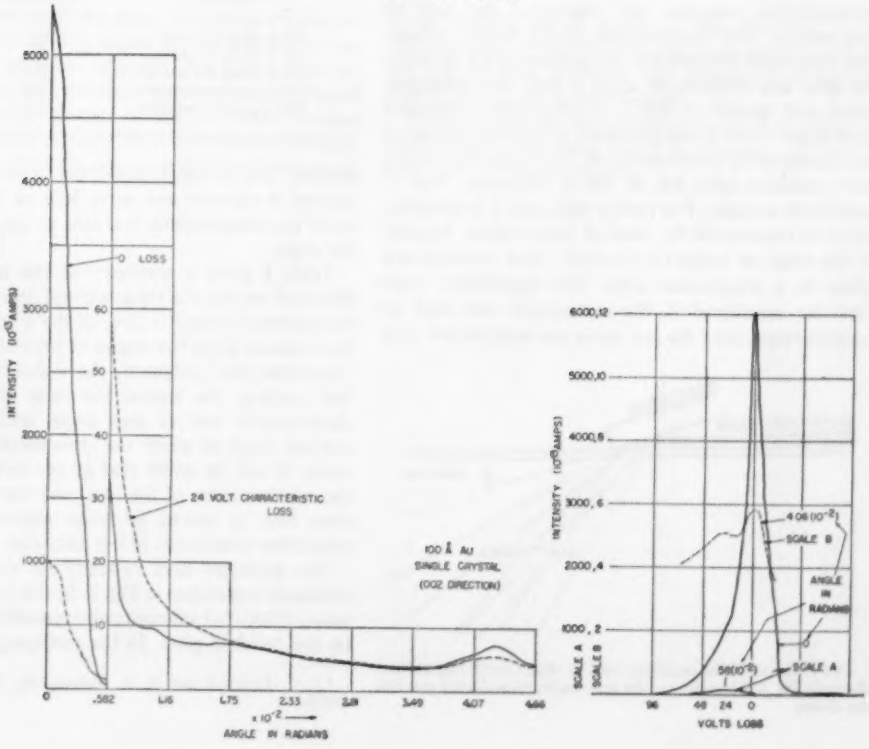

FIG. 5. Left: Graph of scattered intensity as a function of angle. Both elastic and 24-ev characteristic energy loss curves are shown. Right: Graph of scattered intensity as a function of energy loss in ev at selected angles. Single crystal 10 A0 gold, 20-kev incident energy.

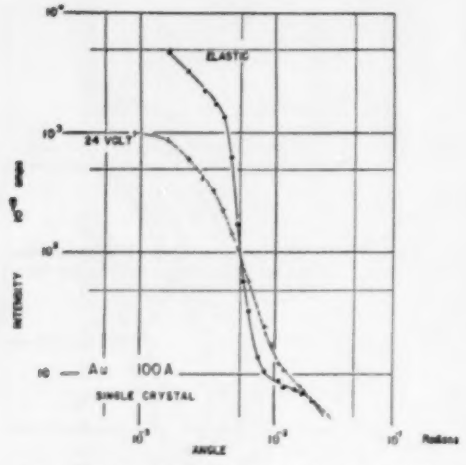

FIG. 6. Data from Fig. 5, left, replotted on log-log scale.

of the energy loss is more precise than the absolute values, for which the error in calibration may be as large as 5 percent of the loss.

The results of a study of scattering of 20-kev electrons by Au is presented in Figs. 2–6. The films of spectrochemically pure gold, which were of different thickness and degree of orientation, were prepared by vacuum evaporation. The degree of orientation in the polycrystalline samples was controlled by rate of evaporation, slow evaporation giving larger crystallites than rapid evaporation. To prepare single crystals, the gold was evaporated upon a rock salt substrate which was heated to 400°C. Under these conditions good single crystals are produced by epitaxy. Figure 2 is a cartographic presentation of the scattering from a polycrystalline gold foil of 100 A thickness. The X coordinate is angle, Y is energy loss, and Z is intensity which is represented by lines of equal value. Because of the range of intensities covered, these contours are given on a logarithmic scale. This logarithmic scale must be considered if the cartographs are read as contour maps, since the low levels are emphasized. It is this fact that makes the portion below the zero axis, which is due to finite line widths and phosphor decay time, appear so prominent. A less distorted view of the energy profile can be seen on the right of Fig. 3. This figure shows that the intensity distribution on a linear scale is a function of energy at selected angles. To the left of Fig. 3 is plotted the intensity as a function of angle at the fixed energy losses of zero ev and 24 ev. It is interesting that from an initially higher value the zero-loss line falls below the characteristic loss at an angle of 20 minutes and continues below until it rises more rapidly and recrosses the loss line at the first diffraction maximum. The fact that the loss line also rises lends support to the suggestion of Farnsworth[7] that the scattering is a two-step process with the loss occurring before or after the diffraction. The long flat region between the initial fall-off and the first diffraction suggests that a screened Coulomb interaction plays a major role.

Figures 4 and 5 present similar data for a gold single crystal of 100-A thickness. The scattering pattern is similar to that just discussed. Figure 6 shows the fall-off of the center maximum plotted on a log log scale. It is obvious that no simple power law is obeyed; the linear portion of the zero-loss curve falls as the sixth power while the characteristic loss falls as the third power of the angle.

TABLE I. Comparison of some scattering characteristics for different degrees of crystal orientation and thickness of gold. I_{el} is the elastic scattering intensity, I_{ch} the characteristic energy loss intensity, and θ the angular position at which $I_{el}/I_{ch}=1$.

Gold film	I_{el}/I_{ch} at zero degrees	θ ($\times 10^{-3}$ radian) at $I_{el}/I_{ch}=1$
100 A single crystal	6	4.9
100 A large crystallite	4	3.9
100 A small crystallite	5	5.5
200 A small crystallite	3.6	4.4
400 A small crystallite	2.9	3.1

Table I gives a summary of the most prominent effects of varying the thickness and degree of crystalline orientation (crystallite size) of the scattering foil. The first column gives the degree of crystalline orientation (crystallite size) judged by the visibility of the diffraction pattern, the second the ratio of the elastic to characteristic loss at zero angle, and the third the smallest angle at which the cross sections are of equal value. It will be noted that as the thickness increases the relative value of the loss peak increases while the cross over is moved to lower angles. The effect of crystalline orientation is less clear-cut.

The geometry used to study Au at almost grazing incidence is sketched in Fig. 7. In this case the specimen was a thick (>1 micron) polycrystalline film deposited on fire polished glass. In the cartograph of Fig. 8, the

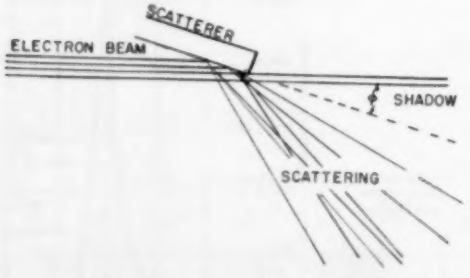

FIG. 7. Sketch of the geometry used to obtain scattering pattern shown in Fig. 8. The source of the zero angle and scattered maxima are shown.

[7] J. C. Turnbull and H. E. Farnsworth, Phys. Rev. **54**, 509 (1938).

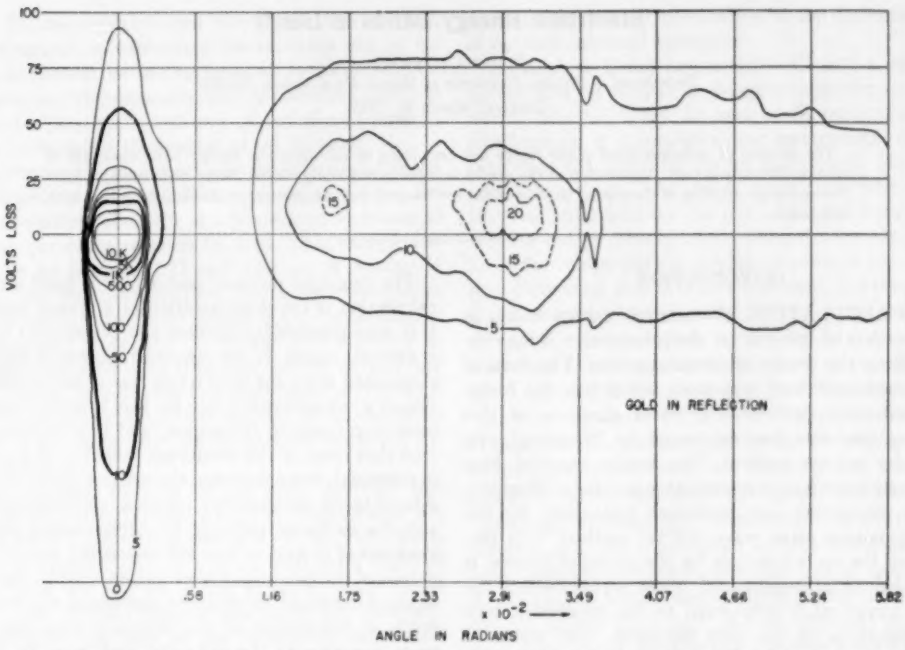

FIG. 8. Cartographic plot of reflection of 20-kev electrons by gold. Note lack of marked specular reflection and wide energy spread of scattered beam. The extreme extension of the contours at zero angle to regions above the zero loss is a result of finite detector time constant and is not significant.

unscattered portion of the initial beam can be seen to the left followed by the region in the shadow of the sample and the region of reflection. It will be noted that even at less than 10^{-2} radian there is no clearly defined specular reflection. Neither of the two small maxima can be definitely identified. The most notable difference between this and the transmission samples is the much wider distribution of energy in the scattered beam. This broadening is to be expected since multiple events are now far more probable. The broadening in angular distribution is similarly explained.

These studies are being extended to other materials while efforts are being made to increase the energy resolution of the instrument.

Electronic Energy Bands in Iron*†

JOSEPH CALLAWAY‡
Department of Physics, University of Miami, Coral Gables, Florida
(Received March 25, 1955)

The method of orthogonalized plane waves has been used to calculate the energy band structure of valence electrons in iron. Application of the results is made to the energy band theory of ferromagnetism. The exchange splitting of the energy bands and the tendency to ferromagnetism at absolute zero have been calculated.

INTRODUCTION

A CALCULATION of electronic energy bands in iron is of interest for the information it may reveal about the theory of ferromagnetism. The form of iron considered here is α iron, which has the body-centered cubic lattice.[1] The band structure of this form of iron was first calculated by Manning,[2] who used the cellular method. The results reported here bear little quantitative resemblance to those of Manning.

The calculation was performed principally by the orthogonalized plane wave (OPW) method.[3,4] In this method, the wave function for the states of interest is expanded in orthogonalized plane waves, which are plane waves made orthogonal to the assumed known eigenfunctions of the core electrons. The states of interest here are those formed from the $3d$ and $4s$ atomic levels. The OPW method requires solution of a determinantal equation of high order and would be impractical if high-speed electronic computing facilities were not available. Success of this method depends on the core functions to which the plane waves are made orthogonal being reasonably close approximations to eigenfunctions of the crystal potential. Because of the inclusion of exchange in the crystal potential where the core functions are formed from a Hartree free atom field, this condition is not satisfied. Consequently the OPW method failed for states of S-like symmetry and these had to be treated by the cellular method.[4] Also, a modification of the OPW method had to be made to obtain reasonable convergence of the expansion for states of D-like symmetry since these are orthogonal by reason of symmetry to all the core eigenfunctions. This is accomplished by adding to the expansion a function having the character of an atomic d function close to any nucleus.[4]

The principal physical problem in a band structure calculation is the determination of a crystal potential. If it were possible to calculate a self-consistent field for a crystal, errors in the assumed potential would be eliminated when the final result was obtained. Calculation of a self-consistent field for iron is impractical with present computing techniques, and it is unfortunately true that some of the results are sensitive to the choice of potential. Some features: the relative positions of the d-band levels at symmetry points in the Brillouin zone, and the exchange splitting of corresponding states of electrons of $+$ and $-$ spin are reasonably insensitive to details of the potential. Other results, such as the width of the d band and the relative position of the $3d$ and $4s$ levels at the center of the Brillouin zone, are much more sensitive to the potential and must be viewed with some reserve.

The calculation can now be outlined briefly. A starting charge density was formed from superposed Hartree charge densities for the d^6s^2 configuration of the free iron atom arranged in the proper crystal lattice. The starting potential was computed from this; exchange effects for a nonmagnetic state were included by means of Slater's free electron approximation to the exchange potential.[5] Convergent OPW expansions were obtained for nine states in the Brillouin zone: Γ_{12}, $\Gamma_{25'}$, Γ_{15}, H_{12}, $H_{25'}$, H_{15}, N_2, N_3, and N_4. An interpolation scheme recently proposed by Slater and Koster[6] was used to extend these results to other states.

The width of the $3d$ band was calculated to be about two electron volts. The separation of the $3d$ levels at the center of the Brillouin zone is considerably smaller than it is at the corners and faces of the zone. The charge density of the $3d$ electrons is more compact than that of the Hartree free atom field. This is due to the inclusion of exchange, and is in agreement with the interpretation of neutron polarization experiments.[7]

The relative position of the $4s$ and $3d$ bands is sensitive to the potential used and is apparently incorrectly given by the potential mentioned. The $4s$ band was predicted to be above the $3d$ band at all points. An improved potential was obtained by assuming seven $3d$ electrons instead of six and by recalculating the exchange potential on the basis of the Hartree-Fock equa-

* Preliminary results were presented at the New York Meeting of the American Physical Society, January 27, 1955 [Phys. Rev. **98**, 1150 (1955)].

† Part of material contained in a thesis submitted to the faculty of Princeton University in partial fulfillment of the requirements for the degree of Doctotor of Philosophy.

‡ National Science Foundation Predoctoral Fellow, 1953–1954.

[1] The lattice parameter is taken to be 2.86645×10^{-8} cm. The radius of the atomic sphere is then 2.667 Bohr units. D. E. Thomas, J. Sci. Instr. **25**, 440 (1948).

[2] M. F. Manning, Phys. Rev. **63**, 190 (1943).

[3] C. Herring, Phys. Rev. **57**, 1169 (1940).

[4] A discussion of some features of the OPW method especially pertinent to this calculation is given by J. Callaway, Phys. Rev. **97**, 933 (1955).

[5] J. C. Slater, Phys. Rev. **81**, 385 (1951).

[6] J. C. Slater and G. F. Koster, Phys. Rev. **94**, 1498 (1954).

[7] J. Steinberger and G. C. Wick, Phys. Rev. **76**, 994 (1949).

tions. It was revealed that the Slater free electron approximation overestimates the exchange energy by about 15 percent for $3d$ electrons and by 20 percent for $4s$ electrons. The improvement in potential taken in first order perturbation theory placed the $4s$ level Γ_1 about 1.4 ev below the bottom of the $3d$ band.

Application was made to the theory of ferromagnetism by calculating from the Hartree-Fock equations the change in potential energy of a $3d$ electron when one $3d$ electron per atom reverses its spin. This energy was found to be between 1.23 and 1.58 ev. A density of states curve was calculated for the unmagnetized state, and the change in kinetic energy upon magnetization was computed to be 0.69 ev. This gives a tendency to ferromagnetism between 0.54 and 0.89 ev at absolute zero. This is considerably too large. Most of the error probably results from underestimation of the change in kinetic energy caused in turn by underestimation of the d-band width.

The exchange splitting of the band structure was considered. Corresponding states of D symmetry are separated by a gap or the order of 3 ev; the S-like levels Γ_1 are separated by about 1 ev. A total band width of 4.1 ev from the bottom of the $4s$ band to the Fermi level in the $3d$ band (magnetized state) was obtained.

Finally, on the basis of this calculation, one would expect a rigorous self-consistent field calculation of the energy levels of electrons in iron would give overlapping d and s bands with a d-band width of the order of that which has been estimated empirically, and would give an energy change on magnetization which might be of the same order as the observed change, or which might be considerably larger (due to neglect of correlation).

CRYSTAL POTENTIAL

The energy band theory of solids is conceptually based on the Hartree-Fock equations. However, it has not been possible to solve the Hartree-Fock equations exactly for a solid. There are two principal difficulties: (1) The effective potential for an electron state $\psi_{\mathbf{k}}{}^i$ (ith irreducible representation of wave vector $\mathbf{k}$) depends on $\psi_{\mathbf{k}}{}^i$ and is different for each state $\psi_{\mathbf{k}}{}^i$. This leads to great complication and is almost never handled exactly. One approximation often used is that each electron moves in the field of an ion. It has also been proposed to simplify the Hartree-Fock equations so that there is a common potential for all states.[5] One convenient method is by means of a free-electron approximation: it is assumed that the exchange potential at any point is determined by the local charge density of electrons of the same spin and is the same as for a free-electron gas of the same density.[5] A somewhat better approximation is to assume that the exchange potential is the same for all states of a given angular momentum and spin,[6] or in the case of a solid, is determined by the predominant angular momentum in the decomposition of $\psi_{\mathbf{k}}{}^i$ into spherical harmonics.

(2) Since it is not practical to calculate a self-consistent field for a solid, a charge distribution or a potential must be chosen. In some cases, particularly the alkali metals, it is possible to use spectroscopic data to determine the potential (or an equivalent). For more complicated cases, recourse is made to a Hartree (or Hartree-Fock) field for the free atom and from this a starting charge density and a potential are computed. Since the charge density around an atom in the crystal may differ from what it is for a free atom, it is sometimes attempted to superpose free atom charge densities arranged on atomic sites in the crystal lattice. The numerical reliability of such procedures is questionable, but it is doubtful whether better methods are available.

In this calculation, free atom charge densities obtained from the Hartree field for the d^6s^2 configuration of atomic iron calculated by Manning and Goldberg[9] placed on lattice sites were superposed. The result was spherically averaged and normalized to 26 electrons in the unit cell. For convenience in calculating exchange potentials, the d electrons were also treated separately. A Coulomb potential was computed from this charge density in the usual way, and an exchange potential was obtained by Slater's free electron approximation for an unmagnetized state with three $3d$ electrons of each spin. In this approximation,

$$V_+ = -6(3\rho_+/4\pi)^{\frac{1}{3}}; \qquad (1)$$

V_+ is the exchange potential in atomic units for an electron of positive spin and ρ_+ is the local charge density of electrons of positive spin.

The observed saturation magnetic moment of iron has been interpreted as indicating there are considerably less than two $4s$ electrons per atom in metallic iron.[10] Also, the reliability of the free electron approximation to the exchange potential can be questioned. When it was found that the results obtained with the potential just described were unsatisfactory in certain respects, it was decided to investigate the effect of assuming that there are seven $3d$ electrons instead of six and of computing the exchange potential from the Hartree-Fock equations. An examination of various methods of averaging exchange potentials has been reported by Herman, Callaway, and Acton.[6] It can be deduced from the data in this paper that the free electron approximation overestimates the exchange energy for a $3d$ electron by about 20 percent compared to the Hartree-Fock equations for the case of a free germanium atom. The situation turns out to be similar for iron.

The Hartree-Fock exchange potential appearing in the wave equation for a state $\psi_{nlm}(r_1)$ may be written

[6] Herman, Callaway, and Acton, Phys. Rev. **95**, 371 (1954).

[9] M. F. Manning and L. Goldberg, Phys. Rev. **53**, 662 (1938).

[10] N. F. Mott, Proc. Phys. Soc. (London) **47**, 571 (1935).

as follows:

$$V_{nlm}(r_1)=\frac{\sum_{n'l'm'}\left[\int\psi_{n'l'm'}^{*}(r_2)\frac{2}{r_{12}}\psi_{nlm}(r_1)dr_2\right]\psi_{n'l'm'}(r_1)}{\psi_{nlm}(r_1)}. \tag{2}$$

The summation over $n'l'm'$ is restricted to all occupied states having the same spin as nlm. If for a given $n'l'$, all the m' states are occupied, the contribution to the exchange potential from those states is independent of m and m'. If a shell is incompletely filled, as is the case for the d electrons (assuming the unmagnetized condition), some assumption has to be made about the occupancy of the m levels. For the purpose of calculating an exchange potential, it is convenient to assume, in the absence of other information, that they are occupied with equal probability. In this case, the exchange potential will be spherically symmetric. In calculating that part of the exchange potential for the state Γ_1 that is due to the interaction of the $3d$ and the $4s$ electrons it is sufficient to use just $n/5$ of the $4s$-$3d$ exchange for a closed $3d$ shell. (Here n is the number of $3d$ electrons of spin parallel to that of the $4s$ electron.)

The situation is more complicated when one considers the $3d$-$3d$ interaction in calculating the exchange potential for a $3d$ state. It can be shown that the exchange potential for a $3d$ electron in a closed shell can be written as[11]

$$V_{3d}(r)=-\frac{2}{r}\left[Y_0(3d,3d,r)+\frac{2}{7}\left\{Y_2(3d,3d,r)+Y_4(3d,3d,r)\right\}\right]+\frac{2}{5r}\sum_{n=1}^{4}Y_2(ns,3d,r)\frac{P_{ns}(r)}{P_{3d}(r)}+\frac{1}{r}\sum_{n=2}\left[\left\{\frac{4}{5}Y_2(np,3d,r)+\frac{18}{35}Y_2(np,3d,r)\right\}\frac{P_{np}(r)}{P_{3d}(r)}\right], \tag{3}$$

where

$$Y_k(nl,n'l',r)=\int_0^r P_{nl}(r_1)P_{n'l'}(r_1)\left(\frac{r_1}{r}\right)^k dr_1+\int_r^\infty P_{nl}(r_1)P_{n'l'}(r_1)\left(\frac{r}{r_1}\right)^{k+1}dr_1, \tag{4}$$

and

$$\psi_{nlm}(r)=\frac{P_{nl}(r)}{r}Y_{lm}(\theta,\phi), \tag{5}$$

and the P_{nl} are normalized to one. Similarly, for the $4s$ state Γ_1 we write (assuming closed shells):

$$V_{4s}=-\frac{2}{r}\frac{1}{P_{4s}}\left[\sum_{n=1}^{4}P_{ns}(r)Y_0(4s,ns,r)+\sum_{n=2}^{3}P_{np}(r)Y_1(4s,np,r)+P_{3d}(r)Y_2(4s,3d,r)\right]. \tag{6}$$

[11] D. R. Hartree and W. Hartree, Proc. Roy. Soc. (London) **A157**, 490 (1936).

Now suppose there are n $3d$ electrons of + spin. A simple argument shows that in order to preserve the spherical symmetry of the potential, one should modify Eq. (3) by multiplying the braces containing Y_2 and Y_4 by $(n-1)/4$, i.e., we have

$$V_{3d}=-\frac{2}{r}\left[Y_0(3d,3d,r)+\frac{2}{7}\frac{(n-1)}{4}\times\left\{Y_2(3d,3d,r)+Y_4(3d,3d,r)\right\}\right]+\cdots, \tag{7}$$

the remainder being unchanged. This prescription will be seen at once to yield the correct result when the $3d$ shell is full, or contains but one electron. To obtain this result for a different case, consider the situation of two $3d$ electrons of + spin. Let one of the electrons be in the state $m=0$; the other is distributed with probability $\frac{1}{4}$ over all other states. The exchange terms in the Hartree-Fock equation, i.e., the coefficient of $Y_2(3d,3d,r)$ and $Y_4(3d,3d,r)$ will be $\frac{1}{4}$ of the closed-shell values plus certain terms which are not spherically symmetric. If we now say that the first electron is distributed with probability $\frac{1}{5}$ over all the m levels, and average the exchange terms in this way, the nonsymmetric terms disappear, and we are left with just $\frac{1}{4}$ of the closed-shell result.

Under the assumption that for the purpose of computing a starting potential, all the m levels can be treated as degenerate, we have the following important result: the change in the exchange potential for a $3d$ electron of + spin when we increase the number of $3d$ electrons per atom with positive spin by one is

$$\Delta V_{+,3d}=\frac{1}{7r}\{Y_2(3d,3d,r)+Y_4(3d,3d,r)\}, \tag{8}$$

where this is to be taken with the proper algebraic sign to decrease the energies of these electrons. This result is useful when we wish to consider the ferromagnetism of iron.

On the basis of these results, an improved exchange potential was calculated from the starting charge density for the unmagnetized state. It was found that the Slater free electron approximation to the exchange potential overestimates exchange badly for small r and is reasonably close for large r to the Hartree-Fock potential. If the expectation value of the difference between the Hartree-Fock and free-electron exchange potentials is found with the $3d$ radial function determined for the state $\Gamma_{25'}$, the result is that the Slater approximation overestimates the exchange energy by 0.49 Rydberg or 15 percent.

The exchange potential for a $4s$ electron was then calculated from (6), using for the $4s$ wave function, the wave function for Γ_1 calculated by the cellular method. Since this function has nodes, the exchange potential has infinities, but these do not contribute to

the exchange energy, being removed when we calculate the expectation value. Except very close to one of the peaks in the exchange potential, it was found that the free-electron approximation overestimates the exchange potential. The error in the exchange energy for the Γ_1 state is 0.23 Rydberg or 20 percent. Most of this error seems to be due to overestimation of the interaction between the 4*s* and the 3*d* electrons.

The usefulness of the free-electron approximation depends on the state considered and the accuracy required. It seems to compare favorably with other methods of averaging exchange potentials.[5] Unfortunately, the dependence of the exchange potential on the wave function for the particular state may be too great to justify use of an exchange potential averaged over all states. Accuracy in the potential is important because of the sensitivity of some features of the band structure to details of the potential.

The effect of using a Coulomb potential computed from a d^7s^1 configuration of the free iron atom was also examined. The principal change comes from the fact that the charge density is now more compact and the potential is less attractive for moderate values of r. The expectation value of this change in potential found with the $\Gamma_{25'}$ function (see next section) is 0.697 Rydberg, while the change in exchange energy occasioned by increasing the number of 3*d* electrons by one is 0.035 Rydberg in the opposite direction. The state Γ_1 is not affected so strongly; the change in the Coulomb energy is 0.122 Rydberg while the change in the exchange energy is -0.020 Rydberg.

It was not feasible to examine the effect of the changes in potential on the bandwidth, since a repetition of the entire band structure calculation would have been required in order to obtain an accurate answer.

BAND STRUCTURE OF THE NONMAGNETIC STATE

OPW expansions were constructed for the levels Γ_1, Γ_{12}, $\Gamma_{25'}$, and Γ_{15} at the center of the Brillouin zone; H_1, H_{15}, $H_{25'}$, and H_{12} at the corner point H, $2\pi/a$ (1,0,0); P_3 and P_4 at the corner P, $2\pi/a(\frac{1}{2},\frac{1}{2},\frac{1}{2})$; and N_1, N_2, N_3, and N_4 at the point N, $2\pi/a(\frac{1}{2},\frac{1}{2},0)$ which is the center of a face. The Brillouin zone for the body-centered lattice is shown in Fig. 1. As indicated in the introduction, the expansions for Γ_1, H_1, and N_1 gave unreasonably low energies. Γ_1 and H_1 were treated by the cellular method. The expansions for P_3 and P_4 apparently did not contain enough plane waves to yield reliable results, but further calculations for P_4 in particular would have required a prohibitively large secular determinant to obtain accuracy commensurate with that obtained at Γ and H. It is believed that reliable solutions from the point of view of convergence of the OPW expansions were obtained for the following nine states: Γ_{12}, $\Gamma_{25'}$, Γ_{15}, H_{12}, $H_{25'}$, H_{15}, N_2, N_3, and N_4. The appropriate determinantal equations were solved on the high-speed electronic computing machine at the

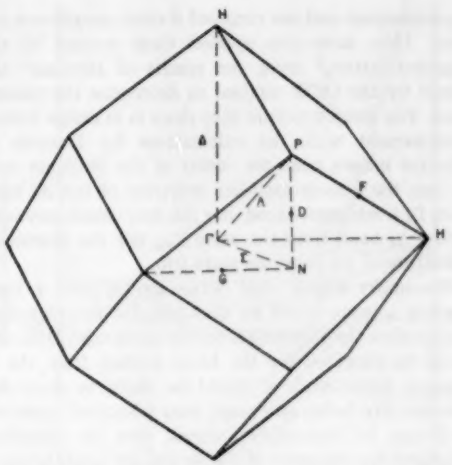

FIG. 1. Brillouin zone for the body-centered cubic lattice. Symmetry points and axes are indicated.

Institute for Advanced Study, Princeton, New Jersey. All the eigenvalues and eigenvectors of the matrices (usually of seventh order) were determined in the process.

The results of the calculation up to this point were unsatisfactory in one respect: the 4*s* level Γ_1 was placed some seven volts above the *d* band. This is contrary to reasonable expectations based on existing knowledge of the transition metals. This result prompted the previously mentioned study of the crystal potential. A potential was constructed, based on a d^7s^1 configuration of the free iron atom (but with the same wave functions as the d^6s^2) and on the Hartree-Fock exchange integrals. The difference between this potential and the one previously used was treated by first order perturbation theory, but only as regards the position of the levels. The Γ_1 level was now found to lie satisfactorily below the 3*d* band.

Slater and Koster have proposed an interpolation scheme for energy bands in crystals based on the tight binding approximation.[6] These authors regard the integrals occurring in the matrix components of the energy between different Bloch sums as disposable parameters to be determined from energy values obtained by other methods at symmetry points in the Brillouin zone. They have applied this scheme to *d* bands in the transition metals for both the body-centered[6] and face-centered cubic lattices,[12] using parameters determined from a previous calculation for nickel.[13] Some of their results, particularly the symmetry about $E=0$ of the density of states for the body-centered lattice, are rather critically dependent on their

[12] G. F. Koster, Quarterly Progress Report of the Solid State and Molecular Theory Group, Massachusetts Institute of Technology, October 15, 1954, (unpublished), p. 4.
[13] G. C. Fletcher, Proc. Phys. Soc. (London) **A65**, 192 (1952).

approximation and are removed if more parameters are used. They have also applied their method to the diamond lattice,[6] using the results of Herman[14] obtained by the OPW method to determine the parameters. The band structure they draw is in rather serious disagreement with the calculations by Herman of effective masses near the center of the Brillouin zone in that the free-electron-like behavior of the Δ_1 band from Γ_1 is not reproduced, nor the downward curvature of the Δ_1 band from the state Γ_{15}, nor the downward curvature of $\Delta_{2'}$ from the state $\Gamma_{25'}$.

We might expect that better fitting with a tight binding scheme could be obtained for the transition metals since the *d* bands are relatively narrow. Difficulty could be expected for the band formed from the 4*s* electron levels since it would be likely to show free electron like behavior except near points of crossover. If it can be reasonably asserted that the distortion produced by crossover of the 4*s* and 3*d* bands is not so great as to effect strongly the density of states, then it might be reasonable to try to use the interpolation scheme to compute the density of states.

FIG. 2. Energy bands in iron parallel to 100 axis (unmagnetized state). Intermediate points are determined by the interpolation scheme. Use of more parameters would remove the degeneracy of Δ_1 and Δ_2; of Δ_5' and Δ_5. Dotted lines show possible alteration of predicted band structure in order to avoid crossover of Δ_1 bands.

[14] F. Herman, Phys. Rev. **88**, 1210 (1952).

It was decided to apply Slater's scheme in the two-center approximation using nearest neighbor interactions only. If we allow for the possibility of different central interactions for the states at $\mathbf{k}=0$, there are five parameters to fit. These parameters were determined from the energies of the levels Γ_{12}, $\Gamma_{25'}$, $H_{25'}$, H_{12}, N_2, N_3, and N_4. Since there are seven levels there are two relations which the matrix elements have to satisfy if the fitting is exact. These relations are not exactly satisfied, but are obeyed sufficiently well to suggest there is some truth in the approximation. This form of the interpolation scheme leaves one unwanted degeneracy: the bands along the 100 axis in the Brillouin zone are split into a doubly degenerate band and a triply degenerate band instead of three nondegenerate bands and one doubly degenerate band. However, the symmetry of the density of states about its midpoint is removed.

By using Slater's interpolation scheme, energy levels were calculated at several points in the Brillouin zone in order to determine the form of the bands and the density of states. The density of states is found in the following way: For various values of k_x and k_y, the band structure parallel to the k_z axis in the Brillouin zone was determined by the interpolation scheme. For each of these curves, the energy was divided into small intervals (0.01 Rydberg) and the relative extent of the k_z axis for which each curve lay within the given energy range was computed. This gives a rough density of states for each band. These curves are step curves and they all have to be added with the proper weighting. The result is a step curve for $\eta(E)$.

Table I gives the lowest eigenvalues for all the representations for which convergent solutions were found. Diagrams of the band structure are shown in Figs. 2 and 3 (intermediate states and also the two N_1 levels have been located by the interpolation scheme). The Δ_1 and Σ_1 bands from Γ_1 are drawn as free-electron bands. Since cross over of equivalent bands is rendered extremely unlikely by group theory, the band structure will be distorted somewhat from the solid lines of these diagrams. A possible modification of the band structure to prevent such cross over is shown by dotted lines in Fig. 2.

The splitting of the 3*d* levels at the center of the Brillouin zone is only 0.3 ev; much less than it is at the corners and faces of the zone. The bottom of the 3*d* band at the point N_1 lies 1.35 ev above the lowest point of the 4*s* band at Γ_1. The location of the top of the *d* band is ambiguous because of the mixing of *s* and *d* states: The state N_4 (which is determined by the OPW method) lies 1.57 ev above the lowest N_1 (which is found by the interpolation scheme). There is another state of type N_1 about 1.8 ev (estimated from a single OPW) above N_4; this may be predominately *S*-like although N_1 contains a mixture of *s* and *d* states. The top of the *d* band is not determined with precision, but

it would be reasonable to say that this calculation gives a d band width of about two electron volts. Unfortunately, these numerical values are sensitive to the potential.

A much smaller splitting of the d-band states at $\mathbf{k}=0$ than at other points of the zone is also a feature of the band structures calculated for nickel by Fletcher[13] and for copper by Howarth.[15] These elements have the face-centered cubic structure. It does not agree with the predictions of Slater and Koster[6] for the body-centered lattice, based on their interpolation scheme.

Some confidence in the relative order of the $3d$ levels among themselves (at least for the ones found from OPW expansions) was furnished by an exploratory calculation for the points Γ and H with a potential which did not include any exchange. Although the magnitudes of the separations were changed the order and relative separation of the levels was the same. The result that the separation of the $3d$ bands at Γ is roughly one third that at H may be viewed with some confidence.

TABLE I. Lowest eigenvalues.

Representation	Energy (Rydbergs)
Γ_1	−0.750
H_{12}	−0.625
N_3	−0.595
$\Gamma_{25'}$	−0.595
N_3	−0.574
Γ_{12}	−0.573
$H_{25'}$	−0.555
N_4	−0.548
H_{15}	+0.154[a]
H_1	+0.64[a]
Γ_{15}	+2.00[a]

[a] Correction to potential not included.

The separation between the levels Γ_1 and H_{15} is 1.238 Rydbergs (16.8 electron volts) before correction of the potential. These levels are presumably the limits of the s-p bands. The width of this band according to the free electron approximation is 1.345 Rydbergs, which is in error by 8.6 percent. It then seems reasonable to draw the $4s$ bands as free-electron bands. Since the states Γ_{15} and H_{15} formed from $4p$ electron levels lie far above the d band, one might conclude that the mixing of p and d states in the d band is small. P_4 is a state where mixing of this kind is permitted by group theory. The form of the OPW expansion, although poorly convergent, suggests that this mixing is small.

There is no experimental information as yet which bears directly on the form of the band structure suggested here. However, experiments on the polarization of slow neutrons by magnetized iron give information as to the charge distribution of a magnetically active electron. These experiments have been analyzed by Steinberger and Wick.[7] Although their cellular method calculation of the wave functions of d electrons was

[15] D. J. Howarth, Proc. Roy. Soc. (London) **A220**, 513 (1953).

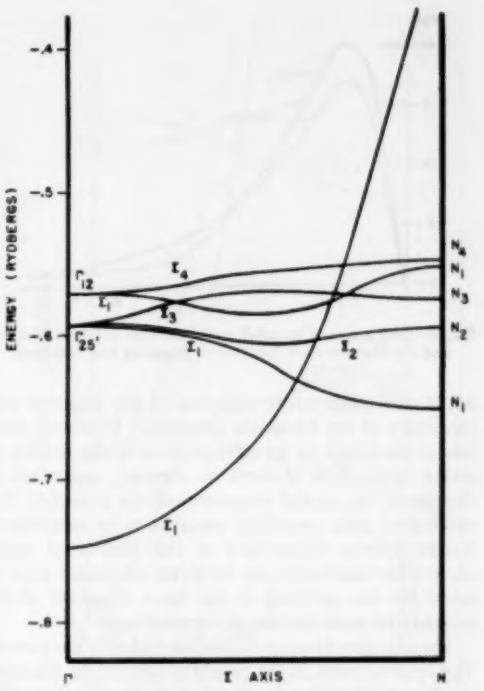

FIG. 3. Energy bands in iron parallel to 110 axis (unmagnetized state). N_1 levels and intermediate points are determined from the interpolation scheme. Effects of prohibiting crossover of Σ_1 bands are not shown.

performed with boundary conditions which are not appropriate for $3d$ electron states, their principal conclusion is probably sound. They find that the charge distribution of a magnetically active electron must be somewhat more compact than are the Hartree functions for a free iron atom.[9] The additional binding is provided by exchange.

The wave function for a $3d$ electron depends, of course, on the particular state in the band. But inspection of the OPW eigenfunctions suggests that the wave function does not change much over the $3d$ band. This result is consistent with the small width of the band. It would seem that a reasonable idea of the radial charge distribution of a $3d$ electron could be obtained by summing the $l=2$ part of the expansion for one of the states. This was done for the state $\Gamma_{25'}$; the result is shown in Fig. 4 where it is compared with the $3d$ radial function of Manning and Goldberg.[9] The $\Gamma_{25'}$ function has been altered in the right direction from the Hartree field.

The density of states for the unmagnetized state obtained from the calculation based on the interpolation scheme is shown in Fig. 5. It has the two-hump structure suggested by information on the electron specific

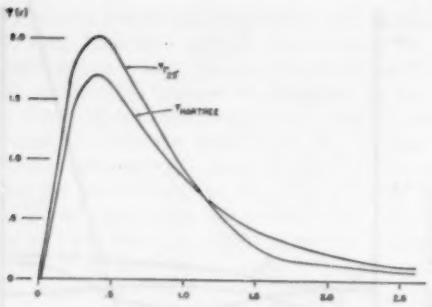

FIG. 4. Comparison of $3d$ radial wave functions obtained from Γ_{25}' and the Hartree wave function of Manning and Goldberg.

heat[16] and temperature variation of the magnetic susceptibility of the transition elements.[17] However, these results are based on an extrapolation of the density of states curve from element to element, regardless of changes in the crystal structure and the potential. The validity of such procedure remains to be established. Before definite comparison of the density of states curve with experiment can be given, allowance must be made for the splitting of the band structure of the magnetized state introduced by exchange.

The calculated energy bands are probably too narrow. The improvement in the potential previously discussed would tend to widen the bands, but it was not possible to calculate this. An accurate calculation of the d-band width must wait for a self-consistent field.

An estimate of the self-consistency of this calculation can be made by comparing the Coulomb potential calculated from the Γ_{25}' function previously discussed with the Coulomb potential of the assumed initial distribution. The potentials are found to disagree considerably since the charge density obtained in this calculation is more compact than the initial one. Consequently, results of this calculation which are dependent on the details of the potential are open to some question.

APPLICATIONS TO FERROMAGNETISM

Equation (8) gives the change in the potential energy of a $3d$ electron in the Hartree-Fock scheme when one $3d$ electron per atom reverses its spin. We shall assume (1) that this potential is the same for all electrons in the d band, (2) that we can calculate its effect by first order perturbation theory, and (3) that the expectation values of this potential are the same to a sufficient approximation for all the states in the d band. This potential was computed by using the radial function for the state Γ_{25}', and also by using the starting charge density for a $3d$ electron. The expectation value of these potentials were found by using the Γ_{25}' function. For the potential constructed from the starting charge density, the expectation value is -1.23 ev. For the potential constructed from the Γ_{25}' function, the value is -1.58 ev. Since the latter potential is derived from a charge distribution that may be too compact and the former from one that is too loose, the correct figure should lie between these limits. The energy computed here represents the lowering of the levels of majority spin electrons from the unmagnetized state, and we must remember that the levels of minority spin electrons are raised by a like amount. Corresponding levels of opposite spin are separated by an energy between 2.46 and 3.16 ev. The figures obtained here from the Hartree-Fock exchange potential agree reasonably well with the corresponding results of Slater's free-electron approximation to the exchange potential.

The change in cohesive energy due to exchange when one $3d$ electron per atom reverses its spin is just one-half the separation between corresponding levels in the magnetized state. The factor of one-half arises from the fact that when we add the one-electron eigenvalues of the Hartree-Fock equations, we have counted the exchange interactions twice. Thus the change in cohesive energy due to spin reversal will be between 1.23 and 1.58 ev. These numbers are slightly larger than those obtained by Slater for the case of nickel by examination of spectroscopic data.[18] Slater obtains a value of 0.99 ev for this quantity. The discrepancy arises from two causes: (1) a different method of averaging the exchange interactions over the $3d$ states, and (2) slightly larger values for the appropriate integrals in this case. The difference in the method of averaging amounts to one fifth of the change in spin energy.

We must now compute the change in the kinetic energy on going to the magnetized state. This can be determined from the density of states curve. We have to calculate the integrals $\int E\eta(E)dE$ for the magnetized

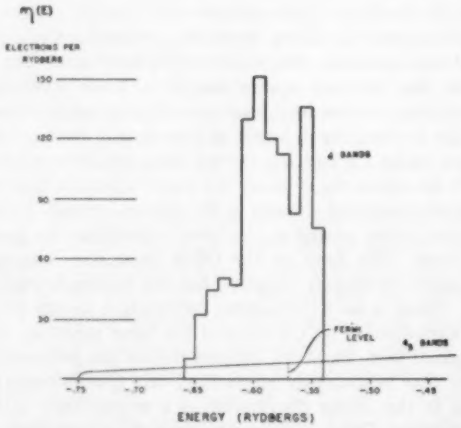

FIG. 5. Density of states for iron (unmagnetized state). The $4s$ band is drawn as a free electron band. $\eta(E)$ for the $4s$ band is enlarged by a factor of ten.

[16] M. Horowitz and J. G. Daunt, Phys. Rev. **91**, 1099 (1953).
[17] C. J. Kreissman and H. B. Callen, Phys. Rev. **94**, 837 (1954).
[18] J. C. Slater, Phys. Rev. **49**, 537 (1936).

and unmagnetized electron distributions. These integrals have been computed and yield the result that the change in Fermi energy upon magnetization is 0.69 ev. This figure is not very accurate since it is the difference between two large numbers. The net energy of magnetization at absolute zero is then between 0.89 and 0.54 ev per atom; a result that is considerably larger than would be suggested by the Curie temperature. Most of this discrepancy may be due to having too narrow a calculated $3d$ band. One might expect that for a band width of 3.0 ev a change in Fermi energy approximately $\frac{3}{2}$ the above value or 1 ev might be obtained.

Although these calculations were made for a situation in which there would be a net magnetic moment of 2.0 Bohr magnetons per atom (neglecting a small contribution from the $4s$ electrons and from the orbital moment), the situation should not be appreciably different for the observed saturation magnetic moment of 2.2 Bohr magnetons per atom.[19]

The principal change in the band structure on passing to the magnetized state is that the levels of electrons of + and − spin will be split. This splitting was calculated to be between 2.46 and 3.16 ev. Since these figures are somewhat greater than the predicted width of the unmagnetized $3d$ band, one might expect that the $3d$ band will be split into halves, the lower being full and containing electrons of the majority spin. There will, of course, be some change in the band form due to the difference in the exchange energies of these states; in particular, the upper band should be somewhat wider than the lower. When this change is estimated using Slater's free electron exchange potential, one finds that the upper band should be about 0.1 ev wider than the lower if the individual halves are about 2.0 ev wide.

The $4s$-electron levels will serve to connect the halves of the d band. The alignment of the spins of the $3d$ electrons will necessarily cause a splitting of the $4s$-electron levels. This splitting is smaller than that of the $3d$ levels. It can be determined from the alteration of the potential of a $4s$ electron:

$$\frac{n}{5}\frac{2}{r}\frac{P_{3d}(r)}{P_{4s}(r)}Y_2(4s,3d,r), \tag{9}$$

when n $3d$ electrons per atom change their spin. The functions P are proportional to r times the radial part of the wave functions, and Y_2 is defined in (4). Here it is assumed that all the $3d$ and all the $4s$ electrons have the same wave function. This potential has been computed using wave functions for the Γ_1 and $\Gamma_{25'}$ states. The expectation value of the potential is -0.040 Rydberg, taken with the Γ_1 function. Thus the Γ_1 levels of + and − spin will be separated by 0.080 Rydberg or 1.1 ev if one $3d$ electron per atom reverses its spin. Consequently there will be an alteration in the relation of the s and d states from that obtaining in the nonmagnetic state and one may expect a small number of $4s$ electrons to participate in the magnetization.

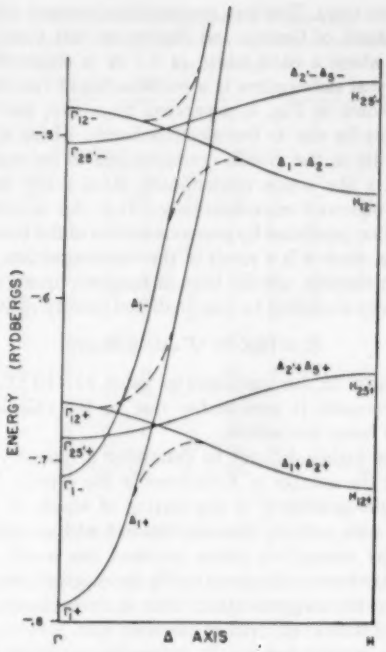

FIG. 6. Energy bands in iron parallel to 100 axis for magnetized state. The $4s$ bands are drawn as free electron bands. Levels of electrons of + and − spin are indicated by + or − sign after the standard symbol. Dotted lines indicate possible elimination of crossover of Δ_1 bands of the same spin.

The band structure along the 100 axis in the Brillouin zone for the magnetized state is shown in Fig. 6 for two excess $3d$ electrons of + spin, under the assumption that the position but not the form of the bands has been altered. The curvature of the $4s$ bands is that of free-electron bands. We have the following picture: the d band is split into halves connected by bands which should show a mixing of s and d states, perhaps predominantely s-like. The Fermi level comes approximately in the middle of the upper d band. The minimum separation of the split d bands is at the point N where they are separated by a gap of the order of one electron volt. However, if the separated d bands are somewhat wider than calculated here, there may be some overlap of predominately d states. Because some of the $3d$ electrons will drop into lower $4s$ states in the magnetic state, the Fermi level will be slightly lower than predicted on the basis of d bands alone. The width of the filled portion of the bands, from the lowest state Γ_1 to the Fermi level will be about 0.30 Rydberg or 4.1

[19] The observed magneton number, 2.2 Bohr magnetons per atom, can be approximately accounted for in terms of two excess spins per atom and a contribution from the orbital angular momentum. C. Kittel, *Introduction to Solid State Physics* (John Wiley and Sons, Inc., New York, 1953).

electron volts. This is in reasonable agreement with the experiment of Gyorgy and Harvey on soft x-ray emission[20] where a band width of 3.7 ev is observed. The density of states curve is a combination of two like the one shown in Fig. 4, separated by a gap, and laced together by the 4*s* free-electron bands. There is a decided dip in the middle corresponding to the region in which *s* like states predominate. Such a dip has not been observed experimentally. This dip is different from that predicted by previous studies of the transition metals, since it is a result of the ferromagnetism.

The electron specific heat of magnetic iron at absolute zero according to this predicted density of states is

$$C_v = 18\times10^{-4}T \text{ cal/mole-deg},$$

compared to the experimental value $12\times10^{-4}T$.[16] The disagreement is presumably due to the calculated *d* bands being too narrow.

It is rather difficult to determine a quantity to be called the number of *s* electrons in the crystal. This is ambiguous because of the mixing of states. If the 4*s* band were entirely free-electron-like and no mixing of angular momentum states occurred, one would obtain 0.11 4*s* electron per atom in the nonmagnetic state and 0.19 in the magnetic state, with an excess in the latter case of 0.07 4*s* electron of majority spin.

The energy balance in magnetization must be recomputed if the role of the 4*s* electrons is taken into account. The result is nearly the same as before. There are three effects which, when added, very nearly cancel: (1) the decrease in energy due to exchange which comes from the 3*d*-4*s* exchange, (2) the increase in kinetic energy upon magnetization, and (3) a decrease in energy due to electrons dropping from higher 3*d* states into 4*s* states. To the accuracy possible here, these effects cancel. Readjustment of the 4*s* levels represents an improvement in the wave function of the system and must lead to a state of lower energy,[21] but this decrease is probably small.

ACKNOWLEDGMENTS

I should like to thank Dr. Conyers Herring, Dr. Walter Kohn, and Professor E. P. Wigner for valuable discussions and comments. I am indebted to Dr. H. H. Goldstine, the members of the electronic computer group at the Institute for Advanced Study, Princeton, New Jersey, and in particular to Mrs. S. Bargmann for very great assistance with the numerical work. Without their help, this calculation would have been impossible. This work was begun while the author was a National Science Foundation Predoctoral Fellow at Princeton University. Finally, I should like to thank the management and staff of Bell Telephone Laboratories, Inc., Murray Hill, New Jersey for their hospitality during the summer of 1954.

[20] E. M. Gyorgy and G. C. Harvey, Phys. Rev. **93**, 365 (1954).
[21] C. Herring (private communication).

APPENDIX

Use of Group Theory to Simplify the Eigenvale Problem

Only those orthogonalized plane waves appear in the expansion for the wave function at a point $\mathbf{k}$ in the Brillouin zone which are formed by adding to $\mathbf{k}$ all reciprocal lattice vectors. In order to obtain a convergent expansion, it is necessary to employ a large number of orthogonalized plane waves (for instance 86 are used in the expansion of the level Γ_{15} at $\mathbf{k}=0$). This would seem to lead to impossibly large secular equations which, for a general $\mathbf{k}$, we should have to solve; but at certain points in the Brillouin zone, a simplification is possible.

Consider the operations belonging to the point group of the reciprocal lattice which carry a point $\mathbf{k}$ of the Brillouin zone into itself or an equivalent point (a point $\mathbf{k}'$ is said to be equivalent to $\mathbf{k}$ if $\mathbf{k}=\mathbf{k}+\mathbf{g}$, where $\mathbf{g}$ is a reciprocal lattice vector). These operations are said to form the group of the point $\mathbf{k}$.[22] For a general $\mathbf{k}$, the group of $\mathbf{k}$ will consist only of the identity. There exist, however, symmetry points in whose group there are several operations. Then the wave function of a state of that $\mathbf{k}$ can be classified according as it belongs to a particular irreducible representation of the group of $\mathbf{k}$. Because the Hamiltonian will have no nonvanishing matrix elements between functions belonging to different irreducible representations, the OPW secular equation can be factored. In particular, we can choose a linear combination of orthogonalized plane waves of a given type which belongs to a (particular row of a) particular irreducible representation. Only combinations belonging to this symmetry type need be considered in setting up the secular equation.

For example, consider the point Γ. The group of Γ consists of the 48 operations of the cubic point group. There are ten irreducible representations of this group: four one-dimensional, two two-dimensional, and four three-dimensional representations. The orthogonalized plane waves which can participate in the expansion of the wave function of one of these representations are: the wave 000, the 12 waves 110, the six waves of type 200, the twenty-four waves of type 211, the twelve waves 220, the twenty-four waves 210, the eight waves 222, the forty-eight waves 321, etc.[23] Suppose we wish to find the lowest energy of a state belonging to the representation $\Gamma_{25'}$. Such a state will be triply degenerate, and if expanded in spherical harmonics will have as harmonic of lowest order a function of type xy/r^2 (or xz, or yz, or a linear combination of these).[24] Since the functions xy, yz, and zx are linearly independent, they form a basis for the expansion of any function

[22] Bouckaert, Smoluchowski, and Wigner, Phys. Rev. **50**, 58 (1936).
[23] $2\pi/a$ is omitted.
[24] F. C. Von der Lage and H. A. Bethe, Phys. Rev. **71**, 612 (1947).

belonging to $\Gamma_{25'}$. Let us choose to construct the expansion of the wave function in $\Gamma_{25'}$ which transforms like xy. To do this, we choose a plane wave of a particular type, say 110, and apply the formula[25]

$$\sum_T D_{xy,\,xy}(T)T\chi_{\mathbf{k}}=\sum D_{xy,\,xy}(T)\chi_{(T\mathbf{k})}. \qquad (10)$$

Here, T runs over all 48 operations of the group of Γ. $D_{xy,\,xy}(T)$ is the xy, xy element of the matrix representing the operation of T on the basis xy, yz, zx. The result is a linear combination of plane waves which transforms according to the xy row of the representation $\Gamma_{25'}$. We then proceed in a similar manner for all of the plane waves we intend to use in the expansion. In this manner, we express the wave function for a state of $\Gamma_{25'}$ as a series in orthogonalized plane waves, taking advantage of symmetry. The Hamiltonian will have no matrix elements between this function and functions belonging to different irreducible representations, or between orthogonal members of this representation.

In the general case, to construct an expansion which will transform according to the ith row of the jth irreducible representation of the wave vector $\mathbf{k}$, we first determine the types of waves which belong in the expansion and construct

$$\sum_T D_{ij,\,ij}(T)T\chi_{\mathbf{k}}, \qquad (11)$$

for all the plane wave types. Only these functions now need be employed in constructing the secular equation. There is one unknown coefficient for each such linear combination.

In the case the representation is nondegenerate, it is sufficient to use[25]

$$\sum_T C_j(T)T\chi_{\mathbf{k}}, \qquad (12)$$

where C_j is the character of the operation T in the jth irreducible representation and $\chi_{\mathbf{k}}$ is an orthogonalized plane wave. The result is a function transforming according to the jth irreducible representation of wave vector $\mathbf{k}$.

[25] E. P. Wigner, *Group Theory and Quantum Mechanics* (Edwards Brothers, Inc., Ann Arbor, 1944).

TABLE II. Wave functions for Γ ($\mathbf{k}=000$).

	Representation									
Wave	Γ_1	$\Gamma_{1'}$	Γ_2	$\Gamma_{2'}$	Γ_{12}	$\Gamma_{12'}$	Γ_{15}	Γ_{25}	Γ_{15}	$\Gamma_{25'}$
110	+	0	0	0	0	0	0	0	+	+
101	+	0	0	0	+	0	0	+	+	0
011	+	0	0	0	−	0	0	−	0	0
$\bar{1}10$	+	0	0	0	0	0	0	0	−	−
$\bar{1}01$	+	0	0	0	+	0	0	+	−	0
$0\bar{1}1$	+	0	0	0	−	0	0	−	0	0
$1\bar{1}0$	+	0	0	0	0	0	0	0	+	−
$10\bar{1}$	+	0	0	0	+	0	0	−	+	0
$01\bar{1}$	+	0	0	0	−	0	0	+	0	0
$\bar{1}\bar{1}0$	+	0	0	0	0	0	0	0	−	+
$\bar{1}0\bar{1}$	+	0	0	0	+	0	0	−	−	0
$0\bar{1}\bar{1}$	+	0	0	0	−	0	0	+	0	0
200	+	0	0	0	+	0	0	0	+	0
020	+	0	0	0	−	0	0	0	0	0
002	+	0	0	0	0	0	0	0	0	0
$\bar{2}00$	+	0	0	0	+	0	0	0	−	0
$0\bar{2}0$	+	0	0	0	−	0	0	0	0	0
$00\bar{2}$	+	0	0	0	0	0	0	0	0	0
(000)	(+)				x^2-y^2			$z(x^2-y^2)$	x	xy

In certain cases, a given irreducible representation may occur more than once in a given plane wave type. For instance, the representation $\Gamma_{25'}$ occurs twice among the plane waves 211. This means that it will be possible to construct two linearly independent wave functions of xy symmetry from the waves 211. Both will have to be included in the expansion. The rule for determining the number of times a particular representation is contained in a particular plane wave type is as follows[21]: (1) Determine the number of plane waves carried into themselves (i.e., *aab* into *aab*) by an operation of the group. (2) Multiply this by the character of the operation. (3) Form the sum of (2) for all operations. (4) Divide the number obtained in (3) by the number of operations contained in the group.

Table II gives the appropriate linear combinations for the first nineteen waves belonging to Γ. The linear combinations for other points may be obtained from the author.

Atomic Energy Levels for the Thomas-Fermi and Thomas-Fermi-Dirac Potential*

RICHARD LATTER
The Rand Corporation, Santa Monica, California
(Received January 24, 1955)

The eigenvalues of the Schrödinger equation have been obtained for the Thomas-Fermi and Thomas-Fermi-Dirac atomic potentials. Electron self-interactions were taken into account by modifying the potentials to give asymptotically the field of a unit charge. All levels were treated from $1s$ to $7d$ for a range of Z-values sufficient to permit easy interpolation. It was found that the energies, for either the Thomas-Fermi or Thomas-Fermi-Dirac potentials, agree in general as well with experimental ionization energies as the Hartree or Hartree-Fock approximations. Applications of the statistical potential to other atomic problems are indicated.

I. INTRODUCTION

QUANTITATIVE estimates of atomic behavior rely heavily upon the self-consistent field method of Hartree[1] and Hartree-Fock[2] for the determination of atomic states. These methods provide the best solution for the atomic ground state in terms of a separable wave function in the sense that this solution is derived from a variational principle which minimizes the total energy. This extremum property cannot be claimed, in general, for excited states since they must be orthogonal to all lower states, and this orthogonality may require a superposition of product type wave functions.

The numerical complexity of the Hartree and Hartree-Fock methods makes it difficult to obtain an overall picture of atomic behavior. At present only isolated solutions of the self-consistent field equations are available, and these mainly for ground state configurations. The difficulty in the methods lies primarily in the lengthy numerical iterations which lead to the self-consistent solutions. Straightforward iterations in the Hartree procedure are not necessarily convergent so that in practice additional numerical complications arise.

It is suggested, however, that these numerical difficulties in the Hartree, or Hartree-Fock, procedure will not be circumvented without loss of accuracy, at least for the ground state configuration. For the excited states it may be possible to find a mathematically simpler method without loss of accuracy since in this case the Hartree procedure is not necessarily optimal. For the ground state, though, the method does give, in principle, the best possible value for the total energy of the atom, subject to the limitation of separable wave functions. Even if the total energy of the atom has been determined accurately, it does not follow that all single electron term values have been accurately determined. In fact, the lowest one-electron term value will be weighted most heavily in the total energy determination for the atom, and presumably is very accurate. Higher single electron term values, which contribute less importantly to the total atom energy, may be only roughly determined. In view of these features of the Hartree, or Hartree-Fock, approximation, consideration has been given to simpler approximations which could be applied to atomic systems in their ground states. An approximation with this general applicability is furnished by the use of the Thomas-Fermi,[3] or Thomas-Fermi-Dirac,[4] statistical potential as a central field for the atomic system. Some term values for circular orbits and for the $5f$ level have been determined by previous investigators[5,6] with this potential, but a general exploration of the results to be obtained has not previously been carried out. The results of such an exploration will be presented here for the isolated, zero-temperature atom for all atomic numbers and for the one-electron term values from $1s$ to $7d$.

II. THEORETICAL CONSIDERATIONS

The description of the many-electron atom which uses an equivalent central potential, such as a statistical potential, is familiar in spectroscopy as the central-field approximation.[7] In this approximation, an equivalent central potential is used to generate a set of energy levels and wave functions under the assumption that the electrons are independent. The one-electron wave functions and energy levels so obtained may be taken as the zero order basis to which corrections can be applied by perturbation theory. The one-electron eigenfunctions and eigenvalues are given by solution of the Schrödinger equation,

$$[-(\hbar^2/2m)\Delta - eV(r)]\phi_i = \epsilon_i\phi_i, \qquad (1)$$

where $V(r)$ is the effective central potential for the atom. In the present discussion, this potential is either the Thomas-Fermi, or the Thomas-Fermi-Dirac, statistical potential. In this zero order, the total energy

* This study was supported by the U. S. Atomic Energy Commission.
[1] D. R. Hartree, Proc. Cambridge Phil. Soc. **24**, 89 (1928).
[2] V. Fock, Z. Physik **61**, 126 (1930).
[3] E. Fermi, Atti. accad. nazl. Lincei **6**, 602 (1927); **7**, 342, 726 (1928); L. H. Thomas, Proc. Cambridge Phil. Soc. **23**, 542 (1927).
[4] P. A. M. Dirac, Proc. Cambridge Phil. Soc. **26**, 376 (1930).
[5] F. Rasetti, Atti accad. nazl. Lincei **7**, 915 (1928); Z. Physik **49**, 546 (1928); R. Gáspár, J. Chem. Phys. **20**, 1863 (1952).
[6] Maria G. Mayer, Phys. Rev. **60**, 184 (1941).
[7] E. U. Condon and G. H. Shortley, *The Theory of Atomic Spectra* (Cambridge University Press, London, 1951).

of the atom is given by

$$E=\sum_{\{i\}}\epsilon_i, \tag{2}$$

and the wave function for the atom, without antisymmetrization, is

$$\psi=\prod_{\{i\}}\phi_i, \tag{3}$$

where $\{i\}$ denotes the set of occupied one-electron levels. This form for the total energy, or for the total wave function, is assumed to apply to the ground state as well as to excited configurations. The analytic simplicity resulting from this assumption is evident and is a consequence of using a fixed potential for all configurations. With the aim of obtaining similar simplicity in the Hartree methods, Roothaan[8] has proposed that the Hartree ground state potential be used as the fixed potential with which excited configurations are determined. This simplification of the Hartree

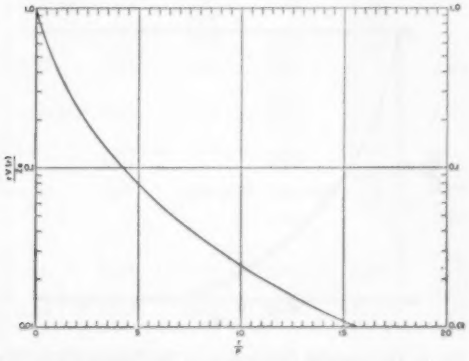

FIG. 1. The potential distribution for the Thomas-Fermi atom.

procedure carries with it, however, the numerical difficulties associated with the determination of the Hartree ground state.

The important error in this application of a fixed central field arises just from the use of the same potential for all configurations of the atom. This error clearly grows with increasing excitation of the atom above the ground state. It will be apparent from the results to be presented here that the statistical potentials give acceptable values for ground state energies and presumably will therefore give semiquantitative predictions for states of low excitation. If highly excited atomic states are determined in this way, the perturbation corrections to the energies and wave functions will certainly become important. These perturbation corrections are determined by the perturbation energy

[8] C. C. J. Roothaan, Revs. Modern Phys. **23**, 69 (1951).

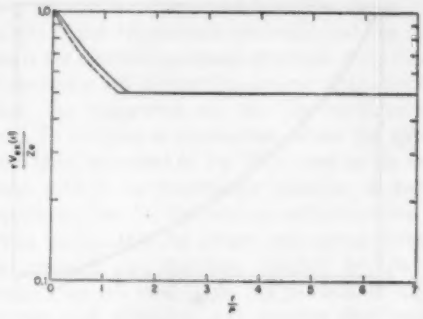

FIG. 2. The potential distribution for the Thomas-Fermi-Dirac atom is shown with the solid line; the dashed line shows the approximation of the universal function of Eq. (9) for $Z=2$.

operator,

$$H_{\text{pert}}=\sum_i\left\{eV(r_i)-\frac{Ze^2}{r_i}+\tfrac{1}{2}\sum_{i\neq j}\frac{e^2}{r_{ij}}+\sum_i\xi(r_i)\mathbf{L}_i\cdot\mathbf{S}_i\right\}, \tag{4}$$

where customary notation[7] has been used. In the present paper, however, the evaluation of term values is limited to the zeroth order even for excited states.

III. DETERMINATION OF THE ATOMIC POTENTIAL

The effective central field potential used in the present calculations is estimated from the statistical model of Thomas-Fermi and from the statistical model including exchange as developed by Dirac. More specifically, these statistical potentials are taken for the isolated atom at absolute zero temperature so that the ground state potential of the atom is the potential under discussion. The potential distribution for the Thomas-Fermi atom, without exchange, has been calculated by Miranda,[9] and has been recalculated with improved accuracy by the author.[10] The analytic fit to this potential function was used for the present calcu-

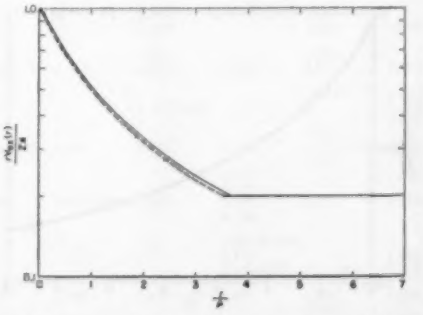

FIG. 3. The potential distribution for the Thomas-Fermi-Dirac atom is shown with the solid line; the dashed line shows the approximation of the universal function of Eq. (9) for $Z=5$.

[9] C. Miranda, Mem. Acc. Italia **5**, 285 (1934).
[10] Unpublished calculations.

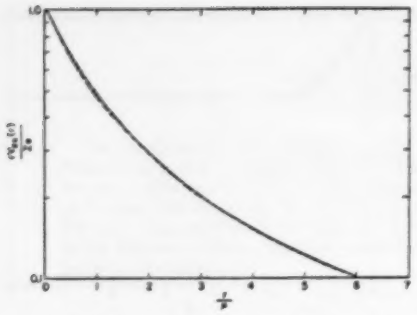

FIG. 4. The potential distribution for the Thomas-Fermi-Dirac atom is shown with the solid line; the dashed line shows the approximation of the universal function of Eq. (9) for $Z=10$.

lations:

$$\phi(r/\mu)=\frac{rV(r)}{Ze}=\Big[1+0.02747(r/\mu)^{\frac{1}{2}}+1.243(r/\mu)$$
$$-0.1486(r/\mu)^{\frac{3}{2}}+0.2302(r/\mu)^{2}$$
$$+0.007298(r/\mu)^{5/2}+0.006944(r/\mu)^{3}\Big]^{-1}, \quad (5)$$

where $\mu=0.8853a_0/Z^{\frac{1}{3}}$ and a_0 is the Bohr radius. The maximum error in this fit to the numerical values is less than 0.3 percent. The potential of Eq. (5) includes the electrostatic self-interaction of the electron whose term value is to be determined, and consequently it leads to significant errors in the higher term values. A number of modifications in the Thomas-Fermi potential have been suggested[11] to remove this source of error in applications to the atomic term-value problem. The Thomas-Fermi ion potential and the Fermi-Amaldi correction have been proposed as more correct fields. These latter have the practical disadvantage of requiring a new solution of the Thomas-Fermi equation for each value of Z. A procedure which does not have this disadvantage replaces the $V(r)$ of Eq. (5) by

$$V(r)=[(Z-1)e\phi(r/\mu)+e]/r, \quad (6)$$

where $\phi(r/\mu)$ is the universal Thomas-Fermi[12] function for the neutral atom of atomic number Z. The predictions of the potential of Eq. (6) for the behavior of the $4f$ and $5f$ electrons have been obtained by Mayer.[6] More extended calculations by the present author with this potential indicated that it over-corrected appreciably for the self-interaction; it consequently gives too large binding energies.

The potential which was used in the present calculations was

$$V(r)=Ze\frac{\phi(r/\mu)}{r}, \quad \text{if} \quad V(r)>\frac{e}{r},$$
$$V(r)=0, \quad \text{otherwise}, \quad (7)$$

and as shown in Fig. 1. This form of potential, which provides the correct asymptotic behavior, was adopted for reason of simplicity. It does not make any modification in the field for self-interaction in the interior of the atom, but over most of this region this neglect should be relatively unimportant.

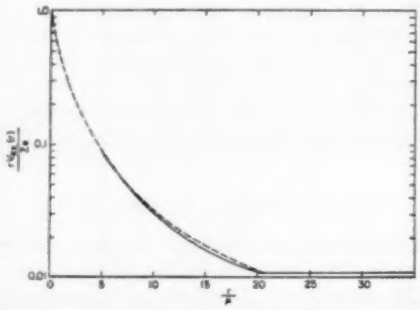

FIG. 6. The potential distribution for the Thomas-Fermi-Dirac atom is shown with the solid line; the dashed line shows the approximation of the universal function of Eq. (9) for $Z=92$.

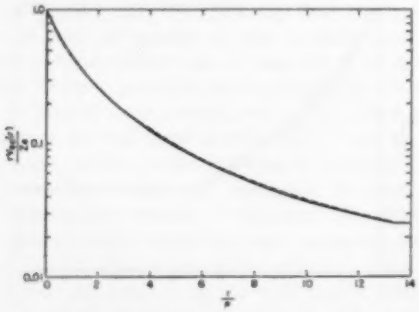

FIG. 5. The potential distribution for the Thomas-Fermi-Dirac atom is shown with the solid line; the dashed line shows the approximation of the universal function of Eq. (9) for $Z=40$.

The Thomas-Fermi potential of Eq. (7) estimates only the electrostatic interaction of the electrons for the atomic ground state. The Dirac extension of the Thomas-Fermi model provides an approximate procedure for including exchange effects. If $\phi_{ex}(r/\mu)$ is the solution for the Thomas-Fermi-Dirac equation,[13] then the effective central field[14] for the one-electron

[11] P. Gombas, *Die Statistische Theory des Atoms* (Springer-Verlag, Berlin, 1949).

[12] P. Gombas (reference 11). The function $\phi(r/\mu)$ used here is the same as Gombas' $\phi(x)$.

[13] P. Gomas (reference 11). The function $\phi_{ex}(r/\mu)$ used here is the same as Gombas' $\psi(x)$.

[14] The physical implications of the discontinuity in the $V(r)$ of Eq. (8) have been discussed by N. H. March, Phil. Mag. **45**, 325 (1954).

Schrödinger equation is

$$V_{ex}(r)=Ze\frac{\phi_{ex}(r/\mu)-\phi_{ex}(r/\mu)(r/r_0)}{r}$$
$$+\frac{Z^{\frac{1}{2}}e}{r_0}\frac{3\sqrt{2}}{2\pi}\left(\frac{r_0}{a_0}\right)^{\frac{1}{2}}\left[\left(\frac{\phi_{ex}(r/\mu)}{r/r_0}\right)^{\frac{1}{2}}+\delta\right], \quad (8)$$
$$\text{for } r<r_0,$$
$$V_{ex}(r)=0, \quad \text{for } r>r_0,$$

where $\delta=(3/32\pi^2)^{\frac{1}{2}}(1/Z^{\frac{1}{2}})(r_0/\mu)^{\frac{1}{2}}$. It should be noted that $\phi_{ex}(r/\mu)$ is the solution of the Thomas-Fermi-Dirac equation for prescribed Z which corresponds to zero pressure at the boundary of the atom; r_0 is the finite radius of the atom required as a consequence of the zero-pressure boundary condition. The first term of Eq. (8) is the electrostatic potential and the second term is the effective exchange potential. As is familiar, the electronic self-interactions are correctly eliminated within the framework of the Thomas-Fermi-Dirac model. In the present application, where the Thomas-Fermi-Dirac potential of Eq. (8) is used as the atomic central field in the Schrödinger equation, it does not properly account for the electron self-interaction since it does not possess the correct asymptotic behavior. The potential was therefore modified by the same procedure as was used to get the potential of Eq. (7). The practical difficulty still remains that separate solutions of the Thomas-Fermi-Dirac equation for $\phi_{ex}(r/\mu)$ are required for each value of Z. This difficulty

TABLE I. Term values in Rydbergs computed with the Thomas-Fermi potential of Eq. (7).

Z	$1s$	$2s$	$2p$	$3s$	$3p$	$3d$	$4s$	$4p$	$4d$	$4f$	$5s$	$5p$
2	1.250×10^{0}	2.775×10^{-1}		1.190×10^{-1}			6.578×10^{-2}					
3	2.665	3.606	2.516×10^{-1}	1.402			7.419				4.582×10^{-2}	
4	5.701	4.329	2.553	1.568	1.129×10^{-1}		8.041	6.331×10^{-2}				
5							8.612					
6	1.628×10^{1}	6.321	2.781	1.950	1.207	1.111×10^{-1}	9.374	6.668			5.494	4.216×10^{-2}
7			3.146		1.321			7.137				
8	3.307	1.312×10^{0}	4.220		1.560		1.139×10^{-1}				6.358	4.871
9		1.976	7.078	2.940	1.840		1.226	8.937				
10	5.637	2.871	1.231×10^{0}	3.231	2.027							5.554
11	7.053	3.992	1.986	3.527	2.152	1.113	1.378	9.950			7.314	
12												
13	1.040×10^{0}	6.957	4.195	3.871	2.254							
14				4.323	2.357	1.114	1.563	1.063×10^{-1}	6.265×10^{-3}		8.021	6.039
15				4.970	2.480			1.104				
16	1.671	1.334×10^{1}	9.379	7.344	2.925		2.028	1.158				6.450
17		1.603		9.317				1.350				7.211
18					4.251							
19	2.462	2.227	1.703×10^{1}	1.516×10^{0}	5.654	1.118	2.548	1.637	6.294		1.112×10^{-1}	8.213
22					1.386×10^{0}		3.012	1.939				
23				3.482		1.128			6.354			9.463
24												
25						1.149			6.518			
26	4.934	5.392	4.556	5.713	3.445	1.240	3.902	2.216	7.522		1.461	1.013×10^{-1}
27						2.773			1.060×10^{-1}			
28						5.951						
29	6.268	7.245	6.269	8.667	5.777	1.005×10^{0}	5.378	2.522	1.103	6.250×10^{-3}	1.730	1.113
30						1.499						
31								2.930				
32								3.273			2.056	
33								3.768				1.387
35						5.244	1.363×10^{0}	5.088	1.122		2.359	1.561
37	1.063×10^{0}	1.373×10^{0}	1.238×10^{0}	2.054×10^{0}								
38					1.752×10^{0}	8.572	2.114		1.131		2.639	
40								1.394×10^{0}	1.142		2.836	1.902
41												
42									1.168		3.067	
44									1.320		3.359	2.054
45												
46									3.021		3.760	
47	1.777	2.517	2.332	4.475	3.751	2.404×10^{0}	5.934	3.767	4.652	6.250	4.021	2.218
50											5.163	2.470
52									1.797×10^{0}			2.754
53												2.957
54											7.961	
57	2.679	4.046	3.813	8.070	7.072	5.190	1.350×10^{0}	9.996	3.981	6.251	1.124×10^{0}	4.524
60											1.554	
61										6.251		7.838
63										6.251		
65	3.537	5.558	5.285	1.186×10^{0}	1.064×10^{0}	8.308	2.252	1.785×10^{0}	9.461	6.252	2.529	1.314×10^{0}
66										6.254		
67										3.391×10^{-1}		
68										7.735		1.849
70										1.789×10^{0}		2.274
72										2.995		
74	4.648	7.571	7.253	1.717	1.568	1.283×10^{0}	3.632	3.020	1.894×10^{0}	4.391	5.188	3.299
76											5.957	
77												4.231
78										7.758	6.795	
82	5.765	9.642	9.284	2.285	2.111	1.779	5.212	4.462	3.065	1.191×10^{0}	8.692	6.125
84												
87										1.826	1.150×10^{0}	8.478
88												
92	7.334	1.261×10^{0}	1.220×10^{0}	3.127	2.922	2.530	7.690	6.760	5.007	2.594	1.482	1.133×10^{0}

TABLE I.—*Continued.*

Z	5d	5f	5g	6s	6p	6d	6f	6g	6h	7s	7p	7d
2												
3				3.108×10^{-3}						2.246×10^{-3}		
4												
5												
6				3.605	2.903×10^{-2}					2.546	2.120×10^{-2}	
7												
8				4.053	3.269						2.344	
9										2.911		
10												
11				4.531	3.731					3.050	2.620	
12												
13					3.890	2.783×10^{-2}				3.267	2.713	2.044×10^{-2}
14												
15												
16				5.584	4.265							
17												
18												
19	4.026×10^{-3}				4.948	2.794				3.994	3.307	2.051
22												
23	4.063			6.968	5.516	2.817					3.612	2.067
24	4.091					2.835						2.079
25	4.169					2.887						2.114
26	4.887					3.352				4.692		2.418
27	6.009					3.872						2.702
28	6.152					3.946						2.745
29	6.203			8.611	6.255	3.974				5.140	4.001	2.762
30												
31	6.252											
32	6.268											
33												
35				1.058×10^{-1}	7.931	4.037				6.004	4.811	
37												2.814
38	6.371					4.072						
40	6.444					4.116						2.850
41	6.510					4.158						2.877
42	6.628			1.260	9.298	4.235				6.848	5.440	2.926
44	7.886					4.986						3.373
45	9.667					5.646						3.688
46	1.041×10^{-1}					5.915						3.819
47	1.069	4.000×10^{-2}		1.487	1.017×10^{-1}	6.033				7.721	5.832	3.881
50	1.097					6.175						3.957
52				1.830	1.175					8.898	6.498	
53												
54												
57	1.121	4.000		2.176	1.436	6.307	2.778×10^{-2}			9.987	7.537	4.033
60		4.001				6.366						
61												
63	1.145	4.001				6.460	2.778			1.112×10^{-1}		4.124
65	1.161	4.001		2.691	1.809	6.577	2.779			1.152	8.758	4.196
66		4.004					2.782					
67	1.197	6.249				6.848	4.000					4.363
68	1.238	6.250				7.165	4.000			1.220	9.099	4.555
70	1.529	6.251				8.808						5.307
72	2.724					1.014×10^{-1}	4.001					5.792
74	4.755	6.251	4.000×10^{-3}	3.704	2.128	1.058	4.001	2.778×10^{-2}	2.778×10^{-2}	1.410	9.854	5.978
76												
77												
78	1.077×10^{0}	6.251			2.359	1.089				1.591	1.059×10^{-1}	6.132
82	1.931	6.251	4.000	6.365	2.788	1.104	4.001	2.778	2.778	1.797	1.175	6.212
84	2.455											
87					4.020						1.380	6.293
88	3.713											
92	5.265	6.252	4.000	1.460×10^{0}	6.609	1.135	4.002	2.778	2.778	2.268	1.573	6.393

may be obviated by the observation that the $V_{ex}(r)$ of Eq. (8) may be approximated by a universal potential of the following form:

$$V_{ex}(r)=Ze\frac{\phi(r/\mu)}{r}+\frac{3\sqrt{2}}{4\pi}\frac{Z^{\frac{1}{2}}e}{a_0^{\frac{1}{2}}}\frac{[\phi(r/\mu)]^{\frac{1}{2}}}{r^{\frac{1}{2}}}, \quad \text{for } V_{ex}(r)>e/r, \tag{9}$$

$$V_{ex}(r)=e/r, \quad \text{otherwise,}$$

where $\phi(r/\mu)$ is defined by Eq. (5), and where the proper cut-off behavior has been included. This universal exchange potential deviated from the Thomas-Fermi-Dirac potentials by less than 5 percent for $5<Z<92$; for values of $Z<5$ the error increases. A comparison of (9) with the Thomas-Fermi-Dirac potentials is shown in Figs. 2–6 for $Z=2$, 5, 10, 40, and 92.

IV. NUMERICAL PROCEDURE

The calculations for the term values with the potentials of Eqs. (7) and (9) were carried out by numerical integration of the Schrödinger equation on an IBM 701 Defense Calculator. If the wave function ϕ_i is written as

$$\phi_i=[\psi_i(r)/r]Y_{lm}(\theta,\phi), \tag{10}$$

then ψ_i satisfies the differential equation

$$\psi_i''-\left[\frac{2m\epsilon_i}{\hbar^2}-\frac{2me}{\hbar^2}V(r)+\frac{l(l+1)}{r^2}\right]\psi_i=0, \tag{11}$$

TABLE II. Term values in Rydbergs computed with the Thomas-Fermi-Dirac potential of Eq. (9).

Z	$1s$	$2s$	$2p$	$3s$	$3p$	$3d$	$4s$	$4p$	$4d$	$4f$	$5s$	$5p$
2	1.613×10^{0}	3.048×10^{-1}		1.284×10^{-1}			6.881×10^{-2}					
3	3.818	3.886	2.569×10^{-1}	1.472			7.677				4.709×10^{-2}	4.055×10^{-2}
4	7.471	4.770	2.729	1.669	1.188×10^{-1}		8.398	6.585×10^{-2}				
5							9.366					
6	1.917×10^{1}	9.540	4.208	2.304	1.530	1.113×10^{-1}	1.044×10^{-1}	7.892			5.964	4.807
7			6.709		1.772			8.698				
8	3.711	2.166×10^{0}	1.100×10^{0}		1.953		1.226				6.699	
9		3.082	1.715	3.293	2.097		1.318	9.772				
10				3.743	2.241							5.872
11	7.633	5.540	3.546	4.387	2.420	1.120	1.563	1.083×10^{-1}			7.982	
12				5.336	2.680							
13	1.110×10^{2}	8.956	6.268	6.692	3.099	1.124	1.895	1.264	6.330×10^{-2}		9.100	6.861
14				8.518	3.789			1.389				
15								1.517	6.376			7.775
16	1.759	1.604×10^{1}	1.224×10^{1}	1.369×10^{0}	6.403		2.385					
17		1.898		1.707		1.144		1.732	6.460		1.110×10^{-1}	8.510
18					1.096×10^{0}				6.539			
19	2.567	2.570	2.070	2.554	1.403	1.176	2.922	1.907	6.694		1.216	9.117
20						1.229			7.131			
21						1.475			8.745			
22					2.668	2.500	3.843	2.205	1.024×10^{-1}		1.436	
23				5.018		4.351			1.070			1.056×10^{-1}
24									1.091			
25						1.004×10^{0}			1.104			
26	5.083	3.912	5.117	7.632	5.282		6.682	3.121	1.113		1.818	1.244
27						1.839						
28						2.363						
29	6.434	7.842	6.915	1.098×10^{1}	8.042	2.961	1.057×10^{0}	4.958	1.137	6.251×10^{-2}	2.103	1.469
30						3.639						
31								7.032	1.158			
32								8.348			2.469	
33								9.860	1.194			
34									1.229			
35						8.265	2.392	1.350×10^{0}	1.293		2.759	1.826
36									1.432			
37	1.085×10^{2}	1.454×10^{0}	1.325×10^{0}	2.393					1.745			
38					2.114×10^{1}	1.212×10^{1}	3.383		2.319		3.309	2.019
39												
40								2.662	4.250		3.862	2.185
41												
42									7.148		4.655	2.427
44											5.672	2.793
46											7.016	
47	1.805	2.625	2.450	4.964	4.257	2.918	7.949	5.656	1.883×10^{0}	6.253	7.808	3.720
50											1.068×10^{1}	5.270
52									3.776			6.711
53												7.558
54											1.588	
55												
56												
57	2.701	4.182	3.960	8.715	7.744	5.886	1.634×10^{1}	1.284×10^{1}	6.509	6.256	2.085	1.186×10^{1}
58										6.257		
59										6.275		
60										2.667×10^{-1}		
61											2.913	1.777
62												
63										1.297×10^{0}		
65	3.576	5.716	5.456	1.264×10^{1}	1.145×10^{1}	9.153	2.616	2.149	1.288×10^{0}	2.195	3.944	2.552
67												3.017
68										3.859		
70										5.184	5.558	3.816
72												
74	4.692	7.554	7.451	1.809	1.664	1.384×10^{0}	4.086	3.480	2.340	8.371	7.133	5.093
77												6.219
78										1.230×10^{1}	8.994	
80												
82	5.814	9.848	9.507	2.390	2.222	1.896	5.750	5.010	3.605	1.701	1.115×10^{1}	8.445
84												
85												
87												1.114×10^{1}
88										2.560		
89												
90												
91												
92	7.390	1.285×10^{0}	1.246×10^{1}	3.249	3.030	2.666	8.336	7.420	5.668	3.240	1.785	1.435

where $V(r)$ is either the potential of Eq. (7) or of Eq. (9). The scheme adopted for the numerical integration of Eq. (11) is similar to one recently suggested by Blanch.[15] Equation (11) was converted into the following integral equation:

$$\psi_l(r)=\psi_l'(0)r+\int_0^r(r-r')\left[\frac{2m\epsilon_l}{\hbar^2}-\frac{2me}{\hbar^2}V(r')+\frac{l(l+1)}{r'^2}\right]\psi_l(r')dr', \quad (12)$$

[15] G. Blanch, Math. Tables and Other Aids to Computation **6**, 219 (1952).

TABLE II.—*Continued.*

Z	5d	5f	5g	6s	6p	6d	6f	6g	6h	7s	7p	7d
2												
3				3.179×10^{-3}	2.810×10^{-3}					2.290×10^{-3}	2.061×10^{-3}	
4												
5												
6				3.851	3.233					2.690	2.322	
7												
8				4.237	3.574							
9											2.595	
10										3.136		
11				4.872	3.935						2.740	
12												
13				5.387		2.807×10^{-3}				3.546	2.951	2.060×10^{-3}
14												
15	4.074×10^{-3}				4.739							
16										3.892	3.292	
17	4.125			6.253		2.856						2.092
18	4.173					2.887						2.113
19	4.273	4.000×10^{-3}		6.698	5.359	2.951				4.224	3.529	2.155
20	4.554					3.128						2.271
21	5.330					3.540						2.514
22	5.852					3.789						2.653
23	6.046			7.892	6.001	3.888				4.802	3.868	2.711
24	6.145					3.942						2.743
25	6.210				6.479	3.978						2.765
26	6.262	4.001				4.007				5.263	4.247	
27												2.798
28												2.815
29	6.404	4.001		9.810	7.578	4.090				5.670	4.640	2.833
30												
31	6.533					4.166						2.880
32	6.631				8.245	4.224				6.065		2.916
33	6.773					4.308					5.046	2.968
34	7.007					4.446						3.051
35	7.428			1.179×10^{-1}	8.835	4.677						3.185
36												
37	9.091					5.383				6.880		3.548
38	9.776				9.492	5.641					5.528	3.676
39	1.020×10^{-1}					5.808						3.761
40	1.046					5.922						3.820
41	1.064					6.005						3.865
42	1.077			1.563	1.075×10^{-1}	6.071				7.960	6.074	3.900
44					1.163							
46												
47	1.121	4.002		1.878	1.314	6.309				9.021	6.807	4.034
50	1.148					6.466						4.124
52	1.173			2.189	1.543	6.617				1.002×10^{-1}	7.815	4.211
53						6.722						4.271
54	1.212					6.861						4.350
55	1.244					7.050						4.454
56	1.290											
57	1.361	4.005		2.578	1.737	7.700	2.781×10^{-3}			1.120	8.508	4.782
58	1.480	4.006					2.783					
59	1.672	4.039				8.731	2.831					5.213
60		6.248					3.999					
61	2.366			3.055	1.910	9.614				1.246	9.114	5.553
62												5.672
63	3.502					1.013×10^{-1}	4.003					5.766
65	5.069	6.254		3.831	2.154	1.044	4.003			1.406	9.910	5.907
67												
68				4.709		1.074				1.539	1.072×10^{-1}	6.056
70	1.092×10^{0}	6.255			2.722	1.090					1.136	6.136
72				6.381			4.004					
74	1.778	6.256	4.000×10^{-3}	7.456	3.605	1.118	4.005	2.778×10^{-3}	2.778×10^{-3}	1.801	1.278	6.291
77												
78	2.686			1.012×10^{0}	5.052	1.152				1.972	1.414	6.484
80	3.229	6.257				1.176						6.620
82	3.837	6.258	4.000	1.355	7.098	1.209	4.007	2.778	2.778	2.155	1.533	6.812
84	4.511											
85		6.262				1.299						7.304
87		6.277		1.901	1.084×10^{0}	1.422	4.028				1.673	7.860
88	6.071	6.385				1.523	6.108			2.503		
89		2.071×10^{-1}										8.565
90		5.608					6.247					
91		5.340				2.082	6.250					9.214
92	7.930	7.263	4.000	2.597	1.579	2.372	6.252	2.778	2.778	2.839	1.828	9.474

where the boundary condition $\psi_i(0)=0$ has been used. For the numerical work, the integral equation was replaced by a difference equation. To insure stability of the difference equation, the integral which is the coefficient of r was evaluated by Cote's rule and the remaining integral was evaluated by Simpson's rule. Division points for the numerical integration were based on a scale of $r^{\frac{1}{2}}$, rather than on r, since the former scale makes the variations in the functions ψ_i more uniform. Improvements on initial guesses of the eigenvalues were obtained by a convergence procedure coded into the machine. This procedure automatically selected new guesses for the eigenvalues based on the requirement that the eigenfunction had the prescribed number

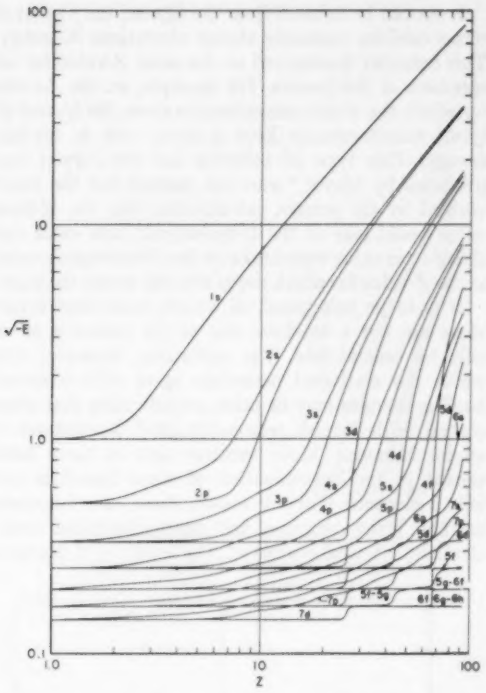

FIG. 7. The square root of the term values of Table I for the Thomas-Fermi atom is shown as a function of Z.

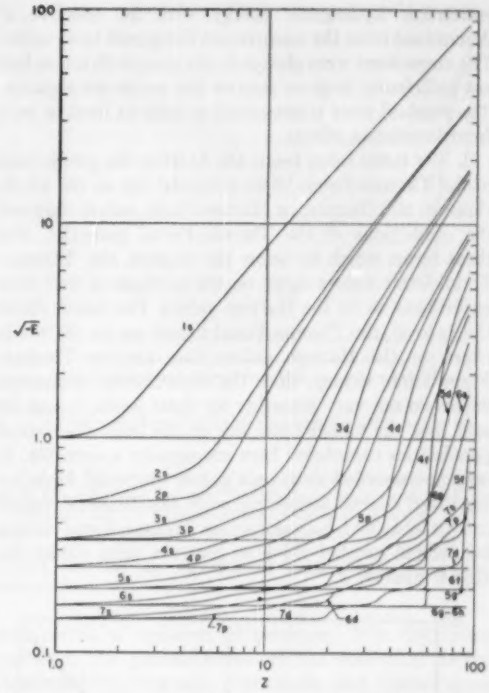

FIG. 8. The square root of the term values of Table II for the Thomas-Fermi-Dirac atom is shown as a function of Z.

of zeros and had a zero at a point distant from the origin where it was estimated to have a value less than 10^{-7} of its maximum value. The solution ψ_i will contain a small amplitude contribution from the irregular solution as a result of inevitable truncation and rounding errors in the numerical scheme. This error in the eigenfunction precludes the possibility of the solution being zero at the prescribed point. The accuracy of the eigenvalue determination is not affected by this difficulty. When the eigenvalue is known, this error in the eigenfunction may be avoided by integrating both inward and outward, and then joining the solutions at a point where the irregular solution is known to be negligible. This latter procedure is now in use in computations of eigenfunctions.

V. RESULTS AND CONCLUSIONS

The results of the present calculations for the one-electron term values $1s$ to $7d$ with the Thomas-Fermi potential of Eq. (7) are summarized in Table I. Similarly, the results for the same one-electron term values with the Thomas-Fermi-Dirac potential of Eq. (9) are shown in Table II. The values computed for Tables I and II include the minimum number of term values necessary to give a survey of the periodic table and also to permit easy graphical interpolation for those term values not tabulated. The numerical values of Tables I and II are shown graphically in Figs. 7 and 8, respectively. A more detailed presentation of the results is given in Figs. 9–12[16] which also include those Hartree, or Hartree-Fock, values which are available in the literature.[17] These figures also give a comparison of the computed values with experimental ionization energies taken from Landolt-Bornstein.[18]

The following conclusions are drawn from the computations with the statistical potentials:

1. There is a discrepancy at large binding energies between experimental term values and computed values whether computed with the statistical potential or with the Hartree procedure. This discrepancy is attributed to relativistic effects. An approximate correction for these relativistic effects was made by using the known

[16] The levels $5g$, $6g$, and $6h$ are not included in these figures since these levels have hydrogenic term values.

[17] A survey of the existing results is given by D. R. Hartree, Repts. Progr. Phys. **11**, 8 (1946–47) and by Landolt-Bornstein (reference 18).

[18] Landolt-Bornstein, *Atom—und Molekularphysik* (Springer-Verlag, Berlin, 1950), Part I.

Note added in proof.—Recently J. C. Slater [Phys. Rev. **98**, 1039 (1955)] has published a revised table of experimental one-electron term values for free atoms with atomic numbers below 41. Some of these term values show large deviations from those of Landolt-Bornstein which are presented in Figs. 9–12. However, these differences do not essentially affect the qualitative comparisons with the theoretical results.

relativistic hydrogenic energy with an effective Z determined from the uncorrected computed term value. The corrections were always in the proper direction but not sufficiently large to remove the entire discrepancy. The residual error is presumed to arise at least in part from correlation effects.

2. For terms lying below the $3s$-level, the predictions of the Thomas-Fermi-Dirac potential are on the whole closer to the Hartree, or Hartree-Fock, values than are the predictions of the Thomas-Fermi potential. For these terms which lie below the $3s$-level, the Thomas-Fermi-Dirac values agree on the average as well with experiment as do the Hartree values. For terms above the $3s$-level, the Thomas-Fermi values are on the whole closer to the Hartree values than are the Thomas-Fermi-Dirac values; since the experimental ionization values do not vary smoothly for these levels, it may be said that the values from any of the three theoretical possibilities considered here are equally acceptable. It may be remarked that, on a purely empirical basis, an improved overall agreement with experimental values can be obtained by taking the Thomas-Fermi values for atomic number $Z+\frac{1}{2}$ to give the term values for atomic number Z.

3. As can be inferred from the figures, the f series of terms exhibits unusually abrupt alterations in energy. This behavior is observed at the same Z-value for all members of the f-series. For example, at the Z-value for which the $4f$-electron enters the atom, the $5f$- and $6f$-levels simultaneously have a sharp rise in binding energy. This type of behavior for the f-series was predicted by Mayer,[6] who also pointed out the result verified by the present calculations, that the $5f$-term value would take on the $4f$-hydrogenic term value and the $6f$-term value would take on the $5f$-hydrogenic value at the Z-value for which the $4f$-electron enters the atom.

It is to be recognized, of course, that term values alone are not a sensitive test of the accuracy of an effective central field. The uniformity, however, with which the statistical potentials agree with observed binding energies may be taken as indicating that these central fields furnish reasonably good descriptions of atomic behavior. More sensitive tests of these fields consist in the determination of wave functions and matrix elements. For this reason, these wave functions are now being computed and photo-absorption coefficients will then be evaluated. The accuracy of the term

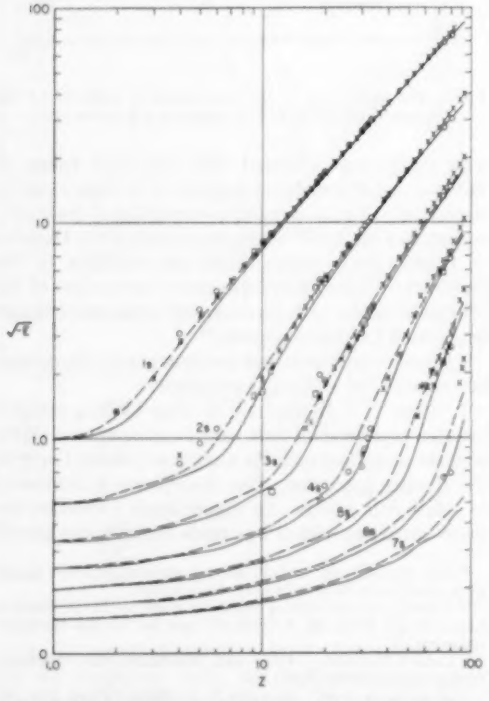

FIG. 9. The square root of the computed s-levels are shown with the solid line for the Thomas-Fermi atom and with the dashed line for the Thomas-Fermi-Dirac atom. The circles (○) are the values computed by the Hartree method; the squares (□) are the values computed by the Hartree-Fock method. The crosses (×) are the experimental values.

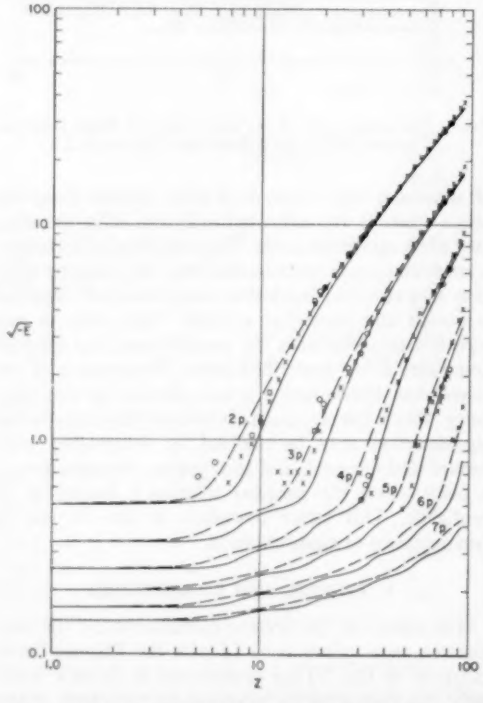

FIG. 10. The square root of the computed p-levels are shown with the solid line for the Thomas-Fermi atom and with the dashed line for the Thomas-Fermi-Dirac atom. The circles (○) are the values computed by the Hartree method; the squares (□) are the values computed by the Hartree-Fock method. The crosses (×) are the experimental values where the doublet energies have been averaged.

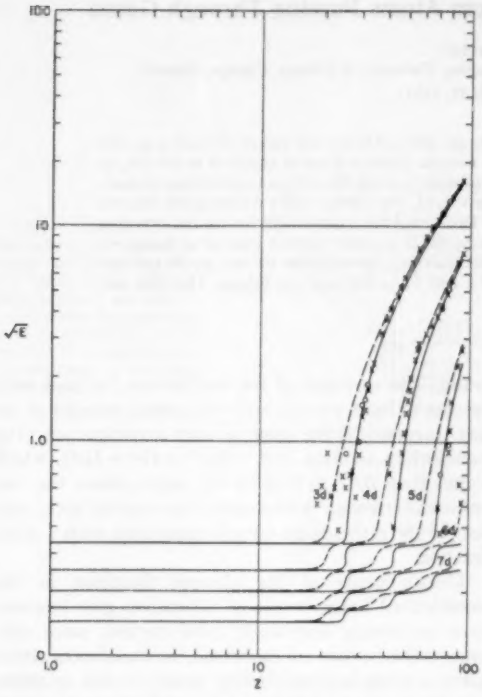

FIG. 11. The square root of the computed d-levels are shown with the solid line for the Thomas-Fermi atom and with the dashed line for the Thomas-Fermi-Dirac atom. The circles (○) are the values computed by the Hartree method; the squares (□) are the values computed by the Hartree-Fock method. The crosses (×) are the experimental values where the doublet energies have been averaged.

values for the statistical potentials suggests further that the perturbation expansion will converge rapidly. It may reasonably be expected, therefore, that the first order perturbation correction to the present zero order term values will comprise the principal part of the residual errors. The verification of this conjecture by calculation of the matrix elements of the perturbation operator of Eq. (4) is now in progress.

The statistical model, with the potential that it determines, makes possible the approximate calculation of other kinds of atomic states. For example, the energies and wave functions of ionized atoms may be computed. One may also treat atoms under pressure

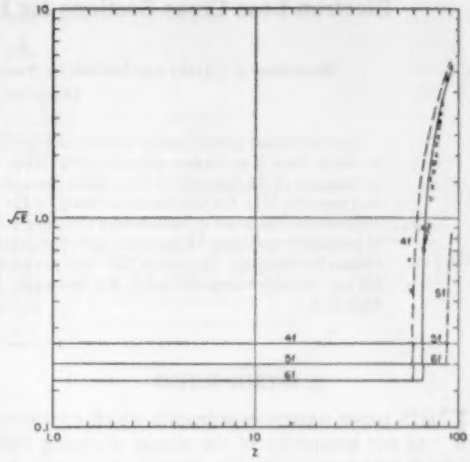

FIG. 12. The square root of the computed f-levels are shown with the solid line for the Thomas-Fermi atom and with the dashed line for the Thomas-Fermi-Dirac atom. The circles (○) are the values computed by the Hartree method; the squares (□) are the values computed by the Hartree-Fock method. The crosses (×) are the experimental values where the doublet energies have been averaged.

and atoms at nonzero temperature. For the latter problem, the generalization of the statistical model developed by Feynman, Metropolis, and Teller[19] gives a potential distribution which may be used as an effective central field. This central field approximates the effective field in the atom averaged over the thermal fluctuations of the electron cloud. The term values and one-electron eigenfunctions computed with this potential are averages which neglect the effects of thermal fluctuations. It may be expected that this approach to the effects of temperature on the atom will be particularly useful in computations of opacity and equations of state. These computations are now in progress.

ACKNOWLEDGMENTS

The author expresses his sincere appreciation to Miss Barbara Batchelder, Miss Ruth Merrill, and Miss Frieda Rosenberg for their capable numerical assistance. The author is indebted to Dr. W. G. McMillan, Dr. A. L. Latter, and Professor M. S. Plesset for many helpful discussions.

[19] Feynman, Metropolis, and Teller, Phys. Rev. **75**, 1561 (1949).

Electron Loss Cross Sections for Helium Atoms Passing Through Gases

SOL KRASNER
Department of Physics and Institute for Nuclear Studies, University of Chicago, Chicago, Illinois
(Received March 31, 1955)

Neutral helium atoms having kinetic energies in the range 100 to 450 kev are passed through a gas cell in which there is an intense magnetic field. When a few microns pressure of gas is admitted to the cell, an attenuation of the transmitted beam takes place, due to collisions in which the helium atoms become ionized, and removed from the unidirectional beam by the magnetic field. The method will not distinguish between collisions in which one or both helium electrons are lost. The sum of the cross sections for the two processes is measured, per atom of gas traversed. The cross sections rise in a rather uniform manner as energy increases in this range. In units of 10^{-17} cm^2 per atom of gas traversed, the values at 100 and at 450 kev are: for air, 30.2±0.8 and 43.9±1.5; for hydrogen, 5.8±0.6 and 12.5±0.8; and for helium, 11.6±0.6 and 16.8±0.4.

1. INTRODUCTION

THIS paper reports experiments which contribute to our knowledge of the charge changing collisions of helium ions passing through gaseous media. The kinetic energies of the ions lie in the range 100–450 kev, where their translational speeds are comparable to the speed of the electrons in the neutral helium atom. The experiment is one which measures the sum of the cross sections for producing magnetically deviable charged ions from moving neutral atoms. Using the notation of Snitzer,[1] where σ_{if} is the cross section for a collision in which the initial positive charge of the moving ion is i and its final charge f, in electron units, the present experiments measure the sum $(\sigma_{01}+\sigma_{02})$, referring to the processes $He^0 \rightarrow He^+ + \epsilon$ and $He^0 \rightarrow He^{++} + 2\epsilon$, respectively.

The experimental results on charge changing collisions in helium as of June, 1953, have been reviewed by Allison and Warshaw.[2] At that time the equilibrium fractions of the various charged states in a helium beam had been measured by Snitzer[1] in the present energy range, and certain scattered data were available on equilibrium ratios and cross sections σ_{12} at energies extending upward from 646 kev were available from Rutherford's work.[3] Since that time Bittner[4] has reported an application of these phenomena in the production of a He^{++} beam for the van de Graaff acceleration. This is accomplished by the preliminary acceleration of the readily available He^+ through 400 kev, followed by stripping to He^{++} by passing through a small amount of gas. Also a group at Oak Ridge[5] have measured the equilibrium charge distribution of helium ions in the range 20–250 kev passing through the gases H_2, He, N_2, O_2, Ne, and A. In the region between 100 and 200 kev, where there is some overlapping of their results with those of Snitzer, the Oak Ridge investigators find approximately 20 percent more He^0 in the equilibrated beam. The variation of the equilibrium fractions with respect to beam energy, and with atomic number of the gas traversed, is the same in both investigations. The equilibrium fraction $He^{++}/(He^{++}+He^+ + He^0)$, which varies from 0.02 to 0.04 in the region where the two researches overlap is essentially the same in both, subject to the rather large error in measuring such a small fraction.

Measurements of the charged fractions in the equilibrated beam do not of themselves give information concerning any single cross section, since only cross-section ratios are concerned. An experiment which gives a cross section directly must involve transient conditions, in which the thickness of the layer traversed is not sufficient to equilibrate the beam. Some cross sections σ_{10} for He^+ ions at energies below 40 kev have been obtained by Stedeford and Hasted.[6] Values of σ_{12} for He^+ ions in various gases at 10 and 20 kev have been reported by Fedorenko.[7] There do not seem to have been any loss cross sections for He^0 measured previously.

2. METHOD OF THE EXPERIMENT

The technique of the experiment is essentially the same as that of Montague[8] and Kanner[9] in their measurements of electron loss cross sections for hydrogen atoms in H_2 and in air. The beam of neutral helium atoms was obtained by allowing the He^+ beam from the University of Chicago's Cockcroft-Walton accelerator (kevatron) to pass through a small amount of gas, and then bending away the charged components, He^+ and He^{++}, from the emergent beam by means of a magnetic field.

The neutral beam then passed through a measuring chamber situated in the magnetic field, and was detected by a secondary electron emission detector at its far end. When gas at a known pressure, p, is admitted into the chamber, some of the neutral helium atoms collide with the gas molecules, are stripped of one, or

[1] E. Snitzer, Phys. Rev. **89**, 1237 (1953).
[2] S. K. Allison and S. D. Warshaw, Revs. Modern Phys. **25**, 779 (1953).
[3] E. Rutherford, Phil. Mag. **4**, 277 (1924).
[4] J. Bittner, Rev. Sci. Instr. **25**, 1058 (1954).
[5] Stier, Barnett, and Evans, Phys. Rev. **96**, 973 (1954).
[6] J. B. H. Stedeford and J. B. Hasted, Proc. Roy. Soc. (London) **A227**, 466 (1955).
[7] N. V. Fedorenko, Zhur. Tekh. Fiz. **24**, 769 (1954).
[8] J. H. Montague, Phys. Rev. **81**, 1026 (1951).
[9] H. Kanner, Phys. Rev. **84**, 1211 (1951).

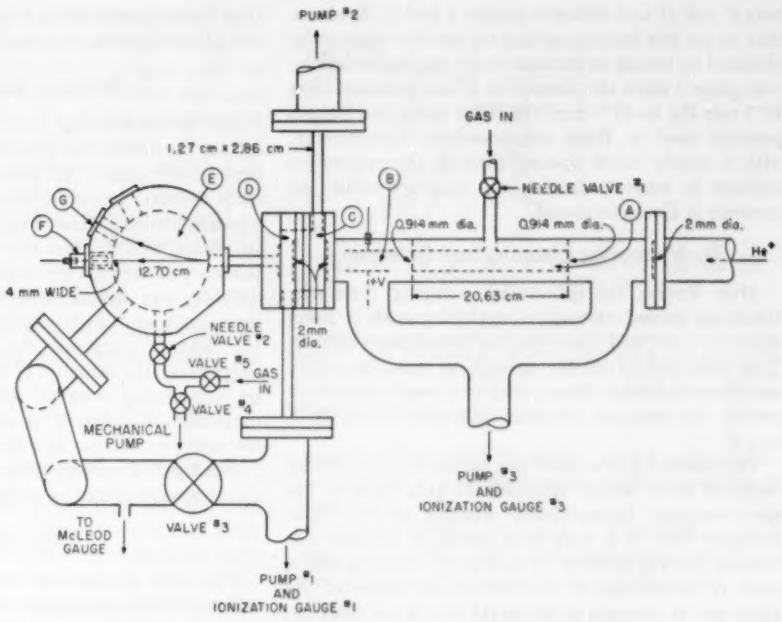

FIG. 1. Apparatus. Neutral helium is produced by charge equilibration of a He^+ beam in the differentially pumped gas cell A. Loss cross sections are measured in chamber E, in the presence of a magnetic field perpendicular to the plane of the figure.

perhaps two electrons, and then are removed from the beam by the magnetic field, thus giving rise to an attenuation of the neutral beam.

The electron loss cross section per atom of gas traversed is given by

$$(\sigma_{01}+\sigma_{02})=\frac{kT}{pl\xi}\ln\frac{R(0)}{R(p)}, \qquad (1)$$

where l is the path length in the measuring chamber, $R(0)$ is the normalized beam intensity with no gas in the chamber, and $R(p)$ that when the gas pressure in the chamber is p dynes/cm^2. k is the Boltzmann constant, T the temperature in °K, and ξ is the number of atoms per molecule in the gas.

3. DESCRIPTION OF THE APPARATUS

A schematic diagram of the apparatus is given in Fig. 1 and will be referred to in the following discussion.

A. Equilibrating Cell

This is cell A of Fig. 1. In it, the beam of He^+ ions is charge equilibrated by passing through a gas. The cell is a pipe 20.63 cm long having small holes, 0.94-mm diameter, at both ends. Diffusion pumps 1, 2, and 3 and the kevatron diffusion pumps have sufficient pumping speed so that when a controlled amount of gas is admitted through needle valve No. 1 no perceptible rise in pressure occurs in the kevatron or the measuring chamber E. Sufficient gas is admitted to establish charge equilibrium, and this can be accomplished without significantly decreasing the average energy of the transmitted beam.

The pressure used in the equilibrating cell was on the order of 10 microns. If one calculates the energy lost by 400-kev helium ions in air, using an energy loss cross section[10] of 84.6×10^{-16} ev×cm^2/molecule, one finds the energy loss is less than one kev. For lower energies, or for lighter gases in the equilibrating cell, the loss would be less.

B. Beam Monitor

The emergent beam, now about 1-mm diameter, next passes through the monitor (B in Fig. 1), which is essentially a parallel plate ionization chamber. The lower plate is connected through an insulated seal to the positive terminal of a 90-volt battery; thence to ground. The upper plate is connected through a well-insulated (10^{13} ohms) Teflon seal to some type of current integrator. With enough gas in the equilibrating cell to establish charge equilibrium, the gas pressure in the monitor region was sufficient to give currents of the order 10^{-10} ampere.

C. Differential Pumping System

Since the monitor current is directly proportional to the gas pressure between the two plates it is essential that the pressure here remain unchanged when gas is admitted to the measuring chamber E. In order to accomplish this it was necessary to install two stages of differential pumping, represented in Fig. 1 by cham-

[10] P. K. Weyl, Phys. Rev. **91**, 289 (1953).

bers C and D and diffusion pumps 1 and 2. Evidence that no gas was backing up into the monitor region was obtained by noting no increase in the reading on ionization gauge 3 when the pressure in E was increased from 10^{-4} mm Hg to 10^{-3} mm; the latter being the highest pressure used in these measurements. Furthermore, with a steady beam passing through the system no increase in monitor current was observed when the pressure in E was increased.

D. Measuring Chamber and Detector

After leaving the differential pumping chambers, the beam passed through a steel plug with a 2-mm diameter hole, and then into the measuring chamber. This hole had to be big enough to pass the entire equilibrated helium beam, and yet small enough to permit the required pressure differential between E and B.

The measuring chamber[11] is a hollow bronze cylinder designed to fit snugly between the pole faces of the electromagnet. Diametrically opposite to the 2-mm entrance hole is a port into which is inserted the neutral particle detector (F in Fig. 1). There is also a port, G, whose axis is directed to the center of the circle and at an angle of 30° to the axis of the detector. At this "thirty-degree" port was placed a glass plate, covered on the inside with ZnS powder. As will be shown later, the effective path length for attenuation depends on the radius of curvature of the ions in the magnetic field. This radius of curvature was maintained constant at all beam energies by adjusting the magnetic field so that the spot from the He^+ portion of the equilibrated beam could always be seen at a fixed point on the ZnS surface.

The detector is the same as that used by Montague.[8] It consists of an inclined beryllium-copper plate in the path of the beam and a grounded electrode parallel to the collecting plate but out of the way of the beam. A saturating negative potential (−67.5 volts) is applied to the collecting plate so that when a neutral atom strikes it, the secondary electrons are driven to the grounded plate. The geometry is such that the electron paths are parallel to the magnetic lines of force. The net positive current to the collecting plate was summed on a small current integrator.

E. Current Integrators

Three different circuits were used as current integrators in the course of these measurements, and every cross section reported here was measured with two or more different combinations of them. In each of the three circuits, the rise of voltage across a high-quality condenser was detected as the condenser was being charged by the current to be measured. This rise in voltage was detected by (1) a quadrant electrometer,[12] (2) a battery-operated dc amplifier of standard design,[13] and (3) a vibrating reed electrometer.[14]

F. Pressure Measurements

For a quick-acting pressure indicator, useful in setting the needle valve, pressures could be read on an Alphatron[15] gauge. All pressures used in calculating cross section, however, were measured on a liquid nitrogen trapped McLeod gauge. At first it was difficult to obtain reliable McLeod readings because of the tendency of the mercury to stick in the capillaries. This difficulty was completely overcome by roughening the inner surfaces of both capillaries with carborundum in the manner suggested by Rosenberg.[16] After this roughening, the diameter of the capillary was measured by introducing weighed amounts of mercury. The calibration of the gauge was also checked by stopping the mercury columns at different points with the same trapped gas. Pressures computed from these measurements always agreed to within 3 percent.

G. Gases

The only precaution taken in admitting air for attenuation measurements was to pass it through a calcium chloride drying tube. There were occasional indications that the gases H_2 and He were contaminated by heavier gases when in the measuring chamber. They were brought to needle valve No. 2 from their storage tanks through short plastic tubing lines in which the gases were kept slightly above atmospheric pressure and constantly flowing. Electrolytic hydrogen was used, with a "Deoxo"[17] catalytic unit to combine the oxygen, followed by a trap immersed in liquid nitrogen to freeze out the water vapor. The helium used was government grade A, 99.9 percent pure.

4. EXPERIMENTAL PROCEDURE

A. Measurement of Attenuation Ratio and Pressure

The procedure in a typical cross-section measurement will be described with reference to Fig. 1. Gas was first admitted through needle valve No. 1 into the equilibrating cell; then with the beam directed so as to pass through the apertures of this cell, the magnetic field on the measuring chamber was adjusted until the He^+ spot appeared at the 30° port.

Then the quantities $R(0)$ and $R(p)$ of Eq. (1) were determined by taking readings of the quantity of charge collected by the detector in the time that the monitor collected a fixed amount of charge, first with

[11] Described more fully in reference 8.
[12] Described in U. S. Atomic Energy Commission Document MDDC-562 (unpublished).
[13] The circuit ("Zeus") is given on the data sheet for the Raytheon CK5697/CK570 electrometer triode.
[14] Built by the Applied Physics Corporation, Pasadena, California.
[15] National Research Corporation, Cambridge, Massachusetts.
[16] P. Rosenberg, Rev. Sci. Instr. 9, 258 (1938).
[17] Baker and Company, Newark, New Jersey.

vacuum in the measuring chamber, and then after gas was admitted. The pressure was then taken. By closing valve 5 and opening valve 4, vacuum could be produced in the measuring chamber without mechanically closing the needle valve No. 2, thus preserving its setting for subsequent gas in, gas out cycles.

Data from a typical experiment are exhibited in Fig. 2. Referring to this figure, if we let $p_{\frac{1}{2}}$ represent the pressure at which the attenuation ratio would be 0.5, as read by extrapolation from the plot, Eq. (1) becomes

$$(\sigma_{01}+\sigma_{02})=0.693(kT)/l\xi p_{\frac{1}{2}}.$$

Using $l=10.11$ cm, $T=287°$K, $k=1.38\times10^{-16}$ erg/°K, $\xi=2$, and $p_{\frac{1}{2}}=(2.98\pm0.10\mu)(1.33)$ dynes/(cm^2 μ), we obtain

$$(\sigma_{01}+\sigma_{02})=(34.1\pm1.1)\times10^{-17}\text{ cm}^2\text{ per air atom.}$$

B. Determination of Attenuation Path Length

The effective path length is less than the diameter of the measuring chamber because ions formed close to the detector do not have their paths deviated sufficiently by the magnetic field to miss the entrance slit to the detector. It is clear that this "ineffective distance" s is determined by the radius of curvature of the He^+ ions in the magnetic field, the width and shape of the beam, and the location of the undeflected, neutral beam in the detector slit opening. As pointed out before, the radius of curvature for He^+ was kept the same (23.7 cm) in all experiments.

The width and location of the beam were measured as follows. A simple circuit was devised by means of which the current through the magnet could be varied continuously from -0.25 to 0.25 ampere, sufficient to sweep the charged component of the beam completely across the slit. The measuring chamber was evacuated; and for each magnet current setting the normalized beam intensity, $R(0)$, and the magnetic field strength were measured. The latter was accomplished with a rotating coil fluxmeter driven by a synchronous motor. The resultant plot of $R(0)$ *versus* fluxmeter reading is shown in Fig. 3.

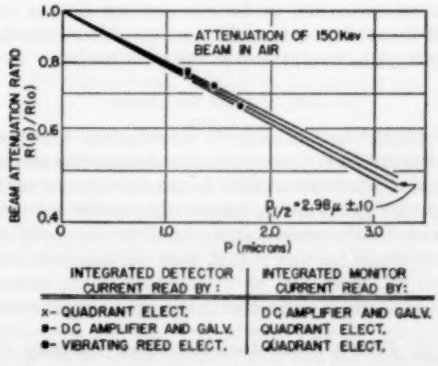

FIG. 2. Typical experimental data. $R(p)/R(0)$ is the ratio of the monitored emergent beam intensity with gas in the cell to its value with the cell evacuated.

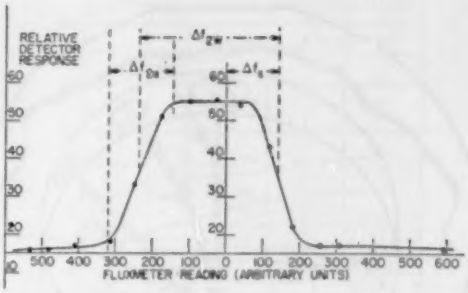

FIG. 3. Response of the detector as the charged component of the beam is swept across the detector aperture by varying the magnetic field. The asymmetry about $H=0$ shows that the neutral beam does not fall exactly in the center of the slit. When cross-section measurements were being made, the charged beam was deflected to the right.

From an inspection of Fig. 4, it is seen that a small linear displacement d of the charged component of the beam, caused by the magnetic field, is given by

$$d=D^2/2\rho, \qquad (2)$$

where ρ is the radius of curvature of He^+ in the magnetic field, and $D=12.70$ cm is the distance from the entrance of the measuring chamber to the detector slit. Since $H\rho$ is constant for a given ion momentum and charge, d is proportional to H and thus to the fluxmeter reading.

Using this proportionality, we may make certain useful calculations. First, we note that the change of fluxmeter reading Δf_{2W} (Fig. 3) corresponds to a displacement of the center of the beam through the known width of the detector slit ($2W=4$ mm). The fluxmeter change Δf_{2a} corresponds to a displacement of the center of the beam a distance equal to the beam diameter $2a$. Thus

$$2a=(\Delta f_{2a}/\Delta f_{2W})(2W)=1.88\text{ mm}. \qquad (3)$$

Furthermore, Δf_s represents the distance from the center of the undeflected beam to the closest edge of the slit, and this distance s is

$$s=(\Delta f_s/\Delta f_{2W})(2W)=1.51\pm0.2\text{ mm}. \qquad (4)$$

Now, to calculate the effective path length, we assume the beam to have a circular cross section of radius $a=0.94$ mm, and average the "ineffective distance" z over the cross section of the beam. One arrives at the formula,

$$\bar{z}=(2\rho)^{\frac{1}{2}}\int_{-a}^{a}[(s-x)(a^2-x^2)]^{\frac{1}{2}}dx\Big/\int_{-a}^{a}(a^2-x^2)^{\frac{1}{2}}dx, \qquad (5)$$

for the average ineffective distance.

Numerical integration of the above formula with $\rho=23.7$ cm gives $\bar{z}=2.59$ cm, so for the effective path

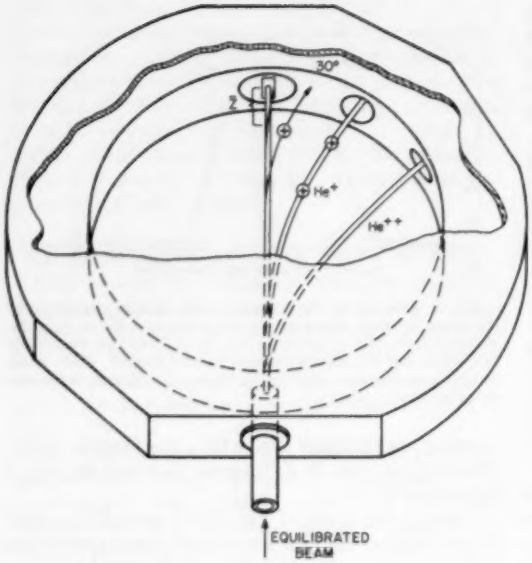

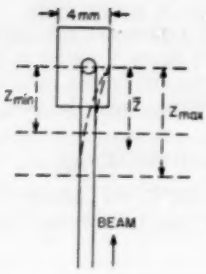

FIG. 4. If a singly charged helium ion is produced from a neutral in the region $\bar{z}$, the magnetic deviation is not sufficient to remove it from the detector aperture.

length for attenuation we have

$$l = D - \bar{z} = 10.11 \text{ cm}.$$

The path length l was also determined by another independent, but less accurate method. The electron loss cross section for 100-kev He atoms in air was measured in the standard magnetic field ($\rho = 23.70$ cm) and also in a larger magnetic field which corresponded to a radius of curvature of 11.2 cm for the He^+ ions. From Eq. (5), we see that $\bar{z}$ varies as $\rho^{\frac{1}{2}}$, so that the two attenuation lengths are $[D-\bar{z}]$ and $[D-\bar{z}((11.2)/(23.70))^{\frac{1}{2}}]$, respectively. Each of these lengths is proportional to the logarithm of the corresponding attenuation ratio, and from the observed ratio of these logarithms at constant pressure it resulted that $\bar{z} = 2.80$. In computing cross sections, however, the value $\bar{z} = 2.59$ was used.

C. Checks for Internal Consistency

(1). *Starting Point for Electron Loss Path*

The effective path length could conceivably be increased because of collisions with gas atoms located between the equilibrating cell and the measuring chamber if the fringing magnetic field were sufficiently strong in this region to separate out the charged ions. This source of error was shown to be negligible by the following experiment, in which the magnetic field was present.

With a certain gas pressure p present in the measuring chamber, the intensity of the attenuated He^0 beam was measured. Then the large valve 3 was opened, and the pressure p re-established in the measuring chamber by considerably increasing the opening of the needle valve No. 2. This greatly increased the gas pressure in chamber D, where the stray magnetic field might operate, but no measurable decrease in beam intensity resulted.

(2) *Saturation of Bias Potential on the Detector*

With chamber E evacuated and the magnetic field on, it was found that $R(0)$ was independent of the bias voltage applied to the collecting plate of the Montague detector if such voltage was more negative than -45 volts. The bias used was -67.5 volts, and since the maximum potentials built up on the detector in the course of measurement were of the order of one volt, saturation was maintained.

(3) *Saturation of Bias Potential on the Monitor*

By measuring $R(0)$ as a function of monitor plate potential, saturation in the collected ion current was found if the drop across the monitor plates exceeded 65 volts; 90 volts was used in the experiments.

(4) *Gas Effect on the Detector*

Montague[5] and subsequent investigators who used this detector for hydrogen charge exchange cross-section measurements found a small increase of detector sensitivity with gas pressure, but for the smaller gas pressures used in the present work, the effect was negligible. The evidence for this is that with the magnetic field turned off, there was no attenuation in the neutral beam when gas was admitted to the measuring chamber.

(5) *Effect of Small-Angle Rutherford Scattering*

The absence of beam attenuation when gas is admitted, but with no magnetic field, shows that the

spreading of the beam by small-angle Rutherford scattering has not diverted an appreciable amount of it outside the aperture of the detector. This is because the beam diameter (1.88 mm) at the detector slit is considerably less than the width and height of the slit (4×4 mm). The absence of an effect was confirmed by a calculation of the scattering to be expected.

5. RESULTS

The results are listed in Table I and plotted in Fig. 5. The errors listed are estimates based on the scatter of the points about the chosen straight lines in the plots of the logarithm of the attenuation against the pressure (see Fig. 2). They do not include possible systematic errors.

Table I also includes values of a parameter γ_i which has the following significance. Suppose the electrons in the complete atom corresponding to the moving ion are numbered serially, 1, 2, $\cdots i$, $\cdots Z$, in order of increasing binding. Suppose that at some point in the path of the moving ion the ith electron is the outermost one,

TABLE I. Experimental results. Sum of the cross sections for the loss of one or both electrons from a moving helium atom.

Kinetic energy of He^+ in kev	V cm/sec ×10⁸	γ_1 [see Eq. (7)]	$(\sigma_{01}+\sigma_{02})\times10^{17}$ square centimeters per atom H_2	He	Air
100	2.20	1.69	5.8±0.6	11.6±0.6	30.2±0.8
120	2.41	1.55	7.8±0.6	···	···
150	2.70	1.38	8.4±0.5	12.6±0.7	34.1±1.1
200	3.12	1.20	9.2±0.4	13.6±0.7	···
250	3.48	1.07	10.3±0.7	13.6±0.7	38.2±1.0
300	3.82	0.98	11.4±0.7	···	···
350	4.12	0.90	···	14.9±0.9	44.6±1.0
400	4.41	0.85	12.7±1.0	16.0±1.5	43.3±1.5
450	4.67	0.80	12.5±0.8	16.8±0.4	43.9±1.5

all the electrons of lesser binding having been lost. Let I_i be the ionization potential which will remove this ith electron from the ion. Then we define a velocity,

$$V_i=(2I_i/m)^{\frac{1}{2}}, \tag{6}$$

to be referred to as the orbital velocity of the outermost electron adhering to the ion. m is the electron mass. If V is the translational velocity of the moving ion,

$$\gamma_i=V_i/V. \tag{7}$$

For the moving neutral helium atom, γ_1 refers to either of the two $1s$ electrons. In this somewhat special case, I_1 is clearly to be interpreted as one-half of the sum of the first and second ionization potentials of helium; $I_1=\frac{1}{2}(54.1+24.5)$ or 39.3 ev, whence $V_1=3.73\times10^8$ cm/sec.

It was found by repeating measurements in air that these cross sections were always reproducible within <7 percent. Unfortunately, this was not true for the other two gases, H_2 and He. It is perhaps significant that the lower values of cross sections obtained for these gases were the more self-consistent, as if, in spite of all precautions, there was occasional contamination with air or heavier gases.

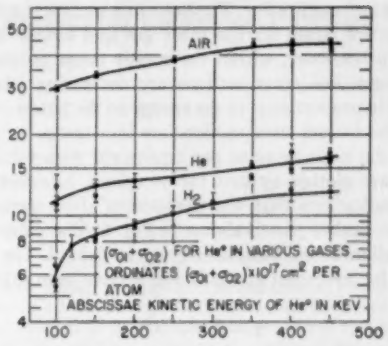

FIG. 5. Experimental values of the cross-section sum $(\sigma_{01}+\sigma_{02})$ in units of 10^{-17} cm² per atom of gas traversed, plotted against translational helium atom energy in kev.

Any error in the path length for attenuation would not affect the relative values of the cross sections since all measurements were made with the same path length. The agreement of the two different methods of measuring this length suggests that the uncertainty in l is less than 5 percent.

6. DISCUSSION

It is of interest to compare the loss cross sections reported here with those measured previously in this laboratory for hydrogen atoms in the kinetic energy range 30 to 325 kev.[8,9] These hydrogen measurements gave the cross sections σ_{01} for hydrogen atoms moving in the gases H_2 and air. The differences are both quanti-

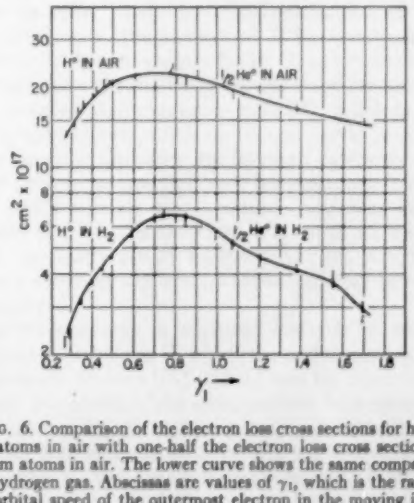

FIG. 6. Comparison of the electron loss cross sections for hydrogen atoms in air with one-half the electron loss cross sections of helium atoms in air. The lower curve shows the same comparison for hydrogen gas. Abscissas are values of γ_1, which is the ratio of the orbital speed of the outermost electron in the moving ion to its translational speed.

tative and qualitative. The loss cross sections for helium atoms are larger for the same gas and kinetic energy, and furthermore, within the energy range studied, the hydrogen loss cross sections are decreasing (they are roughly proportional to the energy to the power -0.70), but the helium cross sections are increasing.

If the cross sections per equivalent removable electron are plotted against the γ_1 values, however, there are indications that the phenomena show some regularity. Such a plot is shown in Fig. 6. The values of γ_1 for helium atoms have been given in Table I. The values of γ_1 for hydrogen atoms in Fig. 6 have been calculated from

$$\gamma_1 = 2.18 \times 10^8 / V, \tag{8}$$

where the numerator is the speed of the electron in the first Bohr orbit of the hydrogen atom, whose translational speed is V. In constructing Fig. 6, the measured helium cross sections have been divided by two, since the neutral helium atom has two identical electrons available for removal. It is seen that the loss cross section per equivalent removable electron seems to be a function of gamma only, with a maximum in the neighborhood of $\gamma_1 = 0.7$. It is very unfortunate that in the energy ranges through which the kevatron is operable the gamma ranges for H^0 and He^0 do not overlap, which prevents an extended test of the suggested simplification.

The rapid decline in the He^0 loss cross section in hydrogen gas as the helium kinetic energies fall below about 150 kev may be due to the approach to the threshold for transfer of the ionization energy from the protons in the hydrogen gas to the helium electrons, and to the increasing efficiency of the screening of the proton charge by the hydrogen electron during the collision. The critical speed for the transfer of 24.5 ev from a moving proton to an electron at rest is 1.47×10^8 cm/sec, which is the translational speed of a 44.5-kev helium atom. The velocities of the electrons in the helium atom will lower and decrease the abruptness of this threshold, but certainly a decrease of cross section in this region is to be expected.

7. ACKNOWLEDGMENTS

The author wishes to express his thanks to Professor S. K. Allison for suggesting this problem, and for his constant interest and helpful advice during its completion. The collaboration of J. Cuevas in taking the data is greatly appreciated.

Atomic Phosphorus Paramagnetic Resonance Experiment Employing Universal Dissociator*

H. G. DEHMELT
Department of Physics, Duke University, Durham, North Carolina
(Received March 29, 1955)

A simple spectrometer for the observation of paramagnetic resonance of free atoms near 9000 Mc/sec is described. This is followed by a detailed discussion of a new dissociation technique employing a carrier gas and a high-temperature arc which is shown to be effective enough to allow oscilloscopic observation of the atomic nitrogen spectrum, previously reported by Heald and Beringer. This dissociation technique which is believed to have universal applicability has been used to produce atomic phosphorus. The spectrum due to its $^4S_{\frac{3}{2}}$ ground state has been observed. It consists of a narrow doublet which arises from magnetic hfs interaction due to the P^{31} nucleus. The separation has been measured as

$$\delta\nu(P^{31}, {}^4S_{\frac{3}{2}}) = 56.2 \pm 1.5 \text{ Mc/sec},$$

and the g_J factor for the ground state has been obtained as

$$g_J(P, {}^4S_{\frac{3}{2}}) = 2.0019 \pm 0.0004,$$

which is only slightly smaller than the free-electron g value. The occurrence of a hfs in the supposedly symmetric $^4S_{\frac{3}{2}}$ ground state as well as the small g_J factor indicate the presence of higher state admixtures. The effects of beginning jj coupling in group V elements are briefly discussed and a sizeable electric quadrupole term in the ground state hfs of Sb and Bi is predicted.

INTRODUCTION

IN the last few years, an appreciable number of free atoms[1–3] has been studied by Beringer and coworkers using microwave paramagnetic resonance techniques. A similar microwave absorption experiment on Cs vapor[4] had been performed earlier. If there are no complications in such paramagnetic resonance experiments the static magnetic field, H_0, the resonance frequency, ν_0, and g_J, the gyromagnetic ratio of the free-atom state of total angular momentum, J, are connected by the well-known relation,

$$\nu_0 = (g_J\beta/h)H_0,$$

β denoting the Bohr magneton. Of the atoms H, O, and N studied so far, only H had been investigated previously by atomic beam resonance deflection techniques.[5] The g_J factor results on the two populated states of O, and the hyperfine structure observed for atomic N, provided interesting information on the higher order interactions of the electrons in these atoms.

The difficulties which have to be overcome in the extension to other atoms of this, in comparison with other methods experimentally easy, technique for the study of magnetic properties of atoms, consisted mainly in getting the free atoms into the microwave cavity in a sufficient concentration to give a detectable absorption. One elegant solution[6] has been suggested by Gordon *et al.* In this method a beam of atoms is magnetically focused[7] into a microwave cavity. As the focuser at the same time rejects the higher or lower of the two states between which transitions take place, a gain of the order of $kT/h\nu$ in intensity in an absorption or stimulated emission experiment can be realized which then offsets the loss in intensity due to the low density which can be used in atomic beams. However, there still remains the problem of dissociation.

In Beringer's experiments, the approach was simply to pass the usually wet molecular gases through a high-voltage discharge at pressures around 0.1 mm Hg, and then pumping the appreciably dissociated discharge products through a short section of tubing whose insides had been poisoned with a suitable anticatalyst to prevent recombination on the walls. Since at these low pressures the diffusion speed, with which the atoms reach the walls, is much greater than practical flow speeds and dissociation rates, this wall poisoning is absolutely necessary to maintain a sufficient concentration of free atoms at a reasonable distance from, and even in, the discharge tube.[8]

On the other hand, the actual mechanism of this wall poisoning is little understood. It has been possible to find suitable anticatalysts for H, O, and N but even for other gases like the halogens, not much success has been reported. As for substances like C, which in the form of gaseous compounds like CO can easily be introduced into the discharge but have an extremely low vapor pressure at practical wall temperatures, it is at least highly unlikely that a suitable poisoning agent will ever be found. Furthermore, it is not at all easy to break up tightly bound molecules like N_2 in a low-pressure discharge and special techniques may have to be employed.

For these reasons, it appeared desirable to test a dissociation technique in which the active component at a pressure between 0.01 and 0.1 mm Hg is added to an inert gas carrier of the comparatively high pressure of 10–100 mm Hg. As at these pressures it is possible to maintain high temperature arcs with gas temperatures up to 6000°K, the simple *thermal* dissociation of *any*

* This work has been supported by a contract with the Office of Ordnance Research, Department of the Army. A short account has already appeared in Bull. Am. Phys. Soc. **30**, No. 1, 42 (1955).
[1] R. Beringer and M. A. Heald, Phys. Rev. **95**, 1474 (1954).
[2] E. B. Rawson and R. Beringer, Phys. Rev. **88**, 677 (1952).
[3] M. A. Heald and R. Beringer, Phys. Rev. **96**, 645 (1954).
[4] Roberts, Beers, and Hill, Phys. Rev. **70**, 112 (1946).
[5] Koenig, Prodell, and Kusch, Phys. Rev. **83**, 687 (1951).
[6] Gordon, Zeiger, and Townes, Phys. Rev. **95**, 282 (1954).
[7] H. Friedburg, Z. Physik **130**, 493 (1951).
[8] R. W. Wood, Phil. Mag. **44**, 538 (1922).

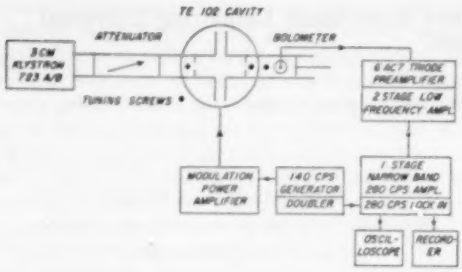

FIG. 1. Block diagram of paramagnetic resonance spectrometer.

molecule into atoms is assured. At the same time the carrier greatly reduces the diffusion speed of the free atoms and thereby effectively eliminates the wall effects. An experiment on atomic phosphorus along these lines shall now be described in some detail.

SPECTROMETER

The paramagnetic resonance spectrometer used, see Fig. 1, was essentially a simplified version of the one described by Beringer *et al.*[1] It operated at a frequency around 9000 Mc/sec. A 723*A*/*B* klystron was used as the power source and great care was taken to reduce the ripple and jitter on the cathode and reflector voltages as far as possible. The reflector voltage was obtained from batteries through a low impedance dividing network. In this simple way it was possible to keep the spurious frequency modulation of the klystron low enough that no significant decrease in noise was noticed for identical power incident upon the bolometer if the power was fed directly from the klystron into the bolometer instead of through the cavity. A rather-low-*Q* rectangular transmission cavity made from standard *X*-band wave guide and silvered afterwards was used. The gas stream entered and left the λ length (TE102) cavity through short tubular sections acting as below-cutoff attenuators.

The use of the rectangular cavity was dictated by the fact that only a magnetron electromagnet of 3-in. diameter and ¾-in. gap was available. Consequently the homogeneity over the largest dimension of the sample, 1 in., was rather poor, namely of the order of 1 oersted. The magnet was powered from 16 ordinary 6-volt car batteries. Mainly in order to increase the ease of field measurements, a proton resonance stabilization system was installed. Simply by changing the frequency of the proton stabilizer, the field at its usual value, around 3300 oe, could be pulled ±200 oe. By mechanically ganging the stabilizer control with the recorder drive, field reproducibility on the recording tape was achieved, which greatly helped with the identifications of weak lines. The magnetic field was modulated by conventional circuits at 140 cps, this frequency being derived from the 60-cps main by dividing and multiplying circuits.

The transmitted microwave power was detected by a commercial (Sperry 821) bolometer. Application of the microwave power increased the Johnson noise of the dc biased bolometer more than would have been due to its corresponding temperature and resistance increase. This indicates some amplitude noise in the klystron output. Provided one considers a factor of 2 or 3 worthwhile, a balanced bolometer circuit would have merits. In such a circuit, one bolometer would obtain its power through the cavity, while the other one would get an equal amount directly from the klystron. The amplitude modulation noise of the klystron could then be cancelled out by bucking the two bolometers against each other. The ac output of the bolometer was fed through a large dc blocking capacitor and over a well-shielded step-up transformer (Thermador TG1) applied to the grid of a triode connected 6AC7 input stage. Tests by grounding the grid of this input stage showed that the Johnson noise of the hot bolometer easily swamped the tube noise a few times. After further amplification by two penthode stages, the signal had to pass a single twin *T* negative feedback narrow band stage tuned to 280 cps before it reached a Schuster-type lock-in detector[9] employing a reference voltage of 280 cps. The lock-in output, which was displayed on a recording milliammeter, corresponded essentially to the second derivative of the absorption lines. The doubling technique greatly enhanced the narrow lines of interest here over broad absorptions due to various spurious causes like free electron cyclotron resonances, etc. It also reduced the pick-up and flicker noise problems. These advantages easily outweigh the inherent loss in modulation efficiency of about 30 percent, as compared with detection at the modulation frequency itself. The spectrometer sensitivity was optimized with the help of a diphenyl-picryl-hydrazil test sample. Peak-to-peak signal-to-noise ratio at 1-sec time constant for a sample of this substance containing 3×10^{15} free electron spins was found to be better than 200 for a line width of about 6 Mc/sec.

DISSOCIATOR AND CARRIER GAS SYSTEM

The helium-argon carrier was supplied in the form of commercial compressed gases (Matheson) of better than 99.9 percent purity. The pressure was reduced to about 1 atmosphere with the usual automatic regulators, followed by small needle valves (Hoke) for further reduction down to the 10–100 mm Hg range. A finer adjustment for partial pressures below 1-mm Hg could be obtained with the Matheson 51 needle valve, which was used for the N_2 addition. It was found that the expensive argon could be replaced by the cheaper helium to a large extent. Pure helium operation led to overheating of the quartz tube. The carrier then passed over white phosphorus contained in a flask which could be heated to cover a P_4 partial pressure range of

[9] N. A. Schuster, Rev. Sci. Instr. 22, 254 (1951).

0.02–1 mm Hg, see Fig. 2. The dissociator consisted essentially of a 15-mm o.d. quartz tube containing two tungsten electrodes. In order to sustain the desired high current arc, the cathode has to get hot enough to thermally emit an electron current of several amperes, which is the case at about 3000°K. To start the arc an ac voltage of more than 800 volts had to be applied in series with the dc operating voltage of 130–250 volts. A choke limited the ac current to 4 amp. After about a minute of high-voltage operation at 100–200 mm Hg the electrodes became suddenly white hot, emitting an intense light, and the gap voltage dropped to a low value. After removal of the ac voltage the arc then operated on the dc supply. The starting procedure was aided by a high-frequency high voltage from a Tesla transformer. The gap voltage in argon for a gap distance of 40 mm in the pressure range of 10–200 mm Hg was around 40–50 volts and was rather independent of the current, which could be raised up to 8 A without melting the electrodes.

In the pressure range of interest, 10–100 mm Hg, it is still not a bad assumption that electron and gas temperature in the arc plasma are nearly equal, and that the current is mainly carried by the electrons. The gas temperature then must be large enough to provide by thermal ionization a sufficient positive ion concentration to neutralize the heavy space charge associated with the large observed electron current densities. Calculations along these lines, as well as experiments, establish gas temperatures[10,11] up to 6000°K. At these temperatures all molecules at the low partial pressures of interest here will be completely dissociated into their atomic constituents. This expectation was tested by adding up to 1-mm N_2, dissociation energy 9.8 ev, to

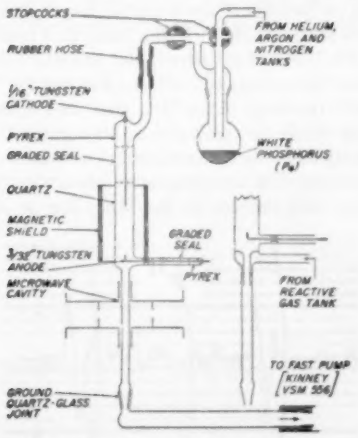

FIG. 2. Universal dissociator employing helium-argon carrier.

[10] W. Elenbaas, *The High Pressure Mercury Vapor Discharge* (Interscience Publishers, Inc., New York, 1951).

[11] J. P. Cobine, *Gaseous Conductors* (McGraw-Hill Book Company, Inc., New York, 1941).

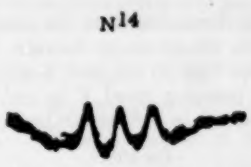

FIG. 3. Atomic N^{14} hfs triplet. Broad-band oscilloscopic display and field modulation at 15 cps were used. The dissociator was an earlier Pyrex water-cooled version.

argon and helium-argon mixtures around 50-mm Hg. The well-known active nitrogen afterglow appeared strongly, and the hfs triplet of the atomic $^4S_{\frac{3}{2}}$ ground state was observed in the paramagnetic resonance spectrometer, compare Fig. 3. Resonance due to atomic hydrogen also was detected with this arrangement.

After these early tests proved successful, attempts were made to obtain the paramagnetic resonance spectrum of atomic phosphorus. Phosphorus was chosen for various reasons: (1) its hfs had not been measured; (2) the dissociation technique could be tested on polyatomic molecules, P_4, which could also be easily admixed to the carrier; (3) its atomic ground state, $^4S_{\frac{3}{2}}$, has no orbital angular momentum. So far a certain setback of the carrier technique has not been discussed. While collisions of the inert nonmagnetic carrier atoms will not broaden resonance lines of *S*-states, since there is no interaction with the sole contributor to the total angular momentum, the electron spin resultant, they will broaden non-*S*-states at a likely rate of 1 Mc/sec/mm Hg carrier pressure. For these states, the electron orbitals of nonvanishing angular momentum provide the handle by which the total angular momentum can be turned over by an impinging carrier atom. Fortunately for a sizeable group of atoms where the orbital momentum carrying electrons are shielded by outer inert shells, like in the $4f^n6s^2$ states of the rare earth elements, this broadening may be appreciably reduced. Even though the associated intensity loss may not be prohibitive, it was clearly desirable to avoid non-*S* atoms at this stage. In spite of these precautions, the early attempts did not meet with success. It was, therefore, decided to have a closer look at the processes by which the free atoms do recombine which definitely have been generated in the arc. It is well known that two single atoms which collide in the gas phase will not stay together long unless the resulting collision complex has a way to get rid of the recombination energy which, of course, is also sufficient for dissociation. To stabilize the collision complex, a third body has to be present to absorb part of the recombination energy. This now may be another molecule or the wall of the container. Triple collisions in the gas phase are too rare and can be neglected here. The worst assumption concerning the wall effect is that every free atom hitting the wall recombines. It follows then that the carrier pressure in a flow system like ours should be high enough to prevent appreciable diffusion to the tube wall before the cavity

is reached. By demanding that the average time, t, an atom travels the arc-cavity distance, S, should be half its diffusion time to the wall, a relation between the necessary pumping speed V in cm³/sec and the diffusion constant D in cm²/sec can be formulated:

$$V \approx 40SD.$$

The tube diameter has conveniently dropped out. As a practical example, we take $V \sim 6000$ cm³/sec and $S=6$ cm and obtain $D_{max}=25$ cm²/sec. If we assume a diffusion coefficient for atomic P into argon of about 0.3 cm²/sec at atmospheric pressure and at room temperature, this calls for a minimum carrier pressure of 10 mm Hg. Because of the much higher temperatures in and immediately after the arc region, this estimate may be considerably too low unless one uses water-cooling of the arc housing. In this way, one shields the dissociator wall with a dense layer of cooler gas. The just-obtained relation should be satisfied in any case unless one wants to rely on wall poisoning. However, in the general case it is not the only condition which has to be satisfied in order to assure a sufficient free atom concentration in the cavity. While for atoms forming only diatomic molecules gas phase losses are completely in the background, this is by no means so when polyatomic molecules are formed.[12] Even though not much will happen if one P atom collides with another one, there will always be an appreciable fraction of fragments P_2, P_3, and also impurities at hand which have not passed through the hottest zone of the dissociator. If a P atom now hits such a fragment, say P_3, the recombination energy in the resulting excited P_4 molecule can spread over many degrees of freedom, which gives the complex a sufficiently long life to be deactivated by a collision with a carrier atom, or it may also break up into two P_2 molecules. Fortunately, not every collision between a free atom and a polyatomic fragment leads to the formation of an excited molecule, as it must clearly make a difference if the fragment can form a bond at the spot where it is hit or not. The whole matter gets rather involved, and the gist of all this is that one may hope for an atom to live over 10 to 100 collisions with polyatomic groups. This places a limit on the partial pressure of the active component which is likely to give an optimum concentration of free atoms. One may arrive at a rough estimate by demanding that a P atom should not collide with more than 10–100 other P atoms during the transit time, t, from the arc to the cavity. With a tube cross section of ½ cm² and the same values for V and S as in our above example, t comes out 5×10^{-4} sec. If one assumes a collision time for P at atmospheric pressure and room temperature of 4×10^{-10} sec, this optimum P pressure will be $10^{-2}-10^{-1}$ mm Hg which should lead to a well-observable paramagnetic resonance signal. It might be emphasized here that the rather stringent general conditions to assure a sufficient free atom concentration can be met in a practical arrangement. Therefore, the carrier dissociation and transport technique should be quite universally applicable. Besides, for H and N, this has so far also been demonstrated for atomic P, whose paramagnetic resonance spectrum was observed after a sufficiently fast pump (Kinney, VSM 556, preceded by 35 l ballast volume) was installed.

The arc may also be used to evaporate metals into the carrier gas. Preliminary experiments employing a graphite anode supporting a ball of molten Cu indicate that even *excited or metastable* Cu atoms are present as far as 20 cm downstream from the arc, as evidenced by the emission of the characteristic green Cu spectrum. The formation of metallic mirrors on the tube wall inside the cavity poses a problem which, however, can be overcome by the design shown in the insert of Fig. 2. Here the carrier stream is sheathed by a thin lamina of reactive gas like Cl_2 or air which reacts with the metal atoms diffusing into it.

ATOMIC P SPECTRUM

It was originally planned to measure the P spectrum, which consists of a narrow doublet (see Fig. 4) centered around roughly the free electron g value, by simultaneously observing it with the atomic N spectrum. The g_J factor of atomic N had been measured with high precision by Heald and Beringer,[3] and this procedure would have eliminated the need for precise measurements of the microwave frequency and the magnetic field at the exact site of the free-atom sample. Unfortunately, however, it was not possible with the present equipment to achieve a suficient concentration of P, as well as N atoms, by simultaneously charging the carrier with P_4 and N_2. Therefore, an intermediate standard in the form of the center high-field line, Mn_{+1}, of the hfs sextet of Mn^{++} in the cubic ZnS host lattice (line width 3 oe was employed. The procedure now was to alternate recordings of the Mn_{+1} line and the N spectrum with recordings of the Mn_{+1} and the P spectrum a few times while the geometrical arrangement of free atom cavity Mn^{++} sample and proton resonance coil was left unchanged. The average proton resonance frequency differences with respect to the Mn_{+1} line as zero are

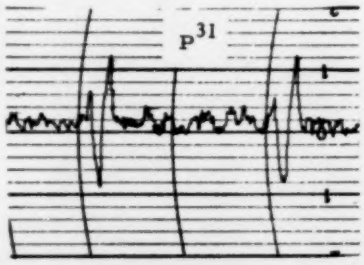

FIG. 4. Hfs doublet of atomic P^{31}. A 1-sec time constant was used in the recording circuit.

[12] Glasstone, Laidler, and Eyring, *The Theory of Rate Processes* (McGraw-Hill Book Company, Inc., New York, 1941).

given in Table I. The proton frequencies were measured with a direct reading frequency meter (Gertsch FM3). The limit of error in these frequencies was about 2 kc or half the observed line width. The spectrum was proven to be independent of the carrier pressure in the region of 20–40 mm Hg. This includes the line width which was found to be 1 oe between zero deflection points and which was exclusively due to the inhomogeneity of the available field. From the values in Table I one calculates for the P^{31} hfs separation 20.0±0.5 oe or

$$\delta\nu(P^{31}) = 56.2 \pm 1.5 \text{ Mc/sec.}$$

The proton frequency corresponding to the center of the P spectrum is only 1.3 kc/sec lower than that of

TABLE I. Proton frequency differences for measured resonance peaks, in kc/sec.

Mn_{+1}	P_{+1}	N_0	P_{-1}
0	−74	−118	−159.5

the N center line, N_0, which is less than the assigned limit of error. With Heald and Beringer's value $g_J(N) = 2.0021$, we consequently obtain

$$g_J(P) = 2.0019 \pm 0.0004,$$

neglecting small correction terms, as the Paschen-Back effect is very nearly complete.

In order to explain the observed splitting as magnetic hfs due to the P^{31} nucleus of nuclear spin $I = \frac{1}{2}$, one has to assume small admixtures of excited states to the predominantly $3s^2 3p^3\ ^4S_{\frac{3}{2}}$ ground state, since this state in pure LS coupling cannot couple to the nuclear magnetic moment. The admixtures most effective in producing a magnetic hfs interaction will be the ones of the type $3s3p^3ns$ $(n = 4, 5 \cdots)$, in which one of the $3s$ electrons has been promoted to a higher s orbital and the two s electrons have parallel spins.[13,14] A total of such admixtures of the order of 1 percent is sufficient to account for the observed hfs in P. For the last members of the series N, P, As, Sb, Bi, however, there will be sizeable contributions from the ground state p electrons to the hfs. This can easily be seen since in pure jj coupling the $J = \frac{3}{2}$ ground state is made up of two antiparallel $p_{\frac{1}{2}}$ electrons and one $p_{\frac{1}{2}}$ electron and, therefore, effectively behaves like a single $p_{\frac{1}{2}}$ electron. Consequently, in jj coupling one will find not only sizeable magnetic dipole and electric quadrupole interactions for the ground state but also a g_J factor of 1.333 instead of 2. There is little doubt that beginning jj coupling is the essential cause for the small g_J values of the last members of the series. While a look at Table II shows that extreme jj coupling is not even reached in Bi, there are definitely observable quadrupole terms to be expected in the ground state hfs of at least Sb and Bi.

TABLE II. Ground state g_J-factors for group V-atoms.

Free electron	N	P	As[a]	Sb[b]	Bi[b]
2.0023	2.0021	2.0019	1.994	1.967	1.65

[a] J. B. Green and W. M. Barrows, Phys. Rev. **47**, 131 (1935).
[b] D. R. Inglis and M. H. Johnson, Phys. Rev. **38**, 1642 (1931).

It is a pleasure to express my thanks to Professor Beringer for stimulating discussions during a visit at Yale University and to Professor Gordy for the use of the facilities of the Duke Microwave Laboratory.

My thanks further go to Mr. H. Mortenson for the construction of the proton resonance field stabilizer system, and I should like to mention the friendly cooperation of Mr. Thomas Henson in building the various quartz dissociators.

[13] A. Abragam and M. H. L. Pryce, Proc. Roy. Soc. (London) **A205**, 135 (1951).
[14] G. F. Koster, Phys. Rev. **86**, 148 (1952).

New Technique for High-Resolution Microwave Spectroscopy*

R. H. Romer† and R. H. Dicke
Palmer Physical Laboratory, Princeton University, Princeton, New Jersey
(Received March 17, 1955)

An experiment is described in which microwave resonance lines have been obtained having widths substantially less than the normal Doppler width. The line shape obtained depends on the properties of a radiating gas when contained in a cavity in the form of a pillbox, of diameter large compared to height. Collisions of molecules with the walls take place in such a manner that the collisions narrow the line instead of broadening it. The 1.25-cm inversion transition in ammonia was observed, and lines one quarter the normal Doppler width of 73 kc/sec obtained; further narrowing appears feasible. The line shapes and widths are in good agreement with the calculations.

BY employing a gas cell of special shape and gas at low pressure, it is possible to produce microwave spectral lines having widths substantially less than Doppler breadth. The essential feature of the gas cell is that it should consist of two flat parallel walls, separated by approximately $\lambda/2$, where λ is the free-space wavelength of the radiation, operating in a mode for which the electromagnetic wave bounces back and forth between the two walls. One suitable form of such a gas cell is a pillbox shaped cavity having a diameter large compared to a wavelength, operating in the TE_{111} mode.

Although these narrow spectral lines should be obtainable using standard microwave absorption detection equipment, some improvement in average signal power is expected from a detection system based on pulse induced coherent spontaneous radiation,[1] and it was this technique which was used in our experiments.

It is somewhat paradoxical that the effect of wall collisions which strongly disturb the internal state of the molecule should be such as to lead to a spectral line more narrow than that obtained in the absence of wall collisions. It was shown by Johnson and Strandberg[2] that the previous simple considerations of the effect of wall collisions on a gas were basically incorrect. These simple considerations had assumed a Lorentz line shape with a line width proportional to the characteristic molecular speed, $v_0=(2kT/m)^{\frac{1}{2}}$, divided by a length characteristic of the gas cell, this length being given by the shortest dimension of the cell in case the cell had one of its dimensions much smaller than the others. In particular, Johnson and Strandberg took as a model of a long wave-guide cell, one of whose cross-sectional dimensions L was considerably shorter than the other, a cell composed of two infinite parallel plates separated by a distance L. They showed that the line shape to be expected from wall collisions alone in such a cell was not a Lorentz line of full width $\Delta\nu\cong 0.2v_0/L$, as had been previously assumed, but was actually far from a Lorentz line, having a logarithmic singularity at the line center. They pointed out that this singularity would be masked by any finite Doppler broadening, resulting from motion of molecules along the wave guide, yielding an effective contribution to the line width arising from wall collisions of approximately $\Delta\nu \cong 0.8v_0/L$. Danos and Geschwind[3] subsequently pointed out that for the power levels commonly employed in microwave spectrometers, the simple theory, although fundamentally incorrect, did in fact give results which were fairly accurate. The non-Lorentz shaped lines predicted were shown to be realizable only for rather unusual operating conditions of extremely low incident power levels. They showed that even if not masked by the Doppler effect, the singularity in the line shape would be removed by power saturation effects, and the effective contribution to the line shape from wall collision effects could be well represented by the simple theory, giving approximately a Lorentz shape.

In the gas cell to be described, the Doppler effect is missing, and by maintaining the proper operating conditions, a line breadth may be realized, arising solely from wall collision effects, which is substantially less than the value $\Delta\nu=v_0/L$, where L is the smallest dimension of the cell. The obtainable line shape is in fact determined primarily not by the smallest cell dimension, but by the other dimensions of the cell. To understand the beneficial effect of the wall collisions in producing a narrow spectral line by avoiding Doppler broadening, it is necessary first to understand that for an absorption spectrometer as well as for the pulse induced emission spectrometer[4] the source of the signal power is an electromagnetic wave radiated by the gas. For an absorption spectrometer, the radiated wave might be called an "absorption wave" in that it is the destructive interference with this wave that reduces the intensity of the incident microwave when absorption by the gas is occurring. The gaseous origin of this signal energy is easily demonstrated experimentally. If the incident wave is suddenly turned off, the gas continues to radiate for perhaps 10 microseconds. From this point

* Experimental work supported by the Signal Corps.
† National Science Foundation Predoctoral Fellow, 1952–55.
[1] R. H. Dicke, Phys. Rev. **93**, 99 (1954).
[2] H. R. Johnson and M. W. P. Strandberg, Phys. Rev. **86**, 811 (1952).
[3] M. Danos and S. Geschwind, Phys. Rev. **91**, 1159 (1953).
[4] The details of a pulse induced emission spectrometer are given in an article to be published in *The Review of Scientific Instruments*.

of view the only effect of the incident electromagnetic wave is to excite the gas into a state in which the individual molecules possess oscillating electric dipole moment expectation values. This results in an oscillating polarization of the gas, the radiation from which can be treated classically. In the pulse induced emission technique, molecules are excited by a microwave frequency pulse into superposition energy states in which each molecule possesses an oscillating electric dipole moment. A given molecule continues to radiate until it hits another molecule or a wall of the container. For the pillbox cavity of height $\lambda/2$ with low gas pressure, the collisions occur primarily at the two large parallel flat surfaces. To understand the beneficial significance of the collision, it need only be noted that if the pillbox height were greater than $\lambda/2$, say λ, with the cavity operating in the TE_{112} mode, then a given molecule, instead of colliding with the wall would continue to move across a nodal plane in the cavity into a region where the electric field is reversed in direction. It here radiates (classically) with the opposite phase with respect to the standing wave in the cavity, and its wave interferes destructively with the waves radiated by molecules which have not crossed a nodal plane. To state it another way, the collisions with the walls are damaging in that molecules are removed from the radiating system. However, collisions are not as serious as the absence of collisions, in which case the molecular motion mixes the oscillating molecules of different phases, resulting in destructive interference between the contributions from individual molecules.

It is now easy to comprehend the origin of the narrow spectral line. For the pillbox cavity, the number of radiating atoms, and hence the amplitude of the radiated wave, since the molecules radiate in phase, falls off after a short time as the reciprocal of the elapsed time after the exciting pulse. (See Fig. 1.) This $1/t$ dependence lasts for a time which is greater the larger the diameter of the pillbox. After about 15 microseconds in the case of ammonia, most of the molecules which have not yet collided with a wall are moving nearly parallel to the flat surfaces. After a sufficiently long period, the effect of the side walls must be included.

For a cylindrical cavity of the same diameter as the pillbox but many wavelengths long, the interference effects, arising from motion of the molecules into regions where the electric field has various phases, as previously discussed, cause the radiated amplitude to fall off as a Gauss error function of the time. The line shape is given by the Fourier transform of this envelope function. This is the usual Gaussian shaped line characteristic of Doppler broadening. On the other hand, for an amplitude variation proportional to the reciprocal of the time, characteristic of the pillbox, the Fourier transform gives a narrow line more sharply peaked than a Lorentz profile. Were it not for the side walls and other practical difficulties, the line shape would have a logarithmic singularity at its center.[2]

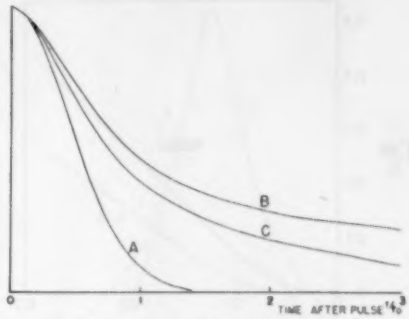

FIG. 1. Calculated envelopes of radiation from ammonia at low pressure and room temperature. Curve A: Large gas cell: normal Gaussian Doppler decay. Curve B: Infinite diameter pillbox cavity, uniform field assumed: asymptotically proportional to $1/t$. Curve C: Finite diameter pillbox, considering field distribution effects. Diameter to height ratio of cavity 9.2. $t_0 = \lambda/2v_0 = 11.5$ microseconds.

In the case of an absorption apparatus, although the details differ, the main conclusion remains the same. In the absence of wall collisions, a destructive interference effect remains which leads to the normal Doppler broadened line, but when a gas cell in the form of a pillbox cavity of height $\lambda/2$ is operated at low gas pressures and low incident power, the molecules with long free paths are strongly favored. They are excited for a long time, giving rise to a large oscillating electric moment, and they radiate for a long period. Because of the long uninterrupted radiation period, these molecules contribute principally to the spectral line intensity at its center, which, because of the strongly oscillating character of these molecules and their long radiation time, becomes strongly peaked.

Consider now in more detail the line shape expected when an infinite diameter pillbox cavity is used. The cavity is formed by two parallel plates of infinite extent, separated by $\lambda/2$. A wave guide couples to the normal mode of the cavity which is a standing plane wave of uniform amplitude over the extent of the plates. A short intense radio-frequency pulse excites the gas. Since the cavity is only of height $\lambda/2$, it is a fair approximation to say that the exciting field is in phase and of equal amplitude throughout the cavity. (If the cavity were, for example, λ in height, then this approximation could not be made, since the exciting field would have opposite phases in different regions of the cavity.) To this approximation, all the molecular dipoles are oscillating with equal amplitude, and in phase with each other. Thus the radiated amplitude is proportional to N, the number of contributing molecules, N being at most equal to the thermal equilibrium difference in population of the two states. Because the electric field actually has a sinusoidal distribution over the gap between the plates, the molecules are actually excited by various amounts dependent upon their location. Also, the radiated amplitude from a molecule

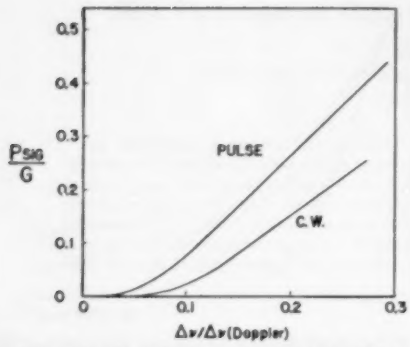

FIG. 2. Calculated available signal power (in units of G), as a function of line width (in units of the normal Doppler width), for pulsed excitation and continuous absorption experiments in infinite diameter pillbox cell. Line width in the two cases is that due to finite interval between pulses in the pulsed experiment, and that due to saturation broadening in the c.w. experiment. $G=Q_0\omega_0^3\mu_0^2n^2\hbar^2/8v(kT)^2$, where Q_0=unloaded Q of cavity; v=volume of cavity; n=total number of molecules in the two energy states; μ_0=absolute value of electric dipole matrix element. $\Delta\nu$ (Doppler) $=(\ln 2)^{\frac{1}{2}}v_0\omega_0/\pi c$ where $v_0=(2kT/m)^{\frac{1}{2}}$.

will depend on its location at the time it is radiating. However, in a relatively short time after the pulse, because of the molecular motion the oscillating dipole moment density of the gas will become uniform, after which time the lack in uniformity of the field strength has no effect. Thus, the assumption of uniformity of the oscillating electric field affects only the initial part of the time dependence of the radiation intensity. This part contributes only slightly to the shape of the line in the vicinity of the line center. In addition to the simplification which results from the assumption of uniformity of the field, there is the additional advantage that a direct comparison can be made with the earlier absorption calculations.[2,3]

If a molecule undergoes a collision, it is restored to a state of thermal equilibrium, or at least the phase of its oscillating moment is disturbed, so that after the collision it is just as likely to be out of phase as in phase with the undisturbed molecules. Molecules which have suffered a collision may be considered to have been removed from the radiating system, since, on the average, they contribute nothing to the macroscopic polarization. Then $N=N(t)$, where t is the elapsed time since the exciting pulse was turned off, and where $N(t)/N(0)$ is the fraction of molecules which have not had a collision since $t=0$. Ignoring radiation damping,[5] and also assuming a pressure low enough so that collisions between gas molecules can be ignored,

$$N(t)/N(0)=\frac{2}{v_0\lambda\pi^{\frac{1}{2}}}\int_0^{\lambda/2}dz\int_{-z/t}^{(\lambda/2-z)/t}\exp(-v^2/v_0^2)dv. \quad (1)$$

[5] In a coherent spontaneous emission process, the line width caused by radiation damping may be as high as $n\hbar\omega\gamma/4kT$, where n is the total number of radiating molecules and γ is the natural line width for one isolated excited molecule. (See reference 1.) This damping cannot be neglected in all cases.

The radiated amplitude is proportional to $N(t)$, and thus the real part of the Fourier transform of $N(t)$ gives the line shape

$$\text{Real part } g(\omega)=\frac{\sqrt{2}}{v_0\lambda\pi}\int_0^\infty\cos(\omega-\omega_0)t\,dt \times\int_0^{\lambda/2}d\int_{-z/t}^{(\lambda/2-z)/t}\exp(-v^2/v_0^2)dv. \quad (2)$$

For large t,

$$\lim_{t\to\infty}N(t)/N(0)=\lambda/(2\pi^{\frac{1}{2}}v_0t). \quad (3)$$

The Fourier transform of a function which is proportional to $1/t$ as t becomes infinite has a logarithmic singularity at $\omega=\omega_0$, and thus, in principle, lines as narrow as desired can be obtained by this method.

By a series expansion and partial integration, the line shape [Eq. (2)] can be transformed into

$$\text{Real part } g(\omega)=\frac{1}{(2\pi)^{\frac{1}{2}}(\omega-\omega_0)} \times\int_0^\infty[1-\exp(-1/x^2)]\sin\left[\frac{(\omega-\omega_0)\lambda x}{2v_0}\right]dx. \quad (4)$$

A line shape of identical form has been calculated by Johnson and Strandberg[2] and later by Danos and Geschwind[3] for a c.w. (continuous wave) absorption experiment in a similar cell, with a vanishingly small amount of incident power. As Danos and Geschwind point out, any nonzero amount of power incident on the gas, which is necessary to produce an observable signal, introduces saturation effects which remove the singularity in the line shape. Similarly, in the pulse experiments considered here, in order to obtain a usable signal, there must be a finite interval between successive exciting pulses. Under these conditions, molecules with velocities parallel to the faces of the cell are not allowed to continue radiating for infinitely long times, and for this reason in addition to others, the singularity in the line shape is removed, by cutting off the $1/t$ decay at a finite time. As the repetition interval is decreased, the signal power and the line width increase, just as in the c.w. experiment, the signal power and line width increase as the incident power is raised. The calculated signal power at the center of the line is given as a function of calculated line width for the two idealized cases in Fig. 2. The line width in the c.w. case is calculated from Danos and Geschwind's results. The line width in the pulsed excitation case is calculated from the transform of $N(t)$, Eq. (1), cut off at the repetition interval T:

$$\text{Real part } g(\omega)=\frac{1}{(2\pi)^{\frac{1}{2}}}\int_0^T N(t)\cos(\omega-\omega_0)t\,dt. \quad (5)$$

The line width is given in units of the normal Doppler width,

$$\Delta\nu(\text{Doppler}) = (\ln 2)^{\frac{1}{2}}\tau_0\omega_0/\pi c.$$

In the experiment performed, the gas was excited by a sequence of rf pulses, the phase of the rf oscillation being preserved from one pulse to the next. After each exciting pulse, the gas radiated a wave of decaying amplitude, whose phase was determined by the phase of the exciting rf. The frequency spectrum of the radiation from the gas then consisted of a component at the center frequency of the exciting pulse, plus side bands above and below this frequency, spaced by the pulse repetition frequency. The detection system selected the frequency component of this radiation at the center frequency of the exciting pulses, and it is the available signal power in this component and not the total radiated power which is plotted in Fig. 2.

Unfortunately, a severe loss is taken in signal to noise ratio in order to achieve narrow spectral lines by using a cavity of this special pillbox shape. First, a low pressure must be used to obtain the required long mean free path, which must be at least comparable to the diameter of the pillbox cavity. Second, only a small fraction of the molecules have the long trajectories that avoid the top and bottom faces of the cavity. The net result is that as the line width is decreased by increasing the cavity diameter, the signal power varies directly with the square of the line width.

The data[6] which Danos and Geschwind used as a check on their wall broadening theory and also the data used by Johnson and Strandberg[2] to check their earlier calculation of the same effect, were based on experiments in an ordinary long microwave absorption cell. In such experiments, the molecules can move many wavelengths in the direction of propagation of radiation, and the full Doppler width is observed, as discussed earlier. Under conditions of low pressure and low incident rf intensity, the major source of broadening in such a cell is the Doppler effect, and wall collision effects are present only as a correction to the Doppler width. The expected width is calculated by adding this correction term in a rather arbitrary manner to the large Doppler width.

In the experiments considered here, however, the exciting field, instead of being propagated parallel to the surfaces of the plates, is approximately a plane wave bouncing back and forth between the plates. In such an experiment, as has been mentioned, it is a fairly good approximation to regard the electric field as being in phase and of uniform amplitude throughout the cell, so that the wall collision effects are the only source of line width. Such an experiment allows a direct comparison of observed and calculated wall collision widths.

[6] Gunther-Mohr, White, Schawlow, Good, and Coles, Phys. Rev. **94**, 1187 (1954).

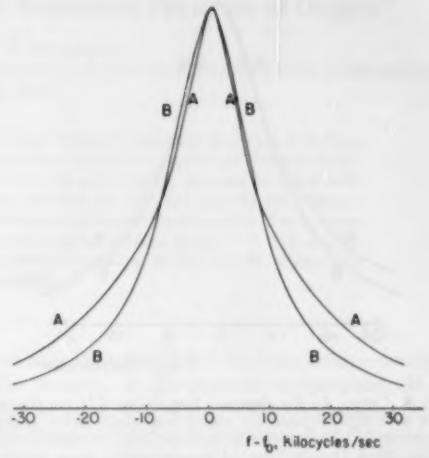

FIG. 3. Curve A: Calculated line shape, 5.75 cm diameter pillbox (diameter to height ratio 9.2). Curve B: Lorentz line shape chosen to have same height and width at half-maximum amplitude as curve A.

In the experiments performed here, the $J=K=3$ inversion transition in ammonia at 24 000 Mc/sec was observed. The gas, at low pressure and at room temperature, was contained in a cylindrical copper cavity of height approximately $\lambda/2=0.62$ cm, diameter 5.75 cm, operating in the TE_{111} mode. The line width was determined by the finite size of the cavity. The addition of side walls at a moderately small radius makes the amplitude decay faster than $1/t$ when molecules begin to suffer collisions with these walls. (See Fig. 1.) For sufficiently low pressures and long pulse repetition intervals, the line width is determined by the diameter of the cavity. A numerical calculation of the line shape to be expected from such a cavity, taking into account the field distribution in the cavity, which was ignored in the previous discussion where the radiated amplitude was taken as strictly proportional to the number of radiating molecules, predicts a line 16.2 kc/sec wide (full width at half-maximum amplitude), of nearly Lorentz shape but slightly sharper at the peak than a Lorentz line of the same width. (The field distribution in the cavity does not have a drastic effect on the line shape. The line computed without taking the field distribution into consideration is of the same general shape, with a width of about 14.5 kc/sec.) The normal Doppler width is 73 kc/sec. Observed lines are about 18 kc/sec wide, with shapes and widths in good agreement with the calculation. The calculated line shape and a Lorentz line of the same width as the calculated line are plotted in Fig. 3. Note that the Lorentz line, chosen to have the same width at half-maximum amplitude, has a somewhat broader peak than does the calculated line. A Lorentz line chosen to have the same curvature at the line center as the calculated line would have a

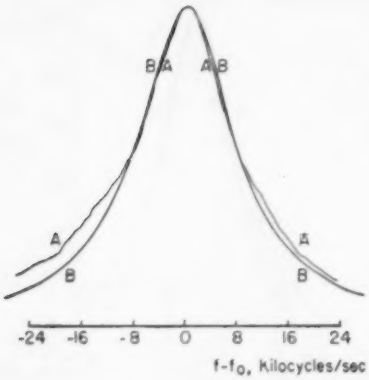

FIG. 4. Curve *A*: An observed line shape, 5.75-cm diameter pillbox with slight asymmetry arising from phase errors in detection system, 17.9 kc/sec wide at half-maximum amplitude. Curve *B*: Calculated Lorentz line, of approximately same width as curve *A* at half-maximum amplitude.

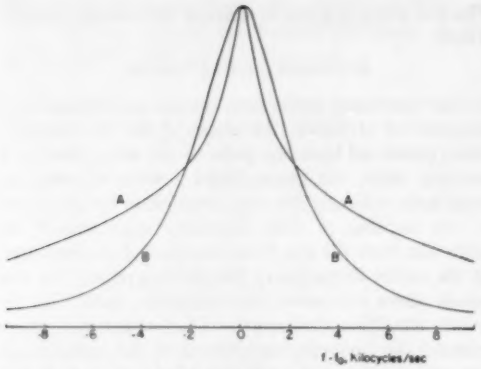

FIG. 5. Curve *A*: Calculated line shape, 62.5-cm diameter pillbox (diameter to height ratio 100). Curve *B*: Lorentz line shape chosen to have same width at half maximum amplitude as curve *A*.

width slightly smaller than that of the calculated line. In Fig. 4 is plotted an observed line, whose width is 17.9 kc/sec. The slight asymmetry of the line may be attributed to slight phase errors in the detection system. Also plotted in Fig. 4 is a Lorentz line chosen to have approximately the same width at half-maximum amplitude as the observed curve. Note that the observed line is slightly sharper at the peak than the Lorentz line of the same width, bearing out qualitatively the predictions of the calculation (Fig. 3). The signal was 35 db above noise in the above measurements for an information bandwidth of 0.5 cycles/sec. The calculated signal to noise ratio, assuming a crystal conversion gain of $\frac{1}{4}$, a crystal noise temperature of 2, and an i-f (intermediate-frequency) amplifier noise figure of 4 (an over-all receiver noise figure of 20, or 13 db), is approximately 42 db for operation at the required low-pressure and low-pulse repetition rate.

By increasing the cavity diameter, it seems feasible to decrease the line width by about another factor of four, but beyond this point, technical problems appear to make further narrowing considerably more difficult.

The calculated line shape for a cavity of diameter 62.5 cm, a diameter to height ratio of 100 to 1, is plotted in Fig. 5, together with a Lorentz line of equal width at half-maximum amplitude. The departure of the calculated line from the Lorentz shape is evident. Note that although the calculated width at half-maximum amplitude is approximately 4 kc/sec, a Lorentz curve with the same degree of sharpness at the line center as the calculated line would have a width of about 1.5 kc/sec. Thus, greater resolution is possible than that implied merely by the value of the width at half-maximum amplitude.

Line Breadths in the Microwave Magnetic Resonance Spectrum of Oxygen*

M. TINKHAM† AND M. W. P. STRANDBERG
Department of Physics and Research Laboratory of Electronics, Massachusetts Institute of Technology, Cambridge, Massachusetts

(Received March 4, 1955)

The line-breadth parameters of a number of lines of the X-band magnetic resonance spectrum of O_2 have been measured and interpreted with the aid of a previously reported theory of the spectrum. The results are that the M-dependence of the line width is negligible, and there is only a slight decrease in width with increasing K. A typical width (half-width at half-intensity) at 300°K is 2.2 (Mc/sec)/mm Hg. At pressures up to 8 mm Hg, the line centers have been found to shift less than 2 percent of the line width. The average temperature dependence of the normalized line breadth parameter $(\Delta\nu/P)$ is found to be $T^{-0.75}$. This may be compared with the theoretical $T^{-0.637}$ and the $T^{-0.88}$ found by previous workers. We find O_2-N_2 collisions to be no less effective than O_2-O_2 collisions in producing broadening.

1. INTRODUCTION

LINE breadths (half-width at half-intensity) in the millimeter microwave spectrum of oxygen have been reported by numerous investigators,[1] and Beringer and Castle[2] have given results for the magnetic resonance spectrum. The various results, however, have not been completely satisfactory. For example, there are sizable discrepancies between the results of Gokhale and Strandberg and those of other investigators of the millimeter spectrum. The results of Beringer and Castle could not be properly converted to frequency widths with the existing theory. Also, there is poor agreement between the experimental temperature dependence of the line breadth and that predicted by theory. In view of this unsatisfactory situation, line-width measurements were made as part of the comprehensive study of the microwave spectrum of the oxygen molecule which was previously reported.[3] The results of these measurements and of the re-evaluation of the measurements of Beringer and Castle are given in this paper.

In the microwave spectrum of a gas at the pressures used in these experiments one may neglect all sources of broadening except collision broadening and the instrumental broadening resulting from any inhomogeneity of the magnetic field over the cavity containing the sample. (The power level was always kept low enough to preclude any saturation broadening effects.) From kinetic theory, the normalized line-breadth parameter for collision broadening, $\Delta\nu/P$, is conveniently expressed as

$$\Delta\nu/P=2b^2/(\pi MkT)^{\frac{1}{2}}, \tag{1}$$

where $\Delta\nu$ is the half-width at half-maximum intensity, P is the pressure, T the absolute temperature, M the molecular mass, and b the "collision diameter." This normalized line breadth is independent of P for the low pressures used. However, it does depend on T, and it will, in general, also vary from line to line in the spectrum because the collision cross section πb^2 for radiation interruption will depend on the quantum state of the molecule. If the molecules acted like hard spheres, b would simply be the diameter of the sphere, and $(\Delta\nu/P)\propto T^{-\frac{1}{2}}$. Actually, the effective collision diameter is greater for slow molecules which have more time to interact during each encounter. Thus b decreases with increasing T, and the total temperature dependence is

$$\Delta\nu/P\propto T^{-n}, \tag{2}$$

where $n>\frac{1}{2}$. One may show that if the interaction potential is proportional to r^{-p}, then

$$n=\frac{1}{2}\frac{p+1}{p-1}. \tag{3}$$

Thus the exponent n is a convenient indicator of the "hardness" of the intermolecular interaction potential.

2. EXPERIMENTAL METHOD

In taking the experimental data, an X-band recording resonance spectrometer with magnetic field modulation was used. This apparatus yields a trace of the derivative of the absorption along an abscissa linear in the magnetic field. Since the modulation amplitude was always less than one-tenth of the line width, the considerations given by Andrew[4] show that the spurious increase in line width introduced by the finite modulation amplitude is less than 1 percent. This was confirmed experimentally by extrapolation. Three independent values of the line width for a Lorentz shape were deduced from each trace by measuring the separations of the points of one-half, three-quarters, and full-maximum signal. The absence of any trend in the discrepancies among these determinations confirms that the shape is indeed Lorentzian, as it should be for collision broadening. Since the deflection

* This work was supported in part by the Signal Corps; the Office of Scientific Research, Air Research and Development Command; and the Office of Naval Research.

† National Science Foundation Fellow; now at the Clarendon Laboratory, Oxford, England.

[1] Those studying the resolved spectrum include: B. V. Gokhale and M. W. P. Strandberg, Phys. Rev. **84**, 844 (1951); Anderson, Smith, and Gordy, Phys. Rev. **87**, 561 (1952); R. M. Hill and W. Gordy, Phys. Rev. **93**, 1019 (1954); J. O. Artman and J. P. Gordon, Phys. Rev. **87**, 227(A) (1952); J. O. Artman, Ph.D. thesis, Physics Department, Columbia University, 1953 (unpublished); J. O. Artman and J. P. Gordon, Phys. Rev. **96**, 1237 (1954).

[2] R. Beringer and J. G. Castle, Jr., Phys. Rev. **81**, 82 (1951).

[3] M. Tinkham and M. W. P. Strandberg, Phys. Rev. **97**, 937 and 951 (1955), referred to in the text as I and II.

[4] E. R. Andrew, Phys. Rev. **91**, 425 (1953).

is stationary at the maximum signal points, the accuracy with which their separation may be determined is rather limited in the presence of noise. Thus, the other two determinations were given the dominant weight when the best experimental value was chosen for each chart. Each piece of raw data is the average of these best widths from two charts of the given line at the same temperature and pressure.

The data obtained in this way were fitted to a dependence of the form

$$\Delta H = (\Delta H)_0 + (\Delta H/P)P \qquad (4)$$

by least squares. Since $(\Delta H)_0$ is the result of field inhomogeneity over the cavity, its value should increase smoothly as one considers lines at increasing fields. On this basis a smoothed set of $(\Delta H)_0$ values was chosen, and from them a new fit for the $\Delta H/P$ values was made. This procedure allows us to obtain some of the advantages of the data on *all* lines in fitting *each* line.

Two completely independent sets of data were taken and fitted in this way. They were made with different cavities and different pole pieces. In each set, data were taken at three to ten different pressures at each temperature. The adjustment procedure described is supported by the fact that the largest adjustments were of opposite sign for the two sets and tended to bring the data toward a common result. Thus we are assured that our procedure only averages out random errors and does not eliminate any actual effect.

3. RESULTS

The results of our measurements are given in Table I. The conversion to frequency widths made use of the computed $d\nu/dH$ factors quoted in II. The indicated errors are estimated limits of error based on the errors of the individual least-squares fittings and on the differences between the results obtained with the two sets of data.

For comparison, let us also consider the results of Beringer and Castle.[2] As far as the transitions were identified in reference 2 (half only to K value), they were correctly assigned except for line 17. However, the calculations of II allow total identification to be made and the proper $d\nu/dH$ factors calculated to convert widths in gauss to widths in megacycles per second. Values for the line widths of reference 2 corrected by a factor of $(H/\nu)(d\nu/dH)$ are also tabulated in Table II.[5] The temperature-dependence exponent, n, is indicated in the last column. To simplify direct comparison with our data, their 85°K data have been converted to 78°K by using an average T-dependence.

TABLE I. Line-breadth data. ($\Delta\nu/P$ is in (Mc/sec)/mm Hg.)

Transition K	J	M	$\Delta\nu/P$ O_2 at 300°K	$\Delta\nu/P$ O_2 at 78°K	$\Delta\nu/P$ Air at 78°K	$\frac{\Delta\nu(\text{air})}{\Delta\nu(O_2)}$	n
1	1	−1→0	2.35 ±0.10	6.13 ±0.3	6.13 ±0.3	1.00 ±0.06	0.71 ±0.04
1	2	1→2	2.20 ±0.10	6.00 ±0.2	6.02 ±0.3	1.00 ±0.06	0.74 ±0.04
1	2	0→1		5.92 ±0.3			
1	2	−1→0	2.23 ±0.14	6.20 ±0.1	6.21 ±0.2	1.00 ±0.04	0.76 ±0.06
3	2	0→−1		5.93 ±0.3	6.63 ±0.3	1.12 ±0.08	
3	4	−1→0	2.00 ±0.10	5.70 ±0.3	6.12 ±0.3	1.07 ±0.06	0.78 ±0.06
5	4	0→−1		6.0 ±0.5			
5	6	−1→0		5.5 ±0.3			

TABLE II. Line-breadth data of Beringer and Castle re-evaluated by our work.

B and C[a] line number	K	Transition J	M	Corrected $\Delta\nu/P$ 300°K	85°K	78°K	n
2	1	1	−1→0	2.24	6.52	6.98	0.85
5	1	2	1→2	2.49	6.98	7.47	0.82
9	1	2	0→1		6.21	6.65	
12	1	2	−1→0	2.08	6.38	6.84	0.89
14	3	2	0→−1		5.83	6.24	
19	3	4	−1→0		6.62	7.09	
3	3	2→4	0→1		6.97	7.47	
4	3	4→2	−2→−1	2.42	7.41	7.94	0.89
17	5	4	0→−1		6.83	7.31	
16	5	4→6	0→1		7.02	7.52	
7	5	6→4	−2→−1	2.18	6.16	6.60	0.825
11	9	8→10	2→3		6.57	7.04	

[a] See reference 2.

4. DISCUSSION

First, let us compare our results with those of reference 2. Our correction has greatly reduced the scatter of these results. However, the agreement with our data is still rather poor. At 300°K, our results agree in the mean but have a mean deviation of roughly ±8 percent. At 78°K our means differ by 14 percent, but the mean deviation about that is only ±5 percent. This difference in behavior at the two temperatures is such that our values of the exponents n are in the vicinity of 0.75, whereas their values are near 0.85. It seems clear that a systematic error is present. One possible source of error is in the measurement of the temperature, particularly of the low temperature. We measured the low temperature with a thermocouple soldered to the cavity wall. This thermocouple was calibrated at the boiling points of N_2 and O_2, as well as at the ice point, and temperatures could be read to a fraction of a degree. It was found that this temperature was always within a degree of 78°K with the liquid N_2 which we used. The data of Beringer and Castle are quoted at 85°K though liquid air was used.[6] The varying composition as the air boils away will cause an error since cavity temperatures are not directly measured.[6] However, even if we presumed that their temperature was as low as 78°K, their line width would still exceed ours. Perhaps a more promising explanation lies in the residual width $(\Delta H)_0$ at zero pressure. No particular effort was made to take field homogeneity into account in the work reported in reference 2.[6] Figure 6 of that paper would indicate the

[5] That the assumption of a linear ν to H relationship implied by the use of ν/H as a conversion factor may introduce large errors was acknowledged by Beringer in Ann. N. Y. Acad. Sci. **55**, 818 (1952).

[6] R. Beringer (private communication).

correction is negligible for 300°K measurements, in agreement with our deduction. The fact that they used a different cavity at low temperatures and at room temperatures would make the observed differential effect possible, especially for measurements at 2 or 3 mm Hg pressure used in reference 2 in the line breadth studies.[6] Since in our work, the same cavity and positioning were used for both temperatures, and since the residual width was carefully handled, it would appear that our data should be reliable.

Considering only our data on O_2 self-broadening, there seems to be a trend toward lower line widths with increasing rotational quantum number K. However, the decrease in signal strength with increasing K has precluded carrying this far enough to establish whether it levels off or continues to drop slowly. In any case, the variation with K is slight. Three transitions with $K=1$, $J=2$ were studied in an attempt to find any M-dependence of the line width. Since the widths of these three lines all agree within the experimental error, we conclude that the dependence on M is negligible, as expected. It should also be remarked that the magnitudes of our line widths are in general agreement with those found for the same value of K by Anderson *et al.*; by Hill and Gordy; and by Artman.

The lines observed in this spectrum each come from a single transition, rather than from a sum of transitions of degenerate M states as in field-free spectroscopy. It was of interest to see if there were any of the pressure shifts that are allowed in phase-shift theories of broadening. Measurements of the positions of line centers over a range of pressures up to 8 mm Hg indicate that any such shifts must be less than two percent of the line width.

We find that the exponent n in the temperature dependence increases slightly with both J and K, but the differences are all within the limits of error. The mean value of n, 0.75, should be compared with the average of 0.87 found by Beringer and Castle and the average of 0.85 found by Hill and Gordy in the 5-mm spectrum.

The theoretical position on line widths in the microwave spectrum of O_2 has been carefully reviewed by Artman using Anderson's[7] semidiabatic method. He finds that the magnetic dipole-dipole interaction, which would give $n=1$, is completely negligible in magnitude. The electric quadrupole-quadrupole interaction, which is the next longest range interaction available, would give $n=0.75$, but again the magnitude would seem to be an order of magnitude too small to account for the entire line width. He finds that a combination of polarizability and exchange interactions dominate. This short range interaction gives $n=0.627$, rather near the hard sphere value of 0.5. In view of these theoretical expectations, our lower value of n is definitely more understandable than the old values. Our data are also in reasonable agreement with Artman's prediction of a line width independent of K except for a slight drop from $K=1$ to $K>1$.

Finally, let us consider the data on the ratio of air-broadening to self-broadening at 78°K presented in Table I. We find that for the three different $K=1$ transitions the ratio is 1.00 ± 0.06; for the two $K=3$ transitions the ratio is 1.10 ± 0.10. These results are rather surprising in view of the fact that both Anderson *et al.* and Artman found N_2 only about 85 percent as effective a broadening agent as O_2. Of course, since both of these investigations were at room temperature and were of the millimeter spectrum, which involves somewhat different states, a direct comparison may not be significant.

5. CONCLUSIONS

On the basis of our data we conclude that the line width is independent of M and decreases slightly with increasing K. We find the average temperature dependence exponent n to be 0.75. This is nearer the theoretically expected value of 0.627 than the previous values of roughly 0.85. The line centers shift less than 2 percent of the line width for pressures up to 8 mm Hg. Finally, we find O_2-N_2 collisions to be no less effective than O_2-O_2 collisions in producing broadening.

[7] P. W. Anderson, Phys. Rev. **76**, 647 (1949).

Absorption Cross Section of Helium and Argon in the Extreme Ultraviolet

PO LEE AND G. L. WEISSLER
Department of Physics, University of Southern California, Los Angeles, California
(Received October 26, 1954)

The absorption of radiation of wavelength between 240 A and 1000 A in helium and argon was measured photometrically in a grazing incidence vacuum spectrograph. For helium a sharp absorption edge was observed at 504.3 A. Near this edge the photoionization cross section at 495.7 A was found to be 6.95×10^{-18} cm². The variation of the cross section as a function of the wavelength was in agreement with the computed curves by Wheeler and Vinti within the experimental error limit. For argon three absorption edges exist at 786.8 A, 778.0 A, and 424.0 A corresponding to the M_2, M_3, and M_1 edges, respectively. Possible autoionization phenomena between the M_2 and M_3 edges were observed. The cross section at the M_2 edge was found to be 3.5×10^{-17} cm² which is comparable with the value computed by Dalgarno.

INTRODUCTION

THE absorption of radiation in the extreme ultraviolet by inert gases was first observed qualitatively by C. Cuthbertson.[1] During the recent years photometric techniques in the vacuum ultraviolet have been improved to such an extent that the determination of absorption cross sections of gases in this spectral region was possible within an experimental error of about ten percent. The cross sections of neon[2] have been measured and were found to be in good agreement with the values computed by Seaton. This work concerns itself with the cross sections of helium and argon. Results were obtained in the same manner as described for neon.[2] Tank helium and argon were supplied by the Air Reduction Pacific Company, Los Angeles, California. The helium contained 1×10^{-4} parts of hydrogen, and argon 10^{-3} parts of oxygen as impurities, fractions too small to introduce serious experimental errors.

The determination of the absorption coefficient was based on Beer's law,

$$I=I_0e^{-kx},$$

where the absorption coefficient, k, is in units of cm^{-1} at N.T.P. The cross section σ is given by

$$\sigma=k/N,$$

where N is Loschmidt's number. In the foregoing equations, I_0 and I are the incident and emergent intensities of light when passing through a layer of the absorbing gas x cm thick at N.T.P. From the photometric determination of the emergent intensities at different pressures of the absorbing gas, the k-values were thus obtained.

TABLE I. Absorption coefficients in helium as a function of the wavelength.

Source line wavelength (A)	k (cm^{-1})	Source line wavelength (A)	k (cm^{-1})
OIV 779.8	0	2× NII 418.9	120
OII 675.7	0	2× OIII 395.6	92
NII 635.1	0	2× OIII 374.0	95
HeI 584.3	75	2×NIII 362.9	84
NII 506.1	0	2×NIII 358.3	98
? 495.7	186	2× OIII 328.1	75
OII 485.6	162	2×NIII 323.6	80
? 452.0	160	2× OIII 306.0	45
2×OIII 445.6	142	2× NIV 283.6	30
2× OII 434.9	115	2× NIV 247.2	25
2× NII 428.2	110	2× OIV 239.6	25

[1] C. Cuthbertson, Proc. Roy. Soc. (London) **A114**, 650 (1927).
[2] Po Lee and G. L. Weissler, Proc. Roy. Soc. (London) **A219**, 71 (1953).

PHOTOIONIZATION CROSS SECTIONS IN HELIUM

Helium is transparent in the wavelength region longer than 504.8 A except for resonance line absorption.

Many source lines near 500 A were available for this investigation, since a mixture of argon and helium was used as a discharge carrier gas in the light source.[3]

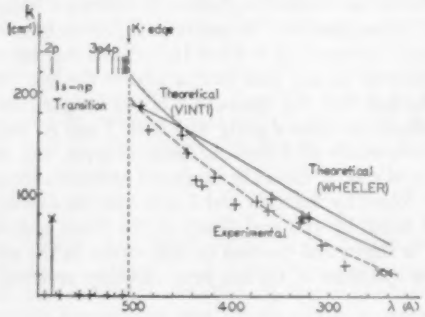

FIG. 1. Absorption coefficients of helium as a function of wavelength. + represents the measured values of the coefficient k and × indicates values whose error limit is larger than 15 cm^{-1} but unknown. The solid curves indicate the absorption contour computed by Vinti and by Wheeler.

A sharp absorbing edge was observed between the source lines AII 504.80 and AII 503.64 which agreed with the computed value 504.27 A from spectroscopic data.[4] The k-values of the adjacent continuum are given in Table I and shown in Fig. 1. The absorption of HeI 584.3, a resonance line of helium, was due to a process of photoexcitation. The continuous absorption

[3] Po Lee and G. L. Weissler, J. Opt. Soc. Am. **42**, 80 (1952).
[4] C. E. Moore, *Atomic Energy Levels*, National Bureau of Standards, Circular No. 467 (U. S. Government Printing Office, Washington, D. C., 1949), Vol. I, p. 4.

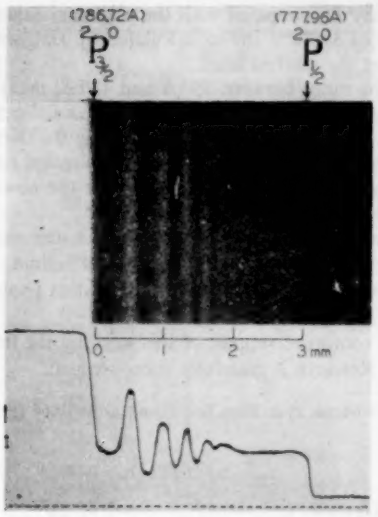

FIG. 2. A photograph of the absorption spectrum of argon between the M_3 and M_2 edges. The lower curve is the corresponding microdensitometer trace.

was obviously due to photoionization in which a 1*s*-electron in the ground state was ejected from the atom by the incident photon. Wheeler[5] and Vinti[6] have computed the absorption coefficient of helium. Their results are shown in the Fig. 1 as solid lines. The theoretical cross section obtained at the spectral head was 7.4×10^{-18} cm², while the experimental value from the extrapolation of the dashed curve in Fig. 1 was 7.3×10^{-18}. The experimental cross sections fall off more rapidly than Wheeler's and seem to follow Vinti's curve more closely, with a probable error in the measurements of about 15 cm^{-1}.

PHOTOIONIZATION CROSS SECTIONS OF ARGON

Since argon has a lower ionization potential than helium, its absorption extended over a comparatively

TABLE II. Absorption coefficients in argon as a function of the wavelength.

Source line wavelength (A)	k (cm^{-1})	Source line wavelength (A)	k (cm^{-1})
AIV 843.7	0	AII 725.5	880
AIV 827.3	0	AIV 700.3	950
? 781.2	520	AIV 683.2	940
OIV 779.8	515	NII 671.7	940
NII 776.0	960	NII 660.3	900
NIII 772.3	920	OII 644.1	900
NIII 771.9	970	AIII 637.2	900
AIII 769.1	890	OIV 625.8	860
NII 747.0	940	OII 617.1	850
NII 745.8	940	AII 602.8	850

[5] J. A. Wheeler, Phys. Rev. **43**, 258 (1933).
[6] J. P. Vinti, Phys. Rev. **44**, 524 (1933).

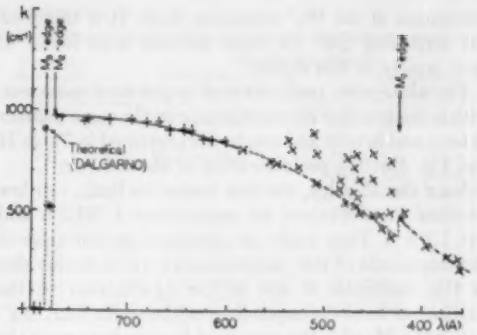

FIG. 3. Absorption coefficients of argon as a function of wavelength. ✦ represents the measured values of the coefficient k and ✖ indicates values whose error limit is larger than 50 cm^{-1} but unknown. ⊙ indicates the value computed by Dalgarno.

larger spectral region. The continuous emission spectrum of molecular helium[7] served in this case as a light source to provide qualitative information on the absorption of argon near its ionization limits. The spectrum thus obtained showed two sharp absorption edges near 786 A. There was a group of resonance absorption lines at longer wavelengths due to $3p\rightarrow nd$ and $3p\rightarrow ns$ transitions. Like helium and neon, the absorption coefficients in these resonance lines were smaller than those in the continuous absorption and are not given here. The print in Fig. 2 shows the absorption spectrum between the edges at 786.72 A and at 777.96 A, respectively. Below the print is the corresponding microdensitometer trace. A series of resonance lines which converged to the M_2 edge as a limit is in evidence. They are diffuse due to the perturbation of the adjacent

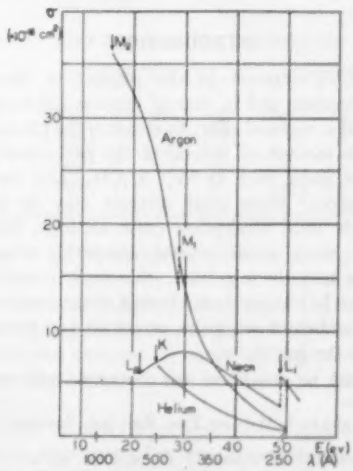

FIG. 4. Absorption cross sections of the three inert gases, argon, neon, and helium.

[7] Y. Tanaka, Sci. Papers Inst. Phys. Chem. Research (Tokyo) **39**, 465 (1942).

continuum of the $^2P_{\frac{1}{2}}^\circ$ ionization limit. It is therefore not surprising that the cross sections were found to vary rapidly in this region.

The absorption coefficients of argon were measured with a discrete line emission source in the same manner as neon and helium and results are presented in Table II and Fig. 3 with a probable error of about 50 cm^{-1}.

Near the M_3 edge, the first ionization limit, two low k-values were obtained for source lines ? 781.2 A and OIV 779.8 A. They might be considered as indicative of the magnitude of the photoionization cross section due to the transition of one of the $3p$-electrons to the continuous level corresponding to the series limit $^2P_{\frac{1}{2}}^\circ$. Below the M_2 edge the measured k-value represents the total contribution of two possible transitions and falls off slowly toward shorter wavelengths At the M_2 edge the cross section was estimated to be 3.5×10^{-17} cm^2. This may be compared with the photoionization cross section of 3×10^{-17} cm^2 as calculated by Dalgarno[8] for argon at the spectral head.

In the range between 550 A and 420 A, many comparatively large k-values were found as indicated by crosses above the dashed curve in Fig. 3. They may possibly be explained as due to autoionization near the M_1 edge. In contrast, below this edge the absorption coefficients were found uniformly lower.

In summarizing the results obtained, the variation of the photoionization cross sections of helium, argon, and neon *versus* the energy of the incident photon are shown in Fig. 4.

The continued support of this work by the Office of Naval Research is gratefully acknowledged.

[8] A. Dalgarno, Proc. Phys. Soc. (London) **A65**, 666 (1952).

PHYSICAL REVIEW VOLUME 99, NUMBER 2 JULY 15, 1955

Photoionization Efficiencies and Cross Sections in O_2, N_2, CO_2, A, H_2O, H_2, and CH_4

N. WAINFAN, W. C. WALKER, AND G. L. WEISSLER
Department of Physics, University of Southern California, Los Angeles, California

(Received October 26, 1954)

The photoionization cross sections of several gases were obtained by making simultaneous measurements of the total absorption cross sections and ionization efficiencies in the wavelength region from 473 A to 1100 A. In each case the total absorption cross sections were in agreement with those reported by others. For O_2, the ionization cross sections were found to be between 5 and 30×10^{-18} cm^2, while those for N_2 were close to 23×10^{-18} cm^2 over almost the entire range studied. The ionization cross section of argon at the onset of ionization was compared with the theoretical estimate made by Dalgarno. The long-wavelength limits for photoionization were determined and were found to yield ionization potentials in good agreement with those obtained by spectroscopic and electron impact methods.

INTRODUCTION

PRESENT interest in the physics of the upper atmosphere and in that of gaseous discharges has motivated a renewed effort to measure the photoionization cross sections of several of the permanent gases. For a few gases, such as Ne,[1] A, CH_4,[2] and the alkali metal vapors,[3] these cross sections may be inferred from their total absorption cross sections. However, since in many gases several competing absorption processes may be expected, the most unambiguous results can be obtained only from a direct measurement of the number of ion pairs produced per photon absorbed in the gas.[4,5]

The work reported here was concerned with measurements of the absolute photoionization cross sections and ionization efficiencies of O_2, N_2, CO_2, A, H_2, H_2O, and CH_4 as a function of wavelength between 473 and 1020 A. Techniques employed in this investigation were essentially the same as those described in an earlier paper containing preliminary results for O_2 and N_2.[6]

APPARATUS AND PROCEDURE

The equipment employed in this study consisted of three major components, a light source and normal-incidence vacuum monochromator, instruments for determining the absolute light intensity at the exit slit, and an assembly of ion chambers, mounted in a gas-filled experiment chamber behind the exit slit, in which the ionization currents and absorption coefficients were measured. The light source and monochromator have been described previously.[6] A line-emitting light source was used in preference to the frequently employed continuum in order to facilitate the separation of first-

[1] P. Lee and G. L. Weissler, Proc. Roy. Soc. (London) **A219**, 71 (1953).
[2] H. Sun and G. L. Weissler, J. Chem. Phys. (to be published).
[3] Ditchburn, Tunstead, and Yates, Proc. Roy. Soc. (London) **A181**, 386–99 (1943).
[4] F. L. Mohler, Phys. Rev. **28**, 46–56 (1926).
[5] Watanabe, Zelikoff, and Inn, AFCRC Technical Report No. 52–53 (unpublished); also, Phys. Rev. **91**, 1155 (1953); K. Watanabe, J. Chem. Phys. **22**, 1564 (1954).
[6] Wainfan, Walker, and Weissler, J. Appl. Phys. **24**, 1318 (1953).

TABLE I. Monochromator wavelengths.

Nominal wavelength in angstroms	Emission lines included: 0.6-mm slits, Approx resolution 10 A	0.3-mm slits, Approx resolution 5 A
473	473.0 AIII 476.4 AIII 473.9 AIII 481.8 AIII	
508	503.6 AII 508.7 AIII 507.4 OIII 510.6 AII 507.7 OIII 511.5 AIII 508.2 OIII 511.6 AIII 508.4 AIII 512.8 AIII 508.6 AIII	
530	525.8 OIII 532.4 AIII 526.5 AII 534.3 AIII 529.9 AIII 535.6 AIII 530.5 AII 536.7 AIII	
550	547.9 AII 554.1 OIV 548.8 AII 554.5 OIV 553.3 OIV 555.1 OII 553.5 AIII	
575	572.0 AII 578.6 AII 573.4 AII 580.3 AII 576.7 AII	
598	597.7 AII 600.6 OII 597.8 OIII 602.9 AII 599.6 OIII	
627	624.6 OIV 625.9 OIV 625.1 OIV 629.7 OV	
644	641.4 AIII 644.6 NII 641.8 AIII 644.8 NII 643.3 AIII 645.2 NII 644.1 OII	
662	661.9 AII 660.4 NII 663.1 O 666.0 AII	
687	683.3 AIV 685.8 NIII 684.9 NIII 686.3 NIII 685.5 NIII 688.5 AIV	684.9 NIII 686.3 NIII 685.5 NIII 688.4 AIV 685.8 NIII
704	702.3 OIII 703.8 OIII 702.8 OIII 704.5 AII 702.9 OIII 704.3 AIV	702.3 OIII 703.8 OIII 702.8 OIII 704.5 AII 702.9 OIII 704.3 AIV
716	Not resolved	715.6 AV 715.7 AV
720	715.6 AV 718.6 OII 715.7 AV 723.4 AII 718.1 AII 725.5 AII 718.5 OII	718.1 AII 718.6 OII 718.5 OII 723.4 AII
728	Not resolved	725.5 AII 730.9 AII
762	Not resolved	759.4 OV 761.5 AIV 760.2 OV 762.0 OIV 760.4 AIV 763.3 NIV 761.1 OV 764.4 NIII
770	763.1 NIV 771.9 NIII 769.2 AIII 772.5 NIII 769.4 OI 776.0 NII 772.9 NIII 779.8 OIV 771.5 NIII 779.9 OIV	770.3 OI 772.5 NIII 772.9 NIII 776.0 NII 771.5 NIII 779.8 OIV 771.9 NIII 779.9 OIV
787	787.9 OIV 790.4 OIV 790.1 OIV	787.9 OIV 790.4 OIV 790.1 OIV
797	796.7 OII	796.7 OII
825	Not resolved	822.2 AV 827.4 AV 827.1 AV
833	827.1 AV 833.7 OIII 827.4 AV 834.5 OIII 832.8 OII 835.1 OIII 832.9 OII 835.3 OIII 833.3 OII	832.8 OII 834.5 OII 832.9 OIII 835.1 OIII 833.3 OII 835.3 OIII 833.7 OIII
843	Not resolved	840.0 AIV 843.8 AIV
850	Not resolved	850.6 AIV
872	Not resolved	871.1 AIII 876.1 AI 875.5 AIII
894	Not resolved	894.3 AI 898.9 OIII
920	915.6 NII 922.0 NV 915.9 NII 923.0 NIV 916.0 NII 923.2 NIV 916.7 NII 923.4 OIV 916.8 AII 923.4 NIV 921.3 OIV	919.8 AII 923.0 NIV 921.3 OIV 923.2 NIV 921.4 OIV 923.4 OIV 922.5 NIV 923.4 NIV
955	955.3 NIV	955.3 NIV
979	979.8 NIII 979.9 NIII	979.8 NIII 979.9 NIII
991	988.6 OI 990.2 OI 988.8 OI 990.8 OI 989.8 NII 991.5 NIII 989.8 NII 991.6 NIII 990.1 OI	988.6 OI 990.2 OI 988.8 OI 990.8 OI 989.8 NIII 991.5 NIII 989.8 NII 991.6 NIII 990.1 OI

order from higher-order spectral components. For most of the gases studied, the photoionization cross sections were established using two 1.5-cm-long ionization chambers spaced 10 cm apart along the light beam. The ionization currents generated in these ion chambers were between 10^{-10} and 10^{-13} ampere and were measured with a Beckman, Model V, micro-microammeter. A windowless Reeder thermopile having a sensitivity in vacuum of 1.05 microvolts per microwatt was used to determine the photon flux at the exit slit.[7] In addition to this, a 1P28 photomultiplier tube, sensitized to ultraviolet radiation by having it view a fluorescent screen (Sodium Salicylate or Apeizon L grease),[8] was calibrated against the thermopile and used as a secondary radiation detector. Primary and exit slit widths of 0.6 mm each limited the resolution of this system to 10 A.

In order to provide a check on the accuracy and to eliminate instrumental errors the work was repeated, for several of the gases, using three, 3 cm long, ionization chambers in tandem, each separated by a distance of

[7] D. M. Packer and C. Lock, J. Opt. Soc. Am. **41**, 699 (1951); see also, K. Watanabe and E. C. Y. Inn, J. Opt. Soc. Am. **43**, 32 (1953).

[8] Johnson, Watanabe, and Tousey, J. Opt. Soc. Am. **41**, 702 (1951).

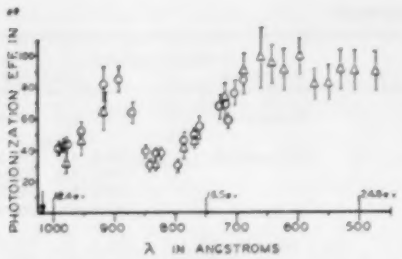

FIG. 1. Photoionization efficiencies of O_2. △ Data taken with 1.5-cm ion chambers, and 10 A resolution. ○ Data taken with 3-cm ion chambers, and 5 A resolution. The first ionization limit at 1019±10 A is indicated on the wavelength axis by an arrow.

25 cm. For use in conjunction with these chambers the Reeder thermopile was replaced by one of the Schwarz-Hilger type. Its increased sensitivity of 9.5 microvolts per microwatt in vacuum eliminated the necessity for the photomultiplier tube and permitted the use of 0.3 mm wide slits which gave a 5 A resolution.

Because of the five- to ten-angstrom resolution of the monochromator, the radiation at each of the nominally assigned wavelengths consisted, in many cases, of a number of individual light source emission lines. Although no detailed identification of these lines was made, spectrograms were taken with a 10-micron wide primary slit and compared with the wavelength table compiled by Boyce and Moore.[9] The possible emission lines falling within each resolved wavelength band are tabulated in Table I. In addition to the line emitting source, a hydrogen glow discharge[8] was used providing a wavelength continuum down to about 900 A. This light source helped to establish the long wavelength ionization limits in O_2 and CH_4.

In order to determine both the photoionization efficiencies and cross sections of a particular gas it was first necessary to determine the absolute absorption coefficient k of the gas. At the working pressure and temperature the value of k is defined by Lambert's law as follows: $k=-\ln(I_d/I_0)/d$. Since the saturated ionization currents are proportional to the intensity of the light beam passing through the ion chambers, this can be written as $k=-\ln(i_2/i_1)/d$, where i_1 is the ion current in the ion chamber nearest the exit slit and i_2 is that in another chamber separated a distance d cm from the first. From a knowledge of k and the incident photon flux at the exit slit the number of photons per second N absorbed in the first ion chamber may be obtained as follows: $N=I_0\{\exp[-kX]-\exp[-k(X+L)]\}$, where I_0 is the photon flux at the exit slit of the gas-filled experiment chamber, X is the distance between the exit slit and the leading edge of the first ion chamber and L is the length of the collector electrode for this ion chamber. The photoionization efficiency γ, in percent, can then be calculated from the ratio of the ionization current in charges per second to the number of photons per second absorbed in the ion chamber, that is, $\gamma=(i_1/N)\times 100$. The total absorption cross section σ, obtained by dividing the value of k by Loschmidt's number, can then be combined with the photoionization efficiency to give the cross section for ionization by all processes from the relation $\sigma_i=\sigma\gamma$.

Test runs made with the experiment chamber evacuated to a pressure of about 5×10^{-5} mm of Hg, as well as the occurrence of sharp ionization onsets, indicated that photocurrents from the ion chamber walls due to reflected or scattered light were negligible. The remaining possible sources for error in the present investigation, included in calculating the probable errors of the photoionization results presented, were the following: (1) an estimated five percent error in the determination of the absolute light intensity, (2) a five percent calibration error in the current recording system, (3) an error in the absolute pressure measurements, and (4) an error in the measured total absorption coefficients. Since the ionization cross section depended directly on the value of the total absorption coefficient, there was some variation in the accuracy of the results for different lines. The probable errors for each line are indicated in the figures.

RESULTS AND DISCUSSION

Because of their importance in upper atmospheric physics, the gases O_2 and N_2 were investigated in detail. In addition several less abundant atmospheric components, CO_2, A, H_2, and H_2O were studied, though less extensively. Theoretical interest also motivated a brief consideration of CH_4.[10]

Oxygen

Ionization efficiencies and cross sections for O_2 are graphically presented in Figs. 1 and 2 and together

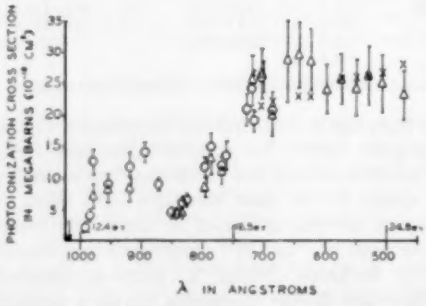

FIG. 2. Photoionization cross sections of O_2. △ Data taken with 1.5-cm ion chambers. ○ Data taken with 3-cm ion chambers. × Estimate of ionization continuum made by Lee and Weissler (reference 14). The first ionization limit at 1019±10 A is indicated on the wavelength axis by an arrow.

[9] J. C. Boyce and J. T. Moore, "Provisional Wavelength Identification Tables for the Vacuum Ultraviolet," Massachusetts Institute of Technology, 1941 (unpublished).

[10] A. Dalgarno, Proc. Phys. Soc. (London) A65, 663 (1952).

TABLE II. Photoionization in O_2.

	With small ion chambers			With large ion chambers		
λ	$\sigma_{abs}\times10^{18}$ cm²	Eff in %	$\sigma_{ion}\times10^{18}$ cm²	$\sigma_{abs}\times10^{18}$ cm²	Eff in %	$\sigma_{ion}\times10^{18}$ cm²
473	26.0±2.6	88.8±13.2	23.1 ±4.1			
508	27.7±2.8	89.9±13.5	24.9 ±4.5			
530	29.0±2.9	90.3±13.5	26.2 ±4.7			
550	29.3±2.9	82.7±12.4	24.2 ±4.4			
575	31.2±3.1	82.0±10.3	25.6 ±4.1			
598	24.0±2.4	99.8±13.0	23.9 ±4.0			
625	31.5±3.2	90.8±13.6	28.6 ±5.2			
644	31.0±3.1	94.9±14.2	29.4 ±5.3			
662	29.0±2.9	98.4±19.7	28.5 ±6.4			
687	21.9±2.2	90.2±11.7	19.8 ±3.3	24.6 ±1.05	83.9±11.8	20.6 ±3.0
704	33.4±3.3	79.2± 9.5	26.5 ±4.1	34.4 ±1.6	75.6± 6.5	26.0 ±2.5
716				32.5 ±1.6	58.4± 4.5	19.0 ±1.7
720	34.6±3.5	73.7± 8.9	25.5 ±4.0	35.2 ±1.5	68.4± 7.4	24.2 ±2.8
728				31.0 ±1.7	67.4± 7.5	20.8 ±2.6
762				24.9 ±2.1	54.5± 7.3	13.6 ±2.2
770	22.7±2.3	47.8± 5.7	10.9 ±1.7	24.1 ±1.2	49.5± 4.5	11.9 ±1.2
787	31.0±3.1	42.1± 6.3	13.1 ±2.4	32.0 ±1.7	46.7± 5.8	14.9 ±2.0
797	35.2±3.5	23.9± 3.0	8.41±1.4	38.2 ±2.3	30.6± 3.0	11.7 ±1.4
825				16.5 ±1.2	38.2± 3.2	6.30±0.70
833	14.5±1.5	32.3± 3.9	4.67±0.75	15.2 ±0.79	38.7± 2.9	5.88±0.54
843				14.3 ±0.96	31.1± 3.7	4.34±0.61
850				11.4 ±0.84	39.6± 4.5	4.50±0.61
872				14.1 ±0.70	63.2± 7.3	8.91±1.1
894				16.1 ±0.63	84.6± 8.1	14.0 ±1.4
920	12.5±1.9	65.1±13.0	8.17±2.0	14.3 ±1.1	81.8±10.6	11.7 ±2.2
955	17.5±2.6	46.0± 9.2	8.05±2.0	16.9 ±2.5	52.4± 5.5	8.86±1.6
979	22.4±3.4	31.4± 6.3	7.04±1.8	28.1 ±3.9	44.6± 3.3	12.5 ±2.0
985				9.2 ±1.2	42.4± 3.4	3.9 ±0.59
991				4.75±1.5	4.13± 3.7	1.96±0.64
	Av of 2 runs (1 at 100 microns, 1 at 50 microns)			Av of 5 runs (2 at 96 microns, 2 at 44 microns, 1 at 23 microns)		

with the total absorption cross sections are compiled in Table II.

The onset of ionization was found at 1019±10 A corresponding to an ionization potential of 12.1±0.1 volts.[11] This value was found to be in good agreement with the 12.1±0.20 volts obtained by Hagstrum[12] for the production of O_2^+-ions by electron bombardment and with the 12.2±0.1 volt result of Price and Collins[13] for the transition $O_2\ X\ ^2\Sigma_g^- \rightarrow O_2^+\ X\ ^2\Pi_g$. Good agreement was also noted between the total absorption cross sections presented and those of Weissler and Lee.[14]

Between the first ionization limit at 1019 A and the second at 763 A most of the photoions were produced in the $O_2\ X\ ^2\Sigma_g^- \rightarrow O_2^+\ X\ ^2\Pi_g$ transition. The possibility of autoionization cannot be excluded entirely because of the existence of strong molecular absorption bands in this region. However, it was impossible to observe this process separately in the present work. Resonance absorption bands reported by Collins and Price,[13] which were found down to about 680 A, coincide with the regions of low-ionization efficiencies. The non-ionizing absorbed photons were assumed to excite those molecular states which give rise to these bands. In the region of continuous absorption below 680 A the high-ionization efficiencies indicated that almost all the absorption occurred by one or more of the energetically possible photoionization processes.

The data for O_2 were obtained for pressures from 23 to 100 microns and within this range the results were found to be independent of the pressure. Thus, it is unlikely that two step ionization events occurred in the gas. In addition the hydrogen glow light source was used to explore the region between the ionization limit and the Lyman α line at 1216 A. No evidence of two step ionization processes preceding the ionization limit was found although currents down to 3×10^{-13} ampere or two orders of magnitude smaller than those measured during the experiment could easily be detected.

Nitrogen

Figures 3 and 4 show the photoionization efficiencies and cross sections in N_2. These results in addition to the total absorption cross sections are compiled in Table III.

From an onset at 792±5 A the ionization efficiency increased rapidly to values near 100 percent at about 700 A, and at wavelengths shorter than this nearly the

[11] The ionization limit presented here is at a slightly longer wavelength than that previously reported by the authors (see reference 6). The present value was obtained after a small error in the wavelength scale of the monochromator had been corrected. It should also be noted that in the previous paper the O_2 ionization limits were stated incorrectly. The correct designations are $O_2^+\ X\ ^2\Pi_g$ for the first ionization limit, $O_2^+\ a\ ^4\Pi_u$ for the second, and $O_2^+\ A\ ^2\Pi_u$ for the third.

[12] H. D. Hagstrum, Revs. Modern Phys. **23**, 185–203 (1951).

[13] W. C. Price and G. Collins, Phys. Rev. **48**, 714–19 (1935).

[14] G. L. Weissler and P. Lee, J. Opt. Soc. Am. **42**, 200–203 (1952).

TABLE III. Photoionization in N_2.

	With small ion chambers			With large ion chambers		
λ	$\sigma_{tot}\times10^{18}$ cm²	Eff in %	$\sigma_{ion}\times10^{18}$ cm²	$\sigma_{tot}\times10^{18}$ cm²	Eff in %	$\sigma_{ion}\times10^{18}$ cm²
473	24.5±2.5	84.5±12.7	20.8±3.8			
508	25.0±2.5	88.5±13.3	22.2±4.0			
530	25.8±2.6	89.0±13.4	23.0±4.2			
550	27.1±2.7	86.0±12.9	23.3±4.2			
575	24.1±2.4	87.5±13.1	21.1±3.8			
598	22.4±2.2	101.0±15.0	22.4±4.0			
625	22.7±2.3	101.5±15.0	22.7±4.2			
644	23.8±2.4	93.1±14.0	22.1±4.0			
662	30.3±4.6	99.0±19.8	30.0±7.5			
687	25.7±2.6	88.8±13.3	22.9±4.1	27.4±1.20	82.4±6.2	22.6±2.0
704	24.0±2.4	89.8±13.5	21.5±3.9	25.4±1.04	91.3±9.5	23.0±2.6
716				26.7±1.20	69.5±6.7	18.6±2.0
720	21.4±2.1	100.7±15.1	21.4±3.8	20.1±1.07	80.3±6.6	16.2±1.6
728				37.5±2.9	69.9±7.3	25.5±3.3
762				32.6±3.7	65.0±5.5	21.2±3.0
770	28.5±2.9	50.2± 7.5	14.3±2.6	31.4±3.2	55.5±5.6	17.5±3.0
787	19.3±1.9	45.6± 6.8	8.8±1.6	17.5±3.1	51.5±7.0	9.0±2.0
	1 run at 100 microns			3 runs (1 at 102 microns, 1 at 43.5 microns, 1 at 29.0 microns)		

entire absorption mechanism appeared to be that of photoionization. The onset limit corresponded to a first ionization potential of 15.6±0.1 volts, which is in good agreement with the 15.7±0.2 volts obtained by Hagstrum[12] and also with the ionization limit of 796 A or 15.58 volts for the transition $N_2\ X\ ^1\Sigma_g^+ \rightarrow N_2^+\ X\ ^2\Sigma_g^+$ as determined from band spectroscopy.[15] Again as in the case of O_2 the total absorption cross sections agreed with previous results.[16]

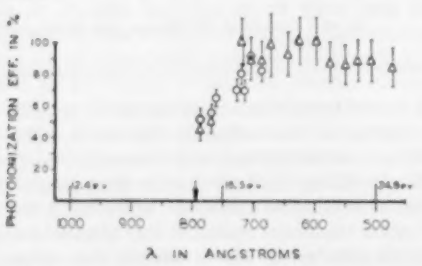

FIG. 3. Photoionization efficiencies of N_2. △ Data taken with 1.5-cm ion chambers, and 10 A resolution. ○ Data taken with 3-cm ion chambers, and 5 A resolution. The first ionization limit at 792±5 A is indicated on the wavelength axis by an arrow.

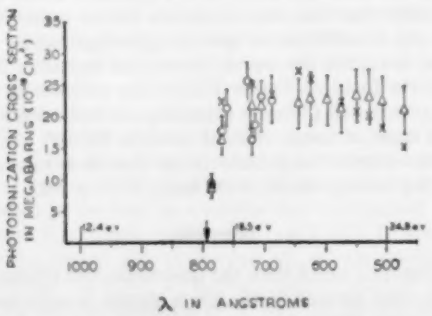

FIG. 4. Photoionization cross sections of N_2. △ Data taken with 1.5-cm ion chambers and 10 A resolution. ○ Data taken with 3-cm ion chambers and 5 A resolution. × Estimate of ionization continuum made by Lee and Weissler (reference 16). The first ionization limit at 792±5 A is indicated on the wavelength axis by an arrow.

Excitation of the σ_u 2*s*-electrons to levels above the first ionization limit made autoionization a possible mechanism in N_2.[17] Since Hagstrum found no N^+-ions appearing at electron impact energies less than 24.3 ev corresponding to a wavelength of 508 A, it was assumed that almost the entire absorption mechanism between 796 and 508 A involved the production of N_2^+-ions by the removal of the σ_g 2*s*- or possibly the σ_u 2*s*-electrons from the molecule.

Carbon Dioxide

Photoionization results for CO_2 are shown in Figs. 5 and 6. An ionization potential of 14.0±0.3 volts corresponding to 883±15 A was observed for this gas. The relatively large uncertainty of ±15 A in the position of the onset was due to a lack of sufficient light source emission lines near this onset. Within the error limits stated the present result agreed with the 13.73±0.01 volt figure obtained by Price and Simpson[18] from an analysis of the absorption spectrum of CO_2. Total absorption coefficients, reduced to N.T.P., varying between 300 and 1500 cm^{-1} were measured in the region from 473 to 883 A and were found to be in excellent agreement with recent results obtained by Sun.[19] Between the onset of ionization and 690 A the rapid fluctuation of the ionization cross sections was pre-

[15] G. Herzberg, *Molecular Spectra and Molecular Structure* (D. Van Nostrand Company, Inc., New York, 1950), p. 459.
[16] Weissler, Lee, and Mohr, J. Opt. Soc. Am. 42, 84 (1952).
[17] E. R. Worley, Phys. Rev. 64, 207 (1943).
[18] W. C. Price and D. M. Simpson, Proc. Roy. Soc. (London) A169, 501 (1939).
[19] H. Sun and G. L. Weissler, J. Chem. Phys. (to be published).

sumably due to the strong molecular absorption bands extending from 1150 to 690 A.[18] Since the acceptance band of the monochromator included a number of emission lines, the presence of these absorption bands caused a considerable difference between data taken at the two different resolutions.

Argon

In Figs. 7 and 8 are presented results for argon. The ionization limit found at 790±5 A, which is equivalent to 15.7±0.1 volts, is in agreement with the 15.76 volt figure listed by Moore.[20] From this threshold the ionization efficiency was observed to rise steeply as would be expected in the case of a monatomic gas. The photoionization cross sections were found to be in good agreement with the estimate of the ionization continuum made by Lee and Weissler.[21] A cross section of 27×10^{-18} cm² was found at 770 A, that is, just beyond the onset. This result agrees with the theoretical estimate made by Dalgarno[10] of 30×10^{-18} cm² at the ionization limit. In this comparison, the 770 A line was chosen since at a 5 A resolution it was the longest wavelength

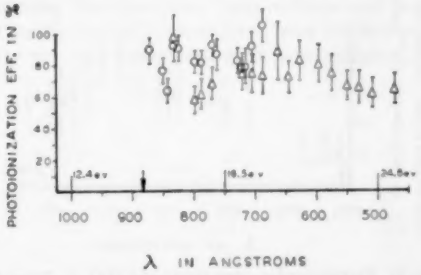

FIG. 5. Photoionization efficiencies of CO_2. △ Data taken with 1.5-cm ion chambers and 10 A resolution. ○ Data taken with 3-cm ion chambers and 5 A resolution. The first ionization limit at 883±15 A is indicated by an arrow on the wavelength axis.

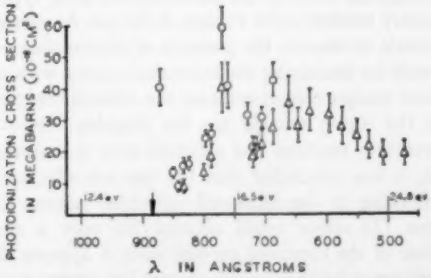

FIG. 6. Photoionization cross sections of CO_2. △ Data taken with 1.5-cm ion chambers and 10 A resolution. ○ Data taken with 3-cm ion chambers and 5 A resolution. The first ionization limit at 883±15 A is indicated on the wavelength axis by an arrow.

[20] C. Moore, *Atomic Energy Levels*, National Bureau of Standards Circular No. 467 (U. S. Government Printing Office, Washington, D. C., 1949), Vol. I, p. 211.

[21] P. Lee and G. L. Weissler, Phys. Rev. (to be published).

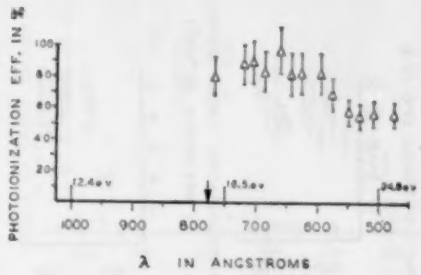

FIG. 7. Photoionization efficiencies of argon. △ Data taken with 1.5-cm ion chambers, and 10 A resolution. The first ionization limit of 790±5 A is indicated on the wavelength axis by an arrow.

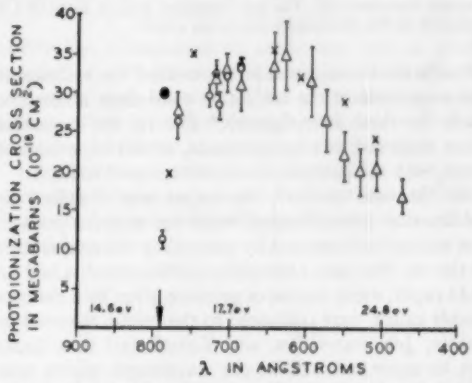

FIG. 8. Photoionization cross sections of argon. △ Data taken with 1.5-cm ion chambers, and 10 A resolution. ○ Data taken with 3-cm ion chambers, and 5 A resolution. × Estimate of the ionization continuum made by Lee and Weissler (reference 21). ● Theoretical estimate of Dalgarno (reference 10). The first ionization limit at 790±5 A is indicated on the wavelength axis with an arrow.

line lying outside the autoionization region of argon. The cross section for this line should therefore correspond to a direct ionization process as assumed by Dalgarno. Within the autoionization region, that is, between 787 A and 778 A, a much smaller cross section was observed.

Hydrogen and Water

Because of the general interest in H_2 and H_2O preliminary results in these gases are presented in Figs. 9, 10, and 11. Total absorption coefficients for H_2 have been measured by Lee and Weissler[22] who reported values varying between 200 and 500 cm^{-1} in the region from the ionization limit at 803.7 A to 680 A, a region containing strong absorption bands. The absorption coefficients observed in the present investigation for H_2, representing averages over a 5 A band width, were found to fall well within the range reported by Lee and Weissler. It should also be noted that the large ioniza-

[22] P. Lee and G. L. Weissler, Astrophys. J. 115, 570 (1952).

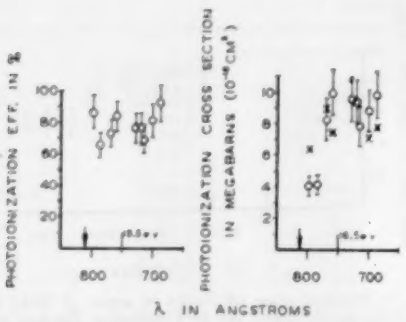

FIG. 9. Photoionization efficiencies and cross sections of H_2. ○ Data taken with 3-cm ion chambers, and 5 A resolution. × Estimate of the ionization continuum made by Lee and Weissler (reference 22). The first ionization limit at 810±15 A is indicated on the wavelength axis by an arrow.

tion efficiencies obtained for H_2 verified the estimate of the magnitude of the ionization continuum absorption made by these investigators.[22] For H_2 the ionization onset observed was in agreement, within experimental error, with the generally accepted value of 803.7 A.

In the case of H_2O, the vapor was obtained by sublimation from distilled water ice and its pressure was maintained constant by controlling the temperature of the ice. The total absorption coefficients obtained for H_2O vapor, using the vapor pressure given by a thermocouple gauge, were compared to the results reported by Astoin, Johannin-Gilles, and Vodar[23] and were found not to agree too well in the wavelength region near 473 A. On the basis of this comparison an estimated probable error of ±30 percent, due to the uncertainty in the pressure determination, was placed on the photoionization cross sections presented in Fig. 11. An ionization limit of 985±5 A corresponding to 12.5±0.1 volts was obtained from the position of the ionization onset in H_2O. This value was in excellent agreement with that obtained by Smith and Bleakney[24] using electron impact techniques.

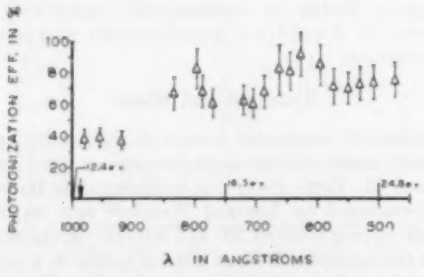

FIG. 10. Photoionization efficiencies of H_2O. △ Data taken with 1.5-cm ion chambers, and 10 A resolution. The first ionization limit at 985±5 A is indicated on the wavelength axis with an arrow.

[23] Astoin, Johannin-Gilles, and Vodar, Compt. rend. **237**, 558–560 (1953).
[24] L. G. Smith and W. Bleakney, Phys. Rev. **49**, 883(A) (1936).

Methane

Preliminary results on photoionization in CH_4 are shown in Fig. 12. Data taken at three pressures of 16.4, 28.5, and 50 microns were found, within experimental error, to be independent of the gas pressure. The total absorption cross sections calculated from these data are presented in Fig. 13 and compared there with the more accurate observations of Ditchburn[25] and of Sun and Weissler in this laboratory.[26] A 12.8±0.2 volt ionization potential, corresponding to 967 A, was obtained which is in accord with the estimate of Sun and Weissler, and with the 12.72 volt value reported by Smith and Bleakney.[24]

In the region from 800 A to 700 A the ionization efficiencies appeared to be larger than 100 percent. Three processes were considered to explain this anomaly; (1) photoelectric emission from the ion chamber walls by photons from the decay of excited states of the ionization products, (2) secondary electron emission by the positive ions collected in the ion chamber, and

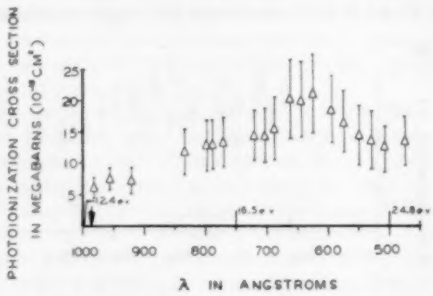

FIG. 11. Photoionization cross sections of H_2O. △ Data taken with 1.5-cm ion chambers, and 10 A resolution. The first ionization limit at 985±5 A is indicated on the wavelength axis by an arrow.

(3) additional positive ion formation by some type of secondary process in the volume of the gas. An attempt was made to observe the presence of photoemission at the walls by measuring the ionization current with and without opaque shields masking the collector electrode from the region outside the ion chamber. Since no difference in readings was obtained with this arrangement, it was concluded that (1) was not effective in contributing to the increased collection current. The process (2) above could account for only a small fraction of the increased current since it appears that the efficiency for this process at very low energy is only of the order of 1 to 2 percent.[27] Thus it seemed probable that the abnormally large ionization efficiencies observed between 800–700 A were due to positive ion production by some, as yet not identified, secondary

[25] R. W. Ditchburn, Proc. Roy. Soc. (London) **A229**, 44 (1955).
[26] H. Sun and G. L. Weissler, J. Chem. Phys. (to be published).
[27] J. H. Parker, Phys. Rev. **93**, 1148 (1954).

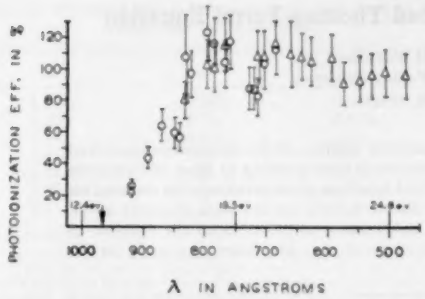

FIG. 12. Photoionization efficiencies of CH_4. △ Data taken at 100 microns with 1.5-cm ion chambers, and a 10 A resolution. ○ Average of data taken with 3-cm ion chambers at 16.4 and 28.5 microns with a 5 A resolution. The first ionization limit at 967±10 A is indicated on the wavelength axis by an arrow.

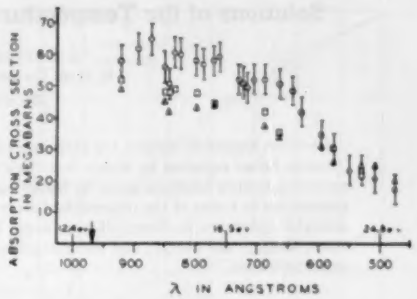

FIG. 13. Absorption cross sections of CH_4. ○ Average of data taken at 50, 28.5, and 16.4 microns. □ Data of Ditchburn. △ Data of Hsiang Sun and G. L. Weissler. The first ionization limit at 967±10 A is indicated on the wavelength axis by an arrow.

process in the body of the gas. For the wavelength region below 700 A where the efficiency is 100 percent the data in Fig. 13 also represent the ionization cross sections. In the region between the onset of ionization and 800 A the ionization cross sections due to all processes, primary and secondary, can be obtained by combining the absorption cross sections and the ionization efficiencies. It seems clear from this preliminary study that more extensive work is needed in CH_4 to clarify the aforementioned anomalies, and to justify comparison with the theoretical results of Dalgarno.[10]

Further work on some of the aforementioned gases and on others is contemplated for the future in order to answer additional as yet unresolved questions.

Our thanks are due to Dr. H Sun and Dr. Po Lee for many helpful discussions and to the Office of Naval Research for its continued support of the work reported here.

Solutions of the Temperature-Perturbed Thomas-Fermi Equation*

J. J. GILVARRY AND G. H. PEEBLES
The Rand Corporation, Santa Monica, California
(Received January 24, 1955)

Previous numerical results are extended by using an analytical solution of the temperature-perturbed Thomas-Fermi equation to obtain boundary and initial parameters corresponding to seven neutral-atom zero-temperature solutions given by Slater and Krutter. Fitted functions given previously for the solution parameters in terms of the unperturbed atom radius are revised to include the new data, to obtain a considerable extension in directly-fitted range. Effects of the temperature perturbation on the equation of state, the internal energy, and parameters related to the equation of state are shown graphically for the extended range.

IN a previous paper[1] by one of the authors, thermodynamic functions for the Thomas-Fermi atom model at low temperature were obtained by a perturbation method. In a further paper,[2] an analytic solution of the temperature-perturbed Thomas-Fermi equation of general order was given in terms of quadratures on the unperturbed Thomas-Fermi function for zero temperature. This quadrature solution yields the boundary and initial parameters of a solution, which enter the thermodynamic functions, as explicit integrals on the zero-temperature function to which the solution refers.

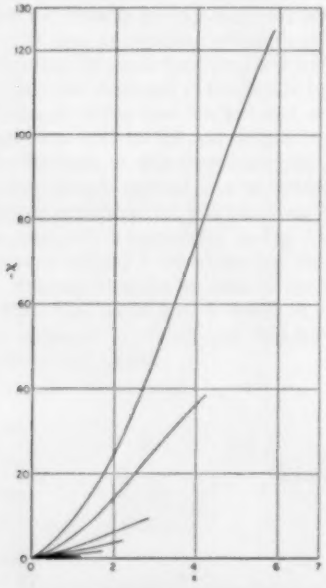

FIG. 1. Solution for the temperature-perturbation function χ as a function of radial distance x in the atom, from data of SK. The solution corresponding to the second parenthetic case in Table I has been omitted.

From these results, accurate values of the boundary and initial parameters of the corresponding first-order temperature-perturbed equation were obtained from six neutral-atom zero-temperature solutions given by FMT.[3] The values of the parameters were fitted semi-empirically by functions of the atom radius having the proper limiting behavior in the cases of an infinitesimal and an infinite atom, to make values of the thermodynamic functions readily accessible without the need for interpolation.

This paper extends the numerical results of II by obtaining the values of the boundary and initial parameters corresponding to seven neutral-atom zero-temperature solutions obtained by SK,[4] as tabulated by Gombas.[5] The solutions of SK refer to considerably smaller atomic volumes than do those of FMT; the smallest volumes approach those corresponding to a degenerate Fermi-Dirac gas. The fitted functions of II have been revised to include the values of the solution parameters derived from the data of both SK and FMT. With this revision, the fitted functions in the tem-

TABLE I. Boundary and initial parameters from data of SK; zero-temperature case.

$-\phi_b'$ (from SK)	ϕ_b	x_b	x_b (from SK)
1.00	1.447	1.194_2	1.19
1.38	0.946_0	1.696_0	1.69
1.50	0.6650	2.20_4	2.20
1.55	0.477_7	2.80_4	2.80
1.58	0.2556	4.24_4	4.23
1.586	(0.150_2)[a]	(5.86_4)[a]	5.85
1.588	(0.073)[b]	(8.5)[b]	8.59
1.58808	0		∞

[a] The values of SK for ϕ in this case have a discontinuity of jump 0.0037 at the point $x=1.46$. It was concluded that the error probably lay in the region $x<1.46$, since subtraction for $x>1.46$ of the saltus 0.0037 to make ϕ and its derivatives continuous yielded a value of ϕ_b (and of χ_b and χ_b') not smooth with respect to the other values of the table. The tabulated boundary values were derived from unchanged data.

[b] In this case, only two figures are given in the data at the boundary, so that this point is of low weight. The point is bracketed by two points from the data of FMT, which yield by interpolation (for the tabulated x_b) a value of ϕ_b differing by about 4 percent from the tabulated ϕ_b. This case was ignored in obtaining the fitted functions of I for ϕ_b and $\phi_b'-\phi_{b,\infty}'$.

* This work was sponsored by the U. S. Atomic Energy Commission.

[1] J. J. Gilvarry, Phys. Rev. **96**, 934 (1954), referred to hereafter as I.

[2] J. J. Gilvarry, Phys. Rev. **96**, 944 (1954), referred to hereafter as II.

[3] Feynman, Metropolis, and Teller, Phys. Rev. **75**, 1561 (1949), referred to hereafter as FMT.

[4] J. C. Slater and H. M. Krutter, Phys. Rev. **47**, 559 (1935); referred to hereafter as SK.

[5] P. Gombas, *Die statistische Theorie des Atoms und ihre Anwendungen* (Springer-Verlag, Vienna, 1949), pp. 53, 357.

TABLE II. Boundary and initial parameters from data of SK, temperature-perturbed case.

x_b	$-\chi_b$	$-\chi_i'$
1.194_2	0.587_5	0.429_8
1.696_9	1.78_5	0.826_8
2.20_4	4.18_7	1.33_2
2.80_4	9.32	2.03_4
4.24_4	38.8_5	4.07_2
5.86_4	$(124._7)$[a]	(6.73_5)[a]
8.5	$(51._1)$[b]	$(11._4)$[b]

[a] It was found that the values of χ_b and χ_i' depend very little on the values of ϕ to the left of the discontinuity noted in Table I for this case, and hence the saltus in ϕ was removed by fairing the data into the value unity at $x=0$. Different but reasonable fairings yielded changes in χ_b and χ_i' less than their corresponding possible errors. The tabulated values for this case seem smooth with respect to the other values of the table.

[b] The values of χ_b and χ_i' are smooth, within less than 0.5 percent, with respect to the bracketing values from the data of FMT, in spite of the difficulty noted in Table I.

perature-perturbed case cover the same directly fitted range of data as do the fitted functions in the zero-temperature case, as given in I.

The notation used is the same as in papers I and II; the subscript 1 is deleted from the symbols corresponding to the first-order temperature-perturbation function χ and to its boundary value χ_b and initial slope χ_i'.

1. NUMERICAL RESULTS

To obtain accurate values of the integrals entering χ_b and χ_i', the tabulated zero-temperature solutions of SK (given in all but one case to four figures at the atom boundary) were used to obtain improved values of the boundary radius x_b (given to only three figures by SK), and of the boundary value ϕ_b (not given by SK). The computed values of ϕ_b and x_b are tabulated in Table I against the initial slope ϕ_i' to which they correspond, with the values of x_b from SK for comparison. Parenthetic values in the table involve minor discrepancies, as noted. With the exception of the second parenthetic case (in the region of which smoothing was used to give major weight to the data of FMT), the values of ϕ_b given in this table are essentially the ones used to obtain the fitted function[6] of I for ϕ_b. As is evident from the table, the number of significant figures given by SK for the initial slope ϕ_i' (or, more important, for the difference $\phi_i'-\phi_{i,\infty}'$, where $\phi_{i,\infty}'$ is the initial slope corresponding to an atom of infinite radius) is not commensurate in general with the number possible in the other parameters, on the basis of the solutions as tabulated.

TABLE III. Coefficients[a] of fitted functions from data of SK and FMT; temperature-perturbed case.

n	C_n	m	D_m
3	-3.205×10^{-1}	$1-\lambda_2=0.2280$	-5.805×10^{-4}
$n'=4.215$	-2.331×10^{-2}	$m'=0.7400$	-1.925×10^{-1}
5	-2.519×10^{-3}	2	-3.120

[a] The coefficients are given to four figures to minimize round-off error.

[6] Boundary and initial parameters, as given by Gombas, corresponding to an eighth solution of SK for large volume, have been ignored in Table I, because of apparent lack of sufficient significant figures in the difference $\phi_i'-\phi_{i,\infty}'$. No solution corresponding to these boundary and initial values is tabulated by Gombas.

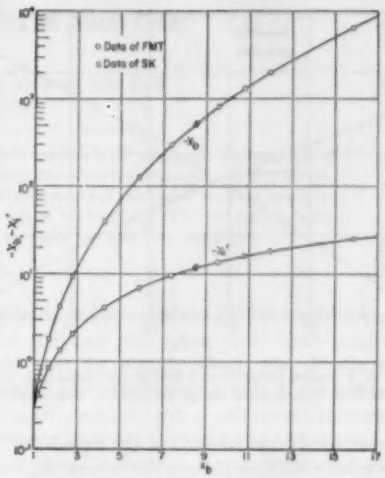

FIG. 2. Fitted functions for χ_b and χ_i' against boundary radius x_b of atom.

With these boundary parameters for the unperturbed case, the values of χ_b and χ_i' corresponding to a temperature perturbation were determined from Eqs. (14) of II by numerical integration on the zero-temperature solutions of SK. The results are tabulated in Table II against the unperturbed radius to which they correspond. The values of χ_i' yield, from Eq. (13) of II, the solutions plotted in Fig. 1 for the temperature-perturbation function χ as a function of radial distance x in the atom. The solutions corresponding to the smaller values of x_b do not differ much from the straight lines

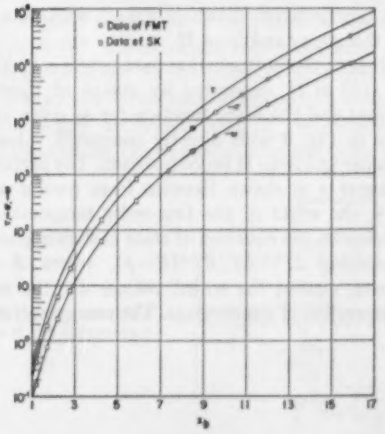

FIG. 3. Perturbation parameters σ, τ, and ω from fitted functions, against boundary radius x_b of atom.

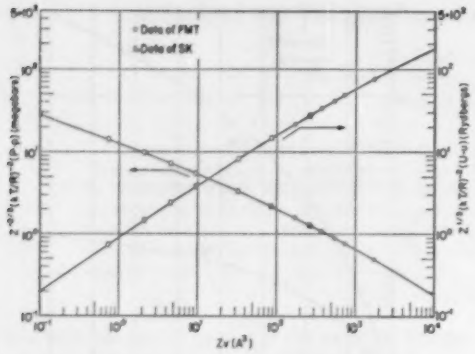

FIG. 4. Scaled pressure and energy perturbations from fitted functions, against scaled volume in cubic angstroms.

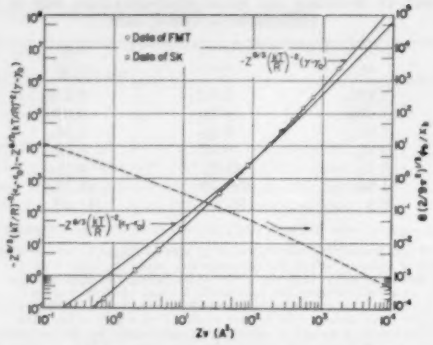

FIG. 5. Scaled perturbations in parameters ϵ_T and γ from fitted functions, against scaled volume in cubic angstroms. The scaled temperature $Z^{-4/3}kT/R$ must be small relative to the quantity shown by the dashed curve.

characteristic (as noted in I) of the Fermi-Dirac limit.

The results of Table II from the data of SK, combined with the results of II from the data of FMT, have been fitted by expressions of the form

$$\chi_b = \sum_n C_n x_b^n, \quad \chi_i' = [\sum_m D_m x_b^{-m}]^{-1}, \qquad (1)$$

in which $n = 3,\ n',\ 5$ and $m = 1-\lambda_2,\ m',\ 2$, where $\lambda_2 = \frac{1}{2}(73^{\frac{1}{2}}-7)$ and n', m' are disposable exponents. As in II, the pair of coefficients C_3, D_2 and the pair C_5, $D_{1-\lambda_2}$ are chosen with their corresponding exponents to yield the proper asymptotic behavior of the fitted functions in the two limits $x_b \to 0$ and $x_b \to \infty$, respectively, so that $C_{n'}$ and $D_{m'}$ are the only disposable coefficients. The values of the disposable coefficients and exponents are tabulated in Table III with the values of the others from II. The corresponding fitted functions reproduce the data of Table II, and the data of Table I in II, within 2.3 percent in χ_b and 1.5 percent in χ_i'. The change in the disposable exponent and coefficient in the fitted function for χ_b or χ_i' is relatively small compared to the corresponding value of II. The fitted functions are shown in Fig. 2, with data points from this paper and from II.

Values of the perturbation parameters σ and ω from Eqs. (16) of II, computed by means of these fitted functions and the fitted function for ϕ_b given in I, are shown in Fig. 3 with directly computed values from this paper and from II for comparison. The perturbation parameter τ is shown likewise from results of I. In Fig. 4, the effect of the first-order temperature perturbation on the equation of state is shown graphically by plotting $Z^{-2/3}(kT/R)^{-2}(P-\bar{p})$, where R is the Rydberg, against the scaled volume $Z\nu$; the ordinate is independent of temperature. The energy perturbation $U-u$ in units of R is shown similarly; the value of $Z^{1/3}(kT/R)^{-1}S$ in $R/°\mathrm{K}$, where S is the entropy, differs from the plotted quantity by the numerical factor 1.27×10^{-5}. In Fig. 5, the dimensionless parameters $\epsilon_T-\epsilon_0$ and $\gamma-\gamma_0$ associated with the equation of state are shown in similar manner; data points corresponding to $\epsilon_T-\epsilon_0$ (for which fitted functions must be used to obtain the necessary derivatives) are omitted. The dimensionless quantity $8(2/9\pi^2)^{1/3}\phi_b/x_b$ shown in Fig. 5 represents a limit relative to which the scaled temperature $Z^{-4/3}\,kT/R$ must be small, for validity of the perturbation method.

2. CONCLUSION

The large extension in directly fitted range of the fitted functions, obtained by inclusion of results from the data of SK, is obvious from the figures.

As pointed out by Umeda,[7] and noted in connection with Table I, minor inconsistencies exist between the data of SK and FMT. The discrepancies point to the existence of small systematic errors in one or both sets of data. Extensive numerical solutions of the Thomas-Fermi equation obtained by Dr. R. Latter yield the same conclusion. As a consequence, limits of accuracy quoted for the fitted functions refer only to the data employed; the actual error may be larger.

The authors wish to thank Miss E. Force for the computational work. In connection with I and II, one of the authors owes acknowledgments to Dr. R. Bellman for valuable discussions.

[7] K. Umeda, Phys. Rev. **83**, 651 (1951).

Scattering of Fast Neon Atoms in Neon Gas*

H. W. BERRY
Physics Department, Syracuse University, Syracuse, New York
(Received March 24, 1955)

The angular distribution of fast neon atoms scattered by neon gas has been measured. The energies of the incident atoms ranged from 0.30 to 3.0 kev and the scattering was observed for angular deviations extending from 16° to 64° in the laboratory system. An interatomic potential was calculated from the measurements and may be represented for atom separations of 0.4 to 1.0 A as $V(r)=10.4\times10^{-9}e^{-4.35r}$ ergs (r in A). The angular distribution of ions produced in the neutral atom collisions has also been measured.

THE elastic scattering of a beam of fast, homogeneous atoms on passage through a gas provides a direct means of investigating the interatomic potential. Since beams of fast neutral atoms with energies from tens of electron volts up are readily produced, the scattering may be observed for a wide range of velocities. With the particle energies available in this experiment, the scattering arises primarily from the repulsive potential characteristic of the close approach of the molecules. Also at these energies, the deflections may be described classically except for a very small angular range in the forward direction.

EXPERIMENTAL METHOD

The present investigation is an extension to neon of the method previously employed for argon.[1] A beam of fast, neutral neon atoms was formed by first producing an ion beam of the desired energy. On passage through a region containing neon gas, a fraction of the ions was neutralized by charge exchange. The resonance character of this transfer ensures that many collisions will occur with little deflection of the neutralized ion.[2] A reversed field removed any ions remaining in the beam on leaving the neutralizing region. In a second chamber, that shown in Fig. 1, the beam directed along the axis was scattered by neon gas at a pressure in the neighborhood of two microns. The scattered atoms were detected by the electron emission produced by the bombardment of tantalum electrode C. To gain in sensitivity this was shaped so as to receive particles for the full azimuthal angle. The collector assembly was movable along the axis of the region shown. A fine wire grid G placed over the entrance slit of the detector prevented the collection of electrons produced by the bombardment of the various metal surfaces of the region. The electrode K was used to measure the incident, unscattered beam.

The ejection of electrons by the bombardment of the scattered atoms on the detector surface depends on the energy of the incident particles and consequently on the angle of scattering as well as on the surface state of the electrode. At the collision energies used here, some inelastic collisions will occur and those resulting in ionization will be directly observable. If the energy transferred to internal energy is only of the order of the ionization potential of neon, it will be small compared to the energy of an elastically scattered atom except at the largest angles of deflection. Hence, neglecting this discrepancy produced by inelastic collisions, the particles entering the collector at a given angle will have a known energy. If the coefficient of electron ejection is known, the number of particles may be determined.

This coefficient, the number of electrons emitted per incident particle, has been measured in a separate experiment[3] for neon ions and neutral atoms on the same undegassed tantalum surface as used here. In general, the electron yield increases with gas adsorption so that an undegassed surface is an advantage. Within the experimental error, the coefficient of electron ejection is the same for both neon ions and atoms and ranges from 0.16 to 1.20 electrons per particle for energies of several hundred to three thousand electron volts. Consequently, one value sufficed for the measurements even though both ions and neutral atoms were incident upon the collector.

As is shown in Fig. 1, each element of the path will contribute to the detector "current"; but will do so with differing angular ranges and with angles of scattering varying from 90° to a minimum angle dependent upon the collector position. As the collector is moved along the axis away from the entrance aperture, this minimum acceptable angle decreases. Also, if the detector is moved a distance dx, thus increasing the scattering path,

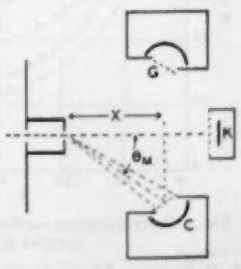

FIG. 1. A schematic diagram of the apparatus.

* Supported by the Office of Naval Research.
[1] H. W. Berry, Phys. Rev. 75, 913 (1949).
[2] H. S. W. Massey and E. H. S. Burhop, *Electronic and Ionic Impact Phenomena* (Oxford University Press, London, 1952), Chap. VIII.
[3] H. W. Berry, Phys. Rev. 74, 848 (1948).

the increase in electron current from the collector is

$$dI = \alpha I_0 N_1 p F(\theta) d\theta dx - N_1 p \sigma_A I dx,$$

where α = ratio of the electron ejection coefficient for particles scattered at angle θ to that for the incident atoms; I_0 = electron current produced by the bombardment by the initial beam of electrode K; $N_1 p$ = number of scattering centers per unit volume; $F(\theta)$ = polar scattering coefficient for incident and knocked-on atoms[4]; and σ_A = cross section for attentuation of the unscattered beam with x. This last is dependent upon the apparatus geometry and the criterion contained therein on what deviations represent a loss from the beam. This cross section was determined by limiting the lower value of the angular range accepted by the collector by a diaphragm with a circular aperture and by measuring the detector current at several positions along the axis. At its largest value, the second term in the equation did not exceed 15 percent of the first term.

RESULTS

There are shown in Fig. 2 the polar scattering coefficients determined as described previously. As expected, the distributions have a minimum in the neighborhood of 45°, but are not symmetric about the minimum partly because of inelastic collisions. The inelastic scattering at any laboratory angle is the sum of two components corresponding to different angles in the center-of-mass system. If the maximum angle is nearly 90° corresponding to a small relative loss of energy to internal motion, one component is small and contributes primarily to the large angles of scattering. In the analysis used emphasis was placed on the lower-angle scattering. Some of the asymmetry may arise from the lower accuracy of the measurements at the larger angles. The design of the apparatus was such that, for angles less than 45°, the increasing angular range accepted by the collector compensated in large part for the decreased scattering with increasing angle of deflection.

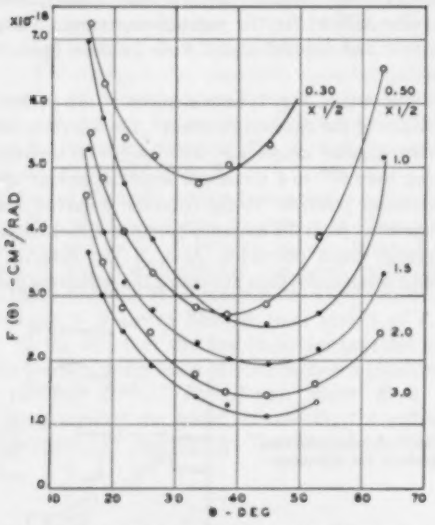

FIG. 2. Polar scattering coefficients with incident beam energies in kev.

[4] E. H. Kennard, *Kinetic Theory of Gases* (McGraw-Hill Book Company, London, 1938), p. 115.

The analysis of the data followed the method described in reference 1. In brief, this consisted of obtaining by numerical integration from the polar distributions a series of cross sections for the scattering of the incident particle outside of a given angle. The usual orbit equation was modified for the case of constant angular momentum and solved for the interaction potential. On choosing a value of the angular momentum within the range of the experimental data, a numerical integration for the potential was performed. The repulsive interaction potential so found for neon-neon collisions is shown in Fig. 3 as the continuous curve. The dashed line is the potential previously found for argon.

Both of the curves in Fig. 2 may be fitted within a few percent by the relation $V(r) = Ae^{-br}$ with $A = 21.9 \times 10^{-9}$ erg for argon and 10.4×10^{-9} erg for neon, and with $b = 4.14$ angstrom^{-1} for argon and 4.25 angstrom^{-1} for neon, with r in angstroms.

ANGULAR DISTRIBUTION OF POSITIVE IONS

Those inelastic collisions which produce ions may be observed alone if secondary electrons are held to the collector by a positive potential. With this arrangement, a background electron current now drawn to the positive collector caused some difficulty so that a small axial magnetic field of less than 50 gauss was added. A further modification used in these measurements was to hold the outer collector fixed and move the inner cylinder to change the angular range. This resulted in a greater stability and was necessary here because of the smaller collector currents imposed by the use of a lower scattering gas pressure.

A serious difficulty in the measurement of the positive ion distribution arises from the large probability for neutralization of an ion in its own gas. This will produce an attenuation of the scattered ion current directed to the receiver which varies with the angle of deflection through the ion energy and the path length. Under the assumption that a charge transfer collision will generally produce a slow ion at a large angle of scattering and hence not collected by the detector, the loss may be expressed in terms of the total cross section for neutralization. Consequently, the polar coefficients for the positive ions were divided by $\exp(-N_1 p \sigma_N d)$, where $N_1 p$ is the number of scattering centers per unit volume, σ_N the cross section for charge transfer, and d the distance from the initial scattering point to the collector. This factor was made as small as possible by the use of

a low gas pressure but still resulted in relative corrections as high as 25 percent. Existing values of the cross section for neutralization[5] do not cover the range of energies required in this experiment and so these were measured as described in reference 3. The cross sections, so found, decrease linearly as a function of the square root of the energy from 14.0×10^{-16} cm² at (300 ev)$^{\frac{1}{2}}$ to 8.5×10^{-16} cm² at (3000 ev)$^{\frac{1}{2}}$.

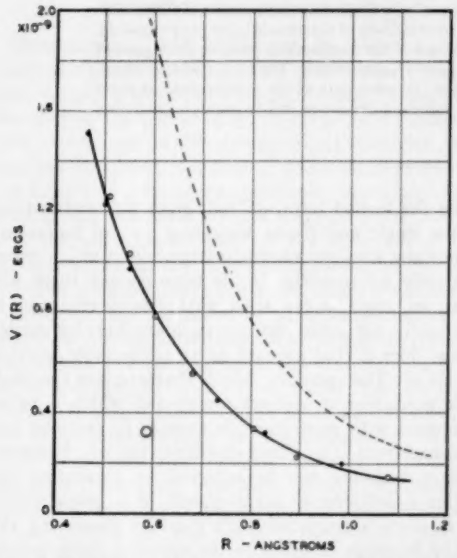

FIG. 3. The interatomic potential for neon-neon is shown by the continuous curve. Open and closed circles represent the potential for two values of the angular momentum. The argon interatomic potential is shown as the dashed curve.

The polar coefficients for positive ions produced in neon-neon neutral atom collisions are shown in Fig. 4. These exhibit a more marked assymetry than the total scattering distributions with an increasing flatness with decreasing energy. The ratio of the positive ion to the

[5] A. Rostagni, Nuovo cimento **12**, 134 (1935); B. Rosen and H. Kallman, Z. Physik **61**, 61 (1930); F. Wolf, Ann. Physik **29**, 33 (1937).

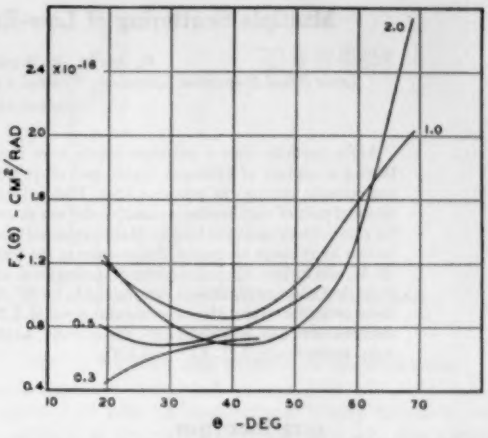

FIG. 4. Polar scattering coefficients for positive ions produced in neon-neon collisions. Energies of the incident particles are given in kev.

total scattering coefficient show, in general, an increase with the angle of scattering. At 40° this ratio has values of 0.07, 0.14, 0.34, and 0.45 for 0.3, 0.5, 1.0, and 2.0 kev respectively. A maximum angle of scattering of the positive ions can be determined to within a degree for the lower beam energies. These were found to be 58°, 65°, and 72.5° for 0.3, 0.50, and 1.0 kev incident particle energies. These angles correspond to a transfer to internal energy in an inelastic collision of an energy of about 45 ev as compared with the ionization potential for neon of 21.6 ev.

Previous measurements of the ionization of gas molecules by fast neutral atoms have been limited to the measurement of a total cross section for ionization. Rostagni and others[6] have measured this cross section for the ionization of neon by neon atoms; and for an energy of 1.0 kev Rostagni found a value of 1.6×10^{-16} cm². For comparison, a cross section for scattering into an angle between 20° and 70° may be found from the results in Fig. 4 for 1.0 kev and is approximately 1.0×10^{-16} cm².

[6] A. Rostagni, Nuovo cimento **13**, 389 (1936); H. F. Batho, Phys. Rev. **42**, 753 (1932); H. Wayland, Phys. Rev. **52**, 31 (1937).

Multiple Scattering of Low-Energy Alpha Particles in a Gas

G. Allen, R. Wedeler, and S. Barile
Lewis Flight Propulsion Laboratory, National Advisory Committee for Aeronautics, Cleveland, Ohio
(Received March 22, 1955)

Alpha particles from a polonium source were slowed down and allowed to enter a cloud chamber containing a mixture of hydrogen, water, and ethyl alcohol at pressures of 12.25 cm, 1.50 cm, and 2.25 cm, respectively, during the sensitive time. Eighty-four sharp tracks of particles which stopped in the illuminated part of the chamber and which did not show any sharp bends due to single scattering were selected for study. Starting at the termini of the projected tracks, the angles between successive chords of three millimeters length were measured, the energies at the first three intersections of the chords being approximately 18, 45, and 85 kev. The magnitudes of the angles at which the tails of the distributions could be distinguished from the Gaussian parts were determined to be 10°, 6° to 8°, and 4°, respectively. The total standard deviations (which included the experimental error of 2.2°) for the Gaussian part of the distributions at these energies were 8.0°, 4.3°, and 3.0°, respectively, so that the standard deviations due to multiple scattering were, respectively, 7.7°, 3.7°, and 2.0°.

INTRODUCTION

In recent years considerable progress has been made in the experimental study and theoretical interpretation of the multiple scattering of charged particles of medium energies in a gas, and the agreement between experiment and theory is moderately good. In the case of low-energy nuclear particles, however, there is still much to be done in this field because, on the one hand, there is a scarcity of experimental work; on the other hand, no satisfactory theory of scattering has been developed in the absence of an adequate treatment of such effects as charge exchange which become important in this energy range. The present communication is devoted to an account of the results of some cloud-chamber experiments on the multiple scattering of alpha particles with energies below one-hundred kev in a mixture of hydrogen and alcohol and water vapor.

In studying the multiple scattering by cloud-chamber techniques it is sufficient to make use of photographs giving the projection of the paths of the individual particles on a single plane, since from measurements of such photographs the multiple-scattering law can be specified just as completely as by measurements of the actual path in three dimension. In the present work the expression "projected path" will be used to mean the projection of the path of a particle on the plane of the photograph of its track. As applied to such projected paths, the results of the theories of multiple scattering are conventionally expressed in terms of the angle φ between two tangents to the projected path at points a given distance l apart. Although differing in details, different theories all give the result that for φ not too large, the number of particles $dF(\varphi)$ for which this angle lies between φ and $\varphi+d\varphi$ is represented by an expression of the form:

$$dF(\varphi)=(2\pi\sigma^2)^{-\frac{1}{2}}\exp(-\varphi^2/2\sigma^2)d\varphi+dF'(\varphi). \quad (1)$$

The first term represents the true multiple-scattering distribution, i.e., the effect of a large number of individual collisions each leading to a small deflection, while the second term, $dF'(\varphi)$, gives the contribution of the single and plural scattering, i.e., of individual deflections through relatively large angles which occur relatively infrequently. If l is large enough there will exist an angle $\varphi_c \gg \sigma$ such that the distribution is essentially Gaussian for $\varphi<\varphi_c$ and only for angles $\varphi>\varphi_c$ does $dF'(\varphi)$ amount to an appreciable fraction of $dF(\varphi)$. The quantity which characterizes the multiple scattering at a given energy and which is to be compared with experiment is then σ. In carrying out measurements on cloud-chamber tracks, however, greater accuracy can be achieved by measuring the angles ω between adjacent chords of a given length ($\approx l$) along a projected path than by measuring the angles between tangents to the curve at these points. It can be shown[1] that for angles $\varphi<\varphi_c$ for which the Gaussian part of Eq. (1) is dominant, the distribution function for ω is Gaussian in form with σ replaced by $\sigma_\omega=(2\sigma^2/3)^{\frac{1}{2}}$. It follows that the angles ω are distributed according to

$$dG(\omega)=(2\pi\sigma_\omega^2)^{-\frac{1}{2}}\exp(-\omega^2/2\sigma_\omega^2)d\omega+dG'(\omega), \quad (2)$$

and that there exists an angle ω_c such that to a good approximation dG' may be neglected for $\omega<\omega_c$. In the case of multiple scattering the experimental problem is then to determine for a given energy and path length the variance σ_ω^2 of the Gaussian part of the distribution in ω and if possible to give an estimate for ω_c. It is impossible to ascertain in advance whether this can be done with any accuracy for a given set of conditions since before analyzing the data one does not know whether the angle at which the distribution starts to deviate from a Gaussian distribution is large compared to the variance σ_ω^2 or not. In the present experiment we obtained the distribution of the angles ω for low-energy alpha particles for the case in which the plane of projection was essentially parallel to the direction of incidence. The distribution of the measured angles ω will have a form like that of Eq. (2) but will not be

[1] Groetzinger, Berger, and Ribe, Phys. Rev. 77, 584 (1950).

identical with it because these values of ω are affected by the experimental errors. We shall therefore have for the experimental distribution the equation

$$d\bar{G}(\omega)=(2\pi\bar{\vartheta}_\omega^2)^{-\frac{1}{2}}\exp(-\omega^2/2\bar{\vartheta}_\omega^2)d\omega+d\bar{G}'(\omega), \quad (2a)$$

where the barred quantities have essentially the same significance as their counterparts in Eq. (2). The analog of ω_e, we shall designate $\bar{\omega}_e$.

EXPERIMENTAL PROCEDURE

Measurements were made on 84 cloud-chamber tracks produced by alphas which entered the chamber with energies of about 500 kev, these tracks having been obtained in the course of an investigation[2] concerned with the ranges of low-energy alpha particles. The chamber employed, which had a diameter of 25 cm, was filled with a mixture of hydrogen, water, and ethyl alcohol, and was operated at a temperature of 20.5°C. In a previous investigation[3] of the operation of this chamber under the conditions used, it was verified that the composition of the filling gases remains essentially constant during the period in which sharp tracks are produced (the sensitive time) and it was determined that at this time the partial pressures amount to 12.25 cm for hydrogen, 1.5 cm for water, and 2.25 cm for ethyl alcohol. In accordance with the aforementioned definition of the sensitive time, the tracks analyzed were selected from a considerably larger number available by excluding those which were thick or fuzzy. An image of each suitable track was projected to full size onto a sheet of transparent celluloid using a Recordak microfilm reader. Starting at the end of the track at which the particles stopped successive points with a 3-mm separation were marked along each track with the aid of a pair of dividers. In each case, the angles between the chords defined by these points were then measured with a drafting machine. Both the plotting of the points and the measurement of the angles between the chords were performed independently by two of us (G. A. and R. W.) and the averages of the resulting measurements of the angles were used as the individual scattering angles ω.

The aforementioned choice of the chord length d was governed by the following considerations. First the most important requirement is that d should be considerably larger than the track thickness in order to avoid unduly large errors of measurement. Second, d should ideally be sufficiently great that the condition $\bar{\omega}_e \gg \bar{\vartheta}_\omega$ be satisfied in order that it be possible to estimate the latter quantity as accurately as possible. Third, if possible, d should be small enough so that the change of energy over the part of the track spanned by a pair of chords be reasonably small in order that the observed value of $\bar{\vartheta}_\omega$ can be properly associated with a reasonably small range of energies. For low-energy alphas the absence of even an approximate theory makes it impractical at present to attempt to apply the second criterion. In any event, however, the tracks obtained are so thick and the energy loss per unit distance is so high in the present case that d is fixed by the first and third conditions alone. On this basis the value of d chosen was 3 mm.

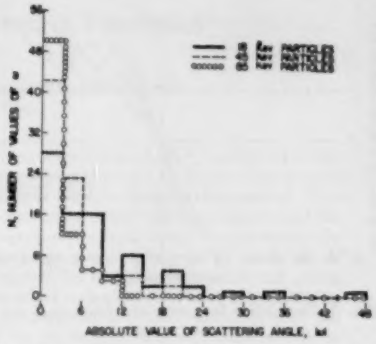

FIG. 1. Frequency distributions of the scattering angles.

The following procedure was used for estimating and correcting the experimental error due to optical distortion and inaccuracy of angular measurement. A straight line and a circle which had a diameter of 3.4 cm were constructed on a sheet of drawing paper. The width of both lines was chosen the same as the average width of a track. The sheet of paper was placed at the proper position in the cloud chamber and photographed. The angles between successive 3-mm segments of the straight line and between successive 3-mm chords of the circle were then measured by the procedure described previously. The standard deviations in the measured values of these angles in these two cases were 2.2°. On the assumption that the multiple scattering angles and the error angles are statistically independent, the variance of the Gaussian part can be corrected by subtracting the error variance.

RESULTS

The energies E_1, E_2, and E_3 at each intersection of adjacent chords was estimated by using the range energy curves for alpha particles in air given by Cook *et al.*[4] together with the value of the air equivalent of the cloud-chamber mixture estimated in a previous paper.[3] These energies were found in this way to be approximately 18, 45, and 85 kev, respectively. The frequency distributions, in intervals of 6°, for the measured values of the corresponding angles are shown in Fig. 1.

In order to determine the value of the quantity ϑ_ω from these results it is, as remarked earlier, necessary to separate the contribution of the Gaussian part of $d\bar{G}$ from that of the tail $d\bar{G}'$ in the total distribution.

[2] Barile, Webeler, and Allen, Phys. Rev. **96**, 673 (1954).
[3] S. Barile and R. Webeler, Rev. Sci. Instr. **25**, 389 (1954).
[4] Cook, Jones, and Jorgensen, Phys. Rev. **91**, 1417 (1953).

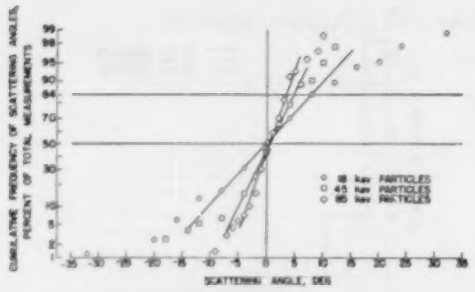

FIG. 2. Cumulative frequency distributions of the scattering angles.

To indicate the method used, it is convenient first to define the quantity $\bar{G}(\omega)$ as equal to $\int_{-\infty}^{\omega} d\bar{G}$. It can then be shown[5] that there exists a function $\Gamma(\bar{G})$ depending on $\bar{\sigma}$ only through $\bar{G}$ such that for $\bar{G}$ Gaussian, the relation

$$\Gamma(\bar{G})-\Gamma(0.5)=[\Gamma(0.8413)-\Gamma(0.5)](\omega-\bar{\mu})/\bar{\sigma}_\omega \quad (3)$$

holds so that $\Gamma(\bar{G})$ varies linearly with ω. In Eq. (3) $\bar{\mu}$ is the average of the measured values of ω and will be close to zero. In order to determine the Gaussian part of the distribution, the experimental points were represented graphically in Fig. 2 with Γ as ordinate and ω as abscissa. It can be seen that in each case these points lie on a straight line over a considerable range centering about $\Gamma(0.5)$. We estimate in each case $\bar{\sigma}_\omega$ from the slope of this line by use of Eq. (3)[6] and took $\bar{\omega}_c$ as the value of ω at which the points began to deviate appreciably from the line. The resulting values are shown in Table I which also gives the values of σ_ω obtained by correcting $\bar{\sigma}_\omega$ for the experimental error. These do not suffice to determine a curve of σ *versus* energy, but it does follow that σ increases much faster than $1/E$ with decreasing energy whereas the usual theories applying to high-energy charged particles predict a $1/E$ dependence.[7] The enhanced low-energy scattering is to be expected, of course, because of the increasing importance of nuclear collisions in this energy range.

[5] R. S. Burington and D. C. May, Jr., *Handbook of Probability and Statistics with Tables* (Handbook Publishers, Inc., Sandusky, Ohio, 1953), p. 109.

TABLE I. Summary of results of the multiple scattering experiment. E is the kinetic energy of the alpha particle; $|\bar{\omega}_c|$ is the maximum magnitude of the angles for which the distribution remained Gaussian; $\bar{\sigma}_\omega$ is the total measured standard deviation; σ_ω is the standard deviation due to multiple scattering.

E, kev	$\lvert\bar{\omega}_c\rvert$, deg	$\bar{\sigma}_\omega$, deg	σ_ω, deg
18	10	8.0	7.7
45	6–8	4.3	3.7
85	4	3.0	2.0

ACKNOWLEDGMENTS

The authors are indebted to Dr. Gerhart Groetzinger and Dr. Philip Schwed for many helpful discussions and Miss Angela Haferd and Mrs. Marcelle Jordan for performing the necessary computations.

[6] A χ^2 test was made of the conclusion that the points within the limits $\bar{\omega}_c$ in each case belonged to a Gaussian distribution with the indicated experimental parameters. The test showed that such a conclusion was not statistically inconsistent with the experimental distribution (reference 5, p. 141).

[7] N. F. Mott and H. S. W. Massey, *The Theory of Atomic Collisions* (Clarendon Press, Oxford, 1949), p. 278.

Relaxation Processes in a System of Two Spins*

I. SOLOMON†
Lyman Laboratory, Harvard University, Cambridge, Massachusetts
(Received March 29, 1955)

Abragam and Pound's method for the calculation of the longitudinal relaxation time T_1 has been extended to the transverse relaxation time T_2. Explicit calculations have been carried out for a pure dipole-dipole interaction, showing that for an interacting pair of like spins, or for nuclei in paramagnetic solution, T_1 is exactly equal to T_2 in the extreme narrow case. For a pair of interacting unlike spins, it is shown that the longitudinal components of the magnetic moments do not have simple exponential decays. This gives rise to a steady and transient Overhauser effect. The transverse components, however, have in all cases, simple exponential decay defined by a single relaxation time T_2. A set of modified Bloch's equations is found, giving the correct equation of motion of the macroscopic magnetic moments of such a system of pairs of unlike spins.

The equality of T_1 and T_2 has been verified in paramagnetic solutions, and a nuclear Overhauser effect has been observed in anhydrous hydrofluoric acid. If one assumes that the extreme narrow case corresponds to the actual motion, the experimental results are not consistent with the picture of a pure dipole-dipole interaction between the hydrogen and fluorine nuclei of a molecule without taking into account the effect of the other molecules.

I. INTRODUCTION

WE consider a particle of spin **I** interacting with another particle of spin **S**. The Hamiltonian of such an interacting pair, in a magnetic field H_0 along the z direction is

$$\mathcal{H}=\mathcal{H}_M-\hbar\gamma_I H_0 I_z-\hbar\gamma_S H_0 S_z+\mathcal{H}'. \tag{1}$$

$\mathcal{H}_M$ is the Hamiltonian of the motion of the particles and commutes with the spin operators. The next two terms are the Zeeman energies of the spins in the constant magnetic field H_0. $\mathcal{H}'$ is the spin-spin interaction term considered as a perturbation. All the explicit calculations will be performed in the case of a dipole-dipole type interaction:

$$\mathcal{H}'=-(\hbar^2\gamma_I\gamma_S/r^5)[3(\mathbf{I}\cdot\mathbf{r})(\mathbf{S}\cdot\mathbf{r})-\mathbf{I}\cdot\mathbf{S}], \tag{2}$$

but any other type of interaction, e.g., electron-coupled interaction $A\mathbf{I}\cdot\mathbf{S}$, can be treated in the same way.

We will consider only spins of value $\frac{1}{2}$ so that there is no quadrupole interaction. Larger values for the spins would make computations more complicated without fundamental changes.

II. TRANSITION PROBABILITIES

If $|m_i\rangle$ and $|m_j\rangle$ are two eigenstates of the unperturbed Hamiltonian with the corresponding energies E_i and E_j, the transition probability per unit time between these two states is, in the first order, given by

$$w_{ij}=\frac{1}{t}\frac{1}{\hbar^2}\left|\int_0^t\langle m_j|\mathcal{H}'(t')|m_i\rangle e^{-i\omega_{ij}t'}dt'\right|^2, \tag{3}$$

with

$$\omega_{ij}=(E_j-E_i)/\hbar.$$

In the case of a randomly fluctuating perturbing Hamiltonian $\mathcal{H}'(t)$, this integral has been calculated by Abragam and Pound.[1] When the fluctuations are rapid, as in liquids and gases, the result is a time-independent transition probability per unit time. In the present case of spin $\frac{1}{2}$, we define four eigenstates of the spins by the following relations:

$$\begin{aligned} I_z|+\rangle&=+\tfrac{1}{2}|+\rangle,\\ I_z|-\rangle&=-\tfrac{1}{2}|-\rangle,\\ S_z|+\rangle&=+\tfrac{1}{2}|+\rangle,\\ S_z|-\rangle&=-\tfrac{1}{2}|-\rangle, \end{aligned} \tag{4}$$

so that the four unperturbed eigenstates of a pair are $|+\rangle|+\rangle$, $|+\rangle|-\rangle$, $|-\rangle|+\rangle$, and $|-\rangle|-\rangle$ with the respective occupation numbers N_{++}, N_{+-}, N_{-+}, and N_{--}.

The transition probabilities per unit time w_0, w_1, w_1', and w_2 between these four states, which we are going to use in the discussion of the motion of the longitudinal component of the magnetic moment are indicated in diagram (A) of Fig. 1.

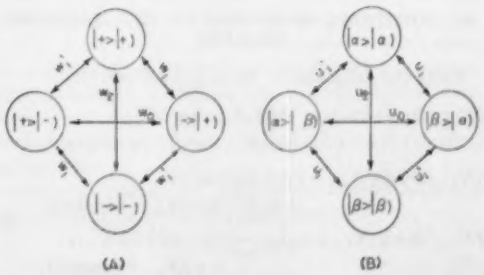

FIG. 1. (A) Transition probabilities between the eigenstates of the longitudinal components of the spin operators. (B) Transition probabilities between the eigenstates of the transverse components of the spin operators.

* This work was supported in part by the joint program of the Office of Naval Research and the U. S. Atomic Energy Commission.

† The author was supported during his residence as Research Fellow at Harvard University by Centre d'Etudes Nucléaires de SACLAY. Present address: C. E. N. de Saclay, GIF-SUR-YVETTE, France.

[1] A. Abragam and R. V. Pound, Phys. Rev. **92**, 953 (1953).

The equations of motion of the transverse components of the magnetic moment involve the operators I_x (or I_y) and S_x (or S_y). So, in similarity to set (4) we define four eigenstates of the spins by

$$\begin{aligned} I_x|\alpha\rangle &= +\tfrac{1}{2}|\alpha\rangle, \\ I_x|\beta\rangle &= -\tfrac{1}{2}|\beta\rangle, \\ S_x|\alpha\rangle &= +\tfrac{1}{2}|\alpha\rangle, \\ S_x|\beta\rangle &= -\tfrac{1}{2}|\beta\rangle. \end{aligned}$$

The four states of a pair $|\alpha\rangle|\alpha\rangle$, $|\alpha\rangle|\beta\rangle$, $|\beta\rangle|\alpha\rangle$, and $|\beta\rangle|\beta\rangle$ are not eigenstates of the energy. However, these four states are orthogonal, so it is still meaningful to speak of the occupation numbers $N_{\alpha\alpha}$, $N_{\alpha\beta}$, $N_{\beta\alpha}$, $N_{\beta\beta}$ and of the transition probabilities per unit time w_0, w_1, w_1', and w_2 between these states as indicated on Fig. 1(B).

To calculate the transition probabilities, we proceed as follows:

Consider two orthogonal states $|a\rangle$ and $|b\rangle$ that are not eigenstates of the energy. They can always be expanded in eigenvectors of the energy.

$$\begin{aligned} |a\rangle &= \textstyle\sum_i a_i|m_i\rangle, \\ |b\rangle &= \textstyle\sum_j b_j|m_j\rangle. \end{aligned} \tag{5}$$

For example, in the present case of spin $\frac{1}{2}$ we have:

$$\begin{aligned} |\alpha\rangle &= (1/\sqrt{2})[|+\rangle+|-\rangle], \\ |\beta\rangle &= (1/\sqrt{2})[|+\rangle-|-\rangle]. \end{aligned} \tag{5'}$$

Using the expansion (5) and the fact that $\langle a|b\rangle=0$, we get a formula generalizing (3). The transition probability per unit time between the states $|a\rangle$ and $|b\rangle$ is

$$w_{ab}=\frac{1}{t}\frac{1}{\hbar^2}\left|\int_0^t \sum_{ij}\langle m_j|\mathcal{H}'(t')|m_i\rangle a_i^* b_j e^{-i\omega_{ij}t'}dt'\right|^2.$$

This integral can be calculated in the same technique as Abragam and Pound[1] used and will be shown to be time independent in the case of rapid motion.

III. EQUATIONS OF MOTION OF THE MAGNETIC MOMENT

From the definltion of the w's, it follows that

$$\begin{aligned} dN_{++}/dt &= -(w_1+w_1'+w_2)N_{++}+w_1'N_{+-} \\ &\quad +w_1N_{-+}+w_2N_{--}+\text{constant}, \\ dN_{+-}/dt &= w_1'N_{++}-(w_0+w_1+w_1')N_{+-} \\ &\quad +w_0N_{-+}+w_1N_{--}+\text{constant}, \\ dN_{-+}/dt &= w_1N_{++}+w_0N_{+-}-(w_0+w_1+w_1')N_{-+} \\ &\quad +w_1'N_{--}+\text{constant}, \\ dN_{--}/dt &= w_2N_{++}+w_1N_{+-}+w_1'N_{-+} \\ &\quad -(w_1+w_1'+w_2)N_{--}+\text{constant}. \end{aligned} \tag{6}$$

The constants are obtained by considering the system at temperature equilibrium by inserting the proper Boltzman's factor, and are unimportant in the computation of the relaxation times.

The experimentally observable quantities are the macroscopic magnetic moments $\bar{I}_z$ and $\bar{S}_z$, distinguishable by their different Larmor frequencies and proportional to:

$$\begin{aligned} (N_{++}+N_{+-})-(N_{-+}+N_{--}) &= K\bar{I}_z, \\ (N_{++}+N_{-+})-(N_{+-}+N_{--}) &= K\bar{S}_z. \end{aligned} \tag{7}$$

Inserting the values (7) in (6) we get:

$$\begin{aligned} d\bar{I}_z/dt &= -(w_0+2w_1+w_2)\bar{I}_z \\ &\quad -(w_2-w_0)\bar{S}_z+\text{constant} \\ d\bar{S}_z/dt &= -(w_2-w_0)\bar{I}_z \\ &\quad -(w_0+2w_1'+w_2)\bar{S}_z+\text{constant}. \end{aligned} \tag{8}$$

These equations along with the results of identical calculations for the transverse components I_x and S_x lead finally to the following set of equations:

$$\begin{aligned} d\bar{I}_z/dt &= -(w_0+2w_1+w_2)(\bar{I}_z-I_0) \\ &\quad -(w_2-w_0)(\bar{S}_z-S_0), \\ d\bar{S}_z/dt &= -(w_2-w_0)(\bar{I}_z-I_0) \\ &\quad -(w_0+2w_1+w_2)(\bar{S}_z-S_0), \end{aligned} \tag{9}$$

$$\begin{aligned} d\bar{I}_x/dt &= -(w_0+2w_1+w_2)\bar{I}_x-(w_2-w_0)\bar{S}_x, \\ d\bar{S}_x/dt &= -(w_2-w_0)\bar{I}_x-(w_0+2w_1'+w_2)\bar{S}_x. \end{aligned} \tag{10}$$

I_0 and S_0 are the equilibrium values of the magnetic moments of the spins **I** and **S**, and make explicit the values of the constants of Eqs. (8). These equations show that, in general, the decay of the observed quantities is not a simple exponential, but rather a linear combination of two exponentials. There are two cases that can easily be seen to give simple exponential decays:

(a) The two spins **I** and **S** are alike ("alike" meaning that $\gamma_I=\gamma_S$). Then the only observable quantities are $\bar{I}_z+\bar{S}_z$ and $\bar{I}_x+\bar{S}_x$. From the definition it follows that $w_1'=w_1$ and $w_1'=w_1$; thus the equation of motion of the two observable quantities is

$$\begin{aligned} \frac{d}{dt}(\bar{I}_z+\bar{S}_z) &= -2(w_1+w_2)(\bar{I}_z+\bar{S}_z-I_0-S_0), \\ \frac{d}{dt}(\bar{I}_x+\bar{S}_x) &= -2(w_1+w_2)(\bar{I}_x+\bar{S}_x). \end{aligned} \tag{11}$$

These are the usual decays with the relaxation times

$$\begin{aligned} 1/T_1 &= 2(w_1+w_2), \\ 1/T_2 &= 2(w_1+w_2). \end{aligned} \tag{12}$$

(b) Nuclei relaxed in a paramagnetic solution. The relaxation of such a nuclear spin **I** will be almost entirely the result of the dipole-dipole interaction $\mathcal{H}'$, when paired with an electronic spin **S** of a paramagnetic ion. On the other hand, this interaction $\mathcal{H}'$ is a negligible relaxation process for the electronic spin **S**, so that, in the time scale of observation of the nuclear magnetic

moment, we may consider to have $\bar{S}_z=S_0$ and $\bar{S}_x=0$. Then Eqs. (9) and (10) show that the nuclear spins **I** have simple decays with relaxation times:

$$1/T_1=w_0+2w_1+w_2,$$
$$1/T_2=u_0+2u_1+u_2. \tag{13}$$

IV. BLOCH'S EQUATIONS FOR A TWO-SPIN SYSTEM

Equations (9), which we will rewrite for convenience as

$$d\bar{I}_z/dt=-\rho(\bar{I}_z-I_0)-\sigma(\bar{S}_z-S_0),$$
$$d\bar{S}_z/dt=-\rho'(\bar{S}_z-S_0)-\sigma(\bar{I}_z-I_0), \tag{14}$$

with

$$\rho=w_0+2w_1+w_2,$$
$$\rho'=w_0+2w_1'+w_2, \tag{15}$$
$$\sigma=w_2-w_0$$

are the usual macroscopic Bloch equations[2] in which we have added a term representing the spin **I**—spin **S** interaction.

It is less straightforward to compare the equation of motion (10) for the transverse components with Bloch's equations because our Eqs. (10) are the equation of motion of the expectation values of the time independent spin operators, and therefore describe the motion of I_x and S_x in coordinates rotating respectively with angular velocity $\omega_I=\gamma_I H_0$ and $\omega_S=\gamma_S H_0$. Nevertheless, let us try to represent the motion of the transverse components of the macroscopic magnetic moment by a set of Bloch's equations similarly modified by adding a spin-spin interaction term. These equations will be in the laboratory coordinates:

$$dI_+'/dt=-i\omega_I I_+'-\nu I_+'-\mu S_+',$$
$$dS_+'/dt=-i\omega_S S_+'-\nu' S_+'-\mu I_+', \tag{16}$$

with

$$I_+'=I_x'+iI_y',$$
$$S_+'=S_x'+iS_y'.$$

Now to compare with Eqs. (10) we shall write Eqs. (16) in the rotating coordinates ($I_+=I_+'e^{i\omega_I t}$ and $S_+=S_+'e^{i\omega_S t}$):

$$dI_+/dt=-\nu I_+-\mu e^{-i(\omega_S-\omega_I)t}S_+,$$
$$dS_+/dt=-\nu' S_+-\mu e^{-i(\omega_I-\omega_S)t}I_+. \tag{17}$$

(a) In the case of like spins, $\omega_S=\omega_I$ and Eqs. (17) give simply: (ν and ν' are obviously equal by symmetry considerations)

$$\frac{d}{dt}(I_++S_+)=-(\nu+\mu)(I_++S_+).$$

That is exactly the second of Eq. (11) with

$$\nu+\mu=2(u_1+u_2). \tag{18}$$

(b) In the case of unlike spins, "unlike" meaning that

$$|\omega_I-\omega_S|\gg\nu, \quad |\omega_I-\omega_S|\gg\nu',$$

the last term of Eq. (17) will average out so that the transverse components have simple exponential decays:

$$dI_+/dt=-\nu I_+,$$
$$dS_+/dt=-\nu' S_+. \tag{19}$$

So these modified Bloch equations of the transverse components, obtained by analogy with the Eq. (14) for the longitudinal components, predict that, in Eqs. (10), we shall have

$$u_2-u_0=0. \tag{20}$$

This will be proven quantum mechanically in the next section. Then Eqs. (17) represent the correct motion of the transverse components in all the cases with the set of values

$$\nu=u_0+2u_1+u_2,$$
$$\nu'=u_0+2u_1'+u_2, \tag{21}$$
$$\mu=u_2-u_0.$$

To summarize, it has been shown in this section, that the Bloch equations do not hold for a two-spin system. However, by a slight modification of these, one can still find a set of equations [Eqs. (14) and (17)] that represent the motion of the macroscopic magnetic moment. It has been seen, too, that unlike the longitudinal components, the transverse components always have a simple exponential decay.

V. STEADY AND TRANSIENT OVERHAUSER EFFECT

In any steady-state condition, the first of Eqs. (14) will give

$$-\rho(\bar{I}_z-I_0)-\sigma(\bar{S}_z-S_0)=0. \tag{22}$$

If we apply an intense rf field at the resonance frequency of the spins S, for example, so that we equalize the populations in state $|+\rangle$ and $|-\rangle$ ("saturation"), we will have

$$S_z=0. \tag{23}$$

Now, inserting the value (23) in Eq. (22) we get the value of I_z, when S_z is saturated:

$$\bar{I}_z=I_0+(\sigma/\rho)S_0. \tag{24}$$

This is the effect first derived by Overhauser,[3] and extended by Bloch[4] to the case of dipole-dipole interaction. It is to be remarked that in the case of nuclear spins, Eq. (24) could be used to determine the relative signs of the gyromagnetic ratios of the two spins: The effect would be an increase of the static magnetic moment if the two signs are the same, and a decrease if the signs are opposite.

A solution of Eqs. (14) of particular interest is the one corresponding to the initial conditions:

$$(\bar{I}_z-I_0)_{t=0}=0,$$
$$(\bar{S}_z-S_0)_{t=0}=S_\delta. \tag{25}$$

The solution, in the case $\rho=\rho'$, is, (the case $\rho\neq\rho'$ gives more complicated formulas, without any funda-

[2] F. Bloch, Phys. Rev. **70**, 460 (1946).

[3] A. Overhauser, Phys. Rev. **89**, 689 (1953); **92**, 477 (1953).

[4] F. Bloch, Phys. Rev. **93**, 944 (1954).

mental difference)

$$\begin{aligned}\dot{I}_z-I_0&=\tfrac{1}{2}S_i[e^{-(\sigma+\sigma_I)t}-e^{-(\sigma-\sigma_I)t}],\\ \dot{S}_z-S_0&=\tfrac{1}{2}S_i[e^{-(\sigma+\sigma_I)t}+e^{-(\sigma-\sigma_I)t}].\end{aligned}\tag{26}$$

These equations show that the relaxation of the spins $\mathbf{S}$ changes the difference of populations of spins $\mathbf{I}$ in time. This could be called a "transient" Overhauser effect and has been studied experimentally. The results will be discussed in Sec. VII.

VI. COMPUTATION OF THE TRANSITION PROBABILITIES

As an illustration of the method given in Sec. II we are going to compute the transition probabilities when the perturbing Hamiltonian $\mathcal{H}'$ is the dipole-dipole interaction (2). This perturbing Hamiltonian will be written as in Bloembergen, Purcell, and Pound's paper[5]:

$$\begin{aligned}\mathcal{H}'=&[I_zS_z-\tfrac{1}{4}(I_+S_-+I_-S_+)]F_0+[I_+S_z+I_zS_+]F_1\\&+[I_-S_z+I_zS_-]F_1^*+I_+S_+F_2+I_-S_-F_2^*,\end{aligned}\tag{27}$$

with

$$\begin{aligned}F_0(t)&=k[1-3\cos^2\theta(t)],\\F_1(t)&=-\tfrac{3}{2}k\sin\theta(t)\cos\theta(t)e^{i\varphi(t)},\\F_2(t)&=-\tfrac{3}{4}k\sin^2\theta(t)e^{2i\varphi(t)},\\k&=\hbar^2\gamma_I\gamma_S/b^3.\end{aligned}\tag{28}$$

We shall assume, as usual, that

$$\langle F(t)F^*(t+\tau)\rangle=\langle|F(0)|^2\rangle e^{-|\tau|/\tau_c},$$

the brackets meaning average among all pairs.

It can be seen[5] that

$$\begin{aligned}\langle F_0^2\rangle&=\tfrac{4}{5}k^2,\\\langle|F_1|^2\rangle&=\tfrac{3}{10}k^2,\\\langle|F_2|^2\rangle&=\tfrac{3}{10}k^2.\end{aligned}$$

Now we can calculate the transition probabilities used in the preceding sections. Equation (3) gives

$$\begin{aligned}w_0&=\frac{1}{t\hbar^2}\left|\int_0^t\tfrac{1}{4}F_0(t')e^{-i(\omega_I-\omega_S)t'}dt'\right|^2,\\w_1&=\frac{1}{t\hbar^2}\left|\int_0^t\tfrac{1}{2}F_1(t')e^{-i\omega_It'}dt'\right|,\\w_1'&=\frac{1}{t\hbar^2}\left|\int_0^t\tfrac{1}{2}F_1(t')e^{-i\omega_St'}dt'\right|^2,\\w_2&=\frac{1}{t\hbar^2}\left|\int_0^t\tfrac{1}{2}F_2(t')e^{-i(\omega_I+\omega_S)t'}dt'\right|^2.\end{aligned}\tag{29}$$

Equation (6) gives, with the use of the expansion (5′),

$$\begin{aligned}u_0=\frac{1}{t\hbar^2}\left|\frac{1}{4}\int_0^t\{(1-\tfrac{1}{4}[e^{-i(\omega_I-\omega_S)t'}+e^{i(\omega_I-\omega_S)t'}])F_0(t')-(e^{-i\omega_It'}-e^{-i\omega_St'})F_1(t')\right.\\\left.+(e^{i\omega_It'}-e^{i\omega_St'})F_1^*(t')-e^{-i(\omega_I+\omega_S)t'}F_2(t')-e^{i(\omega_I+\omega_S)t'}F_2^*(t')\}dt'\right|^2,\\u_1=\frac{1}{t\hbar^2}\left|\frac{1}{4}\int_0^t\{\tfrac{1}{4}(e^{-i(\omega_I-\omega_S)t'}-e^{i(\omega_I-\omega_S)t'})F_0(t')+e^{-i\omega_St'}F_1(t')\right.\\\left.+e^{i\omega_St'}F_1^*(t')-e^{-i(\omega_I+\omega_S)t'}F_2(t')+e^{i(\omega_I+\omega_S)t'}F_2^*(t')\}dt'\right|^2,\\u_2=\frac{1}{t\hbar^2}\left|\frac{1}{4}\int_0^t\{(1+\tfrac{1}{4}[e^{-i(\omega_I-\omega_S)t'}+e^{i(\omega_I-\omega_S)t'}])F_0(t')+(e^{-i\omega_It'}+e^{-i\omega_St'})F_1(t')\right.\\\left.-(e^{i\omega_It'}+e^{i\omega_St'})F_1^*(t')+e^{-i(\omega_I+\omega_S)t'}F_2(t')+e^{i(\omega_I+\omega_S)t'}F_2^*(t')\}dt'\right|^2.\end{aligned}\tag{30}$$

u_1' is obtained from u_1 by interchanging ω_I and ω_S.

It is seen that, before performing the integration, we must distinguish the cases where $\omega_I=\omega_S$ and $\omega_I\neq\omega_S$. We will assume that the motion is rapid, so that $\tau_c w\ll 1$ and $\tau_c u\ll 1$.

(a) Pairs of Like Spins: $\omega_I=\omega_S=\omega$

$$\begin{aligned}w_0&=\frac{\tau_c}{8\hbar^2}\langle F_0^2\rangle,\\w_1=w_1'&=\frac{\tau_c}{2\hbar^2}\langle|F_1|^2\rangle\frac{1}{1+\omega^2\tau_c^2},\\w_2&=\frac{2\tau_c}{\hbar^2}\langle|F_2|^2\rangle\frac{1}{1+4\omega^2\tau_c^2},\end{aligned}\tag{31}$$

$$\begin{aligned}u_0&=\frac{\tau_c}{8\hbar^2}\left[\frac{\langle F_0^2\rangle}{4}+\langle|F_2|^2\rangle\frac{2}{1+4\omega^2\tau_c^2}\right],\\u_1=u_1'&=\frac{\tau_c}{8\hbar^2}\left[\langle|F_1|^2\rangle\frac{2}{1+\omega^2\tau_c^2}+\langle|F_2|^2\rangle\frac{2}{1+4\omega^2\tau_c^2}\right],\\u_2&=\frac{\tau_c}{8\hbar^2}\left[\frac{9}{4}\langle F_0^2\rangle+\langle|F_1|^2\rangle\frac{8}{1+\omega^2\tau_c^2}+\langle|F_2|^2\rangle\frac{2}{1+4\omega^2\tau_c^2}\right].\end{aligned}\tag{32}$$

[5] Bloembergen, Purcell, and Pound, Phys. Rev. 73, 679 (1948).

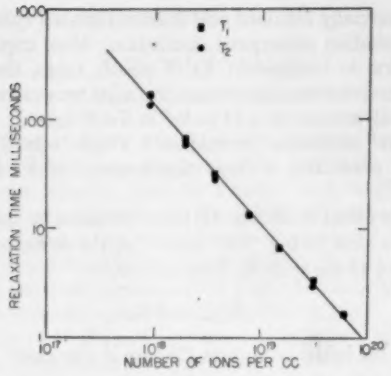

FIG. 2. Longitudinal and transverse relaxation times of protons at room temperature in paramagnetic solutions of ferric ions ($FeNH_4(SO_4)_2+12H_2O$) of different concentrations.

Using these values in Eqs. (12) we get the relaxation times:

$$\frac{1}{T_1}=\frac{6}{20}\frac{\hbar^2\gamma^4}{b^6}\left[\frac{\tau_c}{1+\omega^2\tau_c^2}+\frac{4\tau_c}{1+4\omega^2\tau_c^2}\right],$$
$$\frac{1}{T_2}=\frac{3}{20}\frac{\hbar^2\gamma^4}{b^6}\left[3\tau_c+\frac{5\tau_c}{1+\omega^2\tau_c^2}+\frac{2\tau_c}{1+4\omega^2\tau_c^2}\right]. \tag{33}$$

These results are identical to Kubo and Tomita's.[6] In the extreme narrow case ($\omega^2\tau_c^2\ll 1$), we can see that $T_1=T_2$.

$$1/T_1=1/T_2=\tfrac{3}{2}(\hbar^2\gamma^4/b^6)\tau_c. \tag{34}$$

(b) Pairs of Unlike Spins

The w's give the straightforward generalization

$$w_0=\frac{\tau_c}{8\hbar^2}\langle F_0^2\rangle\frac{1}{1+(\omega_I-\omega_S)^2\tau_c^2},$$
$$w_1=\frac{\tau_c}{2\hbar^2}\langle|F_1|^2\rangle\frac{1}{1+\omega_I^2\tau_c^2},$$
$$w_1'=\frac{\tau_c}{2\hbar^2}\langle|F_1|^2\rangle\frac{1}{1+\omega_S^2\tau_c^2}, \tag{35}$$
$$w_2=\frac{2\tau_c}{\hbar^2}\langle|F_2|^2\rangle\frac{1}{1+(\omega_I+\omega_S)^2\tau_c^2}.$$

In computing the u's, if we suppose that $|\omega_I-\omega_S|\gg 1/T$, so that any integral of the form:

$$\frac{1}{T}\frac{1}{\hbar^2}\int_0^T\int_0^T F^*(t')e^{-i\omega_I t''}F(t'')e^{i\omega_S t''}dt'dt''$$

averages out for any macroscopic time of observation T ($1/T$ is of order of magnitude of the u's) we get

$$u_0=u_2=\frac{\tau_c}{8\hbar^2}\left\{\left(1+\frac{1}{8}\frac{1}{1+(\omega_I-\omega_S)^2\tau_c^2}\right)\langle F_0^2\rangle+\left(\frac{2}{1+\omega_I^2\tau_c^2}+\frac{2}{1+\omega_S^2\tau_c^2}\right)\langle|F_1|^2\rangle+\frac{2}{1+(\omega_I+\omega_S)^2\tau_c^2}\langle|F_2|^2\rangle\right\},$$
$$u_1=\frac{\tau_c}{8\hbar^2}\left\{\frac{1}{8}\frac{1}{1+(\omega_I-\omega_S)^2\tau_c^2}\langle F_0^2\rangle+\frac{2}{1+\omega_S^2\tau_c^2}\langle|F_1|^2\rangle+\frac{2}{1+(\omega_I+\omega_S)^2\tau_c^2}\langle|F_2|^2\rangle\right\}, \tag{36}$$
$$u_1'=\frac{\tau_c}{8\hbar^2}\left\{\frac{1}{8}\frac{1}{1+(\omega_I-\omega_S)^2\tau_c^2}\langle F_0^2\rangle+\frac{2}{1+\omega_I^2\tau_c^2}\langle|F_1|^2\rangle+\frac{2}{1+(\omega_I+\omega_S)^2\tau_c^2}\langle|F_2|^2\rangle\right\}.$$

In the extreme narrow conditions ($\omega_I^2\tau_c^2\ll 1$ and $\omega_S^2\tau_c^2\ll 1$), the above formulas are considerably simplified:

$$w_0=\tfrac{1}{10}\delta,$$
$$w_1=w_1'=(3/20)\delta, \tag{37}$$
$$w_2=\tfrac{3}{5}\delta,$$

$$u_0=u_2=27/80,$$
$$u_1=u_1'=13/80, \tag{38}$$

with $\delta=\hbar^2\gamma_I^2\gamma_S^2\tau_c/b^6$.

With these values, the equation of motion (14) and (17) become

$$\frac{d}{dt}(\bar{I}_z-I_0)=-\delta[(\bar{I}_z-I_0)+\tfrac{1}{2}(\bar{S}_z-S_0)],$$
$$\frac{d}{dt}(\bar{S}_z-S_0)=-\delta[\tfrac{1}{2}(\bar{I}_z-I_0)+(\bar{S}_z-S_0)], \tag{39}$$
$$dI_+/dt=-\delta I_+,$$
$$dS_+/dt=-\delta S_+.$$

And the solution (26) for the longitudinal components is,

$$\bar{I}_z-I_0=\tfrac{1}{2}S_z[\exp(-\tfrac{3}{2}\delta t)-\exp(-\tfrac{1}{2}\delta t)],$$
$$\bar{S}_z-S_0=\tfrac{1}{2}S_z[\exp(-\tfrac{3}{2}\delta t)+\exp(-\tfrac{1}{2}\delta t)]. \tag{40}$$

[6] R. Kubo and K. Tomita, J. Phys. Soc. (Japan) 9, 888 (1954).

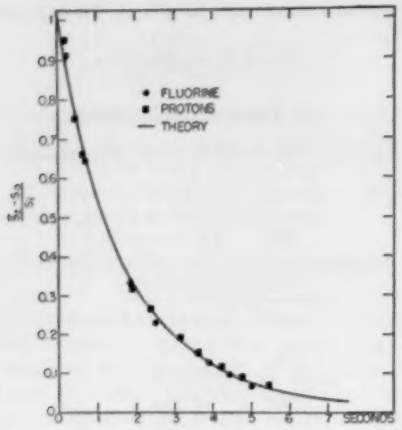

FIG. 3. Motion of the longitudinal component of the magnetic moment of one kind of nuclei toward its equilibrium value in hydrofluoric acid. The equation of the solid curve is

$$(S_z-S_0)/S_i=\tfrac{1}{2}[\exp(-t/D_1)+\exp(-t/T_1)],$$

with $T_1=1.27$ sec and $D_1=2.25$ sec.

(c) Relaxation of Nuclei in Paramagnetic Solution

Inserting the values (35) and (36) in the Eqs. (13) one gets:

$$\frac{1}{T_1}=\frac{1}{10}\frac{\hbar^2\gamma_I^2\gamma_S^2}{b^6}\left[\frac{\tau_c}{1+(\omega_I-\omega_S)^2\tau_c^2}+\frac{\tau_c}{1+\omega_I^2\tau_c^2}+\frac{\tau_c}{1+(\omega_I+\omega_S)^2\tau_c^2}\right],$$

$$\frac{1}{T_2}=\frac{\hbar^2\gamma_I^2\gamma_S^2}{20b^6}\left[4\tau_c+\frac{\tau_c}{1+(\omega_I-\omega_S)^2\tau_c^2}+\frac{3\tau_c}{1+\omega_I^2\tau_c^2}+\frac{6\tau_c}{1+\omega_S^2\tau_c^2}+\frac{6\tau_c}{1+(\omega_I+\omega_S)^2\tau_c^2}\right]. \tag{41}$$

In the extreme narrow case, as expected, $T_1=T_2$:

$$1/T_1=1/T_2=(\hbar^2\gamma_I^2\gamma_S^2/b^6)\tau_c. \tag{42}$$

We have measured the relaxation times of protons in paramagnetic solutions containing different concentrations of ferric ions. As it is shown in Fig. 2, the predicted equality between T_1 and T_2 has been verified within about 2.5 percent.

VII. EXPERIMENTAL RESULTS

The most sensitive test of the theory outlined above appears to be the Overhauser effect discussed in Sec. V. This effect has been observed in anhydrous hydrofluoric acid HF at room temperature. The boiling point of the acid, at atmospheric pressure, is 19.4°C. As a result, the commercially obtained acid is stored in steel cylinders, necessitating subsequent distillation. After triple distillation in transparent Kel-F plastic tubes, the acid became colorless. The resonance studies were carried out in small samples of acid sealed in Kel-F tubes.[7]

Free precession techniques[8,9] ("spin echo") were used, permitting a direct measurement of S_z, I_z, $\bar{I}_z$, and $\bar{S}_z$.

The initial conditions (25) were obtained by applying at the time $t=0$ a "180° pulse" at the resonance frequency of the spins **S**. Then at $t=0$,

$$(\bar{S}_z)_{t=0}=-S_0.$$

So the initial conditions (25) are in this case:

$$\begin{aligned}(\bar{I}_z-I_0)_{t=0}&=0,\\ S_i=(\bar{S}_z-S_0)_{t=0}&=-2S_0.\end{aligned} \tag{43}$$

In the extreme narrow case, we have in Eqs. (14) $\rho=\rho'$. Even if we are not in the extreme narrow case, this equality will hold approximately in hydrofluoric acid, for the Larmor frequencies of hydrogen and fluorine differ by less than 6 percent. In this condition, solution (26) with the initial condition (43) is

$$\begin{aligned}\bar{I}_z-I_0&=S_0[e^{-(\rho-\sigma)t}-e^{-(\rho+\sigma)t}],\\ \bar{S}_z-S_0&=-S_0[e^{-(\rho-\sigma)t}+e^{-(\rho+\sigma)t}].\end{aligned} \tag{44}$$

Figures 3 and 4 show the experimental results, that are, as expected from our simple theory, symmetrical with respect to the hydrogen and fluorine nuclei. The figures show that the experimental points can be fitted very

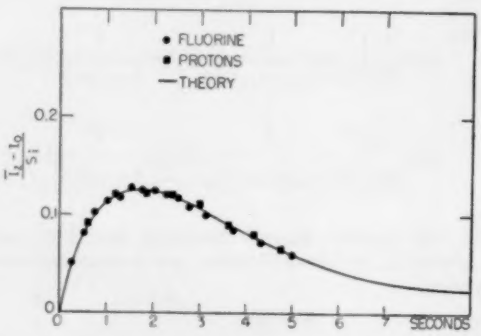

FIG. 4. Motion of the longitudinal component of one kind of spin after having applied a 180° pulse to the other kind of spin in hydrofluoric acid. The equation of the solid curve is

$$(\bar{I}_z-I_0)/S_i=\tfrac{1}{2}[\exp(-t/D_1)-\exp(-t/T_1)],$$

where T_1 and D_1 are the same as in Fig. 3.

[7] The first experiments were performed in Teflon. But after a few days in Teflon, the liquid acid becomes colored and the relaxation times drop considerably, showing that commercial Teflon is not completely inert to hydrofluoric acid.

[8] E. L. Hahn, Phys. Rev. **80**, 580 (1950).

[9] H. Y. Carr and E. M. Purcell, Phys. Rev. **94**, 630 (1954).

well by (44) with the values:

$$T_1=1/(\rho+\sigma)=1.27 \text{ sec},$$

$$D_1=1/(\rho-\sigma)=2.55 \text{ sec}.$$

The estimated error in these times is about 20 percent. These results show a ratio $\sigma/\rho=\frac{1}{3}$. The same ratio is obtained directly from the steady Overhauser effect: Saturation of protons (or fluorine nuclei) increases the magnetization due to fluorine (or to protons if fluorine has been saturated) by a factor of about 30 percent. The static magnetic moments of hydrogen and fluorine being approximately equal, Eq. (24) gives $\sigma/\rho\cong\frac{1}{3}$.

This ratio of $\frac{1}{3}$ is, however, in disagreement with the value $\frac{1}{2}$ calculated for a pure dipole-dipole interaction in the extreme narrow case [Eqs. (39) and (40)].

The decay of the transverse component is, within experimental errors, simply exponential with the same time constant T_2 for protons and fluorine nuclei:

$$T_2=0.43\pm0.015 \text{ sec}.$$

This again is in disagreement with Eq. (39), showing that either the effect of neighboring molecules needs to be taken into account, or that the interaction is not a pure dipole-dipole one, or both. It has been possible to remove the discrepancy by adding to the pure dipole-dipole interaction an electron-coupled exchange interaction $A\mathbf{I}\cdot\mathbf{S}$ of reasonable amplitude. Further experiments on purer hydrofluoric acid are being carried out to investigate this effect.

Figure 5 is an example of the signals obtained: It shows the increase of the magnetization due to fluorine, following a 180° pulse for protons. The magnitude of the longitudinal magnetic moment of fluorine is indicated by the amplitude of the tail following a 90° pulse for fluorine.

On the same photograph are superimposed: (a) the thermal equilibrium value of the magnetic moment of the fluorine obtained by simply applying a 90° pulse for fluorine (tails *a* and *b*). (b) the value of the magnetic moment of the fluorine when the protons are saturated (tail *c*). Similar photographs have been obtained by interchanging the role of hydrogen and fluorine.

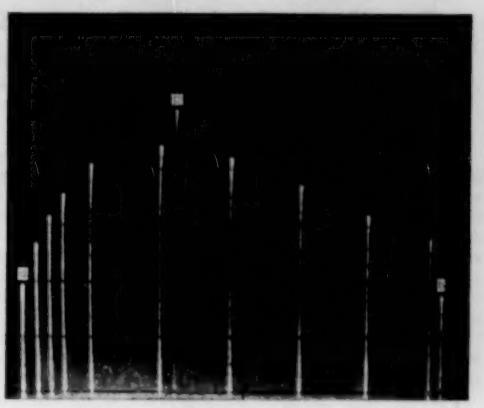

FIG. 5. Amplitude of tails of 90° pulses at fluorine frequency after having applied a 180° pulse at hydrogen frequency in hydrofluoric acid. *a* and *b* represent the amplitude of the tail when no 180° pulse has been applied; *c* represents the amplitude of the tail when the proton resonance has been saturated (steady Overhauser effect).

ACKNOWLEDGMENTS

The experiment was suggested, during a discussion on the subject, by Professor N. Bloembergen. It is a pleasure to thank him for his constant interest in the development of this work and for many valuable suggestions. I wish to thank Dr. K. Tomita and Professor R. V. Pound for many helpful discussions. Professor E. M. Purcell drew my attention to some important theoretical inaccuracies in the early stages of this work. I want to express my gratitude to Dr. G. B. Benedek for having introduced me to the spin echoes techniques and for having kindly revised the manuscript.

Pure Nuclear Quadrupole Spectra of Chlorine and Antimony Isotopes in Solids*

TIEN-CHUAN WANG
Columbia University, New York, New York

(Received March 21, 1955)

Experimental measurements on nuclear quadrupole resonances of chlorine and antimony isotopes in solids have been made to an accuracy of about 0.001 percent. The results are compared in detail with theoretical results for (1) nuclear quadrupole interaction, (2) interaction between quadrupole coupling and thermal vibrations, and (3) effects of a nuclear hexadecapole. The ratio $(eQq)_{Cl^{35}}/(eQq)_{Cl^{37}}$ varies between 1.268736 and 1.268973 while $(eQq)_{Sb^{123}}/(eQq)_{Sb^{121}}$ varies from 1.274714 to 1.274770. These variations may be attributed to zero-point vibrations and to thermal vibrations, so that no clear evidence is found for nuclear polarization by surrounding electric fields. For *p*-dichlorobenzene, the temperature coefficient of the coupling constant of Cl and the variation of isotopic coupling ratio with temperature are shown to be in fair quantitative agreement with the extension of Bayer's theory of vibrational effects. Relaxation times, Zeeman effects, and certain effects due to crystal structure are examined. Small discrepancies in the measured ratios of frequencies of transitions in Sb^{121} and Sb^{123}, which can be attributed to nuclear hexadecapole interactions are found. These indicate a hexadecapole coupling constant in Sb^{120} of 24 kc/sec and a ratio of the Sb^{123} hexadecapole coupling to that of Sb^{121} of 0.8 ± 0.3. A convenient high-sensitivity circuit for observation of nuclear resonances in solids has been developed and is discussed.

I. INTRODUCTION

HYPERFINE structure which arises from the electrical quadrupole interaction between nuclei and their surrounding electrons has been extensively observed in atomic and molecular spectra. The quadrupole coupling constant eQq, which is the main object of these measurements, gives information regarding the distribution of electrons around a nucleus and the deviation of the nucleus from spherical symmetry. This information may, in turn, be utilized to determine molecular[1,2] and nuclear structures and to shed light on solid state phenomena. Because of the inherent difficulty in measuring the small frequency difference associated with the quadrupole hyperfine structure, the value of eQq cannot easily be obtained to high accuracy by using methods of optical or molecular spectroscopy. Experiments on pure nuclear quadrupole resonances yields data of much higher accuracy.[3-6] With the experimental setup of the present experiment, the quadrupole resonance frequencies can be measured to an accuracy of better than 0.001 percent. With this accuracy the ratios of eQq of different isotopes were found to be dependent upon temperature and molecular environment. In order to evaluate these experimental results, it has been necessary to calculate nuclear quadrupole interactions with much greater care than is usual. The effects of several very small interaction terms were included and compared with the experimental data.

II. THEORY

A. General Formulation

The electrical interaction between an atomic nucleus and its neighboring electronic charge can be expressed in a series corresponding to the effects of various electrical multipoles. In this series, the first term represents the interaction of a point charge with the electronic field while the second and third terms describe electric quadrupole and hexadecapole (16th-pole) interactions. These last two terms are not zero only if the shape of nucleus and the distribution of its surrounding electrons depart from spherical symmetry. The Hamiltonian operator for the nuclear quadrupole interaction can be written as

$$H_Q=\frac{eQq}{4I(2I-1)}[(3I_z^2-I^2)+\tfrac{1}{2}\eta(I_+^2+I_-^2)]_{\rm op}. \quad (1)$$

This representation can be obtained by a simplification of the formulation given by Pound,[6] Bersohn,[7] or Dehmelt and Krüger.[8] Here I represents the spin of the nucleus, $I_\pm\equiv I_x\pm iI_y$, Q is the nuclear quadrupole moment,

$$q\equiv\int_{\tau_e}\frac{\rho(\mathbf{r}_e)(3\cos^2\theta_e-1)}{r_e^3}d\tau_e\equiv-\frac{\partial E_z}{\partial z},$$

where r_e and θ_e are polar coordinates of the electronic charge element $\rho d\tau_e$ considered from the center of symmetry, q is the principal value of the field gradient at the nucleus, and

$$\eta\equiv\left(\frac{\partial E_x}{\partial x}-\frac{\partial E_y}{\partial y}\right)\Big/\frac{\partial E_z}{\partial z}$$

is the asymmetry parameter of the field gradient in a plane perpendicular to the z direction. In all cases, $1\geq|\eta|\geq0$. Matrix elements of the operator in Eq. (1)

* Work supported jointly by the Signal Corps, the Office of Naval Research, and the Air Research and Development Command.

[1] C. H. Townes and B. P. Dailey, J. Chem. Phys. **17**, 782 (1949).

[2] C. H. Townes and B. P. Dailey, J. Chem. Phys. **20**, 35 (1952).

[3] In the preliminary result of the present experiment, the ratio $(eQq)_{Cl^{35}}/(eQq)_{Cl^{37}}$ in solid *trans*-dichloroethylene was found to be 1.2682 ± 0.0004. This was the first accurate value obtained. This ratio was quoted by Geschwind, Gunther-Mohr, and Townes, Phys. Rev. **81**, 288 (1951); but the accuracy stated there involves a typographical error. The probable error should read 0.0004 instead of 0.004.

[4] Wang, Townes, Schawlow, and Holden, Phys. Rev. **86**, 809 (1952).

[5] R. Livingston, Phys. Rev. **82**, 289 (1951).

[6] R. V. Pound, Phys. Rev. **79**, 685 (1950).

[7] R. Bersohn, J. Chem. Phys. **20**, 1505 (1952).

[8] H. G. Dehmelt and H. Krüger, Z. Physik **129**, 401 (1951).

can be derived from well-known matrices for quantum-mechanical angular momentum.[9] In an I, m representation, the first term in Eq. (1) gives diagonal elements which are the main parts of the characteristic energies. The second term represents off-diagonal elements corresponding to $\Delta m=\pm 2$. They are nonvanishing only when the asymmetry-parameter η is different from zero.

B. Energy Levels

The nuclear quadrupole moment is zero unless $I\geqslant 1$. For integral values of I, Eq. (1) will lead to solutions for the energy levels which are similar to those of a molecular asymmetric rotor.[10] In general, for the case of half-integral spin, the $2I+1$ energy levels are doubly degenerate, so that the secular equation of degree $2I+1$ can be factored into two identical equations of degree $I+\frac{1}{2}$. If spin I is greater than $\frac{3}{2}$, it is impossible to obtain the exact solution in closed form. However, the energy levels can be obtained by the use of an approximation method to solve the secular equation.

For I equal to $\frac{3}{2}$, the exact solution[2,11] for the energy level is

$$W_{m-\pm 1'}=-\tfrac{1}{4}eQq(1+\tfrac{1}{3}\eta^2)^{\frac{1}{2}},$$
$$W_{m-\pm 1'}=\tfrac{1}{4}eQq(1+\tfrac{1}{3}\eta)^{\frac{1}{2}}, \qquad (2)$$

where the primed m indicates those states which are modified by the asymmetry parameter.

For $I=5/2$, the energy levels which are obtained from the expansion in powers[12] of η^2 are

$$W_{\pm 1'}=\frac{-eQq}{5}\left(1+\frac{4}{9}\eta^2-\frac{172}{729}\eta^4+\frac{15\,332}{59\,049}\eta^6-\frac{1\,717\,580}{4\,782\,969}\eta^8\right), \qquad (3a)$$

$$W_{\pm 1'}=\frac{-eQq}{20}\left(1-\frac{3}{2}\eta^2+\frac{23}{24}\eta^4-\frac{449}{432}\eta^6+\frac{44\,675}{31\,104}\eta^8\right), \qquad (3b)$$

$$W_{\pm 1'}=\frac{eQq}{4}\left(1+\frac{1}{18}\eta^2+\frac{17}{5832}\eta^4-\frac{143}{944\,784}\eta^6-\frac{12\,587}{612\,220\,032}\eta^8\right). \qquad (3c)$$

[9] These matrices are:

$\langle m|I_z|m\rangle=m$,

$\langle I,m|I_\pm|I,m\mp 1\rangle=[(I\pm m)(I\mp m+1)]^{\frac{1}{2}}$,

$\langle I,m|I^2|I,m\rangle=I(I+1)$,

$\langle I,m|I_\pm^2|I,m\mp 2\rangle=[(I\pm m)(I\pm m-1)(I\mp m+1)(I\mp m+2)]^{\frac{1}{2}}$.

[10] King, Hainer, and Cross, J. Chem. Phys. **11**, 27 (1943).

[11] Christopher Dean, dissertation, Harvard University, June, 1952 (unpublished).

[12] Bershon (reference 7) has obtained the solutions for $I=5/2$ up to eighth-order terms. However, his sixth order coefficient of η for $W_{m-\pm 1'}$ differs from the present value. Private communication with him establishes that the fourth term in his Eq. (21a) should read $-(715/472\,392)\eta^6$, which is the same as the present result.

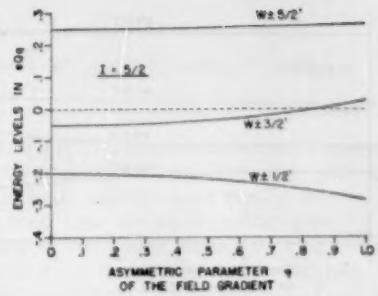

FIG. 1. Energy levels of the quadrupole interaction for $I=5/2$.

Figure 1 shows energy levels as functions of η. If $\eta=0$, the two transitions $\nu_1=W_{\pm 1'}-W_{\pm 1'}$, and $\nu_2=W_{\pm 1'}-W_{\pm 1'}$, have the simple ratio $\nu_2/\nu_1=2$.

Similarly, for spin $I=7/2$, the energy levels are approximately[13]

$$W_{\pm 1'}=-\frac{5}{28}eQq\left(1+\frac{5}{6}\eta^2-\frac{311}{216}\eta^4+\frac{20\,557}{3888}\eta^6-\frac{762\,019}{31\,104}\eta^8\right), \qquad (4a)$$

$$W_{\pm 1'}=-\frac{3}{28}eQq\left(1-\frac{31}{30}\eta^2+\frac{21\,967}{9000}\eta^4-\frac{3\,975\,973}{450\,000}\eta^6+\frac{734\,970\,487}{18\,000\,000}\eta^8\right), \qquad (4b)$$

$$W_{\pm 1'}=\frac{eQq}{28}\left(1+\frac{5}{6}\eta^2+\frac{25}{216}\eta^4-\frac{275}{3888}\eta^6-\frac{25}{93\,312}\eta^8\right), \qquad (4c)$$

$$W_{\pm 1'}=\frac{7}{28}eQq\left(1+\frac{1}{30}\eta^2+\frac{29}{27\,000}\eta^4+\frac{1241}{12\,150\,000}\eta^6+\frac{2263}{1\,458\,000\,000}\eta^8\right). \qquad (4d)$$

Figure 2 gives the dependence of the energy levels on η. If we take $\nu_1=W_{\pm 1'}-W_{\pm 1'}$, $\nu_2=W_{\pm 1'}-W_{\pm 1'}$, and $\nu_3=W_{7/2'}-W_{1'}$, the ratio of transition frequencies $\nu_3:\nu_2:\nu_1$ should be 3:2:1 for the case $\eta=0$.

C. Effects of Thermal Vibrations

It is well known that the quadrupole coupling constant eQq measured in pure nuclear quadrupole resonances is temperature dependent. Dehmelt, Krüger[8] and later Bayer[14] suggested that this temperature dependence was caused solely by thermal vibrations of molecules in crystals and Dean[11] has studied the effects of thermal vibrations on chlorine resonances in a group

[13] R. Bersohn has kindly checked the results of this calculation.

[14] H. Bayer, Z. Physik **130**, 227 (1951).

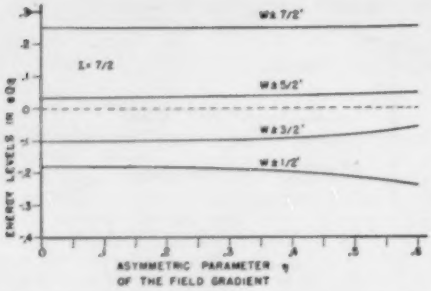

FIG. 2. Energy levels of the quadrupole interaction for $I=7/2$.

of molecular crystals. As molecules execute molecular (torsional) and intramolecular (stretching and bending) oscillations in crystals, the charge distribution in the molecules becomes distorted and the principal axes of the electric field gradient are varied so that a variation[15,16] in q is to be expected. For the sake of illustration one may consider p-dichlorobenzene, a molecular crystal whose principal torsional vibration frequencies have been well identified.[17,18] Since chlorine atoms are bonded to the benzene rings at opposite corners, two modes of thermal vibrations involving rotation around the principal molecular axes perpendicular to the chlorine bonds will be effective in the temperature variation of the q of the chlorine. Because of this effect, the quadrupole Hamiltonian operator becomes

$$H_Q=\frac{eQq'}{4I(2I-1)}[(3I_z^2-I^2)+\tfrac{1}{2}\eta'(I_+^2+I_-^2)]_{00}; \quad (5a)$$

where

$$q'=q[1-\tfrac{3}{4}(\langle\theta^2\rangle_{Av}+\langle\phi^2\rangle_{Av})+\tfrac{1}{2}\eta(\langle\theta^2\rangle_{Av}-\langle\phi^2\rangle_{Av}) +\tfrac{1}{8}(3-\eta)\langle\theta^2\rangle_{Av}\langle\phi^2\rangle_{Av}], \quad (5b)$$

and

$$\eta'=(q/q')[\eta+\tfrac{3}{4}(\langle\theta^2\rangle_{Av}-\langle\phi^2\rangle_{Av})-\tfrac{1}{2}\eta(\langle\theta^2\rangle_{Av}+\langle\phi^2\rangle_{Av}) +\tfrac{1}{8}(3-\eta)\langle\theta^2\rangle_{Av}\langle\phi^2\rangle_{Av}], \quad (5c)$$

express the modifications of q and η due to the thermal vibrations. They are functions of the mean square amplitudes $\langle\phi^2\rangle_{Av}$ and $\langle\theta^2\rangle_{Av}$ of rotation about the two principal axes x and y respectively. According to Bayer's formulation, $\langle\phi^2\rangle_{Av}$ and $\langle\theta^2\rangle_{Av}$ are both functions of the absolute temperature T and of the molecular vibration constants (such as vibration frequencies and moments of inertia around x- and y-axes).

The Hamiltonian operator from Eq. (5a) has exactly the same form as in Eq. (1). The only effect which is caused by thermal vibrations is the change of q to q', and of η to η'. In the case $I=\frac{3}{2}$ which occurs in chlorine nuclei, by neglecting higher order terms in thermal vibration amplitudes, the temperature coefficient for the quadrupole resonance frequency is found to be

$$\frac{1}{\nu_0}\left(\frac{d\nu}{dT}\right)=\frac{-3\hbar^2}{2kT^2}\left[\frac{e^{h\nu_a/kT}}{I_x(e^{h\nu_a/kT}-1)^2}+\frac{e^{h\nu_b/kT}}{I_y(e^{h\nu_b/kT}-1)^2}\right], \quad (6a)$$

where ν_0 is the pure quadrupole resonance frequency for $\eta=0$, I_x and I_y are momenta of inertia of the molecule perpendicular to the bond direction of the chlorines, ν_a and ν_b the corresponding frequencies of torsional vibrations, k = Boltzmann's constant and $\hbar$ = Planck's constant divided by 2π. Under ordinary conditions, $h\nu_a/kT$ and $h\nu_b/kT\ll 1$, so that Eq. (6a) becomes

$$\frac{1}{\nu_0}\left(\frac{d\nu}{dT}\right)=-\frac{3k}{8\pi^2}\left[\frac{e^{h\nu_a/kT}}{I_x\nu_a^2}+\frac{e^{h\nu_b/kT}}{I_y\nu_b^2}\right]. \quad (6b)$$

This equation indicates that the magnitude of the temperature coefficient $\nu_0^{-1}(d\nu/dT)$ decreases as the frequency of the torsional vibration increases. Moreover, for the chlorine resonances,[19] the ratio $(eQq)_{35}/(eQq)_{37}$ will be

$$\frac{(eQq)_{Cl^{35}}}{(eQq)_{Cl^{37}}}=\frac{\nu_{35}}{\nu_{37}}=\frac{(eQq)_{35}^0}{(eQq)_{37}^0} \times\left[1-\frac{3\hbar^2}{8I_{x35}kT}\frac{\Delta I_x}{I_{x35}}-\frac{3\hbar^2}{8I_{y35}kT}\frac{\Delta I_y}{I_{y35}}\right], \quad (7)$$

where $\Delta I=I_{37}-I_{35}$, ν_{35} and ν_{37} are the pure quadrupole resonance frequencies of Cl^{35} and Cl^{37}, and $(eQq)^0$ the quadrupole coupling constant when $\eta=0$ and when there are no thermal vibrations. Equation (7) indicates that $(eQq)_{Cl^{35}}/(eQq)_{Cl^{37}}$ decreases with a decrease of temperature T. Since $1/I_{x35}$ and $1/I_{y35}$ are proportional to ν_a^2 and ν_b^2, the squares of the torsional vibration frequencies, the temperature effect on the ratio of quadrupole coupling constants of isotopes as given in Equation (7) is larger for the higher-frequency modes of torsional vibration. Figure 3 shows the deviation $\Delta\nu$ from ν_0 (or Δq from q_0) of the resonance frequencies with temperature (where for simplicity, it is assumed that only one mode is excited). The solid curve represents the dependence of the quadrupole coupling constant (actually q) of Cl^{37} and the dotted one that of Cl^{35}. The two curves coincide at high temperature, and separate at low temperature due to the slightly different effect of thermal vibrations for different isotopes. Since the ratio of quadrupole moments, Q_{35}/Q_{37}, is constant, the ratio $(eQq)_{35}/(eQq)_{37}$, will vary with temperature as does q_{35}/q_{37} shown in Fig. 3, so that it should decrease with decreasing temperature. When the absolute temperature T approaches zero, zero point vibrations are still effective in changing q and give an appreciable difference between q_{35} and q_{37}.

[15] Fabricand, Carlson, Lee, and Rabi, Phys. Rev. **91**, 1403 (1953).
[16] H. J. Zeiger and D. I. Bolef, Phys. Rev. **85**, 788 (1952).
[17] A. Kastler and A. Rousset, Phys. Rev. **71**, 455 (1947).
[18] B. D. Saksena, J. Chem. Phys. **18**, 1653 (1950).

[19] Both Cl^{35} and Cl^{37} possess spins of $\frac{3}{2}$.

D. Hexadecapole Interaction

As mentioned previously, after the quadrupole term the next term to be considered in the interaction of the nucleus with its surrounding electronic charge is the hexadecapole term. This term can be written as

$$H_{\text{hex}}\equiv\int_{\tau_e}\int_{\tau_n}\rho_e{}^e\rho_n\frac{r_n{}^4}{r_e{}^5}P_4(\cos\theta_{en})d\tau_e d\tau_n$$

$$=\int_{\tau_e}\int_{\tau_n}\frac{\rho_e{}^e\rho_n r_n{}^4}{r_e{}^5}(-1)^m Z_4{}^{(m)}(n)Z_4{}^{(-m)}(e)d\tau_e d\tau_n,\qquad r_e>r_n,\quad (8a)$$

where the $Z_4{}^{(m)}$ are defined as

$$Z_4{}^{(m)}=(-1)^m\left[\frac{(l-m)!}{(l+m)!}\right]^{\frac{1}{2}}\sin^m\theta\frac{d^m}{d^m(\cos\theta)}\times P_4(\cos\theta)e^{im\phi},\quad (8b)$$

$$Z_4{}^{(-m)}=(-1)^m Z_4{}^{(m)};$$

and $\cos\theta_{en}=\cos\theta_e\cos\theta_n+\sin\theta_e\sin\theta_n\cos(\phi_e-\phi_n)$. θ_{en} is the angle between the electronic position r_e and the nuclear position r_n referred to the center of symmetry of the molecules, and θ_n, θ_e, ϕ_n, and ϕ_e are the nuclear and the electronic polar and azimuthal angles respectively. One may define the principal hexadecapole field as

$$m_{16}\equiv-\frac{\partial^3 E_e}{\partial z^3}=\int_{\tau_e}\frac{\rho_e{}^e(r_e)(35\cos^4\theta_e-30\cos^2\theta_e+3)d\tau_e}{r_e{}^5},\quad (9a)$$

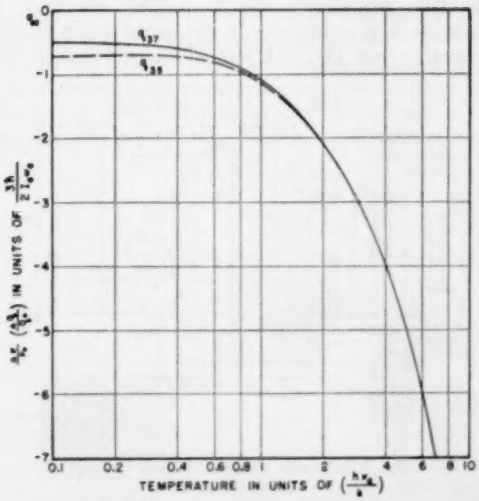

FIG. 3. Dependence of nuclear quadrupole resonance frequencies on temperature. The solid curve is for Cl^{37} and the dotted curve for Cl^{35}.

and

$$eM_{16}\equiv\int_{\tau_n}\psi^*_{I,m=I}r_n{}^4(35\cos^4\theta_n-30\cos^2\theta_n+3)\times\psi_{I,m=I}d\tau_n,\quad (9b)$$

where M_{16} is the nuclear hexadecapole moment, which will be zero unless $I\geq 2$. m_{16} is inversely proportional to $r_e{}^5$ and hence decrease more rapidly with an increase of r_e than does the corresponding quantity q for a quadrupole interaction. Expression (9a) vanishes for either an s or p electron, but not for electrons of higher angular momentum. Hence electrons in d and f orbitals will make the most important contribution to m_{16}. The hexadecapole moment M_{16} is a quantity which describes the second order departure of the nuclear charge distribution from spherical symmetry.

Taking only those operators in Eq. (8b) for which $m=0$, and symmetrizing, one obtains the principal quantity in the Hamiltonian for the nuclear hexadecapole interaction,

$$H_{\text{hex}}=\frac{eM_{16}m_{16}}{128I(I-1)(2I-1)(2I-3)}\times[35I_z{}^4-30I_z{}^2I^2+3I^4+25I_z{}^2-6I^2]_{\text{op}}.\quad (10)$$

This equation applies only where $I\geq 2$, which is the condition required for existence of a hexadecapole moment. The ratio $eM_{16}m_{16}/eQq$ may be seen to be approximately $r_n{}^2/r_{eff}{}^2$, where r_n is the nuclear radius and r_{eff} is an average distance of the electron from the nucleus.

For $I=5/2$, the energy levels for the hexadecapole interaction will be, from Eq. (10)

$$\begin{aligned}W(\text{hex})_{m=\pm\frac{1}{2}}&=(3/96)(eM_{16}m_{16}),\\ W(\text{hex})_{m=\pm\frac{3}{2}}&=-(9/192)(eM_{16}m_{16}),\\ W(\text{hex})_{m=\pm\frac{5}{2}}&=(1/64)(eM_{16}m_{16}).\end{aligned}\quad (11)$$

Similarly, for $I=7/2$, the energy levels are:

$$\begin{aligned}W(\text{hex})_{m=\pm\frac{1}{2}}&=(9/448)(eM_{16}m_{16}),\\ W(\text{hex})_{m=\pm\frac{3}{2}}&=-(3/448)(eM_{16}m_{16}),\\ W(\text{hex})_{m=\pm\frac{5}{2}}&=-(13/448)(eM_{16}m_{16}),\\ W(\text{hex})_{m=\pm 7/2}&=(1/64)(eM_{16}m_{16}).\end{aligned}\quad (12)$$

III. APPARATUS

A. General Considerations

Requirements for a good spectrometer include wide frequency coverage, high sensitivity, and low distortion. Since the resonance frequencies of direct nuclear quadrupole transitions are molecular or atomic properties and there are no laboratory means available for simulating these tremendous fields, the radio-frequency oscillator of the spectrometer should be capable of

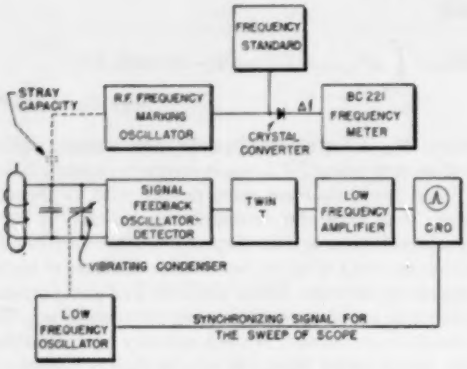

FIG. 4. Block diagram of rf spectrometer for pure nuclear quadrupole resonances.

tuning over a wide frequency range in order to cover the frequencies of quadrupole resonances. To detect the very weak signal of the pure nuclear quadrupole resonance, a spectrometer of high sensitivity is required. Accurate measurements also require that the electronic system incorporated in the spectrometer reproduce the shape of resonance lines accurately. In general the nuclear quadrupole interaction is characterized by a shorter relaxation time than the nuclear magnetic interaction; hence a greater rf field is needed to produce an observable resonance. Neither the Bloch cross-coil nor the Purcell bridge method are capable of giving adequate sensitivity for a pure nuclear quadrupole resonance experiment because of difficulty of balancing out the large primary rf signal which is used to induce the nuclear signal. An unbalanced circuit developed by Pound and Knight[20] would also be inadequate in this application as it operates well only at low rf levels. A super-regenerative system has the advantage of wide frequency coverage and high sensitivity, although it too has important shortcomings. The most important of these is the ambiguity which arises from the presence of spurious signals resulting from the production of sidebands separated by the quenching frequency. In addition, there is empirically observed dependence of line-shape and line width upon the frequency and amplitude of the quenching voltage.[11] A satisfactory circuit, which is called "Signal Feedback Oscillator-Detector" will be discussed later.

The block diagram of the whole system is shown in Fig. 4. The main part of this setup is similar to the system used by Livingston.[21] The crystalline sample is placed in the coil of the rf tank circuit of the oscillator-detector. When the rf oscillator is tuned to the neighborhood of the quadrupole resonance line, the frequency of the oscillator is swept to and fro across the quadrupole resoannces by a vibrating condenser.[22] Because of quadrupole resonance, a minute amount of energy is absorbed from the coil causing the effective Q of the coil to decrease by a small amount. This effect, in turn, will cause a small rf voltage drop across the tank circuit which can be detected by the detecting device in the oscillator. The signal feedback device gives additional amplification directly in the detection tube, and hence avoids possible difficulty due to noise introduced by a subsequent stage of amplification. At the same time it provides amplification over a narrow band width. The low-frequency amplifier[23] amplifies the signal and then delivers it to the verticle deflection system of the scope. The horizontal sweep of the scope is synchronized with the low-frequency oscillator which controls the vibrating condenser. Through this arrangement, the resonance line is displayed on the screen of the scope.

B. Signal Feedback Oscillator-Detector

The circuit arrangement of the signal feedback oscillator-detector is shown in Fig. 5. The 6AK5 tube acts simultaneously as an rf oscillator and a detector. The oscillator is essentially a split-resistance grounded-plate Colpitts circuit with feedback obtained by means of the stray capacitances while the detector is a combination of the grid-leak and plate types. The circuit has been used by Hopkins[24] and Livingston[21] but in their case the tube operates at a different point of its characteristic. The present arrangement has the advantage of only one "hot" lead to the rf tank circuit and avoids an extra detector which would otherwise connect to the tank with attendant decrease in Q. The excitation ratio for the oscillator is governed by the ratio of the "regeneration" resistor to the 1.5-megohm grid-leak. When the vibrating condenser sweeps the oscillator frequency across the nuclear resonance, a decrease in rf voltage due to absorption in the sample appears across the tank and will be detected at the

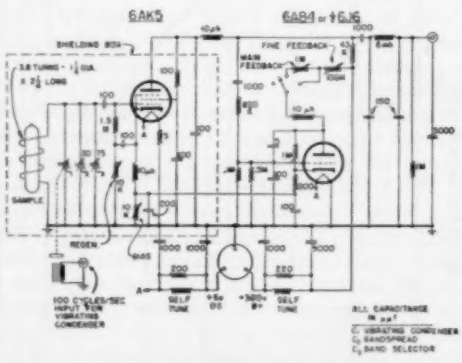

FIG. 5. Schematic diagram of signal feedback oscillator-detector.

[20] R. V. Pound and W. D. Knight, Rev. Sci. Instr. 21, 219 (1950).
[21] R. Livingston, Ann. N. Y. Acad. Sci. 55, 800 (1952).
[22] Part of surplus APN-1 Radio Altimeter.
[23] A. Hewlett Packard amplifier operates with a power amplification of 40 db.
[24] N. J. Hopkins, Rev. Sci. Instr. 20, 401 (1949).

plate of the 6AK5 tube. This signal represents the absorption mode which results from the imaginary part of the nuclear susceptibility.

The mechanism of operation is shown graphically in Fig. 6. By adjusting the "bias" control potentiometer, the dc grid bias is set almost to the cut-off point. Due to the use of the cathode bias system, the cut-off action is extremely slow. The rf grid swing is adjusted to be slightly greater than the bias voltage (on the verge of "Class B_1" and "Class B_2" operation). At the rf peak, the grid is only very slightly positive ("Class B_2"). The circuit parameters are adjusted so as to use the steepest possible slope of the characteristic in order to have good detection. However, when a signal appears, because of grid rectification the bias is decreased slightly as shown in Fig. 6 and cancels out the detection action to some degree. The feedback arrangement counteracts this loss and reinforces the signal.

Another factor which increases the signal-to-noise ratio is the fact that the $R-C$ time constant (about 10^{-3} second) of the coupling network at the grid side of the 6J6 is adjusted to match the reciprocal of the width of the resonance line. Hence a frequency-selective characteristic for the circuit is incorporated within the feedback loop associated with the 6J6 tube. In this way, one can avoid the use of a high-gain narrow-band amplifier in the following stage. The rf level across the tank ranges from 5 to 13 volts. A specially designed high-μ tube which could operate at a high rf level might give more sensitive detection for a nuclear signal of shorter relaxation time. The detection characteristic for the 6AK5 with feedback is shown in Fig. 7.

It was found that Raytheon 5654 tubes were superior to ordinary 6AK5 tubes in this application. Good shielding between the rf and af (audio-frequency) circuits is absolutely essential for the operation of the feedback circuit. In the present apparatus, rf and af circuits are located in separate copper compartments and all feed-through connections are made with button condensers. The complete system is enclosed in a copper box. Two similar circuits were built, one to cover the range from 10–60 Mc/sec and the other from 60–120 Mc/sec.

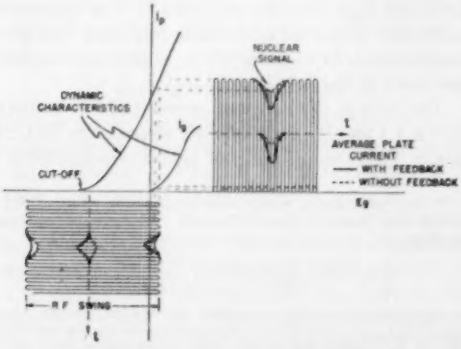

FIG. 6. Operating behavior of signal feedback oscillator-detector.

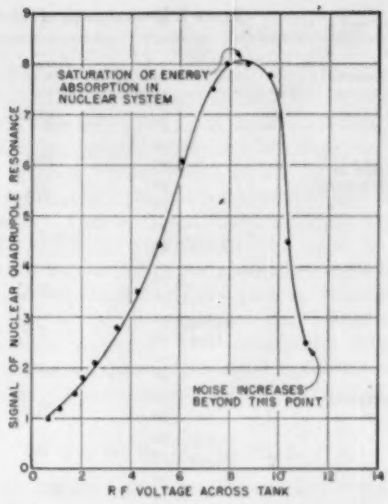

FIG. 7. Detection characteristic of 6AK5 used as signal feedback oscillator-detector (Cl^{35} in a single crystal of p-$C_6H_4Cl_2$ was used).

The signal of the Cl^{35} resonance in $NaClO_3$ at room temperature is shown in Fig. 8. The theoretical signal to noise ratio is about 20.

C. Frequency Measurement

A 100-kc/sec crystal oscillator which is stabilized to several parts in 10^7 with respect to WWV, serves as the frequency standard. By frequency multiplication, harmonics at 5, 20, and 40 Mc/sec are available as references for accurate frequency measurements. Usually the 5 and 20 Mc/sec standard signals are applied together to a 1N34 crystal which serves as mixer and harmonic generator simultaneously. Thus, frequency markers at 5-Mc/sec intervals are available from 5 Mc/sec up to several hundred Mc/sec. A frequency-marking oscillator which interacts with the frequency-modulated oscillator-detector will produce a characteristic pip on the scope. If this pip is placed on the center of the absorption line, the resonance frequency can be determined with a BC-221 frequency meter which measures the beat frequency Δf between the marking oscillator and the nearest frequency marker from the standard. In this way, the absolute frequency can be determined within several hundred cycles, being limited only by the accuracy of the BC-221 meter. A TS-323 frequency meter is used as the marking oscillator and for rough frequency checks. Sometimes a Gertsch FM-3 frequency meter is good enough for the accurate frequency measurement in the region of the fundamental frequency of its searching oscillator. Since the frequency of the quadrupole resonance is sensitive to temperature, the sample temperature is kept constant within 0.1°C by a mercury contact thermostat.

TABLE I. Measurements of chlorine quadrupole resonances in different compounds.

Compound	Isotope	Temp. °C	Resonance freq. (Mc/sec)	Signal to noise	Half-intensity width (kc/sec)	Date of experiment
	Cl^{35}	27.4[a]	34.23324±0.00025	15	1.43	March 19, 1952
	Cl^{37}		26.97952±0.00025	5	1.40	
	Cl^{35}	16.9	34.29402±0.00025	12	1.38	March 17, 1952
Para-$C_6H_4Cl_2$	Cl^{37}		27.02771±0.00025	4	1.23	
(single crystal)	Cl^{35}	0.3	34.34609±0.00025	12		March 20, 1952
	Cl^{37}		27.06887±0.00025	4		
	Cl^{35}	−195	34.77540±0.00025	19	2.74	March 25, 1952
	Cl^{37}		27.40811±0.00025	4		
	Cl^{35}	25.5	19.17496±0.00050	10	2.28	April 1, 1952
	Cl^{37}		15.11125±0.00025	3		
strong lines	Cl^{35}	0.6	19.19916±0.00050	10	2.92	Feb. 26, 1952
	Cl^{37}		15.13058±0.00025	3		
	Cl^{35}	−195	19.30468±0.00050	12	3.56	March 28, 1952
$SbCl_3$	Cl^{37}		15.21522±0.00025	4		
(polycrystal)	Cl^{35}	25.5	20.40739±0.00050	4		April 1, 1952
	Cl^{37}		16.08146±0.00025	1.5		
weak lines	Cl^{35}	0.6	20.47433±0.00050	4		Feb. 26, 1952
	Cl^{37}		16.13457±0.00025	1.5		
	Cl^{35}	−195	20.90767±0.00050	4		March 28, 1952
	Cl^{37}		16.47790±0.00025	2		
p.c.[b]	Cl^{35}	23.8	29.92864±0.00050	9	0.57	July 25, 1952
	Cl^{37}		23.58894±0.00025	3	0.52	
$NaClO_3$ s.c.[b]	Cl^{35}	0.4	30.02468±0.00050	15	1.35	March 7, 1952
	Cl^{37}		23.66998±0.00025	4	1.13	
p.c.	Cl^{35}	−195	30.63017±0.00025	20	1.87	July 9, 1953
	Cl^{37}		24.14228±0.00025	4	1.07	
CH_3Cl	Cl^{35}	−195	34.02341±0.00025	8	5.44	April 17, 1952
(polycrystal)	Cl^{37}		26.81552±0.00025	2		
Trans-$C_2H_2Cl_2$	Cl^{35}	−195	35.9862±0.0008	8	2.6	Dec. 17, 1951
	Cl^{37}		28.3646±0.0008	2		

[a] High-temperature phase (sample heated over 40°C, cooled again). See C. Dean and R. V. Pound, J. Chem. Phys. **20**, 195 (1952).
[b] p.c. = polycrystal; s.c. = single crystal.

IV. CHLORINE SPECTRUM

A. General Aspects

Both of the stable chlorine isotopes (Cl^{35}, Cl^{37}) have a nuclear spin of $\frac{3}{2}$. Each isotope, therefore, has only one pure nuclear quadrupole transition. Results of measurements of these transitions in various molecules at different temperatures are tabulated in Table I. In general, these data are taken at three temperature points (room temperature, temperature of melting ice, and liquid nitrogen temperature). Although no attempt was made to measure the absolute temperature accurately, the relative temperature at each measuring point was kept constant within 0.1°C. The temperature coefficient of nuclear quadrupole resonance frequencies and the ratio, $(eQq)_{Cl^{35}}/(eQq)_{Cl^{37}}$, in different compounds are listed in Table II.[25]

The ratio of the magnetic moment of Cl^{35} to that of Cl^{37} is 1.2 and the ratio of their abundances 75.4/24.6, hence, the expected ratio of signal intensities[26] is 4.2

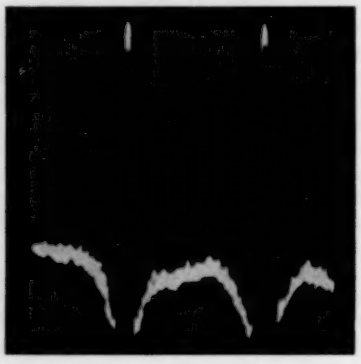

FIG. 8. Signal of pure quadrupole resonances of Cl^{35} in $NaClO_3$ at room temperature. (Double pips appear because of the vibrating condenser sweeping across the resonance frequency twice in one cycle.)

[25] Some preliminary results were published in reference 4.

[26] If one uses the Pound formula (reference 6) with some modification, the signal-to-noise amplitude ratio will be

$$\frac{A_s}{A_n}=\frac{V_0 Q_0 \gamma^{\frac{1}{2}} \eta^{\frac{1}{2}} \gamma N_0 \sin\theta \nu_0^{\frac{1}{2}} T^{*\frac{1}{2}} (I+m)(I-m+1)}{32kT_c(2I+1)(2\pi kT_c BFT_1)^{\frac{1}{2}}}$$

for the pure quadrupole resonances, where θ is the angle between the rf field and q. The ratio of signal intensities for the two isotopes should be proportional to the ratio of natural abundances, the ratio of magnetic moments, the $\frac{1}{2}$ power of the ratio of eQq's, and to the square root of the ratio of the (T_2^*/T_1) values.

to 1. This value is in rough agreement with the experimental values given in Table I. From Table I one may note that the line width increases with a decrease of temperature (from room temperature to liquid nitrogen temperature). This effect might be attributed to an increase of strains in crystals as the temperature of the sample was reduced.

B. Temperature Dependence

It has been shown in Fig. 3 that eQq and therefore the quadrupole resonance frequency will, in general, decrease with an increase of temperature. The experimental negative temperature coefficients of the resonances lines support this prediction. For *para*-chlorobenzene, since the molecular torsional vibrations are well known, the value of the frequency coefficient of the resonances of Cl^{35} as given by Eq. (6) can be easily calculated. At 16.9°C the predicted value of the fractional change in frequency per degree change in temperature is -7.11×10^{-5} whereas the experimental one is -9.16×10^{-5}. Equation (7) also predicts that the ratio $(eQq)_{Cl^{35}}/(eQq)_{Cl^{37}}$, should decrease with a decrease of temperature. The data given in Table II also agrees with this predicted variation. For the case of *para*-dichlorobezene, the calculated change in ratio, $(eQq)_{Cl^{35}}/(eQq)_{Cl^{37}}$, is -2.2×10^{-5} for a decrease of temperature from 289.9°K to 78°K, whereas the measured change is $-(4.7\pm1)\times10^{-5}$. This agreement of theory with experiment indicates that the thermal vibrations proposed by Bayer do play a major role in the temperature dependence of nuclear quadrupole interactions.

In antimony trichloride there are two pairs of resonance frequencies (for Cl^{35} and Cl^{37}), which have different dependence on temperature. From this observation, one may conclude that there are two nonequivalent sites for the chlorine atoms in the crystal lattices. The exact structure of this crystal is as yet not known. For sodium chlorate, the temperature variation of the ratio $(eQq)_{Cl^{35}}/(eQq)_{Cl^{37}}$, shows the same trend as other compounds, but with a considerable smaller magnitude. This might be attributed to the fact that the chlorine atoms are situated near the mass center of molecules, so that the isotopic effect on torsional vibrations is small.

C. Nuclear Polarization

In the earlier measurements of $(eQq)_{Cl^{35}}/(eQq)_{Cl^{37}}$, discrepancies of about two percent were found for different molecular environments. In an attempt to explain this effect, a theory of nuclear polarization by surrounding electric field was suggested.[27] Actually some of tne experimental data of earlier experiments contains errors whose magnitudes are comparable to the aforementioned discrepancies. The data of the present experiment, which have the probable error of about 0.001 percent, show that the variation of the ratio, $(eQq)_{Cl^{35}}/(eQq)_{Cl^{37}}$, is less than 0.024 percent and that it is dependent upon temperature as well as molecular environments (as shown in Table II). It has been pointed out in the last section that this variation of ratio, $(eQq)_{Cl^{35}}/(eQq)_{Cl^{37}}$, is to be attributed largely to molecular torsional vibrations. Moreover, the recent more accurate measurements of the ratio, $(eQq)_{Cl^{35}}/(eQq)_{Cl^{37}}$, in atomic chlorine by the atomic beam method (the ratio is 1.2686 ± 0.0004)[28] and in CH_3Cl (the ratio is 1.2685 ± 0.0002) and SiH_3Cl (the ratio is 1.2687 ± 0.0005) by the microwave absorption method[29] also supports the results of the present measurement. Therefore, it can be concluded that while nuclear polarization by electric field undoubtedly does exist, its effect on the present measured variations of ratio $(eQq)_{Cl^{35}}/(eQq)_{Cl^{37}}$ is largely masked by thermal vibrations.

D. Relaxation Time

In the present experiment, the spin lattice relaxation time T_1 is measured by the saturation of the rf field

TABLE II. Ratio $(eQq)_{Cl^{35}}/(eQq)_{Cl^{37}}$, and temperature coefficients of resonance lines of Cl in different compounds.

Compound	Isotope	Temp. °C	Temp. coef. of reson. freq. (kc/°C)	Ratio $\frac{(eQq)_{Cl^{35}}}{(eQq)_{Cl^{37}}}$
		27.4[a]		1.268860 ±0.00001
Para-$C_6H_4Cl_2$ (single crystal)	Cl^{35}	16.9	−3.14	1.268847
	Cl^{37}		−2.48	±0.00001
		0.3		1.268841 ±0.00001
	Cl^{35}	−195	−2.20	1.268800
	Cl^{37}		−1.74	±0.00001
$SbCl_3$ (polycrystal)	Cl^{35}	25.5	−0.972	1.268920
	Cl^{37}		−0.776	±0.00002
strong lines		0.6		1.268898 ±0.00002
	Cl^{35}	−195	−0.54	1.268774
	Cl^{37}		−0.43	±0.00002
	Cl^{35}	25.5	−2.69	1.269001
	Cl^{37}		−2.13	±0.00002
weak lines		0.6		1.268973 ±0.00002
	Cl^{35}	−195	−2.22	1.268831
	Cl^{37}		−1.76	±0.00002
	p.c.[b] Cl^{35}	23.8	−4.10	1.268757
	Cl^{37}		−3.25	±0.00002
$NaClO_3$	a.c.[b]	0.4		1.268739 ±0.00002
	p.c. Cl^{35}	−195	−3.10	1.268736
	Cl^{37}		−2.44	±0.00001
CH_3Cl (polycrystal)		−195		1.268795 ±0.00001
Trans-$C_2H_2Cl_2$		−195		1.26870 ±0.00006

[a] High-temperature phase.
[b] p.c. = polycrystal; a.c. = single crystal.

[27] Gunther-Mohr, Geschwind, and Townes, Phys. Rev. **81**, 289 (1951).

[28] V. Jaccarino and J. G. King, Phys. Rev. **83**, 471 (1951).
[29] R. L. White (private communication).

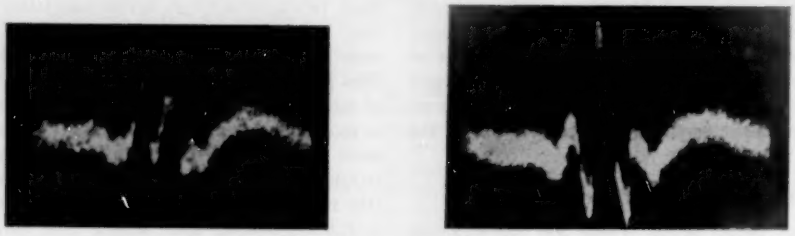

(a) (b)

FIG. 9. Zeeman splittings of pure quadrupole resonance line of Cl^{35} in a single crystal of $NaClO_3$. (a) and (b) indicate different orientation of magnetic field with the crystal.

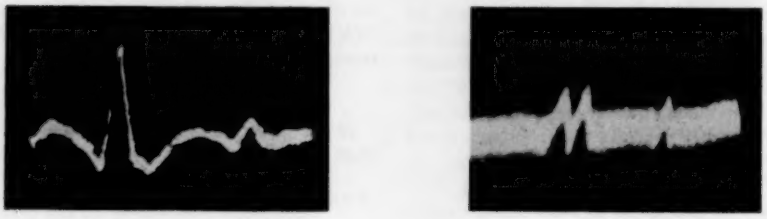

(a) (b)

FIG. 10. Resonance lines of Cl^{35} arising from coexistence of two different phases in a single crystal of *p*-$C_6H_4Cl_2$. (a) Resonance lines. (b) Zeeman splitting.

and the apparent transverse relaxation time T_2^* by the width of the resonance at half-maximum intensity. Results of measurements of these values at room temperature are given in Table III. The measurement of T_1 and T_2^* in $NaClO_3$ is in agreement with the results obtained from a measurements by the free-induction method.[30] The crystal structure of $NaClO_3$ was determined by Zachariasen.[31] This crystal has cubic structure with a unit cell 6.555 A on a side, containing four molemolecules. The Na−Cl distance given by Zachariasen's molecular structure is 1.59 A. However, from the position parameters of sodium and chlorine nuclei in the unit cell as given by the same author, this distance can be evaluated as 4.01 A. It is more likely that the latter value is correct, since the former gives too high a magnetic field at the chlorine nucleus due to the sodium nucleus.

E. Crystal Structure and Zeeman Effect

By introducing a weak magnetic field in the single crystal sample of sodium chlorate, Zeeman splittings of the resonance line of Cl^{35} were observed as shown in Fig. 9(a) and (b). These patterns are different for different orientation of the magnetic field within the crystal. Two Cl^{35} lines in Fig. 10(a) are due to the coexistence of the two phases of *para*-dichlorobenzene. This phenomenon occurs when a single crystal is heated above 40°C and then gradually cooled to room temperature. The interval between these two Cl^{35} lines as shown in Fig. (10a) is about 20 kc/sec. Figure 10(b) shows the difference of Zeeman splitting patterns of two different resonance lines. These differences indicate that the molecules of *para*-$C_6H_4Cl_2$ are oriented differently in the different phases of the crystal.

TABLE III. Measurements of relaxation time T_1 and T_2^*.

Compound	Isotope	T_1 seconds	T_2^* milliseconds
$NaClO_3$	Cl^{35}	0.039	0.56
	Cl^{37}	0.028	0.61
p-$C_6H_4Cl_2$	Cl^{35}	0.022	0.23

[30] E. L. Hahn and B. Herzog, Phys. Rev. **93**, 639 (1954).
[31] W. H. Zachariasen, Z. Krist. **71**, 517 (1929).

V. ANTIMONY SPECTRUM

A. General Discussion

Sb^{121} possesses a spin of 5/2 and Sb^{123} a spin of 7/2, therefore Sb^{121} has two pure quadrupole resonance transitions and Sb^{123} has three.[32] Results of measurements are tabulated in Table IV. Each set of five transitions in one compound was measured at a temperature which was held constant to within 0.1°C. Two sets of data were taken for each molecule at different temperature points. In the last column in Table IV, ν_3^{123}(calc) are values of ν_3^{123} as calculated from measured values of ν_1^{123} and ν_2^{123} from Eq. (4), while ν_3^{123}(meas'd) are experimental values. The $(eQq)_{Sb^{123}}/(eQq)_{Sb^{121}}$ ratio

[32] Pure quadrupole resonances of antimony isotopes in $SbCl_3$ were first observed by H. G. Dehmelt and H. Krüger, see Z. Physik **130**, 385 (1951).

TABLE IV. Measurements of antimony quadrupole resonances in different compounds.

Compound	Temp. °C	Isotope	Transition	Signal to noise	Resonance freq. (Mc/sec)	Half-intensity width (kc/sec)	eQq (Mc/sec)	Remarks (values in Mc/sec)	Date of experiment
$SbCl_3$ (single crystal)	31.07	Sb^{121}	ν_1^{121}	5:1	58.07831	5.18	376.90239	ν_2^{123}(calc) = 102.69226	Aug. 13, 1952
			ν_2^{121}	3:1	112.49849	8.07			
		Sb^{123}	ν_1^{123}	5:1	37.33261	5.32	480.45424	ν_2^{123}(meas'd) = 102.69037	
			ν_2^{123}	3:1	67.72563				
	0.8	Sb^{121}	ν_1^{121}	5:1	58.37421	7.08	378.27006	ν_2^{123}(calc) = 103.05003	Sept. 13, 1952
			ν_2^{121}	3:1	112.87532	5.53			
		Sb^{123}	ν_1^{123}	5:1	37.62624	6.13	482.19602	ν_2^{123}(meas'd) = 103.04629	
			ν_2^{123}	3:1	67.92500				
$SbBr_3$ (single crystal)	31.04	Sb^{121}	ν_1^{121}	5:1	48.35638	9.23	320.01353	ν_2^{123}(calc) = 87.35376	Nov. 6, 1952
			ν_2^{121}	5:1	95.87212	14.00			
		Sb^{123}	ν_1^{123}	3:1	29.84304	11.15	407.92664	ν_2^{123}(meas'd) = 87.35369	
			ν_2^{123}	3:1	58.05708				
	0.4	Sb^{121}	ν_1^{121}	5:1	48.65959	14.32	321.92938	ν_2^{123}(calc) = 87.87824	Nov. 28, 1952
			ν_2^{121}	5:1	96.44099	10.14			
		Sb^{123}	ν_1^{123}	3:1	30.04807	12.29	410.38583	ν_2^{123}(meas'd) = 87.87624	
			ν_2^{123}	3:1	58.39938	11.53			
Sb_2S_3 (single crystal)	30.75	Sb^{121}	ν_1^{121}	3:1	44.33480	9.89	295.54679	ν_2^{123}(calc) = 80.72903	June 5, 1953
			ν_2^{121}	3:1	88.66300				
		Sb^{123}	ν_1^{123}	3:1	26.91568		376.73771	ν_2^{123}(meas'd) = 80.72829	
			ν_2^{123}	2:1	53.81785				
	0.2	Sb^{121}	ν_1^{121}	5:1	44.80731	11.16	298.69326	ν_2^{123}(calc) = 81.59109	June 24, 1953
			ν_2^{121}	3:1	89.60674				
		Sb^{123}	ν_1^{123}	3:1	27.20256		380.70651	ν_2^{123}(meas'd) = 81.58955	
			ν_2^{123}	2:1	54.39268				

and the field asymmetry parameter η are given in Table V.

In general, signals of these antimony resonances are found to be much weaker than those of chlorine resonances. In order to cover the required frequency range, different coils were used and the signal to noise ratio for each line is given in Table IV. Observations of ν_1^{121} and ν_2^{123} were made with the same rf coil. The ratio of natural abundances of Sb^{121} and Sb^{123} is 56/44 and the ratio of their magnetic moments (3.3595)/(2.5470); therefore the theoretical estimated ratio of signal intensities between ν_1^{121} and ν_2^{123} is about 5:3. This value is in good agreement with the experimental values in Table IV. All line widths of the antimony resonances are considerably greater than those of the chlorine resonances. The probable explanation for this broadness lies in the fact that the stronger quadrupole interaction of antimony nuclei shortens the relaxation time.

Single crystals of $SbCl_3$ and $SbBr_3$ used in this experiment were grown in the laboratory, whereas the single crystals of Stibnite (Sb_2S_3) were natural ones.

B. Quadrupole Coupling Constants and Ratios

The temperature dependence of the quadrupole coupling constants of antimony has the same tendencies as those of chlorine; namely an increase of temperature is associated with a decrease of quadrupole coupling constants as shown in Table IV. In Table V, one may note that the ratio, $(eQq)_{Sb^{123}}/(eQq)_{Sb^{121}}$, varies only by 0.005 percent with temperature and with different molecular environments. This small change in the ratio of (eQq) between two antimony isotopes may be attributed to the greater mass of antimony which makes them less sensitive to thermal vibrations. The lack of

TABLE V. Ratio of eQq's and asymmetry parameter, η, of antimony isotopes in different compounds.

Compound	Temp. °C	Isotope	η, asymmetry parameter	Ratio $\frac{(eQq)_{123}}{(eQq)_{121}}$
$SbCl_3$ (single crystal)	31.07	Sb^{121}	±0.15919	1.274744
		Sb^{123}	±0.15923	±0.00001
	0.8	Sb^{121}	±0.16357	1.274740
		Sb^{123}	±0.16354	±0.00001
$SbBr_3$ (single crystal)	31.04	Sb^{121}	±0.08236	1.274717
		Sb^{123}	±0.08217	±0.00001
	0.4	Sb^{121}	±0.08393	1.274770
		Sb^{123}	±0.08363	±0.00001
Sb_2S_3 (single crystal)	30.75	Sb^{121}	±0.0076	1.274714
		Sb^{123}	±0.0077	±0.00001
	10.2	Sb^{121}	±0.0082	1.274754
		Sb^{123}	±0.0073	±0.00002

variation in the coupling ratio $(eQq)_{Sb^{123}}/(eQq)_{Sb^{121}}$ affords no evidence of nuclear polarization for those nuclei. The temperature dependence of this ratio has the same sign as that for the chlorine isotopes, that is the ratio of eQq of the lighter isotope to that of the heavier isotope decreases with a decrease of temperature. The only exception was in the case of $SbCl_3$, in which the ratio, $(eQq)_{Sb^{123}}/(eQq)_{Sb^{121}}$, was found to be constant to within four parts in one million. This variation is less than the probable experimental error.

C. Field Asymmetry Parameter

Values of the field asymmetry parameter, η, as obtained from measurements are shown in Table V. The spins of Sb^{121} and Sb^{123} are different, consequently their energy levels are different. Measurements show that η^{121} and η^{123} agree exceedingly well, especially for $SbCl_3$ which indicates the high consistency of the experimental data. However, a small disagreement (in general less than 0.3 percent in magnitude of η) exists between η^{121} and η^{123}. This difference may be due to the isotopic effect on the thermal vibrations. Moreover, one may note in Table V, that values of η for both isotopes change with temperature as might be expected from effects of thermal vibrations. The frequency, ν_3^{123}, calculated from η_{123} and $(eQq)_{Sb^{121}}$ which are obtained from ν_1^{123} and ν_2^{123} by Eq. (4), shows a disagreement of only several parts in one hundred thousand with the measured ν_3^{123}. The errors (which are evaluated from experimental errors in ν_1^{123} and ν_2^{123}) in ν_3^{123} as calculated by Eq. (4) is less than one kc/sec, and the error of the measured frequency ν_3^{123} is even smaller (about 300 cps). This discrepancy is, in general, two or three times larger than is to be expected. A possible explanation will be given in the next section.

D. Effect of Hexadecapole Interactions

The discrepancy pointed out in the last section is very interesting. It cannot be due to polarization of the nucleus by surrounding electronic charges, since Gunther-Mohr, Geschwind, and Townes[27] have shown that the energy connected with nuclear polarization depends on angle in the same way as that due to quadrupole interactions.

It was shown above (Sec. II-D), that the ratio between the magnitudes of the electric hexadecapole coupling constant and the electric quadrupole coupling constant for an atom is of the order of r_n^2/r_{atl}^2. In the present case, r_n^2, as determined either from the magnitude of their quadrupole moments or from the well-known formula for nuclear radii is about 10^{-24} cm^2 for the antimony isotopes. The valence electrons of antimony are in a $5p$-orbital which may be hybridized with $5d$-orbitals. The $5d$-electrons will be responsible for the hexadecapole field m_{16}. A simple calculation using hydrogenic wave functions shows that $1/r_{atl}^2 > (1/10^{-19})$ cm^{-2} for a Sb $5d$-electron. Therefore, the ratio $(eM_{16}m_{16})/eQq$ is about 10^{-5} for antimony isotopes. This is the same order of magnitude as the discrepancy mentioned above.

The set of data on the quadrupole resonances in $SbBr_3$ at 0.4°C was taken with a great deal of care. By using Eq. (4) and Eq. (12), the constants of Sb^{123} can be evaluated as

$$|(eQq)_{Sb^{123}}| = 410.3814 \text{ Mc/sec},$$
$$\eta^{123} = \pm 0.0836145,$$
$$|(eM_{16}m_{16})_{Sb^{123}}| = 24.0 \pm 5 \text{ kc/sec}.$$

The results of the calculation indicates that $(eM_{16}m_{16})_{Sb^{123}}$ is opposite in sign to $(eQq)_{Sb^{123}}$. The ratio $(eM_{16}m_{16})_{Sb^{123}}/(eQq)_{Sb^{123}}$ is about 10^{-5} which agrees fairly well with the theoretical estimate given above.

One may assume that the asymmetry parameter η for Sb^{121} is 0.0836145, the same as for Sb^{123} at the same temperature. Substituting this η and the measured values of ν_1^{121} and ν_2^{121} given in Table IV into Eq. (3) and Eq. (11) and solving for $(eQq)_{Sb^{121}}$ and $(eM_{16}m_{16})_{Sb^{121}}$, one obtains

$$|eQq_{Sb^{121}}| = 321.93223 \text{ Mc/sec},$$
$$|(eM_{16}m_{16})_{Sb^{121}}| = 30.3 \pm 5 \text{ kc/sec}.$$

As in the case of Sb^{123}, $(eM_{16}m_{16})_{Sb^{121}}$ and $(eQq)_{Sb^{121}}$ are opposite in sign. Similarly, the ratio $(eM_{16}m_{16})_{Sb^{121}}/(eQq)_{Sb^{121}}$ is of the order of 10^{-5}. Furthermore, by taking the ratio, one obtains:

$$\frac{(eQq)_{Sb^{121}}}{(eQq)_{Sb^{121}}} = 1.274745 \pm 0.00001,$$

$$\frac{(eM_{16}m_{16})_{Sb^{123}}}{(eM_{16}m_{16})_{Sb^{121}}} = 0.8 \pm 0.3.$$

One might think that the discrepancy pointed out in Sec. V-C, arose from second order perturbations due to the nuclear quadrupole interaction with the valence electrons or with thermal vibrations. However, simple calculations will show that these effects are too small to explain the present discrepancy.

The second order perturbation of electronic states by the quadrupole interaction will give the energy shift

$$\Delta W_s = -\sum_{n'l'm'} \frac{(eQq_{n'l'm'nlm})(eQq_{n'l'm'nlm})}{E_{n'l'm'} - E_{nlm}},$$

where n', l', m' and n, l, m are quantum numbers which signify different electronic states of energy $E_{n'l'm'}$ and E_{nlm}. It has been pointed out by Townes[1] that $q_{n'l'm'nlm}$ are zero unless $m=m'$, $l=l'\mp 0$ or $l=l'\pm 2$. A good approximation is that $q_{n'l'm'nlm}$ is about one tenth of q (q_{nlmnlm}) for p-electrons and $eQq/(E_{n'l'm'} - E_{nlm})$ is about 10^{-6}, so that ΔW_s will be 10^{-6} eQq.

The effect of second-order perturbation of thermal vibrations by the quadrupole interaction can be cal-

culated by assuming simple harmonic vibrations, with the Hamiltonian

$$H_{\text{vib}}=\frac{P_\theta^2}{2I_\theta}+\frac{K\theta^2}{2},$$

where P_θ is the angular momentum, θ the angular amplitude of the vibration, I_θ the moment of inertia around the angular vibration axis, and K the torsional force constant. Hence, the vibration frequency will be $\omega_\tau=(K/I_\theta)^{\frac{1}{2}}$. The perturbation energy due to the quadrupole interaction is

$$H_Q'=\tfrac{1}{4}eQq(3\cos^2\theta'-1),$$

where $\theta'=\theta_I+\theta$, and θ_I is the angle between nuclear spin and the axis of symmetry of the electric gradient q. By the addition theorem for Legendre polynomials and using $\sin^2\theta\simeq\theta^2$ (for small θ), the perturbing Hamiltonian becomes

$$H_Q'=\tfrac{1}{4}eQq(3\cos^2\theta_I-1)(1-\tfrac{3}{2}\langle\theta^2\rangle_{\text{Av}}),$$

where $\langle\theta^2\rangle_{\text{Av}}$ indicates the average value of θ^2 under thermal vibrations.

Using the quantum-mechanical matrix elements for a simple harmonic oscillator, one obtains the first-order perturbation energy as,

$$\Delta W_1=-\tfrac{3}{8}eQq(3\cos^2\theta_I-1)(n+\tfrac{1}{2})\hbar/(I_\theta K)^{\frac{1}{2}},$$

where n is the vibration quantum number. The effect of this term is linear in $(3\cos^2\theta_I-1)$, so it will not change the interval rule of the nuclear quadrupole energy levels. This result is in agreement with Eq. (5).

The energy term due to the second-order perturbation is

$$\Delta W_2=\frac{9}{256}(eQq)^2(3\cos^2\theta_I-1)^2\frac{(2n+1)\hbar}{\omega_\tau I_\theta K}.$$

This energy depends on $(3\cos^2\theta_I-1)^2$, so it will give rise to a pseudo-hexadecapole effect. Taking $n=1$ for the first excited state, one obtains

$$\Delta W_2=\frac{27}{256}(eQq)(3\cos^2\theta_I-1)^2\frac{eQq}{\omega_\tau}\frac{\hbar}{I_\theta K}.$$

Substituting the appropriate molecular constants in the foregoing equation and simplifying, one obtains

$$\Delta W_2/h=5\times10^{-9}(eQq/h)(3\cos^2\theta_I-1)^2.$$

E. The Relation of Quadrupole Resonance to the Crystal Structure of Anitmony Compounds

The structure of stibnite, Sb_2S_3, has been determined.[33] It is known that the crystal forms a prolonged chain of indefinite length in a direction parallel the surfaces of cleavage. Each antimony atom is bonded to three sulfur atoms in a plane parallel to the chain axis. There are auxilliary Sb−S bonds existing in the crystal, which do not contribute considerably to the eQq of antimony. It is obvious that the field gradient q's for antimony atoms are in directions perpendicular to the chain axis. When the crystals were placed with their chain axis parallel to the rf coil axis (direction of the rf magnetic field), signals of pure quadrupole resonances due to antimony were observed with fairly good intensity. After the crystals were reorientated, with the chain axis perpendicular to the rf field, the signal disappeared. This behavior is to be expected from a theoretical consideration which shows that the signal intensity should vary with the sine of the angle between the rf field and the field gradient q.

Stibnite melts at 550°C. Crystals were heated to 450°C in an oven, then left there to anneal. When these annealed crystals were used as samples, the signal intensity was doubled. This effect indicates that the stibnite crystals were under some tension which was removed by annealing. When this is done, the field gradient q becomes more uniform and the signal strength is increased.

The very large asymmetry parameter η found in $SbCl_3$ and $SbBr_3$ indicates some type of intermolecular bonding in these crystals as has been shown to occur in I_2.[2] The two different sets of Cl resonances in $SbCl_3$ are probably also connected with intermolecular bonds.

ACKNOWLEDGMENTS

The author would like to thank Dr. V. W. Cohen of Brookhaven National Laboratory for the loan of the TS-323 frequency meter used as a marking oscillator. He also wishes to express his gratitude to Professor C. H. Townes for his guidance and encouragement during the experiment.

[33] W. Hofmann, Z. Krist. **86**, 225 (1933).

New Approach to Nonequilibrium Processes*

PETER G. BERGMANN AND JOEL L. LEBOWITZ
Department of Physics, Syracuse University, Syracuse, New York
(Received March 23, 1955)

In this paper we propose a new model for the description of irreversible processes, which permits the construction of a Gibbs-type ensemble and the employment of the general techniques of statistical mechanics. The internal dynamics of the system that is engaged in the process is assumed to be described fully by its Hamiltonian. Its interaction with the driving reservoirs is described in terms of impulsive interactions (collisions). The reservoirs themselves possess definite temperatures, are inexhaustible, and free of internal gradients. The ensemble obeys an integro-differential equation in Γ space, containing both the terms of the Liouville equation and a stochastic integral term that describes the collisions with the reservoirs. It is shown in this paper (1) that the ensemble will approach canonical distribution in the course of time in the presence of a single driving reservoir, (2) that it will approach a stationary nonequilibrium distribution in the presence of several reservoirs at different temperatures, and (3) that in the latter case, and for small temperature differences, Onsager's reciprocal relations are satisfied by the stationary distribution.

1. INTRODUCTION

THE purpose of this paper is to propose a statistical-mechanical model for nonequilibrium processes that leads naturally to the existence of a stationary state, approached by an ensemble in the course of time, which is independent of the initial ensemble distribution. In the stationary state, the ensemble is not in thermodynamic equilibrium. It remains in its state only because its surroundings maintain gradients inside the thermodynamic system; in the simplest case, these are temperature gradients.

In statistical mechanics, the concept of temperature is based on the canonical distribution with respect to the energy of the whole system. If the ensemble is not canonical, temperatures may still be definable on canonical or quasi-canonical distributions of partial energies; we speak of local temperature, kinetic temperature, temperature of the nuclear spins, etc. The first pioneering work in the theory of irreversible processes was based on the assumption that such partial temperatures could be defined significantly.[1,2] Other workers succeeded in formulating general rules by adopting modified versions of Boltzmann's assumptions: That is that certain fluctuating variables are always statistically uncorrelated to each other.[3] Later refinements of Boltzmann's "Stosszahlansatz," in which the single-particle occupation numbers are assumed to be uncorrelated, make similar assumptions about higher (n-particle) distribution functions.[3] None of these theories clarifies completely the nature of irreversibility of a process which in its internal dynamics obeys deterministic laws of motion. Some of the assumptions made, i.e., Boltzmann's original assumptions, are demonstrably inconsistent with the classical laws of motion. It appeared impossible, with a closed system, to overcome Zermelo's classical argument, either in classical or in quantum mechanics, according to which the solutions of Liouville's equation are either periodic or almost periodic and, hence, cannot exhibit true irreversibility.[4] The argument that Poincaré cycles have such enormous periods that in practice they cannot be observed is not wholly unsatisfactory. Nevertheless, the fact that a Poincaré cycle may be longer than the total period since the development of the present physical universe (10^9 to 10^{10} years) does not entitle us to the positive conclusion that the specific assumptions made by various workers[2,3] will lead to valid approximations for realistically observable periods of time.

The most satisfactory approach, so it appears to us, is to construct models that permit treatment in terms of Gibbs-type ensembles, in which the openness of the system, and with it the possibility of true irreversible behavior, is explicitly introduced. Klein and Prigogine have considered such a model,[5] which represents a perfect one-dimensional crystal. In this model the mean free path of phonons is infinite; hence there can be no internal gradient. The spectral distribution of phonons is everywhere the same; hence the Klein-Prigogine model does not lend itself to a study of internal gradients and internal dissipation. Our paper will present a new and somewhat more general attempt to construct a system that interacts with its surroundings, in such a fashion that Gibbsian ensembles can be constructed; their development in the course of time, i.e., their dynamics, becomes the subject of mathematical investigation.

For a truly stationary process to be possible, the reservoirs that maintain the gradients within the system must be inexhaustible. They must possess an infinite

* This work was supported by the Office of Scientific Research, Research and Development Command, United States Air Force.

[1] L. Onsager, Phys. Rev. **37**, 405 (1931); **38**, 2265 (1931).

[2] For other authors who have used similar approaches leading essentially to macroscopic (phenomenological) laws, see E. W. Montroll and M. S. Green, Ann. Rev. Phys. Chem. **5**, 449 (1954). The same review article also contains an extensive bibliography of work based on different approaches, *viz.*, kinetic theory, Markov chains, etc.

[3] M. Born and H. S. Green, *A General Kinetic Theory of Liquids* (Cambridge University Press, Cambridge, 1949); J. G. Kirkwood, J. Chem. Phys. **14**, 180 (1946); **15**, 72 (1947).

[4] P. and T. Ehrenfest, Encykl. d. Math. Wiss. **4**, 2ii, September, 6 (1911).

[5] G. Klein and I. Prigogine, Physica **19**, 74, 89 (1953).

number of degrees of freedom, in such a manner that they present to the system to be considered always the same appearance. Hence their canonical coordinates cannot be fully included in the description of the process in phase space (or in Hilbert space, in a quantum description). What should be included is the (fluctuating) interaction between system and reservoirs. Again, if in this interaction we disregard the effects of fluctuations, i.e., if we simply add to the internal Hamiltonian of the system the interaction energy with the reservoirs, averaged at each point of system-phase space over the possible values of the reservoir coordinates, then the resulting Liouville equation in system-phase space will not differ from one with fixed external forces, and no disspation will result.

How, then, is the action of the reservoir(s) to be introduced? There appear to be two possibilities. They represent, respectively, continuous and impulsive interaction. In both it is assumed that any part of the surroundings that will interact with the system will be statistically independent of the state of the system at the beginning of such interaction. But once the interaction has begun, the statistical independence will be lost; in fact one can show that with a continuous interaction Hamiltonian the correlation function between system and reservoir(s) satisfies a number of differential equations that preclude continued statistical independence. At any instance the interaction term in the Hamiltonian will depend on the previous history. We have been unable as yet to discover a simple mathematical scheme that would represent such finite interaction.

The second possibility is to treat the interaction impulsively. If the reservoir interacts for brief spans of time only, but then strongly, it may be assumed that the net effect of such impulsive interaction will be to move the representative point in system-phase space a finite distance, that depends both on its original location and on the state of the reservoir just prior to interaction. If we further simplify the reservoir by assuming that it consists of a sensibly infinite number of disconnected and similar parts, that each such part interacts with the system but once, and that prior to interaction there is statistical independence between that reservoir component and the system, then we can average over the possible states of the reservoir (i.e., of that portion of the reservoir about to interact impulsively with the system). The result of this averaging operation will be the determination of a contingent probability $K(x',x)dx'dt$, which tells us the probability that the representative point of the system, known to be at the location x (in system-phase space) will be thrown into the volume element dx' (a finite distance from x) within the time interval dt. Once we know the function K, then the Liouville equation for the probability density μ in system-phase space will take the form

$$\frac{\partial\mu(x,t)}{\partial t}+(\mu,H)_x = \int_{x'}[K(x,x')\mu(x')-K(x',x)\mu(x)]dx'. \quad (1.1)$$

The remainder of this paper will be concerned with an investigation of the structure of the function K (Sec. 2), with the approach toward thermal equilibrium in the presence of a single reservoir at a definite temperature (Sec. 3), with a proof that in the presence of several reservoirs ensembles obeying Eq. (1.1) approach a stationary state in the course of time (Sec. 4), and with the Onsager reciprocal relations (Sec. 5).

Before we enter these somewhat more detailed discussions, it may be in order to justify further the form of Eq. (1.1). We are well aware of the fact that impulsive interaction represents an asymptotic limit, which is not always realistic. But it is possible to construct model interactions that approach this limit arbitrarily closely. By assuming this particular form of interaction, and by suppressing the influence that the several components of the reservoir exert on each other, we are able to introduce into the mathematical formulation the notion of the inexhaustible reservoir. We need not neglect recoil (i.e., the reaction of the system back on the reservoir); and we are able to maintain the reservoirs at definite temperatures (or other thermodynamic potentials) without allowing for thermal or other gradients within the reservoirs.

2. STOCHASTIC KERNEL

The expression $K(x',x)$ in Eq. (1.1) represents a transition probability density in the phase space of the system. It is a so-called contingent probability, dealing with the rate of transitions from the state x to the state x' (we shall always write the arguments of such transitions going from right to left) on the assumption that the system is known to be initially in the state x. Hence the value of K will be independent of the probability distribution of the ensemble of systems in the system phase space.

The likelihood of such a transition will depend on the distribution of the reservoir (or reservoir components) as well as on the intrinsic probability of a collision (something like the collision cross section) if both system and reservoir are known to be in suitable states for a collision of the type considered. We shall have to consider both these factors.

As for the distribution of the reservoir, we shall consider it as part of the basic concept of reservoir that its parts are in a canonical distribution, characterized by a definite temperature. Considering the components of such a reservoir in their own phase space (i.e., the phase space of any one of the infinitely many identical reservoir components, usually called the μ space of

such a composite), we may write this distribution in the standard form

$$\mu_r = \frac{1}{Z_r} e^{-E_r/kT} = \frac{1}{Z_r} e^{-\beta E_r}. \tag{2.1}$$

The subscript r indicates that these quantities belong to a reservoir component (and not to our system).

Next, we come to the much more delicate problem of the intrinsic reaction constant (or collision cross section). All microscopic laws, both classical and quantum theoretical, are reversible with respect to the direction of time. That is to say, there exists a transformation involving (in a suitable coordinate system) a change in the signs of the time coordinate and of all the momentum coordinates with respect to which these laws are invariant. In classical mechanics, the Hamiltonian is an even function of the canonical momentum components; in quantum mechanics (in a wave mechanical representation), the same transformation is accomplished if we change the sign of the time coordinate and at the same time replace the wave function by its complex conjugate. Hence, under this transformation the Hamiltonian remains the same function of its arguments. Each point of phase space (or of Hilbert space) is mapped on another point. We shall denote this mapping or transformation by a bar: $x \to \bar{x}$. Given a point in classical phase space with the coordinates x (standing for both q_k and p_k), there will be a point $\bar{x}$. If a trajectory in phase space is given by the function $x(t)$, then $\bar{x}(-t)$ is a trajectory, also consistent with the equations of motion.

Microreversibility must also apply to the impulsive interactions between system and reservoir. If a certain initial state of the system x_s and initial state of the reservoir x_r go over into a final state x_s', x_r' through discontinuous impulsive interaction, then the initial state $\bar{x}_s'$, $\bar{x}_r'$ must go over into the final state $\bar{x}_s$, $\bar{x}_r$ by means of the exactly reversed impulsive interaction, and the cross sections for these two corresponding processes must be equal. We may assume that the energy of the reservoir component associated with the point x_r equals the energy associated with the point $\bar{x}_r$, and likewise the energies at the two points x_r' and $\bar{x}_r'$ equal each other. We may, therefore, conclude that the ratio between the transition rates from x to x' and from $\bar{x}'$ to $\bar{x}$, (contingent on the initial state of the system but not on that of the reservoir) equals $\exp[\beta(E_r'-E_r)]$, because of Eq. (2.1). But impulsive interactions conserve the energy; hence the difference in reservoir energies equals the negative difference in system energies. Accordingly, we shall find that the ratio of the contingent proabilities of transition of the system from x_s to x_s' and transition from $\bar{x}_s'$ to $\bar{x}_s$ equals $\exp[\beta(E_s-E_s')]$,

$$K(x',x) = e^{\beta(E_r-E_s')} K(\bar{x},\bar{x}'), \quad E_s = \bar{E}_s, \quad E_s' = \bar{E}_s'. \tag{2.2}$$

This result appears unexceptionable, but it is insufficient to achieve our purpose. We have, therefore, gone one step further and assumed that microreversibility (i.e., equal cross sections) holds not only for the transition from x to x' and the "properly reversed" transition $\bar{x}'$ to $\bar{x}$, but also for the "directly reversed" transition x' to x. This additional assumption is sufficient to assure the monotonic decrease of the Helmholtz potential of a system in thermal contact with a single temperature reservoir until the ensemble of systems becomes canonical. However, our assumption may not be necessary for this result to hold. In fact though one can conceive of many forms of interaction in which the strengthened form of symmetry between a transition and its "direct reverse" holds, because of some special *geometric* symmetry of the model, it appears likely that the assumption made in this paper will have to be generalized, i.e., weakened, so that the approach proposed here is applicable to a wider class of models and phenomena. This possibility is now being investigated.

In what follows we shall accept the strongest form of symmetry of interaction, that is to say, equality between the cross sections of any transition and its direct reverse. If there are several reservoirs present, each with its own peculiar coupling to the system, then the kernel K of Eq. (1.1) will be the sum of such individual kernels K_a,

$$K = \sum_a K_a, \tag{2.3}$$

each representing the effects of one (the ath) reservoir. The kernel K_a will correspond to both the requirements of strong microreversibility (equality between the cross sections of direct reverses) and of canonical distribution of each reservoir. It will satisfy the equality:

$$\begin{aligned} K_a(x,x') &= e^{\beta_a[H(x')-H(x)]} K_a(x',x), \\ K_a(x,x') &= e^{\beta_a H(x')} L_a(x,x'), \quad L_a(x,x) = L_a(x'x) \geqslant 0. \end{aligned} \tag{2.4}$$

This condition on the stochastic kernel introduced into the Liouville equation (1.1) represents the point of departure of this paper. In the next section we shall show that with only one reservoir present the assumption (2.3) brings about the monotonic approach of the system governed by Eq. (1.1) toward the canonical distribution.

3. APPROACH TO THERMAL EQUILIBRIUM

We shall first consider an ensemble of systems each of which is in thermal contact with a reservoir at a definite temperature T. In that case the Liouville equation (1.1), with (2.4), assumes the form

$$\frac{\partial \mu}{\partial t} + (\mu, H) = \int_{x'} [e^{\beta H(x')} \mu(x') - e^{\beta H(x)} \mu(x)] L(x,x') dx'. \tag{3.1}$$

We shall now examine the solutions of this integro-differential equation with arbitrary initial conditions.

Of course, we cannot require that the entropy of the system will always increase as a result of its interaction with the reservoir. After all, energy is being exchanged; depending on initial conditions, it is quite possible that the system on the average transfers energy to the reservoir. We shall show, instead, that as the result of the interaction the total entropy, i.e., the sum of the entropies of the system and the reservoir, will increase. True, we have no detailed description of the reservoir. But as our reservoir is inexhaustible and, at the same time, possesses a definite temperature, it is to be assumed that the change in its entropy equals the amount of energy transferred to it, divided through by its absolute temperature. In other words, the rate of change of total entropy equals

$$dS_{\text{total}}/dt=\sigma=\dot{S}-k\beta\dot{U}. \tag{3.2}$$

Of course, the Hamiltonian of the system is assumed to be explicitly time-independent, i.e., no work is being performed on the system.

Our conjecture is, then, that the quantity $(S-k\beta U)$ will increase monotonically with time. If we multiply this expression by T and reverse the sign, we obtain the Helmholtz potential F,

$$F=U-ST=\int\mu(H+\beta^{-1}\ln\mu)dx, \tag{3.3}$$

which is to decrease monotonically in the course of time. We shall now proceed to prove this assertion.

The form of Eq. (3.1) suggests that instead of the variable μ we introduce ν,

$$\nu=\mu e^{\beta H}. \tag{3.4}$$

In terms of ν, Eqs. (3.1) and (3.3) read

$$\frac{\partial\nu}{\partial t}+(\nu,H)=e^{\beta H}\int_{x'}[\nu(x')-\nu(x)]L(x,x')dx',$$
$$F=\beta^{-1}\int_x e^{-\beta H}\nu\ln\nu dx, \tag{3.5}$$

respectively. The time derivative of the Helmholtz potential then becomes

$$\dot{F}=\beta^{-1}\int_x e^{-\beta H}(\ln\nu+1)\dot{\nu}dx$$
$$=\beta^{-1}\int_x\int_{x'}[\ln\nu(x)+1][\nu(x')-\nu(x)]L(x,x')dx'dx$$
$$+\beta^{-1}\int_x e^{-\beta H}(\ln\nu+1)(H,\nu)dx. \tag{3.6}$$

It can be shown immediately that the second integral on the right-hand side vanishes. We make use of the fact that the integral over a Poisson bracket can be converted into a surface integral through integration by parts and hence vanishes when extended over the whole phase space, provided only the variables under the integrand satisfy reasonable boundary conditions (the analogous statement in quantum mechanics is that the trace of a commutator vanishes). All we need to do then is to carry out the obvious transformation of the integrand

$$e^{-\beta H}(\ln\nu+1)(H,\nu)=((\ln\nu+1)H,e^{-\beta H}\nu)$$
$$=((\ln\nu+1)H,\mu), \tag{3.7}$$

and the desired result follows as a matter of course. The rate of change in the Helmholtz potential is therefore determined wholly by the first integral on the right-hand side of Eq. (3.6). By interchanging the role of the two sets of variables of integration, x and x', and by adding the resulting expression to the original form of the integral, we obtain this expression for

$$\dot{F}=(2\beta)^{-1}\int_x\int_{x'}[\ln\nu(x)-\ln\nu(x')]$$
$$\times[\nu(x')-\nu(x)]L(x,x')dxdx' \tag{3.8}$$
$$\leqslant 0.$$

The integrand on the right is manifestly negative-definite. Thus we have shown that the Helmholtz potential is bound to decrease with time. This decrease will be nonzero as long as there is any stochastic interchange between any two regions in phase space at which the ratio of the densities has not yet assumed the canonical value corresponding to the temperature $T=(\beta k)^{-1}$.

It remains to be shown that the Helmholtz potential assumes its absolute minimum for this canonical distribution. To examine the expression (3.3) for minima, we form its variation,

$$\delta F=\int\left[H+\frac{1}{\beta}(\ln\mu+1)\right]\delta\mu dx, \tag{3.9}$$

but subject to the restriction that the variations are not to violate the normalization requirement,

$$\int\delta u dx=0. \tag{3.10}$$

It follows that the only distributions stationary with respect to the variation (3.9), (3.10) are proportional, and therefore equal, to the canonical distribution. We can form the second variation as well, in order to determine whether the stationary solution represents a maximum, minimum, or saddle point. We have

$$\delta^2F=\int[(H+\beta^{-1}\ln\mu)\delta^2\mu+\beta^{-1}(\delta\mu)^2]dx$$
$$=\beta^{-1}\int[(\delta\mu)^2-\ln Z\delta^2\mu]dx \tag{3.11}$$
$$=\beta^{-1}\int(\delta\mu)^2dx>0.$$

The absence of any additional stationary solutions guarantees that the canonical distribution is not only a relative but the absolute minimum. The value of this minimum is, of course $F=-\beta^{-1}\ln Z$.

Our conclusion is, then, that the Helmholtz potential decreases monotonically in the course of time and that its absolute minimum corresponds to the canonical distribution at the temperature of the (single) reservoir. This result is not quite equivalent to the assertion that the canonical distribution is reached asymptotically. It is possible, first of all, that certain regions of phase space do not interact with each other through the stochastic kernel. Such a contingency is equivalent to the existence of quantities that are absolute constants of the motion, in the sense that they change their value neither under the influence of the internal forces nor under the impact of collisions with the surroundings. Such absolute constants of the motion are known, e.g., the symmetry character of the wave function with respect to indistinguishable particles in quantum mechanics. The existence of such absolute constants of the motion will make it possible to subdivide the phase space into invariant subspaces, each of which is ergodic with respect to the motion of Eq. (3.1).

Another possibility is that the stochastic kernel L converges to zero near certain points or regions and that there is insufficient non-stochastic flux into them, (see the discussion at the end of Sec. 4). This possibility is well known in a special case, namely the interaction of a Knudsen gas with the walls. Molecules of very low velocity take a long time to reach the wall. If the number of collisions per second drops too rapidly with velocity, then the approach to canonical distribution will not be uniform or even certain. Apart from these two possibilities, our system will approach the canonical distribution.

4. APPROACH TO STATIONARY NONEQUILIBRIUM STATES

In this section we shall prove that for a wide class of kernels $K(x,x')$ the distribution $\mu(x,t)$ will approach asymptotically some stationary distribution $\mu_s(x)$, which is independent of the initial distribution $\mu(x,0)$,

$$\lim_{t\to\infty}\mu(x,t)=\mu_s(x). \tag{4.1}$$

Our proof will be based on a general theorem by Doeblin,[6,7] which applies to all Markoffian processes.

If the initial distribution of the ensemble in phase space corresponds to a definite location, at the point x',

$$\mu(x,0)=\delta(x-x'), \tag{4.2}$$

we shall denote the distribution at any subsequent time t by the symbol $P(x,x'/t)$. For an arbitrary initial distribution $\mu(x,0)$, we then have

$$\mu(x,t)=\int_\Gamma P(x,x'/t)\mu(x',0)dx', \tag{4.3}$$

$$P(x,x'/t)\geq 0,\quad \int_\Gamma P(x,x'/t)dx=1,\quad t\geq 0. \tag{4.4}$$

The probability that at the time t the system will be in some particular region in phase space A (i.e., A might be the region between two energy surfaces E_1 and E_2) will be denoted by $\mu(A,t)$; it is given by

$$\mu(A,t)=\int_A \mu(x,t)dx=\int_\Gamma P(A,x'/t)\mu(x',0)dx'. \tag{4.5}$$

The integral

$$P(A,x'/t)=\int_A P(x,x'/t)dx \tag{4.6}$$

represents the (contingent) probability that a system, initially at the point x', will be found in the domain A at the time t. It is usually called a transition probability. Obviously $P(\Gamma,x'/t)=1$ for all t. It follows from the time independence of the Hamiltonian, and of the kernel $K(x,x')$ in Eq. (1.1) obeyed by $\mu(x,t)$, that $\mu(x,t+\tau)$ is determined by $\mu(x,\tau)$, again through Eq. (4.3); i.e.,

$$\begin{aligned}\mu(x,t+\tau)&=\int_\Gamma P(x,x'/t)\mu(x',\tau)dx'\\&=\int\int P(x,x'/t)P(x',x''/\tau)\mu(x'',0)dx''dx'\\&=\int P(x,x''/t+\tau)\mu(x'',0)dx''.\end{aligned} \tag{4.7}$$

Because $\mu(x'',0)$ is arbitrary, it follows that

$$P(x,x''/t+\tau)=\int P(x,x'/t)P(x',x''/\tau)dx'. \tag{4.8}$$

Equation (4.8) is a special case of the Chapman-Kolmogorov equation, which holds for all stationary Markov transition functions:

$$P(A,x''/t+\tau)=\int_\Gamma P(A,x'/t)P(dx',x''/\tau). \tag{4.9}$$

In this equation, $P(dx',x''/\tau)$ is the probability that the system will pass from the initial point x'' to the "infinitesimal" set $(x',x'+dx')$ in time τ, and the integral is a Lebesgue integral. In the case where a transition density exists, $P(dx',x''/t)=P(x',x''/t)dx'$.

If the Hamiltonian of Eq. (1.1) were explicitly time-dependent, then we should have a nonstationary

[6] W. Doeblin, Ann. Sci. Ecole Norm. Sup. (3) **57**, 61 (1940).
[7] J. L. Doob, *Stochastic Processes* (John Wiley and Sons, Inc., New York, 1953).

Markov process, for which Eqs. (4.7), (4.8), and (4.9) do not hold. In that case, there could be no approach to stationary equilibrium in the strict sense, though it is not excluded that in the presence of a periodic Hamiltonian (e.g., spin resonance in the presence of dissipative processes) the solution of Eq. (1.1) may approach periodic behavior. In this paper we are not concerned with that possibility.

We shall now state Doeblin's theorem for the function $P(A, x'/t)$ that satisfies Eq. (4.9): If there exists an $\epsilon>0$, an $s>0$, and a set measure $\Psi(A)$ in Γ space, normalized so that $\Psi(\Gamma)=1$, and if these quantities can be chosen so that

$$P(A, x'/s)<1-\epsilon, \tag{4.10}$$

whenever $\Psi(A)<\epsilon$, for all x', then the limit

$$\lim_{t\to\infty}\{P(A, x'/t)\}$$

exists. The convergence is uniformly exponentially fast.

When the above conditions for the existence of the limit are satisfied for some time s, then they will also be satisfied for all times $t>s$, because

$$P(A, x'/t)=\int_\Gamma P(A, x''/s)P(dx'', x'/t-s) \leqslant \max\{P(A, x''/s)\}<1-\epsilon. \tag{4.11}$$

Intuitively, the conditions on $P(A, x/t)$ in Doeblin's theorem require that the stochastic process spread distributions that are concentrated initially in regions of measure zero into domains possessing a nonvanishing measure. This requirement excludes, for instance, the case of an isolated system, one that does not interact with a random reservoir. The ensemble distribution of such a system in its phase space obeys the unmodified Liouville equation, which maps distributions initially concentrated in a point on another point without spreading. Such a distribution, as is well known, will never become stationary if it is not stationary to begin with.

The requirement in Doeblin's theorem that $\psi(A)$ be normalized means that the measure of infinitely far regions in phase space is zero with respect to ψ. Hence with any transition function $P(A, x'/t)$ which satisfies the Doeblin conditions we must be able to find a finite region B in Γ space such that the probability of finding the system in B at any time $t>s$ is uniformly bounded away from zero (i.e., the bound is independent of the initial state of the system).

The assumptions made in Eq. (4.10) are sufficient but not necessary conditions for the asymptotic approach to a stationary distribution. As an illustration of this point we may use an example cited by Doob[7] for this purpose. Let

$$P(A, x'/t)=[2\pi(1-\rho^{2t})]^{-\frac{1}{2}}\int_A \exp\left[-\frac{(x-\rho^t x')^2}{2(1-\rho^{2t})}\right]dx, \quad 0<\rho<1. \tag{4.12}$$

Then

$$\lim_{t\to\infty} P(A, x'/t)=\frac{1}{(2\pi)^{\frac{1}{2}}}\int_A \exp(-\tfrac{1}{2}x^2)dx. \tag{4.13}$$

This convergence is not uniform in x': if A is any finite set, $P(A, x'/t)$ can be made arbitrarily small for any t, by choosing x' sufficiently large. Hence the conditions under which Doeblin's theorem was proved are not satisfied in this case.

We shall now turn to the conditions to be satisfied by the transition rate $K(x,x')$, Eq. (1.1), in order that Doeblin's theorem be applicable to the distribution $P(A, x'/t)$ whose time dependence obeys the generalized Liouville equation (1.1), We shall expand $P(x, x'/t)$ into a series with respect to the number of collisions between the reservoir and the system during the time t.

The system can pass from x' to x in time t without any collisions only if $x=x_t'$, where x_t' is the position at time t of a system initially at x', according to its Hamiltonian equations of motion. The probability of zero collisions, $\eta(x',t)$, is

$$\eta(x',t)=\exp\left(-\int_0^t p(x_s')ds\right), \tag{4.14}$$

where

$$p(x')=\int_\Gamma K(y,x')dy \tag{4.15}$$

is the rate at which collisions with the reservoir occur at the point x'. Hence

$$P^{(0)}(x, x'/t)=\left[\exp\left(-\int_0^t p(x_s')dx\right)\right]\delta(x-x_t'). \tag{4.16}$$

The probability that the system will experience exactly one collision in the interval t, given that at the beginning of the interval the system was at x' and at the end of the interval at x, will be a product of the following three probabilities: (1) there was no collision up to some time λ, $0\leq\lambda\leq t$, which is given by $\eta(x',\lambda)$; (2) there was a collision during the time interval $(\lambda, \lambda+d\lambda)$, which caused the system to make a discontinuous jump from x_λ' to $x_{(\lambda-t)}$ [the probability for this event is $K(x_{(\lambda-t)}, x_\lambda')d\lambda$]; (3) there was no collision between $(t-\lambda)$ and t, $\eta(x, \lambda-t)=\eta(x_{(\lambda-t)}, t-\lambda)$. Since λ is arbitrary, we have to add the different possibilities. Hence

$$P^{(1)}(x, x'/t)=\int_0^t d\lambda \exp\left[-\int_{\lambda-t}^0 p(x_s)ds\right] \times K(x_{\lambda-t}, x_\lambda')\exp\left[-\int_0^\lambda p(x_s')ds\right]. \tag{4.17}$$

By analogous reasoning we find the probability for the system to have two collisions with the reservoir to

be

$$P^{(2)}(x, x'/t) = \int_\Gamma dy \int_0^t d\beta \int_0^{t-\beta} d\lambda \left\{ \exp\left[-\int_{\lambda+\beta-t}^{0} p(x_s) ds \right] \times K(x_{\lambda+\beta-t}, y_\beta) \exp\left[-\int_0^\beta p(y_s) ds \right] \times K(y, x_\lambda') \exp\left[-\int_0^\lambda p(x_s') ds \right] \right\}. \quad (4.18)$$

Following up this analysis, we can get all the terms $P^{(n)}(x, x'/t)$. The total transition density $P(x, x'/t)$ is the sum of all these different possibilities

$$P(x, x'/t) = \sum_{n=0}^{\infty} P^{(n)}(x, x'/t). \quad (4.19)$$

This expansion can also be obtained by means of an entirely different, nonprobabilistic, scheme. It is the result of a perturbation expansion of $\mu(x,t)$ in powers of $K(x,x')$. The same type of perturbation theory is commonly used in quantum mechanics for the wave function $\psi(q,t)$ which, like $\mu(x,t)$, obeys a first-order differential equation in time. Let us rewrite Eq. (1.1) in an operator form thus

$$\partial\mu/\partial t = (H,\mu) - p(x)\mu + \int K(x,x')\mu(x')dx' = (\mathfrak{K}+V)\mu, \quad (4.20)$$

where

$$\mathfrak{K}\mu = (H,\mu) - p(x)\mu, \quad V\mu = \int K(x,x')\mu(x')dx'.$$

The operator $\mathfrak{K}$ is singular, but V is regular, bounded, and positive definite, hence we shall expand $\mu(x,t)$ as a power series in V. For this purpose we shall first convert the integro-differential equation for $\mu(x,t)$ into an integral equation,

$$\mu(x,t) = \exp(t\mathfrak{K})\mu(x,0) + \int_0^t \exp[(t-\lambda)\mathfrak{K}] V \mu(x,\lambda) d\lambda. \quad (4.21)$$

Expanding now in V we get

$$\mu(x,t) = \exp(t\mathfrak{K})\mu(x,0) + \int_0^t d\lambda \{\exp[(t-\lambda)\mathfrak{K}] V \exp(\lambda\mathfrak{K})\}\mu(x,0) + \int_0^t d\gamma \left\{ \exp[(t-\gamma)\mathfrak{K}] V \int_0^\gamma d\lambda [\exp((\gamma-\lambda)\mathfrak{K}) V \exp(\lambda\mathfrak{K})] \right\} \mu(x,0) + \cdots. \quad (4.22)$$

Now $\exp(t\mathfrak{K})f(x,0) = f(x,t)$ is the solution of the equation

$$\partial f(x,t)/\partial t = (H,f) - p(x)f. \quad (4.23)$$

More explicitly, this solution has the form

$$f(x,t) = \exp\left[-\int_0^t p(x_{s-t}) ds \right] f(x_{-t}, 0). \quad (4.24)$$

Substituting this expression back into Eq. (4.21) for the case when $\mu(x,0) = \delta(x-x')$ and hence $\mu(x,t) = P(x, x'/t)$, we see that the expansions of Eqs. (4.22) and (4.19) are identical.

We can now prove that if $K(x,x')$ is bounded by an integrable function $v(x)$[8]

$$K(x,x') < Mv(x), \quad \int_\Gamma v(x)dx = 1, \quad (4.25)$$

then our $P(x, x'/t)$ satisfies the Doeblin conditions. There are no additional restrictions imposed on $K(x,x')$ if $v(x)$ is made a function of $H(x)$ alone, $v(x) = v(H(x))$. This last assumption implies that $v(x_t) = v(x)$ for all t.

[8] This condition is somewhat more restrictive than absolutely necessary but it simplifies the proof considerably.

It now follows from (4.17), (4.18) that

$$P^{(1)}(x, x'/t) < M \int_0^t v(x_{\lambda-t}) d\lambda = Mtv(x), \quad (4.26)$$

$$P^{(2)}(x, x'/t) < \frac{(Mt)^2}{2!} v(x),$$

and in general

$$P^{(n)}(x, x'/t) < \frac{(Mt)^n}{n!} v(x), \quad n \geq 1. \quad (4.27)$$

Hence, from (4.19),

$$P(x, x'/t) < \exp\left[-\int_0^t p(x_s') ds \right] \delta(x - x_t') + (e^{Mt} - 1)v(x). \quad (4.28)$$

In order that our system should approach a stationary state independent of its initial position, x', in phase space, we must, of course, assume that there are no trajectories in Γ space on which the system can move without ever getting into a region where it can collide with the reservoir. Otherwise if the system is initially in a state x' which lies on such a trajectory, it would

behave as if there were no reservoir, and the density $\mu(x,t)$ would always be $\delta(x-x_i')$ without ever becoming stationary. More precisely, we assume that there exists a time t_1, such that for any time $t>t_1$, the system will spend at least an interval τ, $\tau=\alpha(t-t_1)$, $\alpha>0$ in such a region in phase space where the probability per unit time, $p(x)$, of its undergoing a collision is greater than some positive number m. Hence

$$P(x,x'/t)<\exp[-m\alpha(t-t_1)]\delta(x-x_i') + (e^{Mt}-1)v(x), \quad t>t_1, \tag{4.29}$$

and

$$P(A,x'/t)<\exp[-m\alpha(t-t_1)]+(e^{Mt}-1)\Psi(A), \tag{4.30}$$

where

$$\Psi(A)=\int_A v(x)dx. \tag{4.31}$$

When $\Psi(A)<\epsilon$, then

$$P(A,x'/t)<\exp[-m\alpha(t-t_1)]+(e^{Mt}-1)\epsilon, \tag{4.32}$$

which is less than $(1-\epsilon)$ whenever

$$\epsilon<e^{-Mt}(1-\exp[-m\alpha(t-t_1)]), \quad t>t_1. \tag{4.33}$$

Thus whenever $K(x,x')$ satisfies (4.25), $P(A,x'/t)$ satisfies (4.10); Doeblin's theorem applies, and

$$\lim_{t\to\infty} P(A,x'/t)=P(A,x') \tag{4.34}$$

exists, The limiting distribution $P(A,x')$ will be independent of x' if there are no noninteracting regions in phase space. Otherwise, the stationary state will depend on the initial distribution between these invariant subspaces. This requirement of ergodicity is the same as in the case of a single reservoir discussed at the end of Sec. 3.

5. STATIONARY STATE WITH SEVERAL RESERVOIRS: ONSAGER RELATIONS

We shall now consider an ensemble of systems in contact with n reservoirs at temperatures $T_i=(k\beta_i)^{-1}$, $i=1,\cdots,n$. Equation (1.1) then assumes the form

$$\frac{\partial\mu}{\partial t}+(\mu,H)=\sum_{i=1}^{n}\int_{x'}[e^{\beta_i H(x')}\mu(x')-e^{\beta_i H(x)}\mu(x)] \times L_i(x,x')dx'. \tag{5.1}$$

The rate of entropy production σ will be given, in analogy with Eq. (3.2), by

$$\sigma=\dot{S}-k\sum_{i=1}^{n}\beta_i J_i, \tag{5.2}$$

where J_i is the average rate of energy flow from the ith reservoir to the system. The rate of change of the mean energy U is equal to the sum of the flows

$$\dot{U}=\int_\Gamma H\frac{\partial\mu}{\partial t}dx=\sum_{i=1}^{n}J_i=\sum_{i=1}^{n}\int_x dx \times\int_{x'}dx'[e^{\beta_i H(x')}\mu(x')-e^{\beta_i H(x)}\mu(x)]H(x)L_i(x,x') =\sum_{i=1}^{n}\int_x dx\mu(x)\int_{x'}dx'\,e^{\beta_i H(x)}L_i(x,x')[H(x')-H(x)], \tag{5.3}$$

$$J_i=\int_x dx\mu(x)\int_{x'}dx'e^{\beta_i H(x)}L_i(x,x')[H(x')-H(x)] =\int_x dx\mu(x)f_i(x). \tag{5.4}$$

It can be shown by methods analogous to those used in the derivation of Eq. (3.8) that $\sigma\geq 0$. The equality can hold only if all the β_i are equal to each other.

When the ensemble becomes stationary, $\partial\mu/\partial t=0$, the internal entropy remains constant, $\dot{S}=0$, and Eq. (5.4) reduces to

$$\sigma=-k\sum_{i=1}^{n}\beta_i J_i\geq 0. \tag{5.5}$$

Since in the stationary state the mean energy U is constant, it follows that

$$\dot{U}=\sum_{i=1}^{n}J_i=0. \tag{5.6}$$

Here we may solve for some particular flow J_m in terms of the other flows

$$J_m=-\sum_{i\neq m}{}' J_i \tag{5.7}$$

in a stationary ensemble. Substituting this expression into Eq. (5.5), we get

$$\sigma=k\sum_{i\neq m}{}'(\beta_m-\beta_i)J_i=\sum_{i\neq m}{}'\gamma_i J_i(\gamma_i), \tag{5.8}$$

where the J_i are now independent flows.

It follows from this expression for the total entropy production that in our model, the J_i and the γ_i, are the currents and the forces respectively, which are used in the Onsager theory.[1] Onsager's reciprocal relations state that in the linear approximation the dependence of J_l on γ_k is the same as that of J_k on γ_l. In other words, when the reservoir temperatures are close to each other (i.e., where the γ_i's are small), when we can set

$$J_l=\sum_{k\neq m}{}' A_{lk}\gamma_k, \tag{5.9}$$

then

$$A_{lk}=\left(\frac{\partial J_l}{\partial\gamma_k}\right)_{\gamma_i=0}=\left(\frac{\partial J_k}{\partial\gamma_l}\right)_{\gamma_i=0}=A_{kl}. \quad (5.10)$$

We shall now prove the validity of Eq. (5.10) for our model. Since the J_m chosen in Eq. (5.7) was arbitrary, the symmetry relations should be independent of that choice. They will be if and only if

$$J_{lk}=\left(\frac{\partial J_l(\beta_i)}{\partial\beta_k}\right)_{\beta_i=\beta}=\left(\frac{\partial J_k(\beta_i)}{\partial\beta_l}\right)_{\beta_i=\beta}=J_{kl}, \quad (5.11)$$

for $l, k=1, \cdots, m, \cdots n$. We shall, therefore, prove Eq. (5.11) rather than Eq. (5.10). Generally, $J_{lk}=-A_{lk}$, $l, k\neq m$.

From Eq. (5.3), we get

$$\frac{\partial J_l}{\partial\beta_k}=\int_\Gamma dx\left[\frac{\partial\mu(x)}{\partial\beta_k}f_l(x)\right], \quad l\neq k, \quad (5.12)$$

since $f_l(x)$ depends only on β_l. Solving for $\partial\mu/\partial\beta_k$, in the stationary state, from the time independent form of Eq. (5.1), we get

$$\left(\frac{\partial\mu}{\partial\beta_k},H\right)=\sum_{i=1}^{n}\int_{\Gamma'}\left\{e^{\beta_i H(x')}\frac{\partial\mu(x')}{\partial\beta_k}-e^{\beta_i H(x)}\frac{\partial\mu(x)}{\partial\beta_k}\right\}L_i(x,x')dx'$$
$$+\int_{\Gamma'}\left\{\mu(x')e^{\beta_k H(x')}\left[H(x')L_k(x,x')+\frac{\partial L_k}{\partial\beta_k}\right]-\mu(x)e^{\beta_k H(x)}\left[H(x)L_k+\frac{\partial L_k}{\partial\beta_k}\right]\right\}dx'. \quad (5.13)$$

We shall now evaluate this equation when all the β_i's equal to β. Under these conditions $\mu(x)=(1/Z)e^{-\beta H(x)}$, as derived in Sec. 3, and Eq. (5.13) reduces to

$$(\mu_k,H)=\int_\Gamma[\mathfrak{L}(x,x')e^{\beta H(x')}\mu_k(x')]dx'-q(x)\mu_k(x)+\frac{1}{Z}e^{-\beta H(x)}f_k^0(x), \quad (5.14)$$

where

$$\mu_k=\left(\frac{\partial\mu}{\partial\beta_k}\right)_{\beta_i=\beta}, \quad \mathfrak{L}(x,x')=\sum_{i=1}^{n}[L_i(x,x')]_{\beta_j=\beta}=\mathfrak{L}(x',x),$$

$$q(x)=\int_{\Gamma'}\mathfrak{L}(x,x')e^{\beta H(x)}dx'=p(x)\,|_{\beta_i=\beta}.$$

Multiplying Eq. (5.14) by $Ze^{\beta H(x)}\mu_l(x)$ and integrating over Γ, we get

$$J_{kl}=\int_\Gamma f_k^0(x)\mu_l(x)dx$$
$$=Z\int_\Gamma\left\{e^{\beta H(x)}\mu_l(x)(\mu_k(x),H(x))-\int_{\Gamma'}\mathfrak{L}(x,x')e^{\beta[H(x)+H(x')]}\mu_k(x')\mu_l(x)dx'+\mu_k(x)\mu_l(x)q(x)e^{\beta H(x)}\right\}dx. \quad (5.15)$$

Hence

$$J_{kl}-J_{lk}=Z\int_\Gamma e^{\beta H(x)}[\mu_l(x)(\mu_k(x),H(x))-\mu_k(x)(\mu_l(x),H(x))]dx \quad (5.16)$$
$$=2Z\int_\Gamma e^{\beta H}\mu_l(\mu_k,H)dx-\beta^{-1}Z\int_\Gamma(\mu_k\mu_l,e^{\beta H})dx.$$

The last term vanishes. In order to evaluate the remainder in (5.16), it is convenient to separate $\mu_i(x)$ into a symmetric and an antisymmetric part with respect to the momentum variables of the system:

$$\mu_i(x)=E_i(x)+O_i(x), \quad E_i(x)=E_i(\bar{x}), \quad O_i(x)=-O_i(\bar{x}). \quad (5.17)$$

A Poisson bracket between even functions is odd, and between an even and an odd function even, etc. Because H is an even function, its Poisson bracket with $E_i(x)$ is odd, and with $O_i(x)$ even. Since the integral of an odd function over the whole phase space vanishes, it follows that

$$J_{kl}-J_{lk}=2Z\int_\Gamma[E_l(O_k,H)+O_l(E_k,H)]e^{\beta H}dx \quad (5.18)$$
$$=2Z\int_\Gamma[O_l(e^{\beta H}E_k,H)-O_k(e^{\beta H}E_l,H)]dx.$$

We can now solve for $(e^{\beta H}E_k,H)$ from Eq. (5.14), remembering that it follows from the way we arrive at Eq. (2.3) that $L(x,x')=L(\bar{x},\bar{x}')$. Thus

$$(e^{\beta H}E_k,H)=\int_{\Gamma'}\mathfrak{L}(x,x')e^{\beta[H(x)+H(x')]}O_k(x')dx'-e^{\beta H(x)}q(x)O_k(x). \quad (5.19)$$

Substituting (5.19) into (5.18) we arrive at our desired result,

$$J_{kl}-J_{lk}=0. \quad (5.20)$$

This derivation of the Onsager relations requires no reference to fluctuation theory, nor does it involve an

assumption that the laws connecting the macroscopic variables are Markoffian.

6. CONCLUSION

In this paper we have developed in classical (nonquantum) mechanics a model for a stationary irreversible process that is capable of being treated with the methods of statistical mechanics due to Gibbs. Our model is based on the assumption that no essential features of the real process are lost if the interaction of the system with the driving reservoirs is pictured in terms of instantaneous impulsive interactions. The reservoirs themselves are described as infinitely large composites consisting of identical noninteracting components in canonical distribution. Thus each reservoir has a definite temperature, infinite heat capacity, and vanishing internal heat conductivity. No special assumptions are made concerning the structure of the system; its internal dynamics are governed by some nonsingular Hamiltonian.

We have succeeded in showing that our model, with arbitrary initial ensemble distribution, will approach the canonical distribution if driven by a single reservoir, will approach a stationary (noncanonical) distribution if driven by several reservoirs at different temperatures, and in the stationary state will obey the Onsager relations if the driving temperature gradients are small.

Further work will be devoted to a more detailed investigation of the stochastic kernels that represent the action of the reservoirs, the introduction of more general thermodynamic forces than temperature gradients, and the transition to quantum mechanics.

PHYSICAL REVIEW VOLUME 99, NUMBER 2 JULY 15, 1955

Lagrangians Linear in the "Velocities"*

EZRA NEWMAN† AND PETER G. BERGMANN
Department of Physics, Syracuse University, Syracuse, New York

(Received March 16, 1955)

Lagrangian linear in the first time derivatives are of sufficient importance in physics (particle fields, general relativity in the Palatini formulation, Einstein-Strauss type unified field theory, etc.) to warrant special consideration. Our treatment is patterned after Dirac's more general exploration of Lagrangians leading to algebraic relations between the canonical variables. In our case, the number of such constraints is at least as large as the number of configuration coordinates. The secondary constraints are free of canonical momentum densities. We have examined all the possibilities that may arise—incompatibility of the field equations, proper Cauchy-Kowalewski problems, and the appearance of arbitrary functions in the solutions. Appropriate quantization procedures for the compatible cases will be indicated.

1. INTRODUCTION

MANY physical theories are derivable from Lagrangians that are linear in the first time derivatives of the field variables. We have investigated in this paper the compatibility of the field equations of such a theory, methods of constructing a Hamiltonian formalism, and quantization procedures. The formalism developed is capable of handling such diverse theories as the Pauli-Fierz equations, gravitational theory in the Palatini form (i.e., considering the components of the affine connection as independent variables), the Einstein-Strauss unified field theory, and Maxwell theory with the vector potentials treated as variables independent of **E** and **H**.

Our treatment is based on Dirac's[1] study of theories for which the momenta canonically conjugate to the field variables are not all algebraically independent of the field variables and their spatial derivatives themselves. Dirac reduces all cases to Lagrangians that are homogeneous of the first degree in the "velocities" (derivatives of the field variables with respect to the chosen time coordinate); any Lagrangian can be given this form by the device of parametrization. Lagrangians that are (inhomogeneously) linear in the velocities do not require this treatment. They can be discussed quite successfully without the introduction of a parameter. They are of sufficient importance in physics that they warrant a specialized treatment.

There are two general types of linear Lagrangians (in our sense). They all lead to differential equations that are free to accelerations and are linear in the velocities. The first type leads to equations in which the matrix of the coefficients of the velocities is nonsingular, the second to equations in which the same matrix is singular. The first case can be treated completely and in full generality. The second case has a number of subcases. Whenever the matrix of the coefficients is singular, then there exists a number of linear combinations of the (Lagrangian field) equations that are free of velocities. These combinations may be empty; if they are not, their time derivatives may be independent of the original field equations. In the latter case, new combinations

* This work was supported by the Office of Naval Research.
† Submitted to the Graduate School of Syracuse University as a thesis for the master's degree.
[1] P. A. M. Dirac, Can. J. Math. **2**, 129 (1950); **3**, 1 (1951).

free of velocities may be formed, and so forth. Roughly, these subcases may then lead to systems of equations that (a) are incompatible, (b) lead to proper initial value problems (Cauchy-Kowalewski systems), or (c) possess solutions incorporating a number of arbitrary functions of the coordinates.

In all cases, we have endeavored to indicate appropriate procedures for quantizing the theory.

2. BASIC EQUATIONS

We consider Lagrangian densities of the form

$$L=f^{A\rho}y_{A,\rho}+Q^*(y_B)=f^A(y_B)\dot{y}_A+Q,\quad \rho=1\cdots4$$
$$f^A=f^{A4},\quad Q=Q^*+f^{As}y_{A,s},\qquad (2.1)$$
$$A=1\cdots N,\quad s=1,2,3,$$

where y_A are the field variables and $y_{A,s}$ their spatial derivatives. The Euler equations are

$$L^A=\{\partial^A f^{B\rho}-\partial^B f^{A\rho}\}y_{B,\rho}+\partial^A Q^*$$
$$=\{\partial^A f^B-\partial^B f^A\}\dot{y}_B+\delta^A Q=0,\qquad (2.2)$$

where

$$\partial^A f^B\equiv\partial f^B/\partial y_A,\quad \partial^{As}f^B\equiv\partial f^B/\partial y_{A,s},$$
$$\delta^A Q\equiv\partial^A Q-(\partial^{As}Q)_{,s}.$$

The equations have been written first in four-dimensional notation and then with the time variable singled out. In the remainder of this paper, only the latter will be used. We shall write

$$\partial^A f^B-\partial^B f^A\equiv f^{AB}.\qquad (2.3)$$

Because f^{AB} is skewsymmetric, its determinant will vanish if there are an odd number of field variables. If for this or any other reason, $\det|f^{AB}|=0$, then we cannot solve the Euler equations algebraically for $\dot{y}_A$. Even then it may happen that the field equations are of the Cauchy-Kowalewski type. This statement will be amplified in Sec. 5.

To go over to the Hamiltonian formalism we introduce the momentum densities conjugate to the y_A,

$$\pi^A=\partial L/\partial\dot{y}_A=f^A.\qquad (2.4)$$

Ordinarily, the defining equations for the canonical momentum densities are used in turn to express the time derivatives of the field variables, the $\dot{y}_A$, in terms of the canonical variables and to eliminate them from the standard expression for the Hamiltonian density,

$$\mathcal{H}=\dot{y}_A\pi^A-L.\qquad (2.5)$$

Our Eq. (2.4) contains no reference to the $\dot{y}_A$. Hence the usual procedure is not feasible. However, it may be possible to obtain expressions for the "velocities" directly from the field equations (2.2) and to use these expressions to obtain the Hamiltonian density. Such a determination will be unique if the determinant of the f^{AB} does not vanish. If it does, the lack of uniqueness in the determination of the $\dot{y}_A$ from Eq. (2.2) may give rise to a certain arbitrariness in the Hamiltonian density. This contingency will be taken up in detail in Secs. 4 and 5. At any rate, if

$$\dot{y}_A=\mu_A(y_B,y_{B,s})\qquad (2.6)$$

is a particular solution of the field equations (2.2), we may substitute this solution into the expression for the Hamiltonian and obtain

$$\mathcal{H}=\mu_A\pi_A-f^A\mu_A-Q=\mu_AC^A-Q,\qquad (2.7)$$

with μ_B satisfying

$$f^{AB}\mu_B+\delta^AQ=0.\qquad (2.8)$$

The expressions C^A, which we have introduced in Eq. (2.7),

$$C^A\equiv\pi^A-f^A=0,\qquad (2.9)$$

vanish because of Eq. (2.4). They represent conditions on the canonical field variables that are free of velocities. We call such conditions constraints. More particularly, the C^A are "primary constraints," because they result directly from the defining Eq. (2.4). Even though the C^A vanish, their partial derivatives will appear in the canonical field equations. The canonical field equations have the form

$$\dot{y}_A=\partial\mathcal{H}/\partial\pi^A=\mu_A,$$
$$\dot{\pi}^A=-\delta^A\mathcal{H}=\delta^AQ+\mu_B\partial^Af^B-C^B\delta^A\mu_B.\qquad (2.10)$$

Presumably, Eqs. (2.9) and (2.10) determine the behavior of the field in the Hamiltonian formalism. For this system of equations to be consistent, the time derivatives of the constraints must vanish. In some theories with constraints, this set of conditions leads to additional constraints (the secondary constraints), whose time derivatives must again vanish, etc. In this instance, these consistency conditions are satisfied automatically. We have

$$\dot{C}^A=\dot{\pi}^A-\dot{y}_B\partial^Bf^A$$
$$=\delta^AQ+f^{AB}\mu_B-C^B\delta^A\mu_B.\qquad (2.11)$$

The first two terms on the right-hand side will vanish together if the choice (2.6) for μ_A was made correctly, i.e., in accordance with the Lagrangian field equations (2.2). The last term will vanish if the constraints (2.9) are satisfied. Similarly, the time derivatives of the expressions (2.11) will again vanish modulo Eqs. (2.2), (2.6) and (2.9). It follows that if we satisfy the canonical field equations (2.10) at all times and the constraints (2.9) at least at one time t_0, then the constraints will remain satisfied at all times. This set of conditions,—(2.9) at one time, (2.7), (2.10) at all times,—is then equivalent to the Lagrangian field equations (2.2), possibly specialized (if $\det|f^{AB}|=0$) by the choice (2.6).

A relationship which will be useful in the remainder of the paper is the Poisson bracket between two constraints. A short calculation shows

$$(C^A(x),C^B(x'))=f^{AB}\delta(x-x').\qquad (2.12)$$

Attempts to quantize a theory with constraints in the usual manner, i.e., by equating the commutators of the quantum-theoretical observables with the Poisson brackets of the c-number theory run into a characteristic difficulty. One might be tempted to require of the constraints that they are identically zero, i.e., that all matrix elements of the corresponding operators vanish. Such an assumption is: inconsistent with the requirement that some of the commutators of these constraints with other observables (which may also be constraints, though they need not be) are different from zero. Frequently, this difficulty, which also arises in quantum electrodynamics, has been circumvented by the requirement that the constraints do not vanish identically, but only that the wave vectors are eigenvectors of the constraints, belonging to the eigenvalue zero. This alternative is not entirely satisfactory, either. If the constraints have nonvanishing Poisson brackets, as they do in our case [see Eq. (2.12)], then the requirement that the state vector is a null vector of both of the constraints involved leads to the self-contradictory requirement that it also be a null vector of the commutator. Similar though different difficulties arise when the constraints have c-number commutators with other field variables, a situation that arises in electrodynamics.

Dirac[1] has suggested a modification of the usual quantization procedures that can be applied to theories incorporating constraints. He classifies constraints (within the c-number theory) into two categories, those that have vanishing Poisson brackets with all other constraints ("first-class constraints") and those that do not ("second-class constraints"). By replacing a given set of constraints by a new set of linear combinations, he first maximizes the number of first-class constraints. The remaining second-class constraints, say R in number (R in our case equals the rank of the matrix f^{AB}) will then have a set of Poisson brackets whose determinant does not vanish. He then introduces a new type of bracket symbol, which is now usually called a Dirac bracket, defined in terms of the Poisson bracket (M,N) as follows:

$$\{M,N\}=(M,N)-\int\int(M,\theta^\alpha(x'))F_{\alpha\beta}(x',x'')\times(\theta^\beta(x''),N)d^3x'd^3x''. \quad (2.13)$$

The quantities θ^α represent the totality of all new second-class constraints, and have Poisson brackets

$$(\theta^\alpha(x),\theta^\beta(x'))=\Phi^{\alpha\beta}(x,x'),\qquad \Phi^{\alpha\beta}(x,x')=-\Phi^{\beta\alpha}(x',x) \quad (2.14)$$

and $F_{\alpha\beta}$ is the reciprocal to the $\Phi^{\alpha\beta}$,

$$\int\Phi^{\alpha\beta}(x',x)F_{\beta\gamma}(x,x'')d^3x=\delta(x'-x'')\delta_\gamma{}^\alpha. \quad (2.15)$$

By direct computation, Dirac has shown that his bracket satisfies the Jacobi relationship, i.e.,

$$\{A,\{B,C\}\}+\{B,\{C,A\}\}+\{C,\{A,B\}\}=0. \quad (2.16)$$

This fact alone suggests that the Dirac bracket represents a group-theoretical commutator, just as the ordinary Poisson bracket does.[2] At any rate, inasmuch as the Dirac bracket between any θ^α and any dynamical variable vanishes identically, it is possible to set the θ^α identically zero, and thereby replace the whole phase space of $2N$ dimensions (per space point) by the $(2N-R)$-dimensional hypersurface $\theta^\alpha=0$. On this hypersurface, our theory will still have $(N-R)$ first-class constraints (per space point). The quantization procedure applies to this reduced theory; Dirac brackets, rather than Poisson brackets, are related to the commutators of the quantum-mechanical observables. Dirac has also shown that for the correct Hamiltonian

$$\dot{y}_A=(y_A,H)=\{y_A,H\},\qquad \dot{\pi}^A=(\pi_A,H)=\{\pi^A,H\}. \quad (2.17)$$

In other words, the Dirac bracket is capable of taking over completely the role that is played by Poisson brackets in theories without second class constraints.

The field equations of Lagrangians linear in the velocities belong to one of three main types.

(1) They may determine the "velocities" $\dot{y}_A$ uniquely and algebraically as functions of y_A and $y_{A,s}$ (Sec. 3).

(2) It may be impossible to determine the "velocities" uniquely (Sec. 4).

(3) We may be able to derive conditions of compatibility, which, together with the original field equations, determine the "velocities" (Sec. 5).

3. "VELOCITIES" DETERMINED BY EULER EQUATIONS

The first case is characterized by $\det|f^{AB}|\neq 0$. In this case, the Hamiltonian H is a uniquely defined function of the y_A, $y_{A,s}$ and π^A. Since the rank of f^{AB} is N, all constraints and all the π^A's can be eliminated by means of Dirac's method. Wherever a quantity π^A occurs we replace it by the corresponding f^A. Thus the Hamiltonian reduces to $\mathcal{H}=-Q$. The canonical equations are now obtained in terms of the Dirac brackets. We shall derive some properties of the Dirac bracket for this case.

Choosing for θ^α all the C^A's and thus making $\Phi^{\alpha\beta}$ equal to $f^{AB}\delta(x-x')$, and defining a new set of quantities f_{AB} by

$$f^{AB}f_{BC}=\delta_C{}^A, \quad (3.1)$$

[1] P. G. Bergmann, and I. Goldberg, Phys. Rev. 98, 531 (1955).

we get from Eq. (2.13)

$$\{y_A(x),y_B(x')\}$$
$$=(y_A(x'),y_B(x'))-\int\int(y_A(x),C^D(x''))$$
$$\times f_{DE}(x'',x''')\delta(x''-x''')(C^E(x'''),y_B(x'))d^3x''d^3x'''$$
$$=\delta_A{}^D f_{DE}\delta_B{}^E\delta(x-x')=f_{AB}\delta(x-x'). \tag{3.2}$$

We can write the Dirac bracket between any two functionals of the y_A and $y_{A,s}$ by using Eq. (3.2). The result is

$$\{M,N\}=\int\frac{\delta M}{\delta y_A}f_{AB}\frac{\delta N}{\delta y_B}d^3x. \tag{3.3}$$

If we substitute $N=-\int Qd^3x=H$ and $M=y_A$ followed by $M=f_A$, we get from Eqs. (2.17) and (3.3),

$$\dot{y}_A=-\delta^B Qf_{AB} \quad \text{or} \quad \dot{y}_A+\delta^B Qf_{AB}=0, \tag{3.4}$$

and

$$\dot{f}_C=\partial^A f^C\dot{y}_A=\{f^C,H\}=-\partial^A f^C\delta^B Qf_{AB}$$

or

$$(\dot{y}_A+\delta^B Qf_{AB})\partial^A f^C=0.$$

The first of these is exactly equal to the Euler equations when we multiply by f^{CA}.

The quantization procedure is now as follows. Instead of relating the Poisson bracket to the commutator, we relate the Dirac bracket. Therefore the operators y_A satisfy the commutator relation

$$[y_A(x),y_B(x')]=i\hbar f_{AB}\delta(x-x'). \tag{3.5}$$

The Schrödinger equation is

$$i\hbar\frac{\partial\Psi}{\partial t}=-\int Qd^3x\Psi. \tag{3.6}$$

Terms in Q must be ordered so as to make Q Hermitian. No mention need be made of either the constraints or the momentum densities.

Although this formalism can be applied among other examples to the Pauli-Fierz[3] equations, we will illustrate it with a much simpler example. Consider the Lagrangian for the Schrödinger equation, the ψ and ψ^* taken as classical field variables,

$$L=\tfrac{1}{2}i\hbar(\psi^*\dot{\psi}-\dot{\psi}\psi^*)-\tfrac{1}{2}(\hbar^2/m)\psi^*{}_{,s}\psi_{,s}. \tag{3.7}$$

Hence,

$$f^{AB}=i\hbar\begin{pmatrix}0 & -1\\ 1 & 0\end{pmatrix}$$

and

$$f_{AB}=\frac{1}{i\hbar}\begin{pmatrix}0 & 1\\ -1 & 0\end{pmatrix}.$$

From Eq. (3.5), we see that $[\psi(x),\psi^*(x')]=\delta(x-x')$, the usual commutator in the second-quantized theory (if the particles are bosons).

[3] W. Pauli and M. Fierz, Helv. Phys. Acta **12**, 297 (1939).

4. UNDETERMINED VELOCITIES

The more difficult and mathematically more interesting case is that of $\det|f^{AB}|=0$. A general solution to Eq. (2.8) is

$$\mu_A=\bar{\mu}_A+\xi^i u_{iA}, \tag{4.1}$$

where ξ^i are a set of functions of the y_A, $y_{A,s}$ and x^a, for the moment unspecified, with i going from 1 to $(N-R)$ (R is the rank of the matrix f^{AB}); u_{iA} are a complete set of linearly independent vectors satisfying the homogeneous equation $f^{AB}u_{iB}=0$, and $\bar{\mu}_A$ is any particular solution of Eq. (2.8). $\bar{\mu}_A$ is then a known algebraic function of y_A and $y_{A,s}$.

If we multiply Eq. (2.2) by u_{iA}, we see that the following $(N-R)$ conditions must be satisfied if solutions of Eq. (2.8) (or the Euler equations) are to exist:

$$u_{iA}\delta^A Q=0. \tag{4.2}$$

These conditions may be satisfied identically, in analogy to the Bianchi identities of general relativity. But it may also happen, instead, that these conditions restrict solutions of our Euler equations to hypersurfaces in configuration or phase space. They contain only the field variables y_A and their spatial derivatives, $y_{A,s}$. We call constraints of this type secondary constraints and label them

$$C_i=u_{iA}\delta^A Q. \tag{4.3}$$

If Eqs. (4.2) are identities, we shall write them with an identity sign, otherwise with an ordinary equality sign. It may be that in a particular problem both types of vector u_{iA} [those that satisfy Eq. (4.2) identically and those that impose constraints] will appear.

We consider first the case of all the C_i vanishing identically, i.e. $u_{iA}\delta^A Q\equiv 0$ for all i. The ξ^i of Eq. (4.1) are completely arbitrary functions. The equation $u_{iA}\delta^A Q\equiv 0$ is empty and we cannot derive additional conditions for the ξ^i, as we can when $u_{iA}\delta^A Q=0$. (We shall study the use of the secondary constraints for determining the ξ^i in the next section.) The Hamiltonian for the present problem is

$$\mathcal{H}=\bar{\mu}_A C^A+\xi^i u_{iA}C^A-Q. \tag{4.4}$$

We can better understand the appearance of the arbitrary ξ^i in the canonical formalism if we use $\xi^i u_{iA}C^A=C$ as the generator of an infinitesimal canonical transformation,

$$\delta y_A=\partial C/\partial\pi^A=\xi^i u_{iA}. \tag{4.5}$$

The functional change in the Lagrangian is given by[4]

$$\delta' L=-C^a{}_{,a}-L^A\delta y_A \tag{4.6}$$

where the C^a is arbitrary and the L^A are the field equations. Putting Eq. (4.5) into Eq. (4.6) and noting that

$$L^A\delta y_A=L^A\xi^i u_{iA}=(f^{AB}\dot{y}_B+\delta^A Q)u_{iA}\xi^i\equiv 0,$$

[4] P. G. Bergmann and R. Schiller, Phys. Rev. **89**, 4 (1953).

we see that $\delta' L = -C^{\alpha}{}_{,\alpha}$. This is the condition for a continuous group of invariant transformations which depend on the arbitrary functions ξ^i. In other words, for a solution y_A of the field equations satisfying certain initial conditions, $y_A' = y_A + \xi^i u_{iA}$ is also a solution satisfying the same initial conditions if ξ^i and its spatial derivatives vanish at $t=0$. The choice of a particular set of ξ^i is equivalent in Maxwell theory to a particular gauge frame and in general relativity to particular coordinate conditions.

In order to quantize this type of theory by Dirac's procedure, we must maximize the number of first class constraints. As was explained in Sec. 2, this is done by taking linear combinations of the old constraints, the coefficients being the coefficients of the orthogonal matrix which borders the singular matrix f^{AB}. Since f^{AB} is of rank R, there will be R second-class constraints and $(N-R)$ first-class constraints. We use these R new second-class constraints to form the Dirac bracket and to eliminate R variables from the theory. The quantum-mechanical commutation relations are associated with the Dirac bracket rather than with the Poisson bracket, and the $(N-R)$ first-class constraints $C^{*\alpha}$ give rise to $(N-R)$ Schrödinger equations:

$$C^{*\alpha}\Psi = 0, \tag{4.7}$$

in addition to the usual one:

$$i\hbar \frac{\partial \Psi}{\partial t} = -\int Q d^3x \Psi. \tag{4.8}$$

5. COMPATIBILITY CONDITIONS WHEN $\det|f^{AB}| = 0$

When Eq. (4.2) is not an identity (i.e., when we have secondary constraints) there are so many subcases that it has been difficult for us to give a systematic analysis of it. The simplest way to see the various possibilities is to consider a theory with a finite number of degrees of freedom (i.e., a problem in mechanics) rather than one with an infinite number of degrees of freedom (a field). The Lagrangian analogous to Eq. (2.1) is

$$L = f^{\alpha}(x)\dot{x}_{\alpha} + Q(x). \tag{5.1}$$

The Euler equations are

$$L^{\alpha} = f^{\alpha\beta}\dot{x}_{\beta} + \partial^{\alpha}Q = 0, \tag{5.2}$$

$$f^{\alpha\beta} \equiv \frac{\partial f^{\beta}}{\partial x_{\alpha}} - \frac{\partial f^{\alpha}}{\partial x_{\beta}}, \quad \partial^{\alpha}Q \equiv \frac{\partial Q}{\partial x_{\alpha}}.$$

The case we are considering now is that of $\det|f^{\alpha\beta}| = 0$ and $u_{i\alpha}\partial^{\alpha}Q = 0$ where $u_{i\alpha}$ satisfies the homogeneous equation $f^{\alpha\beta}u_{i\beta} = 0$. For compatability the time derivative of the secondary constraint, $C_i = u_{i\alpha}\partial^{\alpha}Q$, must vanish. These time derivatives, which are homogeneous in the velocities, have the form

$$\partial^{\beta}(u_{i\alpha}\partial^{\alpha}Q)\dot{x}_{\beta} = 0. \tag{5.3}$$

These equations (5.3), together with the original Euler equations, form an extended set of field equations. Three possibilities may arise: (a) There may exist no algebraic solutions of these equations for the velocities, in this case the original Euler equations are incompatible; (b) Eqs. (5.3), (2.2) may uniquely determine the velocities in terms of the x's, so that our equations are of the Cauchy type (i.e., we have an initial value problem); (c) algebraic solutions may exist without being unique. In the last case there may be linear combinations of the extended field equations that do not contain velocities, different from the ones we have already obtained, $u_{i\alpha}\partial^{\alpha}Q = 0$. We must then extend the field equations further by taking their time derivatives. This procedure is repeated until the velocities are uniquely determined by all the extended field equations or when the last linear combination of field equations free of velocities is identically zero. In the latter case, there will appear in the Hamiltonian an arbitrary function, and our theory will have similar invariance properties as those of the previous section. The quantization of problems of this type must be handled individually; no general procedure can be set up because of the extreme complexity of the problem.

When the velocities are uniquely determined by the extended field equations, the Hamiltonian is also a unique function. However, to the canonical equations of motion we must adjoint not only the primary constraints, $C^{\beta} = p^{\beta} - f^{\beta} = 0$ but also the secondary constraints, i.e., all the independent linear combinations of the extended field equations that are free of velocities. In order to apply Dirac's procedure for quantization, we must form the matrix whose elements are the Poisson brackets between all the constraints, primary and secondary. It will be of order $N+M$, where N is the number of degrees of freedom of the mechanical system and M is the number of secondary constraints. The matrix will be of the form

$$F = \begin{pmatrix} f^{\alpha\beta} & (C_i, C^{\beta}) \\ (C^{\alpha}, C_i) & 0 \end{pmatrix}. \tag{5.4}$$

The terms in the lower right-hand corner are zero because the C_i contain only configuration space variables. In general the rank of F will be less than $N+M$, though there are interesting cases for which it is equal to $N+M$. In the latter case, all the constraints are, in Dirac's terminology, second-class constraints. The Dirac bracket is formed with these constraints and $N+M$ variables are removed from the canonical formalism. The quantum-mechanical commutation relations are then associated with the Dirac bracket and we have only one Schrödinger equation because there are no first-class constraints.

If the rank, R, is less than $N+M$, we must take a linear combination of all the constraints and maximize the number of first-class constraints, as was done in the

previous section. The Dirac bracket is then constructed from the new second-class constraints. When we quantize, there will be $(N+M-R)$ first-class constraints that will go over into Schrödinger equations in addition to the usual one, Eqs. (4.7) and (4.8).

To help clarify the procedures outlined in this section, we will apply them to a simple example. Consider the Lagrangian density L with five independent field variables u and u_α $(\alpha=1, 2, 3, 4)$:

$$\begin{aligned} L&=-u_\alpha u_{,\alpha}+\tfrac{1}{2}u_\alpha{}^2-\tfrac{1}{2}\kappa^2u^2 \\ &=u_4\dot{u}-u_s u_{,s}+\tfrac{1}{2}u_s{}^2-\tfrac{1}{2}u_4{}^2-\tfrac{1}{2}\kappa^2u^2, \qquad (5.5) \\ c&=1, \quad \kappa=(m/\hbar)^2, \quad u_{,\alpha}\equiv\partial u/\partial x^\alpha, \quad s=1, 2, 3. \end{aligned}$$

The Euler equations are

$$\dot{u}_4-u_{s,s}+\kappa^2u=0, \quad u_s=u_{,s}, \quad \dot{u}=u_4. \qquad (5.6)$$

These two sets of equations are obviously equivalent to the Klein-Gordon equation, but the Lagrangian is in such a form that we can apply our procedure. A simple calculation shows that there are only three secondary constraints,

$$C_s\equiv u_s-u_{,s}=0. \qquad (5.7)$$

The time derivatives of these constraints,

$$\dot{u}_s-\dot{u}_{,s}=0 \qquad (5.8)$$

plus the Euler equations, allow us to solve for the velocities, though the Euler equations by themselves are insufficient to determine $\dot{u}_s$:

$$\dot{u}_4=u_{s,s}-\kappa^2u, \quad \dot{u}_s=u_{4,s}, \quad \dot{u}=u_4. \qquad (5.9)$$

Since the momenta are defined as

$$\pi^\alpha=\partial L/\partial\dot{u}_\alpha=0, \quad \pi=\partial L/\partial\dot{u}=u_4, \qquad (5.10)$$

we obtain the five primary constraints:

$$C^\alpha=\pi^\alpha=0, \quad C=\pi-u_4=0. \qquad (5.11)$$

The matrix, whose elements are the Poisson brackets of all the 8 constraints, (5.7) and (5.11), is

$$\begin{pmatrix} 0 & 0 & 0 & 0 & 0 & 0 & 0 & 1 \\ 0 & 0 & 0 & 0 & 0 & 0 & 1 & 0 \\ 0 & 0 & 0 & 0 & 0 & 1 & 0 & 0 \\ 0 & 0 & 0 & 0 & 1 & 0 & 0 & 0 \\ 0 & 0 & 0 & -1 & 0 & 0 & 0 & 0 \\ 0 & 0 & -1 & 0 & 0 & 0 & 0 & 0 \\ 0 & -1 & 0 & 0 & 0 & 0 & 0 & 0 \\ -1 & 0 & 0 & 0 & 0 & 0 & 0 & 0 \end{pmatrix}. \qquad (5.12)$$

Since its rank is eight, all the constraints are second-class, and eight variables can be eliminated. The most convenient choice for elimination is u_α and π^α. The Hamiltonian density,

$$\begin{aligned} \mathcal{H}&=\dot{u}_4\pi^4+\dot{u}_s\pi^s+\dot{u}\pi-L \\ &=\dot{u}_4C^4+\dot{u}_sC^s+\dot{u}C+u_{,s}u_s-\tfrac{1}{2}(u_s{}^2-u_4{}^2-\kappa^2u^2), \qquad (5.15) \end{aligned}$$

then reduces to

$$\mathcal{H}=\tfrac{1}{2}(\pi^2+u_{1s}{}^2+\kappa^2u^2). \qquad (5.16)$$

The Dirac bracket between any two functionals becomes simply

$$\{M,N\}=\int\left(\frac{\delta M}{\delta u}\frac{\delta N}{\delta\pi}-\frac{\delta M}{\delta\pi}\frac{\delta N}{\delta u}\right)d^3x. \qquad (5.17)$$

We see that our procedure reduces to the usual quantization procedure for the Klein-Gordon equation.

6. CONCLUSION

Theories that are linear in the derivatives of the field variables lend themselves particularly well to a detailed examination of the Dirac bracket formalism and its applicability to the problem of quantization, because of the comparatively lesser formal complexity of such theories. Despite some simplification, there remain both fundamental and computational difficulties that must be overcome before essentially nonlinear theories (such as the general theory of relativity) can be quantized successfully with the help of the formalism described in this paper.

The principal fundamental difficulty is the formulation of rules that will permit the ordering of noncommuting factors in the Hamiltonian. Presently it appears that the requirements of general covariance will greatly restrict the freedom of choice in this respect, but without leading to a unique determination; we have not yet succeeded in clearing this question up definitely.

The investigation of this fundamental question is closely related to the computational difficulty involved in handling very large systems of simultaneous algebraic equations. In general relativity, in the Palatini formulation, there are altogether 50 field variables, 10 components of the metric tensors and 40 components of the affine connection. Though some degree of separation of the system of equations that determines the null vectors of the matrix f^{AB} is possible, the remaining problem is still formidable. We hope that these difficulties will be overcome in the near future.

Letters to the Editor

PUBLICATION of brief reports of important discoveries in physics may be secured by addressing them to this department. The closing date for this department is five weeks prior to the date of issue. No proof will be sent to the authors. The Board of Editors does not hold itself responsible for the opinions expressed by the correspondents. Communications should not exceed 600 words in length and should be submitted in duplicate.

Temperature Effects in the Annihilation of Positrons*

ROBERT T. WAGNER AND FRANK L. HEREFORD
Department of Physics, University of Virginia, Charlottesville, Virginia
(Received May 12, 1955)

A COMPONENT of anomalously long lifetime was first observed by Bell and Graham[1] in the decay of positrons in several condensed materials. In order to account for this component, which we shall call the τ_2 component, they postulated the existence of triplet state positronium which was being converted to the singlet state and subsequently annihilating. Several of the substances which exhibited the τ_2 component also showed a dependence of τ_2 on the temperature of the annihilation medium. This was particularly true in the case of Teflon. Graham and Stewart[2] further observed that as the temperature was reduced, the three-photon annihilation rate in Teflon decreased, thus establishing a correlation between τ_2 and three-photon annihilations as a function of temperature. We have further investigated the effects of reduced temperature in several other substances which show a τ_2 component. Among these were methyl alcohol, water, and glycerine, each containing a small amount of $Na^{22}Cl$ in solution.

The $Na^{22}Cl$ of about one mC activity was first dissolved in 5 ml distilled water, this aqueous solution later being evaporated to the salt residue and redissolved in methyl alcohol and glycerine for the determinations in these liquids. The active solution was placed in a small Pyrex volumetric flask and submerged in the various refrigerating agents such as liquid helium, liquid nitrogen, solid carbon dioxide in alcohol, and freezing mixtures of ice and salt. The refrigerants were placed inside a Dewar which was contained in a second Dewar. NaI(Tl) scintillation counters placed at 120° relative to one another were used as radiation detectors. A fast triple coincidence circuit was built to record the number of three- and two-photon coincidences. Provisions were made to lift one of the counters out of the coplanar position of source and counters by 45° in order that triple coincidences other than from the three-photon annihilation of positrons could be measured. The coplanar to noncoplanar ratio was 1.86. Twofold coincidences were measured by placing two of the counters at 180° with respect to one another and coplanar with the source. The counting rates thus obtained were not absolute rates inasmuch as the counter efficiencies had not been determined. Care was exercised in maintaining a constant mass of material surrounding the sample when changing refrigerants. For example, at higher temperatures wood alcohol (density 0.806 g/cm³) replaced the liquid nitrogen (density 0.804 g/cm³) used in the outer Dewar for the measurements at 4.2°K. Also, the constancy of the twofold coincidence rate for the various refrigerants showed that the absorptivity of the different refrigerants did not change. Room temperature twofold and threefold coincidences were taken first, followed by the rates at the reduced temperature, and finally the room temperature rates were remeasured to assure that counting rates had not drifted during the course of a determination. The results are plotted in Fig. 1, where the normalized threefold coincidence rate has been shown as a function of temperature. The normalization factor was determined by comparison of twofold coincidence rates for the various runs.

A decrease in the threefold coincidence rate is apparent after the annihilation medium has become solid due to freezing. In this connection, the water solution solidified at 260°K, methyl alcohol at 176°K, and glycerine began to solidify at about 290°K. The threefold rate was also measured for annihilation of Zn^{65} positrons in the zinc. No temperature effect was found, which observation is consistent with the absence of a τ_2 component in metals.

These data then support the correlation between the anomalous τ_2 component and the increased three-photon counting rate. A similarity in the effects of temperature on these two phenomena is also apparent. The most significant aspect of the data presented here is the indication that the temperature effect occurs only

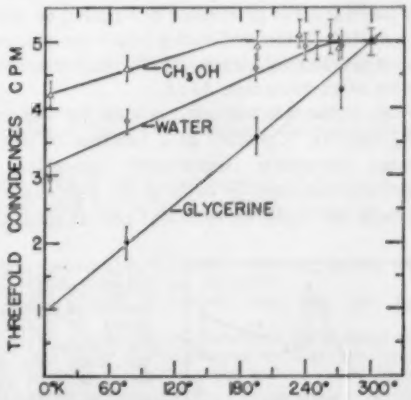

FIG. 1. Three-photon annihilation rate as a function of temperature. Open circles—annihilation in water; closed circles—glycerine; triangles—methyl alcohol. Rates for different materials were arbitrarily normalized at 300°K.

after solidification of the materials. Sufficient experimental data are not yet available to draw definite conclusions about the nature of the state responsible for the τ_2 lifetime and increase three-photon rate nor about the mechanism of its destruction. However, our results suggest the importance of the order and structural state of the materials and perhaps such factors as the dielectric constant which is known to be temperature-dependent.

* Supported by the Office of Ordnance Research.
[1] R. E. Bell and R. L. Graham, Phys. Rev. **90**, 644 (1954).
[2] R. L. Graham and A. T. Stewart, Can. J. Phys. **32**, 678 (1954).

Effect of Elastic Strain upon Electrical Resistance when Cold-Work Induced Imperfections are Present

E. W. KAMMER

Naval Research Laboratory, Washington, D. C.
(Received May 3, 1955)

MOLENAAR and Aarts[1] have shown that the increase in electrical resistance produced in copper by cold work at liquid nitrogen temperature can be partially removed by annealing the specimen at room temperature. Experiments by Manintveld[2] indicate that the resistance contribution removable by this mild heat treatment is due to vacancies or aggregates of vacancies since the activation energies correspond closely with theoretically estimated values.[3] The experiment reported here is concerned with the effect of elastic strain upon the electrical resistance after the metal has been subjected to various amounts of cold-work. By means of simple tension, permanent elongation was produced in an annealed copper wire (diameter 0.001 inch) while submerged in liquid nitrogen. At certain increments of permanent elongation, an elastic strain cycle was performed during which the change in resistance per unit resistance, $\Delta R/R$, was measured as a function of elastic strain, $\Delta L/L$.

In Fig. 1 the quantity, G, defined by the ratio $(\Delta R/R)/(\Delta L/L)$, is plotted as a function of percent permanent elongation. Immediately preceding the measurement indicated by point A the wire was withdrawn from the liquid nitrogen and kept at room temperature for several hours. Without further cold work the specimen was again cooled and the ratio, G, represented by the point A, was determined. After a small increase in permanent elongation the wire was removed from the liquid nitrogen and the value of G was determined under room temperature conditions. This point is designated by B.

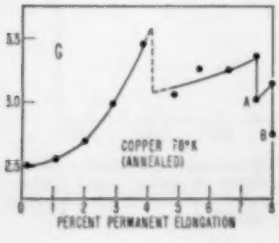

FIG. 1. The ratio, $G = (\Delta R/R)/(\Delta L/L)$, as a function of plastic elongation in copper at liquid nitrogen temperature. Each point represents the slope of an electrical resistance *versus* elastic strain relation measured at the indicated state of deformation.

The strain sensitivity factor, G, changes in much the same manner and degree as did the resistivity in the experiment of Molenaar and Aarts after the room temperature anneal. This behavior suggests that each type of imperfection makes its own contribution to the factor G. In this case vacancies generated by cold-work influence the relationship between elastic strain and resistivity to an easily measurable degree. The graph is also evidence that the factor G can experience large changes in magnitude during the deformation process, independently of the annealing treatment. Evidently there is a complicated interplay between the imperfection generation and escape or annihilation processes.

[1] J. Molenaar and W. H. Aarts, Nature, **166**, 690 (1950).
[2] J. A. Manintveld, Nature **169**, 623 (1952).
[3] T. Broom, Advances in Phys. **3**, 74 (1954).

Angular Correlation of Photons from Positron Annihilation in Solids

A. T. STEWART

Physics Division, Atomic Energy of Canada Limited, Chalk River, Ontario, Canada
(Received April 11, 1955)

MEASUREMENTS of the angular correlation of photons from positron annihilation have been continued[1] with better resolution, and two new effects have been observed.

The shape of the angular correlation curve varies considerably throughout a series of some dozen metals from Be to Pt. Figure 1 shows typical coincident counting rates, $I(\varepsilon)$, as a function of ε, the angle between the annihilation photons. These data, when corrected for instrument resolution,[2] have yielded the average momentum distribution, $N(k)dk$, of annihilating electron-positron pairs by using the fact that $\varepsilon dI/d\varepsilon$ is proportional to $N(k)$.

For the light metals the momentum distribution of annihilating pairs resembles that found by other means[3] for the conduction electrons alone. For the heavier metals a component of higher momentum appears.[4] Figure 2 shows typical distributions for Zn and Mg. Results for a number of metals show that the higher momentum component increases with the fractional volume occupied by the ion cores, possibly indicating an increased number of annihilations with bound electrons or an excluded volume effect[5] in the annihilation with conduction electrons.

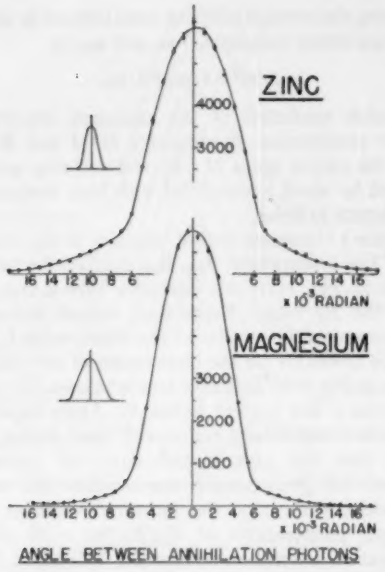

FIG. 1. Observed angular correlations of photons from positron annihilation in Zn and Mg. The instrument resolution is indicated.

In amorphous nonconductors, as Page *et al.*[6] have already shown, the angular correlation has a broad base and somewhat sharper peak than is observed for most metals. An example of this can be seen by comparing Fig. 1 and Fig. 3. In Teflon, the maximum coincident counting rate increases gradually with increase in temperature. In Fig. 3, the results for Teflon at two temperatures, 77°K and 525°K, are shown. If it is supposed that positrons in Teflon annihilate by two processes, corresponding to narrow and wide components of the observed curves, then it appears that as the temperature is raised the narrow component becomes narrower or its intensity increases at the expense of the other component. It is probable that these two annihilation processes may be related to the two modes of decay observed by Bell and Graham,[7] one of which also showed a temperature effect.

The observed lifetimes of positrons in solids, the three quantum annihilation rate experiments,[8] and the present measurements all suggest that the mechanism of positron annihilation in metals and crystalline solids is different from that in amorphous nonconducting materials.

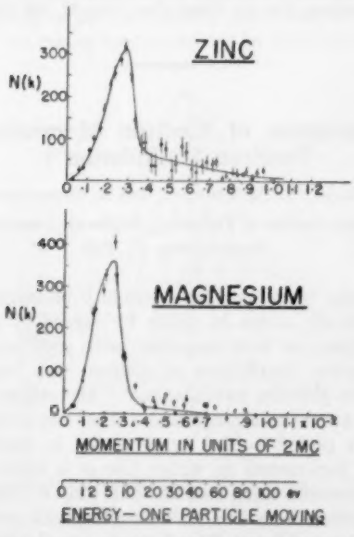

FIG. 2. Momentum distribution of annihilating pairs in Zn and Mg.

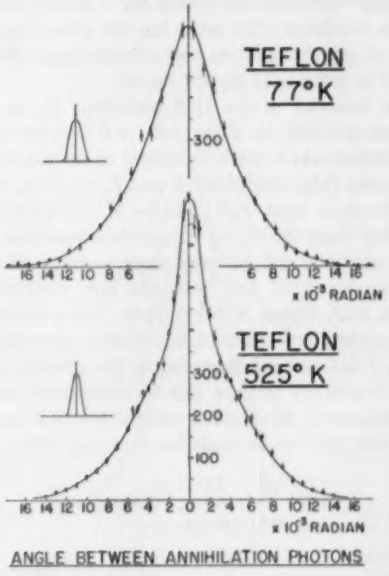

FIG. 3. Observed angular correlation of photons from positron annihilation in Teflon. The instrument resolution is indicated.

This work is being continued and a full account will be submitted for publication in the *Canadian Journal of Physics*.

[1] R. E. Green and A. T. Stewart, Phys. Rev. **98**, 486 (1955).
[2] C. Eckart, Phys. Rev. **51**, 735 (1937).
[3] For example, W. B. Skinner, Trans. Roy. Soc. (London) **A239**, 95 (1946).
[4] Through the courtesy of Professor S. DeBenedetti we have learned that similar results have been obtained in his laboratory.
[5] DeBenedetti, Cowan, Konneker, and Primakoff, Phys. Rev. **77**, 205 (1950).
[6] Page, Heinberg, Wallace, and Trout, Phys. Rev. **98**, 206 (1955) and L. A. Page (private communication).
[7] R. E. Bell and R. L. Graham, Phys. Rev. **90**, 644 (1953).
[8] R. L. Graham and A. T. Stewart, Can. J. Phys. **32**, 678 (1954); T. A. Pond, Phys. Rev. **93**, 478 (1954).

Hall Theory in *n*-Type Germanium*

LOUIS GOLD
Lincoln Laboratory, Massachusetts Institute of Technology, Lexington, Massachusetts
(Received April 7, 1955)

A STUDY of the galvanomagnetic properties of the eight-[111] and six-[100] ellipsoidal models, appropriate respectively for the energy surfaces in *n*-type germanium and silicon, has been in progress for some time in the Lincoln Laboratory.[1] Using the assumption of energy-independent scattering time τ which has already been employed to explain cyclotron resonance,[2] theoretical calculations have been carried out. Preliminary comparison of the angular and magnetic field B dependence of the magnetoresistance reveals essential agreement with the energy-dependent τ theories,[3,4] although admittedly the constant τ assumption is restrictive. The latter has the advantage, however, of greatly reducing the computational effort required in arriving at explicit results.

The behavior of the Hall coefficient R_H in *n*-germanium is as follows: Plots of R_H *vs* B have two asymptotic values which are independent of orientation—the saturation (high-field) limit is just $R_\infty = 1/Nqc$, while in the low-field limit $R_0 = [3K(K+2)/(2K+1)^2]R_\infty$. In between these limits, an orientation-dependent minimum occurs which becomes more pronounced as the current density J and magnetic field directions are chosen with higher Miller indices. The occurrence of such minima for τ characteristic of lattice scattering was pointed out earlier.[5] However, in the present description, it is easier to show this for diverse orientations; and moreover, for a given orientation of $\mathbf{J}$ and $\mathbf{B}$, a universal plot can be made for R_H *vs* $\omega\tau$, where

$$\omega = \frac{qB}{m^*c}\cdot\frac{3K}{2K+1}, \quad K = m_1/m_2,$$

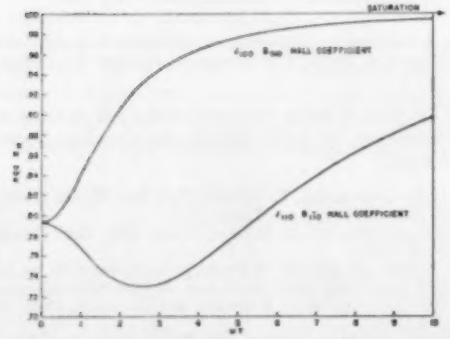

FIG. 1. Behavior of Hall coefficient plotted in terms of the universal parameter $\omega\tau$ which simultaneously depicts the effect of magnetic field and scattering time: (a) The case $\mathbf{J}_{100}$, $\mathbf{B}_{010}$; (b) the case $\mathbf{J}_{110}$, $\mathbf{B}_{1\bar{1}0}$.

m^* being the average effective mass defined in terms of the mass tensor components m_1 and m_2, by

$$3/m^* = 1/m_1 + 2/m_2.$$

Favorable resolution of the minimum requires the proper combination of symmetry for $\mathbf{J}$ and $\mathbf{B}$ along with the proper range of $|B|$ and τ, being generally abetted by small τ associated with high temperatures and impure samples.

Figure 1 illustrates typical behavior of the universal plots. The arrangement $\mathbf{J}_{100}$, $\mathbf{B}_{010}$ exhibits the behavior shown in Fig. 1(a); the minimum here is coincident with the R_0 value. Experiment indeed indicates a minimum very close to $B=0$.[6] The situation for $\mathbf{J}_{110}$, $\mathbf{B}_{1\bar{1}0}$ is more amenable for the observation of the minimum which as Fig. 1(b) indicates occurs at $\omega\tau \sim 2.5$ with an R_H value a few percent below R_0. Again experiment seems to be essentially in line with this.[6] So far, it appears that the experimental data fall somewhere between the predictions of the constant and energy-dependent τ theories; the measured value at liquid nitrogen temperatures of R_∞/R_0 for $\sim$10 ohm-cm material at room temperature lies between 1.27 and 1.08 in these respective theories, for K about 19.[6]

I would like to thank Miss M. Clare Glennon of the Lincoln Laboratory Computer Group for carrying out the calculations and W. M. Bullis and W. Krag for permission to refer to their research still in progress.

* The research reported in this document was supported jointly by the Army, Navy, and Air Force, under contract with the Massachusetts Institute of Technology.

[1] L. Gold and L. M. Roth (to be published).
[2] Lax, Zeiger, and Dexter, Physica **20**, 818 (1954).
[3] B. Abeles and S. Meiboom, Phys. Rev. **93**, 1121 (1954).
[4] M. Shibuya, Phys. Rev. **95**, 1385 (1954).
[5] W. Krag and W. M. Bullis (to be published).
[6] Dresselhaus, Kip, and Kittel, Phys. Rev. **98**, 368 (1955).

Measurement of Electron Momentum by Positron Annihilation*†

G. LANG,‡ S. DEBENEDETTI, AND R. SMOLUCHOWSKI
Carnegie Institute of Technology, Pittsburgh, Pennsylvania
(Received May 27, 1955)

IN order to explore the possibility of investigating electronic states in solids by means of positron annihilation we have measured, with good resolution, the angular distribution of gamma rays from two-quantum positron annihilations[1–4] in various metals. The experimental arrangement utilizes two scintillation counters placed behind vertical slits in lead blocks located two meters on either side of a vertical strip of the material being studied. This strip is bombarded by positrons from two Na^{22} sources which are placed on opposite sides of it and which are shielded from direct view of the fixed counter. The movable counter

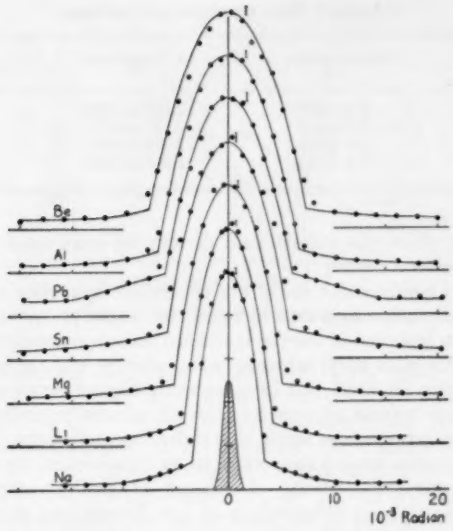

FIG. 1. The shaded curve is the calculated resolution. The central parabolas are computed from density, atomic weight, and valence, assuming an ideal Fermi gas at zero temperature. The abscissas of the sharp corners correspond to computed maximum momenta.

rotates about a vertical axis passing through the sample. The slits are 2 mm wide and the sample has, in each case, an effective width of 1 mm as seen from the counter positions. We estimate the resolution curve to have a width at half-maximum of about 1.3 milliradians.

The experimental results are plotted as a function of the angular deviation from 180°. This deviation, expressed in radians, is equal to the z component of the momentum of the annihilating pair, measured in units of mc. All curves are normalized to the same height at the center. The standard deviation, shown only for the highest point of each curve, varies as the square root of the counting rate. The background at high angles is explainable in terms of random coincidences. A correction for the finite resolution of the instrument would not appreciably alter the position of the points.

The curves of Fig. 1 consist of two parts, a central parabola and a large-angle tail. The parabolas are the computed z-momentum distribution of electrons of a Fermi gas having the same density as that of free electrons in the metal, assuming the number of free electrons per atom equal to the number of the corresponding column in the periodic table. The curves of the tails have been traced through the experimental points.

It is interesting that the momentum distribution of the annihilating pairs should correspond so closely to that of a Fermi gas. This fact seems to imply (a) that the positrons annihilate at rest, (b) that they seldom annihilate with the electrons of the atomic cores, (c) that this type of experiment does not reveal significant local effects of the lattice upon the electrons, (d) that the annihilation probability is independent of the electron velocity. It is also interesting to note that Al, Sn, and Pb show alkali-like angular distributions in spite of the presence of overlapping bands. This may indicate that we are sampling electrons only in interstitial regions.

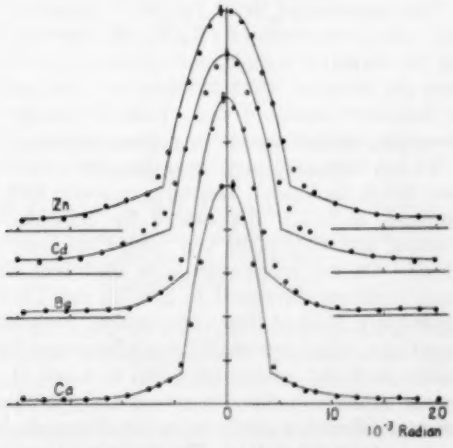

FIG. 2. Other examples of the angular distribution of annihilation radiation. See caption of Fig. 1.

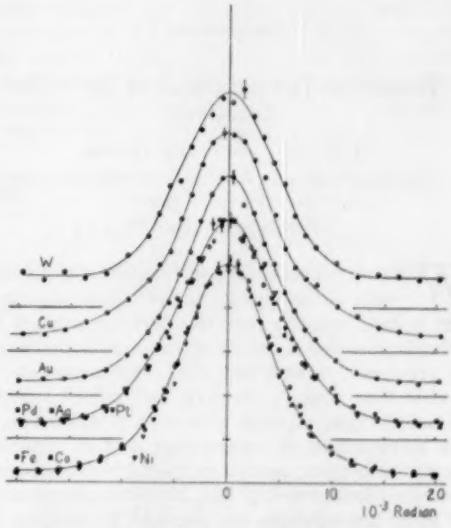

FIG. 3. Angular distributions from transition and noble metals. Curves are experimental.

For the elements of Fig. 2, the decomposition of the curves into two parts is more ambiguous since the tails blend more smoothly with the central peaks. However, a treatment similar to that of Fig. 1 gives reasonable results.

In Fig. 3, transition metals and noble metals, the analysis in terms of parabolas is not possible because of the large size of the tails. Since the cores are close to each other in these elements, one is tempted to associate these tails with the electron of the atomic cores.[5] To the accuracy of this experiment Fe, Co, and Ni are indistinguishable; the same is true of Pd, Pt, and Ag.

* This work is being supported by the National Science Foundation.

† Paper submitted (by G. L.) in partial fulfillment of the requirements for the degree of Doctor of Science at Carnegie Institute of Technology, 1955.

‡ Sylvania Electric Products Company, Predoctoral Fellow.

[1] DeBenedetti, Cowan, Konneker, and Primakoff, Phys. Rev. **77**, 205 (1950).

[2] Page, Heinberg, Wallace, and Trout, Phys. Rev. **98**, 206 (1955).

[3] R. E. Green and A. T. Stewart, Phys. Rev. **98**, 486 (1955); also A. T. Stewart (personal communication of more recent work).

[4] Ambrosino, Houbaut, and Maignan, Compt. rend. **237**, 708 (1953).

[5] J. Des Cloizeaux and G. Ambrosino, Compt. rend. **237**, 1069 (1953).

Transition Temperatures of He^3-He^4 Solutions

J. G. Dash and R. Dean Taylor

University of California, Los Alamos Scientific Laboratory, Los Alamos, New Mexico

(Received April 11, 1955)

WE are currently engaged in an experimental study of the superfluidity of dilute solutions of He^3 in He^4, including pure He^4. Measurements of the behavior of a torsion pendulum immersed in the liquids, as previously carried out[1] yield information on the normal fluid density, viscosity, and critical velocity. This technique, together with certain refinements in the measurement of temperature and of pendulum oscillation periods, permits us to make quite accurate determinations of the λ points. Transition temperatures of individual solutions are obtained by locating the discontinuity in slope of the torsion period *versus* temperature, which is equivalent to finding the temperature

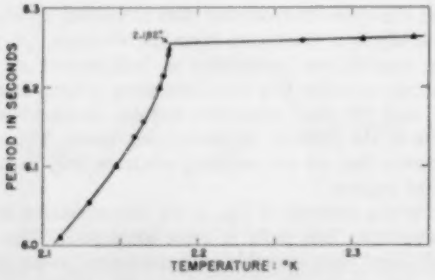

FIG. 1. Behavior of pendulum period in the vicinity of the λ point: pure He^4.

TABLE I. The λ temperatures of solutions.

Concentration x%	λ Temperature °K
Pure He^4	2.182±0.0005
3.65±0.2	2.127±0.002
6.0 ±0.2	2.096±0.002
9.2 ±0.2	2.045±0.002

at which the normal fluid density becomes equal to the total density.

Liquids under study are condensed in a glass cell surrounded by a bath of liquid He^4. Vapor pressures of the bath and of the cell liquid are read on manometers filled with butyl sebacate, whose density and thermal expansion coefficient have been carefully measured in a large volume pycnometer. The oil manometer readings are expressed in terms of standard mercury level differences, using a conversion factor composed of the oil density, the density of mercury at 20°C,[2] and the gravitational accelerations at Los Alamos and at sea level. Estimated accuracy of the manometry is ±0.2 mm oil, corresponding to ±0.014 mm Hg. Vapor pressures are converted to temperatures on the 1948 "agreed" liquid helium scale.[3] Bath temperatures are stabilized by an electronic regulator of the Sommers type,[4] to within 0.1 millidegree in the vicinity of the λ point. The oscillating system is composed of a fine torsion wire suspending a stack of 50 closely spaced Al disks centered in the glass cell. The pendulum has a period of 5.2680 seconds *in vacuo* and a period of 6.250 seconds in He I near the λ point. Times of several oscillations are measured with the aid of an electronic chronograph to about 1 millisecond accuracy. Sensitivity and accuracy of the method are suggested by Fig. 1, which shows the behavior of the period in the vicinity of the transition, for the case of pure He^4.

When solutions of He^3 in He^4 are condensed in the cell, molar concentration $x=N_3/N_3+N_4$ (where N_3, N_4 are the respective isotopic concentrations) is obtained from the measured vapor pressures and interpolation of Sommers'[5] smoothed data. Table I presents the transition points of pure He^4 and three solutions.

We find 38.00±0.05 mm Hg as the vapor pressure of pure He^4 at the λ point. This value compares with the pressures 38.3±0.2 mm quoted by Schmidt and Keesom[6] and 38.10±0.02 mm quoted by Long and Meyer.[7] On the temperature scale used here, these vapor pressures correspond to 2.185°K and 2.183°K, respectively. Both of these investigations consisted of detecting a vapor pressure difference between a liquid helium bath and helium condensed in a cell at the bottom of the bath. The disappearance of a detectable pressure difference is attributed to the abnormally high heat conductivity of He II. This technique appears to be less direct than the present method.

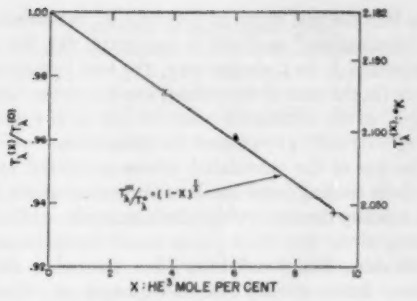

FIG. 2. Variation of λ point with He^3 concentration.

Numerous theoretical calculations[8] of the effect of He^3 on He^4 give predicted slopes $dT_\lambda^{(x)}/dx$ varying from -6 to -1.6 degrees/mole fraction in the concentration range of the present study. Our results yield a slope of -1.47 ± 0.03 degrees/mole fraction for small x. King and Fairbank[9] report a slope of -1.5 degrees/mole fraction for concentrations up to 4.3 percent.

The experimental λ temperatures are in excellent agreement, to within 2 millidegrees, with the function $T_\lambda^{(x)}=T_\lambda^0(1-x)^{\frac{1}{3}}$ given by Goldstein.[10] This simple dependence arises from the asymptotic Bose-Einstein model, when neglecting the effect of He^3 on the *total* liquid density. Our experimental points, together with the above empirical law, are shown in Fig. 2.

The present work is being continued, and will be reported in more detail in the future.

[1] E. L. Andronikashvilli, J. Phys. (U.S.S.R.) **10**, 201 (1946); A. C. Hollis-Hallett, Proc. Roy. Soc. (London) **A210**, 404 (1951).
[2] *Handbook of Chemistry and Physics* (Chemical Rubber Publishing Company, Cleveland, 1948), thirtieth edition.
[3] H. van Dijk and D. Shoenberg, Nature **164**, 151 (1949).
[4] H. S. Sommers, Jr., Rev. Sci. Instr. **25**, 793 (1954).
[5] H. S. Sommers, Jr., Phys. Rev. **88**, 113 (1952).
[6] G. Schmidt and W. H. Keesom, Physica **4**, 963 (1937).
[7] E. Long and L. Meyer, Phys. Rev. **83**, 860 (1951).
[8] J. G. Daunt, Advances in Phys. **1**, 209 (1952).
[9] J. C. King and H. A. Fairbank, Phys. Rev. **91**, 489 (1953).
[10] L. Goldstein, Phys. Rev. **95**, 869 (1954).

Ferromagnetism in Noble Metal Alloys Containing Manganese

F. A. OTTER, JR., P. J. FLANDERS, AND E. KLOKHOLM
Laboratories for Research and Development, The Franklin Institute, Philadelphia, Pennsylvania
(Received May 16, 1955)

IN the course of investigating the electrical resistivities and thermopowers of some noble metal binary alloys,[1] it was noted that the resistivity of the alloys containing more than about eight atomic percent manganese deviated from linearity at low temperatures as shown in Fig. 1. Similar behavior has been reported by others.[2] The temperature at which the break in the resistivity occurs increases with increasing manganese content.

TABLE I. Ferromagnetic properties of three specimens.

Alloy	T (°K)	σ_s (emu/g)	T_c (°K)	$N_{eff}(\mu_B)$
Au+18.64 at. % Mn	180	4.78	317	1.3
Au+13.01 at. % Mn	83	3.88	139	1.9
Ag+14.58 at. % Mn	84	1.33	163	0.25

Magnetic moment measurements on three of our specimens showed that they are ferromagnetic. Since other ferromagnetic substances show definite changes in the slope of the resistivity *vs* temperature curves at the Curie temperatures,[3,4] one would then suspect that all of the noble metal alloys with more than about eight atomic percent manganese are ferromagnetic[5] with Curie temperatures that increase with increasing manganese content.

Table I shows the saturation moments at the indicated temperatures, the Curie temperatures, and the approximate number of Bohr magnetons per manganese atom based on extrapolations to 0°K. The magnetic moment of the Au+18.64 atomic percent Mn specimen also possessed a paramagnetic component at high fields so that the total moment could be written as

$$M=\sigma_s+\chi H,$$

where

$$\chi=C/(T-\Theta) \text{ (Curie-Weiss law).}$$

If χ is mass susceptibility, the values of Θ and C are

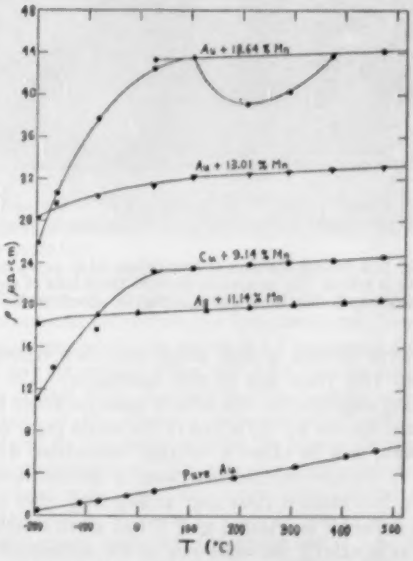

FIG. 1. Typical resistivity curves for Cu-Mn, Ag-Mn, and Au-Mn alloys.

58°K and 1.65×10^{-2}, respectively. The coexistence of two types of magnetism in the same specimen would seem to be consistent with the existence of a partial state of order that has been proposed to explain the resistivity anomaly around 230°C. We are planning to investigate these and other alloys in the same composition range at temperatures in the liquid helium range.

[1] F. A. Otter, Jr., Phys. Rev. **98**, 1552(A) (1955).
[2] A. L. Norbury and K. Kuwada, Phil. Mag. **4**, 1338 (1927); A. N. Gerritson and J. O. Linde, Physica **17**, 573 (1951).
[3] R. M. Bozorth, *Ferromagnetism* (D. Van Nostrand Company, Inc., New York, 1951), p. 763.
[4] F. J. Donahoe, Acta Metallurgia (to be published).
[5] Au_2Mn was reported ferromagnetic by Roub, Zwicker, and Baur, Z. Metallkunde **44**, 312 (1953).

Spin Echoes with Four Pulses

G. J. B. Crawford
Radiation Laboratory, McGill University, Montreal, Canada
(Received May 23, 1955)

RECENTLY, Das and Roy,[1] in extending previous analyses of the spin echo experiments[2,3] to the case of four pulses, have drawn attention to an unexplained echo (occurring at $t=2\tau_3-\tau_2+\tau_1$) specially characteristic of such a pulse sequence. Figure 1 shows

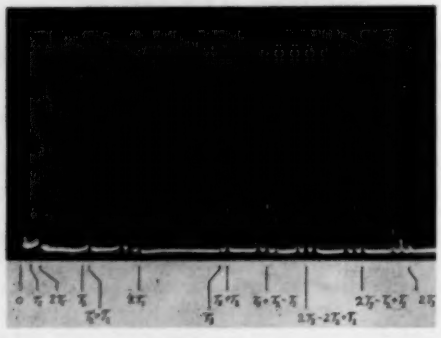

FIG. 1. A typical sequence of four pulses (at 0, τ_1, τ_2, and τ_3) and their echoes. The separation between the echoes in any particular group of three is τ_1. The pulses are all approximately 120°.

a typical pattern of four pulses and their echoes obtained two years ago in this Laboratory. The echo spacing suggests that the echo in question arises in the normal manner by the action of the fourth pulse (at τ_3) on what may be called a "virtual" stimulated echo at $\tau_2-\tau_1$. Vector considerations[4] and a detailed analysis do in fact make it clear that at any time after τ_2 the spin ensemble is oriented as if it had given a signal at $\tau_2-\tau_1$ in exactly the same way as the stimulated echo at $\tau_2+\tau_1$ was produced. The analysis also shows that this "virtual" echo is the one transformed by the fourth pulse into the real signal at $2\tau_3-\tau_2+\tau_1$, in accord with the "mechanism" outlined in paragraph (e), Sec. III, of reference 1. In a similar way, the four "pentanary" echoes (in the case of five pulses) are due to the "mirror images" of the stimulated echoes at $\tau_3+\tau_1$, $\tau_3+\tau_2-2\tau_1$, $\tau_3+\tau_2-\tau_1$, and $\tau_3+\tau_2$ about the pulse at τ_3.

The use of the stimulated echoes generated by the fourth or reading pulse has been suggested[4] as the basis of a memory device in which the amplitude, width, and spacing of the first three pulses would form the coding mechanism. The possibilities of a somewhat simpler system have already been explored at Stanford University.[5]

The author gratefully acknowledges discussions on this problem with Professor J. S. Foster and Professor J. D. Jackson of this Laboratory.

[1] T. P. Das and D. K. Roy, Phys. Rev. **98**, 525 (1955).
[2] E. L. Hahn, Phys. Rev. **80**, 580 (1950).
[3] T. P. Das and A. K. Saha, Phys. Rev. **93**, 749 (1954).
[4] G. J. B. Crawford, Ph.D. thesis, McGill University, 1954 (unpublished).
[5] S. Fernbach and W. G. Proctor, J. Appl. Phys. **26**, 170 (1955).

Effect of Screening on Solute Diffusion*

F. J. Blatt
Physics Department, University of Illinois, Urbana, Illinois
(Received May 13, 1955)

RECENT experiments[1,2] on the diffusion of cadmium, indium, tin, and antimony into silver have shown that the activation energy for diffusion decreases as Z, the valence difference between solute and solvent atoms, increases. Lazarus[3] proposed an explanation of these results, invoking the electrostatic interaction between solvent and solute ions in the metallic lattice. A critical parameter of his theory is the screening radius r_s of the screened Coulomb potential used to represent the solute ion. Lazarus used a screening radius derived from the Fermi-Thomas model and obtained good agreement between theory and experiment. Since in the Fermi-Thomas approximation r_s is independent of the valence of the solute atom, the theory predicted that H, the activation energy for solute diffusion, is given by

$$H=H_0-H_1Z,$$

where H_0 is the activation energy for self-diffusion of the solvent, and H_1 is a function only of the properties of the solvent, and not of the solute.

Now it is well known that in some instances, for example a calculation of the resistivity of dilute alloys,[4] the Fermi-Thomas model gives incorrect numerical results. Recently, Friedel has shown[5] that the Fermi-Thomas model is only a first approximation in an evaluation of the appropriate screening radius; if this parameter is determined by satisfying the quasi self-consistent condition that the total screening charge

TABLE I. Screening radius as a function of valence difference for impurities in silver.

Z	-3	-2	-1	$+1$	$+2$	$+3$	$+4$
r_s (A)	0.73	0.7	0.665	0.5	0.485	0.473	0.468

equal the valence difference (Friedel sum rule), one then finds the r_s is, for a given solvent metal, also a function of Z.

The correct screening radii for fulfilling the Friedel condition have been evaluated for impurities in silver. The results are listed in Table I. The form of the potential, namely $(Z/r)\exp(-r/r_s)$, was assumed *a priori*, and r_s was treated as an adjustable parameter. In Fig. 1 are shown the activation energies for solute diffusion calculated from these screening radii using the formula derived by Lazarus, as well as the experimental activation energies and those obtained by using the screening radius predicted by the Fermi-Thomas model.

There may be a number of reasons for the discrepancy between the calculated and experimental results. The theory proposed by Lazarus is admittedly only semi-quantitative. Also, the assumption of a screened Coulomb potential neglects all effects due to the size of the ion core, although this may play a significant role.

In any case, a significant feature of the results is the marked asymmetry of the calculated activation energies about the point $Z=0$. This asymmetry is a consequence of the dependence of r_s on Z, shown in Table I, which gives rise to much larger screening radii for negative than for positive Z values. One may, therefore, predict from this dependence of r_s on Z that the absolute magnitude of the difference in activation energies for solute and self-diffusion should be significantly larger for solutes which are electropositive relative to the solvent than for the corresponding electronegative solutes. This conclusion appears to be confirmed by preliminary measurements on the diffusion of ruthenium in silver.[6]

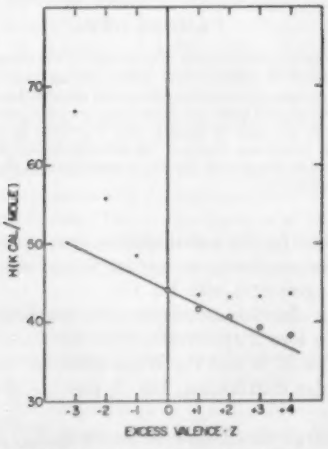

FIG. 1. Calculated and experimental activation energies for solute diffusion in silver. The straight line results from the use of a constant screening radius given by the Fermi-Thomas model. The solid points were calculated with the screening radii listed in Table I. The circles show the experimental results.

The author is grateful to Professor D. Lazarus, Professor L. Slifkin, and Dr. C. T. Tomizuka for several stimulating conversations, and to Dr. S. Machlup for his generous help in preparing the numerical work for machine computation by the ILLIAC.

* Supported by the Office of Naval Research.
[1] Sonder, Slifkin, and Tomizuka, Phys. Rev. **93**, 970 (1954).
[2] C. T. Tomizuka and L. Slifkin, Phys. Rev. **96**, 610 (1954).
[3] D. Lazarus, Phys. Rev. **93**, 973 (1954).
[4] N. F. Mott, Proc. Cambridge Phil. Soc. **32**, 281 (1936).
[5] J. Friedel, Advances in Phys. **3**, 446 (1954).
[6] C. T. Tomizuka (private communication).

Energy Distribution of Neutrons Scattered by Paramagnetic Substances

B. N. BROCKHOUSE

Physics Division, Atomic Energy of Canada Limited, Chalk River, Ontario, Canada

(Received April 26, 1955)

SLOW neutrons, when scattered magnetically by a paramagnetic material, undergo an energy change which depends on the degree of coupling of the magnetic ions. Van Vleck[1] has calculated the energy changes expected for paramagnetic substances in which the coupling arises from exchange forces. In a high-temperature approximation he finds that the rms energy change

$$(\delta E)_{\text{rms}}=k_B|\Delta|[6/ZS(S+1)]^{\frac{1}{2}}, \qquad (1)$$

where k_B is Boltzmann's constant, Z is the number of interacting neighbors, S is the spin of the ion and Δ is the Weiss constant determined from the measured susceptibility by fitting to the Curie Weiss law $\chi=C/(T-\Delta)$. Van Vleck was not able to obtain a detailed energy distribution but a calculation of the fourth moment suggested that a Gaussian might be a fair approximation.

By using the apparatus shown in Fig. 1, the energy distribution of neutrons scattered by a number of paramagnetic substances has been measured. Neutrons of wavelength λ_0 in the region of 1.3 angstroms (energy 0.05 ev) are selected from the *NRX* reactor spectrum by a crystal (*X*1). A small fraction (usually about 10 percent) of the resulting monoenergetic neutrons is scattered by the specimen, and the energy distribution of those scattered at some particular angle ϕ is examined by means of an analzying crystal spectrometer (*X*2). Background is obtained by turning the crystal (*X*2) by an amount such that the Bragg law can no longer be satisfied for any neutron energy. This is done automatically at intervals during a run. A background so

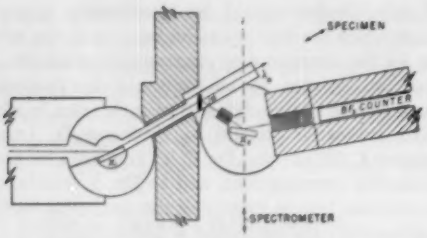

FIG. 1. Schematic diagram of the apparatus. The angle of scattering ϕ can be changed by moving the specimen and the spectrometer as indicated.

determined has been subtracted in the results following. The energy distributions are normalized to the counting rate obtained with the counter looking directly at the specimen and can be put on an absolute basis by comparison with similar measurements on a vanadium standard. The scattering by vanadium metal, which is almost completely incoherent, consists,[2,3] of a widely spreading inelastic component which increases with angle of scattering and temperature, and a truly elastic component which falls off with angle of scattering and temperature according to a Debye-Waller factor. The shape of this elastic peak is taken to represent the resolution function of the instrument at the incident energy. A rough intensity calibration has been obtained by theoretical considerations[4] and by measuring the energy distribution of neutrons scattered by a thick (~10 mean free paths) paraffin scatterer and assuming them to be Maxwellian.

Measurements were made on anhydrous specimens of $MnSO_4$ and Mn_2O_3.

$MnSO_4$.—In this substance the coupling between the manganese ions is small as indicated by the Weiss constant[5] of $\Delta = -24°$ and the fact that the transition temperature is less than 14°K. The angular distribution of the scattered neutrons,[6] Fig. 2, shows no structure which might be attributable to effects of coupling.

The energy distribution of neutrons scattered with the momentum change $4\pi \sin(\phi/2)/\lambda_0 = 0.97$ A^{-1} is shown in Fig. 3(a). The points were fitted to the resolution function for the instrument by area normalization. Within the accuracy, no perceptible energy changes occur, in agreement with Eq. (1).

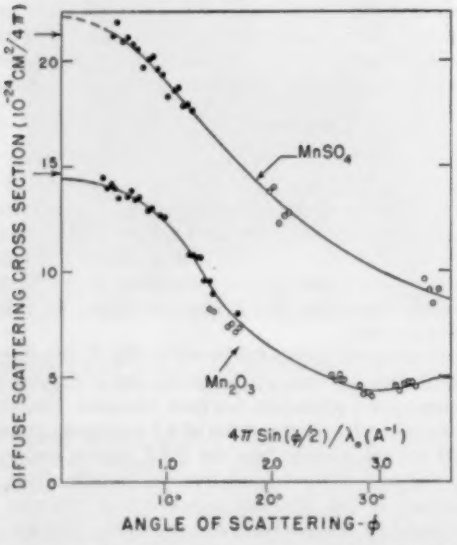

FIG. 2. Differential cross section (barns/4π steradians) of $MnSO_4$ and Mn_2O_3 for 1.12 A neutrons at 295°K. The observed scattering is composed of magnetic and thermal diffuse scattering, the latter being almost zero at zero angle of scattering. Multiple and incoherent scattering has been subtracted. The horizontal arrows indicate the theoretical magnetic cross sections at zero scattering angle for 5 spins and 4 spins. Different symbols indicate the results of different experiments.

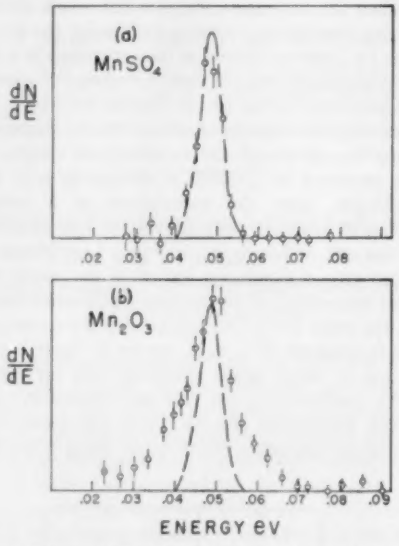

FIG. 3. Energy distributions of neutrons of wavelength 1.28$_8$ A after scattering by $MnSO_4$ and Mn_2O_3 at an angle of 11°20′. Within the accuracy the spectra contain all the scattered neutrons. A component of each spectrum is multiply scattered amounting to 11 percent in the case of $MnSO_4$ and 9 percent in the case of Mn_2O_3. The resolution function for the instrument is shown as dashed lines. In the case of $MnSO_4$ it was fitted to the points by area normalization.

Mn_2O_3.—In this substance the coupling between manganese ions is appreciable since the transition temperature[7] is 80°K and the Weiss constant[8] $\Delta = -176°$. The angular distribution, Fig. 2, possibly shows some structure.

The energy distribution is shown in Fig. 3(b). The distribution is asymmetrical by about the amount of a Boltzmann factor, $\exp(-\delta E/k_B T)$. The half-width of the distribution is somewhat greater than that given by Eq. (1) (0.0043 ev or 51°K), but by no more than might

be expected from the uncertainties in both the theory and the experiment.

Work has been done on a number of other materials including MnO, Cr_2O_3, and $ZnFe_2O_4$ and is being continued with a view to studying the dependence of the energy distribution on the temperature, the angle of scattering, and the degree of magnetic order. An account of this work will be submitted to the *Canadian Journal of Physics*.

The author is indebted to Dr. D. G. Henshaw for the excellent aluminum crystals used in these experiments.

[1] J. H. Van Vleck, Phys. Rev. **55**, 924 (1939).
[2] J. M. Cassels, *Progress in Nuclear Physics* (Academic Press, Inc., New York, 1950), Vol. 1.
[3] Energy distributions of neutrons scattered by vanadium metal under several different conditions have been measured by the author with results in agreement with the theory. This work is being continued with a view to obtaining the frequency distribution of the normal modes in vanadium metal.
[4] G. E. Bacon and R. D. Lowde, Acta Cryst. **1**, 303 (1948).
[5] de Haas, Schultz, and Koolhass, Chem. Abstracts **34**, 2222[2] (1940); Physica **7**, 57 (1940).
[6] See also Shull, Strauser, and Wollan, Phys. Rev. **83**, 333 (1951).
[7] E. G. King, J. Am. Chem. Soc. **76**, 3289 (1954).
[8] Bhatnagar, Cameron, Harbard, Kapur, King, and Prakash, J. Chem. Soc. 1433 (1939).

Annealing Process in Neutron-Irradiated LiF

D. Binder and W. J. Sturm
Oak Ridge National Laboratory, Oak Ridge, Tennessee
(Received May 12, 1955)

THE previous work[1] on neutron irradiated LiF crystals showed that the lattice expansion was caused by equal numbers of vacancies and interstitial atoms. It was also shown, by analyzing the annealing data for nonuniformly irradiated crystals, that the annealing process was of order higher than one. We will now derive a more exact order, an activation energy, and a jump frequency for the lattice defects causing the expansion by analyzing the annealing data for uniformly irradiated crystals.

As described previously,[1] two crystals were covered with 0.03 in. of cadmium during irradiation to insure a uniform irradiation. The lattice parameter changes as derived from density measurements, $(\Delta a/a)_\rho$, for the crystals after irradiation and after 10-minute anneals at successively higher temperatures, are summarized in Table I. The probable error in $(\Delta a/a)_\rho$ is $\pm 1.3\times 10^{-5}$, and the blank spaces represent anneals not performed.

Table I. The lattice parameter changes after irradiation and successive thermal anneals.

Condition	$10^5(\Delta a/a)_\rho$ Crystal Cd-3	Crystal Cd-4
Irradiated	8.02	8.51
315°C anneal	7.65	8.16
345	6.64	7.08
375	4.62	5.18
410	2.06	...
425	...	1.25

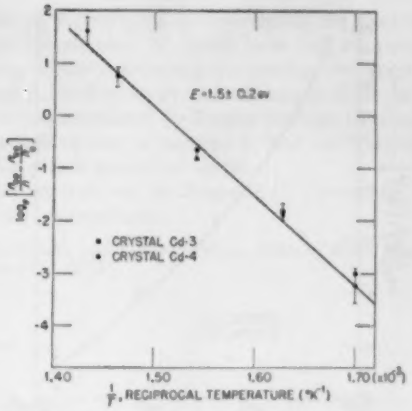

FIG. 1. Annealing data assuming a second-order process.

Assume that the lattice defects change position by a random walk process. Then if we have a single rate process with activation energy E for unit motion, the probability for taking one step at temperature T varies as $e^{-E/kT}$, and the rate of change of the total defect concentration n is

$$dn/dt = -cn^\gamma e^{-E/kT},$$

where c is a constant and γ is the order of the reaction. The solution of this equation for $\gamma > 1$ may be expressed in the form,

$$\log_e\{(n_{00}/n)^{\gamma-1} - (n_{00}/n_0)^{\gamma-1}\} = \log_e\{(\gamma-1)n_{00}^{\gamma-1}ct\} - E/kT, \quad (1)$$

where n_{00} is the defect concentration for the irradiated condition and n_0 is the concentration for the start of each anneal at temperature T.

We assume n is proportional to $(\Delta a/a)_\rho$ so that both n_{00}/n and n_{00}/n_0 may be determined from ratios of the data in Table I. Since the anneals were performed for a fixed time interval, the plot of $\log_e\{(n_{00}/n)^{\gamma-1} - (n_{00}/n_0)^{\gamma-1}\}$ *versus* $1/T$ should be a straight line for the correct order γ, and the slope should determine the activation energy. A straight line is obtained for $\gamma = 2$, as shown in Fig. 1, and the slope indicates an activation energy of 1.5 ± 0.1 ev. The possibility of $\gamma = 1$ was eliminated in reference 1, and the plot for $\gamma = 3$ is curved as shown in Fig. 2. The annealing process is then of the second order as expected from the random recombination of non-neighboring, isolated vacancies and interstitials, or Frenkel defects.

Keating[2] has suggested that the irradiation-induced distortion cannot be due to isolated vacancies and interstitials, but to large aggregates of imperfections. His data show a lattice expansion only one-tenth as

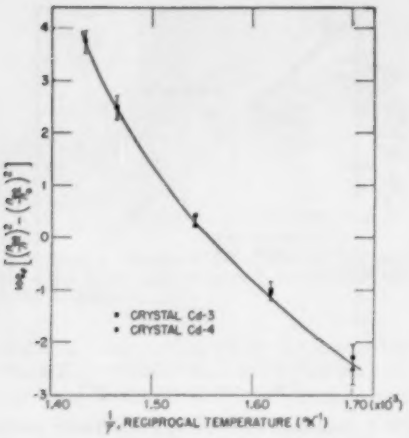

FIG. 2. Annealing data assuming a third-order process.

large as the data of reference 1 for equivalent irradiations. It is possible that the temperature of irradiation was much higher in Keating's experiment, annealing the lattice expansion.

The jump frequency, or frequency with which the defect takes an atomic step, may be estimated from our data. The fractional rate of decrease of the defect concentration is $-(1/n)(dn/dt)$, and the number of random atomic steps taken before a vacancy meets an interstitial is $1/n$. Therefore, the jump frequency is

$$\nu = -(1/n^2)(dn/dt) = ce^{-E/kT}.$$

For the temperature T_0 at which the left-hand side of Eq. (1) is zero, we have

$$c = (1/n_{00}t)e^{E/kT_0}.$$

The temperature T_0 may be obtained from Fig. 1, but n_{00} can only be estimated. We take n_{00} as equal to $(\Delta a/a)_\rho$ (for the irradiated condition) within an order of magnitude. Then $n_{00} \approx 8\times10^{-4}$, $t = 600$ sec, $1/T_0 = 1.52\times10^{-3}$, and the jump frequency is

$$\nu \approx 6\times10^{11}e^{-E/kT} \text{ sec}^{-1}.$$

[1] D. Binder and W. J. Sturm, Phys. Rev. **96**, 1519 (1954).
[2] D. T. Keating, Phys. Rev. **97**, 832 (1955).

Anisotropy of Bremsstrahlung and Pair Production in Single Crystals

F. J. DYSON, *Institute for Advanced Study, Princeton, New Jersey*
AND
H. ÜBERALL, *Laboratory of Nuclear Studies, Cornell University, Ithaca, New York*

(Received May 18, 1955)

IT has been pointed out by Landau[1] that the Bethe-Heitler formulas for bremsstrahlung and pair production will need modification for electrons and photons of energy greater than 10^{12} ev passing through condensed matter. The Bethe-Heitler theory requires that charged particle and photon interact coherently over a path length of the order of

$$L = \lambda[1-(v/c)\cos\theta]^{-1}, \quad (1)$$

where λ is the photon wavelength, v the charged particle velocity, and θ the angle between the directions of charged particle and photon. When the charged particle energy E is relativistic, the angles of emission will in general be such that

$$L \sim \lambda E^2/m^2. \quad (2)$$

Landau observes that multiple Coulomb scattering will reduce the longitudinal distance traveled by the electron by

$$\Delta = KL^3/E^2, \quad (3)$$

over a path length L, where K is the Coulomb scattering constant of the material. The Bethe-Heitler theory will break down when $\Delta > \lambda$, i.e., when

$$K\lambda E^2 > m^4. \quad (4)$$

In lead, this condition is satisfied for all photons when the electron energy reaches 5×10^{12} ev.

We here consider a quite different effect of the coherent path-length idea, which should be easily observable at energies of the order of 500 Mev, for example with the Cornell synchrotron beam. Suppose an electron is incident on a single crystal of lead, at an angle α to a line of nearest-neighbor atoms, i.e., at an angle $(90°-\alpha)$ to a (110) plane. The spacing of the atoms in the line is $d = 3.5$ A. The number of atoms included within the path length (2) will be

$$N = (\lambda_0/d)(E/m) = 7\times10^{-3}(E/m) \quad (5)$$

for photon energy equal to E, and will be greater than this for photons of lower energy. Here $\lambda_0 = 24\times10^{-11}$ cm is the Compton wavelength. Thus for $E = 500$ Mev, $N \geq 7$ for all photons. Now a large matrix element for bremsstrahlung arises when the electron passes through an atom within the Thomas-Fermi screening radius

$$R = a_0Z^{-\frac{1}{3}} = 1.2\times10^{-9} \text{ cm}. \quad (6)$$

When the angle α is less than

$$\alpha_0 = (R/Nd) = 137Z^{-\frac{1}{3}}(m/2\pi E) = 0.3°, \quad (7)$$

the effective matrix element will be multiplied by N each time such a passage occurs, while the effective number of targets will be reduced by a factor N.

We expect therefore that the total bremsstrahlung intensity will be enhanced by a factor $N \sim 7$ when the electron beam is within 0.3° of a line of nearest neighbor atoms. Exact quantum-mechanical calculations are being undertaken to confirm the existence of the effect and to estimate its magnitude. Even if the crude classical argument in this letter is optimistic by a factor of

50, the effect should be easily visible. The softer part of the bremsstrahlung spectrum should show a more intense enhancement over a finer range of angles.

Calculations have shown that the coherence effect disappears when averaged over crystal orientation, to a high degree of accuracy. The Bethe-Heitler theory therefore remains valid for polycrystalline materials, except at very much higher energies when the Landau effect becomes important.

It occurs to us that the bremsstrahlung anisotropy might in certain circumstances be a useful adjunct to x-ray crystallography, in determining the structure of organic molecules. It would have the advantage of giving direct information concerning the angles between pairs of atoms in the molecule, without the complications introduced by Fourier analysis. Of course, an experimental test is required to find out whether this will be either possible or useful.

We are indebted to Professor G. Cocconi for some helpful conversations.

[1] L. Landau and I. Pomeranchuk, Doklady Akad. Nauk. **92**, 535 and 735 (1953).

PHYSICAL REVIEW VOLUME 99, NUMBER 2 JULY 15, 1955

Proceedings of the American Physical Society

Minutes of the 1955 Spring Meeting Held at Washington, D. C., April 28–30, 1955

(Corresponding to *Bulletin of the American Physical Society*, Volume 30, No. 3)

THE 1955 Spring Meeting of the American Physical Society was held at Washington, D. C., on Thursday, Friday, and Saturday, April 28–30, 1955. Though neither the time nor the place of this meeting deviated from tradition, there were three new features which deserve special mention. First, the heavy task of administering the meeting fell upon a new Chairman of the Local Committee, R. D. Huntoon of the National Bureau of Standards. He was ably assisted by W. R. Tilley also of the Bureau, serving as Secretary of the Local Committee, and by the other members of the Committee, who were Ralph Alpher (APL), D. F. Bleil (NOL), Wayne C. Hall (NRL), R. J. Seeger (NSF), and Howard Tatel (DTM), Mrs. L. S. Taylor, who served Chairman of the Ladies' Programme Committee, and by nearly one hundred others. We must not forget either that Hugh Odishaw, Huntoon's predecessor, lent the aid afforded by his long experience. Warmest thanks to all!

Second, all of the sessions were held in the Sheraton Park Hotel, excepting six in the East Building of the National Bureau of Standards and one of which there will be further mention. We thus attained a degree of compactness not previously achieved in Washington since the old days when there were not more than three simultaneous sessions and the Bureau could receive them all. It is somewhat astonishing that one hotel could provide so many halls, and in spite of the fact that the largest hall in the building was not quite ready for our sessions.

Third, we borrowed the Lisner Auditorium of George Washington University (and for the gratuitous use thereof we owe thanks to President Marvin of the University) for one of the most impressive sessions in the history of the Society—a memorial to Enrico Fermi. H. L. Anderson, E. J. Konopinski, Emilio Segrè, Frederick Seitz, and W. H. Zinn gave a series of excellent papers that reviewed Fermi's life and work from the beginning to the end of his glorious career. These papers were not without allusions to other work that sprang directly from Fermi's own. The Chairman of this memorial session, H. A. Bethe, was also its organizer. Those who did not hear it, and also those who did, will welcome the news that these speeches will be published in *Reviews of Modern Physics*. The hall with its 1500 seats was full.

The remaining invited speakers of the meeting were chosen, as is the custom, mainly but not altogether from the Washington area. Elias Burstein selected three in semiconductor physics, and the Division of Chemical Physics arranged a Symposium. Contributed papers numbered 394, not quite up to last year's total. Registration amounted to 1832.

The banquet of the Society was held on Friday evening. I should have listed a fourth unprecedented feature: this banquet was the very first event in the history of the new Main Ballroom of the Sheraton Park Hotel, in which Ballroom workmen were still putting on the finishing touches less than half-an-

hour before the dinner began. The after-dinner speakers were John von Neumann and R. W. G. Wyckoff. They deserved a larger audience than they had.

The Nominating Committee met on Friday afternoon to select candidates for the various offices in the Society, terms to begin at the end of the 1956 Annual Meeting. Their choices were: for the *Presidency*, E. P. Wigner; *Vice-Presidency*, H. D. Smyth; *Treasurership*, G. B. Pegram; *Secretaryship*, K. K. Darrow; *Managing Editorship*, S. A. Goudsmit; *Council*, S. K. Allison, C. D. Anderson, D. M. Dennison, N. F. Ramsey; *Board of Editors*, J. Bardeen, G. Chew, L. H. Fisher, A. Rose, L. Spitzer (foregoing with special assignment to *The Physical Review*), E. Segrè and J. A. Wheeler (special assignment to *Reviews of Modern Physics*). Of these, Wigner, Pegram, Darrow, and Goudsmit were also nominated from the membership at large.

The Council met on the Wednesday afternoon preceding the meeting. As usual, the main theme of its lengthy debate was the unending parlous situation of the finances of the Society resulting from the unending increase in the rate of submission of manuscripts to *The Physical Review*. In the Toronto Bulletin the Managing Editor has given a fuller account of the outcome than will be given here. For the record be it mentioned that the page charge goes up to $25 and the charge for a Letter to the Editor to $25, both changes being put into effect on July 1, 1955; and that the membership subscription rate (*for The Physical Review*) goes up to $10 in addition to dues and the nonmember domestic subscription rate to $40, both changes to go into effect on January 1, 1956. These increases come too late to assure us of a balanced budget on 1955 operations, and we must invade the 1953 surplus.

The Council created the posts of Deputy Secretary and Deputy Treasurer, and appointed to these posts W. W. Havens, Jr., and S. L. Quimby, their terms to run until the end of the 1956 Spring Meeting.

The Council elected to Fellowship nine candidates and to Membership 92 candidates; their names are appended.

Elected to Fellowship: M. K. Brachman, J. N. Cooper, P. H. Dike, Herbert Friedman, D. L. Hill, M. L. Merritt, E. C. Nelson, G. T. Pelsor, and Richard Tousey.

Elected to Membership: [a]Philip W. Alley, Leon Arnell, Charles M. Askey, [a]Anthony Charles L. Barnard, [a]David M. Bernstein, Richard Andrew Bolz, Raymond Bowers, Robert D. Brown, Ernst Brun, [a]Robert Stowe Caldwell, [a]Robert Wilfred Campbell, [a]Robert Harry Chambers, Robert J. Clark, Franklin Steele Coale, Ulric Eugene Dennis, Henry Marshall Dixon, III, William Djinis, Lloyd C. Downes, Nelson S. D'Andres DuBois, Jr., Nicholas Fabijanic, [a]Thomas Clark Farrar, Archibald T. G. Ferguson, [a]Donald Dennis Fitts, [a]Thomas Joseph Flautt, Jr., [a]John Brendan Freely, [a]Garth William Gobeli, [a]Robert Boyd Gordon, [a]Roger Leland Hall, [a]Walter Ashley Harrison, [a]Mazhar Hasan, Elmer Ellsworth Haskins, Tchang Fong Hoang, [a]Daniel Joseph Horen, Jack Thomas Humphries, Robert Frederick Johnson, [a]Thomas Everett Johnson, Jr., William Harper Johnston, [a]Hubert Whitney Joy, Yoshiya Kanda, [a]Raymond Hal Kelley, David P. Kennedy, [a]Ottmar C. Kistner, [a]Robert Seiple Knox, William Claire Knudsen, Sol Henry Krasner, [a]Paul Henry Latimer, [a]Myron Levitsky, Shu-hua Li, Joseph Granville Logan, Jr., [a]Victor Arvid Madsen, [a]Finley Warren Markley, John William McClain, [a]Mark Nordman McDermott, Eugenie Verburger Mielczarek, Stanley Richard Mielczarek, Walter Bert Mitchell, [a]Franz Mohling, Dan Neuberger, [a]James Allan Niederer, Minoru Oda, [a]Wilfred Palmer, William Howard Parth, [a]Sheldon Penman, Eugene A. Plassmann, [a]Melvin Pomerantz, [a]Manfred Raymond Pyka, [a]Karl S. Quisenberry, Jr., [a]Isaac Richman, [a]Joseph Hindle Robinson, III, William Buford Rose, Shirley M. Rosser, [a]Sheldon Schultz, [a]Arthur B. Shaw, [a]Paul Joseph Shlichta, [a]Peter Stuart Signell, [a]James Edward Simmons, John T. Sinnette, Jr., Alberto Sirlin, [a]Alan Sobel, Kelley Roderick Spearman, [a]William George Spitzer, John June Spokas, Robert Weir Stanley, Hiroshi Suura, [a]Robert Earl Thomas, Lien Yueh Tu, [a]Albert Ray Turley, Stanely Henry Vegors, Leila Mae Virtue, [a]Harry Jean Watters, Joan P. Welker, and G. A. Wolff.

KARL K. DARROW, *Secretary*
American Physical Society
Columbia University
New York 27, New York

[a]—Student.

Errata Pertaining to Papers A6, C2, D4, FA9, K1, K4, KA4, KA7, PA6, R6, S7, UA2, X8, XA1, XA3, and ZA1

A6, by Peter Meyer and J. A. Simpson. In line one instead of "Forbush has recently shown that the cosmic-ray intensity increased by ionization chambers has increased" read "Forbush has recently shown that the cosmic-ray intensity measured by ionization chambers has increased."

C2, by Jerome Rothstein. In line 10 instead of "tan*kat*" read "tan*hat*."

D4, by H. P. Noyes. In line six instead of "range is negative, implying at least two bound states of $I=\frac{1}{2}$," read "range is negative, implying at least one bound state of $I=\frac{1}{2}$."

FA9, by A. Fafarman and M. H. Shamos. The following sentence should be added: "However, the experimental ratio is uncertain because of Compton degradation of the oxygen $2p-1s$ radiation."

K1, by John L. Johnson and William S. Porter. Insert a footnote to JLJ: "†Now at Westinghouse Electric Corporation, Industrial Atomic Power."

K4, by S. A. Cox and R. M. Williamson. In line 10 instead of "function for which the channel spin = 1" read "function calculated for 25 percent of $S=1$ and 75 percent of $S=2$."

KA4, by George E. Hudson and Alfred Saenger. Instead of "boundary conditions—has been" read "boundary conditions has been" and instead of "first acoustic harmonic" read "first acoustic overtone."

KA7, by J. W. Corbett and W. W. Watson. Instead of $(q_1)^{0.33}$ read $(q_1)^{\frac{1}{3}}$.

PA6, by R. M. Williamson and S. A. Cox. In line 15 instead of "−0.14" read "−0.60." In line 16 instead of "+0.30" read "−0.40." In line 20 delete the word "not."

R6, by R. K. Smither. Instead of $\delta^2=1+\frac{2I_{de}}{I_0}$ read $\delta=1+\frac{I_{de}}{I_0}$.

S7, by W. K. H. Panofsky and G. B. Yodh. Instead of "The results are $X_s=0.0256\pm0.0030$ and $X_s=0.0199\pm0.0022$ at" read "The results are $X_s=0.0183\pm0.0010$ at pion energies." Instead of "energies of 55 and 75 Mev, respectively" read "energies near 60 Mev." Instead of "The results are consistent with either electric-dipole or magnetic-dipole absorption" read "The results require a cutoff of the contribution of large momentum transfers of the electrons to the process."

UA2, by Robert J. Rubin and B. A. Fleishman. Instead of the equation

$$w_i^{(2)}=\frac{3k}{8M}P(1-P)\sin^4\frac{i\pi}{2(N+1)}\left\{\frac{\cos i\pi/(N+1)}{(N+1)(\sin^2 i\pi/(N+1))}+\frac{1}{i\pi\sin i\pi/(N+1)}\right\}$$

read

$$w_i^{(2)}\,\Sigma^2=-\frac{12k}{M}\frac{P(1-P)}{N+1}\,\Sigma^2\tan^2\frac{i\pi}{2(N+1)}.$$

X8, by Stirling A. Colgate. In line 11 instead of "$N^{14}(p,p^1)\alpha$" read "$N^{14}(p,p')\gamma$." In line 12 instead of "$N^{14}(p,p^2)\alpha$" read "$N^{14}(p,p')\gamma$."

XA1, by V. W. Hughes and J. S. Geiger. A footnote should be added to the title: "*This research has been supported in part by the Office of Naval Research."

XA3, by Louis Pierce. Instead of "$A=106\,534.45$ Mc, $B=13\,349.10$ Mc, $C=11\,834.14$ Mc" read "$A=106\,534.74$ Mc, $B=13\,348.95$ Mc, $C=11\,834.30$ Mc."

ZA1, by A. S. Wightman and D. Hall. In line 24 the definition of β should read $\beta=[(P_{12}\cdot P_{34})^2-m_{12}^2m_{34}^2][(Z_{12}\cdot Z_{34})^2-Z_{12}^2Z_{34}^2]$.

PROGRAMME

THURSDAY MORNING AT 10:00

Main Ballroom

(R. B. BRODE presiding)

Cosmic Rays

A1. Altitude Effect on Cosmic-Ray Fine Structure. DANA T. WARREN,* *Colorado A & M College.*—Cosmic ray intensities have been measured at zenith-angle intervals of 2½° in the four principal geomagnetic azimuths at Fort Collins, Colorado. This is at the same magnetic latitude as Missouri, where fine structure was previously observed, but is at an altitude of 5000 instead of 1000 feet. The irregularity near the zenith, which is azimuthally unsymmetrical in Missouri, appears as a significantly low-zenith reading in all azimuths. However, the azimuthally symmetrical irregularities that are so marked in Missouri could not be found. The chi-test shows reasonably good agreement with parabolas (omitting the zenith reading), although the measurements covered both the same zenith-angle range and air-path range in which the effects were previously found. Combining residuals from the various azimuths shows no symmetrical irregularities greater than half the size of those in Missouri. Also, less accurate measurements in the north and south with 103 g/cm² of lead absorber shows one high point at 35°, probably not statistically significant. Thus the altitude effect confirms the difference previously deduced between these two kinds of fine structure.

* Now at the University of California Radiation Laboratory, Livermore, California.

A2. Azimuthal Effect for Cosmic-Ray Protons and Alpha Particles Using a Cerenkov Counter.* J. R. WINCKLER AND L. PETERSON, *University of Minnesota.*—Data has been obtained with a large Čerenkov telescope containing two five-inch diameter end-window photomultipliers. The work is an extension of earlier experiments.[1] These experiments consistently showed too small an azimuthal effect for agreement with the accepted spectrum of primary protons. Alpha particles, however, should undergo less atmospheric scattering and have a much closer directional correlation with primary nuclei following collisions. The telescope was flown at 11 g/cm² atmospheric depth at geomagnetic latitude 40° for six hours at a 60° zenith angle. The pulse-height distributions in each azimuthal sector are compared in an absolute sense with the distribution for relativistic particles (sea level mesons). Preliminary analysis of part of the data shows that a large fraction of the singly charged particles at 11 g/cm² are distributed in velocity below $\beta=1$ and are of secondary origin. The results for the alpha component will be discussed and compared with the proton component and the alpha primary spectrum obtained in other ways.

* Supported by the joint program of the Office of Naval Research and the U. S. Atomic Energy Commission.
[1] J. R. Winckler and K. Anderson, Phys. Rev. **93**, 596–605 (1954).

A3. Latitude Effect on the Nucleon and Hard Components of Cosmic Rays. D. C. ROSE AND J. KATZMAN, *National Research Council, Canada.*—During the summer of 1954 cosmic-ray measurements were taken aboard the Canadian Navy Icebreaker Labrador during a cruise through the Northwest Passage and circumnavigating the North American Continent. The apparatus consisted of a neutron monitor or pile of lead and paraffin with BF_3^{10} neutron counters and a triple coincidence Geiger-counter telescope with five inches of lead shielding. The results show that for the nucleon component the knee in the latitude effect is at about 54° north geomagnetic latitude. The results for the hard or mesonic component are complicated by difficulties in temperature correction but show the latitude knee to be somewhat higher in latitude than previous measurements.

A4. Variation of the Position of the Cosmic-Ray Neutron Intensity Maximum with Geomagnetic Latitude.* R. K. SOBERMAN, A. BEISER, AND S. A. KORFF, *New York University.*—It has been experimentally demonstrated that there exists a maximum in the cosmic-ray neutron intensity when plotted as a function of altitude or pressure. The position of this maximum at various geomagnetic latitudes in the northern hemisphere has been measured by experiments which used balloon borne unshielded BF_3 counters with various enrichments of the B^{10} isotope. It has been found that the position of the maximum varies approximately parabolically when plotted as a function of geomagnetic latitude. The range of variation is from about 120 millibars at the equator to about 70 millibars at the north geomagnetic pole. The experimental results will be compared with theory.

* Supported by the Office of Naval Research.

A5. Geomagnetic Albedo at Rocket Altitudes at the Equator. H. GRIEM AND S. F. SINGER, *University of Maryland.*—Cosmic-ray secondaries above the "top" of the atmosphere ("albedo") present an unknown contribution in experiments designed to measure the flux of primary protons. The question of albedo is of particular importance at the geomagnetic equator; it enters into all considerations connected with the primary spectrum, in particular the energy balance. At the present time our knowledge of the equatorial albedo is sparse: it is >35 percent of the total flux at 45° zenith angle and made up mainly of minimum ionizing particles.[1] In attacking the albedo problem theoretically, we note that at the equator the magnetic field confines charged secondaries to the altitude region in which they are produced. Depending on altitude and range they can make many loops between production and absorption, thus enhancing their contribution to the counting rate. This process has been studied in detail for protons and electrons of various energies, and their relative contribution to the albedo is discussed.

[1] S. F. Singer, Phys. Rev. **80**, 47 (1950).

A6. Changes in the Low-Energy Primary Spectrum and the Low-Energy Particle Cutoff of Cosmic Radiations. PETER MEYER AND J. A. SIMPSON, *The University of Chicago.*—The solar magnetic dipole field can no longer be invoked to account for the low-energy particle cutoff in the primary spectrum. Neutron detectors in high-altitude aircraft were used to measure changes in the cut-off particle rigidity and total intensity in 1948, 1951, and 1954. It was observed between 1948 and 1951 that the cut-off rigidity decreased to permit particles not present in the 1948 spectrum to reach the earth. Furthermore, the total primary particle intensity was observed to increase in such a way as to increase the exponent of the assumed power law spectrum at low-particle rigidities. There is evidence that the phenomenon is not of terrestrial

origin. Forbush has recently shown that the cosmic-ray intensity increased by ionization chambers has increased between 1947 and 1950, and that this change appears to be associated with the cycle of solar activity. If both changes are due to the same process then the low-energy particle cutoff is a property of the solar system.

A7. Energy Spectrum of Medium and Heavy Primaries at $\lambda = 61°$.* J. E. NAUGLE, P. S. FREIER, AND E. P. NEY, *University of Minnesota.*—A stack of 83 emulsions was flown at a geomagnetic latitude of 61° (Saskatoon, Canada) for the purpose of detecting and stopping medium- and heavy-primary nuclei. The stack was kept at an altitude of 10.8 ± 0.6 grams/cm² for 7.15 hours. The stack was flown upside down during ascent so that particles which stopped during ascent could be eliminated. The outside of the stack has been scanned for particles with I/I min $\geqslant 25$ as measured by delta rays. Particles with I/I min $\geqslant 30$ and with a possible range in the stack of $\geqslant 19.6$ grams/cm² of emulsion are being followed until they interact, leave the stack, or end; 210 particles have been followed, of which 85 have ended in the stack. The charge of the ending particles is being measured by delta-ray densities *vs* range and by a densitometer measurement of the width and opacity of the end of the track. The two methods agree to within about ± 0.5 unit of Z. A preliminary energy spectrum in the region from 180 to 620 Mev/nucleon will be presented. The charge distribution in the same energy interval will also be presented.

* Supported in part by the joint program of the U. S. Atomic Energy Commission and the Office of Naval Research and by a grant from the Graduate School of the University of Minnesota.

A8. High-Energy Nucleonic Component in the Atmosphere.* L. ALTMAN, H. S. BRIDGE, AND R. W. WILLIAMS, *M.I.T.*—An experiment on high-energy cosmic-ray nucleons in the atmosphere has been performed at mountain altitudes using a large double ionization chamber which provides a measure of the energy of π^0 mesons created in nuclear interactions. The interactions considered were initiated by nucleons (or pions) in an energy range of 200 to 2000 Bev. Preliminary analysis yields the following: absorption mean free path in air (corrected for Gross transformation), approximately 105 g/cm²; integral frequency spectrum (deduced from the energy of π^0's), $\sim E^{-1.4}$. There is an increasing degree of association between the nucleonic and electronic components of the cosmic radiation at the higher energies.

* Supported in part by a joint program of the Office of Naval Research and the U. S. Atomic Energy Commission.

A9. Rocket Observations on Soft Radiation at Northern Latitudes.* F. B. MCDONALD, R. A. ELLIS, AND M. B. GOTTLIEB, *State University of Iowa.*—A combination Geiger counter and crystal scintillation counter telescope has been developed for rocket use to study the properties of a new soft radiation observed recently at high altitudes in northern latitudes.[1] The crystal (Na-I-Th activated) is mounted below a single thin-walled Geiger counter in the nose of the rocket. The Geiger counter gates the output of the photomultiplier so that the pulse height distribution of particles traversing the Geiger counter and entering the crystal is obtained. In addition the counting rate of the Geiger counter is scaled and telemetered. Three successful flights were made with this apparatus at a geomagnetic latitude of 70°N in July, 1954 using the Iowa balloon-launched rocket technique. Two flights gave anomalously high single Geiger-counter counting rates above 220 000 ft. The telescope rate did not show a significant increase—a result which is consistent with the observed atmospheric absorption of the soft radiation, in view of the additional material between Geiger counter and crystal. Complete data from the three flights will be shown and discussed, and measurements of the vertical cosmic-ray flux as a function of altitude will be given.

* Assisted by the Office of Naval Research and the U. S. Atomic Energy Commission.

[1] Meredith, Gottlieb, and Van Allen, Phys. Rev. 97, 201 (1955).

A10. Double Geiger-Tube Study of Soft Radiation at Northern Latitude.* J. A. ELLIS, M. B. GOTTLIEB, AND L. H. MEREDITH, *State University of Iowa.*—The soft radiation previously detected above 50 km in northern latitudes,[1] with a thin-walled Geiger tube carried in a balloon-launched Deacon rocket was studied further in July, 1954 using two nearly identical Geiger tubes and a photoelectric rocket-orientation indicator. One Geiger tube was shielded only by its 30 mg/cm² skin and the 160 mg/cm² wall of the rocket, and by varying amounts of atmosphere. The other Geiger tube was surrounded by an additional absorber of thickness 150 mg/cm². Two successful flights were made and the effect was detected in the second flight. After subtracting the cosmic-ray background, the ratio of counting rate for the tube without the absorber to counting rate for the tube with the absorber was about 3 for the upper part of the flight (90 to 100 km) and was about 2 around 50 km where the soft radiation was first encountered.

* Assisted by the Office of Naval Research and the U. S. Atomic Energy Commission.

[1] Meredith, Gottlieb, and Van Allen, Phys. Rev. 97, 201 (1955).

A11. High-Altitude Rocket Measurements with Scintillation Counters at Northern Latitudes.* ROBERT A. ELLIS, *State University of Iowa and Tennessee A. and I. State University.*—Two rocket flights of Na I scintillation crystals to about 90 km altitude were made at geomagnetic latitude 70°N in July, 1954. The crystals were flat cylinders 3.18 cm diameter and 1.0 cm thick. The counting rate of pulses larger than 1 Mev yields a value of charged particle intensity in agreement with previous Geiger counter results, i.e. $J \sim 0.5$ (cm² sec sterad)$^{-1}$. Detailed results and the interpretation of smaller pulses will be presented.

* Assisted by the Office of Naval Research and the U. S. Atomic Energy Commission.

A12. Interpretation of Soft Radiation Observed at High Altitudes in Northern Latitudes. J. A. VAN ALLEN, *State University of Iowa.*—The previously reported soft radiation has been further studied as reported in accompanying papers. The probability of occurrence was about 0.5 during July, 1954 at $\lambda = 70°$. Absorption mean free path is of the order of 180 mg/cm² in aluminum and 220 mg/cm² in the atmosphere. Discussion of alternative interpretations in terms of gamma rays of energy about 20 kev, electrons of energy about 1 Mev, or protons of energy about 15 Mev will be presented.

A13. Identification of Cosmic-Ray Shower Particles in Emulsions. A. HUSAIN, C. J. D. JARVIS,* AND E. PICKUP, *National Research Council, Canada.*—An experiment is in progress to identify medium energy particles ($pB \sim 50$ Mev $-$ 1 Bev) emitted in cosmic-ray stars formed at high altitudes in Ilford G5 emulsions, by means of grain counting and scattering. Pions, K-mesons (mass $\sim 950 m_e$), protons, hyperons, and deuterons have been identified, and there is some indication of particles with a mass intermediate between that of the 950-m_e group and the proton group. The most recent results will be reported.

* National Research Laboratory Postdoctorate Fellow.

A14. Experimental Results on the Arrival Times and Lateral Distribution of Air-Shower Particles.* G. CLARK, *M.I.T.*—The experiments on the distribution of arrival times of air shower particles described by Bassi, Clark, and Rossi[1] have been extended using improved apparatus for which the

standard deviation in the determination of the difference of arrival times of two particles at two counters is 3×10^{-9} second. From new data we find that the flux of "first" electrons in showers with sizes near 10^5 particles can be represented by the

$$\sim 0, \quad t<0$$

function $f(t)\sim\epsilon^{-t/\tau}$, $t>0$, where $\tau=(7\pm1)\times10^{-9}$ second. The mean arrival time of "first" particles which penetrate 15 cm of lead does not differ from the mean arrival time of "first" electrons by more than 5×10^{-9} second. A lower limit on the average radius of curvature of the shower fronts is 400 m. The projected zenith angle distribution can be fitted by the function $I(\theta)=I_0(\cos\theta)^{10\pm1}$. An array of eight large-area electron-density detectors was operated in coincidence with the timing array for part of the time. We will present data on the lateral distribution and density fluctuations of electrons in individual showers.

* This work was supported in part by the joint program of the Office of Naval Research and the U. S. Atomic Energy Commission.
[1] Bassi, Clark, and Rossi, Phys. Rev. **92**, 441 (1953).

A15. Positive Excess of High-Energy μ Mesons.* ROBERT B. BRODE AND MARVIN J. WEBER, *University of California, Berkeley.*—With counter spacing of 4 meters and an iron block 1.35 meters thick with a magnetic induction of 1.8 webers per square meter, it is possible to resolve the μ-meson spectrum into bands between 55 and 14 Bev, mean energy 24 Bev and 14 and 4 Bev mean energy 9.2 Bev. The ratio of positive to negative μ mesons is 1.30 ± 0.02 for the band with mean energy of 24 Bev and 1.31 ± 0.02 for the band with a mean energy of 9.2 Bev. These values are higher than the measurements reported by Owen and Wilson and by Filosofo *et al.* The counting ratio in each of the energy intervals is of the order of 100 per day. Within the precision of the existing measurements the ratio of positive to negative μ mesons appears to be constant at energies above two billion volts. The decrease in this ratio below two billion can be explained by the production of μ mesons by secondary neutrons.

* Assisted by the joint program of the Office of Naval Research and the U. S. Atomic Energy Commission.

THURSDAY MORNING AT 10:00

Burgundy Room

(W. W. HAVENS, JR. presiding)

Neutron Physics, I

B1. Radiation Widths in the Slow Neutron Resonances of Iridium.* H. H. LANDON, *Brookhaven National Laboratory.*—The parameters in the lowest-energy resonances in iridium have been determined from total cross-section measurements, using the Brookhaven crystal spectrometer. Preliminary results give the radiation width of the 0.654-ev resonance as 75 ± 5 mv. Activation measurements indicate that this resonance is most probably in Ir^{191}. The radiation width of the 1.305-ev resonance is 86 ± 3 mv. Activation at this resonance confirms the previous assignment by Goldhaber *et al.*[1] to Ir^{193}. Results for the 5.36-ev resonance, and the remaining one-level parameters for each resonance will be presented.

* Research performed under contract with the U. S. Atomic Energy Commission.
[1] Goldhaber, Lowry, and Sunyar, BNL-C-9, 96 (unclassified) (1949).

B2. Total Neutron Cross Section of Rhenium.* G. IGO, *Brookhaven National Laboratory.*—The resonances in rhenium at neutron energies between 1 and 14 ev have been studied with the BNL Crystal Spectrometer. The total cross-section data have been analyzed to determine the radiation width and peak cross-section parameters of the strong resonance at 2.157 ev. The method of analysis used to take account of Doppler effect and the effect of a finite resolution will be presented. The limits of error of these results will be discussed. The radiation width of the 2.157-ev resonance is 49 mv. The previously observed radiation widths, when plotted as a function of atomic weight, show a minimum of approximately 50 Mev at $A\simeq180$.

* Research performed under contract with the U. S. Atomic Energy Commission.

B3. Slow Neutron Resonance Scattering in Indium.* J. MOORE, *Brookhaven National Laboratory and Columbia University.*—The technique of using "thick-thin" target geometry[1] has been employed to study the scattering spectrum of indium below 10 ev. The levels at 1.458 ev, 3.85 ev, and 8.85 ev were clearly observed. Scattering from the level at 1.458 ev has been observed previously.[2,3] The values of Γ_n/Γ and σ_p can be determined for all the levels with an accuracy of about 15 percent from these data and $\sigma_0\Gamma^2$ obtained from total cross-section measurements.[4] A complete analysis is being worked out assuming independent Breit-Wigner levels and correcting each level for the presence of the others by using a method of successive approximations. An attempt is being made to make spin assignments.

* Research performed under the auspices of the U. S. Atomic Energy Commission.
[1] H. L. Foote, Jr. and J. Moore, Bull. Am. Phys. Soc. **30**, No. 1, 22 (1955).
[2] B. N. Brockhouse, Can. J. Phys. **21**, 448 (1953).
[3] L. B. Borst, Phys. Rev. **90**, 859 (1953).
[4] V. L. Sailor and L. B. Borst, Phys. Rev. **87**, 161 (1952).

B4. Total Neutron Cross Sections of Na, K, and Rb, in the 0.03- to 10-ev Region.* E. G. JOKI, L. G. MILLER, AND J. E. EVANS, *Phillips Petroleum Company.*—Transmission measurements have been made with the MTR-crystal spectrometer on Na, K, and Rb metal samples,[1] 8.73 cm (8.48 g/cm^3), 30.0 cm (26.1 g/cm^3), and 5.04 cm, respectively. The free-atom scattering cross sections, as determined from these data, are 3.2 ± 0.1 b for Na and 2.04 ± 0.1 b for K. The Rb data are to be corrected for a 5-weight percent Cs contamination in the sample.

* Work performed under the auspices of the U. S. Atomic Energy Commission.
[1] We are indebted to Dr. W. K. Ergen of the Oak Ridge National Laboratory for supplying the samples.

B5. Resonance Parameters in Ta.* F. B. SIMPSON, R. G. FLUHARTY, AND O. D. SIMPSON, *Phillips Petroleum Company.*—In a continuation of the Ta studies at the MTR,[1] fast chopper transmission measurements have been used to determine parameters above 10 ev. New levels have been found at 23 and 36 ev. Sets of Breit-Wigner level parameters have been determined on five levels, and fairly constant values of Γ_γ are observed. The values of Γ_n have been determined for other levels, and the ratio $(\Gamma_n{}^0)/\bar{D}$ will be discussed. From a combination of crystal and fast chopper spectrometer data, the resonance absorption integral has been calculated.

* Work performed under the auspices of the U. S. Atomic Energy Commission.
[1] Evans, Joki, and Smith, Phys. Rev. (to be published).

B6. Total Neutron Cross Section of Np-237 in the 0.02- to 3-ev Region.* M. S. SMITH, R. R. SMITH, E. G. JOKI, AND J. E. EVANS, *Phillips Petroleum Company.*—Previous MTR crystal-spectrometer measurements,[1] which provided evidence for the existence of a second natural Ta isotope, have demonstrated the feasibility of total cross-section measurements on samples with macroscopic cross sections as small as 0.04 cm^{-1}. When a 154-mg sample of Np became available,[2] transmission measurements were made in the 0.02- to 3-ev region. The Np sample was a 0.5-cm^2 solution of the nitrate in D_2O. A special elevator-type sample changer provided for precise location of the sample in a Bragg beam 0.35 cm^2. Prominent resonances were found at 0.489, 1.34, and 1.49 ev. The Breit-Wigner parameters for the first resonance are $E_0=0.489\pm0.005$ ev, $\sigma_0=2600$ b, $\Gamma=0.032\pm0.003$ ev, and $g\Gamma_n=0.016$ mv. Values of $\sigma_0\Gamma$ for the 1.34- and 1.49-ev resonances are $\sim$29 and $\sim$140 ev·b, respectively.

* Work performed under the auspices of the U. S. Atomic Energy Commission.
[1] Evans, Joki, and Smith, Phys. Rev. (to be published).
[2] We are grateful to Dr. Wallmann of the University of California Radiation Laboratory for providing the Np sample.

B7. Analysis of Low-Energy Neutron-Resonance Cross Sections.* B. MARGOLIS, O. KOFOED-HANSEN, AND E. NAGEL, *Columbia University.*—A neutron cross section formula is derived using the Wigner-Eisenbud[1] procedure with the following assumptions: (1) an average level spacing can be used, (2) the square roots of the products of the reduced neutron and radiation widths have alternating signs in order to approximate a random sign distribution, and (3) for energies near any level, the contribution from other levels is representable by average level widths. Estimates of the deviations from the one level Breit-Wigner formula in the wings of the resonances are obtained. Comparison with experimental data will be made.

* This work partially supported by the U. S. Atomic Energy Commission.
[1] E. P. Wigner and L. Eisenbud, Phys. Rev. **72**, 29 (1947).

B8. Recent Developments in the Analysis of Neutron Resonances and Results of Fast Chopper Measurements on Tantalum.* V. E. PILCHER, D. J. HUGHES, AND J. A. HARVEY, *Brookhaven National Laboratory.*—The area method for the determination of resonance parameters has proved to be very useful for the analysis of neutron resonances in the ev region. However, for cases in which the samples used are neither very thick ($n\sigma_0\gg1$) nor very thin ($n\sigma_0\ll1$), the usual method of obtaining the parameters from the area requires an excessive amount of computation.[1] In order to facilitate the rapid analysis of data from a large number of resonances, we have calculated a set of universal curves relating the areas of transmission dips to resonance parameters for various values of Doppler broadening. With the aid of these curves, resonance parameters may be determined from the measured area above a transmission dip in a small fraction of the time required by the older methods. It is also a simple matter to determine the uncertainty in the parameters arising from various experimental errors. The application of the new procedure to the analysis of Brookhaven fast chopper measurements on tantalum will be discussed. In tantalum, 20 resonances were observed up to 130 ev. The average level spacing per spin state, $\bar{D}$, is 9 ev (based on the first 10 levels) and the average Γ_n^0/D is $(1.8\pm0.3)\times10^{-4}$.

* Work carried out under contract with the U. S. Atomic Energy Commission.
[1] Seidl, Hughes, Palevsky, Levin, Kato, and Sjöstrand, Phys. Rev. **95**, 476 (1954).

B9. Fast Chopper Measurements of Radiation Widths.* A. STOLOVY AND J. A. HARVEY, *Brookhaven National Laboratory.*—Further investigations have been made of the radiation widths of nuclear energy levels for isotopes in the regions of the neutron-magic numbers using the Brookhaven fast chopper. Neutron transmission measurements were made on low-energy resonances in the following isotopes: Sr^{87}, Sb^{121}, Sb^{123}, Ba^{135}, La^{139}, Nd^{145}, and Pt^{195}. The resonances were analyzed to obtain the Breit-Wigner level parameters. Good measurements of radiation widths were possible only when radiative neutron capture predominated over neutron scattering. The fluctuations in the measured radiation widths are not large, and they can be correlated with the shell model through the dependence of the radiation width on the excitation energy and the level spacing. The essential features of this dependence seem to be given by the modified single-particle transition theory of Blatt and Weisskopf, using their level density formula. Evidence from this investigation also indicates that the radiation emitted by excited nuclei is primarily electric dipole radiation.

* Work carried out under contract with the U. S. Atomic Energy Commission.
[1] J. S. Levin and D. J. Hughes, Bull. Am. Phys. Soc. **30**, No. 1, 22 (1955).

B10. Energy Distribution of Cold Neutrons Scattered by Lattice Vibrations.* R. S. CARTER, D. J. HUGHES, AND H. PALEVSKY, *Brookhaven National Laboratory.*—Both x-rays and neutrons can be used to investigate the fundamental problem of the spectrum of the lattice vibrations of a crystal. Neutrons offer a more direct method of attacking the problem because they are available with energies comparable to those of the lattice vibrations making it possible to measure directly the energy changes resulting from the neutron interacting with the lattice. The energy distribution of the neutrons scattered inelastically by a crystal is almost completely dependent on the lattice vibrations of the crystal if the energy of the incident neutrons is small compared to the energy of the scattered neutrons. A filtered beam of neutrons has been obtained from the Brookhaven reactor with wavelengths greater than 4.5 A and a flux of about 10^4 neutrons/cm^2-sec over an area of 7 square inches. Preliminary results have been obtained on beryllium and vanadium by analyzing the scattered neutrons by the gold-absorption method. The major fraction of the neutrons scattered from Be is found to have wavelengths of about 1.5 A in agreement with simple theoretical arguments. Higher energy components were also observed. The scattering of neutrons from vanadium is almost completely incoherent elastic scattering and, as expected, the major part of the scattered neutrons exhibited the same energy as the incident neutrons.

* Work carried out under contract with the U. S. Atomic Energy Commission.

B11. Inelastic Scattering of Cold Neutrons by the Lattice Vibrations of Crystalline Solids.* H. PALEVSKY, D. J. HUGHES, AND R. L. ZIMMERMAN, *Brookhaven National Laboratory.*—For neutrons of wavelengths longer than twice the largest lattice spacing of a crystalline sample, the Bragg condition is satisfied only in the forward direction. The measured cross section in a transmission experiment arises from the nuclear absorption, inelastic scattering from the lattice vibrations of the solid and incoherent elastic scattering. By choosing substances having small nuclear absorption and investigating the variation of the total cross section with sample temperature and neutron wavelength it is possible experimentally to determine the inelastic scattering with good accuracy. Such investigations have been carried out with the Brookhaven slow chopper for the past several years, using samples of Be, C, Mg, Al, Fe, Cu, Zr, Pb, and Bi. These have simple crystal structure and cover a wide range of masses and Debye temperatures. Typical sample temperatures varied from 100° to 1000°K and the energies of the incident neutrons corresponded to temperatures between 2.5° to 60°K. The exact theoretical calculations (assuming a Debye frequency spectrum) for these interactions is very involved, and a number of papers have been published dealing with approximation methods. The agreement of ex-

periment and theory for a few elements is good, but for most of the samples investigated the agreement with theory is poor.

* Work carried out under contract with the U. S. Atomic Energy Commission.

B12. Neutron Velocity Distribution in an Infinite Scattering Medium with Finite Absorption.* JOHN W. NIESTLIE, JR., AND ARTHUR I. BERMAN, *Pratt & Whitney Aircraft.*—The hardening of the neutron spectrum with respect to the Maxwellian distribution has been calcu'ated[1] for a medium of constant scattering cross section in which small amounts of material of high absorption cross section (varying inversely with velocity) are introduced. Scattering probabilities derived by Wigner and Wilkins[2] for monatomic media whose atoms are in classical motion were used in the formulation. The integral neutron conservation equation, obtained by cutting off the distribution at an arbitrary high velocity, and introducing a source of neutrons degraded from a high velocity constant flux, was solved by an iterative method with an IBM 701 computer.

* Work carried out under contract with the U. S. Atomic Energy Commission.

[1] An independent solution was recently obtained by H. D. Brown and D. S. St. John (unpublished). The problem is being solved using a Monte Carlo technique by R. Osborne and R. Coveyou.

[2] E. P. Wigner and J. E. Wilkins, Jr., Atomic Energy Commission Document 2275.

THURSDAY MORNING AT 10:00

Exhibit Hall I

(P. KUSCH presiding)

Radiofrequency Spectroscopy, I

BA1. Hyperfine Structure in the Paramagnetic Resonances in Solutions of Manganous Salts. JOSEPH E. GEUSIC AND DUDLEY WILLIAMS, *Ohio State University.**—Studies of paramagnetic resonance absorption by the Mn^{++} ion in solutions of manganese salts have revealed well resolved hyperfine structure. The observed line pattern is predicted by the expression,

$$H = h\nu/g - Am - \frac{A^2g\beta}{2h\nu}\{I(I+1) - M^2 + M(2M-1)\},$$

in which the symbols have their usual meaning. The value for the hyperfine splitting parameter $A = 95.3 \pm 1.0$ gauss is in agreement with the value previously obtained by Tinkham, Weinstein, and Kip[1] but in disagreement with the value reported by Schneider and England.[2] The variation of line width with concentration will be discussed.

* Supported by a contract with Office of Scientific Research, Air Research and Development Command, U. S. A. F.

[1] Tinkham, Weinstein, and Kip, Phys. Rev. **84**, 848 (1951).

[2] Schneider and England, Physica **17**, 221 (1951).

BA2. Paramagnetic Resonance of Irradiated Hydrogen Sulfide and Hydrazine Chloride at Liquid Air Temperature.* WILLIAM B. ARD, JR., AND WALTER GORDY, *Duke University.*—The paramagnetic resonance of solid H_2S and D_2S has been observed at 8900 Mc after irradiation by x-rays at 77°K. A resolved hyperfine structure is observed. A doublet with a separation of 28 gauss is found at g value 2.00 and seems to be independent of crystal orientation and isotopic substitution. Other lines with g values larger than 2 vary with crystal orientation. The doublet is tentatively interpreted as arising from the S^+H radical in a $^2\Sigma_1$ state. Resonance has also been found in irradiated $N_2H_6Cl_2$. This resonance shows a hyperfine structure which has been observed over a range of about 430 gauss. A weak line, which seems to be independent of crystal orientation, is found at a field 250 gauss lower than the free electron value. It may be the lower component of the atomic hydrogen doublet. Resonances were also observed in irradiated N_2H_4 and H_2Se.

* Work supported by the Office of Ordnance Research.

BA3. Nuclear Spin of Rb^{81}—Method of Measurement.* J. P. HOBSON,† J. C. HUBBS, W. A. NIERENBERG, AND H. B. SILSBEE, *University of California.*—The zero moment method of atomic beams was applied to the measurement of the nuclear spin, magnetic moment, and hyperfine splitting of Rb^{81} (4.7 hours). The isotope was produced by α-bombardment of $BaBr_2$ in the 60-inch cyclotron. About 70 millicuries of Rb^{81} were produced, and were chemically extracted with 5 mg of normal RbBr as carrier. A beam of Rb was produced from the reaction $Ca + 2RbBr \rightarrow CaBr_2 + 2Rb$. A specially designed oven loader inserted the channeled oven from air to its position under high vacuum in three minutes. The beam after passing a conventional single magnet and detector slit fell on either a hot wire detector or on a sulfur button which could be extracted from vacuum in a few seconds to be counted. The x-rays from 2 kev to 60 kev resulting from K-capture decay of Rb^{81} were counted in a NaI−TlI scintillation counter with a very small crystal.

* Research supported by the Office of Naval Research.

† Now at National Research Council, Ottawa, Canada.

BA4. Spin and Magnetic Moment of (4.7-Hour) Rubidium-81.* J. C. HUBBS,† J. P. HOBSON, W. A. NIERENBERG, AND H. B. SILSBEE, *University of California, Berkeley.*—The spin and hyperfine splitting of neutron-deficient Rb^{81} have been determined to be $\frac{3}{2}$ and 5000 ± 150 megacycles by the zero-moment method of atomic beams. From the hfs, spin, and magnetic moment of other rubidium isotopes and these values, the nuclear magnetic moment of Rb^{81} is deduced to be 2.00 ± 0.06 nuclear magnetons. The isotope was identified from its chemistry and from its half-life and decay scheme. A study of the angular distribution of material emitted from highly channeled ovens has shown substantial agreement between experiment and the theory of Silsbee[1] for the fraction per unit solid angle of atoms emitted in the forward direction. The collection of ions and atoms on various surfaces has been investigated by tracer techniques. Sulfur is found to retain substantially all incident thermal rubidium atoms.

* Research supported by the Office of Naval Research.

† National Science Foundation Predoctoral Fellow: now at Columbia University.

[1] H. B. Silsbee, Ph.D. thesis, Harvard University, 1950.

BA5. Fine Structure of Singly Ionized Helium.* ROBERT NOVICK, EDGAR LIPWORTH, AND PAUL F. YERGIN,† *Columbia University.*—The energy difference (δ) between the $2^2S_{\frac{1}{2}}$ and $2^2P_{\frac{1}{2}}$ states of ionized helium has been measured by a pulse technique described by Yergin *et al.*[1] As a result of an improvement in the detection efficiency, the signal-to-noise ratio has been increased by a factor of ten. In addition a study has been made of the various phenomena that determine the shape of the resonance curve. As a result of this study a number of

small corrections to the observed resonance center have been discovered and evaluated. The present value of δ for He^+ is 14 043±13 Mc/sec. The stated uncertainty is equal to three times the standard deviation plus an estimated 2 Mc/sec for the uncertainty in the systematic corrections. This result is consistent with the previous results[1,2] and is in good agreement with the present theoretical value of 14 047.3±2.6 Mc/sec. The relation of the present results to those obtained in hydrogen and deuterium will be discussed. Further measurements of δ in He^+ are in progress.

* Work supported jointly by the Signal Corps, the Office of Naval Research and the Air Research and Development Command, and the National Science Foundation.
† Present address: University of Pennsylvania.
[1] Yergin, Lamb, Lipworth, and Novick, Phys. Rev. 90, 377(A) (1953).
[2] W. E. Lamb, Jr., and M. Skinner, Phys. Rev. 78, 539 (1950).

BA6. Hyperfine Structure of Gallium Isotopes in the Ground State. A. Lurio and A. G. Prodell, *Columbia University.*—The hyperfine structure of the $^2P_{\frac{1}{2}}$ state of both Ga^{69} and Ga^{71} have been measured by the atomic beam magnetic resonance method. The measured values are, $\Delta\nu^{69}=2677.9875\pm0.0010$ mc/sec and $\Delta\nu^{71}=3402.6946\pm0.0013$ mc/sec. The ratio of the measured $\Delta\nu$'s equals the ratio of the magnetic interaction constants α within experimental errors. Both the $^2P_{\frac{1}{2}}$ and the $^2P_{\frac{3}{2}}$ states may be characterized by a hyperfine structure anomaly constant, $\Delta=(\mu''/\mu^{69}-\alpha^{71}/\alpha^{69})\times(\mu^{69}/\mu^{71})$. We find that the differential constant $\delta=\Delta_{\frac{1}{2}}-\Delta_{\frac{3}{2}}=31.5\pm2.4\times10^{-4}$. The values of δ predicted by Bohr and Weisskopf[1] from a consideration of the magnetic effect of the penetration of the electron into the nucleus is 13×10^{-4} (odd particle in nucleus model). The difference between the experimental and theoretical value of δ may arise from the finite distribution of the coulomb charge within the nucleus or from other effects. The hyperfine structure of the metastable $^3P_{\frac{1}{2}}$ states of Ga^{69} and Ga^{71} were also remeasured in view of the discrepancy between the results of Daly and Holloway[2] and those of Kusch and Becker.[3] Our results agree with those of Daly and Holloway within our present experimental error of ±3 kc.

[1] Bohr and Weisskopf, Phys. Rev. 77, 94–98 (1950).
[2] Daly and Holloway, Phys. Rev. 96, 539–540 (1954).
[3] Kusch and Becker, Phys. Rev. 73, 584–91 (1948).

BA7. Nuclear Spins and Hyperfine Separations of Au^{198} and Au^{199}.* J. B. Reynolds, R. L. Christensen,† D. R. Hamilton, A. Lemonick,‡ F. M. Pipkin,§ and H. H. Stroke, *Princeton University.*—The Princeton focusing atomic beam apparatus[1] has been used to measure the spin of Au^{198} (2.7 days) and the spin and hyperfine separation, $\Delta\nu$, of Au^{199} (3.2 days). The value of H in the transition field was determined by a K^{39} resonance; resonances at several values of H were observed for each gold isotope. We obtain $I=\frac{3}{2}$ for Au^{198}, in agreement with the $d_{\frac{3}{2}}$ proton prediction of the shell model. The spin of Au^{199} is 2, in agreement with Nordheim's "weak" rule applied to a $d_{\frac{3}{2}}$ proton and a $p_{\frac{1}{2}}$ neutron. $\Delta\nu$ for Au^{199} is 10 850±150 mc/sec. $\Delta\nu$ for Au^{198} is greater than 14 000 mc/sec. Further measurements are being made to determine $\Delta\nu$ for Au^{198} as well as the signs of both magnetic moments.

* Work supported by the U. S. Atomic Energy Commission and The Higgins Scientific Trust Fund.
† Whiton Fellow.
‡ Now at Haverford College.
§ Now at Harvard University.
[1] Lemonick and Pipkin, Phys. Rev. 95, 1356 (1954).

BA8. Nuclear Resonance Fluorescence in Ge^{74} and Pr^{141}.* Franz R. Metzger, *Bartol Research Foundation.*—Using a germanium metal scatterer[1] and a gaseous source of As^{74}, a large resonance fluorescence effect due to the 596 kev excited state of Ge^{74} has been observed. Angular distribution measurements characterize the transition as quadrupole. From the magnitude of the resonance fluorescence effect a lifetime τ_γ of $(2.4\pm1)\times10^{-11}$ second was calculated for the 596 kev transition. This lifetime is one order of magnitude shorter than expected for an electric quadrupole transition on the basis of the single particle model. Using the 145 kev gamma rays from a source of Ce^{141}, resonance fluorescence from a praseodymium oxide[2] scatterer has been observed. Preliminary results indicate a lifetime τ_γ of $(3.5\pm1)\times10^{-9}$ second for the 145 kev magnetic dipole transition in Pr^{141}. This lifetime is two orders of magnitude longer than expected on the basis of the single particle model.

* Assisted by the joint program of the Office of Naval Research and the U. S. Atomic Energy Commission.
[1] Loaned by the Bell Telephone Laboratories, Murray Hill, New Jersey.
[2] Loaned by Dr. F. Spedding, Ames Laboratory of the U. S. Atomic Energy Commission, Ames, Iowa.

BA9. Spin, Magnetic Moment, and Electric Quadrupole Moment of La^{138}, and the Magnetic Moment of Cl^{36}. P. B. Sogo and C. D. Jeffries, *University of California, Berkeley.*—By nuclear induction we have observed the nuclear magnetic resonance of the rare odd-odd isotope La^{138} using both natural and enriched samples, supplied by Oak Ridge National Laboratory. The ratio of the resonance frequency to that of La^{139} is $\nu(La^{138})/\nu(La^{139})=0.93407\pm0.00003$. By a detailed comparison of the relative signal amplitudes, polarities, and line widths of La^{138} and La^{139}, and using the known moments of La^{139}, we find the spin $I(La^{138})=5$, and the magnetic moment $\mu(La^{138})=+(3.6844\pm0.0004)$ nm, without diamagnetic correction. From the observed thermal relaxation times and the reasonable assumption that the relaxation process is chiefly via the nuclear electric quadrupole moment Q we find $Q(La^{138})/Q(La^{139})\cong3$, which yields $|Q(La^{138})|\cong2.7\times10^{-24}$ cm^2 from the measured value $Q(La^{139})$ of Murakawa and Kamei. Using the experimentally determined g factors for the adjacent nuclei Ba^{137} and La^{139} we calculate on a simple jj coupling model $\mu(La^{138})=+3.70$ nm We have observed the magnetic resonance from 250 μc of Cl^{36}, obtaining for the magnetic moment $\mu(Cl^{36})=+(1.2838\pm0.0002)$ nm. A jj coupling calculation similar to the foregoing yields $\mu(Cl^{36})=1.16$ nm. This work has been supported in part by the U. S. Atomic Energy Commission.

BA10. Nuclear Magnetic Moment and Mass of Chlorine-36.* P. C. Fletcher and L. C. Aamodt, *Columbia University.*—The magnetic moment of the Cl^{36} nucleus was measured by observing the Zeeman splitting in the electric quadrupole hyperfine pattern of the molecule CH_3Cl^{36} ($J=0\rightarrow1$, $K=0$, $F=2\rightarrow2$). Its magnitude, as measured in a rectangularly cross-sectioned absorption cell, was found to be 1.32±0.08 nuclear magnetons. Its sign, determined in a circularly cross-sectioned absorption cell allowing circular polarization, was found to be positive. These observations favor the nuclear configuration $(d_{\frac{3}{2}})^3(d_{\frac{3}{2}})^p$ which is that expected from nuclear shell theory. Measurements of the quadrupole spectrum without a magnetic field gave the following information: the spin of Cl^{36} was confirmed to be 2, the mass difference ratio $(M_{Cl^{36}}-M_{Cl^{35}})/(M_{Cl^{37}}-M_{Cl^{35}})$ was found to be 1.00168±0.04 percent, the molecular rotational constant for CH_3Cl^{36} was found to be 13 187.604±0.015 Mc and its quadrupole coupling constant to be −15.83±0.20 Mc.

* This work supported jointly by the Signal Corps, the Office of Naval Research, and the Air Research and Development Command.

BA11. Quadrupole Resonances of Chloro and Bromobenzene Derivatives. P. J. Bray, *Rensselaer Polytechnic Institute,** and R. G. Barnes, *University of Delaware.*†—All available nuclear quadrupole resonance data for chloro and bromobenzene derivatives, including some work not yet published, have been correlated with the Hammett sigma parameter.[1–3] Regression lines have been fitted to the data by the method of least squares. These indicate that in the bromobenzene case the experimental values can be represented by the equation, $f=227.19+8.18\sigma$ megacycles per second. Evaluation of the correlation coefficient shows that approxi-

mately 90 percent of the observed frequency behavior may be ascribed to the sigma parameter. *Ortho*, *meta*, and *para* substituent positions correlate with nearly equal validity. In the chlorobenzene case, the correlation is less satisfactory, with only 60 percent of the frequency behavior determined by sigma in meta and para examples, and 83 percent determined in ortho examples. A brief discussion of some alternative views on this problem will be given.

* Research supported by a grant from the National Science Foundation.
† Research supported by the Office of Ordnance Research and the Research Corporation.
[1] L. P. Hammett, *Physical Organic Chemistry* (McGraw-Hill Book Company, Inc., New York, 1940).
[2] H. C. Meal, J. Am. Chem. Soc. **74**, 6121 (1952).
[3] P. J. Bray and R. G. Barnes, J. Chem. Phys. **22**, 2023 (1954).

BA12. Nuclear Magnetic Relaxation in Ethane Derivatives.* S. L. LINDER, *Washington University*.—It has been found that hydrogen and fluorine nuclei in certain of the ethane derivatives exhibit very long thermal relaxation times at liquid nitrogen temperature. The substances CH_2Cl-CH_2Cl and CH_2Cl-CF_2Cl have been examined and in both cases the proton relaxation time is about 30 seconds, while the fluorine relaxation time is about 10 seconds. The line widths of these resonances are all of the order of 10 gauss. In the Bloch notation, this situation can be described as $\alpha \ll \beta$, $\beta \gg 1$, and, for the values of H_1 used in this experiment, $\alpha \ll 1$. If the rf field is turned on suddenly, the derivative of the nuclear signal is observed to saturate with a time constant which can be related to T_1, the thermal relaxation time. The experiment permits an estimation of the saturation factor, which is a measure of the deviation of the line shape from a pure Lorentzian.

* Assisted in part by the joint program of the Office of Naval Research and the U. S. Atomic Energy Commission.

THURSDAY MORNING AT 10:00

Exhibit Hall II

(C. ZENER presiding)

Metals

C1. An Effect of Order-Disorder on the Low-Temperature Resistance Maximum. R. W. SCHMITT, *General Electric Research Laboratory*.—The addition of Mn to a Cu_3Au alloy is found to produce a maximum in the low-temperature resistance of the alloy similar to the maxima found in Cu, Ag, or Au upon adding Mn.[1] Moreover, the temperature at which the resistance maximum occurs depends on the heat treatment of the alloy in a way that suggests a connection between this temperature and order-disorder in the matrix. An alloy containing ≈ 0.17 atomic percent Mn has been investigated and an upward shift in the temperature of the resistance maximum of as large as 0.4°K has been observed in going from a "disordered" matrix to a "well-ordered" matrix.

[1] A. N. Gerritsen and J. O. Linde, Physica **17**, 573 (1951); **18**, 877 (1952).

C2. Monomolecular *vs* Bimolecular Relaxation Kinetics in Cu_3Au and Beta Brass. JEROME ROTHSTEIN, *Signal Corps Engineering Laboratories*.—Consider the elementary act of disordering in binary alloy as barrier-opposed AB interchange, "wrong" configuration metastable, interchange of nearest neighbors only permitted. If a wrong A-atom has "right" nearest B-neighbors it can migrate, while remaining wrong, from its original partner and be "righted" by interchange with a wrong B-atom not the original partner, leading to bimolecular isothermal relaxation kinetics (cot*kt* or tan*kt* laws) as expected[1] and observed[2] for Cu_3Au. If wrong A has only right A nearest neighbors except for the original partner (wrong B), "righting" is only by interchange with the original partner, leading to monomolecular isothermal relaxation kinetics ($\exp -\alpha t$ law); this is expected for beta brass. For comparable barrier heights and frequency factors monomolecular relaxation is much the faster by many orders of magnitude, particularly so at temperatures appreciably below T_c. Ease of quenching in disorder in Cu_3Au and absence of disorder in severely quenched beta brass support this expectation of monomolecular relaxation kinetics for the latter.

[1] J. Rothstein, Phys. Rev. **94(A)**, 1429 (1954).
[2] F. Burns, Phys. Rev. **94(A)**, 1429 (1954).

C3. Thermoelectric Powers of some Palladium Alloys. J. C. TAYLOR AND B. R. COLES,* *Imperial College, London* (introduced by J. E. Goldman).—Thermoelectric powers (S) have been measured in the range 0° to −200°C for the palladium-silver alloys and for some palladium-rhodium alloys. In the former system S is found to be highly sensitive to the presence of unoccupied d-band states. A marked variation of S with composition occurs in alloys with more than 90 percent of either element. This behavior can be ascribed to a contribution to conduction by d-band holes in the palladium-rich alloys, and to departure of the Fermi surface from an absolutely spherical form as the electron concentration increases in the silver-rich alloys. Estimates of S for the pure metals, made on the basis of simple theoretical models which ignore these complications, show close agreement with values obtained by extrapolating experimental results for alloys where these effects are absent. The composition dependence of S in alloys containing no d-band holes supports the view[1] that the relaxation time for impurity scattering has an energy dependence different from that for lattice scattering. Initial additions of rhodium to palladium produce effects which are consistent with the behavior in the alloys with silver, but larger additions give anomalous effects.

* On leave of absence at Carnegie Institute of Technology.
[1] C. A. Domenicali and F. A. Otter, Phys. Rev. **95**, 1134 (1954).

C4. Thermodynamic Properties of Alpha Ag-Cd and Alpha Au-Cd Alloys.* P. HERASYMENKO, *New York University*.—Measurements of partial pressure of cadmium were made over alpha solid solutions in the Ag-Cd and Au-Cd systems. Thin weighed wires of pure silver or gold were placed at different positions along a temperature gradient in an evacuated quartz tube in which a constant pressure of cadmium vapor was maintained. The wires absorbed cadmium until the alloys formed reached equilibrium with the vapor. Cadmium content was obtained from the weight increase of the wires. Several hundred alloys were obtained in the alpha field of each system at different cadmium pressures and for different temperature ranges (mostly above 550°C). The evaluation shows that sharp increases in relative partial entropy of cadmium occur at 8.33 at. percent Cd in the Ag-Cd system, and at 16.66 and 25.0 at. percent Cd in the Au-Cd system. The results indicate that a considerable ordering takes place in the alpha (f.c.c.) solid

solutions at compositions where the ratio of solute to solvent atoms is 1/11, 1/5, and 1/3.

* The study was sponsored by the Office of Ordnance Research.

C5. Mutual Solubilities of Iron and Osmium. S. S. SIDHU AND D. D. ZAUBERIS, *Argonne National Laboratory.*—The electronic structures of 3*d* and 4*s* shells of iron are identical with those of 5*d* and 6*s* of osmium. In the "free" or gaseous state each *d*-shell contains 6 electrons and each *s*, 2. The metallic radii of iron are about 6.1 percent and 6.7 percent smaller than those of osmium for coordination numbers of 8 and 12 respectively. These factors favor an extensive solubility of one metal in the other. From a series of substitutional solid solutions of iron in osmium and osmium in iron, prepared at 2000°–2700°C and cooled to room temperature, it is found that iron dissolves in osmium to the extent of 80 atomic percent, and osmium in iron to about 10 atomic percent. The region between 80 and 90 atomic percent iron in osmium is a transformation region in which the two phases coexist. As iron dissolves in osmium the osmium lattice contracts, but with increasing solubility of osmium in iron the iron lattice expands. At room temperature the volumes of the unit cells of osmium metal and of electrolytic α iron used in this investigation were: 27.98×10^{-24} cm³ and 23.49×10^{-24} cm³ respectively. At the solubility limits they approached the value of approximately 24×10^{-24} cm³.

C6. Small-Angle X-Ray Scattering from Cold-Worked Metals.* R. H. NEYNABER, W. G. BRAMMER, AND W. W. BEEMAN, *University of Wisconsin.*—The diffuse small angle scattering from cold-worked metals is presumed caused by the collection of lattice vacancies into small cavities. Some of our recent experimental results are difficult to explain on this model. We observe in annealed Ni, Cu, and Al foils sharp scattering peaks at 1° or 2° scattering angle (Fe K_α radiation). We believe these arise from two successive Bragg scatterings by adjacent and slightly-tilted grains. We will discuss the possibility that some or all of the diffuse scattering in cold-worked foils is due to a similar mechanism. Foils cold worked at liquid air temperature show immediately the usual diffuse scattering. There is no evidence for the growth of cavities by the diffusion of vacancies as the foil is warmed. Below annealing temperatures the intensity of the diffuse scattering decreases and increases reversibly with increasing and decreasing foil temperature. This is understandable with double scattering (the Debye factor) but difficult with a cavity model. Arguing against double scattering is our failure to find scattering curves intermediate between the occasional sharp peaks from annealed samples and the continuous diffuse scattering from slightly cold-worked samples.

* Supported by the Office of Scientific Research, Air Research Development Command, and the Wisconsin Alumni Research Foundation.

C7. Dislocation Relaxations at Low Temperatures and the Limiting Shear Stress in Metals. W. P. MASON, *Bell Telephone Laboratories.*—Recent measurements of the ultrasonic attenuation[1,2] in four face-centered metals have shown relaxations in the temperature range from 35°K to 150°K. For lead the relaxation frequency follows Eq. (1a). At higher temperatures, a loss shown by Eq. (1b) results for lead. Thus

$$\omega_0 = 2\pi f_0 = 2.9\times10^{9} e^{-790/RT} \quad (1a); \qquad Q^{-1} = 1.8 e^{-4190/RT}. \quad (1b)$$

TABLE I.

Metal	Temp. of max. atten.	Act. eng. cal/mole	b in A°	μ dynes/cm²	T_{13_0} dynes/cm²	T_{13_0}/μ
Pb	35°K	790	3.5	7.3×10^{10}	3.9×10^{5}	5.3×10^{-6}
Cu	85°K	1910	2.55	4.0×10^{12}	1.9×10^{8}	4.7×10^{-5}
Al	100°K	2260	2.86	2.5×10^{11}	1.6×10^{7}	6.4×10^{-5}
Ag	60°K	1350	2.88	2.5×10^{11}	1.0×10^{7}	4.0×10^{-5}

Furthermore, 790 cal/mole correlates with the energy required to displace a dislocation loop from one minimum energy to an adjacent one against the limiting shearing stress $T13_0$. From the activation energies measured one can determine the limiting shearing stress $T13_0$ for the four metals as shown by Table I.

[1] P. C. Bordoni, J. Acoust. Soc. Am. 26, 495 (1954).
[2] H. E. Bömmel, Phys. Rev. 96, 220 (1954).

C8. Conductivity of Thin Films in a Longitudinal Magnetic Field. ERNEST KOENIGSBERG AND LEON FINDLEY, *Midwest Research Institute.*—The conductivity of thin *films* in a strong magnetic field (i.e., radius of curvature of electron paths less than half the film thickness) can be expressed in closed form.[1] We have calculated the conductivity in weak fields by numerical integration of the expression resulting from the free electron approach described in reference 1. This integration was performed on the Card Program Calculator at Midwest Research Institute. Calculation errors range from less than 1.0 percent for thick films to 3.0 percent (due to slow convergence) for relatively thin films in very weak fields. Comparison is made with Chamber's[2] results for thin *wires*. In a given field, the conductivity of a film is greater than that of a wire of the same material whose diameter is equal to the film thickness. At present, experimental results are not available for comparison.

[1] E. Koenigsberg, Phys. Rev. 91, 8 (1953).
[2] R. G. Chambers, Proc. Roy. Soc. (London) A202, 378 (1950).

C9. Tensile Strengths of Silver Films of Various Thicknesses at Different Temperatures.* J. B. BREAZEALE, W. L. BART, AND J. W. BEAMS, *University of Virginia.*—Silver films are electrodeposited on the periphery of cylindrical ferromagnetic rotors which are then spun until the films are thrown off. Both tensile strength and adhesion may be measured by this method,[1] but in these experiments care was taken in the electrodeposition process to reduce adhesion to a negligible value. The rotors were magnetically suspended in glass vacuum chambers and driven by rotating magnetic fields. At low temperatures the vacuum chamber was surrounded by two dewars. The outer Dewar contained liquid nitrogen; and the inner one contained liquid helium or liquid nitrogen, depending upon the desired operating temperature. At room temperature the tensile strength is independent of film thickness and equal to about that of bulk silver for thicknesses from 10^{-2} cm to approximately 2.9×10^{-6} cm. For film thicknesses less than about $2.9\pm0.3\times10^{-3}$ cm (the exact value depends slightly upon the plating current) the tensile strength increases many fold. At liquid nitrogen temperature for film thicknesses from 10^{-2} cm to roughly 2.9×10^{-6} cm the tensile strength is constant and equal to approximately 2.3×10^{8} dynes/cm². For thinner films a large increase in tensile strength is observed.

* Supported by the Office of Ordnance Research.
[1] Beams, Walker, and Morton, Phys. Rev. 87, 524 (1952).

C10. A Technique for the Study of Thin Metallic Films. R. L. KELLY, *Stanford Research Institute.*—A method will be described which permits the determination of resistivity and thermoelectric emf of thin metallic films. The films are formed by vacuum evaporation in a sealed-off glass tube and kept under high vacuum during the electrical measurements. The tube will be described in detail and some preliminary data on iron films will be presented.

C11. Micromachining with Virtual Electrodes. A. UHLIR, JR., *Bell Telephone Laboratories.*—Minute holes have been drilled in germanium, iron, copper, silver, and tungsten carbide by a new technique for machining by electrolytic etching. The flow of current is localized by a nonconducting partition in the electrolyte. The partition may be a glass tube drawn down to a tip as small as one micron in diameter. A variety of shapes can be produced by moving the tip with respect to the work. Localized plating has also been accomplished with the technique.

THURSDAY MORNING AT 10:00

Continental Room

(N. P. HEYDENBURG presiding)

Fission; Coulomb Excitation

CA1. Energy Spectrum of the Delayed Gamma Rays from Uranium Photofission.* J. M. WYCKOFF AND H. W. KOCH, *National Bureau of Standards.*—The delayed gamma rays from uranium samples irradiated by 18.5 Mev electrons from a 50 Mev betatron were studied in the range of 30 kev to 5 Mev with a 4 in. long, 5 in. diameter, NaI(Tl) spectrometer. After bombardment times of 1, 2, 10, and 90 minutes, photographs of two ten-channel pulse-height analyzers taken at regular intervals recorded the pulse-height distribution and decay rate. The location of the spectrometer was such that there was no neutron activation of the crystal. Three uranium samples, 0.02, 0.09, and 0.30 cm thick, were used in order to assess the effects of buildup of gamma intensity in the bombarded target and self-absorption, backscattering, and self-excitation of the $K\alpha$ x-rays on the measured spectrum. The measured energy spectrum above 360 Kev during the first 100 seconds was a fairly smooth straight line on a semi-log plot dropping 3.5 decades by 5 Mev. In the delay time interval between 10 and 42 minutes the slope of the exponential spectrum decreased, thus decreasing the mean and the apparent maximum energy. An estimate of the number of gammas per fission above 200 kev is 2.7.

* Supported by the Department of Defense, Air Force Special Weapons Project.

CA2. Neutron Induced Fission Excitation Curve for Am^{241}.* R. A. NOBLES, R. L. HENKEL, AND R. K. SMITH, *Los Alamos Scientific Laboratory.*—The Am^{241} fission cross section has been measured for several neutron energies between 0.5 and 7 Mev by simultaneously counting fission events from known foils of Am^{241} and U^{235} irradiated by the same neutron flux. U^{235} fissions were counted by a conventional ionization chamber. Due to the high specific activity of Am^{241}, a fast counting system was developed to prevent obscuring the fission pulses by multiple pile-up of alpha pulses. The Am^{241} pulses were counted in a xenon scintillation counter using a tetraphenylbutadiene loaded plastic film to shift the ultraviolet radiation to the visible spectrum for viewing by an RCA-6342 photomultiplier. Pulse height stability was achieved by maintaining the temperature of this counter at 0°C. The pulse output of the photomultiplier was clipped to 2×10^{-9} second, amplified sent to a fast crystal discriminator which was biased to remove alpha pulses. The remaining fission pulses were lengthened to 1 μsecond, amplified and counted with conventional circuits. Using the known U^{234} fission cross section, the excitation curve for Am^{241} was determined. The cross section has a threshold at 0.5 Mev neutron energy, rises until 1.5 Mev, is constant up to 6 Mev and rises above 6 Mev.

* Work performed under the auspices of the U. S. Atomic Energy Commission.

CA3. Angular Distribution of Fragments from Neutrons-Induced Fission of U^{233}.* J. E. BROLLEY, JR., AND R. L. HENKEL, *Los Alamos Scientific Laboratory.*—$\sigma_f(0°,E_n)/\sigma_f(90°,E_n)$ for U^{233} was measured at a number of neutron energies from the threshold near 1 Mev to 20 Mev. A double fission chamber whose common center high-voltage electrode was also a collimator[1] served to detect fissions in a given direction. A coincidence requirement between the two chambers served to minimize background effects. In the threshold region the anisotropy rises rapidly to a maximum and then declines. Thereafter it exhibits the same behavior as U^{235}, climbing rapidly up to seven Mev and slowly declining from 14 to 20 Mev. At seven Mev the angular distribution $\sigma_f(\theta,7)$ has a shape of the form $1+A\cos^2\theta+B\cos^4\theta$, with the cosine fourth term dominant, similar to the curve for U^{235} previously obtained.

* Work performed under the auspices of the U. S. Atomic Energy Commission.

[1] Brolley, Dickinson, and Henkel, Phys. Rev. **95**, 651 (1954).

CA4. Spontaneous Fission Neutron Multiplicities.* R. V. PYLE, D. A. HICKS, AND JOHN ISE, JR., *University of California, Berkeley.*—Further measurements of the prompt neutron multiplicity spectra from the spontaneous fission of some of the actinides have been made in a liquid scintillator moderator and detector.[1] Using the average number of neutrons per spontaneous fission of Cf^{252}, $\bar{\nu}=3.53\pm0.15$, we found the efficiency for detecting one neutron to be $\epsilon=0.772\pm0.029$. The data from two nuclides have been analyzed and the ratio $\bar{\nu}$ $Cf^{252}/\bar{\nu}$ $Cm^{244}=1.344\pm0.015$ obtained (probable errors shown throughout), giving ν $Cm^{244}=2.63\pm0.11$. Higgins *et al.* have measured $\bar{\nu}$ $Cm^{244}=2.60\pm0.12$. If $P(n)$ is the observed multiplicity distribution and $F(\nu)$ is the actual distribution,

$$F(\nu)=\sum_{n=\nu}^{n=n_{\max}} P(n)\left[\frac{n!}{\nu!(n-\nu)!}\right]\epsilon^{n-\nu}(\epsilon-1)^{n-\nu}.$$

Based on 6594 Cm^{244} fissions and 5429 Cf^{252} fissions, the values of $F(\nu)$ (normalized to unity) are

$\nu=$	0	1	2	3	4	5	6	7
Cm^{244}	0.013 ±0.006	0.140 ±0.021	0.315 ±0.019	0.340 ±0.018	0.157 ±0.021	0.030 ±0.006	0.004 ±0.002	0.0009 ±0.0006
Cf^{252}	0.005 ±0.002	0.032 ±0.012	0.145 ±0.032	0.336 ±0.022	0.304 ±0.014	0.117 ±0.016	0.053 ±0.010	0.003 ±0.002

* This work was done under the auspices of the U. S. Atomic Energy Commission.

[1] Hicks, Ise, and Pyle, Phys. Rev. **97**, 564 (1955).

CA5. Coulomb Excitation of States in Thallium and Lead. P. H. STELSON AND F. K. MCGOWAN, *Oak Ridge National Laboratory.*—Gamma rays of 205-, 279-, and 410-kev energy are observed when thallium is excited by proton bombardment. Coincidence measurements indicate that 410-kev γ rays are coincident with both the 205- and 279-kev γ rays. It is thought that states of 279- and 682-kev energy are excited in Tl^{203}, and states of 205- and 615-kev energy are excited in Tl^{205}. The reduced transition probabilities for $E2$ excitation, $B(E2)$, are $(13.5\pm2.7)\times10^{-50}$ cm^4 e^2 and $(14.6\pm2.9)\times10^{-50}$ cm^4 e^2 for the 279- and 682-kev states in Tl^{203}, respectively. The values of $B(E2)$ and information obtained from studies of the decay of Hg^{203} and Pb^{203} give evidence that the $B(M1)$ for the 279-kev state is a factor of 2000 less than single particle estimate and that the $B(E2)$ for the 410-kev transition is 100 times larger than that expected for a transition between single-particle proton states. Gamma rays of 570- and 810-kev are observed when lead is excited by proton bombardment. The yield of the 810-kev γ ray increased when radiogenic lead enriched to 88 percent Pb^{208} was bombarded. These γ rays are thought to result from the excitation of the first excited states of Pb^{207} and Pb^{206}. The $B(E2)$ for excitation of the 570-kev and 820-kev states are $\left(2.8^{+0.6}_{-1.1}\right)\times10^{-50}$ cm^4 e^2 and $\left(13^{+2.6}_{-4.5}\right)\times10^{-50}$ cm^4 e^2, respectively.

CA6. Electric Excitation of Palladium, Cadmium, and Molybdenum by Protons.* GEORGE PAULISSEN AND HANS MARK, *M.I.T.*—Energy levels in enriched isotopes of cadmium, palladium, and natural molybdenum have been studied by electric excitation with protons. The following γ rays are observed: Pd^{105}, 270 and 430 kev; Pd^{106}, 500 kev; Pd^{108}, 425 kev; Pd^{110}, 365 kev; Cd^{110}, 290 kev; Cd^{114}, 545 kev. A 199 kev γ ray from natural molybdenum is observed which is probably due to a previously observed[1,2] level in Mo^{95}. Energies of the levels in the even A isotopes of palladium and cadmium increase with decreasing neutron number while the reduced transition probabilities decrease. The reduced transition probability of the 270-kev level in Pd^{105} is seven times smaller than that of the 430-kev level. Coincidence experiments and yield curve measurements are in progress on a number of odd A isotopes where two or more γ rays are observed to measure branching ratios and clarify level structures.

* Supported by the joint program of the Office of Naval Research and the U. S. Atomic Energy Commission.
[1] G. M. Temmer and N. P. Heydenburg, Phys. Rev. **93**, 351 (1953).
[2] Huber, Medicus, Preiswerk, and Steffen, Phys. Rev. **73**, 1211 (1948).

CA7. Internal Conversion Electrons from Electric Excitation.* E. M. BERNSTEIN AND H. W. LEWIS, *Duke University.*—Using a magnetic beta-ray spectrometer similar to the one used by Huus and Bjerregaard,[1] we have observed the internal conversion electrons from electric excitation of several nuclei. Alpha particles and protons of energy 2–4 Mev were used as the bombarding particles. The elements and levels investigated were: Mn, 128 kev; Ag, 320 kev; 420 kev; Ta, 137 kev, 166 kev; W, 102 kev, 112 kev, 124 kev; Au, 77 kev, 191 kev, 277 kev. The K/L conversion ratio for the Au 277 kev line leads to a 60 percent $M1$ and 40 percent $E2$ mixture for the transitions from this level to the ground state. This is in agreement with the gamma-ray angular distribution measurements of Cook *et al.*[2] Electron spectra and K/L ratios for other elements will be discussed.

* This work was supported by the U. S. Atomic Energy Commission.
[1] T. Huus and J. Bjerregaard, Phys. Rev. **92**, 1579 (1953).
[2] Cook, Class, and Eisinger, Phys. Rev. **96**, 638 (1954).

CA8. Angular Distribution of Gammas from Coulomb Excitation of Thin Platinum.* W. I. GOLDBURG, *Duke University.*—Measurements have been made of the angular distribution of gamma rays from spin 2 levels near 345 kev resulting from proton bombardment of natural platinum. Preliminary analysis of the data indicates that the proton energy dependence of the anisotropy is more rapidly changing[1] than the predictions of present Coulomb excitation theory.[2,3] The proton energy range was 2–4 Mev. The 0.0001-inch platinum was backed by 0.005-inch uranium. The bremsstrahlung contribution from the backing was measured and subtracted out.

* This work was supported in part by the U. S. Atomic Energy Commission.
[1] P. H. Stelson and F. K. McGowan, Bull. Am. Phys. Soc. **29**, No. 7, 34 (1954).
[2] K. Alder and A. Winther, Phys. Rev. **91**, 1578 (1953).
[3] K. Alder and W. Winther, Phys. Rev. **96**, 237 (1954).

CA9. Energy Levels in Ru, Pd, and Cd by Coulomb Excitation. G. M. TEMMER AND N. P. HEYDENBURG, *DTM, Carnegie Institution of Washington.*—We have excited the following gamma rays in Ru, Pd, and Cd nuclei by 6-Mev alpha-particle bombardment (*mass number*, followed by transition energy in kev). *Ru: 100*, 540; *102*, 473; *104*, 355. *Pd: 104*, 550; *105*, 266, and 433; *106*, 510; *108*, 424; *110*, 370. *Cd: 110*, 654; *111*, 340; *112*, 620; *113*, 290, and 550(?); *114*, 550; *116*, 508. Enriched isotopes[1] were used for Pd and Cd. All gamma rays in the even-even nuclei represent transitions to the first-excited 2^+ states. Their transition probabilities (lifetimes) have been determined and will be presented. None of the lifetimes can be measured with presently available coincidence techniques ($\lesssim 10^{-11}$ sec). The lifetimes are of the order of 20 times *faster* than would be expected on the basis of single-particle transitions. Both the positions and lifetimes of these states are found to follow systematic trends interpretable on the basis of "deformation" of these nuclei.[2] A number of these $E2$ transitions as well as some in the odd-mass nuclei had not been observed before.

[1] Kindly lent by G. Scharff-Goldhaber.
[2] A. Bohr and B. R. Mottelson, Kgl. Danske Videnskab. Selskab, Mat.-fys. Medd. **27**, No. 16 (1953).

CA10. Energy Levels in Ti, Fe, Ge, and Mo by Coulomb Excitation. N. P. HEYDENBURG AND G. M. TEMMER, *DTM, Carnegie Institution of Washington.*—We have observed Coulomb-excited gamma rays with 6-Mev alpha particles on Ti, Fe, Ge, and Mo. Enriched targets (supplied by Oak Ridge) were used in the case of Mo; for the other elements, the identification was made from known transitions. The following gamma rays (energies in kev) were observed: Ti^{48}, 750 and 990; Ti^{46}, 890; Fe^{56}, 854; Ge^{73}, 830; Ge^{74}, 590; Mo^{93}, 786; Mo^{100}, 528. With the exception of the 750 kev line in Ti^{48}, all lines are due to quadrupole excitation of first-excited 2^+ levels. Transition probabilities will be given for these gamma rays. The excitation curve of the 750 kev line of Ti^{48} was not consistent with Coulomb excitation of this energy and has been assigned to the reaction $Ti^{48}(\alpha,n\gamma)Cr^{51}$; a gamma ray of the same energy was also observed in the reaction $V^{51}(p,n\gamma)Cr^{51}$.[1] Results for Ge^{76} and Mo^{98} will also be reported.

[1] A neutron group to this level was previously seen by Stetson, Preston, and Goodman, Phys. Rev. **80**, 287 (1950).

THURSDAY MORNING AT 9:30

Caribar Room

(C. N. YANG presiding)

Theoretical Physics, I; Meson Theory

D1. Numerical Calculation of Meson-Nucleon Scattering.* M. H. KALOS, *Cornell University*, AND R. H. DALITZ, *Institute for Advanced Study.*—The solution of the integral equations for pion-nucleon scattering proposed by Dyson *et al.*[1] has been programmed for the UNIVAC computer,[2] paying particular attention to the singular nature of these equations. Phase shifts obtained behave qualitatively in accord with the rough solutions previously given. The wave functions and phase shifts will be presented for the s-, p-, d-states for which renormalization is not necessary, for energies up to 1 Bev. Calculations will also be presented for the corresponding integral equations of the relativistic p-wave theory in which the nucleon pair-creation graphs are omitted.

* This work was supported by the U. S. Atomic Energy Commission and the Office of Naval Research.
[1] Dyson *et al.*, Phys. Rev. **95**, 1644 (1954).
[2] The cooperation of the staff of the U. S. Atomic Energy Commission Computing Facility at New York University is gratefully acknowledged.

D2. Scattering of Pions by Nucleons in Intermediate Coupling. M. H. FRIEDMAN AND T. D. LEE, *Columbia University.*—The scattering of pions from nucleons has been investigated by considering a symmetrical pseudoscalar meson field coupled to an extended fixed nucleon using gradient coupling. In treating this Hamiltonian one uses the intermediate coupling approximation[1] which is based on a variational procedure and does not depend on the strength of the coupling constant nor the number of mesons in the field. The problem divides into two parts. The first is the solution of the ground state (i.e., physical nucleon) using the Tomonoga approximation.[2] In order to describe the scattering of a meson by a physical nucleon one multiplies this ground-state wave function by a scattering function for the meson. This latter is then determined by a variational technique. The resulting α_{33} phase shift agrees with experiment, if the coupling constant $f^2=0.712$ and the cut-off $\omega_{max}=6.21\mu$ where μ is the meson mass. (This corresponds to a renormalized coupling constant $f_r^2=0.105$.) The α_{31} and α_{11} phase shifts are small, *e.g.* being $-1.60°$ and $5.99°$ respectively at 200 Mev.

[1] T. D. Lee and R. Chiristian, Phys. Rev. **94**, 1760 (1954).
[2] S. Tomonaga, Progr. Theoret. Phys. **2**, 6 (1947).

D3. Correlation of Meson-Nucleon Scattering and Nuclear Forces. ABRAHAM KLEIN* AND BRUCE H. MCCORMICK, *Harvard University.*—The general form of the interaction kernel for the relativistic two-nucleon equation has been constructed by means of the technique of functional differentiation with respect to external sources. If the nonlinear propagation of mesons (meson-meson interaction) can be neglected, the corresponding potential can be expressed completely in terms of the meson scattering and production matrices for the individual nucleons (off the energy shell) and of the meson Green's functions. The circumstance can be exploited to obtain information about the fourth-order nuclear forces, for example, by making a momentum-energy expansion of the meson-nucleon scattering amplitude and choosing the coefficients to fit the data in the low-energy region. This procedure has in effect already been applied to the isotopic-spin independent part of the *S*-wave scattering.[1] It can equally well be applied to the isotopic-spin dependent *S*-wave scattering and the *P*-wave scattering. The corresponding modifications of the long-range nuclear forces will be discussed.

* Society of Fellows.
[1] A. Klein, Phys. Rev. **95**, 1061 (1954).

D4. Effective Range Analysis of the Pion-Nucleon *S*-Waves.* H. P. NOYES, *University of Rochester.*—The photomeson-Panofsky effect result[1] that $|a_1-a_3|/k=0.19$ ($k=p_\pi/\mu c$) and low-energy scattering data[1] imply a_1 increases more rapidly than k below 60 Mev. Then either the effective range is negative, implying at least two bound states of $I=1/2$, or shape dependent corrections are enormous, requiring a pathological interaction. If, however, interpretion of the Panofsky effect is in error due (for example) to charge dependent corrections, all other data[1] are consistent with $a_1\sim 0.173k$, $a_3\sim -0.097k$. Introducing a hard core,[2] the shape independent approximation may be written $a_l=\mathrm{ctn}^{-1}(-1/a_lk+r_{0l}k/2)-r_{0l}k$. If one fits the slopes and $a_1=+10°$, $a_3=-13°$ at $k=1.3$, the curves are essentially independent of r_{01} if $r_{01}\lesssim\hbar/\mu c$. The parameters (units $\hbar/\mu c$) are

r_{03}	a_1	r_{01}	a_3	r_{03}
0	−0.434	0.761	−0.564	0.661
1	−0.222	0.049	−0.322	0.419

* Work supported in part by the U. S. Atomic Energy Commission.
[1] For recent data see *Proceedings of the Fifth Annual Rochester Conference* (Interscience Publishers, Inc., New York, 1955) (to be published).
[2] H. P. Noyes and A. E. Woodruff, Phys. Rev. **94**, 1401 (1954) and references.

D5. Energy Distribution of γ Rays from π^0 Decay.* R. M. STERNHEIMER, *Brookhaven National Laboratory.*—The energy distribution of γ rays resulting from the decay of π^0 mesons produced by a high-energy proton beam is related in a simple manner to the differential cross-section $f(E_\pi,\theta_\pi)$ for π^0 production, where $E_\pi=\pi^0$ total energy and $\theta_\pi=$angle of π^0 to the incident beam. The angle ψ in the laboratory system between the observed γ and the decaying π^0 must be $\leq\psi_{max}=\sin^{-1}(\tilde{k}/k)$, where $k=$laboratory energy of γ, $\tilde{k}=\gamma$ energy in π^0 rest system. At high γ energies, ψ_{max} is small (e.g., 3.9° for $k=1$ Bev). Hence the γ-energy distribution for large k at an angle θ_γ to the beam involves only values of $f(E_\pi,\theta_\pi)$ for a narrow range of $\theta_\pi\approx\theta_\gamma$. If $P(k,\theta_\gamma)$ is the number of γ rays per unit energy interval dk and per unit solid angle at θ_γ, $f(k,\theta_\gamma)$ is given by $-(k/2nN)\partial P(k,\theta_\gamma)/\partial k$, where $n=$number of incident protons, $N=$number of target nuclei/cm^3. This expression is valid for $k\gtrsim 500$ Mev and can be used to obtain $f(E_\pi,\theta_\pi)$ from measurements with a γ-ray spectrometer set at various angles to the proton beam. This result has been extended to an arbitrary two-body decay.

* Work performed under the auspices of the U. S. Atomic Energy Commission.

D6. Pion Production in Proton-Proton Scattering.* D. B. LICHTENBERG, *University of Illinois.*—A calculation of the cross section for the reaction $p+p\rightarrow\pi^+ +d$ has been carried out, using the cut-off form of the Yukawa theory.[1] The diproton and deuteron wave functions have been treated phenomenologically. Two types of terms have been taken into account: (1) those due to direct emission of the pion and (2) those due to resonance scattering of the pion by the proton in the state of angular momentum 3/2 and isotopic spin 3/2.[2] These terms were found to be of comparable magnitude. Since the diproton state is one of high energy, the results are very sensitive to the details of the wave functions chosen for the deuteron and diproton, but with any reasonable choice, the correct qualitative features of the p-wave part of the production amplitude emerge. In particular, the absolute value of the experimental cross section is consistent with a coupling constant of the same order as that determined by pion-nucleon scattering and photoproduction.

* Supported in part by the Office of Naval Research.
[1] G. F. Chew, Phys. Rev. **95**, 1669 (1954).
[2] K. A. Brueckner, Phys. Rev. **86**, 106 (1952).

D7. Pion Production for Polarized Protons. F. MANDL AND T. REGGE, *University of Rochester* (introduced by R. E. Marshak).—The production of pions and deuterons in proton-proton collisions is analyzed using the statistical operator methods. We derive (1) the production cross section for s-, p-, and d-waves and (2) the polarization of the deuteron for both polarized and unpolarized incident protons with the restriction to s- and p-waves. The deuteron polarization gives new information about the production amplitudes for an unpolarized proton beam for the p-wave production only and for a polarized one for s-waves as well. With polarized protons a triple-scattering experiment is required. The experimental possibilities of the triple scattering experiment (in the energy-range 400 to 600 Mev) will be discussed.

D8. Pion Production in Electron-Proton Collisions.* R. H. DALITZ, *Institute for Advanced Study.*—The main part of the direct pion production from protons by the virtual electromagnetic field of a scattered electron may be predicted from the pion-photoproduction data, if only the outgoing pion is measured, since small angle scattering in which this field is transverse then predominates. New information is contained in the deviations from such an estimate; these deviations reflect (a) the momentum dependence of the (off-diagonal) matrix elements for excitation by the transverse field and (b) the electric transitions induced by the longitudinal field. Transverse and longitudinal excitations will generally interfere and, since the momentum transfer is large, the matrix elements (b) are different from those for the corresponding

transverse excitations. Photoproduction data and matrix-element estimates based on fixed-source meson theory suggest that the observable deviations will give information mainly on the momentum dependence of the $M1$ excitation of the resonant state and on the longitudinal $E1$ excitation. The experimental data available will be discussed.

* This work has been supported by the program of the Office of Naval Research at Stanford University and Cornell University.

D9. A Model for Multiple Meson Production. E. M. HENLEY, *University of Washington*, AND T. D. LEE, *Columbia University*.—A quantum-mechanical model, analogous to the classical treatment of Lewis, Oppenheimer, and Wouthuysen,[1] is proposed to study the production of mesons in nucleon-nucleon collisions. The colliding nucleons are pictured as bare cores surrounded by arbitrary numbers of mesons. The structure of the meson cloud surrounding each core and the scattering states for various numbers of mesons are determined by an intermediate coupling calculation. The strength of the meson-nucleon coupling constant and the size of the core are determined by comparison with meson-nucleon scattering experiments. In the collision process, mesons are produced by an exchange of ordinary spin and isotopic spin between the cores. Although absolute cross sections cannot be obtained from this model, production ratios for various processes are completely determined. Results will be presented for the production of one and two mesons at collision energies of the order of a few Bev.

[1] Lewis, Oppenheimer, and Wouthuysen, Phys. Rev. **73**, 127 (1948).

D10. Structure of the Mesonic Cloud Associated with a Nucleon. G. SALZMAN, *University of Illinois*.—Experimental evidence for the spatial extent of the charges and currents associated with a physical nucleon is becoming available. The effects of this extension may, for each nucleon, be described in terms of two invariant functions (form factors) F_1 and F_2, where $\epsilon_0 F_1$ is the nucleon's effective charge, ϵ_0 its static charge, $\mu_0 F_2$ its effective anomalous magnetic moment, and μ_0 its static anomalous magnetic moment. The functions F_1 and F_2 may be expressed as power series in $(\Delta p)^2[=\Delta p_\nu \Delta p_\nu]$, the square of the four momentum transferred to the nucleon in the collision under discussion. The terms of F_1 and F_2 which depend on the first power of $(\Delta p)^2$ are being calculated to second order in the nucleon meson coupling using the cut-off theory with neglect of nucleon recoil. These results, and their comparison to experiment will be reported.

D11. Nuclear Radius and Nuclear Forces.* S. D. DRELL, *M.I.T.*—The difference between the "radius" of the nuclear matter distribution and the nuclear-force radius ($r_n \sim 1.45A^{\frac{1}{3}} \times 10^{-13}$ cm) for $A \gtrsim 50$ is interpreted as a consequence of the finite range of nuclear forces. Assuming that the matter distribution coincides with the charge distribution as determined at Stanford ($r_c \sim 1.2A^{\frac{1}{3}} \times 10^{-13}$ cm), we sum up the nuclear interactions of an incident nucleon for various proposed internucleon potentials, $V(r)$. We also evaluate induced spin, matter, and charge polarizations of the nuclear matter due to an impinging nucleon as a test of the convergence of these calculations. The aim here is to see what ranges and strengths of $V(r)$ are appropriate, say, to overcompensate the Coulomb barrier for protons at a distance $\sim r_n$. This approach is sensitive, in first order, only to the long-range behavior of the spin and charge independent portion of $V(r)$. It leads to the following conclusions. Either the neutron distribution extends at least 10 percent beyond the proton one or $V(r)$ must contain a sizeable amount of Wigner interaction with the range of a meson Compton wavelength. Such an interaction is not found in recent meson theoretically deduced $V(r)$. This result is insensitive to details of the tail of the charge distribution.

* This work was supported in part by the joint program of the Office of Naval Research and the U. S. Atomic Energy Commission.

D12. The Two-Nucleon Potential from the Cut-Off Yukawa Theory. S. GARTENHAUS, *University of Illinois*.—Using the Yukawa theory with cut-off, the two-nucleon interaction is calculated up to fourth order in the coupling constant. The resulting potential at large distances ($\gtrsim 10^{-13}$ cm) is similar to the well-known potential with no cut-off.[1] At small distances, however, the tensor potential approaches zero, and the central potential is strongly repulsive. All details are completely determined by two parameters, the coupling constant and cut-off. The Schrödinger equation for the two-nucleon problem at low energies is solved using the Blatt-Kalos routine on the Illinois electronic computer, and values are obtained for the binding energy, the quadrupole moment, and the four n-p scattering parameters. It is found that all experimental values are reproduced (to within 15 percent) with the same coupling constant and cut-off required to explain pion-nucleon scattering and photoproduction.[2]

[1] Taketani *et al.*, Progr. Theoret. Phys. **7**, 45 (1952); K. A. Brueckner and K. M. Watson, Phys. Rev. **92**, 1023 (1953); E. M. Henley and M. A. Ruderman, Phys. Rev. **92**, 1036 (1953).
[2] G. F. Chew, Phys. Rev. **95**, 1669 (1954).

D13. On the Singlet *S*-State Nucleon-Nucleon Potential.* R. B. RAPHAEL, *University of California, Berkeley*.—A knowledge of the singlet S-phase shift over only a limited energy region implies a corresponding limitation in the extent to which the S-state nuclear force may be determined from the scattering data. It will be shown, by means of a rapidly convergent approximation procedure suggested by Schwinger, that it is possible to know the value of the nuclear force at a discrete set of radial points only, whose number and distribution depend upon the energy range over which the S-phase shift is accurately represented. Thus the lowest approximation, corresponding to a knowledge of the S-phase shift between 0 and 10 Mev, produces a value at a single point, and is thus consistent with the shape-independent approximation. The next approximation, valid for scattering energies between 0 and 50 Mev, specifies the potential at three points within its range; when one uses the S-phase shifts appropriate to the usual potential shapes, the method reproduces these shapes with qualitative accuracy. When applied to the actual scattering data, the procedure produces an S-state potential having a repulsive core of radius $\sim 0.3 \times 10^{-13}$ cm. The effect on these results of alternate fits of the data and extensions of the method will be mentioned.

* This work was performed under the auspices of the U. S. Atomic Energy Commission.

D14. Anomalous τ-Meson Decay. TETSUO EGUCHI,* *Iowa State College*.—The possibility that a τ meson decays into two π mesons and a photon is considered by perturbation calculation under the assumption that the τ meson ordinarily decays into three π mesons via a virtual nucleon pair. Both processes are allowed if the τ-meson field is a pseudoscalar with pseudoscalar coupling to the nucleon field. If the neutral τ meson exists, the decay $\tau^0 \to \pi^+ + \pi^- + \gamma$ would look like a θ^0 event with a Q-value less than the normal value 214 Mev. The calculation shows that the probability of this decay with an apparent Q-value between 75 and 214 Mev is of the order of a few percent of that of the normal τ-meson decay. The possibility of interpreting the anomalous θ^0 events observed by Thompson[1] and others[2] in this manner will be discussed.

* Institute for Atomic Research, on leave from Kyushu University, Fukuoka, Japan.
[1] R. W. Thompson, Proceedings of the Fourth Annual Rochester Conference (1954).
[2] Van Lint, Anderson, Cowan, Leighton, and York, Phys. Rev. **94**, 1732 (1954).

D15. The $\Lambda^0 - \theta^0$ Ratio in Pb and C. MARTIN M. BLOCK* AND ROBERT JASTROW, *Naval Research Laboratory*.—The yields of Λ^0 and θ^0 particles have been calculated by Monte

Carlo techniques for 1.9-Bev π^- mesons incident on Pb and C. Associated production (π^-+N(nucleon)$\rightarrow\Lambda^0+\theta^0$) is assumed and the histories of the unstable particles are followed via elastic scattering and the exchange reaction (1) $\theta^0+N\rightarrow\Lambda^0+\pi$. Reaction (1) increases the Λ^0 to θ^0 ratio and is exothermic. The analogous reaction (2) $\Lambda^0+N\rightarrow\theta^0+2N$, which converts Λ^0's to θ^0's, is effectively prohibited by its high threshold (~740 Mev), which lies above typical Λ^0 energies. Results will be reported for several assumptions on the relative probability of (1).

* On military leave of absence from Duke University, Durham, North Carolina.

THURSDAY MORNING AT 10:00

NBS, East Building

(E. BURSTEIN presiding)

Invited Papers on Semiconductors

DA1. Polar Semiconductors. W. W. SCANLON, *U. S. Naval Ordnance Laboratory.* (30 min.)

DA2. Impact Ionization of Impurities in Germanium. N. SCLAR, *U. S. Naval Research Laboratory.* (30 min.)

DA3. Photoconductivity in Germanium. W. W. TYLER, *General Electric Company.* (30 min.)

DA4. Structure of Energy Bands in Semiconductors. F. HERMAN, *RCA Laboratories.* (30 min.)

THURSDAY AFTERNOON AT 2:00

Main Ballroom

(S. A. KORFF presiding)

Invited Papers on Photoproduction of Mesons and on Cosmic Rays

E1. The Photoproduction of Mesons in Hydrogen and Deuterium. R. L. WALKER, *California Institute of Technology.* (30 min.)

E2. Photopion Production from Nuclei. K. M. CROWE, *Stanford University.* (30 min.)

E3. Recent Results Concerning Hyperons and Heavy Mesons. G. T. REYNOLDS, *Princeton University.* (30 min.)

E4. *K*-Mesons and Hyperons in the Cosmic Radiation. M. M. SHAPIRO, *Naval Research Laboratory.* (30 min.)

E5. Cosmic-Ray Intensity near the North Magnetic Pole in 1954. H. V. NEHER, *California institute of Technology.* (30 min.)

THURSDAY AFTERNOON AT 2:00

Burgundy Room

(H. W. NEWSON presiding)

Neutron Physics, II

F1. Neutron Resonances in the Kilovolt Region: Cl^{35}, Cl^{37}, K^{39}, and K^{41}.* L. A. TOLLER, J. R. PATTERSON, AND H. W. NEWSON, *Duke University.*—Neutron cross section curves have been measured by the transmission method between 2 and 200 kev for Cl and 2 to 120 kev for K. The strengths of the resonant spectra increase decidedly with atomic weight. Below 110 kev there are 9 resonance peaks in K^{41}, 9 in K^{39}, 6 in Cl^{37}, and 2 in Cl^{35}. However, the fractional loss of peaks is undoubtedly considerably greater for the lighter nuclides. Widths for some of the peaks have been estimated by the area method: K^{41}, 39(0.9); K^{39}, 43(0.3), 58(0.6), 68(0.8); Cl^{35}, 26.5(0.34); Cl^{37}, 8.8(0.09), 26.5(0.33), 47.4(0.20), 55.5(0.18), 65.0(0.18), and 94.2(0.80). The estimated value of the width (kev) is shown in parentheses next to the neutron energy of the peak. Compensating samples were used to cancel out any isotopic impurity greater than 5 percent; the frequency with which both isotopes have resonances at the same energy makes this precaution necessary. Peaks at 26.5, 141, and 190 kev are found in the cross section curves for both isotopes of Cl; and both K isotopes show peaks at 10, 23, 58, 96, and 110 kev. No plausible model is known which can account for the surprising frequency of this effect. The separated isotopes were prepared at Oak Ridge National Laboratory by C. P. Keim and his associates.

* This work was supported by the U. S. Atomic Energy Commission.

F2. Total Neutron Cross Sections in the Kilovolt Region: Zr^{90}, Zr^{92}, and Zr^{94}.* P. F. NICHOLS, R. G. SMITH, AND H. W. NEWSON, *Duke University.*—The total cross sections of Zr^{90}, Zr^{92}, and Zr^{94} were measured as oxides by the transmission method over a neutron energy range from 5–140 kev. The neutron collimation-detection equipment has been previously reported.[1] The most prominent resonances in Zr^{90} occur at 18(0.12) and 42(0.40) kev; in Zr^{92} at 7(0.05) and 48(0.35) kev; and in Zr^{94} at 20(0.11), 44(0.20), and 68(0.50) kev. The figures in parentheses are the estimated widths. Weaker resonances were found in each isotope. The resonances in Zr^{90} are somewhat more prominent than in the others, but the apparent level spacings are about the same. Better resolution will be required to find the variation of level spacing near neutron number 50. The separated isotopes were prepared at Oak Ridge National Laboratory by C. P. Keim and his associates.

* This work was supported by the U. S. Atomic Energy Commission.
[1] J. H. Gibbons, Phys. Rev. **94**, 773 (1953).

F3. Angular Distributions of Scattering of Moderate Energy Neutrons. A. LANGSDORF, JR., AND R. O. LANE, *Argonne National Laboratory.*—Measurements of the angular distributions of the scattering of 0.1–1.5-Mev neutrons by various nuclei have been made at five laboratory angles, 22°, 54°, 92°, 112° and 144° with neutrons from the $Li^7(p,n)Be^7$ reaction: Five detectors, one at each angle, count simultaneously each with an efficiency of over 15 percent and a resolution of 1° to 5°. Detection is accomplished with oil-immersed BF_3 counters, and the response with energy in this range is flat to better than 10 percent when calibrated with a long counter. No discrimination is made between elastic and inelastic scattering. These data were obtained with an energy resolution of 50–100 kev. Though corrections for multiple scattering have not been made, they are minimized by the use of scatterers of at least 90 percent transmission. Differential scattering cross sections are calculated from integration of the angular distribution for carbon and its known smoothly varying cross sections in this range. Scattering cross sections obtained in a similar manner for the various elements measured are in good agreement with prior published values.[1]

[1] M. Walt and H. H. Barschall, Phys. Rev. **93**, 1062 (1954).

F4. Elastic Scattering of 14.6-Mev Neutrons. W. G. CROSS AND R. G. JARVIS, *Chalk River Laboratories.*—The differential cross sections for elastically-scattered 14.6-Mev neutrons have been measured at 25 angles between 10° and 125° for Mg and Bi, and over a smaller angular range for Ca, Cd, and Ta. A beam of neutrons from the $T(d,n)\alpha$ reaction is defined by counting only neutrons in coincidence with a collimated beam of α particles from the reaction.[1] Plastic scintillators are used for both the α and neutron counters. The neutron counter bias rejects neutrons of less than 11 Mev. Gamma rays from inelastic scattering are rejected because of their flight time. To reduce the background (mainly accidental coincidences) a copper bar shields the neutron counter from the source. The disk-shaped scatterers scatter five to 10 percent of the incident neutrons, the thicker scatterers being used for measurements at large scattering angles. Angular resolution is about ±3°. Minima in the angular distributions were found at the following angles (in degrees): Mg, 44±2, 113±5; Ca, 40±2, 75±2; Cd, 38±2, 85±5; Ta, 30±1; Bi, 27±1, 57±2.

[1] G. K. O'Neill, Phys. Rev. **95**, 1235 (1954).

F5. Interaction of 3.7 Mev Neutrons with Al, S, Fe, and Cu.* IRA L. MORGAN, *University of Texas.*—Neutrons of energy 3.7 Mev from the *d-d* reaction have been used to investigate the differential elastic scattering cross section of Al, S, Fe, and Cu, and gamma rays from inelastic scattering were also measured. A ring type geometry was employed with an overall resolution of 10° and scattering angles were varied from 10° to 150°. The detector and monitor were ZnS(Ag) buttons. Data for Fe and Al are in general agreement with earlier work.[1] Comparison of elastic scattering curves to certain theories will be presented. A NaI(Tl) crystal detector was placed at a scattering angle of 90°, and gamma rays produced by inelastic scattering were analyzed with a 20-channel analyzer. Gamma-ray energies were found to be generally consistent with earlier results,[2] obtained with 3.2 Mev neutrons. However, we find additional gamma rays of higher energy from Fe and Cu, and the intensities are markedly different. Further work on excitation functions for inelastic scattering is in progress.

* Assisted by the U. S. Atomic Energy Commission.
[1] W. D. Whitehead and S. C. Snowdon, Phys. Rev. **92**, 114 (1953).
[2] Scherrer, Allison, and Faust, Phys. Rev. **96**, 386 (1954).

F6. Scattering of 4.4 Mev Neutrons by C, Ca, Fe, and Zr.* J. B. WEDDELL AND B. JENNINGS, *Westinghouse Research Laboratories,* AND R. L. HELLENS, *Westinghouse Electric Corporation.*—The neutron spectra from the scattering of 4.4 Mev neutrons at 90° by carbon, calcium, and zirconium have been measured by the proton recoil photographic method. Previously reported results from iron[1] have been revised after additional measurements. The results permit location of energy levels in Fe^{56} and Zr, and the estimation of differential elastic and inelastic scattering cross sections. Differential elastic cross sections at 90° are: C, 0.061±0.016 b/sterad; Ca, 0.053±0.013 b/sterad; Fe, 0.076±0.020 b/sterad; Zr, 0.096±0.024 b/sterad. Differential inelastic scattering cross sections for the first four excited states in Fe^{56} are: (0.85 Mev), 0.036±0.010 b/sterad; (2.05 Mev), 0.021±0.007 b/sterad; (2.58 Mev), 0.012±0.006 b/sterad; (2.90 Mev), 0.020±0.013 b/sterad. Results for Zr are: (2.2 Mev), 0.009±0.004 b/sterad; (2.8 Mev, existence doubtful), 0.008±0.004 b/sterad. The results will be compared to predictions based on the theory of Feshbach, Porter, and Weisskopf.[2]

* Assisted by the joint program of the Office of Naval Research and the U. S. Atomic Energy Commission.
[1] Jennings, Weddell, and Hellens, Phys. Rev. **95**, 636 (1954).
[2] Feshbach, Porter, and Weisskopf, Phys. Rev. **96**, 448 (1954).

F7. Gamma Radiation from the Interaction of 4.4-Mev Neutrons with Germanium and Tungsten.* ROLF M. SINCLAIR, *Westinghouse Research Laboratories.*—Gamma radiation from samples of germanium and tungsten bombarded by 4.4±0.1-Mev neutrons has been observed. A single NaI(Tl) crystal, shielded from the direct neutron beam by a "heavy metal" wedge, was used as the detector. Germanium emits gamma rays of energy 0.52±0.02 (presumably annihilation radiation), 0.59±0.02, 0.82±0.02, 1.03±0.02, and 1.23±0.05 Mev. The 0.59 and 0.82-Mev gamma rays correspond in energy to transitions from known[1] excited states of Ge^{74} and Ge^{72}, respectively. Tungsten emits two discrete gamma rays, of energy 0.63±0.02 and 0.75±0.02 Mev.

* Supported by the joint program of the Office of Naval Research and the U. S. Atomic Energy Commission.
[1] G. Scharff-Goldhaber, Phys. Rev. **90**, 587 (1953), and references cited therein.

F8. Analysis of Inelastic Neutron Scattering Data for Mn, Fe, and I.* D. A. LIND AND J. J. VAN LOEF, *University of Wisconsin.*—Data on the inelastic scattering of neutrons by Fe, Mn and I have been reported.[1] The excitation curves reported have been analyzed using the transmission coefficients T_l calculated for a square well potential of the form $V=42$ Mev $(1+i\xi)$ and $R=1.45\ A^{\frac{1}{3}}\times10^{-13}$ cm with the theory developed by Hauser and Feshbach.[2] It is impossible to determine spin assignments unambiguously from the data. A $7/2^+$ assignment to the 128 kev level in Mn^{55} gives the best fit. The Fe^{56} excitation curve is fit best by the assignment of 2+ but 1+ or 1− would give equally good fits. These are ruled out by the angular distribution of the 850-kev gamma

radiation. The distribution is given by $W(\theta)=1+a_2P_2(\theta)+a_4P_4(\theta)$ where $a_2=0.38\pm0.10$ $a_4=0.16\pm0.05$. The best fit of these data with theory is obtained for a $\zeta=0.2$. No unique spin assignment can be made on the basis of the excitation curves for the 62, 208, 435, and 632-kev levels of I. A comparison of the total inelastic scattering cross section for I^{127} with the capture cross section calculated on the basis of theory indicates that a value of $\zeta=0.2$ is needed.

* Research was supported by the U. S. Atomic Energy Commission and the Wisconsin Alumni Research Foundation.
[1] Van Loef and Lind, Bull. Am. Phys. Soc. 29, No. 7, B5 (1954).
[2] Hauser and Feshbach, Phys. Rev. 87, 366 (1952).

F9. Fast Neutron Reactions in KI(Tl) Crystals. MARY JEAN SCOTT AND RALPH E. SEGEL, *Johns Hopkins University.*—The heavy charged particle spectrum resulting from the bombardment of KI(Tl) with neutrons has been investigated. Thin (~15 mil) KI(Tl) crystals were mounted on photomultiplier tubes and the pulse-height spectra recorded in a 99 channel analyzer. For fast monoenergetic neutrons of energy less than 3.5 Mev, a single peak was observed in the spectrum. The pulse height varied correctly with neutron energy if the group is identified with the reaction $K^{39}(n,p)A^{39}$. At higher neutron energies, a broad peak appears in the spectrum at lower pulse height. This broad peak has been tentatively ascribed to transitions to two excited states of A^{39} which have been previously reported at 1.33 and 1.68 Mev.[1] The potentialities of KI(Tl) crystals for counting neutrons in various energy ranges will be discussed.

[1] Nussbaum, Van Lieshout, and Wapstra, Phys. Rev. 92, 207(L) (1953).

F10. Secondaries from High Energy Neutron Interactions with Tungsten.* R. W. WANIEK, L. GARRIDO, R. GOLOSKIE, AND E. G. SILVER,† *Harvard University.*—With the technique previously described,[1,2] Tungsten wires of 13 microns diameter embedded in Ilford G5 emulsions were exposed to neutrons of 40, 70, and 110 Mev maximum energy. The neutron spectra were hardened by inserting one mean free path of CH_2 at the respective energies. The spectra of the ejected protons and alpha particles are all peaked at energies far below the conventional Coulomb barrier. There is some evidence for the presence of a few peaks in the proton spectra. The angular distributions of the secondaries with energies below 10 Mev is anisotropic. Some evidence for localized interactions leading to the emission of nuclear fragments is provided by a few instances. The process could be compatible with the assumption of an asymmetric fission-like mechanism excited by specialized oscillations of the nucleus.

* Supported by the joint program of the Office of Naval Research and the U. S. Atomic Energy Commission.
† Now at Oak Ridge School of Reactor Technology.
[1] Waniek, Fox, Garrido, and Silver, Bull. Am. Phys. Soc. 30, No. 1, 9 (1955).
[2] E. G. Silver and R. W. Waniek, Rev. Sci. Instr. 25, 119 (1954).

Invited Paper

F11. Widths and Spacings of Nuclear Energy Levels. D. J. HUGHES, *Brookhaven National Laboratory.* (30 min.)

THURSDAY AFTERNOON AT 2:00

Exhibit Hall I

(E. M. PURCELL presiding)

Radio-Frequency Spectroscopy, II; Optical and Atmospheric Physics

FA1. Interpretation of the Knight Shift in Metallic Sodium. T. KJELDAAS, JR., *Westinghouse Research Laboratories,* AND W. KOHN, *Carnegie Institute of Technology.*—The Knight shift of the nuclear resonance frequency in metals is due to the interaction of the magnetic moments of nuclei and those of the conduction electrons.[1] The fractional shift is proportional to the product of χ_p, the electron spin susceptibility, and P_F, the average probability density of conduction electrons at the nucleus.[1] A calculation of P_F for metallic sodium has been carried out, similar to one recently reported for lithium.[2] The resulting value of $P_F=0.61\ a_0^{-3}$ is in good agreement with the result of reference one, and when combined with the experimental value of the shift,[3] yields $\chi_p=(0.86\pm0.03)\times10^{-6}$ cgs mass units, in excellent agreement with the theoretical value of Pines.[4] The volume dependence of P_F was found to be small; this would seem to rule out the possibility that the observed[5] large low-temperature anomaly is due to a change of P_F in a phase transformation.

[1] Townes, Herring, and Knight, Phys. Rev. 77, 852 (1950).
[2] W. Kohn, Phys. Rev. 90, 590 (1954).
[3] H. S. Guttowsky and B. R. McGarvey, J. Chem. Phys. 20, 1472 (1952).
[4] D. Pines, Phys. Rev. 95, 1090 (1954).
[5] W. D. Knight, Phys. Rev. 90, 861 (1954).

FA2. Calculation of a Spin Resonance Equation. J. I. KAPLAN, *United States Naval Research Laboratory.*—A method is given for calculating the spin resonance equations under the following conditions: (1) the rf field may have any magnitude relative to the constant magnetic field; (2) the frequency of the rf field is monochromatic; (3) the system is defined by one relaxation time; (4) the rf intensity is assumed constant over the sample but the constant field may be inhomogeneous.

FA3. Theory of Magnetic Resonance Saturation.* E. P. GROSS, *Syracuse University.*—We use equations which are generalizations of the Karplus and Schwinger type to study saturation in magnetic resonance absorption. Spin-spin interactions are in the Liouville term, while spin lattice interactions are represented by the stochastic term. For gases, the magnetization satisfies equations differing from those of Bloch in the transverse components tend to relax to the instantaneous value of applied field. When spin-spin interactions are important, a solution is obtained for line width small compared to the Larmor frequency. The solution agrees with Redfield's[1] postulate that the density matrix is canonical in the rotating coordinate system for circularly polarized rf fields. The defects of Bloch's equations are traced to using perturbation theory in analyzing the statistical behavior of a system in weak interaction with a reservoir. We develop a generalization of the Weisskopf-Wigner approach and find generalizations of the equations used in the foregoing. The restriction to processes near equilibrium made in irreversible thermodynamics is artificial. We require that the line width due to reservoir interaction be small compared to the separation of combining

system levels; the spin system can deviate arbitrarily from equilibrium.

* Supported by Office of Scientific Research, U. S. Air Force.
[1] A. G. Redfield, Bull. Am. Phys. Soc. **30**, No. 1, 43 (1955), abstract R4.

FA4. Indirect Exchange Coupling of Nuclear Moments by Electrons in Semiconductors and Insulators. P. W. ANDERSON, *Bell Telephone Laboratories.*—The indirect exchange mechanism for nuclear moments proposed by Ramsey[1] for molecules and Kittel and Ruderman[2] for metals has been worked out for simple models of semiconductors and insulators. The mechanism nvolves the virtual excitation of triplet states by the hyperfine interaction. The result is rather similar to, but in some ways more general than, that of Bloembergen.[3] It appears from our results that even for the case of metals considered by Ruderman and Kittel, as well as for the present case in particular, the electronic states of interest have rather large energies relative to the Fermi level. This has two interesting physical consequences: (a) Coulomb interaction effects such as exciton formation are not important. (b) The accuracy of all such calculations is severely limited by the fact that effective mass approximation as well as constancy of the hyperfine interaction constants cannot be expected to hold well over such large energy ranges. Within the rather wide margin for error allowed by (b), comparison with the experimental results of Shulman, Mays, and McCall[4] for InSb and GaSb is satisfactory.

[1] N. F. Ramsey, Phys. Rev. **91**, 303 (1953).
[2] M. A. Ruderman and C. Kittel, Phys. Rev. **96**, 99 (1953).
[3] N. Bloembergen, Bull. Am. Phys. Soc. **30**, 44 (1955) (to be published).
[4] Shulman, Mays, and McCall, Bull. Am. Phys. Soc. **30**, 43 (1955), abstracts R2 and R3.

FA5. Quantum Theory of Dielectric Relaxation.* JOEL L. LEBOWITZ AND E. P. GROSS, *Syracuse University.*—Dielectric relaxation in compressed gases has been studied[1] using a classical theory involving impacts of duration that are short compared to the resonant period, the period of the applied field, and time between collisions. The present work deals with the unified treatment of the discrete rotational lines at low pressures, the continuous absorption determined by quantum and inertial effects at intermediate pressures, and the Debye absorption at high pressures. This is accomplished with the impulsive model by using the Wigner distribution function to construct quantum kinetic equations from the classical theory. Our quantum characterization of impulsive collisions is that the diagonal elements of the density matrix in the position representation are unchanged by collisions. Analysis of the resulting absorption justifies using classical theory to estimate inertial effects at higher pressures, and confirms the connection between collision frequency and Debye relaxation time noted earlier.

* Supported by Office of Scientific Research, U. S. Air Force.
[1] E. P. Gross, Phys. Rev. **97**, 395 (1955); Bull. Am. Phys. Soc. **30**, No. 1 (1955), abstract TA14.

FA6. An Application of the Photomultiplier to the Interference Spectroscope.* JOSEPH G. HIRSCHBERG, *University of Wisconsin.*—Following ideas developed especially by P. Jacquinot[1] and in this laboratory, the liquid-air cooled photomultiplier is applied to the study of fine details in complex spectrum lines with the Fabry-Perot interferometer. Sweeping is accomplished alternatively by varying air pressure or by actually varying the spacer distance mechanically. The interferometer is coupled with a 21-foot concave grating in a double-pass modified Wadsworth mounting[2] and the two are swept in synchronism. The system is applied to the spectrum of helium.

* Supported by the Wisconsin Alumni Research Foundation and by the Office of Ordnance Research.
[1] Private communication.
[2] E. Hulthén and E. Lind, Arkiv Fysik **2**, 253 (1950).

FA7. Isotope Shift Nonlinearities in the Spectrum of Cadmium. W. M. CLOUD, *University of Wisconsin.**—Measurements of spectrograms of cadmium, taken with an atomic beam source (constructed under the direction of Dr. Arroe) and a Fabry-Perot interference spectrograph (with dielectric coatings supplied by Professor Jacquinot) yield tentative results for the transition $_{48}$Cd II, σ22640, ($4d^{10}5p^2P_{3/2}^0 - 4d^9 5s^2\,{}^2D_{5/2}$) in fair, but not complete, agreement with other work[1–4] on the same line, as shown in the following table of shifts in mK (where S refers to the strongest component):

Isotope	106	108	111.5	110	113.5	112	114	116
S W[1]				0		54	105	
M[2]	−106	−56	−20	0	35	55	109	147
H K R[3]				0.0		53.3	101.2	135.6
W S[4]	−112.2	−51.2	−15.2	0.0	39.4	53.1	99.9	135.6
This work	−113.2	−52.1	−18.9	0.0	35.2	53.5	98.4	134.0

* Supported by Office of Naval Research and Office of Ordnance Research.
[1] H. Schüler and H. Westmeyer, Z. Physik **82**, 685 (1933).
[2] K. Murakawa, Phys. Rev. **93**, 1232 (1954).
[3] Hindmarsh, Kuhn, and Ramsden, Proc. Phys. Soc. (London) **A67**, 478 (1954).
[4] E. C. Woodward and D. R. Speck, Phys. Rev. **96**, 529(A) (1954); see E. C. Woodward, Phys. Rev. **93**, 948(A) (1954).

FA8. Isotope Shift in the Ionized Spectrum of Carbon.*† C. R. BURNETT, *Pennsylvania State University.*—The isotope shift between C^{13} and C^{12} in the $2s2p^3\,{}^3P - 2p^3\,{}^3D$ transitions of ionized carbon has been resolved using a Fabry-Perot interferometer. Preliminary measurements are 0.94 K for λ2512 $2s2p^3\,{}^3P_{3/2} - 2p^3\,{}^3D_{3/2}$ and 0.89 K for λ2509 $2s2p^3\,{}^3P_{1/2} - 2p^3\,{}^3D_{3/2}$ with the C^{12} component at higher frequency in both cases. The calculated normal mass effect is 0.14 K. The difference in shift for the two lines appears to be real, as is also the case for the $2s2p^3\,{}^3S - 2s^23p^3P$ transitions.[1] Excitation of the enriched sample of C^{13} consisted of a mild condensed discharge in a hollow cathode source cooled with liquid nitrogen. It is to be noted that the above configurations differ in the number of $2s$ electrons and should thus be sensitive to nuclear volume effects. It is planned to continue this study using an enriched sample of C^{14}.

* This study was initially supported at South Dakota State College by Engineering and Science Research funds.
† This project is now supported by a grant from the Research Corporation.
[1] C. R. Burnett, Phys. Rev. **80**, 494 (1950).

FA9. Mesonic X-Rays from Capture of Cosmic Ray Mu Mesons in a Chemical Compound. A. FAFARMAN AND M. H. SHAMOS, *New York University.*—Measurements of the x-rays emitted by mesonic carbon and oxygen atoms have been made, using a different experimental arrangement than that reported for Pb. A tank (~4 liters) of liquid scintillator, dioxane, $C_4O_2H_8$, (plus 10 g/l of p-terphenyl) served as the absorber and as the detector for the stopping of cosmic ray mu mesons. The mesons were identified by the method of delayed coincidences ($\mu-\beta$ event). The mesonic x-rays from the dioxane were detected by a coincidence scintillation spectrometer (γ pulse), which included a 4 in. diam × ½ in. thick NaI crystal together with a 5 in. diam 6364 photomultiplier. Those γ pulses in coincidence with the μ of $\mu-\beta$ events ($\mu\gamma-\beta$ events) were lengthened and their pulse height recorded on a recording milliammeter. The time distribution of the delayed coincidences ($\mu\gamma-\beta$ events) was recorded by a 4-channel delay discriminator over the delay interval 0.5 to 8.0 μsec. It was possible to study the mesonic x-rays with essentially no background, and with no contribution from nuclear absorption gamma radiation nor from (decay beta particle) bremsstrahlung. The measured $2p-1s$ transition energies of 82 kev and 145 kev for carbon and oxygen respectively agree with the simple Bohr orbit calculations. The observed ratio of captures by oxygen and carbon (0.33 ± 0.04) does not agree with the Z dependence predicted by Fermi and Teller for mesonic atom formation by this chemical compound (0.67), nor with the simple stopping power calculation (0.50).

FA10. Dispersion Electrons and Refractive Index in the Soft X-Ray Region.* D. E. Bedo and D. H. Tomboulian, *Cornell University.*—Recent investigations indicate that the continuous soft x-ray spectrum emitted by electrons accelerated in a synchrotron[1] may serve as a source of known spectral distribution. In conjunction with expressions[2] for the reflecting power of a glass grating, the spectrum of such a source was utilized to evaluate the refractive index of the grating material. The index is found to increase from 0.915 at 180 A to 0.950 at 380 A. The real decrement of the refractive index has the form $A\lambda^2Q$. If the material of the grating be regarded to possess the SiO_2 structure, and if Q may be assumed to represent the number of dispersion electrons per SiO_2 molecule, then computed values of Q drop from almost 24 at 180 A to 3 at 380 A. This suggests that at the shorter wavelength all L and M shell electrons of the molecule participate in the dispersion process, while at the higher wavelength only the M electrons are effective.

* Supported by the Office of Ordnance Research, U. S. Army.
[1] P. L. Hartman and D. H. Tomboulian, Phys. Rev. **91**, 1577 (1953).
[2] G. C. Sprague (to be published).

FA11. Preliminary Experiments on X-Ray Microscopy by Reconstructed Wave Fronts.* Hussein M. A. El-Sum and Albert V. Baez, *University of Redlands.*—The point-focus x-ray tube at the University of Redlands has been used for making shadow projection microradiographs of biological and metallurgical objects. Depending on the geometrical arrangement of source, object, and film, the shadow may lose its sharpness and exhibit a diffraction pattern of the object. Using continuous radiation from Al, Ag, and Au targets, holograms of simple objects like single wire, fine grid and sharp edge were made, showing up to three fringes. The appearance of the diffraction fringes in these holograms differs from those using visible radiation, due to the absorption of the x-rays by the diffracting object. Any possible discrepancy between our results and our formula connecting source size, number of registered fringes, film resolution, wavelength, and geometrical parameters can be attributed to the fact that nonmonochromatic x-radiation was used. The reconstruction of such x-ray holograms using visible radiation will be discussed.

* Supported in part by grants-in-aid from the Research Corporation, the Office of Naval Research and the American Cancer Society upon recommendation of the Committee on growth of the National Research Council.

FA12. Atmospheric Attenuation of Solar Millimeter Wave Radiation. H. H. Theissing and P. J. Caplan.—The instrumentation consisted of a 60 in. searchlight parabola, $f=25.5$ in., in the focus of which was a thermal detector with a sensitive area about 8 mm in diameter, which approximately equals the geometric image of the sun. A set of black filters suppressed the powerful visible and near infrared solar intensity. A filter method was chosen to determine the intensity distribution of the millimeter spectrum. These spectral measurements, which will be described in a separate publication, showed a peak at about 1 mm. For this spectrum the atmospheric attenuation α (per km per percent H_2O vapor) was measured by observing the solar signal during greatly varying humidity conditions At the same time, the percentage water concentration (c) from ground level up to 20 000 feet was known from balloon data, which made it possible to treat the upright path as if it were a horizontal path. If $\bar{c}$ is the average water vapor concentration in the sun's total atmospheric path d—varying with various elevation angles—the observed signal S will be proportional to $\exp(-\alpha\bar{c}d)$. Plotting, therefore, $\log S$ *vs* $\bar{c}d$ actually furnishes a plot of $-\alpha\bar{c}d$ *vs* $\bar{c}d$, which should be a straight line with the slope $-\alpha$. The experimental value of α obtained in this way was compared with atmospheric attenuation data computed by T. F. Rogers.*

* Atmospheric millimeter absorption data computed and presented at the Navy Millimeter Wave Conference in Washington, 1953, by T. F. Rogers, Air Force Cambridge Research Center (unpublished).

FA13. A Comparison of Observed Drop-Size Distributions in Clouds and Rain with Proposed Analytical Expressions.* Shepard Bartnoff, *Tufts College.*—The two functions, $y(x)=(m\ln 2)x^{m-1}\exp(-x^m\ln 2)$ derived from Best's[1] formula and $y_a(x)=AX^{(a/b)-1}(2-x^{1/b})^b$ developed by Atlas and Bartnoff,[2] are compared and are found to be nearly identical with respect to distribution parameters obtained from natural clouds and rain. The moments μ_2, μ_3, and μ_4 computed from individual distributions are found to be highly correlated with similar moments obtained from the family of curves described by Best's function, indicating that natural distributions in clouds and rain can be satisfactorily represented analytically.

* This work is supported by a contract with the Air Force Cambridge Research Center.
[1] A. C. Best, Quart. J. Roy. Meteorol. Soc. **76**, 16–36 (January, 1950).
[2] D. Atlas and S. Bartnoff, J. Meteorol. **10**, 143–148 (1953).

Thursday Afternoon at 2:00

NBS, East Building

(J. Bardeen presiding)

Semiconductors, I

G1. Ionization and Solubility of Impurities in Semiconductors.* C. S. Fuller and Howard Reiss, *Bell Telephone Laboratories.*—Impure semiconductors like Ge and Si behave like dilute aqueous solutions in that, in both instances, the equilibrium solubilities of ionic impurities in them depends on the ionization of the media as well as upon the ionization of other solutes present.[1] Using simple mass action law arguments, relations have been developed[2] for the specific case of the equilibrium solubility of the donor Li in silicon as a function of known dopings of the acceptor boron at different temperatures. These relations have been tested experimentally by determining the changes in resistivity of a series of specimens of p-type silicon containing up to 5.6×10^{18} boron/cm³. The observed solubilities are found to be in satisfactory agreement with theory thus validating the empirical mobilities as well as the essential correctness of the theory. The maximum in the solubility curve of Li in undoped Si as a function of temperature previously observed[3] can be explained by the increase in intrinsic electron concentration with temperature.

* J. Chem. Phys. (to be published).
[1] H. Reiss, J. Chem. Phys. **21**, 1209 (1953).
[2] H. Reiss and C. S. Fuller, Phys. Rev. **97**, 559 (1955).
[3] C. S. Fuller and J. A. Ditzenberger, Phys. Rev. **91**, 193 (1953).

G2. Electron Capture Probability of the Upper Copper Acceptor Level. J. F. Battey and R. M. Baum, *Sylvania Electric Products.*—Copper has been diffused into originally n-type germanium to such an extent that the upper acceptor levels introduced by the copper atoms are approximately half

populated.[1] It has been shown previously that the upper copper levels in germanium act as recombination traps.[2] Using approximations appropriate to the circumstances, the minority carrier lifetime[3] is expected to be inversely proportional to the electron capture probability of the levels over the temperature range investigated. It is found in contrast to previously reported measurements[4] on samples with unknown recombination level structures that the lifetime decreases exponentially with increasing temperature. A suggested interpretation is that only electrons of energy greater than 0.22 ev above the bottom of the conduction band can enter the upper copper acceptor levels.

[1] J. F. Battey and R. M. Baum, Phys. Rev. **94**, 1393 (1954).
[2] J. A. Burton *et al.*, J. Phys. Chem. **57**, 853 (1953).
[3] W. Shockley and W. T. Read, Jr., Phys. Rev. **87**, 835 (1952).
[4] R. N. Hall, Phys. Rev. **87**, 387 (1952).

G3. Two-Carrier Model of p-type Germanium at 77°K. E. N. Adams, R. E. Davis, and Colman Goldberg, *Westinghouse Research Laboratories.*—The conduction mobility at liquid air temperature was studied for samples of p-type germanium ranging in impurity content from about 10^{13} to 4×10^{14}. Appreciable dependence of the mobility on impurity content was found even for samples of impurity content less than 10^{14}. The field dependence of the Hall constant and magnetoresistance was measured for each sample. An analysis of these data suggest that for samples with impurity concentrations below 10^{14} the dependence of the mobility on impurity content originates in impurity scattering of fast holes. Preliminary interpretation of the data on a two-carrier model indicates that the parameters which give the best fit are somewhat different from those found at higher temperatures.[1]

[1] Herman, Willardson, and Beer, Phys. Rev. **96**, 1512 (1954).

G4. Mobility of Holes in Germanium-Silicon Alloys. A. Levitas, *Sylvania Electric Products.*—Hall and resistivity measurements have been performed on nine samples of p-type germanium-silicon alloys ranging in composition from 100 percent germanium to 100 percent silicon. The measurements were performed in a temperature range extending from 80°K to 390°K. Brooks[1] has predicted that alloy scattering will have a significant effect on the mobilities of the alloys, and the measured mobilities are consistent with this prediction. At reduced temperatures the mobilities depart from a power law in temperature in a manner which suggests the operation of a mechanism which becomes increasingly important as the composition of the alloy is changed from 100 percent of one constituent toward a 50 percent alloy. This mechanism is presumably alloy scattering. The behavior is masked to some extent by impurity scattering, and an attempt will be made to correct for this effect.

[1] H. Brooks (private communication).

G5. Modulation of Schottky Emission from Metal Point Contacts to Germanium. G. Wallis and J. F. Battey, *Sylvania Electric Products.*—A new confirmation has been found for the Schottky emission diode theory of reverse current by Simpson and Armstrong.[1] The surface barrier, ϕ, of germanium diodes (15 to 25 ohm-cm, n-type with pulsed tungsten whiskers) was modulated by the ambient cycle dry oxygen, wet oxygen, ozone.[2] Changes in ϕ on the free surface were monitored by contact potential measurements. Simultaneously measured changes in pulsed reverse diode current, i, were consistent with theory, if it was assumed that ϕ under the whisker changed in the same direction as on the free surface. Theory[1] predicts the observed voltage dependence of the current changes with ambient, $\Delta i/i\cong-A\Delta\phi(1-B/V^{\frac{1}{2}})$, where A and B are positive constants for a given contact, V is the reverse bias, and Δi and $\Delta\phi$ are the changes with ambient in i and ϕ. Such analysis of high voltage diodes shows ϕ to be between 0.60 and 0.65 ev, the field due to the holes at the contact to be about 5×10^5 volts/cm, the field due to V about 10^4V volts/cm.

[1] J. H. Simpson and H. L. Armstrong, J. Appl. Phys. **24**, 25 (1953).
[2] W. H. Brattain and J. Bardeen, Bell System Tech. J. **32**, 1 (1953).

G6. Forward Characteristic of Germanium Point Contact Rectifiers. M. Cutler, *Hughes Aircraft Company.*—A quantitative discussion of the forward characteristic is given for point contact rectifiers. It is based on the combined solution of the emission equations for the barrier[1] and the diffusion equations for the bulk region.[2] It shows that the theoretical value of $d\ln I/dV$ in the exponential region is nearly q/kT, and that the experimental slopes which are a fraction of this value cannot be the result of the spreading voltage. Recombination of injected carriers has little effect except at large currents beyond the exponential region. Relations are derived for the limit of very large currents, which show that gamma approaches a value smaller than $(1+b)^{-1}$, the hole concentration at the contact approaches a maximum value proportional to the equilibrium concentration of holes at the surface, and the spreading voltage becomes a linear function of the current.

[1] M. Cutler, Phys. Rev. **96**, 255 (1954).
[2] J. A. Swanson, J. Appl. Phys. **25**, 314 (1954).

G7. Silicon Conductivity Modulated Diffused $p-n$ Junction Rectifier. M. B. Prince, *Bell Telephone Laboratories.*—Impurity diffused type silicon rectifiers[1] can now be made incorporating the feature of conductivity modulation. These devices, using areas of 0.1 cm², conduct more than 35 amperes at 1 volt in the forward direction. It will be shown that complete conductivity modulation of the device leads to a constant voltage drop independent of the forward current. Thus the effective series resistance of the device is about 0.005 ohm for 0.1 cm² wafers.

[1] G. L. Pearson and C. S. Fuller, Proc. Inst. Radio Engrs. **42**, No. 4 (1954).

G8. Sensitization of Photoconductivity in PbSe. James N. Humphrey, *U. S. Naval Ordnance Laboratory, and University of Maryland.*—The sensitization of PbSe films has been investigated using oxygen, sulfur, selenium, and the halogens as sensitizers. Each sensitizer acts as an acceptor impurity, converting n-type films to p-type, at the condition of maximum resistance. At −195°C each sensitizer produces photoconductivity with minimum time constants of about 15 microseconds. At 25°C measurable sensitivity ($\tau\sim1$ microsecond) results only if oxygen is introduced, alone or with another sensitizer. It is believed that each sensitizer produces surface states giving the resistance maximum and change of carrier sign. At −195°C the observed 15 microsecond time constant is identified with that of recombination centers which are present independent of sensitization. Any sensitizer able to raise the dark resistance will produce photoconductivity with this τ. At 25°C the recombination center time constant is shorter, probably 10^{-6} second or less. This is too short to yield measurable photoconductivity. Oxygen, however, in addition to producing surface states, enters the lattice. The resulting ions represent traps with very short capture times and longer decay times (~1 microsecond at 25°C). These traps compete with the recombination centers, capturing optically excited electrons and delaying recombination. The resulting free holes produce photoconductivity having a $\tau\sim1$ microsecond.

G9. Silicon Analysis for Boron by Thermal Neutrons. E. G. K. Schwarz, *Signal Corps Engineering Laboratories.*—Simultaneous alpha counting under thermal neutron irradiation offers an extremely sensitive method to analyze ultra pure silicon for boron impurities. Alpha-counting rates were calculated in terms of boron concentration and thermal neu-

tron flux for a thin alpha-saturated flat silicon sample. The most suitable technique for this analysis is scintillation counting by means of a silver activated zinc-sulfide screen in connection with a photomultiplier tube. It was estimated that the sensitivity of spectrochemical analysis can be surpassed by more than four orders of ten when the highest available thermal neutron fluxes are utilized. Interferences originating from gamma background radiation and from Li^6 traces which may be present in the neighborhood of the detector are discussed.

G10. Hall Effect and Conductivity of InSb. H. J. Hrostowski, F. J. Morin, T. H. Geballe, and G. H. Wheatley, *Bell Telephone Laboratories.*—High purity InSb has been prepared by zone refining.[1] Single crystal samples with total impurity concentration of 10^{15} cm^{-3} have electron and hole mobilities much higher than previously reported.[2] Hall mobilities at 78°K are 3.7×10^5 cm^2/volt sec for electrons, and approximately 10^4 cm^2/volt sec for holes. Impurity scattering contributes appreciably to the observed electron mobility up to 300°K. Lattice scattering mobilities of both electrons and holes have temperature dependence different from $T^{-\frac{3}{2}}$. With an effective electron mass of 0.015 m the electron lattice scattering mobility is proportional to $T^{-1.7}$. Determination of Hall mobility for positive holes is complicated by the variation of the Hall coefficient with magnetic field[3] in p-type material. Estimation of the ratio of Hall to conductivity mobility indicates nonspherical energy surfaces in the valence band. Low temperature measurements show no ionization of donors. In p-type InSb below 10°K impurity band conduction is observed.[4] Above 10°K acceptors are ionized. The activation energy is $7\pm1\times10^{-3}$ ev. An effective hold mass between 0.1 m and 0.25 m is required to fit the experimental data.

[1] W. G. Pfann, Trans. Am. Inst. Mining Met. Engrs. **194**, 747 (1952).
[2] O. Madelung and H. Weiss, Z. Naturforsch. **9a**, 527 (1954).
[3] Harman, Willardson, and Beer, Phys. Rev. **95**, 699 (1954).
[4] C. S. Hung and J. R. Gliessman, Phys. Rev. **96**, 1226 (1954).

G11. Effects of Hydrostatic Pressure on the Conductivity of InSb. Robert W. Keyes, *Westinghouse Research Laboratories.*—The effect of high hydrostatic pressures on the electrical conductivity of n and p type specimens of InSb has been measured in the temperature range −80° to +270°C. Pressures up to 12 000 kg/cm^2 were employed. The energy gap was found to increase at a rate 1.5×10^{-6} ev/atmos, a value slightly less than that found by Long and Miller.[1] The variation of the carrier mobilities with pressure is obtained from the changes in conductivity in the exhaustion range. The mobility of the electrons decreases with increasing pressure and is approximately inversely proportional to the energy gap. The mobility of the holes is almost independent of pressure. A simple picture of the band shapes which allows these mobility effects to be understood and which is in accord with other data on InSb will be suggested.

[1] D. Long and P. H. Miller, Jr., Bull. Am. Phys. Soc. **30** No. 1, 53 (1955), abstract V8.

Thursday Afternoon at 2:00

Exhibit Hall II

(R. Pepinsky presiding)

Ferroelectricity and Ferromagnetism

GA1. Guanidine Aluminum Sulfate Hexahydrate—A New Ferroelectric Material. A. N. Holden, B. T. Matthias, W. J. Merz, and J. P. Remeika, *Bell Telephone Laboratories.*—Guanidine aluminum sulfate hexahydrate[1] is ferroelectric over a large range of temperatures including room temperature. It is the parent of a family of materials in which the aluminum cation and the sulfate anion can be replaced by the anions and trivalent cations which form alums, for example Ga^{3+}, Cr^{3+}, and $SeO_4^{=}$. Replacement of guanidine has so far proved impossible. The material is trigonal, with perfect cleavage in the basal plane; the trigonal axis is the ferroelectric direction. The space group is $C_3{}^1(2)$—$P31m$, and the unit cell contains three molecules. It can be readily grown from water solution by standard techniques.[2]

[1] Ferraboschi, Cambridge Phil. Soc. **14**, V, 473 (1908).
[2] Holden, Discussion Faraday Soc. No. 5, 312 (1949).

GA2. Electrical Properties of Guanidine Aluminum Sulfate Hexahydrate (G.A.S.H.) and Some Isomorphs. W. J. Merz, J. P. Remeika, A. N. Holden, and B. T. Matthias, *Bell Telephone Laboratories.*—At room temperature very symmetrical and square hysteresis loops can be obtained with G.A.S.H. The spontaneous polarization is about $P_s=0.35$ microcoulomb/cm^2. G.A.S.H. is thus a weak ferroelectric crystal similar to rochelle salt and in contrast to $BaTiO_3$. The coercive field strength is strongly frequency dependent; 60 cycles per sec $E_c\cong1500$ volts per cm. The small signal dielectric constant is only about 15 along the ferroelectric axis and about 5 perpendicular to it. Very little change in the dielectric constant is observed when the crystal is heated. Above 100°C, where the crystal starts to lose water of crystallization, no reproducible results can be obtained, and hence no determination of the Curie point could be made. The polarization P_s decreases linearly with increasing temperature suggesting a Curie temperature of about 200°C–300°C. The coercive field E_c increases rapidly at low temperatures. The ferroelectric properties of the isomorphs are very similar to those of G.A.S.H. If crystals are subjected to square electrical pulses the switching time t_s becomes shorter the higher the applied field, as in the case of $BaTiO_3$,[1] though the switching time of G.A.S.H. is longer.

[1] W. J. Merz, Phys. Rev. **95**, 690 (1954).

GA3. Oxygen Parameters of the $FeFe_{(2-x)}Cr_xO_4$ Spinel System.* H. J. Yearian and W. D. Derbyshire, *Purdue University.*—Oxygen parameter measurements of powdered samples of spinels of the $FeFe_{(2-x)}Cr_xO_4$, $0\leq x\leq2$, system have been made at room temperature by x-ray diffraction intensity methods. The value of the parameter, which measures the space available to the cation in a tetrahedral position, was found to vary monotonically from 0.378 ± 0.002 at $x=0$

to 0.387 ± 0.002 at $x=2$. The samples were prepared according to the process described by Yearian, Kortright and Langenheim.[1] They interpreted the lattice parameter measurements of these spinels as indicating that: from $x=0$ to $x=0.3$ the structure is completely inverse; from $x=1.28$ to $x=2.0$ it is completely normal; between these two regions is a region in which the structure undergoes a transition between these two types. The results of this investigation support this interpretation. In the region from $x=1.28$ to $x=2.0$ the oxygen parameter is essentially constant and in the region from $x=0.3$ to $x=1.38$ it increases in an approximately linear manner. The accuracy of the results is not sufficient to indicate if the oxygen parameter is essentially constant in the region from $x=0$ to $x=0.3$.

* Supported, in part, by the Office of Naval Research.
[1] Yearian, Kortright, and Langenheim, J. Chem. Phys. **22**, 1196 (1954).

GA4. Ionic Equilibrium in a Series of Magnesium-Manganese Ferrites.* C. J. KRIESSMAN AND S. E. HARRISON, *Remington Rand Inc.*—Samples of $Mg_yMn_{1-y}Fe_2O_4$ with values of $y=0$, 0.10, 0.25, 0.50, 0.75, 0.90, 1.0 have been sintered at 1500, 1400, and 1300°C and quenched from various temperatures in both air and water. Saturation magnetization and x-ray measurements have been made to determine the fraction x of Mg^{++} ions on A sites. For samples sintered at 1400°C the saturation magnetization, μ_0, decreases from 5.0 to 2.6 Bohr magnetons as y increases from 0 to 0.75; as y increases to 1.0, μ_0 increases to 3.2. $Mg_{0.9}Mn_{0.1}Fe_2O_4$ has been sintered at various high temperatures up to 1500°C and quenched from temperatures between 1500°C and 400°C; saturation magnetization values and the resulting ionic distributions have been determined. These data fit a Boltzmann type distribution in which the activation energy is dependent on x: $\theta=\theta_0-\theta_1 x$. This behavior is analogous to the previously reported data on $MgFe_2O_4$.[1] The effects of sintering temperature, rapidity of quench, and chemical decomposition on the magnetic moments of this system will be discussed.

* Supported in part by the Office of Naval Research.
[1] Kriessman, Harrison, and Callen, Bull. Am. Phys. Soc. **30**, No. 2, 39 (X4) (1955).

GA5. Effect of Aluminum on the Saturation Magnetic Moments of Iron-Cobalt Alloys. B. R. COLES* AND W. R. BITLER, *Carnegie Institute of Technology* (introduced by J. E. Goldman).—It is well known that the saturation moment of iron (expressed in Bohr magnetons per iron atom) is almost unchanged by the addition of small amounts of such elements as zinc, aluminum, and silicon. This behavior is in marked contrast to that of nickel and it has been suggested that 3*d*-band holes of both spin directions exist in pure iron. It has further been suggested[1] that such a picture of iron leads to a reasonable interpretation of the flat maximum in the saturation moment against composition curve for iron-cobalt alloys. The saturation moments of various iron-cobalt alloys with additions of 5 percent and 10 percent of aluminum have been measured, and the preliminary results seem to bear out the above suggestions. Small aluminum additions decrease markedly the saturation moments of alloys on the cobalt-rich side of the iron-cobalt saturation moment maximum, but the saturation moment per transition metal atom of the iron-rich alloys is little affected by initial aluminum additions.

* On leave of absence from Imperial College, London, England.
[1] B. R. Coles and W. Hume-Rothery, Advances in Phys. **3**, 149 (1954).

GA6. Ferromagnetic Structure of Uranium Hydride. M. K. WILKINSON, C. G. SHULL, AND R. E. RUNDLE,* *Oak Ridge National Laboratory.*—Neutron diffraction patterns have been obtained for polycrystalline samples of UD_3 and UH_3 at various temperatures from 20°K up to room temperature in an investigation of the ferromagnetic structure which develops below 175°K. Coherent ferromagnetic scattering is found in several reflections at low temperatures and these disappear at temperatures in the vicinity of the reported Curie temperature. From these ferromagnetic reflections it is established that the lattice ordering is of simple ferromagnetic type with all atomic moments possessing closely the same moment value and oriented in the same direction. Paramagnetic diffuse scattering is seen at the higher temperatures and this taken with the ferromagnetic scattering suggests a magnetic form factor for the uranium ion which has strong orbital moment characteristics. Comparisons will be drawn between the observed form factor and those calculated for various electronic configurations of the uranium ion.

* At Ames Laboratory, Iowa State College.

GA7. Ferromagnetism of Iron. JOSEPH CALLAWAY, *University of Miami.*—A previous calculation of energy bands in unmagnetized iron[1] has been extended by the inclusion of magnetic effects. The change in exchange energy when one 3*d* electron per atom reverses its spin has been calculated from the Hartree Fock equations using a 3*d* wave function calculated for one of the unmagnetized crystal states. This energy is between -1.58 and -1.23 ev. The 3*d*–4*s* exchange tends to magnetize the 4*s* electrons, and about 0.1 4*s* electron per atom will participate in the magnetization. The magnetization tends to split the *d* bands into halves occupied by the different spins; corresponding levels are split by between 2.5 and 3.2 ev. The magnetization of a few 4*s* electrons is important in computing the increase in kinetic energy which opposes magnetization; this increase is computed from the density of states curve to be about 1.13 ev. The residual ferromagnetic tendency at absolute zero is thus between 0.10 and 0.45 ev per atom. Correlation effects are estimated to be small.

[1] J. Callaway, Bull. Am. Phys. Soc. **30**, No. 1, C1 (1955).

GA8. Calculation of the Discontinuity in the Specific Heat of Gadolinium.* HARRY A. BROWN, *Oberlin College.*—Using the cluster approach of Bethe-Peierls-Weiss[1] and adding the approximation that the spins can be considered to be classical vectors (gadolinium has a spin of 7/2) it is possible to calculate the discontinuity which occurs in the specific heat curve as it passes through the Curie temperature. The value predicted is 5.5 cal/M. The measured value[2] is 7.0 cal/M which is satisfactory in view of the limitations of the cluster approach. The theory also predicts a $1/T^2$ decrease above the Curie temperature which is verified by the experimental data.

* This research has been assisted by the Wisconsin Alumni Research Foundation.
[1] P. R. Weiss, Phys. Rev. **74**, 1493 (1948).
[2] Griffel, Skochdopole, and Spedding, Phys. Rev. **93**, 657 (1954).

Invited Paper

GA9. Spin-Wave Resonance in Ferromagnetic Metals. G. T. RADO, *U. S. Naval Research Laboratory.* (30 min.)

THURSDAY AFTERNOON AT 2:00

(S. DE BENEDETTI presiding)

Continental Room

Invited Papers

H1. Yields of Mesonic *K* and *L* Series X-Rays. J. B. PLATT, *University of Rochester.* (30 min.)

H2. Intensities and Energy Shifts of Transitions in Pi-Mesonic Atoms. M. B. STEARNS, *Carnegie Institute of Technology.* (30 min.)

H3. Electric Quadrupole Transitions in Nuclei. A. W. SUNYAR, *Brookhaven National Laboratory.* (30 min.)

H4. Low-Energy Physics from a High-Energy Standpoint. L. I. SCHIFF, *Stanford University.* (30 min.)

THURSDAY AFTERNOON AT 2:00

Caribar Room

(E. P. WIGNER presiding)

Theoretical Physics II, Mainly Scattering Theory

HA1. (Abstract withdrawn.)

HA2. Variational Treatment of Elastic Scattering of Electrons from Hydrogen.* M. C. NEWSTEIN,† *M.I.T.* (introduced by P. M. Morse).—Stationary expressions are derived for the direct and exchange scattering amplitudes.[1] Calculations are made of the direct amplitudes corresponding to scattering from a static, as well as from the actual, potential. Comparison of these two results shows that for 1.2 volts the major effect of polarization is to greatly decrease the direct cross section, while for 3.4 and 9.5 volts the major effect is a reduction in the forward and backward values of the direct amplitude. Calculations made of the complete cross sections including exchange give results in good agreement with those of Morse and Allis[2] for 3.4 and 9.5 volts. A cross-section theorem used by Boyet and Borowitz[3] is found to be not applicable to the determination of total cross sections when Born fields are used with the stationary expressions.

* Supported by the Office of Naval Research.
† Now at the Harvard College Observatory.
[1] The expression for direct scattering is the same as the one given by Borowitz and Friedman, Phys. Rev. **80**, 441 (1953).
[2] Allis and Morse, Phys. Rev. **44**, 269 (1933).
[3] Boyet and Borowitz, Phys. Rev. **93**, 1225 (1954).

HA3. Many Body Effects in Nuclear Scattering of Electrons. R. R. LEWIS, JR.,* *University of Michigan.*—Most present calculations of the nuclear scattering of electrons neglect transitions out of the ground state, in which case the scattering depends only on the ground-state charge distribution. In principle the scattering will actually depend as well on the pair distribution function, etc. The existence of these terms in second-order perturbation theory has been investigated,[1] and calculations have been made for light nuclei. The calculation involves a twofold assumption: that only plural scattering is important, and that the proton velocities are small compared to the electron velocity. These assumptions pertain to light nuclei, at not too high electron energies (<300 Mev). In the calculations a phenomenological pair distribution function is assumed for simplicity. Correction terms depending on the proton velocity are estimated as well. The dependence on the pair distribution function in the model independent region will also be discussed.

* Now at University of Notre Dame.
[1] Similar calculations have been discussed by L. I. Schiff, Bull. Am. Phys. Soc. **29**, No. 8, Q8 (1954).

HA4. Proton Bremsstrahlung. KERSON HUANG AND S. D. DRELL, *M.I.T.*—The differential cross section for proton bremsstrahlung is calculated for low-energy x-rays emitted by $E=2$ Mev protons which scatter in the field of tin nuclei ($Z=50$). This is essentially a classical problem of the dipole radiation from a proton moving in a Coulomb field since the proton's deBroglie wavelength is much shorter than the distance of closest approach to the nucleus. However, the classical orbit calculation for x-rays emitted at 90° to the proton beam in a 3 kev energy interval about $\hbar\omega=150$ kev predicts a differential cross section, $\sigma_c(90°)=2.1\times10^{-31}$ cm², in disagreement with the experimental result of H. Mark,[1] $\sigma_{exp}(90°)=1.3\pm0.5\times10^{-31}$ cm². Since corrections due to shielding by the orbital electrons and due to higher multipoles are negligible, this discrepancy must be due to quantum corrections resulting from the energy loss to radiation. We have expanded the exact quantum-mechanical matrix element for dipole bremsstrahlung, as derived by Sommerfeld, in a power series in $\hbar\omega/E$. Keeping the zero- and first-order terms, we have carried out the necessary integrations and have obtained a correction which lowers the calculated cross section by 25 percent in agreement with experiment.

H. Mark, Bull. Am. Phys. Soc. **29**, No. 8, Berkeley Meeting, 1954.

HA5. Quantum Calculation of Coulomb Excitation. L. C. BIEDENHARN, *The Rice Institute.*—The usual treatment of Coulomb excitation employs a semiclassical approximation, and the validity of this approach has been the subject of recent investigations.[1] The quantum treatment[2] of the excitation, and the directional correlation parameters, reduces ultimately to consideration of radial Coulomb matrix elements for arbitrary angular momenta. These integrals define in general functions of the Appell type. (The electric dipole radial matrix elements are found to be the exception.) The relevant properties of these matrix elements, recursion formulas, series, and asymptotic expansions will be given; comparison will be made to approximate evaluations. The more amenable special cases of *1.* no energy loss, and *2.* the approach to the classical limit will be discussed in detail.

[1] G. Breit and P. B. Daitch, Phys. Rev. **96**, 1447 (1954); P. B. Daitch *et al.*, Phys. Rev. **96**, 1449 (1954); L. C. Biedenharn and C. M. Class, submitted to Phys. Rev.
[2] L. C. Biedenharn and M. E. Rose, Oak Ridge Natl. Lab. 1789, Sept. 1954.

HA6. Multiple Coulomb Scattering Including Nuclear Size Effects.* WILLIAM T. SCOTT, *Smith College.*—An alternative method to that of Cooper and Rainwater[1] has been developed for calculating the multiple Coulomb scattering in thick layers of fast-charged particles sufficiently energetic to show a noticeable influence of the finite size of nuclei. The usual Molière theory is modified by the inclusion of a suitable nuclear form factor, expressed as a single or double Fourier transform integral. The correction term to the Molière exponent can be written as the form factor integral with the Fourier kernel replaced by a modified expression involving only elementary functions, thus readily allowing the inclusion of various form factors. For the Born approximation, the integral on evaluation reduces to terms of Molière type plus terms whose exponentials can be fitted to within 1 percent by a sum of Gaussians. The final calculation amounts to a re-use of Molière's tables with different coefficients and normalizations. These results, and calculations with Cooper and Rainwater's form factor, will be presented and compared with other calculations and available experimental results on μ-meson scattering.

* Work performed while the author was a visitor at Brookhaven National Lab. and at the Nat. Bur. Standards. Research being continued under a grant from the Nat. Sci. Foundation.
[1] L. N. Cooper and J. Rainwater, Phys. Rev. **97**, 492 (1955).

HA7. Proton-Proton Scattering at High Energies. ROBERT SERBER, *Columbia University,* AND WILLIAM RARITA, *Brooklyn College.*—The elastic proton-proton scattering distribution at 1 Bev as measured at the Brookhaven Cosmotron by Smith, McReynolds, and Snow agrees remarkably well within experimental error with a simple model. We assume that each proton acts as a classical black sphere of radius R for the wave of the other. Thus the total cross section is $2\pi R^2$, and the angular distribution is proportional to $J_1^2(kR\sin\theta)/\sin^2\theta$. Using the total cross section measured by Chen, Leavitt, and Shapiro, we determine R. As k is known from the energy, the shape of the distribution is now uniquely established. A by-product of the calculation is the total elastic cross section which is estimated to be 20.7 mb.

HA8. Elastic Scattering of 17 Mev Protons by Nuclei.* W. ARON, J. S. MCINTOSH, AND G. SCHRANK, *Princeton University,* AND J. H. BIGELOW, *Institute for Advanced Study.*—A five-parameter optical model based upon a complex well with a phenomenological spin-orbit term is employed to analyze the elastic scattering data for 17 Mev protons on various nuclei obtained by Schrank[1,3] and Dayton.[1,3] The nuclear potential chosen consists of a complex square well with its edge adjusted to join smoothly at bottom and zero by a third degree polynomial. The nuclear spin-orbit term is of the Thomas type, with adjustable real magnitude. The charge density is taken to be proportional to the well depth, and the corresponding Coulomb potential calculated. From this potential, wave functions are calculated, phase shifts determined, and cross sections obtained. These calculations are performed on the electronic computer at the Institute for Advanced Study.

* Work supported by the Atomic Energy Commission and the Higgins Fund.
[1] I. Dayton and G. Schrank, Phys. Rev. (to be published).
[3] G. Schrank, Bull. Am. Phys. Soc. (this issue).
[3] I. Dayton, Phys. Rev. **95**, 754 (1954).

HA9. Nucleon Scattering by Nuclei at High Energies. I. I. SHAPIRO, *Lincoln Laboratory,* AND R. J. GLAUBER, *Harvard University.*—The accuracy of the optical approximation for both neutron and proton scattering has been tested by comparing with exact phase-shift calculations. The potential employed was a complex square well combined with the coulomb potential of a uniformly charged sphere. Parameters were chosen appropriate to carbon at 96 Mev. For proton scattering the results show excellent agreement. The Coulomb interference region is reproduced quite accurately, and the comparison extends satisfactorily to substantially larger angles. For neutrons better agreement is found than has been reported,[1] probably due to a different approximation in the correspondence of parameters. Comparison of the neutron and proton results shows considerable Coulomb interference for angles smaller than 20° and negligible effects beyond 25°. Calculations of Coulomb interference effects in the proton polarizations resulting from spin-orbit potentials will also be discussed.

[1] S. Pasternack and H. Snyder, Phys. Rev. **80**, 921 (1950).

HA10. Theory of Nucleon Transfer.* G. BREIT, *Yale University.*—In the calculation of nuclear cross sections, it is helpful to obtain the adiabatic approximation wave function for a particle which is shared by two nuclei. Applications of the Rayleigh-Schrödinger perturbation method can be awkward on account of the entrance of wave functions for the continuum which do not have the barrier penetration properties characteristic of the actual function. A method employing Green's function for the wave equation in the absence of localized nuclear potentials has been worked out leading to expansions free of the difficulty mentioned. The eigenvalue problem contains depths of localized potentials as parameters. There is a restriction in the method regarding absence of overlap of the potentials. A correction for the change in energy is included. The method is intended for cross-section calculation in heavy-particle bombardment reactions.

* Supported by the Office of Ordnance Research, U. S. Army.

HA11. Inelastic Scattering of Nucleons by a Dynamic Nuclear Wall. DAVID M. CHASE, *Los Alamos Scientific Laboratory.*—The coupling between collective- and individual-particle motions envisaged in the collective model provides in nuclear scattering a mechanism for energy exchange between incident nucleon and target nucleus. For target nuclei near closed shells this nucleon-nuclear wall interaction would excite principally the fairly pure vibrational levels expected for such nuclei; for target nuclei far from closed shells and strongly deformed, the interaction would excite principally rotational levels. A one-dimensional model has been used to study numerically the features of such interaction, estimate the magnitude of the resulting cross sections, and compare two different methods of calculation. One method is that formulated by Bohr and Mottelson.[1] The other is based on the use of adiabatic nucleonic wave functions for the scattering process and seems especially appropriate when the coupling is strong and the collective levels of the target closely spaced. It is proposed subsequently to apply this method to the calculation of cross sections for rotational excitation. The results in one

dimension indicate average cross sections for neutrons of the order of several percent of geometric at moderate energies.

[1] A. Bohr and B. Mottelson, Kgl. Danske Videnskab. Selskab, Mat.-fys. Medd. 27, No. 16 (1953).

HA12. Deuteron Cross Sections at High Energies. R. J. GLAUBER, *Harvard University.*—Recent experiments indicate lack of additivity of the neutron and proton cross sections in deuterium at energies as high as 1.4 Bev. For example, direct measurement of the n–p total cross section there gives[1] $\sigma(n,p)$ $=43$ mb. while, with incident protons, deuterium-hydrogen subtraction yields[2] $\sigma(p,d-p)=33$ mb. To consider these effects, a generalization of the optical model has been constructed for the treatment of collisions with two-body systems in the high-energy limit. We assume that the incident particle wavelength is smaller than the ranges of interaction, and that the ranges at these energies are smaller than the deuteron. It may then be shown generally that the deuteron total cross section is $\sigma_d=\sigma_n+\sigma_p+4\pi\lambda^2\,\mathrm{Re}[f_n(0)f_p(0)]\langle r^{-2}\rangle_D$ where σ_n and σ_p are the free neutron and proton cross sections, $f_n(0)$ and $f_p(0)$ are the elastic forward scattering amplitudes, and r is the neutron-proton separation, whose inverse square is averaged in the deuteron. In particular, for purely absorptive interactions the forward amplitudes are imaginary and $\sigma_d=\sigma_n+\sigma_p$ $-(4\pi)^{-1}\sigma_n\sigma_p\langle r^{-2}\rangle_D$, a result easily interpreted in terms of an eclipsing effect. Estimates of the interference term for incident protons are 9 and 17 mb. for deuterons with square-well and Hulthén potentials, respectively.

[1] Coor, Hill, Hornyak, Smith, and Snow. Phys. Rev. (to be published).
[2] Chen, Leavitt, and Shapiro (private communication). See also Phys. Rev. 95, 663 (1954).

HA13. Scattering and Potential. JOHN A. WHEELER, *Princeton University.*—For spherically symmetrical potentials satisfying a certain boundedness condition, it is known that the potential is uniquely determined by the phase shifts (1) for all l's and all energies, provided the data are mutually consistent; or (2) for one l and all energies, provided that for this l value either (a) there exist no bound states or (b) one knows for each bound state its energy and a certain number defined by Jost and Kohn characteristic of that state. It is shown that these quantum results and the characteristic numbers of Jost and Kohn possess a simple interpretation in the JWKB semi-classical analysis of the connection between phase shift and potential. This same analysis leads to a third conclusion, that the potential is uniquely determined by the phase shifts for a single energy and all l.

HA14. Scattering Approximations Using Plane Wave Trial Functions. J. MAYO GREENBERG, *Rensselaer Polytechnic Institute.*—Several approximations to the total amplitude of scattering by a potential involve integrations similar to those required for evaluating the second Born approximation. This is certainly obvious in the Schwinger variational principle. It is also true for another variational principle[1] in case the trial functions are restricted to those of the plane-wave type. It can then be shown that the imaginary part of the scattering amplitude, which is an integral of a product of scattering amplitudes, can be put in a form which is the imaginary part of the second Born approximation. The required integration is apparently only possible with plane wave trial functions and has already been performed independently by numerous authors for the Yukawa potential (or for linear combinations thereof). It can also be done approximately, under suitable conditions, for the square well and, in fact, exactly for zero-angle scattering. Calculations are now in progress which will aid in the choice of the most successful approximation which for analytical simplicity requires plane-wave trial functions.

[1] J. M. Greenberg, Bull. Am. Phys. Soc. 30, No. 1, 50 (TA1).

HA15. Scattering Analysis. WILLIAM RARITA, *Brooklyn College and Case Institute of Technology.*—The elastic-scattering cross section usually expressed in terms of the phase shifts δ_l becomes complicated when there is interference among the phases. However, if the real parts of the phase amplitudes i.e. of the $1-\exp 2i\delta_l$ are employed as variables the scattering distribution is then simple and, in fact, merely algebraic in nature. The great advantage of such a representation is in the ease of following the analytic behavior of the solutions, say, as a function of the energy. In the case of π^+-P at low energies we can solve for each $\cos 2\delta_l$ in terms of measurable quantities. If there is absorption we have to introduce the imaginary parts of the phase amplitudes as extra variables. Results for the π^+-P and $P-P$ scattering will be discussed.

FRIDAY MORNING AT 9:30

Lisner Auditorium

(H. A. BETHE presiding)

Symposium in Memory of Enrico Fermi

J1. The Fermi Statistics and Its Applications. F. SEITZ, *University of Illinois.* (25 min.)
J2. Beta Decay. E. KONOPINSKI, *University of Indiana.* (25 min.)
J3. Neutron Physics. EMILIO SEGRÈ, *University of California, Berkeley.* (30 min.)
J4. Atomic Energy. W. H. ZINN, *Argonne National Laboratory.* (30 min.)
J5. Mesons. H. L. ANDERSON, *University of Chicago.* (30 min.)

FRIDAY MORNING AT 9:30

Bergundy Room

(E. L. HUDSPETH presiding)

Transmutation and Nuclear Energy Levels, I

K1. A Study of the Reactions $H^3(d,n)\alpha$ and $He^3(d,p)\alpha$.* JOHN L. JOHNSON AND WILLIAM S. PORTER, *Yale University.*—The total cross sections for the reactions $H^3(d,n)\alpha$ and $He^3(d,p)\alpha$ have been fitted with the Breit-Wigner one level formula using S-wave deuterons, assuming that only one total angular momentum state is effective. A fit to the differential

scattering cross section for deuterons on He^3 consistent with the reaction fits has been obtained using a one-body model with the Coulomb field cut off by a square nuclear well. Satisfactory fits to the reaction data were found using several types of energy dependence[1] of the Γ suggested by different models of the resonance. The effect of varying the nuclear radius has been investigated. Comparison of widths reduced in the above manner is consistent with charge symmetry of the nuclear forces within the accuracy of the calculations.

* This research was supported by the Office of Ordnance Research, U. S. Army.

[1] G. Breit, Phys. Rev. **58**, 506 (1940); **69**, 472 (1946), E. P. Wigner, Phys. Rev. **70**, 15 (1946); **70**, 606 (1946).

K2. Energy Levels of the Isobars Li^6-He^6. K. W. ALLEN, E. ALMQVIST,* AND C. B. BIGHAM,* *University of Liverpool, England.*—The reactions $Li^7(He^3,\alpha)Li^6$ and $Li^7(t,\alpha)He^6$ have been studied. Excitation energies in Mev of the levels observed in Li^6 with their widths given in brackets are: 2.19 (<0.1), 3.56±0.06 (<0.1), 4.3±0.02 (?), 5.35±0.07 (<0.1), 6.63 ±0.08 (<0.2), and 7.40±0.10 (0.6). Less certainly identified are levels at 5.6±0.2 (2.0), 8.37±0.08 (<0.2), and 9.3±0.2 (0.6). Recoil Li^6 ions of energy corresponding to the 3.56 Mev level were observed, showing that it does not emit heavy particles and is the γ-emitting state identified by Day and Walker.[1] The levels at 2.19 and 4.3 Mev are also observed in the scattering of deuterons by helium[2] and hence have isotopic spin T=0. In He^6, levels at 1.71 (<0.1) and possibly 3.4 (<0.3) were observed. These appear to be analogs of the levels in Li^6 at 5.35 and 6.63 Mev. The sharp 5.35 level in Li^6, therefore, probably has T=1 and properties 2^+, and is not the 1^+ state required near this energy by the (d,α) scattering analysis. However, the reaction data are consistent with a broad 1^+ level at 5.6 Mev.

* Present address Chalk River Laboratory.

[1] Day and Walker, Phys. Rev. **85**, 582 (1952).

[2] Galonsky and McEllistrem, Phys. Rev. **96**, 826A (1954).

K3. He^3 and T Reactions in Some Light Elements. E. ALMQVIST,* K. W. ALLEN, AND C. B. BIGHAM,* *University of Liverpool, England.*—By equipping the Liverpool 1-Mev accelerator with a gas recovery system it was possible to make a systematic study of He^3 and triton reactions. Ten ml of He^3 and 10 ml of hydrogen containing a few percent tritium were available. A proportional counter, a magnetic analyzer, a NaI crystal spectrometer, and photographic emulsions were used to study the charged reaction products. Targets of Li^6, Li^7, Be^9, B^{10}, B^{11}, C^{12}, C^{13}, N^{14}, O^{16}, and F^{19} were bombarded. Energy distributions of the reaction products of (1) $Li^6(He^3,\alpha)Li^5$, (2) $Li^6(He^3,p)Be^8$, (3) $Li^7(He^3,p)Be^9$, (4) $B^{10}(t,\alpha)Be^9$, and (5) $B^{10}(He^3,\alpha)B^9$ will be reported. The proton distributions from Li^6 and Li^7 agree with those of the Oak Ridge group.[1] In reaction (3) were observed the following levels in Be^9, with widths shown in brackets: 1.80±0.1 (<0.4), 2.39±0.08 (<0.2), 3.06±0.08 (<0.3), 4.74±0.08 (1.2) Mev, and possibly one at 9.1±0.2 (1.2) Mev. Also deuterons from the reaction $Li^7(He^3,d)Be^8$ were observed. Reaction (4) shows levels at 2.39 and 3.06 in Be^9. Reaction (5) shows only one excited state of B^9 at 2.58±0.13 Mev. Reaction (1) shows α peaks of 8.3 and 7.5 Mev energy.

* Present address Chalk River Laboratory.

[1] Moak, Good, and Kunz, Phys. Rev. **96**, 1363 (1954).

K4. Angular Distributions and Angular Correlations in $Be^9(d,p)Be^{10}$, and $B^{10}(d,p)B^{11}$.* S. A. COX AND R. M. WILLIAMSON, *Duke University.*—Angular correlation measurements have been made in the reactions $Be^9(d,p)Be^{10}$ and $B^{10}(d,p)B^{11}$ for the purpose of investigating the validity of the angular correlation theory[1] in stripping reactions. The angular distribution of group P_1 in $Be^9(d,p)Be^{10}$ has been measured previously[2] and is characteristic of $L_{neutron}=1$. Using the known ground state spins of Be^9 and Be^{10} and assuming $J=2$ for the 3.37 Mev state in Be^{10}, the correlation functions corresponding to the two possible channel spins have been calculated. The measured correlation agrees well with the function for which the channel spin =1. The angular distributions of the five longest range proton groups in $B^{10}(d,p)B^{11}$ have been measured from $\theta_p=15°$ to 130°. At $E_d=3.90$ Mev groups P_0, P_3, and P_4 have strong stripping peaks between 25 and 30 degrees corresponding to $L_{neutron}=1$ in agreement with previous data at $E_d=7.7$ Mev.[3] Angular correlation measurements were made on groups P_2 and P_4. The measured correlations will be compared with the possible theoretical correlation functions.

* This work was supported in part by the U. S. Atomic Energy Commission.

[1] Biedenharn, Boyer, and Charpie, Phys. Rev. **88**, 517 (1952).

[2] Fulbright, Bruner, Bromley, and Goldman, Phys. Rev. **88**, 700 (1952).

[3] N. T. S. Evans and W. C. Parkinson, Proc. Phys. Soc. (London) **A67**, 684 (1954).

K5. Energy Levels of B^{11}, C^{13}, C^{12}, and F^{21}. C. B. BIGHAM,* K. W. ALLEN, AND E. ALMQVIST,* *University of Liverpool, England.*—The long range particles emitted from targets of B^{10}, B^{11}, C^{13}, C^{12}, N^{14}, O^{16}, and F^{19} bombarded by 900 kev He^3 and T ions have been studied using photographic emulsion and NaI crystal techniques. In each case the observed proton groups yield information about the level structure of the residual nucleus with an estimated error in energy of less than ±0.1 Mev. In B^{11}, levels were observed at excitations of 0.94, 1.65, 2.61, 3.37, 3.75, and 4.46 Mev; in C^{13} at 4.43, 7.77, 9.61, 10.75, 11.83, 12.76, 13.31, 13.97, 15.10, 16.04, and 16.57 Mev; in C^{12} at 3.08, 3.77, 6.89, 7.63, 8.96, 10.00, 10.99, and 11.67 Mev. The reaction $F^{19}(t,p)F^{21}$ was observed. The data yield a mass defect for F^{21} of 6.37±0.1 Mev, and it is stable against heavy-particle breakup. Excited states of F^{21} at 0.89 Mev and possibly 3.34 and 4.01 Mev were observed.

* Present address Chalk River Laboratory.

K6. $C^{12}(p,pn)C^{11}$ Cross Section for 340 Mev Protons.* W. E. CRANDALL, W BIRNBAUM, G. P. MILLBURN, AND R. V. PYLE, *University of California, Berkeley.*—The cross section for the $C^{12}(p,pn)C^{11}$ reaction was measured by monitoring the proton beam with a Faraday cup and the C^{11} decay with a 4π gas counter. The self-absorption of the thin polystyrene foils was measured by uniformly activating thin foils and counting these foils singly and in combinations to eliminate the foil weight from the determination. Also simultaneous activation of plastic scintillators determined a zero foil thickness point by β–γ coincidence technique. The effects of the self-absorption curve on the cross section previously determined with thin polystyrene foils will be discussed.

* This work was performed under the auspices of the U. S. Atomic Energy Commission.

K7. Protons from the Deuteron Bombardment of C^{12}.† T. W. BONNER, ALFRED A. KRAUS, JR., J. T. EISINGER,* AND J. B. MARION, *The Rice Institute.*—Excitation functions and angular distributions of the reaction $C^{12}(d,p)C^{13}$ have been measured from $E_d=2.0$ Mev to $E_d=5.0$ Mev, where E_d is the deuteron energy. Excitation functions were taken at angles of observation of 30°, 90°, and 150°. Resonances were found at $E_d=2.53$, 2.73, 3.02, 3.34, 3.93, and 4.76 Mev. These resonances show interference effects. Excitation functions were measured at 10°, 50°, 60°, 70°, 80°, 90°, 100°, 110°, 120°, and 130° for $E_d=3.2$ Mev to $E_d=4.2$ Mev. The analyses of these data will be discussed in terms of Butler stripping and resonant compound nucleus formation. The angular distribution at 3.29 Mev is in agreement with that of Holmgren *et al.*[1]

† Supported by the U. S. Atomic Energy Commission.

* Now at Bell Laboratories, Murray Hill, New Jersey.

[1] Holmgren, Blair, Simmons, Stratton, and Stuart, Phys. Rev. **95**, 1544 (1954).

K8, (d,p) Reactions from C^{13} and C^{14}.* J. N. McGruer, E. K. Warburton, and R. S. Bender, *University of Pittsburgh.*—Observations have been made of the proton groups resulting from the deuteron bombardment of a thin carbon target. 14.5 Mev deuterons were incident upon a target of elemental carbon[1] (enriched to 60 percent C^{13}) and outgoing protons were analyzed with a magnetic spectrometer. Seven previously reported levels were observed in C^{13} and four in C^{14}. In addition twelve new levels were observed, three in C^{13} at 7.47, 9.50 and 9.90 Mev, and nine in C^{14} at 6.59, 7.35, 8.32, 9.80, 10.43, 10.59, 12.60, 12.85, and 12.96 Mev.

* Work done at the Sarah Mellon Scaife Radiation Laboratory and assisted by the joint program of the Office of Naval Research and the U. S. Atomic Energy Commission.
[1] We are indebted to T. Lauritsen for furnishing the target.

K9. Differential Cross Sections for $C^{13}+d$ Reactions.* M. T. McEllistrem, Ren Chiba, R. A. Douglas, D. F. Herring, and E. A. Silverstein, *University of Wisconsin.*—Differential cross sections for laboratory angles between 24 degrees and 167 degrees have been measured in a differentially pumped gas scattering chamber as a function of deuteron energy (2.5–3.4 Mev) for elastic scattering, and for the (d,p) reactions to the ground and 3.08-Mev level of C^{13}. Absence of systematic errors was indicated by also measuring the p–p cross sections. The ground state data confirm and extend our earlier measurements. Resonances in the elastic scattering were observed at 2.51, 2.74, 2.96, 2.99, 3.12, and 3.39 Mev. The resonances at 2.51 and 2.74 Mev were also observed in the (d,p) reactions. The combined effect of some or all of the resonances at 2.96, 2.99, and 3.12 Mev was also observed in the (d,p) data. An angular distribution for the (d,p) reaction to the first excited state on the 2.74-Mev resonance showed a large cross section for angles near 180 degrees. Above the resonance, the forward stripping peak (corresponding to $l_n=0$) increased markedly, whereas the large angle cross sections were greatly diminished. Interference between stripping and compound nuclear contributions to the (d,p) reactions is clearly indicated. Some success has been attained in attempts to analyze the data into compound nuclear and stripping contributions.

* Work supported by the U. S. Atomic Energy Commission and the Wisconsin Alumni Research Foundation.

K10. Energy Dependence of the Cross Sections for the Reactions $C^{13}(d,n)N^{13}$ and $C^{13}(d,t)C^{11}$ up to $E_D=20$ Mev.* D. H. Wilkinson,† *Brookhaven National Laboratory.*—The energy dependence of the integrated cross section for the reaction $C^{13}(d,n)N^{13}$ leading to the *ground state of N^{13} only* has been measured as a function of deuteron energy up to $E_D=20$ Mev. The cross section falls rather smoothly above $E_D=6$ Mev, rather more slowly than is suggested by the simple Born approximation stripping theory, and substantially more slowly than would be expected on the basis of compound nucleus formation. The cross section at $E_D=8$ Mev is 100 mb. The cross section for the reaction $C^{13}(d,t)C^{11}$ rises rapidly from threshold ($E_D=14.5$ Mev) to $E_D=20$ Mev where the cross section (to all available states of C^{11}) is 10 mb. This cross section may not be explained on the basis of the compound nucleus model even under the rather unlikely assumption of a triton reduced width as great as that for a neutron, and it seems most likely that pickup is involved.

* Work done under the auspices of the U. S. Atomic Energy Commission.
† On leave from Cavendish Laboratory, Cambridge, England.

K11. Angular Distribution of Proton Groups from the $N^{14}(d,p)N^{15}$ Reaction.* R. D. Sharp, A. Sperduto, and W. W. Buechner, *M.I.T.*—A study of the angular distribution of the proton groups for the $N^{14}(d,p)N^{15}$ reaction has been undertaken with the ONR-MIT electrostatic generator in conjunction with the new broad-range spectrograph. A series of exposures have been made at a deuteron bombarding energy of 7 Mev and at angles between 5 and 55 degrees in 5-degree steps, and between 60 and 110 degrees in 10-degree steps. The target consisted of a thin nylon film supported by an evaporated layer of gold. The energy spectrum observed over the 30-inch length of nuclear track plates was such that sixteen proton groups[1] from the $N^{14}(d,p)N^{15}$ reaction were recorded simultaneously at each angle. These groups covered the region of excitation in N^{15} from the pair of levels at 5.3 Mev to about 11 Mev. Angular-distribution curves for a number of these groups have thus far been obtained. Spin and parity assignment for the various levels are being made on the basis of a Butler-type stripping analysis.

* This work has been supported in part by the joint program of the Office of Naval Research and the U. S. Atomic Energy Commission.
[1] Sperduto, Buechner, Bockelman, and Browne, Phys. Rev. **96**, 1316 (1954).

K12. A 2-State at 8.85 Mev. in O^{16}.* B. J. Toppel, D. H. Wilkinson,† and D. E. Alburger, *Brookhaven National Laboratory.*—The bombardment of F^{19} by 3.1- to 4.1-Mev protons from the Brookhaven National Laboratory research Van de Graaff gives rise to a gamma ray of energy 2.73 ± 0.02 Mev as determined by single crystal NaI(Tl), and by three crystal pair spectrometer measurements. This gamma ray is shown to be in coincidence with the 6.14-Mev gamma ray from the 3-state of O^{16} and therefore comes from a state in O^{16} formed in the reaction $F^{19}(p,\alpha)O^{16}$ which is stable against alpha-particle emission although such emission is energetically possible. A weak gamma ray of 1.71 ± 0.02 Mev is found to be in coincidence with gamma radiation between 6.3 and 8 Mev, as is a yet weaker line of 1.92 ± 0.02 Mev. These latter transitions are to the $1-$ and $2+$ states at 7.12 and 6.91 Mev, respectively. These observations fix the new state in O^{16} at 8.85 ± 0.02 Mev and, together with the observation that the ground state transition is not seen, imply its characteristics as $2-$. The implications of this result for the alpha-particle model of O^{16} will be discussed. The occurrence of the 1.92 Mev line is in violation of the isotopic spin selection rule on $E1$ radiations in self-conjugate nuclei.

* Work done under the auspices of the U. S. Atomic Energy Commission.
† On leave from Cavendish Laboratory, Cambridge, England.

K13. Inelastic Scattering at 19 Mev Protons by O^{16}: (A) Proton Groups.* R. Sherr and W. F. Hornyak,† *Princeton University.*—The α-particle model of O^{16} predicts the existence of $2\pm$ doublets which have been unsuccessfully looked for in the past. To investigate this problem, 19.0-Mev protons were used to excite O^{16} by inelastic scattering. The external beam of the Princeton cyclotron was automatically controlled to ±10 kev in mean energy. Scattered protons were detected with a NaI(Tl) crystal whose energy response was calibrated by p-p scattering. Observations on O^{16} were made at 10 angles between 40° and 165° using targets of cellulose acetate, PbO_2, and U_3O_8. In addition to the doublets at 6.1 and 7.0 Mev (unresolved in this experiment) seven states were found: 8.85, 9.84, 10.34, 11.08, 11.51, 12.03, and 12.52 Mev; the average energy deviation in the various determinations for each level was approximately 30 kev. The 11.08 and 12.03 levels are new; the others agree within 20 kev with previously published values, except for the 8.85 Mev level previously reported as 8.6 ± 4 Mev. The integrated cross sections in millibarns are roughly 58 and 34 for the 6- and 7-Mev doublets and 28, 8, 8, 20, 11, 6, and 11, respectively, for the higher levels.

* Work supported by the U. S. Atomic Energy Commission and The Higgins Fund.
† On leave from Brookhaven National Laboratory.

K14. Inelastic Scattering of 19 Mev Protons by O^{16}: (B) Gamma Radiation.* W. F. Hornyak† and R. Sherr, *Princeton University.*—The spin and parities of the levels of

O^{16} listed in the preceding abstract are known from C^{12} (α,α) and N^{15} (p,α) work, except for the levels at 8.85, 11.08, and 12.03 Mev. If any of the latter states are 2^- they could not decay by α-particle emission and would decay by γ-ray emission. With a 30 mμsec NaI(Tl) coincidence apparatus, coincidence spectra for both protons at 150° and γ rays at 90° were observed. In addition to p-γ coincidences for the protons leading to the 6- and 7-Mev states, conspicuous p-γ coincidences were observed only for the groups to the 8.85, 11.08, and 12.52-Mev levels. The 12.52-Mev level showed a ~4-Mev coincidence γ ray consistent with decay by α-particle emission to the first excited state in C^{12}. Only cascade γ transitions through the states at 6- and 7-Mev were observed for both the 8.85 and 11.08 states. A reasonable interpretation assigns a spin and parity of 2^- to the latter levels, and assumes cascading through the 3^- level at 6.13 Mev and the 1^- level at 6.9 Mev. The weak proton group leading to the 12.03-Mev state also showed probable p-γ coincidences.

* Work supported by the U. S. Atomic Energy Commission and The Higgins Fund.
† On leave from Brookhaven National Laboratory.

Friday Morning at 9:30

Caribar Room

(H. L. Dryden presiding)

Fluid Dynamics; General Physics

KA1. Radiation from a Strong Shock Front in Krypton.* E. B. Turner, *University of Michigan.*—Petschek[1] observed that a very strong shock front in argon is usually seen as a bright luminous line. We have shown from wave-speed photographs in krypton with a revolving drum camera at an angle to the shock tube, that the luminosity is homogeneous across the front and not a wall effect. Another series of wave-speed photographs were made with a wedge interference filter placed in front of a horizontal slit on the shock tube. These showed mainly line radiation, but the lines were not those of krypton. At the suggestion of C. W. Peters, a spectrum was obtained by rotating the film drum at such a speed that the image of the shock front was stationary on the film. The Swan bands of carbon, which arise from organic vapors, as well as the lines of Ca and Na were observed. The sharp luminous front is apparently due to inelastic collisions between these vapors and krypton atoms in the zone where translational equilibrium is not yet established.

* Supported by the Air Research and Development Command.
[1] H. E. Petschek, Phys. Rev. **84**, 614(A) (1951).

KA2. Reflection of a Compression Wave from a Symmetrical Wedge. R. W. Skulski* and D. Weimer,† *Armour Research Foundation.*—Compression waves generated by paper pistons accelerated by shock waves in a shock tube have been reflected from symmetrical wedges. Studies of the density fields in the interaction region have been made with an interferometer and the parameters, "wave age," distance up the wedge, and angle of incidence have been investigated over a range of incidence angles from 25° to 80° and "effective shock strengths" from $\xi=0.5$ to $\xi=0.9$. The limit of regular reflection for this type of wave is shown to exist theoretically and this limit has been verified experimentally. Beyond this limit a type of Mach reflection occurs.

* Askania Regulator, Chicago.
† Mechanics Research Department, American Machine and Foundry Co., Chicago.

KA3. Shock Wave Spectroscopy. Richard J. Rosa, *Cornell University.**—A moving film technique has been developed for photographing strong shock spectra. If the film is made to move at a velocity within 5 percent of that of the shock wave image, the exposure time is increased by twenty and the light from different regions of the shock is separated on the film. Space resolved spectra of Mach No. 10 shocks in argon were obtained. These indicate that the luminosity of the front[1] is due to impurities, specifically, carbon bearing compounds. It could be expected that the light emitted by minute traces of impurities would dominate the spectrum at the theoretical equilibrium temperatures at this Mach number. Experiments with a probe filled with liquid N_2 also indicate impurities are responsible. The spectra show the Swan bands of C_2 confined to a narrow region at the front, and the violet CN bands reaching a maximum intensity close to the front and tailing off behind. Lines due to metallic impurities such as Hg and Na are observed to start at or near the front and continue with constant intensity to the entropy line. Preliminary results of air spectra above $M=15$ will also be presented.

* This work was partially supported by the Office of Naval Research.
[1] H. E. Petschek, Phys. Rev. **84**, 614 (1951).

KA4. Periodic Shock Production in Resonating Gas Columns. George E. Hudson and Alfred Saenger, *New York University.*—Observations have been made of periodic shock waves produced in a tube closed at one end by a rigid wall and at the other by a piston vibrating in sinusoidal motion. Although the piston's amplitude is small, shocks are produced when the frequency is near the acoustic resonance frequency of the gas column. With a condenser pickup, pressure variations at several points at the tube wall have been measured as a function of frequency, as has the relative phase between the piston's motion and the peak pressure. A solution of the exact one—dimensional compressible flow equations subject to the first order (isentropic) shock boundary conditions—has been found for the comparable case of oscillating motion of a gas in a tube closed rigidly at both ends. The computed maximum gas displacement corresponding to our observed pressures indicates that the maximum gas displacement at the tube center is about the same as that computed from acoustic theory. Observations have also been made of two shocks colliding periodically at the tube center when the driving frequency is near that of the first acoustic harmonic.

KA5. The Sonoluminescence of Water.* D. Srinivasan and L. V. Holroyd, *University of Missouri.*—An effort has been made to establish the origin of the weak luminescence produced when water is irradiated by an intense ultrasonic beam. In order to promote cavitation it is necessary that the water be saturated with a gas. Water saturated with the following gases was studied separately using 800 kilocycle acoustic radiation: argon, oxygen, nitrogen, and helium. The intensity of luminescence increased with increasing solubility of the gas. The spectral distribution of this luminescence was determined with a photon counter in the interval from 2800 A

to 5500 A. The spectrum is continuous and corresponds to that of a blackbody at a temperature of the order of 10 000°K. An absorption spectrophotometer was used to determine the nature and quantity of any chemical products formed during the ultrasonic irradiation. Hydrogen peroxide was found in the case of oxygen saturated water but no chemical products were observed either in argon or helium solutions. Theoretical considerations of cavitation in Liquids by Noltingk and Neppiras[1] suggest the possibility of the production of high temperatures in the cavitation bubbles and our results seem to support this view.

* Supported in part by the National Science Foundation.
[1] B. E. Noltingk and E. A. Neppiras, Proc. Phys. Soc. (London) **B63**, 674 (1950).

KA6. One-Dimensional Dispersion of Mass by Molecular and Turbulent Diffusion.* B. A. FLEISHMAN, *Applied Physics Laboratory* (introduced by R. A. Alpher).—A given one-dimensional distribution of matter is dispersed under the combined action of molecular diffusion and turbulence. We derive here a formula for the mean concentration of dispersed matter, as a function of x and t, in terms of the initial distribution, the coefficient of molecular diffusion, and the statistical properties of the turbulent velocity field. First the initial value problem for the diffusion-convection differential equation (for an arbitrary bounded convection field) is solved for the concentration σ by perturbing with respect to the "magnitude" of the convection velocity. Then, assuming that we have a random convective velocity field (i.e., an ensemble of velocity fields) rather than one specific convection field, we take an ensemble average of the infinite series for $\sigma(x,t)$ obtained previously. In the resulting series for $\bar{\sigma}(x,t)$, the *mean* concentration, the zero-order term involves only the molecular diffusion coefficient and the initial distribution, while the nth-order term contains in addition the nth-order space-time correlation coefficient of the turbulent velocity field. The result is valid at small dispersion times or for small intensities of turbulence.

* This work was supported by the Bureau of Ordnance, U. S. Department of the Navy.

KA7. Maximizing the Separation Factor of a Thermal Diffusion Column.* J. W. CORBETT† AND W. W. WATSON, *Yale University*.—The separation factor, q, of a hot-wire thermal diffusion column for gaseous operation is a function of the radius, r, pressure, p, and temperature differential in the column. The relation describing the maximized q with respect to r is $K_d = 2K_c$,[1] with K_c and K_d the convection- and diffusion-remixing factors, respectively. The condition describing maximized q with respect to p is $K_d = K_c$. (For want of information on parameter dependence the parasitic remixing factor, K_p, has been omitted from consideration.) The magnitude of the maxima for both criteria goes as $1/r$ (or p^1), therefore the smallest radius constructionally feasible should be chosen. The ratio of q for $K_d = K_c$ (designated q_1) to that q for $K_d = 2K_c$, evaluated at constant r, goes as $(q_1)^{0.33}$, hence for the desired case of large q, the advantage of operating at $K_d = K_c$ (i.e., a higher pressure) is not inconsequential. The relationship between q and the temperature difference is not a simple function and no general conditions can be established. A maximum of q with respect to temperature may, or may not, occur in the operating region, and each case must be investigated numerically.

* Supported in part by the U. S. Atomic Energy Commission.
† General Electric Coffin Fellow.
[1] Jones and Furry, Revs. Modern Phys. **18**, 151 (1946).

KA8. A Determination of Current in Absolute Measure. RAYMOND L. DRISCOLL, *National Bureau of Standards* (introduced by F. B. Silsbee).—A steady current was measured in an absolute sense using a Pellat type electrodynamometer; simultaneously the same current was passed through a resistance whose value was known in units maintained at this Bureau. The current was adjusted beforehand to make the potential difference across the resistance equal to the emf of a standard cell whose value was known in units of emf as currently maintained. The numerical value of a current in terms of standards of emf and resistance has been found to be larger than its numerical value obtained from absolute measurements by 19 parts per million. Known uncertainties in the absolute measurement are estimated to be 6 parts per million.

KA9. Transient Response of Cavity Resonator. C. W. HOOVER, JR., *Bell Telephone Laboratories*.—The general transient response of a cavity resonator to pulse-modulated radio frequency power input is obtained by solution of the differential equations representing the resonator and coupling loop. The solution obtained gives the normalized resonator response in the undercoupled, critically coupled, and overcoupled cases when the rf input is at or near the resonator center frequency. In the critical and overcoupled cases it is shown that the response is modified by a cosinusoidal modulation factor when the frequency of the source is different than the frequency of maximum response, or the frequency remaining constant when the coupling between source and resonator is changed. This modulation factor gives rise to large amplitude oscillations in the response. The solution obtained is of interest where close coupling is used between power source and resonator as in linear accelerators and klystrons. The solution is approximate but the maximum error in the amplitude of the normalized response is $1/2Q_0$. The observed response of a particular cavity resonator is given and is shown to agree with the predicted response.

KA10. Counting Efficiency of Electromechanical Message Registers. GREGORY THEOCLITUS, *Air Prehealer Corporation*, AND HOMER C. WILKINS, *Alfred University*.—The effect of the dead-time of nonjamming message registers on recorded counting rates has been investigated. A nonjamming message register is one which, when fed pulses at an increasingly high rate, will record at a rate asymptotically approaching the reciprocal of the dead-time. Using the Poisson distribution law for random events, the expected observed counting rate has been computed for various true counting rates in applications in which such a message register is preceded by electronic scaler circuits of various scale factors. It has been found that the expected curve of observed counting rate *versus* true counting rate is linear up to counting rates about one-half the asymptotic value, and then has several points of inflection and minima before leveling off at the asymptotic value of observed counting rate. Experiments using Geiger counters as sources of random pulses give results in good agreement with the theory. A discussion of the derivation of the curves and also an explanation of the minima will be given.

KA11. Automatic Pressure Control System.* D. F. HERRING, *University of Wisconsin*.—A constant pressure control system for a differentially pumped gas scattering chamber has been developed. An octoil-*S* filled manometer monitored by two photocells is used as a pressure detector. The octoil in the manometer is used as a cylindrical lens which focuses the light beams on the photocells. The signals from the two photocells are balanced against each other, thus making the instrument a null detector. The resulting error signal is then amplified and made to control the current through a gas flow regulating device. This device consists of a glass capillary of 15 mils inside diameter, through which is passed a nichrome wire of 10 mils diameter. By heating this wire with the current, the viscosity of the gas is altered, thus controlling the rate of flow of gas through the capillary. The present system controls the pressure to ± 0.03 mm of octoil. Details of construction and operation will be presented.

* This work is supported by the U. S. Atomic Energy Commission and the Wisconsin Alumni Research Foundation.

KA12. Ultra High Speed Cine-Microscopy and Time Resolved Spectroscopy. GEORGE HAUVER AND LOUIS ZERNOW, *Ballistic Research Laboratories.*—The technique previously described[1] for combining an ultra high-speed framing camera (framing rates $>10^6$/second) with a microscope in order to obtain cine-microscopic sequences of physical phenomena has been extended to higher magnifications ($>200\times$). Considerably greater magnifications are still possible. Limiting factors will be discussed. Studies of the explosion of thin conducting films by means of electrical discharges will be described. A simple method for using the ultra high-speed framing camera for time-resolved spectroscopy will also be described and illustrated with spectrograms of exploding wires.[2]

[1] L. Zernow and G. Hauver, Bull. Am. Phys. Soc. **30**, No. 2, 28 (1955), abstract Q11.
[2] J. A. Anderson and Sinclair Smith, Astrophys. J. **64**, 295 (1926).

KA13. Steady-State Calibration of Vibration Transducers at Accelerations up to ±4000 g. T. A. PERLS, C. W. KISSINGER, AND D. R. PAQUETTE, *National Bureau of Standards.*—Details are presented for a new steady-state method for calibrating small vibration pickups at peak accelerations up to ±4000 g. The method uses a commercial vibration generator and 70-watt power amplifier designed for a maximum of ±50 g, together with a selection of resonant beams made from a fatigue-resistant chrome-vanadium steel. The mechanical Q of the resonant system, which includes the beam, a clamping device, and the shaker armature, is of the order of 100 to 200. Beams with shapes other than rectangular have been tried in an effort to distribute the stresses, and one of the tapered beams has resulted in the highest accelerations so far. Sharp discontinuities in the beams, in particular holes used for clamping purposes, have to be avoided since they result in stress concentrations and in the initiation of cracks. Sample linearity data of small $BaTiO_3$ accelerometers will be shown. The method may also have application to fatigue testing.

KA14. Rotational Oscillations of Electrostatically Charged Conductors. OLEG YADOFF AND SOPHIE YADOFF.—When two or more fine wires are charged electrostatically (+) and (−), they commence evenly to rotate, the amplitudes and frequencies of rotation being functions of the potential, their diameters, and their distances from one another. These rotations occur whether the wires be arranged parallelly, obliquely, or perpendicularly to one another. In darkness the rotations of (+)-charged wires cut whitish-violet loops, whereas the rotations of the (−)-charged wires describe distinct luminous circles. The phenomenon occurs in air and various gases. Generally, amplitudes and frequencies are greater with ( ) charges. Rotations persist if only one wire is charged and the other is grounded or left suspended in the air. Authors' mathematical analysis follows current methods.

FRIDAY MORNING AT 9:30

NBS, East Building

(W. H. BRATTAIN presiding)

Semiconductors, II

L1. Microwave Magnetoconductivity Bridge for Semiconductors.* SIMON FONER, H. J. ZEIGER, R. L. POWELL, AND BENJAMIN LAX, *Lincoln Laboratory.*—A sensitive microwave bridge at 9200 Mcps has been constructed to measure the magnetoconductivity of semiconductors. The apparatus permits rotation of the magnetic field relative to crystal orientation. Such measurements should yield information on the shape of the energy surfaces associated with the carriers. Variation of the temperature should provide information on the average effective mass of carriers as well as the temperature dependence of the scattering.[1] The method allows investigation of semiconductors which can not at present be studied by cyclotron resonance because of sample impurity. Many of the difficulties inherent in dc measurements, particularly at low temperatures, are eliminated, i.e., contact problems, thermal effects, etc. Furthermore, theoretical analysis of the data is simplified because conductivity rather than resistivity is measured. Changes of 0.04 percent in conductivity can be observed at present. Preliminary investigations of a number of semiconductors will be discussed.

* The research in this document was supported jointly by the Army, Navy, and Air Force under contract with the Massachusetts Institute of Technology.
[1] J. M. Goldey and S. C. Brown, Bull. Am. Phys. Soc., **30**, No. 1, 53 (1955), abstract V3; T. S. Benedict and W. Shockley, Phys. Rev. **89**, 1152 (1953).

L2. Microwave Magnetoconductivity Effects in InSb.* R. N. DEXTER AND BENJAMIN LAX, *Lincoln Laboratory.*—Using cyclotron resonance techniques[1] we have observed the magnetoconductivity of electrons and holes in polycrystalline and single-crystal InSb. The observations thus far have shown the nonresonant microwave absorption characteristic of $\omega\tau<1$, where ω is the angular frequency and τ is the scattering time. Low values of τ result from impurities and imperfect stoichiometry of the compound. In the most nearly perfect (polycrystalline) samples it was possible by means of curve fitting to determine that $\tau=0.2\times10^{-11}$ second (i.e. $\omega\tau=0.3$ at 23 000 Mcps). The average effective masses of electrons and holes were found to be approximately 0.02 m_0 and 0.3 m_0 respectively where m_0 is the free-electron mass. These values are consistent with those obtained from optical measurements.[2] In n-type samples the electrons had not frozen into the traps at 1.2°K resulting in carrier densities of the order of $10^{13}-10^{14}$ per cc. Complicated absorption effects in samples of thickness of about 0.3 mm arose from variations of microwave skin depth relative to sample thickness as a function of magnetic field and possibly from depolarization and plasma effects.[3]

* The research in this document was supported jointly by the Army, Navy, and Air Force under contract with the Massachusetts Institute of Technology.
[1] Dexter, Lax, Kip, and Dresselhaus, Phys. Rev. **96**, 222 (1954).
[2] E. Burstein, Phys. Rev. **93**, 632 (1954).
[3] C. Kittel, Physica (to be published).

L3. Recombination Processes in Tellurium.* DAVID REDFIELD,† *University of Pennsylvania.*—The statistical treatment of recombination processes in semiconductors developed by Shockley and Read[1] has been applied to tellurium using a proposal advanced by Rittner.[2] Data reported earlier on the photoconductivity of tellurium as a function of light intensity at 100°K showed a transition from linear to square root dependence that was suggestive of direct recombination.[3] However, Rittner's considerations indicated the possibility of explaining such a dependence by recombination through traps under certain conditions. This possibility has been analyzed

for p-type material, and the physical consequences of these conditions considered in the light of available information on tellurium. Without any assumptions regarding the magnitude of the recombination coefficients involved, it seems possible to distinguish between the different recombination mechanisms. On the basis of such analysis, direct recombination appears to be dominant in tellurium.

* This work supported in part by the Office of Naval Research and the U. S. Air Force.
† Socony-Vacuum Oil Company Fellow.
[1] W. Shockley and W. T. Read, Phys. Rev. **87**, 835 (1952).
[2] E. S. Rittner, *Photoconductivity* (to be published).
[3] D. Redfield, *Photoconductivity* (to be published).

L4. Galvanomagnetic Effects in Single Crystals of Antimony.* H. J. Juretschke and S. J. Freedman, *Polytechnic Institute of Brooklyn*, and S. Epstein, *Signal Corps Engineering Laboratory*.—At room temperature the change of the resistivity tensor of antimony with magnetic field H can be expressed as a rapidly converging power series in H. For $H \leq 15$ kgauss terms up to and including H^3 are important. Contributions from H^4 also play a small role. This effect has been mapped out by measurements of longitudinal and transverse voltages on Sb single-crystal rods, as a function of H and of the directions of the primary current and of the magnetic field with respect to crystal axes. The results are described in terms of a set of phenomenological coefficients of various products of the magnetic field components, compatible with the crystal symmetry of Sb. For H in kgauss, the ratio of second- and third-power coefficients to the first-power Hall constants is of the order of 10^{-2} and 10^{-3}, respectively, although not all of the higher-order coefficients are of the same magnitude.

* This work has been supported in part by the Office of Naval Research.

L5. Magnetoresistance in Germanium at Low Temperatures.* F. J. Darnell and S. A. Friedberg, *Carnegie Institute of Technology*.—Magnetoresistance measurements have been carried out for oriented single crystals of n- and p-type germanium at temperatures down to 4.2°K. Magnetic fields up to 5400 gauss were applied in the longitudinal direction and in various transverse directions with respect to the current. The region in which $(\Delta\rho/\rho) \propto H^2$ is quite small, being exceeded at 77°K, for example, by applied fields of a few hundred gauss and by still smaller fields at lower temperatures. The effects observed above nitrogen temperatures are similar to those reported by Pearson and Suhl.[1] For high-purity n-type material the results down to 20°K are in reasonable accord with the strong-field theory of Abeles and Meiboom[2] allowing only for scattering by lattice vibrations. The very large effects observed at 4.2°K may be treated with the same theory if impurity scattering is included. The applicability of this theory to p-type material at these temperatures will be considered.

* Work supported in part by the National Science Foundation and the Office of Naval Research.
[1] G. L. Pearson and H. Suhl, Phys. Rev. **83**, 768 (1951).
[2] B. Abeles and S. Meiboom, Phys. Rev. **95**, 31 (1954).

L6. Conductivity of Nickel Oxide as a Function of Temperature and Surrounding Atmosphere.* Robert Lindsay and John J. Banewicz, *Southern Methodist University*.—The electrical conductivity of NiO has been determined from temperatures of 200°C to 1000°C in atmospheres containing oxygen at partial pressures of 3 to 760 mm of Hg. Samples prepared by two different methods were used. One sample was made by sintering NiO prepared by the decomposition of $Ni(OH)_2$. The second sample was formed by treating nickel metal in air at 1000°C. Both samples had platinum potential probes embedded in them. For each atmosphere, reproducible curves were obtained. In all temperature regions the $\log\sigma$ *vs* $1/T$ plot was approximately linear. Characteristic temperatures were noted for each atmosphere at which the slopes of the plots changed. In the upper temperature regions the conductivity of NiO was found to increase with increasing oxygen pressure in the manner noted by Baumbach and Wagner.[1]

* Assisted by a grant from the Research Corporation.
[1] Baumbach and Wagner, Z. Physik. Chem. **B24**, 59 (1934).

L7. Electronic Interaction of Imperfections in Semiconductors and Insulators. R. L. Longini, *Westinghouse Research Laboratories*.—The concentrations of electrons and holes in semiconductors and insulators are modified by the introduction of impurities or of vacancies into an otherwise perfect crystal. As a result of this modification, certain electronic energies are added to the free energy of solution of these "particles." In particular, if a crystal becomes very n-type, the p-type impurities or vacancies can go into the crystal much more easily than in the intrinsic material and furthermore, n-type impurities have greater difficulty in entering the crystal. Similarly, p-type impurities or vacancies in large quantity reduce the ease with which further p-type impurities or vacancies can come into the crystal and increase the solubility of n-type impurities. The extent of this effect is shown to depend drastically on the energy gap, such that in insulators almost any excess of n-type impurities will cause either p-type impurities or vacancies to go into the lattice. This electronic interaction also affects the diffusion of substitutional impurities in such a way that n-type impurities will have a tendency to diffuse more rapidly than p-type.

L8. Comparison of the Condon and the Adiabatic Approximations for an Impurity Center. Jordan J. Markham, *Zenith Radio Corporation*.—For most purposes wave functions of an electron trapped at an impurity in a crystal are approximated by the product of two functions, one involving the lattice coordinates and the other the position of the electron. The electronic function may be determined for the equilibrium position of the lattice (Condon approximation) or one may assume that the electronic wave function continuously adjusts itself to the instantaneous position of the lattice (adiabatic approximation). The first approach underestimates the kinetic energy and overestimates the potential energy, while the second does just the reverse. The author has compared the two approximations using the variational principle. Although the formal treatment is quite general and includes all the effects for harmonic vibrations, the actual terms were evaluated for a simple model. The calculations show that for extremely shallow traps the Condon approximation is slightly superior while for deep traps the adiabatic should be used. For traps of depths less than 0.2 ev the methods are essentially equivalent; in any of these calculations, other approximations are made and they are of greater importance than the slight difference between the properly used Condon or adiabatic approximations.

L9. A Combined Tight Binding and Perturbation Theory of Graphite π States. J. C. Slonczewski and P. R. Weiss, *Rutgers University*.—Apparently the Fermi surface of graphite lies in the neighborhood of the π-band zone edges parallel to the hexagonal z-axis. A special method is used to estimate the energies in this region. The dependence of energy on k_z is obtained by a tight binding method in which a Bloch sum is formed of solutions of the isolated layer approximation. The dependence of energy on k_x and k_y is obtained by perturbing the states whose wave vectors lie on the edge of the zone with the operator $\hbar^2/im(k_x\partial/\partial_x + k_y\partial/\partial_y)$. Here k_x and k_y are measured from the zone edge. This method yields simple relations between variable x- and y-components of tensor mass and certain "vertical" energy gaps. Interaction between second-nearest layers results in band overlap. Spin-orbit coupling is found to modify the results stated.

L10. Propagation and Plasma Oscillation in Semiconductors.* BENJAMIN LAX AND LAURA M. ROTH,† *Lincoln Laboratory.*—The classical magnetoionic theory[1] can be extended to semiconductors whose energy surfaces in the Brillouin zone are ellipsoidal or warped spherical surfaces possessing cubic symmetry. The conductivity tensors in either case are evaluated in a coordinate system in which the magnetic field is along one of the axes. The tensor is substituted in Maxwell's equations and solutions are obtained for the propagation constant in terms of an effective conductivity. The effective conductivity is tabulated for the ellipsoidal models for longitudinal and transverse propagation for the high symmetry [001], [110], and [111] crystal directions. Polynomial equations for the plasma oscillation frequencies are obtained for each of these cases when the propagation constant is equated to zero. The theory is being extended to warped surfaces since approximate expressions for the conductivity tensor have been obtained in this case.[2] Modifications of the results when depolarizing effects[3] have to be taken into account will also be discussed.

* The research in this document was supported jointly by the Army, Navy, and Air Force under contract with the Massachusetts Institute of Technology.
† Now at Harvard University, Cambridge, Massachusetts.
[1] E. V. Appleton, U.R.S.I. Reports, Washington (1927).
[2] H. J. Zeiger (private communication).
[3] C. Kittel, Physica (to be published).

L11. Radiation Effects in Gallium Antimonide. J. W. CLELAND AND J. H. CRAWFORD, JR., *Oak Ridge National Laboratory.*—The conductivity of *n*- and *p*-type GaSb[1] of high-carrier concentration decreases monotonically under fast neutron irradiation and approaches saturation before any intrinsic behavior is observed. The removal rate of current carriers is approximately equal for both types of material for high carrier concentrations and is quite temperature dependent. Measurements of the Hall constant after exposure indicate the production of electron traps in *n*-type and hole traps in *p*-type and low-temperature (~120°C) heating indicates that some of these irradiation produced traps are thermally annealable. Extended high-temperature (~500°C) vacuum anneal, however, increases greatly the acceptor concentration of irradiated *p*-type specimens but does not markedly alter the acceptor concentration of unirradiated companion samples. A similar decrease in effective donor concentration of irradiated *n*-type material permits the formation of samples with a lower initial-carrier concentration. Reirradiation then indicates that the removal rate of current electrons in *n*-type material is not dependent upon initial-electron concentration. The removal rate of holes in *p*-type material, however, decreases rapidly for material of lower initial-hole concentration.

[1] We are indebted to Dr. Raymond L. Smith of the Franklin Institute for the *p*-type samples and to Dr. H. P. R. Frederikse of the National Bureau of Standards for the *n*-type samples used in these experiments.

FRIDAY MORNING AT 10:00

Continental Room

(B. L. CRAWFORD presiding)

Chemical Physics

LA1. Improved Symmetrized Cell Theory of Liquids. J. DAHLER AND J. O. HIRSCHFELDER, *University of Wisconsin.*—To obtain practical results from the cell theory of liquids, it seems necessary to assume a simple symmetry for the distribution of a molecule about its lattice site. This is accomplished by replacing the interaction of the molecule with its neighbors by some "suitably averaged" interaction. In the Lennard-Jones and Devonshire treatment, the pair interaction is replaced by its spatial average. We find that a Boltzmann-type average is much more satisfactory. For an assumed symmetry of the distribution, our procedure provides an extension of Kirkwood's theory such that the resulting integral equation for the distribution function can be solved by numerical methods. We have found the function L defined by the double surface integral,

$$\iint_{s_1 s_2} f(\rho, r_1, r_2, R)\, d\sigma_1 d\sigma_2 \Big/ \iint_{s_1 s_2} d\sigma_1 d\sigma_2 = \int_{\rho_{\min}}^{\rho_{\max}} f(\rho, r_1, r_2, R) L(\rho/R, r_1/R, r_2/R)/R\, d\rho$$

to be extremely useful. Here, r_1 and r_2 are the radii of two spheres, R the separation of their centers, ρ the separation of points on the two spheres, and f an arbitrary function of its arguments. L is found to be a quadratic function of ρ, different for various subranges of the interval $(\rho_{\min}, \rho_{\max})$. For a variety of physical problems such as x-ray and electron diffraction, L may have application.

LA2. (Abstract withdrawn.)

LA3. Temperature-Pressure-Structure Effects on the Viscosity of Several Higher Hydrocarbons.* D. A. LOWITZ, W. WEBB, AND R. W. SCHIESSLER, *The Pennsylvania State University.*—The viscosity of several very pure high molecular

weight hydrocarbons has been determined at six temperatures ranging from 100°F to 275°F and at pressures ranging from 15 to 50 000 psi by use of a rolling-ball viscometer. For three of the hydrocarbons for which pressure-density data were not available, the density was determined over the same limits of pressure and temperature by use of a flexible bellows piezometer. The group varies in molecular weight from 240 to 429 and comprises several structural families of chain to ring and cyclohexyl to benzenoid ring structure. When the pressure-viscosity data are plotted in the form $\log \eta/d$ *vs* $[(v_0/v)^4 - K(v_0/v)^2]$, where η is the viscosity at pressure P, v_0 is the specific volume at atmospheric pressure, v is the specific volume at P, and K is a constant chosen for each compound, it is found that reasonably good straight lines are obtained.

* Research supported in part by America Petroleum Institute Project 42.

LA4. A Study of the Compressions of Several High Molecular Weight Hydrocarbons.* W. G. CUTLER, R. W. SCHIESSLER, AND W. WEBB, *The Pennsylvania State University.*—Using the Bridgman sylphon bellows technique, compressions for several very pure liquid hydrocarbons have been measured to pressures as high as 150 000 psi at 100°F, 140°F, 175°F, 210°F, 239°F, and 275°F. The hydrocarbons have a molecular weight range of 170 to 351 and include normal paraffins, cycloparaffins, fused ring aromatics, and fused ring napthenes. The Tait equation, $v_0 - v = C \log(1 + P/B)$, provided a good empirical fit for the isotherms. In the above equation C and B are constants, v is the specific volume at pressure P, and v_0 is the specific volume at atmospheric pressure. The Hudleston relation, $\log[v^4 P/(v_0^4 - v^4)] = a - b(v_0^4 - v^4)$, where a and b are constants and other symbols have the same meaning as above, has also been examined. Isobars and isochores have been drawn and studied over the full range of pressure and temperature. The effect of molecular structure on the compressibility of the hydrocarbons has been examined.

* Part of the work of Research Project 42 of the American Petroleum Institute.

LA5. Statistical Mechanics of Isotopic Systems with Small Quantum Corrections.* JACOB BIGELEISEN, *Brookhaven National Laboratory.*—The differences in the thermodynamic properties of isotopic molecules, which can be described by the first quantum correction ($u^2/24$ law), depend on the difference in the reciprocal masses of the atoms in the molecule, and are, therefore, independent of all masses except for those atoms isotopically substituted. This theorem provides a rigorous proof of the rule of the geometric mean for gaseous molecules. The theorem shows that the partition function ratio for double labelled molecules is equal to the appropriate ratio for single labelled molecules. The rule of the geometric mean for the vapor pressures can be derived using the assumption that the internal energy states are the same in the liquid and gas. The vapor pressures of the liquid hydrogens can be calculated in good agreement with experiment from the vapor pressures of any two, e.g., H_2 and HD. The partition function ratios for molecules of the type XY_n, $XY_{n-1}Y'$ can be expressed in terms of the masses Y and Y' and the symmetrical stretching frequency. This permits an evaluation of the experimental data on the fractionation of H_2O^{18} and H_2O^{18} by cations in terms of the breathing frequency. The results are in agreement with predictions from an electrostatic model.

* Research carried out under the auspices of the U. S. Atomic Energy Commission.

LA6. Derivation of a Quantum-Statistical Transport Equation for Dilute Gases. A. W. SÁENZ, *Naval Research Laboratory.*—We have derived a quantum-statistical transport equation for dilute gases composed of particles of spin zero using the properties of Wigner distribution functions (d.f.'s), Kirkwood's method of time averaging over a suitable interval τ,[1] and the formal time-dependent scattering theory. Our main assumptions may be stated roughly as follows: (i) the hypothesis of binary collisions; (ii) the effect of the statistics need only be taken into account for pairs; (iii) the d.f.'s are slowly varying over suitable microscopic regions and the time-averaged d.f.'s depend only secularly on time; (iv) an assumption of molecular chaos appropriate to bosons. The collision terms of our equation of transport contain an exact cross section: they reduce to those given by Kirkwood and Ross[2] when we evaluate this cross section according to the first Born approximation. The relation of our work to that of Mori and Ono,[3] Ono,[4] and Kirkwood and Ross[2] will be mentioned.

[1] J. G. Kirkwood, J. Chem. Phys. **14**, 180 (1946); 15, 72 (1947).
[2] J. G. Kirkwood and J. Ross, J. Chem. Phys. **22**, 1094 (1954).
[3] H. Mori and S. Ono, Progr. Theoret. Phys. **8**, 327 (1952).
[4] S. Ono, Progr. Theoret. Phys. **12**, 113 (1954).

LA7. Einstein-Bose Gas Below the Critical Temperature. J. FORD AND T. H. BERLIN, *Johns Hopkins University.*—The canonical partition function for an ideal Einstein-Bose gas is often expressed as a contour integral and then evaluated by the method of steepest descent. It had previously been thought that this method failed below the critical temperature, since the saddle point then became congruent with a singularity of the integrand. This difficulty can be overcome by using an indented contour. The partition function thus evaluated yields the same expressions for thermodynamic variables as are obtained by other procedures.

LA8. Statistical Mechanical Calculation of the Data of State of the Helium Isotopes at Intermediate Temperatures and Densities.* ABRAHAM S. FRIEDMAN AND IRWIN OPPENHEIM, *National Bureau of Standards.*—Series expansions for the quantum mechanical partition functions, distribution functions, and thermodynamic functions, which were developed previously,[1] have been applied to the computation of the quantum mechanical compressibility factors for the isotopes of helium. DeBoer's quantum corrected values of the Lennard-Jones 6-12 intermolecular force constants were used, and the differences in compressibility factors, $Z_{He^3} - Z_{He^3}$ and $Z_{He^4} - Z_{He^4}$ were computed over a wide temperature and pressure range.

* Supported in part by the U. S. Atomic Energy Commission, Division of Research.
[1] I. Oppenheim, Bull. Am. Phys. Soc. **29**, No. 8, 10 (1954), abstract D6.

LA9. Ideal Gas Thermodynamic Functions of the Isotopic Hydrogen Sulfides.* LESTER HAAR, JOE C. BRADLEY, AND ABRAHAM S. FRIEDMAN, *National Bureau of Standards.*—The ideal gas thermodynamic functions for H_2S, D_2S, T_2S, HDS, HTS, and DTS were calculated from molecular data. The recent spectroscopic data for H_2S and D_2S by Allen[1] were employed. The zero-order frequencies and the moments of inertia of the other isotopes were calculated from the H_2S and D_2S data. The partition functions are obtained in closed form. The calculations include high-temperature corrections for vibrational anharmonicity, rotation-vibration coupling, centrifugal stretching, and a low-temperature correction for nonclassical rotation, in addition to a correction for the ortho-para effect.[2] The statistical calculations were performed on the National Bureau of Standards digital computer—SEAC. Tables of C_p^0/R, $(H^0 - E_0^0)/RT$, $-(F^0 - E_0^0)/RT$, and S^0/R, have been calculated at close temperature intervals from 50°–5000°K.

* Supported in part by the U. S. Atomic Energy Commission, Division of Research.
[1] H. C. Allen, Jr. (private communication).
[2] H. W. Woolley (in preparation).

FRIDAY MORNING AT 10:00

Exhibit Hall II

(U. FANO presiding)

Invited Papers from the National Bureau of Standards

M1. Direct Measurement of Negative-Ion Affinities. L. M. BRANSCOMB, *NBS.* (30 min.)
M2. The Theory of Electron Penetration. L. V. SPENCER, *NBS.* (30 min.)
M3. Elastic Scattering of Photons from 5 to 30 Mev. E. G. FULLER, *NBS.* (30 min.)
M4. Nuclear Orientation at Low Temperatures. ERNEST AMBLER, *NBS.* (30 min.)

FRIDAY AFTERNOON AT 2:00

Main Ballroom

(E. SEGRÈ presiding)

Scattering and Polarization of Nuclei

N1. Polarization Effects in Proton-Proton Scattering at 210 Mev.* EMANUEL BASKIR,† JOHN TINLOT, AND SIDNEY SPITAL, *University of Rochester.*—Measurements have been made of the angular dependence of proton polarization produced by p-p collisions at 210-Mev laboratory energy. A highly-polarized beam of protons, produced by scattering from a carbon or a beryllium target at $15°\pm1°$, is scattered from a second target and is counted in a multicrystal telescope mounted on a rotatable arm. The mean beam energy is 210 ± 2 Mev; full width at half maximum, 10 ± 2 Mev. Both polyethylene and liquid hydrogen second targets have been used to cover the barycentric angular range from 20° to 90°. Preliminary measurements have also been made at lower energies, e.g. 130 ± 10 Mev and indicate agreement with results obtained at Harwell.[1] A least squares fit to the 210-Mev data will be presented, and comparison made to results obtained at other energies.

* Work supported by the U. S. Atomic Energy Commission.
† National Science Foundation Predoctoral Fellow.
[1] Dickson and Salter, Nature 173, 946 (1954).

N2. Polarization of 210-Mev Protons Elastically Scattered from Carbon.* W. G. CHESNUT, E. M. HAFNER, AND R. HARDING, *University of Rochester.*—The angular dependence of scattering asymmetry has been measured using a carbon scatterer in the highly-polarized external 210-Mev proton beam from the Rochester cyclotron. Data were taken simultaneously in several energy intervals near the elastic peak by means of seven scintillation counters and differential absorbers mounted on the rotating telescope arm. This system allows several checks upon success in separating elastically scattered protons from those which leave the carbon nucleus in its 4.4-Mev excited state. The results indicate small contamination of inelastically scattered protons in the count obtained for the channel of highest energy. The observed asymmetry that is believed to represent principally elastic scattering reaches a maximum at approximately 17°, shows a decided dip to a minimum at 30°, and then rises sharply up to 37.5° in the laboratory which is the largest angle at which measurements have so far been made. Estimates of the absolute values of $(d\sigma/\partial\omega)_R$ and $(\partial\sigma/\partial\omega)_L$ will be given.

* Work supported by the U. S. Atomic Energy Commission.

N3. Phase-Shift Analysis of 210-Mev Proton Polarization.* E. M. HAFNER AND W. CHESNUT, *University of Rochester.*—Attempts have been made to describe the results of the preceding paper in terms of sets of 40 phase shifts for partial waves up to $l=10$. The optical model of Taylor,[1] and the $l\cdot s$ potential suggested by Fermi[2] and developed by Sternheimer,[3] were used as guides in this work. A spin-independent potential intermediate between a square well and a harmonic-oscillator well, combined with a harmonic-oscillator spin-dependent potential, produce a qualitative description of the results. The phase shifts can then be perturbed in such a way as to give an accurate fit to the data up to $\vartheta=30°$, but they predict stronger polarization at larger angles than is actually observed. Possible causes of this discrepancy will be discussed.

* Work supported by the U. S. Atomic Energy Commission.
[1] T. B. Taylor, Phys. Rev. 92, 831 (1953).
[2] E. Fermi, Nuovo cimento 11, 407 (1954).
[3] R. M. Sternheimer, Phys. Rev. 95, 587 (1954).

N4. Negative Pressure Pentane Bubble Chamber Used in High-Energy Experiments.*† RICHARD J. PLANO‡ AND IRWIN A. PLESS, *The University of Chicago.*—A negative pressure isopentane bubble chamber has been constructed and used to examine high-energy proton interactions with hydrogen and carbon. The sensitive fluid is contained in an all glass system with inside dimensions $13\times13\times27$ mm. The flat walls were polished to allow precision photography. The chamber was operated at a temperature of 127°C, compressed with a positive pressure of 40 atmospheres, and expanded to a negative pressure of 2.5 atmospheres. The recycling time was typically two seconds and included the following operations. The chamber was expanded to the desired negative pressure after which the cyclotron was pulsed. The incident protons passed through a counter telescope in front of the chamber, giving a coincidence pulse which was delayed 4 microseconds and used to trigger a light flash of duration 3/4 microsecond. Two 35-mm cameras were used in a 90° stereo arrangement to permit maximum accuracy in angular measurements.

* Abstract placed in this session at special request.
† Research supported by a joint program of the Office of Naval Research and the U. S. Atomic Energy Commission.
‡ National Science Foundation Predoctoral Fellow.

N5. A Study of 456-Mev Proton Interactions with Hydrogen and Carbon.* IRWIN A. PLESS AND RICHARD J. PLANO,† *The University of Chicago.*—The negative pressure bubble chamber described in the preceding abstract was used to investigate high-energy proton interactions with hydrogen and carbon. Proton-proton elastic scatterings are distinguished from proton-carbon interactions down to a laboratory angle of 4°. The accuracy on our angular measurements exceeds 1°. A typical hour of scanning will reveal on the order of one proton-proton scattering, three elastic proton-carbon scatterings, and five proton-carbon inelastic reactions. Total cross sections obtained are in good agreement with published data. The carbon-star prong distribution will be presented, as will

histograms describing the angular distribution of elastic proton-proton, elastic proton-carbon, and quasi-elastic proton-nucleon scatterings.

* Research supported by a joint program of the Office of Naval Research and the U. S. Atomic Energy Commission.
† National Science Foundation Predoctoral Fellow.

N6. $P-P$ Interactions at 3 Bev.* A. KERNAN† AND R. CESTER, *University of Rochester.*—Ilford G-5 emulsions were exposed to the internal beam of the Brookhaven proton synchrotron in order to study proton-proton interactions in emulsion; the incident beam energy was determined to be 3 Bev by the relative scattering technique.[1] The plates were examined under high magnification using the along-the-track scanning technique. Only those events were accepted for analysis having an even number of prongs (exclusive of the incident proton) and satisfying certain kinematical criteria necessary to insure their compatibility with an initial nucleon-nucleon interaction; i.e. either with an H-atom of the emulsion or a proton of an emulsion nucleus. Of twenty events completely analyzed to date 3 are elastic scatterings, 10 represent single π-meson production and 7 represent multiple π production ($\geq 2\pi$ mesons). Additional data will be presented and the cm angular distribution for the single π production will be given. The data obtained for the inelastic events will be compared with current theoretical predictions.

* This research supported in part by the U. S. Atomic Energy Commission.
† American Association of University Women Fellow.
[1] M. Koshiba and M. F. Kaplon, Phys. Rev. **97**, 193 (1955).

N7. Elastic Scattering of 40-Mev Alpha Particles from Heavy Nuclei.* HARVEY E. WEGNER, R. M. EISBERG, AND G. IGO, *Brookhaven National Laboratory.*—Recent experiments[1] on the elastic scattering of alpha particles from heavy nuclei have been successfully interpreted by several theoretical methods. In this experiment we have measured the angular distribution for the elastic scattering of 40-Mev alpha particles from Th, Pb, Au, Pt, W, and Ta, in order to provide additional data which may be used to differentiate between these methods. The scattered particles were detected, at laboratory angles ranging from 20 to 55 degrees, by a thin NaI (Tl) crystal mounted on a Dumont 6292 photomultiplier tube. The elastically-scattered alpha particles were separated from the other particles by pulse height analysis. Slides will be shown giving the ratio of the observed cross section to the Coulomb cross section as a function of laboratory angle. This ratio decreases approximately exponentially for scattering angles greater than a certain critical angle. In order to provide a simple comparison of the results of this experiment with previous data, slides will be shown giving the ratio of the observed cross section to the Coulomb cross section as a function of parameters which are common to all three experiments, such as the momentum transfer or the apsidal distance of the classical trajectory.

* This work has been carried out at the Brookhaven 60-inch cyclotron under the auspices of the U. S. Atomic Energy Commission.
[1] G. W. Farwell and H. E. Wegner, Phys. Rev. **95**, 1212 (1954).

N8. Absolute Angular Distribution of 20-Mev Protons Elastically Scattered by Oxygen and Nitrogen.* RICHARD H. CHOW† AND BYRON T. WRIGHT, *University of California, Los Angeles.*—The absolute angular distributions of 20-Mev protons scattered elastically by O^{16} and N^{14} were determined using the externally deflected beam of the U.C.L.A. synchro-cyclotron. The scattered protons were detected with angular resolution of about $\pm 1.3°$ by an NaI (Tl) scintillation detector with about 1.5 percent energy resolution full width at half maximum. The low-counting rate at 60° and beyond for O^{16} was overcome by scattering from a solid LiOH target about 6½ mgm per cm² thick and resolving the various groups of elastically-scattered protons. The relative distribution so obtained was normalized at 60°. For N^{14}, at 45° and beyond the protons were scattered from the gas confined at one atmosphere pressure in a small cylinder constructed of 0.0005-in. duraluminum and 0.001-in. "Mylar" polyester foils. The various methods were cross checked and agreed within statistics. The resultant angular distributions for the two elements were similar but the minima in the oxygen curve were slightly deeper. In terms of the optical model this feature can be interpreted qualitatively as less absorption in the case of O^{16}.

* Assisted by the joint program of the Office of Naval Research and the U. S. Atomic Energy Commission.
† Now at the Atomic Energy of Canada Limited, Chalk River, Ontario.

N9. Elastic Scattering of 17-Mev Protons by Nuclei.* G. SCHRANK, *Princeton University.*—Angular distributions of 17-Mev protons elastically scattered by Ta, W, and Bi have been obtained. Data was taken every five degrees from 20° to 172° with an absolute standard-deviation error of three percent. A five-parameter optical model, based on a complex potential with a fuzzy boundary, and including a nuclear spin-orbit term of the Thomas type, is used in an attempt to fit the data. In addition, angular positions of the second diffraction minimum for about twelve light nuclei have been experimentally determined with an accuracy of about 0.2 percent. The usefulness of this data in observing local variations in nuclear "radii" will be indicated.

* Work supported by the U. S. Atomic Energy Commission and The Higgins Fund.

N10. Differential Cross Sections for Elastic Scattering of Nitrogen by Nitrogen. H. L. REYNOLDS AND A. ZUCKER, *Oak Ridge National Laboratory.*—The angular distribution of nitrogen elastically scattered by nitrogen was measured for laboratory energies from 13 to 22 Mev. A gas target at a pressure of approximately ½ cm of mercury was used with Ilford D-1 nuclear emulsions as the particle detectors. The incident beam was collimated to ± 1 deg while the angular acceptance of the detector was ± 1 deg. Absolute values for the differential cross sections were obtained by normalizing the angular distributions to the calculated Coulomb cross sections at small angles, where nuclear forces did not contribute to the cross sections. At the lower energies the interference term in the Mott Coulomb-scattering formula clearly appears, illustrating the known spin and statistics of nitrogen. As the energy is increased the differential cross section falls below that predicted for Coulomb scattering because of the increasing importance of the nuclear interaction. At 22 Mev the differential cross section at 45 deg in the laboratory system is about ½ of the Coulomb cross section, with the deviation from the Coulomb cross section beginning at about 25 deg.

N11. Energy Levels of Na^{21}.*† W. HAEBERLI, *University of Wisconsin and Duke University.*—A phase-shift analysis of $Ne^{20}(p,p)Ne^{20}$ cross-section data[1] has been performed. Resonance phase shifts have been extracted by a new method which will be discussed. The analysis indicates resonances with the following resonant energies (E_p, Mev), total widths (kev), angular momenta and parities: 1.81, 180, $3/2^-$; 1.953, 6, $5/2^+$; 2.135, 17, $3/2^+$; 3.176, 110, $1/2^+$; 3.566, 25, $3/2^-$; 3.828, 6, $5/2^-$, or $7/2^-$; 4.28, 150, $3/2^+$, or $5/2^+$; corresponding to virtual states of Na^{21} at 4.18, 4.31, 4.49, 5.48, 5.85, 6.10, and 6.53 Mev respectively. With the exception of the 6.10-Mev state, all these levels are found to have an elastic width $\Gamma_e > 0.7\Gamma$. An anomaly in the cross section observed at $E_p = 2.7$ Mev cannot be analyzed in terms of a single resonance. Also unassigned so far is a narrow resonance at $E_p = 3.552$ Mev ($\Gamma \sim 2$ kev) and a resonance with a small elastic width ($\Gamma_e < 0.1\Gamma$) at $E_p = 3.42$ Mev ($\Gamma \sim 20$ kev).

* Abstract placed in this session at special request.
† This work was supported by the Wisconsin Alumni Research Foundation and the U. S. Atomic Energy Commission.
[1] Haeberli, Galonsky, Goldberg, and Douglas, Phys. Rev. **91**, 438 (1953).

FRIDAY AFTERNOON AT 2:00

Exhibit Hall I

(E. O. SALANT presiding)

Mostly Hyperons and Heavy Mesons

P1. Production of Heavy Mesons at the Bevatron.* L. T. KERTH, D. H. STORK, R. W. BIRGE, R. P. HADDOCK, AND M. N. WHITEHEAD, *University of California, Berkeley.*—Heavy mesons produced at 90° to the 5.7-Bev proton beam at the Berkeley bevatron have been focused by quadrupole magnets and deflected into a shielded region by means of an analyzing magnet. The target was copper, $\frac{1}{4}$ in. high and 1 in. in the beam direction. The distance from target to image was nine feet and the vertical and horizontal magnifications were 2.5 and 0.6, respectively. The focusing characteristics and momentum dispersion were investigated by placing nuclear plates at the image and determining the range and spatial distributions of protons produced at the target. A small emulsion stack has been exposed to 135 Mev positively charged K's. The processed emulsions were scanned by searching for nonminimum tracks and following each track to the end of its range. Background was sufficiently low so that 17 K's with a single lightly ionizing secondary track and 3τ's were found in 24 man-hours of scanning. On the basis of past experience this represents an increase in scanning efficiency of about two orders of magnitude.

* This work was performed under the auspices of the U. S. Atomic Energy Commission.

P2. β Decay of *K*-Mesons.* G. YEKUTIELI, M. F. KAPLON, AND J. KLARMANN, *University of Rochester.*—Two events in emulsion have been observed that are interpretable as the decay of a K-meson into an electron and two neutral particles. In the first, the decay track is emitted at minimum ionization with an energy of 260 Mev; identification rests upon the fact that it loses 110 Mev in 4.6 cm with no change in ionization, an abnormal loss for a π or μ meson but not for an electron. In the second, the secondary is emitted with 20 Mev at minimum ionization; in terms of known particles it must be an electron. For both particles the primary mass is $\sim 1000\ m_e$. In view of these and other recent observations on the K-electron decay[1] it now seems conclusive that a K-meson exists decaying into an electron and two neutral massless particles (this is implied by the first event above). It is thus interesting to inquire as to whether those K-decays giving a continuous electron or μ meson spectrum may not be alternate modes via a Fermi interaction. The branching ratio is of order unity and the lifetime $\sim 10^{-9}$ second assuming a universal Fermi interaction.[2] A survey of the observations on K-meson decay in emulsion shows that the data do not contradict this hypothesis.

* This research was supported in part by the U. S. Air Force through the Office of Scientific Research, Air Research and Development Command.
[1] Recent observations reported by G. Goldhaber and M. G. K. Menon at Fifth Annual Rochester Conference.
[2] A. M. L. Messiah (unpublished).

P3. High-Energy Cosmic-Ray Soft Showers in Nuclear Emulsion.* M. KOSHIBA AND M. F. KAPLON, *University of Rochester.*—A stack of stripped emulsion flown in Sky-Hook Balloons at 41° geomagnetic latitude has been scanned for high-energy soft showers. More than twenty cases of pure electron showers have been observed and analyzed for which the apparent origin consists of a single electron pair in emulsion. The nature of these showers (initial pair energy in the region of 10 Bev) as well as the initial cascade development has been investigated, with special attention to the trident process[1] in the early development. Most of these showers are consistent with the assumption that they originate from the conversion of the decay photons from locally produced π^0 mesons. However, there are a few anomalous cases[2] not easily reconcilable with our present knowledge.

* This research was supported in part by the U. S. Air Force through the Office of Scientific Research, Air Research and Development Command.
[1] M. Koshiba and M. F. Kaplon, Phys. Rev. **97**, 193 (1955).
[2] Schein, Haskin, and Glasser, Phys. Rev. **95**, 855 (1954); A. Debenedetti *et al.*, Nuovo cimento **12**, 954 (1954); and N. Dallaporta (private communication).

P4. "*V*-Particles" in Nuclear Emulsion.* J. KLARMANN, M. F. KAPLON, AND G. YEKUTIELI, *University of Rochester.*—Emulsion stacks are well suited for precise energy determinations and identification of relatively energetic charged particles (effective energy limit determined by stack size) since they can be stopped and their energy determined by range measurement while identification is assisted by the characteristics of the track terminus. Emulsion stacks should thus afford the most precise Q-value determinations for unstable particles if they can be detected and their decay fragments stop. We have searched for "V-particles" by tracing back trajectories of σ mesons; for those events in which the meson originates from a 2-prong star, the other prong being an ending proton, we calculate a Q-value assuming decay of a neutral particle into a proton and π^- meson. Very precise Q-values are reported for the Λ^0 decay in this way.[1] At present 12 V-particles selected this way in our laboratory give a spectrum of Q-values including 3 between 36.6 and 37 Mev and two with 30.3 and 30.5 Mev, respectively. The latter two (having no counterpart in cloud chamber investigations) suggest a possible background of simulated V-particles in emulsion coinciding with the Λ^0.

* This research was supported in part by the U. S. Air Force through the Office of Scientific Research, Air Research and Development Command.
[1] Nuovo cimento Suppl. **2**, 461 (1954). The data reported here seems deficient in low Q-values.

P5. Comparison of Ionization-Range Methods of Mass Estimation. F. W. O'DELL AND M. M. SHAPIRO, *Naval Research Laboratory.*—For charged particles which come to rest by ionization loss in nuclear emulsion, two principal methods of mass estimation based on the variation of ionization with residual range (I-R) have been employed: grain density *versus* range and mean gap length *versus* range. These methods are particularly applicable, respectively, to relatively long ranges (where the track is "grainy") and to short ones (where the track is dense). For the first method (gain density *vs* R) the subjectivity of counting grains in "blobs" has been circumvented by measuring blobs and employing the convention that the grain count for a blob is proportional to its length. This procedure yields high reproducibility and satisfactory mass evaluation. A third method, utilizing as an index of ionization the ratio of integrated blob length to gap length, has been explored for its possible applicability, especially at shorter ranges. This technique, as well as the other two, has been applied to protons, pions, and K-mesons with a view to comparing the precisions obtainable with the three I-R methods when comparable times are invested in measurement.

P6. Stopped *K*-Mesons Observed near the Geomagnetic Equator. B. STILLER, M. M. SHAPIRO, AND N. SEEMAN, *Naval Research Laboratory.*—Stacks of stripped emulsions were exposed to the cosmic rays at an atmospheric depth of 12 g/cm² and geomagnetic latitude 10°N. Application of scattering-

range and ionization-range measurements to 16 K-meson tracks,[1] as well as to calibration tracks of stopped protons and pions, shows that I-R methods are capable of greater precision for comparable effort and available track length than S-R. Mass histograms for the group of K-primaries exhibit "best values" somewhat lower than but compatible with the tau-meson mass. For those K-mesons which exhibit a single fast charged decay product, ionization and $p\beta$ values were obtained for secondary tracks of sufficient length. These results are employed to infer the relevance of the respective schemes $K_{\mu 2}\rightarrow\mu+\nu$ and $\chi\rightarrow\pi+\pi^0$ to those K-decays. Measurements of the star products arising from the capture of negative K-mesons are also reported. A "complete" positive-tau meson event, including the star origin and all three terminating pion secondaries, is analyzed.

[1] Seeman, Shapiro, and Stiller, Bull. Am. Phys. Soc. **30**, No. 1, 63 (1955), abstract Z2.

P7. Recent Results on S-Particles.* H. DeStaebler, Jr., H. S. Bridge, B. Rossi, and B. V. Sreekantan, *M.I.T.*—Data concerning K-mesons observed to decay at rest in a multiplate chamber (S-events) are reported. The distribution of the secondary ranges clearly exhibits two peaks, one at about 75 g cm^{-2} copper and another at about 45 g cm^{-2} copper. The first group supports the two-body decay proposed by the Paris group: $K_{\mu 2}\rightarrow\mu+\nu$. The second group provides strong additional evidence for the χ meson originally proposed by the Bristol group. According to our results the neutral particle in this decay must be a π^0 meson *viz.*; $\chi\rightarrow\pi+\pi^0$. Since the secondary range distribution is not continuous it is improbable that an appreciable fraction of the secondary particles arise from a three-body decay process.

* This work was supported in part by the joint program of the Office of Naval Research and the U. S. Atomic Energy Commission.

P8. Timing Measurements on Penetrating Cosmic Ray Showers.* Kenneth W. Robinson,† *Princeton University.*—Time delays in local penetrating cosmic-ray showers have been measured using scintillation and Čerenkov detectors and a chronotron. After correcting for background a single exponential decay curve is obtained corresponding to a mean lifetime of 8.00±0.72 millimicroseconds. These delayed events may be interpreted as decays of stopped K-mesons.[1] The background is analyzed into accidental and $\pi-\mu-e$ events and a ratio of π^+ to K of 8 to 1 is obtained, uncorrected for relative detection efficiencies. An associated Geiger counter hodoscope gives an average particle multiplicity of 6 for the delayed events interpreted as K-particles. Preliminary analysis of the data obtained from an experiment in which the Čerenkov detectors were surrounded alternately with thin Pb plates and equivalent Al plates indicates that gamma rays are associated with some of these delayed events. Comparisons will be made with a similar previous experiment.[2]

* Supported by the joint program of the Office of Naval Research and the U. S. Atomic Energy Commission.
† National Science Foundation, Predoctoral Fellow.
[1] H. Bridge, Nuovo cimento 12, 81 (1954).
[2] L. Mezzetti and J. W. Keuffel, Phys. Rev. 95, 858 (1954).

P9. Momentum and Ionization Measurements on Charged V-Particles.* W. B. Fretter, E. W. Friesen, G. E. Kepler, and L. Lagarrigue, *University of California, Berkeley.*—We have made several direct measurements of the mass of the primaries of charged V-particles by ionization-momentum measurements in a cloud chamber[1] at sea level. We have also measured the momentum p^* of the secondaries in the center of mass system. To make this calculation, we can use two independent methods. The first is to obtain the velocity of the primary directly from the ionization measurement. The second is to use the measured momentum and an assumed mass. One negative particle has a mass of 1150±140 electron masses. The p^* for the secondary is 171±18 Mev/c for a μ meson and 165±18 for a π meson, by the ionization method. If we assume that the mass of the primary is 955 M_e we find $p^*=157$ ±16 for a π secondary. This particle does not appear to be a π^-, θ^-, or $K\mu^-{}_2$, but could be a $K\mu^-{}_2$. The ionization measurements on the secondaries indicate that most of them are light mesons and not electrons.

* Assisted by the joint program of the Office of Naval Research and the U. S. Atomic Energy Commission.
[1] W. B. Fretter and E. W. Friesen, Rev. Sci. Instr. (to be published).

P10. Angular Correlations in V^0-Particle Decays.* B. V. Sreekantan, A. Pevsner, and G. Sandri, *M.I.T.*—Thirty-four cases of neutral V-particles produced inside the plates of a multiplate cloud chamber, by charged primaries, have been analyzed to find whether there exists any correlation between the production and decay planes of neutral V-particles. In twenty-four cases the limits on the Q-values of the V^0-particles could be determined, and the particles could be identified as probable Λ^0's. All these cases are inconsistent with θ^0's. In the remaining ten cases the V^0-particle could not be identified. The distribution of the dihedral angle between the production and decay planes, based on these thirty-four cases, appears to be consistent with an isotropic distribution and does not show any marked tendency for the two planes to be parallel. Several more cases of single V's and a few cases of double (V_0, V_0), and (V_0, V_{ch}) are being analyzed. Data on all these cases will be presented.

* This work was supported in part by the joint program of the Office of Naval Research and the U. S. Atomic Energy Commission.

P11. Evidence for Charge Asymmetry of $V^\pm$-Particles.* Y. B. Kim, J. R. Burwell, R. W. Huggett, and R. W. Thompson, *Indiana University.*—It was previously reported[1] that the p_ν-distributions and the distributions of decay points in the chamber indicate a $V^\pm$ charge asymmetry. Further analysis indicates that the V^--lifetime is of the order of 10^{-10} but might be as long as 10^{-9} second. The V^+-lifetime appears to be considerably longer. Although the statistics are limited, the V^+-events suggest a long lived $K^+\rightarrow(L^++$one neutral) of mass about 1000 m_e. The mean value of p' for $3\,V^+$-events is 222±5 Mev/c, in excellent agreement with the $K_{\mu 2}$.[2] If a substantial number of V^+-particles[3] are θ^+, the lifetime of θ^+ is probably considerably longer than θ^0. Although the statistics are limited, the p_ν-distribution of V^- does not suggest an isotropic[4] two-body decay process of a homogeneous group.

* Assisted by the Office of Ordnance Research and by a grant of the Frederick Gardner Cottrell Fund of the Research Corporation.
[1] Kim, Burwell, Huggett, and Thompson, Phys. Rev. 96, 229 (1954).
[2] Gregory, Lagarrigue, Leprince-Ringuet, Muller, and Peyrou, Nuovo cimento 11, 292 (1954).
[3] Hudson, Ballam, Arnold, Harris, Rau, Reynolds, and Trieman, Phys. Rev. 96, 1089 (1954).
[4] The Princeton group reports that V^--secondaries are emitted backward in the C-M system (Rochester Conference, 1955).

P12. Multiplicity Distribution of O+N$_p$ Stars. D. T. King, *Naval Research Laboratory.*—A track-following method has been used to find 149 stars, comprised only of thin or gray tracks, in G5 emulsions which had been exposed to the cosmic radiation. The stars are selected according to the requirements that (1) at least two charged particles appear to emerge and (2) the ionization of all tracks corresponds to velocities exceeding ~0.3 c. These criteria describe collisions of fast incident particles with hydrogen nuclei or edge nucleons of heavier nuclei in the emulsion. Among these stars, 19 percent are attributable to doubly-charged primaries, 72 percent to singly-charged primaries and 9 percent show no charged primary. The distribution in the number N of emergent tracks for the 107 stars of type O+N$_p$ will be discussed.

P13. Analysis of Properties of Secondary Particles in Nucleon-Nucleon Collisions at Very High Energy.* R. G. GLASSER, D. M. HASKIN, AND MARCEL SCHEIN, *University of Chicago.*—The momentum of the individual particles emitted in the "outer cone" of the *S*-star[1] was measured. This star has a primary energy of 2×10^{13} ev. In addition a lower limit to the momentum of the particles in the "inner cone" was obtained. It was found that one of the particles in the inner cone had an energy of 50 Bev from track-to-track scattering. On transforming the trajectories of the tracks from the laboratory (*L*-) system to the center-of-mass (*C*-) system for the nucleon-nucleon collision, the inner cone becomes the forward cone and the outer cone the backward cone. These two cones have a half-angle of about 20° each in the *C*-system, assuming in the transformation that all particles are pions. The symmetry in the *C*-system is satisfactory under this assumption, but from the properties of the Lorentz transformation, it can be shown that the presence of proton-antiproton pairs would distort this symmetry and that the energy of such pairs would be appreciably greater than that of the pions. The results of this investigation are compared with theories of multiple meson production including those of Landau and Heisenberg.

* Supported in part by the joint program of the Office of Naval Research and the U. S. Atomic Energy Commission.
[1] Lord, Fainberg, and Schein, Phys. Rev. **80**, 970 (1950); R. G. Glasser and Marcel Schein, Phys. Rev. **90**, 218 (1953).

P14. Further Investigations on the Photon Event.* MARCEL SCHEIN, D. M. HASKIN, AND R. G. GLASSER, *University of Chicago.*—The high-energy photon event found in a pellicle stack exposed in the stratosphere above Texas in 1954[1] has been analyzed carefully. The longitudinal and radial distribution of pair origins has been accurately determined, providing evidence for the convergence of pair origins in a distance of several centimeters from the entry of the event into the pellicle stack. The angular spread of the event is estimated to be 2×10^{-4} radian. Energy measurements from multiple scattering on most of the pairs will be presented. At very high energies track-to-track scattering was employed. Possible interpretations of the photon event will be discussed.

* Supported in part by the joint program of the Office of Naval Research and the U. S. Atomic Energy Commission.
[1] Schein, Haskin, and Glasser, Phys. Rev. **95**, 855 (1954).

FRIDAY AFTERNOON AT 2:00

Burgundy Room

(T. W. BONNER presiding)

Transmutation and Nuclear Energy Levels, II

PA1. The Angular Distribution of Protons from the $O^{16}(d,p)O^{17}$ Reaction as a Function of the Bombarding Energy.* J. C. GROSSKREUTZ, *University of Texas.*—The distribution in angle of the protons from the $O^{16}(d,p)O^{17}$ reaction has been measured for incident deuteron energies of 2.4, 2.2, 2.0, 1.78, 1.6, 1.4, and 1.1 Mev. Two groups of protons corresponding to the ground and first excited states of the residual nucleus O^{17} were detected using a thin CsI crystal and Du Mont 6291 photomultiplier tube mounted inside a 23-inch diameter scattering chamber. A number *vs* energy curve was taken for each proton group at 14 different angles between 5 and 160 degrees in the laboratory system. The results show that the stripping process takes place down to at least 1.1 Mev for the ground-state protons, while for the lower-energy group, the forward maximum has almost completely disappeared at that energy. Competition from compound nucleus formation is clearly evident, especially near resonances in the total yield of the reaction.[1] The data join smoothly the results of Van Patter *et al.*[2] who have investigated the reaction at energies above 2.6 Mev.

* Supported in part by the Office of Scientific Research, Air Research and Development Command.
[1] N. P. Heydenburg and D. R. Inglis, Phys. Rev. **73**, 230 (1948).
[2] Van Patter, Simmons, Stratton, and Zipoy, Phys. Rev. **96**, 825 (1954)

PA2. Deuteron Capture by O^{16}. J. W. BUTLER, *Naval Research Laboratory.*—The cross section for radiative capture of the deuteron by O^{16} has been measured by bombarding a 0.05-mil NiO foil and counting the positrons from the residual F^{18} nuclei. The positrons were counted with a 2-crystal coincidence counter actuated by the 2-annihilation quanta. The contribution of F^{18} from the $O^{17}(d,n)F^{18}$ reaction was determined by bombarding a similar target enriched[1] to 0.89 percent O^{17}. The cross section for the $O^{16}(d,\gamma)F^{18}$ reaction is of the order of 10 microbarns at 1.7-Mev bombarding energy. The cross section for the $O^{17}(d,n)F^{18}$ reaction at the same energy is some 3000 times higher.

[1] The enriched O^{17} was kindly supplied by Professor A. O. C. Nier.

PA3. Gamma Rays from Proton Bombardment of O^{18}.* EMMETT L. HUDSPETH, IRA L. MORGAN, AND JOSEPH T. PEOPLES, *University of Texas.*—A thin target of gaseous CO_2 enriched[1] 14 percent in O^{18} has been bombarded with protons of energy 0.3 to 2.6 Mev. The gas was contained in a cell of 2 cm depth, and the proton beam entered through a 0.05-mil Ni foil. Target thickness was estimated as 20 kev for 2.0 Mev protons. A $1\frac{1}{2}$ in.$\times1\frac{1}{2}$ in. NaI(Tl) crystal detector was used with a 20-channel analyzer. The excitation curve for ground-state transitions shows seven resonances, indicating levels in F^{19} tentatively evaluated as 8.49, 8.76, 9.65, 9.83, 10.04, 10.15, 10.22, 10.28, and 10.36 Mev. The first two levels are also known from $O^{18}(p,\alpha)$; these are the least intense of the levels found in the present work. The excitation curve shows a sudden drop at the $O^{18}(p,n)$ threshold. A pulse-height analysis has been made of gamma radiation produced at a bombarding energy of 2.20 Mev. It shows transitions to known excited states of F^{19}, in addition to ground-state transitions.

* Supported in part by the Office of Scientific Research, Air Research and Development Command.
[1] The enriched CO_2 was obtained from the Temple University Research Institute.

PA4. Excitation Curve for $F^{19}(n,\alpha)N^{16}$.* NORMAN A. BOSTROM, EMMETT L. HUDSPETH, AND IRA L. MORGAN, *University of Texas.*—The cross section for the reaction $F^{19}(n,\alpha)N^{16}$ has been measured as a function of neutron energy from 3.5 to 6.2 Mev. Neutrons were obtained by bombarding thin deuterium gas targets with deuterons from the University of Texas Van de Graaff generator. The energy spread

of the neutrons was approximately 25 kev at $E_d=1$ Mev. A ring of CaF_2 was irradiated with neutrons for a few seconds; the generator was then turned off and the 7.35-second activity of N^{16} was followed for several half-lives. Fluctuations in the deuteron-beam current were corrected by use of a circuit of a type previously described.[1] Resonances for this reaction appeared at neutron energies of 4.17, 4.68, 5.04, 5.40, 5.59, 5.90, and 6.08 Mev. The apparent threshold for the reaction is 3.88 Mev, which is 2.31 Mev above the calculated threshold of 1.57 Mev. These results are consistent with a spin assignment of $2(-)$ to N^{16}. This reaction offers possibilities for detection of fast neutrons in the presence of intense gamma radiation.

* Assisted by the U. S. Atomic Energy Commission.
[1] S. C. Snowdon, Phys. Rev. **78**, 299 (1950).

PA5. Some Energy Levels of Na^{23}.* C. P. Browne and W. C. Cobb, *M.I.T.*—The $Mg^{24}(d,\alpha)Na^{22}$ reaction has been used to observe levels in Na^{22} up to 3-Mev excitation. Thin targets of natural magnesium metal were bombarded with deuterons accelerated by the MIT–ONR electrostatic generator to energies of 5, 6, and 7 Mev. The energies of alpha particles emitted at 90 degrees to the incident beam were measured with the new broad-range spectrograph. Ten groups of alpha particles have been identified with this reaction. At 7-Mev incident energy, all ten groups appear on the nuclear track plate in a single exposure. Preliminary results give a ground-state Q-value of 1.954 Mev and excited states at 0.59, 0.89, 1.53, 1.94, 1.99, 2.22, 2.58, 2.98, and 3.07 Mev. The assignment of the group indicating a level at 2.22 Mev is somewhat less certain than for the other groups. At 6-Mev incident energy the groups leading to the ground state and first two excited states have approximately equal intensity. Of course, if the isotopic spin-selection rule holds, $T=1$ levels in Na^{22} will not be observed with this reaction. The energy of the first state observed here agrees with the 593-kev gamma ray previously observed.[1] In view of the observed intensities, it is unlikely that this level is the expected low-lying $T=1$ level.[2]

* This work has been supported by the joint program of the Office of Naval Research and the U. S. Atomic Energy Commission.
[1] G. M. Temmer and N. P. Heydenburg, Phys. Rev. **93**, 351 (1954).
[2] S. A. Moszkowski and D. C. Peaslee, Phys. Rev. **93**, 455 (1954).

PA6. Angular Distributions and Angular Correlations in $Mg^{24}(d,p)Mg^{25}$.* R. M. Williamson and S. A. Cox, *Duke University*.—The yields as a function of deuteron energy (2–4 Mev) of the nine longest range proton groups resulting from the $Mg^{24}(d,p)$ reaction have been obtained at selected angles between 15° and 135°. The proton detector was a thin crystal scintillator having a resolution of 2.5 percent for 8-Mev protons. Strong interference effects are observed in the yield curves, especially at the angles of the stripping peaks. The observed angles of the stripping peaks near 4-Mev deuteron energy are in agreement with other data.[1] The angular correlation between protons and gammas from the 3.40-Mev ($L_{neutron}=1$) level in Mg^{25} has been measured at several deuteron energies. The correlation predicted by stripping theory[2] is $W(\theta)=1-0.14\cos^2\theta$. The measured anisotropies range between 0 and +0.30, the latter chamber corresponding to the most strongly peaked proton angular distributions. The presence of an anisotropy confirms the assigned[2] spin of $\frac{1}{2}$ for this level. The sign of the anisotropy indicates that stripping theory may not be applied in this deuteron energy and target Z region.

* This work was supported in part by the U. S. Atomic Energy Commission.
[1] P. M. Endt and J. C. Kluyver, Revs. Modern Phys. **26**, 95 (1954).
[2] Biedenharn, Boyer, and Charpie, Phys. Rev. **88**, 517 (1952).

PA7. Gamma-Ray Cascades in Al^{28}. A. E. Litherland, E. B. Paul, G. A. Bartholomew, and H. E. Gove, *Chalk River Laboratories*.—The decay schemes of gamma rays in Al^{28} from the $Mg^{24}(p,\gamma)$ reaction at the five resonances in the range of proton energies 0.8 to 2.1 Mev have been established by coincidence measurements employing two 5 in. by 4 in. NaI(Tl) crystals and associated electronics. All the resonances except that at 1.49 Mev ($J=7/2-$) showed direct transitions to at least two of the lowest three states. The relative intensities of these primaries have been measured and compared with predicted theoretical values for single-particle transitions and in one case with the mirror reaction $Mg^{24}(n,\gamma)$.[1] In general the agreement is not very good. At two of the resonances cascades occur through levels which are themselves unstable against proton emission, while at the 1.49 Mev resonance (3.72 Mev in Al^{28}, $J=7/2-$) the strongest transition is via a level at 1.81 Mev in Al^{25} rather than the $5/2+$ ground state.

[1] B. B. Kinsey and G. A. Bartholomew, Phys. Rev. **93**, 1260 (1954).

PA8. Gamma Rays from Proton Bombardment of Mg^{24}. E. B. Paul, G. A. Bartholomew, H. E. Gove, and A. E. Litherland, *Chalk River Laboratories*.—A thin (10 kev) target of separated Mg^{24} isotope[1] has been bombarded by protons in the energy range 0.8 to 2.1 Mev using the Chalk River electrostatic generator. The emitted gamma-rays have been studied in a 5 in. diameter by 4 in. long NaI(Tl) crystal coupled to a Dumont K-1198 photomultiplier. The five resonances found by elastic proton scattering[2] in this region have been observed. By measuring the angular distribution of the ground-state proton capture gamma ray at the 1.49 Mev resonance, the spin of this f-wave[3] resonance is shown to be 7/2. The absolute yield of gamma rays has been measured at some of the resonances. At the 2.01 Mev resonance the absolute yield of the 1.38 Mev gamma-ray indicates the partial width for inelastic scattering may be as much as 25 percent of the total width.[3]

[1] Obtained from Atomic Energy Research Establishment, Harwell, England.
[2] Mooring, Koester, Goldberg, Saxon, and Kaufmann, Phys. Rev. **84**, 703 (1951).
[3] L. J. Koester, Phys. Rev. **85**, 643 (1952).

PA9. Magnetic Analysis of Protons from $Al^{27}(d,p)Al^{28}$. W. W. Buechner, A. Sperduto, and Marcos Mazari.* *M.I.T.*—In a previous investigation,[1] using 2-Mev deuterons, fifty proton groups from this reaction were measured and assigned to levels in Al^{28} between the ground state and 6.31 Mev. In the present work, using higher bombarding energies, a broad-range magnetic spectrograph[2] has been used to study these groups and to extend the region of excitation investigated up to neutron binding in Al^{28}. The assignment of most of the observed groups to this reaction is based on the agreement of the Q-values measured in observations at 90 degrees with deuteron energies of 6 and 7 Mev and observations at 35 and 10 degrees using 7-Mev deuterons. The previous work has been confirmed in detail, and a number of new levels have been established. The spectrum is complex, with at least 100 well-resolved levels between the ground state and neutron binding (7.72 Mev). This work has been supported in part by the joint program of the Office of Naval Research and U. S. Atomic Energy Commission.

* On leave from the National University of Mexico.
[1] Enge, Buechner, and Sperduto, Phys. Rev. **88**, 963 (1952).
[2] Buechner, Browne, Enge, Mazari, and Buntschuh, Phys. Rev. **95**, 609 (1954).

PA10. The $Si^{28}(p,p'\gamma)Si^{28}$ Reaction. H. O. Cohn, J. K. Bair, J. D. Kington, and H. B. Willard, *Oak Ridge National Laboratory*.—Work with platinum target backings indicated a strong 1.8-Mev gamma ray when bombarded with protons from the ORNL 5.5-Mev Van de Graaff generator.

It has been shown that this is due to a thin surface contamination of silicon. The gamma rays are produced by inelastic scattering of protons by the first excited state of Si^{28} at 1.78 Mev. A 3 in. × 3 in. NaI(Tl) crystal was used to detect the gamma rays. Yields of this reaction have been measured at 0° with respect to the protons from 1.8- to 4.7-Mev bombarding energy. Resonances were observed at $E_p = 3.11$ Mev ($\Gamma = 12$ kev), 3.35 Mev ($\Gamma = 11$ kev), 3.58 Mev ($\Gamma = 70$ kev), 3.71 Mev ($\Gamma = 40$ kev), 4.25 Mev ($\Gamma = 22$ kev), and 4.44 Mev ($\Gamma \cong 100$ kev, this may be a superposition of two broad levels). Excitation energies in the compound nucleus P^{29} are 5.73, 5.96, 6.18, 6.31, 6.82, and 7.01 Mev, respectively.

PA11. Gamma-Ray Resonances in the Reaction $Si^{30}(p,\gamma)P^{31}$.* S. MILANI, JOHN N. COOPER, AND J. C. HARRIS, *Ohio State University.*—Both thick and thin targets of electromagnetically separated[1] silicon-29 have been bombarded with protons of energies between 300 and 1000 kev. In addition to the gamma-ray resonances reported by Endt, Kluyver, and Van der Leun,[2] prominent resonances were observed at proton energies of approximately 696, 727, 917, and 956 kev. Preliminary data reveal several other resonances at energies between 1000 and 1200 kev. Measurements by scintillation spectrometer of the gamma-ray energies from the 414-kev resonance show the decay is predominantly by a cascade with gamma rays of 5.9 and 0.7 Mev as reported by Kluyver *et al.* At the 696-kev resonance the gamma-ray energies suggest decay through the 0.7- and 2.0-Mev levels[3] with relatively weak transitions to the level at 1.4 Mev. At the 727-kev resonance strong decay through the 1.4-Mev level is indicated.

* Supported in part by the U. S. Atomic Energy Commission through a contract with the O. S. U. Research Foundation.
[1] Supplied by Oak Ridge National Laboratory.
[2] Endt, Kluyver, and Van der Leun, Phys. Rev. **95**, 580 (1954).
[3] Mandeville, Swann, Chatterjee, and Van Patter, Phys. Rev. **85**, 193 (1952).

PA12. Gamma Rays from Proton Bombardment of Phosphorus.* B. D. KERN AND L. W. COCHRAN, *University of Kentucky.*—The spectrum of the gamma rays from the proton bombardment of a thick phosphorus target has been obtained at several proton energies using a 1½ inches in diameter × 1 inch in length NaI(Tl) crystal in a scintillation spectrometer. Gamma rays whose energies vary with the proton energy are identified at 12.0, 9.7, 7.0, and 7.5 (±0.2) Mev, at $E_p = 1.3$ Mev ($Q = 10.7$ Mev). Gamma rays whose energies do not vary with the proton energy are seen at 2.3 and 1.6 (±0.1) Mev, poorly resolved; the 1.6-Mev gamma ray is tentatively identified as arising from the $P^{31}(p,\alpha\gamma)Si^{28}$ reaction. The spectrum of only those gamma rays of lower energy which are in coincidence with higher-energy gamma rays has been obtained and shows considerably better resolution. In it, gamma rays are identified at 0.5 (annihilation radiation), 2.25, 2.56, and 4.40 (±0.05) Mev. Levels in S^{32} are indicated at 2.25, 4.40, and 4.81 Mev, in reasonable agreement with earlier reports.[1,2]

* This work was supported in part by the U. S. Atomic Energy Commission.
[1] R. H. Dicke and J. Marshall, Jr., Phys. Rev. **63**, 86 (1943).
[2] S. C. Snowdon, Phys. Rev. **87**, 1022 (1952).

FRIDAY AFTERNOON AT 2:00

Continental Room

(J. E. MAYER presiding)

Division of Chemical Physics

Symposium on Nonequilibrium Processes

Q1. Statistical Mechanics of Irreversible Processes. ILYA PRIGOGINE, *Harvard University and Free University of Brussels.* (30 min.)

Q2. Fluctuations and Irreversibility. HERBERT CALLEN, *University of Pennsylvania.* (30 min.)

Business Meeting of the Division of Chemical Physics

Q3. Theory of Sound Dispersion in Dilute Gases. MARK KAC, *Cornell University.* (30 min.)

FRIDAY AFTERNOON AT 2:00

Exhibit Hall II

(E. P. WIGNER presiding)

Post-Deadline Papers, If Any

FRIDAY AFTERNOON AT 2:00

NBS, East Building

(L. MARTON presiding)

Electron Physics

R1. An Ultra-High Vacuum Valve.* D. G. BILLS AND F. G. ALLEN, *Harvard University.*—An all-metal vacuum valve with a minimum leakage conductance of 10^{-13} l/sec has been described by Alpert.[1] We have found, however, using an Alpert-type seal that reproducible conductances of 10^{-13} l/sec are difficult to obtain, the usual minimum value for a typical valve being about 10^{-10} l/sec. By completely confining the softer metal in the seal we have produced simplified and enlarged valves with conductances which are continuously variable from 1 l/sec to less than 10^{-14} l/sec. Presumably the conductance may be made as small as desired. All of the advantages of Alpert's design have been retained in the new design.

* Supported in part by the Office of Naval Research, the Signal Corps of the U. S. Army, the U. S. Air Force, and the Air Force Cambridge Research Center.

[1] D. Alpert, J. Appl. Phys. **24**, 860 (1953).

R2. Ambipolar Diffusion in a Magnetic Field. ALBERT SIMON, *Oak Ridge National Laboratory.*—Diffusion of ions in an arc plasma across a magnetic field is shown to be *not* ambipolar in character in most experiments. Owing to the highly anisotropic conductivity of the medium, the ions diffuse across the field at their own intrinsic rate. Space-charge neutralization is maintained by slight adjustment of the currents in the direction of the magnetic field lines. Previous experiments by Bohm, Burhop, Massey, and Williams[1] on calutron arcs had indicated a discrepancy of greater than 10^2 between the experimental diffusion coefficient and the coefficient calculated by the usual ambipolar theory. This discrepancy is now resolved and no additional mechanisms, such as plasma oscillations, need be postulated. Both an intuitive and formal proof of the effect will be presented.

[1] A. Guthrie and R. K. Wakerling, *The Characteristics of Electrical Discharges in Magnetic Fields* (McGraw-Hill Book Company, Inc., New York, 1949), NNES I-5, Chapter 9.

R3. A Possible Explanation of Moving Striations in Discharge Tube. SATOSI WATANABE AND NORMAN OLESON, *U. S. Naval Postgraduate School.*—It is theoretically shown that there can exist in the positive column a traveling wave of densities and electric field along the axis, superimposed on the average drift current and the well-known uniform ambipolar diffusion in the radial direction. The wavelength of this type of oscillations is given in the lowest approximation by $\lambda=(2\pi R/\mu)[1+a^2(Ee/kT)^2]$ and its propagation velocity is of the order of magnitude of the sound velocity of the neutral gas in the tube; R = tube radius, $\mu=2.4$, a = electronic Debye-Hückel radius, E = electric field, k = Boltzmann constant, T = electron temperature, and e = electronic charge.

R4. Cyclotron Resonance of Free Electrons in a Nitrogen Afterglow. R. V. JONES, W. DOBROWOLSKY, W. B. KUNKEL, AND C. D. JEFFRIES, *University of California, Berkeley.*—Nitrogen gas at a few mm pressure containing a trace of oxygen is pumped through a discharge into a TE_{011} mode cavity, which is the sensitive element of a paramagnetic resonance absorption spectrometer operating at 8600 mc/s. We observe simultaneously the paramagnetic resonance of atomic N in the ground state[1] and the cyclotron resonance of free electrons[2] produced by the self-ionization of active nitrogen. This provides a means of comparing the relative abundances of atoms and electrons, which should be useful for afterglow studies. Also the method is quite sensitive to electrons, densities down to 10^2 electrons/cc being detectable. The resonance line width is directly related to the mean collision time of the electrons in the gas, and varies from a few gauss at low pressures up to about 10^3 gauss at higher pressures and microwave powers. These results are in reasonable agreement with theory. We have not observed the paramagnetic resonance of atomic N metastable states. This research has been supported in part by the Research Corporation and the U. S. Atomic Energy Commission.

[1] M. A. Heald and R. Beringer, Phys. Rev. **96**, 645 (1954).
[2] J. W. Benson, J. App. Phys. **23**, 757 (1952).

R5. (Abstract withdrawn.)

R6. The Measurement of the Coefficient of Secondary Electron Emission with a Resonant Cavity. R. K. SMITHER, *Yale University.*—Under certain conditions a secondary electron-resonant discharge process occurs in the electrical field regions of a resonant cavity. If a dc field is added to the rf field in the discharge region a net flow of current is observed which can be related to the coefficient of secondary electron emission (δ). When the proper dc field is applied, the square of the coefficient of secondary emission is given by

$$\delta^2=1+\frac{2I_{dc}}{I_0},$$

where I_{dc} is the current supplied by the dc bias and I_0 is the current in the secondary electron resonance discharge. Since the measured quantities appear only in the difference between the square of the coefficient of secondary emission and one, it is possible to obtain good accuracy even when the coefficient is approximately one.

R7. Measurement of Low-Energy Electron Absorption in Metals and Insulators. E. J. STERNGLASS AND M. M. WACHTEL, *Westinghouse Research Laboratories.*—A direct method for studying the absorption of slow electrons in solids has been developed. Slow secondary electrons (~0–10 ev) are generated uniformly throughout deposits of 25, 50, and 100 A

±10 percent of Au and 1150, 2600, and 5200 A ±10 percent of KCl supported on a 120 A film of SiO, using 2–20 kev penetrating electrons. The ratio of the low-energy yields Δ measured at 14–20 kev on the exit side of layers of different thicknesses d gives the diffusion-length L of the slow electrons according to

$$\frac{\Delta_2}{\Delta_1}=\frac{1-\exp(-d_2/L)}{1-\exp(-d_1/L)}.$$

Taking ratios of yields minimizes possible surface effects. Simultaneous measurements of the transmitted primaries serve as check on thickness determinations and absence of pin-holes. For Au, the yield increases little with thickness, the ratio being $\leq 1.23\pm0.04$ for the two thinnest layers. This leads to $L\leq 18$ A, indicating that electrons capable of inelastic collisions can diffuse only a few atomic layers. In sharp contrast, the corresponding ratio for KCl is 1.71 ± 0.06, making $L=2300\pm600$ A and demonstrating long diffusion paths of slow electrons able to make only elastic collisions.

R8. Surface Recombination of Cadmium Sulfide. S. H. LIEBSON AND E. J. WEST, *United States Naval Research Laboratory*.—Increased surface recombination of photoconductive cadmium sulfide has been reported by Bube[1] for crystals in a humid atmosphere. Liebson[2] has observed a decrease in the red luminescence of cadmium sulfide in an atmosphere containing electronegative gases. We have measured this decrease in luminescence as a function of oxygen pressure from about 2×10^{-4} to approximately 500 mm Hg for crystals which were photoconductive and high impedance as well as those which were low impedance at room temperature. The results indicate a linear variation of the logarithm of the luminescence *vs* the pressure. Several interpretations are discussed based on the formation of an electric field at the surface due to electrons on chemisorbed oxygen.

[1] R. H. Bube, J. Chem. Phys. 21, 1409 (1953).
[2] S. H. Liebson, J. Electrochem. Soc. 101, 359 (1954).

R9. Cross Sections for the Characteristic Energy Loss of Electrons. LEWIS B. LEDER AND L. MARTON, *National Bureau of Standards*.—Previous measurements[1] of the characteristic energy losses of electrons in solids have been made primarily using photographic detection. We have now improved our apparatus so that we can measure absolute intensity relationships using a calibrated photomultiplier detector. The detector system consists of a phosphor coated glass window over a 1P21 photomultiplier. The multiplier signal is fed to a logarithmic amplifier the output of which is recorded on a Speedomax. The recorded signal is calibrated with a Faraday cage and quartz fiber electrometer. From these measurements we can determine the ratio of the elastic scattering to the characteristic scattering peak intensities as well as the differential cross sections for these events. The rectangular detector slit defines an acceptance angle of 10^{-3} radian in one direction and 10^{-4} radian at right angles. Thus the differential cross sections measured are given for a solid angle of $(10^{-3})^2$ or 10^{-6} steradian. At a primary energy of 30 kev the ratio elastic/characteristic for 400-A gold is 3.4 and for 100-A carbon is 7.4. The variation of these ratios and of the differential cross sections with thickness and primary energy will be given.

[1] L. Marton and L. B. Leder, Phys. Rev. 94, 203 (1954) (earlier references are given here).

R10. Angular Dependence of the Characteristic Energy Loss of Electrons Passing Through Metal Foils.* R. A. FERRELL, *University of Maryland*.—From the Bohm-Pines[1] electron plasma theory of metals, an electron of energy, E, upon passing through a metal foil of thickness t, excites a plasma oscillation of quantum energy ΔE and scatterers into the solid angle $d\Omega$, with probability $td1/\lambda=t/2\pi a_0\cdot\theta_E/\theta_E^3+\theta^2\cdot d\Omega$, where $\theta_E=\Delta E/2E$ θ = angle of scattering $\leq pc/(2mE)^{\frac{1}{2}}$, pc = cut-off momentum, and a_0 = Bohr radius. Although other mechanisms, such as atomic excitation, in general compete with plasma oscillations in producing characteristic energy losses, the angular dependence should identify the mechanism in any given case. For example, recent experimental measurements[2] of the angular distribution of 20-kev electrons scattered by 100 A gold foils show a peaking of the 24-ev loss at small angles ($<10^{-2}$ radian), in qualitative agreement with the expressions for $d1/\lambda$, but not easily interpretible in terms of atomic excitation, (which would give a broader angular dependence). Improvements in $d1/\lambda$ to allow for elastic scattering by the lattice will be discussed.

* Research supported by the Office of Naval Research.
[1] D. Bohm and D. Pines, Phys. Rev. 92, 609 (1953) and D. Pines, Phys. Rev. 92, 626 (1953).
[2] Marton, Simpson, McGraw, Mendlowitz, Mendlowitz, and Marton, Bull. Am. Phys. Soc. 30, No. 1, 29 (1955), abstracts LA2 and LA1.

R11. Mean Free Path for Discrete Electron Energy Losses in Metallic Foils. R. D. BIRKHOFF, A. W. BLACKSTOCK,* AND R. H. RITCHIE, *Oak Ridge National Laboratory*.—The discrete energy losses observed when a beam of electrons passes through a thin foil have been studied as a function of incident energy. Foils of Al, Mg, and Cu ranging in thickness from 14 to 85 $\mu g/cm^2$ have been bombarded with electrons of energies 25 to 115 kev. Losses appear at multiples of 14.9 ev and 10.7 ev, respectively, for Al and Mg whereas only one loss is found in Cu at 22.6 ev. Mean free paths for the losses lie in the range 25 ± 10 $\mu g/cm^2$, 165 ± 55 $\mu g/cm^2$, and 90 ± 30 $\mu g/cm^2$ for the three metals. The magnitudes of the losses agree with the plasma oscillation theory of Pines and Bohm for Al and Mg if the number of free electrons per atom is chosen about equal to the valence. In addition the mean free path as a function of energy for Al agrees closely with the theoretical curve.

* Oak Ridge Institute of Nuclear Studies Fellow from North Carolina State College.

FRIDAY AFTERNOON AT 2:00

Caribar Room

(L. I. SCHIFF presiding)

Theoretical Physics III, Mainly Nuclear Theory

RA1. On the Imaginary Part of the Potential in the Optical Model of the Nucleus. A. M. LANE AND C. F. WANDEL, *M.I.T.* (introduced by V. F. Weisskopf).—The dependence of the imaginary part of the "Weisskopf" potential on the neutron bombarding energy is calculated by an extension of the semiclassical method of Goldberger.[1] The nucleus is described by the statistical model. Using the nucleon-nucleon experimental cross section, and taking the Pauli exclusion principle into account, we calculate an effective total cross section in nuclear matter. The Pauli principle is assumed to forbid colli-

sions which do not bring both particles outside the Fermi momentum sphere in momentum space. Assuming an analytic expression ($1/E$ law) for the nucleon-nucleon cross section, the integrations over the Fermi distribution can be carried out in closed form. Given the effective cross section, a mean-free path and an imaginary potential can be computed. Despite the crude model used, a good fit with experimentally determined imaginary potentials is obtained. In the range from 0 to 100 Mev bombarding energies $|V_{im}|$ increases from 2 to 11 Mev. This, we believe, confirms the importance of the Pauli principle in explaining the long mean free path inside nuclear matter at low energies.[3]

[1] M. L. Goldberger, Phys. Rev. **74**, 1269 (1948).
[2] V. F. Weisskopf, Science **113**, 101 (1951).

RA2. Nuclear Oscillator Potential. D. C. PEASLEE, *Purdue University.*—Some consequences are considered of constructing an effective harmonic oscillator well to fit the single-particle interpretation[1] of the photonuclear "giant resonances." Consistency with 0–4-Mev neutron scattering on the optical model with $r_0 \approx 1.2\times10^{-13}$ cm implies an effective nucleon mass in the nucleus of order $M^* \sim \frac{1}{4}M$. The depth of the corresponding effective parabolic well approaches 200 Mev. Under these conditions, the Thomas (relativistic) term is sufficient to account for the spin-orbit splitting in the shell model, which then has no direct relation to polarization effects in high-energy scattering. The value $g_L \approx 1$ for protons in nuclei indicates that the velocity-dependent forces responsible for M^* involve only the radial momentum component, for which a plausibility argument can be given.

[1] D. H. Wilkinson, Bull. Am. Phys. Soc. **30** (1), 25 (1955), paper IA4.

RA3. Collective Modes in Nuclei. F. COESTER, *State University of Iowa.*—The Hamiltonian of the "unified model" of Bohr[1–3] and Mottelson[2] has been derived from many-particle quantum mechanics. A point transformation in the configuration space of the N nucleons of the core introduces 6 collective coordinates describing the size and shape of the nucleus and $3N-6$ internal coordinates. It is assumed that the wave function Ψ of the nucleus for the ground-state and the low-lying excited states can be approximated by the product $\Psi_0\Phi$ where Ψ_0 depends only on the internal coordinates of the core and Φ depends on the collective coordinates of the core and the coordinates of the external nucleons. $\Psi_0\Phi$ is treated as a trial function in the Schrödinger variational principle. For fixed Ψ_0 this yields a Schrödinger equation for Φ. The Hamiltonian in this equation is the Hamiltonian of Bohr and Mottelson plus certain correction terms. Ψ_0 influences the values of the constant parameters occurring in this Hamiltonian, but not its structure.

[1] A. Bohr, Kgl. Danske Videnskab. Selskab, Mat.-fys. Medd. **26**, No. 14 (1952).
[2] A. Bohr and B. R. Mottelson, Kgl. Danske Videnskab. Selskab, Mat.-fys. Medd. **27**, No. 16 (1953).
[3] A. Bohr, thesis, Copenhagen (1954).

RA4. The Variational Approach to Collective Nuclear Behaviour. JAMES J. GRIFFIN, *Princeton University.*—A "temporary potential" is assumed, the shape of which depends upon one or more deformation coordinates. The wave equation is solved for a fixed value of the deformation. The wave function is multiplied by an arbitrary function of deformation and integrated over deformation. The resultant pure n-particle wave function is used to evaluate the expectation value of the energy of the system. The integrations over particle coordinates are performed explicitly. The resultant energy is a function of the undetermined deformation weighting function. The condition of minimum energy determines a wave equation (integral equation) for this "collective wave function."[1] The kernels in the collective wave equation have been evaluated in special instances of a single deformation coordinate, and will be discussed. Their form suggests comparison with a simplified problem where the kernel is the product of a quadratic function with a Gauss function. This comparison allows one to estimate a decrease of the order of ~2 Mev in the ground-state energy as a result of allowing a fluctuation in deformation (collective vibration) as compared with the conventional treatment with fixed deformation and fixed potential.

[1] David L. Hill and John A. Wheeler, Phys. Rev. **89**, 1102 (1953).

RA5. Coupling of $2s_{\frac{1}{2}}$ and $1d_{\frac{1}{2}}$ Orbitals. P. GOLDHAMMER AND E. FEENBERG, *Washington University.**—Coupling between $2s_{\frac{1}{2}}$ and $1d_{\frac{1}{2}}$ nucleon orbitals through the mediation of surface waves has been investigated in the mass range 29 to 37. A single nucleon description appropriate for $_{14}Si_{15}$ and $_{15}P_{14}$, and a three nucleon description with $T=\frac{3}{2}$ appropriate for $_{16}Si_{17}$ and $_{17}Cl_{20}$ (3 proton holes) have been treated by the intermediate coupling procedure considering only states with 0, 1, and 2 surfons. $(2s_{\frac{1}{2}})^2(1d_{\frac{1}{2}})^1$, $(2s_{\frac{1}{2}})^1$ $(1d_{\frac{1}{2}})^2$, and $(1d_{\frac{1}{2}})^3$ configurations are coupled in the three nucleon systems. $M1$ transition matrix elements between $I=\frac{1}{2}^+$ and $I=\frac{1}{2}^+$ are small, but not "l-forbidden" as they are for pure $1d_{\frac{1}{2}}\rightarrow 2s_{\frac{1}{2}}$ transitions. The "l-forbidden" $\frac{1}{2}^+\rightarrow\frac{1}{2}^+$ G.T. matrix element in the decay $_{15}P_{14}\rightarrow{}_{14}Si_{15}$ has the value 0.026 (experimental value 0.040).† The correction to the $\mu_{\frac{1}{2}}$ Schmidt moment in $_{14}Si_{15}$ is about one half the experimental deviation; while the correction to the $\mu_{\frac{1}{2}}$ Schmidt moment for $_{17}Cl_{20}$ is 0.788, compared to 0.552 observed. Quadrupole moments appear too large by a factor of three. Similar calculations for three nucleon systems with $T=\frac{1}{2}$ yield results applicable to $_{15}P_{16}$ and $_{18}A_{19}$.

* Assisted in part by the joint program of the Office of Naval Research and the U. S. Atomic Energy Commission.
† Roderick, Lönsjö, and Meyerhof, Phys. Rev. **97**, 97 (1955).

RA6. Intermediate Coupling in the $1p$ Shell. DIETER KURATH, *Argonne National Laboratory.*—Since neither the LS or the jj limit of the independent particle model provides a satisfactory picture for nuclei in the region between He^4 and O^{16}, it is of interest to see whether spin-orbit coupling of intermediate strength can explain the observation. A calculation has been made including all possible configurations within the $1p$ shell using the Argonne electronic digital computer (AVIDAC). The strength of spin-orbit coupling is taken from O^{16}, N^{16} where the $1p_{\frac{1}{2}}-1p_{\frac{3}{2}}$ splitting is about 6.3 Mev. The two-body interaction used is the central force mixture of 0.8 Majorana and 0.2 Bartlett with an inverted Gaussian spatial dependence. Energy levels, magnetic moments, and quadrupole moments will be presented.

RA7. Particle States in a Spheroidal Potential.* STEVEN A. MOSZKOWSKI, *University of California.*—To study the effect of deviations from sphericity on nuclear energy levels and wave functions, some spheroidal potentials have been considered, especially that of a spheroidal box (axes $D^{-\frac{1}{3}}R_0$, $D^{-\frac{1}{3}}R_0$, DR_0). For this case, define $x'=D^{\frac{1}{3}}x$, $y'=D^{\frac{1}{3}}y$, $z'=D^{-\frac{2}{3}}z$. In the primed coordinate system, the difference between this spheroidal box and a spherical one with the same R_0, wave functions $\psi_i(\mathbf{r})$ and energies E_i is a change in the *kinetic* energy, for which matrix elements, taken between zero order states $\psi_i(\mathbf{r}')$ are easily computed. The resulting secular equation reads: $(E-E_i')\psi_i(\mathbf{r}')=\Sigma_k H_{ik}\psi_k(\mathbf{r}')$ where $3E_i'=(2D+D^{-2})E_i$. $3H_{ik}\cong -2(D-D^{-2})\,|P_2(\theta)|_{ik}E_i$, if i and k are in the same major shell and is small otherwise. This method was used to calculate energy levels of a spheroidal box, both without and with an additional spin-orbit term of essentially the form $k\boldsymbol{\sigma}\cdot\mathbf{l}$. For more general spheroidal potentials $V(r')$ which increase monotonically with r' and which are reasonably flat for small r', the above results still hold approximately with the following modifications: In $\psi_i(\mathbf{r}')$, E_i' and H_{ik}, D is replaced by D^f, where f is the ratio of kinetic energy to total energy, measured from the bottom of the well.

* Work partially supported by the Office of Naval Research and the Office of Ordnance Research.

RA8. Nuclear Forces and the Beta Decay of C^{14}.* WILLIAM M. VISSCHER AND RICHARD A. FERRELL, *University of Maryland.*—The long C^{14} lifetime, apparently in contradiction with beta-decay theory (allowed Gamow-Teller transition), and with the experimentally observed allowed spectrum,[1] can be accounted for by a sufficiently large admixture of tensor force, as has been shown by Talmi and Jancovici.[2] We find that there is a wide range of values of the nuclear force parameters for which the beta-decay matrix element, calculated using harmonic oscillator p-state wave functions and Gaussian potentials, is arbitrarily small. Parameters chosen to vary were tensor force strength and range, and spin-orbit strength. The results, fairly insensitive to tensor force range, require that the tensor strength be roughly proportional to the spin-orbit strength. Large or small values for both are permitted. The spin-orbit strength indicated by experiment corresponds to a tensor force strong enough to cause a considerable mixing of d-configuration, whose effect on the beta lifetime may be calculated, leading to a corrected relation between the force parameters.

* Supported by the Office of Naval Research.
[1] A. Moljk and S. C. Curran, Phys. Rev. **96**, 395 (1954).
[2] B. Jancovici and I. Talmi, Phys. Rev. **95**, 289 (1954).

RA9. Interaction Contribution to Nuclear Isomerism. A. ROTENBERG AND L. SPRUCH, *New York University.*—It has been observed[1] that certain magnetic dipole transitions offer the possibility of distinguishing between the effects of interaction moment operators and of impure wave functions, but at that time[1] only a few estimates of transition lifetimes were available. Many accurate measurements have since been made of the lifetimes of so-called forbidden magnetic dipole transitions and also of a few lifetimes which seem to be forbidden magnetic octupole transitions. Transition probabilities were calculated using the shell model and interaction moment operators. In the dipole case, the operators considered were the three used in a phenomenological analysis of magnetic moment data,[2] only one of which gives a nonvanishing contribution. In the octupole case, the operator was obtained by an extension of a calculation performed by Villars and Weisskopf.[3] The calculations indicate that it is possible to explain most of the data on the Mayer model, which is a desirable feature for those transitions not readily explainable on a Bohr-Mottelson model.

[1] M. Ross, Phys. Rev. **88**, 935 (1952).
[2] A. Russek and L. Spruch, Phys. Rev. **87**, 1111 (1952).
[3] F. Villars and V. F. Weisskopf (unpublished).

RA10. Theoretical Results on Orbital Capture. H. BRYSK AND M. E. ROSE, *Oak Ridge National Laboratory.*—A detailed survey of the theory of orbital capture has been carried out. Transition probabilities for the K-shell and all three L-subshells have been examined for all orders of forbiddenness through second-forbidden, using wave functions corrected for the finite size of the nucleus and the effect of screening, and considering the variation in the wave functions over the nuclear volume (Oak Ridge National Laboratory 1830). Some of the conclusions that can be drawn are: The L_I/K branching ratio agrees with Rose and Jackson's values, and is independent of the order of forbiddenness provided that the neutrino energy is large compared to the difference in binding energy between the two shells. The effect on the L_I/K capture ratio of nonadiabatic electron transitions is unimportant. The p-electron contribution to orbital capture becomes dominant for low-energy transitions involving an angular momentum change of two or more. Angular correlations exist among the electromagnetic radiations associated with orbital capture (inner bremsstrahlung photon, atomic x-ray, gamma ray from an excited daughter nucleus) (Oak Ridge National Laboratory 1862). In most cases of interest, however, there is isotropy. In fact, the conditions required for the observation of anisotropy are at present experimentally unattainable.

RA11. Nuclear Charge Distribution in Pb^{208}.* DAVID L. HILL AND BURTON E. FREEMAN, *Los Alamos Scientific Laboratory,* AND KENNETH W. FORD, *Indiana University.*—The cross section according to the exact Dirac-Darwin-Mott theory for the elastic scattering of fast electrons from various conceivable spherically symmetric nuclear charge distributions has been evaluated accurately and compared with recent Stanford data taken at 83, 153, and 186 Mev with a Pb^{208} target. We find that the data can be fit within the limits set by experimental uncertainties, and that the same charge distribution gives the best fit at each energy. This charge distribution has a radial dependence given by $1-\frac{1}{2}\exp[-n(1-x)]$ for $x=(r/R)\leq 1$ and given by $\frac{1}{2}\exp[-n(x-1)]$ for $x\geq 1$, with $n=10$, and $R=6.7\times 10^{-13}$ cm. Appreciable peaking of the charge distribution either at the center or surface of the nucleus evidently does not exist. The value of R here found agrees within 1 or 2 percent with the value earlier determined[1] by an analysis of mu-mesonic x-ray data. Radiative corrections omitted in this analysis of electron scattering probably are unimportant in determining the charge distribution, and corrections for inelastic scattering are negligible in Pb^{208}. The analysis indicates a high degree of determination for the nuclear charge distribution as the experimental data becomes more complete.

* Work done under the auspices of the U. S. Atomic Energy Commission.
[1] D. L. Hill and K. W. Ford, Phys. Rev. **94**, 1617 (1954).

RA12. Validity of Deformation-Potential Theory in N-Type Ge. R. ROSENBERG* AND M. LAX, *Syracuse University.*—The Bardeen-Shockley deformation-potential theory, based on a model of spherical energy surfaces about the origin of the Brillouin zone, predicts electron scattering only by the long-wavelength longitudinal acoustic modes of lattice vibration. In N-type Ge, however, the multi-ellipsoid model of energy surfaces applies, and the electron is scattered by all three acoustic branches and by the three optical branches of the vibrational spectrum. Moreover, the electron can make "intra-ellipsoid" and "inter-ellipsoid" transitions. The present analysis of electron-lattice scattering employs an interaction Hamiltonian which is a linear form in the displacements of the lattice particles from their equilibrium positions. The properties of the coefficients of the particle displacements are determined from the symmetry group of the crystal. Seven matrix elements of the linear form (one of which is E_1, the constant appearing in deformation-potential theory) are required to specify electron-lattice scattering processes in N-type Ge, on the assumption that the energy minima occur near the boundary of the Brillouin zone. Symmetry arguments are used to reduce this number. N-type Si is also discussed.

* This work was supported in part by the Office of Naval Research, and constitutes part of a Ph.D. thesis in preparation at Syracuse University.

RA13. Dynamics of the Klein Particle. DAVID FINKELSTEIN, *Stevens Institute of Technology and New York University.*—A notion of a covariant rigid localized system has been defined.[1] It has been shown that all such can be obtained by imposing covariant constraints upon a particular covariant system of six degrees of freedom which is due to F. Klein.[2] The previous discussion was limited to the kinematics of these systems. Now the classical and quantum dynamics will be treated. Two choices of action integral will be presented. The first action is chosen with an eye to obtaining a Dirac-like particle as one of the spin states of the Klein particle, and is linear in the velocity. The second action is mathematically more natural, being merely the arc length on the configuration space, but this leads to a nonlocal wave equation for the quantized particle. For the present purposes, the canonical quantization procedure is adequate.

[1] D. Finkelstein, Bull. Am. Phys. Soc. **30**, No. 1, 36 (1955), abstract OA5.
[2] F. Klein, *The Mathematical Theory of the Top* (Princeton University Press, Princeton, New Jersey, 1896).

RA14. Elementary Particle Models. T. F. MORRIS, *McGill University.*—Theories of elementary particles are investigated, which are characterized by the existence of an incompatibility between mass and space-time position measurements. Several mass operators with positive definite spectra have been obtained. In momentum space the wave function is easily decomposed into components which transform according to various representations of the inhomogeneous Lorentz group. Hence the quantization of the theory is straightforward. Although the introduction of subsidiary variables, similar to those used by Yukawa, is necessary, the interpretation remains within the scope of local fields. Several types of interaction are considered.

RA15. Certain Matters Pertaining to the Internal Structure of Nucleons.* W. F. G. SWANN, *Bartol Research Foundation.*—In 1948, the writer[1] criticized the statement that the mass-energy relation for rest mass is contained in the restricted theory of relativity. It was shown that the statement could be validated by regarding each nucleon as composed of a very large number of subparticles of negligible rest mass, moving with velocities very nearly equal to the velocity of light. In the present paper, the foregoing idea is crystalized into more concrete form by assuming that the motions of the subparticles are axially symmetrical within a nucleon. The discussion then pertains to the elements involved and the mathematical possibilities open in providing for the spin characteristics of the various nucleons. Finally, insofar as the macroscopic concept of a potential energy V for the forces between nucleons turns out to be $\Sigma_i M_{0i}c^2$, where M_{0i} is the rest mass of the ith nucleon in the configuration to which V applies, a discussion is made of the possibilities as regards ultimate forces, between the subparticles, necessary to provide for the correlation between V and $\Sigma_i M_{0i}c^2$ consistent with experience.

* Assisted in part by the joint program of the Office of Naval Research and the U. S. Atomic Energy Commission.
[1] Phys. Rev. **74**, 202 (1948).

FRIDAY EVENING AT 7:00

Sheraton Park, Continental Room

(R. T. BIRGE presiding)

Banquet of the American Physical Society

After-dinner speakers: R. W. G. Wyckoff and John von Neuman

SATURDAY MORNING AT 9:30

Exhibit Hall I

(S. W. BARNES presiding)

Mesons, I

S1. Electromagnetic Production of μ Mesons.* G. E. MASEK, A. J. LAZARUS, AND W. K. H. PANOFSKY, *Stanford University.*—We have made measurements on the yield of negative μ mesons emitted from a $\frac{1}{4}$-radiation-length copper target at 10° and 30° to an incident 550-Mev electron beam. The angle of emission and the momentum of the mesons are selected by a magnet system. Various absorbers give a maximum rejection of μ^- from π^- decay in flight and the μ^-'s from electromagnetic production are stopped above a triple-coincidence counter telescope. The decay electrons are counted with the telescope through delayed electronic gates. If it is assumed, and it has been verified, that the π production is substantially isotropic, then any large difference from isotropy between 10° and 30° is attributed to μ-pair production. The purely electromagnetic (including nuclear-size effect) cross sections for a single member of the μ pair have been calculated at 10° and 30° by Rawitscher[1] to be $d^2\sigma/d\Omega dT_\mu = 2.1\times10^{-28}$ cm²/(sterad ×Mev×equivalent quanta) at 10°, and 550-Mev bremsstrahlung and 225-Mev meson kinetic energy. (For 30° the cross section is 1/50 of this.) Our results show that the experimental cross section is not larger than and might be compatible with this number.

* Supported by the Office of Naval Research and the U. S. Atomic Energy Commission.
[1] G. Rawitscher, Bull. Am. Phys. Soc. **29**, No. 8, 24 (1954), abstract O6.

S2. μ−e Decay Spectrum.* R. H. HELM, K. M. CROWE, AND G. W. TAUTFEST, *Stanford University.*—The preliminary analysis of an experiment on the μ–e decay spectrum has yielded data which seem to be relatively simple to interpret. Delayed positrons from the $\pi^+\to\mu^+\to\beta^+$ decay in a Li or C target in the 500-Mev bremsstrahlung beam are magnetically analyzed by a 180° point-focusing spectrometer and counted by a thin-crystal telescope. The maximum positron energy occurs at a field of 4500 gauss. The net resolution is observed to be 4–10 percent full width at half-maximum, depending on the size of targets and detectors, and arising mainly from energy loss of positrons leaving the target. The spectrum obtained is being analyzed in terms of the ρ parameter introduced by Michel.[1] The best value of ρ is 0.55 ± 0.10. The stated error is divided among: our statistics, the resolution (which is currently being recomputed), and systematic uncertainties (background, etc.). This value is in agreement with a number of other measurements of roughly the same accuracy, but is inconsistent with the extremely accurate values reported by Sagane *et al.*[2]

* Supported by the Office of Naval Research and the U. S. Atomic Energy Commission.
[1] L. Michel, Proc. Phys. Soc. (London) **A63**, 514 (1950).
[2] Sagane, Dudziak, and Vedder, Phys. Rev. **95**, 863 (1954).

S3. Mesonic Decay of an Ejected Triton. HERMAN YAGODA, *National Institutes of Health.*—A heavy fragment is ejected from a star of type $21+5p$ which decays at rest into three charged particles. Gap counts indicate that the excited fragment is singly charged and heavier than a proton. The mass of the particle, as estimated by constant sagitta scattering along its range of 1330 microns, is 2.93 ± 1.36 proton masses. All three secondary particles terminate their range, and one of them can be identified as a negative pi meson of 26.6 ± 0.9 Mev kinetic energy. Two short recoil tracks, if assumed to be protons, have kinetic energies of 1.43 ± 0.04 and 2.31 ± 0.15 Mev, respectively. Momenta balances applied to several decay schemes suggest that the event probably represents $H^{3*}\rightarrow H^1+H^1+n^0+\pi^-+Q=31.5\pm1$ Mev. The binding energy of the excited triton, 5.4 ± 1 Mev, is found to be less than that of the normal triton (8.48 Mev). The time of flight of the particle is 4.2×10^{-11} sec. The event was recorded in a G-5 emulsion, 1500 microns thick, exposed to cosmic radiation in the stratosphere. This example of the mesonic-decay of a "*V*-triton" is in close agreement with theory.[1]

[1] W. Cheston and H. Primakoff, Phys. Rev. **92**, 1541 (1953).

S4. Cross Section for $p+p\rightarrow\pi^++p+n$.* D. STORK AND S. WHETSTONE, *University of California, Berkeley.*—The 0° cross section for $p+p\rightarrow\pi^++p+n$ (1) has been measured as a function of pion energy for protons of energy 338 Mev. The pions were detected in flight by means of scintillation-counter, pulse-height techniques. A combination of quadrupole and wedge magnetic focusing provided a pion energy resolution of ±0.7 Mev. With a spread of proton beam energy of ±1.2 Mev the pion energy continuum of reaction (1) was separated from the peak caused by the reaction $p+p\rightarrow\pi^++d$ (2). The ratio of the total cross sections $(d\sigma/d\Omega)$ for reactions (1) and (2) is in good agreement with the Watson-Brueckner phenomenological theory.[1] However, the shape of the energy spectrum of reaction (1) shows a considerable deviation from that given by the phenomenological theory for *P*-wave pions and a final two-nucleon *S*-state.[2]

* This work was performed under the auspices of the U. S. Atomic Energy Commission.
[1] K. M. Watson and K. A. Brueckner, Phys. Rev. **83**, 1 (1951).
[2] A. H. Rosenfeld, Phys. Rev. **96**, 139 (1954).

S5. π^+/π^- Ratios Produced by 340-Mev Protons at 0°. J. E. CAROTHERS AND C. G. ANDRE,* *University of California.*—The π^+/π^- ratio has been measured for several elements at 0° to the 340-Mev proton beam of the Berkeley cyclotron. The detection scheme and the ratios obtained for deuterium have been described in a previous letter.[1] The most important feature of the detection scheme is that it allows a direct comparison of the positive and negative yield. A magnetic field separates the mesons from the proton beam and separates the different charges. When the field is reversed, particles of the opposite sign are counted by the detectors. The ratios obtained

TABLE I.

Energy (Mev)	$D(\pi^+/\pi^-)$	$He(\pi^+/\pi^-)$	$Be(\pi^+/\pi^-)$	$C(\pi^+/\pi^-)$	$Pb(\pi^+/\pi^-)$
30	5.8 ± 2.5	3.4 ± 2.2	4.3 ± 1.2	4.5 ± 1.6	0.83 ± 0.6
60	22.1 ± 3.5	10.8 ± 2.1	9.2 ± 1.2	10.9 ± 1.6	1.7 ± 1.0
120		35.1 ± 18.3	12.7 ± 1.8	14.5 ± 1.9	6.7 ± 3.2

* Now at Calvin College, Grand Rapids, Michigan.
[1] J. Carothers and C. G. Andre, Phys. Rev. **88**, 1426 (1952).

are listed in Table I. The energies listed are those accepted by the magnetic channel. The large errors are the result of the very low π^- production, which lead to low counting rates.

S6. Pion Production by Neutrons on Helium.* PETER H. MOULTHROP, *University of California, Berkeley.*—A helium-filled 36-atmosphere diffusion cloud chamber in a pulsed 21 000-gauss magnetic field was operated in the 300-Mev neutron beam of the 184-inch cyclotron. Two hundred and ninety five negative pions were found. The dominant reactions were $\alpha(n,p\pi^-)He^3$ and $\alpha(n,d\pi^-)He^3$, each contributing about 30 percent to the total cross section for negative pion production. The reaction $\alpha(n,p\pi^-)\alpha$ contributed less than 10 percent. Partial cross sections, energy, and angular distribution data will be presented.

* This work was performed under the auspices of the U. S. Atomic Energy Commission.

S7. Pion Production from Hydrogen by 600-Mev Electrons.* W. K. H. PANOFSKY AND G. B. YODH, *Stanford University.*—The ratio of bremsstrahlung-produced to electron-produced pions from hydrogen has been measured using a liquid-hydrogen target. Pions of 55 and 75 Mev at 75° to a 600-Mev electron beam were observed. The data have been reduced to "effective radiation lengths" for electron-pion production, X_e, which is the thickness of a fictitious radiator that would double the yield with electrons directly. The results are $X_e=0.0256\pm0.0030$ and $X_e=0.0199\pm0.002$ at pion energies of 55 and 75 Mev, respectively. The results are consistent with either electric-dipole or magnetic-dipole absorption.

* Supported by the Office of Naval Research and the U. S. Atomic Energy Commission.

S8. π^+ Photomeson Production at 143°. R. STEPHEN WHITE, MARK J. JAKOBSON, AND GORDON W. REPP, *University of California, Berkeley.*—Liquid hydrogen and deuterium targets have been bombarded by the bremsstrahlung from the Berkeley synchrotron; π^+ mesons were observed at 143° to the beam. The detection of π^+ mesons was by means of a coincidence between the stopping π^+ meson and the positron from the μ^+ meson decay in a single plastic crystal. For thin absorbers (low-energy mesons) pulse-height analysis was done on the π^+-meson pulse. Absolute cross sections were obtained with the help of emulsions exposed to $\pi^\pm$ mesons from deuterium. The excitation function at 143° for π^+-meson production from hydrogen and deuterium-hydrogen ratios will be given. The data will be compared to those of other laboratories and with theoretical predictions.[1] This work was performed under the auspices of the U. S. Atomic Energy Commission.

[1] Geoffrey F. Chew, Phys. Rev. **95**, 1669 (1954).

S9. Neutral Photomesons from Hydrogen.* F. E. MILLS† AND L. J. KOESTER, JR., *University of Illinois.*—Total cross sections for the photoproduction of π^0 mesons in hydrogen have been measured from threshold to 240 Mev. One of the π^0-decay γ rays from a liquid-hydrogen target was detected in a scintillation-counter telescope. The detection efficiency of this telescope was calculated by a Monte Carlo method. Counting rates at laboratory angles of 84° and 130° were measured as the betatron energy was varied in 10 Mev steps. Analysis of these data by the photon difference method yields the cross sections for production of decay γ rays. The kinematics of the decay process establish relations between these γ-ray cross sections and the π^0 cross sections. In this energy range, the 84° γ-ray cross section proves to be a measure of the π^0 total cross section. An $S-P$ interference term is indicated by the comparison between the 84° and 130° γ-ray cross sections. These results will be compared with other experiments and with theory.

* Supported in part by the Office of Naval Research and the U. S. Atomic Energy Commission.
† Now at Cornell University, Ithaca, New York.

S10. Neutral Photomesons from Hydrogen.* L. J. KOESTER, JR., *University of Illinois.*—Differential cross sections for the reaction $h\nu+p\rightarrow\pi^0+p$ have been measured for incident photon energies between 180 and 215 Mev and around 280 Mev. The recoil protons from a liquid-hydrogen target were detected in nuclear emulsions. The c.m.s. angle of the π^0 was 135° at the lower energies and 110° at 280 Mev. By comparison with

measured total cross sections (preceding abstract) the 135° cross sections indicate a backward asymmetry in the angular distribution which can be explained as interference between S- and P-waves. The magnitude of the interference term agrees with results of Watson's analysis[1] and of the Chew-Low theory.[2]

* Supported in part by the Office of Naval Research and the U. S. Atomic Energy Commission.
[1] K. M. Watson, Phys. Rev. **95**, 228 (1954).
[2] G. F. Chew and F. E. Low (private communication).

S11. Neutral Meson Photoproduction at Forward Meson Angles.* DALE R. CORSON, *Cornell University*, AND WILLIAM S. MCDONALD AND VINCENT Z. PETERSON, *California Institute of Technology*.—The recoil protons from cold, high-pressure hydrogen gas exposed to the 596-Mev bremsstrahlung of the CalTech synchrotron have been detected in C-2 600 micron emulsions placed within the target chamber. The minimum detectable proton energy is 5 Mev. Pairs of emulsions on opposite sides of the beam were used to minimize errors in beam centering. Range and angle with respect to the beam are measured, the angle being a sensitive measure of the photon energy. Most background tracks may be eliminated by measurement of dip angle. The net background correction, estimated from protons beyond the maximum recoil angle (71°), is 5 percent. Preliminary measurements yield the following cross sections (center of mass) for the reaction $\gamma+P\rightarrow P+\pi^0$:

Photon energy	θ_π (cm)	$(d\sigma/d\Omega)$ (μb/sterad)
260–340 Mev	45°–60°	14.6 ± 2.3
260–340 Mev	26°–45°	9.3 ± 2.0
340–420 Mev	26°–45°	9.2 ± 2.1
420–500 Mev	26°–37°	3.8 ± 2.0

An extrapolation of the data of Oakley and Walker[1] at larger meson angles, using their angular distribution coefficients, is consistent with the present data.

* This work was supported in part by the U. S. Atomic Energy Commission.
[1] D. Oakley and R. Walker, Phys. Rev. (to be published).

S12. A Search for the Photoproduction of Meson Pairs in Hydrogen.* M. SANDS, M. BLOCH, J. G. TEASDALE, AND R. L. WALKER, *California Institute of Technology*.—An attempt has been made to detect negative mesons from the interaction of photons with hydrogen. The existence of negative mesons would imply meson pair production. Mesons produced in a high-pressure hydrogen target by the 500-Mev bremsstrahlung of the CalTech synchrotron were detected by the magnet spectrometer used for other measurements.[1] Accidental coincidences and the electron background were reduced by adding a third counter to the detection apparatus and requiring 3-fold coincidences. Measurements at 73° with respect to the photon beam and using a meson energy window about 10-Mev wide at 47 Mev gave a negative meson intensity for hydrogen $(1.5 \pm 0.3) \times 10^{-4}$ of the intensity of positive mesons of the same energy. Most of the negative mesons were absent in measurements repeated with a 375-Mev bremsstrahlung beam. Lacking further measurements, this number must be considered an *upper bound* for the negative meson intensity. Measurements made at laboratory angles of 30° and 104° will also be reported.

* Supported in part by the U. S. Atomic Energy Commission.
[1] Walker, Teasdale, and Peterson, Phys. Rev. **92**, 1090 (1953).

SATURDAY MORNING AT 9:30

Main Ballroom

(A. M. WEINBERG presiding)

Apparatus of Nuclear Physics, I

T1. Four-Pole Permanent-Magnet Rings for Focusing Beams of Charged Particles.* J. P. BLEWETT, N. C. CHRISTOFILOS, AND A. M. VASH, *Brookhaven National Laboratory*.—The transverse-gradient magnetic-field pattern necessary for alternating gradient focusing of beams of charged particles can be set up inside a cylinder of permanent magnet material by using suitable procedures for magnetization. Gradients of about 800 gauss per cm have been achieved with good linearity in cylinders having an inside diameter of one inch. The present work is aimed at a focusing system for a proton linear accelerator. An approximate analysis of the field pattern to be expected in a cylinder having given magnetic properties indicates that higher gradients should be attained when the four-pole magnetizing system is inside rather than outside the cylinder. It indicates, moreover, that the attainable field gradients using materials of the Ferroxdur, Indox, or Ferrimag class should be materially higher than those reached with Alnico V or Cunico. Both of these predictions have been verified by experiment. The fields are examined by rotating the cylinder about its axis and observing the output of a fixed search-coil. Harmonic analysis of the search coil output permits a study of the various nonlinear terms and an evaluation of the displacements of the magnetic axis from the geometrical axis of the cylinder.

* Work carried out under contract with U. S. Atomic Energy Commission.

T2. Nonlinearities in the Alternate-Gradient Synchrotron.* E. D. COURANT, *Brookhaven National Laboratory*.—The equations of motion in an alternating-gradient accelerator necessarily contain nonlinear terms. One may hope that these will ameliorate the effect of the resonance instabilities predicted by the linear theory[1]; one may also fear that the nonlinearities will introduce further instabilities. Numerical computations have been performed on the UNIVAC for a variety of nonlinear problems. It is found that stable equilibrium orbits generally exist, whether or not the corresponding linear problems are stable. If the parameters of the problem are slowly varied during the course of the computation these equilibrium orbits move. The particles generally follow the equilibrium orbits, but under certain conditions they jump from the region of influence of one equilibrium orbit to another; if the nonlinearity is too strong the motion may even become completely unstable. These jumps can be correlated with the resonances of the linear theory. It appears doubtful whether nonlinearities can permit the machine designer to ignore any of the resonances; on the other hand, moderate nonlinearities do not appear to give rise to any deleterious effects not predicted by the linear theory.

* Work carried out under contract with U. S. Atomic Energy Commission.
[1] E. D. Courant, Phys. Rev. **91**, 456A (1953).

T3. Design Studies for Alternating-Gradient Magnets. Part I: Field Distributions Computed by the Relaxation Method.* M. HILDRED BLEWETT, *Brookhaven National Laboratory*.—The magnet for an alternating-gradient proton synchrotron must produce a field with a uniform gradient over an aperture

determined by the possible excursions of the particles and should use as little steel as possible. At the same time, saturation effects should appear at as high fields as possible. As a guide in the design of the Brookhaven 25-Bev proton synchrotron, a number of relaxation studies have been made of the field patterns around and in the steel, and in the exciting coils, for a variety of possible magnet configurations. The computed field patterns have indicated several possible modifications in magnet and coil geometry to improve magnet efficiency. In making relaxation computations, with the rather complex boundary conditions necessary for a high-gradient magnet, the ordinary methods involving computation of a vector potential have been found to yield insufficient accuracy in the derived field gradient. A modified potential function has been developed which reduces the computational labor and from which gradients can be computed to better than 1 percent accuracy for magnet-pole contours of arbitrary shape. Conclusions from these studies are being tested on model magnets.

* Work carried out under contract with U. S. Atomic Energy Commission.

T4. Design Studies for Alternating-Gradient Magnets. Part II: Model Measurements.* GLEN R. LAMBERTSON,† C. LASKY, AND ROBERT H. PHILLIPS, *Brookhaven National Laboratory.*—Measurements have been made of the dc fields of alternating-gradient synchrotron magnet models of *C*-type configuration with an n of approximately 325. The models measured have a ratio of gap width to mid-gap height equal to 3.5. Gradient measurements using preliminary pole-face contours show a gradient uniform within 2 percent over approximately one half the width of the pole tip. Below 8000 gauss, saturation effects do not appreciably reduce this region. The region narrows rapidly as saturation increases, and above 10 000 gauss attaining the required aperture constitutes a problem. Results of modifying the pole-face contours to extend the usable aperture to higher flux densities will be reported. The measurements are encouraging with respect to the feasibility of accomplishing the alternation of the gradient by reversal of the pole tips on the yoke.

* Work carried out under contract with U. S. Atomic Energy Commission.
† On leave from the Radiation Laboratory, University of California, Berkeley, California.

T5. Precision Vibrating-Coil Magnetic-Gradient Recorder.* MARTIN GRAHAM, *Brookhaven National Laboratory.*—The accurate measurement of a magnetic-field gradient is required in the testing of magnets for accelerators under development at Brookhaven National Laboratory. An instrument has been built which vibrates a search coil in the magnetic field, and vibrates a reference coil on the same shaft in a reference magnet. The voltages induced in the two coils are compared in a modified bridge circuit whose null is set by a self-balancing arrangement which also runs a recorder pen. The entire device produces graphs of normalized gradient *versus* radial position in the magnet gap. The ranges of $\partial B/\partial r$ are 0 to 1 gauss/centimeter, and 9 to 10 gauss/centimeter (suppressed zero). Multiplication factors up to 10^5 are available by use of an attenuator in the search-coil circuit. The performance is limited by thermal noise in the search coil to about $\frac{1}{4}$ percent at the response speeds used.

* Work carried out under contract with U. S. Atomic Energy Commission.

T6. Scattering of Electrons in a Strong Focusing Synchrotron.* MICHAEL J. MORAVCSIK AND J. MICHAEL SELLEN, JR., *Cornell University.*—Calculations of the scattering loss are carried out for the 1-Bev Cornell "mesotron" under construction. "Elastic" scattering by nuclei and "inelastic" scattering by atomic electrons are considered. Screening effects are accurately taken into account (by using the Hartree wave function for the smallest scattering angles) because the very small angles relevant in the problem correspond to large impact parameters. Because of these small angles the contribution of the inelastic scattering is just as important as that of the elastic process. It is shown that the total cross section in the highly relativistic limit as given by the Born approximation is independent of energy for any physical central potential where large angle scattering is unimportant. In applying the scattering formula to the synchrotron representative points are selected in the field lattice and the results are averaged over these points. Vertical and radial scattering are treated separately and the cross section for each of these is taken to be half of the whole cross section. The radial case will be complicated by the synchrotron oscillations. Two different injection conditions are considered and it is found that they give roughly the same results because of the damping of oscillations as the energy increases.

* Assisted by the joint program of the Office of Naval Research and the U. S. Atomic Energy Commission.

T7. A Method for the Prompt Destruction of the Electron Beam in a Conventional Synchrotron.* C. L. HAMMER AND A. J. BUREAU, *Iowa State College.*—By passing current through coils wrapped around a section of the donut of a synchrotron it is possible to change the fall off index of a part of the guide field while leaving the remaining guide field unaltered. This technique is used on the Iowa State College 70-Mev synchrotron and complete beam destruction is found experimentally to occur in approximately 0.08 microsecond. The buildup of the radial oscillation is analyzed and it is estimated that complete destruction of the beam is accomplished in approximately 10 revolutions or 0.06 microsecond. The analysis also shows that this technique can be a valuable aid in the extraction of an electron beam from a synchrotron or betatron.

* Work was performed in the Ames Laboratory of the U. S. Atomic Energy Commission.

T8. Betatron Oscillations in a Fixed-Field Alternate-Gradient Accelerator with Spirally-Ridged Poles. L. JACKSON LASLETT, *Iowa State College** *and Midwestern Universities Research Association.*†—An analysis has been made of the particle trajectories to be expected in a spirally-ridged fixed-field accelerator similar to that described previously by Kerst, *et al.*[1] The field in the median plane is taken to be of the form

$$H = -H_0(r/r_0)^k[1 + f\sin(w^{-1}\ln(r/r_0) - N\theta],$$

with the result that the basic character of the oscillations remains unaffected by the gradual increase of mean radius during the acceleration cycle. The periodic solution of the equations of motion suggests an equilibrium orbit which is appreciably scalloped. Stability conditions and other features of the betatron motion about this orbit are significantly affected by this scalloped character of the reference orbit. Approximate formulas and numerical examples are presented to illustrate these points.

* Institute for Atomic Research and Ames Laboratory of the U. S. Atomic Energy Commission.
† Assisted by the National Science Foundation.
[1] Kerst, Terwilliger, Symon, and Jones, Bull. Am. Phys. Soc. **30**, No. 1, 14 (1955), abstract D5.

T9. Synchro-Microtron Requiring No Static Magnetic Guide Field. H. F. KAISER, *Naval Research Laboratory.*—A previous paper[1] proposed an electron accelerator in which a magnetic field rising stepwise in time is superposed locally on a given static field microtron orbit. Subsequent finite and stepwise electron energy increases are then matched by step increases in magnetic guide field, allowing the particle to reach at constant orbit radius any energy attainable with the superposed field. The theory is now extended to the case where the usual static magnetic field is absent and the particle energy and field increase stepwise from the outset. In previous theory

the step operation began with particle velocity nearly c making the difference in particle and field wave speeds $[\beta_p c - 1/(LC)^{\frac{1}{2}}]$, small and nearly constant. Now the major problem is adjustment of field wave speed to the large charges in β_p occurring in the initial turns. Phase conditions resulting from various choices of fixed-field wave velocity are studied and also some schemes for keeping wave and particle speed equal by automatic electronic variation of the field line parameters (L,C) such as gas discharge or ferrite line loading techniques.

[1] H. F. Kaiser, Bull. Am. Phys. Soc. **29**, No. 7, 18 (1954), abstract I8.

T10. Cyclotron Energy Measurement by Time-of-Flight.* S. D. Bloom, C. O. Muehlhause, and H. E. Wegner, *Brookhaven National Laboratory.*—In the course of developing time-of-flight techniques for the study of neutrons generated by a cyclotron, the energy and time dispersion of the machine were determined. An unfocused proton beam traveled along an evacuated tube striking a gamma producing target whose position along the flight path could be varied. The gamma rays could be detected with any of the fast organic phosphors or NaI (Tl) in conjunction with either an RCA type 1P21 or 5819 photomultiplier tube. A fast delayed coincidence between the cyclotron radio-frequency (18.56 Mc) and the detector pulse was required, as well as a slow coincidence between the fast coincidence output and a slow channel discriminator pulse. At a fixed time delay in the rf leg of the fast coincidence circuit the spatial distribution of the proton was determined for two positions. These positions were separated in flight time by one rf period (54 mμsec). The following operating parameters were measured: exit orbit circumference, 114±1 cm; proton energy, 2.31±0.02 Mev; time dispersion, 2.5 mμsec. Since no change in time dispersion was observed for the two proton positions and since different spatial sections of the beam were the same energy, it was concluded that the beam is monochromatic to ~1 percent.

* Work done under auspices of the U. S. Atomic Energy Commission.

T11. An 8-Mev Variable Energy Cyclotron. H. W. Fulbright, D. A. Bromley, and J. A. Bruner, *University of Rochester.*—Details of the construction and successful operation of the new 27-in. variable energy cyclotron and beam-handling system at the University of Rochester will be described. A proton beam of energy easily and quickly adjustable to any energy from 1.5 to 8 Mev having a narrow energy spread and a current (after analysis) of several tenths of a microampere is produced. Deuterons of 4.5 Mev and alpha particles of 9 Mev have also been generated. The cyclotron employs a single dee and a variable-frequency oscillator.

Saturday Morning at 9:30

Burgundy Room

(A. J. Allen presiding)

Transmutation and Nuclear Energy Levels, III

TA1. Gamma Rays from Protons on P^{31}.* J. W. Olness and H. W. Lewis, *Duke University.*—Gamma rays from P^{31} bombarded by protons of 1.4 to 3.36 Mev have been studied with a scintillator. Targets, of thickness less than 10 kev at 2 Mev, were prepared by evaporation of zinc phosphide on thick tantalum. Above 2.30 Mev, twenty-one resonances were observed for the production of a 1.26-Mev gamma ray, attributed to the reaction $P^{31}(p,p')P^{31}$. Rather large inconsistencies occur in previously reported energies for the low-lying states of P^{31}; we believe that our value for this state is correct to ±15 kev. No evidence for other low-lying states was observed. The gamma spectrum above $E_p = 2.47$ Mev showed the presence of a 1.8 Mev gamma ray, attributed to $P^{31}(p,\alpha\gamma)Si^{28}$, with a resonance structure similar to that of the 1.26 Mev gamma ray. We have also measured the yield of gamma rays greater than 3 Mev in energy, corresponding to capture radiation. All resonances above $E_p = 2.1$ Mev correspond to previously unreported levels in S^{32}. Further work with thinner targets and observation of charged particles is planned.

* This work was supported by the U. S. Atomic Energy Commission.

TA2. The Reaction $P^{31}(p,\alpha)Si^{28}$. R. L. Clarke, E. Almqvist, and E. B. Paul, *Chalk River Laboratories.*—Zinc phosphide targets have been bombarded by protons of 1.0 to 2.5 Mev energy. Alpha particles leading to the ground state of Si^{28} were observed by means of a double-focusing magnetic spectrometer mounted to detect particles at 90° to the beam. Sixteen well separated resonances were observed. Of these, only two show a measureable γ-ray yield, although many resonances in the $P^{31}(p,\gamma)S^{32}$ reaction have been observed in this region.[1] These two resonances are at 1.90 and 2.03 Mev. The widths and differential cross sections at 90° are listed below for the resonances more than 4 kev wide:

E_R(Mev)	Γ(kev)	$d\sigma/d\Omega(90°)$ (barns/sterad)
1.52	9.0	0.022
1.64	~5	0.025
1.90	27	0.043
2.03	18	0.037

The lowest resonance observed in this work is at 1.03 Mev, and overlaps the work of Freeman and Seed.[2]

[1] Gove, Paul, Litherland, and Bartholomew, Phys. Rev. **95**, 650(A) (1954).
[2] J. M. Freeman and J. Seed, Proc. Phys. Soc. (London) **A64**, 313(L) (1951).

TA3. Neutrons from the Proton Bombardment of S^{33} and S^{34}.* F. Ajzenberg and A. Rubin, *Boston University,* and J. G. Likely, *Princeton University.*—An isotopic sulfur target, 50 kev thick, and an enriched CdS target, 100 kev thick, have been bombarded by 17.5-Mev protons from the Princeton cyclotron. The sulfur target was prepared by the method of Nielsen and Weinstein[1] while the enriched[2] CdS was painted on a polystyrene foil. Preliminary measurements of proton recoil tracks in Ilford C-2 emulsions at 30 and 150 degrees (1500 tracks) indicate four neutron groups corresponding to states in Cl^{32} and five neutron groups corresponding to states in Cl^{34}. An attempt will be made to correlate the results of these neutron spectra measurements with the picture of the $Cl^{34}-S^{34}$ decay derived from β-decay measurements.[3]

* This work was supported in part by the U. S. Air Force, through the Office of Scientific Research, and in part by the U. S. Atomic Energy Commission.
[1] E. Nielsen and A. Weinstein, Rev. Sci. Instr. **24**, 1146 (1953).
[2] The CdS, on loan from the Stable Isotopes Division of the U. S. Atomic Energy Commission, was enriched to 14.92 percent S^{34}.
[3] P. M. Endt and J. C. Kluyver, Revs. Modern Phys. **26**, 95 (1954).

TA4. Protons from the Alpha Bombardment of A^{38} and A^{40}.* ROBERT B. SCHWARTZ, JAMES W. CORBETT,† AND WILLIAM W. WATSON, *Yale University.*—Gas targets 150 kev thick of natural argon (99.6 percent A^{40}; 0.34 percent A^{36}) and of argon enriched in A^{38} (97.4 percent A^{38}; 2.5 percent A^{40}) have been bombarded with 7.4-Mev alphas from the Yale cyclotron. Protons at 90° to the incident beam have been studied by means of 50-μ Ilford C-2 emulsions, placed 19 cm from the target. The ground-state Q-value for the $A^{38}(\alpha,p)K^{39}$ reaction is -1.29 Mev, with excited states at 2.60 and 2.81 Mev. The ground state Q for $A^{40}(\alpha,p)K^{43}$ is -3.55 Mev, with excited states at 0.44 and 1.01 Mev. The ground-state Q-values are in good agreement with the Q's computed from mass spectrometer and beta-decay data.[1] The rather high energy of the first excited state in K^{39} follows the trend of the first excited states in the other 20-neutron nuclei whose $d_{\frac{3}{2}}$ proton shell is being filled. The cross section for the $A^{40}(\alpha,p)K^{43}$ reaction is quite low—only 4 percent of the cross section for the A^{38} reaction.

* Supported in part by the U. S. Atomic Energy Commission.
† General Electric Coffin Fellow.
[1] R. W. King, Revs. Modern Phys. **26**, 327 (1954); Duckworth, Hogg, and Pennington, Revs. Modern Phys. **26**, 463 (1954).

TA5. Angular Distribution of Proton Groups from $Ca^{42}(d,p)Ca^{43}$ Reaction.* C. K. BOCKELMAN, C. M. BRAAMS, W. W. BUECHNER, AND D. B. GUTHE, *M.I.T.*—Thin CaO targets were prepared by evaporating $CaCO_3$ of isotopic constitution 65 percent Ca^{42} and 35 percent Ca^{40}. These targets were bombarded with 7-Mev deuterons accelerated by the MIT–ONR generator. The proton spectrum was recorded with nuclear emulsions in the broad-range magnetic spectrograph at fifteen angles between 10 and 100 degrees. Results for the groups of greatest yield have been obtained. They indicate that both the ground state and 1.00-Mev state in Ca^{43} are fitted by $l_n=3$ Butler curves, if the radius is chosen as 7.5×10^{-13} cm. The state at 0.60 Mev shows a distribution characteristic of $l_n=1$. Results on the Ca^{41} levels are in general agreement with those of Holt and Marsham.[1]

* This work has been supported in part by the joint program of the Office of Naval Research and the U. S. Atomic Energy Commission.
[1] J. R. Holt and T. N. Marsham, Proc. Phys. Soc. (London) **A66**, 565 (1953).

TA6. The Stripping Reactions $Fe^{55}(d,p)Fe^{57}$ and $Fe^{57}(d,p)Fe^{58}$.* CHARLES E. MCFARLAND, FRANKLIN B. SHULL, ALEXANDER J. ELWYN, AND BENJAMIN ZEIDMAN, *Washington University.*—Targets of concentrated Fe^{57} (74.6 percent) and natural Fe^{56}, both in the form of Fe_2O_3, were bombarded with 10-Mev deuterons. Energy spectra of the protons emitted were observed at intervals of 5° in the forward hemisphere with the aid of a proportional counter telescope and an absorber stack of variable thickness. Q-values measured for the $Fe^{56}(d,p)Fe^{57}$ reaction are 5.53 (ground state) and 4.24 Mev. Those for the $Fe^{57}(d,p)Fe^{58}$ reaction are 7.09 (ground state), 6.26, 5.15, and 3.72 Mev. By comparison with curves calculated from Butler's theory of stripping reactions,[1] the angular distribution of each of these groups was found to correspond to the capture of neutrons having one unit of orbital angular momentum. The spin of each of the two observed states of Fe^{57} is hence either $\frac{1}{2}$ or $\frac{3}{2}$ and the parity of both states is odd. The spin of each of the observed states of Fe^{58} is 0, 1, 2, or 3, and their parities are all even.

* Supported by the U. S. Air Force through the Office of Scientific Research of the Air Force Research and Development Command.
[1] S. T. Butler, Proc. Roy. Soc. (London) **208**, 559 (1951).

TA7. The $O^{18}(d,n\gamma)F^{19}$ Reaction. H. D. HOLMGREN AND J. W. BUTLER, *Naval Research Laboratory.*—The "gamma-ray threshold" technique[1] of observing energy levels has been applied to the $O^{18}(d,n\gamma)F^{19}$ reaction to study the energy levels of F^{19} in the region of excitation extending from 6.0 Mev to 7.6 Mev. The apparatus was adjusted so as to observe thresholds for gamma rays in the energy range between 4.0 and 7.5 Mev. The only threshold observed was at a bombarding energy of 350 kev, corresponding to a level in F^{19} at an excitation of 6.04 Mev. In addition to a gamma ray of 6.04 Mev, there appears also to be a threshold for a 4.37-Mev gamma ray at 350-kev bombarding energy. A detailed study of the gamma ray spectrum at a bombarding energy of 1.40 Mev confirms our belief that there are no other levels in this region which decay predominantly to any level below the 1.59-Mev level of F^{19}, since no gamma rays with an energy higher than 4.5 Mev were observed with an intensity greater than 10 percent of that of the 6.04-Mev gamma ray.

[1] J. W. Butler, Bull. Am. Phys. Soc. **29**, No. 7, 26 (1954), abstract R7.

TA8. Inelastic Scattering of Protons from Fe^{54} and Fe^{56}.† G. C. PHILLIPS, C. R. GOSSETT, J. P. SCHIFFER, AND P. M. WINDHAM, *The Rice Institute.*—The Rice Institute 180° magnetic spectrometer has been used to study the low-energy levels of iron by bombarding thin targets of separated isotopes* with protons at energies up to 5.7 Mev. Only one level in each isotope was observed for excitation energies below 1.5 Mev. These levels are: Fe^{54}, 1.413 ± 0.005 and Fe^{56}, 0.845 ± 0.005 Mev. The operation of the spectrometer with the Van de Graaff generator for inelastic scattering measurements will be discussed. The resolution attained is $\Delta\rho/\rho=5\times10^{-4}$. Typical spectra will be presented.

† Supported in part by the U. S. Atomic Energy Commission.
* Supplied by the Oak Ridge National Laboratory.

TA9. Inelastic Scattering of Protons from Isotopes of Mn, Ni, and Cu.* J. P. SCHIFFER, P. M. WINDHAM, C. R. GOSSETT, AND G. C. PHILLIPS, *The Rice Institute.*—The Rice Institute 180° magnetic spectrometer has been used to study the low-lying excited states of five isotopes by inelastic scattering of protons. Thin evaporated targets of enriched isotopes[1] were bombarded with protons using energies from 4.6 to 5.7 Mev.

Isotope	Levels excited Mev
Mn^{55}	0.128 ± 0.007
Ni^{58}	1.453 ± 0.005
Ni^{60}	1.329 ± 0.005
Cu^{63}	0.669, 0.968, 1.326, 1.410, 1.549 all ±0.005
Cu^{65}	No levels observed below 1.5 Mev

* Supported in part by the U. S. Atomic Energy Commission.
[1] Supplied by the Oak Ridge National Laboratory.

TA10. The reaction $Ni^{58}(\alpha,\gamma)Zn^{62}$. H. MORINAGA, *Purdue University.*—The yield of Zn^{62} from the alpha-particle bombardment of natural nickel was studied as a function of the energy of the alpha particles. The 9.3-hour activity due to Zn^{62} (produced by the (α,γ) reaction on Ni^{58}) was compared with the 38-minute activity of Zn^{65} (produced by the (α,γ) reaction on Ni^{62}) after chemical separation of zinc from the targets. At alpha-particle energies of 12.0, 13.9, 15.7, and 17.2 Mev, the cross sections are 0.30, 0.49, 0.47, and 0.42 mb, respectively. The order of magnitude is in good agreement with the estimate for the de-excitation of the compound nucleus by electric dipole transitions. The energy dependence of the cross section can be calculated from the statistical theory assuming reasonable level densities. The ratio of the experimental value to the calculated value increases considerably with energy, indicating the reduction of the dipole transition rate at lower energy or some enhancement at the energy corresponding to the giant resonance observed in photonuclear reactions.

TA11. Gamma Rays from the Proton Bombardment of Cu-63 and Cu-65.* C. E. WELLER AND J. C. GROSSKREUTZ, *University of Texas.*—Gamma radiation from the bombardment of the separated isotopes Cu-63 and Cu-65 with 1.9-Mev protons was observed by means of a NaI crystal and a 20-channel analyzer. From Cu-63 we detected 0.995-Mev gamma rays, and from Cu-65 1.04- and 0.824-Mev gamma rays, all

presumably due to the inelastic scattering of the protons. The 0.995- and 1.04-Mev radiations correspond to transitions from known excited states of Cu-63 and Cu-65, respectively.[1] The 0.824-Mev gamma ray we assign to either a new level in Cu-65 at 0.824 Mev or to a transition from the 1.04 level to a level at 0.210 Mev. Evidence for the latter level has been previously reported.[2] We have as yet been unable to detect a 0.210-Mev gamma ray. A continous gamma-ray spectrum up to at least 10 Mev was also observed, most probably due to proton capture. Thick target yield curves of the two 1-Mev gamma rays will also be shown. The onset of the (p,n) reaction in Cu-65 is clearly evident just above 2.0 Mev.

* Supported in part by the Office of Scientific Research, Air Research and Development Command.
[1] *Nuclear Data* (United States Department of Commerce, National Bureau of Standards, September 1, 1950).
[2] R. A. Cohn and J. D. Kurbatov, Phys. Rev. **78**, 318 (1950).

TA12. Gamma-ray Spectrum of $Cd^{113}(n,\gamma)Cd^{114}$.* HENRY MOTZ, *Brookhaven National Laboratory.*—Nine gamma rays superimposed upon an unresolved continuum have been observed from cadmium while being irradiated by slow neutrons. The energies and intensities have been determined by the K x-ray-K photopeak coincidence method, using a thin lens spectrometer[1] with a resolution of 3 percent.

Energy (kev)	Intensity per neutron captured
557 ±3	0.89
651 ±4	0.20
728 ±5	0.07
803 ±5	0.07
1215 ±8	0.10
1308 ±8	0.10
1388 ±8	0.13
1500 ±15	0.05
1655 ±10	0.06

These values fit well with the high-energy data of Kinsey and Bartholomew.[2] A discussion of the level scheme for Cd^{114} will be presented.

* Under the auspices of the U. S. Atomic Energy Commission.
[1] Henry Motz, Phys. Rev. **90**, 355(A) (1953).
[2] Kinsey and Bartholomew, Can. J. Phys. **31**, 1051 (1953).

TA13. (p,γ), (p,α), (p,He_3), (p,t), and (p,Be^7) Cross Sections. B. L. COHEN, H. G. BLOSSER, D. J. COOMBE, G. H. MCCORMICK, AND E. NEWMAN, *Oak Ridge National Laboratory.*—Activation cross sections for several (p,γ), (p,α), (p,He_3), and (p,t) reactions were measured using 22-Mev protons from the Oak Ridge National Laboratory 86-inch cyclotron. Reduced energies were obtained with absorbers; radiochemical processing was used in most cases. (p,γ) cross sections vary only slightly with bombarding energy and target mass; this is strongly contrary to expectations from compound nucleus interaction. The absolute cross sections (~1 mb) are consistent with a direct interaction interpretation. (p,α) cross sections are in general agreement with the predictions of statistical theory; this includes cases for $A=54-202$ and is in sharp contrast to the findings of Paul and Clarke[1] for (n,α) reactions. (p,t) and (p,He_3) cross sections are also in good agreement with the predictions of statistical theory; this indicates that, after correcting for Coulomb and energetic effects, emission of tritons, He^3 ions, and alpha particles in nuclear reactions is just as probable as emission of neutrons or protons. A search for (p,Be^7) reactions was made with 30-Mev protons from the Berkeley linac.[2] Preliminary results indicate $\sigma(p,Be^7)<0.1$ mb in fluorine, oxygen, and sodium.

[1] E. B. Paul and R. L. Clarke, Can. J. Phys. **31**, 268 (1953).
[2] We are greatly indebted to Dr. L. Alvarez for the use of the University of California Radiation Laboratory linear accelerator.

SATURDAY MORNING AT 9:30

NBS, East Building

(R. T. BIRGE presiding)

Invited Papers on Thermodynamics and Cryogenics

U1. Carnot's Concept of Entropy, and Modern Presentations of Thermodynamics. V. K. LA MER, *Columbia University.* (30 min.)

U2. New Definition of the Kelvin Scale Adopted by the Tenth General Conference on Weights and Measures. F. G. BRICKWEDDE, *National Bureau of Standards.* (30 min.)

U3. The Theory of Liquid Helium. R. P. FEYNMAN, *California Institute of Technology.* (40 min.)

U4. Structure of the Intermediate State in Superconductors. A. L. SCHAWLOW, *Bell Telephone Laboratories.* (30 min.)

SATURDAY MORNING AT 9:30

Exhibit Hall II

(J. W. DAVISSON presiding)

Various Topics in Solid-State Physics

UA1. Low Frequency Vibrational Spectrum of F.C.C. Lattice. L. SALTER, *Wabash College* (introduced by F. E. Throw).—Houston's method[1,2] is applied to the problem of determining the normal mode distribution function for the face-centered cubic lattice in the low-frequency limit. The method yields explicit expressions for the coefficients a_i, $g(\omega)=a_1\omega^2+a_2\omega^4+a_3\omega^6\cdots$, in terms of the force parameters occurring in the dynamical matrix for the problem. Experimental values of c_{11}, c_{12}, and c_{44} are used to discuss the variation of the equivalent Debye Θ in the low-temperature range for several substances of interest.

[1] W. V. Houston, Revs. Modern Phys. **20**, 161 (1948).
[2] E. Bauer, Phys. Rev. **92**, 58 (1953).

UA2. On The Frequency Spectrum of a One-Dimensional Isotopic Crystal Mixture.* ROBERT J. RUBIN AND B. A.

FLEISHMAN, *Applied Physics Laboratory.*—We use a perturbation method to obtain the first- and second-order corrections to the vibration frequencies of a one-dimensional crystal composed of a random arrangement of two isotopes of mass M_A and M_B in the proportions $P:(1-P)$. The zeroth-order approximation is chosen to be a uniform crystal composed of particles with the average mass $M=M_AP+M_B(1-P)$. The average first-order correction is zero where the average is taken over all possible arrangements of the isotopes. The average second-order correction to the square of the ith frequency is

$$\omega_i^{(2)}=\frac{3k}{8M}P(1-P)\sin^4\frac{i\pi}{2(N+1)}\times\left\{\frac{\cos i\pi/(N+1)}{(N+1)\sin^2 i\pi/(N+1)}+\frac{1}{i\pi\sin i\pi/(N+1)}\right\},$$

where k is the force constant and $\epsilon^2=(M_A-M_B)^2/4M^2$. The second-order correction as might be expected diverges at high frequencies ($i\sim N$). The existence of this divergence has a bearing on a perturbation calculation of the zero-point energy of a one-dimensional isotopic crystal mixture.

* This work was supported by the Bureau of Ordnance, Department of the Navy.

UA3. On the Optical Properties of Solids. HERBERT B. ROSENSTOCK, *Naval Research Laboratory.*—Accepted first-order theory asserts that a nonvanishing dipole moment is associated with only those vibrations of a lattice whose propagation vector is zero.[1] This result is based on the use of the so called "cylic" boundary conditions in the normal mode analysis of the lattice. Application of exact boundary conditions[2] to the problem indicates, however, that the dipole moment is a quasi-continuous and ordinarily nonvanishing function of the propagation vector with a strong peak at the point predicted by first-order theory. It follows that the $3n-3$ (or fewer) sharp lines which make up the first-order infrared absorption spectrum (also the reflection- and the first-order Raman spectrum)[3] of a crystal with n atoms per unit cell should be broadened and that "absorption edge" effects should be observed at the frequencies at which singularities[4] appear in the frequency spectrum of the solid.

[1] M. Born and M. Goeppert-Mayer, *Handbuch der Physik* (Verlag Julius Springer, Berlin, Germany, 1933), **24/2**, 623, Sec. II.
[2] M. Born, Proc. Phys. Soc. (London) **54**, 362 (1942).
[3] M. Born and M. Bradburn, Proc. Roy. Soc. (London) **A188**, 161 (1947).
[4] L. van Hove, Phys. Rev. **89**, 1189 (1953); H. B. Rosenstock, Phys. Rev. **97**, 290 (1955).

UA4. Change in Length of Alkali Halide Crystals Caused by X-Ray Irradiation.* LAN-YING LIN AND B. R. RUSSELL, *University of Pennsylvania.*—Potassium and sodium chloride crystals (about 12 mm×7 mm×1.5 mm) at room temperature were irradiated with x-rays in a thermostated enclosure regulated to 10^{-2} °C. The crystals were about 2¼ inches from the x-ray-tube beryllium window. The change in length of the largest dimension of the crystal was measured during the irradiation by a capacitance-type dilatometer with sensitivity 10^{-5} cm. The F center density calculated from the increase in length per unit length (assuming one ion pair at the surface for each pair of lattice vacancies) agreed within 5 percent with the number of color centers determined subsequently by optical absorption measurement. For example: $\Delta l/l=6.1\times10^{-7}$, n(calculated) $=4.1\times10^{16}$ cm^{-3}, n(optical, colored portion) $=3.9\times10^{16}$ cm^{-3} for NaCl; $\Delta l/l=1.36\times10^{-6}$, n(calculated) $=6.6\times10^{16}$ cm^{-3}, n(optical) $=6.7\times10^{16}$ cm^{-3} for KCl. These crystals were uncolored in about 30 percent of their volume as they were larger than the x-ray beam. Using a slightly smaller crystal to get uniform coloration throughout the whole crystal, $\Delta l/l=4.3\times10^{-7}$, n(calculated) $=2.1\times10^{16}$ cm^{-3}, n(optical) $=2.0\times10^{16}$ cm^{-3} for KCl.

* This research was supported by the U. S. Air Force, through the Office of Scientific Research of the Air Research and Development Command.

UA5. X-Ray Diffraction Studies of Radiation Damage of Germanium Single Crystal.* SIGMUND WEISSMANN AND ROGER CHANG, *Rutgers University.*—A germanium single crystal (impurities 1 part in 10^9, resistivity 35 ohm-cm) was acid-cut into two halves. One half of the crystal was subjected to neutron irradiation at a temperature of 160–200°C. The slow neutron flux was measured to be 1.43×10^{13} n.v.t., the fast neutron flux was estimated to be half this value. Rocking curves were performed for both the irradiated and unirradiated specimens using a calcite crystal as first crystal and testing the specimens in the (1, −1) position with CuKα_1 radiation. The halfwidths for the (111) reflection obtained were: unirradiated specimen 56 seconds of arc; irradiated specimen 3½ minutes of arc. The irradiated germanium crystal exhibited also considerable diffuse scattering. Precision lattice parameter determination yielded: unirradiated specimen, $a_0=5.657_7A$; irradiated specimen $a_0=5.659_3A$. The increase in lattice parameter (about 0.02 percent) for the irradiated specimen is insufficient to account for the observed 3-fold increase in halfwidth. An explanation of the observed phenomena is being advanced.

* Work supported by the U. S. Atomic Energy Commission.

UA6. Slip Systems and Creep in Oxide Crystals. J. B. WACHTMAN, JR., AND L. H. MAXWELL, *National Bureau of Standards.*—Single crystals of periclase, rutile, and sapphire deform by slip at temperatures above one-half their absolute melting temperature. Slip systems are (100), (110), and (111) with $[1\bar{1}0]$ in periclase, (011) and (201) in rutile, and (0001) with $[11\bar{2}0]$ in sapphire. Temperature of about 1600°C is required for deformation other than slip on the (0001) plane. There is a rather well-defined stress required to cause creep to begin in sapphire. This creep yield stress is 780 kg/cm^2 resolved shear stress at 900°C and falls monotonically to about 130 kg/cm^2 at 1400°C. Sapphire containing about 0.75 percent chromia has a value about twice that of pure sapphire at 1300°C. The typical creep curve for sapphire under constant load has a distorted "S" shape. Creep begins very slowly at first, rises to a maximum rate, and finally falls off to a very slow rate. At 1300°C a final stage of fast creep apparently leading to failure sometimes occurred. The modulus of rupture of sapphire measured in short-time tests rises from about 3800 kg/cm^2 at 800°C to about 6200 kg/cm^2 at 1000°C. This is interesting as plastic deformation in long-time tests begins about 900°C.

UA7. Relationship between Activation Energy for Slip in Crystalline Solids and Applied Stress Based on a Dislocation Model. ROGER CHANG, *Rutgers University.*—Attempts have been made by many investigators[1–3] to find a theoretical relationship between activation energy for slip in crystalline solids and applied stress with only limited success. The present theory assumes that the activation energy for the movement of a dislocation line against an array of obstacles is equal to the maximum work done by the tension in the dislocation line to move the dislocation against the obstacle one interatomic distance in the slip direction. A simple derivation yields $U=-(Gb^2/4\pi)\ln(\tau/\tau_0)$, where U is the activation energy, G shear modulus, b Burger's vector, ln natural logarithm, τ applied shear stress, $\tau_0=(Gb/4\pi\Omega_0)$, Ω_0 being the effective radius of that region around the dislocation line within which Hooke's law fails ($\Omega_0\cong2b$). The agreement between theory and experimental data is remarkably good. Further work based on the theory is being carried on by the author to develop a generalized theory of creep in crystalline solids.

[1] F. R. N. Nabarro, Advances in Phys. **1**, 336 (1952).
[2] A. H. Cottrell and B. A. Bilby, Proc. Phys. Soc. (London) **62A**, 49 (1949).
[3] T. Yokobori, J. Physiol. Soc. Japan **7**, 44 (1952).

UA8. Cavity Formation in Iron Oxide.* D. W. JUENKER,† R. A. MEUSSNER, AND C. E. BIRCHENALL, *Princeton Uni-*

versity.—A study has been made of the formation of oxide scale on iron in an oxygen atmosphere at temperatures above 700°C. Apart from the expected behavior,[1,2] there was observed a phenomenon not reported by previous investigators; when an iron sample is oxidized to an "FeO" composition and permitted to homogenize in argon, there may be found within the oxide a cavity, of geometry nearly identical with that of the original iron sample, surrounded by oxide walls of uniform thickness, and containing no more than a residual filament of the original specimen. From this behavior and other evidence, one may infer that the iron core sometimes separates completely from the surrounding oxide, with iron transport continuing despite the absence of substantial oxide-iron contact. The mechanism of this transport of iron from the separated core to the interior surface of the oxide is in doubt.

* This research was supported by the United States Air Force, through the Office of Scientific Research of the Air Research and Development Command.
† Presently with the Department of Physics, University of Notre Dame.
[1] Davies, Simnad, and Birchenall, Trans. Am. Inst. Mining Met. Engrs. 191, 889 (1951).
[2] Dunnington, Beck, and Fontana, Corrosion 8, 2 (1952).

UA9. Energy Transport in the Scintillation Process.* E. R. HARDWICK† AND W. G. MCMILLAN, *University of California at Los Angeles.*—In scintillation solutions, the transfer of excitation energy from solvent to solute (phosphor) molecules theoretically may occur through either photons or excitons. Against a prevalent thesis that *all* transfer occurs via photons it may be argued that (a) transfer has been observed using *UV* excitation, even when solvent-emission and phosphor-absorption bands do not appreciably overlap; (b) the decay time of a pulse ($\sim 10^{-9}$ sec) seems rather too short to permit an appreciable number of photon emission-reabsorption steps. While the exciton theory appears to avoid these particular difficulties, there is little doubt but that some effects, such as the transfer through glass observed by Ageno and Querizoli,[1] require the photon mechanism. Certainly at least the reabsorption of scintillation photons constitutes a mechanism of (long-range) energy transfer. We have studied experimentally three aspects of the scintillation process: (a) quenching and self-quenching of α-particle induced scintillations; (b) transfer distances, recorded photographically following Ageno; and (c) destruction of the surface of anthracene crystals by α-particles, monitored by the consequent decline in scintillation efficiency. The bearing which these measurements have upon the questions raised above will be discussed.

* This work was assisted by a grant in aid from the Institute for Geophysics, University of California at Los Angeles.
† Present address: National Research Council, Ottawa 2, Canada.
[1] M. Ageno and R. Querizoli, Nuovo Cimento 9, 196, 282 (1952).

UA10. Hall Effect and Resistivity Study of Photoconducting PbS Films. JOSEPH F. WOODS, *U. S. Naval Ordnance Laboratory, and Catholic University of America.*—Hall coefficient (R) and resistivity (ρ) have been measured on chemically-deposited PbS photoconducting films* under varying degrees of illumination sufficient to produce current increases of 3 to 167 percent of the dark current. R is measured by a d–c method utilizing a vibrating reed electrometer and recorder. Values of the ratios $\Delta R/R_0$ and $\Delta\rho/\rho_0$ are accurate to within 3 percent, where R_0 and ρ_0 are the dark values of R and ρ respectively, and ΔR and $\Delta\rho$ are the corresponding changes produced by the illumination. It is found that under a given value of illumination $\Delta R/R_0$ is equal to $\Delta\rho/\rho_0$ within 7 percent. R is basically a measure of the number of carriers within the crystallites while ρ depends both on the number of carriers and on the mobility which is limited by barriers in the film. Hence, these results suggest that the mobility does not change significantly under illumination and that the photoconductive effect is caused directly by an increase in the number of carriers.

* The author wishes to acknowledge the cooperation of the Eastman Kodak Company in preparing the lead sulfide films used in these studies.

UA11. *The Absorption of Alkali-Halides in the Far Ultra-Violet. J. R. NELSON, J. G. SIEGFRIED, AND P. L. HARTMAN, *Cornell University.*—To augment photoconductivity measurements to be made on NaCl and KCl, the absorption spectrum of these substances has been obtained at two temperatures, in the region from 900A to 1750A. Measurements on evaporated films by transmission and on bulk crystals by reflectivity are in fair agreement but not in strict accord with the data of Schneider and O'Bryan. Curves will be shown illustrating new regions of the spectrum and points of difference with previous measurements. The effect of narrowing and resulting appearance of fine structure of the presumed exciton peak at low temperature will be presented.

* Supported in part by the Office of Naval Research.

SATURDAY MORNING AT 9:30

Continental Room

(M. GOLDHABER presiding)

Radioactive Substances, I

V1. Gamma Rays from P^{34}, Cl^{34}, and P^{30}.* E. BLEULER AND H. MORINAGA, *Purdue University.*—The gamma rays following the beta decays of P^{34}, Cl^{34}, and P^{30} were investigated with NaI scintillation spectrometer and a twenty-channel analyzer. In addition to the two known 2^+ levels at 2.16 and 3.24 Mev in S^{34}, another 2^+ level was found at 3.9 Mev. The *ft* values of the beta decays to the first and the third excited state are lower than average from P^{34} and higher than average from the 3^+ isomeric state of Cl^{34}. For the second excited state the situation is reverse. The decay from P^{30} to the first excited state of Si^{30} was found to be slower than an average allowed transition. The results are discussed in terms of mixed configurations; appreciable mixing is suspected to exist in the 0^+ ground state of S^{34} (and Cl^{34}) which possibly explains the unusual $T=1$ ground state of Cl^{34}.

* Supported by U. S. Atomic Energy Commission.

V2. Radioactive Decay of Ca^{47}.* L. J. LIDOFSKY, N. BENCZER, AND V. K. FISCHER, *Columbia University.*—The results of several recent investigations[1–3] on the decay properties of Ca^{47} are in considerable disagreement as to the maximum energies of the negatron groups, the number of associated gamma rays and the half-lives. We have reinvestigated the decay in an attempt to resolve these disagreements and to understand certain of its features. The Ca^{47} half-life is found to be 4.7 ± 0.2 days and a beta spectrum is

observed which can be resolved into groups of maximum energy 1.92±0.02 Mev and 0.65±0.03 Mev. Gamma rays of 1.31±0.02 Mev, 0.82±0.02 Mev, and 0.48±0.02 Mev are found. Gamma-gamma coincidences are observed only between the 0.82 Mev and the 0.48 Mev radiations. We see no other gamma rays unambiguously attributable to Ca^{47}. The results of these investigations and others in progress on the $A=47$ isobars will be discussed.

* This work partially supported by the U. S. Atomic Energy Commission.
[1] Luis Marquez, Phys. Rev. **92**, 1311 (1953).
[2] Cork, LeBlanc, Brice, and Nester, Phys. Rev. **92**, 367 (1953).
[3] Aten, Grenell, and Van Dijk, Physica **19**, 1049 (1953).

V3. Decay of Sc^{44}.* J. W. Blue and E. Bleuler, *Purdue University.*—The decay of Sc^{44} has been reinvestigated using a magnetic-lens spectrometer adapted to coincidence measurements. The fraction of transitions going by electron capture has been measured to be 0.06±0.01, in agreement with theory. With this branching ratio the total conversion coefficients of the 270-kev isomeric transition and of the 1.16-Mev gamma ray in Ca^{44} are 0.132±0.002 and 6.36±0.13×10^{-3} respectively. This indicates an $M4$ or $E4$ transition for the 270-kev gamma ray and an $E2$ transition for the 1.16-Mev gamma ray. The continuous electron spectrum, reported by Bruner[1] to accompany 4 percent of the positron decays, has been studied in coincidence with the nuclear gamma ray and with the positrons. The intensity was observed to be very dependent on the thickness of the source and backing. Using vacuum evaporated sources on 0.6 mg/cm² Al backing, the electron intensity between 30 and 150 kev was found to be ¼ of that previously reported. The coincidence measurements show that ¾ of these electrons are not in coincidence with the full-energy nuclear gamma ray and hence are created by the gamma ray.

* Supported by the U. S. Atomic Energy Commission.
[1] J. A. Bruner, Phys. Rev. **84**, 282 (1951).

V4. Inner Bremsstrahlung from V^{49}. R. W. Hayward and D. D. Hoppes, *National Bureau of Standards.*—The x-radiation and inner bremsstrahlung from the electron capturing V^{49} have been studied by means of an argon-methane proportional counter and a well-type sodium-iodide scintillation spectrometer. The observed internal bremsstrahlung spectrum is corrected for background, energy resolution, Compton and escape electrons, gamma-ray detection and geometrical efficiency of the crystal, and source-absorption effects. The spectrum may be essentially accounted for over most of the energy range by the theory of Glauber and Martin[1] incorporating p-electron capture and Coulomb effects. The total disintegration energy of V^{49} as determined from the spectrum is 610±10 kev. A recent determination of the half-life of 334±20 days by Lyon[2] leads to a logft=6.16±0.03, a value consistent with other allowed spectra with transitions within the $f_{7/2}$ shell.

[1] R. J. Glauber and P. C. Martin, Phys. Rev. **95**, 572 (1954).
[2] W. S. Lyon, Phys. Rev. **97**, 121 (1955).

V5. The Internal Conversion Coefficient of Cr—51. Z. O'Friel and A. H. Weber,* *Saint Louis University.*—The internal conversion coefficient of V^{51} (parent, Cr^{51}) was measured (using a thin lens β-ray spectrometer) employing the Compton electron spectrum for determination of the number of unconverted nuclear photons,[1] following the Thomas-Lauritsen analysis.[2] The value of α_K is (1.38±0.13)×10^{-3}. This value compares with 1.5×10^{-3} of von D. Maeder, *et al.*[3] who used a scintillation detector for the measurement of atomic x-rays and nuclear photons. These values correspond to an $M1$ transition in the Rose-Goertzel tables. Since Cr^{51} decays by K-capture to the ground state of V^{51}, the Compton electron method is particularly applicable.

* Supported in the initial phases of the work by the U. S. Atomic Energy Commission.
[1] Sturcken, O'Friel, and Weber, Phys. Rev. **93**, 1053–1056 (1954).
[2] R. G. Thomas and T. Lauritsen, Phys. Rev. **88**, 969–986 (1952).
[3] von D. Maeder, Preisweik, and Steinemann, Helv. Acta Phys. **25**, 461–463 (1952).

V6. The Decay of Rh^{104} and Rh^{104m}.* M. E. Bunker, J. P. Mize, and J. W. Starner, *Los Alamos Scientific Laboratory.*—The radiations of Rh^{104} (44 sec) and Rh^{104m} (4.3 min) have been investigated with β- and γ-scintillation spectrometers and a magnetic lens. The dominant radiation of Rh^{104} is the well-known 2.5-Mev ground-state β transition (98.5 percent). β–γ coincidence studies have revealed two other Rh^{104} β groups with energies and intensities of ~1.9 Mev (1.4 percent) and ~0.7 Mev (0.08 percent). Associated with the lower-energy β groups are γ rays of energy 0.556 and 1.24 Mev. These two gammas are in coincidence. Although Rh^{104m} decays predominantly by gamma emission to Rh^{104}, it is also β unstable (~0.1 percent of the disintegrations), giving rise to γ transitions in Pd^{104} of energy 0.556, 0.74, 0.78, and 1.53 Mev. γ–γ coincidence studies indicate the existence of additional γ rays of energy ~0.92 and ~1.34 Mev which are presumably also associated with the decay of Rh^{104m}. Possible spin assignments for the levels of Pd^{104} will be discussed.

* Work performed under the auspices of the U. S. Atomic Energy Commission.

V7. Decay of Neutron Deficient Rhodium Isotopes.* Donald J. Farmer, *University of Washington.*—Observation of the decay of internal conversion electrons from active rhodium using a beta-ray spectrometer with sources prepared from the rhodium fractions of proton- or deuteron-bombarded ruthenium, and additional studies with a NaI(Tl) scintillation coincidence spectrometer using sources prepared by proton bombardment of natural and separated isotopes of ruthenium reveals radiations having the following characteristics: Rh mass ≤99, half-life 15.0±0.2 days, gamma rays 0.086 Mev ($K/L/M\approx25/5/1$) and 0.353 Mev, coincidences between these radiations and with annihilation radiation; Rh mass <102, half-life 5±1 years, gamma rays 0.127 Mev ($K/L\approx8$) and 0.198 Mev, coincidences between these radiations, no coincidences with annihilation radiation. These radiations were previously attributed to Rh^{102} (220 day).[1,2] The mass assignments of 4.5 day Rh^{101} and 21 hour Rh^{100} are confirmed, as are the assignments of the higher-energy gamma radiations of Rh^{102}. Gamma-ray coincidence studies have been made on the latter isotope.

* Supported in part by the U. S. Atomic Energy Commission.
[1] L. Marquez, Phys. Rev. **95**, 67 (1954).
[2] D. B. Kochendorfer and D. J. Farmer, Phys. Rev. **96**, 855A (1954).

V8. Attenuation of the Cd^{111} Directional Correlation in Liquid In^{111} Sources. R. M. Steffen, *Purdue University.*—Directional Correlation measurements[1] on viscous liquid sources of In^{111} indicated the presence of a small but not negligible attenuation of the Cd^{111} gamma correlation in dilute aqueous solutions of In salts. The attenuation effect is due to the interaction of the nuclear quadrupole moment in the first excited Cd^{111} state with the rapidly fluctuating fields which are present in the liquid. This time-dependent interaction is characterized by a parameter λ_2. Measurements of the directional correlation of the Cd^{111} gamma rays as a function of the delay-time between the emission of the first and the second gamma ray enabled us to measure λ_2 directly for different liquid sources. In dilute aqueous solutions $\lambda_2=(6\pm1)\times10^8$ sec^{-1}. Viscous sources (aqueous solutions of $InCl_3$ +glycerin) show considerably larger values of λ_2; however, λ_2 does not increase as rapidly as the macroscopic viscosity of the liquid. The unperturbed directional correlation of the Cd^{111} gamma cascade, as obtained from these measurements, is: $W(\theta)=1-(0.18\pm0.01)P_2(\cos\theta)$.

[1] P. B. Hemmig and R. M. Steffen, Phys. Rev. **92**, 832 (1953).

V9. A Fast Favored First Forbidden Beta Transition.* Michael J. Glaubman, *Princeton University.*—The ground state of Sb^{129} is known to be $2-$[1]; the ground state of the even-even Sn^{128} nucleus is presumably $0+$. The transition between

the two states is parity favored and therefore unique (Tensor), and the K/β^+ ratio depends only on the energy and certain well-defined electronic wave functions.[2] We have measured the positron intensity (by measuring the annihilation radiation in a calibrated source) and compared it with the intensity of the K capture to the ground state as determined in a previous experiment.[3] Our preliminary results are: $K/\beta^+ = 300 \pm 130$; $W_0 = 2$ (mc^2); $\log(W_0^2 - 1)ft = 9 \pm 0.15$. The $\log ft$ value indicates that the positron decay is speeded up by a factor of 10 compared to the negatron decay.[1] This fact can be explained in terms of the purity of configurations of magic nuclei and the favorable configuration of Sb^{122} ($g_{7/2}h_{11/2}$) for this type of transition ($\Delta J = 2$, $\Delta L = 1$).

* Supported by the Atomic Energy Commission and The Higgins Fund.
[1] M. J. Glaubman and F. R. Metzger, Phys. Rev. **87**, 203 (1952).
[2] R. E. Marshak, Phys. Rev. **61**, 431 (1942).
[3] M. J. Glaubman, to be published in the Phys. Rev.

V10. Radiations from $_{50}Sn^{125}$ (9.7 *d* and 9.5 *m*).* S. B. Burson, J. M. LeBlanc, and D. W. Martin, *Argonne National Laboratory.*—The radiations from $_{50}Sn^{125}$ (9.7 *d* and 9.5 *m*) have been studied using the scintillation coincidence spectrometer and the decay scheme deduced. Enriched Sn^{124} was irradiated with reactor neutrons and chemically purified. From the NaI(Tl) pulse-height distribution, the presence of seven gamma rays associated with the 9.7-day activity is concluded. These have energies: 1.98 ± 0.02, 1.41 ± 0.02, 1.07 ± 0.01, 0.90 ± 0.01, 0.81 ± 0.01, 0.47 ± 0.01, and 0.34 ± 0.01 Mev. An anthracene crystal was used for beta-ray detection. The aluminum-absorption curve of the total beta spectrum shows, in addition to a predominant component of about 2.3 Mev, a weak low-energy branch. Coincidence-absorption curves taken with selected gamma rays show this inner spectrum itself to be complex. Two components of ~0.4 Mev and ~1.3 Mev are so resolved. The foregoing results, together with gamma-gamma coincidence measurements, lead to a decay scheme for the 9.7-day activity believed to be unique. Four excited states in the Sb^{125} nucleus with energies 1.07, 1.41, 1.88, and 1.97 Mev are shown to exist. In the 9.5-m activity, a weak gamma ray of 1.41 Mev is observed in addition to the known 0.326-Mev transition.

* Work done under auspices of U. S. Atomic Energy Commission.

V11. Radioactive Decay of Cs^{134}. H. H. Forster and J. S. Wiggins, *University of Southern California.*—The beta- and gamma-ray spectra of (2.3*y*) Cs^{134} have been investigated with a double-thin lens beta-ray spectrometer of 1.5–2.5 percent resolution and a NaI scintillation spectrometer with a single-channel pulse-height analyzer. The source material was CsCl in acid solution obtained from Oak Ridge. An analysis of the beta spectrum showed evidence of four beta groups with approximate endpoint energies of 87, 220, 405, and 655 kev. Gamma lines obtained through internal and external conversion had energies of 475, 562, 569, 604, 662, 796, 802, 1036, 1170, 1368, and 1401 kev. No definite evidence for the 202 kev gamma mentioned by Cork[1] has been observed. Details of the spectrum will be presented, and the decay scheme will be discussed.

[1] Cork, LeBlanc, Nester, Martin, and Brice, Phys. Rev. **90**, 444, (1953).

Saturday Morning at 9:00

Caribar Room

(E. Montroll presiding)

Theoretical Physics, IV

VA1. Application of Operator Calculus to Irreversibility. U. Fano, *NBS.*—A small system A interacting with a large system B experiences irreversible effects, analyzed conveniently[1] by Feynman's operator calculus. To describe the state of A we consider the Heisenberg representation $\mathfrak{F}(t) = \exp(iHt) \times F \exp(iHt)$ of operators F acting on A only, and average it over the initial state of B ($\mathfrak{F}(t)$ operates on B through $H = H_A + H_B + V$). An improved version of an earlier[1] formula is now presented:

$$\langle \mathfrak{F}(t) \rangle_B = F \exp \int^t dt' \{ i[H_A + \langle V \rangle_B, I] - \int^{t'} du \langle [\mathfrak{V}(-u), (\mathfrak{V}, I)] \rangle_B + \cdots \},$$

where operators on left of I act left of F. This equation is exact and displays the qualitative aspects of the problem. $\langle \mathfrak{F}(t) \rangle_B$ varies by infinitesimal transformations $\exp dt' \{ \cdots \}$ which operate not in succession but interlocked because $\mathfrak{V}(-u)$ acts at $t' - u$ instead of t'. The time variations of $\langle \mathfrak{F}(t) \rangle_B$ obey a first-order differential equation only if this interlocking can be discounted in view of short life of autocorrelations and of other circumstances.

[1] U. Fano, Phys. Rev. **96**, 869 (1954).

VA2. Green's Function for Heat Conduction-Convection Problems with Given Motion of the Boundaries. H. Kurt Forster, *University of California.*—The equation for combined heat conduction and convection in an incompressible fluid contains the explicitly time varying term $v(r,t) \cdot \operatorname{grad} T$; consider conditions $T = 0$ or $\operatorname{grad} T = 0$ along boundaries which may move; general methods are hardly developed for such problems. We show that a solution, to any desired degree of accuracy, may be obtained along these lines: Subdivide t into intervals $t_1 t_2 \cdots t_n$; let the temperature distribution at t_i be $T_i(r')$ and $G_i[r, r', (t_{i+1} - t_i)]$ the known Green's function for the pure heat-conduction problem for the domain at t_i. Solve the pure conduction problem from t_i to t_{i+1} by $\Theta(r) = \int G_i \cdot T_i dr'$; then $T_{i+1}(r') = \Theta[r' - h(r')]$, where $h(r)$ represents the fluid displacement (convection) in time $(t_{i+1} - t_i)$, gives an approximation to the temperature distribution at t_{i+1}. Let $P_n(r,t)$ be the result of this process applied successively to the n intervals, and let the initial temperature be an instantaneous unit source, the convergence of P_n, as $n \to \infty$, to the exact Green's function of the heat conduction-convection problem is then assured on physical grounds and the boundary conditions remain satisfied throughout. This method was applied to an actual problem;[1] a mean for P_1 (between the two possible paths leading to P_1) gave good agreement with experiment.

[1] H. K. Forster, J. Appl. Phys. **25**, 1067 (1954).

VA3. Numerical Solution of the Integral Transport Equation. Daniel Schiff, *Westinghouse Electric Corporation.*—The transport equation for particles which interact only with the constituents of a relatively dense medium, and not with one another, is expressed in the form of an inhomogeneous linear integral equation. The unknown function in this equation is the directional flux, or in an alternate formulation, the

ith generation of directional birth-rate density. There is in the general case a quadruple integral over the space, angle, and energy variables, the kernel being a product of a cross section, an exponential attenuating factor, and a scattering function. The equation is made amenable to computation by employing discrete variables and replacing the integrals with sums over the space lattice, angular divisions, and energy groups. All physical processes may be included, the approximation being only in the size of the above intervals. With the aid of an electronic digital-computer multienergy group, multiregion problems have been calculated which include capture, fission, elastic, and inelastic scattering of neutrons and photoelectric absorption, pair production, and Compton scattering of gamma rays. Simple cases have been calculated for comparison with analytic solutions of the differential integral form of the transport equation, and they yield satisfactory results.

VA4. Asymptotic Spatial Trend of Electron Penetration. L. V. SPENCER, *NBS.*—The equation describing electron penetration in the continuous slowing-down approximation[1] is reduced to an interlinked system of ordinary differential equations by a Fourier transform in the spatial coordinate and a Legendre transform in angle. In an approximation suited to deep penetration this system reduces further to a partial differential equation having the simple but apparently nonseparable form of a Schrodinger oscillator equation with time-dependent force constant. This equation is in fact separable and has both eigenfunction and point solutions. The point solutions are of most interest and yield the desired deep penetration spatial trend. In the limit of small-energy losses, the point solutions express analytically the summation of the series solutions of Yang.[2] The treatment of this schematic equation can be generalized to yield a method for solving the more realistic linked system of ordinary differential equations. This approach supports and complements a theory recently submitted by the author to the Physical Review.

[1] H. W. Lewis, Phys. Rev. **78**, 526 (1950).
[2] C. N. Yang, Phys. Rev. **84**, 599 (1951).

VA5. Diffusion Equation of Nucleonic Component of Cosmic Rays.* S. OLBERT, *M.I.T.*—A linear integro-differential equation of the type:

$$\frac{\partial N(E,x)}{\partial x}=\frac{-1}{\lambda}N(E,x)+\frac{1}{\lambda_s}\int K(E,E')N(E',x)dE'+Q(E,x)$$

is investigated theoretically with particular reference to the diffusion of the nucleonic component of high-energy cosmic rays in the atmosphere. The kernel function $K(E,E')$ is chosen so as to incorporate the basic features of Fermi's model of multiple production of meson and (possibly) antinucleons. It is shown that, using reasonably simplified forms of $K(E,E')$, one can find general analytic solution of the above equation. The results obtained are compared with the experimental data.

* This work is supported in part by the joint program of the Office of Naval Research and the U. S. Atomic Energy Commission.

VA6. Exchange in the Thomas-Fermi-Dirac Model.* W. G. MCMILLAN, *University of California at Los Angeles and The RAND Corporation.*—In the statistical model of the atom at zero temperature, the maximum local electron-momentum P is related to the electrostatic potential V by $P^2/2m-\lambda e^2P/\pi\hbar=eV+\mu$, where μ is the electron chemical potential. The coefficient λ is zero for the Thomas-Fermi (TF) case, and unity for the Dirac (TFD) modification. March has recently given compelling arguments for interpreting the zero-pressure TFD atom (which has a finite radius) as a constituent of a metallic phase rather than of a dilute gas, and has cited the atomic radii of the alkali metals in support. Generally, however, this model predicts much too large atomic volumes. The Dirac exchange correction is calculated using plane waves, and thus assumes that the electrons involved in the exchange come from regions of the same density, and therefore same P. Actually, the electron density within a normal atom changes markedly over (radial) distances comparable to the electron wavelength. Near the atomic boundary this has a most pronounced effect on P and thus on the predicted normal volume. Assuming the exchange correction to be of the Dirac form, but with λP in place of P, λ has been determined from Latter's solutions so as to give agreement with experimental atomic volumes. The resulting values of $\mu(=1.29\lambda^1$ ev), then agree semiquantitatively with experimental photoelectric work functions.

[1] R. Latter (to be published).

VA7. A Variant on the Yang Lee Theory of Condensation. M. B. LEWIS AND A. J. F. SIEGERT, *Northwestern University.*—The pressure defined in the work of Yang and Lee[1] is not the average pressure in the grand canonical ensemble, but is defind by averaging the latter once more over all volumes smaller than the volume of the systems in the grand canonical ensemble.[2] While there is little doubt that these two definitions become equivalent in the limit of infinite volume, a rigorous proof of this equivalence would have to be based again on properties of the *canonical* partition function such as van Hove's theorems.[3] We have, therefore, made more rigorous a variant of the Yang Lee theory suggested by one of us.[4] This variant replaces the grand canonical ensemble by the pressure ensemble and deals only with quantities which can be operationally defined even for finite systems. The proof is based primarily on some of van Hove's theorems.[3]

[1] C. N. Yang and T. D. Lee, Phys. Rev. **87**, 404 (1952).
[2] C. N. Yang, "Special problems of statistical mechanics I" (mimeographed lecture notes, Seattle, 1952), p. 31.
[3] L. van Hove, Physica **15**, 951 (1949).
[4] A. J. F. Siegert, Phys. Rev. **96**, 243 (1954).

VA8. An Exact New Reformulation of the Many Body Problem. J. K. PERCUS, *New York University Institute of Mathematical Sciences,* AND G. J. YEVICK, *Stevens Institute of Technology.*—In previous work,* we have introduced collective coordinates $(\Sigma\exp(ikx_i))$ for the purpose of transforming the N-body problem into that of a set of linear harmonic oscillators. The justification for this method is that the resulting oscillators appear to be dynamically independent. Up to now, the error inherent in the independent-oscillator picture eluded us. We here present the exact reformulation of the Lagrangian in terms of collective coordinates, utilizing for this purpose a set of very simple identities. The general procedure is first illustrated with the external potential terms in the Lagrangian, in which the concept of dynamical fourier coefficient is first introduced. The same procedure is applied to the internal potential terms, and now we obtain twofold dynamical fourier coefficients, the most significant terms being the "diagonal" coefficients which can be expressed by the two-particle correlation function of the system. The two-particle correlation function is seen to play an important role in the dynamical theory, as indicated in previous work on the superfluid, Helium II. Finally, a similar technique is used to recast the kinetic-energy term.

* Detailed papers have been submitted to Phys. Rev.

VA9. The Exact Classical and Quantum Mechanical Equations of Motion for N Particles Using Collective Coordinates. G. J. YEVICK, *Stevens Institute of Technology,* AND J. K. PERCUS, *New York University Institute of Mathematical Sciences.*—First, the exact quantum-mechanical Schrodinger

equation in collective coordinates can be obtained in a simple, nonforced manner by the methods of the preceding abstract. The only change is in the quantum-mechanical kinetic-energy operator, which is handled in a general fashion. Specific quantum-mechanical terms appear which can be suitably eliminated. The statistics are made manifest by the special form of the boundary conditions in q-space. Next, the exact classical equations of motion for the collective coordinates are presented. These equations represent a set of N-coupled harmonic oscillators which correspond in various approximations to the equations considered in previous work. An interesting feature in the above is that only $2N$ collective coordinates are required in the exact theory as opposed to the infinite number which one would expect. These higher dependent q_k's (which we can express in terms of the N independent coordinates) play a paramount role in the understanding of finer physical details in the general dynamical theory of N-particles. The solution of the classical equations of motion has been initiated by means of the method of variation of parameters, which allows one to make a detailed study of such problems as the transition from order to chaos.

VA10. Particle Motion in Nonrelativistic Quantum Theory. RALPH SCHILLER, *Stevens Institute of Technology.*—In the nonrelativistic quantum theory of a spinning electron it is found that the usual transition to classical mechanics cannot be made via the route of ray optics. The velocity of the particle can no longer be written as the gradient of a scalar function so that the Hamilton-Jacobi theory must be generalized for a transition to classical mechanics to be effected. In this generalization the velocity field for the particle must be written $v=\nabla s+\xi\nabla\eta$,[1] which is the Clebsch decomposition for an arbitrary vector field. We show that for a nonrelativistic particle of arbitrary spin whose motion is determined by a Schrodinger-type equation, the velocity field always has the Clebsch form, $v=\nabla\varphi+\cos\theta\nabla\chi$ where θ, χ, and φ are the Euler angles of rotation. If the field describes a particle that is capable of distortion in addition to rotation (the particle might have a varying quadrupole moment) then the velocity field depends on the parameters of distortion as well as the parameters of rotation.

[1] Bohm, Schiller, and Tiomno, Nuovo cimento (to be published).

VA11. Applications of Topology to General Relativity. C. W. MISNER,* *Princeton University.*—We look upon the set of homogeneous differential equations consisting of the Einstein field equations together with Maxwell's equations and the Dirac equation for a neutrino in general relativistic form as the statement of an as yet unquantized unified field theory. The topological content of these equations implied by the theorems of Hodge and de Rham is pointed out. A relationship between critical points of the metric (where $(-g)^{\frac{1}{2}}=0$) and annihilation of the "particles" of this theory is given. The existence of nontrivial solutions of the field equations is not established.

* Proctor Fellow.

VA12. Flat Picture of Curved Space. F. J. BELINFANTE, *Purdue University.*—Gupta's quantization of Einstein's gravitational field suggests simplifying nature's laws in systems S "flat" at infinity and satisfying De Donder's coordinate condition, by introducing an auxiliary tensor $\gamma_{\mu\nu}=\delta_{\mu\nu}(1-2\delta_{\mu 0})$ in one such system $S_0(ct,x,y,z)$, thus singling out a Lorentz group. Not being uniquely determined, $\gamma_{\mu\nu}$ is subject to "gauge transformations" (=variety of choice). Therefore, Rosen's geometrical interpretation of $\gamma_{\mu\nu}$ (Phys. Rev., 1940) is unjustified, and the question of "gauge invariance" of Gupta's quantization deserves attention. From S_0 conventionally obtain a polar coordinate system $S_r(ct,r,\theta,\varphi)$, and find the static spherical empty-space solution of Einstein's equations for the metric $g_{\mu\nu}$ around the origin in S_r. Comparison with Schwarzschild's solution shows $r=\rho-m$, if $\rho=$Schwarzschild's radical variable. Radial distances $R=\int(g_{\rho\rho})^{\frac{1}{2}}d\rho$ for points with $\rho<2m$ are imaginary; thence, points $r<m$ not corresponding to real points in space should be omitted from the quantum-field theoretically useful flat picture of curved space S_r on scale $(\gamma_{\mu\nu}dx^\mu dx^\nu)^{\frac{1}{2}}$: $(g_{\mu\nu}dx^\mu dx^\nu)^{\frac{1}{2}}$. In spacetime this provides tubelike holes as "worldtubes" of particles. ("Swiss-cheese model"). Fields surrounding actual particles may prevent such holes in the "flat" picture of space.

VA13. Defining Invariants of Metric Spaces. ARTHUR KOMAR, *Princeton University.*—The importance of the problem of characterizing the metric spaces of General Relativity by sets of invariants, as a more precise formulation of Mach's Principle is presented. It is found that two n-dimensional spaces are locally applicable if the equating of the sets of all fundamental scalars of orders up to $n+2$ in derivatives of the metric, of both spaces, form a consistent set of equations for the solution of the coordinate transformations which are to take one from one metric to the other. In this sense these scalars form a (in general highly overdetermined) set of invariants which define the space.

VA14. A Formulation of Relativity. HUSEYIN YILMAZ, *Stevens Institute of Technology.*—The two principles of special relativity; namely, the covariancy of natural laws and the invariancy of the velocity of light are derived from a common principle called the principle of superposition. It is shown that the quantities which satisfy the principle are scalars, vectors, tensors, and spinors. Covariant and the contravariant components arise from the fact that for any solution of the principle there is another solution which is dual to the first. Therefore, for any description of nature there is a dual description. The metric character of physics then follows from the requirement that the two descriptions must lead to the same physical conclusions. Other interesting aspects are discussed.

VA15. A Classical Microphysics. GERTRUDE T. SCHWARZMANN.—Interpretation of wave and corpuscle state as alternate, equivalent states of the entities of light and matter, of particle waves as alternating currents with a direct-current component, of their velocities those of the associated particles, of spin motion as full-fledged motion is the foundation to a classical microphysics. The composite character of revolution, sense of revolution always equal to sense of spin, allows of differentiating earthial from mercurial motion. For earthial motion the spinning corpuscle ring alters; for mercurial motion it maintains its orientation relative to its radius vector, so that its spin component is transformed into a second revolutional component. Assuming that the cutting of magnetic lines of force by the spinning corpuscle ring is prerequisite to the transition corpuscle into wave, the electron, mercurially spiraling towards the nucleus, cannot emit radiation, interpreted as wave phenomenon. Interpolated between mercurial spirals and earthial stationary orbits are the earthial transition orbits wherein the electron, on transition from an mth into an nth orbit spinning $2n$ times per revolution, is transformed into the associated electron wave which decomposes at the perihelion into the corresponding light wave of frequency $R.c.(m^2-n^2)/n^2\cdot m^2$ and electron wave of frequency $v_n^2\cdot m_2/h$, whereupon both component waves revolve around the nucleus.

SATURDAY AFTERNOON AT 1:30

Burgundy Room

(M. A. TUVE presiding)

Apparatus of Nuclear Physics, II

W1. An Occluded-Gas Ion Source.* LAWRENCE RUBY AND JAMES D. GOW, *University of California, Berkeley.*—An occluded-gas-pulsed ion source has been developed which embodies a method of obtaining large quantities of ions and electrons from hydrogenated titanium. The plasma is released when a spark is initiated on the surface of the metal. To achieve this in vacuum, a capacitor or pulse line is discharged across a sandwich of titanium separated by a thin insulator. A stack of such metal-insulator elements is used to average out individual variations in the sparks. A typical stack is ¼ in. diameter by 1 in. long. With axial geometry and a 3/32-in. source opening, 10 ma at 10 KV has been extracted with an aperture electrode and 250 ma, correspondingly, with a grid electrode. With radial geometry, ions have been extracted using a slot electrode. Pulse lengths have ranged from 10 μsec to 1 msec at rates as high as 5 pps. H^+ dominates H_3^+ by a factor of 3 in the mass-emission spectrum. The composition of the insulators influences the spectrum. Advantages of the source are its high output, compact size, high ratio of atomic to molecular ions, independence of a magnetic field, and gas economy.

* This work was done under the auspices of the U. S. Atomic Energy Commission.

W2. Triggering a Fast Two-Crystal Compton Scintillation Spectrometer with Iodine-Escape X-Rays from the NaI(Tl) Primary Crystal. P. R. HOWLAND AND N. E. SCOFIELD, *U. S. Naval Radiological Defense Laboratory.*—Using the 133.5 kev[1] line in $Ce^{144}-Pr^{144}$ a peak has been observed in the pulse-height spectrum of a Compton scintillation spectrometer which corresponds to the usual escape peak observed in single-crystal spectrometers but which differs in the mechanism of observation in that the escape peak is triggered by escape x-rays which leave the primary crystal and are incident on the secondary crystal. This escape peak for the 133.5-kev line has an energy of 98±3 kev. By discriminating against the secondary crystal pulses up to and including weighted average energy of the escaping iodine *K* x-rays, it is possible to make the escape peak disappear. This method gives a possible means of distinguishing photoelectric processes from Compton processes at incident energies up to about 200 kev.

[1] Cork, Brice, and Schmid, Phys. Rev. **96**, 1295 (1954).

W3. Monte Carlo Calculation of the Response of NaI(Tl) Scintillation Spectrometers. MARTIN J. BERGER AND JOHN A. DOGGETT, *NBS.*—Measurements of γ rays with NaI(Tl) crystals yield pulse-height distributions related to the true energy spectrum by an integral equation whose kernel (response function) is the probability that an incident photon of energy E will give rise to a pulse of size E'. We have calculated this function for photons with energies from 0.279 to 4.45 Mev, incident on cylindrical crystals ranging from ½ in. (diameter)×½ in. (length) to 5 in.×9 in. Most of the calculations pertain to collimated sources, some to incident broad beams and point isotropic sources. Compton scattering and absorption were treated by the Monte Carlo method. A total of 50 000 random walks were computed and analyzed on the NBS automatic computer. Analytical corrections were made for the escape of annihilation radiation and bremsstrahlung. The shape of the response function is determined in first approximation by a characteristic parameter p = (area under photopeak)/(area under entire pulse-height spectrum), a smooth function of (crystal length×diameter)$^{\frac{1}{2}}$. For small crystals, our values of p are in good agreement with those obtained by Maeder *et al.*[1] by an approximate analytical calculation.

[1] Maeder, Müller, and Wintersteiger, Helv. Phys. Acta, **27**, 3 (1954).

W4. Oxygen Quenching and Wavelength Shifters in Liquid Scintillators. C. A. ZIEGLER, H. H. SELIGER, AND I. JAFFE, *NBS.*—We have investigated the effects of oxygen quenching and of the addition of a wavelength shifter under more well-defined conditions of oxygen removal than reported previously.[1,2] Oxygen-free solutions prepared and flame-sealed under vacuum were compared with oxygen-saturated solutions using the γ rays from $Cs^{137}-Ba^{137}$ and a Dumont 6292 PMT in a reproducible geometry. The integral of the pulse-height distribution curve was assumed to be proportional to the light output. We have found that the major contribution of the wavelength shifter α naphthylphenyloxazole is to compete with dissolved oxygen for the energy in the solution, the former emitting light and the latter de-exciting by other processes. The 23 percent gain in sensitivity to be expected on the basis of the shift in the emission spectrum is almost completely compensated for by the approximately 83 percent efficiency for the energy transfer from solute to shifter. Data with *p*-terphenyl, 2,5-diphenyloxazole and α napththylphenyloxazole in zylene will be presented.

[1] Pringle, Black, Funt, and Sobering, Phys. Rev. **92**, 1582 (1953).
[2] J. R. Arnold, Science **119**, 155 (1954).

W5. Response of a Sodium-Iodide Spectrometer to High-Energy Electrons.* H. W. KOCH, J. M. WYCKOFF, AND B. PETREE, *NBS.*—Monoenergetic electrons from a 50-Mev betatron operated between 1 and 20 Mev were used to study the performance of a 5 in. by 4 in. and a 5 in. by 9 in. NaI(Tl) total-absorption spectrometer.[1] The pulse-height distributions produced by bombardment of the central axis of the large crystals show very peaked distributions with small tails. The energy resolution reaches its optimum value at 10 Mev where the total width at half maximum is 4 percent, whereas the comparable resolution for 10-Mev x-rays would be 9 percent.[1] This added width to the x-ray pulse-height distribution results largely from the escape of one annihilation photon from the crystal. Synthesis of the x-ray distributions from the electron distributions and the linearity of spectrometer response to electron energy will be discussed.

* Supported in part by the U. S. Office of Scientific Research of the Air Research and Development Command.
[1] R. S. Foote and H. W. Koch, Rev. Sci. Instr. **25**, 746 (1954).

W6. A Fast Multichannel Coincidence Circuit.* T. H. BRAID AND R. W. DETENBECK,† *Princeton University.*—For delayed coincidence and time of flight experiments, it is advantageous to measure the time distribution of coincidences in a multichannel device. The condenser discharge principle used in the present circuit is due to Rossi and Nereson.[1] The first signal cuts off a diode, allowing a condenser to discharge slowly through a resistance. The delayed signal stops the discharge. The amplitude of the pulse from the CR circuit is proportional to the delay time T if $CR \gg T$. These pulses are fed to a twenty-channel pulse-height analyzer, gated by a slow conventional coincidence circuit so that single pulses are not

recorded. We have used the circuit so adjusted as to be linear up to 0.1 microsecond delay and have obtained a resolving time $2\tau = 3.10^{-9}$ second. This was measured with Na^{22} annihilation quanta (one side artificially delayed) and terphenyl crystals as detectors.

* Supported by the U. S. Atomic Energy Commission and the Higgins Fund.
† National Science Foundation Predoctoral Fellow.
[1] Rossi and Nereson, Rev. Sci. Instr. 17, 65 (1946).

W7. A Precision Monitor for Electron Beams.* G. W. TAUTFEST AND K. L. BROWN, *Stanford University.*—Two Faraday-cup electron beam monitors have been developed which are capable of measuring the absolute integrated beam current of the Stanford linear accelerators to an accuracy of better than $\pm\frac{1}{2}$ of one percent and ± 2 percent, respectively. The combined energy range of these integrators is from 1 Mev to better than 300 Mev. With the techniques employed, it is evident that with only minor modifications in size, the useful range of such beam monitors can be extended to energies beyond 1 Bev. Design principles and construction details will be discussed. Such monitors have proved to be especially valuable in conjunction with the Stanford linear accelerators where large peak currents of small cross-sectional area are frequently used.

* Supported by the Office of Naval Research and the U. S. Atomic Energy Commission.

W8. A New Multichannel Recording Time-Delay Analyzer.* P. G. KOONTZ, C. W. JOHNSTONE, G. R. KEEPIN, JR., AND J. D. GALLAGHER, *Los Alamos Scientific Laboratory.*—A new time-delay analyzer encompassing a wide, flexible time base will be described. The system includes three basic units: (1) a four-decade gated scaler with pulsed reset; (2) a crystal controlled interval timer; and (3) a coincidence readout circuit which duplicates the instantaneous reading of the gated scaler at intervals established by pulses from the timer unit. Time channels of 0.001-, 0.01-, 0.1-, 1-, and 10-sec width are provided; these may be combined either in progressive sequence starting with a preselected channel width, or used individually on continuous operation at a single channel width. Provision is made for either photographic recording or electrical print-out on electrosensitive paper. Data obtained with the new analyzer agree with a conventional ten-channel time-delay analyzer over the limited range of the latter. A simple procedure is available for checking correct operation of the system. The development of this analyzer was prompted by the need for such an instrument to study the complex decay of delayed neutron emitters produced in the fission process. However, it was purposely developed as a versatile system capable of handling a wide range of problems requiring time-delay analysis.

* Work performed under the auspices of the U. S. Atomic Energy Commission.

W9. A New Type of Lens for Charged Particles.* NATHANIEL P. CARLETON, *Harvard University* (introduced by O. Oldenberg).—An electrostatic lends for charged particles can be made by producing a potential which varies continuously with the distance along a cylindrical surface coaxial with the beam of particles. In particular, when the potential varies along the cylinder as the square of the distance from some original plane, then the equations of motion for a charged particle in the cylinder are easily solvable and the particle trajectories found analytically. From the trajectories one sees that this potential configuration acts as a positive or negative lens which has no aberrations when both object and image are in the field and other special conditions are also met. The aberrations of this lens when it is used with the object and image outside the field have not been calculated, but use of the lens to focus low-energy protons indicates that aberrations may be smaller than those of conventional focusing fields. The lens can be perfectly realized by depositing a conducting film of variable thickness inside a glass cylinder and passing a current through it. In tests, the theory was realized approximately by a succession of closely spaced rings, maintained at the proper potentials.

* This work was partially supported by the Air Force Cambridge Research Center.

SATURDAY AFTERNOON AT 1:30

Main Ballroom

(M. DEUTSCH presiding)

Invited Paper

X1. The Transuranium Elements. A. GHIORSO, *University of California, Berkeley.* (40 min.)

Various Topics in Nuclear Physics

X2. An Attempt to Detect Neutrinos by the Reaction $Cl^{37}(\bar{\nu},e^-)A^{37}$.* RAYMOND DAVIS, JR., *Brookhaven National Laboratory.*—Large volumes of carbon tetrachloride have been irradiated adjacent to the Brookhaven reactor in an effort to observe the reaction $Cl^{37}(\bar{\nu},e^-)A^{37}$ induced by fission-product neutrinos. The experiments have demonstrated that radioactive A^{37} can be removed from 1000-gallon quantities of carbon tetrachloride by sweeping with helium gas. The background amounts of A^{37} induced in carbon tetrachloride by the nucleonic component of cosmic radiation, and fast neutrons has been measured. An upper limit to the cross section was set of 2×10^{-46} cm² per atom. The background effects prevented observing lower values of the cross section. The possibility of observing the theoretically calculated cross section of 4×10^{-45} cm² per atom will be discussed.

* Research carried out under the auspices of the U. S. Atomic Energy Commission.

X3. Annihilation Radiation from Positrons Stopping in Superconducting Lead. S. M. SHAFROTH AND J. A. MARCUS, *Northwestern University.*—Coincident two-quantum annihilation radiation from positrons stopping in lead at 4.2°K was observed alternately in a magnetic field of 750 gauss and with no field. Thus the lead was alternately in its normal state and in its superconducting state. The lead was shown to be superconducting in a separate experiment. In a manner similar to Pond's[1] method we look for differences in the two-quantum

coincidence rate which would indicate an enhancement of the three quantum radiation when the lead was superconducting as was first suggested by Dresden.[2] The source was Na^{22} surrounded by lead disks 0.010 in. thick. It was immersed in liquid helium, and then placed between the poles of an electromagnet. Two scinillation counters were connected in coincidence to a circuit with a resolving time of 2×10^{-8} sec. The counters were placed 180° apart with a source half way between them. Solid angles of 10^{-3} and 3×10^{-4} steradian were employed. No difference in counting rate from superconducting to nonsuperconducting was observed to within a statistical accuracy of 0.10 percent.

[1] T. A. Pond, Phys. Rev. **93**, 478 (1954).
[2] M. Dresden, Phys. Rev. **93**, 1413 (1954).

X4. Temperature Effects in the 3-Quantum Annihilation of Positrons.* R. T. WAGNER AND F. L. HEREFORD, *University of Virginia*.—The ratio of three-quantum to two-quantum annihilation of positrons in ice and zinc has been investigated in the 4°–300°K temperature range. The positron source (Na^{22}) was prepared by dissolving sodium chloride in distilled water in a 5-ml flask which was then placed at the bottom of a Dewar. The ratio of three-photon to two-photon annihilations at various fixed low temperatures was then measured using a triple coincidence circuit. An approximately linear decrease in this ratio is noted with decreasing temperature in the ice similar to results in teflon.[1] Using the same apparatus, this ratio was measured by positron annihilations in zinc in which the positron emitter (Zn^{65}) was the absorber. Here no temperature effect is observed. The correlation of these results with the data[2] on positron lifetimes will be discussed.

* Supported by Office of Ordnance Research.
[1] R. L. Graham and A. T. Stewart, Can. J. Phys. **32**, 678 (1954).
[2] R. E. Bell and R. L. Graham, Phys. Rev. **90**, 644 (1953).

X5. Angular Correlation of Two-Quantum Annihilation in Condensed Materials.* L. A. PAGE, M. HEINBERG, O. J. WALLACE, AND T. W. TROUT, *University of Pittsburgh*.—Positron annihilation is being studied in apparatus similar to that of DeBenedetti *et al.*[1] with the addition of slits to shield the gamma detectors from the 5-mC Na^{22} source. A narrow component has been isolated in fused quartz, comprising about 20 percent of the total annihilations, with width-at-half-maximum no greater than 3×10^{-3} radian. Other materials having the long lifetime component as listed by Bell and Graham,[2] exhibit an angular distribution similar to fused quartz, while materials listed as having no long lifetime have, by comparison, a structureless distribution. To date, from data at room temperature, the former group is fused quartz, teflon, polystyrene, polyethylene, paraffin, and lucite; the latter group is crystalline quartz, aluminum, magnesium, copper, and graphite. Preliminary magnetic quenching experiments[3] increase the amount of narrow component by applying a strong field to fused quartz and teflon, but give no observable change for crystalline quartz. Quantitative comparison of this effect with expectation based on measured[2] lifetimes and percentage long-life component will be made.

* Work done in Sarah Mellon Scaife Radiation Laboratory, supported by the Office of Ordance Research.
[1] DeBenedetti, Cowan, Konnecker, and Primakoff, Phys. Rev. **77**, 205 (1950).
[2] R. E. Bell and R. L. Graham, Phys. Rev. **90**, 644 (1953).
[3] Compare M. Deutsch and E. Dulit, Phys. Rev. **84**, 601 (1951).

X6. Internal Pair Creation in Negatron Decay.* J. S. GREENBERG AND M. DEUTSCH, *M.I.T.*—Using a fairly thin and uniform source of P^{32} (about 25 millicuries in one milligram), it was found that the negatron decay of P^{32} is accompanied by the emission of electron positron pairs with an abundance of $0.9\pm0.6\times10^{-3}$ per beta decay. This corresponded in the experiment to an average counting rate of 3.5 positrons per hour from the source. The fractional contribution to this number by secondary effects in the source material could not be determined due to uncertainties in the source thickness and composition. However, the results indicate that the ratio of positrons emitted to negatron decays is probably not greater than 1.5×10^{-3}, which is of the order of magnitude predicted by the theory of Arley and Möller.[1] The method of detection used was to employ a magnetic field to focus the positrons emitted by the source onto a beryllium catcher placed longitudinally along the magnetic field. The annihilation of the positrons in the beryllium catcher was then detected by means of the characteristic 180° coincidences of the 0.51-Mev gamma rays. Appropriate baffles and shielding were used to prevent detection of positrons that were not produced in the source.

* Supported in part by the joint program of the Office of Naval Research and the U. S. Atomic Energy Commission.
[1] Arley and Möller, Det. Kgl. Danske Vid. Selskab. **15**, 9 (1938).

X7. Z-Dependence of Bremsstrahlung.* K. L. BROWN, W. C. BARBER, A. I. BERMAN,† AND W. D. GEORGE, *Stanford University*.—The relative amounts of bremsstrahlung produced by the elements Cu, Ta, Pb, and U for incident electrons of energy 24 and 34 Mev were measured using the $Cu^{63}(\gamma,n)Cu^{62}$ reaction as the photon detector. This reaction has a cross section with an effective absorption energy of 17.5 Mev and a width at half maximum of 5 Mev so that photons were detected in a comparatively narrow energy band. The electron beam was monitored by a Faraday cup placed immediately behind the radiator and detector foils. Corrections were applied to account for ionization and radiation losses of the electrons and for pair production and Compton losses of the photons. The experimentally determined "thin-target" bremsstrahlung cross sections relative to copper were 5.681 ± 0.13, 6.959 ± 0.16, and 8.221 ± 0.19 per atom for Ta, Pb, and U, respectively, at 24 Mev; and 5.583 ± 0.08, 6.770 ± 0.09, and 8.172 ± 0.12 at 34 Mev. These results are from five to thirteen percent lower than the corresponding ratios calculated from the Bethe-Heitler theory (including screening and radiation produced in collision with atomic electrons). The results are consistent with a deviation from theory of $(1.44\pm0.1)\times10^{-3}Z^2$ percent.

* Supported by the joint program of the Office of Naval Research and the U. S. Atomic Energy Commission.
† Now with Pratt-Whitney, Hartford, Connecticut.

X8. Prediction of Auroral Gamma Rays.* STIRLING A. COLGATE, *University of California, Livermore*.—The aurora has been explained by protons from the sun. The mean depth of atmospheric penetration of 110 km predicts a primary proton energy of 300 kev. A few aurora have been observed to penetrate to 70 km, implying 6-Mev protons. Störmer's calculations would limit such particles to magnetic latitudes much closer to the magnetic pole than the observed incidence, implying that the proton energy is greater than that derived from the range. If the incident proton energy is greater than 2.6 Mev (the lowest level of N^{14}) the N^{14} (pp^1) α reaction should give rise to an observable gamma flux. The N^{14} (pp^2) α cross section has been measured at 7.4 Mev. A measurement was made by the author of the gammas from 31-Mev protons stopping in air. The Mev gammas per proton stopping in air is approximately $10^{-5}E_p^3$, $3<E_p<30$ Mev. The incident proton flux divided by the solid angle to the observer can be estimated from the intensity of total light, or from the intensity of the H_α emission as $10^7/E_p$ protons/sec per (cm² solid angle) at the observer. For 3-Mev incident protons, this gives 10^2 Mev γ's/cm²/sec above the earth's atmosphere and approximately 10^3 Mev γ's/cm²/sec at 50 000 feet.

* This work was performed under the auspices of the U. S. Atomic Energy Commission.
[1] Fan and Meinel, Astrophys. J. **118**, 205 (1953).
[2] Bennett and Hulburt, Phys. Rev. **95**, 315 (1954).

X9. Radiation Dosage from Thermonuclear Explosions. M. S. STEINBERG, *Yale University* (introduced by A. Einstein).—It is of interest to demonstrate a method for estimating thermonuclear explosion radiation dosage using publicly available data from the Japanese ship, Fukuryu Maru. The world-average cumulative dose is given by $R_s = \dot{R}_s(t_0)D^{-1}(t_0)K_s^{-1}(t_0) \times \int D(t)K_s(t)dt$, where the dosage rate $\dot{R}(t)$ due to fallout is proportional to the gross decay factor $D(t)$ and to the surface density of fallen matter $K(t)$ in the effective area of exposure. It is assumed that the measured shipboard fallout was characteristic of the general fallout. Subscripts e and s refer to earth and ship respectively, and the integration extends over the genetically significant exposure time; $K_s(t)$ is assumed to increase linearly during fallout and thence to remain constant at K_{s0} while $D(t)$ is assumed of the form t^{-p}. The rate of fallout is determined from Stokes' Law; K_{s0} is obtained from the excavated matter estimate of Martin; $\dot{R}_s$ (16 days) has been measured by Nishiwaki; and K_s (16 days) and p are estimated from Kyoto University studies on the shipboard fallout. For the spring, 1954 explosions we find $R_s \sim 5$ roentgens, excluding effects of fallout ingestion.

SATURDAY AFTERNOON AT 1:30

Exhibit Hall II

(E. K. PLYLER presiding)

Microwave and Band Spectra

XA1. Two Quantum Transitions in the Microwave Zeeman Spectrum of Atomic Oxygen. V. W. HUGHES AND J. S. GEIGER, *Yale University*.—The three extra lines observed by Rawson and Beringer[1] in the microwave spectrum of ground state $^3P_2$ atomic oxygen have been identified as arising from two quantum transitions between Zeeman levels with the selection rule $\Delta M = \pm 2$. Each of the three lines is observed at the mean frequency of the two corresponding $\Delta M = \pm 1$ transitions to within the experimental accuracy of a few ppm. The line width of the two quantum transitions is approximately one half that of the normal transitions, and the line intensity varies more rapidly with rf power, both in agreement with the theory. One extra two quantum line is predicted for the $^3P_1$ Zeeman spectrum; however, this line would be weak and also would occur at the frequency of a line in the $^3P_2$ Zeeman spectrum. This line has not been observed. Multiple quantum transitions have been previously reported in the electric quadrupole radiofrequency spectrum of RbF and in the Zeeman spectrum of O_2 and K.[2] The theory of such transitions has been discussed.[3]

[1] Rawson and Beringer, Phys. Rev. **88**, 677 (1952).
[2] Hughes and Grabner, Phys. Rev. **79**, 314 (1950); **82**, 561 (1951); P. Kusch, Phys. Rev. **93**, 1022 (1954).
[3] Hughes and Grabner, Phys. Rev. **79**, 829 (1950); Preprint from H. Salwen.

XA2. Microwave Spectrum of the Ozone Molecule.* E. K. GORA, *Providence College*.—The frequencies and intensities of 191 absorption lines of ozone in the microwave domain between 0 and 11 cm^{-1} have been calculated. All the lines have been taken into consideration from which a measurable contribution to microwave absorption is to be expected. This has made it necessary to extend the calculations to transitions between levels of rotational quantum numbers as high as $J = 50$. For the calculation of the transition frequencies standard methods have been employed, but for the calculation of the intensities a simplified computational procedure has been developed. The mathematical methods for the intensity calculations described by previous authors become very cumbersome for transitions between levels of high rotational quantum numbers, but the simplified computational procedure has made it comparatively easy to determine all the ozone line intensities. The sub-branch structure of the spectrum is described in detail.

* Supported by the U. S. Air Force through the Air Force Cambridge Research Center.

XA3. Centrifugal Distortion Effects in Ozone.* LOUIS PIERCE, *Harvard University*.—The microwave spectrum[1,2] of ozone has been reanalyzed to include the effect of centrifugal distortion. Using the energy expression given by Kivelson and Wilson,[3] it was possible to fit eighteen lines of the rotational spectrum to within a mean deviation of ± 1.5 Mc. The rotational constants determined in this manner are $A = 106\,534.45$ Mc, $B = 13\,349.10$ Mc, $C = 11\,834.14$ Mc. The four distortion constants obtained in this analysis predicted vibrational frequencies which were of the right order of magnitude. The relation of these constants to the vibrational spectrum will be discussed in terms of the theory developed by Kivelson and Wilson.[4]

* Supported by the Office of Naval Research.
[1] R. H. Hughes, J. Chem. Phys. **21**, 959 (1953).
[2] Trambarulo, Ghosh, Burrus, and Gordy, J. Chem. Phys. **21**, 851 (1953).
[3] D. Kivelson and E. B. Wilson, Jr., J. Chem. Phys. **20**, 1575 (1952).
[4] D. Kivelson and E. B. Wilson, Jr., J. Chem. Phys. **21**, 1229 (1953).

XA4. Microwave Spectra of Indium Chloride and Bromide.* A. H. BARRETT AND M. MANDEL, *Columbia University*.—The pure rotational spectra of indium monochloride and indium monobromide have been observed using a high-temperature spectrometer.[1] Internuclear distances and vibration-rotation interaction constants determined are

Molecule	r_e(A)	α_e(Mc/sec)
$In^{115}Cl^{35}$	2.4012 ±0.0001	15.34 ±0.15
$In^{115}Br^{79}$	2.5408 ±0.0001	5.706 ±0.025
$In^{115}Br^{81}$		5.605 ±0.018

Since the nuclear spins of In^{115}, $Cl^{35,37}$, and $Br^{79,81}$ are 9/2, 3/2, and 3/2, respectively, the spectra are complicated by hyperfine structure resulting from the interaction of each electric quadrupole moment with the molecular field. The spectrum of $In^{115}Cl^{35}$ yielded values of -655 ± 6 Mc for the In^{115} coupling constant and -24 ± 2 Mc for the Cl^{35} coupling constant. The quadrupole structure was not sufficiently resolved to allow a determination of the coupling constants in $In^{115}Br$. Interpretation of the results in terms of ionic character and bond hybridization of these molecules will be discussed.

* Work supported jointly by the Signal Corps, the Office of Naval Research, and the Air Research and Development Command.
[1] Stitch, Honig, and Townes, Rev. Sci. Instr. **25**, 759 (1954).

XA5. Theory of the Fine Structure of the Microwave Spectrum of NO_2.* CHUN C. LIN† *Harvard University*.—The theory of hyperfine structure of NO_2 first proposed by McAfee[1] has been re-examined and revised to include the case where the spin-rotation interaction and the dipole-dipole coupling are of the same order of magnitude. This theory satisfactorily accounts for the frequency of the ten lines observed by Bird.[2] Some small deviations, however, do exist. The origin of these

discrepancies is not clear; they are probably due to second order effects of the magnetic interactions. The predicted intensities of the ten lines also agree with observation within the experimental accuracy. The magnetic coupling constants obtained from this investigation are rather bizarre and may furnish interesting information about the electronic structure of NO_3. The theory of the Zeeman effect is also being studied and compared with experiment.

* Supported in part by the Office of Naval Research.
† duPont Company Predoctoral Fellow.
[1] K. B. McAfee, Jr., Phys. Rev. **78**, 340(A) (1950); Phys. Rev. **82**, 971 (1951).
[2] G. R. Bird, Bull. Am. Phys. Soc. **30**, 21 (1955), abstract H6.

XA6. Internal Motion in Methyl Amine.* D. KIVELSON, *M.I.T.*, AND D. R. LIDE, JR., *N.B.S.*—The microwave spectrum[1,2] of methyl amine exhibits hindered internal rotation of the NH_2 group with respect to the CH_3 group, as well as inversion doubling arising from the fact that there are two equally likely orientations of one NH bond with respect to the other. An approximate theory has been worked out for these two internal motions and their mutual interaction. By a suitable choice of variable the kinetic energies can be completely separated; the potential energy can be reduced to a term accounting for inversion, a term accounting for hindered internal rotation, and an interaction term. If the latter is neglected the two internal motions can be treated independently except for their interrelated dependence upon the periodic boundary conditions. The interaction term can be treated by a Van Vleck transformation. This theory is applied to methyl amine.

* This work was supported in part by the Signal Corps; the Office of Scientific Research, Air Research and Development Command; and the Office of Naval Research.
[1] D. R. Lide, Jr., J. Chem. Phys. **20**, 1812 (1952); **21**, 571 (1953).
[2] Shimoda, Nishikawa, and Itah, J. Chem. Phys. **22**, 1456 (1954); J. Phys. Soc. Japan **9**, 974 (1954).

XA7. Molecular-Beam Microwave-Absorption Spectroscope.* M. PETER AND M. W. P. STRANDBERG, *M.I.T.*—A microwave absorption spectroscope has been developed, whose absorption-line half-power—half-width is determined by the average time that the molecules under observation are exposed to the microwave field. This is an improvement over the similar previous device by Strandberg and Dreicer,[1] in which the Stark modulation frequency limited the resolution. In both devices the Doppler broadening, which limits the resolution of the usual microwave spectroscopes, is eliminated. An improvement by a factor of twelve is now obtained over such usual systems, and a half-power—half-width of 3 kc has been observed. To use such resolution it has been necessary to develop a stabilization circuit which maintains the phase of a *K*-band klystron to within a few degrees of the phase of some harmonic of a very stable quartz oscillator. The resolution of the present system is therefore limited only by geometry and may thereby be improved by use of longer average observation times, i.e., use of longer molecular beams.

* This work was supported in part by the Signal Corps; the Office of Scientific Research, Air Research and Development Command; and the Office of Naval Research.
[1] M. W. P. Strandberg and H. Dreicer, Phys. Rev. **94**, 1393 (1954).

XA8. Excited Torsional States in Asymmetric Hindered Rotors.* P. R. SWAN AND M. W. P. STRANDBERG, *M.I.T.*—The $J=0\rightarrow1$ transition of methyl alcohol is being investigated. Because of internal torsion in this type of molecule the transition is split into a series of doublets, each doublet corresponding to a particular internal torsion state. A preliminary model used was that of a rigid symmetric top attached at an arbitrary angle to a rigid asymmetric frame and allowed to rotate about its symmetry axis under the influence of a threefold cosine potential barrier. The resulting Hamiltonian was found to be incapable of predicting the torsional splitting when applied to the methyl-alcohol molecule. A semiempirical combination of Kivelson's[1] formula for the corresponding transition in a symmetric hindered rotor with matrix elements from this methyl-alcohol Hamiltonian was found to give a close fit to the observed spectrum. An additional feature of the methyl-alcohol spectrum is the large fourth-order Stark effect of one of the lines of the $J=0\rightarrow1$ series. The Hamiltonian necessary to describe these rotation-torsion interaction effects will be discussed.

* This work was supported in part by the Signal Corps; the Office of Scientific Research, Air Research and Development Command; and the Office of Naval Research.
[1] D. Kivelson, J. Chem. Phys. **22**, 1733 (1954).

XA9. Electronic Contribution to Effective Nuclear Masses in Molecules.* M. W. P. STRANDBERG, *M.I.T.*—The problem of the interaction of molecular rotational and electronic states has been extensively investigated in the past.[1-5] Quite briefly stated, it has been demonstrated that the molecular electrons contribute to the molecular moment of inertia tensor an amount which is directly and simply related to the molecular magnetic moment tensor. Examples of this correction have been made with the experimental results on several molecules, and the measured corrections to the principal moments of inertia arising from the molecular electrons have been discussed. The authors of a recent paper[6] reporting the deuterium-tritium mass ratio evaluated from microwave measurements attempted a discussion of this correction without apparently realizing that it is a matter which may be reduced to measurement. The electronic correction to spectroscopic mass ratio measurements will be discussed in terms of past work.

* This work was supported in part by the Signal Corps; the Office of Scientific Research, Air Research and Development Command; and the Office of Naval Research.
[1] H. B. G. Casimir, *Rotation of a Rigid Body in Quantum Mechanics* (J. B. Wolters', The Hague, 1931), Vol. 3.
[2] Gokhale, Johnson, and Strandberg, Phys. Rev. **83**, 881 (1951).
[3] H. R. Johnson and M. W. P. Strandberg, J. Chem. Phys. **20**, 687 (1952).
[4] B. F. Burke and M. W. P. Strandberg, Phys. Rev. **90**, 303 (1953).
[5] M. W. P. Strandberg, *Microwave Spectroscopy* (Methuen and Company, Ltd., London, 1954), Chap. VII.
[6] B. Rosenblum and A. H. Nethercot, Jr., Phys. Rev. **97**, 84 (1955).

XA10. "Average" Internuclear Separations Arising in the Study of Molecular Band-Systems.* R. W. NICHOLLS AND W. R. JARMAIN, *University of Western Ontario*.—The concept of an "average" internuclear separation or "r-centroid" $\bar{r}_{v'v''}$ associated with the radiation of the $(v'\rightarrow v'')$ molecular band will be discussed. Methods of computation of arrays of $\bar{r}_{v'v''}$ will be described. The properties of the r-centroid, and its application to the interpretation of band intensities will be reviewed.

* This research is assisted by the Air Force Cambridge Research Center.

XA11. The Vibrational Spectrum of Tetrabromoethylene.* D. E. MANN, JANET HAWKINS MEAL,† AND EARLE K. PLYLER, *National Bureau of Standards*.—The infrared spectrum of C_2Br_4 has been observed and measured in the range from 3 to 100 microns. These data, together with the older Roman spectra and a new force constant analysis, have enabled an essentially complete and satisfactory vibrational assignment to be achieved for the first time. In particular, the values of the angular fundamentals in the b_{1u}, b_{2u}, and b_{3u} species have been established. The vibrational assignments for C_2F_4, C_2Cl_4, and C_2Br_4 are now fully concordant.

* This work was supported in part by the Office of Naval Research.
† National Research Council—National Bureau of Standards Postdoctoral Research Associate.

Invited Paper

XA12. Temperature-Measurement from Molecular Band Spectra (Nonequilibrium). H. P. BROIDA, *National Bureau of Standards*. (30 min.)

SATURDAY AFTERNOON AT 1:30

NBS, East Building

(L. R. MAXWELL presiding)

Cryogenics

Y1. Intradomain Magnetic Saturation for Iron. WARREN E. HENRY, *U. S. Naval Research Laboratory.*—Studies have been made of the magnetization of polycrystalline, 99.9 percent iron (Westinghouse) as a function of magnetic field for temperatures between 1.5°K and 300°K, in magnetic fields up to 60 000 gauss. For a given temperature, the magnetization rises with nearly constant slope with field until a certain field (about 8000 gauss for a sphere) is reached, which depends on the shape of the sample. The slope then goes quickly to zero and remains zero for fields up to 60 000 gauss. In the helium range (1.5°K−4.2°K), the saturation magnetization remains constant to within experimental error (0.2 percent). No appreciable remanence is observed in zero field. A ballistic, moving sample method[1] for measuring the magnetization was used. Analysis of the data is made in terms of departures from the quantum mechanical "$T^{\frac{3}{2}}$ Bloch law" (applicable over part of the range) and from the Weiss molecular field relation; empirical relations are put forth to correlate the data. Comparison is made between our data and previous work[2] done in more limited ranges of temperature and magnetic field.

[1] W. E. Henry, Phys. Rev. **88**, 559 (1952).
[2] M. Fallot, Ann. phys. **10**, 291 (1938).

Y2. Thermodynamic Properties of Chrome Alum.* L. D. JENNINGS AND MELVIN A. HERLIN,† *M.I.T.*—A new method was applied to the measurement of the thermodynamic properties of potassium chromium alum in the region of temperatures reached by adiabatic demagnetization. The method requires the measurement of adiabatic magnetization curves which approach an asymptotic value at large fields characteristic of the analogous ideal paramagnetic gas at the same entropy. The entropy of the actual salt is then given as that of the ideal salt which has the same large field magnetization. The temperature of the salt is given by a method, previously described,[1] which makes use of the deviation of the behavior of the actual salt from that of the ideal. Each adiabat is identified by T^*, the magnetic temperature at that entropy. We find good agreement with other workers for $T(T^*)$, but less satisfactory agreement for $S(T^*)$ in the region $T^*=0.1$ to $T^*=0.2$. This discrepancy is attributed to a failure of the usual computation of entropy near 1°K, to our need to extrapolate our results at high magnetic fields, or to an actual difference among samples.

* This work was supported in part by the Signal Corps; the Office of Scientific Research, Air Research and Development Command; and the Office of Naval Research.
† Now at Lincoln Laboratory, M.I.T.
[1] M. A. Herlin, Proc. Intern. Conf. Low Temp. Physics (Oxford, 1951), p. 144.

Y3. An Ultra-Low-Level Voltage Detector Using Bismuth and Superconductors. JULIUS BABISKIN, *Naval Research Laboratory.*—A direct-current or low-frequency amplifier which should be capable of detecting 10^{-12} volt in low-impedance circuits at low temperatures is under development. A single layer of bismuth wire is wound between two oppositely-wound layers (~0.1 microhenry) of superconducting lead wire. A superconducting lead shield eliminates stray magnetic fields. Current changes in the superconducting winding caused changes in the concentrated magnetic field over the bismuth activating its magnetoresistance. To eliminate bismuth calibration problems, the magnetoresistance minimum was chosen at a sacrifice in sensitivity as the balance point affording an absolute null point independent of the cyclical reproducibility, temperature, and thermal emf's of bismuth. For preliminary measurements on a prototype detector, the smallest detectable current change was 10^{-6} amp at the magnetoresistance minimum. Obvious design improvements should increase the detection limit considerably. Compared with a superconducting galvanometer,[1] the detector is simple, rugged, compact, and independent of vibration. This detector allows impedance matching between low-impedance voltage sources (e.g. temperature or magnetic field sensitive) in the superconducting circuit and measuring instruments at room temperature in the bismuth circuit.

[1] A. B. Pippard and C. T. Pullan, Proc. Cambridge Phil. Soc. **48**, 188 (1952).

Y4. On the Superconductivity of Hafnium. R. A. HEIN, *Naval Research Laboratory, and The Catholic University of America.*—The magnetic susceptibility and the electrical resistance of a hafnium rod[1] have been observed between 0.06°K and 4.22°K. The susceptibility measurements failed to reveal any evidence of superconductivity as previously reported.[2,3] The electrical resistance, which was constant in the liquid-helium range, started to decrease at 0.20±0.02°K and was still falling at the lowest temperature attained [$(R0.06°K/R0.20°K)=0.6$]. Since this effect was sensitive to small magnetic fields, a quasi-critical field curve was obtained. Susceptibility measurements made subsequent to a high-vacuum anneal again failed to indicate any superconductivity; however, the resistance of the annealed specimen did show an abrupt decrease at 0.15±0.03°K. This is in disagreement with the results of other workers.[3] The sensitivity of the magnetic measurements was such that if 10 percent of the hafnium had gone superconducting it would have been readily detectable.

[1] Supplied by the Materials Section, Wright Air Development Center, Dayton, Ohio, and had a stated purity of 98.92 percent.
[2] N. Kurti and F. Simon, Proc. Roy. Soc. (London), **A151**, 610 (1935).
[3] T. S. Smith and J. G. Daunt, Phys. Rev. **88**, 1172 (1952).

Y5. Superconductivity of Tin Whiskers.* O. S. LUTES, *NBS and University of Maryland,* AND E. MAXWELL,† *NBS.*—The superconducting resistance transitions of several tin whiskers[1] have been observed in the liquid-helium temperature range. The results are compared with those for larger wires and significant differences are found. In particular the transitions in a transverse magnetic field are discontinuous at temperatures substantially lower than the zero-field transition temperature. This result differs from that for larger wires,[2] which show intermediate resistance at these temperatures.

* This research was supported by the Office of Scientific Research of the Air Research and Development Command.
† Permanent address: Lincoln Laboratory, Massachusetts Institute of Technology, Cambridge, Massachusetts.
[1] Compton, Mendizza, and Arnold, Corrosion **7**, 327 (1951).
[2] E. R. Andrew, Proc. Roy. Soc. (London) **A194**, 80 (1948).

Y6. Displacement of the Superconducting Critical Field by Pressure.* N. L. MUENCH† AND H. E. RORSCHACH, JR., *The Rice Institute.*—An ice-bomb technique[1] (water is frozen in a constant-volume cell) has been used to obtain pressures of 1900 atmospheres to study the shift in the critical field of several superconductors. Data have been obtained at sufficiently low temperatures to determine the temperature dependence of $(\partial H_c/\partial P)_T$. For tin, one obtains $(\partial H_c/\partial P)_T = (\partial H_c/\partial P)_{T_c}[0.6+0.4(T/T_c)^2]$. This value is such that the

geometry[2] of the transition curve is preserved: $(H_0/T_c)_P = (H_0/T_c)_{P=0}$. H_0 is the value of the critical field H_c at $T=0$. The shift of H_0 with pressure and the shift resulting from a change in isotopic mass can be used to calculate the dependence of H_0 on the lattice parameters and on the Debye θ_D. The result indicates that H_0 is an order of magnitude more sensitive to fractional changes in lattice dimensions (θ_D constant) than to fractional changes in θ_D (lattice dimensions constant), i.e., $(\partial H_0/\partial \log V)_{\theta_D} \sim 10(\partial H_0/\partial \log \theta_D)_V$.

* Supported in part by the National Science Foundation.
† Magnolia Petroleum Company Fellow in Physics.
[1] B. Lazarev and L. Kan, J. Phys. (USSR) **14**, 439 (1944).
[2] E. Maxwell, Phys. Rev. **86**, 239 (1952).

Y7. Surface Energies in Superconductors. H. W. LEWIS, *Bell Telephone Laboratories.*—It is well known that the London phenomenological theory of superconductivity fails to account for the existence of a positive surface energy at the boundary between a normal and a superconducting region of a material. Modifications due to Landau and Ginsburg, and to Bardeen, make it possible to understand the positive surface energy as a specifically quantum-mechanical effect. However, these modifications change the London equations to a pair of coupled nonlinear differential equations, and only numerical solutions exist. A variational procedure for evaluating the surface energy within this framework will be discussed, and numerical results will be presented. These are relevant to the recent experiments of Schawlow. The possible existence of a gap in the electronic energy spectrum, and its effect on the predicted surface energy at low temperatures will be discussed, as well as the effect of a short electronic mean free path.

Y8. A New Method for Measuring the Absolute Viscosity of Liquid Helium II.* HENRY H. KOLM AND MELVIN A. HERLIN,† *M.I.T.*—A new type of static viscometer for use in liquid helium II was developed; its inner cylinder is suspended within a rigidly fixed, coaxial outer cylinder by a servomechanically controlled magnetic bearing of the type used by Beams and others[1] in vacuum ultracentrifuges. The inner cylinder is accelerated electromagnetically; the absolute viscosity of the medium is determined from the deceleration observed when it is permitted to coast freely. Bearing friction is negligible, and there is no inherent lower limit to the speed of this measurement. Reproducible viscosity values were obtained in gaseous helium, but $1/TS$-damping from thermomechanical flow induced by eddy current heating in the rotor was observed in liquid helium II. This effect was reduced considerably by elaborate precautions for isolating the apparatus from ground vibrations; further improvement would require more favorable location of the apparatus. At higher speeds, the anomalous behavior reported elsewhere[2] was again observed, which eliminates the attempted "mutual friction" explanation. The absolute viscosity increased discontinuously to a higher value as the speed increased.

* This work was supported in part by the Signal Corps; the Office of Scientific Research, Air Research and Development Command; and the Office of Naval Research.
† Now at Lincoln Laboratory, Massachusetts Institute of Technology, Cambridge, Massachusetts.
[1] Beams, Ross, and Dillon, Rev. Sci. Instr. **22**, 77 (1951).
[2] A. C. Hollis-Hallet, Proc. Roy. Soc. (London) **A210**, 404 (1952) and Proc. Cambridge Phil. Soc. **49**, 717 (1953).

Y9. Ultrasonic Measurements in Magnetically-Cooled Liquid Helium.* C. E. CHASE† AND MELVIN A. HERLIN,† *M.I.T.*—Measurements were made of the velocity and attenuation of ordinary (first) sound in liquid helium between 0.1°K and 1°K, at 12.1 Mc/sec. These temperatures were produced by adiabatic demagnetization of ferric ammonium alum from a starting temperature near 0.9°K, produced by a large oil diffusion pump. Since helium was admitted by an arrangement of concentric thin-walled stainless-steel cones (originated by Dr. J. Ashmead, Mond Laboratory), the demagnetization chamber could be isolated or placed in direct communication with the bath. Warmup times approximating one hour were obtained. The velocity remains essentially constant below 1°K at 240±5 m/sec. Although the inherent difficulty of a fixed path length makes it less accurate than the earlier 239±2 m/sec found above 0.85°K,[1] the value shows that no gross changes occur. The attenuation passes through two clearly resolved maxima slightly below 1°K, falls smoothly toward zero as absolute zero is approached. This agrees qualitatively with Khalatnikov's theory[2,3] which explains the anomalously high absorption of helium II in terms of two relaxation times.

* This work was supported in in part by the Signal Corps; the Office of Scientific Research, Air Research and Development Command; and the Office of Naval Research.
† Now at Lincoln Laboratory, Massachusetts Institute of Technology, Cambridge, Massachusetts.
[1] C. E. Chase, Proc. Roy. Soc. (London) **A220**, 116 (1953).
[2] I. M. Khalatnikov, J.E.T.P. (U.S.S.R.) **20**, 243 (1950).
[3] I. M. Khalatnikov, J.E.T.P. (U.S.S.R.) **23**, 8 (1952).

Y10. The Amplitude Dependence of the Velocity of Second Sound.* ALEXANDER J. DESSLER AND WILLIAM M. FAIRBANK, *Duke University.*—When second-order terms are considered in the theory of liquid helium II, Temperley[1] and Khalatnikov[2] have shown that the velocity of second sound is amplitude dependent and can be written in the form $C_2 = C_{20} + \tau_2 v_n$ where C_{20} is the velocity of second sound at zero amplitude, v_n is the velocity of the normal fluid and τ_2 is a function of the temperature. Osborne[3] has qualitatively verified this equation by observing the shape of the shock wave in second sound pulses of large amplitude. We have measured τ_2 as a function of temperature; v_n was varied by superimposing a small marker pulse on top of a large carrier pulse of duration long compared with the length of the marker pulse. The time of flight of the marker pulse was measured as a function of the amplitude of the carrier pulse. Measurements of τ_2 have been made from 2.1°K to 1.4°K. The experimental results will be compared with the theories.

* This project has been supported by contracts with the Office of Ordnance Research, U. S. Army.
[1] H. N. V. Temperley, Proc. Phys. Soc. (London) **A64**, 105 (1951).
[2] I. M. Khalatnikov, Doklady Acad. Nauk. U.S.S.R. **79**, 237 (1951).
[3] D. V. Osborne, Proc. Phys. Soc. (London) **A64**, 114 (1951).

Y11. Kinetic Theory of Liquid Helium II: Heat Transfer.* C. A. REYNOLDS, *University of Connecticut.*—A simple hydrodynamical treatment of two oppositely flowing, noninteracting fluids cannot be the proper method of handling heat transfer in helium II because of the microscopic interactions which must take place and which assure thermodynamic equilibrium or near thermodynamic equilibrium. Instead a phenomenological kinetic theory approach is used here. It is assumed that some of the atoms are in the condensed state and the others are "normally excited," following the ideas of the Bose-Einstein condensation. It is further assumed that the energy transfer may be broken up into two types—transfer of energy from atom to atom and transfer by motion of an atom with its associated energy. The former corresponds to a solid or phonon type of transfer and is not treated here. From a consideration of the latter type of transfer one can understand: the decrease in "conductivity" as the temperature is lowered; the existence of a maximum in the "conductivity"—temperature relationship; the shift in the maximum to higher temperatures as the slit width is reduced; the decrease in the heat "conductivity" as the slit width is reduced; and the "critical velocity."

* Supported in part by the Research Corporation, the National Science Foundation, and the Office of Naval Research.

Y12. Heat Transfer in Fine Channels of Helium II.* HAROLD FORSTAT AND CHARLES A. REYNOLDS, *University of Connecticut.*—An apparatus has been constructed for the measurement of heat transfer by liquid helium II in fine channels in packed rouge. It consists of a glass bulb containing a

heater and thermometer. Above this is a length of packed rouge; above this a glass-metal seal for the purpose of assuring thermal contact with the bath; and above this a glass viewing section. The bulb and rouge region are surrounded by a vacuum jacket. Helium is condensed into this system from a supply outside of the Dewar. The temperature below the rouge is measured by the thermometer in the bulb and the temperature above the rouge is measured by a thermometer placed inside of the metal seal. After heat is supplied one waits until the level in the viewing region comes to rest, assuring zero net mass transfer, and then notes the temperatures. The results will be compared with other data on heat transfer[1] and with theory.[2]

* Supported in part by the Research Corporation, the National Science Foundation, and the Office of Naval Research.
[1] W. H. Keesom *et al.*, Physica **13**, 153 (1947).
[2] F. London and P. R. Zilsel, Phys. Rev. **74**, 1148 (1948); C. A. Reynolds, preceding abstract, Bull. Am. Phys. Soc. **30**, No. 3, 69 (1955).

Y13. The Slope of the λ Curve of Liquid Helium.* K. R. ATKINS, *University of Pennsylvania.*—Landau's theory of liquid helium has been developed to give an approximate value for the slope of the λ curve in terms of the quantities $(\rho/\Delta)(\partial\Delta/\partial p)$, $(\rho/\rho_0)(\partial\rho_0/\partial p)$, and $(\rho/\mu)(\partial\mu/\partial p)$. From the experimental data on the coefficient of expansion and the pressure variation of the velocities of first and second sound, the following numerical values are derived for these quantities: $(\rho/\Delta)(\partial\Delta/\partial p) = -0.57$, $(\rho/\rho_0)(\partial\rho_0/\partial p) = +0.26$, and $(\rho/\mu)(\partial\mu/\partial p) = -1.8$. The negative slope of the λ curve can then be explained and its magnitude predicted with an accuracy of about 15 percent.

* Work supported in part by the U. S. Atomic Energy Commission.

Y14. PV Isotherms of He^3 Gas between 1.5 and 3.8°K. WILLIAM E. KELLER,* *Los Alamos Scientific Laboratory.*—With the same apparatus[1] used recently to determine the equation of state of He^4, PV isotherms of 99.75 percent He^3 gas have been measured at 3.786°, 2.991°, 2.161°, 1.818°, and 1.515°K ("agreed" scale). Using the inverse volume virial expansion we obtain for the second virial coefficient, B, the respective values −65.4, −86.3, −117.9, −142.3, and −169.5 cc/mole. Only for the isotherms at the two highest temperatures is it necessary to include a quadratic term in the analytical expression in order to give a good fit to the experimental points. Discussions based on the properties of the isotherms will be presented on: the relation of the measured B's to the recently calculated values[2]; the density of the saturated vapor as a function of temperature; and corrections to the "agreed" temperature scale below 4°K.

* Work done under the auspices of the U. S. Atomic Energy Commission.
[1] W. E. Keller, Phys. Rev. **97**, 1 (1955).
[2] Kilpatrick, Keller, Hammel, Phys. Rev. **97**, 9 (1955).

Y15. Theorem on the Many-Body Quantum Ground State. P. J. PRICE, *I. B. M. Watson Laboratory.*—Let $\Psi_0(\mathbf{r}_1, \cdots \mathbf{r}_N)$ be the wave function of the ground state for a large number, N, of interacting particles (helium atoms, for example). We may construct a wave function for $N-1$ particles proportional to $\int \phi^*(\mathbf{r}_1)\Psi_0 d^3\mathbf{r}_1$. Then the condition that the energy expectation be not less than the energy of the ground state for $N-1$ particles gives an inequality for each function $\phi(\mathbf{r})$. If ϕ is chosen proportional to $\exp(i\mathbf{k}\cdot\mathbf{r})$, we find

$$\hbar^2k^2/2m + 2w(\mathbf{k}) \gtrless h, \tag{1}$$

where h is the enthalpy per particle (partial enthalpy, for one species of several) and $w(\mathbf{k})$ is defined in terms of the reduced density matrices and may be interpreted (for zero external field) as the expectation of potential energy of a particle *when its momentum is* $\hbar\mathbf{k}$. Averaging (1) over the probabilities of different momenta gives the result that the total interaction potential energy cannot exceed PV. Consequences of these results will be discussed.

SATURDAY AFTERNOON AT 1:30

Continental Room

(R. W. HAYWARD presiding)

Radioactive Substances, II

YA1. Radiations from Ce^{143} (33 hr).* D. W. MARTIN, J. M. CORK, AND S. B. BURSON, *Argonne National Laboratory.*—The radiations from Ce^{143} (33 hr) have been studied with the scintillation coincidence spectrometer and with magnetic photographic spectrographs. Enriched Ce^{142} was irradiated with reactor neutrons. Gamma rays of 1.10±0.01, 0.861 ±0.005, 0.724±0.002, 0.668±0.002, 0.565±0.005, 0.493 ±0.002, 0.351±0.001, 0.294±0.001, 0.232±0.001, and 0.0574±0.0002 Mev are found to decay with the 33-hr period in the NaI(Tl) pulse-height distribution. Conversion lines are seen for all but the 1.10- and 0.57-Mev transitions. Gamma-gamma and beta-gamma coincidence data define the decay scheme with considerable certainty. The Pr^{143} nucleus is shown to have excited states at 0.0574, 0.232 (or 0.493), 0.351, 0.724, 0.918, and 1.16 Mev. Qualitative observations of the beta-ray components were made by observing the pulse-height distributions from an anthracene crystal in coincidence with the principal gamma components. In addition to the known strong components at 1.38, 1.09, and 0.71 Mev, two distinct weak components at ~0.5 and ~0.3 Mev are observed, coincident with radiations from the 0.918- and 1.16-Mev levels respectively. The pulse distribution coincident with the 57-kev gamma ray is indistinguishable from the non-coincidence distribution above 1 Mev. Thus, the 1.38-Mev beta ray feeds the 58-kev level, and any ground-state beta transition is of low intensity.

* Work done under auspices of U. S. Atomic Energy Commission.

YA2. The Excited States of Ce^{140}.* C. H. PRUETT, H. H. BOLOTIN, P. L. ROGGENKAMP, AND R. G. WILKINSON, *Indiana University.*—Scintillation and magnetic beta ray spectrometry have been applied to the study of the more important levels of Ce^{140}. Coincidence experiments verify that successive levels are at 1.60, 2.09, 2.42, and 2.53 Mev above the ground state and correspond to gamma rays of energies 1.60, 0.815, 0.490, 0.438, and 0.328 Mev. The relative intensities of the gamma rays are found to be 2.50, 1.15, 1.25, 0.15, and 1.00, respectively. The energies and relative intensities of two high energy transitions have been determined by means of a scintillation pair spectrometer. Values of 2.50±0.05 and 3.00±0.20 Mev are obtained with corresponding intensities of one percent and 0.04 percent of the 1.60 Mev gamma ray. The beta-ray measurements substantiate the relative intensities and end-point energies of the beta-ray groups which have been reported by others. In addition, it has been possible to estimate the internal

conversion coefficients and K/L ratios. The angular correlation of four cascade pairs of the above gamma rays has been studied. The results obtained, together with the beta ray and internal conversion data, are most consistent with the assignment 0+, 2+, 4+, 3+ for the ground state and first three excited states. The assignment 0+, 2+, 4+, 4+ cannot be definitely excluded.

* Supported by the joint program of the Office of Naval Research and the U. S. Atomic Energy Commission.

YA3. The Radioactive Decay of Yb^{175}.* J. P. MIZE, M. E. BUNKER, AND J. W. STARNER, *Los Alamos Scientific Laboratory.*—The radiations from 4.2 day Yb^{175} have been investigated and a decay scheme with spin and parity assignments proposed. Radioactive sources were obtained by irradiating normal ytterbium oxide with thermal neutrons. Examination of the beta spectrum with a magnetic lens spectrometer and a $\beta-\gamma$ coincidence scintillation spectrometer revealed the existence of three beta groups with end points 468, 355, and 72 kev and relative intensities $\sim$(90:4:6), respectively. Scintillation spectrometer studies showed that gamma transitions of 113, 137, 145, 251, 283, and 396 kev occur. The decay scheme was established with the help of coincidence measurements. The multipolarities of the various gamma rays were determined from measured values of K/L ratios, L subshell conversion ratios, and K conversion coefficients. The levels in Lu^{175} excited by the decay of Yb^{175} have the following energies: 113.6$\pm$0.2 kev, 251.0$\pm$0.3 kev, and 396.6$\pm$0.3 kev. The possibility that the 113.6 kev and 251.0 kev levels are the first and second rotational levels, respectively, of Lu^{175} predicted by the strong coupling approximation of the Bohr-Mottelson theory[1] will be discussed.

* Work done under the auspices of the U. S. Atomic Energy Commission.
[1] A. Bohr and B. R. Mottelson, Kgl. Danske Videnskab. Selsk., Mat.-ys. Medd. **27**, No. 16 (1953).

YA4. $\beta-\gamma$ Angular Anisotropy in Re^{186}.* F. T. PORTER, M. S. FREEDMAN, T. B. NOVEY, AND F. WAGNER, JR., *Argonne National Laboratory.*—The $\beta-\gamma$ directional correlation between the beta group leading to the first excited state in Os^{186} and the ensuing 137-kev gamma ray has been measured as a function of β energy from 200 to 900 kev. The anisotropy is consistent with the form $W(\theta)=1+A(E_\beta)\cos^2\theta$. The coefficient $A(E_\beta)$ increases with β energy to a maximum $\simeq$0.16 for energies near the end point. The integrated value of A (200–900 kev) is 0.11$\pm$0.02. The existence of this $\beta-\gamma$ anisotropy supports the nonallowed nonunique shape of the β transition, $\Delta I=1$, yes, (see following abstract) and makes necessary a correction to the coincidence β spectrum as observed in a magnetic spectrometer. For the Argonne double lens with 3 percent geometry for the gamma detector behind the source and with β acceptance between cones of half angles 13° and 33°, the correction has the form[1] Observed Spectrum/$[1+0.4A(E_\beta)]\simeq$True Spectrum.

* Based on work performed under the auspices of the U. S. Atomic Energy Commission.
[1] Roland F. Herbst (private communication).

YA5. Nonunique First Forbidden Beta Transitions in Re^{186}.* M. S. FREEDMAN, F. T. PORTER, T. B. NOVEY, AND F. WAGNER, JR., *Argonne National Laboratory.*—The main inner beta group ($E_0=936$ kev) in Re^{186} has been observed, in the Argonne double-lens spectrometer, in coincidence with the 137-kev gamma, to deviate from the statistical shape. The effect on the spectrum due to the beta-gamma angular anisotropy (see preceding abstract) has been computed, and with an appropriate subtraction the ground state beta ($E_0=1073$ kev) has been likewise found to deviate from the statistical shape, both distributions consistent with $\Delta J=1$, yes transitions. An analysis of the spectral shapes and values for the fitting parameters will be presented.

* Based on work performed under the auspices of the U. S. Atomic Energy Commission.

YA6. Radiations from Platinum (197).* V. R. POTNIS,† C. E. MANDEVILLE, AND JOHN S. BURLEW,‡ *Bartol Research Foundation.*—The radiations of Pt^{197} have been examined with coincident spectrometers of NaI$-$Tl and anthracene. Gamma rays have been detected at 77, 191, and 279 kev, the unconverted quantum radiations having relative intensities of 30, 3.9, and 1.0. Coincidence measurements revealed the presence of three beta spectra of maximum energies 670, 479, and 468 kev, terminating at levels in Au^{197} at 77, 268, and 279 kev which are also excited[1,2] in the decay of Hg^{197} and by coulomb excitation.[3] These beta spectra have intensities in order of decreasing end-point energy of 90.6, 8.4, and 1.0 percent. These estimates are based upon the observed gamma-ray intensities and upon previously determined conversion coefficients, experimental[1,2] and theoretical.[4] In the same order, values of logft are 6.4, 6.88, and 7.8.

* Assisted by the joint program of the Office of Naval Research and the U. S. Atomic Energy Commission.
† Permanent address, Gwalior (M.B.), India.
‡ The Franklin Institute.
[1] Huber, Humbel, Schneider, de Shalit, and Zuentj, Helv. Phys. Acta **24**, 127 (1951).
[2] J. W. Mihelich and A. de Shalit, Phys. Rev. **91**, 78 (1953).
[3] N. P. Heydenburg and G. M. Temmer, Phys. Rev. **93**, 906 (1954).
[4] Rose, Goertzel, Spinrad, Harr, and Strong, Phys. Rev. **83**, 79 (1951).

YA7. Angular Correlation Measurements in Hg^{197}.* HORACE H. COBURN AND SHERMAN FRANKEL, *University of Pennsylvania.*—The results of measurements of the various angular correlations in the 165 kev$-$134 kev cascade in Hg^{197} will be discussed. The experimental values of A_2, corrected for geometry, are $HgNO_3(K-\gamma)$ 0.11; $Hg(K-\gamma)$ 0.11; $HgNO_3(L-\gamma)$ 0.12; $Hg(L-\gamma)$ 0.10; $HgS(L-\gamma)$ 0.09; $HgO(NH_3)NO_3(L-\gamma)$ 0.10; $HgO(L-\gamma)$ 0.08; $HgCo_2(L-\gamma)$ 0.11; $HgNO_3(M-\gamma)$ 0.11; $Hg(M-\gamma)$ 0.11; $HgNO_3(L+M-K)$ 0.19. Those data are accurate to $\pm$0.02 and indicate that the various correlations are insensitive to chemical environment. The theoretical $(K-\gamma)$ correlation is 0.221, so that there is appreciable wipeout. The "hard core" value is 0.044, so that the insensitivity cannot be due to complete saturation of the correlation by static external fields. The $HgNO_3(L+M-L)$ correlation was measured as a function of delay using a resolving time $t_0=0.5\tau$ where $\tau=8\times10^{-9}$ sec is the intermediate state half-life. Measurements at delays $\delta=-0.2\tau$, 0, 0.6τ, and 1.2τ gave the (uncorrected) results 0.21, 0.19, 0.19, 0.18($\pm$0.02). Since the correlation does not fall off rapidly with delay, we conclude that the wipeout effects result from the excitation of the Hg atom following K, L, or M conversion, that the resulting perturbations are short lived ($\approx<10^{-9}$ sec) and that the wipeout is not due to the fields of neighboring stoms.

* This work supported in part by the U. S. Office of Ordnance Research.

YA8. The Excited States of Hg^{199}.* HERBERT H. BOLOTIN AND ROGER G. WILKINSON, *Indiana University.*—Scintillation coincidence counting techniques have been applied to the study of the cascade gamma rays which occur in the decay of the 45 min Hg^{199} isomer. The K conversion coefficient for the 0.159 Mev radiation is found to be 0.34$\pm$0.03 in agreement with an $E2$ transition and with previous work.[1] α_K for the 0.368 Mev radiation is found to be 0.98$\pm$0.04 and a value of 1.78$\pm$0.10 is obtained for the total conversion coefficient of this transition. The measured α_K for the higher energy transition differs by a factor of four from the value expected for an $M4$ transition. Angular correlation measurements of the gamma rays yield a negative anisotropy of -14.5 ± 8 percent instead of a positive 37 percent which would arise from a pure 2^2–2^4 cascade. The conclusion is that the 0.368 Mev transition is a mixture of $M4$ and $E5$ radiation. A mixing ratio of $E5/M4$ of 30$\pm$20 percent is suggested. A half-life of 42$\pm$1 minutes was obtained for the decay.

* Supported by the joint program of the Office of Naval Research and and the U. S. Atomic Energy Commission.
[1] A complete list of authors appears in Hollander, Perlman, and Seaborg, Revs. Modern Phys. **25**, 469 (1953).

YA9. Photoproduction of Pb^{207m}. W. L. BENDEL, M. E. TOMS, AND R. A. TOBIN, *Naval Research Laboratory.*—An 0.8-second activity has been observed by bombardment of lead with bremsstrahlung from the Naval Research Laboratory 22-Mev betatron. Data were obtained by cycling the apparatus. This activity is attributed to the reaction $Pb^{208}(\gamma,n)Pb^{207m}$. The pulse-height distribution observed with a scintillation counter is consistent with this assignment. The half-life was measured as 799±13 milliseconds. The apparent threshold is at approximately 10.2 Mev. The absence of any observable activity below 10.2 Mev indicates that the $Pb^{207}(\gamma,\gamma')Pb^{207m}$ reaction is negligible and also that this state is not measurably produced by neutron capture in Pb^{206}. The difference between this apparent threshold and the energy differential of 9.0 Mev (neutron binding energy plus energy of the metastable state) may be due to the spin change required (0 to 13/2) to reach this state.

YA10. Metastable States in Re^{180}, Ir^{191}, Au^{193}, Pb^{201}, and Pb^{203}.*† VERA KISTIAKOWSKY FISCHER, *University of California Radiation Laboratory and Columbia University.*—Activities produced in W, Ir, Pt, Au, and Tl targets by bombardment with 31.5-Mev protons were studied with scintillation and proportional counters. A grey-wedge pulse height analyzer was used for determination of gamma-ray energies. Excitation function studies were the basis for making assignments. Decay schemes will be proposed. The 7.4 sec Au^{197m} and the 30 sec Au^{195m} were also seen and their observed properties and excitation functions were used as a check on the interpretation of the other results.

Assignment	Half-life	Gamma rays	Particles	Produced by
Re^{180m}	145±4 sec	0.88, (0.51), 0.11 Mev, *K* x-rays	1.1 Mev β^+ electrons	$W^{182}(p,3n)$
Ir^{191m}	4.91±0.14 sec	0.14 Mev, *K* x-rays	electrons	$Ir^{191}(p,p)$ $Ir^{191}(p,p2n)$
Au^{193m}	3.88±0.25 sec	0.26 Mev, *K* x-rays	electrons	$Pt^{194}(p,3n)$ $Pt^{194}(p,2n)$
Pb^{201m}	60.1 ±4.4 sec	0.65 Mev, *K* x-rays	electrons	$Tl^{203}(p,3n)$
Pb^{203m}	6.73±0.44 sec	0.86 Mev, *K* x-rays	electrons	$Tl^{203}(p,n)$ $Tl^{205}(p,3n)$

* This work was sponsored in part by the U. S. Atomic Energy Commission.
† Grateful acknowledgment is made of the Sarah Berliner Fellowship (1953–54) of the American Association of University Women which made this work possible.

YA11. Internal Conversion Coefficients of Tl^{203} (parent, Hg^{203}). R. K. DOERNER AND A. H. WEBER,* *Saint Louis University.*—A method for internal conversion coefficient measurement is described utilizing an electron scintillation pulse-height spectrometer and consisting essentially in the measurement of the number of coincidences within the anthracene crystal between conversion electrons and the electrons from the continuous beta spectrum. This number divided by the number of noncoincident events yields the total conversion coefficient. For Tl^{203} (parent, Hg^{203}) the conversion coefficient so measured is 0.11. When compared to 0.164 (by direct comparison of area under conversion and beta-spectrum curves) and 0.16 (from the ratio of *K* plus *L* x-rays to 280 kev gamma rays) this value, although low is sufficiently close to make the method feasible. The weighted mean value of the coefficients measured by the three indicated methods is $\alpha_K=0.147\pm0.002$ and $\alpha_L=0.045\pm0.001$; giving $K:L=3.29$. It is thus tentatively assumed that the 280 kev gamma ray is about 75 percent *E*2 plus 25 percent *M*1. According to the shell model the first excited state of Tl^{203} is a $d_{3/2}$ state. The large amount of mixing should increase considerably the ratio $E2/M1$ compared to single particle estimates.

* Supported in initial phases of the work by the U. S. Atomic Energy Commission.

YA12. Alpha-Gamma Directional Correlation in Am^{241}.* T. B. NOVEY, *Argonne National Laboratory.*—Previous studies[1,2] of the alpha-60 Mev gamma directional correlation in liquid film sources of Am^{241} have been continued. It is found that the attenuation due to electron quadrupole interaction in the liquid can be varied by the presence of ions of varying complexing strength and concentration. The results of a series of measurements involving ions of increasing complexing strength are as follows:

Solutions	Anisotropy [W(180°)−W(90°)]/W(90°)
1*N* $HClO_4$	−0.17±0.03
1*N* HCl	−0.19±0.04
6*N* HCl	−0.12±0.03
1*N* H_2SO_4	−0.11±0.03
1*N* HNO_3	−0.07±0.03
1*N* acetic acid	+0.03±0.03
1*N* $HClO_4$+1*N* citric acid	−0.02±0.04
1*N* $HClO_4$+1*N* versene	−0.04±0.03

These measurements were made with a resolving time, 2τ, of 0.15 microseconds. Measurements with shorter resolving times and varying delay times give an extrapolated anisotropy at zero delay of −0.22.

* Work done under the auspices of the U. S. Atomic Energy Commission.
[1] T. B. Novey, Phys. Rev. **96**, 547 (1954).
[2] Raboy, Novey, and Krohn, Bull. Am. Phys. Soc. **30**, No. 1, 48 (1955), abstract S9.

SATURDAY AFTERNOON AT 1:30

Exhibit Hall I

(W. K. H. PANOFSKY presiding)

Mesons, II

Z1. Pion Pair Production by Photons.* R. M. FRIEDMAN, K. M. CROWE, AND HANS MOTZ,† *Stanford University.*—In view of the anomalously large pair production of pions in nucleon-nucleon collisions and the considerable interest in the interpretation of pair-production processes, we report our attempts to observe pion pairs from 500- to 600-Mev bremsstrahlung on hydrogen. The method consists of looking for π^- mesons produced by bremsstrahlung on liquid hydrogen; μ^- mesons are counted by delayed coincidences[1] resulting from the decay in flight of the π^- meson. By subtracting the target-empty signal, we obtain a H_2 count which we hope to identify as π^-'s by observing: (1) proper deflection (~30°) in a magnetic field; (2) proper half-life for μ decay into electrons; and (3) disappearance below kinematic threshold. To date the signal we obtain does not fully meet these requirements so that our results are to be interpreted as upper limits. The ratio of π^- to π^+ mesons at 55 Mev, 75° lab angle, with 590-Mev bremsstrahlung, is less than 3.7±0.4 percent. The results of a number of runs will be given and evidence concerning a lower limit will be presented.

* Supported by the Office of Naval Research and the U. S. Atomic Energy Commission.
† Now at the Engineering Laboratory, Oxford University.
[1] Crowe, Friedman, and Motz, Bull. Am. Phys. Soc. **29**, No. 8, 20 (1954), abstract L3.

Z2. π^-/π^+ Ratios in Photoproduction.* HANS MOTZ,† K. M. CROWE, AND R. M. FRIEDMAN, *Stanford University.*—We have observed variations of $-/+$ photopion production ratios for asymmetric nuclei which seem to be correlated with the difference in binding energy of the ground state of the residual nuclei for the negative and the positive production. For 280-Mev bremsstrahlung, a plot of the $-/+$ ratio *vs* $\Delta M = M_{Z+1,A} - M_{Z-1,A}$ gives a straight line for all elements measured, confirming the results of Littauer and Walker.[1] (In the event no stable isobar exists, the sum of the masses of the reaction products is used.) We have also measured $-/+$ ratios for Be, Li, and C, as well as Ca and Pb for various primary electron energies. At high energies (500 Mev) the $-/+$ ratio seems to tend toward the neutron-proton ratio within the experimental errors. Our results are consistent with the measured excitation functions (linear over a reasonably wide range) and the calculated threshold variations due to binding energy.

* Supported by the Office of Naval Research and the U. S. Atomic Energy Commission.
† Now at the Engineering Laboratory, Oxford University.
[1] R. M. Littauer and D. Walker, Phys. Rev. **86**, 838 (1952).

Z3. π^+ Photoproduction in Carbon.* K. M. CROWE, R. M. FRIEDMAN, AND HANS MOTZ,† *Stanford University.*—By varying the energy of the Stanford linear electron accelerator, we have measured the yields of positive photopions of 60 ± 10 Mev energy at 75° lab angle for 250- to 600-Mev bremsstrahlung. Our resolution and monitoring are checked with pions from hydrogen. The "efficiency" per proton, $\epsilon = \sigma_C/6\sigma_H$, is a slowly-varying function of the primary electron energy which approaches 0.95 at 500 Mev. A large fraction ($\sim\frac{1}{3}$) of the yield is obtained from photons of energy larger than 350 Mev. This corresponds to leaving the residual nucleus excitation energy of 100–300 Mev. Similar results are obtained for 40 ± 10-Mev π^{+}'s and 100 ± 10-Mev π^{+}'s. Various interpretations of this effect are considered and will be discussed qualitatively: (a) internal momentum distribution of the protons in the nucleus,[1] (b) variation of the production matrix element for free nucleons with angle and energy, (c) surface production and absorption effects, (d) coherent production, (e) density of final states in the residual nucleus for large excitation energies, and (f) form-factor effects.

* Supported by the Office of Naval Research and the U. S. Atomic Energy Commission.
† Now at the Engineering Laboratory, Oxford University.
[1] M. Lax and H. Feshbach, Phys. Rev. **81**, 189 (1951).

Z4. Positive Pion Scattering by Hydrogen at 300 Mev.* R. S. MARGULIES, *Brookhaven National Laboratory.*—The Brookhaven six-foot diffusion chamber has been used at the Cosmotron to study elastic scattering of π^+ mesons on hydrogen at 300 Mev. Assuming a total cross section of 75 mb,[1] the 115 events so far analyzed have c. m. angular distribution $d\sigma/d\Omega = 2.27 + 2.40\cos\theta + 11.1\cos^2\theta$ mb/sterad. The Fermi-type phase shifts, assuming only S- and P-waves are found to be $\alpha_3 = -12°$, $\alpha_{31} = -10°$, $\alpha_{33} = 126°$. This experimental distribution strongly favors the theoretically predicted "track I" solution of de Hoffman, *et al.*[2]

* Work performed under the auspices of the U. S. Atomic Energy Commission.
[1] S. J. Lindenbaum and L. C. L. Yuan (private communication).
[2] de Hoffman, Metropolis, Alei, and Bethe, Phys. Rev. **95**, 1586 (1954).

Z5. Scattering of 22-Mev Positive Pions on Protons.* S. WHETSTONE AND D. STORK, *University of California, Berkeley.*—A beam of positive pions was passed through a $3\frac{1}{2}$-inch thickness of liquid hydrogen contained in a polyethylene-lined styrofoam target. The pions entered the hydrogen with a mean energy of 25.0 ± 0.5 Mev, and traversed the target parallel to the face of a stack of G. 5 nuclear emulsions, 6 inches long and $1\frac{1}{2}$ inches high, placed 1 inch from the beam edge. Tracks of scattered pions, identified at the end of their range in the emulsion by the characteristic decay-at-rest, can be followed back to the front surface of the stack, where measurements of the entrance angles can be made. It is possible to determine the scattering angle and energy for each event. We can therefore distinguish hydrogen events from elastic carbon scatters occurring in the 0.004-inch polyethylene liner. The pion beam was obtained by selecting pions produced at 0° in the reaction $p+p \rightarrow \pi^+ + d$, using quadrupole magnets to "strong-focus" the electrostatically-deflected 340-Mev proton beam of the Berkeley synchrocyclotron. Advantage was taken of the double-focusing properties of a wedge-shaped analyzing magnet. Fourteen scatters from hydrogen established to date yield a preliminary cross section of 3 mb for scattering in the interval 45°–135° in the laboratory.

* This work was done under the auspices of the U. S. Atomic Energy Commission.

Z6. Scattering of Negative Pions Near 15 Mev in Hydrogen.* M. C. RINEHART, K. C. ROGERS, AND L. M. LEDERMAN, *Columbia University.*—The Nevis hydrogen-filled diffusion cloud chamber was employed in a search for low-energy negative pion scatterings of protons. The incident flux had a mean energy of 15 Mev, with a half-width of about 7 Mev. Significant contributions to the flux extended from 2.5 to 30 Mev. Twenty-six interactions were observed satisfying angular criteria based on length of recoil protons. The distribution of events in angle and energy was analyzed by the method of maximum likelihood. In this analysis, the Coulomb and p-wave contributions are treated as known and all of the data are used to determine the best s-wave phase shift, assumed to vary linearly over the energy interval. The result is $\alpha_3 + 2\alpha_1 = (0.25\pm0.05)\eta$ in radians. If this result is combined with $\alpha_1 - \alpha_3$ obtained from the Panofsky effect *via* detailed balance, the quantity $\alpha_1 + 2\alpha_3$ is positive. If, however, the charge exchange scattering results of Tinlot and Roberts and Spry are used, $\alpha_1 + 2\alpha_3$ is negative, in agreement with p_1 mesic x-ray results.[1] The latter choice yields $\alpha_1 = +0.17\eta$, $\alpha_3 = -0.10\eta$ in agreement with Orear's suggestion.

* Supported by the joint program of the Office of Naval Research and the U. S. Atomic Energy Commission.
[1] Stearns, Stearns, DeBenedetti, and Leipuner, Phys. Rev. **97**, 240 (1955).

Z7. Pion-Proton Total Cross Sections Near 4 Bev.* K. C. BANDTEL, H. A. BOSTICK, B. J. MOYER, R. W. WALLACE, AND N. F. WIKNER, *University of California, Berkeley.*—Measurements are in progress of the total cross section subtended by protons and other nuclei for collision with pions of energies in the region of 4 Bev. When the Berkeley bevatron is operating at 10^{10} protons per pulse a negative pion beam of 4.4-Bev energy is available at 50 feet from the target with an intensity of about 0.4 pion per cm² per pulse. These conditions are typical of the energy-selected positive and negative pion beams in use. The muon contamination in these beams is at present estimated to be in the neighborhood of four percent, though further work on this point remains to be done. At the time of writing of this abstract, the π^--proton cross section measured at 4.4 Bev is 30 ± 5 millibarns, and by the time of presentation of this work the limits of error should be reduced, and cross-section values for other nuclei are expected to be available. Measurements are made with a geometry which is calculated with respect to the Coulomb scattering of the mesons, and also with regard to the elastically scattered and secondary charged particles which might be detected in the final counter telescope.

* This work was performed under the auspices of the U. S. Atomic Energy Commission.

Z8. Pion-Proton Elastic-Scattering Cross Sections at 43 Mev and $37\frac{1}{2}°$. S. W. BARNES, D. MILLER, J. RING, G. GIACOMELLI, R. SUMMERS, AND H. R. CHILDS, *University of Rochester.*—The differential π–p scattering cross section of 43 ± 3 Mev pions has been measured at a laboratory scattering angle of $37\frac{1}{2}{}^{+10°}_{-7°}$. The pions were scattered in a liquid hydro-

gen target, detected by a doubles telescope of two annular crystals and identified by the pulse heights yielded by the second annular crystal. The geometry of the detecting telescope was such that pions scattered from the walls of the hydrogen target were not counted. On the basis of the 200 pions of each sign scattered to date the π^- and π^+ cross sections in the center-of-mass system are, respectively, 0.54 ± 0.08 mb/sterad and 0.27 ± 0.04 mb/sterad. The uncertainties given are mean deviations based on the counting statistics. Both the cross sections are approximately twice the value predicted by the recent Bethe-de Hoffman set of phase shifts.

Z9. (Abstract withdrawn.)

SATURDAY AFTERNOON AT 1:30

Caribar Room

(A. S. WIGHTMAN presiding)

Theoretical Physics, V: Field Theory

ZA1. Universal Singular Functions In Local Relativistic Quantum Field Theory. A. S. WIGHTMAN AND D. HALL, *Princeton University.*—The vacuum expectation value of a product of n Heisenberg operators is, from translation invariance, a function of the $n-1$ variables x_1-x_2, x_2-x_3, $\cdots$, $x_{n-1}-x_n$. If no negative-energy states exist, it can be extended to an analytic function of the variables $z_{12}=x_1-x_2-i\eta_1$, $z_{23}=x_2-x_3-i\eta_2$, $\cdots$, where η_1, $\eta_2\cdots$ vary in the interior of the forward-light cone. By virtue of Lorentz invariance the vacuum expectation value therefore becomes a sum of integrals with respect to invariant weight functions of certain universal singular functions which are the boundary values of analytic functions. For scalar fields, these latter functions can be written: $\Delta=\int d\mu(\Lambda)\exp -itr(\Lambda M)$, where Λ is a homogeneous Lorentz transformation, $d\mu(\Lambda)$ is an invariant volume element on the group manifold, and $M^{\mu\nu}=\sum_{j=1}^{n-1} p_{j,j+1}{}^{\mu}z_{j,j+1}{}^{\nu}$. For $n=2$, one gets the well-known formula

$$\Delta=m^{-2}\Delta_m{}^{(+)}(z)=H_1{}^{(1)}[m(z_{12}{}^2)^{\frac{1}{2}}][8\pi im(z_{12}{}^2)^{\frac{1}{4}}]^{-1}.$$

For $n=3$ the analogous formula is

$$\Delta_{m_{12},m_{23},m_{13}}(z_{12},z_{23},z_{13})=[H_0{}^{(1)}((\alpha-(2\beta)^{\frac{1}{2}})^{\frac{1}{2}}) -H_0{}^{(1)}((\alpha+(2\beta)^{\frac{1}{2}})^{\frac{1}{2}})](2\beta)^{-\frac{1}{4}}(8\pi i)^{-1},$$

where

$$\alpha=m_{12}{}^2z_{12}{}^2+m_{23}{}^2z_{23}{}^2+2(p_{12}\cdot p_{23})(z_{12}\cdot z_{23})$$

and

$$\beta=[(p_{12}\cdot p_{23})^2-m_{12}{}^2m_{23}{}^2]^{\frac{1}{2}}[(z_{12}\cdot z_{23})^2-z_{12}{}^2z_{23}{}^2]^{\frac{1}{2}}.$$

For spinor and tensor fields similar universal singular functions exist. They are obtained from the above by appropriate differentation and multiplication by γ matrices.

ZA2. Some Simple Results of Feynman Field Theory. J. R. H. DEMPSTER, *Princeton University.*—The "sum over histories" in Feynman's method of quantization can be evaluated for any system with a quadratic Lagrangian, including noninteracting field theories.[1] However, the techniques for dealing with such quantities in field theory, involving differentiation and integration of functionals, are quite unfamiliar. In the simple example of a real scalar field, it is shown that these techniques present no especial difficulty and give consistent results, even though many of the integrals appear at first sight to be undefined. While the noncommutative operators of the usual quantum-field theory need never appear in this formalism (matrix elements of time-ordered operator products are given directly by Feynman sums), it is instructive to relate the two approaches by a direct calculation using the sum over histories. In this straightforward way an explicit form is obtained for these operators, in a representation in which the field strength is diagonal, and their commutation rules are derived.

[1] R. P. Feynman, Revs. Modern Phys. **20**, 367 (1948); Phys. Rev. **84**, 126 (1951).

ZA3. A Generalization of Feynman's Integral Over-All-Paths Formulation of Quantum Mechanics. Y. TAKANO AND J. L. ANDERSON, *University of Maryland.**—Schwinger's action principle[1] is applicable only to those problems where the kinetic energy is pure quadratic in the velocities. It is not at all evident how his formalism can be extended to deal with kinetic-energy terms of the form $\frac{1}{2}\dot{q}_iG^{ij}\dot{q}_j$ where G^{ij} may depend explicitly on the coordinates. Feynman's formulation,[2] to which Schwinger's action principle can be shown to be equivalent, does appear to lend itself to a natural generalization for Lagrangians of the type considered. The arguments which led to this modification were based upon the results of an examination of the effect of changing variables in the original Feynman formulation. As was to be expected, it was found necessary to include the Jacobian of the transformation in the transformed integral. For a nonlinear transformation a pure-quadratic energy term goes over to the form considered above, and the Jacobian is $\sqrt{g}$ where g is the determinant of G^{ij}. We propose therefore to include such a term in the general statement of Feynman's Postulate.

* Supported by Office of Naval Research.
[1] J. Schwinger, Phys. Rev. **82**, 914 (1951).
[2] R. P. Feynman, Revs. Modern Phys. **20**, 367 (1948).

ZA4. Functional Integration and *S*-Matrix Theory. JAMES L. ANDERSON, *University of Maryland.**—Ordering operators have been introduced into S-matrix theory[1] which allows one to write down the T-product of a functional of the field variables directly in terms of N- or normal-products of these variables. The rules for this expansion originally involved exponentials of functional differential operators and as such offered little hope

for practical application. In this paper it will be shown that, by introducing the concepts employed in functional integration, it is possible to convert these differential operators to integral form. When this is done, it is not surprising to find that the expressions obtained thereby are equivalent to Feynman's integral-over-all-paths formulation of quantum mechanics.[3] However, the expressions derived via *S*-matrix theory provide a simple rule for defining the normalization constant in Feynman's Theory. Also, these expressions allow one to express Feynman's integral in several alternate forms which might prove more convenient for actual calculation.

* Work supported by Office of Naval Research.
[1] J. L. Anderson, Phys. Rev. **94**, 703 (1954).
[2] R. P. Feynman, Revs. Modern Phys. **20**, 367 (1948).

ZA5. Spectrum of a Bethe-Salpeter Equation.* FREDERICK L. SCARF, *M.I.T.*—The spectrum of Wick's two-body equation[1] is investigated rigorously for arbitrary binding energy ϵ. It is verified that for ϵ nonzero this singular equation has a complete point spectrum labeled by n, l, m, and k. The limit of zero ϵ is investigated, and it is shown that *all* eigenvalues tend to zero. This contradicts Wick's results which are shown to be based on an unreliable approximation. It is found that the set of eigenvalues $\lambda_n(k=0)$ give the best fit to the Balmer formula. The Bethe-Salpeter amplitudes on a space-like surface are also investigated. It is demonstrated that all amplitudes obey every known boundary condition at any ϵ. It is also shown that the amplitudes are all well behaved and all are fairly good approximations to the hydrogen-atom wave functions in the N.R. region, but that those with $k=0$ give the best fit. While the solutions with $k=0$ seem to correspond to nonrelativistic ones, no rigorous criterion has been found to reject the "spurious" solutions.

* Assisted in part by the joint program of the Office of Naval Research and the U. S. Atomic Energy Commission.
[1] G. C. Wick, Phys. Rev. **96**, 1124 (1954).

ZA6. Space Inversion and Charge Conjugation for Fermion Fields.* B. P. NIGAM AND L. L. FOLDY, *Case Institute of Technology*.—While the space-inversion transformation of a fermion field is fixed only to within an arbitrary phase factor, the space-inversion and charge-conjugation transformations commute only for a particular choice of this phase *modulo* π. Since situations exist (e.g. positronium) in which both transformations are diagonal, it would appear (paradoxically) that these would fix the phase. This point has been examined by constructing explicit representations of these transformations, with an arbitrary phase factor associated with each, in a form independent of an expansion of the fields in a set of orthonormal functions. The commutator has been found to be proportional to $\sin(\theta Q)$, where θ is the space-inversion phase and Q the total-charge operator. Since charge conjugation can be diagonal only for states where $Q=0$, the commutator thus vanishes for such states independently of the value of θ, thus resolving the apparent paradox. These special explicit representations of the transformations may be of value for other calculations.

* Supported by the National Science Foundation and the U. S. Atomic Energy Commission.

ZA7. Re-examination of the Neutrino Theory of Light. O. W. GREENBERG* AND A. S. WIGHTMAN, *Princeton University*.—Pryce's[1] formal argument that the requirements of relativistic invariance and Bose commutation rules are mutually inconsistent is not complete, in that he did not consider the most general bilinear combination of neutrino (and antineutrino) creation and annihilation operators. His argument has been extended to cover this case. The essential difference between the three-dimensional theory (which does not work) and the one-dimensional theory (which does) can be understood from the following schematic argument. The creation operator c_1^* for the right circularly polarized photon of lowest momentum for a given direction contains the typical terms $a_j^{(+1)*}a_j^{(-1)}$, $b_j^{(+1)*}b_j^{(-1)}$, and $a_j^{(+1)*}b_j^{(+1)*}$, where $a_j^{(\pm 1)}$ is the annihilation operator for a right (left) circularly polarized neutrino of momentum j, and b is the corresponding operator for an antineutrino. Note that in these operators angular momentum conservation requires adjoint for right circular polarization and no adjoint for left. This implies that the lowest two-photon state vanishes: $(c_1^*)^2\Phi_0 \propto c_1^*a_1^{(+1)*}b_1^{(+1)*}\Phi_0 \propto (a_1^{(+1)*}b_1^{(+1)*})^2\Phi_0=0$, where Φ_0 is the vacuum state. This contradicts Bose statistics. In the one-dimensional case, there is no polarization, c_1^* no longer commutes with $a_1^*b_1^*$, and the two-photon state doesn't vanish.

* National Science Foundation Predoctoral Fellow.
[1] M. H. L. Pryce, Proc. Roy. Soc. (London) **165A**, 247 (1938).

ZA8. On Covariant Calculations of Polarization in Nucleon-Nucleon Scattering. BURTON D. FRIED, *The Ramo-Wooldridge Corporation*.—As is well known, the polarization calculated from nonrelativistic, quantum mechanics using conventional, spin-dependent potentials, vanishes in lowest-order Born approximation (unless, as in the recent optical model calculations of polarization in nucleon-nucleus scattering, a complex potential is assumed). In higher orders it is possible to obtain a nonzero result if there are intermediate states whose energy coincides with that of the initial state, for these give rise to an imaginary component in the effective potential. The situation is quite similar in the relativistic case. In fact, if the interaction between nucleons arises from a quantized meson field, then it is possible to demonstrate that, to all orders of perturbation theory, contributions to polarization come entirely from "displaced poles" in the Feynman-Dyson-Wick formalism. Since only the imaginary component of the potential is needed, the polarization is considerably easier to compute, to a given order, than is the total cross section. (At an appropriate stage of the calculation, $(x-i\epsilon)^{-1}$ can be replaced by $\pi i\delta(x)$, which reduces by one the number of integrations over Feynman parameters.) Calculations of the n–p and p–p polarization are being carried out using ps–ps meson theory.

ZA9. Canonical Transformations of the Pseudo-vector Field. M. EISNER, *Texas A. & M. College*.—A series of canonical transformations are employed to reduce the pseudo-vector Hamiltonian with pseudo-vector and tensor coupling to nucleons to a form which allows splitting of the field into longitudinal and transverse parts. Although the interaction term contains more complicated operators than in the original representation, this offers no difficulty in the strong coupling treatment of nuclear forces, self energy, and isobar energy problems. Agreement is obtained with the results of Rüdenberg[1] for strong coupling for pseudo-vector and tensor coupling alone. A simplification of the general interaction operator is discussed in terms of dichotomic variables implying extra degrees of freedom.

[1] K. Rüdenberg, Helv. Phys. Acta **24**, 89 (1951).

ZA10. Approximately Relativistic Equations. M. KLERER* AND R. D. HATCHER, *New York University*.—A modified Breit equation for two particles, with anomalous moments, has been examined. The Foldy-Wouthuysen method is used for reduction to a Pauli form. A previously used procedure of replacing the spin operator σ by $\mu\sigma$, where μ is the actual magnetic moment in units of Bohr (or nuclear) magnetons, is shown to be inconsistent with the modified equation. The limits of applicability of the previous procedure, in transforming to the actual magnetic moment, is discussed as a function of the mass. This phenomenological treatment yields good results when applied to the fine structure and hyperfine structure of hydrogen. Effects due to the finite mass and magnetic moment of the proton are directly reduced from the two-body equation.

An examination is made of certain terms usually neglected in applications of the normal Breit equation. Difficulties arising from application of an approximately relativistic one body equation to hyperfine structure are discussed and an alternate method is proposed. The relationship of the Foldy-Wouthuysen method to that of "large components" is also examined.

* Now at The City College, New York City.

ZA11. On the Lee Model. KATSUMI TANAKA, *Argonne National Laboratory.**—Lee[1] has treated some simple one-particle problems of interacting fields that are both renormalizable and solvable in order to obtain some deeper insight as to the nature of the renormalization procedure without the use of perturbation method. One of the peculiar results of Lee is that the renormalized coupling constant cannot be realized by any limiting process if g, the unrenormalized constant, is restricted to be on the real axis. We have treated the two-particle state within Lee's formalism and obtained an integral equation that determines the binding energy of the two particles, if there are bound states. It is expressed in terms of the renormalized mass and coupling constant which were obtained from the one-particle state. It is shown that when the upper limit in momentum space goes to infinity, the integral equation for the binding energy involves divergent integrals. In other words, Lee's formalism for two particles is not free from divergent integrals. The reasons for this are given.

* Work done under the auspices of U. S. Atomic Energy Commission.
[1] T. D. Lee, Phys. Rev. **95**, 1329 (1954).

ZA12. On Quantum Electrodynamics and the Mass Operator. W. WESSEL, *U. S. Air Force Institute of Technology.*—In a theory of the electron proposed by the author,[1] quantization of the electromagnetic field is accomplished by the choice of infinite matrices in place of Dirac's. The mass term is then of the form[2] $m=m(I,K)(I^2+K^2)^{\frac{1}{2}}$, where I and K are the invariants of the momentum tensor and $m(I,K)=m_0\sinh(\Gamma K)$ with $\Gamma=(3/2)(\hbar c/e^2)=205.5566\pm0.0024$. In a K-representation the infinite matrices are represented by difference operators,[3] which makes the square root very unwieldy. It has been found, that the nonlinear difference equation $(1/2i)[\theta(K+i)-\theta(K-i)]=K/\theta(K)$, which may be considered as the quantum analog of $\partial(I^2+K^2)^{\frac{1}{2}}/\partial K=K/(I^2+K^2)^{\frac{1}{2}}$, has a simple solution $\theta(K)$. With its substitution for $(I^2+K^2)^{\frac{1}{2}}$ the rest mass problem may be reduced to a difference equation with a periodic coefficient, that admits a closed solution for spin $\frac{1}{2}$, if Γ can be approximated by a rational multiple of π. With $\Gamma=64\pi+10\pi/7=205.54992\cdots$ one finds one mass eigenvalue m/m_0 at -1 and two complex conjugate ones close to $+1$ on the unit circle. The complex ones may be interpreted by the fact that quantization of the ψ-field has not yet been accomplished.

[1] W. Wessel and S. J. Czyzak, Phys. Rev. **91**, 986 (1953).
[2] W. Wessel, Phys. Rev. **83**, 1031 (1951).
[3] W. Wessel, Z. Naturforsch. **7a**, 583 (1952).

ZA13. Transformation Groups in Configuration Space.* IRWIN GOLDBERG AND ALLEN JANIS, *Syracuse University.*—The canonical type transformations in the Lagrangian formalism[1] have been studied to determine whether the analogue of the Dirac bracket transformations[2] can be identified. The group theoretical commutators are used to construct the group of transformations in configuration space which has a normal subgroup the transformations generated by the constraints. The factor group of this subgroup has a one to one correspondence with the permissible generators. The observables of the quantized theory are to be identified with the permissible generators.

* Supported by Office of Naval Research.
[1] P. G. Bergmann and R. Schiller, Phys. Rev. **89**, 4 (1953).
[2] P. G. Bergmann and I. Goldberg, Phys. Rev. (to be published).

ZA14. Peierls' Introduction of Canonical Transformations into the Lagrangian Formalism.* PETER G. BERGMANN, *Syracuse University.*—It will be shown that an approach due to Peierls[1] and one due to Bergmann and Schiller,[2] to define canonical transformations in the Lagrangian formalism, are equivalent, at least in the realm of theories considered by Peierls, in which the matrix of coefficients of the terms quadratic in the velocities is regular. The extension of the Lagrangian formalism to theories with singular matrix will be discussed in a separate abstract by Goldberg and Janis. Peierls has suggested quantization on the basis of so-called c-number variations. From the present discussion a different possibility emerges: To construct the group of permissible and interesting transformations in the c-number theory, to retain only those observables that generate these transformations, to determine the commutators group-theoretically, and for consistency to test that the proposed set of infinitesimal transformations forms indeed a group. Work designed to test the efficacy of this approach is now in progress.

* Supported by Office of Naval Research.
[1] Proc. Roy. Soc. (London) **A214**, 143 (1952).
[2] P. G. Bergmann and R. Schiller, Phys. Rev. **89**, 4 (1953).

ZA15. Expansion of Two-Dimensional Wave Fields in Powers of $1/\rho$.* HARVEY EINBINDER, *Technical Research Group.*—If solutions of the two-dimensional wave equation exist of the form $\frac{e^{ik\rho}}{\rho^{\frac{1}{2}}}\sum_{n=0}^{\infty}\partial_n(\theta)\rho^{-n}$, a recurrence relation connecting successive coefficients is obtained formally by substituting this series into the wave equation, namely:

$$2ik(n+1)\partial_{n+1}=(n+\tfrac{1}{2})^2\partial_n+\frac{\partial^2\partial_n}{\partial\theta^2}.$$

This expansion is then derived by steepest descents from an integral representation of the solution from which it is shown that the series is asymptotic and cannot converge for more than a single value of θ regardless of the aperture field. This is in contrast to three-dimensional wave fields where such expansions are uniformally and absolutely convergent. However, the total field in two dimensions is uniquely determined by the values of the far field by means of an integral representation. These results are illustrated by the cylindrical waves $H_\nu^{(1)}(ke)$.

* This research was supported by the Air Force Cambridge Research Center.

SUPPLEMENTARY PROGRAMME

SP1. Production of Electrostatic Charges by Rotation of a Permanent Magnet. OLEG YADOFF.*—A slender cylindrical magnetized rod, long in relation to its diameter, which rotates rapidly about its longitudinal axis, engenders thereby electrostatic charges on its surface and produces in the surrounding medium a strong electrostatic field. Conditions under which this occurs have been determined experimentally. The direction of rotation determines the sign of the electrostatic field. If two rods rotate in opposite directions, the fields obtained have opposing directions: (+) and (−). The two rods then undergo mutual attraction, under Coulomb's law, which provides also for the converse, namely that like fields are mutually repellent. The complexity of the electromagnetic processes involved in the occurrences both within and around the rod is such that no definite conclusion has as yet been possible. Nevertheless, these observations tend to support the hypothesis, put forward by the author some time ago, that in general so-called electrostatic fields should be considered as but one aspect of the basic electromagnetic phenomenon.

* To be called for at the end of Session KA if the Chairman rules that time permits.

SP2. An Energy Control for External Cyclotron Beams.* G. SCHRANK, *Princeton University*.†—In order to eliminate the uncertainty in energy of the external 18-Mev proton beam from Princeton's *FM* cyclotron without the manufacture of large steering magnets, a device was constructed which stabilizes the mean energy of the beam to better than 0.1 percent. The device looks at the end of the range of a sample of protons which are elastically scattered from a very thin intercepting foil. This group of scattered protons is allowed to spend most of its range in aluminum and then enters and stops in an argon filled parallel-plate ionization chamber. By a double electrode arrangement which collects the ions produced at the end of the range, the mean energy of these protons is determined, and by feeding the difference signal from these two collectors back into the cyclotron magnet-current control, the energy is automatically stabilized. Better than 0.1 percent control can be achieved with as few as 500 protons entering the ion chamber per second.

* Work supported by the Atomic Energy Commission and The Higgins Fund.

† To be called for at the end of Session T if the Chairman rules that time permits.

SP3. Physical Significance of the Three Quantum Numbers. GERTRUDE T. SCHWARZMANN.*—The stationary orbits described by the satellite electrons are eccentric circular, earthial orbits. Upon the motion therein is imposed the quantum condition $2r_n pi = 2n \cdot \lambda$ as prerequisite to the fulfillment of the particular law of conservation of orbital angular momentum imposed upon the interaction between electrons and photons; this law explains the origin of the always positive, multivalued spin-quantum number: "The fraction of the spin component transformed in the transition orbit into a second revolutional component increases if emitting electron and emitted photon revolve in opposite senses; it decreases if they revolve in the same sense, by the magnitude of the orbital angular momentum of the photon," which revolves about the nucleus in a circular orbit, its radius the perihelion value $k \cdot r_n/2n$ $(k = 1, 2, \cdots n)$ of the radius vector of the electron in its particular nth orbit. Computation shows that the electrons describing transition orbits with perihelion value $k \cdot r_n/2n$ emit the corresponding lines of the nth series as $(k-1)$st harmonics. When energy from without is added to hydrogen atoms in the normal state, the emission of the Lyman and Balmer series tells that the emitting electrons have described the transition orbits leading to the first and second orbit, respectively.

* To be called for at the end of Session VA if the Chairman rules that time permits.

Author Index to Papers Presented at the 1955 April Meeting at Washington

Adams, E. N., R. E. Davis, and Colman Goldberg—G3
Ajzenberg, F., A. Rubin, and J. G. Likely—TA3
Allen, K. W., E. Almqvist, and C. B. Bigham—K2
Almqvist, E., K. W. Allen, and C. B. Bigham—K3
Altman, L., H. S. Bridge, and R. W. Williams—A8
Ambler, Ernest—M4
Anderson, H. L.—J5
Anderson, James L.—ZA4
Anderson, P. W.—FA4
Ard, Jr., William B. and Walter Gordy—BA2
Aron, W., J. S. McIntosh, G. Schrank, and J. H. Bigelow —HA8
Atkins, K. R.—Y13
Babiskin, Julius—Y3
Bandtel, K. C. H. A. Bostick, B. J. Moyer, R. W. Wallace, and N. F. Wikner—Z7
Barnes, S. W., D. Miller, J. Ring, G. Giacomelli, R. Summers, and H. R. Childs—Z8
Barrett, A. H. and M. Mandel—XA4
Bartnoff, Shepard—FA13
Baskir, Emanuel, John Tinlot, and Sidney Spital—N1
Battey, J. F. and R. M. Baum—G2
Bedo, D. E. and D. H. Tomboulian—FA10
Belinfante, F. J.—VA12
Bendel, W. L., M. E. Toms, and R. A. Tobin—YA9
Berger, Martin J. and John A. Doggett—W3
Bergmann, Peter G.—ZA14
Bernstein, E. M. and H. W. Lewis—CA7
Biedenharn, L. C.—HA5
Bigeleisen, Jacob—LA5
Bigham, C. B., K. W. Allen, and E. Almqvist—K5
Bilis, D. G. and F. G. Allen—R1
Birkhoff, R. D., A. W. Blackstock, and R. H. Ritchie—R11
Bleuler, E. and H. Morinaga—V1
Blewett, J. P., N. C. Christofilos, and A. M. Vash—T1
Blewett, M. Hildred—T3
Block, Martin M. and Robert Jastrow—D15
Bloom, S. D., C. O. Muehlhause, and H. E. Wegner—T10
Blue, J. W. and E. Bleuler—V3
Bockelman, C. K., C. M. Braams, W. W. Buechner, and D. B. Guthe—TA5
Bolotin, Herbert H. and Roger G. Wilkinson—YA8
Bonner, T. W., Alfred A. Kraus, Jr., J. T. Eisinger, and J. B. Marion—K7
Bostrom, Norman A., Emmett L. Hudspeth, and Ira L. Morgan —PA4
Braid, T. H. and R. W. Detenbeck—W6
Branscomb, L. M.—M1
Bray, P. J. and R. G. Barnes—BA11
Breazeale, J. B., W. L. Bart, and J. W. Beams—C9
Breit, G.—HA10
Brickwedde, F. G.—U2
Brode, Robert B. and Marvin J. Weber—A15
Broida, H. P.—XA12
Brolley, Jr., J. E. and R. L. Henkel—CA3
Brown, Harry A.—GA8
Brown, K. L., W. C. Barber, A. I. Berman, and W. D. George —X7
Browne, C. P. and W. C. Cobb—PA5
Bryak, H. and M. E. Rose—RA10
Buechner, W. W., A. Sperduto, and Marcos Mazari—PA9
Bunker, M. E., J. P. Mize, and J. W. Starner—V6
Burnett, C. R.—FA8
Burson, S. B., J. M. LeBlanc, and D. W. Martin—V10
Butler, J. W.—PA2
Callaway, Joseph—GA7
Callen, Herbert—Q2
Carleton, Nathaniel P.—W9
Carothers, J. E. and C. G. Andre—S5
Carter, R. S., D. J. Hughes, and H. Palevsky—B10
Chang, Roger—UA7
Chase, C. E. and Melvin A. Herlin—Y9
Chase, David M.—HA11
Chesnut, W. G., E. M. Hafner, and R. Harding—N2
Chow, Richard H. and Byron T. Wright—N8
Clark, G.—A14
Clarke, R. L., E. Almqvist, and E. B. Paul—TA2
Cleland, J. W. and J. H. Crawford, Jr.—L11
Cloud, W. M.—FA7
Coburn, Horace H. and Sherman Frankel—YA7
Coester, F.—RA3
Cohen, B. L., H. G. Blosser, D. J. Coombe, G. H. McCormick, and E. Newman—TA13
Cohn, H. O., J. K. Bair, J. D. Kington, and H. B. Willard —PA10
Coles, B. R. and W. R. Bitler—GA5
Colgate, Stirling A.—X8
Corbert, J. W. and W. W. Watson—KA7
Corson, Dale R., William S. McDonald, and Vincent Z. Peterson—S11
Courant, E. D.—T2
Cox, S. A. and R. M. Williamson—K4
Crandall, W. E., W. Birnbaum, G. P. Millburn, and R. V. Pyle —K6
Cross, W. G. and R. G. Jarvis—F4
Crowe, K. M.—E2
——, R. M. Friedman, and Hans Motz—Z3
Cutler, M.—G6
Cutler, W. G., R. W. Schiessler, and W. Webb—LA4
Dahler, J. and J. O. Hirschfelder—LA1
Dalitz, R. H.—D8
Darnell, F. J. and S. A. Friedberg—L5
Davis, Jr., Raymond—X2
Dempster, J. R. H.—ZA2
Dessler, Alexander J. and William M. Fairbank—Y10
DeStaebler, Jr., H., H. S. Bridge, B. Rossi, and B. V. Sreekantan—P7
Dexter, R. N. and Benjamin Lax—L2
Doerner, R. K. and A. H. Weber—YA11
Drell, S. D.—D11
Driscoll, Raymond L.—KA8
Eguchi, Tetsuo—D14
Einbinder, Harvey—ZA15
Eisner, M.—ZA9
Ellis, J. A., M. B. Gottlieb, and L. H. Meredith—A10
Ellis, Robert A.—A11
El-Sum, Hussein M. A. and Albert V. Baez—FA11
Fafarman, A. and M. H. Shamos—FA9
Fano, U.—VA1
Farmer, Donald J.—V7
Ferrell, R. A.—R10
Feynman, R. P.—U3
Finkelstein, David—RA13
Fischer, Vera Kistiakowsky—YA10
Fleishman, B. A.—KA6
Fletcher, P. C. and L. C. Aamodt—BA10
Foner, Simon, H. J. Zeiger, R. L. Powell, and Benjamin Lax —L1
Ford, J. and T. H. Berlin—LA7
Forstat, Harold and Charles A. Reynolds—Y12
Forster, H. H. and J. S. Wiggins—V11
Forster, H. Kurt—VA2
Freedman, M. S., F. T. Porter, T. B. Novey, and F. Wagner, Jr.—YA5
Fretter, W. B., E. W. Friesen, G. E. Kepler, and L. Lagarrigue —P9

Fried, Burton D.—ZA8
Friedman, Abraham S. and Irwin Oppenheim—LA8
Friedman, M. H. and T. D. Lee—D2
Friedman, R. M., K. M. Crowe, and Hans Motz—Z1
Fulbright, H. W., D. A. Bromley, and J. A. Bruner—T11
Fuller, C. S. and Howard Reiss—G1
Fuller, E. G.—M3
Gartenhaus, S.—D12
Geusic, Joseph E. and Dudley Williams—BA1
Ghiorso, A.—X1
Glasser, R. G., D. M. Haskin, and Marcel Schein—P13
Glauber, R. J.—HA12
Glaubman, Michael J.—V9
Goldberg, Irwin and Allen Janis—ZA13
Goldberg, W. L.—CA8
Goldhammer, P. and E. Feenberg—RA5
Gora, E. K.—XA2
Graham, Martin—T5
Greenberg, Howard and Sidney Borowitz—HA1
Greenberg, J. Mayo—HA14
Greenberg, J. S. and M. Deutsch—X6
Greenberg, O. W. and A. S. Wightman—ZA7
Griem, H. and S. F. Singer—A5
Griffin, James J.—RA4
Gross, E. P.—FA3
Grosskreutz, J. C.—PA1
Haar, Lester, Joe C. Bradley, and Abraham S. Friedman LA9
Haeberli, W.—N11
Hafner, E. M. and W. Chesnut—N3
Hammer, C. L. and A. J. Bureau—T7
Hardwick, E. R. and W. G. McMillan—UA9
Hauver, George and Louis Zernow—KA12
Hayward, R. W. and D. D. Hoppes—V4
Hein, R. A.—Y4
Helm, R. H., K. M. Crowe, and G. W. Tautfest—S2
Henley, E. M. and T. D. Lee—D9
Henry, Warren E.—Y1
Herasymenko, P.—C4
Herman, F.—DA4
Herring, D. F.—KA11
Heydenburg, N. P. and G. M. Temmer—CA10
Hill, David L., Burton E. Freeman, and Kenneth W. Ford —RA11
Hirchberg, Joseph G.—FA6
Hobson, J. P., J. C. Hubbs, W. A. Nierenberg, and H. B. Silsbee—BA3
Holden, A. N., B. T. Matthias, W. J. Merz, and J. P. Remeika —GA1
Holmgren, H. D. and J. W. Butler—TA7
Hoover, Jr., C. W.—KA9
Hornyak, W. F. and R. Sherr—K14
Howland, P. R. and N. E. Scofield—W2
Hrostowski, H. J., F. J. Morin, T. H. Geballe, and G. H. Wheatley—G10
Huang, Kerson and S. D. Drell—HA4
Hubbs, J. C., J. P. Hobson, W. A. Nierenberg, and H. B. Silsbee—BA4
Hudson, George E. and Alfred Saenger—KA4
Hudspeth, Emmett L., Ira L. Morgan, and Joseph T. Peoples —PA3
Hughes, D. J.—F11
Hughes, V. W. and J. S. Geiger—XA1
Humphrey, James N.—G8
Hussin, A., C. J. D. Jarvis, and E. Pickup—A13
Igo, G.—B2
Jennings, L. D. and Melvin A. Herlin—Y2
Johnson, John L. and William S. Porter—K1
Joki, E. G., L. G. Miller, and J. E. Evans—B4
Jones, R. V., W. Dobrowolsky, W. B. Kunkel, and C. D. Jeffries—R4
Juenker, D. W., R. A. Meussner, and C. E. Birchenall—UA8
Juretschke, H. J., S. J. Freedman, and S. Epstein—L4
Kac, Mark—Q3
Kaiser, H. F.—T9
Kalos, M. H. and R. H. Dalitz—D1
Kaplan, J. I.—FA2
Keller, William E.—Y14
Kelly, R. L.—C10
Kern, B. D. and L. W. Cochran—PA12
Kernan, A. and R. Cester—N6
Kerth, L. T., D. H. Stork, R. W. Birge, R. P. Haddock, and M. N. Whitehead—P1
Keyes, Robert W.—G11
Kim, Y. B., J. R. Burwell, R. W. Hugget, and R. W. Thompson —P11
King, D. T.—P12
Kivelson, D. and D. R. Lide, Jr.—XA6
Kjeldaas, Jr., T. and W. Kohn—FA1
Klarmann, J., M. F. Kaplon, and G. Yekutieli—P4
Klein, Abraham and Bruce H. McCormick—D3
Klerer, M. and R. D. Hatcher—ZA10
Koch, H. W., J. M. Wyckoff, and B. Petree—W5
Koenigsberg, Ernest and Leon Findley—C8
Koester, Jr., L. J.—S10
Kolb, Alan—R5
Kolm, Henry H. and Melvin A. Herlin—Y8
Komar, Arthur—VA13
Konopinski, E.—J2
Koontz, P. G., C. W. Johnstone, G. R. Keepin, Jr., and J. D. Gallagher—W8
Koshiba, M. and M. F. Kaplon—P3
Kriessman, C. J. and S. E. Harrison—GA4
Kurath, Dieter—RA6
Lambertson, Glen R., C. Lasky, and Robert H. Phillips—T4
La Mer, V. K.—U1
Landon, H. H.—B1
Lane, A. M. and C. F. Wandel—RA1
Langsdorf, Jr., A. and R. O. Lane—F3
Laslett, L. Jackson—T8
Lax, Benjamin and Laura M. Roth—L10
Lebowitz, Joel L. and E. P. Gross—FA5
Leder, Lewis B. and L. Marton—R9
Levitas, A.—G4
Lewis, H. W.—Y7
Lewis, M. B. and A. J. F. Siegert—VA7
Lewis, Jr., R. R.—HA3
Lichtenberg, D. B.—D6
Lidofsky, L. J., N. Benczer, and V. K. Fischer—V2
Liebson, S. H. and E. J. West—R8
Lin, Chun C.—XA5
Lin, Lan-Ying and B. R. Russell—UA4
Lind, D. A. and J. J. Van Loef—F8
Linder, S. L.—BA12
Lindsay, Robert and John J. Banewicz—L6
Litherland, A. E., E. B. Paul, G. A. Bartholomew, and H. E. Gove—PA7
Longini, R. L.—L7
Lowitz, D. A., W. Webb, and R. W. Schiessler—LA3
Lurio, A. and A. G. Prodell—BA6
Lutes, O. S. and E. Maxwell—Y5
Mandl, F. and T. Regge—D7
Mann, D. E., Janet Hawkins Meal, and Earle K. Plyler —XA11
Margolis, B., O. Kofoed-Hansen, and E. Nagel—B7
Margulies, R. S.—Z4
Markham, Jordan J.—L8
Martin, D. W., J. M. Cork, and S. B. Burson—YA1
Masek, G. E., A. J. Lazarus, and W. K. H. Panofsky—S1
Mason, W. P.—C7

McDonald, F. B., R. A. Ellis, and M. B. Gottlieb—A9
McEllistrem, M. T., Ren Chiba, R. A. Douglas, D. F. Herring, and E. A. Silverstein—K9
McFarland, Charles E., Franklin B. Shull, Alexander J. Elwyn, and Benjamin Zeidman—TA6
McGruer, J. N., E. K. Warburton, and R. S. Bender—K8
McMillan, W. G.—VA6
Merz, W. J., J. P. Remeika, A. N. Holden, and B. T. Matthias—GA2
Metzger, Franz R.—BA8
Meyer, Peter and J. A. Simpson—A6
Milani, S., John N. Cooper, and J. C. Harris—PA11
Mills, F. E. and L. J. Koester, Jr.—S9
Misner, C. W.—VA11
Mize, J. P., M. E. Bunker, and J. W. Starner—YA3
Moore, J.—B3
Moravcsik, Michael J. and J. Michael Sellen, Jr.—T6
Morgan, Ira L.—F5
Morinaga, H.—TA10
Morris, T. F.—RA14
Moszkowski, Steven A.—RA7
Motz, Hans, K. M. Crowe, and R. M. Friedman—Z2
Motz, Henry—TA12
Moulthrop, Peter H.—S6
Muench, N. L. and H. E. Rorschach, Jr.—Y6
Naugle, J. E., P. S. Freier, and E. P. Ney—A7
Neher, H. V.—E5
Nelson, J. R., J. G. Siegfried, and P. L. Hartman—UA11
Newstein, M. C.—HA2
Neynaber, R. H., W. G. Brammer, and W. W. Beeman—C6
Nicholls, R. W. and W. R. Jarmain—XA10
Nichols, P. F., R. G. Smith, and H. W. Newson—F2
Niestlie, Jr., John W. and Arthur I. Berman—B12
Nigam, B. P. and L. L. Foldy—ZA6
Nobles, R. A., R. L. Henkel, and R. K. Smith—CA2
Novey, T. B.—YA12
Novick, Robert, Edgar Lipworth, and Paul F. Yergin—BA5
Noyes, H. P.—D4
O'Dell, F. W. and M. M. Shapiro—P5
O'Friel, Z. and A. H. Weber—V5
Olbert, S.—VA5
Olness, J. W. and H. W. Lewis—TA1
Page, L. A., M. Heinberg, O. J. Wallace, and T. W. Trout—X5
Palevsky, H., D. J. Hughes, and R. L. Zimmerman—B11
Panofsky, W. K. H. and G. B. Yodh—S7
Paul, E. B., G. A. Bartholomew, H. E. Gove, and A. E. Litherland—PA8
Paulissen, George and Hans Mark—CA6
Peaslee, D. C.—RA2
Percus, J. K. and G. J. Yevick—VA8
Perls, T. A., C. W. Kissinger, and D. R. Paquette—KA13
Peter, M. and M. W. P. Strandberg—XA7
Phillips, G. C., C. R. Gossett, J. P. Schiffer, and P. M. Windham—TA8
Pierce, Louis—XA3
Pilcher, V. E., D. J. Hughes, and J. A. Harvey—B8
Piano, Richard J. and Irwin A. Pless—N4
Platt, J. B.—H1
Pless, Irwin A. and Richard J. Piano—N5
Porter, F. T., M. S. Freedman, T. B. Novey, and F. Wagner, Jr.—YA4
Potnis, V. R., C. E. Mandeville, and John S. Burlew—YA6
Price, P. J.—Y15
Prigogine, Ilya—Q1
Prince, M. B.—G7
Pruett, C. H., H. H. Bolotin, P. L. Roggenkamp, and R. G. Wilkinson—YA2
Pyle, R. V., D. A. Hicks, and John Ise, Jr.—CA4
Rado, G. T.—GA9
Raphael, R. B.—D13
Rarita, William—HA15
Redfield, David—L3
Reynolds, C. A.—Y11
Reynolds, G. T.—E3
Reynolds, H. L. and A. Zucker—N10
Reynolds, J. B., R. L. Christensen, D. R. Hamilton, A. Lemonick, F. M. Pipkin, and H. H. Stroke—BA7
Rinehart, M. C., K. C. Rogers, and L. M. Lederman—Z6
Robinson, Kenneth W.—P8
Rogers, K. C.—Z9
Rosa, Richard J.—KA3
Rose, D. C. and J. Katzman—A3
Rosenberg, R. and M. Lax—RA12
Rosenstock, Herbert B.—UA3
Rotenberg, A. and L. Spruch—RA9
Rothstein, Jerome—C2
Rubin, Robert J. and B. A. Fleishman—UA2
Ruby, Lawrence and James D. Gow—W1
Saenz, A. W.—LA6
Salter, L.—UA1
Salzman, G.—D10
Sands, M., M. Bloch, J. G. Teasdale, and R. L. Walker—S12
Scanlon, W. W.—DA1
Scarf, Frederick L.—ZA5
Schawlow, A. L.—U4
Schein, Marcel, D. M. Haskin, and R. G. Glasser—P14
Schiff, Daniel—VA3
Schiff, L. I.—H4
Schiffer, J. P., P. M. Windham, C. R. Gossett, and G. C. Phillips—TA9
Schiller, Ralph—VA10
Schmitt, R. W.—C1
Schrank, G.—N9, SP2
Schwartz, Robert B., James W. Corbett, and William W. Watson—TA4
Schwarz, E. G. K.—G9
Schwarzmann, Gertrude T.—VA15, SP3
Sclar, N.—DA2
Scott, Mary Jean and Ralph E. Segel—F9
Scott, William T.—HA6
Segrè, Emilio—J3
Seitz, F.—J1
Serber, Robert and William Rarita—HA7
Shafroth, S. M. and J. A. Marcus—X3
Shapiro, I. I. and R. J. Glauber—HA9
Shapiro, M. M.—E4
Sharp, R. D., A. Sperduto, and W. W. Buechner—K11
Sherr, R. and W. F. Hornyak—K13
Sidhu, S. S. and D. D. Zauberis—C5
Simon, Albert—R2
Simpson, F. B., R. G. Fluharty, and O. D. Simpson—B5
Sinclair, Rolf M.—F7
Skulski, R. W. and D. Weimer—KA2
Slonczewski, J. C. and P. R. Weiss—L9
Smith, M. S., R. R. Smith, E. G. Joki, and J. E. Evans—B6
Smither, R. K.—R6
Soberman, R. K., A. Beiser, and S. A. Korff—A4
Sogo, P. B. and C. D. Jeffries—BA9
Solem, A. D. and L. Jansen—LA2
Spencer, L. V.—M2, VA4
Srinivasan, D. and L. V. Holroyd—KA5
Sreekantan, B. V., A. Pevsner, and G. Sandri—P10
Stearns, M. B.—H2
Steffen, R. M.—V8
Steinberg, M. S.—X9
Stelson, P. H. and F. K. McGowan—CA5
Sternglass, E. J. and M. M. Wachtel—R7
Sternheimer, R. M.—D5
Stiller, B., M. M. Shapiro, and N. Seeman—P6
Stolovy, A. and J. A. Harvey—B9
Stork, D. and S. Whetstone—S4
Strandberg, M. W. P.—XA9

Sunyar, A. W.—H3
Swan, P. R. and M. W. P. Strandberg—XA8
Swann, W. F. G.—RA15
Takano, Y. and J. L. Anderson—ZA3
Tanaka, Katsumi—ZA11
Tautfest, G. W. and K. L. Brown—W7
Taylor, J. C. and B. R. Coles—C3
Temmer, G. M. and N. P. Heydenburg—CA9
Theissing, H. H. and P. J. Caplan—FA12
Theoclitus, Gregory and Homer C. Wilkins—KA10
Toller, L. A., J. R. Patterson, and H. W. Newson—F1
Toppel, B. J., D. H. Wilkinson, and D. E. Alburger—K12
Turner, E. B.—KA1
Tyler, W. W.—DA3
Uhlir, Jr., A.—C11
Van Allen, J. A.—A12
Visscher, William M. and Richard A. Ferrell—RA8
Wachtman, Jr., J. B. and L. H. Maxwell—UA6
Wagner, R. T. and F. L. Hereford—X4
Walker, R. L.—E1
Wallis, G. and J. F. Battey—G5
Waniek, R. W., L. Garrido, R. Goloskie, and E. G. Silver—F10
Warren, Dana T.—A1
Watanabe, Satosi and Norman Oleson—R3
Weddell, J. B., B. Jennings, and R. L. Hellens—F6
Wegner, Harvey E., R. M. Eisberg, and G. Igo—N7
Weissman, Sigmund and Roger Chang—UA5
Weller, C. E. and J. C. Grosskreutz—TA11
Wessel, W.—ZA12
Wheeler, John A.—HA13
Whetstone, S. and D. Stork—Z5
White, R. Stephen, Mark J. Jakobson, and Gordon W. Repp—S8
Wightman, A. S. and D. Hall—ZA1
Wilkinson, D. H.—K10
Wilkinson, M. K., C. G. Shull, and R. E. Rundle—GA6
Williamson, R. M. and S. A. Cox—PA6
Winckler, J. R. and L. Peterson—A2
Woods, Joseph F.—UA10
Wyckoff, J. M. and H. W. Koch—CA1
Yadoff, Oleg and Sophie Yadoff—KA14
Yadoff, Oleg—SP1
Yagoda, Herman—S3
Yearian, H. J. and W. D. Derbyshire—GA3
Yekutieli, G., M. F. Kaplon, and J. Klarmann—P2
Yevick, G. J. and J. K. Percus—VA9
Yilmaz, Huseyin—VA14
Ziegler, C. A., H. H. Seliger, and I. Jaffe—W4
Zinn, W. H.—J4